Twelfth Annual Conference on Mass Spectrometry and Allied Topics

June 7-12, 1964
Montreal, Canada

Arranged by the Officers of
ASTM Committee E-14

Twelfth Annual Conference on Mass Spectrometry and Allied Topics

June 7-12, 1964
Montreal, Canada

Arranged by the Officers of
ASTM Committee E-14

PREFACE

This volume is a collection of papers presented at the Twelfth Annual Conference on Mass Spectrometry and Allied Topics*, held in Montreal, Canada, June 7-12, 1964. It is intended that this volume be distributed only to registrants of the Twelfth Annual Conference, and therefore, should not be considered as a publication.

A particular acknowledgement is due to Dr. A. B. King for handling the details of program arrangements and for assembling and editing this volume.

N. D. Coggeshall, Program Chairman

* Arranged by the officers of the ASTM Committee E-14.

R. E. Fox, Chairman
N. D. Coggeshall, Vice-Chairman
A. G. Sharkey, Jr., Vice-Chairman
H. E. Lumpkin, Secretary
S. Meyerson, Member-at-Large
A. L. Wahrhaftig, Member-at-Large

TABLE OF CONTENTS

TWELFTH ANNUAL CONFERENCE ON MASS SPECTROMETRY AND ALLIED TOPICS

Montreal, Canada, June, 1964

MASS SPECTRAL STUDIES OF FREE RADICALS, ATOMS AND EXCITED MOLECULES — Page No.

1.* Pyrolysis Studies By Mass Spectrometry
Jacques E. Collin,
University of Liege,
Liege, Belgium 1

2.* Vertical Ionization Potentials of C_2F_5, C_3F_7 and CF_2 Radicals
I. P. Fisher and F. P. Lossing,
National Research Council,
Ottawa, Ontario 5

3.* Mass Spectrometric Study of the Heterogeneous Recombination of CH_3 and C_2H_5 Free Radicals
P. Le Goff, A. Cassuto and A. Pentenero,
Universite de Nancy,
Nancy, France 6

4.* Mass Spectrometric Sampling and Detection of Intermediates for Gaseous Reactions
J. Cuthbert,
United Kingdom Atomic Energy Authority,
Berkshire, England 15

5.* Stern-Gerlach Experiments Using Mass Spectrometric Detection
J. Berkowitz and L. S. Goodman,
Argonne National Laboratory,
Argonne, Illinois 31

6.* Some Recent Developments in the Study of Ionization Processes
James D. Morrison,
C.S.I.R.O.,
Melbourne, Australia 32

7.* The Photoionization and Dissociation of Some Di- and Tri-Atomic Molecules
D. C. Frost, D. Mak, C. A. McDowell, and
D. A. Vroom,
University of British Columbia,
Vancouver, B.C. 39

8.* Mass Spectrometric Detection of Reaction Intermediates from Flash Photolysis
P. Kebarle, R. P. Massmer, O. P. Strausz,
and H. E. Gunning,
University of Alberta,
Edmonton, Alberta 49

9.* Mass Spectrometric Studies of Oxygen Atom Reactions
John T. Herron and Fritz S. Klein,
National Bureau of Standards,
Washington, D. C. 50

10.* Kinetics of O_3 Formation in a Stream of Electrically Discharged O_2
A. Mathias and H. I. Schiff,
McGill University,
Montreal 59

* Invited Paper

TABLE OF CONTENTS - Continued

MASS SPECTRAL STUDIES OF FREE RADICALS, ATOMS AND EXCITED MOLECULES - Continued — Page No.

11.* Ion-Molecule Reactions in Combustion Plasmas and Atomic Diffusion Flames
W. J. Miller, H. F. Calcote, and A. Fontijn, AeroChem Research Laboratories, Inc., Princeton, New Jersey 67

BASIC INSTRUMENT ADVANCES

12.* The Mass Spectrometry of Ions in Glow Discharges
P. H. Dawson, P. F. Knewstubb, and A. W. Tickner, National Research Council, Ottawa, Ontario 80

13.* Advances In Time-Of-Flight Mass Spectrometry
D. C. Damoth, The Bendix Corporation, Cincinnati, Ohio 84

14.* Basic Properties of Electron Multiplier Ion Detection and Pulse-Counting Methods in Mass Spectrometry
Leonard A. Dietz, Knolls Atomic Power Laboratory, Schenectady, N. Y. 91

15.* The Application of Thermal Imaging Techniques to Mass Spectrometric Studies of High Temperature Chemistry
Richard P. Burns and Andrew J. Jason, University of Chicago, Chicago, Illinois 105

16.* Recent Atomic Mass Determinations at McMaster University
R. C. Barber, H. E. Duckworth, B. G. Hogg, J. D. Macdougall, W. McLatchie, and P. Van Rookhuyzen, McMaster University, Hamilton, Ontario 106

FUNDAMENTAL ASPECTS -- I

17. Ionization Studies Using "Mono-energetic" Electrons
C. E. Brion, D. C. Frost, and C. A. McDowell, University of British Columbia, Vancouver, B. C. 118

18. Effect of Molecular Structure on the Ionization Probabilities of Aromatic Molecules
F. T. Deverse and A. Bruce King, Gulf Research & Development Company, Pittsburgh, Pennsylvania 125

19. Effects of Electron Energy Distributions on Ion Appearance Potential Measurements
Dwight A. Hutchison, Argonne National Laboratory, Argonne, Illinois 134

20. An Effect of Electronic Space Charge on Ionization Curves Probability
P. Marmet, Université Laval, Québec 140

* Invited Paper

TABLE OF CONTENTS - Continued

FUNDAMENTAL ASPECTS -- I - Continued

Page No.

21. Determining Appearance Potentials from Non-ideal Ionization Efficiency Curves
Harry J. Svec and Gerard D. Flesch,
Iowa State University,
Ames, Iowa 145

22. Comparison of Metastable Spectra from Single and Double Focusing Mass Spectrometers
M. Barber and R. M. Elliott
Associated Electrical Industries Limited,
Manchester, England 150

23. Direct Observation of Pairs of Positive Ions Resulting from the Decomposition of CO_2^{++}
K. E. McCulloh, T. E. Sharp, and H. M. Rosenstock,
National Bureau of Standards,
Washington, D. C. 158

24. Ion-Molecule Reactions in Methane at Low Ion Energies
A. G. Harrison and T. W. Shannon,
University of Toronto,
Toronto, Ontario 160

25. Cross Sections for the Ion-Molecule Reaction $H_2 + H_2^{+*} = H_3^+ + H$ as a Function of the Vibrational State of the H_2^+ Ion
A. Weingartshofer and E. M. Clarke,
St. Francis Xavier University
Antigonish, Nova Scotia 166

26. Thermal Rate Constants for Ion-Molecule Reactions by a Pulse Technique
Keith R. Ryan and Jean H. Futrell,
Aerospace Research Laboratories,
Wright-Patterson Air Force Base, Ohio 169

INSTRUMENTATION -- I

27. A High Duty Cycle, Radio-Frequency, Time-Of-Flight Mass Spectrometer
R. M. Mills,
National Bureau of Standards,
Washington, D. C. 177

28. Analyzer Sensitivity Parameters in a Double Focusing Mass Spectrograph
C. W. Hull,
Consolidated Electrodynamics Corporation,
Pasadena, California 183

29. A Cold Electron Mass Spectrometer Ion Source
M. K. Testerman, B. E. Gilliland, and E. M. King,
University of Arkansas,
Little Rock, Arkansas 192

30. Monopole Mass Spectrometer (Withdrawn)
Richard F. Herzog,
Geophysics Corporation of America,
Bedford, Massachusetts 193

31. A Simple Mass Spectrometer for Analysis of Argon at Ultra-High Vacuum
E. Farrar, R. M. MacIntyre and Derek York,
University of Toronto,
Toronto, Ontario 194

TABLE OF CONTENTS - Continued

INSTRUMENTATION -- I - Continued

Page No.

32. Apparatus for the Simultaneous Observation of Electrical Conductivity and Gas Diffusion in Crystals
P. P. Pronko and H. R. Krouse,
University of Alberta,
Edmonton, Alberta 201

33. A New Counting Method for Mass Spectrometry
George W. Barton, Jr., Ronald Jene Dupzyk, and
Laurin F. Tolman,
University of California,
Livermore, California 208

34. Electron Multipliers for Use in Mass Spectrometry
B. R. F. Kendall,
Nuclide Corporation,
State College, Pennsylvania 211

35. Comparison of 21-103 Electrometer and Electron Multiplier Spectra
R. A. Meyer,
North American Aviation Science Center,
Canoga Park, California 218

36. Electron Multiplier Detectors in Mass Spectrometry
Heinz G. Boettger,
Consolidated Electrodynamics Corporation,
Pasadena, California 224

37. Simple Data Display System for Fast-Scanning Mass Spectrometer
D. G. H. Marsden, W. Forst, and K. K. Feng,
Université Laval, Québec, and
K. Park,
C.A.R.D.E.,
Quebec 229

TECHNIQUES OF MASS SPECTROSCOPY OF SOLIDS

38.* On the Production of Positive Ions From Solids
Richard E. Honig,
RCA Laboratories,
Princeton, New Jersey 233

39.* Sources of Fluctuations in the Mass Spectroscopic Analysis of Solids by Vacuum Discharge Techniques
J. Franzen, K. D. Schuy, and H. Hintenberger,
Max Planck-Institut fur Chemie (Otto Hahn Institute),
Mainz, Germany 251

40.* Photographic Emulsions as Ion Detectors in Quantitative Mass Spectrography
Edward B. Owens,
Massachusetts Institute of Technology,
Lexington, Massachusetts 271

41.* Mass Spectrographic Microprobe Analysis
W. M. Hickam and G. G. Sweeney,
Westinghouse Research Laboratories,
Pittsburgh, Pennsylvania 280

* Invited Paper

TABLE OF CONTENTS - Continued

FUNDAMENTAL ASPECTS -- II

Page No.

42. Mass Spectra of Ortho-Substituted Diarylmethanes
Seymour Meyerson,
American Oil Company, and
H. J. Drews and E. K. Fields,
Amoco Chemicals Corporation,
Whiting, Indiana 281

43. Mass Spectral Fragmentation of Phenyl-n-Alkanes
A. Bruce King,
Gulf Research & Development Company,
Pittsburgh, Pennsylvania 288

44. Mass Spectrometric Study of Photoionization of Acetylene, Acetylene-d_2, Benzene, Benzene-d_6
Vernon H. Dibeler and Robert M. Reese,
National Bureau of Standards,
Washington, D. C. 300

45. Ionization of Polyatomic Molecules in Collisions with Excited Metastable Noble Gas Atoms
V. Cermak and Z. Herman,
Czechoslovak Academy of Science,
Prague, Czechoslovakia 308

46. Rare Gas Ion Reactions with Pentaborane-9
G. R. Hertel and W. S. Koski,
The Johns Hopkins University,
Baltimore, Maryland 315

47. The Migration of the Oxygen Atom in Unimolecular Ion Decomposition
I. Omura,
Hitachi Central Research Laboratory,
Tokyo, and
Y. Nakajima and H. Sato,
Hitachi Naka Works,
Ibaragi Perfecturey, Japan 321

48. Ion Decomposition Mechanisms
F. W. McLafferty, R. S. Gohlke, and
R. C. Golesworthy,
The Dow Chemical Company,
Framingham, Massachusetts 331

49. Mass Spectrometry in Carbohydrate Chemistry: Dithioacetal-Peracetate Derivatives
Don C. DeJongh, Wayne State University,
Detroit, Michigan 334

50. Mass Spectrometric Studies of Unsaturated Methyl Esters
W. K. Rohwedder, A. F. Mabrouck, and E. Selke
Northern Regional Research Laboratory,
Peoria, Illinois 339

51. Radiofrequency Absorption Experiments in the Omegatron
P. M. Llewellyn and D. P. Littlejohn,
Varian Associates,
Palo Alto, California 346

SOLID SOURCE STUDIES

52. Interatomic Properties of Solids Demonstrated in Spark Ion Source
Berge B. Goshgarian and Andreas V. Jensen,
Air Force Rocket Propulsion Laboratory,
Edwards, California 350

SOLID SOURCE STUDIES - Continued

Page No.

53. Spark Source Mass Spectrographic Analysis of Some Nickel and Iron Base Alloys
H. D. Cook, T. Kessler, and L. T. Beeles,
Bettis Atomic Power Laboratory,
Pittsburgh, Pennsylvania 358

54. Mass Spectrographic Analysis of Rare Earth Metals
J. W. Guthrie,
Sandia Corporation,
Albuquerque, New Mexico 359

55. The Analysis of Solids in Reactor Moderator by Spark Source Mass Spectrometry
P. Chastagner,
E. I. du Pont de Nemours & Company,
Aiken, South Carolina 365

56. Mass Spectrometric Analysis Using a DC Spark Source
J. S. Halliday, A. Harrison and A. Riddoch,
Associated Electrical Industries Limited,
Manchester, England 369

57. Energy Distribution of Ions Formed in the RF Spark Source -- II. Individual Species
J. Rogers Woolsten and Richard E. Honig,
RCA Laboratories,
Princeton, New Jersey 377

58. Electron Induced Surface Ionization Mass Spectrometry
David Lichtman,
Honeywell Research Center,
Hopkins, Minnesota 384

59. The Mass Analysis of Small Samples Utilizing a Sputtering Ion Source
James A. McHugh and James C. Sheffield,
Knolls Atomic Power Laboratory,
Schenectady, New York 388

60. Sputtering Ion Source for Solids
Helmut J. Liebl and Richard F. K. Herzog,
Geophysics Corporation of America,
Bedford, Massachusetts 393

61. Mass Spectrometric Studies of Sputtered Particles From Copper Monocrystals
A. L. Southern,
Oak Ridge National Laboratory,
Oak Ridge, Tennessee 398

ANALYTICAL PROBLEMS AND DEVELOPMENTS

62.* Some Uses, Misuses and Abuses of the Time-Of-Flight Mass Spectrometer
R. S. Gohlke,
The Dow Chemical Company,
Framingham, Massachusetts 404

63.* Mass Spectrometric Investigation of Gases From Flash and Laser Irradiation of Coal
A. G. Sharkey, Jr., J. L. Shultz and
R. A. Friedel,
Bureau of Mines,
Pittsburgh, Pennsylvania 405

* Invited Paper

ANALYTICAL PROBLEMS AND DEVELOPMENTS - Continued

Page No.

64.* Use of the Mass Spectrometer in the Space Industry
N. A. Mackie and C. P. Boebel,
Valley Forge Space Technology Center,
Philadelphia, Pennsylvania 411

65.* Alkanes-Records of Prehistoric Life
W. G. Meinschein,
Esso Research & Engineering Company,
Linden, New Jersey 418

HIGH RESOLUTION ORGANIC ANALYSIS

66. Analysis of Sub-Microgram Samples of Organic Compounds by Mass Spectrometry
R. M. Elliott, T. O. Merren, and W. A. Wolstenholme,
Associated Electrical Industries Limited,
Manchester, England 419

67. Analysis of A Trinuclear Aromatic Petroleum Fraction by High Resolution Mass Spectrometry
H. E. Lumpkin,
Humble Oil & Refining Company,
Baytown, Texas 423

68. Techniques in the High-Resolution Mass Spectrometry of Complex, Polyfunctional Organic Molecules
P. Bommer, W. McMurray, and K. Biemann,
Massachusetts Institute of Technology,
Cambridge, Massachusetts 428

69. Computer Techniques for the Fast and Facile Conversion of Line Positions to Elemental Compositions of Ions Recorded on Photographic Plates
D. Desideri and K. Biemann,
Massachusetts Institute of Technology,
Cambridge, Massachusetts 433

70. High-Resolution Mass Spectra of Compounds Emerging from a Gas Chromatograph
J. T. Watson and K. Biemann,
Massachusetts Institute of Technology,
Cambridge, Massachusetts 438

71. High-Resolution Mass Spectra of Organic Molecules and Their Use for Structure Determination
K. Biemann, W. McMurray, and P. Bommer,
Massachusetts Institute of Technology,
Cambridge, Massachusetts 442

72. Photographic Recording of Mass Spectra of Heavy Organic Molecules
N. Sasaki,
Kyoto University,
E. Watanabe, M. Naito, M. Samura, T. Aoyama,
S. Enomoto, and M. Ishibashi,
Japan Electron Optics Laboratory Company, Ltd.,
Akishima, Tokyo, Japan 447

73. A New Highly Resolving Commercial Mattauch Type Mass Spectrometer for the Analysis of Organic and Inorganic Samples
Karleugen Habfast,
Atlas Mess-und Analysen Technik-GMBH,
Bremen, Germany 451

* Invited Paper

INSTRUMENTATION -- 11

Page No.

74. Quadrupole Mass Spectrometer for Atmospheric Studies in the 50- to 90-Kilometer Range
Wilson M. Brubaker, Norton W. Bell, and Frank B. Wiens, Bell & Howell Research Center, Pasadena, California 456

75. Quadrupole Mass Spectrometer for Energetic Particle Measurements
L. G. Hall and M. R. Ruecker, Consolidated Systems Corporation, Monrovia, California 463

76. A Quadrupole Mass Spectrometer for Isotope Ratio Studies of Plasma Constituents
M. A. Mosharrafa and H. J. Oskam, University of Minnesota, Minneapolis, Minnesota 473

77. Time-Of-Flight Mass Spectrometric Analyses of a Multi-Kilowatt Plasma
G. J. O'Halloran and L. W. Walker, The Bendix Corporation, Southfield, Michigan 479

78. Performance of the High Voltage Engineering Corporation Isotope Separator
George W. Barton, Jr., Abe Tilles, and J. R. Walton, University of California, Livermore, California, and Richard J. Connor and Thomas C. Smith, High Voltage Engineering Corporation, Burlington, Massachusetts 480

79. Flash Vaporization of Solid Material for Mass Spectrometry by Intense Thermal Radiation
Kenneth A. Lincoln, U. S. Naval Radiological Defense Laboratory, San Francisco, California 481

80. Negative Ions of I, II, and III Elements
Kumasaburo Kodera, and Tutomu Makita, Kyoto University, Kyoto, Japan, and Brown University, Providence, R. I. 486

81. Microtrace Analysis of Lithium Isotopes in Metal Targets Bombarded by High Energy Protons
R. Bernas, M. Epherre, E. Gradsztajn, R. Klapisch, and F. Yiou, Laboratorie Joliot-Curie, Orsay (Seine-et-Oise), France 489

ANALYTICAL APPLICATIONS

82. A Mass Spectrometer Method for Analysis of Alkylates for Bio-Soft Detergents
F. J. Galbraith, D. J. Skahan, N. P. Kilargis, and P. J. Contino, The Atlantic Refining Company, Philadelphia, Pennsylvania 493

83. Determination of Phenyl Position Distribution in N-Alkyl-benzenes by Mass Spectrometry
Harrell T. Ford, Continental Oil Company, Ponca City, Oklahoma 499

ANALYTICAL APPLICATIONS - Continued

Page No.

84. Ion Chamber Modifications and Sampling Techniques for Obtaining the Mass Spectra of Low Vapor Pressure Substances
Gregor A. Junk and Harry J. Svec,
Iowa State University,
Ames, Iowa 500

85. Chromatographic Efficiency During Combined Mass Spectrometric Gas Chromatographic Analysis
W. H. McFadden, R. Teranishi, T. R. Mon, and Janet Wasserman,
Western Regional Research Laboratory,
Albany, California 506

86. A Mass Spectrometric Procedure for the Identification and Measurement of Trace Components in Noncondensable Media
W. J. Lambdin, Jr. and H. E. Persinger,
Union Carbide Corporation,
South Charleston, West Virginia 512

87. Simplified Mass Spectra
Graham G. Wanless and George A. Glock, Jr.,
Esso Research & Engineering Company,
Linden, New Jersey 517

88. The RMU-6D -- A Versatile Single/Double Focusing Mass Spectrometer System
Y. Nakajima and T. Noda,
Hitachi Naka Works,
Ibaraki, Japan, and
H. Tsuyma and J. Okamoto,
Hitachi Central Research Laboratory,
Tokyo, Japan 524

89. Design Considerations for a Miniaturized Time-Of-Flight Aerospace Partial Pressure Sensor
J. F. Betts, G. J. O'Halloran, and G. T. Wassell,
The Bendix Corporation,
Southfield, Michigan 531

90. Mass Spectrometric Analysis of Gaseous Impurities in Refractory Metals
J. D. Reynolds,
General Dynamics/Fort Worth
Fort Worth, Texas 532

91. Analysis of Trace Contaminants in Permanent Gases
John Roboz,
Air Reduction Company, Inc.,
Murray Hill, New Jersey 536

GENERAL

92. Characteristics of Ion-Sensitive Emulsions for Mass Spectroscopy
J. M. McCrea,
United States Steel Corporation,
Monroeville, Pennsylvania 541

93. A Computer Program for the Quantitative Interpretation of Mass Spectrograph Plates
Philip R. Kennicott,
General Electric Research Laboratory,
Schenectady, New York 550

94. Plate Reader for Mass Spectrograph
George D. Perkins,
Bell & Howell Research Center,
Pasadena, California 553

TABLE OF CONTENTS - Continued

GENERAL - Continued

Page No.

95. An Electronic Data System for Spark Source Spectrometry
R. J. Dupzyk, G. W. Barton, Jr., R. D. Carver, and R. A. Thomas,
Lawrence Radiation Laboratory,
University of California,
Livermore, California 557

96. Mass Spectrometric Study of the Mass Yields in the Thermal Neutron Fission of Pu^{241}
H. Farrar,
Atomics International,
Canoga Park, California,
W. B. Clarke,
University of California,
LaJolla, California, and
R. H. Tomlinson and H. G. Thode,
McMaster University,
Hamilton, Ontario 562

97. Mass Spectrometric Determination of the Ratio of the Neutron Capture to Fission Cross-Sections of U-235
M. Lounsbury, I. H. Crocker, R. W. Durham, and A. Okazaki,
Atomic Energy of Canada Limited,
Chalk River, Ontario 569

98. The Effect of an Axial Temperature Gradient on the Apparent Pressure in a Knudsen Effusion Cell
Edmund K. Storms,
University of California
Los Alamos, New Mexico 573

99. Mass Spectrometry and the Properties of Condensed Systems at High Temperatures (Withdrawn)
P. Breisacher,
Aerospace Corporation,
El Segundo, California 580

100. The Use of a Mass Spectrometer to Demonstrate the Existence of Gaseous $Ba(OH)_2$
R. S. Newbury, A. W. Searcy, and G. W. Barton, Jr.,
Lawrence Radiation Laboratory,
University of California,
Livermore, California 581

101. A Twin-Crucible Study of the Lithium Fluoride-Beryllium Fluoride System
Alfred Buchler and James L. Stauffer,
Arthur D. Little Inc.,
Cambridge, Massachusetts 582

BIBLIOGRAPHY OF PUBLISHED AND UNPUBLISHED PAPERS ON MASS SPECTROMETRY FOR 1963 587
Subcommittee II Fundamental Aspects 588
Subcommittee III High Molecular Weights and Techniques 641
Subcommittee V Instrumentation and Techniques . . 651

Pyrolysis studies by mass spectrometry(*)

by Jacques E.Collin

Institut de Chimie générale,
Université de Liège
LIEGE (Belgique)

I. Experimental.

1.Working conditions.

The purpose of this work is the study, by means of a Bendix-TOF-Model 14 mass spectrometer, of the behaviour of organic compounds at high temperatures in conditions corresponding to an intermediate situation between homogeneous and heterogeneous decomposition. Biphenyl and ethylnitrite were investigated. A small hole,0.3 mm. Ø, in the wall of the ion source, was used to sample directly the gases from the reaction chamber where the furnace was located.

The reactor is a quartz tube, inside 8 mm Ø, length around 70 mm.,heated by a tantalum wire and surrounded by a double tantalum heat reflector, and a cooling element. Temperatures were measured in the central axis of the furnace by means of a Pt/Pt-Rh thermocouple, and were regulated within 0.5%, up to 1100°C. The gas under study was introduced at pressures of the order of 30-80 microns, and was pumped off by means of a 80 l./sec. oil diffusion pump.

No carrier gas was used and the residence times of molecules in the reactor were estimated to be of the order of 50 to 100 millisec. In those conditions, it was considered that the observed reactions were probably neither purely heterogeneous nor purely homogeneous, and the free radical yield, if any, was expected to be low.

2. Difficulties.

Variation of the wall conditions during an experiment, and degassing, particularly at high temperatures, result in the appearance of species which vary from one experiment to the other. It is thus very difficult to use background spectra and to estimate possible by-products. The nature of products and their contribution to the mass spectrum are difficult to ascertain. In some cases, the use of deuterated compounds was of great help.

The real temperature of the molecules in the ion chamber is not known. If they have the same temperature as in the furnace, a correction factor should be applied and gives minimum decomposition yields, whereas without correction, these values are maximum. A mean value has been adopted as probably closer to the real situation.

II. Pyrolysis of Biphenyl.

1. Introduction.

With helium as a carrier gas, and for short residence times, it has been observed that biphenyl decomposes homogeneously only above 1300°C, and the products were traces of phenyl radical, H_2, C, C_2H_2, C_2H_4, C_4H_6 and C_6H_6[1].

At high pressures on the contrary, decomposition has been reported already at 400°C[2], the activation energy being 74 Kcal/mole, and the products were H_2, CH_4, C_2H_6, C_3H_8, C_4H_{10} and polyphenyls.

2. Experimental results.

a) Decomposition.

In the conditions of our experiments, we note already appreciable decomposition of biphenyl above 400-450°C, at pressures of the order of 20 microns. The results are given in table I where maximum and minimum are indicated. The same results were obtained with deuterated biphenyl $C_{12}D_{10}$.

* Work done in part under Euratom Contract N° 049-61-12-ORG B.

Table 1

Decomposition of Biphenyl (in %)

Temperature °C		400	450	500	550	600	650	700
$C_{12}H_{10}$:	min.	-	-	-	-	-	4	8
	max.	1	4	5	8	10	15	20
	prob.	.5	2	3	4	5	9.5	14
$C_{12}D_{10}$	prob.	-	2	3	6	9	13	18

Temperature °C		750	800	850	900	950	1000
$C_{12}H_{10}$:	min.	16	16	24	30	41	55
	max.	28	29	38	42	52	64
	prob.	20	23	31	36	47	60
$C_{12}D_{10}$	prob.	25	28	32	37	-	-

b) Products of decomposition.

A search for C_3H_3 and C_6H_5 free radicals was undertaken, suggested by the important increase of the corresponding mass peaks at high temperature. Simultaneous recordings of the parent ion intensity and mass 39 (C_3H_3) , or the parent and mass 77 (C_6H_5) were taken at low electron energy (11 ev.) The results are shown in figure 1 for the C_3H_3 ion. A similar curve is obtained for C_6H_5. Although the sensitivity is poor at low voltage, the experimental evidence indicates the presence of these two radicals.

Fig.1

The qualitative analysis is difficult and some possible products were rejected after analysis of the results obtained with deuterated biphenyl. Different pumping speeds were used to help elucidate the mechanisms.

The following conclusions could be drawn:

(1) There was no formation of CH_4 or C_2H_6.

(2) No propylene was obtained but a fair amount of propyne.

(3) Benzene is formed and a compound of formula C_6H_4, possibly hexadiyne-1,5-ene-3.

(4) There is indication of formation of C_2H_3 radicals, although these could not be detected at low voltage.

(5) Vinylacetylene C_4H_4 is formed.

(6) The C_3H_3 and C_6H_5 free radicals are present.

(7) Above 800°C, great amounts of carbon atoms are observed.

3. Discussion.

The molecular diagram of biphenyl, excited biphenyl and ionized biphenyl has been calculated by Burr and al.(3) (see table 2), and an examination of the mass spectrum of biphenyl indicates that the relative abundances of groups of ions corresponding to a given bond breakage follow qualitatively the bond orders. An analogous behaviour might be expected for the breakdown of the neutral molecule when thermally excited, leading principally to the opening of the central C-C bond.

Table 2

Bond orders for Biphenyl and Biphenyl Ion[3]

Bond	Ground State	Excited State	Ionic State
1-2,1-6, 9-10, 10-11	.6601	.5845	.6043
2-3,5-6, 8-9, 11-12	.6766	.7605	.7186
3-4,4-5, 7-8, 7-12	.6188	.4087	.5137
4-7	.3697	.6161	.4929

Decomposition is unexpectedly already observed at 400-450°C, although the central C-C bond is calculated to be equal to 103 kcal, whereas the experimental activation energy of decomposition was previously found to be 74 kcal[2].

This is the probable origin of phenyl radicals, their recombination being known not to be favoured [4].

Hydrogen abstraction may then lead to the formation of benzene molecules and of polyphenyls, however not detected in this research: $C_6H_5 + C_6H_5.C_6H_5 \longrightarrow C_6H_6 + {}^{\bullet}C_6H_4.C_6H_5 \longrightarrow$ polyphenyls. If some molecules are in excited state, to which corresponds a drastic change in bond orders, the bond adjacent to the central one becomes weaker and an opening there might happen leading possibly to 1-phenyl-2,6-diene-4-yne-hexane, where C-C bond rupture would give the C_2H_3, C_4H_3, C_6H_5 radicals too.

The origin of the C_3H_3 free radical is not clear, nor its structure. An open non rearranged radical such as $C_6H_5-{}^{\bullet}C = CH - CH = CH - CH = CH^{\bullet}$, possibly excited, might lead to such fragment.

III. Pyrolysis of Ethylnitrite.

1. Decomposition.

Experiments have been made between 25°C and 600°C; after deduction of the nitrite contribution to the mass spectrum, the following percentages of total ionization remained:

T°	200	250	300	350	400	450	500
% total ioniz.	19.80	59.06	88.45	97.53	98.94	99.75	100.0

Decomposition is then practically complete above 400°C, in agreement with previous results of conventional kinetics experiments[5].

2. Products of decomposition and reaction.

The formation of ethanol is observed and is attributed to the reaction of ethoxy radicals with ethylnitrite, the ethoxy radical being the primary product of decomposition, as a consequence of the very low dissociation energy for the RO-NO bond in nitrites[6].

$$C_2H_5ONO \longrightarrow C_2H_5O + NO$$

$$C_2H_5O + C_2H_5ONO \longrightarrow C_2H_5OH + CH_3CHONO \longrightarrow CH_3CHO + NO$$

Simultaneous formation of acetaldehyde is indeed observed. Mass 30 is important and not more than about 1/6 of its abundance may be shown to be due to CH_2O, the remaining being essentially NO, and possibly some ethane.

A considerable decrease of the alcohol contribution and of the acetaldehyde contribution was observed above 350°C. At the same time, ethylene, water, CO and probably methane appear, suggesting that around 350°C, ethylalcohol undergoes deshydration to give ethylene and water, whereas acetaldehyde decomposes into methane and carbone monoxide.

It is hoped to get a more accurate description of the decomposition by studying the case of deuterated nitrite C_2D_5ONO, which should help in distinguishing species such as CH_4, $^{13}CH_3$ and O; C_2H_4 and CO; C_2H_6NO and CH_2O, appearing normally at the same mass number.

Financial assistance of the European Commission for Atomic Energy (Euratom) is gratefully acknowledged.

References

(1) F.P.Lossing, K.V.Ingold. Can.J.Chem. 31, 30, 1963

(2) D.R.de Halas: 2d Atomic Energy Conference, Geneva, 29, 287, 1958

(3) J.G.Burr, J.M.Scarborough, R.H.Shudde.J.Phys.Chem. 64, 1359, 1960

(4) G.W.Taylor.Can.J.Chem. 35, 739, 1957

(5) P.Gray. Trans.Far.Soc. 52, 344, 1956

(6) F.O.Price, E.L.Rodowskas. J.Am.Chem.Soc. 55, 350, 1937.

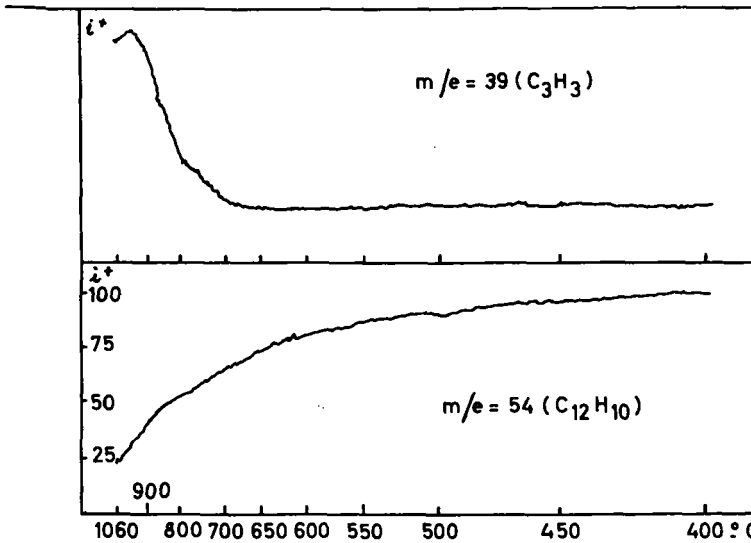

Vertical Ionization Potentials of C_2F_5, C_3F_7 and CF_2 Radicals

I. P. Fisher and F. P. Lossing

Division of Pure Chemistry, National Research Council, Ottawa

ABSTRACT

The C_2F_5, n-C_3F_7 and iso-C_3F_7 radicals have been produced by the thermal decomposition of $(C_2F_5)_2N_2$ and $Hg(C_3F_7)_2$ in a reactor coupled to a mass spectrometer. The vertical ionization potentials were found to be C_2F_5 9.98v, n-C_3F_7 10.06v, and iso-C_3F_7 10.50v. The increase from C_2F_5 to iso-C_3F_7 shows that the CF_3 group acts as a strongly electrophilic substituent. Substitution on the adjacent carbon has only a slight effect, as shown by the near equality of $I(C_2F_5)$ and $I(n\text{-}C_3F_7)$. In terms of simple group interactions the present findings cannot be reconciled with $I(CF_3)$ = 10.2v found by direct ionization of CF_3 radicals, but would require $I(CF_3)$ to be 9.5 - 9.6v. This is closer to the value $I(CF_3)$ = 9.3v proposed by Dibeler et al. Owing to a lack of information on the ionization potentials of fluorinated hydrocarbons the validity of group-orbital calculations for fluorocarbon radicals is questionable, however.

At furnace temperatures above 950°C, C_2F_5 radicals dissociated to form CF_3 and CF_2 radicals. Measurements on CF_2 gave $I_{vert}(CF_2)$ = 11.7v. Taken with $A(CF_2^+)$ from C_2F_4, this value gives $D(CF_2 = CF_2) \sim 81$ kcal/mole and $\Delta H_f(CF_2) \sim -36$ kcal/mole. Such large stability for CF_2 is consistent with the observed thermal dissociation of C_2F_5 into $CF_3 + CF_2$, rather than into $C_2F_4 + F$.

MASS SPECTROMETRIC STUDY OF THE HETEROGENEOUS

RECOMBINATION OF CH_3 AND C_2H_5 FREE RADICALS

by P. LE GOFF, A. CASSUTO and A. PENTENERO

Centre de Recherches de Cinétique Physico-Chimique (C.N.R.S.)

Université de NANCY - France

For ten years, we have been studying by mass spectrometry various heterogeneous gas-solid reactions in various reactors. To day, I would like to discuss the theory of the operation of tubular reactors and its application to the study of the recombination of CH_3 and C_2H_5 free radicals (ref. 6-7).

Figure 1 presents the principle of one of our apparatus : the gas to be decomposed travels through a reactor composed of a quartz tube 2 mm diameter and 25 mm length that can be heated to 1000° C ; the reactor opens in a large vessel with a pumping rate of 400 l/sec. ; the ionization chamber is located in the stream coming out from the reactor, so that the mean gas concentration in the chamber is 50 times that in the vessel.

The reactions that have been studied are the decompositions of dimethyl mercury and diethyl mercury and of mixtures of these substances. But, before speaking of experimental results, we must study in details the flow pattern of gases in the reactor and in the ionization chamber.

PART I : STATISTICAL ANALYSIS OF THE OPERATION OF A REACTOR IN KNUDSEN FLOW

Let us study a reactor through which a gas is travelling at a very low pressure. The molecules come from a vessel situated before the reactor, that we shall call pre-reactor. In the reactor, these molecules undergo many collisions upon the walls. The molecules zigzag, going backwards almost as much as forwards. At the end of such path, some molecules will leave the reactor through the lower mouth (the "EXIT") and others will go back to the pre reactor through the upper-mouth of the reactor (the "ENTRANCE"). (See fig. 2).

For N molecules coming in the reactor, $N\phi$ molecules come out through the exit. They will be called particles of the direct type ; $N(1-\phi)$ are particles of the opposite type, i. e. molecules coming back into the pre-reactor. ϕ is the transparency of the reactor.

Because of the chemical reaction, the N reactive particles entering the reactor can be finally divided into 4 classes according to the following table :

TABLE 1

PARTICLES BALANCE IN AN OVERALL REACTOR

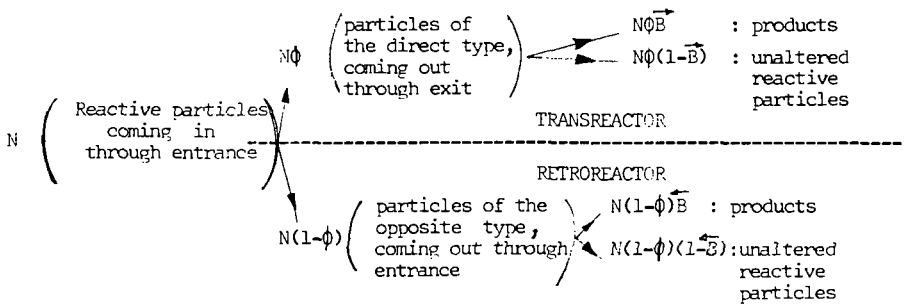

In such cases, the real reactor appears as a superposition of two fictitious and distinct reactors :

- the transreactor would only contain the particles of the direct type leaving the reactor through the exit,

- the retroreactor would only contain the particles of the opposite type, leaving the reactor through the entrance.

Let us call "efficiency $\vec{B}$" of the transreactor, the probability that a particle coming out through the exit will have suffered the chemical transformation. Similarly $\overleftarrow{B}$ is the retroreactor efficiency.

Operation of the transreactor :

We shall now study the only exemple of the transreactor, but obviously an almost similar study might be carried out for the retroreactor.

Let us consider a molecule coming into the reactor, collinding many times against the reactive surface, then going out of the reactor with a "collision" upon the exit mouth.

Let us call $\vec{P}_n$ the probability that one molecule will undergo n collisions on the reactive surface. In the course of each collision, the molecule is likely to react with the probability b. Under such conditions, the probability that the molecule will undergo n collisions without reacting before going out is : $(1-b)^n \vec{P}_n$.

Then, the overall probability of travelling through the reactor with any number of collisions without reacting is

$$\sum_{n=o}^{\infty} (1-b)^n . \vec{P}_n$$

Whence :

$$\vec{B} = 1 - \sum_{n=o}^{\infty} (1-b)^n . \vec{P}_n$$

This is the general relationship between the reactor efficiency $\vec{B}$ and the collision efficiency b.

Theoretically, the problem is solved, except that one should know every probability $\vec{P}_n$. These probabilities are pure numbers depending only upon the geometrical shape of the reactor and they can be computed, theoretically at least, irrespective of any chemical reaction.

Case of short reactors :

Let us recall that, by definition $\vec{P}_n$ is the probability that each molecule will undergo a first collision, then a second one, then a third one, till it goes out, since the (n + 1) collision takes place on the exit mouth. $\vec{P}_n$ represents the product of elementary probabilities :

$$\vec{P}_n = \pi_1 \pi_2 \pi_3 .. \pi_n (1-\pi_{n+1})$$

In the particular case when the length of the reactor is not very different from its average diameter, each molecule has the same average probability of colliding against the reactive surface whatever its position in the reactor may be. Then, the elementary probability π may be taken as constant and in this particular case, the reactor efficiency is easily computed as follows :

$$\vec{B} = \frac{\vec{\vartheta}_1 b}{1 + \vec{\vartheta}_1 b} \qquad \text{with} \qquad \vec{\vartheta}_1 = \frac{\bar{\pi}}{1 - \bar{\pi}}$$

...

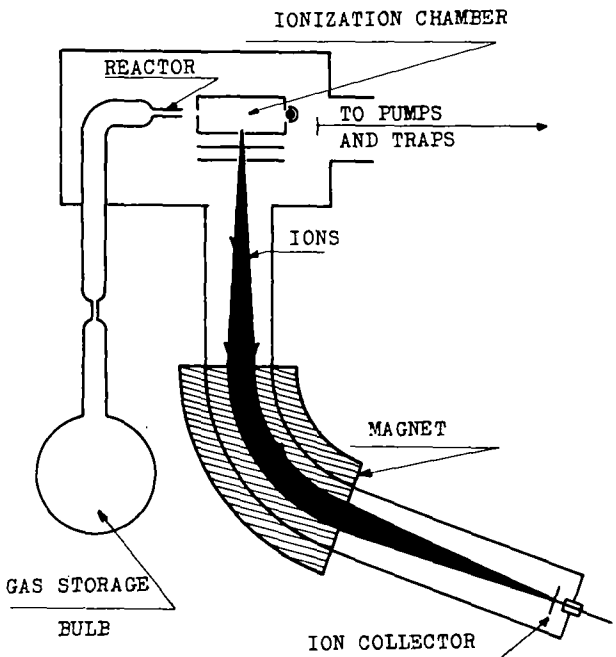

FIG. 1

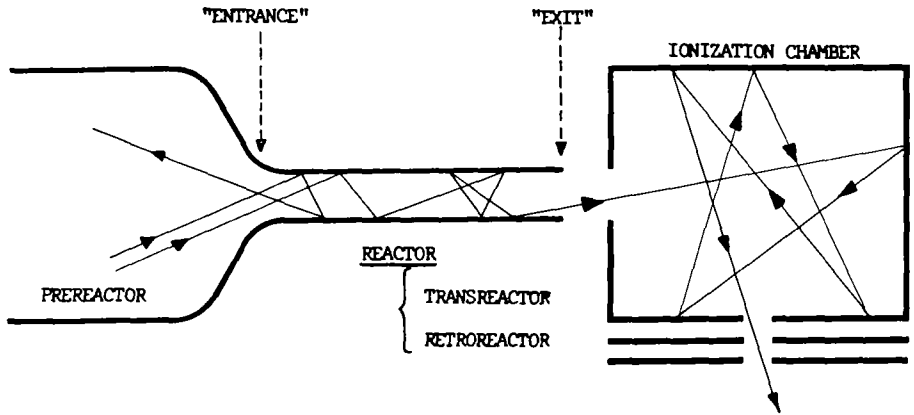

FIG. 2

LONG CYLINDRICAL REACTORS

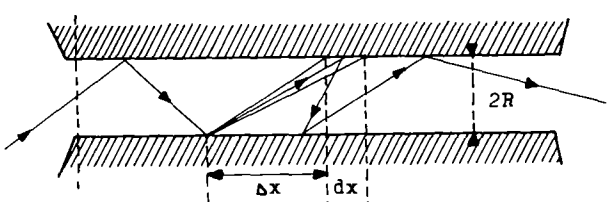

Probability that a particle will cover one step between Δx and $(\Delta x + dx)$

$$d\pi = 1 - \left[\frac{\lambda(\lambda^2 + 6)}{(\lambda^2 + 4)^{3/2}}\right]\frac{d\lambda}{2} \quad \text{with } \lambda = \frac{\Delta x}{R}$$

FIG. 3

$\bar{\nu}_1$ is the average number of collisions of each particle on the reactive surface when it travels through the reactor ; $\bar{\nu}_1$ is computed through mere geometrical considerations. This relationship has been used previously (ref. 1, 2, 3) to explain various heterogeneous kinetic experimental results (hydrocarbon decompositions and oxidations). It can be used also for interpretating the free radicals recombination upon the walls of the ionization chamber of a mass spectrometer.

In our apparatus, each particle undergoes on the average 55 collisions against the walls of the ionization chamber.

We shall come back to this problem later on, but now will be discussed the statistical theory of the decomposition reactor : this is the subject of part 2.

PART 2 : SIMULATION OF MOLECULAR PATHS IN A DIGITAL COMPUTER (MONTE-CARLO METHOD)

We study now the general case of long cylindrical reactors, the length of which is much longer than the average diameter. Let us consider one molecule that has just collided against the wall (fig. 3). The probability that this molecule will cover one step Δx and will undergo the next collision against the surface of a ring dx in thickness, at a distance Δx from its starting point, is given by the probability function :

$$d\pi = 1 - \frac{\lambda(\lambda^2 + 6)}{(\lambda^2 + 4)^{3/2}} \frac{d\lambda}{2}$$

Where $\lambda = \frac{\Delta x}{R}$ is the reduced absciss.

Simulation of the molecular path

We are then able to simulate on a digital computer, the succession of steps allowing particle to progress along the cylinder and go out. This technique of computation, based on the Monte-Carlo method, consists in submitting random numbers in a computer to similar conditions as those of a molecule in the reactor. The principle of the computation only will be presented here (see ref. 4, 5).

First, in the memory of the machine is placed the table of the values expressing the probability that a molecule will go beyond Δx, calculated through integration of the previous function.

Let us then divide this probability function into 100 parts equally probable, numbered from 0 to 99. Thus to each two figures number corresponds a certain step Δx ; the simulation of a step may be decomposed as follows :

1 - emission of a random number between 0 and 99
2 - reading in the table the corresponding step Δx,
3 - addition : $X_n = X_{n-1} + \Delta x$
4 - comparison between X_n and the interval (0, L) which represents the length of the cylindrical reactor.

If X_n is outside the intervals (0, L), the computer will tell that the molecule went out of the cylinder through one side of the other ; on the contrary, if X_n is inside the interval, the machine will register one more collision against the wall. Then, the machine will go through the same operation again and again.

As the computation is going on, and as new molecules are symbolically inserted into the machine, the latter goes on, keeping accounts of all fluctuating quantities, the number of collisions, the densities of collisions, the direction of emission of molecules etc...

Finally by consulting the memory of the machine, we get all these informations.. - As an example, the table hereafter shows the average numbers of collisions undergone by each molecule in the trans- and the retroreactor (without chemical reaction).

FIG. 4

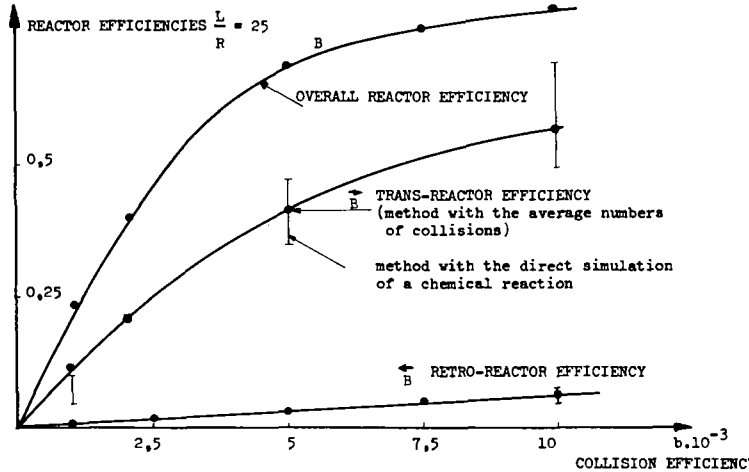

FIG. 5

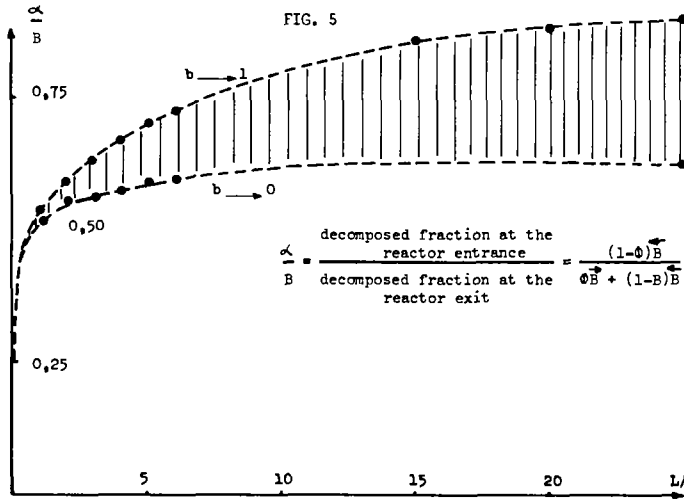

FIG. 6

INFLUENCE OF THE SURFACE TEMPERATURE

UPON THE HETEROGENEOUS REACTIONS OF METHYL FREE RADICALS

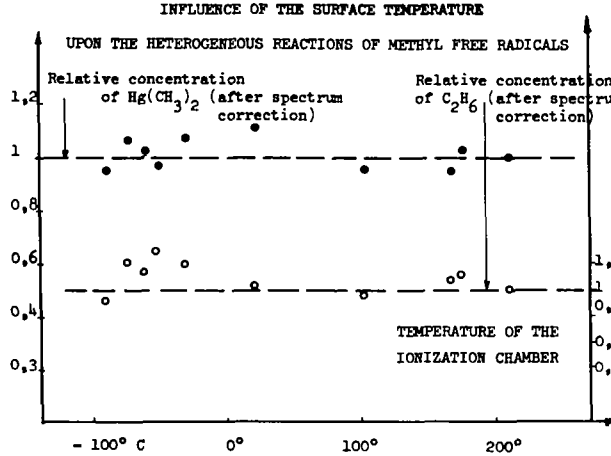

TABLE 2

AVERAGE NUMBER OF COLLISIONS AGAINST THE WALLS OF A TRANS-REACTOR AND OF A RETRO-REACTOR (without chemical reaction)

L/R	1	2	3	4	5	6	25
$\vec{\nu}_1$	0.7	1.9	3.2	4.9	6.8	9.4	123,
$\overleftarrow{\nu}_1$	1.6	2.26	2.9	3.55	4.3	5	17.4

Moments of a higher order have also been computed because they are used in the complete theoretical expression of the reactor efficiency (ref. 6).

Simulation of the chemical reaction

To go further, we have asked the computer to simulate the chemical reaction itself. - The simulation of the chemical reaction consists in ordering the machine to insert a subsidiary stochastic step whenever a collision happens on the wall ; the computer gives thus directly a new estimation of the reactor efficiency (ref. 4).

Let us come back to the experimental system shown on figure 1 : the gas contained in the storage bulb under constant pressure, diffuses through the capillary leak, flows through the pipe we called "pre-reactor", then goes into the cylindrical reactor and, finally, arrives in the large vacuum vessel. But, the reactor transparency is small (ϕ = 0,093 for L/R = 25). In such conditions, 91 per cent of the molecules coming into the reactor, retro-diffuse and go back to the pre-reactor, stay there, then go back again in the reactor. 91 per cent of these molecules are to retrodiffuse again, then go back into the reactor etc... As shown on table 2, for this shape of reactor, the average numbers of collisions are 123 in the transreactor and 17.4 in the retroreactor. It is easier than it seems to be at first sight, to compute this complicated situation.

Writing the matter balance in the prereactor leads directly to the expression of the overall efficiency

$$B = \frac{\phi\vec{B} + (1 - \phi)\overleftarrow{B}}{\phi + (1-\phi)\overleftarrow{B}}$$

This is the general relationship between a reactor overall efficiency B, its transparency ϕ , the transreactor and retroreactor efficiencies $\vec{B}$ and $\overleftarrow{B}$.

Figure 4 shows the results obtained with the digital computer for the retro-reactor, the transreactor and the overall reactor efficiencies. As can be seen, it would not be correct to mistake B for $\vec{B}$, even for small efficiencies. The retrodiffusion plays an important role.

PART 3 : FREE RADICAL REACTIONS IN A LONG REACTOR AND ITS PREREACTOR

Retrodiffusion is particularly important relative to free radicals formed in the reactor : an important number of these particles are to go back into the prereactor, accumulate in it and produce a fairly important stationnary concentration.

For that purpose, the ratio α/B defined on fig. 5 has been computed

$$\frac{\alpha}{B} = \frac{(1 - \phi)\vec{B}}{\phi\vec{B} + (1 - \phi)\overleftarrow{B}}$$

...

In fact, this ratio would be equal, except of a few stoechiometric coefficients, to the proportion of free radical concentrations at the entrance and at the exit of the reactor if no recombination occurred in the prereactor.

Figure n° 5 shows the variation of the ratio with the length of the reactor. Two extreme cases are to be considered, whether the collision efficiency b tends to zero or to one.

It can be seen that all curves are situated in a small hatched intermediate zone ; the ratio α/B becomes great and constant as soon as L/R is more than about 5. These curves show how important the retro-diffusion proves to be in the overall efficiency of the reactor. Practically, the transreactor influence is no longer of any account in comparison with that of the retroreactor, when L/R is more than about 5.

The free radical concentration at the entrance of the reactor would then be comprised between 50 and 80 per cent of the free radical concentration at the exit of the reactor in the case when no recombination occurs. But when back in the prereactor, the free radicals undergo a great number of collisions on its walls, before going out thanks to a new complete transfer through the reactor.

For instance, with a prereactor composed of a pipe 7 cm in length, 1 cm in diameter, and followed by a reactor 2 mm inner diameter, it has been computed that each particle coming back into the prereactor undergo more than 700 collisions. Let us recall that the number of collisions for each particle is 123 in the transreactor, 17 in the retroreactor and 55 in the ionization chamber. Then, the conclusion is that the DISAPPEARING of FREE RADICAL TAKES PLACE ESSENTIALLY IN THE PREREACTOR. Our experiments consisted in studying the influence of temperature of the prereactor, in fixing on the prereactor a subsidiary pumping mouth to alter the average number of collisions upon the walls etc...

This problem has been dealt with the same mathematical theory as the one stated above : the prereactor is considered as a recombination reactor for free radicals (réf. 6).

The application of previous general formula leads to a relation between the free radical stationary concentration at the entrance of the reactor and the recombination collision efficiency of each free radical on the walls of the prereactor.

PART 4 - APPLICATIONS TO METHYL AND ETHYL FREE RADICAL RECOMBINATION

These radicals are formed in the decomposition of dimethyl mercury and diethyl mercury. The results we obtained can be summarized as follows :

1° - A first conclusion concerns the kinetic order of the reactions : all the reactions of free radical recombination on silica proved to be of the first order in the pressure range : 10^{-2} to 10^{-5} mm Hg. This result implies a Rideal mecanism, that is a reaction through collision of a gaseous free radical on a radical already adsorbed.

For instance, the successive steps of the diethyl mercury decomposition are :

Decomposition : $Hg(C_2H_5)_2$ + wall $\longrightarrow$ Hg + $2C_2H_5$

Adsorption : C_2H_5 + bare wall $\longrightarrow$ (C_2H_5)ads

Recombination : $C_2H_5 + (C_2H_5)_{ads} \longrightarrow C_4H_{10}$

Disproportionation : $C_2H_5 + (C_2H_5)_{ads} \longrightarrow C_2H_4 + C_2H_6$

2° - The second conclusion concerns the ethyl radical disproportionation. We obtain 80 per cent butane and 20 per cent ethane and ethylene independantly of concentration. In the dimethylmercury decomposition, the methyl free radical recombination gives ethane mainly ; methane in very low concentration was observed too.

3° - The third point concerns the possible reactions of free radicals, upon the cooled walls of the ionization chamber. As an example, we consider the decomposition of dimethyl mercury.

Passing through the reactor at 1000° C, dimethylmercury is decomposed at more than 50 per cent. The stream coming out from the reactor consists of an excess of dimethylmercury, mercury free atoms and CH_3 free radicals. When the ionization chamber is at room temperature, the successive reactions are as follows :

1) CH_3 + wall $\longrightarrow$ CH_3 ads.

2) $CH_3 + CH_3$ads. $\longrightarrow$ C_2H_6

3) Hg + CH_3ads $\longrightarrow$ $HgCH_3$ads

4) $CH_3 + HgCH_3$ads $\longrightarrow$ $Hg(CH_3)_2$

$\searrow$ C_2H_6

But now, suppose that the ionization chamber is cooled below - 10° C, the mercury condenses on the walls of the chamber and an additional reaction may happen :

$$CH_3 + Hg_{cond} \longrightarrow Hg\ CH_3ads \longrightarrow ?$$

A modification of the reaction mecanism must then be expected at about - 10°, since below this temperature, the wall is covered with a "mirror" of condensed mercury.

Figure 6 shows experimental results. It is observed that between - 100 and + 200°, the concentration of recombination products, dimethyl mercury and ethane remain practicaly constant. The probabilities of recombination by collision are very small : less than 1.10^{-3} in any case : there is no rapid reaction of CH_3 radicals, neither on stainless steel, nor even on the mercury surface that is ceaselessly renewed and henceforth always clean.

4° - The absolute values of recombination collision efficiencies are as follows :

for CH_3 $\quad b = (1.8 \pm 0.2).\ 10^{-4}$ between + 20 and+500° C

for C_2H_5 $\quad b = (4 \pm 2).\ 10^{-4}$ between + 20 and + 400° C

Variations with temperature are negligible. Activation energies are practically zero.

5° - We also studied the simultaneous decomposition of dimethyl mercury and diethyl mercury

<u>ADSORPTIONS</u> : CH_3 + wall $\longrightarrow$ CH_3ads.

C_2H_5 + wall $\longrightarrow$ C_2H_5ads.

<u>RECOMBINATIONS</u> (RIDEAL) "PURE"

$CH_3 + CH_3$ads. $\longrightarrow$ C_2H_6

$C_2H_5 + C_2H_5$ads $\longrightarrow$ C_4H_{10}

$\searrow$ $C_2H_6 + C_2H_4$

"CROSSED"

$CH_3 + C_2H_5$ads $\longrightarrow$ C_3H_8

$C_2H_5 + CH_3$ads. $\longrightarrow$ $CH_4 + C_2H_4$

<u>Pure</u> recombinations of methyl and ethyl free radicals involve the formation of butane, ethane, ethylen and methan but the <u>crossed</u> recombinations are the only giving propane.

The stationary concentrations of these substances have been measured in the case of various relative concentrations of dimethyl mercury and diethyl mercury.

...

The main points of these results are summarized on figure (7). The ratio of the surfaces occupied by chemisorbed methyl and ethyl radicals varies linearly with the ratio of the stationary concentrations of both substances. The small diagram above shows the relative importance of free radical collision efficiency on adsorbed layers : when "u" is the unknown value of the collision efficiency of a free CH_3 radical on an adsorbed CH_3 radical, the other three elementary collision efficiencies have relative values : u - 1,5 and 2 u ; all these numbers are given with an accuracy of ∓ 20 per cent.

Upon the whole, we can state that crossed recombinations are as important as pure recombinations and that the recombination rates of CH_3 and C_2H_5 radicals are practically the same.

As a conclusion, we observe that few results have so far been obtained on recombination rates of atoms and free radicals on the surface of solids.

Mass spectrometry is practically the only experimental technique to study these reactions. In contrast to the electronic paramagnetic resonance, it analyses not only the free radicals but also all molecules stable or unstable that are formed by recombination. Thus the mass balance can easily be calculated. Besides, mass spectrometry is the only technique of analysis operating under so low pressures (10^{-4} to 10^{-6} mm Hg) so that it prevents any possible recombination in the gaseous phase.

REFERENCES

1 - P. LE GOFF - J. Chim. Phys. 1956 - p. 369-379
2 - P. LE GOFF et M. LETORT - J. Chim. Phys. 1956 - p. 480-92
3 - L.P. BLANCHARD et P. LE GOFF - Advances in Mass Spectrometry 1959 p. 570-89
4 - A. PENTENERO - Génie Chimique 1962 avril - vol. 87 n° 4 - p. 97-107
5 - P. LE GOFF - A. PENTENERO et A. CASSUTO - J. Chim. Phys. (to be published)
6 - A. CASSUTO -Thèse Annales de Chimie 13e série - t. 7 - 1962
7 - P. LE GOFF - A. CASSUTO and A. PENTENERO - Industrie Chimique Belge n° 4 1964

SIMULTANEOUS RECOMBINATION OF METHYL AND ETHYL FREE RADICALS

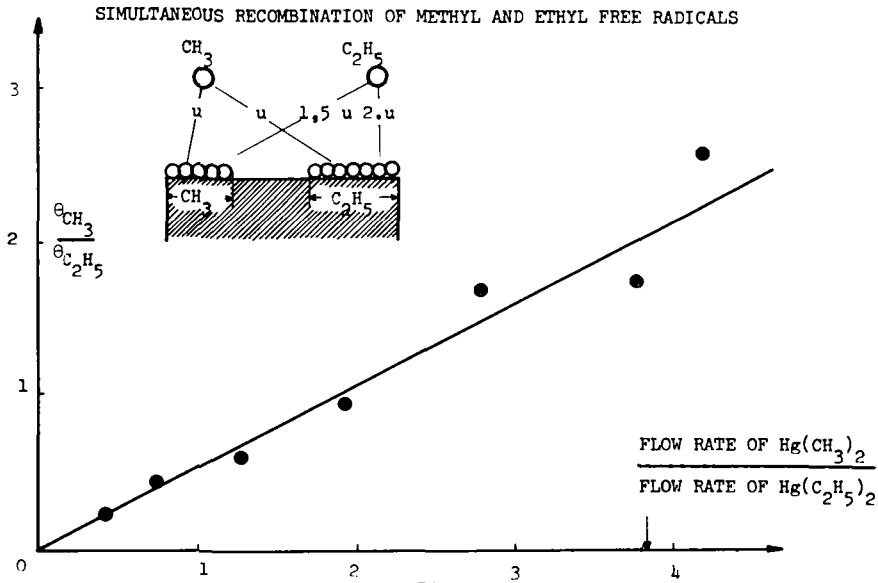

FIG. 7

MASS SPECTROMETRIC SAMPLING AND DETECTION OF INTERMEDIATES IN GASEOUS REACTIONS

J. Cuthbert

United Kingdom Atomic Energy Authority,

Chemistry Division, A.E.R.E., Harwell, Berks, England.

Abstract

Isentropic expansion is shown to take place in sampling through a small pinhole in mass spectrometric studies of gaseous reactions at pressures above a few torr. The flow of CO_2, N_2 and H_2 through a typical pinhole is described by an equation giving a transition region from ~5 to ~500 torr in which the flow changes from molecular effusion to isentropic expansion; the fractionation of a mixture is discussed briefly. Observations of ions $(CO_2)_n^+$ (n=1 to 12) shows that isentropic expansion of CO_2 from several atmospheres pressure may give rise to condensation in the sample.

Pyrolysis of sample molecules on the ion source filament and heterogeneous removal of free radicals at the ion source walls are examined theoretically. For a mass spectrometer with simple pinhole sampling and a separately pumped filament box, wall reactions may reduce the concentrations of sample radicals at least sixfold and there may be a high probability of detecting pyrolysis products. In a molecular beam mass spectrometer these effects may be negligible, although a much larger sample is required.

Introduction

The application of mass spectrometry to the study of chemical reactions offers, in principle, many advantages; mass spectrometers are frequently used to detect trace components (at part-per-million level) in gas mixtures, they are applicable to all substances and the large amount of information produced by even one mass spectrum might suggest that the main problem would be data handling. Nevertheless, in the detection of trace intermediates, and especially of free radicals and atoms, and in the measurement of the kinetics of elementary reaction steps, mass spectrometry has not lived up to its early promise[1,2]; although there have been many studies of interesting reaction systems at pressures of several torr to atmospheric (e.g. work on flames[3,4]), very few quantitative results have been produced on the rates of radical reactions; a large amount of work has been done on the thermochemical properties of radicals, notably organic ones[5], and the heterogeneous production and reactions of free radicals have been extensively studied in mass spectrometers[6].

The purpose of this article is to examine some of the difficulties involved in using a mass spectrometer to sample continuously from a chemical reaction at pressures from a few torr to several atmospheres (i.e. to observe homogeneous gas-phase reacting systems): the corresponding problems for the study of low pressure reactions (i.e. in the Knudsen region) have been discussed by le Goff and by Cassuto[7]. The problems which will be discussed here will be those involved in transferring a sample of gas from the reaction vessel into the mass spectrometer ion source, which involves a reduction in pressure of 4 to 9 orders of magnitude; it will be shown that the initial, rapid, pressure reduction of more than 2 orders of magnitude may be so complicated as to seriously hinder the deduction of the composition of the gas in the reaction vessel from the mass spectrum. The problems of reaction of sample molecules in the ion source will also be discussed.

Sampling

The rapid reduction of pressure when a gas expands into a vacuum through a pinhole leak, and the possibility of so arranging this that the minimum surface is exposed to the gas should enable a chemical reaction to be stopped and the sample to be simultaneously transferred to the ion source; this sampling method has been used to study chemical reactions at pressures from a few torr to atmospheric[2,3,4,8], but it has recently become clear that the sampling process itself may introduce complications[9,10] which it is appropriate to consider in detail.

Table 1

Pinhole leak, d = .00165 cms, 1 = .00120 cms, 1/d = 0.727, k_c = 1.705

Gas	K	Std. devn.	α	Std. devn.	C	Std. devn.	Residual variance
CO_2	1.705	-	11	0.6	0.74	0.017	0.0020
	1.1	.07	15	0.9	0.80	0.01	0.0007
N_2	1.705	-	7	2.1	0.66	0.09	0.031
	0.8	0.1	13	2.7	0.79	0.05	0.011
	1.1	-	10	1.7	0.74	0.05	0.013
H_2	1.705	-	44	8	0.59	0.01	0.009
	2.0	0.7	37	16	0.58	0.03	0.009

Table 2

Parameter and units		Case A	Case B
$\bar{c}$	$cm.sec^{-1}$	$4(10^4)$	$4(10^4)$
$\bar{X}$		1	1
ξ, ζ		1	1
λ		1	1
ψ		N.A.	0.01 and 1
A_c	cm^2	0.1	0.1
A_f	cm^2	0.3	0.3
A_f'	cm^2	0.05	0.05
A_e'	cm^2	0.032	0.032
d_s	cm	0.50	0.5 and 3.5
d_i	cm	1.0	1.0
d_f	cm	0.15	0.15
V_c	litres	0.25	0.25
δ_c	cm	1.0	1.0
V_i	litres	0.0075	0.0075
δ_i	cm	0.30	0.30
V_f	litres	0.001	N.A.
δ_f	cm	0.50	N.A.
S_f	litres sec^{-1}	10, 1 and 0.1	N.A.
A_a	cm^2	.1, .032 and .008	N.A.
A_i	cm^2	1.2 and .232	1.2

The molecular effusion of a gas into vacuum through a thin-edged orifice is given by[11]

$$Q^o = \left(\frac{RT_o}{2\pi M}\right)^{\frac{1}{2}} P_o A_1 \text{ cc.torr.sec}^{-1} \text{ (lusecs)} \qquad (1)$$

and allowance for the length of a real orifice is made by putting $Q = Q^o/k$ where k^{-1} is the Clausing factor[12, 1)].

Molecular effusion only occurs when the mean free path is much larger than the orifice dimensions, whereas for a pinhole leak sampling gas at several torr to atmospheric pressure, the mean free path will generally be comparable with, or less than the orifice dimensions (it is not usually practicable to use an orifice much smaller than 0.001 cms in diameter or length). The nature of gas flow under these conditions is not entirely understood; at very high pressures the flow tends to one of several limits depending upon the l/d value of the orifice; thus Carlson[13] has shown that, for large l/d, the flow may tend to the Knudsen limit, Q^o, (for l = o) because the orifice fills up with gas at the high pressure, and molecules "boil off" the gas surface at the end of the tube. For small l/d the flow tends to a limit determined by isentropic expansion, which is given, for an inviscid gas, by[14]

$$Q_Z = C \left[\frac{\gamma RT_o}{M} \frac{Ma^2}{(1+\frac{1}{2}(\gamma-1)Ma^2)^{\frac{\gamma+1}{\gamma-1}}}\right]^{\frac{1}{2}} P_o A_1 \text{ cc.torr.sec}^{-1}$$

where C, the discharge coefficient, accounts for the formation of a <u>vena contracta</u> and boundary layer phenomena. Maximum flow occurs in a constant area nozzle at Mach 1:

$$Q_{Imax} = C \left[\frac{\gamma RT_o}{M} \left(\frac{2}{1+\gamma}\right)^{\frac{\gamma+1}{\gamma-1}}\right]^{\frac{1}{2}} P_o A_1 \text{ cc.torr.sec}^{-1} \qquad (2)$$

Liepmann[15] shows that the flow through a thin slit or orifice will reach a maximum at higher Mach numbers, and Frankl[16] calculates C = 0.85 for maximum flow at Mach 2.76 through a thin-edged slit for $\gamma = 1.4$; for an orifice the critical Mach number will be higher and C lower, as indicated by Liepmann's measurements of C from 0.81 for Ar ($\gamma = 1.67$) to 0.83 for CO_2 ($\gamma = 1.3$)[15].

For a pinhole of diameter 0.002 cms and l/d = 1 the Knudsen effusion equation will apply below about 5 torr and the isentropic expansion equation above about 500 torr; the transition region is obviously of great interest to the chemical kineticist but, unfortunately, there is no good description of the flow in this region. Knudsen[11] explained the transition from molecular effusion to viscous flow for l/d > 100 and small pressure differentials by:-

$$Q_k = \left\{\frac{1+C_1P_o}{1+C_2P_o}\left(\frac{RT_o}{2\pi M}\right)^{\frac{1}{2}}\frac{1}{k} + \frac{d^2}{32\eta l}\,\frac{1333P}{2}\right\} P_o A_1 \text{ cc.torr.sec}^{-1} \qquad (3)$$

Where $C_1 = (d/\eta)(RT/2\,M)^{\frac{1}{2}}\,1333 \text{ torr}^{-1}$ and $C_2 = 1.235\,C_1$, and this equation has been used to describe mass spectrometric sampling through capillaries. Creutz and Zumwalt[17] replace the first term in equation (3) by

$$\left(\frac{1}{k} - \frac{3\,d}{4\alpha l}\right)\left(\frac{RT}{2\pi M}\right)^{\frac{1}{2}} \cdot \frac{(6\pi\eta/\alpha d)(RT/2\pi M)^{\frac{1}{2}}}{(6\pi\eta/\alpha d)(RT/2\pi M)^{\frac{1}{2}} + 1333P_o} + \frac{3\pi d}{4\alpha l} \qquad (4)$$

where the last term is related to "free molecule viscosity" and $\alpha d/4$ is the effective mean free path at very low pressures (for molecules passing through the orifice); this describes the low pressure end of the transition region rather better than equation (3).

The transition between molecular effusion and isentropic expansion is more difficult theoretically, especially when considering real gases, which are viscous; for viscous isentropic flow equation (2) should be divided by $(1 + C^2F)^{\frac{1}{2}}$ where F is a friction factor[14], dependent on P, η, γ, l and d, which has been tabulated for large orifices. For pinholes, using the viscous flow term of equation (3) as an analogy F is taken here arbitrarily to be $32l/dRe$ where $Re = \rho ud/\eta$ (Reynold's number); there is no rigorous justification for this choice of F and although it has a suitable dependence on all the relevant factors its use will be justified empirically. The

---

1) See list of symbols at the end of this article, for units etc.

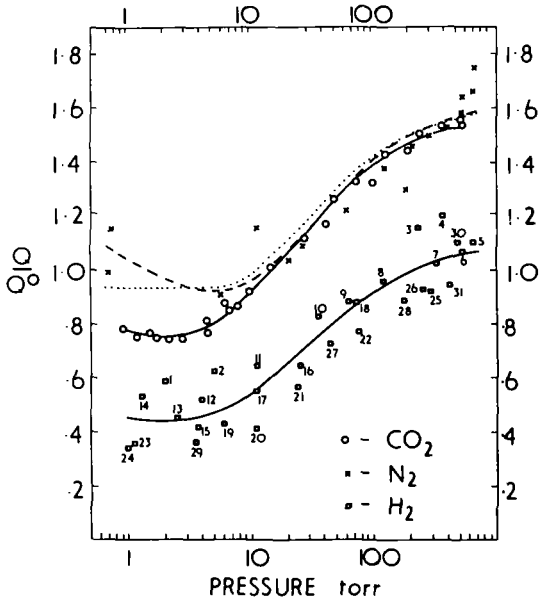

FIG. 1. FLOW THROUGH PINHOLE

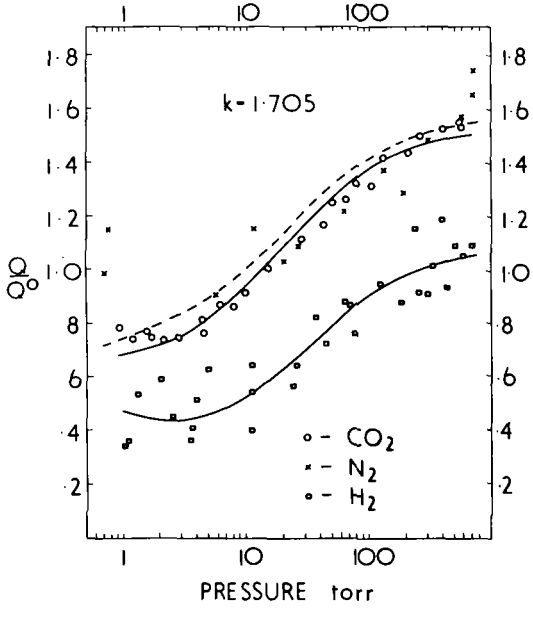

FIG. 2. FLOW THROUGH PINHOLE

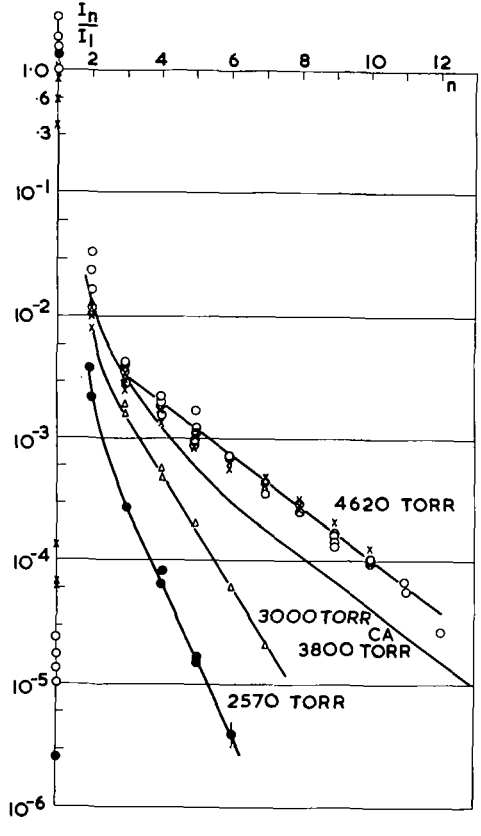

FIG. 3. VARIATION OF INTENSITY OF $(CO_2)_n^+$ IONS WITH n.

modified isentropic expansion term (equation (2)) can now be added to equation (4) to give

$$Q_{MI} = \left\{ \left(\frac{1}{k} - \frac{3\,d}{4\alpha l}\right) \frac{(6\pi\eta/\alpha d)(RT_o/2\pi M)^{\frac{1}{2}}}{(6\pi\eta/\alpha d)RT_o/2\pi M)^{\frac{1}{2}} + 1333P_o} + \frac{3\pi d}{4\alpha l} + \left[\left(\frac{2}{1+\gamma}\right)^{\frac{\gamma+1}{\gamma-1}} \frac{2\,\gamma d Re C^2}{dRe + 321C^2}\right] \right\}$$

$$\left(\frac{RT_o}{2\pi M}\right)^{\frac{1}{2}} P_o A_1 \text{ cc.torr.sec}^{-1} \qquad (5)$$

Where $$Re = \frac{1333P_o d}{\eta} \left[\frac{\gamma M}{RT_o} \frac{Ma^2}{(1+\frac{1}{2}(\gamma-1)Ma^2)^{\frac{\gamma+1}{\gamma-1}}}\right]^{\frac{1}{2}}$$

Equation (5) has been fitted by a least squares method to data, obtained in our laboratory, for hydrogen, nitrogen and carbon dioxide effusing from an orifice with $l/d = 1$; the optimum values of α and C for $k = 1.705$ (the Clausing[12] value) and the optimum k, α and C for best fit are given in Table 1 with the resulting curves in Figures 2 and 1 respectively. Since the nitrogen curve (broken line, Figure 1) is very dependent on the (inaccurate) low pressure results a further optimization was made of α and C for $k = 1.1$ (the best fit value for CO_2) and this (dotted line, Figure 1) is seen to be as good as the best (unrestricted) fit for N_2. The CO_2 curve for optimum $k = 1.1$ (Figure 1) is an appreciably better fit than that for the Clausing value of $k = 1.705$ (Figure 2) and this is confirmed by the residual variances shown in Table 1; perhaps the first term in equation (5) should be modified so that the Clausing value of k can be used, or some other method of estimating k may be required. The simplest explanation of the hydrogen results is that the pinhole was partially blocked giving apparent high values for k and α and a low value for C; moreover, if the pinhole became blocked gradually during the experiment, much of the scatter is explained, as shown by the numbering of the points in Figure 1, corresponding to the order in which the results were obtained.

Table 1 and Figures 1 and 2 show that the isentropic flow term in equation (5) is not unreasonable; the optimum values of C are a little lower than Liepmann predicts[15] and it may be that the best form of the friction parameter, F, has not been found. Nevertheless it is likely that an equation similar to (5) will describe the transition from molecular effusion to isentropic expansion for effusion into vacuum through a real pinhole.

An important corollary is the extent of fractionation in a mixture; equation (5) predicts a complex dependence on η, γ and M, so that calculation of the expected fractionation is difficult, especially as a mixture will flow as a unit at high pressures and as independent components at low pressures. The fractionation in a mass spectrometer leak has recently been discussed by Barber et.al.,[18] who assumed that the flow transition was completed over a small pressure range centred on 17 torr and that the flow was essentially inviscid isentropic expansion well below their maximum pressure of about 55 torr; the similarity of their leak ($d = 0.0013$ cms, $l/d = 2$) to that used for Figures 1 and 2 suggests that they were studying the transition region. Assuming a Mach number of unity and no viscous effects (equation (2)) they showed that the fractionation should be given by[2)]:

$$\frac{\partial n_i}{\partial P_i} \Big/ \frac{\partial n_i^o}{\partial P_i^o} = \left[\frac{M_i}{\sum x_i M_i} \frac{\gamma}{\gamma_i^o} \left(\frac{2}{1+\gamma}\right)^{\frac{\gamma+1}{\gamma-1}} \left(\frac{1+\gamma_i^o}{2}\right)^{\frac{\gamma_i^o+1}{\gamma_i^o-1}}\right]^{\frac{1}{2}} \qquad (6)$$

where subscripts i refer to the molecular species and superscripts o to the pure component. Their results are in reasonable agreement with equation (6), although they show that errors of up to 30% may occur in calculating the partial pressures of mixture components even when using this correction; the fractionation appeared to be independent of viscosity. In supersonic molecular beam systems enrichment of heavier molecules has been found[26] and Greene et.al.[25] have recently found the enrichment to be directly proportional to M_i.

It is clear that much more data is required covering all aspects of this problem over a wide range of pressures and orifice dimensions; considerable experimental accuracy is required in order adequately to test the theories.

---

2) This equation is given incorrectly on page 295 of reference 18, although their results are calculated correctly.

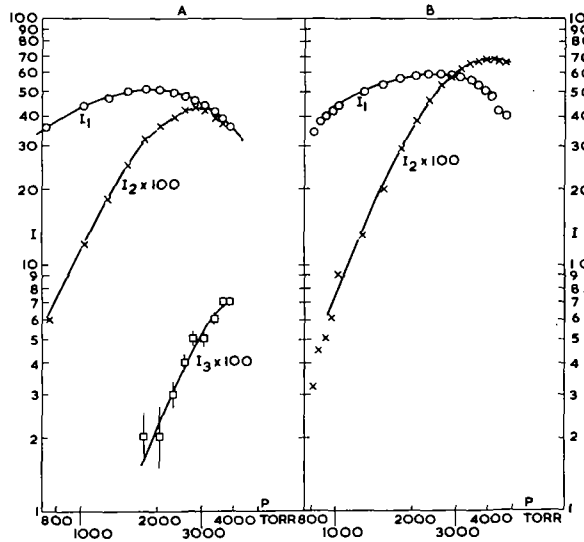

FIG. 4. VARIATION OF INTENSITY, WITH PRESSURE OF $(CO_2)^n$ FOR n = 1,2,3.

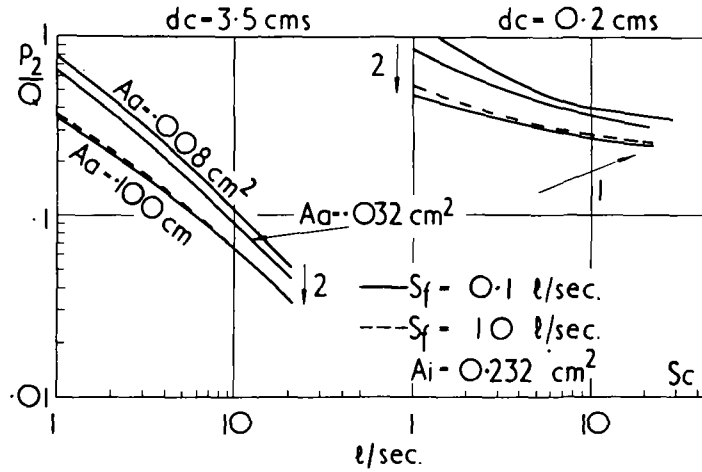

FIG. 5. SENSITIVITY – SIMPLE MASS SPEC.

Reactions during sampling

The most important consequence of the sampling process is the possibility that the composition of the sample will change as it passes through the orifice. The relations between pressure, temperature and velocity for isentropic expansion are:-

$$P/P_o = [1 + \tfrac{1}{2}(\gamma - 1)Ma^2]^{\frac{-\gamma}{\gamma-1}} \text{ and } T/T_o = [1 + \tfrac{1}{2}(\gamma - 1)Ma^2]^{-1} \qquad (7)$$

so that the gas will emerge from the low pressure end of a thin-edged orifice with P/P_o = 0.0172, 0.0390, 0.0465 and T/T_o = 0.192, 0.396, 0.490 for γ = 1.67, 1.4 and 1.3 respectively; e.g. for T_o = 295°K the gas temperatures will be 56.5, 117 and 145°K respectively. In many cases the ambient pressure in the vacuum chamber on the low pressure side of the pinhole will be less than 0.001 P_o so that the gas must expand further into the vacuum by further isentropic expansion, and some distance downstream of the orifice temperatures will be even lower than the above figures; temperature of 55°K have been observed along the flow axis for CO_2 in a molecular beam system[9] and complete accommodation of internal degrees of freedom was found so that the gas might be expected to freeze.

Experiments with a molecular beam system coupled to a mass spectrometer[10,19,20] have shown that CO_2 does condense after expansion through a pinhole from pressures above atmospheric. Polymeric ions $(CO_2)_n^+$ were observed as shown by Figure 3[10] (where the line labelled CA is taken from reference 19 for P_o = 3800 torr). The points at the lower end of the ordinate axis give the detection limits for various experiments, this being mainly determined by the gain of an electron multiplier; the degree of polymerization observed clearly depends upon the detection limit and it is probable that the true limit is the condensed phase. The experiments at 4620 torr originally formed a series of parallel lines when plotted with I_1 = 1 and it was thought that the variations were due to day-to-day changes in the ion source and molecular beam system, so the results were replotted to fall on the same line giving a spread of points for I_1.

The variations in polymeric ion intensity with pressure are shown in Figure 4[10] where the curves are the best fit of equations $I_1 = k_1P \exp(-P/P_1)$; $I_2 = k_2P^3 \exp(-P/P_2)$ and $I_3 = k_3P^6 \exp(-P/P_3)$ where k_n and P_n are constants. These equations assume that the polymers are formed by a suitable series of tertiary collisions and they are present close to the low pressure side of the pinhole, the variation in intensity with P_o being largely due to scattering of the molecules in the first stage of the molecular beam system, a phenomenon which gives a maximum intensity for a pressure such that the mean free path of the molecules is equal to the path length in the first beam stage[3,8]. The optimum values of P_n are P_1 = 1900, P_2 = 1000 and P_3 = 900 torr (from Figure 4A) and P_1 = 2400, P_2 = 1350 torr (from Figure 4B) the differences between the two sets of results being due to different pumping speeds in the first molecular beam stage for these two experiments. The scattering increases from monomer to trimer and, assuming that the scattering constant P_n for n-mers is proportional to σ_{1n}^{-2} (where σ_{1n} is the collision diameter for an n-mer-monomer collision, since the scattering gas is mainly monomeric CO_2 which has collided many times with the walls of the first molecular beam chamber) and that $2\sigma_{1n} = \sigma_{11} + \sigma_{nn}$, it can be shown that σ_{22}/σ_{11} = 1.7 and σ_{33}/σ_{11} = 1.9[10]; these are very reasonable values for dimers and trimers of a linear molecule such as CO_2. Further evidence that the polymers were present in the first molecular beam stage was the disappearance of polymers when baffles were placed in such a way that a collision-free path from the first stage to the ion box was impossible[10]. Polymers were also observed for SO_2 and N_2O[10] and, at higher pressures, for Ar, N_2 and O_2[21]; the degree of polymerization depends on γ, on the boiling point of the gas and on pressure suggesting that it is indeed due to the temperature decrease due to isentropic acceleration to high Mach numbers, the extent of the reaction depending on the extent to which this occurs before the pressure has fallen to a value at which insufficient collisions occur to produce condensation.

Polymeric ions of hydrocarbons and hydrated protons $H^+(H_2O)_n$ are observed in mass spectrometric sampling of flames by Sugden et.al, who attribute them to possible reactions in or near the sampling leak[4]; Milne and Greene[20,27] find these same ionic species from electron impact dissociation of polymers in supersonic H_2O beams.

When isentropic expansion occurs in the sampling pinhole, the mass spectrometer is analysing molecules travelling by collision free paths from a region, downstream of the pinhole, which may be non-homogeneous in pressure, temperature, velocity and composition; there are many difficulties in relating the mass spectrum to the conditions on the high pressure side of the pinhole, and the applicability of this to the study of high pressure reactions needs further study. On the other hand, the very rapid (~1 μsec) expansion and cooling will effectively quench quite fast

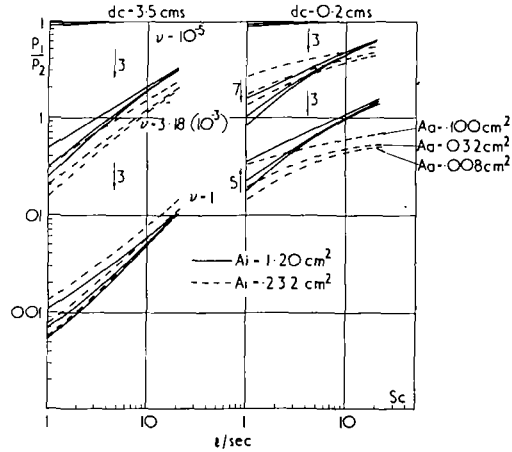

FIG 6 RADICAL DEPLETION-SIMPLE MASS SPEC.

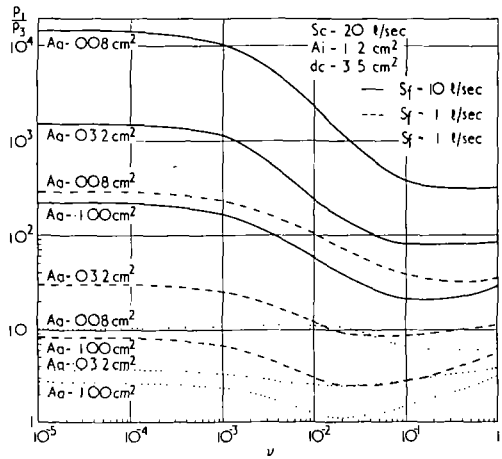

FIG. 7. PYROLYSIS DISCRIMINATION-SIMPLE MASS SPEC

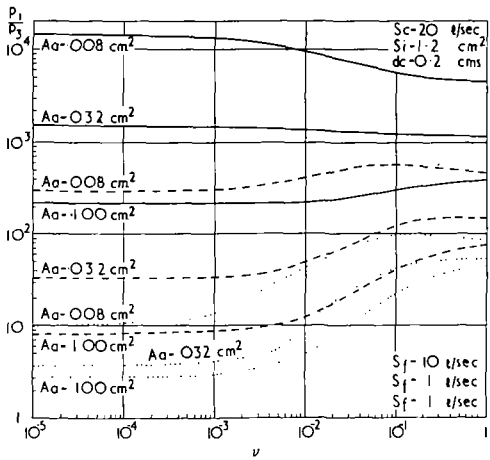

FIG 8 PYROLYSIS DISCRIMINATION-SIMPLE MASS SPEC

reactions; sampling effectively occurs from a region 1 or 2 orifice diameters away from the walls of the reaction vessel and this may be >>100 mean free paths, so that homogeneous reactions can be studied without much heterogeneous contribution.

Ion source reactions

The detection of unstable species such as free radicals or atoms is hindered by pyrolysis of the sample on the hot ion source filament and nearby metal surfaces thereby creating appreciable concentrations of unstable species or reaction intermediates (which may be precisely those being sought) and by collision of sample molecules with the walls, causing recombination or other removal of radicals. These effects have been used[6] to study heterogeneous reactions, although many workers[1,5,22] shield the filament from the sample and provide a collision free path from the sampling pinhole to the electron beam. Fairlure to observe specific radicals whose presence could be inferred with reasonable certainty has often been attributed to recombination in the sampling leak or on the ion source walls[23].

In order to show the magnitude of pyrolysis and wall reaction effects and to obtain guidance for the design of an instrument to study unstable reaction intermediates some calculations have been made for two types of system in common use; case A is a Nier-type ion source with a simple pinhole leak placed close to the ion repeller (which has a hole in it to provide a collision free path from pinhole to electron beam) and the filament is enclosed in a box with its own pumping system, communicating with the ion box only by the hole for the electron beam[5,22]; case B is a molecular beam passing without collisions through an open ion source and into a pumping system, with the filament shielded from the ion box but not separately pumped[3,10]. Various statistical assumptions are made, e.g. that the residence time in any chamber is V/S secs during which time a molecule makes $\bar{c}V/S\delta$ collisions giving an effective pumping speed, due to wall reactions, of $\nu\bar{c}V/\delta$ l/sec; a cosine law is assumed for the distribution of molecules emerging from the sampling pinhole or from the electron beam orifice, although factors (ξ and ζ respectively) are included to allow for deviations. The sample is assumed to consist of equal parts of a free radical (subscript 1) and a stable molecule (subscript 2) both of which pyrolyse on the filament, the stable molecule giving a radical (subscript 3).

In case A the sample pressure in the ionisation region (that part of the electron beam from which ions are collected by the ion accelerating system) due to collision free access from the pinhole is $p_o = 10^3\xi/(\pi(d_c + d_s)^2\bar{c})$ mtorr; the sample entering the ion box without collision (but not necessarily passing directly into the electron beam) is $Q_{IB} = \xi A_c Q/(\pi d_c^2)$ lusecs and the sample entering the ion box after collisions in the outer chamber is $Q_c = 11.4A_iQ/(S_c + 11.4 A_c + \nu_1\bar{c}V_o/\delta_c).(1-A_o\xi/\pi d_c^2)$ lusecs. The removal of sample from the ion box occurs by several mechanisms; diffusion into the outer chamber followed by disappearance into the pumping system or by wall reaction, $S_1 = 11.4A_i (S_o + \nu_1\bar{c}V_o/\delta_c)/(S_c + 11.4A_i + \nu_1\bar{c}V_o/\delta_c)$ l/sec, a similar mechanism for the filament chamber $S_2 = 11.4 A_a (S_f + \nu_1\bar{c}V_f/\delta_f + 11.4 A_f\lambda X)/S_f + 11.4 A_a + 11.4 A_f \lambda X + \nu_1\bar{c}V_f/\delta_f)$ l/sec, which includes pyrolysis on the filament, and wall reactions in the ion box $S_w = \nu_1\bar{c}V_i/\delta_i$ l/sec; molecules which pass into the filament box have a chance of hitting the filament without previous collision and the consequent rate of pyrolysis is $S_p = 11.4 A_a\zeta 10^3/(\pi\bar{c}d_f^2)$. $11.4 A_f\lambda 11.4 A_a/(S_f + 11.4 A_a + 11.4 A_f\lambda X + \nu_1\bar{c}V_f/\delta_f)$ l/sec, where the factor $X = 1 - 11.4 A_a\zeta 10^3/(\pi\bar{c}d_f^2)$. The sample radical pressure in the ionization region is

$$p_{1A} = p_o + \frac{Q_{IB} + Q_c}{S_1 + S_2 + S_w + S_p} \text{ mtorr} \qquad (8)$$

The corresponding pressure, p_2, for stable molecules is obtained by setting $\nu_1 = 0$.

The pressure of stable molecules in the filament box is $p_f = 11.4 A_a p_2/(11.4 A_a + S_f)$ mtorr and these react on the filament at a total rate $11.4 A_f\lambda$ l/sec; those reacting within the area A_f' can reach the ionisation region by a collision free path giving a pressure of radical (species 3) $p_{3o} = 11.4 A_f'\lambda\zeta 10^3 p_f/(\pi(d_f + d_i)^2\bar{c})$ mtorr; the remainder may reach the ionization region after collisions only in the filament box ($p_{3f} = 11.4(A_f - A_f')\lambda 10^3 p_f\zeta/(\pi\bar{c}d_i^2)$. $11.4 A_a/(S_f + 11.4 A_a + \nu_3\bar{c}V_f/\delta_f)$m torr) or after collisions in all chambers $p_{3e} = \lambda 11.4 (A_f - A_f')(1 - \zeta A_e/\pi d_i^2)p_f$. $11.4 A_a/[(S_f + 11.4 A_a + \nu_3\bar{c}V_f/\delta_f)$. $(S_1 + S_2 + S_w + S_p)]$ mtorr; the pressure of radicals produced by pyrolysis is then

$$p_{3A} = p_{3o} + p_{3f} + p_{3e} \text{ mtorr} \qquad (9)$$

In case B the sample reaching the ionization region without collision gives a pressure p_o (as before), but, since the beam passes through the open ion box without

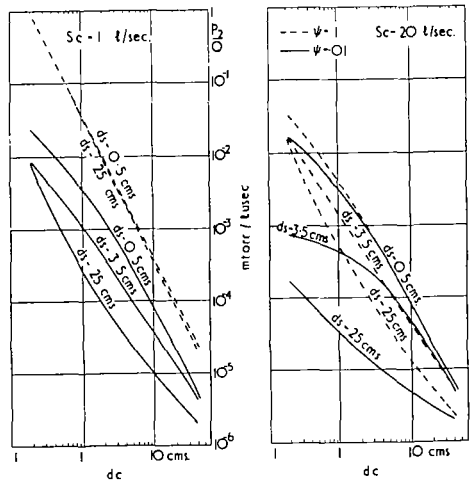

FIG. 9 SENSITIVITY - MOLECULAR BEAM MASS SPEC.

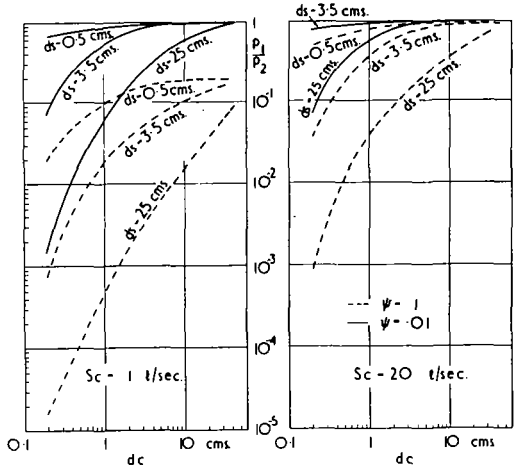

FIG 10. SAMPLE RADICAL DEPLETION - MOLECULAR BEAM MASS SPEC.

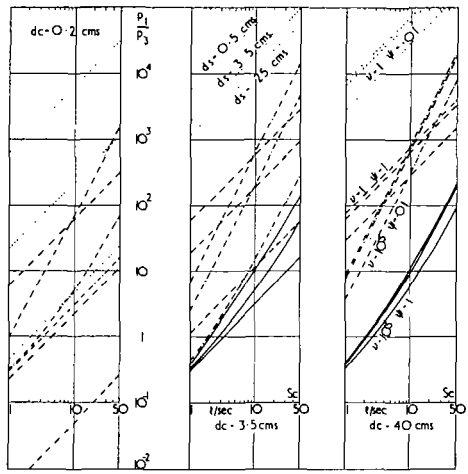

FIG. 11 PYROLYSIS DISCRIMINATION - MOL. BEAM MASS SPEC

collision, the remainder consists only of ψQ_{IB} lusecs scattered back from the pumping system, of which $Q_s = 11.4\ A_i \psi Q_{IB}/(S_c + 11.4\ A_i + \nu_1 \bar{c} V_c/\delta_c)$ lusecs enters the ion box from which it is removed at a rate $(S_1 + S_w)$ l/sec, so that

$$p_{1B} = p_o + Q_s/(S_1 + S_w) \quad \text{mtorr} \qquad (10)$$

and $p_2 = p_1$ for $\nu_1 = o$, as before.

The filament reaction is now assumed to affect only the gas in the outer chamber (the filament is shielded from the ion box, but quite open to the outer chamber); the pressure of stable molecules near the filament is $p_{2f} = \psi Q_{IB}/S_c$ mtorr and if this expression replaces p_f in p_{3o} (case A) the pressure in the ionisation region of pyrolytically produced radicals is

$$p_{3B} = p_{3o} + \frac{11.4\ A_i}{S_c + 11.4 A_i + \nu_3 \bar{c} V_c/\delta_c} \cdot \frac{p_{2f}}{S_1 + S_w} \cdot 11.4 (A_f - A_f') \lambda \left(1 - \frac{\zeta A_e}{\pi d_i^2}\right) \text{mtorr} \qquad (11)$$

To evaluate the design of instruments the sensitivity, p_2/Q mtorr/lusec, the relative sensitivity for radicals, p_1/p_2 and the "pyrolysis discrimination factor", p_1/p_3 are shown in Figures 5 through 11 for the parameters of Table 2; the pyrolysis discrimination factor, p_1/p_3, is the chance that a radical detected in the mass spectrum comes from the sample and not from pyrolysis of the sample for the case that species 1 and 3 are identical (e.g. for a hypothetical sample of CH_3 in CH_4 where the CH_4 pyrolyses to CH_3 on the filament). Figures 5 to 8 refer to case A; Figure 5 shows the increase in sensitivity due to collision free paths from the pinhole, especially at high pumping speeds, S_c (arrow 1) and the reduction in sensitivity due to pyrolysis reactions, depending mainly on the orifice between the ion box and the filament box (A_a) rather than on the filament box pumping speed, S_f (arrow 2). Figure 6 shows the effectiveness of wall removal reactions in depleting sample radical concentrations (arrow 3) the importance of wall reactions in the outer chamber when the pinhole is too far from the ion repeller (difference between $d_c = 3.5$ and 0.2 cms) and the improvement in very unstable ($\nu = 1$) radical concentrations with increasing communication between ion box and filament chamber (A_a), due to pyrolysis affecting the stable molecules more than the radicals (even for equal λ because the radicals have already been depleted by wall collisions) (arrow 5); at high source pumping speeds (S_c) with the pinhole close to the repeller ($d_c = 2$ mms) wall removal of radicals in the ion box is important and an open ion box (large A_i) gives more chance of detecting radicals (as shown by the difference between the full lines and broken lines), whereas at low pumping speeds and especially at moderate wall reaction efficiencies ($\nu_1 \sim 10^{-3}$) there is a high probability of radicals withstanding many collisions in the ion box, so that a relatively closed ion box is desirable (arrow 7 - difference between full and broken lines).

Figures 7 and 8 show the pyrolysis discrimination factor (p_1/p_3) against wall removal efficiency ($\nu_1 = \nu_3$) for various parameters of the filament shielding (A_a) and pumping (S_f), at two values of the repeller-pinhole distance (d_c); as expected p_1/p_3 increases with S_f, with decreasing A_a and with decreasing d_c; it is noteworthy that, for $d_c = 3.5$ cms, $A_a = 0.1$ cm^2 and $S_f = 0.1$ l/sec, values which are probable for a simple (modified analytical?) mass spectrometer, there is a 50% chance that a detected radical might be a pyrolysis product; on the other hand, with reasonable care in providing differential filament pumping the pyrolysis discrimination can be made very large ($p_1/p_3 > 100$) although it then varies considerably with ν; in an instrument (the A.E.I. made M.S.2/R) designed in this way[22] a pyrolysis discrimination factor of more than 3000 was measured,[4)] comparing well with the presently predicted values from about 5000 for $\nu = 10^{-5}$ to 120 for $\nu = 1$[5)]; unfortunately the present theory shows that the relative radical sensitivity (p_1/p_2) for this instrument varies from 0.98 at $\nu = 10^{-5}$ (a very stable "radical") through 0.06 at $\nu = 3.2\ (10^{-3})$ (e.g. H, O, CH_3 on many surfaces) to 0.003 at $\nu = 1$ and it is not surprising that unstable radicals have not been detected in this instrument; the theory also predicts a sensitivity of 0.1 mtorr/lusec for the M.S.2/R, comparing well with the measured value of 0.05 mtorr/lusec, using the sampling pinhole of reference 22.

---

4) The value of >100 quoted in reference 22 refers to the pyrolytic production of H_2S and HCl from HCHO and surface impurities; if the production of CO (the main product) is considered one arrives at the value of 3000 given here.

5) The predicted value of >40000 given in reference 22 is based on a greatly over-simplified calculation.

Figures 9 through 11 show the results of equations 10 and 11 for case B; it is clear that the highest possible pumping speed, S_c, is desirable for best relative radical sensitivity and for pyrolysis discrimination, and the absolute sensitivity is not so much affected by S_c because the main sample pressure in the ionisation region is due to direct beam (the cross-section of the electron beam should be larger than that of the molecular beam and it is desirable to have high ion collection efficiency from the whole of the volume common to the two beams). Thus Figure 9 shows that increasing the length of the molecular beam system (d_c) and increasing the ion source size (d_s) at small d_c are the main factors detrimental to sensitivity. On the other hand, Figure 10 shows that large d_c and small d_s are desirable for high radical sensitivity (because the molecular beam is then better collimated); reducing back-scatter from the pumping system (ν) is important at low pumping speeds and low d_c. Figure 11 shows that a large d_c and high S_c with low back-scattering and small d_s are desirable for maximum pyrolysis discrimination, which actually improves with high wall removal efficiencies ($\nu_1 = \nu_3$), because pyrolytically produced radicals must collide several times in the outer chamber before reaching the ionisation region. The instrument used in reference 10 should have $p_2/Q = 5(10^{-6})$mtorr/lusec, $p_1/p_2 = 0.9$ and p_1/p_3 varying from 3000 at $\nu = 10^{-5}$ to $2(10^5)$ at $\nu = 1$; the experimental sensitivity was $2(10^{-6})$ mtorr/lusec, and detection of the presumably very unstable frozen "polymers" of CO_2 suggests a high value for p_1/p_2.

For a simple instrument the most important factors in detecting free radicals are the pinhole-electron beam distance, which must be small, and the provision of a separately pumped filament box with as high a pumping speed as possible because merely shielding the filament, however thoroughly, is not enough[22]; a high source pumping speed, an open ion box and a restricted electron beam orifice are secondary factors. Even with $S_c = 20$ l/sec, a very open ion box and a pinhole only 2 mms from the ion repeller, a sixfold reduction in concentration of very reactive radicals can be expected (Figure 6).

A molecular beam instrument without separate filament pumping can have negligible depletion of radical concentrations if a high pumping speed, S_c, is combined with efficient molecular beam trapping (low ν) and if the beam is very well collimated; the distance from the final molecular beam orifice to the electron beam, d_s, (which should be small) is a secondary factor; the sample which must be removed from the system under investigation may be up to 10^5 times greater than for a simple mass spectrometer if the sensitivity is to be comparable, and the method of removing this sample and of disposing of the 99.9% which is rejected in the first molecular beam chamber, present some difficulties.

Two comments are necessary on the calculation of pyrolysis effects and on some of the assumptions contained in it. Firstly although it has been assumed that pyrolysis occurs only on the filament, and in the numerical calculations with a unit collision efficiency, it is known[22] that pyrolysis occurs at least as much on hot surfaces near the filament and that such reactions probably have a collision efficiency <<1; nevertheless, the substitution of some very much larger pyrolysing area for A_f and much smaller collision efficiency for would not make much difference to the results. Secondly, the pyrolysis discrimination factor p_1/p_3 has been calculated for a hypothetical sample where $P_1 = P_2$; in many cases of chemical interest free radicals will be present only in small concentrations (P_1/P_2 <<1) and p_1/p_3 would be reduced in the same ratio; in other words a pyrolysis discrimination calculated to be 10^4 by the above treatment means that $p_1/p_3 = 1$ when $P_1/P_2 = 10^{-4}$, that is that a pyrolytic origin for an observed radical must be considered a strong possibility when it is observed to have a concentration of 100 p.p.m. In order to be able to detect radicals at very low concentrations in the sample, it is necessary to show a correspondingly high pyrolysis discrimination factor when this is calculated using the above treatment and assumptions.

Conclusion

Isentropic expansion in sampling gas into a mass spectrometer has been shown to involve previously unrecognised effects, notably due to cooling and possible condensation of the sample; many intermolecular collisions must occur during the sampling process, as shown by the extent of condensation in gases such as CO_2[10], but these processes hopefully may provide the means of quenching fast reactions. Calculations of the effects of pyrolysis and wall reactions show that it is possible to reduce these either by differential filament pumping or by a well-collimated

molecular system, the latter arrangement being better for the detection of free radicals, although it requires the removal of a larger sample from the reaction vessel which, in itself, makes the use of an isentropic expansion sampling pinhole more probable.

These effects may account for the paucity of quantitative work on relatively high pressure chemical reactions in which mass spectrometers have been used to detect unstable intermediates. It may be that a more fruitful technique for precise quantitative work would be the study of individual reaction steps using, perhaps, crossed molecular beam systems and mass spectrometric analysis; the disadvantages of isentropic expansion could possibly be turned into advantages by constructing supersonic molecular beam systems[24], although the presence of condensed species should be remembered in interpreting the results of crossed beam studies.

Acknowledgements

Some of the results of Figures 1 and 2 were obtained by Mr. D. Teesdale of King's College, Newcastle-upon-Tyne during a temporary appointment at A.E.R.E., Harwell. Previously unpublished data on the M.S.2/R instrument were obtained during the author's tenure of an I.C.I. Ltd. Research Fellowship at Oxford University. All calculations were performed on the I.B.M. 7030 computer at A.W.R.E., Aldermaston. The author is indebted to many friends for helpful discussions of many of the topics discussed here.

Notation

Q flow rate in co.torr.sec^{-1} (lusecs)

R gas constant, ergs. deg^{-1} mole^{-1}

T temperature, ^{o}K

M molecular weight, a.m.u.

P_o pressure of sample, torr

A_1 area of sampling pinhole, cm^2

l length of sampling pinhole, cm

d diameter of sampling pinhole, cm

γ specific heat ratio, C_p/C_v

M_a Mach number (local velocity/local sonic velocity)

η gas viscosity, gm. cm^{-1} sec^{-1} (poise)

Re Reynold's number

p gas density, gm. cm^{-3}

u local gas velocity, cm.sec^{-1}

n molecular concentration in ion source, cm^{-3}

I_n intensity of ion beam for n-mer, arbitrary units

σ collision diameter, cm.

d_c distance from pinhole to ion repeller or final molecular beam orifice, cm.

A_c area of hole in ion repeller of final molecular beam orifice, cm^2.

d_s distance from ion repeller or final molecular beam orifice to ionisation region, cm.

V_i volume of ion box, litres

A_a area of electron beam orifice, cm^2

A_i area of all other openings in ion box, cm^2

d_i distance from centre of ionisation region to electron beam orifice, cm.

d_f distance from electron beam orifice to filament, cm.

A_f area of filament, cm^2

A_f' area of filament with collision free access to electron beam orifice, cm^2.

V_f volume of filament box, litres.

S_f pumping speed from filament box, litres. sec^{-1}

V_c volume of outer vacuum chamber containing ion source, litres

Sc pumping speed from outer chamber, litres. sec^{-1}

11.4 A pumping speed of area A cm^2, litres. sec^{-1}

A_e cross sectional area of electron beam in ionisation region, cm^2

$\bar{\sigma}$ mean molecular velocity, $cm.sec^{-1}$

δ average distance between wall collisions, cms.

λ collision efficiency of filament pyrolyses

ν collision efficiency of wall reactions

ψ fraction of molecular beam scattered back from pumping system

p pressure in ion source, mtorr.

Captions to figures

Figure 1 Flow through pinhole. Curves are theoretical best fittings of equation (5) with parameters as in Table 1.

Figure 2 Flow through pinhole. As Figure 1, but with theoretical Clausing coefficient.

Figure 3 Variation of intensity of $(CO_2)_n^+$ ions with n.

Figure 4 Variation of intensity, with pressure of $(CO_2)_n^+$ for n = 1, 2, 3.

Figure 5 Sensitivity, simple mass spectrometer.

Figure 6 Radical relative sensitivity, simple mass spectrometer.

Figure 7 Pyrolysis discrimination, simple mass spectrometer.

Figure 8 " " " " "

Figure 9 Sensitivity, molecular beam mass spectrometer.

Figure 10 Radical relative sensitivity, molecular beam mass spectrometer.

Figure 11 Pyrolysis discrimination, molecular beam mass spectrometer.

References

(1) G.C. Eltenton. J. Chem. Phys., 20, 907 (1952)

(2) F.P. Lossing. Ann. New York Acad. Sci., 67, 499 (1957); J. Cuthbert, Quarterly Reviews (London), 13, 215 (1959); reviews and early bibliography.

(3) S.N. Fener, and R.L. Hudson. J. Chem. Phys., 21, 1374 (1953).

(4) P.F. Knewstubb, and T.M. Sugden. Nature, 181, 474 (1958); Proc. Roy. Soc., A255, 520 (1960).

(5) F.P. Lossing, et. al. J. Amer. Chem. Soc., 81, 281 (1959); 82, 519 (1960).

(6) P. le Goff. J. Chim. Phys. 53, 369, 480 (1956); Compt. rend., 239, 970 (1954); L.P. Blanchard and P. le Goff. Canad. J. Chem., 35, 89 (1957); 37, 515 (1959); P. le Goff and M. Letort. Zhur. fiz. Khim., 32, 481 (1958); O. Osberghaus and R. Taubert, Z. Phys. Chem., 4, 264 (1955).

(7) P. le Goff. J. Chim. Phys., 51, 312 (1954); 53, 359 380 (1956); A Cassuto, Annales de chimie, 7, 249 (1962).

(8) C.W. Nutt, J.S M. Botterill, C. Thorpe, and G.W. Penmore. Trans. Faraday Soc., 55, 1500 (1959).

(9) O. Hagena, and W. Henkes. Z. Naturforsch, 15a, 851 (1960).

(10) J. Cuthbert, E.R. Preece and A.H. Turnbull. Appl. Spect., (in press).

(11) M. Knudsen. Ann. Physik. 28, 999 (1909).

(12) P. Clausing. Ann. Physik., 12, 961 (1932); Z. Physik. 56, 471 (1930).

(13) K.D. Carlson. Report No. ANL-6156 (Argonne Natnl. Lab.).

(14) A.B. Campbel and B.H. Jennings. Gas Dynamics, (McGraw Hill) 1958.

(15) H.W. Liepmann. J. Fluid Mech., 10, 65 (1961).

(16) F.I. Frankl. Trans. Acad. Sci., U.S.S.R. 58, No. 3 (1947).

(17) E.S. Creutz and L.R. Zumwalt. J. Appl. Phys., 2883 (1962).

(18) M. Barber, J. Farren and J.W. Linnett. Proc. Roy. Soc. A274, 293 (1963).

(19) P.G. Bentley. Nature, 190, 432 (1961).

(20) F.T. Greene and T.A. Milne. J. Chem. Phys. 39, 3150 (1963).

(21) R.E. Leckenby and E.J. Robbins. U.K.A.E.A. Risley, England. (private communication).

(22) M. Barber, J. Cuthbert, J. Farren and J.W. Linnett. Proc. Roy. Soc. A274, 285 (1963).

(23) L.F. Phillips and H.I. Schiff. J. Chem. Phys. 37, 1233 (1962); J. Berkowitz and S. Wexler, ibid, p. 1476; A.G. Harrison and F.P. Lossing, Canad. J. Chem., 38, 554 (1960).

(24) R. Campargue. Rev. Sci. Instr., 35, 111 (1964); E.W. Becker and K. Bier, Z. Naturforsch, 9a, 976, (1954); J. Dekkers and J.B. Fenn, Rev. Sci. Instr., 34, 96 (1963).

(25) F.T. Greene, J. Brewer and T.A. Milne. J. Chem. Phys., 40, 1488 (1964).

(26) E.W. Becker, W. Beyrich, K. Bier, H. Burghoff and F. Zigan. Z. Naturforsch. 12a, 609 (1957).

(27) T.A. Milne and F.T. Greene (private communication) to be published in Proc. 10th Symposium on Combustion, Cambridge, 1964.

STERN-GERLACH EXPERIMENTS USING MASS SPECTROMETRIC DETECTION*

J. Berkowitz and L. S. Goodman
Argonne National Laboratory
Argonne, Illinois

Although experiments of the Stern-Gerlach type[1] have largely been supplanted by the resonance technique introduced by Rabi[2] in 1938, there remain a number of problems that are more amenable to solution by the simple deflection method.

Stern and his school, in a classic series of papers,[1] were able to demonstrate spacial quantization and to measure the magnetic moments of a number of atoms (K, Na, Tl, H, Bi, Li) and one molecule, O_2[3]. A serious limitation was imposed upon the scope of their research by the system used to detect their molecular beams. Although condensation, chemical reaction, surface ionization, space charge depression, thermal and manometric techniques were employed, some knowledge of the composition of the beam had to be assumed. In many cases of interest, however, it may be difficult or impossible to produce a molecular beam containing only the species to be investigated, or even primarily the desired species.

Mass spectrometric detection offers a means of studying even a minor molecular component of a molecular beam. This device is indeed already being used for resonance experiments of the Rabi type on molecules.[4] A limitation of the resonance experiments with molecules, however, is the smearing that is frequently caused by a large distribution of thermally populated rotational states.

In many problems of spectroscopic and thermodynamic interest, one is merely interested in deciding between two alternatives for the electronic ground state of a molecule. If one of the alternatives gives rise to a magnetic moment and the other does not, a Stern-Gerlach experiment with mass spectrometric detection offers a direct approach.

We have employed a molecular beam apparatus specifically designed for resonance studies but incorporating a mass spectrometric detector, to answer the following questions.

1. Are the various sulfur molecular species produced under different conditions chain-like or rings?

2. Can the molecule BaOH be produced in significant quantities by the reaction of water with BaO?

3. What are the electronic ground states of molecules such as TiO and ZrO?

A description of the experimental apparatus, and the results obtained therewith will be discussed.

---

* Work performed under the auspices of the U.S. Atomic Energy Commission.

1 "Recent Research in Molecular Beams," I. Estermann, ed., Academic Press, New York (1959), p 1-7.

2 S. Millman, I. I. Rabi and J. R. Zacharias, Phys. Rev. 53, 384 (1938).

3 R. Schnurmann, Zeits. f. Physik 85, 212 (1933).

4 M. R. Baker, H. M. Nelson, J. A. Leavitt and N. F. Ramsay, Phys. Rev. 121, 807 (1961).

SOME RECENT DEVELOPMENTS IN THE STUDY OF IONIZATION PROCESSES

James D. Morrison

Frick Chemical Laboratory, Princeton University, Princeton, New Jersey, U.S.A., and Chemical Research Laboratories C.S.I.R.O. Melbourne, Australia

Electron impact has been used in a mass spectrometer to study the energy states of molecules for some 30-40 years. Throughout this time the progress of the subject has been hindered mainly by the difficulty of obtaining ionizing beams of electrons with low spreads in energy. The wide energy spread in the ionizing electrons smears out all of the wealth of fine detail which spectroscopy shows must be present. To the energy spread might be added one other reason, the natural tendency of most experimentalists, when faced with a set of points, to try to draw straight lines through them. This may seem trivial, but in fact has led to many errors and disagreements about interpretation of data.

Reduction of Energy Spread using Selectors

There have been many attempts to reduce the energy spread. The Fox gun[1] was for years the most successful of these. More recently, Marmet and Kerwin[2] developed the first really satisfactory electron velocity selector. During the last two years, the author and his colleagues have devoted a lot of effort to building such selectors into mass spectrometers. One runs into many difficulties. Under some conditions, ions may be formed on the walls of the ionization source, at energies different from those in free space, and these ions may subsequently diffuse into the mass analyser, and give rise to spurious detail in IE curves. To combat these wall effects, which seem to be aggravated by the use of electron velvet, chambers have been built from 98% transparent gauze. It has been attempted, not very successfully, to build a chamber with hot walls. To date, the most successful chamber is machined out of a block of soft graphite. With this, one can at best obtain electron beams with an energy spread of around 0.02 ev. This is determined from the sharpness of the initial break in the Xe^+ curve. It is never possible to get an equally sharp break for He^+, the initial curvature extending over 0.05 ev, and it is believed that this is due in this case to the Doppler effect.

The maximum electron current obtainable at this energy spread is low, of the order of 10^{-8} amps, making mass analysis of the ionized products difficult. By increasing the operating voltages of the selector, one can obtain $\sim 10^{-7}$ amps, at a half width of 0.08 ev. A typical run obtained at this setting is shown in Figure 1. It is interesting to note that this curve does not show any sign of vibrational structure in the lowest state of the N_2^+ ion. The step in the curve at 16.25 ev due to autoionization shows up very clearly.

Currents of the order of 10^{-7} amps. are hardly sufficient to get good IE curves for many fragment ions, or for the study of free radicals. As one tries to reduce the energy spread by a given amount, the current obtainable goes down by a much larger factor, e.g. a 10 fold improvement in energy spread is accompanied by a 500 fold drop in electron current.

Reduction of Energy Spread by an Analytical Method

The possibility of removing the electron energy spread from experimental data by an analytical approach[3] has been explored recently. It turns out that within certain limitations this can be cone. One has to exchange signal-to-noise ratio for resolution, but unlike the situation where a selector is used, the loss in signal-to-noise ratio for a given degree of improvement in resolution is no more than theoretical. One can fairly readily obtain effective energy spreads of 0.1 ev or less, from data measured using an ordinary ion source with an electron energy spread of 0.6 ev.

Figure 2 shows a methane CH_4^+ curve which has been treated in this way. The original curve was recorded using a CEC 21.103 mass spectrometer. Appreciable curvature still remains at the foot of the curve. The smoothed 2nd differential curve indicates that the vertical ionization potential is approximately 13.0 ev., while the adiabatic IP is $\lesssim$ 12.8 ev. These results support a photon impact (P.I.) study of this molecule made by the author's colleague Dr. Nicholson.

It is of interest to treat some other worker's data in this way. The results obtained by Lossing, Ingold and Henderson[4] for C_2H_2 and allyl radical are shown as curves $i(V)_1$ and $i(V)_2$ in figure 3. The curves are different, but it is hard to say where the difference lies. The curves obtained by processing are shown as $I(E)_1$ and $I(E)_2$. This is not a favorable case in that the scatter becomes serious, but the difference between the two curves also shows up more clearly.

By now everyone is aware of the significance of the detailed shape of ionization efficiency curves, not only for the accurate measurement of threshold energies but also for the identification of the class of the process leading to the ion, and the detection of higher energy states. The threshold law must be taken into account in determining the energy. The higher energy values are of especial importance, in view of recent interest in semiempirical methods of calculating these energies.[5] It is all the more important then that a clear distinction be made between the vertical and the threshold IP. It is the vertical IPs which can be approximately equated to the one electron eigenvalues obtained in the Huckel type calculations. In some cases, it is possible to measure a complete set of these orbital energies from the electron impact (E.I.) data, and to use these to find best values for the parameters in the Huckel treatment.

Configuration of fragment ions

While the absolute energies obtained in this type of calculation are not very good, the minimum total energy would appear to be a good criterion for determining the correct configuration. Accordingly, some calculations of this kind have been carried out, by the method of Hoffman,[6] on some common radical ions. Surprisingly, for the species $C_3H_3^+$, a linear structure turns out to be slightly more stable than an equilateral triangle.

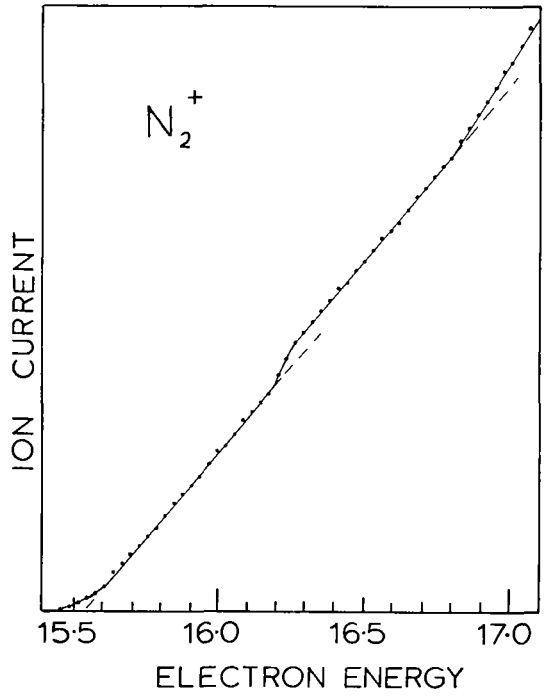

Figure 1 - Ionization efficiency curve for N_2^+, measured using electron selector source.

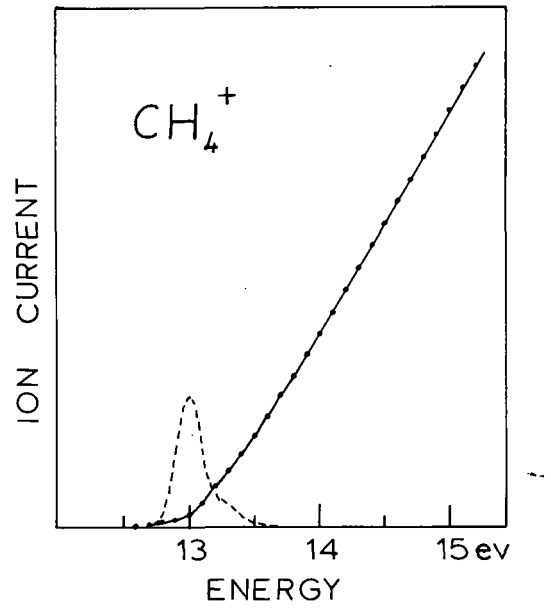

Figure 2 - Ionization efficiency curve for CH_2^+ calculated from ordinary data by analytical method. A smoothed 2nd differential plot obtained from this is shown at the bottom of the figure. The energy scale was calibrated using Kr.

Breakdown of Threshold Law at Higher Energies

It is generally accepted that the threshold law for single ionization is a linear function of the excess energy for E.I. and a step function for P.I. If this were exactly so, the 1st derivative of the P.I. curve and the 2nd derivative of the E.I. curve would give the electronic transition probability curve. In very few cases, however, does the threshold law hold for any very great range. It is hard to decide just how far it does extend, because of the presence of excited states of the ion, and of autoionization phenomena. With electron impact the range over which the threshold law is followed within 1% in approximately 10 ev for He^+, but may be as little as 2 ev for heavier molecule-ions. With photon impact, the behavior would appear to be much as for electrons.

There appear to be two distinct kinds of behavior at higher energies, one a gradual departure from the threshold law, and the other abrupt. This is very evident in the curves for doubly charged molecules, compare for example benzene, ωCH_3, CO and CO_2 with NH_3 and NO.

There is unfortunately also evidence that the slope of the IE curve at higher energies is dependent on the surface cleanliness of the ion source, and the kind of spectrometer used. Using the electron selector and a 60° sector mass analyser, the curve for He^+ is exactly linear for 8-10 ev, before deviating gradually. Using a CEC 21.103 with a slightly modified source the curve may be linear over 2 ev or so, before gradually curving over.

The analytical method mentioned earlier can be used to correct for instrumental effects of this kind. If it is assumed that the curve for He^+ is in fact linear, the actually observed He^+ curve can be used to correct all other curves measured on the same instrument. Figure 4 shows such a correction carried out on a Ne^+ curve. Naturally such correction must be applied with caution.

Accuracy of Measurement of Ionization Energies

Since ionization energies were first measured by EI, there have been discrepancies between values found, and spectroscopic values obtained from Rydberg series. It is sometimes still stated[7] that the spectroscopic value is adiabatic, while the impact value is vertical. Photon impact has provided a large series of very accurate values, and it is true that the discrepancies which are found are almost always such that EI $\sim$ PI.

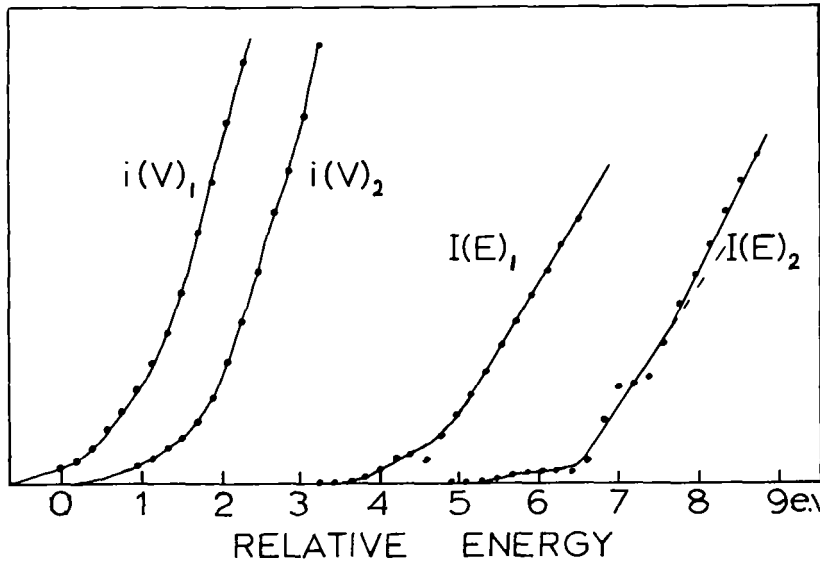

Figure 3 - Effect of correction method when energy spread is not known accurately. $i(V)_1$ and $i(V)_2$ are the curves for $C_2H_2^+$ and allyl$^+$ taken from Lossing and colleagues.[4] $I(E)_1$ and $I(E)_2$ are the corresponding calculated curves using a 'guess' at the electron energy spread of 0.5 ev half width.

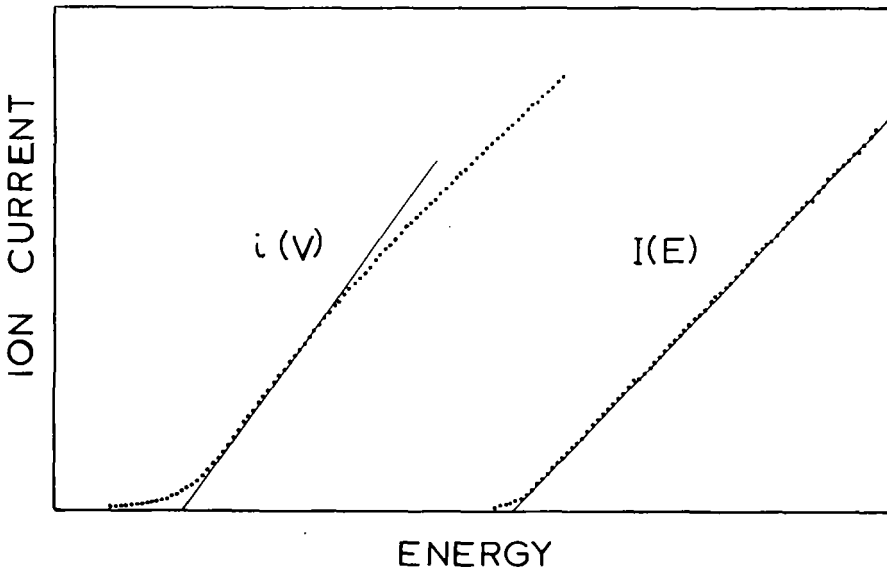

Figure 4 - L.H.S. Directly measured Ne^+ curve. R.H.S. Corrected curve, making use of He^+ curve run on same instrument.

Table 1

Table showing discrepancy between ionization potentials measured by electron and photon impact.

Substance	Ionization Potential e.v.	
	Photon Impact	Electron Impact
CH_4	12.99	13.13
CH_3	9.83	9.95
C_2H_4	10.52	10.8
Propylene	9.73	9.81
C_6H_6	9.245	9.3-9.57
CO_2	13.788	13.80

It has been suggested recently[8] that there may be another theoretical reason why the IPs measured by photon and electron impact should be different. The two processes of energy transfer have very different time scales. Photons are much larger than electrons, and are able to interact with a molecule for a considerably longer time, say 10^{-15} sec., as compared with 10^{-16} - 10^{-17} for electrons. The ionization potentials measured using photons are therefore more likely to correspond to Hartree-Fock orbital energies, while those measured using electrons will correspond to more localized orbitals. A careful examination has been made of the few cases where accurate electron and photon impact data are available, and it is concluded that this effect, if present at all, does not cause a discrepancy of more than 0.05 ev in the ionization energy.

The large majority of electron impact values quoted in the literature have been determined by the critical slope method. Because it is reproducible, this method is still used, especially in measurements on free radicals, and it has always been believed that it gave close to the vertical value. To test this, three likely cases were assumed, and the ionization efficiency curves which would be obtained from these were calculated, using a typical electron energy spread with a half width of 0.5 ev. All three give good semilog plots, as is shown in figure 5. Unfortunately, neither the point at which the curve deviates from linearity, nor the point of 2/3 gradient, bears very much relation to either the vertical or the adiabatic threshold, and can be in error by as much as 0.25 ev. In these particular cases, simple linear extrapolation of the direct curves gives values almost the same as those given by the critical slope method. In view of this result, it is suggested that the use of this method be discontinued, or that a more realistic absolute error be quoted.

References:

1. R.E. Fox, W.M. Hickam, T. Kjeldaas and D.J. Grove Phys. Rev. 84, 859 (1951 Rev. Sci. Instr. 26, 1101 (1955)

2. P. Marmet and L. Kerwin Can. J. Phys. 38, 787,972 (1960)

3. J.D. Morrison J. Chem. Phys. 39, 200 (1963)

4. F.P. Lossing, J.U. Ingold and I.H.S. Henderson J. Chem. Phys. 22, 621 (1954)

5. N.S. Hush and J.A. Pople Trans. Faraday Soc. 51, 600 (1955) also R. Hoffman J. Chem. Phys. 39, 1397 (1963

6. R. Hoffman J. Chem. Phys. 40, 2480 (1964)

7. F.P. Lossing chap. in "Mass Spectrometry" ed. by C.A. McDowell McGraw Hill (1964)

8. S. Berry personal communication

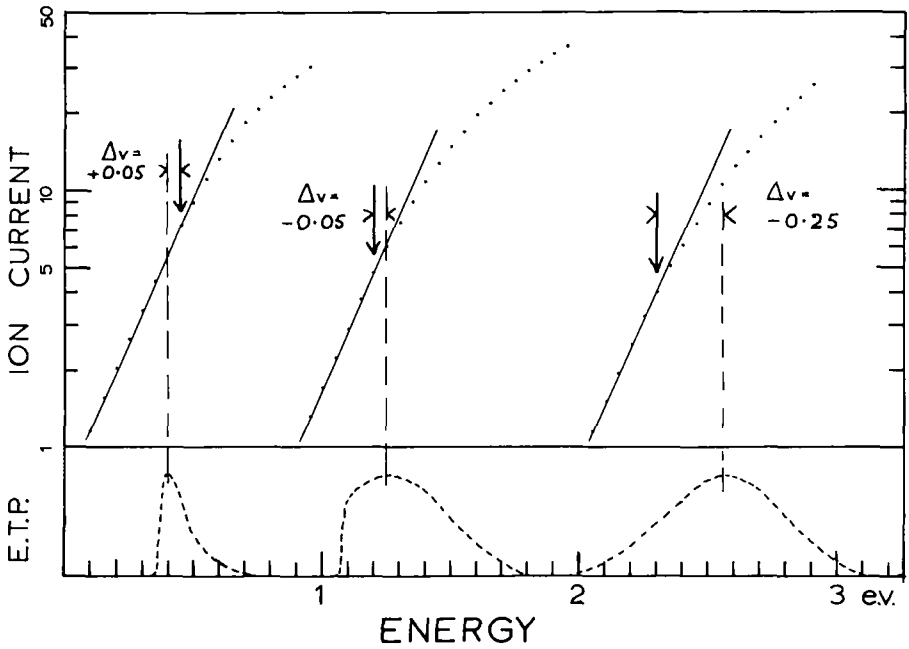

Figure 5 - Lower:- Envelope of the vibronic transition probabilities to be expected in cases where the stable configuration of the molecule-ion is progressively different from that of the neutral molecule.

Upper:- Semilog plots of the ionization efficiency curves calculated from these, assuming an electron energy spread of 0.5 ev half-width. The relation of the critical slope value to the electronic transition probability is indicated by broken lines.

"The Photoionization and Dissociation of some di- and tri-atomic Molecules."

by D. C. Frost, D. Mak, C. A. McDowell and D. A. Vroom
Chemistry Department, University of British Columbia
Vancouver, B.C.

Abstract

A vacuum u-v monochromator and a mass spectrometer have been used to study photoionization processes as a continuous function of energy between 12 and 20 ev. The light source, a repetitive condensed discharge in helium, provides a continuum of radiation.

Photoionization efficiency curves for Xe^+, CO^+, and HF^+ show structure which is interpreted in terms of direct- and pre-ionization processes. The curve for Ar^+ shows no structure above the $^2P_{1/2}$ level, a result at variance with earlier photoionization work.

Appearance potentials of fragments from H_2S and C_2H_4 are used to evaluate certain bond dissociation energies.

Experimental

The mass spectrometer and monochromator are shown in diagramatic form in figure 1.

The mass spectrometer is basically a 60 degree sector, 15 cm. radius of curvature Nier type instrument of resolving power 200. With the exception of the stainless steel tube, all the vacuum enclosures are of brass. Figure 2 shows the ion source. The ion chamber is open at each end to allow unrestricted passage for incident radiation, and is at a potential equal to that of the monochromator exit slit. This prevents any photoelectrons generated on the slit face entering the ionization region to cause spurious ion currents, and as an additional safeguard two deflector plates provide an electric field across the monochromator side of the slit.

Electrodes 4 and 6 define the ion beam, with 2, 3 and 5 providing focussing and beam centering control.

In electron impact work, where the incident beam energy spread is to be minimized, ionization should occur in a field free region. This usually requires pulsing techniques and magnetic screening of the ion source. With photons the situation is simplified, since, uncharged, they remain unaffected by fields. The ion repeller may therefore be adjusted for maximum ion beam with no deterioration in photon monochromicity.

A 17-stage Be/Cu open-ended photomultiplier followed by a vibrating reed electrometer and strip-chart recorder are used for ion current measurement.

The monochromator employs a 15,000 lines/inch aluminized diffraction grating, radius of curvature 1 meter, rotation of which is all that is required to vary the emergent photon beam energy. The general design follows that of Seya (1).

Differential pumping - 140 and 400 liter/min. rotary pumps at the light source end of the monochromator and a 650 liter/sec. oil diffusion pump with water-cooled baffle at the grating housing - prevents any measurable increase in mass spectrometer background pressure (2×10^{-6} mm. Hg) when the light source gas flow is turned on.

The monochromator may be isolated from the mass spectrometer, for maintenance purposes, by a $2^1/_2$ inch high vacuum valve (not shown in the diagram).

The vacuum u-v radiation strikes a sodium salicylate - coated RCA 9816 photomultiplier tube on leaving the ion chamber, and the resultant fluorescence produces a photocurrent proportional to the incident light intensity. The multiplier output is fed to a d-c amplifier and a recorder.

Figure 3 is a diagram of the McPherson model 630 vacuum u-v water and air-cooled light source.

An air-blown, mercury lamp-irradiated spark gap in series with the power supply and lamp triggers the discharge. The continuum intensity falls off with trigger frequency (optimum value 1400/sec.) and helium pressure, becoming unusable below 5 mm.

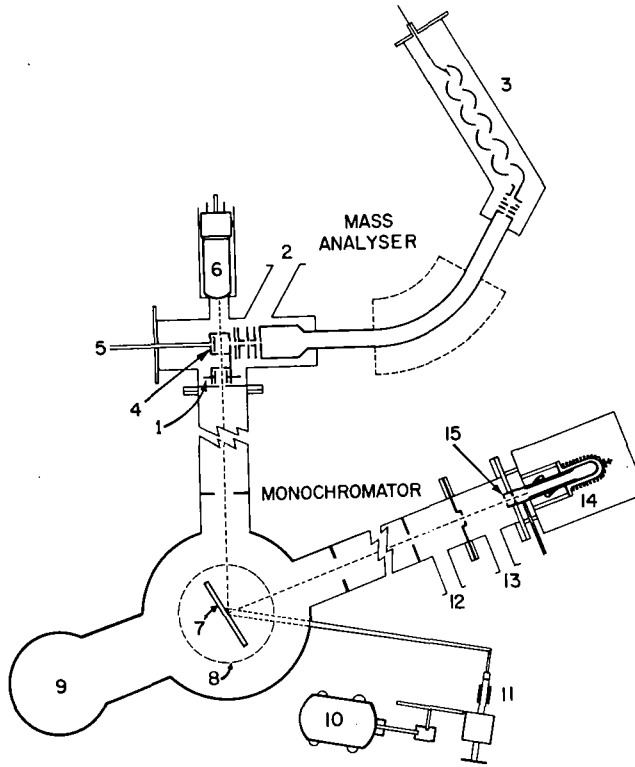

1. Mass Spectrometer and Monochromator.
1 - Secondary electron deflection plates, 2 - mass analyser pump, 3 - 17 stage Be/Cu multiplier, 4 - ion source, 5 - gas sample inlet, 6 - photon detector, 7 - grating, 8 - grating table, 9 - monochromator pump, 10 - grating drive motor, 11 - micrometer screw, 12 and 13 - light source differential pumping, 14 - light source, 15 - inlet slit.

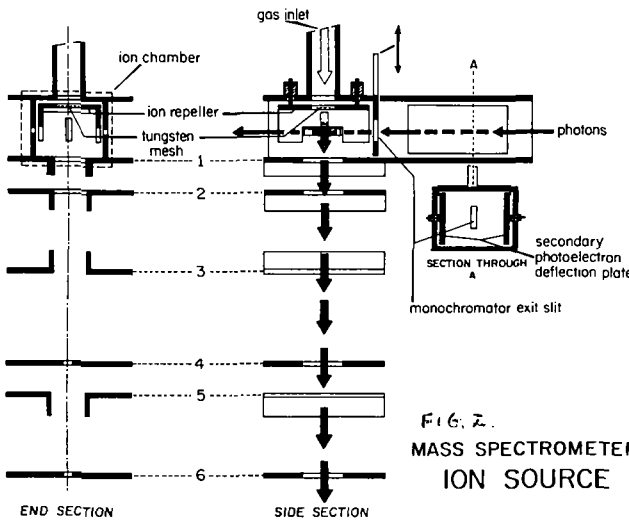

FIG. 2.
MASS SPECTROMETER
ION SOURCE

Hg. Broad peaks in the spectrum occur at approximately the same wavelengths as those reported by Tanaka (2).

The monochromator resolution is about 6 Å, corresponding to an energy spread of 0.08 ev for nominally 13 ev photons.

The grating angle, and hence the photon energy, may be altered by moving a 12 inch arm connected through a vacuum seal to the grating table. A micrometer screw bearing on the end of this arm is calibrated in terms of wavelength after observations on known emission lines from a variety of gases.

A suitably geared motor drives the monochromator screw to vary the photon wavelength over the desired range, usually at a rate of 10 A/minute, and the ion and photon intensities are recorded simultaneously. This enables the photoionization efficiency curve, or the ions/photon ratio in arbitrary units, to be plotted as a continuous function of the incident photon energy.

Results and Discussion

1. Xenon

The photoion efficiency curve for Xenon is shown in figure 4. The peaks near the ionization threshold have been reported by Beutler (3) as preionized in his absorption spectrum, and that they are indeed due to this type of process has been recently confirmed by Nicholson (4) in a total ionization apparatus.

The present work extends the curve up to 16 ev, and was done with mass analysis and much lower sample pressures (10^{-5} mm. Hg.) than those used by Nicholson (20-100 μ). Atom-atom and ion-atom reactions are therefore virtually eliminated. At energies slightly above the $^2P_{1/2}$ level of Xe^+ (13.44 ev) we have evidence for further preionization.

A comparison between peak energies found in this and previous work is given below, together with values for the first I.P.

Table I

Peak Energies for Xe^+ (ev)

Nicholson (4)	12.129(I.P.)	12.48	12.86	13.05	13.16	13.25		
Beutler (3)		12.45	12.82	13.02	13.14	13.21		
This work	12.12(I.P.)	12.43	12.81	13.03	13.18	13.23	13.45	13.63

2. Argon

The curve for Ar^+ (figure 5) shows a sharp onset, with the photoion efficiency at higher energies almost constant. With the present monochromator resolution we do not expect to resolve any structure between the $^2P_{3/2}$ and $^2P_{1/2}$ levels, shown by arrows in the diagram. That preionization peaks should appear in this region has been demonstrated by the total absorption experiments of Huffman et. al. (5).

Comes and Lessman (6) find several peaks in their Ar^+ curve up to 18 ev, and they correlate these with breaks found by various workers using electron impact methods. We would expect to be able to resolve most of the peaks appearing in the Comes and Lessman curve, however we find no evidence for them. The main difference between the two sets of data lies in the light source - the Comes and Lessman data was obtained using a line spectrum, and ours using a continuum.

3. Hydrogen Fluoride

The ionization potential of HF has previously been determined by electron impact methods only. These values and our photoionization figure are given in Table II. Since the ionization threshold of HF corresponds to the removal of what is essentially a non-bonding fluorine 2p electron, the energy of greatest slope at the onset of the photoion efficiency curve is expected to give the ionization potential for the o-o transition.

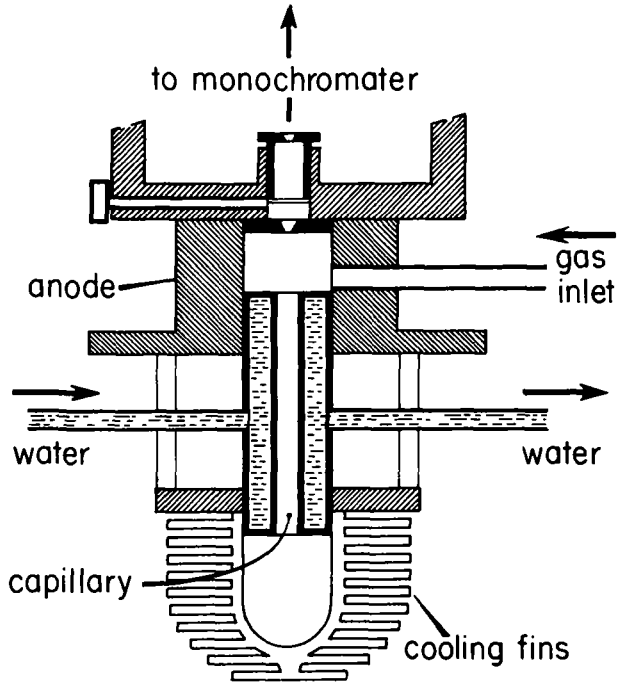

FIG. 3. LIGHT SOURCE

McPherson Model 630 Light Source.

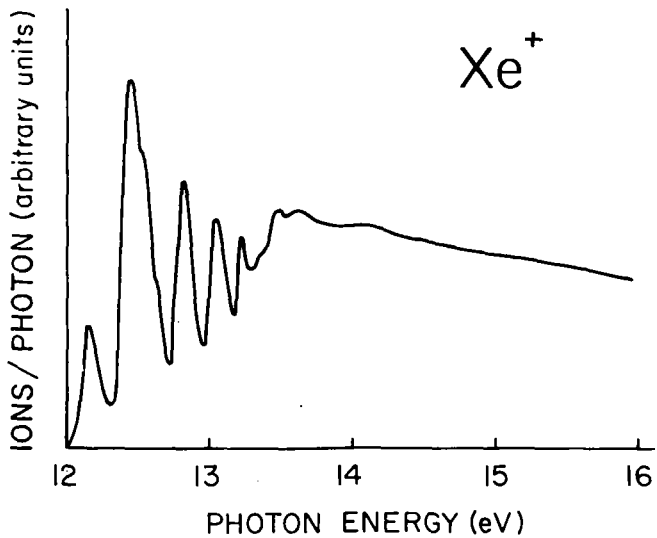

4. P.E. Curve for Xe^+.

The spin-orbital separation for the $HF^+(^2\Pi)$ ground state doublet is predicted to be 0.04 ev, and will therefore not be resolved here.

Table II

Ionization Potentials of HF

Method	Value (ev)	Reference
electron impact	16.38 ± 0.05 *	7
electron impact	16.0 ± 0.2	8
electron impact (R.P.D.)	15.77 ± 0.02* and 16.91 ± 0.1 *($A^2\Sigma^+$)	9
photoionization	16.04 ± 0.05	This work

*Standard Deviation.

The photoionization technique should give a more accurate value for (in this case) the adiabatic ionization potential. In the R.P.D. experiment, the break at 16.91 ev was taken to refer to formation of the HF^+ ion in its $^2\Sigma^+$ (first excited) state through ionization from the σ-bonding orbital.

Several peaks are evident in our curve for HF^+ (figure 6). They are probably due to preionization, however there is no spectroscopic evidence to support or deny this.

The R.P.D. break occurs near to a step in the HF^+ curve, and this may corroborate the assignment of the break to an inner ionization potential. However whether the 'step' is one in reality or a closely spaced series of preionization peaks must be decided by higher resolution experiments.

4. Carbon Monoxide

Figure 7 shows the ion efficiency curve for CO^+. The peaks are probably due to preionization,- several fit peaks in the absorption spectrum known to be preionized (10)(11).

Our value for the ionization potential (making allowance for photon bandwidth), 14.0 ev, agrees with the spectroscopic value of 14.01 ev. Field and Franklin's "preferred" electron impact value is 14.1 ev (12).

The sharp onset of ionization is predicted from the Franck-Condon principle, there being little difference between the ground state internuclear separations of CO and CO^+. The $CO^+(^2\Pi_i)$ state, on the other hand, is considerably displaced from CO and the maximum transition probability is expected to be to the v=3 or 4 ionic level. The higher members of Rydberg series leading to the 0, 1 and 2 vibrational levels of this state are marked in the diagram.

The ion efficiency curve, rising slowly from the o-o energy at 16.5 ev to a maximum at 17.3 ev, illustrates the relatively low ionization probability at the threshold. The steps may indicate ionic vibrational levels or preionization associated with a Rydberg series leading to the CO^+ ($B^2\Sigma^+$) state (marked beneath the curve).

Kaneko (13) has found the R.P.D. curve for CO^+ to show 'hump' thresholds, which he attributed to preionization, at energies denoted by asterisks under our curve. Referring to the Rydberg levels suspected to be preionized, and the peaks in our curve, the asterisks do not correlate at all with preionization thresholds. However they do appear where the density of preionized levels is starting to increase rapidly as the series' converge to their limits.

This photoionization work demonstrates clearly that preionization is widespread, and that even with an electron beam 0.1 ev wide it is a change in the density of preionized states and not a preionization threshold that causes apparent breaks in the electron impact curve for CO^+.

This, of course, does not mean that a break cannot appear in the electron impact curve at an inner ionization potential, but it does point out the extreme care necessary in the interpretation of curves obtained by using electrons of energy bandwidth greater than the adjacent preionization step separation for the particular

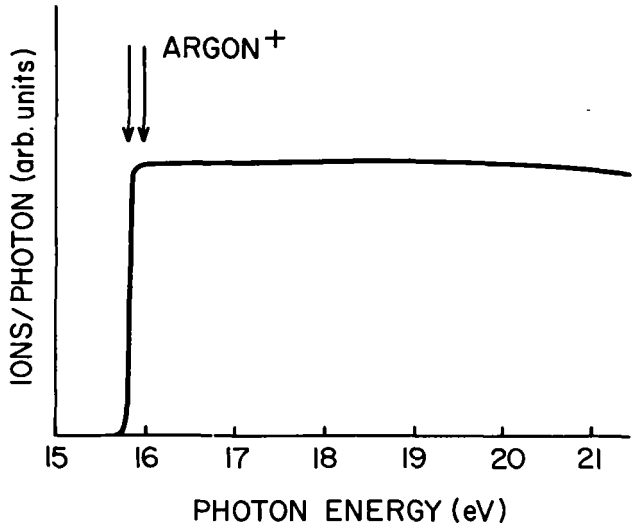

5. P.E. Curve for Ar^+.

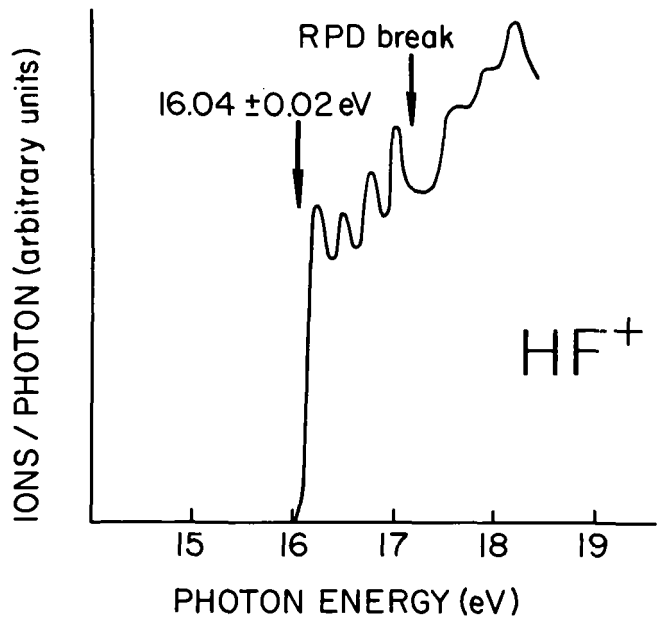

6. P.E. Curve for HF^+.

species under study.

5. Hydrogen Sulphide

Figure 8 shows the ionization efficiency curve for H_2S^+ up to 10.7 ev, and the curve for the fragment SH^+ up to 16 ev. The ionization potential of H_2S is found to be 10.44 ± 0.02 ev, in agreement with Watanabe's photoionization value of 10.46 ev (14).

The SH^+ ion arises through the process

$$H_2S + h\nu \longrightarrow H + SH^+ + e^- + K.E. + E.E.$$

Our value for the SH^+ appearance potential, and previous electron impact values, are summarized below.

Table III

Workers	$A(SH^+/H_2S)$ev.	Reference
Neuert and Clasen (1952)	15.2 ± 0.5	15
Palmer and Lossing (1962)	14.43 ± 0.1 and I(SH)=10.5 ± 0.1	16
Dibeler and Rosenstock (1963)	14.4 ± 0.2	17
This work (photoionization)	14.1 ± 0.1	

We have, using the photoionization value -

$$D(SH\text{-}H) \leqslant A(SH^+/H_2S) - I(SH)$$

$$14.1 \text{ ev} \qquad 10.5 \text{ ev}$$

$$\leqslant 3.6 \pm 0.2 \text{ ev}$$

$$\text{or } 83 \pm 5 \text{ kcal/mole.}$$

6. Ethylene

The photionization efficiency curves for ethylene and the fragments $C_2H_2^+$ and $C_2H_3^+$ are shown in figure 9. Apart from these species, only C_2H^+ and CH_2^{++} from ethylene have appearance potentials less than 20 ev, and their abundance is too low to permit study with our present photon intensity.

Several methods have been used to determine the ionization potential, and the various figures are in good agreement. Some of these are listed in Table IV.

Table IV

The Ionization Potential of Ethylene

Method	I.P. (ev)	Reference
Spectroscopic	10.51	18
Electron impact	10.48	19
Photoionization	10.516	14
Theoretical	10.75	20
Photoionization	10.5 ± 0.1 ev.	This work

The threshold energy is difficult to determine accurately owing to the relatively low probability of ionization to the ground ionic state. The process occurring at about 12.2 ev, however, does so much more easily. This is to be expected if we remove a strongly bonding π electron at 10.5 ev, and ionize from the σ(C-H) orbital at 12.2 ev. The former process, giving rise to a much greater difference in shape between molecule and ion than the latter will, is expected to occur with a correspondingly lower probability.

A further break occurs in the parent curve at 15.0 ± 0.1 ev, which eventually approaches zero slope at about 18 ev. Since the fragment CH_2^+ appears at 18.2 ev there would seem to be a connection between this and the $C_2H_4^+$ curve levelling off.

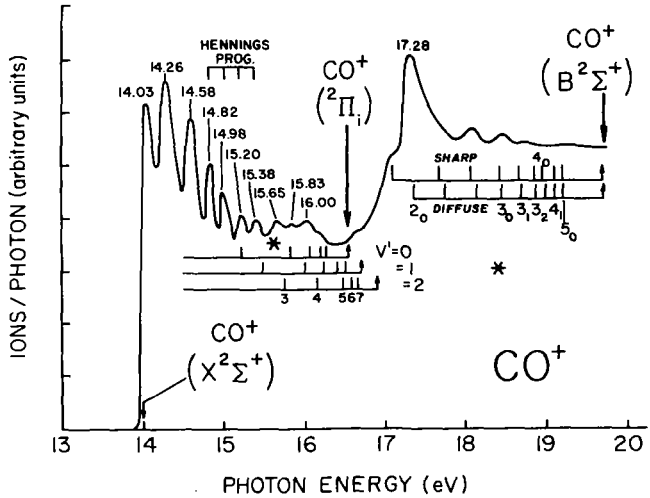

7. P.E. Curve for CO^+.

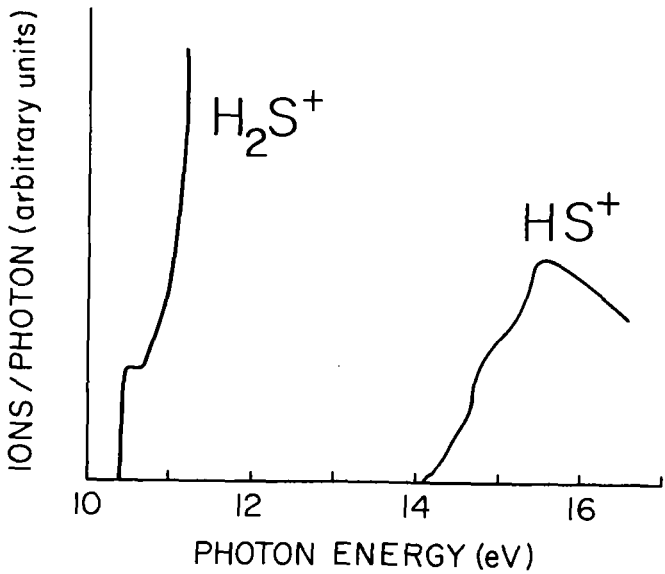

8. P.E. Curve for H_2S^+ and SH^+/H_2S.

The $C_2H_3^+$ fragment is predominantly formed through one process only, at 13.7 ± 0.1 ev, and an upper limit of 4.3 ev for $D(C_2H_3\text{-}H)$ can be derived from

$$A(C_2H_3^+) \geqslant D(C_2H_3\text{-}H) + I(C_2H_3)$$

if one takes $I(C_2H_3)$ to be 9.4 ev (21).

The fragment $C_2H_2^+$ is formed by processes at 13.1 ± 0.1 and 16.0 ± 0.1 ev. The former is clearly

$$C_2H_4 + h\nu \rightarrow C_2H_2^+ + H_2 + e^- + K.E. + E.E.$$

which means energetically

$$A(C_2H_2^+) \geqslant I(C_2H_2) + D(C_2H_3\text{-}H) + D(C_2H_2\text{-}H) - D(H_2)$$

Using $A(C_2H_2^+) = 13.1 \pm 0.1$ ev (above)

$I(C_2H_2) = 14.41$ ev (14)

$D(C_2H_3\text{-}H) \leqslant 4.3 \pm 0.1$ ev (above)

$D(H_2) = 4.72$ ev

we find $D(C_2H_2\text{-}H) \leqslant 2.1 \pm 0.2$ ev. The two H atoms must leave the intermediate as H_2, or the value obtained for $D(C_2H_2\text{-}H)$ would be negative.

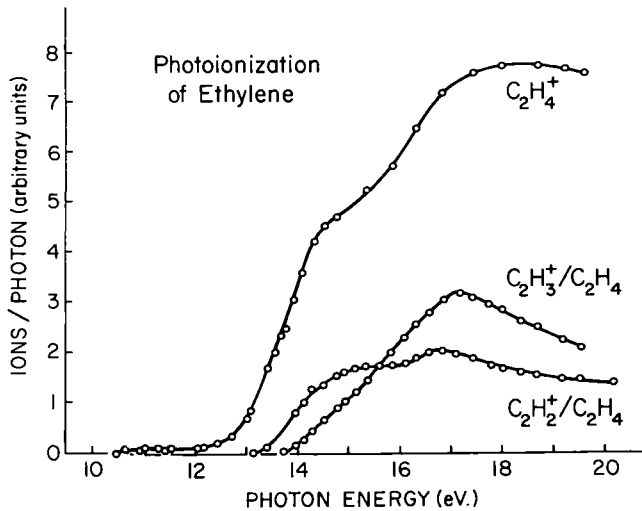

9. P.E. Curve for $C_2H_4^+$ and fragments

References

1. M. Seya, Sci. of Light (Tokyo) 2, 8, 1952; also see T. Namioka, ibid. 3, 15, 1954.
2. Y. Tanaka, A. S. Jursa and F. J. LeBlanc, J. Opt. Soc. Am. 48, 304, 1958.
3. H. Beutler, Z. Physik 93, 177, 1935.
4. A. J. C. Nicholson, J. Chem. Phys. 39, 954, 1963.
5. R. E. Huffman, Y. Tanaka and J. C. Larrabee, J. Chem. Phys. 39, 902, 1963.
6. Von F. J. Comes and W. Lessman, Z. Naturforschg. 16a, 1396, 1961.
7. J. F. Burns, Carbide and Carbon Chemicals Co., K-25 Plant, Report K-1147.
8. R. Thorburn, Proc. Phys. Soc. 123, 122, 1959.
9. J. A. R. Coope, D. C. Frost and C. A. McDowell, Nature 179, 1186, 1957.
10. H. J. Henning, Ann. Physik 13, 599, 1932.
11. Y. Tanaka, Sci. Papers Inst. Phys. Chem. Research (Tokyo) 39, 447, 1942.
12. F. H. Field and J. L. Franklin, "Electron Impact Phenomena", Academic Press Inc., 1957.
13. Y. Kaneko, J. Phys. Soc. Japan 16, 1587, 1961.
14. K. Watanabe, J. Chem. Phys. 26, 542, 1957.
15. H. Neuert and H. Clasen, Z. Naturforsch., 7a, 410, 1952.
16. T. F. Palmer and F. P. Lossing, J. Am. Chem. Soc. 84, 4661, 1962.
17. V. H. Dibeler and H. M. Rosenstock, J. Chem. Phys. 39, 3106, 1963.
18. W. C. Price and W. T. Tutte, Proc. Roy. Soc. A174, 207, 1940.
19. J. E. Collin, Bull. Soc. Chem. Belge. 71, 15, 1962.
20. Y. I'Haya, Molecular Physics, 3, 513, 1960.
21. A. Harrison and F. P. Lossing, J. Am. Chem. Soc. 82, 519, 1960.

MASS SPECTROMETRIC DETECTION OF REACTION INTERMEDIATES FROM FLASH PHOTOLYSIS

P. Kebarle, R. P. Messmer, O. P. Strausz and H. E. Gunning
Chemistry Department
University of Alberta
Edmonton, Alberta, Canada

Early attempts to apply mass spectrometric detection to flash photolysis met with only limited success. The present method uses a conventional sector field instrument. The flash lamp and reactor are mounted in the immediate vicinity of the ion source which is of open construction. A pinhole bleeds the gas to the ion source and a pumping capacity of 100 liters/sec at the source provides for rapid removal of the sampled gas. The concentration change of a radical is followed by sitting on one representative peak for the duration of the reaction. Several flashes the peaks have to be used to complete the analysis. The number of necessary flashes is reduced by making conventional mass spectrometric analysis of the stable products after the flash. The method has the advantage of high sensitivity and instrumental simplicity. A drawback of the present arrangement is the relatively long time required for the passage of the sample from the reactor to and out of the ion source ($\sim$ 2 milli sec.) This limits the time resolution so that only the kinetics of systems where the intermediates persist for several milliseconds can be studied. For radicals and atoms, recombining by third order kinetics, reaction conditions meeting the above requirement can be created.

Mass Spectrometric Studies of Oxygen Atom Reactions

John T. Herron and Fritz S.Klein

Mass Spectrometry Section
National Bureau of Standards
Washington, D.C. 20234

Introduction

The reactions of O atoms with NO and NO_2 have been the subject of several recent studies, using different experimental approaches.[1] Ford and Endow [2] in a study of the photolysis of NO_2 determined the rates of these reactions relative to the rate of the reaction of O atoms with O_2. Direct measurements of the rate of the NO reaction have been reported by Kaufman[3], and by Harteck, Reeves, and Manella[4], using the "air-afterglow" method, by Ogryzlo and Schiff[5], using the isothermal catalytic probe method, and by Kistiakowsky and Volpi[6], using a mass spectrometric method. The only direct measurement of the NO_2 reaction is a mass spectrometric study by Phillips and Schiff[7]. The partial pressure of atomic oxygen was not measured directly in either of the mass spectrometric studies.

A common feature of the above methods used to study atomic oxygen reactions is their lack of generality. A particular method is limited in the reactions to which it can be applied. There is evidently a need for a more general method for the measurement of oxygen atom partial pressures, suitable for obtaining self consistent chemical kinetics for the whole range of atomic oxygen reactions. We wish to describe here a mass spectrometric method which fulfills this requirement. It can be used to study very fast as well as moderately fast reactions, over a wide range of temperatures, under varying conditions of flow and pressure. This method will be applied in the first case to a study of the reactions of O atoms with NO and NO_2, and some isotopic exchange reations.

Experimental

1. Apparatus

The reactions were studied in a fast flow system in which reactants and products were continuously analyzed with a mass spectrometer.

The instrument used in this work was 6" radius of curvature, 60° sector field mass spectrometer. It was designed so that gas flowing through an orifice connecting the reaction zone with the mass spectrometer, passed directly through the "open" type ion source into a large pumping line. Ion currents were measured with a combination of electron multiplier, vibrating reed electrometer, and pen recorder.

The reactors used in this work were modified versions of the Eltenton reactor[8]. A typical reactor and its relation to the ion source is shown in figure 1. Atomic reactant and carrier gas flow in and along the central tube, while other reactants could be added through two additional inlets. The reacting gas stream impinged on a 10 μ orfice made by puncturing with a spark a thin glass diaphram mounted on the base of the reactor.

The reaction zone could be heated with a coiled Nichrome wire heater, or cooled with a stream of chilled air. Temperature was measured with a pair of platinum - platinum 10% rhodium thermocouples suspended in the central reactant inlet tube. Temperature uniformity was ± 2° at ambient and above, and ± 4° at lower temperatures.

The geometry of the reactor was modified according to the rate of the particular reaction under study. Thus for the NO reaction, which is relatively slow, the reactor had a diameter of 1.35 cm., and a length of 19.4 cm., whereas for the NO_2 reaction, the reactor was 0.78 cm in

Table I

"Room Temperature" Rate Constants for the Reactions
$O + NO + M \longrightarrow NO_2 + M$, and $NO_2 + O \longrightarrow NO + O_2$

REACTION	METHOD	k	M	REF.
NO+O+M	PHOTOLYSIS	3.0×10^{16} cc.^{2}moles.$^{-2}$sec.$^{-1}$	N_2	2*
	AIR-AFTERGLOW	2.5±0.3	O_2	3
	AIR-AFTERGLOW	2.76±0.18	Ar,O_2	4
	CATALYTIC PROBE	1.85±0.1	O_2	5
	MASS SPEC.	4.6	N_2	6
	MASS SPEC.	3.73±0.19	N_2	THIS WORK
NO_2+O	PHOTOLYSIS	3.4×10^{12} cc.moles.$^{-1}$sec.$^{-1}$	-	2*
	MASS SPEC.	1.5±0.4	-	7
	MASS SPEC.	3.28±0.33	-	THIS WORK

* Following Benson (Reference 10) we have increased the original values by a factor of 1.6.

Table II

Rate Constants for the Elementary Steps in the Reactions of O Atoms with NO, NO_2, and O_2.

	NO	NO_2	O_2
k_A cc mole^{-1} sec^{-1}	2.0×10^{12}	9.5×10^{12}	0.9×10^{12}
k_B sec^{-1}	3.2×10^{9}	5.3×10^{4} b/	3.5×10^{9}
k_C cc mole^{-1} sec^{-1}	$6. \times 10^{13}$ a/	1.6×10^{9} b/	9.2×10^{11} c/
k_D sec^{-1}	8.0×10^{-20}	3.3×10^{4} b/	3.5×10^{9}

a. reference 12.
b. recalculated from results of present paper and reference 14.
c. references 10 and 11.

diameter and 4 to 7 cm long.

Reaction time is taken as the ratio of the volume of the reactor from the point of reactant inlet to sampling orifice, and the volume flow rate. Flow was measured by collecting the pump effluents in a gasometer. The flow rates obtained in this manner were checked against a National Instruments Labs. "Vol-O-Flo" flowmeter, having a stated accuracy of 0.25% full scale. The two values differed by less than 1%.

Pressure was measured through the second reactant inlet tube (with no reactant flowing), by means of a calibrated diaphram type absolute pressure gauge (Decker Model 311) with a range of 0-3 torr, and an accuracy of better than 0.4%. (i.e. the limit of our method of calibration)

2.Materials

Nitric oxide and nitrogen dioxide were commercially available materials, purified by repeated trap to trap vacuum distillation. Oxygen was prepared by condensation and trap to trap vacuum distillation of ordinary tank oxygen. Pre-purified grade nitrogen and ordinary tank argon were used without further treatment.

3. Procedure

Two methods of producing atomic oxygen were used. In the first, nitrogen was passed through a 2450 Mc/s electrodeless discharge, resulting in about 1% decomposition into nitrogen atoms. To this stream of gas sufficient NO was added through jet No.I.(figure 1.) to remove all the N atoms and to produce an equivalent number of O atoms via the very fast reaction $NO+N \rightarrow N_2+O$.[6] In the second method a mixture of 1 to 3 percent oxygen in argon was passed through the discharge resulting in the direct formation of atomic oxygen.

Mass spectrometric analysis for stable reactants and products were directly obtained from the appropriate ion currents measured at 50 e.v. ionizing energy, and a knowledge of the individual sensitivities (i.e. units of ion current/units of partial pressure) measured in separate experiments.

In the case of oxygen atoms the procedure was more complex as it was necessary to distinguish between O^+ ions arising from the ionization of oxygen atoms and O^+ ions produced by the dissociative ionization of O_2,NO, NO_2, etc. To do this it was necessary to work at reduced ionizing energy (20 e.v. nominal) where such secondary processes were minimized and the necessary corrections small and readily made. The resultant O^+ ion current was a measure of the relative O atom partial pressure. It could be put on an absolute basis using the NO_2 titration (see further).

The experiments were carried out as follows:

NO. For this reaction it was necessary to know only the relative O atom partial pressure as a function of the NO partial pressure. Oxygen atoms were produced by the reaction of N atoms with NO, at jet No.1, and then reacted with additional NO added at jet No. 2. The reaction was studied between 2 and 3 torr total pressure, at linear flow rates of about 200-400 cm/sec, over a temperature range of 307 to 505 °K. It should be noted that under ambient conditions, the temperature of the reactor was always higher than room temperature.

NO_2. In this reaction it was necessary to know the absolute partial pressures of both NO_2 and O. With no NO_2 flowing, the discharge was turned on and the O^+ ion current measured. Sufficient NO_2 was then added to consume all the O atoms. If the stoichiometry of the reaction is $O+NO_2 \longrightarrow NO+O_2$, then the difference in partial pressure of NO_2 with discharge on and off is a direct measure of the oxygen atom partial pressure.

To follow the rate of the reaction the amount of NO_2 was reduced until oxygen atoms were again detectable.

As the final partial pressures of the reactants were only a small fraction (5 to 10%) of the initial partial pressures, it was necessary to set the later partial pressures about equal so that both reactants were present in measurable amounts at the point of sampling. This

reaction was studied at pressures of 1-3 torr at linear flow rates of about 1000 cm/sec, over the temperature range 278 to 374 °K.

Exchange Reactions. The exchange reactions were carried out in a reactor similar to that used for the $O+NO_2$ reaction. The ^{18}O atoms were produced by the decomposition of about 1% oxygen -18 (97.0 atom percent ^{18}O) in argon. Molecular reactants, O_2, NO, and NO_2, all of natural isotopic abundance were added through the inlet jet to the reactant stream the oxygen atom concentration was measured as above by means of the NO_2 "titration".

Results

NO The mechanism of the reaction of NO with O is well established[1] to be:

$$O+NO+M \longrightarrow NO_2 + M \qquad (1)$$

followed by the very fast reaction

$$O+NO_2 \longrightarrow NO + O_2. \qquad (2)$$

In general we can neglect other reactions leading to the comsumption of oxygen atoms as the recombination reaction $O+O+M \longrightarrow O_2+M$ is about 100 times slower than reaction (1) and other reactions first order in oxygen atoms will not affect our final results.[1]

The rate of decay of oxygen atoms can be written as

$$-\frac{dO}{dt} = 2\,k_1\,(NO)\,(O)\,(M)$$

which on integration becomes

$$\log\,(O) = \frac{2\,k_1 t\,(NO)\,(M_o)\,(1+NO/N_2)}{2.303} + C$$

making the substitution $M=M_o(1+NO/N_2)$.

M_o is the total pressure measured with no reactant flowing. To compensate for the change in M as reactant is added, we have assumed that for $NO/N_2 \ll 1$, N_2 and NO are equivalent third bodies in this reaction and therefore the effective M is:

$$M=M_o+NO=M_o\,(1+NO/N_2).$$

A typical set of data is shown in figure 2 where log (O) is plotted as a function of $NO\,(1+NO/N_2)$. From the slope of figure 2, $2\,k_1 t\,(M_o)/2.303$, we calculate k.

The reaction was not studied at temperatures higher than 505 °K, as we observed that at this temperature the recombination coefficient of oxygen atoms had increased about tenfold over its value at room temperature.

A plot of log k vs $1/T$ is shown in figure 3. A least-squares fit of the data give $k_1=(1.44\pm0.20)\times10^{15}\exp(1930\pm100/RT)$ cc^2. $moles^{-2}$ $sec.^{-1}$ At 298°K, $k_1= 3.73\pm0.13\times10^{16}$ cc^2 $moles^{-2}$ sec^{-1}. The uncertainties given here are a measure of the reproducibility rather than the accuracy of the results. On the basis of uncertainties in measuring mass spectrometric sensitivities, and in exactly defining the reactor volume (as it pertains to gas mixing and flow properties) we estimate our values of k_1 to be accurate to ±5%.

NO_2. Reaction (2) is a simple bimolecular reaction the rate of which can be calculated from the usual integrated rate expression

$$k_2= \frac{2.303}{t[(O)_o-(NO_2)_o]}\log\left\{\frac{(NO_2)_o\,(O)_t}{(NO_2)_t\,(O)_o}\right\}$$

A plot of log k_2 vs $1/T$ is shown in figure 3. A least-squares fit of the data give $k_2=(1.95\pm0.61)\times10^{13}\exp.(-1060\pm200/RT)$ cc. moles $^{-1}$ sec^{-1}. At 298°k, $k_2=3.28\pm0.33\times10^{12}$ cc, $moles^{-1}$ sec^{-1}. The accuracy of the results is probably comparable with the reproducibility.

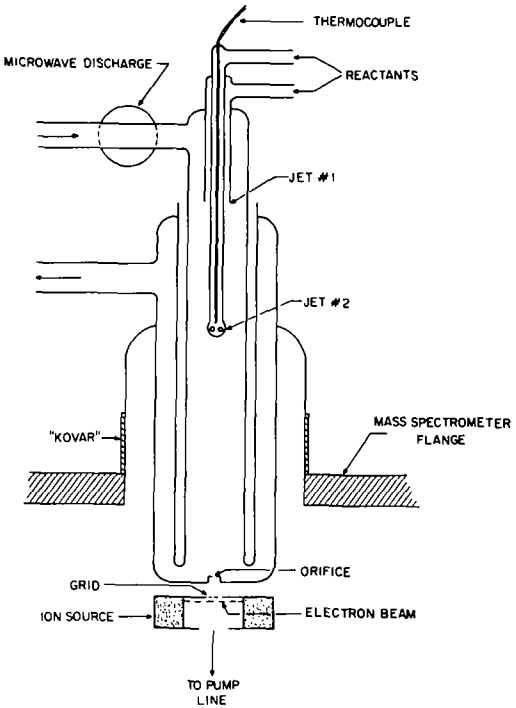

Fig. 1. The reactor and its position relative to the ion source of the mass spectrometer.

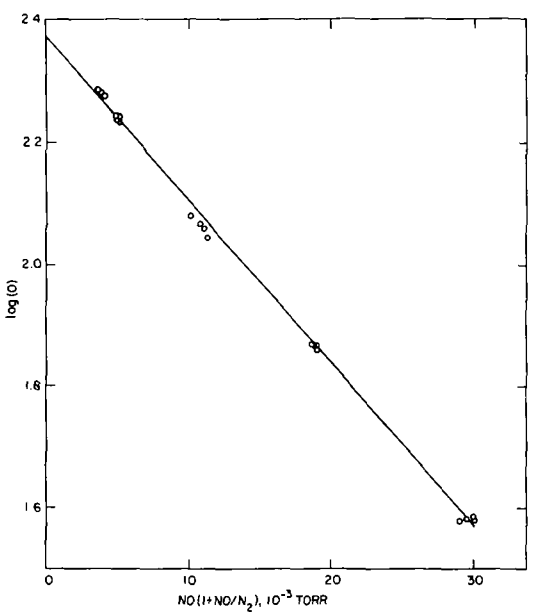

Fig. 2. Plot of log (O) vs. $NO(1 + NO/N_2)$ for the reaction $O + NO + M \longrightarrow NO_2 + M$.

Exchange Reactions. The path from the experimental data to the rate constants is complex and will not be given in detail. However, the following had to be considered:

A. In the exchange with molecular oxygen, the calculation has to include the simultaneous exchange of $^{16}O^{16}O$, $^{16}O^{18}O$ (formed during the reaction) and $^{18}O^{18}O$ (present due to incomplete dissociation in the discharge) with ^{18}O and ^{16}O atoms. The best results were obtained by observing the rate of change in $^{16}O^{16}O$ concentration, since atom-atom recombination affects this species least.

B. In the NO exchange the contribution from $^{18}O^{18}O$ exchange has to be included in the calculation of the equilibrium isotope concentration of $N^{16}O$, which again proves the most accurate in determining the rate of change of isotope composition.

C. The NO_2 isotope exchange turns out to be comparable in rate to the reaction $NO_2+O \longrightarrow NO+O_2$, so that allowance has to be made for the decrease in total NO_2 concentration during the exchange and for the loss in exchanged $N^{16}O^{18}O$ due to the above reaction.

Discussion

In table I we compare the "room" temperature values of the rate constants obtained in this work with values reported by other workers. It is apparent from the table that the NO-O reaction is one of the most thoroughly studied of all atomic oxygen reactions. In spite of the variety of methods used, the range of the rate constants is less than a factor of three. Our value lies somewhat higher than the average of all values (3.1×10^{16} cc.^{2} mole^{-2} sec^{-1}).

The value given by Kistiakowsky and Volpi is based on measurements of the O_2 produced in the overall reaction rather than on a direct measurement of the oxygen atom partial pressure and is therefore probably less accurate.

The catalytic probe method used by Ogryzlo and Schiff is open to criticism on account of its lack of specificity, although these workers have attempted to take this into account. A more significant point of comparison than the actual room temperature rate constants, is the reported activation energy. Thus, over the interval 203 to 293°K, they find that the rate (for $M=CO_2$) changes only by about 10%, corresponding to a negative activation energy of 0.24 kcal/mole. On the basis of our measured activation energy, E= -1.9 kcal/mole, we would predict a fourfold change in k_1.

Our measured activation energy receives support from a value E=-1.5 kcal/mole estimated by Kaufman[1], from a comparison of k_1 at 1000°K ($M=CO_2$), with k_1 at room temperature ($M=O_2$), accounting for the different efficiencies of the third body.

The difference between values obtained using the air afterglow technique and the present method (about 30%) would seem to indicate sources of experimental error in either or both methods not yet determinable.

In the case of the NO_2 reaction our value of the rate constant agrees well with that of Ford and Endow, but is about a factor of two larger than that of Phillips and Schiff. The latter work suffers from the necessity of calculating the partial pressure of oxygen atoms from the stoichiometry of the reaction rather than measuring it directly. The activation energy of the $O+NO_2$ reaction is reported here for the first time.

A detailed mechanism for the reaction of oxygen atoms with NO or NO_2 can be given in its simplest form by the general scheme:

$$O+XO \underset{B}{\overset{A}{\rightleftharpoons}} [O\ X\ O]^* + M \xrightarrow{C} XO_2 + M$$
$$[O\ X\ O]^* + M \xrightarrow{D} X + O_2$$
$$[O\ X\ O]^* + M \xrightarrow{E} XO_2 + h$$

where an excited intermediate $[O\ X\ O]^*$ is formed in step A by binary collision of reactants O and XO. This intermediate can dissociate back

into original reactants by step B or in the case of isotopical unbalance, give isotopically exchanged reactants. Step C, collision between $[O\ X\ )]^*$ and molecule M causes the intermediate to deexcite by energy transfer giving product XO_2. Step D dissociation of $[O\ X\ O]^*$, gives X and, generally, an excited O_2. In the case of the NO reaction the radiative deexcitation step E, to produce XO_2, is also observed. The same scheme is also applicable to the reaction of oxygen atoms with molecular oxygen. Some of these reaction steps and the nature of the excited intermediate have been discussed by several authors[5,6,9-14] making various assumptions as to collision efficiencies, lifetime and energy states of the intermediates.

The overall rate constants for these reactions and the isotopic exchange rates[15], permit a re-evaluation of the rate constants of the above elementary reaction steps. The rate constant k_A is equal to the exchange rate corrected for the isotopic substitution ratio. The ratio k_B/k_C was calculated from the overall rate of the reaction $O+XO+M \rightarrow XO_2+M$ and the isotopic exchange rates[16]. Using the values of k_C given in Table II, the corresponding k_B values were calculated. In the same way the ratio k_D/k_B was derived from the rate constant of the overall reaction $O+XO \rightarrow X+O_2$, and the exchange rates[17]. The rate k_D was then calculated. Table II summarizes the values of the rate constants of these elementary reactions.

As most of these reactions presumably have small activiation energies a qualitative comparison of the room temperature rate constants will be instructive with regard to the nature of bonds formed and broken. For reaction A, the formation of the excited intermediate, the rate constants lie within one order of magnitude in all three cases. Evidently a similar process of bond formation is operative. Small differences in activation energy may explain the differences in rates observed. Comparing the rates of bimolecular deexcitation k_C, the realtive efficiencies of collision are obviously a function of the stability of the intermediate or the number of "contributing modes of vibration."

The rates of unimolecular decomposition of either "two-bond" rupture k_D or "one-bond" rupture k_B are about the same in the case of NO_3^*, indicating that a similar type of activation precedes both decompositions, and giving some clue concerning the configuration of the intermediate (see below). The ratio of the decomposition rates of NO_2^*, $k_B/k_D=10^{28}$, clearly shows the difficulty of a two bond rupture compared to the splitting off of one oxygen atom. There is of course no difference in rates in the case of the O_3^* intermediate.

With regard to the relative stability of these intermediates, measured in terms of the life time $\tau_B = 1/k_B$, the values for NO_2^* and O_3^* are of the same order of magnitude, 10^{-10} sec, whereas the lifetime of NO_3^* is 10^{-5} sec. For NO_3^*, the time appears to be long enough to permit internal rearrangments of the loosely bonded oxygens so that isotopic exchange may be observed without the intermediate necessarily having a symmetric configuration.

It should be remarked at this point that Benson's[10] arguments regarding the exchange experiment of Clyne and Thrush[9], although qualitative in nature are certainly correct in principle. While the reaction was allowed to proceed to competion, sufficient isotopically labelled NO_2 was formed by exhange so that within the accuracy of the experiment "equilibrated" products would be obtained in any case.

A more rigorous test for intermediate configuration is the isotopic exchange observed[15] between ^{18}O atoms and NO_2, which at first sight would indicate a symmetric configuration . It is however quite possible, considering the relatively long life-time of the NO_3^* intermediate, that an assymmetric configuration, such as

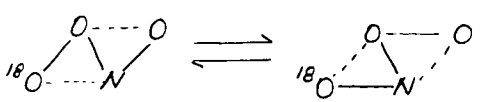

undergoes isotopic mixing by the rearrangement indicated and still requires only an N-O bond rupture to decompose by either reaction B or D to show about equal reaction rates.

Acknowledgement

We wish to thank Mr. W.R. Shields for supervising the design and construction of the mass spectrometer used in this work.

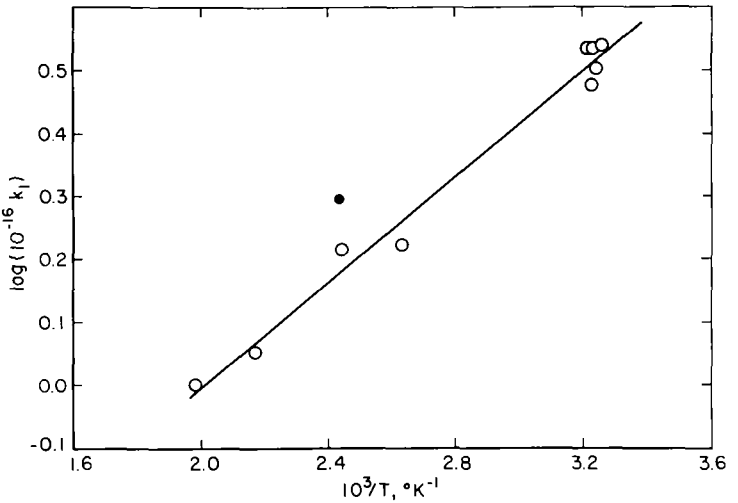

Fig. 3. Plot of log k_1 vs. T^{-1}. The shaded point was not used in determinging the slope or intercept.

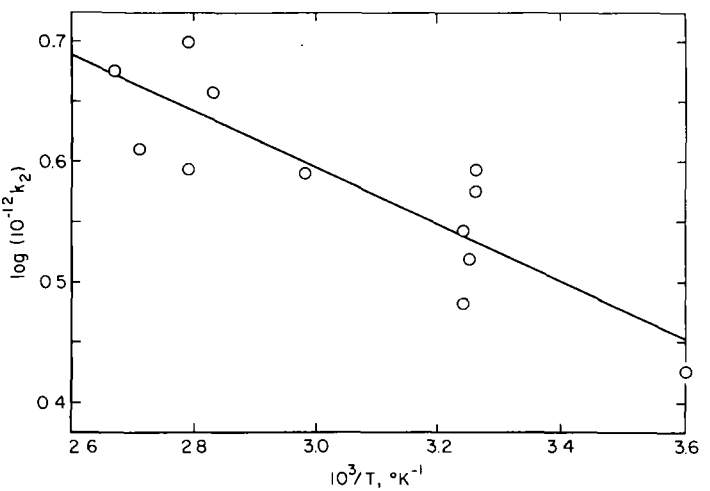

Fig. 4. Plot of k_2 vs. T^{-1}.

REFERENCES

* On Sabbatical leave from the Isotope Department, Weizmann Institute of Science, Rehovoth, Israel.

1. For a review, see F. Kaufman in "Progress in Reaction Kinetics," Volume I (Pergamon Press, New York, 1961).

2. H.W. Ford and N. Endow, J. Chem Phys. 37, 1156 (1957).

3. F. Kaufman, J. Chem. Phys. 28, 352 (1958): Proc. Roy Soc.(London) A247, 123 (1958).

4. P. Harteck, R.R. Reeves, and G. Manella, J. Chem. Phys. 29, 1333 (1958).

5. E.A. Ogryzlo and H.I. Schiff, Can. J. Chem. 37, 1690 (1959)

6. A. B. Kistiakowsky and G.G. Volpi, J. Chem. Phys. 27, 1141 (1957)

7. L.F. Phillips and H.I. Schiff, J. Chem. Phys. 36, 1509 (1962)

8. G.C. Eltention, J. Chem. Phys. 15, 455 (1947); J.T. Herron, J. Res. N.B.S. 65A, 411 (1961).

9. M.A.A. Clyne and B.A. Thrush, Trans. Faraday, Soc. 58, 511 (1962); J. Chem. Phys. 38, 1252 (1963).

10. S. W. Benson, J. Chem. Phys. 38, 1251(1963).

11. S.W. Benson and A.E. Axworthy, Jr., J. Chem. Phys. 26, 1718 (1957).

12. H.P.Broida, H.I. Schiff and T. M. Sugden, Trans. Faraday Soc. 57, 259 (1961).

13. H.W. Ford, Can. J. Chem. 38, 1780 (1960).

14. H.W. Ford and S. Jaffe, J. Chem. Phys. 38, 2935 (1963).

15. J.T. Herron and F.S. Klein, J. Chem. Phys. 40, (1964)

16. The overall rate for $O + NO + M$ was taken from this paper; for $O + NO_2 + M$ from ref. 2; and for $O + O_2 + M$ from ref. 11 The latter's value was increased by a factor of 1.6.

17. The overall rate for $O + NO_2$ was taken from this paper; for $O + NO \longrightarrow N_2 + O$ from F. Kaufman and L.J. Decker, 7th Combustion Symposium, (Butterworths, London, 1959), p. 57.

KINETICS OF O_3 FORMATION IN A STREAM OF ELECTRICALLY DISCHARGED O_2

By A. Mathias and H.I. Schiff

Upper Atmosphere Chemistry Group, McGill University, Montreal, Canada

Perhaps the most important chemical reactions which occur in the stratosphere are those which determine its ozone content. Aside from photolytic processes, these are primarily

$$O + O_2 + M \rightarrow O_3 + M \qquad (1)$$

$$O + O_3 \rightarrow 2\ O_2. \qquad (2)$$

The rate constants for these reactions are therefore of great importance in chemical aeronomy. Unfortunately they are not known with any unanimity.

Laboratory studies of these reactions are frequently performed with flow systems containing small percentages of atoms produced from electrically discharged O_2. The homogeneous recombination rates in such systems are usually equated to $2k_1[O][O_2][M]$. However, such studies have produced a large spread in the reported values of k_1.[1] These values are also appreciably lower than those which are deduced from studies of the thermal and photolytic decomposition of O_3.[2,3]

A value for k_2 has recently been obtained[4] from measurements of the rate of disappearance of O_3 added to a stream of discharged O_2. Although it agreed reasonably well with the results of one study on the thermal decomposition of O_3,[5] it was considerably higher than the results of other such investigations.[6] An even higher value[7] was obtained from the reaction of O_3 with O atoms produced by the titration reaction of 'active' nitrogen with NO. However, the titration reaction also produces[8,9] excited N_2 molecules which are capable of decomposing O_3.

The present paper reports an attempt to resolve these differences by an independent method. A mass spectrometric study was made of the O_3 concentration in a stream of discharged O_2. If only reactions (1) and (2) were operative, a steady state concentration would be established:

$$[O_3]_{ss} = (k_1/k_2)[O_2]^2,$$

from which the ratio of rate constants could be readily evaluated. This relationship was, however, not found to be valid, which showed the occurrence of other processes.

EXPERIMENTAL

The mass spectrometer used was identical to the one described earlier[4] except that rhenium filaments were used throughout and the sampling hole was 15 μ wide and 20 μ deep. Linde U.S.P. grade O_2, containing less than 0.1% N_2, was used directly since samples purified by liquefaction gave identical results. The oxygen was passed through a 100 cm length of quartz tubing 10 mm int. diam., over the mass spectrometer sampling 'leak' and thence to the pump. The mass flow rate was controlled by a fine needle valve and measured with a calibrated capillary flow meter. The pressure in the system was varied at constant mass flow rate by throttling a valve located between the mass spectrometer leak and the pump. The pressure was measured just beyond the mass spectrometer leak either with a Consolidated micromanometer or with a McLeod gauge. Although there was a considerable pressure drop down this long length of relatively narrow tubing, the results of these experiments indicated that the O_3 concentration adjusted to the local pressure in the system so that the pressure at the leak was the significant parameter.

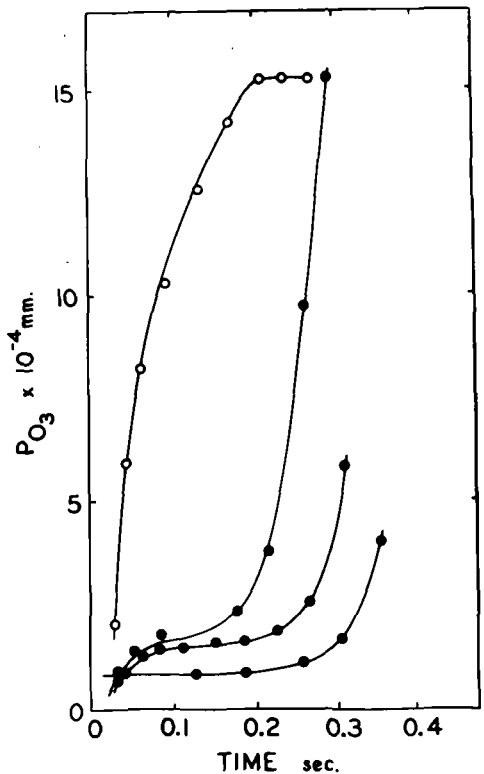

Fig. 1 : O_3 concentration as a function of time:

O - values obtained without traps cooled to 77°K.
● - values obtained with traps cooled to 77°K.

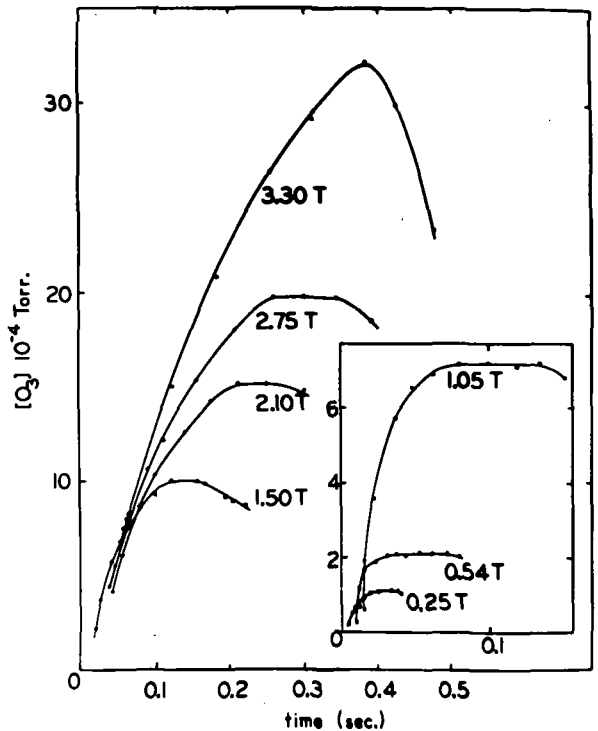

Fig. 2 : O_3 concentrations as a function of time at different pressures. The gas has been passed through traps cooled to 77°K.

The oxygen was dissociated to the extent of a few % in a cylindrical microwave cavity powered by a Microtherm unit. This cavity could be slid along the quartz tubing to alter the distance (and hence the time) between the discharge and the mass spectrometer leak.

The mass spectrometer was calibrated for O_3 by introducing part of the effluent gas from a laboratory ozonizer into the flow system and measuring the mass 32 and 48 peak heights. Simultaneously, a known volume of the same gas was diverted through an aqueous 2% KI solution, and its O_3 content determined by conventional thiosulphate titration.

RESULTS

Experiments with this arrangement gave results for the dependence of O_3 concentration on time which are typified by the plots of the open circles shown in Fig. 1. Curves of this sort were irreproducible but all had the general characteristic of a rise to a relatively flat portion followed by a further rapid increase at longer reaction times. However, when traps cooled by liquid air were inserted directly before the quartz tube, reproducible curves similar to the one through the closed circles were obtained.

A family of such curves at different pressures is shown in Fig. 2. It will be seen that the O_3 concentrations reach maximum rather than steady-state values and that the maxima become sharper as the pressure increases.

The dependence of the maximum O_3 concentration on pressure is shown in Fig. 3. The lines are drawn through two sets of experiments performed with different flow tubes and microwave generators. The linear pressure dependence is also at variance with the quadratic relationship for the steady-state concentration based on reactions (1) and (2). These results strongly suggest the presence of other reactive species.

To test for the existence of such species, the apparatus was modified in the following manner. A section of 10 mm int. diam. Pyrex tubing, containing an inlet through which other reactants could be added to the gas stream, was inserted between the mass spectrometer leak and the quartz tube. This inlet, similar to those described previously[4,10], was located 25 cm from the mass spectrometer leak. Excess NO_2 was added through this inlet to determine the O-atom concentration in the discharged O_2 stream. Alternately, a relatively large flow of pure O_3 was introduced through the inlet to determine the maximum amount which could be destroyed by the discharged O_2. The amount of O_3 which was decomposed was always found to be greater than the O-atom concentration, thus providing direct evidence for the presence of some other species capable of decomposing O_3, most likely excited molecules, O_2^*:

$$O_2^* + O_3 \rightarrow O_2 + O_2 + O. \qquad (3)$$

The concentration of excited molecules can be derived from the relation $[O_2^*] = \frac{1}{2}\{\Delta[O_3] - \Delta[NO_2]\}$ where $\Delta[NO_2]$ and $\Delta[O_3]$ are the amounts of NO_2 and O_3 respectively which can be destroyed by the discharged oxygen stream. The inclusion of $\frac{1}{2}$ in the expression results from reaction (3) being followed by (1) which consumes an additional O_3 molecule.

A number of experiments were performed to determine the concentration of O atoms and O_2^* molecules at reaction times which produced the maxima in the $[O_3]$-time curves. The distance between the discharge and mass spectrometer leak which gave the maximum O_3 concentration was first determined and the value of $[O_3]_{max}$ noted. The discharge was then moved back 25 cm so that the $[O_3]_{max}$ position now occurred at the inlet. The values of [O] and $[O_2^*]$ were then determined as described in the previous paragraph. The results of these experiments are shown in Table I.

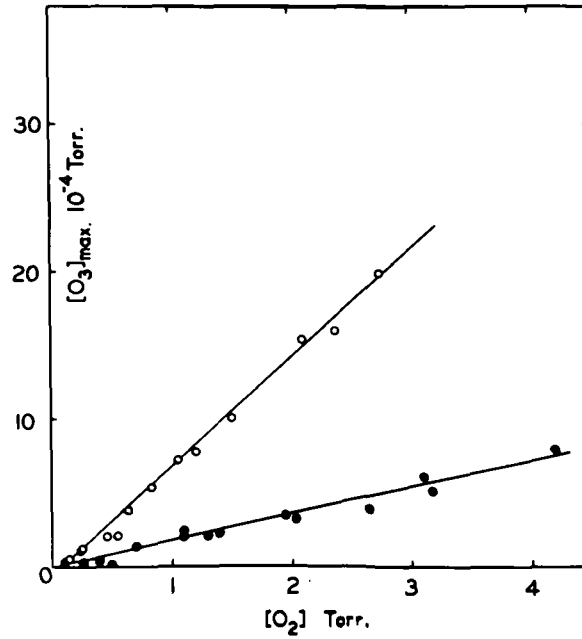

Fig. 3 : The dependence of the maximum O_3 concentration on pressure. The two curves were obtained with different flow tubes.

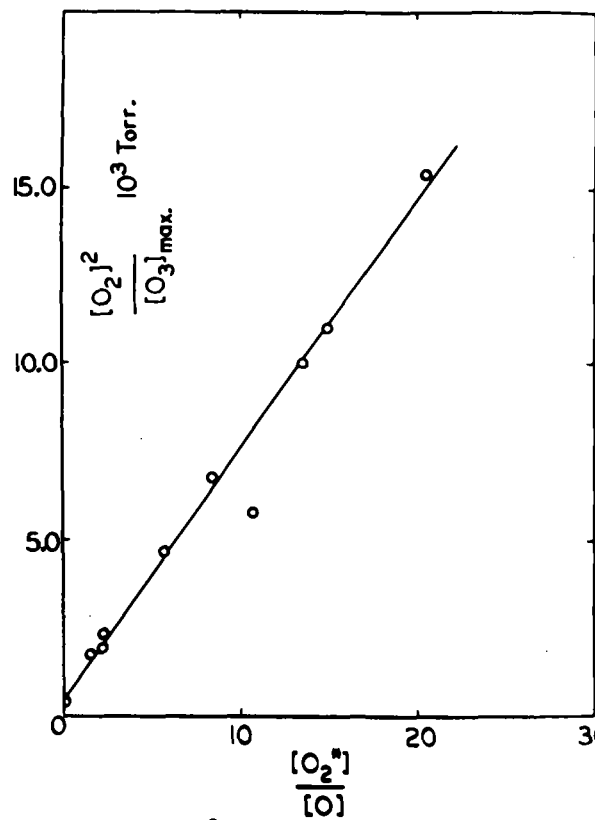

Fig. 4 : A plot of $[O_2]^2/[O_3]$ against $[O_2^*]/[O]$ obtained at reaction times corresponding to maximum O_3 concentrations.

Table I

CONCENTRATIONS OF REACTANTS CORRESPONDING TO $[O_3]_{max}$

$[O_2]$ torr	$[O_3]_{max}$ 10^{-4} torr	$[O]$ 10^{-4} torr	$[O_2^*]$ 10^{-3} torr
0.25	1.58	19.4	0.06
0.62	1.67	9.33	2.11
0.73	2.76	19.4	4.40
1.04	6.10	35.7	5.40
1.20	2.12	5.52	4.65
1.45	3.64	12.4	13.4
1.85	7.31	20.8	12.0
1.95	3.81	14.5	19.9
2.30	4.81	12.4	18.6
3.20	6.62	7.89	16.2

DISCUSSION

The behaviour shown by the lower curves in Fig. 1 can be understood if it is assumed that water vapour is the impurity removed by the traps. It is well known that water vapour is largely dissociated in an electrical discharge. The reaction of H atoms with O_3,

$$H + O_3 \rightarrow OH + O_2, \qquad (4)$$

has a rate constant[11] which is at least 10^3 times larger than the rate constant of reaction (1). Thus, if one H atom is formed per H_2O molecule, then in a discharged gas stream containing a few % of O atoms, (4) will dominate over (1) whenever the H_2O content of the original gas exceeds one part in 10^5. Moreover, the OH radicals formed either in the discharge or as a result of (4) will undergo the rapid reaction,[12]

$$O + OH \rightarrow O_2 + H. \qquad (5)$$

Reactions (4) and (5) therefore constitute an H-atom catalyzed equivalent to reaction (2). The overall kinetics will be indistinguishable from (1) and (2) alone, so that the rate of O-atom recombination should remain unaltered.* On the other hand, the O_3 concentration will be lowered to a pseudo steady-state value given approximately by $k_1[O][O_2]^2/k_4[H]$, which can be associated with the flat portions of the curves in Fig. 1. The O_3 concentration will increase again only after the H atoms are removed by relatively slow three-body processes. Other evidence for the catalytic effect of H atoms in O-atom recombination has recently been reported.[7]

If (1), (2) and (3) are the predominant reactions in dried, discharged oxygen, a steady-state O_3 concentration will not be produced. Instead, a maximum will be reached given by

---

*A similar argument might be invoked for nitrogeneous impurities which could yield NO in the discharge. The catalytic O_3 decomposition could then occur by the counterpart reactions $NO + O_3 \rightarrow NO_2 + O_2$ (4') and $NO_2 + O \rightarrow NO + O_2$ (5'). However, the rate constant for (4') is not significantly larger than for (2), so that this reaction cannot be significant.

$$[O_3]_{max} = \frac{k_1[O][O_2]^2}{k_2[O] + k_3[O_2^*]} .$$

This expression can be rearranged to the form

$$\frac{[O_2]^2}{[O_3]_{max}} = \frac{k_2}{k_1} + \frac{k_3}{k_1}\frac{[O_2^*]}{[O]} .$$

Thus, if this mechanism is operative, a plot of the left-hand side of this expression against $[O_2^*]/[O]$ should yield a straight line. Such a plot is shown in Fig. 4 for the data of Table I. Least-mean-square treatment of the data yields the equation

$$[O_2]^2/[O_3]_{max} = 4.02 \times 10^2 + 6.98 \times 10^2[O_2^*]/[O] \text{ (torr)}$$

Fig. 3 shows that $[O_3]_{max}$ is proportional to $[O_2]$ and independent of $[O]$ or $[O_2^*]$. Inspection of the expression for $[O_3]_{max}$ shows that this result will be consistent with the proposed mechanism only if $[O_2^*]/[O]$ is a linear function of $[O_2]$; i.e.

$$\frac{k_2}{k_1} + \frac{k_3}{k_1}\frac{[O_2^*]}{[O]} = \alpha[O_2],$$

where α is some constant. Fig. 5 shows that within admittedly large experimental error such a relationship seems to apply for a set of data obtained under similar conditions. However, α probably depends on the purity of the gas and other discharge parameters, and there is no reason why it should remain unaltered if discharge conditions are changed. This is probably why the data of Fig. 3, obtained with two different experimental arrangements, lie on curves with different slopes. The increase of $[O_2^*]/[O]$ with $[O_2]$ also explains why the maxima in Fig. 2 get narrower with increasing pressure, since the rate of reaction (3) will then increase relative to the rate of reaction (2).

The value of $k_2/k_1 = 1.2 \times 10^{19}$ molecules cm^{-3} is in good agreement with the results of a careful re-investigation[3] of the phololysis of O_3, and in satisfactory agreement with the revised data from thermal O_3 decomposition studies. Kaufman and Kelso[13] have recently reported a value of 7.5×10^{-34} cm^6 $molecule^{-2}$ sec^{-1} for k_1 from studies in flow systems uncomplicated by the presence of excited O_2. Combination of this value with the result of the present study yields a value of $k_2 = 9.0 \times 10^{-15}$ cm^3 $molecule^{-1}$ sec^{-1} which is appreciably lower than the value of 2.5×10^{-14} reported by Phillips and Schiff.[4] However, their results may have been too high, since no particular precautions were taken to dry their oxygen. Also no corrections were made for possible reaction with O_2^*. This may not have been too serious in their case because the same authors found[14] that the maximum O_3 decomposition never exceeded the O-atom concentration by more than 10%. This is probably because most of their experiments were at lower pressures where the present results show that the $[O_2^*]/[O]$ ratios are small, and probably because the ratio may also depend on gas purity.

From Fig. 4 it may be concluded that $k_3 = 1.7\ k_2$. Reaction (3) may, however, be composite, since some measurements of the rates of O_2^* disappearance indicated the presence of more than one excited species. Arnold and Ogryzlo[15] have also reported that the concentration of $O_2(^1\Delta_g)$ decreases slowly and $O_2(^1\Sigma_g^+)$ more rapidly when O_3 is added to a stream of discharged O_2. A similar decrease in $O_2(^1\Sigma_g^+)$ molecules was reported by Clyne et al.,[7] although they estimate their concentration to be less than 1%. In the present work O_2^* concentrations amounting to

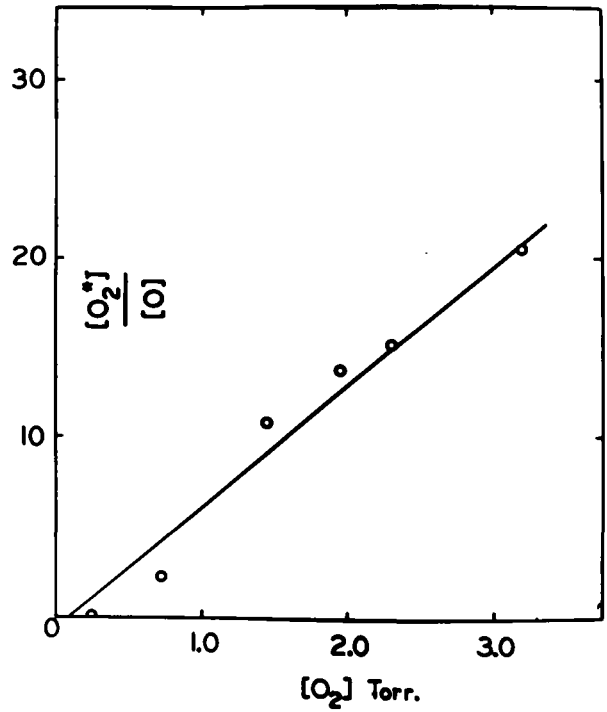

Fig. 5 : The dependence on pressure of the $[O_2^*]/[O]$ ratio obtained at reaction times corresponding to maximum O_3 concentrations.

several % were observed. Mass spectrometric studies[16,17] of discharged O_2 have indicated up to 20% of excited molecules which were tentatively identified as $O_2(^1\Delta_g)$. The excitation energy of this state is some 2 kcal less than the dissociation energy of O_3. This is not, however, inconsistent with the deduction that k_3 is of the same order of magnitude as k_2 which is known to have an activation energy between 4 and 6 kcal $mole^{-1}$. Positive identification of the different species and their relative importance must await further study. However, the inclusion of reaction (3) does provide an explanation for the spread in the reported values of k_1 and permits reconcilation of the work on discharged O_2 and on O_3 decomposition.

REFERENCES

1. F. Kaufman and J.R. Kelso, 'Chemical Reactions in the Lower and Upper Atmosphere' (Interscience, New York, 1961), p. 255.
2. E.S. Campbell and C. Nudelman, AFOSR TN-60-502 (1960).
3. E. Castellano and H.J. Schumacher, Z. physik. Chem., 34, 198 (1962).
4. L.F. Phillips and H.I. Schiff, J. Chem. Phys., 36, 1509 (1962).
5. J.A. Zaslowsky, H.B. Urbach, F. Leighton, R.J. Wnuk, and J.A.Wojtowicz, J. Am. Chem. Soc., 82, 2682 (1960).
6. S.W. Benson and A.E. Axworthy, 'Ozone Chemistry and Technology', (American Chemical Society, Washington,1959)series 21, p.388.
7. M.A.A. Clyne, B.A. Thrush, and R.P. Wayne, Nature, 199, 1057 (1963).
8. L.F. Phillips and H.I. Schiff, J.Chem.Phys., 36, 3283 (1962).

9. J.E. Morgan, L.F. Phillips, and H.I. Schiff, Disc. Faraday Soc., 33, 118 (1962).
10. J.E. Morgan and H.I. Schiff, Can. J. Chem., 41, 903 (1963).
11. L.F. Phillips and H.I. Schiff, J. Chem. Phys., 37, 1233 (1962).
12. F.P. Del Greco and F. Kaufman, Disc. Faraday Soc., 33, 128 (1962).
13. F. Kaufman and R.J. Kelso, Disc. Faraday Soc., in press.
14. L.F. Phillips and H.I. Schiff, J. Chem. Phys., 37, 924 (1962).
15. J. Arnold and E.A. Ogryzlo, Abstr. 46th Conf. Chem. Inst. Canada; Chem. in Can., 15, 54 (1963).
16. S.N. Foner and R.L. Hudson, J. Chem. Phys., 25, 602 (1956).
17. J.T. Herron and H.I. Schiff, Can. J. Chem., 36, 1159 (1958).

ION-MOLECULE REACTIONS IN COMBUSTION PLASMAS AND ATOMIC DIFFUSION FLAMES*

W. J. Miller, H. F. Calcote and A. Fontijn

AeroChem Research Laboratories, Inc.
P. O. Box 12, Princeton, New Jersey 08540

ABSTRACT

Premixed hydrocarbon-oxygen flames and low-temperature atomic diffusion flames (resulting from the reaction of oxygen atoms with hydrocarbon) have been examined mass spectrometrically for both positive and negative ion content. The results indicate that two separate primary chemi-ionization reactions are operative in both systems, namely:

$$(1) \qquad CH \text{ (or } CH^*) + \rightarrow CHO^+ + e$$

and

$$(2) \qquad CH^* + C_2H_2 \rightarrow C_3H_3^+ + e$$

Individual positive ion profiles are interpreted in terms of secondary ion formation mechanisms. Among the reactions found plausible are:

$$(3) \qquad CH_2O + CHO^+ \rightarrow CH_2OH^+ + CO$$

$$(4) \qquad CH_3OH + CHO^+ \rightarrow CH_3OH_2^+ + CO$$

$$(5) \qquad C_2H_2O + CHO^+ \rightarrow C_2H_3O^+ + CO$$

$$(6) \qquad CH_3CHO + CHO^+ \rightarrow CH_3CHOH^+ + CO$$

Negative ions have been found in premixed combustion flames in concentrations on the order of 10^{-9} mole fraction; the ions observed include O^-, OH^-, C_2^- and O_2^-. These ions are thought to arise from dissociative attachment processes involving carbon-containing species. The first negative ion formed in these reactions is almost surely C_2^-, which is thought to arise from

$$(7) \qquad e^- + C_2H_2O \rightarrow C_2^- + H_2O$$

Negative ions have also been found in the cool atomic diffusion flames and at maximum concentrations are approximately equal to the positive ion concentrations. Several ions have been identified in this system, and work is continuing toward the elucidation of attachment mechanisms under these conditions.

INTRODUCTION

Chemi-ionization in hydrocarbon-oxygen reactions has been under investigation at AeroChem for several years. Two separate but complimentary study programs have evolved; one uses flat-flame, low-pressure burners of a type commonly encountered in combustion research, and the other employs electrical discharge flow systems in which atomic oxygen reacts with hydrocarbon gas. In general, these studies have been conducted at pressures below about 20 Torr. Several experimental techniques have been employed. In addition to mass spectrometry, these include Langmuir probes, thermocouple probes and optical spectroscopy. Results of these latter studies will not be discussed here, except when necessary for interpretation of mass spectrometer data.

Reacting systems have been probed for both positive and negative ion content, and the results are interpreted in terms of both primary and secondary ion formation mechanisms. At the outset, it is perhaps worth emphasizing that the mass spectrometer employed in these studies contains no ion sources; we are looking, here, at ions produced as the direct result of chemical processes.

* This work was sponsored by the Office of Naval Research under Contract Nonr-3809(00), and the Air Force Cambridge Research Laboratories under Contract AF 19(628)3302, ARPA Order 42.

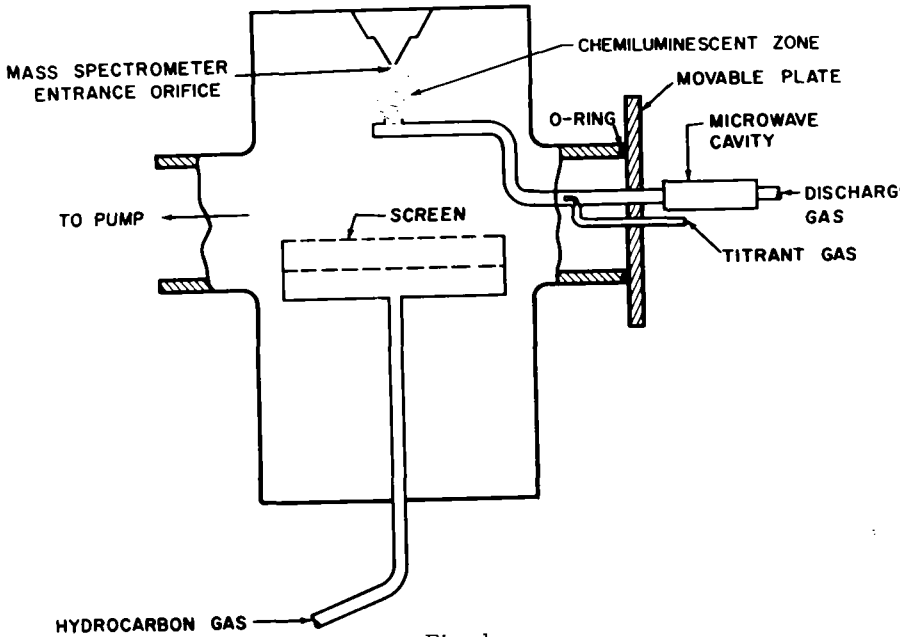
MASS SPECTROMETER ENTRANCE ORIFICE
CHEMILUMINESCENT ZONE
MOVABLE PLATE
O-RING
MICROWAVE CAVITY
DISCHARGE GAS
TO PUMP
SCREEN
TITRANT GAS
HYDROCARBON GAS

Fig. 1

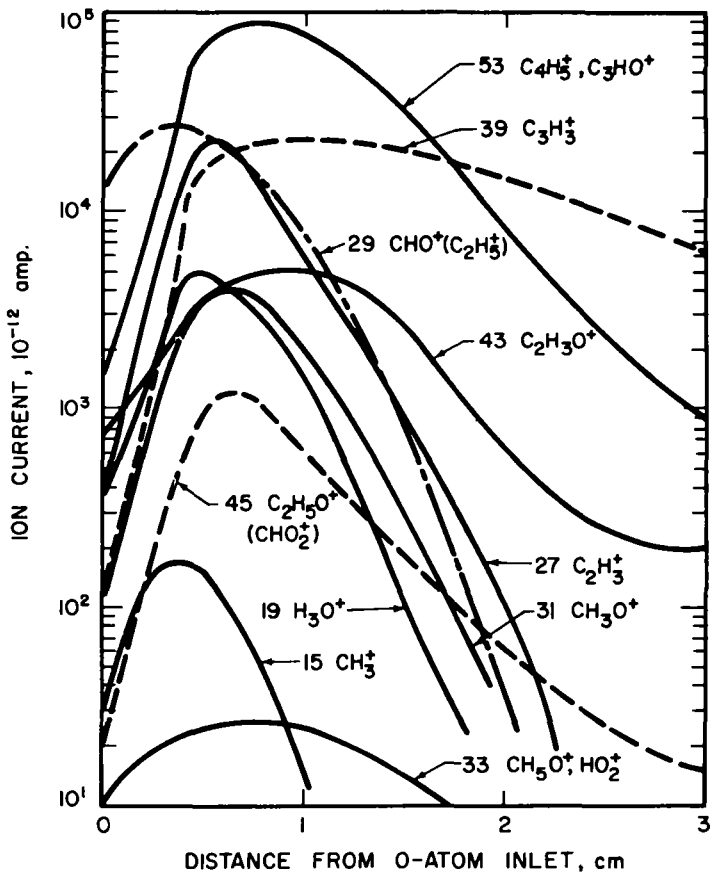
53 $C_4H_5^+$, C_3HO^+
39 $C_3H_3^+$
29 $CHO^+(C_2H_5^+)$
43 $C_2H_3O^+$
45 $C_2H_5O^+$ (CHO_2^+)
27 $C_2H_3^+$
31 CH_3O^+
19 H_3O^+
15 CH_3^+
33 CH_5O^+, HO_2^+
ION CURRENT, 10^{-12} amp.
10^5
10^4
10^3
10^2
10^1
0
1
2
3
DISTANCE FROM O-ATOM INLET, cm

Fig. 2

EXPERIMENTAL

The mass spectrometer and flat-flame burner have been described in great detail in Refs. 1 and 2. The apparatus was used as described there with several notable revisions. Electronic modifications have been made to facilitate the isolation and identification of negative ions; sensitivity of the mass spectrometer has been increased by roughly an order of magnitude. In addition, several changes have been made in the burner assembly, the most notable being enlargement of the housing from 6 in. to 12 in. diameter, enlargement of the burner to 6 in. diameter, and an increase in the pumping efficiency on the mass spectrometer housing. Valves have been added which permit independent control of the pressure in the mass spectrometer housing. Upon reduction of pressure within the ion detector, noise level decreases and sensitivity increases; the pressure is now about 5×10^{-6} Torr. The useful range of the instrument has been extended from 4 to more than 6 orders of magnitude.

The atomic diffusion flame[17 18] was created by allowing oxygen atoms to flow through a 10 mm ID tube into the same 300 mm ID Pyrex reaction chamber as used in combustion experiments into which the hydrocarbon flowed, as shown in Fig. 1. The resulting "flame" was thus O-atom-rich in earlier stages of the reaction near the O-atom inlet and hydrocarbon-rich in the later stages of the reaction. The oxygen atom outlet to mass spectrometer entrance orifice distance could be varied as in the combustion work to obtain ion profiles. Flow rates were measured with calibrated sonic orifice meters. The O-atoms were produced either by a microwave discharge through a 96% He - 4% O_2 mixture or by a microwave discharge through N_2, followed by NO titration of the resulting N-atoms to the equivalence point.[19] The reaction pressure was changed at constant flow rates by throttling the pump connection.

RESULTS AND DISCUSSION

Positive Ions

The reaction of O-atoms with C_2H_2 produces an ellipsoidal luminous reaction zone just above the O-atom inlet. This "flame" consists of an intense blue inner zone surrounded by a diffuse mantle of green (presumably due to CH and C_2 emission, respectively). At a pressure of 1 Torr and a total flow rate of 30 cc sec^{-1}, the blue zone is approximately 3 cm long and 1 cm in diameter. Mass spectrometric probing of the reaction zone reveals predominately masses 27, 29, 39 and 53, with smaller amounts of others. Ion profiles, i. e., ion current as a function of distance from the O-atom inlet, are given in Fig. 2. It should be noted that, of all the ions, mass 29--presumably CHO^+--maximizes closest to the O-atom inlet and that, in this region, it is the dominant ion. The remaining ions all maximize further downstream at approximately the position of maximum visual CH emission. Only masses 39, 43 and 53 persist to any considerable extent downstream of the visible reaction zone.

As the result of experiments in which C_2D_2 was substituted for C_2H_2 as the fuel component in the reaction, the following unambiguous mass assignments have been made: mass 43 is $C_2H_3O^+$, mass 15 is CH_3^+, mass 27 is $C_2H_3^+$, mass 31 is CH_3O^+, mass 39 is $C_3H_3^+$, mass 43 is $C_2H_3O^+$ and mass 53 is a mixture of $C_4H_5^+$ and C_3HO^+. Unfortunately, mass 29 cannot be positively identified in this manner; either $C_2H_5^+$ or CHO^+ satisfy the observations. On the basis of combustion work (e. g., Refs. 3 and 4), however, and from consideration of the argument that nonoxygenated ions are unlikely to appear as dominant ions as close to the oxygen atom inlet as does mass 29, it seems reasonably safe to conclude that this mass is predominantly CHO^+. Heavier masses have been observed in all these diffusion flames but little attempt has been made to identify them. They all have profiles which maximize well downstream and result from ion-molecule polymerization reactions or charge exchange reactions involving already-polymerized molecules. In this respect, these cool atomic diffusion flames are distinctly different from hot combustion flames at these pressures where such polymerization has not been observed. At one atmosphere Sugden and coworkers (e. g., Ref. 6) have observed large concentrations of heavy ions in combustion flames.

The oxygen atom-ethylene reaction gave rise to a much weaker luminous zone. Two distinct differences between the ions produced in this reaction and in the C_2H_2-O reaction are observed--the replacement of masses 39 and 53 in C_2H_2-O reactions by masses 41

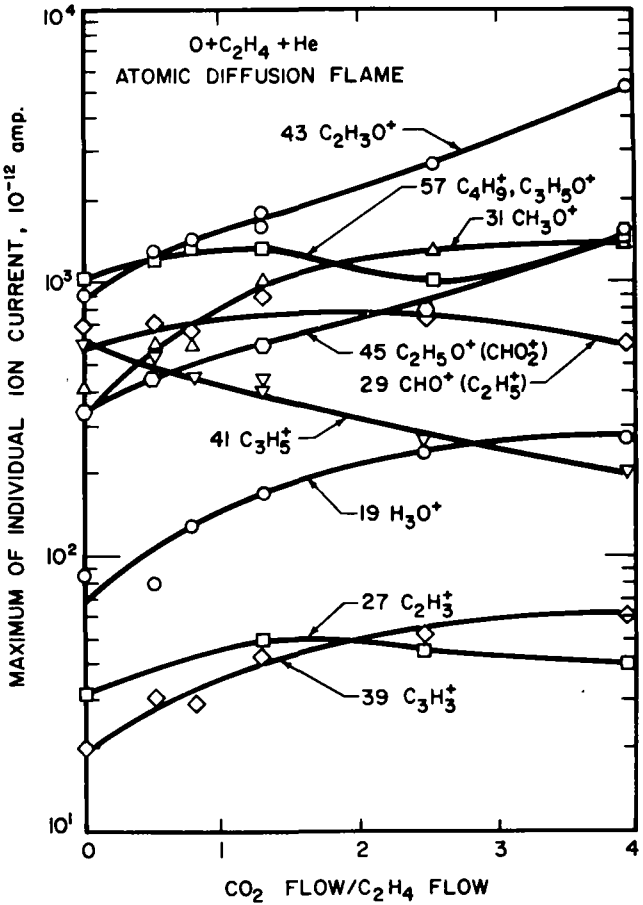
O+C2H4 +He
ATOMIC DIFFUSION FLAME
43 C2H3O+
57 C4H9+, C3H5O+
31 CH3O+
45 C2H5O+ (CHO2+)
29 CHO+ (C2H5+)
41 C3H5+
19 H3O+
27 C2H3+
39 C3H3+
MAXIMUM OF INDIVIDUAL ION CURRENT, 10-12 amp.
CO2 FLOW/C2H4 FLOW

Fig. 3

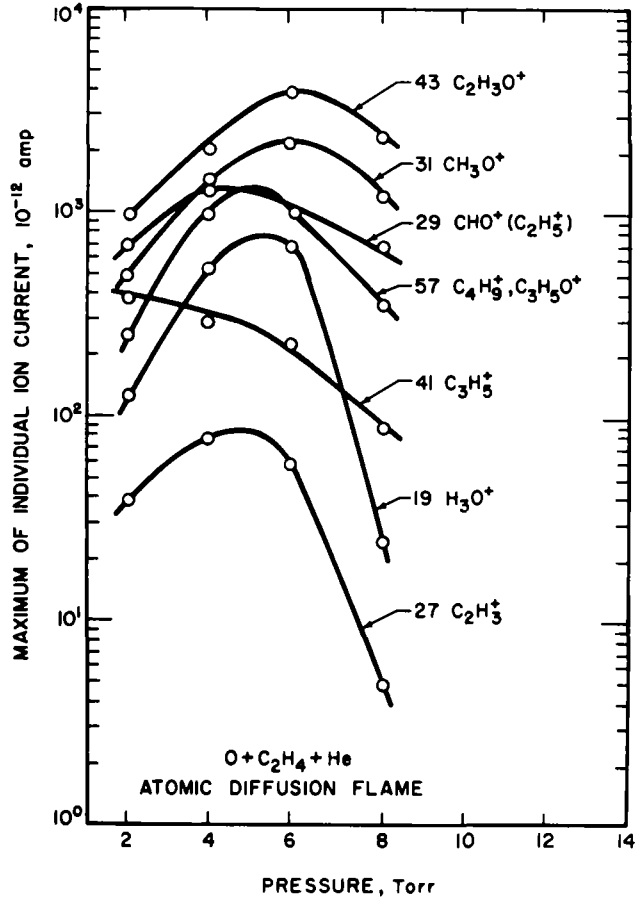
43 C2H3O+
31 CH3O+
29 CHO+ (C2H5+)
57 C4H9+, C3H5O+
41 C3H5+
19 H3O+
27 C2H3+
O+C2H4+He
ATOMIC DIFFUSION FLAME
MAXIMUM OF INDIVIDUAL ION CURRENT, 10-12 amp
PRESSURE, Torr

Fig. 4

and 57, respectively, as dominant ions. Although no deuterated ethylene experiments have been performed, mass 41 is surely $C_3H_5^+$, and mass 57 is probably $C_3H_5O^+$.

The addition of CO_2 to the C_2H_4-O reaction has a marked effect upon the individual ion concentration maxima (Fig. 3). It can be seen that $C_3H_5^+$ demonstrates a monotonic decrease, while all the other ions remain essentially unchanged or actually increase. Almost the same effect may be achieved by increasing the pressure, although under these conditions the other ion maxima optimize around 4-5 Torr (Fig. 4). It should be noted that this is exactly the pressure range in which the temperature, total positive ion concentration and, presumably, reaction rates are at a maximum (Fig. 5). These results indicate that all the ions in the ethylene system arise from a common source with the notable exception of $C_3H_5^+$. This ion is the C_2H_4 analog of the $C_3H_3^+$ ion observed in the C_2H_2 reaction and in hydrocarbon combustion.[3,4] It is quite likely, then, that both of these ions arise through direct reaction of C_2H_4 and C_2H_2, respectively and that, in all probability, the mechanism for $C_3H_5^+$ formation in the C_2H_4 system is different from that for all other ions.

Examination of the ion profiles from a hot C_2H_2-O_2 combustion flame reveals that mass 39, $C_3H_3^+$, is the dominant ion in the flame front. The same is true for all hydrocarbon fuels studied. There has been substantial agreement[2-4] for a number of years that

$$(1) \qquad CH + O \rightarrow CHO^+ + e^-$$

is an important chemi-ionization, i.e., primary ion formation reaction. If this were the only important reaction, then one must account somehow for the high concentration of $C_3H_3^+$ by ion-molecule reactions. Several such reactions have been proposed but they all have been objected to on different bases, e.g., Ref. 20. The evidence from the present study indicates that, instead of being an ion-molecule reaction product, $C_3H_3^+$-- like CHO^+-- is mainly present as a primary ion. The probable mechanism is thought to be

$$(2) \qquad CH^* + C_2H_2 \rightarrow C_3H_3^+ + e^-$$

That the CH in this reaction is in an excited state is indicated by the preferential $C_3H_5^+$ reduction in the C_2H_4-O reactions upon CO_2 addition, presumeably through quenching of CH^*.[18] This effect has also been observed in CO_2 addition experiments in the combustion flame. Figure 6 exhibits the results of these experiments for the ions CHO^+ and $C_3H_3^+$, using N_2 and CO_2 as additives. The effect on $C_3H_3^+$ of 45 cc/sec added CO_2 (fuel-oxygen mixture flow rate = 70 cc/sec) is 10 times as great as its effect on CHO^+; CO_2 is on the order of 20 times more effective than N_2 in suppressing $C_3H_3^+$ concentration. Since both CH^* and C_2H_2 are present in high concentrations in rich flames, it is to be expected that, if Reaction (2) takes place, ionization and especially $C_3H_3^+$ concentration will peak in rich flames. Figure 7 shows the effect of variations in equivalence ratio (ϕ)* on various ion concentrations in C_2H_2 combustion flames. It is important to note that $C_3H_3^+$ does maximize on the fuel-rich side of stoichiometry and that it is the only ion which does so. However, the total ion current in Fig. 7 peaks at stoichiometry or slightly lean. Apparently, then, Reaction (2), although responsible for an important fraction of the ions present, is not the only ionization reaction. The atomic diffusion flame studies likewise[18] indicate that both Reactions (1) and (2) are responsible for primary ion formation. The possibility that further chemi-ionization reactions occur in these systems cannot be excluded.

Although it has been generally assumed that ions other than CHO^+ and $C_3H_3^+$ observed in hydrocarbon combustion flames are due to charge exchange processes, very little experimentation has been performed in attempts to verify or substantiate this. The ion species observed in both systems are mainly the same (cf. Table I). Relative concentrations, of course, vary from one system to the other. The secondary ions present in both systems in large concentrations are CH_3O^+, CH_5O^+, C_2H_3O and $C_2H_5O^+$. These ions will now be discussed in terms of the following reactions:

---

*Equivalence ratio, ϕ, is defined as the ratio of fuel to oxygen ratio in the experiment to fuel to oxygen ratio at stoichiometric.

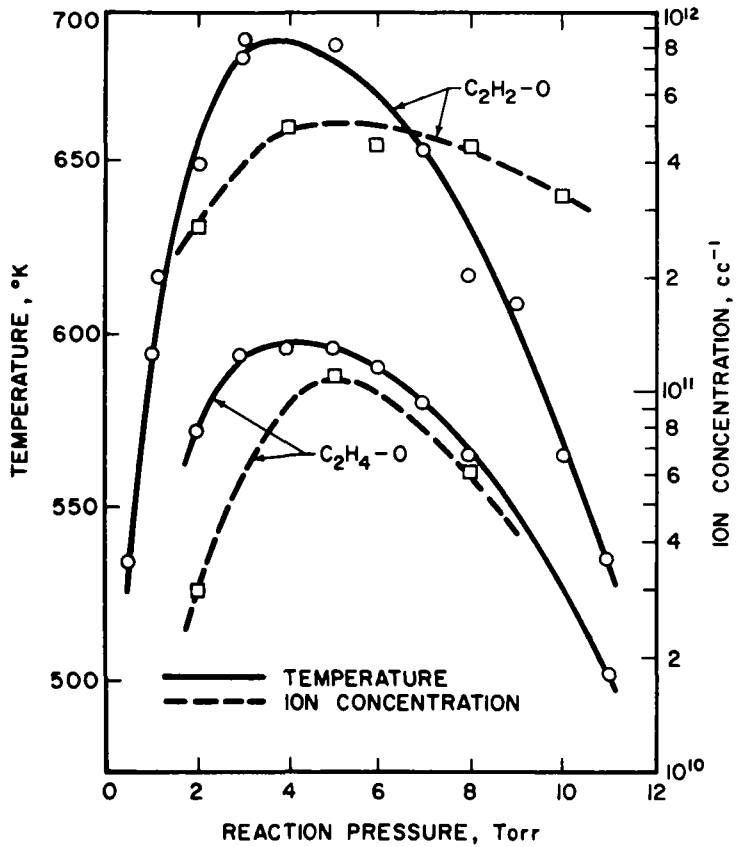
TEMPERATURE, °K
ION CONCENTRATION, cc⁻¹
REACTION PRESSURE, Torr
C2H2-O
C2H4-O
TEMPERATURE
ION CONCENTRATION

Fig. 5

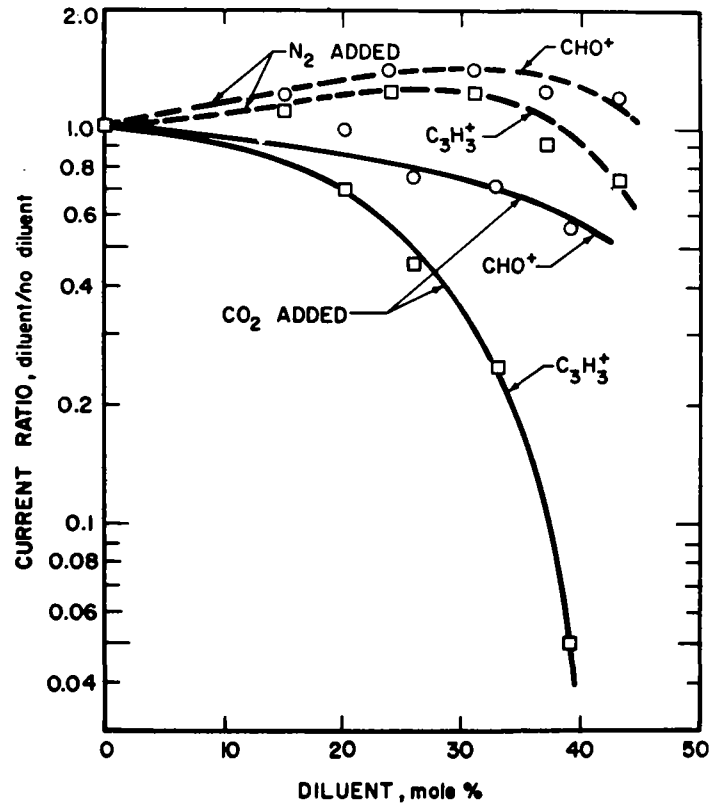
CURRENT RATIO, diluent/no diluent
DILUENT, mole %
N2 ADDED
CO2 ADDED
CHO+
C3H3+

Fig. 6

		ΔH, ev
(3)	$CH_2O + CHO^+ \rightarrow CH_2OH^+ + CO$	-2.7
(4)	$CH_3OH + CHO^+ \rightarrow CH_3OH_2^+ + CO$	-2.7
(5)	$C_2H_2O + CHO^+ \rightarrow C_2H_3O^+ + CO$	-2.3
(6)	$CH_3CHO + CHO^+ \rightarrow CH_3CHOH^+ + CO$	-0.2

Heats of reaction have been calculated from thermochemical data presented in a review by Bernecker and Long.[7]

TABLE I

COMPARISON OF POSITIVE IONS FOUND IN PREMIXED COMBUSTION FLAMES AND ATOMIC DIFFUSION FLAMES

Mass	Ion	Flame: Atomic	Flame: Premixed
15	CH_3^+	x	x
19	H_3O^+	x	x
27	$C_2H_3^+$	x	
29	CHO^+	x	x
31	CH_3O^+	x	x
33	CH_5O^+ (HO_2^+)	x	x
37	$H_5O_2^+$		x
39	$C_2H_3O^+$	x	x
45	$C_2H_5O^+$ (CHO_2^+)	x	x
53	$C_4H_5^+$ (C_3HO^+)	x	x

In order to demonstrate the feasibility of the above processes, we have examined the effect of adding CH_2O, CH_3OH and CH_3CHO to the atomic diffusion flame. Upon addition of these reactants to the fuel stream, pronounced increases were observed in the respective ion currents at masses 31, 33 and 45. Although these results do not prove that charge exchange processes such as those written are responsible for the secondary ions observed in high-temperature combustion plasma, they do, at least, show that these reactions can occur in the presence of such possible combustion intermediates as CH_2O, CH_3OH and CH_3CHO.

Since all the hydrocarbon and oxygenated hydrocarbon ions peak at about the same point in the flame front, the reactions by which they are formed from the primary ion must be very fast. The charge exchange processes discussed above are thought to be fast, but, with $C_3H_3^+$ emerging as a primary ion, the possibility must be considered that other ions arise from it by a chain of oxidative degradation reactions.

Negative Ions

In recent papers on combustion flame ionization phenomena (see, e.g., the Ninth Combustion Symposium) persistently troublesome points have been concerned with the concentrations of negative ions in combustion plasma. Langmuir probe results in both low-pressure and 1-atm combustion flames indicated the presence of large negative ion concentrations. The principal objections to these results were based on the fact that negative ions failed to appear in mass spectrometer experiments except for mass 17 in very small concentrations[8] and in seeded flames.[9] Since that time, Knewstubb and Sugden[10] have reported finding a wide variety of negative ions but only well downstream of seeded flames at 1 atm. However, Van Tiggelen has recently reported finding large numbers of negative ions in hydrocarbon flames at 1 atm and this paper reports our negative ion observations in low-pressure flames.

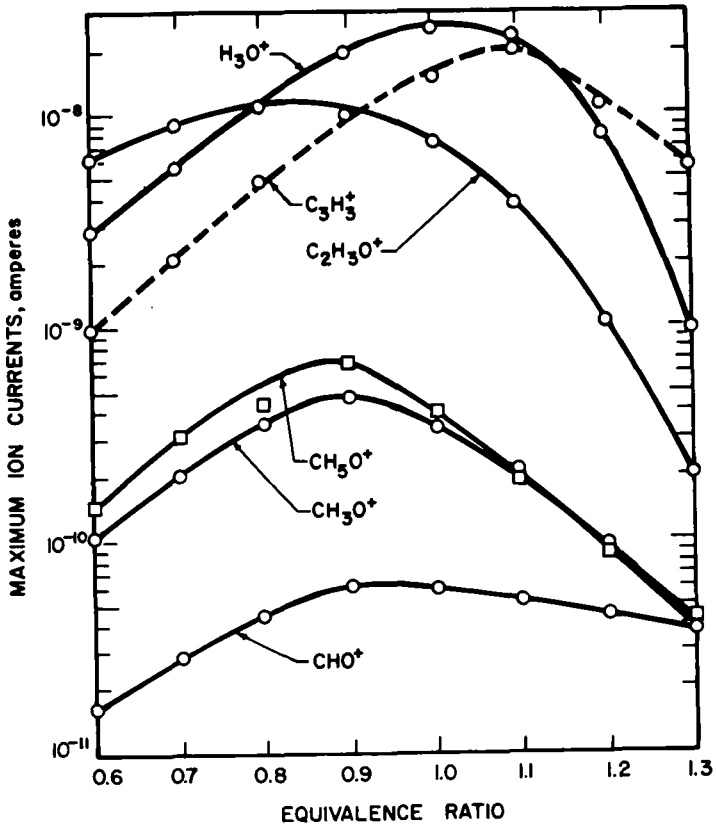
MAXIMUM ION CURRENTS, amperes
EQUIVALENCE RATIO
H_3O^+
$C_3H_3^+$
$C_2H_3O^+$
CH_5O^+
CH_3O^+
CHO^+
10^{-8}
10^{-9}
10^{-10}
10^{-11}
0.6
0.7
0.8
0.9
1.0
1.1
1.2
1.3

Fig. 7

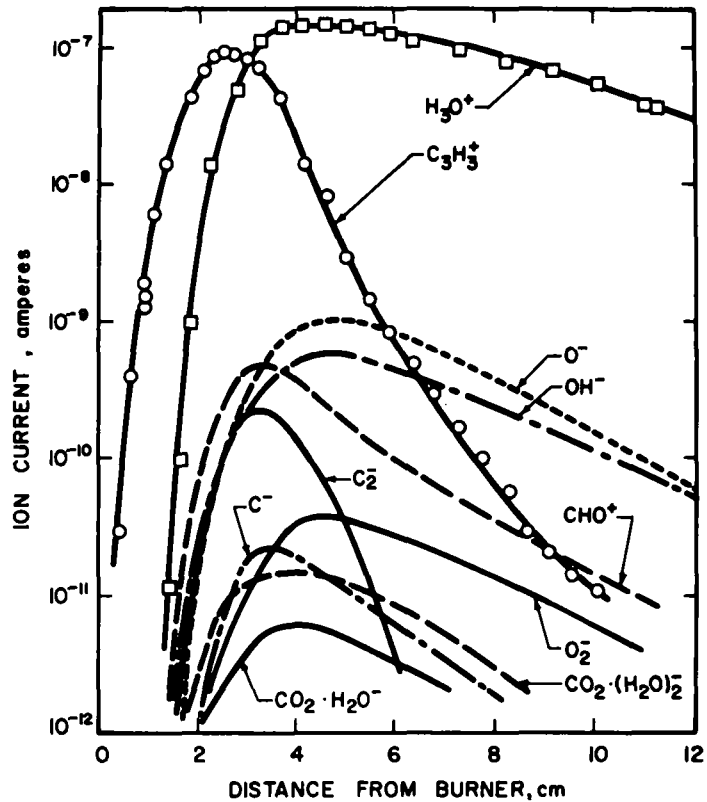
ION CURRENT, amperes
DISTANCE FROM BURNER, cm
H_3O^+
$C_3H_3^+$
O^-
OH^-
C_2^-
C^-
CHO^+
O_2^-
$CO_2 \cdot (H_2O)_2^-$
$CO_2 \cdot H_2O^-$
10^{-7}
10^{-8}
10^{-9}
10^{-10}
10^{-11}
10^{-12}
0
2
4
6
8
10
12

Fig. 8

Figure 8 shows the profiles of the most abundant negative ions in a C_2H_2-O_2 flame at 1 Torr. The positive ions H_3O^+, $C_3H_3^+$ and CHO^+ have been superimposed for reference; C^- and C_2^- are the ions which maximize closest to the flame front. All other ions appear to peak further downstream, behind the flame front. Under the experimental conditions $\phi = 1$, p = 1 Torr, O^- is the dominant ion, followed closely by OH^-; downstream, these are the only important ions. Ions at masses 62 through 64 and 80 through 82 (the limit of resolution as used in this experiment) have been tentatively identified as $CO_2\ H_2O^-$ and $CO_2\ (H_2O)_2^-$. They may also be SO_2^- and $SO_2\ H_2O^-$ formed from SO_2 impurity in the supply gases.

Increasing the pressure indicates that, at pressures above about 2.5 Torr, OH^- will be the dominant ion. It should also be pointed out that, with the exception of OH^-, these negative ions disappear very rapidly with increasing pressure - far more rapidly than do their positively charged counterparts. The negative ions observed here are undetectable at burner pressures above about 4 Torr.

The effect of flame equivalence ratio variations (see Fig. 9) is quite startling, since it might reasonably have been expected that the most electronegative compounds, and therefore the most abundant negative ions, would be compounds containing several oxygen atoms. Comparison of Fig. 7 with Fig. 9 lends to the conclusion that fuel-rich flames have the highest n_-/n_+ ratio. Electrons, surprisingly enough, will be most abundant in lean flames.

The appearance of the negative ion profiles for O^-, OH^- and C_2^- in the early stages of the reaction zone leads to consideration of initial ion-forming reactions involving these species. Since substantial amounts of positive ions and electrons appear ahead of the negative ions, it is reasonable to first consider the negative ion formation process as one of electron attachment; this reduces to finding attachment processes with a large enough cross-section to produce the observed ion concentrations. This can be done by equating the rates of ion formation to the rates of ion loss at the maximum negative ion concentration. Roughly, neglecting diffusional losses of the same order of magnitude as recombination we may write:

$$\beta(n_x)_{max} = \alpha(n_-)_{max}$$

where n_x is the concentration of electron-attaching species, α is the recombination coefficient and β the attachment coefficient. With $\alpha n_- \sim 2 \times 10^{-7} \times 2 \times 10^9$ sec^{-1} (n_- from the Langmuir probe was 2×10^{10} cc^{-1}; from the mass spectrometer, 2×10^8 cc^{-1}), for the direct attachment process to be considered plausible, βn_x must be $\sim 4 \times 10^2$ sec^{-1}. The maximum possible value for n_x is the total molecular concentration, which is $\sim 4 \times 10^{15}$ molecules cc^{-1} for the flame in Fig. 8; thus, a $\beta > 10^{-13}$ cc sec^{-1} is required to produce negative ions by attachment. This is a somewhat high value compared with the attachment coefficients reported for the species of interest, given as $\sim 10^{-15}$ cc sec^{-1} [11,12] or less, depending on the process involved. Direct attachment processes are therefore considered unimportant.

Some dissociative attachment processes have fairly large attachment cross-sections, σ_a; e.g., for SF_6, $\sigma_a = 5.7 \times 10^{-16}$ cm^2 at its maximum, occurring at an electron energy of 0.0 ev.[13] The maximum cross-section for H_2O is 4.8×10^{-18} cm^2, occurring at an electron energy of 6.4 ev. At energies above or below their optimum, σ_a is quite low since attachment cross-sections usually exhibit a sharp maximum with electron energy.

The attachment coefficient is given by $\beta = v_e\sigma_e$ and, since v_e is about 10^7 cm sec^{-1} in this flame, for an ideal dissociative attachment process, β could be as high as $\sim 6 \times 10^{-9}$ cc sec^{-1}. Assuming such a high value for β, then $n_x > (4 \times 10^2/6 \times 10^{-9}) \approx 10^{11}$; i.e., the species attaching must be present in concentrations > 0.002 mole percent. It should be realized that the latter calculation is based on the very large attachment coefficient for SF_6. As mentioned above, low-molecular-weight flame constituents (e.g., H_2O) have much smaller cross-sections (5×10^{-18} cm^2) even at optimum electron energies, and, at the energies prevalent in these flames, many cross-sections will be extremely small. With large molecules which can dissociate into highly electronegative fragments, however, one can reasonably expect to find high dissociative attachment cross-sections.

The rapid loss rate of C_2^- in Fig. 8 closely parallels that of $C_3H_3^+$; the relatively high concentration attained requires a rapid rate of formation for C_2^-. This requirement, together with its location in the flame front and the high concentrations attained in rich flames (Fig. 9), strongly suggests that this is a primary negative ion. This ion may very well be formed by the sequence of reactions:

$$(7) \qquad C_2H_2 + O \rightarrow C_2H_2O^*$$

$$(8) \qquad C_2H_2O^* \rightarrow CH_2 + CO$$

$$(9) \qquad C_2H_2O^* + e \rightarrow C_2^- + H_2O, \Delta H = 2.0 \text{ ev}$$

Assuming the above mechanism[14 15] for oxidation of acetylene, rather large concentrations of $C_2H_2O^*$ can be expected. The attachment reaction above is 2 ev exothermic if all the exothermocity of the first step is retained in $C_2H_2O^*$. This molecule could, in fact, lose considerable energy prior to electron attachment. A question exists as to whether the lifetime of $C_2H_2O^*$ before decomposition, Reaction (9), will be sufficient to allow electron attachment collisions. Two points favor a sufficient lifetime: (i) the time required for rearrangement prior to decomposition and (ii) the anticipated electronic structure should present a large cross-section to electron capture.

The picute that emerges is that the main source of negative ions is dissociative attachment of electrons to $C_2H_2O^*$ with, possibly, some contribution from electron attachment to O_2, O and/or OH. Ions other than C_2^- are then formed by ion-molecule reactions; e.g.,

		ΔH, ev
(10)	$C_2^- + H_2O \rightarrow C_2H + OH^-$	+0.6
(11)	$C_2^- + OH \rightarrow C_2H + O^-$	-0.8
(12)	$C_2^- + CO_2 \rightarrow C_2 + CO_2^-$	-0.7
(13)	$C_2^- + O_2 \rightarrow C + CO_2^-$	-5.5
(14)	$C_2^- + O \rightarrow CO + C^-$	-3.0

If O^- and OH^- were the first negative ions produced, there would be no difficulty in writing reasonable reactions for producing C_2^-, because of its large electron affinity. Thus:

		ΔH, ev
(15)	$O^- + C_2 \rightarrow O + C_2^-$	-1.6
(16)	$OH^- + C_2 \rightarrow OH + C_2^-$	-1.3
(17)	$O^- + C_2H \rightarrow OH + C_2^-$	-0.2

The molecular oxygen ion might be produced by:

$$(18) \qquad O^- + H_2O \rightarrow O_2^- + H_2 \qquad \Delta H = 0.94 \text{ ev}$$

It is thus possible to explain all of the ions observed by reasonable arguments. There is still some difficulty, however, in rationalizing the position in the flame at which negative ions appear; i.e., why do they not appear coincidentally with the formation of $C_3H_3^+$, at which point the electron concentrations should be high and the concentration of $C_2H_2O^*$ even greater? As a first intermediate in acetylene oxidation, C_2H_2O should appear early in the flame front and rapidly decay toward the end of the luminous zone where the ion concentrations peak.

It is possible, of course, that the negative ions are formed intrinsically in a chemiionization reaction not contributing significantly to total positive ion concentrations, e.g.,

$$(19) \qquad CH(^2\Sigma^+) + O_2 \rightarrow CHO^+ + O^- \qquad \Delta H = -2.1 \text{ ev}$$

Other excited states of CH would also be possible precursors and, as has been previously shown,[16] the concentrationoof reactants may be sufficient for such processes. This mechanism is also consistent with the position in the flame at which C_2^- and CHO^+ peak.

The atomic diffusion flame has just recently been examined for negative ions. Preliminary experiments indicate the presence of negative ions in approximately the same concentrations as positive ions. The position at which they maximize relative to the O-atom inlet, however, lies much further downstream outside the luminous zone. The environment in this region is nearly all unreacted C_2H_2 and He diluent. Some of the ions present have been identified. Their mass numbers and tentative empirical formulae appear in Table II.

TABLE II

COMPARISON OF NEGATIVE IONS FOUND IN PREMIXED COMBUSTION FLAMES AND ATOMIC DIFFUSION FLAMES

Mass	Ion	Flame: Atomic	Flame: Premixed
16	O^-		x
17	OH^-	x	x
24	C_2^-	x	x
25	C_2H^-	x	
32	O_2^-		x
36	C_3^-	x	x
42	$C_2H_2O^-$	x	
46	$CH_2O_2^-$	x	
53	$C_4H_5^-(C_3HO^-)$	x	
58	$C_2H_2O_2^-$	x	
62	$CO_2H_2O^-$	x	x

The work on negative ion content of the diffusion flame is continuing. More complete results and discussion will be available shortly.

REFERENCES

1. Calcote, H. F. and Reuter, J. L. : J. Chem. Phys. 38, 310 (1963).
2. Calcote, H. F. : Ninth Symposium (International) on Combustion, p. 622, Academic Press, 1963.
3. Green, J. A. and Sugden, T. M. : Ninth Symposium (International) on Combustion, p. 697, Academic Press, 1963.
4. Bulewicz, E. M. and Padley, P. J. : Ninth Symposium (International) on Combustion, p. 638, Academic Press, 1963.
5. Knewstubb, P. F. and Sugden, T. M. : Proc. Roy. Soc. (London) A255, 520 (1960).
6. Green, J. A. and Sugden, T. M. : Ninth Symposium (International) on Combustion, p. 607, Academic Press, 1963.
7. Bernecker, R. R. and Long, F. A. : J. Phys. Chem. 65, 1565 (1961).
8. Van Tiggelen, A. : Ninth Symposium (International) on Combustion, Discussion, p. 634, Academic Press, 1963.
9. Knewstubb, P. F. : ibid, Discussion, p. 635.
10. Knewstubb, P. F. and Sugden, T. M. : Nature 196, 1312 (1962).
11. Loeb, L. B. : Handbuch der Physik, p. 445, Springer-Verlag, 1956.
12. Branscomb, L. M. : Atomic and Molecular Processes (D. R. Bates, Ed.) p. 100, Academic Press, 1962.

13. Buchel'nikova. J.: J. Exper. and Theor. Phys. (USSR) 35, 1119 (1958).

14. Haller, I. and Pimentel, G. C.: J. Am. Chem. Soc. 84, 2855 (1962).

15. Fenimore, C. P. and Jones, G. W.: J. Chem. Phys. 39, 1514 (1963).

16. Calcote, H. F.: Combustion and Flame 1, 385 (1957).

17. Fontijn, A. and Baughman, G. L.: J. Chem. Phys. 38, 1784 (1963).

18. Fontijn, A., Miller, W. J. and Hogan, J. M.: Tenth Symposium (International) on Combustion, The Combustion Institute, Pittsburgh, Pa. To be published 1965.

19. Morgan, J. E., Elias, L. and Schiff, H. I.: J. Chem Phys. 33, 930 (1960).

20. Calcote, H. F., Kurzius, S. C. and Miller, W. J.: Tenth Symposium (International) on Combustion, The Combustion Institute, Pittsburgh, Pa. To be published 1965.

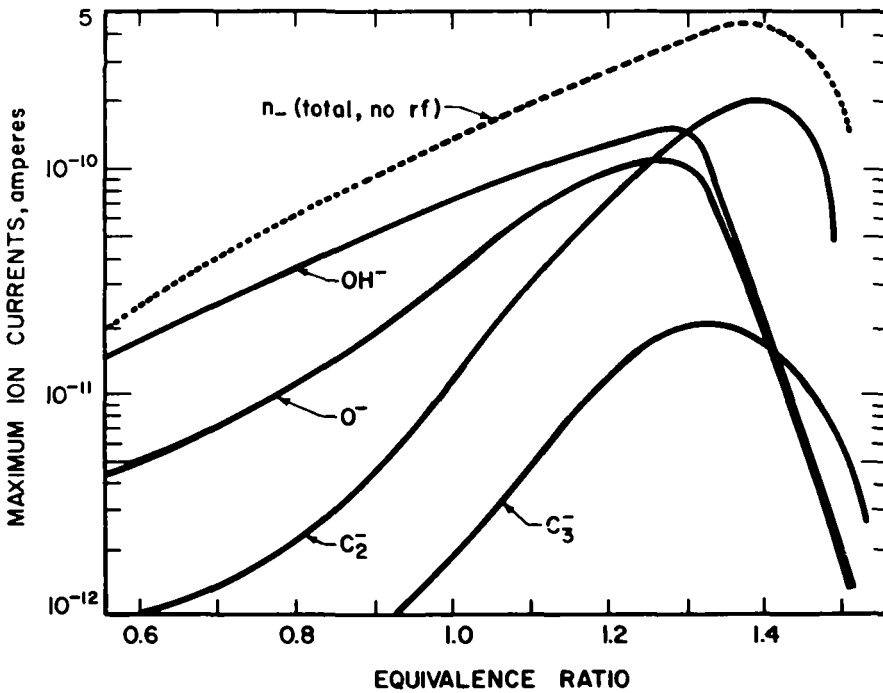

Fig. 9

LIST OF FIGURES

Fig. No.

1 MASS SPECTROMETER ATOMIC DIFFUSION FLAME FLOW SYSTEM

2 ION PROFILES IN C_2H_2-O SYSTEM

P = 1 Torr; C_2H_2 Flow = 17.0 cc(STP) sec^{-1}; He Flow = 14.5 cc(STP) sec^{-1}; O_2 Flow = 0.6 cc(STP) sec^{-1}

3 EFFECT OF ADDED CO_2 ON INDIVIDUAL ION CURRENT MAXIMA IN A C_2H_4-O SYSTEM

C_2H_4 Flow = 26.0 cc(STP) sec^{-1}; He Flow = 14.5 cc(STP) sec^{-1}; O_2 Flow = 0.6 cc(STP) sec^{-1}

4 EFFECT OF PRESSURE ON INDIVIDUAL ION CURRENT MAXIMA IN A C_2H_4-O SYSTEM

Reactant Flow Rates As In Fig. 3

5 TEMPERATURE AND ION CONCENTRATION AS A FUNCTION OF PRESSURE IN C_2H_2-O AND C_2H_4-O SYSTEMS

Reactant Flow Rates As In Figs. 2 and 3; The ion concentration is the maximum concentration for the given flow conditions, as measured by the Langmuir probe.

6 EFFECT OF N_2 AND CO_2 DILUENTS ON CHO^+ AND $C_3H_3^+$ CONCENTRATIONS IN AN ETHYLENE-OXYGEN FLAME

Equivalence Ratio = 1.0; Pressure = 2.0 Torr

7 EFFECT OF FLAME COMPOSITION ON MAXIMUM POSITIVE ION CURRENTS FOR ACETYLENE-OXYGEN FLAMES

Pressure = 4.0 Torr; Total Flow (STP) = 70 cc sec^{-1}

8 POSITIVE AND NEGATIVE ION PROFILES FOR ACETYLENE-OXYGEN FLAMES

Equivalence Ratio = 1.0; Pressure = 1.0 Torr; Total Flow (STP) = 70 cc sec^{-1}

9 EFFECT OF FLAME COMPOSITION ON MAXIMUM NEGATIVE ION CURRENTS FOR ACETYLENE-OXYGEN FLAMES

Pressure = 2.0 Torr; Total Flow (STP) = 70 cc sec^{-1}

THE MASS SPECTROMETRY OF IONS IN GLOW DISCHARGES

P. H. Dawson*, P. F. Knewstubb† and A. W. Tickner

National Research Council, Ottawa, Canada

Introduction

For the last few years the authors have been interested in chemical reactions in electric discharges. The last decade has brought increasing recognition of the great chemical reactivity of ions and it was decided to use the technique of mass spectrometry to study directly the ions in such systems. The dc glow discharge in particular was chosen for study as one which offered a variety of conditions of excitation. A detailed discussion of the properties of the discharge itself is given in Ref. 1.

Experimental Technique

The mass spectrometer used in this work is a double-focusing instrument of conventional design. Its construction and operation have been described in earlier papers[2,3].

The discharge tube which is the source of the ions is shown here as Fig. 1. A movable cathode allows the various discharge regions to be moved across the sampling probe so that ions may be sampled from all parts of the discharge. A more detailed description of its operation, of the mechanism of ion sampling and of the distribution of ion energies is given in Ref. 2.

Results and Discussion

In most of the work so far the region of greatest interest has been the negative glow and this paper will be mainly concerned with results obtained from that part of the discharge. The negative glow is a region in which preliminary ionization occurs by electron impact under conditions of low electrical field. Ions from the interior of the glow are lost mainly to the wall, to which they drift under the influence of a low radial field. At the pressures of 0.1 to 1.0 torr used here the residence time of an ion in the interior of the glow is estimated to be of the order of 10^{-4} sec so that a typical ion makes many collisions at energies close to thermal before it is sampled. As a result it is possible to observe ionic species, such as weakly bound ion clusters, which are difficult to observe in a conventional mass spectrometer ion source even when it is operated at comparable pressures.

The types of information which can be obtained will be illustrated by considering briefly some of the systems which have been studied. In general, the results take the form of plots of ion current sampled by the probe, which is proportional to the ion concentration in front of the probe, versus distance from the cathode. This variation with distance is related to the mechanism of ionization so that it is possible to distinguish between ions formed in different ways.

The simplest cases are those of the rare gases and a typical distribution of ion concentrations is shown for an argon discharge in Fig. 1 of Ref. 3. When the ions are formed directly by relatively high energy electron bombardment, such as occurs in the negative glow, the distribution of ion concentrations along the discharge are very similar. This is shown very strikingly for a mixture of Ar and Kr in Fig. 5 of the same paper.

* General Electric Research Laboratory, Schenectady, New York.
† Dept. of Physical Chemistry, Cambridge University, Cambridge, England.

When ions are formed by some less direct process this is usually apparent as a shift in distance from the cathode relative to the distribution of ions formed by electron bombardment. This can be seen in Fig. 4a of Ref. 3 for a helium discharge to which 2.8% Ar has been added. Here Ar^+ is formed mainly by the interaction of metastable He atoms with Ar (Penning effect) and reflects the distribution of metastable He atoms in the negative glow. A similar effect accounts for the Xe^+ in Fig. 5 of the same paper.

It is possible to use the effect described in the preceding paragraph in a quantitative way to estimate the relative cross sections for the ionization of both rare and molecular gases by metastable He atoms. If to a helium discharge about 0.1% of another gas is added, direct ionization of the second gas by electron impact is negligible and ionization by charge exchange is small and can be allowed for. Thus it is possible to compare areas under the curves for different added gases and to obtain values for the relative cross sections for ionization by He metastables. This has been done for several gases[4] and the results are summarized in Table I. The cross sections have been calculated relative to that of argon and are compared with those of other workers.

TABLE I. RELATIVE CROSS SECTIONS FOR IONIZATION BY METASTABLE HELIUM ATOMS

Gas	Ions from Negative Glow	Sholette and Muschlitz[5]	Benton, Ferguson Matsen and Robertson[6]
Ar	1.0	1.0	1.0
Kr	1.3	1.2	1.6
Xe	1.7	1.6	2.1
O_2	2.2	1.8	-
N_2	1.8	0.9	1.0
CO	6.0	0.9	-
H_2	0.39	0.34	0.91
CH_4	3.6	-	-
NH_3	3.6	-	-

Good agreement is found for the rare gases and for O_2 but for N_2 and especially CO the results appear to be high. The reason for this is not understood but may be due to some accidental coincidence of excited states. For H_2 our results agree with Sholette and Muschlitz[5] rather than with Benton et al[6]. For CH_4 and NH_3 no comparisons can be made and in view of the other results these values should be taken as upper limits.

Another important way in which ions may be formed in the negative glow is by ion-molecule reactions. This is illustrated for Ar containing about 1% H_2 in Fig. 6 of Ref. 3. Here the distribution of ArH^+ does not coincide exactly with that of Ar^+ and the maximum occurs slightly farther from the cathode. This is presumably due to the lower field and the resulting greater cross section for the reaction

$$Ar^+ + H_2 \longrightarrow ArH^+ + H$$

in the interior of the glow. It is worth noting that the mechanism of formation of ArH^+ must be quite different in the positive column.

A more complicated case is encountered when the ion formed by electron bombardment reacts readily with the gas from which it is formed. Hydrogen is a good example of this as can be seen in Fig. 1 of Ref. 7. At the cathode edge of the negative glow H_2^+ is the most abundant ion but in the region of low field in the interior of the glow it reacts readily according to

$$H_2^+ + H_2 \longrightarrow H_3^+ + H$$

Under these conditions the main ion in the negative glow is not the one formed by electron impact but is the ion which results from its reaction with the parent gas.

The observations on hydrogen also illustrate another property of the negative glow as an ion source, i.e. the ability to detect very weakly bound clusters. In the figure referred to in the preceding paragraph significant quantities of H_5^+ are observed. This ion had been suggested by Schaeffer and Thompson[8] as a possible intermediate in the radiation induced exchange of H_2 and D_2 and its detection here give additional support to their view that the exchange takes place via H_3^+. A corresponding study[9] has been made of the exchange in the dc glow discharge and of the effect of added rare gases and it is interesting to note that in experiments with added Kr the ion KrH_3^+ was observed.

When the gas used is polar in nature and hydrogen bonding may be a factor it is possible using this type of ion source to observe the formation of much larger ion clusters. In water, for example, clusters ranging up to $H_3O^+.5H_2O$ were observed[10] and even this limit is considered to be set mainly by the sensitivity of detection of the instrument. It was concluded from a study of the distribution of ion energies that the first three molecules of water were much more strongly bound to the central H_3O^+ than the remainder - a picture which agrees well with the hydration shell structure postulated by Eigen[11].

Recently, similar observations have been made with ammonia[12]. Here clusters up to $NH_4^+.4NH_3$ are observed and the results seem to indicate that the fourth molecule of NH_3 is much more weakly bound to NH_4^+ than are the first three.

Summary

The results given above illustrate some of the properties of the dc glow discharge and especially of the negative glow when used as a source of ions.

There are, of course, a number of limitations, many of which stem from the fact that the various discharge parameters are interrelated. For example, for a particular gas at a given pressure a discharge will operate stably only over a certain range of current densities, and for a given current density the discharge voltages and therefore the electron energies are fixed.

On the other hand glow discharges have properties which differ in several useful ways from those of conventional ion sources. In the negative glow the decrease in energy of the bombarding electrons with increasing distance from the cathode allows one to distinguish between ions formed directly and those resulting from a number of different secondary processes. Ions in the interior of the glow are almost in thermal equilibrium with the gas and this plus the fact that ions may be sampled readily from the edge of the plasma with few collisions enables weakly bound clusters to be observed.

The case of ammonia provides an example of the way in which observations with a conventional "high-pressure" mass spectrometer ion source and those using a glow discharge may complement one another. The conventional ion source study[13] provides much information on the ion-molecule reactions but gives no evidence of the ion clusters which stand

out very strongly in the discharge results. Since clusters may also play an important part in the radiation chemistry of ammonia, it is important that their existance be known. It is interesting to note that a decrease in the yield in the radiolysis of ammonia at pressures of about 100 atmospheres had been attributed to the onsent of clustering[14] whereas the discharge results indicate that clusters in ammonia form readily at much lower pressures.

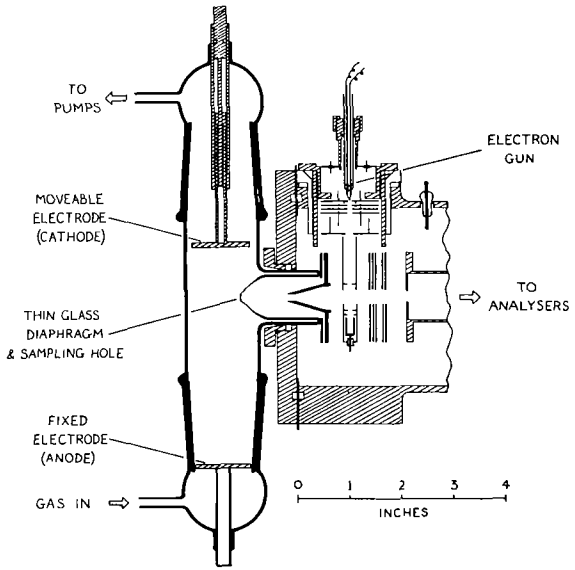

Fig. 1. Discharge tube ion source

References

1. G. Francis, Handbuch der Physik, edited by S. Flugge (Springer-Verlag, Berlin, 1956), Vol. 22.
2. P. F. Knewstubb and A. W. Tickner, J. Chem. Phys. 36, 674 (1962).
3. P. F. Knewstubb and A. W. Tickner, J. Chem. Phys. 36, 684 (1962).
4. P. H. Dawson and A. W. Tickner, to be published.
5. W. P. Sholette and E. E. Muschlitz, J. Chem. Phys. 36, 3368 (1962).
6. E. E. Benton, E. E. Ferguson, F. A. Matsen and W. W. Robertson, Phys. Rev. 128, 206 (1962).
7. P. H. Dawson and A. W. Tickner, J. Chem. Phys. 37, 672 (1962).
8. O. A. Schaeffer and S. O. Thompson, Radiation Research 10, 671 (1959).
9. P. H. Dawson and A. W. Tickner, to be published.
10. P. F. Knewstubb and A. W. Tickner, J. Chem. Phys. 38, 464 (1963).
11. M. Eigen and L. DeMaeyer, "The Structure of Electrolytic Solutions", edited by W. J. Hamer (John Wiley and Sons, Inc., New York, 1959). Chapter 5.
12. P. H. Dawson and A. W. Tickner, J. Chem. Phys. 40 (1964) (in press).
13. G.A.W. Derwish, A. Galli, A. Giardini-Guidoni and G. G. Volpi, J. Chem. Phys. 39, 1599 (1963).
14. Y. Toi, D. B. Peterson and M. Burton, Radiation Research 17, 399 (1962)

ADVANCES IN TIME-OF-FLIGHT MASS SPECTROMETRY

Donald C. Damoth
The Bendix Corporation
Cincinnati, Ohio

The development and expansion of the field of mass spectrometry is quite apparent. It is due to many factors, such as the natural tendency to develop the most sophisticated data possible and the availability of resources to do this. In the past, mass spectrometry was a field unto itself, with the scientist, whatever his basic objectives in using this tool, intimately involved with the apparatus and technique. Now a new type of researcher is beginning to acquire mass spectrometry apparatus. He is not concerned with the intricacies of the apparatus, but only wishes to inject a bit of material into its inlet and have as completely reduced data as possible, emerge from its readout, as quickly and accurately as possible.

Many of those who developed the now familiar research and analysis techniques find them being honed to a fine edge by virtue of widespread usage. The pioneering spirit drives them to new techniques and applications where they can exercise ingenuity and receive the rewards of the first arrivals.

The increased usage of mass spectrometry attracts new companies to supply the equipment needed to help these people in their efforts. These companies bring with them new thoughts and new ways of doing which advance the state of the art.

In order to keep pace with the changes in the field, continuing development of instruments and principles must occur. The refinement of the various types of mass spectrometers is controlled by variables appropriate to each. Some of the impediments to the development of the Time-of-Flight Mass Spectrometer principle have been a lack of confidence by many leaders in the field of mass spectrometry that the principle would be developed very far and a reluctance of manufacturers to work on basic principles.

These impediments seem to have been overcome now, and significant improvements in Time-of-Flight mass spectrometry are being made with increasing frequency by both independent researchers using the tool and by instrument manufacturers.

Probably the first parameter inquired of any mass spectrometer is its resolution. The TOF has traditionally been characterized by resolution of about 150 (1% adjacent peak height interference). Now it is recognized that the resolution must be classified for low or high initial energy species such as inorganic parent ions or organic ions. That is to say, the space focussing of the TOF has been good, while the energy focussing has been less satisfactory in the conventional pulsed mode of operation.

Dr. Studier of Argonne National Laboratories pointed the way to improve energy focussing with a new way of operating the source which also increases sensitivity. Unfortunately, this mode suffers the disadvantages of being difficult to adjust and sensitive to slight contamination of the source.

Studies on this mode of operation to simplify the adjustments while retaining the high sensitivity and improved resolution led to the development of an improved ion source configuration and mode. This new mode provides the improvements in operation while being more simple to adjust for focus.

For many years, the ion source of the Time-of-Flight Mass Spectrometer has been of the configuration shown in Figure 1. The spacings between the backing plate and first ion grid and between the first and second ion grid are 0.240 inches. The electron beam is 0.070 inch from the backing plate. The electron beam is pulsed on from 0.3 to 1.5 microseconds at the start of each 100 microsecond cycle. Then a pulse of about 250 volts amplitude with a rise time of 0.1 microsecond is applied to ion grid number one to draw the ions out of the ionization region. After passing through the first ion grid, the ions are accelerated to 2800 volts energy by the second ion grid. After passing the second ion grid, the ions drift inside a screen which is also at 2800 volts until they hit the cathode of the electron multiplier. Some of the shortcomings of this arrangement will be pointed out in the description of the new mode.

Dr. Studier wished to study thermally ionized species with the TOF. It was not possible to turn the source of ions off and on at the high rate which was required with the pulsed mode source just described. That mode gave poor results with a continuous source of ions. Studier then proceeded to investigate the "Trapping Grid" mode which was incorporated into some of the TOF instruments, but found this unsatisfactory. While investigating the "Trapping Grid" operation, he discovered and developed the "Studier Mode" of operation. An approximation of this mode is shown in Figure 2. Another ion grid is utilized with the voltage configuration shown. The essence of this mode of operation seems to be that a delicate balance of potentials exists between the backing plate and first ion grid to achieve a type of energy focussing in which the less energetic ions are trapped in the potential well of the electron beam while the more energetic ions are drawn to the backing plate and neutralized. When the drawout pulse is applied to the first ion grid, the strong field deflects the electron beam away from the normal ionization region and the ions are drawn out. This mode yields a sensitivity increase of 10 to 100 times due to the increased average ionizing beam current of about 100 microamperes compared to about one microampere in the standard mode. The resolution for high initial energy species is increased and a resolution of 300 for organic species is obtained.

This mode has disadvantages, however, which limit its use. First, the potentials in the ionization region prohibit having an electric field free region during the ionization process which is desirable for ionization potential and ion-molecule studies. In addition, the sorting action of the electron beam potential well trapping might be undesirable in some molecular beam experiments. The controls to adjust the source for optimum performance in this mode interact and since there are three or four controls, a fair amount of skill and time is required to achieve good operation. And, since the potentials in the source region under optimum conditions are small, the source is quite susceptible to contamination and must be cleaned frequently to maintain best performance.

In order to retain the best features of the original pulsed mode and the Studier mode, the new ion source configuration and operating mode has been developed as shown in Figure 3. The distance between the backing plate and first ion grid is 0.070 inch, with the electron beam axis 0.030 inch from the front surface of ion grid #1.

Calculations and observations have shown that there is a considerably different value of drawout pulse height in the original ion source configuration for optimum space focussing and optimum energy focussing. By moving the electron beam axis nearer to ion grid #1, the field values for optimum space and energy focussing are brought much closer together, and by bringing the backing plate closer to ion grid #1, the potential needed on grid #1 for a particular field value is reduced. Thus, with this configuration we obtain better focussing with smaller demand on the electronic circuitry.

Ion grid #1 is now comprised of sheets of high transmission molybdenum mesh welded to both sides of a 0.020 inch thick stainless steel plate. The nickel mesh previously used has too high of a magnetic susceptibility and is not usable in this configuration because the #1 grid is so close to the electron beam. Gold and silver

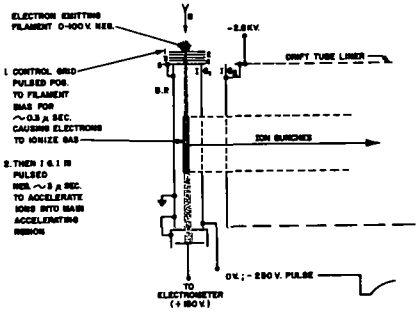

S-12-101 OPERATION
(PULSED IONIZATION)
Fig. 1

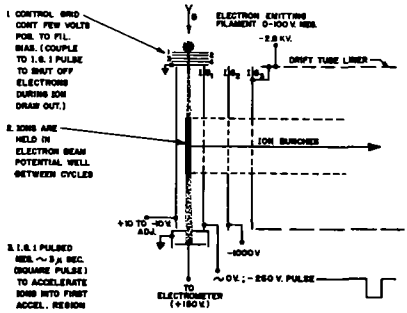

S-12-107 OPERATION
(CONTINUOUS IONIZATION)
Fig. 2

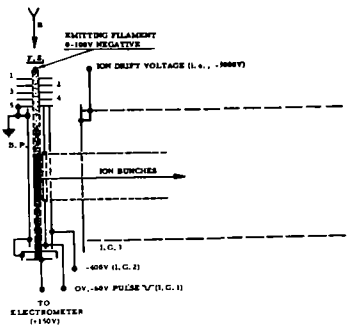

1000 SERIES ION SOURCE
TIME-OF-FLIGHT MASS SPECTROMETER
Fig. 3

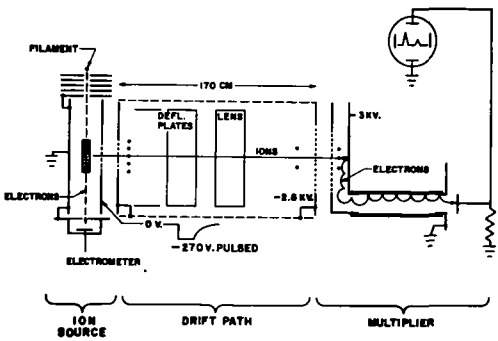

T.O.F.M.S. SCHEMATIC
Fig. 4

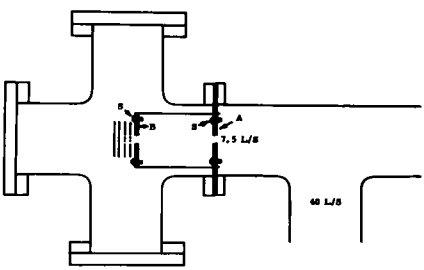

SOURCE PUMPING BAFFLE LOCATIONS

Fig. 5

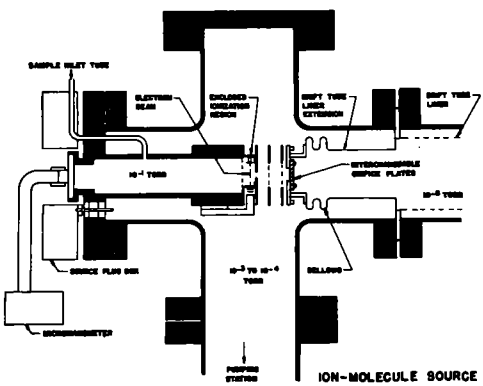

Fig. 6

are out because they amalgamate with mercury and do not have sufficient tensile strength. The double screen on both sides of the stainless plate provides a finite thickness grid which essentially eliminates electric field peek-through and disturbance of the electron beam and ions during the ionization process. The more rigid mesh welded in place under tension provides a more nearly planar accelerating field which tends to accelerate the ions directly toward the multiplier, thus increasing sensitivity. Loose mesh in the grid structure will bow under the force of the electrostatic fields and will accelerate the ions with an appreciable radial ion velocity component causing many of them to miss the cathode of the magnetic electron multiplier.

This source configuration provides improved resolution on organic species with large average ionization currents. It is not particularly susceptible to contamination under constant usage, it has low random ion noise characteristics and the focussing adjustment is accomplished with a single control. Inasmuch as the development and optimization of this new source configuration has not been completed at this time, the resolution figures are not firm, but it appears that the resolution will exceed 300 for organic compounds and 600 for inorganic compounds.

Factors other than the ion source can affect the resolution of a Time-of-Flight Mass Spectrometer. Short term cyclic variations such as mains frequency ripple on high voltage points in the spectrometer can degrade resolution. Better power supply regulation and by-passing A. C. components to ground has improved this condition.

The ion transit time to the cathode of the electron multiplier is critical and small differences become important as resolution is increased. The time difference between mass peaks differing by one amu at mass 400 is about 60 nanoseconds with a 170 cm flight path at 2800 volts. This corresponds to a difference in flight path of 0.04 mm. Thus, the angle of the cathode plate shown in Figure 4 upon which the ions impinge is critical. Careful alignment of the cathode plate to be precisely parallel to the axis of the drift tube makes higher resolution possible.

The development of better electronic circuitry to provide faster, sharper gating pulses for the electron multiplier gating section permits better recorded resolution. With the improvement of resolution to yield the new narrower mass peak pulses, the gates have been made narrower to be able to transfer the analog signal to the recorder; the analog gates have now been made about 20 nanoseconds wide instead of the previous width of about 50 nanoseconds. The oscilloscope output has also been increased in frequency response to keep up with the improved resolution. The former 20 megacycle system has been replaced with an oscilloscope system with a 50 megacycle response.

With the improved resolution, the collisions in the drift path have become increasingly important. With the new 180 cm drift path, the pressure must be kept below 1×10^{-6} Torr in the analyzer to reduce the collisions to an insignificant level. This requires keeping liquid nitrogen in the cold trap when maximum resolution is required.

The sensitivity of the TOF has been increased markedly. Perhaps the most obvious means of increasing the sensitivity was to increase the duty-cycle of the ion source. With a 10 kcs operating frequency which gives a 100 microsecond cycle, the 0.3 microsecond duration ionizing electron beam pulse yields an average trap current of about 1.0×10^{-6} amperes. Increasing the duty cycle by a factor of over 100 to about 50 microseconds has increased the trap current by a like amount and the sensitivity has increased considerably. The new ion source configurations and modes have been making this increase in duty cycle possible while retaining a satisfactory random ion noise ratio. With the former configuration this was not possible.

The ion transmission efficiency was also increased as pointed out earlier by improving the ion grid mesh mounting procedures to eliminate grid bowing and off axis acceleration. The source pressure was increased during the analysis of non-

condensible species as shown in Figure 5. Formerly, there was no pumping baffle between the ion source and cold trap. This resulted in a pumping speed of about 30 liters/second for nitrogen at the ion source. Installation of a 7.5 liter/second baffle at A increased source pressure for a given gas input by a factor of 4. In later instruments, the baffle location was moved to B to decrease the length of the increased pressure region through which the ions had to travel. The baffles are removable by loosening the mounting screws for fast reaction work or molecular beam work where high pumping speeds are desirable.

The effective sensitivity of the instrument for certain applications, such as gas chromatograph - mass spectrometry combinations has been increased by the innovation of pre-dynode gating. This is a method of eliminating one or a small number of ion bunches due to large sample components from entering the multiplying region of the magnetic electron multiplier. The magnetic electron multiplier saturates on peaks in excess of 1×10^{-7} amperes output and if any peaks exceed this value by several hundred percent, the whole spectrum becomes non-linear.

To permit operating at high multiplier gain in the presence of a high level component such as helium, the electrons due to that particular mass are prevented from entering the multiplying region between the glass strips by pulsing the fields in the front end of the multiplier into a cut-off condition at the appropriate time.

The usable sensitivity of the instrument has also been extended by decreasing the noise levels in the output amplifier by over an order of magnitude. The dynamic range now extends from 1×10^{-7} amperes output (1×10^{-5} Torr) to below 1×10^{-14} amperes (1×10^{-12} Torr).

The quantitative accuracy of the TOF has also been improved. Never having been capable of doing quantitative analysis well enough to warrant its use in that application before, the quantitative capability currently being developed will constitute a significant change. Several basic design changes have been instituted toward this end. The circuits supplying the voltages to the various elements of the magnetic electron multiplier have been improved to give voltage stabilities equivalent to gain changes of better than $\pm 0.1\%$ short term and $\pm 1\%$ long term.

The configuration of the deflection plates in the drift region, used for checking out the magnetic compensation of the ion source, and the voltage circuits supplying the deflection voltages was found to cause variations in the ion beam position. Shortening the deflection plates and stabilizing the circuits has improved this condition. Additional electronic circuit improvements such as stabilization of the trap current regulator for the ion source and refinement of the electrometer amplifiers in the analog output has also helped. The net result of these improvements in the quantitative factors in the instrument has not yet been evaluated, but it is expected that an isotope ratio measurement capability of 0.1% and a quantitative capability of 1% for mixtures will be obtained.

Another quantitative aspect in a different parameter is the ability to determine the mass number of an unknown peak. Heretofore, it has been necessary to use indirect methods, such as comparison of unknown spectra with spectra of calibrating materials or by slow direct methods such as counting individual peaks or measuring distances on recorded scans. Now an accessory has been developed which records a staircase pattern with a step every ten mass units up to 400 amu. The device works by comparing the voltage which triggers the gating pulse in the analog scanners, that is, the scan voltage, to a series of reference voltage points. As the scanning voltage passes the adjustable reference points, the output steps to that new value. The output of the mass marker is fed to one channel of the same recorder which is tracing out the mass spectrum. It follows any scan rate equally well.

The repetition frequency of the TOF has been increased to 100 kcs where needed. This permits data points to be obtained every 10 microseconds in fast reaction investigations. One difficulty encountered in operating at frequencies in this range is the overlap of spectra in the output. The ions are started so often that lighter ions from later spectra overtake heavier ions from earlier spectra. This problem can be handled up to about 100 kcs by using higher accelerating voltages and shorter drift paths, or by juggling the frequency so the overlap is inconsequential.

The recording of single cycle spectra at high repetition rates has been improved by researchers along two lines. The direct approach of using continuous film strip cameras has been improved by development of better photographic techniques and new oscilloscopes with brighter spots, both by better focussing and by better phosphors. Also, the development of the light streak recording technique for qualitative monitoring of several tens of mass peaks in conjunctions with the Z-axis gating technique for following two peaks quantitatively has simplified recording the peaks cycle-by-cycle.

The maximum analog scan rate for recorded spectra has been increased so that the spectrum from 0 to 800 amu can be recorded in a single sweep in 1.5 seconds. One problem which arises both in single cycle recording as in fast reaction studies as well as in the very fast analog scans is the statistical variation in the peak heights due to the varying numbers of ions, even with constant sample pressure. Thus it is implicit in any fast scanning mass spectrometer that the fastest scan rates cannot be used at the highest sensitivities. Improvement in this respect comes about by increasing the number of ions formed in the source, such as by increased duty cycle or by improved ion transmission.

A repetitive scan device has been developed which causes the scan to recycle continuously at periods from 0.08 seconds to 800 seconds. The mass range covered is a function of the scan rate. Another interesting device is the total output integrator. This is another analog plug-in but does not scan the mass spectrum. This analog unit remains inactive for ten cycles and operates only on the eleventh cycle. It turns on during that cycle and gates all the electron multiplier output into a single channel, integrating the output due to all the peaks in the spectrum. The start of integration during that cycle can be delayed up to mass 50 so that the lighter ions are not added into the sum.

A TOF has been developed which records either positive or negative ions with the ion source at ground potential. This makes it feasible to investigate negative ions generated outside the mass spectrometer. Recording of negative ions is accomplished by floating the electron multiplier and the analog electrometers. Special power supplies are also floated at the high voltage. The electrometers are A. C. coupled to amplifiers at ground potential which drive the recorders. This method of analyzing negative ions is more demanding of the basic circuitry but permits retaining all the basic functions of the mass spectrometer for negative ions.

Since a reasonable concensus has been reached that ionization potential modes such as the Retarding Potential Difference method, or variations thereof, are valid and reliable, circuitry for performing such measurements is being developed. A refinement of this technique using an audio frequency oscillator to modulate the ionization potential as in the Fox method and a phase sensitive detector to detect the output variations caused by the modulator is under development. This device will permit ionization potential measurements to be made considerably faster than before.

The addition of a simple planar shield located behind the emitting filament as shown in Figure 3 and operating at the filament potential shields the filament from the ground potential of the vacuum housing. This and the reduction of the ion accelerating voltage peek-through into the ionization region by use of the double ion drawout grid have improved ionization potential measurement accuracy.

An ion source configuration has been developed which permits formation of ions in a region of pressures to above 0.1 Torr making it very useful for studying ion-molecule reactions. This is shown schematically in Figure 6. The ionization region is tightly enclosed as opposed to the usual open configuration in the TOF. The only apertures for gas to leave the source region are the electron beam entrance slits and the ion exit orifice in the drawout grid. These have a combined pumping speed of about 0.1 liter/second for mass 28. Gas enters the source through the small inlet tube near the center of the large chamber behind the source. The ionization region is defined electrically on the back by a high transmission mesh. This has a low impedance for the sample gases. A micromanometer is attached to the sample chamber at the source header. This arrangement permits obtaining uniform, measurable pressures in the source region. Differential pumping reduces pressure so that collisions outside the source region are inconsequential.

The ion drawout grid was later modified to reduce the distance the ions have to travel through the higher pressure region after the drawout pulse is applied. This new arrangement acts as a double grid and cuts down field penetration into the ionization region reducing the ion noise caused by unsyncronized drawout. Some minor noise problems remain, and these are being investigated.

This source permits generation of ions in a field free environment so field effects can be studied. The variable delay on the ion drawout pulse permits precise determination of reaction times. The electronic circuitry is being changed so that the analog gates are syncronized with the start of the ion drawout pulse instead of a master pulse. This causes the analog gates to remain positioned on chosen mass peaks as the time between ion formation and onset of the drawout pulse is varied. This will make it a simple matter to plot the intensity of several peaks as a function of residence time in the source.

Another source configuration variation which is significant is the "nude source" shown in Figure 7. This configuration was originally developed for residual gas analysis in large chambers, and now is finding application in shock tube studies and other molecular beam work. The advantage of this arrangement is that the ionization region is within two centimeters of the outline of the source, permitting short travel between practically any reactor configuration and the ionization region.

Some success has also been obtained with a TOF source operated without collimating or compensating magnets. This is advantageous for the study of low energy externally generated ions. This configuration utilizes an electron beam path length of about 13 millimeters. The resolution and sensitivity are both degraded, but are still quite usable.

This, then has been a summary of many of the changes in the basic Time-of-Flight Mass Spectrometer. There have also been extensive changes in instrument layout and inlet systems which markedly improve the operability of the whole system.

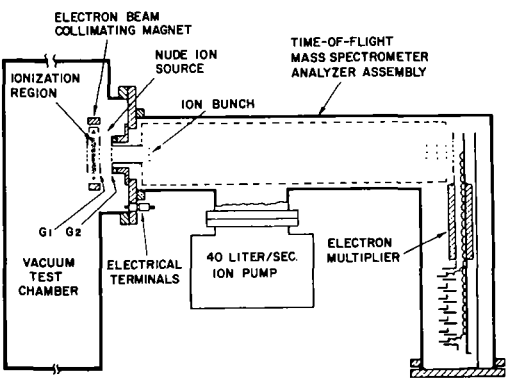

Fig. 7

Basic Properties of Electron Multiplier Ion Detection and Pulse-Counting Methods in Mass Spectrometry

L. A. Dietz

General Electric Company, Knolls Atomic Power Laboratory*,

Schenectady, New York

INTRODUCTION

At the Knolls Atomic Power Laboratory, development of techniques for the precise comparison of two ion currents by pulse counting has required a detailed study of factors which limit the current-measuring accuracy of electron multipliers. Recently published theoretical and experimental work on anode pulse-height distributions in photomultipliers(1-3) indicates that the critical role played by focusing between dynodes and the secondary electron gain of the first stage in determining pulse-height distribution and detection efficiency has not been appreciated fully. Inefficient focusing and low gain distort the anode pulse-height distributions and limit the accuracy of measuring electron or ion currents with an electron multiplier.

This morning I would like to describe several basic properties of electron multipliers and pulse-counting methods. For example, the cascading electron multiplication process will be analyzed in terms of compound Poisson statistics and statistical models will be developed to explain current-measurement bias in electron multipliers used in either the dc or pulse-counting modes. It will be shown how the results can be applied to correct an observed isotope ratio for this bias. The design of a new electron multiplier of high gain, high speed, and high efficiency will be described, along with experimental data obtained during its evaluation. Finally, a new all solid state discriminator and pulse amplifier with a speed in excess of 100 Mc/sec will be described briefly and operating characteristics of the new detector system will be given. The pulse-counting system described in this paper is an outgrowth of the early work of White and Collins(4), who used an electron multiplier in the pulse-counting mode to improve the detection sensitivity of a surface ionization mass spectrometer.

---

*The Knolls Atomic Power Laboratory is operated by the General Electric Company for the U. S. Atomic Energy Commission.

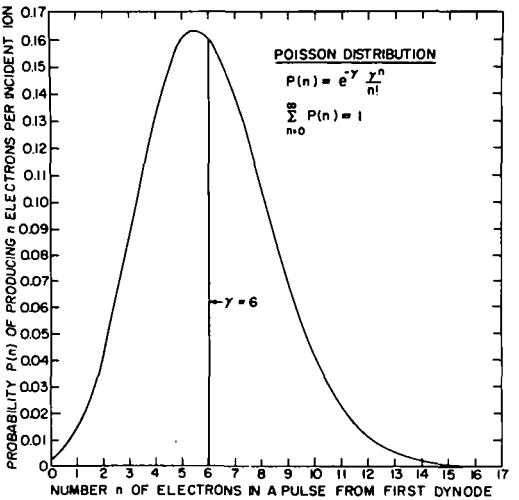

Fig. 1

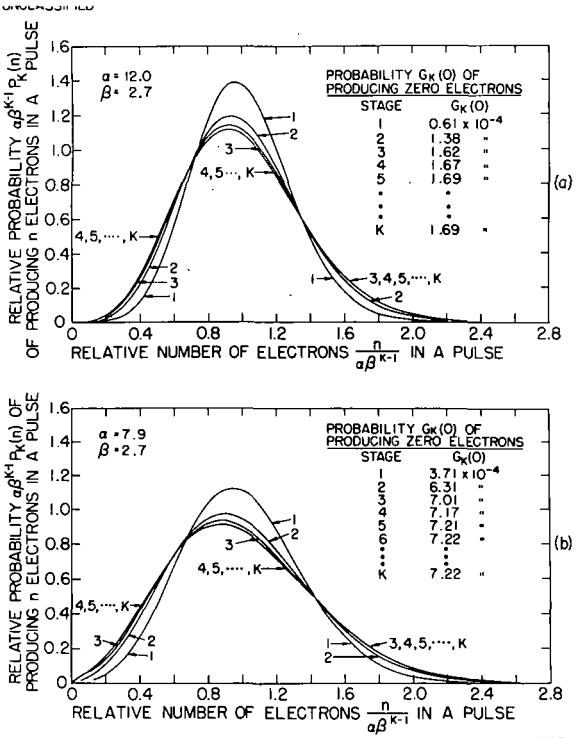

Fig. 2

KS-54523

STATISTICS OF SECONDARY ELECTRON MULTIPLICATION

The following analysis of secondary electron multiplication for the case of ion detection in an electron multiplier uses the elegant generating function technique(5) which Lombard and Martin(6) used in an investigation of photomultiplier statistics. Changes have been made in their notation to avoid confusion in separating first stage gain from those of all succeeding stages. First stage gain is defined as α secondary electrons/incident ion, and those of all succeeding stages as β secondary electrons/incident electron. This distinction is necessary for electron multipliers used for detecting ions, since in this case α and β generally are unequal. By "stage gain" is meant that fraction of the average number of secondary electrons emitted from a dynode surface which arrive at the following dynode to continue the chain multiplication process. In a well-focused multiplier structure, stage gain is slightly less than or equal to the average secondary electron yield of a dynode surface. The difference between yield and gain must be kept in mind, since the following statistical development is in agreement with the experimental data only when the gain equals or is nearly equal to the yield.

The hypothesis of Poisson statistics for each stage of multiplication is plausible if one considers the production of secondary electrons from a surface by high velocity ions or electrons to involve random processes. An energetic ion or electron, during its passage through an activated dynode surface which usually is an oxide layer, causes excitation of many electrons below the surface so that some of them can surmount the surface potential barrier if they gain sufficient energy and if their momenta are properly oriented. If the number of excited electrons per incident charged particle is large and if the probability of escape of any given excited electron is small compared with unity, then for single ion or electron impacts with a surface it can be shown that the expected frequency distribution for producing $n = 0, 1, 2, \ldots, n$ secondary electrons is given by the Poisson distribution, $\exp(-\gamma)\,\gamma^n/n!$, where γ is the average secondary electron yield. An example is shown in Fig. 1, where $\gamma = 6$. The distribution is bounded at zero probability for electrons by an intercept of $\exp(-\gamma)$ and is unbounded for large n. For two or more stages in cascade, this simple Poisson distribution becomes a compound Poisson distribution according to probability theory.

Assuming single ion inputs and Poisson statistics for each stage, secondary electron production in an electron multiplier of K stages can be described by a statistical generating function $G_K(s)$ for a compound Poisson distribution,

$$G_K(s) = \sum_{n=0}^{\infty} P_K(n)\, s^n = \exp\alpha \left\{ -1 + \exp\beta_1 \left[-1 + \ldots + \exp\beta_{K-1}(s-1) \right] \right\}, \quad (1)$$

where the compound exponential cascades upward through K exponentiations; s is a generating function parameter; α is the average gain of the first stage; and $\beta_1, \ldots, \beta_{K-1}$ are the average gains of the second through Kth stage, respectively. The coefficients of s^n can be expressed as a Maclaurin series in $P_K(n)$. Thus, the probability of generating 0, 1, 2,..., n secondary electrons after K stages of multiplication is given by Eq. (2),

UNCLASSIFIED

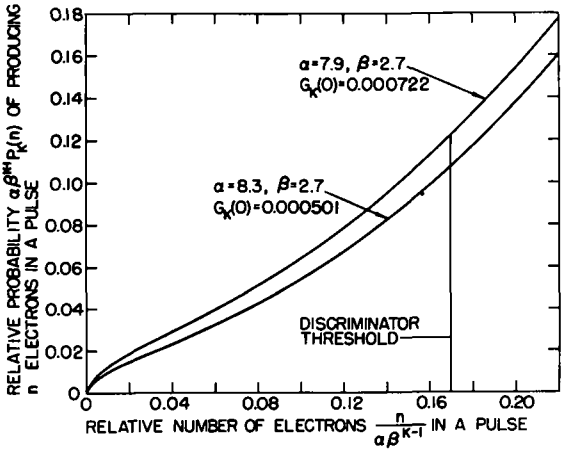

Fig. 3

KS-54520
UNCLASSIFIED

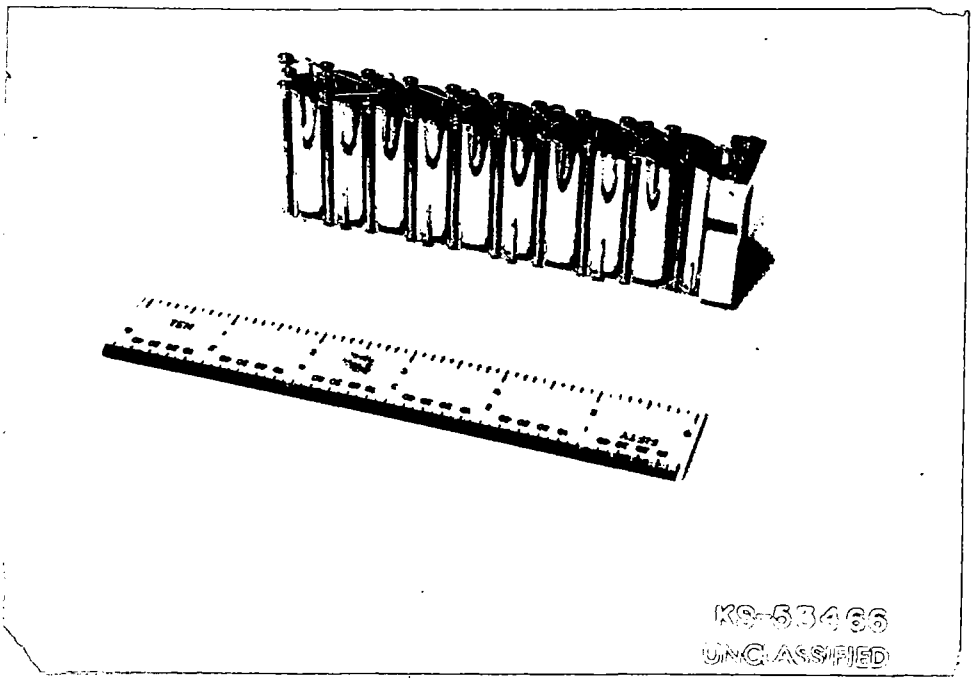

Fig. 4

$$P_K(n) = \frac{\alpha}{n} \sum_{i=0}^{n-1} (n-i)\, P_K(i)\, E_{K-1}(n-i), \text{ where } n \neq 0 \text{ and } K \geq 2. \tag{2}$$

In Eq. (2), $P_K(i)$ and $E_{K-1}(n-i)$, respectively, are derivitives of the generating functions $G_K(s)$ and $E_{K-1}(s)$ evaluated at $s = 0$. These derivitives are defined by Eqs. (3) and (4).

$$P_K(i) = \frac{1}{i!} \frac{d^i}{ds^i} G_K(s)\Big|_{s=0} \tag{3}$$

$$E_{K-1}(n-i) = \frac{1}{(n-i)!} \frac{d^{n-i}}{ds^{n-i}} E_{K-1}(s)\Big|_{s=0}, \text{ where} \tag{4}$$

$$E_{K-1}(s) = \exp\beta_1 \left\{ -1 + \exp\beta_2 \left[-1 + \ldots + \exp\beta_{K-1}(s-1) \right] \right\} \tag{5}$$

The generating function $E_{K-1}(s)$ arises when Leibnitz' rule for differentiating the product of two functions is applied in the differentiation of $G_K(s)$. The generating function $G_K(s)$ describes the overall gain characteristics of a multiplier and is a function of α and β; whereas $E_{K-1}(s)$ describes the gain characteristics of all stages beyond the first and is a function of the β's only. For convenience in the following development we assume that all the β's are equal.

The probability of collecting zero secondary electrons at the multiplier anode is treated separately. From Eqs. (3) and (1) it can be shown to be

$$P_K(0) = G_K(0) = \exp\alpha \left\{ -1 + \exp\beta \left[-1 + \ldots + \exp(-\beta) \right] \right\}. \tag{6}$$

The magnitude of $P_K(0)$ is determined by the fraction of ions which produce zero secondary electrons on the first dynode and by the fraction of secondary electron pulses which die out before reaching the anode. Both processes are included in the $P_K(0)$ term, but are easily separated by noting that the loss at the first dynode surface is $\exp(-\alpha)$.

Calculations of pulse-height distributions were made on a Philco 2000 digital computer. Probability coefficients for each stage were calculated until their sums exceeded 0.9999 -- i.e.

$$\sum_{n=0}^{N} P_K(n) > 0.9999,$$

where N is the final term and all coefficients for $n > N$ are taken as zero. The sum of all the probability coefficients from $n = 0$ to $n = \infty$ is unity. Therefore, one can define the detection efficiency of an electron multiplier by Eq. (7), since, at least in principle, any non-zero pulse of electrons reaching the anode should be detectable.

$$\text{EFFICIENCY} = 1 - G_K(0) = \sum_{n=1}^{\infty} P_K(n) \tag{7}$$

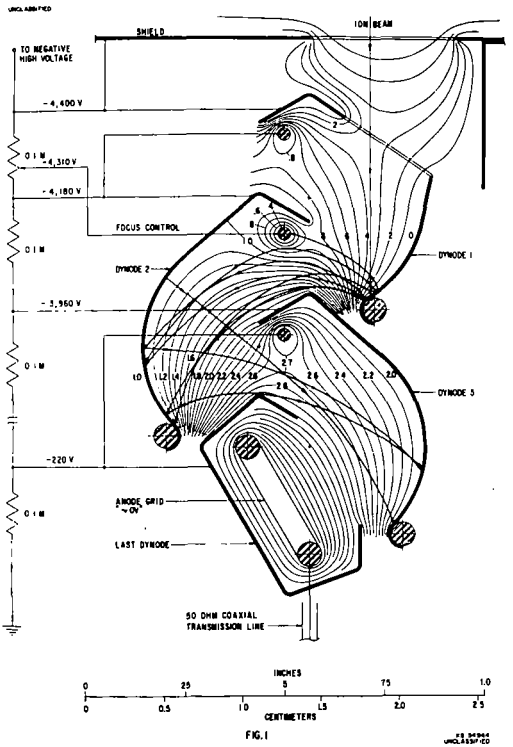
UNCLASSIFIED
SHIELD
ION BEAM
TO NEGATIVE HIGH VOLTAGE
-4,400 V
0.1 M
-4,310 V
-4,180 V
FOCUS CONTROL
0.1 M
DYNODE 2
DYNODE 1
-3,960 V
0.1 M
DYNODE 3
-220 V
0.1 M
ANODE GRID
LAST DYNODE
50 OHM COAXIAL TRANSMISSION LINE
INCHES
CENTIMETERS
FIG. 1
UNCLASSIFIED

Fig. 5

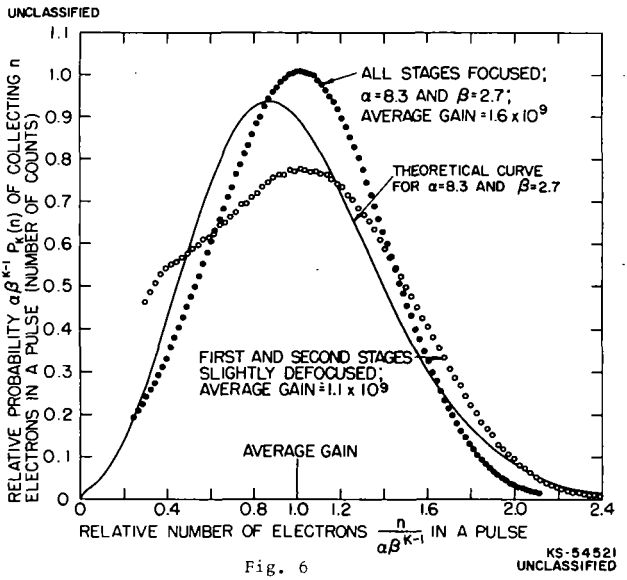
UNCLASSIFIED
RELATIVE PROBABILITY $\alpha\beta^{K-1} P_K(n)$ OF COLLECTING n ELECTRONS IN A PULSE (NUMBER OF COUNTS)
ALL STAGES FOCUSED; α=8.3 AND β=2.7; AVERAGE GAIN = 1.6 x 10^9
THEORETICAL CURVE FOR α=8.3 AND β=2.7
FIRST AND SECOND STAGES SLIGHTLY DEFOCUSED; AVERAGE GAIN = 1.1 x 10^9
AVERAGE GAIN
RELATIVE NUMBER OF ELECTRONS $\frac{n}{\alpha\beta^{K-1}}$ IN A PULSE
KS-54521
UNCLASSIFIED

Fig. 6

In Fig. 2 are shown distributions which were calculated for two different values of α, for the condition $\alpha > \beta$. They change shape progressively from a simple Poisson distribution for the first stage to a compound Poisson distribution of constant shape after only a few stages. It is clear that the first stage gain largely determines the shape of the expected pulse-height distribution. The first moment of the distribution gives the average electron current gain through stage K as $\alpha\beta^{K-1}$. It is shown normalized to the average value taken as unity. The resulting curve labeled 4, 5, ..., K is what one would expect to see on a multi-channel pulse-height analyzer. Because $P_K(0)$ is not included in the normalized curves, the area under a given curve really represents overall multiplier efficiency through that stage.

Specular reflection of a portion of the ion beam striking the surface of the first dynode plays an insignificant role in beam detection losses. McHugh and Sheffield(7) could find no evidence of its existence for various ion species striking a target at normal incidence. They placed an upper limit of 10^{-6} on the ratio of reflected to incident ions.

STATISTICAL MODELS FOR MEASUREMENT BIAS

Bias depends primarily on the secondary electron gain of the first stage and is different for the dc and pulse-counting modes of detecting ions. Before developing suitable expressions to correct for bias, we note that $G_K(0)$ in Eq. (6) can be rewritten in a simpler but equivalent form,

$$G_K(0) = \exp\left[\alpha(b-1)\right] , \tag{8}$$

where b equals $E_{K-1}(0)$ and can be evaluated readily from Eq. (5). To do this, one sets K successively equal to 2, 3, ..., K and calculates values of the corresponding expressions for $E_{K-1}(0)$ until b reaches a constant value. The constant b is the fraction of events lost in all stages beyond the first and is always much less than unity in any practical multiplier. It follows that multiplier efficiency may be expressed as

$$\text{EFFICIENCY} = 1 - \exp\left[\alpha(b-1)\right] . \tag{9}$$

The gain α of the first stage is a variable quantity. It depends on many things, among which may be ion mass, energy or velocity, atomic or molecular structure of an ion, kind of secondary emitting surface, angle of entry into the surface, and optical transmission between first and second dynodes. Since no simple relationship exists for predicting α in all cases, in a given experimental situation it is best to measure it for specific ions. This may not always be accomplished easily.

In the dc mode of operation, an electron multiplier converts an ion beam into a highly amplified current of electron pulses, which are measured as a dc current. The observed anode current is the product of the true primary current of ions striking the first dynode, the multiplier efficiency, and the average current gain. If it can be assumed that multiplier dark

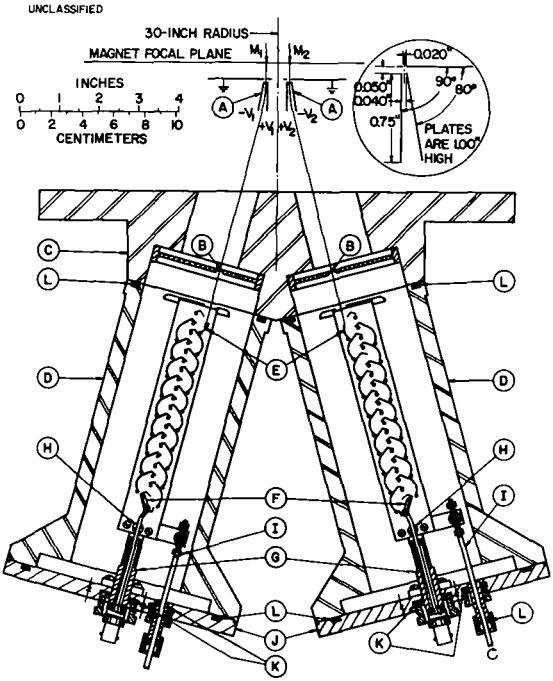

Fig. 7

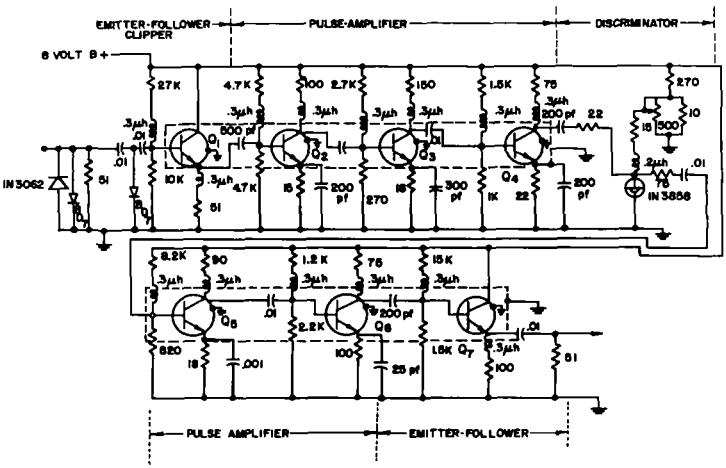

HIGH SPEED INTEGRAL DISCRIMINATOR WITH WIDE DYNAMIC RANGE

Fig. 8

KS-54368
UNCLASSIFIED

current is negligible compared with the anode current or can be calibrated accurately, then the ratio R_{12} of two primary ion currents, corrected for multiplier bias, defines a measured isotope ratio as given by Eq. (10),

$$R_{12} = \frac{I_1}{I_2}\frac{\alpha_2}{\alpha_1}\frac{1 - \exp\left[\alpha_2(b-1)\right]}{1 - \exp\left[\alpha_1(b-1)\right]}, \tag{10}$$

where I_1 and I_2, respectively, are the observed anode currents for isotopes 1 and 2. From Eq. (10) we can conclude that detection bias in an isotope ratio measurement is considerably less than that in either of the two separate ion current measurements used in forming the ratio. For example, if β is 2.5, b converges to 0.11 after 6 stages; and if α_1 and α_2 are large, say 6 or more, then the detection efficiency for each ion beam is nearly unity and Eq. (10) reduces to the expression $R_{12} = I_1\alpha_2/I_2\alpha_1$. For this case the bias correction factor is the ratio of the first stage gains, α_2/α_1.

In the pulse-counting mode, the anode current of electron pulses undergoes electronic amplification, then is passed into a pulse-height discriminator and pulse shaper where all pulses above a threshold voltage are accepted for pulse counting in a high speed electronic scaler. A definite fraction of the total number of pulses always is below the discriminator threshold voltage and is not counted. Therefore, current-measurement bias may be defined as the total fraction of these events (single ions) which is not counted. The detection efficiency for pulse counting an ion beam is given by the multiplier efficiency minus the discriminator losses, i.e.

$$\text{DETECTION EFFICIENCY} = 1 - G_K(0) - \sum_{n=1}^{m} P_K(n),$$

where m is the number of electrons necessary to produce a voltage pulse with an amplitude equal to the discriminator threshold voltage. Detection efficiency will depend on such things as the amplitude distribution of pulse heights, whether or not a coaxial transmission line joins the anode to any external electronic circuitry, and the amount of electronic amplification used between the multiplier and pulse-height discriminator.

In practice, pulse-counting background is negligible and can be calibrated when necessary. Therefore, an isotope ratio R_{12} defined as the ratio of two pulse-counting rates is given by the expression,

$$R_{12} = \frac{p_1}{p_2}\frac{1 - G_{K2}(0) - \sum_{n=1}^{m} P_{K2}(n)}{1 - G_{K1}(0) - \sum_{n=1}^{m} P_{K1}(n)}, \tag{11}$$

where p_1 and p_2, respectively, are observed pulse-counting rates for isotopes 1 and 2, and the other terms have been defined. In the pulse-counting system described here, amplified pulses can be made sufficiently high and the discriminator threshold voltage sufficiently low so that more than 99% of all

pulse heights exceed the threshold voltage. For small mass differences, the summation terms are negligible and can be ignored. If α_1 and α_2 are approximately 6 and β is 2.5, then detection efficiency is close to unity and Eq. (11) reduces to the expression $R_{12} = p_1/p_2$. Obviously, this result is not valid in an experimental situation where α is only 1 or 2, or when a large fraction of the pulses are not counted.

Because $P_K(n)$ is a sensitive function of α, the fraction of pulses below the discriminator threshold can be expected to change as shown in Fig. 3. Here 1.0% and 0.9% of the distributions with α's of 7.9 and 8.3, respectively, are below the discriminator threshold and hence are not counted. Therefore, a 5% difference in first stage gain would result in approximately 0.1% detection bias, even when 99% of the pulses are counted. This bias is represented by the area between the two pulse-height distributions and the discriminator threshold. Corresponding detection bias for the dc mode would be 5%.

It is apparent that a high first stage gain and a high overall multiplier gain are essential in obtaining an efficient electron multiplier pulse-counting system which is insensitive to fluctuations in gain. In either the dc or pulse-counting modes of operation, multiplier efficiency places an upper limit on the fraction of an ion current which can be detected, but in a given experimental situation it is possible to make suitable corrections for current-measurement bias.

ELECTRON MULTIPLIER DESIGN AND OPERATING CHARACTERISTICS

Precision isotope ratio measurements impose very stringent requirements on the basic design and performance of an electron multiplier, particularly in the simultaneous measurement of two ion beams. These limitations can be minimized by paying attention to details of multiplier design which are of special importance in mass spectrometry.

The first stage is the crucial region in an electron multiplier which is used for pulse counting. We have achieved high secondary electron yields which are stable over long periods of time by using Al_2O_3 as the activated surface of the first dynode. Yields average 7-8 secondary electrons for a 20 KV monatomic positive ion striking the first dynode at about 50° incidence to the surface. In a manner similar to Daly's technique(8), aluminum is vacuum deposited onto a polished stainless steel first dynode. Then it is assembled between mica insulating slabs, along with the remaining BeOu dynodes and the anode grid. A prototype multiplier is shown in Fig. 4. The entire structure is activated at approximately 630°C in a low partial pressure of oxygen. It is then sealed and stored in the quartz tube in which it was activated. After activation the aluminized surface has a dull finish. All dynodes are 1.5-in long so that end effects in the electric fields between dynodes are unimportant, especially in the first few stages. The combination of high yield, close dynode spacing, and good electron optics between first and second dynodes insures a high first stage gain. An important secondary benefit of high first stage gain is that almost all noise pulses, especially those initiated by single electrons emitted thermionically at room temperature from the first or second dynodes, are below the threshold of the pulse-height discriminator.

The electron multiplying stages and collector region are similar to a design reported by Pietri(9) for the 56 AVP photomultiplier. Details of an electrostatic field plot and ray tracing are shown in Fig. 5. Double electrostatic shielding of the first dynode surface insures isolation of the first stage from external stray electric fields. Focusing in the first and second stages is optimized by adjusting the potential on the focus rod, which shapes the electric field and increases its intensity to provide a downward deflecting force on the secondary electrons as they pass by the outer edge of the third dynode. Maximum dc anode current corresponds to maximum peaking in the pulse-height distribution. When interdynode voltages exceed 220 v/stage, electron-optical transmission between adjacent dynodes is high; in the first stage it is approximately unity. Ray paths on either side of the two principal rays, which are perpendicular to the first dynode surface, are calculated for 5v initial energy in a direction tangent to the surface at the point of emission.

Operating characteristics of the new multiplier are as follows. The aluminized first stage and nineteen additional stages of amplification with activated 2% Be, 98% Cu dynodes produce current gains exceeding 10^9 electrons/incident ion, at inter-dynode voltages of 250-300 v. Even though activated BeCu dynodes have low photosensitivity, care must be exercised in shielding a multiplier from the uv discharge of a sputter-ion pump. The 20-stage multiplier can provide much more gain than is needed initially, but as it ages, inter-stage voltage must be increased periodically to maintain the operating gain at 1×10^8, approximately. All dynode resistors are mounted outside the vacuum system. Complete magnetic shielding is provided by a hollow circular cylinder of Armco iron which surrounds the multiplier. A special 50 ohm coaxial connector was designed for high vacuum use. It transmits anode pulses to solid state electronic circuits outside the high vacuum. Pulse width at the rf connector is less than 5 nsec, and average anode pulses are about 200 mv high for the condition of equal inter-dynode voltages, a 50 ohm terminating resistor, and an average current gain of 1×10^8. At this gain, overall detection efficiency of the multiplier and counting system exceeds 95%, typical background pulse-counting rates at room temperature are less than 1 count/min, and typical anode dark currents are less than 10^{-12} amp dc. Low dark current and operating life of a multiplier depend at least partly on continuously maintaining a high vacuum of 10^{-8} Torr between dynodes. This is accomplished with sputter-ion pumps.

First dynode yields at 20 kv impact energy were measured as 7-8 secondary electrons/incident ion for the monatomic ions Rb^+, Ba^+, and U^+. For the polyatomic ion $Na_2BO_2^+$ at mass position 89 it is approximately 16 electrons/incident ion with 20 kv energy. The yield measurements were determined under actual operating conditions by using a battery-operated electrometer to measure the ion current incident on the first dynode. The first dynode was made a Faraday collector with the surrounding dynodes and focus rods acting as secondary electron repellers.

SUPPORTING DATA FOR POISSON STATISTICS

The statistical analysis of secondary electron multiplication suggests two kinds of experiments to test its validity. In the first experiment, predicted pulse-height distributions are compared with distributions observed on a multi-channel pulse-height analyzer. In the second experiment, the probability of producing zero electrons at the multiplier anode is measured in terms of multiplier efficiency, which can be determined from the ratio of the anode pulse-counting rate to the dc ion current striking the first dynode.

Pulse-height analysis was made with a 512-channel transistorized pulse-height analyzer. Pulse-height distributions obtained for Ba^{138+} are shown in Fig. 6. Above 1×10^9 gain, pulse amplitudes are progressively attenuated in going from small to large pulses. Apparently the yield properties of the dynode surfaces limit the maximum number of electrons in a pulse. For the defocused condition, the secondary electrons from the first dynode are allowed to strike the second dynode above the center of its circular arc. As the optical transmission deterioriates, the pulse-height distribution changes from a sharply peaked one to a quasi-exponential distribution, even though the gain does not change markedly.

The number of low amplitude pulses is very sensitive to inter-dynode focusing. From the statistics, one can see that a low optical transmission, especially in the first few stages, reduces the gain and increases the probability of occurance of small pulses. Other factors probably are important too.

At comparable average current gains for the electron multiplier, pulse-height distributions obtained for the $Na_2BO_2^+$ ion are approximately the same as those obtained for barium, even though the compound ion has a secondary electron yield which is twice that of the monatomic ion.

A combination of linear and geometrical voltage division was tried. Inter-dynode voltages of the first three stages were made 1.8 times as high as the last 11 stages; intermediate voltages were reduced by 10%/stage. Because this combination was not significantly better than a linear one, the linear distribution was chosen for its simplicity and ease of interpretation.

Multiplier efficiency was measured for Ba^{138+} at an observed average random pulse-counting rate of 2 Mc/sec and was corrected for counting losses and for the fraction of pulses below the discriminator threshold. The discriminator output was fed into a 200 Mc/sec solid state scaler. Multiplier gain was reduced to about 4×10^7 so that the anode current could be kept below 15 μamp dc. Counting losses were 2%, since the dead time of the counting ststem is 10 nsec. The fraction of pulses below the discriminator threshold of 10 mv was determined from integral-bias curves of counting rate vs discriminator setting. This correction was less than 10% with an uncertainty of about 1%. With the measured values of $\alpha = 7.0$ and $\beta = 2.5$, multiplier efficiency should be about 99.8%. The measured value was unity, within the calibration error of a few percent of the electrometer. More work will be done on this measurement to extend it to lower values of first stage gain.

SIMULTANEOUS DETECTION

A scheme for pulse-counting two ion beams simultaneously is shown in Fig. 7. It is mounted on a large 30-in radius double-focusing Dempster type mass spectrometer which was described at this meeting two years ago(10). Data for this paper were obtained from either multiplier operated singly. The simultaneous pulse-counting scheme will be evaluated after the completion of this experiment on the statistics of electron multipliers used as ion detectors.

SOLID STATE ELECTRONICS

A solid state discriminator and pulse-shaping system was designed and constructed by F. H. Sawada(11) at KAPL. It has a resolving time of less than 10 nsec. A schematic diagram of the electronics for the prototype system is shown in Fig. 8.

Output pulses from the electron multiplier are randomly distributed in amplitude and in time. The function of the discriminator/pulse amplifier circuit is to transform random pulse heights into standardized output pulses of constant amplitude and shape, so that they can be counted accurately by a high speed scaler. The discriminator/pulse amplifier will accept a dynamic range of pulse amplitudes which vary by more than 100:1. Input sensitivity of the discriminator is 10 mv and output pulse height is 2 v, approximately. Standard 50 ohm high frequency techniques are used throughout the detection system.

The discriminator works as follows. A pulse with negative input polarity enters the emitter-follower first stage. The larger the negative signal amplitude in, the closer the NPN transistor approaches cutoff. This limits the amplitudes of pulses above 40 mv by providing a non-linear clipping action. The pulses undergo linear amplification in three pulse-amplifier stages ahead of the tunnel diode discriminator. Two additional stages of pulse amplification after the tunnel diode bring the standardized signal level up to about 2.5 v. The emitter-follower output stage matches the output impedence to that of the high speed scaler input.

A photograph of a prototype discriminator is shown in Fig. 9. The transistors are imbeded in a circular brass strip of approximately 1/4-in cross sectional area. The strip is an electrostatic shield and ground which isolates the active electronic elements from each other. It also is an effective heat sink. The discriminator is designed to mount on standoff supports from the multiplier flange.

Even though the overall dead time of the entire counting system is 10 nsec, random pulse-counting rates of 100 Mc/sec are never used with this counting system. A system which counts pulses that are randomly distributed in time will jam and stop counting long before the average random counting rate has reached the maximum value implied by the reciprocal of the dead time. In the counting system described here, the maximum useful counting rate is about 2 Mc/sec, for which the corresponding counting loss is 2%. The main value of a high speed counting system is that it improves the statistical accuracy of measuring small ion currents by allowing more counts to be detected in a given operating time. It also improves the accuracy of counting loss corrections to observed counting rates. A further reason for keeping the maximum average counting rate below 2 Mc/sec is that multiplier life is shortened by drawing too much anode current. Based on our results with the new multiplier, we are limiting the maximum continuous anode current to 10 μamp dc. This is determined as average current gain of the multiplier x average rate at which ions strike the first dynode x electronic charge.

In closing, I wish to acknowledge that I am greatly indebted to the following people for their dedicated support throughout this experiment: J. H. Thomas contributed many useful suggestions about reducing the multiplier design to practice and made several prototype electron multipliers; J. R. Schmid and T. A. McGovern developed the computer program for calculating probability coefficients; F. H. Sawada designed and developed the solid state discriminator/pulse amplifier; J. A. Leathem and J. C. Sheffield helped in the pulse-height analysis; and L. R. Hanrahan, G. A. Land, and A. B. Hance helped construct the dual counting system.

REFERENCES

(1) M. Bertolaccini and S. Cova, Energia Nucleare, 10, 259 (1963).

(2) M. Brault and C. Gazier, Compt. rend. 256, 1241 (1963).

(3) L. G. Hyman, R. M. Schwarcz, and R. A Schulter, Rev. Sci. Instr. 35, 393 (1964).

(4) F. A. White and T. L. Collins, Appl. Spectroscopy 8 No. 1, 17 (1954).

(5) W. Feller, An Introduction to Probability Theory and Its Applications (John Wiley & Sons, Inc., New York, 1957), 2nd ed., Chap XI XII.

(6) F. J. Lombard and F. Martin, Rev. Sci. Instr. 32, 200 (1961).

(7) J. A. McHugh and J. C. Sheffield, J. Appl. Phys. 35, 512 (1964).

(8) N. R. Daly, Rev. Sci. Instr. 31, 264 (1960).

(9) G. Pietri, IEEE Trans. on Nucl. Sci. NS-9, 62 (1962).

(10) L. A. Dietz, Annual Meeting of ASTM Committee E-14 on Mass Spectrometry, New Orleans, Louisiana (June, 1962).

(11) F. H. Sawada, Knolls Atomic Power Laboratory, to be published.

In Fig. 8, transistors Q_1 through Q_7 are either RCA 2N2857 or TI 2N2865; and backward diode BD7 is GE, 0.4 nsec switching time.

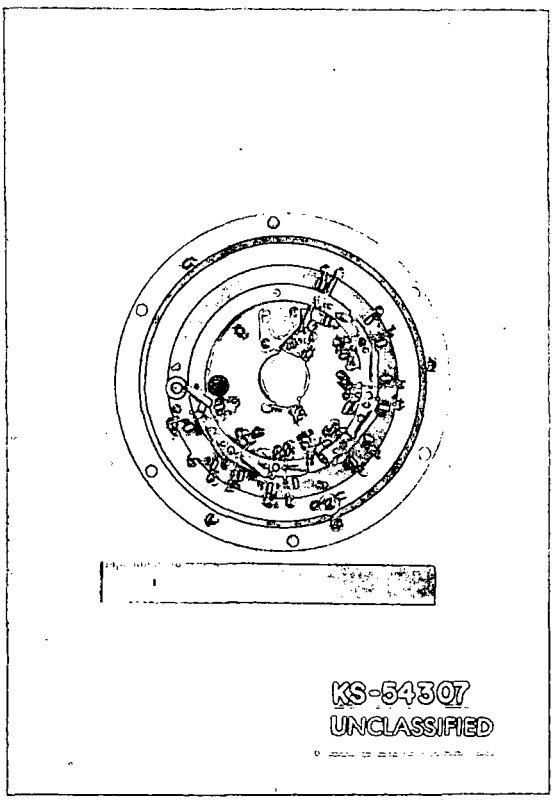

Fig. 9

THE APPLICATION OF THERMAL IMAGING TECHNIQUES TO MASS SPECTROMETRIC STUDIES OF HIGH TEMPERATURE CHEMISTRY

Richard P. Burns and Andrew J. Jason
Department of Physics
The University of Chicago
Chicago 37, Illinois

The radiation from a thermal source such as a stabilized electric arc has been imaged onto the surface of a solid sample in the vacuum system of a mass spectrometer in such a way that only the surface of the sample is at high temperature. In this way many undesirable reactions between the substance at high temperature and its environment have been minimized.

The application of a thermal imaging device in a mass spectrometric system will be discussed, and the approach used in the construction of the sample support, the vacuum system, the molecular beam defining apertures, and the ion source will be presented. A comparison of the relative merit of several ion sources will be given.

Experimental data illustrating studies of the rate of vaporization will include ionization efficiency curves, measurements of surface temperature, and the kinetic energy distribution of ions produced from atoms and molecules evaporating from the surface.

RECENT ATOMIC MASS DETERMINATIONS AT McMASTER UNIVERSITY*

by

R.C. Barber, H.E. Duckworth, B.G. Hogg, J.D. Macdougall,
W. McLatchie and P. Van Rookhuyzen

McMaster University
Hamilton, Ontario, Canada

In reporting the work being done at McMaster University, we shall first describe the large mass spectrometer and then present some recently obtained data in the rare earth region.

A. Description of the Mass Spectrometer

1. Geometry

The mass spectrometer employs a first-order direction-plus-velocity focusing arrangement consisting of a 90° radial electrostatic analyser followed by a 180° uniform magnetic field as indicated in Fig. 1. Both analysers are used symmetrically so that the magnification in each is unity, and the radii of curvature, r_e and r_m, are equal. The radii are approximately 9 ft. The total length of the ion path is approximately 47 ft.

The various slits indicated in the figure have the widths given and perform the following functions. S_1 and S_5 are the principal and collector slits, respectively. S_2 defines the angular extent of the ion beam such that the half angular spread, α, is 8×10^{-4} radians. S_3 is used to limit the height of the ion beam that enters the magnetic analyser. This ensures that the magnetic field encountered by the transmitted beam possesses adequate uniformity over the height of the beam. S_4 determines the range of energies which can be transmitted by the instrument.

The second order image aberrations are given by

$$y_B = r_m \left(B_{11}\alpha^2 + B_{12}\alpha\beta + B_{22}\beta^2\right)$$

where the symbols are those used by Hintenberger and König[1]. The coefficients have the values

$$B_{11} = 0.702, \quad B_{12} = -0.365, \quad B_{22} = -2.12.$$

Thus, although the instrument possesses no second-order focusing, the aberrations corresponding to the second order terms are unusually small. Indeed, the combined effect of the $\alpha\beta$ and β^2 terms appears to be even smaller than in the several instruments that provide partial second-order direction focusing (that is, $B_{11} = 0$).

2. Ion Source

The source which has been used to date is a conventional electron bombardment source, fitted with either a gas leak or some suitable form of oven. The source potential ($\sim$30 kV) is derived from a commercial unit (Beta Electric type 2069) and has a short term stability of one part in 30,000. It has been found, by decreasing the width of S_4, that the energy spread amongst the ions emerging from the source is less than 3 volts, corresponding to $\beta < 5 \times 10^{-5}$.

3. Electrostatic Analyser

Each of the two plates of the cylindrical condenser consists of eleven gold-plated iron blocks which are carefully fitted together to form an accurate, continuous surface. Each block is supported by three 0.625 in. thick alumina insulators which rest in turn on the steel base plate. The surfaces between which the field is established were positioned relative to the inner edge of the base plate so that the gap was 1.000 ± 0.003 in. The plates are 4.0 in. high and roughly 3 in. thick. Grounded diaphragms, positioned in accordance with Herzog's theory[2], terminate the electric field at the physical boundaries of the condenser.

* This work was supported by the U.S. Air Force through the Air Force Office of Scientific Research of the Air Research and Development Command, and by the National Research Council of Canada.

Three ball bearing supports provide for easy movement of the analyser about the point at which the ions enter the magnetic field. This arrangement makes it possible to vary the angle of entry, ϵ_m', to the magnetic field without altering any of the parameters of the electrostatic analyser.

4. Magnetic Analyser

The 180° magnetic field consists of 28 equal angle sectors, each of which is in itself, a "C" electromagnet. The pole pieces are 7.0 in. wide and have a nominal separation of 0.810 in. The field strength may be adjusted from sector to sector by means of trimming rheostats in series with each coil. The variation of the field within a given sector may be adjusted by tilting the upper pole piece of the sector.

A numerical calculation[3] was performed to determine the effect of non-uniformities on the focusing properties of the magnet. The non-uniformities considered were those in which the field varies along the ion path, and those in which it varies radially.

It was found that random variations of 1% from sector to sector would not destroy the double focus although its position might be shifted slightly. However, radial variations in the field of the order of 0.02% per in. could shift the direction and velocity foci by differing amounts so that a double focus would not be formed.

In our instrument, the velocity focus is most sensitive to radial non-uniformities in the region of 45° from the entrance boundary while the direction focus is most sensitive to those in the region of 90° from the entrance boundary. During the initial focusing it was necessary to adjust certain of the magnet pole pieces accordingly.

A soft iron diaphragm was introduced at the entrance boundary of the magnetic field to reduce the extent of the fringing field. The fringing field was measured with a Hall generator and the effective boundary found to be 0.39 in. outside the physical boundary.

The magnet current is regulated by a combination D.C. plus A.C. amplifier circuit described by Garwin et al[4] and modified slightly for this application. Long term stability is about one part in 10^5 and appears to depend primarily on the stability of the reference voltage. The short term regulation is better than one part in 10^6.

5. Ion Detection

On passing through the collector slit, the ion beam is detected by a 14 stage Allen type electron multiplier with a gain of about 10^6. The multiplier output is amplified and viewed on an oscilloscope screen. When the sawtooth voltage from this oscilloscope is used to modulate the electrostatic analyser voltage, the ion beam is swept across the collector slit and a peak is seen on the oscilloscope screen.

6. Focusing Procedure

In the initial focusing, the principal slit was set at its theoretical position with respect to the electrostatic analyser. The distance between the electrostatic analyser and the magnet was also set at its theoretical value. With the electrostatic analyser thus set up, the value of ϵ_m' was varied in order to bring, in turn, the direction and velocity foci to the collector.

The velocity and direction foci are identified as follows. If, on every second sweep of the oscilloscope, the source potential is changed by 15 volts, lack of velocity focusing results in a peak being displaced with respect to itself. Coincidence occurs for some value of ϵ_m'. The direction focus is characterized by a very marked increase in the sharpness of the peaks as ϵ_m' passes through its optimum value. The relative positions of the two foci may be deduced from the geometry.

The next two figures show the peaks as they appear on the oscilloscope screen when these tests are carried out. In Fig. 2 the instrument is adjusted for direction focusing without velocity focusing. Alternate sweeps are displaced with respect to each other to facilitate viewing. In Fig. 3 the instrument is adjusted to give velocity focusing but not direction focusing.

When ϵ_m' is varied, the field necessary to bring ions to the same stage of the trace on the oscilloscope screen is a maximum for normal entry. If the final direction focus occurs at this same angle, this is an indication that the direction focus of the electrostatic analyser is formed at the entrance boundary of the magnetic field. Having thus established that the electrostatic analyser was focusing properly, the magnet pole pieces were adjusted in the manner described above to bring the two foci into coincidence.

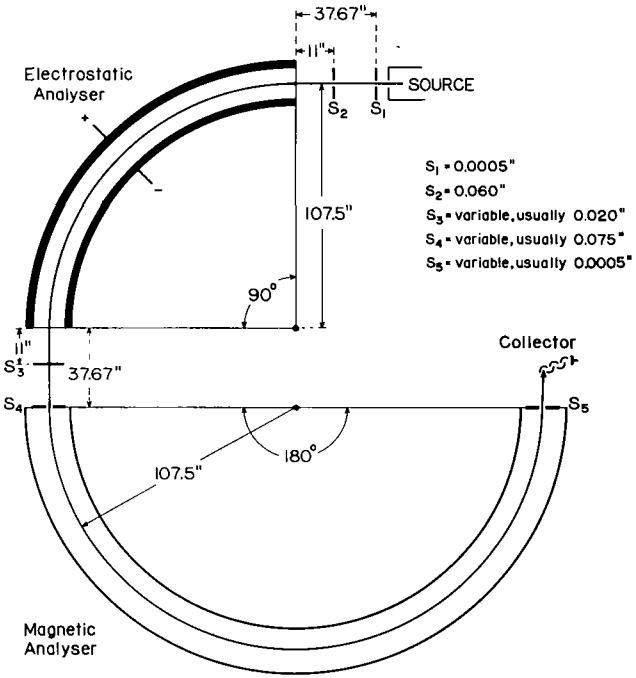
37.67"
11"
Electrostatic Analyser
SOURCE
S_2
S_1
S_1 = 0.0005"
S_2 = 0.060"
S_3 = variable, usually 0.020"
S_4 = variable, usually 0.075"
S_5 = variable, usually 0.0005"
107.5"
90°
11"
S_3
37.67"
Collector
S_4
S_5
180°
107.5"
Magnetic Analyser

Figure 1.

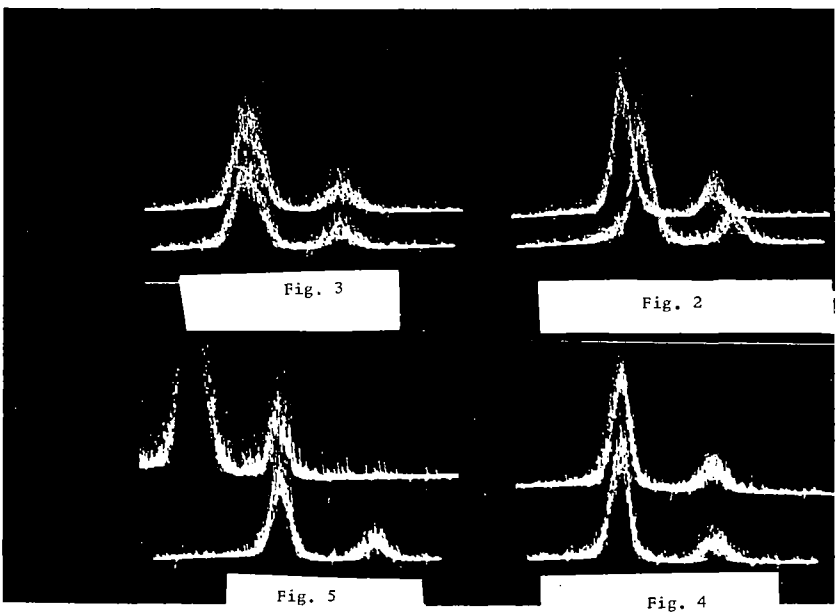
Fig. 3
Fig. 2
Fig. 5
Fig. 4

Thereafter, the routine focusing operation consists of varying ϵ_m' to determine the relative positions of direction and velocity foci, and then making any small adjustment of l_e' that is necessary to bring the direction and velocity foci into coincidence.

Fig. 4 shows the doublet of the previous figures after these adjustments have been completed. The mass separation of this doublet is 1/45,000, indicating that the resolution on this occasion was approximately 1/100,000. For this picture the width of the collector slit was equal to the width of the image. Among the doublets that have been previously reported[5], is one for which the separation is 1/126,000 and one for which the separation is only 1/130,000. In these cases it was necessary to have a resolution of about 1/200,000. This figure was attained regularly for the period needed by reducing the width of the collector slit. The actual resolution under these conditions still agreed with the theoretical value.

7. Peak Matching

The spacing of a doublet is measured in the following way. Let us suppose that, for a given magnetic field and electrostatic analyser voltage V, ions of mass M are arriving at the collector. If, then, on every second sweep of the oscilloscope, the voltage is changed an amount ΔV to $V + \Delta V$, a peak due to ions of mass $M - \Delta M$ will be brought to the same stage of the oscilloscope sweep. At the same time, the source potential must also be switched by an amount ΔV_a on alternate sweeps. The matching procedure is illustrated in Fig. 5. There are, of course, two ways of doing this: the lighter ion may be matched to the heavier one or vice versa.

When the doublet spacing is close, the error in measuring V is larger than the magnitude of ΔV. Accordingly the mass difference for either of these two cases is given by

$$\Delta M = \frac{\Delta V}{V} \cdot M$$

Considering the two methods of matching, the two directions of sweeping the ion beam, and the fact that one trace on the oscilloscope may be made to appear either above or below the other, we see that there are 8 possible matching situations. The 8 values so obtained constitute one "run" and the mean of these values is the value of the run. By adopting this procedure we believe that we have eliminated the possibility of significant errors arising in the switching mechanism or in the operator's judgment of the matched condition.

The electrostatic analyser voltage, V, is supplied by twelve 45 volt batteries which are stable to one part in 10^4 during a day and to better than one part in 10^6 over two or three minutes. A differential voltmeter is used to measure V with an accuracy of 0.03%. A potentiometer with an accuracy of 0.015% is used to measure ΔV.

8. Calculation of Errors

Twenty to thirty runs are made in order to determine a doublet spacing, and from these values the probable error is computed in the usual way. This probable error, which represents the reproducibility of the results, must then be combined with the errors in V and ΔV in order to arrive at the final probable error. It should be noted that this procedure treats the errors ascribed to the voltage measurements as if they were 50% confidence limits. We understand these values to represent limits of error rather than 50% confidence limits. Because of this, we should expect the final error associated with a doublet to be somewhat conservative.

9. Consistency of the Results

The probable error representing just the reproducibility of the results gives a measure of the inherent precision with which a mass difference may be determined with this instrument. Judging from the results over the past two years, we have found that a working value for this precision has been about one part in 10^8 of the mass at which the doublet occurs.

As we shall see later, further checks on the reliability of these measurements may be made by means of closed loops.

A further remark regarding the reliability of the doublet measurements should also be made. We have made extensive use of doublets which are peculiar in that the two members of the doublet are chemically identical (e.g. $Nd^{144}\ Cl^{35} - Nd^{142}\ Cl^{37}$). For such a doublet the two ion groups emerge from the source with the same distribution in angle and energy. The amount, ΔV_a, that the source potential should be changed in switching from one doublet member to the other is calculated from the doublet spacing and set accurately with a volt-

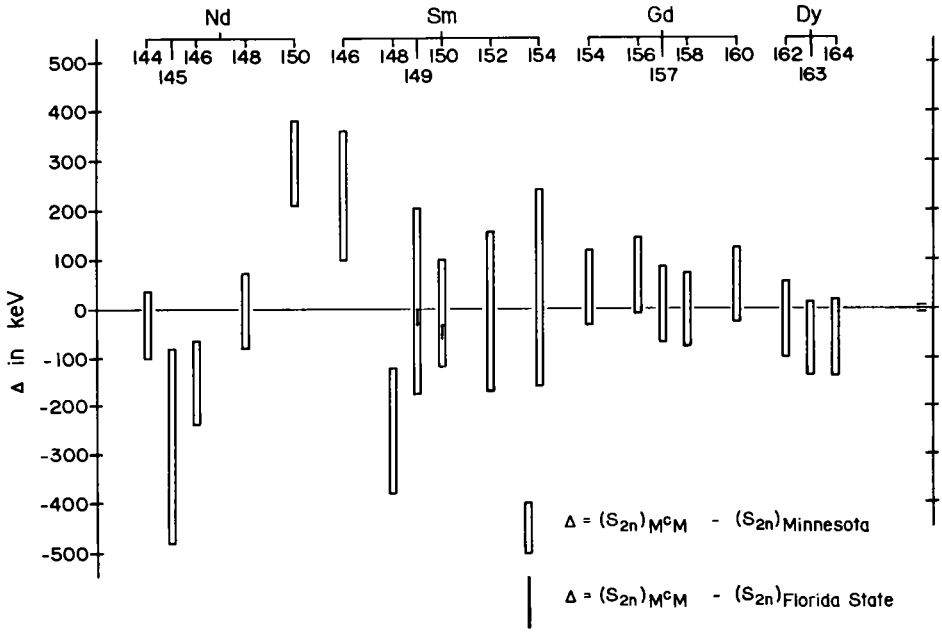
Nd
Sm
Gd
Dy
144 146 148 150
145
146 148 150 152 154
149
154 156 158 160
157
162 164
163
500
400
300
200
100
0
-100
-200
-300
-400
-500
Δ in keV
Δ = (S2n)MCM - (S2n)Minnesota
Δ = (S2n)MCM - (S2n)Florida State

Fig. 6

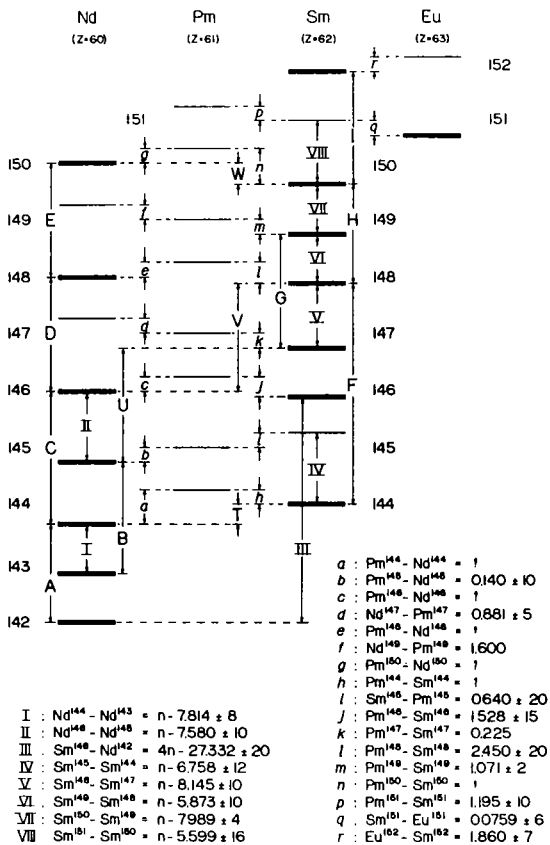
Nd
(Z=60)
Pm
(Z=61)
Sm
(Z=62)
Eu
(Z=63)
152
151
150
149
148
147
146
145
144
143
142
A
B
C
D
E
F
G
H
U
V
W
I
II
III
IV
V
VI
VII
VIII
a : Pm144 - Nd144 = 1
b : Pm145 - Nd145 = 0.140 ± 10
c : Pm146 - Nd146 = 1
d : Nd147 - Pm147 = 0.881 ± 5
e : Pm148 - Nd148 = 1
f : Nd149 - Pm149 = 1.600
g : Pm150 - Nd150 = 1
h : Pm144 - Sm144 = 1
i : Sm145 - Pm145 = 0.640 ± 20
j : Pm146 - Sm146 = 1.528 ± 15
k : Pm147 - Sm147 = 0.225
l : Pm148 - Sm148 = 2.450 ± 20
m : Pm149 - Sm149 = 1.071 ± 2
n : Pm150 - Sm150 = 1
p : Pm151 - Sm151 = 1.195 ± 10
q : Sm151 - Eu151 = 0.0759 ± 6
r : Eu152 - Sm152 = 1.860 ± 7
I : Nd144 - Nd143 = n - 7.814 ± 8
II : Nd146 - Nd145 = n - 7.580 ± 10
III : Sm148 - Nd142 = 4n - 27.332 ± 20
IV : Sm145 - Sm144 = n - 6.758 ± 12
V : Sm148 - Sm147 = n - 8.145 ± 10
VI : Sm149 - Sm148 = n - 5.873 ± 10
VII : Sm150 - Sm149 = n - 7.989 ± 4
VIII Sm151 - Sm150 = n - 5.599 ± 16

Fig. 7

meter. This procedure will eliminate the effect of second order terms on the doublet spacing. For this reason, results from this type of doublet should be particularly reliable.

In a doublet where the members are chemically dissimilar it may be that, for a given source potential, the two ion groups possess different energies after passing through the electrostatic analyser. This may be verified in our instrument because an intermediate direction focus is formed and because the energy resolving power of the electrostatic analyser is high. It has been confirmed that such an energy difference may occur and that it may be as large as 6 eV. Accordingly, when doublets of this type are studied, precautions are taken to ensure that this energy difference is always less than 1 eV.

B. Recent Results

During the past several months we have studied some 22 doublets involving stable nuclides in the mass region 142 to 164. This region is, of course, of particular interest since nuclei in the mass region from about 150 to 190 are known to be strongly deformed in the ground state. Such a nuclear deformation may be interpreted to imply the existence of a special bond between those nucleons acting co-operatively to produce the deformation in addition to the usual force by which they are bound to the nucleus as a whole. Hence the onset of this mode of collective motion should manifest itself as an increase in the nucleon binding energy.

Such an increase in the nucleon binding energy was first observed in 1953 by Hogg and Duckworth[6] when they plotted, against neutron number, differences between experimental masses and the semi-empirical masses of Metropolis and Reitweisner. Using experimental values with an accuracy of about 600 keV they observed a broad general increase in binding energy for nuclides with neutron numbers between 90 and 114.

Subsequently, in 1957, Johnson and Nier[7] obtained values accurate to 100 keV and showed the effect to be particularly pronounced at N = 90 in agreement with certain other facts (e.g. quadrupole moments, Coulomb excitation energy levels) that had emerged in the meantime from nuclear spectroscopy.

1. Experimental Results

In Table I we present the particular doublets which we have studied along with their spacings. The ions needed to form these doublets were produced by electron bombardment of the vapours of $NdCl_3$, $SmCl_3$, $GdCl_3$ and $DyCl_3$. Of these values, all except K carry errors smaller than 6 keV. The error associated with K is larger as it was necessarily the result of a relatively small number of measurements.

When these values are combined with the known value of the Cl^{37}-Cl^{35} mass difference (1961 Mass Table[8]), the mass differences between the corresponding rare earth nuclides are obtained. Most of these differences may then be expressed in the more convenient form (2n - Q) where n is the neutron mass and Q is the MeV. (For F we have 4n - Q). Then for all of the doublets down to S (except F) Q is S_{2n}, the double neutron binding energy, or the energy in MeV required to remove two neutrons from the heavier nuclide.

In passing, we note that the last 4 doublets provide cross-links between Nd and Sm. In particular T and W are of interest since they are the first direct determinations of the mass differences between pairs of stable isobars.

2. Double Neutron Separation Energies

Inasmuch as the primary data yield directly accurate S_{2n} values we shall emphasize this quantity in our discussion. The S_{2n} values derived directly from the primary data are compared with previous S_{2n} values in Fig. 6. We plot here differences between the new S_{2n} values and previous values from (a) mass spectroscopic work at the University of Minnesota[7,9,10] and (b) (d,p) Q-values from Florida State University[11]. We see that the agreement is fairly good although there are some important differences. Moreover, in 3 cases the errors are now reduced by factors of 3 to 5 while for the remainder the errors are reduced by factors ranging from 10 to 40.

By combining our new data with existing reaction and disintegration Q-values a number of additional S_{2n} values may be obtained. In Fig. 7 and Fig. 8 we show the ground state energies of the various nuclides indicated. Capital letters represent the mass differences given by our doublet values. Roman numerals give (n,γ)[12,13], (d,p)[11,14] and alpha-decay Q-values while the lower case letters indicate total β decay energies[16,17,18,19]. Then, as an example,

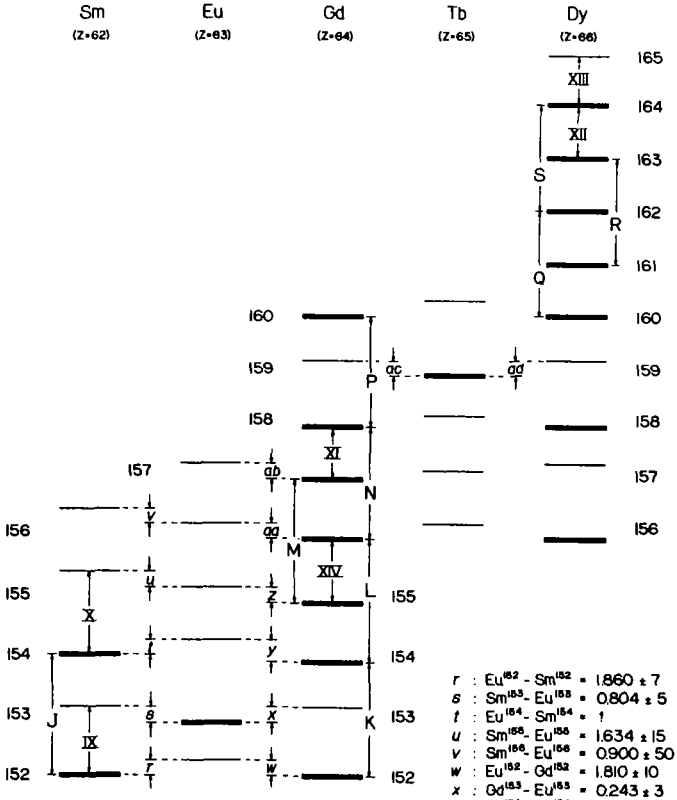
Sm (Z=62)
Eu (Z=63)
Gd (Z=64)
Tb (Z=65)
Dy (Z=66)
IX : Sm155 - Sm152 = n - 5.909 ± 12
X : Sm156 - Sm154 = n - 5.809 ± 12
XI Gd158 - Gd157 = n - 7.932 ± 4
XII : Dy164 - Dy163 = n - 7.659 ± 5
XIII : Dy165 - Dy164 = n - 5.639 ± 5
XIV. Gd156 - Gd155 = n - 8.531 ± 5
r : Eu152 - Sm152 = 1.860 ± 7
s : Sm153 - Eu153 = 0.804 ± 5
t : Eu154 - Sm154 = 1
u : Sm156 - Eu156 = 1.634 ± 15
v : Sm156 - Eu156 = 0.900 ± 50
w : Eu152 - Gd152 = 1.810 ± 10
x : Gd153 - Eu153 = 0.243 ± 3
y : Eu154 - Gd154 = 1.970 ± 20
z : Eu155 - Gd155 = 0.247 ± 3
aa : Eu156 - Gd156 = 2.430 ± 10
ab : Eu157 - Gd157 = 1.270 ± 50
ac : Gd159 - Tb159 = 0.947 ± 7
ad : Dy159 - Tb159 = 0.380 ± 20

Fig. 8

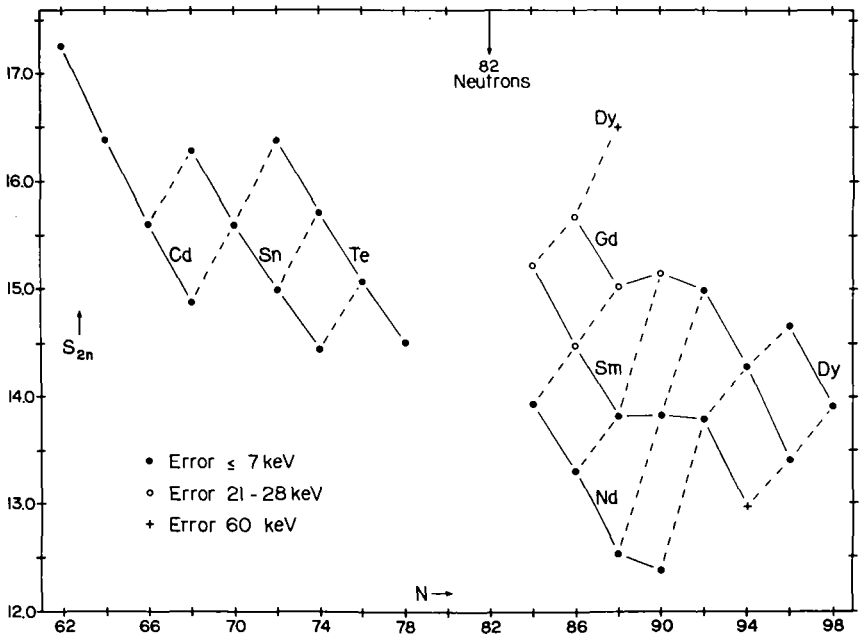
82 Neutrons
Cd
Sn
Te
Dy+
Gd
Sm
Nd
Dy
S2n
N→
• Error ≤ 7 keV
∘ Error 21 - 28 keV
+ Error 60 keV
17.0
16.0
15.0
14.0
13.0
12.0
62
66
70
74
78
82
86
90
94
98

Fig. 9

the S_{2n} value for Sm^{156} is calculated as follows:

$$Sm^{156} - Sm^{154} = 2n - S_{2n} = t - y + L + aa + v$$

In Fig. 9 we show the new S_{2n} values plotted as a function of N (where N is even) along with some previously-published values for a number of even-even isotopes of Cd, Sn and Te. The solid curves join points belonging to the same element. The dotted lines join nuclides with the same difference between neutron number and proton number (N - Z) -- i.e. they are isodiapheric curves. The solid curves for Cd, Sn and Te are strikingly regular as are the corresponding curves for Nd and Sm in region N = 84 to 88. In addition, their slopes are not unlike those for Cd, Sn and Te, especially if one allows for the fact that such curves immediately following a closed shell (82) slope more steeply than those immediately preceeding one. Further, the two points for Gd suggest that its curve in this region is also more or less normal.

But at N = 88 the Sm and Gd curves undergo a dramatic change, corresponding to the onset of nuclear deformation. Similarly a marked, although smaller, effect is present in Nd.

We also see from the Sm and Gd curves that the dislocation corresponding to the onset of collective motion extends for a range of 4 neutrons, after which essentially "normal" behaviour resumes. An extrapolation of the Dy curve to lower neutron numbers is also consistent with the hypothesis that any dislocation in that curve also terminates at N = 92. The curves for Sm, Gd and Dy are again virtually parallel in the region beyond N = 92.

The isodiapheric curves also undergo a marked change in slope at N = 88. In the region N = 88 to 92 the three lines shown are parallel. For N greater than 92 the curves are again roughly parallel and have about the same slope as those for N less than 88.

New S_{2n} values for odd N are plotted similarly in Fig. 10. Again we show the even-N curves for Cd, Sn and Te. The odd-N points for these elements fall almost exactly on these curves. In both Nd and Sm the points for N = 89 are higher than would be expected from "normal" behaviour. Although fewer points are available, the effect is again shown in Sm and, in both Sm and Gd, we see that normal behaviour is nearly resumed at N = 93.

It then appears that, for even N, the effect is confined to the region N = 88 to 92, suggesting that the nuclear distortion exhibited by nuclei in this region of the mass table is established during the addition of the 89th, 90th, 91st and 92nd neutrons.

3. Single Neutron Separation Energies

The new data may also be used with the reaction and disintegration data to derive single neutron separation energies. These are plotted in Fig. 11 as a function of neutron number. Within a given element these curves naturally divide into two groups depending on whether N is even or odd. Accordingly, points for a given element for either even-N or odd-N are connected.

We see again the mass effect as N exceeds 88 although it is less obvious in these curves. The effect is again seen to be larger for Sm than for Nd. The even-N curves indicate the resumption of "normal" behaviour as N exceeds 92. However, the odd-N curves seem to indicate that "normal" behaviour may not be fully resumed with the addition of the 93rd neutron.

4. Neutron Pairing Energies

The pairing energy associated with the last pair of neutrons in a nucleus with even neutron number is

$$P_n = S_n\ (Z,N) - S_n\ (Z,N - 1),\ N \text{ even.}$$

The pairing energies deduced from the new S_n values are shown in Fig. 12 plotted as a function of N.

These new values confirm the marked increase in the neutron pairing energy about N = 90 observed in the earlier mass spectroscopic work of Johnson and Nier[7], although the new values differ somewhat. The increase in pairing energy is largest in Sm, but is also marked in Nd and Gd. The Dy curve, which does not extend as far as N = 90, seems to follow the same trend as the other curves.

From these curves we see that the marked changes in the S_{2n} -versus-even-N curves in the region N = 88 to 92 do not simply reflect a change in the pairing energy of the last pair of neutrons. If this were the case, (1) the curves for the pairing energies of Sm and Gd would have to be similar and (2) the values for the pairing energies for N = 92 would have to be approximately the same as those for N = 90.

TABLE I

Mass Differences in Rare Earth Region (on scale C^{12} = 12u)

	Doublet	Spacing in u
A.	$Nd^{144}Cl^{35}$ - $Nd^{142}Cl^{37}$	5329 ± 3
B.	$Nd^{145}Cl^{35}$ - $Nd^{143}Cl^{37}$	5744 ± 5
C.	$Nd^{146}Cl^{35}$ - $Nd^{144}Cl^{37}$	6003 ± 3
D.	$Nd^{148}Cl^{35}$ - $Nd^{146}Cl^{37}$	6740 ± 4
E.	$Nd^{150}Cl^{35}$ - $Nd^{148}Cl^{37}$	7006 ± 5
F.	$Sm^{148}Cl^{35}_2$ - $Sm^{144}Cl^{37}_2$	8710 ± 5
G.	$Sm^{149}Cl^{35}$ - $Sm^{147}Cl^{37}$	5257 ± 4
H.	$Sm^{150}Cl^{35}$ - $Sm^{148}Cl^{37}$	5452 ± 4
I.	$Sm^{152}Cl^{35}$ - $Sm^{150}Cl^{37}$	5429 ± 4
J.	$Sm^{154}Cl^{35}$ - $Sm^{152}Cl^{37}$	5479 ± 3
K.	$Gd^{154}Cl^{35}$ - $Gd^{152}Cl^{37}$	4016 ± 30
L.	$Gd^{156}Cl^{35}$ - $Gd^{154}Cl^{37}$	4199 ± 4
M.	$Gd^{157}Cl^{35}$ - $Gd^{155}Cl^{37}$	4316 ± 4
N.	$Gd^{158}Cl^{35}$ - $Gd^{156}Cl^{37}$	4956 ± 4
P.	$Gd^{160}Cl^{35}$ - $Gd^{158}Cl^{37}$	5890 ± 5
Q.	$Dy^{162}Cl^{35}$ - $Dy^{160}Cl^{37}$	4555 ± 6
R.	$Dy^{163}Cl^{35}$ - $Dy^{161}Cl^{37}$	4758 ± 3
S.	$Dy^{164}Cl^{35}$ - $Dy^{162}Cl^{37}$	5347 ± 5
T.	Sm^{144} - Nd^{144}	1951 ± 3
U.	$Sm^{147}Cl^{35}$ - $Nd^{145}Cl^{37}$	5305 ± 4
V.	$Sm^{148}Cl^{35}$ - $Nd^{146}Cl^{37}$	4656 ± 3
W.	Nd^{150} - Sm^{150}	3633 ± 4

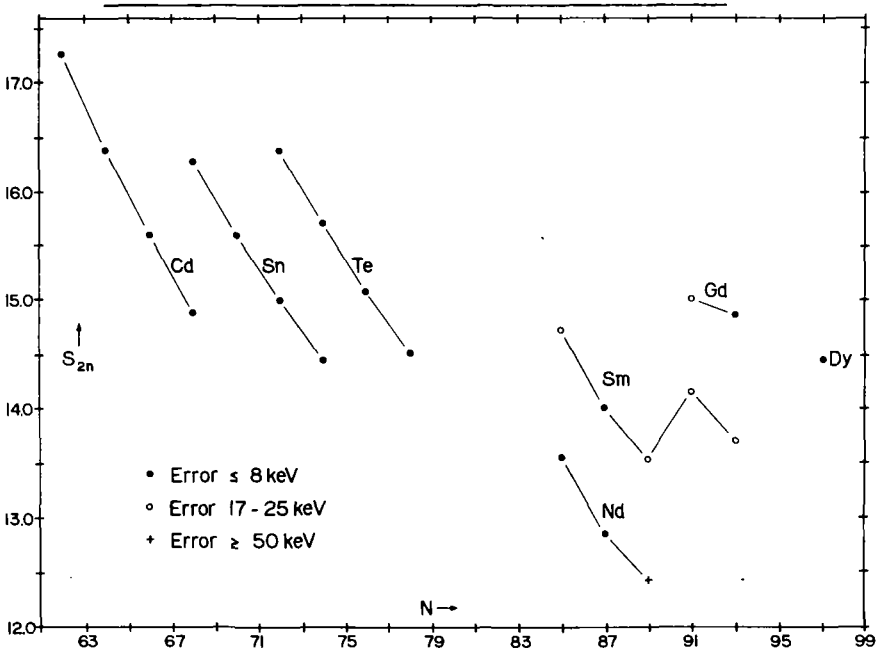

Fig. 10

5. Direct Determinations of the Sm^{144}-Nd^{144} and Nd^{150}-Sm^{150} Energy Differences

As was pointed out earlier, two of the primary data are direct determinations of the energy differences between pairs of stable isobars.

In Fig. 13 we show the decays at 144 and at 150 together with what is known concerning the total decay energies of the intermediate isobars Pm^{144} and Pm^{150}.

The total energy available for the Pm^{144}-Nd^{144} decay has never been determined, although it is known that it must exceed 1.78 MeV. Beta decay systematics suggest that it has the value 2.6 ± 3 MeV, in which case our result would indicate 0.8 ± 3 MeV is available for the unobserved Pm^{144}-Sm^{144} decay.

The decay of Pm^{150} has been the subject of a good deal of study, prompted in part by curiosity as to the stability or instability of Nd^{150}. As shown here, the currently accepted value of the Pm^{150}-Sm^{150} decay energy is 3.43 ± 6 MeV, based on two measurements[20,21]. This unfortunately leads to a value 46 ± 60 keV for the Pm^{150}-Nd^{150}energy difference so that the question regarding the stability of Nd^{150} remains. It is hoped that a more accurate value for the Pm^{150}-Sm^{150} decay will resolve this problem.

6. Closed Loop Calculations

Referring to Fig. 7 we see that we can form a closed loop involving only the new data, viz.

$$C + D + E - W - H - F - T = 0 \qquad (1)$$

Here as in some other cases the Cl^{37}- Cl^{35} mass difference drops out of the calculation. Substituting the measured values into (1) we obtain the value + 3 ± 10 keV.

Using V we see that the two halves of this loop also close independently:

$$\text{Upper half:} \quad D + E - W - H - V = 5 \pm 9 \text{ keV} \qquad (2)$$

$$\text{Lower half:} \quad C + V - F - T = -2 \pm 7 \text{ keV} \qquad (3)$$

The data I and II are accurate (n, γ) values from the Chalk River laboratory[12] and may be used in a small closed loop, namely:

$$I + C - II - B = +8 \pm 14 \text{ keV} \qquad (4)$$

A loop involving the most accurate of the (d,p) Q-values from Florida State University[11] and one of the Chalk River values[12] is as follows:

$$I + C + D + E - W - VII - G - U - B = -1 \pm 14 \text{ keV} \qquad (5)$$

Finally, referring to Fig. 8 we see that a small closed loop may be formed as follows:

$$M + XI - N - XIV = +3 \pm 10 \text{ keV} \qquad (6)$$

Summary

1. The mass effect associated with the onset of nuclear deformation begins suddenly as N exceeds 88 neutrons.
2. The magnitude of the mass effect depends on Z, being large for Sm (Z = 62) and Gd (Z = 64), but smaller for Nd (Z = 60).
3. The S_n and S_{2n} curves for even-N indicate that nuclear deformation is established during the addition of the 89th, 90th, 91st and 92nd neutrons. The corresponding curves for odd-N show that the effect may extend beyond N = 92.
4. The new results are shown to be internally consistent to the extent to which they may be tested.

References

1. H. Hintenberger and L. A. König, Advances in Mass Spectrometry, Edited by J. D. Waldron, p.16, London: Pergamon Press, 1959.
2. R. Herzog, Z. Phys., 97, 596 (1935).
3. L. A. Cambey, J. H. Ormrod and R. C. Barber, Can. J. Phys. 42, 103 (1964).
4. R. L. Garwin, D. Hutchinson, S. Penman and G. Shapiro, Rev. Sci. Instr. 40, 105 (1959).
5. R. C. Barber, R. L. Bishop, L. A. Cambey, H. E. Duckworth, J. D. Macdougall, W. McLatchie, J. H. Ormrod and P. Van Rookhuyzen, Proceedings of the Second International Conference on Nuclidic Masses, Edited by W. H. Johnson, p.251. Vienna: Springer Verlag, 1964.
6. B.G. Hogg and H. E. Duckworth, Phys. Rev. 91, 1289 (1953).
7. W. H. Johnson and A. O. Nier, Phys. Rev. 105, 1014 (1957).

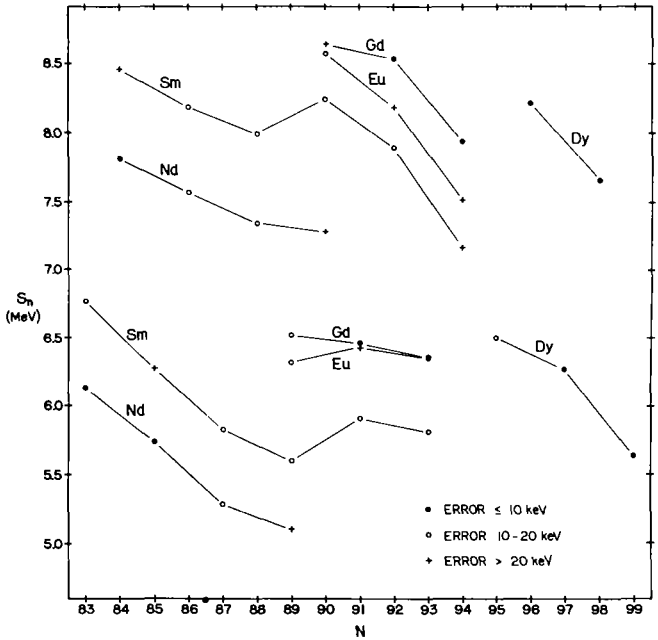
Sm
Nd
Gd
Eu
Dy
Sm
Nd
Gd
Eu
Dy
S_n (MeV)
N
• ERROR ≤ 10 keV
○ ERROR 10-20 keV
+ ERROR > 20 keV

Fig. 11

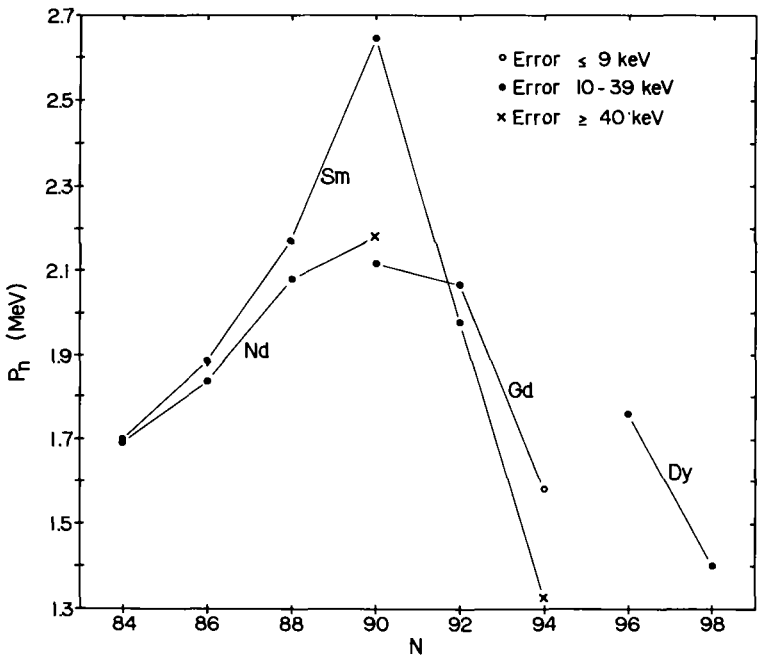
○ Error ≤ 9 keV
• Error 10-39 keV
× Error ≥ 40 keV
Sm
Nd
Gd
Dy
P_n (MeV)
N

Fig. 12

8. L. A. König, J. H. E. Mattauch and A. H. Wapstra, Nuc. Phys. 31, 18 (1962).
9. W. H. Johnson and V. B. Bhanot, Phys. Rev. 107, 1669 (1957).
10. V. B. Bhanot, W. H. Johnson and A. O. Nier, Phys. Rev. 120, 235 (1960).
11. R. A. Kenefick and R. K. Sheline, private communication.
12. L. A. König, J. H. E. Mattauch and A. H. Wapstra, Nuc. Phys. 28, 1 (1961).
13. W. N. Shelton and R. K. Sheline, private communication.
14. L. V. Groshev, A. M. Demidov, V. A. Ivanov, V. N. Lutsenko and V. I. Pelekov, Doklady Akad. Nauk SSSR. 141, 59 (1961).
15. A. Siivola, private communication.
16. Nuclear Data Sheets, Edited by Katharine Way (National Academy of Sciences, National Research Council, Washington 25, D.C.) (1959-64).
17. R. P. Sharma, S. H. Devare and B. Saraf, Phys. Rev. 125, 2071 (1962).
18. E. G. Funk, J. W. Mihelich and C. F. Schwerdtfeger, Phys. Rev. 120, 1781 (1960).
19. G. T. Ewan, R. L. Graham and J. S. Geiger, Nuc. Phys. 29, 153 (1962).
20. N. B. Gove and G. D. O'Kelley, private communication to the Nuclear Data Group.
21. V. K. Fischer and E. A. Remler, Bull. Amer. Phys. Soc. 3, No. 1, 63 (1952) and private communication to the Nuclear Data Group.

Figure Captions

Fig. 1. Geometry of the mass spectrometer.
Fig. 2. Focusing test -- direction focus only.
Fig. 3. Focusing test -- velocity focus only.
Fig. 4. Focusing test -- double focus.
Fig. 5. Matched doublet. The doublet spacing is about 1/45,000.
Fig. 6. Comparison of new S_{2n} values with previous values.
Fig. 7. Schematic diagram showing the ground state energies of the nuclides of Nd, Pm, Sm and Eu.
Fig. 8. Schematic diagram showing the ground state energies of the nuclides of Sm, Eu, Gd, Tb and Dy.
Fig. 9. Double neutron separation energies plotted as a function of N for even-N. Solid lines join nuclides of the same element. Broken lines join nuclides having the same neutron excess (N-Z).
Fig. 10. Double neutron separation energies plotted as a function of N for odd-N.
Fig. 11. Single neutron separation energies plotted as a function of N. For a given element curves join points for either even-N or odd-N.
Fig. 12. Pairing energies for the last pair of neutrons plotted as a function of neutron number.
Fig. 13. Decay schemes for A = 144 and A = 150.

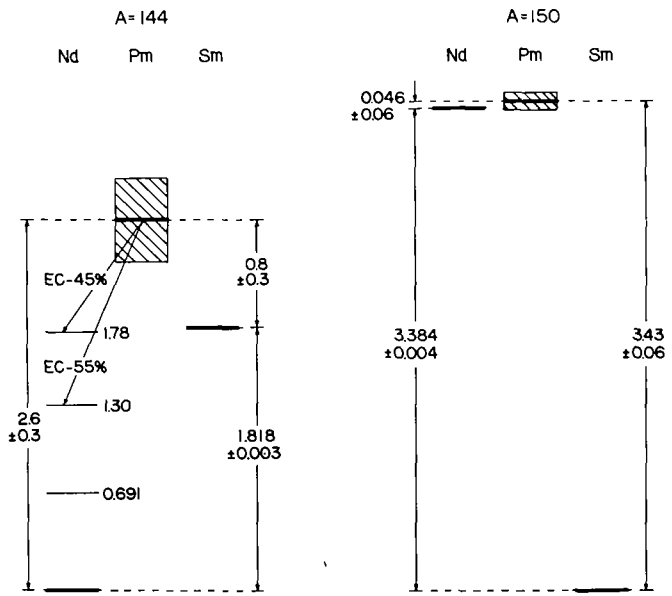

Fig. 13

Ionization Studies using Mono-energetic electrons.

C. E. Brion, D. C. Frost and C. A. McDowell

Department of Chemistry, University of British Columbia

Introduction

Over the past few decades a great deal of effort has been put into the study of the electron impact induced ionization of atoms and molecules. However the majority of the techniques employed have suffered from the disadvantage of a wide energy spread in the ionizing electron beam. Such "low resolution" techniques permit only the determination of the first ionization potential. Any structural features in the ionization efficiency curve due to excited states of the ion are generally obscured. It is therefore impossible to obtain higher ionization potentials and information on such phenomena as autoionization and threshold laws.

All these quantities are of particular concern to the theoretical chemist and with the rapidly advancing interest in radiation chemistry there has been a renewed effort in the development of suitable measuring techniques.

For the study of molecular energy states it is desirable that the energy band width of the ionizing electron beam be less than 0.1 e.V. Early attempts to produce such sources were made by Lawrence (1), Nottingham (2), Clarke (3) and Sugden (4).

A great advance was made with the introduction of the R. P. D. method by Fox (5) in 1951. The technique has since been used quite extensively in many laboratories and has enjoyed considerable success. However the method must be considered as indirect and often tedious. In addition it has not seemed possible to reduce the effective energy spread to less than 0.1 e.V. This has precluded the study of closely spaced electronic and vibrational energy levels.

The use of an electrostatic energy selector provides in principle a more direct approach and two types of selector have received attention in recent years. In one class we have the parallel plate energy selector used by Hutchison (6) and also by Foner and Nall (7). The selected electron beams are of low intensity and the resulting ion currents are difficult to measure. The second type, the 127° electron velocity selector appears more promising mainly as a result of the work of Marmet and Kerwin (8). Marmet and Morrison (9) have combined such a selector with a mass spectrometer and studied the ionization of several molecules. The results are somewhat difficult to interpret due to the low ion currents observed and also the possibility of wall reactions in the ion chamber.

Some of these difficulties have been overcome in the work presented in this paper.

Instrumentation

Several different experimental arrangements have been used. Each will be described in turn.

Firstly a selector and analyser unit were constructed similar to that described by Marmet and Kerwin (8). A low electron reflective surface was designed to function in the same fashion as the "electron velvet" described by the above workers. The surface is covered with fine metallic needles (and was used to line the catcher electrode as well as the ion chamber). An electron beam current of 10^{-8} amps was obtained with a half width of 0.027 volts. This selector was then built into the Nier type ion source of a 60° sector mass spectrometer. It was assumed that the energy distribution was not appreciably disturbed. However the best test of the usefulness of a selected electron beam is its ability to resolve closely spaced energy levels. The ion source is operated and designed to ensure that field penetration into the ionization region is reduced to a minimum. The electron energy is varied continuously and linearly with time by a motor scanning assembly. This enables the direct recording of ionization efficiency curves.

Early attempts at measuring ionization efficiency curves for argon met with little success due to the low ion yield. However with the use of ion counting

techniques some structure was indicated. In view of the magnitude of the electron beam the extremely low ion yield was surprising. Many more ions must be formed but somehow lost before they could leave the ion chamber. It can only be concluded that ions were lost to the walls and it is possible that the "electron velvet" which is so effective at absorbing electrons might have the same effect for ions. Removal of the "electron velvet" from the ion chamber gave an immediate increase in ion intensity of several orders of magnitude.

A second selector and analyser assembly has been designed involving simplified and improved accuracy of construction (12). The overall height of the selector is increased to minimise "end effects". This enables elimination of the vertical focussing grids. No "electron velvet" is used and all surfaces are gold plated. An electron current of 10^{-7} amps with a half width of 60 millivolts can be obtained. Some experiments were performed by total ionization to increase the measured ion intensity. It must be stressed that such measurements are only possible when the gas under study has a lower ionization potential than any of the background gases. With this experimental arrangement we have been able to study the vibrational excitation of ions. The new selector and analyser have now been built into the mass spectrometer. The measured distribution "in situ" under operating conditions is 0.08 volts.

Experimental Results

Krypton:- Figure 1 shows the I. E. curve for krypton obtained with the first selector using mass analysis. The noise level is appreciable but the study of many curves indicates the structural features shown. Direct scanning has the advantage that results are obtained rapidly thus minimising effects of instrumental drift. However as a check several integration runs were made. A typical curve is shown in the upper plot of figure 1. The two curves are very similar. The first break above the $^2P_{3/2}$ threshold correlates with the $^2P_{1/2}$ state of Kr^+ while the higher onsets may be due to autoionization. No other published work is available for comparison at these higher energies.

Argon:- Figure 2 shows the ionization efficiency curve for argon obtained with the second selector and mass analysis. Similar results were obtained with the first selector as can be seen from Table 1 where I and II refer to this work. Taken as a whole the table shows some general trends and the existence of certain structural features in the curves can be established. It is of particular interest to consider the photoionization work of Comes and Lessman (f). Several of the levels above $^2P_{1/2}$ correlate quite well with peaks in the photoionization efficiency curve. It seems reasonable to postulate that some of the breaks observed in electron impact could be due to autoionization processes. The photoionization work of Frost et al however (paper 7 of this meeting) shows the Ar^+ photoionization efficiency to be essentially constant above the $^2P_{1/2}$ level in disagreement with the findings of Comes and Lessman.

Oxygen:- The results for argon, though in fair agreement with other electron selector work are at variance with RPD data where in general none of the postulated autoionizing states are observed.

It was felt that it would be interesting to study the ionization of a simple diatomic molecule such as oxygen which has been studied by the R. P. D. method and also by spectroscopy. The R. P. D. method has been the subject of much criticism though it must be pointed out that many workers in different laboratories have used the method with some success.

In addition Wacks and Krauss (10), from theoretical considerations of vibrational transition probabilities, were unable to produce the segmented ionization efficiency curve of oxygen reported by Frost and McDowell (11). A study (12) has been made of O_2 in an attempt to resolve these conflicting reports.

Figure 3 diagrammatically shows our observed I. E. curve compared with the R. P. D. data. The two curves are almost identical. The electronic transition thresholds observed by Frost and McDowell for excited states of O_2^+ are therefore substantiated. Further evidence for the linear segments of the O_2^+ I. E. curve is provided firstly by the work of Melton (13) who used the R. P. D. gun together with a time of flight mass spectrometer. He obtained a similar curve. In addition Curran (14) in studying ion molecule reactions using the R. P. D. gun has discussed the formation

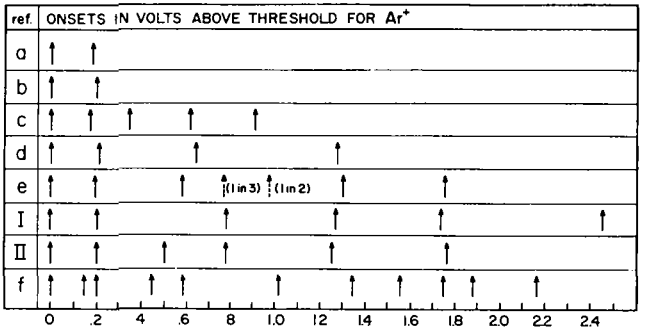

TABLE I

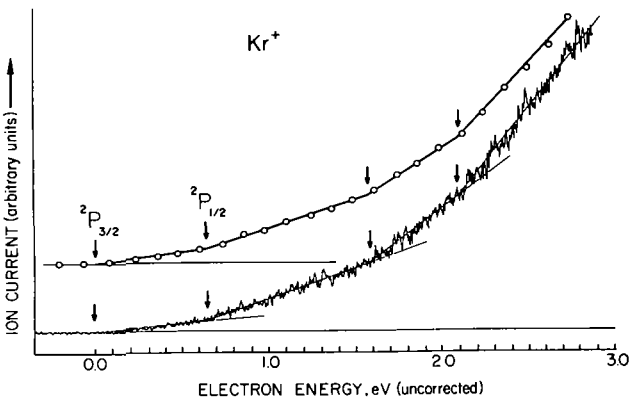

FIGURE 1

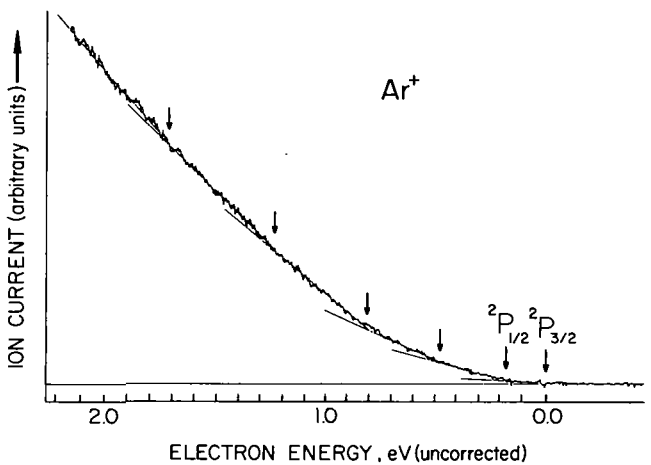

FIGURE 2

of O_3^+ and O_4^+. He concludes that both ions are formed from O_2^+ $^2\Pi_u$. Both appearance potentials are close to the observed ionization potential ($O_2 \longrightarrow O_2^+$ $^2\Pi_u$) and the I. E. curves are linear to within 0.1 e.V. of threshold. They show no evidence of the vibrational excitation of O_2^+ which might be expected from the theoretical considerations.

Table II shows the observed ionization potentials.

Table II Ionization Potentials of O_2

Electronic State	This Work	RPD (11)
$^2\Pi_g$	12.20 ± 0.05	12.21 ± 0.04
$^4\Pi_u$	16.24 ± 0.03	16.30 ± 0.03
$^2\Pi_u$	17.12 ± 0.04	17.18 ± 0.02
$^4\Sigma_g^-$	18.40 ± 0.03	18.42 ± 0.02
?	21.29 ± 0.04	21.34 ± 0.02

It is observed that the threshold of the ionization efficiency curve is non linear for about 0.8 e.V. above the $^2\Pi_g$ threshold. This was also found by Frost and McDowell. The extent of this tailing is much too great to be accounted for by energy spread alone and it seems reasonable to suggest that it is due to vibrational excitation of O_2^+ $^2\Pi_g$.

This threshold region has been examined in some detail using the second selector in a total ionization apparatus. Figure 4 shows a typical curve which is composed of a series of linear or near linear segments.

The observed discontinuities correlate quite well with the known vibrational quanta. Results are shown in table III. Relative transition probabilities may be estimated from the slopes of the segments and are compared with the values computed by Wacks and Krauss in table IV.

Table III Vibrational Quanta for O_2^+ ($^2\Pi_g$)

Transition	Quantum (e.V.)
0-1	0.26 ± 0.02
1-2	0.25 ± 0.02
2-3	0.24 ± 0.02

Table IV Relative transition probabilities to Vibrational levels of O_2^+ ($^2\Pi_g$) from the ground state of O_2.

Vibrational level	0	1	2
This work	0.3	1.0	0.8
Theory	0.6	1.0	0.7

In accord with theory and the difference in internuclear separation of O_2 and O_2^+ $^2\Pi_g$ the most probable transition is to the second vibrational level.

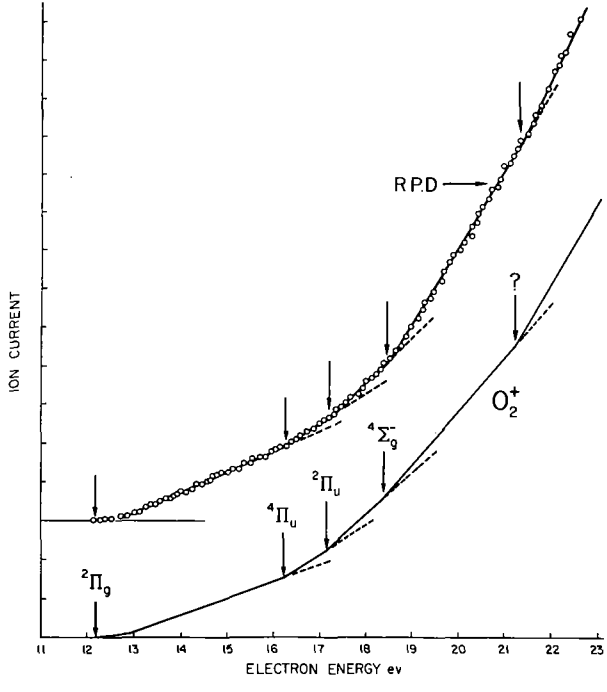

FIGURE 3

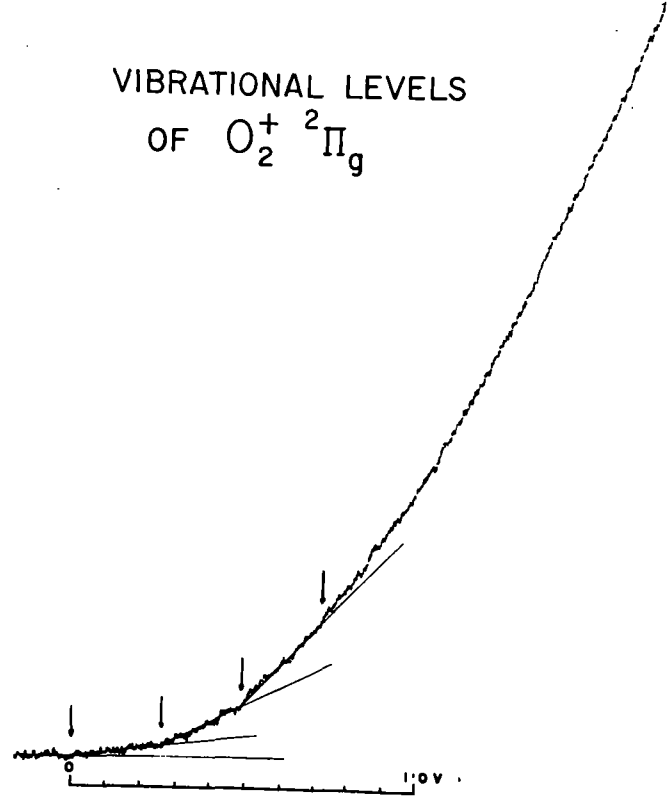

FIGURE 4

Conclusions

127° electron selectors can be combined with mass spectrometers to provide information on the energy states of ions.

The studies of oxygen are interesting in that to date little or no confirmatory work had been performed with electron selectors at energies much in excess of 1 e.V. above any ionization threshold. This work would also appear to validate the R. P. D. method over a wide range of energy for at least the study of oxygen. Secondly all the experimental evidence on the formation of O_2^+ indicates that, for all electronic states other than the ground $^2\Pi_g$ state, the computations of Wacks and Krauss are not applicable to electron impact induced ionization. Unfortunately the applicability to photon impact cannot be tested since any vibrational structure would be obscured by the large number of autoionizing peaks (15, 16). The apparatus of Turner (17) would presumably clarify this point since autoionization is not observed with this technique.

However the experimental studies have clearly shown that there is an appreciable transition probability to the first three vibrational levels of O_2^+ $^2\Pi_g$ in agreement with the theory. It should be noted that this is not in agreement with Morrison's "deconvoluted" ionization efficiency curve of O_2^+ (18) which is linear to the ionization threshold of O_2^+ $^2\Pi_g$. Since Morrison's measured ionization potential is essentially in agreement with the spectroscopic adiabatic ionization potential of O_2 this would imply that the Franck-Condon principle does not apply i.e. we have only a non-vertical transition to the V=0 level of O_2^+ $^2\Pi_g$. Furthermore it is surprising to find a similar situation for N_2^+ where earlier work by Marmet and Morrison (19, 20) showed excitation of several vibrational levels as might be expected. However Morrison's "deconvoluted" curve (18, 21) for N_2^+ is linear in the threshold reason. Further studies of these phenomena are evidently required.

References

(1) Lawrence E. O. Phys. Rev. 28, 947, 1926.

(2) Nottingham W. B. Phys. Rev. 55, 203, 1939.

(3) Clarke E. M. Can. J. Phys. 32, 764, 1954.

(4) Sugden T. M. and Price W. C. Trans. Farad. Soc. 44, 116, 1948.

(5) Fox R. E., Hickam W. M. and Kjeldaas T., Phys. Rev. 89, 555, 1953.

(6) Hutchison D. A. Adv. Mass. Spectry. 2, 527, 1963.

(7) Foner S. N. and Nall B. H., Phys. Rev. 122, 512, 1961.

(8) Marmet P. and Kerwin L., Can. J. Phys., 38, 787, 1960.

(9) Marmet P. and Morrison J. D., J. Chem. Phys., 36, 1238, 1962.

(10) Wacks M. E. and Krauss M., J. Chem. Phys. 35, 1902, 1961.

(11) Frost D. C. and McDowell C. A., J. Am. Chem. Soc., 80, 6183, 1958.

(12) Brion C. E., J. Chem. Phys. 40, 2995, 1964.

(13) Melton C. E., private communication.

(14) Curran R. K., J. Chem. Phys., 38, 2974, 1963.

(15) Nicholson A. J. C., J. Chem. Phys., 39, 454, 1963.

(16) Frost D. C. and McDowell, to be published.

(17) Al-Joboury M. I. and Turner D. W., J. Chem. Soc., page 5141, 1963.

(18) Morrison J. D., Bull. Soc. Chim. Belg., 73, 399, 1964.

(19) Marmet P. and Morrison J. D., J. Chem. Phys., 36, 1238, (1962).

(20) Marmet P., Kerwin L. and Clarke E. M., Advan. Mass Spectry., 2, 522, (1963).

(21) Morrison J. D. Paper 6 this meeting.

(a) Moore C. N. B. S. circular 467 (1949).

(b) Fox R. E., Westinghouse Research Laboratories, Report 60-94439-4-R2 (1956).

(c) See reference (6).

(d) See reference (7).

(e) See reference (20).

(f) Comer Von F. J. and Lessman W. Z. Naturforschg., 16a. 1396, (1961).

EFFECT OF MOLECULAR STRUCTURE ON THE IONIZATION PROBABILITIES OF AROMATIC MOLECULES

F. T. Deverse and A. Bruce King
Gulf Research & Development Company
Pittsburgh, Pennsylvania 15230

The ion yield vs. electron energy has been measured for the parent ions of a number of aromatic compounds immediately above the threshold. From the slopes of the linear portion of these curves, the relative ionization probability per molecule is determined. It is found that the ionization probabilities increase with the size of the π electron system and correlate quantitatively with the electron donating ability of the substituents. Disubstituted benzenes show an additivity of the effect of the substituents on the ionization probability with the meta isomer giving slightly higher values than the ortho and para isomers. Polyphenyl methanes and ethanes show considerably greater ionization probability than fused aromatic compounds with the same number of π electrons.

INTRODUCTION

It was shown by Kearns, et al,[1] that the sensitivity of alkylbenzenes at a fixed electron energy near the threshold was strongly dependent on the degree of substitution. More recent studies[2] have shown that the slope of the ionization efficiency curves of alkylbenzenes varies approximately linearly with the number of substitutents. Similar observations in this laboratory of an increasing slope of the ionization efficiency curve with the number of alkyl groups adjacent to the double bond has been found for some of the simple olefins.[3]

The threshold law for ionization by electron impact has been extensively studied by Morrison and others.[4] For the case of n-fold ionization by electron impact, the threshold law is simply that the transition probability to a particular level depends on the nth power of the excess energy, that is

$$\sigma(E) = C\ (E-E_o)^n \qquad (1)$$

where $\sigma(E)$ is the cross-section at electron energy E, E_o is the threshold energy, C is a constant, and n is the degree of ionization. It has been suggested that this law may be extended to other processes, e.g., photoionization, where n+1 is the total number of electrons emerging from the reaction complex.[4b,5]

From theoretical studies of this problem, a simple qualitative explanation of the nature of the threshold law, as exemplified by equation (1), has been suggested.[6-8] The excess energy $(E-E_o)$ must be divided among the emerging electrons for momentum restrictions leave only a negligible portion as kinetic energy of the ion. When there are n+1 electrons, there are n degrees of freedom for this excess energy. That is, the number of possible combinations of energy states of the electrons is proportional to $(E-E_o)^n$ which gives rise to the energy dependent factor in equation (1), or "freedom factor".[8] For a quantum mechanical formulation of the ionization cross-section, the proportionality constant C of equation (1) will include contributions that are characteristic of the wave functions of the molecule and the state of the ion being formed. By analogy with the transition probability in optical spectra, we shall henceforth use the term ionization probability in referring to the constant C of equation (1).* For the case of single ionization, the relative ionization probability is thus determined from the slope of the ionization efficiency curve with suitable correction to place the ionization efficiency on the same basis, e.g. per molecule or per mole.

Although many experimental studies of ionization efficiency curves have been made with regard to threshold behavior and, more generally, threshold energies, practically no studies of the relative ionization

---

* Dorman and Morrison (ref. 8) have defined this same quantity as the "structural factor".

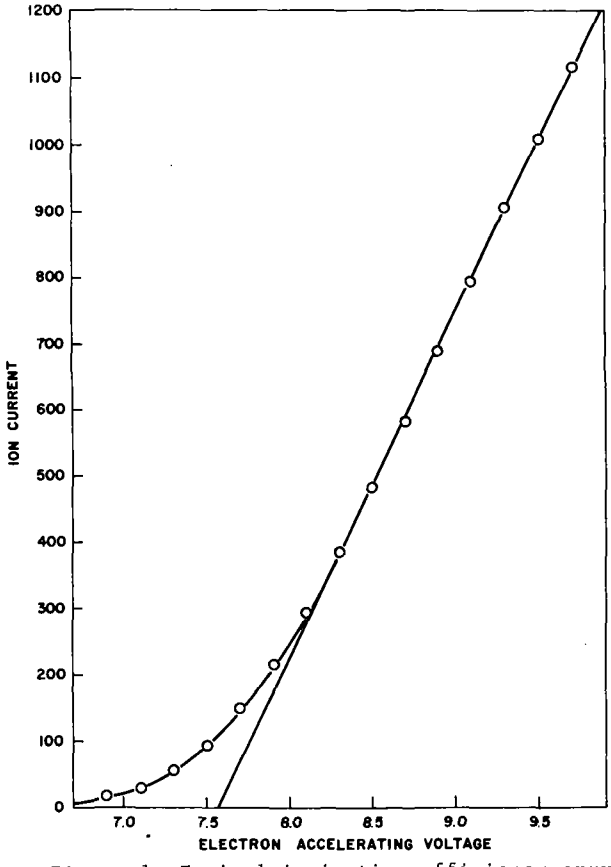

Figure 1 Typical ionization efficiency cruve observed in this study. A curve of toluene is shown.

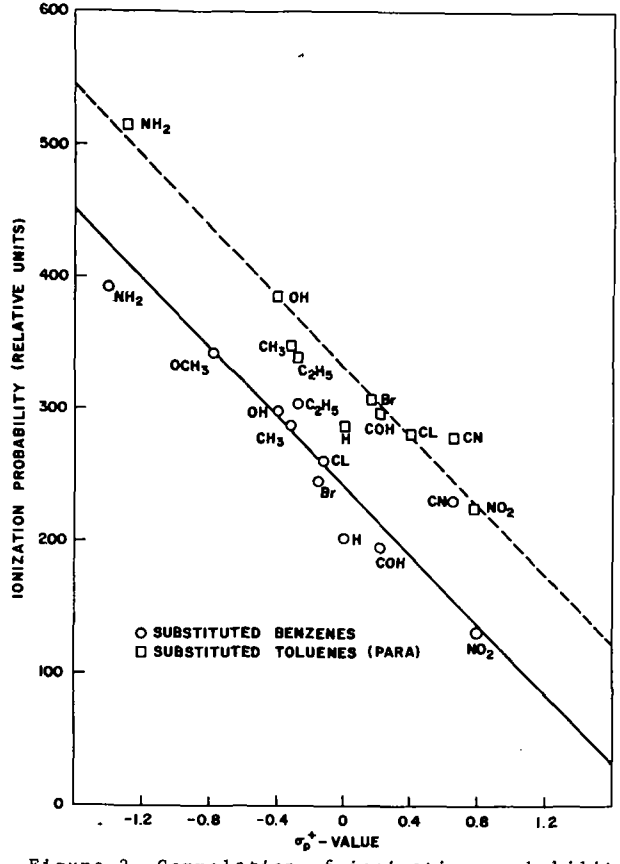

Figure 2 Correlation of ionization probability of substituted benzenes and toluenes with Brown's σ_p^+-value.

probabilities have been reported. Experimental measurements[9] of the relative ionization probabilities of the vibrational levels of H_2^+ were found to agree well with theoretical predictions.[10] No studies have been reported however of a comparison of the relative ionization probabilities of different compounds. The purpose of this paper is to present data obtained for a variety of aromatic compounds so that the structural parameters affecting the ionization probability may be better understood. The aromatic compounds were selected for the study because the ionization occurs from the vicinity of the π electron system and hence these molecules represent one of the simplest systems for study of the effect of molecular parameters on this phenomena.

EXPERIMENTAL

The data were obtained on a Consolidated Electrodynamics Corporation 21-103C mass spectrometer equipped with an all-glass heated inlet system. The inlet was operated at either 175°C. or 350°C. depending on the volatility of the compounds being studied. Operating conditions: repellers- +1.5 volts; anode- +200 volts (both with respect to ion source block), anode current- 20μ amp, ion source temperature- 250°C. The electron accelerating potential (ion source to filament center-tap) was measured with a shielded voltage divider and potentiometer and this procedure gave precision of better than ± .01 volts. In general, the ionization efficiency curve was determined by repeated scans of the parent peak for 0.2 volt intervals from near threshold to about 12 volts.

Most of the compounds studied were obtained from commercial suppliers, e.g. Eastman Kodak, Aldrich, and K&K Laboratories, in the highest available purity and used as received.

It is important in this work to compare the relative ionization probabilities of the compounds studied on a per molecule basis. All the relative ionization probabilities are reported on the basis of benzene = 200.0. These data were obtained by concurrent measurements of the slope of the ionization efficiency curve of the compound under study and that of benzene (or frequently toluene as a secondary standard) using the same liquid volume for both compounds. Identical liquid volumes were introduced using micro-pipettes of volume approximately one lambda. The sample was introduced through a gallium covered fritted disk[11] and repeated introductions were made to confirm that the same volume had been introduced. All compounds which were solid at room temperature were melted and induced in liquid form with the pipette. The ratio of slopes was converted to a relative ionization probability on a molar (or molecular) basis by multiplying by the ratio of the molar volumes. For the compounds which were solid at room temperature, the density of the liquid at the melting point, if available, was used. Otherwise the molar volume was approximated using the room temperature density of the solid. The ratios of the slopes were corrected for C^{13}, D, Cl^{37}, etc., to make the relative ionization probabilities monoisotopic.

In Figure 1, the ionization efficiency curve is shown for toluene which is typical of the shape and energy intervals for the "tail" and linear portions of the curve observed for all of the compounds studied. The onset of linearity corresponds to the voltage at which the energy of the lowest energy electrons in the beam equals the ionization potential. In all cases this energy was found to be .8 ± .2 eV below the ionization potential. This energy scale shift agrees quite well with the magnitude of the combined estimated effects of the repellers (0.75 eV) and contact potentials (probably ± .2 eV).

The total ionization yield vs. electron energy is the sum of the ion yield from the various levels of the ion. Each term in the summation is of the form of equation (1) with its own threshold energy and ionization probability. The total ionization probability, which is the slope of the linear region of the total ionization efficiency curve, may include contributions from several states of the ion. Although fragment ions are formed from the higher states of the ion, by confining the study to the parent ion, only the lower states of the ion are involved in the ionization probability thus determined. The "tail" of all of the experimental ionization efficiency curves of the

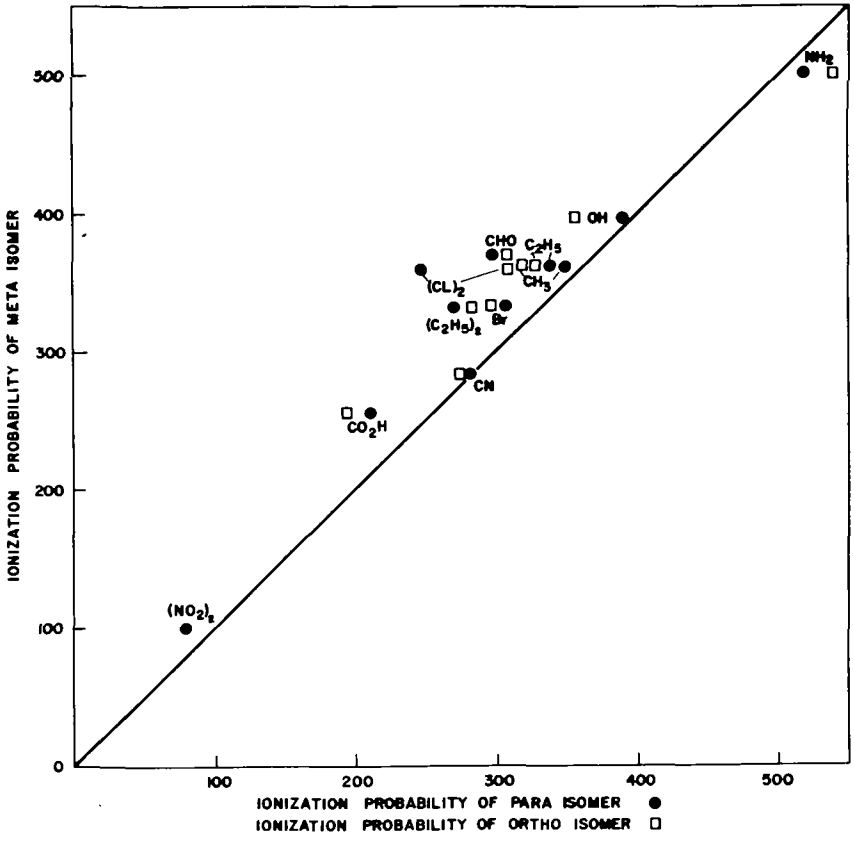

Figure 3 Comparison of ionization probabilities of isomers of disubstituted benzenes. Where only one substituent is listed, the second substituent is a methyl group.

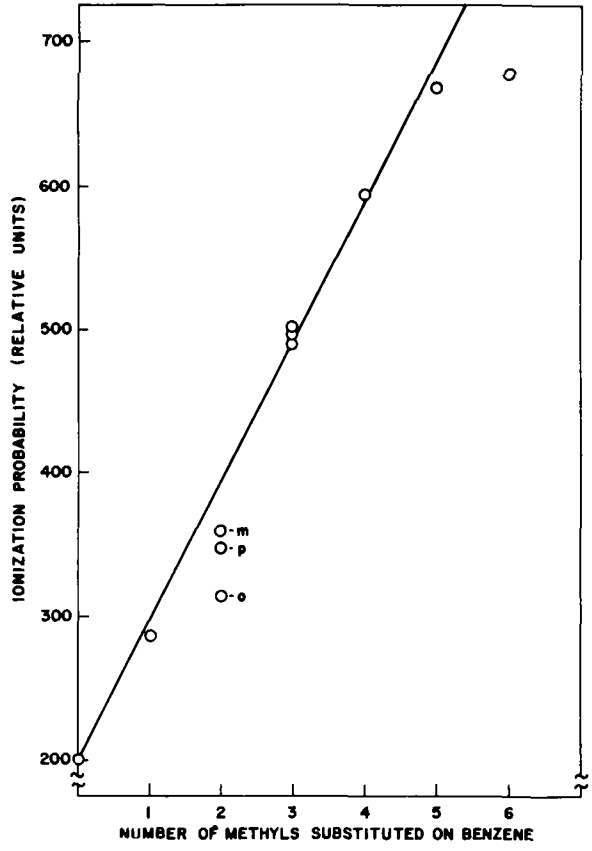

Figure 4 Ionization probabilities of the polymethyl benzenes.

parent ions (e.g. Figure 1) is generally no greater than 1.5 eV and the length of the linear region is 1.0 - 2.5 eV. Thus, if more than one state of the ion makes a significant contribution to the ionization probability of the parent ion, it must be within 1.5 eV of the lowest threshold where its onset would be hidden by the electron energy spread. Secondly, no other states of the region 1.5 - 2.5 eV, or more, above the lowest threshold make observable contributions as they would cause noticable curvature. Therefore in the subsequent discussion, the ionization probabilities refer to the sum of the ionization probabilities for one or more states within about 1.5 eV of the ionization potential.

RESULTS AND DISCUSSION

The ionization probabilities of the C_7-C_{12} n-alkylbenzenes are given in Table I. The slopes for this carbon number range show a relative constancy with toluene slightly lower than the rest, indicating the effect of the chain length beyond the alpha carbon atom makes only a minor contribution to the ionization probability. The constancy of the molecular ionization probability for the monoalkylbenzenes is implied in the low voltage volume sensitivity vs. reciprocal molecular weight relationships[1,12] when one considers the constant ionization potential for this series and the constant liquid density. The

TABLE I

IONIZATION PROBABILITIES OF ALKYLBENZENES

COMPOUND	IONIZATION PROBABILITIES (RELATIVE UNITS)
Toluene	287
Ethylbenzene	303
n-Propylbenzene	301
n-Butylbenzene	305
n-Pentylbenzene	313
n-Hexylbenzene	311
Isopropylbenzene	296
sec-Butylbenzene	289
tert-Butylbenzene	264

TABLE II

IONIZATION PROBABILITIES OF SUBSTITUTED BENZENES

COMPOUND	IONIZATION PROBABILITIES (RELATIVE UNITS)	COMPOUND	IONIZATION PROBABILITY OF ISOMERS (RELATIVE UNITS)		
			ORTHO	META	PARA
Aniline	389	Toluidine	537	501	516
Phenol	298	Cresol	352	398	388
Anisole	340	Xylene	315	361	349
Toluene	287	Ethyltoluene	327	362	330
Ethylbenzene	303	Chlorotoluene			283
Chlorobenzene	262	Bromotoluene	280	334	306
Bromobenzene	247	Tolualdehyde	307	369	298
Benzaldehyde	192	Tolunitrile	274	283	280
Benzonitrile	233	Toluic acid	192	254	211
Benzoic acid	169	Nitrotoluene			223
Nitrobenzene	132	Diethylbenzene	287	334	270
		Dichlorobenzene	309	360	258
		Dinitrobenzene		101	78

TABLE III

IONIZATION PROBABILITIES OF POLYAROMATICS

COMPOUND	IONIZATION PROBABILITIES (RELATIVE UNITS)	COMPOUND	IONIZATION PROBABILITIES (RELATIVE UNITS)
Tetralin	223	3,4,3',4'-Dixylylethane	586
Indan	282	2,3,3',4'-Dixylylethane	616
Indene	410	Diphenylmethane	704
α-Methylstyrene	421	Stilbene	608
Naphthalene	364	Anthracene	677
α-Methylnaphthalene	445	Phenanthrene	781
β-Methylnaphthalene	453	α-Phenylnaphthalene	726
Acenaphthene	498	Pyrene	759
Biphenyl	463	Fluoranthene	809
Acenaphthylene	473	Chrysene	811
Fluorene	515	Triphenylmethane	1477
		Perylene	855

ionization probability of several of the simple branched alkyl benzenes are also given in Table I. One notes that there is a definite decrease in the ionization probability with additional substitution on the α-carbon.

The effect of the electron donating ability of the substituent on the ionization probability of the benzene nucleus was investigated. In Table II are listed the relative ionization probabilities for a number of mono-substituted benzenes. These data are plotted in Figure 2 vs. Brown's σ_p^+ -value for the substituent.[13,14] The linearity and relative magnitude of the slope of this plot clearly indicates the importance of the electron donating ability of the substituent on the ionization probability. It is noted that the greater electron donating ability of the substituent (more negative value of σ_p^+-value) corresponds to the greater ionization probability.

It has been previously reported[16,17] that there is also a close linear relationship between the ionization potential of substituted benzenes and Brown's σ_p^+-value for the substituent. It is thus possible to express a linear relationship between the ionization probability and the ionization potential for the mono-substituted benzenes. Although it may be suggested that one of these quantities is derived in some manner from the other, it is our contention that the variation of the ionization potential and probability for this class of compounds are both effects from the same cause, i.e., the electron donating ability of the substituent.

The ionization probabilities of a number of disubstituted benzenes are also listed in Table II. The data for the para-substituted toluenes are also plotted in Figure 2 vs. Brown's σ_p^+-values. One finds as good a linear relationship as was observed for the substituted benzenes. In addition, the slope of the plot is parallel to the benzene curve and shifted by an amount equal to the difference in the ionization probabilities of toluene and benzene. These results thus show an additivity of the effect of substituents on the ionization probability of the benzene nucleus.

The ionization probabilities of a number of disubstituted benzenes from Table II are shown in Figure 3 to illustrate the differences between the value for the meta and the ortho and para isomers. In all but one case, the meta isomers show somewhat greater ionization probability than the ortho and para. In addition the magnitude of the differences between the ortho and para isomers are much less and the sign of the difference varies. These observations suggest the contributions of resonance stabilization of the ion to the ionization probability. Thus for the disubstituted benzenes, the resonance effects of the substituents on the ionization sites of the ring are reinforced for the meta isomers, but not for the ortho and para isomers. These effects should be considered in any formulation of a quantum mechanical model for the ionization probability by electron impact in the threshold-law region.

The effect of more than two substituents on the ionization probability of benzene was also studied. Data for the three trimethyl benzenes, durene, and penta- and hexamethyl benzene were obtained. The ionization probability for the entire series of polymethyl benzenes are shown in Figure 4. Except for unexplained slightly lower values for the xylenes, a fairly linear increase of the ionization probability is observed for up through five methyl groups. We believe that the deviation of hexamethylbenzene from this behavior is real and that it is the result of complete substitution of the ring.

Thus far, we have only discussed the ionization probabilities of substituted benzenes. As variations of the π electron system will presumably affect the ionization probability, it is of value to examine other π electron systems. The ionization probabilities of a number of additional aromatic compounds were obtained and the data are listed in Table III. The number of compounds that could be run was greatly restricted by availability as well as sufficiently low melting point to permit introduction of a reproducable volume with the pipette. Because of the diversity of types of structure in this list of compounds, it is difficult to separate effects due to the size of the π electron system, substituents on the aromatic rings, etc. However, in Figure 5, a plot of the ionization probability is given vs. the total number of π electrons. It is apparent from the figure that one of the major parameters in the ionization probability of aromatic compounds is the number of π electrons, and thus, presumably, the size of the π electron system.

Several interesting aspects of the data in Figure 5 should be mentioned. The difference between the ionization probabilities for toluene and benzene is identical with the difference between naphthalene and the methyl naphthalenes. In addition the contribution of a condensed saturate ring is frequently less than that for the corresponding dialkyl compound (e.g. indan and tetralin vs. ortho-xylene).

Considerably larger ionization probabilities are observed for the polyphenyl methanes than for the corresponding fused aromatic compounds with the same number of π electrons. The large difference between biphenyl and diphenylmethane points to a considerable enhancement of the ionization probability when the rings are separated by one carbon atom. In addition there is a considerable decrease in the ionization probability for the dixylyl ethanes as compared with diphenyl methane. There are two effects contributing to this difference: The additional substitution on the phenyl groups and the methyl substitution on the α-carbon atom. Since the former effect increases the ionization probability, the observed decrease indicates that alkyl substitution at the α-carbon atom considerably reduces the ionization probability. This observation, coupled with the previously discussed effect of branching on the ionization probability of monoalkylbenzenes, suggests that substitution at the α-carbon atom plays a major role in determining the ionization probability. Alkyl substitution at this site tends to decrease the ionization probability while phenyl substitution increases it considerably.

CONCLUSIONS

It is shown that it is possible to obtain quantitative correlation of the slope of the ionization efficiency curve (herein defined as the ionization probability) of aromatic compounds with their molecular structure. The ionization probability is found to be approximately proportional to the number of π electrons. From studies of substituted benzenes the ionization probability is observed to correlate quantitatively with the electron donating ability of the substituent on the benzene ring. Additivity of the effects of the substituents is observed for the ionization probabilities of poly-substituted benzenes. For the disubstituted benzenes, higher ionization probabilities are found for the meta isomers, suggesting resonance effects. The results for polyphenyl methanes and ethanes suggest the importance of substitution at the α-carbon atom on the ionization probability with an increase for aryl substitution and a decrease for alkyl substitution.

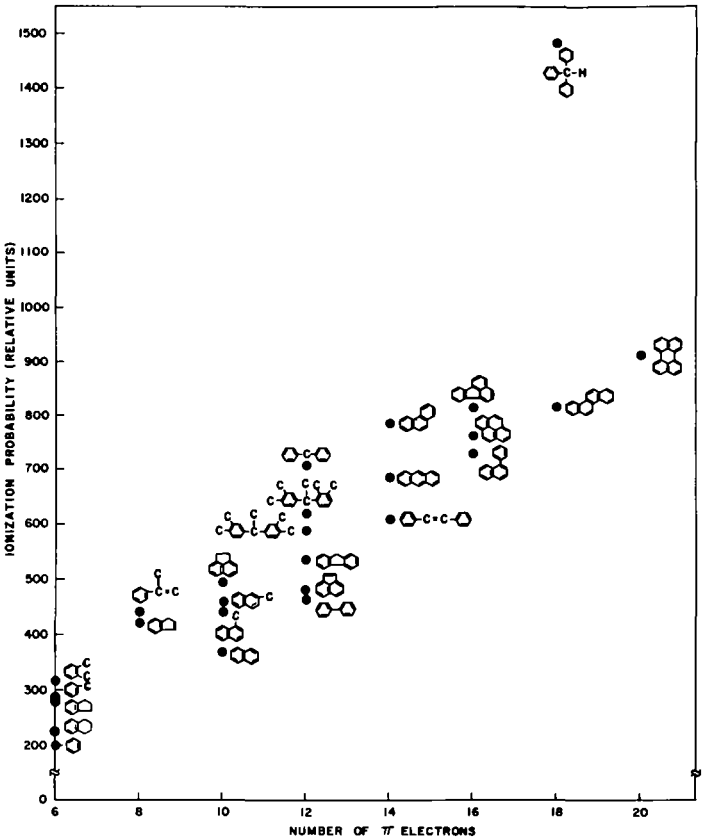

Figure 5 Ionization probabilities of polynuclear aromatic compounds vs. number of π electrons.

It should be emphasized that all of these observations of the effect of structure on the ionization probability have one thing in common: structural features which give increased stability of the ion also enhance the ionization probability.

ACKNOWLEDGEMENTS

The authors wish to thank Dr. J. C. Schug for several helpful discussions and Mr. H. T. Best for obtaining some of the experimental data.

REFERENCES

1 G. L. Kearns, N. C. Maranowski, and G. F. Crable, Anal. Chem. 31, 1646 (1959).

2 H. E. Lumpkin and T. Aczel, Anal. Chem. 36, 181 (1964).

3 A. D. Wentzel, Jr., unpublished results, 1960.

4 For recent reviews see: (a) M. Krauss and V. H. Dibeler, in Mass Spectrometry of Organic Ions, F. W. McLafferty, ed., Academic Press, N.Y. (1963), pp. 117-161, and (b) J. D. Morrison, Rev. Pure Appl. Chem. 12, 117 (1963).

5 J. D. Morrison, J. Appl. Phys. 28, 1409 (1957).

6 G. H. Wannier, Phys. Rev. 100, 1180 (1955).

7 S. Geltman, Phys. Rev. 102, 171 (1956).

8 F. H. Dorman and J. D. Morrison, J. Chem. Phys. 34, 578 (1961).

9 P. Marmet and L. Kerwin, Canad. J. Phys. 38, 972 (1960).

10 M. Krauss and A. Kropf, J. Chem. Phys. 26, 1776 (1957).

11 M. J. O'Neal, Jr., and T. P. Wier, Jr., Anal. Chem. 23, 830 (1951).

12 H. E. Lumpkin, Anal. Chem. 30, 321 (1958).

13 H. C. Brown and Y. Okamoto, J. Am. Chem. Soc. 80, 4979 (1958).

14 A σ_p^+-value of +.22 for -CHO was estimated from the electron impact ionization potential of benzaldehyde[15] and the previously established relationship between ionization potentials and σ_p^+-value.[16,17]

15 M. R. Basila and D. J. Clancy, J. Phys. Chem. 67, 1551 (1963).

16 J. M. S. Tait, T. W. Shannon and A. G. Harrison, J. Am. Chem. Soc. 84, 4 (1962).

17 G. F. Crable and G. L. Kearns, J. Phys. Chem. 66, 436 (1962).

Effects of Electron Energy Distributions on Ion Appearance Potential Measurements*

Dwight A. Hutchison

Argonne National Laboratory, Argonne, Illinois

Abstract

Electron beams with variously shaped energy-distribution functions were formed from a hot tungsten filament and an electrostatic lens system. The distribution functions were measured by means of a parallel-plate electrostatic energy analyzer. Combination of a linear ionization threshold function with the measured energy distributions for first ionization by electron impact of gases allows a possible explanation of the differences of published values of ion-appearance potential measurements.

Introduction

It has been assumed in past studies that a Maxwellian energy distribution of electrons emitted at a particular temperature of a hot metal filament is representative of the electron-energy distribution used in the determinations of ion-appearance potentials by electron impact. Actually, we find that measured energy distributions obtained under usual operating conditions for a typical electron-impact ion-source are quite different from a Maxwellian distribution and seldom approach one. Various experimental conditions which cause this are well known. They consist of the voltage drop across a filament caused by the heating current, the varying temperature along the filament, the physical displacement of a filament due to heating, the contact potentials, the difference of potential between the filament center-tap and the point of maximum emission in an a.c. heated filament, and, not least, the space charge effects between the filament and first defining slit electrode.

We have measured electron-energy distributions under the usual operating conditions for a typical electron-impact ion-source so as to find the magnitude of the effects of the distribution on the shape of the appearance potential curve. The measured distributions combined with a linear first-ionization threshold law allowed calculations of the appearance potential curves from which we could observe the effects sought.

Description of Apparatus

A schematic of the electron-energy analyzer is shown in Fig. 1. It consists of a heated tungsten filament, a line-focus electrostatic lens of the double cylinder type, a plane-parallel plate electrostatic energy selector, and an electron collector with electrodes for prevention of loss of secondary emission electrons. The procedure for measuring an energy distribution was: set the nominal potential (that between the filament and the next electrode) at a desired value, adjust the lens-electrode potentials for best focus on the analyzer entrance slit, scan the potential across the parallel plates while recording the current to the collector by means of a strip-chart recorder. Correction of the recorded currents typical for this type analyzer was made.

Typical Electron-Energy Distributions

In Fig. 2 we show an electron-energy distribution measured for nominal 50.0 e.v. electrons. The pressure in the analyzer was 5×10^{-7} mm Hg

* Based on work performed under the auspices of the U. S. Atomic Energy Commission.

and the total electron emission measured at the first electrode next to the filament was 0.25 mamps. It may be seen that there is more tailing of the distribution on the low energy side than on the high energy side. The spread of energies effective in causing ionization is about 6 volts.

An electron-energy distribution for nominal 35.0 volt electrons is shown in Fig. 3. Other conditions were the same as those for Fig. 2. It is seen that the spread of energies effective in producing ionization is about 14 volts. Thus, a reduction in the nominal electron energy from 50.0 to 35.0 volts with other conditions unchanged causes an increase greater than a factor of two in the effective energy spread together with the appearance of three distinct groups of electrons. The spread and maxima may be accounted for qualitatively by changes in space charge occurring between the filament and the first defining slit electrode. The important point is that a large change of this sort can occur under usual operating conditions of a typical electron-impact ion source and an observer without benefit of an energy analysis would not be cognizant of the large change.

Typical of electron-energy distributions at energies near many appearance potential measurements are those given in Fig. 4 for nominal 15.0 volt beams. The experimental conditions are similar to those of preceding figures except for unknown changes occurring from one day to the next. It is seen that under nominally similar operation one curve has a width at half-maximum of about 1.5 volts and the other about 1.7 volts while the base widths effective in ionization are about the same, near 6 volts.

Calculated Appearance Potential Curves

With a known electron-energy distribution it is possible to calculate the appearance potential curve resulting from the distribution if the threshold law for ionization is assumed. The method of sweeping a known electron distribution f(U) through an ionization probability function P(E) is depicted schematically in Fig. 5. As the maximum energy V is increased the upper limit E_2 of the distribution starts to effect ionization when it reaches a critical energy E_c. Ionization increases with V until the entire distribution is operative at $E_1 > E_c$. The ion appearance potential function $i_+(V)$ may be expressed as

$$i_+(V) = C \int_{V-a}^{V+b} f(U)P(E)dE \ . \qquad (1)$$

If the form of P(E) is assumed linear with the excess energy over the critical energy E_c, we may express Eq. (1) as

$$i_+(V) = C \int_{-a}^{+b} f(\overline{E})(\overline{E}+V-E_c)d\overline{E} \qquad (2)$$

where $E = U + V$, and $\overline{E} = E - V$. Using the measured electron-energy distributions functions f(U) from Fig. 4, we have employed Eq. (2) to calculate the appearance potential functions $i_+(V)$. The integrations were made numerically using Simpson's Rule and performed on an IBM 704 computer. The results are plotted in Fig. 6. Ionization onset between 3 and 4 volts on these curves are arbitrary units corresponding to the maximum limit E_2 of about 19 volts shown in Fig. 4. It is seen that the curved regions extend over a 5 volt range approximately equal to the base widths of the distributions in Fig. 4. The curve with linear portion of steeper slope in Fig. 6 corresponds to the electron distribution in Fig. 4 with the greater area beneath it. It may be seen that the relative magnitude of these areas determines the relative slopes of the calculated curves. Extrapolation of the linear portions of the calculated curves to the energy axis yields appearance potentials differing by about 1.2 volts. This demonstrates the effect which the area under the electron distribution may have in determining an appearance potential. In practice the

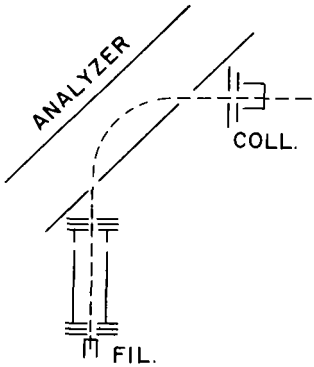

SCHEMATIC OF BEAM ANALYZER

Figure 1. Schematic of electron-beam energy analyzer.

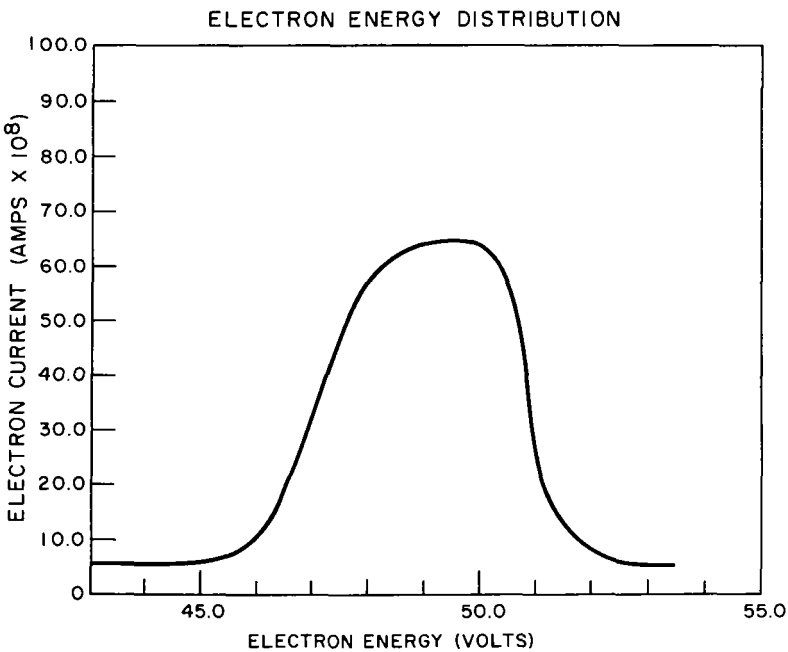

Figure 2. Typical energy distribution measured using nominal 50.0 e.v. electrons.

various methods of extrapolation in common use employ ion currents only about 1-2 volts above the first measurable current. It appears from this that most workers must be extrapolating from the curved part of the appearance potential curve which is caused by the base width of the electron distribution. Because of this it is not surprising to find variations in reported appearance potentials as much as 1.0 to 1.5 volts.

Conclusions

Knowledge of the energy-distribution function for a beam of electrons used in appearance curve measurements is a necessity for appearance potential determinations. Without the distribution it appears impossible to establish a well-founded basis for extrapolation of the appearance potential curve to an appearance potential value. Lack of knowledge of the electron distribution in most reported appearance potential values may possibly account for the large discrepancies that exist.

Acknowledgment is due Mr. Louis G. Pobo for his careful assistance in the collection of the electron-distribution data.

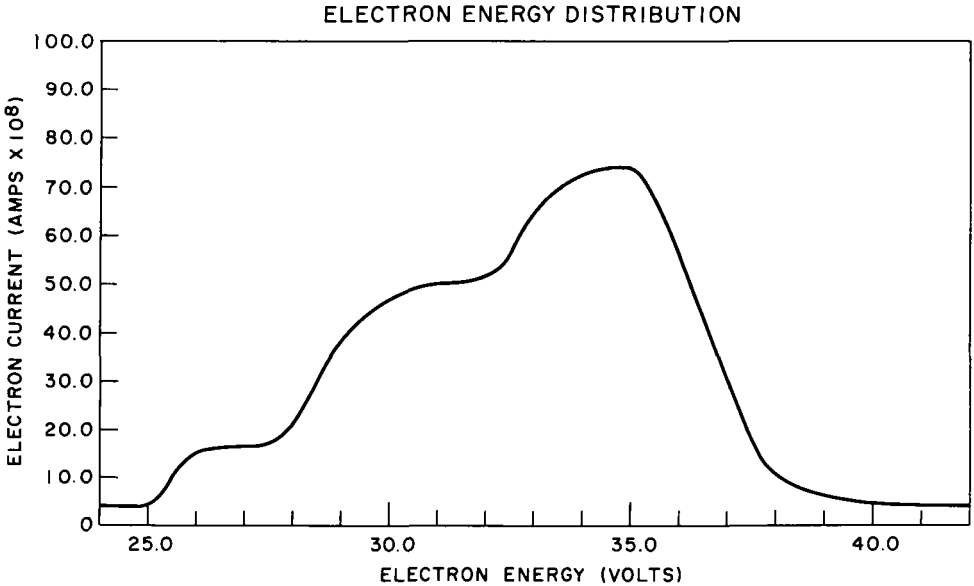

Figure 3. Typical energy distribution measured using nominal 35.0 e.v. electrons.

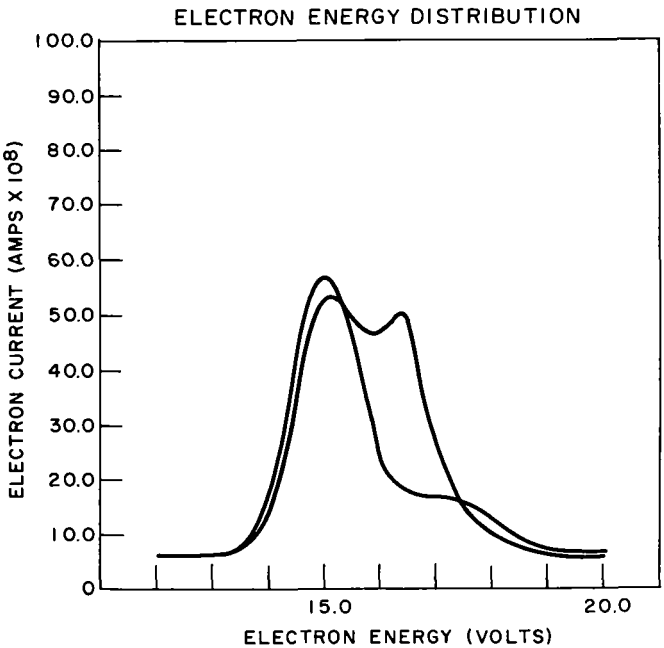

Figure 4. Typical energy distributions measured using nominal 15.0 e.v. electrons.

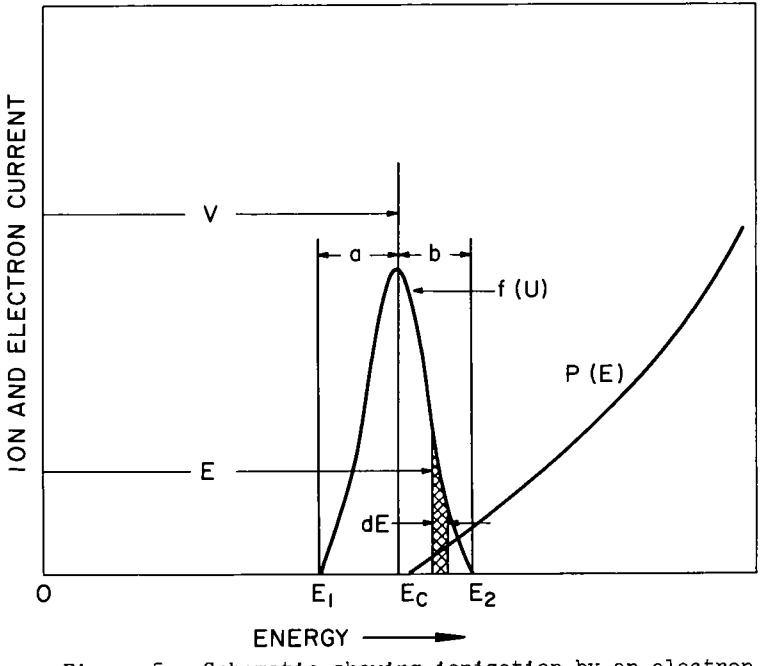

Figure 5. Schematic showing ionization by an electron-energy distribution.

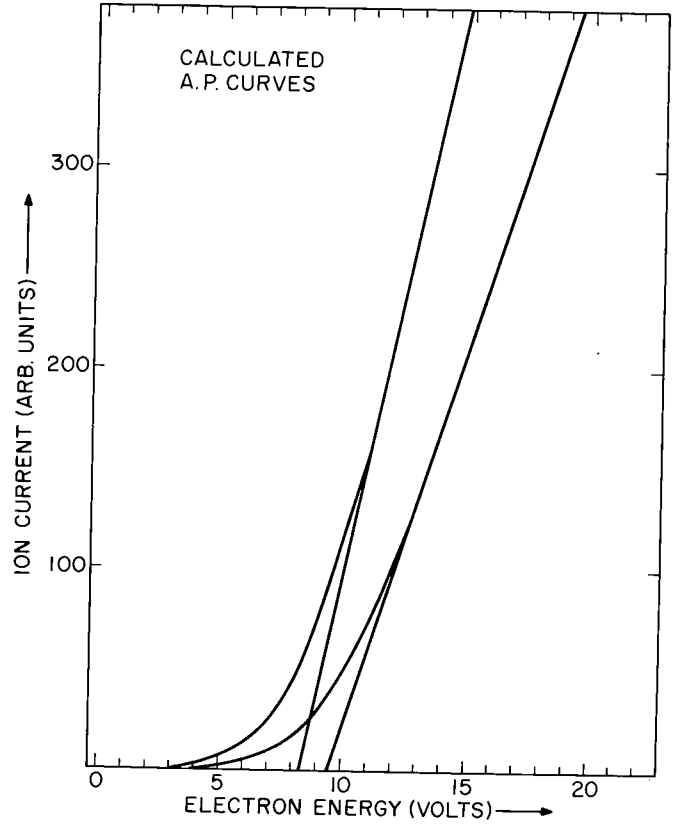

Figure 6. Ionization efficiency curves calculated from two electron-energy distributions of Fig. 4.

An effect of electronic space charge on ionization curves probability.

P. Marmet

Centre de Recherches en Spectrométrie de Masse
Dept de Physique, Université Laval, Québec.

Abstract

In electron impact studies, the difference between the ideal curve which would be obtained with monoenergetic electrons, and the experimental curve produced with a certain energy distribution is usually interpreted using the Maxwellian distribution of thermally emitted electrons and assuming that the electronic space charge and accelerating potential do not modify the energy distribution. Several recent papers (e.g. D. Hartwig and K. Ulmer 1963) mention contrarily that there is a redistribution of energy after a relaxation time. It will be shown that the influence of this redistribution of energy on ionization efficiency curves is different for different ion sources. It devolves that in some cases, instrumental effects can be explained, and that the electron energy distribution cannot be simply deduced from the sharpness of the discontinuities in the ionization efficiency curve.

1 - Introduction.

Maxwellian energy distribution has been used recently by Asundi and Kurepa (1) to show that, from an analysis of the ionization probability curve, and assuming a linear extrapolation, it is possible to determine on an absolute scale the ionization potential of several gases to $\pm$ 0.08 eV. Unfortunately the electron energy distribution has arbitrarily been assumed to be unchanged when an accelerating potential was applied.

A careful study of electron beams performed by Boerch (2) and Hartwig and Ulmer (3) shows that several processes disturb the energy distribution in the beam. It is evident that the final energy distribution observed by those authors (2)(3) will produce a result different from the one expected by Asundi and Kurepa (1). Before studying the influence of the perturbed electron beam on ionization probability curves, let us recall briefly the effects observed by Hartwig and Ulmer.

2 - New perturbing factors according to Hartwig and Ulmer.

The difference between the Maxwellian and the new distribution can be described by the four following perturbations:

a) A change in energy distribution produced by a geometrical effect of the electron source.
b) A change in the average energy produced by the discrimination against slow electrons by the space charge surrounding the filament.
c) A widening of the energy distribution produced by a relaxation between the axial and radial velocity distribution of the charged particules of the beam.
d) A modification of the energy distribution so that it becomes symetric about the average energy.

To complete the description of those perturbations it is demonstrated (3) that a complete relaxation should modify the distribution from the original ΔE_o to the final ΔE according to the relation:

$$\Delta E = \left(\frac{32}{3} \right) \left(E_1 \Delta E_o \right)^{1/2} \qquad (1)$$

where E_1 is the maximum energy of the electron beam.

Furthermore it has been observed experimentally that the relaxation is usually incomplete. For the detailed explanation of these perturbations, the reader must refer to the original article (3).

3 - General consequences for various types of source.

It is obvious that these effects must be taken into account if we are to give a correct interpretation of experimental results. We shall now see that their influence is different for different kind of ion sources. We shall consider three sources, frequently used in mass spectrometers.

A - Perturbation in the "Nier" type source.

In the simple case of a "Nier" type source being used without a magnetic field, the influence of the perturbation on the ionization probability curve is relatively small, because the low energy resolution cannot resolve fine structure in the curve. However, from perturbations a and b, we expect to observe displacements in the energy, similar to the effect of contact potential. We recall that the effect produced by a depends on the geometry, and the one produced by b on the space charge in front of the filament. b therefore depends on a, the temperature, and the electrostatic field surrounding the filament.

From eqn (1) we see that the energy spread is widened when the potential is increased. Consequently the discontinuities in the ionization probability curve should be more and more smoothed with increasing electron energy.

From these conclusions it is easy to realize that even in the absence of classical difficulties already discussed (1)(4)(5), it is extremely difficult to reconstruct all experimental conditions, because the exact geometry, and all the working conditions are not usually published in detail.

An overall conclusion, however, is that the electron energy resolution of a Nier source will not be quite as good as one would expect from consideration of its filament temperature alone, and worsens as electron energy is increased.

When a magnetic field is used in conjunction with this source, the influence of these perturbations is still more important because of the greater path length taken by the electrons.

B - Perturbations of the R.P.D. method.

This method developped by Fox et al. (6) has been able to resolve fine structure in the ionization probability curve, by cutting most of the tail produced by the electron energy spread. It is an ingenious and highly successful method. The importance of space charge effects has been recognize from the very beginning (4) but it has not hitherto been possible to predict its influence.

However, using the observations mentioned by Hartwig and Ulmer, we find that after the relaxation (c), and symetrization (d), the ionizing electrons once past the retarding electrode have a symetric distribution whether the retarding potential is applied or not. The difference between the two relaxed beams becomes:

1) A change in the total electron beam intensity (because slow electrons are eliminated before the second relaxation).
2) A displacement in the average electron energy, for the same reason.

Figure (1) qualitatively shows distributions A and B corresponding to the relaxed distributions of the retarded and non retarded electron beam. Let us consider separately the two changes just mentionned. To do so, we draw on the figure an intermediate state B' in such a way that the distribution B' corresponds to the same current as A, but has the same energy as B. Let us chose arbitrarily narrow bands of electrons having a width ε , in the middle of the distributions A, B and B'. We will show later that the relaxation perturbs the ionization probability curve the same way whether we use the narrow bands α , β and β' or if we use the wide distributions A, B and B'.

When an electron beam α at energy ε_A produces ionization, the ion current $I_{i\alpha}$ is given by the relation:

$$I_{i\alpha} \propto \varphi(\varepsilon_A)\, I_{e\alpha} \qquad (2)$$

Where $\varphi(\varepsilon_A)$ is the ionization cross section for electrons having energy ε_A $I_{e\alpha}$ is the electron current.

Similarly,

$$I_{i\beta'} \propto \varphi(\varepsilon_{B'})\, I_{e\beta'} \qquad (3)$$

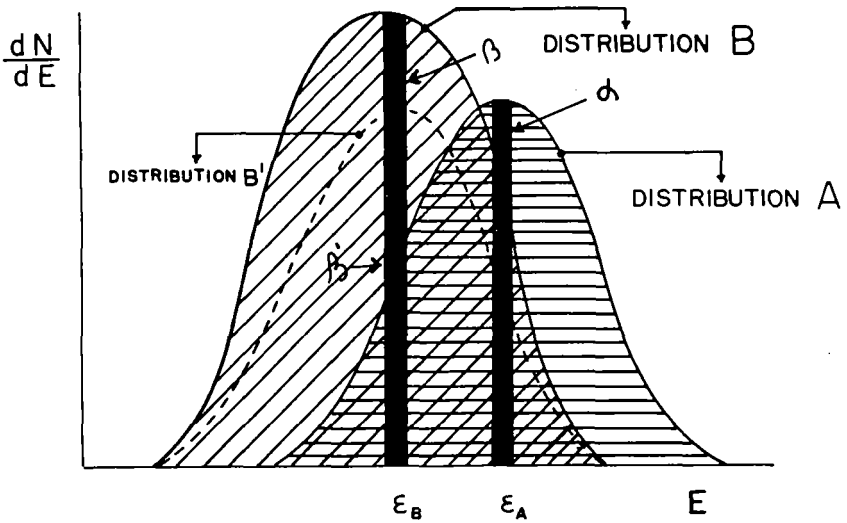

Fig. I

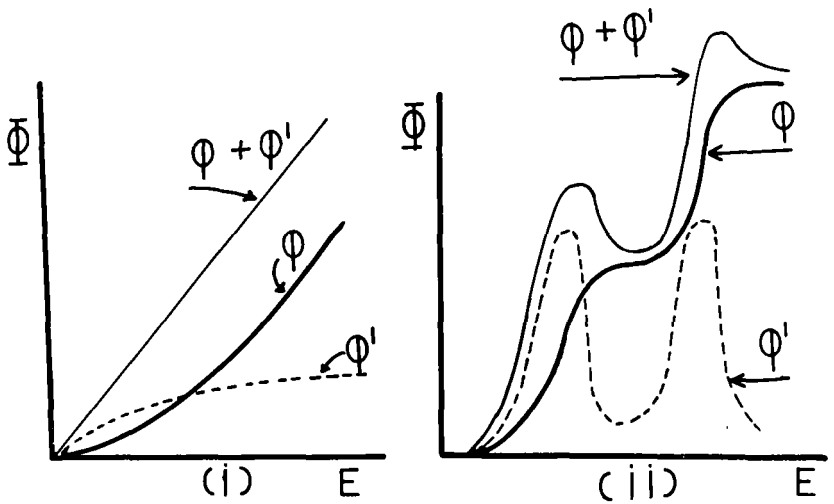

Figure II

By definition $I_{e\alpha} = I_{e\beta'}$

If $\mathcal{E}_A$ is close to $\mathcal{E}_{B'}$ then

$$\Delta I_{i(\alpha \rightarrow \beta')} \propto \Delta \left\{ \varphi (E) \right\} I_{e\alpha} \qquad (4)$$

When we pass from β' to β

we have in β' $\qquad I_{i\beta'} \propto \varphi(\mathcal{E}_{B'}) \; I_{e\alpha} \qquad (5)$

in β $\qquad I_{i\beta} \propto \varphi(\mathcal{E}_B) \; I_{e\beta} \qquad (6)$

By definition

$$\mathcal{E}_{B'} = \mathcal{E}_B \qquad (7)$$

Therefore

$$\Delta I_{i(\beta' \rightarrow \beta)} \propto \varphi(\mathcal{E}_B) \Delta I_e \qquad (8)$$

Thus when we pass from distribution α to β we have:

$$\Delta I_{i(\alpha \rightarrow \beta)} = K_1 \Delta \left\{ \varphi (E) \right\} I_{e\alpha} + K_2 \; \varphi(E) \Delta I_e \qquad (9)$$

where K_1 and K_2 are arbitrary constants.

That same demonstration could be applied to any other band " $\mathcal{E}$ " in A when we try to find its relation to the corresponding one in B and B' and we find a similar result. The total change in current is then given by the sum of the ΔI_i's corresponding to each " $\mathcal{E}$ ", i.e. will be the sum of $\Delta \left\{ \varphi (E) \right\} I_\alpha$ terms plus the sum of φ (E) Δ I terms.

Therefore

$$\Delta I_{iT} = \Delta I_{i(\alpha \rightarrow \beta)} = \sum^{m} K_1 \Delta \left\{ \varphi (E) \right\} I_\alpha + \sum^{n} K_2 \; \varphi(E) \Delta I \qquad (10)$$

In other words, the change in ion current is produced by the sum of terms containing the change of cross section $\Delta \varphi$ plus another sum containing the cross section φ itself.

In the R.P.D. method, the "ion current" plotted is just such a difference of two ion currents obtained with different $\sum \mathcal{E}$'s . Therefore the R.P.D. ion current is a function of the cross section plus its derivative $\Delta\varphi$, the two being added in various proportions depending on K_1 and K_2 .

Typical curves.

Curve φ figure 2i shows a curve having the typical aspect of an ionization curve using an electron beam with a certain energy spread. We have used the function $\varphi = e^{-E} + E - 1$ where E is the electron energy. The derivative φ' is plotted on the same figure, and also $\varphi + \varphi'$. It is interesting to notice that from eq. 11 we expect to get with the R.P.D. method " $\varphi + \varphi'$ " which gives straighter lines and sharper breaks even if the electron energy is not improved. Figure 2ii shows how step functions with electron energy spread (function φ) could appear using the R.P.D. method ($\varphi + \varphi'$). Such a curve $\varphi + \varphi'$ has been obtained experimentally (7). Finally we must not forget that all the perturbations existing in the "Nier" source also exist when the R.P.D. method is used, so that its resolution should diminish with electron energy.

Variation of source parameters (such as drawing out potential and retarding potential) will affect the constants K_1 and K_2, and thus the shape of the ionization probability curve. This has been observed (8).

C - Electrostatic electron selector.

When an electrostatic electron selector is used (e.g. ref 9), the energy distribution is determined by the instrument and we do not expect a Maxwellian energy distribution. Therefore perturbation a is not pertinent.

The electron selector as a whole is not a space charge limited electron source. Consequently perturbation b does not exist.

When the selector is working normally, the space charge in the discrimination region inside the instrument do not produce scattering or relaxation. Ordinarily the electron current is so low that a well designed ion box could be made to avoid any other relaxation. In the absence of this relaxation, perturbations c and d are eliminated. Consequently we may expect the selector to give ionization probability curves with fine structure and no component proportional to their derivatives.

The author wish to thank Dr L. Kerwin, Mr. J.D. Carette and N. Papp for their encouragement and helpful discussions throughout the progress of this work.

4 - References.

(1) Asundi and Kurepa J. Sci Inst Vol 40 P. 183 (1963).
(2) H. Boerch Z. Phys. 139 No 2 P. 115-46 (1955).
(3) D. Hartwig and K. Ulmer Z. Phys Vol 73 No 3 P. 294-320 (1963).
(4) J.A. Simpson Rev. Sci. Inst. 32, 1283 (1961).
(5) P. Marmet and J.D. Morrison J. Chem Phys 36 1238 (1962).
(6) Fox et al. Phys. Rev. 84, 859 (1951).
(7) G. Schulz Phys. Rev. 106, 1179 (1957).
(8) D.C. Frost and C.A. Mc Dowell Proc. Roy Soc A 232, 230 (1955).
(9) P. Marmet and L. Kerwin Can J. of Physics 38, 972 (1960).

Captions for Figures

Figure 1 — Electron energy distribution after relaxation.
Distribution A: when retarding potential is applied.
Distribution B: when retarding potential is not applied.

Figure 2 (i) — Ionization probability curve with a certain electron energy distribution.

$\Phi = \varphi I_e$

$\varphi = e^{-E} + E-1$ with Nier source

$\varphi + \varphi' = E$ with R.P.D. method

(ii) — Autoionization probability curve

$\varphi =$ with Nier Source

$\varphi + \varphi' =$ with R.P.D. method.

DETERMINING APPEARANCE POTENTIALS FROM NON-IDEAL IONIZATION EFFICIENCY CURVES*

Harry J. Svec and Gerald D. Flesch

Institute for Atomic Research and Department of Chemistry
Iowa State University, Ames, Iowa

For several years electron bombardment studies of volatile inorganic compounds have been going on in our laboratories at Iowa State University. Among the general classes of compounds studied are oxychlorides and oxyfluorides of transition elements such as Cr and V; fluorides of xenon, the noble metals and other elements and hydrides of the Group VI and V elements. The compounds are generally very reactive or they are unstable. They are excellent halogenating agents and react with the materials in the sample system and the ion source or they decompose in the mass spectrometer leaving a variety of non volatile residues. As a result of this compound reactivity and/or instability, contact potentials in our ion sources are generally quite high. It has not been unusual for these to be between 2.5 and 4.0 V and we have observed them as high as 6.0 V. It is imperative then that a calibrating gas be ever present.

Additionally, we are frequently concerned with a sampling situation in which a constant decrease in the amount of sample entering the instrument is observed. Accordingly, whenever ionization efficiency measurements are made, we cannot simply observe an ion current as a function of electron accelerating voltage but must use a ratio of currents even while making the measurements in order to obtain meaningful data. Thus we collect data by alternately measuring ion currents first at a predetermined reference electron accelerating voltage and then at diminishing voltages. By this means we hope to obviate errors due to the pressure drop.

The fragment ions from these compounds are of interest because we are concerned with learning as much as possible about the ion source chemistry. Therefore in the treatment of ionization efficiency data it is expedient that we have a method which will give information from which one may possibly infer what chemical reactions are taking place. We are not primarily concerned with excited states in these molecules; the compounds are either much too complex or ill behaved to have been amenable to spectroscopic treatment and electron bombardment information about possible excited states has little or no meaning at this time. We are, however, concerned with the possible and probable chemistry in the ion source and the potential use of our observations to obtain thermochemical information about the compounds.

A survey of standard references in mass spectroscopy will tell you that some methods for determining ionization potentials from ionization efficiency data are preferable to others. Unfortunately, some of those which produce reasonably good ionization potentials for molecules of well behaved materials are not simple to apply. In our search for a method of treating both molecule and fragment ionization efficiency data we have compared several methods and have found a couple methods ourselves. These latter methods are the topics of discussion in this paper.

We intend to compare the linear extrapolation method, the semi-logarithm plotting methods, the extrapolated difference method, an ion current ratio extrapolation method based on a changeable electron accelerating voltage reference and a "parallel slope" method which is an adaptation of the critical slope method. Of these methods, there is no need to discuss the mechanics of the first three since they are well known. It is necessary, however, to discuss the other two methods since they are not generally known, although the ion current ratio extrapolation method has been described in one of our papers.

The mechanics of preparing ionization efficiency curves by this method are shown in Fig. 1. The gas is argon and the ion A^+. First a

* Work was performed in the Ames Laboratory of the U. S. Atomic Energy Commission.

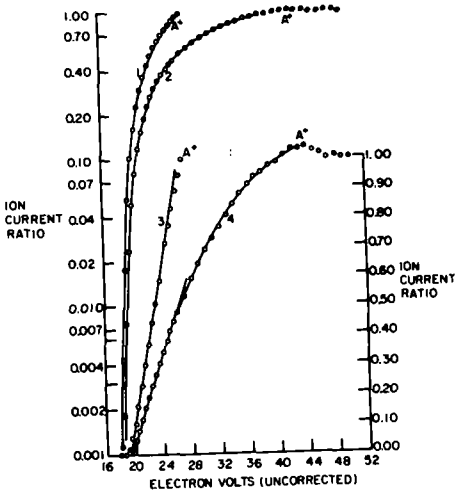

Fig. 1. Mechanics of preparing ratio extrapolation plots of ionization efficiency data.

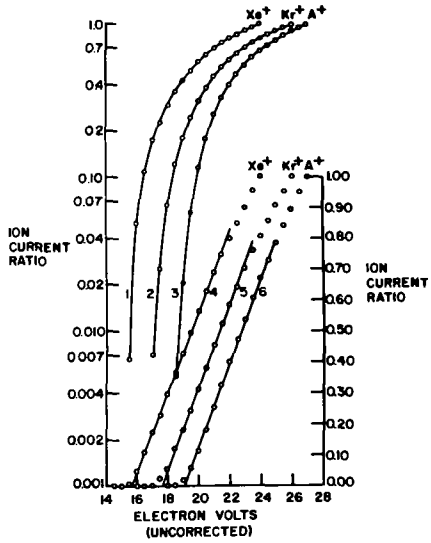

Fig. 2. Ratio extrapolation and semi-log plots of ionization efficiency data for Xe^+, Kr^+ and A^+.

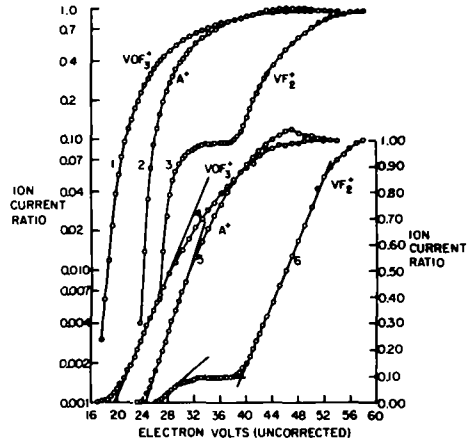

Fig. 3. Ratio extrapolation and semi-log plots of ionization efficiency data for VOF_3^+, A^+ and the fragment ion VF_2^+ from VOF_3.

rapid determination of the ionization efficiency is made by taking data at 0.5 V intervals. Curve 4 on this figure shows a plot of the data so obtained as the ratio of the ion current at a particular ionizing voltage to that at 50 V. There is no reason for this choice of reference voltage other than the fact that 50 V is a reference point commonly used for the semi-log plotting method of obtaining appearance potentials. The ordinate of plots 3 and 4 is on the right and represents a ratio of ion currents. A straight line can be drawn through the initial points on Curve 4 but at some point above the onset, the data deviates from linearity. A new reference voltage is chosen one volt above this point of deviation. A new ratio is then obtained using this new reference voltage and a plot of these new data made as shown in Curve 3. Of course the linear portion of the new curve extends over a considerable fraction of the plot. Similar plots are then made for all other ions of interest and the gas standard, which is running into the mass spectrometer simultaneously with the sample. Such plots have some rather interesting additional properties which will be discussed later. Curves 1 and 2 are semi-log plots (ordinate on the left) of the same ratios used in Curves 3 and 4, and show that this method of handling data has little effect on the character of semi-log plots.

For well behaved materials, one usually depends upon the parallelism of ionization efficiency plots to indicate whether or not the ionizing probabilities occurring in a sample are similar to those occurring in the reference gas. Figure 2 shows both semi-log plots and variable reference ratio plots of the singly charged ions from Xe, Kr and A. In these cases each set of three curves shows that indeed the ionizing probabilities are the same as was to be expected.

Two methods were used to obtain ionization potentials from these plots and both give comparable results. In the case of the ratio plots 4, 5 and 6, the most convenient values are obtained by extrapolating to an ordinate value of zero. In the case of the semi-log plots 1, 2 and 3, the most consistent values for the ionization potentials are obtained from points on the curves where the slopes are parallel. It has been found that in well behaved gases like these, it doesn't matter where the points are chosen. Indeed, comparison of slopes at several points is an excellent way of deciding whether or not the ionization efficiency curves represent the same ionizing process in each sample.

A summary of the results obtained when these two methods were applied to the data shown in Fig. 2 is given in Table I. The differences

Table I Differences in the ionization potential of rare gases in electron volts

Rare gas ions		Spectroscopic	Extrap. differences	Dibeler method semi-log	Parallel slope semi-log	Ratio extrap.
Xe	Kr	1.87	1.30	1.65	1.85	1.96
Xe	A	3.63	3.00	3.05	3.55	3.53
Kr	A	1.76	1.72	1.40	1.70	1.57

of the ionization potentials obtained by other methods using the same data are also given. Column 2 represents spectroscopic values; column 3, values obtained with the method of extrapolated differences; column 4 by the method used by Dr. Vernon Dibeler in conjunction with semi-log plots; column 5, the parallel slope method applied to semi-log plots; and column 6, the ratio extrapolation plots. The agreement with spectroscopic values is found generally to be better for the last two methods than for the other two. We did not include values based on Lossing's 1 % level for semi-log plots because our method of plotting ratios based on a changeable reference, rules out legitimate application of this method.

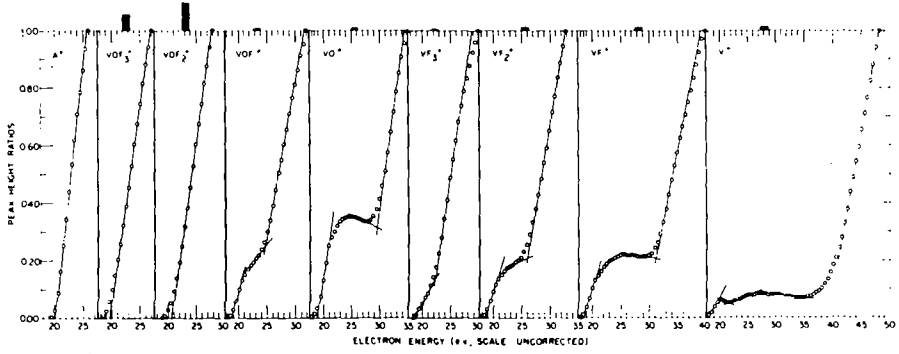

Fig. 4. Ratio extrapolation plots of ionization efficiency data for the positive ions from VOF_3.

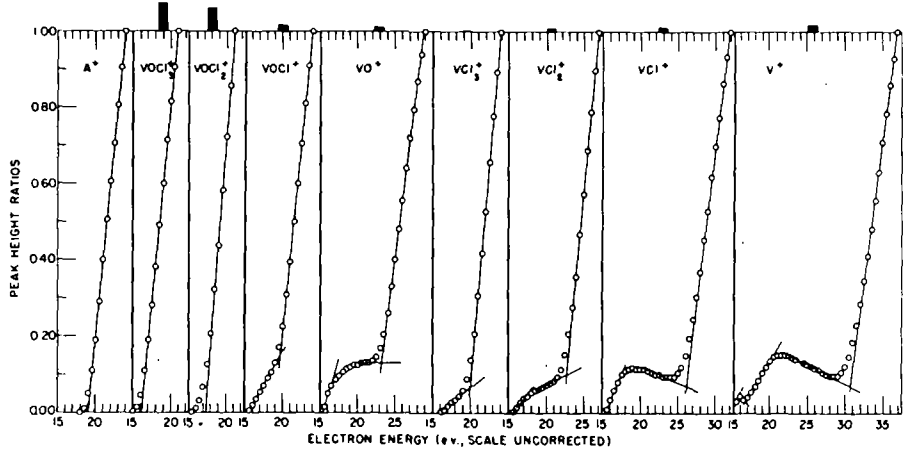

Fig. 5. Ratio extrapolation plots of ionization efficiency data for positive ions from $VOCl_3$.

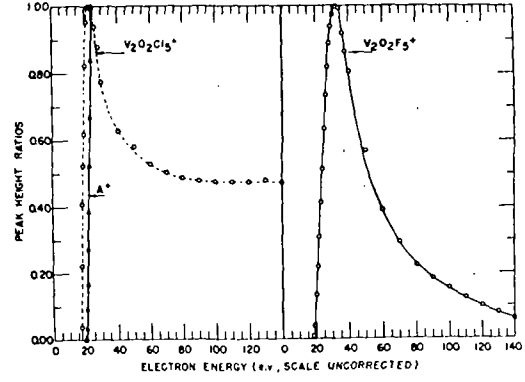

Fig. 6. Ratio extrapolation plots of ionization efficiency data for $V_2O_2Cl_5^+$ and $V_2O_2F_5^+$.

The real purpose, however, is not to belabor one or another of the ionization efficiency plotting methods but to present a means by which we can treat data for all ions we observe from these inorganic compounds. For this reason the remainder of the paper will be devoted to a description of the treatment of data obtained from the vanadium oxyhalides. To illustrate some of the problems, Curves 4, 5 and 6 of Fig. 3 show the rough ionization efficiency curves for the molecule ion, VOF_3^+, and the fragment ion, VF_2^+, based on an electron accelerating reference of 50 V. In addition a similar plot of A^+ is presented. In this figure Curves 1, 2 and 3 are semi-log plots of the same data. Curves 4 and 6 appear to have similar portions although these are certainly not parallel to Curve 5. The foot of Curve 6 indicates that the ion source chemistry is indeed complex. Curves 1 and 2 appear to be similar but very much different from Curve 3. Despite the similar appearance of Curves 1 and 2, inconsistent results are obtained for the ionization potential of VOF_3^+ when the parallel slope method is applied at several points on the curves. Thus the ionizing process for VOF_3^+ is considered to be more complex than would be suspected and the ionization efficiency curves probably represent two or more processes closely related energetically.

These and similar data for the remaining ions from VOF_3, have been replotted according to the variable reference method and are shown in Fig. 4. Note that the curves still indicate strongly the complexity of the ion source chemistry but that all have portions indicating that at least some of the ionizing processes are similar to that of argon. Furthermore, the ion current intensities varied widely, as indicated by the histogram over each fragment from VOF_3. It was, however, unnecessary to adjust the sample pressure so that any of these ion currents matched that of the reference gas. It was also unnecessary to resort to any plotting tricks to force the curves to be parallel and no arbitrary reading points were used to obtain appearance potentials. To indicate that this was not fortuitous, similar data from $VOCl_3$ are plotted and shown in Fig. 5. It is apparent that the main ionizing process is the same as that which occurs when argon is ionized.

If one considers the initial portion of the curves representing fragments which are the result of multiple bond ruptures, the onset voltages obtained from the value of the initial upward break are in each case less than the ionization potential of the parent ion. A discussion of these results is the subject of another paper but one can state here that the process responsible for ion fragments at these electron energies is due to chemi-ionization involving excited molecules in the gas phase and adsorbed on surfaces in the ion source. Appearance potentials for the main ionizing process at high electron energies are obtained from intercepts as are shown on the figure.

This method of handling data is applicable to a large variety of ion source situations. For example, ionization efficiency curves for $V_2O_2Cl_5^+$ and $V_2O_2F_5^+$ ions are shown in Fig. 6. These ions are formed in the ion source when appropriate vanadium oxyhalides are in the mass spectrometer. The curves suggest the existence of some kind of resonance process. A plot of argon data is also shown on the left. Even in this case the parallelism of the plots is evident in spite of the fact that the ion intensities differ by a factor of three or four.

In summary, this method of handling ionization efficiency data is submitted for your consideration. We feel that this ion current ratio extrapolation method of treating ionization efficiency data is reliable and accurate enough to be applied to fragment ions as well as molecular ions. While it does not enable us to ascertain certain details of the energy states of the molecules and fragment ions we are concerned with, the handling problems connected with these compounds introduce uncertainties which make the use of more sophisticated methods of dubious value considering the extra effort entailed in their use. Recent calorimetric values for Heats of Formation of representative compounds among those we've studied are in very good agreement and thus we feel justified in our assumptions concerning the ion source processes and values obtained for appearance potentials using this ratio extrapolation procedure.

COMPARISON OF METASTABLE SPECTRA FROM SINGLE AND DOUBLE FOCUSING MASS SPECTROMETERS

M. Barber and R.M. Elliott,

Associated Electrical Industries Limited,
Manchester, England.

ABSTRACT

Metastable peaks are of great interest in the field of qualitative identification and structure of unknown organic compounds because of the information they provide on fragmentation mechanisms, often indicating the identity of large fragments of the molecule not otherwise obvious from the normal mass spectra. Some examples of this type of application are given.

In the qualitative field, it is an advantage to have intense metastable peaks, in contrast with conventional quantitative work where it is desirable to suppress them. It is also of value if the mean mass of a metastable peak can be estimated accurately, so that the origin of the ion can be deduced. Relative intensity and accuracy of mass estimation are considered in detail with reference to 180° and sector field single-focusing and Nier-Johnson and Mattauch-Herzog double-focusing mass spectrometers. The particular advantages of the Nier-Johnson geometry are demonstrated experimentally.

INTRODUCTION

The proof of the existence of an ionic decomposition process $m_1^+ \rightarrow m_2^+ + m_3$ is of great practical significance in qualitative organic analysis. One of the most positive proofs that such a process is occurring is the observation of a so-called "metastable" peak at mass m_2^2/m_1 (1). The knowledge is useful in three ways:

(i) it may confirm that an ion m_2^+ is a true fragment ion and not due to a decomposition product. Figure 1 shows the parent peak region of a triglyceride spectrum. The group of peaks 18 mass units lower than the parent peak group might be interpreted as being due to thermal decomposition in the inlet system, but the prominent metastable at mass 822.4 due to the process 858 $\rightarrow$ 840 + 18 (presumably H_2O) indicates that to a large extent at least the water molecule is lost in an ionic fragmentation process occurring after ionization of the complete molecule.

(ii) the existence of such a process may indicate that a particular group m_3 exists as an entity. Thus in the spectrum of dihydrorobustic acid (2), $C_{22}H_{22}O_6$, the fragment peak at mass 234 is known by mass measurement to be $C_{13}H_{14}O_4$. The existence of a metastable peak at mass 143.4 corresponding to the process $C_{22}H_{22}O_6^+ \rightarrow C_{13}H_{14}O_4^+ + C_9H_8O_2$ indicates that the $C_9H_8O_2$ group exists as a structural unit in the molecule. Other possibilities which might have been considered for the formation of the 234 peak, such as the loss of CH_3O followed by the loss of another group C_8H_5O, are ruled out.

(iii) on the other hand, evidence for the successive loss of such groups is very useful in organic structure work in elucidating the breakdown mechanisms at work in a particular group of compounds. For example, in the case of the fragment peak at mass 179 ($C_9H_7O_4$) in dihydrorobustic acid there is no metastable peak at mass 83.9 corresponding to the single stage process $C_{22}H_{22}O_6^+ \rightarrow C_9H_7O_4^+ + C_{13}H_{15}O_2$ but there is a metastable peak at 136.4. This

corresponds to the second stage of the process

$$C_{22}H_{22}O_6^+ \longrightarrow C_{13}H_{15}O_4^+ + C_9H_7O_2$$

$$C_{13}H_{15}O_4^+ \longrightarrow C_9H_7O_4^+ + C_4H_8$$

indicating that the C_4H_8 group is lost separately and therefore may well be located in a quite different part of the molecule from the $C_9H_8O_2$ group previously shown to exist.

In addition, since metastable peaks correspond to a direct observation of an actual fragmentation process they are of great interest in theoretical studies of mass spectra.

It is therefore desirable, for a variety of reasons, that the metastable peaks due to these transitions should be readily observable. In particular the peaks should be of reasonable intensity, they should stand out clearly from the normal spectrum, and it should be possible to measure the mass at which the peak occurs with fair accuracy in order to deduce the masses m_1 and m_2 involved in the transition. Different instrument configurations are compared below in terms of these criteria.

OBSERVATION OF METASTABLE PEAKS IN DIFFERENT ANALYSER SYSTEMS

Figure 2 shows, for the most common types of analyser system, the regions where metastable transitions can occur which give rise to collectable ion currents. In general the region in which the transitions must take place in order to give rise to the usual broad but nevertheless distinct peaks is the straight portion of the ion path preceding the magnetic analyser, and the length of this portion is the main parameter determining the intensity of the peaks.

180° Magnetic Instruments

In 180° instruments there is no ion path preceding the analyser, but because of a special property of the 180° analyser (3) there is a short portion of the path within the magnetic field where observable transitions can take place. Nevertheless, because the path length is short the peaks are of low intensity. They are also unsymmetrical, so that the position in the mass scale is uncertain and may differ from the nominal mass m_2^2/m_1 by a few tenths of a mass unit. It is probably for this reason that metastable peaks have not been considered as useful, or used with the same confidence, by users of 180° instruments as in the case of sector instruments.

Magnetic Sector Instruments

The 90° sector single-focusing analyser shown in Figure 2 is identical with the magnetic analyser of the Nier-Johnson double focusing system shown beneath. A similarity in the metastable spectra obtained from two such instruments would therefore be anticipated. Figure 3 shows portions of spectra of n-hexadecane obtained from two instruments of this kind, the double focusing instrument being the A.E.I. MS9. A comparison of the two sets of spectra indicates the following:

(i) the intensities of the metastable peaks are virtually identical for equal values of resolution. It has been suggested that metastables are more intense in double focusing instruments. These spectra show that they certainly are of good intensity but that the geometry of the magnetic analyser is the important factor and not the double focusing principle.

(ii) the collector slit plays a major role in determining intensity (4). In each set of spectra increased resolution was achieved by narrowing the collector slit only, the height of the normal peaks being kept constant.

(iii) at high resolution the intensity of the metastable peaks

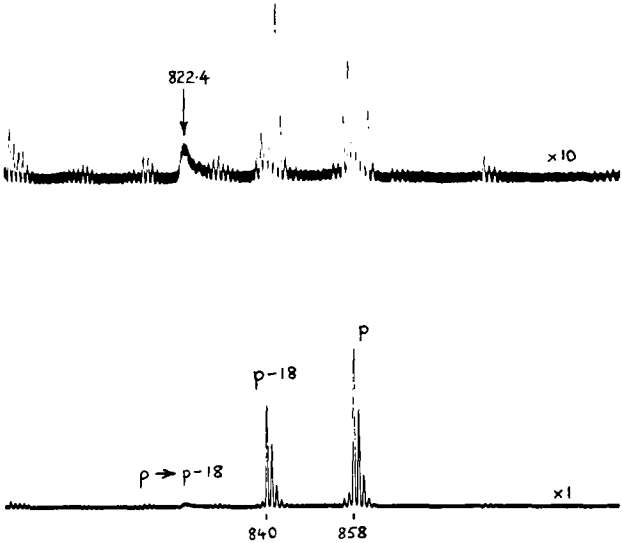

Fig. 1 PALMITO-DIOLEIN — PARENT PEAK REGION

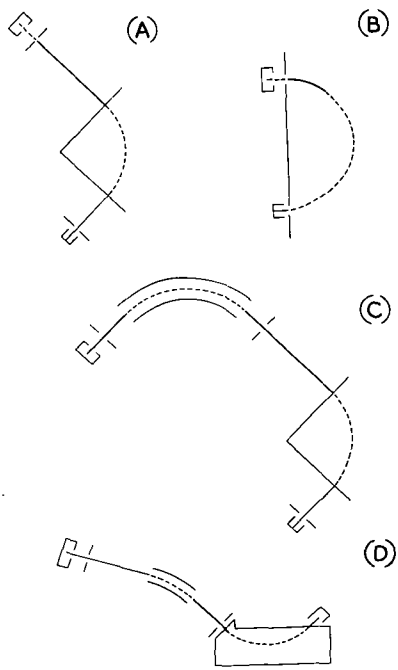

Fig. 2 REGIONS OF FORMATION OF METASTABLES.

——— Collected at discrete mass
- - - - Collected as continuum

is far too low for practical use. On the other hand, at low resolution the metastable peaks are intense but are rather difficult to distinguish from the normal peaks. The optimum condition is evidently a resolution in the region of 1000, where the intensity is still reasonable but the normal and metastable peaks appear as two distinct and easily distinguishable sets.

(iv) the metastable peaks are of uniform and symmetrical shape and in both cases appear at the correct nominal mass at least to within 0.1 mass unit.

For metastables to be readily observed under optimum conditions the ideal instrument should therefore be double focusing, so that a resolution of 1000 is readily obtained, but should have an easily adjustable collector slit so that operation is not restricted to high resolution conditions.

Mattauch-Herzog Instruments

The length of the relevant portion of the ion path, between the analysers, is usually shorter in Mattauch instruments than in the sector types described above. A more fundamental reason for lower intensity in the Mattauch case arises from the focusing properties. The fragment ions resulting from a transition are usually formed with kinetic energy, and therefore form a divergent beam. In the Nier geometry there is an intermediate image between the analysers so that a divergent beam originating at this point will be refocused at the collector, and even for other points along the ion path there is some degree of focusing. In the Mattauch geometry the ions must form a parallel beam between the analysers in order to be focused at the collector so that a diverging beam arising at any point along this portion of the path will not be focused.

Figure 4 shows the same portion of the n-hexadecane spectrum obtained on the A.E.I. MS7 Mattauch-Herzog instrument under conditions otherwise identical with those of Figure 3. The intensity of the metastable peaks is about one order of magnitude less than in the spectra for the other two instruments in Fig.3.

Photographic Plate Detection

The photographic plate is not a favourable detector for metastable peaks, as Figure 5 shows. The upper curve represents the intensity distribution in the ion beams as they approach the collector. As the collector slit width is increased, more and more of the wide metastable beam is accepted and the observed intensity rises by a significant factor relative to the normal peaks. On the photoplate, however, the response is identical with the beam intensity distribution. Since relative intensities of metastable peaks are usually below one per cent even with wide collector slits, very few metastable peaks will be observable at all using the photoplate as a detector.

SPECIAL FEATURES OF THE NIER-JOHNSON SYSTEM

The ion optical system of a Nier-Johnson instrument gives it two further advantages for observation of metastable peaks.

Suppression of Metastable Continuum

In single focusing instruments transitions occurring during acceleration of the ions in the ion source give rise to a continuum stretching down from the mass m_2^2/m_1 of the metastable peak to the mass m_2 of the daughter ion. In some circumstances this may lead to distortion of the shape of the metastable peak. In a double focusing instrument these ions will not normally reach the collector but a continuum may be observed due to a different cause, namely transitions occurring in the electric analyser. However, in the Nier-Johnson case this can also be suppressed.

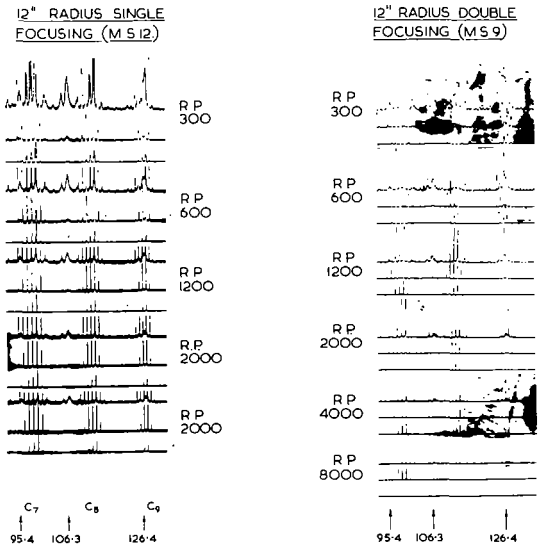

Fig. 3 - METASTABLE PEAKS IN n—HEXADECANE.

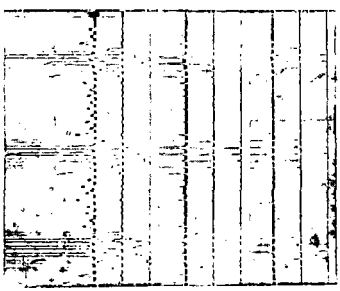

Figure 4

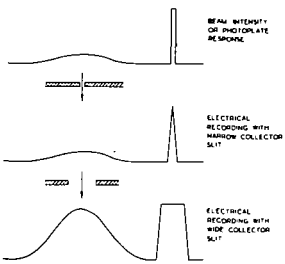

Fig. 5 DETECTION SENSITIVITY FOR METASTABLE PEAKS

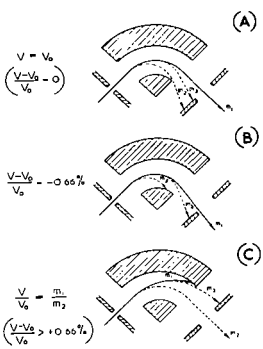

Fig. 6

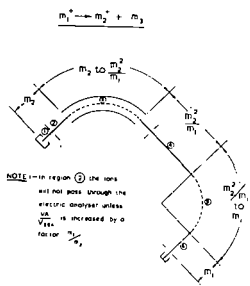

Fig. 8

In Figure 6(a) the m_2^+ ions arising from transitions before or in the electric analyser, having an energy of only $m_2/m_1 \cdot V_o$, are deflected more than the normal ions with energy V_o. If the normal beam passes through the centre of the intermediate slit, some of the metastable ions can pass through the lower half of the slit and will be recorded as part of the continuum mentioned above. Whether the whole or only part of the continuum is observed depends upon the difference in mass between m_2 and m_1 and the width of the intermediate slit. However, the continuum can be completely suppressed by operating the electric analyser in such a manner that the normal ion beam passes just above the lower edge of the intermediate slit as shown in Figure 6(b). This mode of operation is readily achieved by keeping the analyser deflector plate voltage constant and reducing the ion accelerating voltage; in the case of the MS9 the required change is 0.66% of the nominal accelerating voltage.

In Figure 7, which shows a series of metastable peaks in the spectrum of n-hexadecane, the first trace corresponds to this recommended condition; on increasing the ion accelerating voltage to a value 0.6% above nominal, where the normal ion beam passes just inside the upper edge of the intermediate slit, a portion of the continuum due to transitions $C_3H_7^+ \rightarrow C_3H_5^+$ occurring in the electric analyser appears. This not only distorts the shape of the peak at mass 39.1 but could also be erroneously interpreted as a genuine metastable peak of mass 39.4.

In observing metastable peaks it is therefore most important to suppress the continuum in the manner described. It is only possible to do this satisfactorily in instruments such as the Nier-Johnson type where an intermediate image and a true energy spectrum is formed at the intermediate slit.

When these precautions are taken the peaks are quite symmetrical and an accuracy of mass measurement of 100 ppm is possible. This would be sufficient, for instance, to distinguish between metastable peaks due to the loss of HCN and C_2H_3 from ions up to about mass 100.

Suppression of Normal Peaks - Observation of Pure Metastable Spectrum

Fig. 6(c) shows the situation when the ion accelerating voltage is increased beyond the point 0.66% above the nominal value. The normal ions cannot now pass through the intermediate slit and are not recorded. However, at the point where the ion accelerating voltage reaches a value $m_1/m_2 \cdot V_o$ the ions having undergone a transition $m_1^+ \rightarrow m_2^+$ in the region between the ion source and the electric analyser have just the right energy to pass through the intermediate slit. Because these ions have mass m_2 on entering the double focusing analyser system, they are observed at mass m_2 irrespective of their energy. Examples are shown in Figure 7(c) and (d). Peaks are observed corresponding to $m_2 = 38$ and 39 in Fig.7(c) and $m_2 = 37$, 39 and 40 in Fig. 7(d).

Observing metastable peaks in this manner, the transition involved is completely specified by the mass at which the ions are observed (m_2) and the ratio by which the ion accelerating voltage is increased (m_1/m_2). This is in contrast to the normal metastable peaks where only the mass m_2^2/m_1, is observed, for which an infinite number of pairs of values m_1 and m_2 exist. This technique therefore provides a means of identifying the transition leading to particular metastable peaks unambiguously. This may be particularly useful:

(i) where two possible transitions exist which would both give the same metastable mass (ii) where the metastable peak occurs precisely at the mass of an intense normal fragment ion so that it is difficult to observe (iii) where two metastable peaks occur so close together that they are not resolved. An example of this kind occurs in Fig.7. Two obvious possibilities exist leading to metastable peaks at a mass just over 37:

(1) $C_3H_3^+$ (39) $\rightarrow$ $C_3H_2^+$ (38); metastable peak mass 37.03

(2) $C_3H_5^+$ (41) $\rightarrow$ $C_3H_3^+$ (39); metastable peak mass 37.10

Examination of Figure 7(a) indicates that both are probably present but it is impossible to resolve them from each other or from the adjoining metastable peak. However, in the first case m_1/m_2 = 1.0263 and in the second m_1/m_2 = 1.0465. The two processes can therefore be observed quite separately by increasing the ion accelerating voltage by 2½% as in Fig.7(c), when a peak is observed at mass 38 corresponding to (1), and by 5% as in Fig.7(d) when a peak is observed at mass 39 corresponding to (2).

Finally, the ability to observe transitions occurring in two distinct portions of the flight of the ion raises the interesting possibility that rate constants for fragmentation processes could be directly measured by observing the relative numbers of transitions taking place in the two regions. For example, compare the height of the peak at mass 39 in Fig.7(d) with the maximum possible peak height which could be attributed to mass 37.10 in Fig.7(a). It is clear that a far greater number of transitions $C_3H_5^+ \rightarrow C_3H_3^+$ are occurring in the 6-inch length of ion path before the electric analyser than in the 21-inch length between the analysers. An estimate of the relative numbers of transitions per unit time in the two regions (37), together with the knowledge that the time taken for ions of mass 40 to travel the intervening distance is 4×10^{-6} sec., enables the time constant for this fragmentation process to be estimated as $4 \times 10^{-6}/\log_e 37 = 1.1 \times 10^{-6}$ sec. In less complicated cases it should be possible to obtain quite accurate values for processes having time constants in the 10^{-7} to 10^{-4} sec. range.

ACKNOWLEDGEMENTS

The authors wish to thank the Directors of Associated Electrical Industries Limited for permitting publication of this paper.

REFERENCES

(1) Hipple and Condon, Phys. Rev. 68, 54 (1945).

(2) Pelter, Johnston and Barber, Tetrahedron Letters (1964).

(3) Coggeshall, J.Chem. Phys. 37, 2167 (1962).

(4) Beynon, Saunders and Williams, Industrie Chimique Belge, No.4 (1964).

FIGURE CAPTIONS

Fig.1. Parent peak region of palmito-diolein spectrum.

Fig.2. Formation of metastables in (A) 90° sector (B) 180° (C) Nier-Johnson double focusing (D) Mattauch-Herzog double focusing instruments.

Fig.3. Comparison of metastable spectra in the C_7 - C_9 region of n-hexadecane for single and double focusing mass spectrometers with identical 90° sector magnetic analysers.

Fig.4. Metastable spectra in the C_7 - C_9 region of n-hexadecane for a Mattauch-Herzog double focusing mass spectrometer (A.E.I. MS7) for resolutions of 200, 600 and 1200.

Fig.5. Comparison of detection sensitivity for metastable peaks by photographic plate and electrical recording.

Fig.6. Trajectories of normal and "metastable" ions in the electric analyser (Nier-Johnson type) for different values of ion accelerating voltage V (V_0 = nominal value).

Fig.7. Metastable spectra recorded on the A.E.I. MS9 mass spectrometer in the mass 40 region of n-hexadecane for various settings of the ion accelerating voltage V.

Fig.8. Diagram showing the mass at which metastable ions appear for different regions of formation in the Nier-Johnson analyser system.

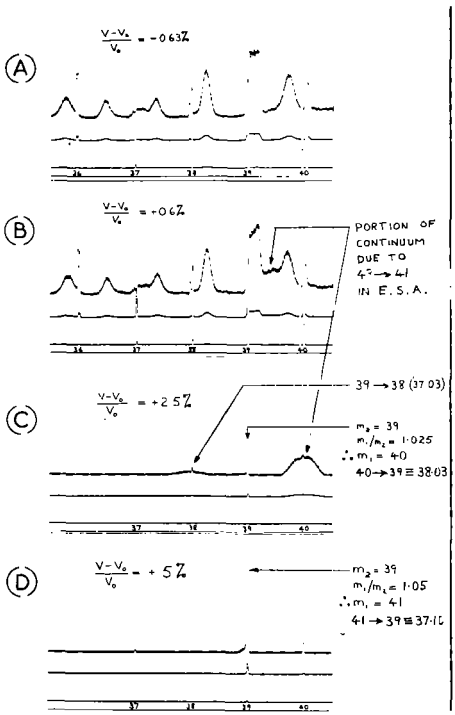

Fig. 7

Direct Observation of Pairs of Positive Ions Resulting from the Decomposition of CO_2^{++}

K.E.McCulloh, T.E.Sharp* and H.M. Rosenstock

Physical Chemistry Division
National Bureau of Standards
Washington,D.C. 20234

The origin of high kinetic energy fragment ions in mass spectra is a matter of controversy. Some authors(1-5) attribute these ions to the decomposition of doubly charged parent ions into two singly charged fragments, the high kinetic energy arising from coulomb repulsion. Others (6,7) propose that these ions result from decomposition, without randomization of the excitation energy, of singly charged ions from repulsive potential surfaces.

An unambiguous test of the first proposal has been made by detecting both charged fragments and proving that they originated from the same molecule. The method employs multiple delayed coincidence techniques. Ionization by a 1 kv electron beam occurs in a uniform electrostatic field. Low energy electrons, ejected upon ionization, are accelerated to an electron multiplier which starts a delay generator. Ions are accelerated in the opposite direction through the uniform field to a second multiplier. The mass of a fragment ion is established by its arrival time at this detector, in delayed coincidence with the ejected electron (8). Positive ion pairs are observed by three-particle delayed coincidence, in which the time of arrival of the second fragment ion is also recorded.

In the present apparatus, initial ion kinetic energies of several electron volts produce pronounced effects on the ion travel times. These have been observed for the ion pairs in question leading us to conclude that the ion pairs have several volts kinetic energy. Although this represents only a crude estimate the results are in essential agreement with those of other workers (1-5).

Using this method the process

$$CO_2^{++} \rightarrow O^+ + CO^+ \qquad (1)$$

has been observed in carbon dioxide.

In addition the products $C^+ + O^+$ have been observed in delayed coincidence. It is not clear whether these ions result

from $CO_2^{++} \rightarrow C^+ + O^+ + O$ as suggested by Dorman and Morrison(9) (2)

or $CO^{++} \rightarrow C^+ + O^+$ (3)

or $CO_2^{+*} \rightarrow C^+ + O^+ + O^-$ (4)

---

* National Academy of Sciences- National Research Council Postdoctoral Resident Research Associate.

Finally, a search revealed no C^+ and O_2^+ in coincidence, indicating that the process $CO_2^{++} \rightarrow C^+ + O_2^+$ (5) is either relatively unimportant (less than 5% of process(1)) or does not occur at all.

The recovery time of the electronics did not permit a search for $O^+ + O^+$ in coincidence.

By elimination of other alternatives, Hall (10) has cited process (1) as the probable source of high kinetic energy O^+ in the 70 V mass spectrum of carbon dioxide. However, he was unable to detect a corresponding high kinetic energy CO^+. A process similar to (1), the decomposition of metastable CO_2^{++}, has recently been reported by Newton and Sciamanna (11).

Although the processes we observe are initiated by 1 kv electrons, it may be assumed that the same processes do occur at lower electron energies, as has been shown in other cases(12). Conversely, the absence of reactions (5) at 1 kv is good proof that this reaction is absent at lower electron energies.

Ion pairs have also been detected in N_2O, CH_4, CF_4 and C_3H_6. The results on C_3H_6 support the decomposition mechanisms proposed by Tsuchiya(5).

REFERENCES

1. P. Kusch, A. Hustrulid, and J.T. Tate, Phys. Rev. 52, 843 (1937).
2. A. Hustrulid, P. Kusch, and J.T. Tate, Phys. Rev. 54,1037 (1938).
3. F.L. Mohler, V. H. Dibeler, and R.M.Reese, J. Chem. Phys. 22, 394 (1954).
4. J. Bracher, H. Ehrhardt, R. Fuchs, O. Osberghaus, and R. Taubert, Adv. in Mass Spectrometry, 2, 285 (1962) Pergamon Press, New York.
5. T. Tsuchiya, Bull. Chem. Soc. Japan 36, 1290 (1963).
6. J.E. Monahan and H.E. Stanton, J. Chem. Phys. 37, 2654 (1962).
7. J.A. Olmstead, UCRL 10687 (1963).
8. H.M. Rosenstock, U.S. Patent 2, 999, 157.
9. F. H. Dorman and J.D. Morrison, J. Chem. Phys. 35, 575 (1961).
10. R.M.S. Hall, Nature, 187, 683 (1960).
11. A.S. Newton and A. F. Sciamanna, J. Chem. Phys. 40, 718 (1964).
12. P. Kebarle and E.W. Godbole, J. Chem. Phys. 36, 302 (1962).

ION-MOLECULE REACTIONS IN METHANE AT LOW ION ENERGIES

A. G. Harrison and T. W. Shannon
Department of Chemistry,
University of Toronto,
Toronto 5, Canada.

ABSTRACT

A pulsed ion source has been constructed which permits variation of the time between ion formation and ion withdrawal for analysis. With this source the ion-molecule reactions in methane and various deuterated methanes have been studied and rate constants obtained for the reaction of thermal energy ions. A technique has been developed for measuring the average residence time in the ion source in the presence of an electric field established by the repeller and rate constants have been obtained for the reactions of ions accelerated by this field. The results show that the rate constant as a function of repeller field has a minimum at low repeller fields.

INTRODUCTION

The reactions of ions with molecules in the gas phase have been studied extensively in the past ten years by mass spectrometry (1, 2). The usual technique has been to operate the ion source at a relatively high pressure with the result that the primary ions formed by electron impact undergo reactive collisions with neutral molecules as they move out of the ionization chamber under the influence of electric fields. The kinetic data thus obtained refers to the reaction of ions accelerated by these fields. Kinetic data for the reaction of thermal energy ions is highly desirable particularly for application to radiation chemistry.

Tal'roze and Frankevich (3) and, more recently, Hand and von Weyssenhoff (4) have reported experiments in which the time between ion formation and ion withdrawal could be varied and hence the reaction of quasi-thermal ions could be studied using reaction time as the experimental variable. The present paper reports the modification of a magnetic deflection instrument to permit operation of the ion source in a pulsed mode and the study by this technique of the hydrogen transfer ion-molecule reactions in methane and deuteromethanes for thermal energy ions.

EXPERIMENTAL

The modifications necessary for operation with a pulsed ion source were made to an A.E.I. MS-2 mass spectrometer. The major modifications were to the ion source and the potential supplies to the source. The modified source, similar in many respects to that used by Tal'roze and Frankevich (3), is shown schematically in Figure 1. The modifications consisted in the addition of an electron beam retarding plate to the electron gun and the enlargement

of the ionization chamber. The electrons, emitted from a directly heated tungsten or rhenium cathode, enter the ionization chamber through slits 0.5 x 3.0 mm. The distance from the centre of the electron beam to the repeller and to the exit slit are each 4.8 mm. The distance from the centre of the beam to the side walls is 6.9 mm.

In operation the spectrometer was focussed on an ion beam of interest during continuous operation. The electron beam was then arrested by applying a bias, negative with respect to the filament, to the beam retarding plate. A bias of 3-5 volts was sufficient as indicated by the disappearance of the ion beam. A positive pulse of 0.1 to 0.5 μsec. duration was then applied to the slit to admit the electron beam. With the electron beam pulsing a small positive potential was applied to the ion withdrawal slit to prevent withdrawal of the ions by penetration of the accelerating field. The ions were pushed out of the ionization chamber by a positive pulse of 2 μsec. duration applied to the repeller plate. The time between the two pulses and hence the reaction time for the ions in the ion source could be varied.

One of the problems in the study of ion-molecule reactions at low repeller voltages has been the possibility that space charges may alter the ion residence times appreciably from the times calculated assuming no space charge effects. A variation of the pulsed operation has proven useful in determining whether such effects are important in the present case and in determining directly the ion residence times. With the electron beam pulsing and a continuous repeller field pulses of ions are produced and accelerated out of the source by the repeller field. A known and variable time later a second short pulse is applied to one-half of the split focus plate. Any ions passing the focus plate at the time of the second pulse will be deflected and will not reach the collecter resulting in a diminution of the recorded ion current. By varying the time between the two pulses a time profile of the ions passing the focus plate is obtained. Typical results for the CH_4^+ ion at two repeller voltages are shown in Figure 2; in both cases the ionizing and deflecting pulses were each 0.2 μsec. In the absence of space charge the time, τ, for the ion to travel from the point of origin to the focus plate is given by the equation

$$\tau = [d(m/2s)^{1/2} + (2sm)^{1/2}] \quad (eE)^{-1/2} \qquad [1]$$

where d is the distance from the ion exit slit to the focus plate, s the distance from the point of origin to the exit slit, m the mass of the ion, e the charge on the ion, and E the repeller field. Figure 3 shows the average withdrawal time for the CH_4^+ ion, determined from the maxima of time profiles such as shown in Figure 2, plotted as a function of $E^{-1/2}$. The straight line obtained shows that space charge effects are not important in the present system down to 2 volts cm^{-1} and therefore that the calculated residence times can be used with confidence.

RESULTS AND DISCUSSION

For the general ion-molecule reaction

$$RH^+ + RH \longrightarrow RH_2^+ + R \qquad [2]$$

the integrated rate expression where reaction time is the experimental variable becomes

$$\log(1 + I_s/I_p) = k[RH]\, t/2.303 \qquad [3]$$

assuming the concentration of RH to remain constant and assuming equal collection efficiencies for both ionic species. A plot of the log

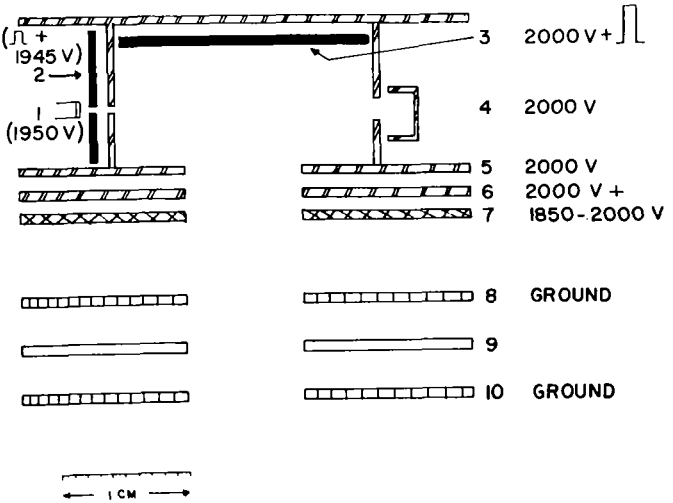

FIGURE 1

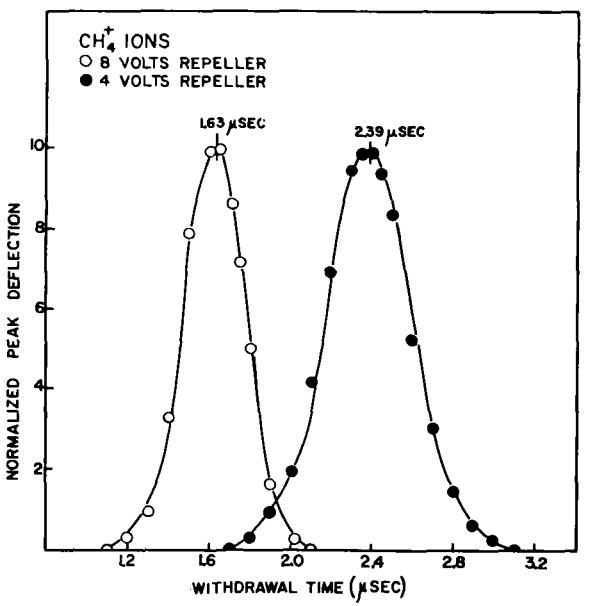

FIGURE 2

term versus reaction time or delay time between the ionizing and repelling pulses should give a straight line with a slope proportional to k. Typical results obtained for the transfer of H and of D in CH_2D_2 are shown in Figure 4. The dotted lines represent the uncorrected experimental data plotted in the manner of equation [3]. The lower curves give the variation of I_{18}/I_{17} and I_{18}/I_{16} as a function of delay time. Since only a small fraction of the ions are reacting the increase in these ratios must indicate preferential loss of the lighter ion from the region being sampled due to its higher thermal velocity. We have used this data to correct the observed I_s/I_p ratios leading to the points shown and satisfactory straight lines. From the slopes of such plots the rate constant data summarized in Table 1 were obtained. Each rate constant is the average of three or more determinations.

TABLE 1

HYDROGEN TRANSFER REACTION IN METHANES

MOLECULE	RATE CONSTANT (cc molecule^{-1} sec^{-1}) x 10^{10}			$kCH_4 \times (\mu H/\mu D)^{1/2}$
	k(per H)	k(per D)	k(total)	
CH_4	1.53		6.12	6.12
CH_3D	1.49	1.30 1.14	5.77	5.94
CH_2D_2	1.35	1.08 1.25	4.84	5.77
CHD_3	1.64	1.12 1.46	5.01	5.61
CD_4		1.18	4.71	5.46

The overall rate constant for the reaction in CH_4 is almost a factor of two lower than the values of 11.6 x 10^{-10} and 11 x 10^{-10} reported by Tal'roze and Frankevich (3) and Hand and von Weyssenhoff (4) respectively. This discrepancy would appear to be slightly greater than the combined limits of error. It might be noted that although the absolute error in the rate constant determination is rather large relative values such as reported in Table 1 can be obtained considerably more accurately. From columns 2 and 3 it is seen that the rate constant per hydrogen and the rate constant per deuterium remain essentially constant throughout the series of deuteriomethanes and lead to $k_H/k_D = 1.28$. The total rate constant for hydrogen transfer therefore decreases with increasing deuterium substitution as shown in column 4. This decrease is considerably greater than predicted by a reduced mass effect on the number of collisions. This is shown by comparison of the observed rate constants with the values calculated in the final column by multiplying k_{CH_4} by the appropriate ratio of the reduced masses. We would suggest that this large effect of deuterium substitution may indicate that an appreciable fraction of the initial collision complex reverts to the reactant species (equation [4]).

$$CH_xD_y^+ + CH_{x}DY \rightleftarrows CH_xD_y\text{-}\overset{+}{-}\text{-}CH_xD_y \begin{cases} \rightarrow CH_{x+1}D_y^+ \\ \rightarrow CH_xD_{y+1}^+ \end{cases} \qquad [4]$$

With increasing deuterium substitution the transfer step in the collision complex is slowed down with the consequence that a greater fraction of the complex reverts to the reactants. The net result

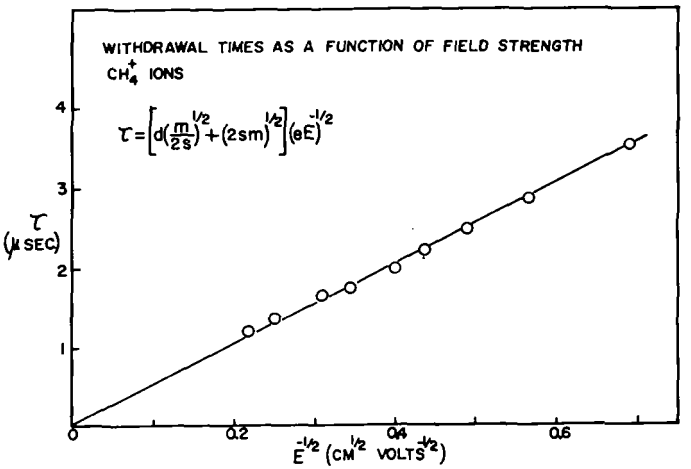

FIGURE 3

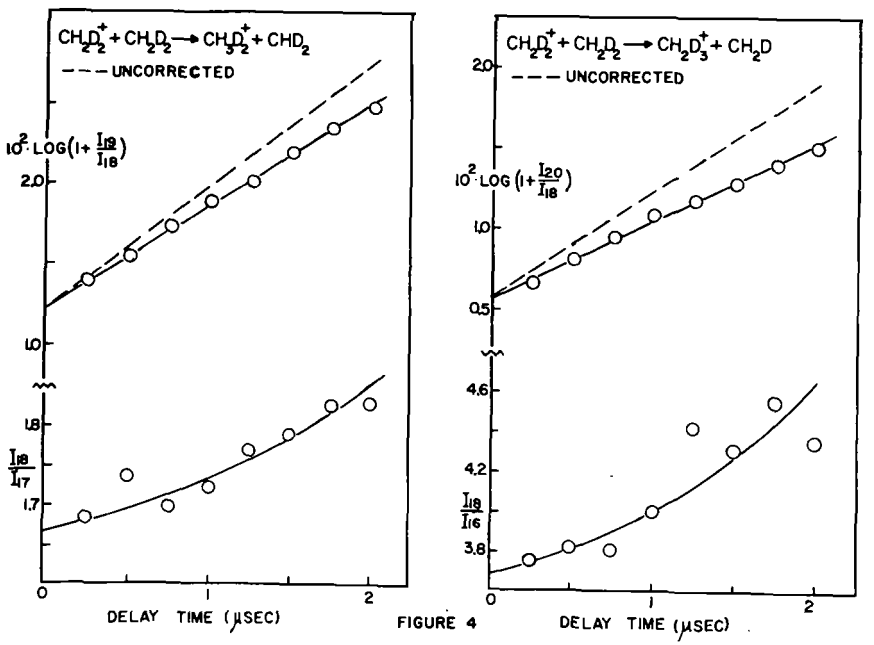

FIGURE 4

is reduced formation of the product secondary ions.

Figure 5 shows preliminary results obtained in the present work for the variation of the apparent rate constant with repeller voltage. Since the distance from the repeller to the exit slit is 9.6 mm. the abscissa of Figure 5 is also approximately the repeller field strength. The solid points were obtained with the electron beam pulsing in the presence of a constant repeller field. Under these conditions the ion residence time is well defined (see above and Figure 3). The open points were obtained with continuous ionization at 6 μamps trap current but otherwise identical conditions. The dip in the rate constant under pulsing conditions appears to be reproducible and, further, the curve obtained with continuous operation approaches that obtained in the pulsing mode as the ionizing current is reduced. It is distinctly possible that with continuous ionization at high emission space charge effects may seriously affect the ion residence timed at low repeller fields leading to anomolously high calculated rate constants. Further studies of repeller dependences are in progress.

REFERENCES

1. C.E. Melton, "Ion-Molecule Reactions" in Mass Spectrometry of Organic Ions, Academic Press, New York, 1963.

2. D.P. Stevenson, "Ion-Molecule Reactions" in Mass Spectrometry. McGraw-Hill, New York, 1963.

3. V.L. Tal'roze and E.L. Frankevich, J. Phys. Chem. (USSR), 34, 1275, (1960) (English Translation).

4. C.W. Hand and H. von Weyssenhoff, Can. J. Chem., 42, 195, (1964).

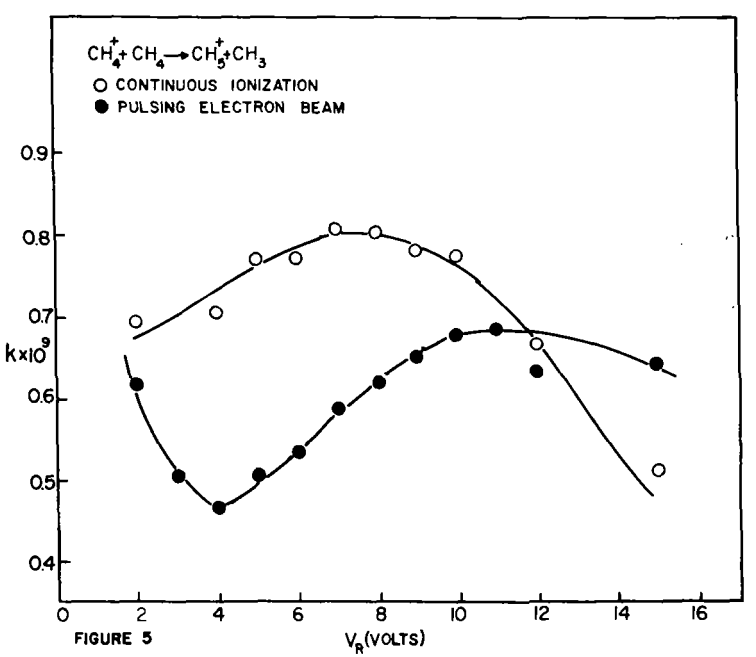

FIGURE 5

Cross Sections for the Ion-Molecule Reaction $H_2 + H_2^{+*} = H_3^+ + H$ as a function of the Vibrational State of the H_2^+ Ion.

A. Weingartshofer and E. M. Clarke
Department of Physics
Saint Francis Xavier University
Antigonish, Nova Scotia, Canada

ABSTRACT

Appearance potential curves are presented for the reactant H_2^+ ion and for the product H_3^+ ion partaking in the ion-molecule collision reaction $H_2^+ + H_2 = H_3^+ + H$ as a function of the vibrational state of the H_2^+ ion. It is found that the dominant contribution to the production of H_3^+ is from the first four vibrational states of H_2^+. The relative cross sections corresponding to the states v = 0, 1, 2, and 3 for H_2^+ are respectively 1.0, 0.5, 0.4 and 0.5. Monoenergetic electrons were used in the formation of the H_2^+ ions, and a mass-spectrometer for analysis of products.

INTRODUCTION*

Kerwin and Marmet at Laval University and Clarke at Saint Francis Xavier University have investigated the process of ionizing H_2 molecules into the various vibrational states of the H_2^+ ion (2, 3, 4). These authors have used a monoenergetic electron beam produced with an electrostatic selector and they have established the important fact that this process occurs according to the Franck-Condon Principle. Franck-Condon factors for these ionization transitions have been computed (5,6,7) and these values show that the probabilities for the transitions 0-2, 0-1, and 0-3 are maximum while they are smaller for the 0-0 and 0-4 transitions. This predicted trend is characteristic and is always observed in our ionization efficiency curves.

RESULTS AND DISCUSSION

Clarke has carried out his experiments with an electrostatic selector built into a mass spectrometer. Counting techniques are employed to measure the ion current. This instrument can be used to investigate energy states of molecules as well as to measure relative cross-sections of ion-molecule reactions. In the present case the H_2^+ formed in a certain vibrational state reacts with the excess H_2 molecules to form H_3^+,

$$H_2^+ \ (\text{Vib.}) + H_2 = H_3^+ + H$$

This reaction is exothermic (8) and occurs very readily (9).

Fig 1. shows the appearance potential curves of H_2^+ and H_3^+. The measured points for the H_3^+- curve fall nicely along very distinct straight-line segments and it is found that they correspond exactly with the vibrational levels of the H_2^+- curve. However, two noticable differences should be observed: (1) In the H_2^+- curve we can see as many as five, sometimes six segments, while for the H_3^+- curve only four, (2) The changes of slope for the segments in the two curves are different.

The interpretation of ion-molecule reactions from appearance potential curves has been discussed by McGowan and Kerwin (10) and following their recommendations it can be shown that the relative cross section σ_v for the formation of H_3^+ ions produced from a colliding H_2^+ in a given vibrational level v is

$$\sigma_v = \alpha_v' / \alpha_v$$

---

* See reference (1) for more information. The outline in this communication will be general and in some respects complementary.

where the α's in the numerator and denominator are respectively the changes in slope of the H_3^+ and the H_2^+- curves.

We have measured the α's of several pairs of curves and the calculated values for the cross sections corresponding to the various levels v of H_2^+ are shown in Table I.

Table I. Values of the relative cross section σ_v for the formation of the H_3^+ ion for various vibrational levels v for the colliding H_2^+ ion.

v	0	1	2	3	4	5
σ_v	1.0	0.5	0.4	0.5	0.0	0.0

The maximum deviation was 10% and the dip at v=2 is quite real.

Fig. 2 represents a plot of the ratio H_3^+ / H_2^+ as a function of the energy of the ionizing electrons. One can see how this ratio drops quickly in the interval of the first four vibrational levels, it then continues dropping slowly and finally levels off at higher electron energies. This graph again brings out the fact that it is only the first four vibrational levels that contribute significantly towards the formation of the H_3^+, the higher vibrational states of the H_2^+ will only dilute the composition in the reaction chamber. Values reported in the literature (11, 12, 13) for the absolute cross section of this reaction have only been obtained at high ionizing electron energies.

This graph resembles in a general way the one published by Tunitskii et. al. (14) except that ours shows fine detail that is entirely lacking in the work of the Russian authors.

It should be mentioned that our interpretation is based on the assumption of identical collection efficiencies for H_3^+ and H_2^+ ions. Evidence for this has been discussed extensively by Reuben and Friedman (11). Experiments with retarding potentials are presently being attempted in this laboratory to confirm the above assumption.

The authors would like to acknowledge the helpful advice and encouragement from Dr. William McGowan and financial support from the National Research Council of Canada.

REFERENCES

1. A. Weingartshofer and E. M. Clarke, Phys. Rev. Letters 12, 591 (1964).
2. P. Marmet and L. Kerwin, Can. J. Phys., 38, 972 (1960).
3. L. Kerwin, P. Marmet, and E. M. Clarke, Can J. Phys. 39, 1240 (1961).
4. L. Kerwin, P. Marmet, and E. M. Clarke, Advances in MassSpectrometry (Pergamon Press, New York, 1963, Vol. 2, p. 522.
5. M. Kraus and A. Kropf, J. Chem. Phys., 26, 1776 (1957).
6. H. von Koch and L. Friedman, J. Chem. Phys. 38, 1115 (1963).
7. M. E. Wacks (to be published). J. Res. Natl. Bur. Stnds., 68A (1964).
8. J. O. Hirschfelder, J. Chem. Phys., 6, 795 (1938).
9. D. P. Stevenson and D. O. Schissler, J. Chem. Phys., 29, 282 (1958).
10. Wm. McGowan and L. Kerwin, Can. J. Phys., 41, 334 (1963).
11. B. G. Reuben and L. Friedman, J. Chem. Phys., 37, 1936 (1962).
12. H. Gutbier, Z. Naturforsch., 12A, 499 (1957).
13. G. F. Giese and W. B. Maier, J. Chem. Phys., 39, 739 (1963).
14. N. N. Tunitskii, P. M. Smirnova, and M. V. Tikhomirov, Daklady Akad. Nauk. S.S.S.R., 101, 1083 (1955).

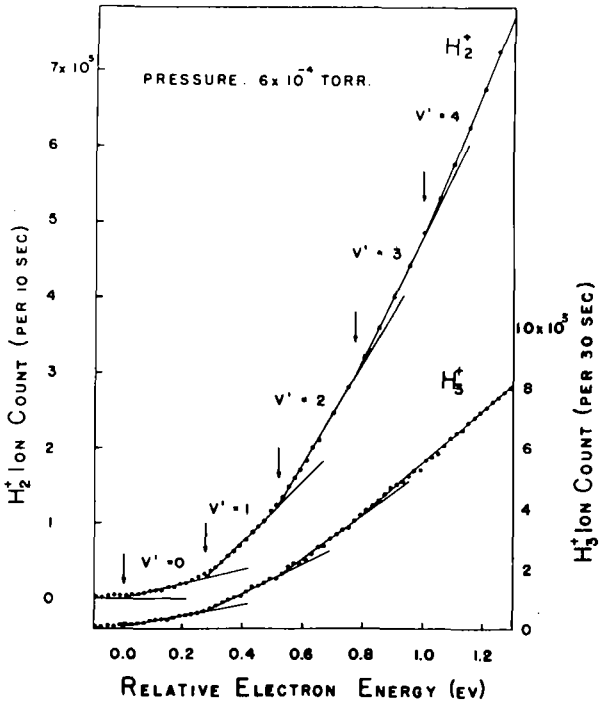

FIG. 1. Appearance potential curves for H_2^+ and H_3^+, plotted as a function of energy above threshold. (Note different ordinate axes.)

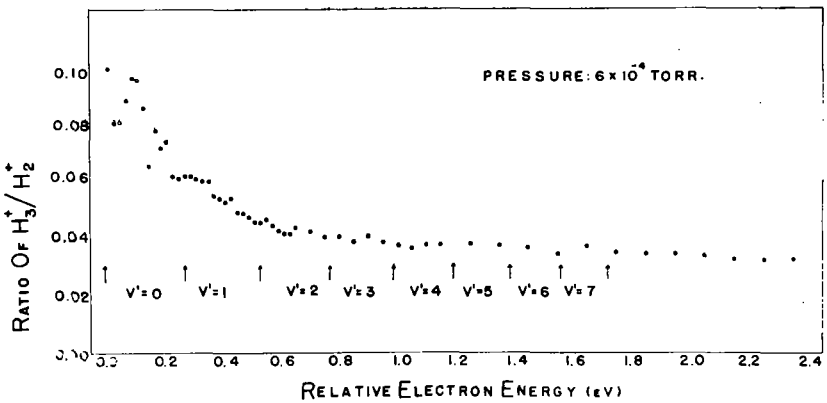

FIG. 2. Plot of the ratio H_3^+ / H_2^+ as a function of the energy above threshold of the ionizing electrons.

THERMAL RATE CONSTANTS FOR ION-MOLECULE REACTIONS BY A PULSE TECHNIQUE

Keith R. Ryan and Jean H. Futrell

Aerospace Research Laboratories
Wright-Patterson Air Force Base, Ohio

ABSTRACT

A combination of a pulsed ionizing beam followed by a variable time delay ion extraction pulse has allowed the determination of thermal rate constants for several ion-molecule reactions using a Consolidated 21-103C 180° mass spectrometer.

These results are compared with the field strength dependent values obtained in the same source operated in the conventional manner. The thermal rate constant for methane, 9.6×10^{-10} cm^3 $molecule^{-1}$ sec^{-1} for a source temperature of 250°C, is within experimental error equal to that reported for continuous mode at 10V/cm. It is also approximately one third the estimated thermal rate constant obtained in earlier work by an extrapolation of higher field strength measurements. Measurements of rate constants at 10V/cm in the continuous mode at electron currents of 0.1μ A yield results significantly lower than those reported in the literature.

INTRODUCTION

It is well known that the cross section for the reaction between a gaseous ion and a gaseous molecule is dependent upon the relative velocity of the reacting pair.[1] For simple systems with few internal degrees of freedom it has been demonstrated that the phenomenological cross section can be defined by

$$Q = k \left(\frac{2m_p}{eE_r \ell} \right)^{1/2} \qquad -(1)$$

where k is the specific reaction rate, m_p the mass of the reactant ion, E_r the electric field in which the reaction takes place and ℓ the reaction path length. Theoretical examination of the problem by Giomousis and Stevenson following the treatment of Langevin revealed that for simple systems the results expressed in Equation (1) could be predicted.[2]

For reactions between ions and molecules which possess internal degrees of freedom it has been shown that the dependence of cross section on velocity is not that given by Equation (1).[3] Concern over the velocity dependence of the reaction cross section arises primarily because of the way in which the reaction is studied. Almost all of the reactions reported so far have been studied using the ion source of a conventional mass spectrometer. The method of ion extraction in these instruments requires that the velocity of the ion beam vary continuously from its point of origin to the point where it emerges from the source.

Talroze has described a technique which allows the determination of the specific reaction rate between ions and molecules when the reacting partners have thermal energies only.[4] The method involves a combination of pulsed ionizing current followed at a known delay time by a repeller pulse which both stops the reaction and extracts the precursor and product ions for mass analysis. The specific reaction rate may be calculated from

$$\frac{i_s}{i_p} = k\, n_o\, t$$

where i_p/i_p is the ratio of product to precursor ion, n_o is the molecular concentration and t the time available for reaction. Because reaction may occur during the ionizing pulse and also during the extracting pulse, the specific reaction rate is most readily obtained from a plot of i_s/i_p against t, the repeller delay time.

Table I. COMPARISON OF PULSE RATES AND 10v/cm RATES

REACTION	Pulse rate. Kp $cm^3\ mol^{-1}\ sec^{-1} \times 10^{10}$	10v/cm rate. K_{10}. $cm^3\ mol^{-1}\ sec^{-1} \times 10^{10}$	$\frac{Kp}{K_{10}}$
$H_2 + H_2^+ \rightarrow H_3^+ + H$	6.6	20.0	.33
$D_2 + D_2 \rightarrow D_3^+ + D$	4.73	14.0	.33
$CO^+ + H_2 \rightarrow COH^+ + H$	15.3	14.1	1.1
$CH_4^+ + CH_4 \rightarrow CH_5^+ + CH_3$	9.6	6.1	1.57
$NH_3^+ + NH_3 \rightarrow NH_4^+ + NH_2$	13.0	6.2	2.1
$H_2O^+ + H_2O \rightarrow H_3O^+ + OH$	11.7	9.8	1.20
$C_2H_3^+ + C_2H_4 \rightarrow C_2H_5^+ + C_2H_2$	10.1	4.3	2.35
$CH_3CHOH^+ + CH_3CH_2OH \rightarrow CH_3CH_2OH_2^+ + CH_3CHO$	31.4	30.3	1.04

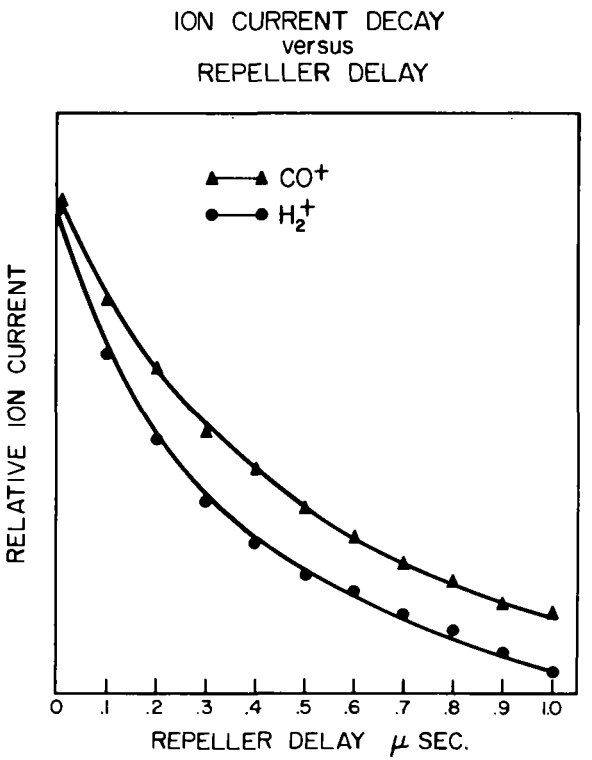

Figure I.

Talroze constructed a special ion source for his investigations and concluded that the specific reaction rate obtained for methane using this technique was not significantly different from that obtained using conventional ion-molecule techniques at 10V/cm field strength. It is the purpose of this paper to report measurements made using pulse circuitry applied to a C.E.C. 21-103C isatron source and to examine the results obtained for several systems.

EXPERIMENTAL

The instrument used in this study was a Consolidated Electrodynamics 21-103C to which the following modifications were made. By adding a Consolidated electron multiplier the detection sensitivity was extended by a factor of 10^6. As required the electrometer originally supplied with the instrument could be used as the detector. In all measurements using the pulse circuits the electron multiplier was used as the detector.

To minimize the effects of stray fields in the ionization region, two precautions were taken. The electron trap was held at 1.5 volts positive to the source by means of a dry cell. In addition the ion exit slit as well as the aperture through which the electrons enter the source were both covered with fine nickel mesh of 100 lines per inch and with a transmission of some 70%.

The dimensions of the ion source are such that an ion with thermal energy and mass 30 a.m.u. will reach the walls in about 3μ seconds. An ion of mass 2 a.m.u. with thermal energy will travel the same distance in approximately 0.7μ seconds. Considerations of this kind govern the repeller delay times to be used and hence the type of pulse circuitry required. Ionizing and repeller pulses are derived from a free-running multivibrator timer. The output of this timer is differentiated and fed into two separate one shot multivibrators one of which has a variable square wave output. Differentiation and comparison of the two signals serves as the time base for the repeller pulse. The ionizing pulse and the repeller pulse are each amplified and clipped in order to restore a square wave appearance to the pulse. Each pulse has a rise time of 0.05μ sec.

A filament assembly serial No. 25597 of the type formerly used in the C.E.C. M401 instrument has been used in this study. This assembly includes a control grid adjacent to the filament. The electron beam is controlled by holding this grid 20 v negative to the filament. The ionizing pulse, which is about 1μ second in duration and has a repetition frequency of about 10 k.c./sec, raises the potential of this grid to two volts positive to the filament. In order to extract the ions, a repeller pulse of 15 volts and 1.5μ second duration can be switched on at any time from 0 to 10μ seconds after the ionizing pulse is switched off. If desired both pulses may be operated simultaneously. In the results reported here the maximum repeller delay used was 1.0μ sec while the increments in delay time used were 0.1μ second.

For the systems described in this paper the specific reaction rate was also determined as a function of field strength. The experimental techniques used for this set of investigations are similar to those described previously.[5]

RESULTS

In Figure 1 we show the dependence of primary ion current on repeller delay time. Results are reported for H_2^+ and CO^+ where it can be seen that, as expected, the rate of decay for H_2^+ is greater than the rate of decay for CO^+. Figure 2 shows the way in which the decay curve for CH_4^+ depends upon the ion accelerating voltage at which the ions are brought to focus.

The amount of decay during the period of one microsecond is in all cases much higher than would be expected from the thermal ion source lifetimes. This might seem to cast doubt on the feasibility of applying the pulse technique to this particular ion source. It must be remembered however that in order to calculate the specific reaction rate the ratio of secondary to primary ion current is used. The important assumption here is that the ratio of secondary to primary ions in the volume of the source from which the analyzer selects the ions represents the state of the reaction at the time of sampling. As long as this condition is satisfied the poor decay curves shown in Figures 1 and 2 are not an indication

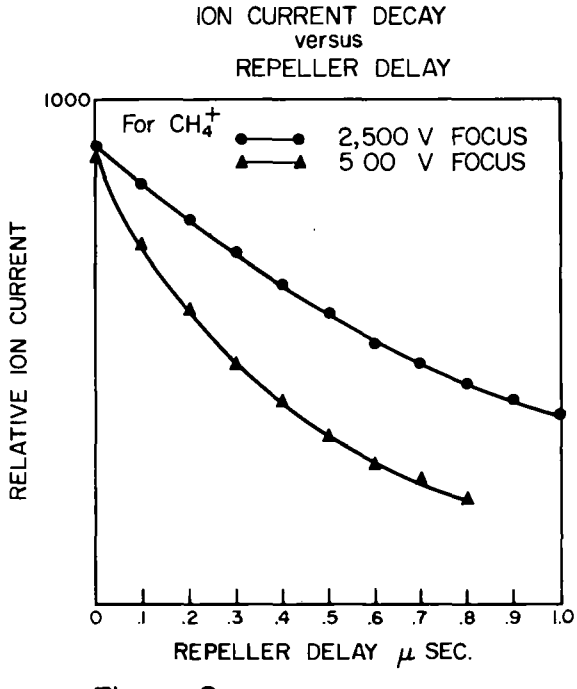

Figure 2.

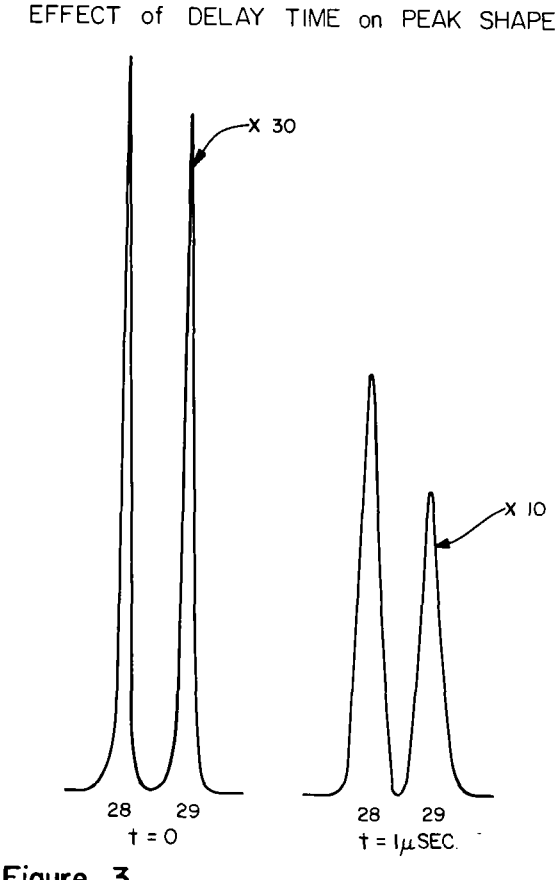

Figure 3.

of the failure of the technique but are really related to the focusing properties of the source.

Figure 3 shows the way the peak shape changes with delay time. The ions shown in this figure are those involved in the reaction

$$CO^+ + H_2 \rightarrow COH^+ + H \qquad (1)$$

It is readily seen that both CO^+ and COH^+ become considerably broader when the delay time changes from 0μ sec to 1.0μ seconds. Although the peak shapes have changed, the profiles for both ions have changed in the same way and the ratio of peak heights may still be taken as the required ratio of ion intensities.

Results for the reaction

$$CH_4 + CH_4^+ \rightarrow CH_5^+ + CH_3 \qquad (2)$$

are shown in Figure 4, the specific reaction rate calculated from these results was 9.6×10^{-10} cm^3 $molecules^{-1}$ sec^{-1}. This value was reproducible to within 5% and is to be compared with a value of 11.6×10^{-10} cm^3 $molecules^{-1}$ sec^{-1} reported by Talroze. It should be pointed out that Talroze had an estimated absolute error of 25% in his experimental work.

In view of the fact that we are assuming a field free reaction zone and further, because of the dependence of the decay current on ion focus voltage, we have determined the specific rate of reaction (2) as a function of the voltage at which CH_4^+ is brought to focus. The results, which are shown in Figure 5, demonstrate that the magnitude of the ion accelerating field has a negligible effect on the observed specific reaction rate.

Having obtained specific reaction rates for a number of systems by this technique it seemed necessary to demonstrate that the values truly represent reactions occuring between particles with thermal energies only. Perhaps the simplest way to do this is to study the dependence of the specific reaction rate on the repeller voltage used to extract the ions from the source. This extrapolation approach to the problem was first used by Field, Franklin and Lampe, and, as these workers pointed out the technique has inherent limitations at very low repeller voltages.[3]

One of the reactions for which k is known to vary with source field strength is

$$C_2H_3^+ + C_2H_4 \rightarrow C_2H_5^+ + C_2H_2 \qquad (3)$$

Field, Franklin and Lampe reported the field strength dependence of k for this reaction noting that, in common with several other systems studied, the specific reaction rate appeared to pass through a maximum at low field strengths. These maxima were attributed to experimental effects arising from an imprecise knowledge of the conditions in the ion source.

In our experiments we also found that the specific reaction rate passed through a maximum value at low field strength. In the case of reaction (3) the position of the maximum was not reproducible nor was it as sharp as the maximum occuring for reaction (2). A typical result for reaction (3) is shown in Figure 6.

For experiments in which results such as Figure 6 were obtained the trapped electron current was held at 10μ A. When the trap current was reduced to 0.1μ A the field strength dependence became quite reproducible and for reaction (5) took on the shape shown in Figure 7. We are currently investigating further the dependence of k, the specific reaction rate on the trapped electron current. However indications at the moment are that the dependence obtained for a current of 0.1μ A is a much better representation of the actual energy dependence than the results obtained at currents of the order of 10μ A.

In Table I is presented a summary of the results obtained for the system studied. We tabulate the specific reaction rate for the pulse technique (K_p), the specific reaction rate obtained at 10V/cm, (K_{10}), and the ratio of the two $\frac{K_p}{K_{10}}$. In the case of the reactions

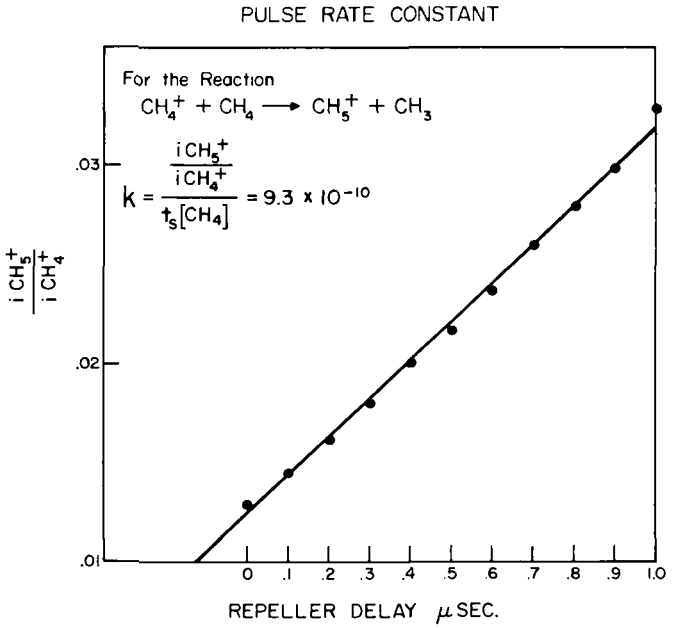

Figure 4.

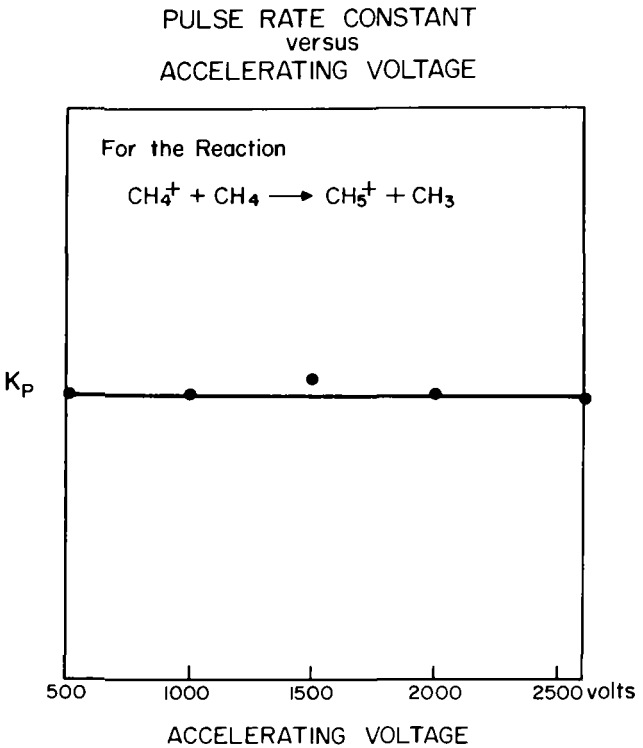

Figure 5.

$$H_2 + H_2^+ \rightarrow H_3^+ + H \quad (4)$$

and

$$D_2 + D_2^+ \rightarrow D_3^+ + D \quad (5)$$

it should be noted that the mass of the product ion is 50% greater than the precursor ion. Furthermore the source residence times of the precursor ions are much shorter than for the ions in any other systems studied. Both these facts suggest that there may be considerable error in the observed values of K_p for both (4) and (5). For this reason we are not inclined to place much significance on the observed ratio of $\frac{K_p}{K_{10}}$.

The other systems appear to divide themselves into two classes, those in which $K_p \sim K_{10}$ and those in which K_p is significantly greater than K_{10}. For this second class we suggest that the transition state ion-molecule complex at low field strength differs from the structure which predominates at 10V/cm. It would appear for slow moving ions the possibility exists that a tighter complex can form leading to a higher observed value of k. This conclusion is in disagreement with Talroze who concluded that the specific reaction rates both for reaction (2) and

$$H_2O + H_2O^+ \rightarrow H_2O^+ + OH \quad (6)$$

are not significantly different from the values obtained by conventional techniques. We would agree in the case of reaction (6) but not reaction (2).

REFERENCES

1. Stevenson, D. P., "Ion-Molecule Reactions in Mass Spectrometry", Edited by M. Dowell, McGraw Hill, 1963.

2. Giomousis, G. and Stevenson, D. P., J. Chem. Phys., 29, 294 (1958).

3. Field, F., Franklin, J., and Lampe, F., J. Am. Chem. Soc., 79, 2419 (1957).

4. Talroze, U. L. and Frankevich, E. L., J. Phys. Chem. (USSR), 34, 1275 (1960).

5. Ryan, K. R., Sieck, L. W., and Futrell, J. H., J. Chem. Phys. To be published.

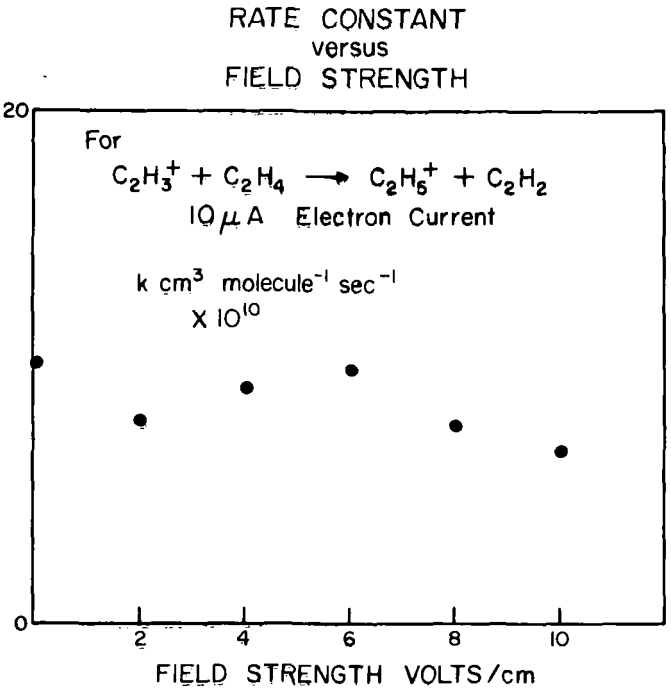

Figure 6.

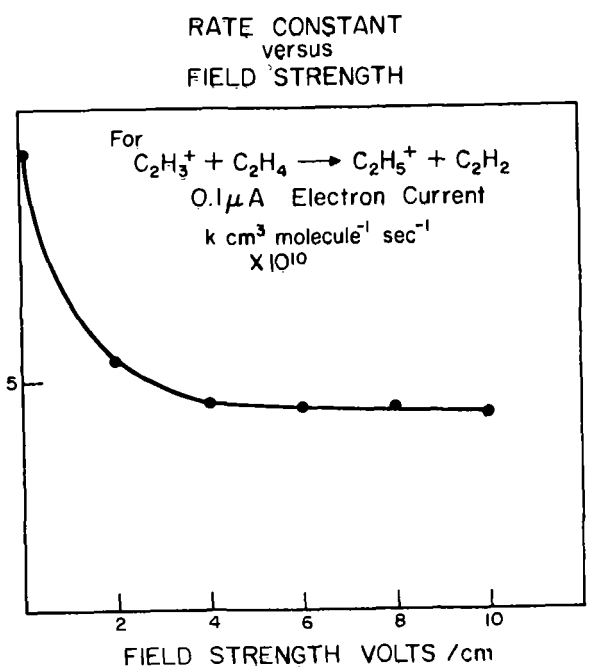

Figure 7.

A HIGH-DUTY CYCLE, RADIO-FREQUENCY, TIME-OF-FLIGHT MASS SPECTROMETER

by

R. M. Mills

A new type of time-of-flight mass spectrometer has been developed for use in studying ions in flames and the properties of compounds which are good flame inhibitors [1]. This instrument is simple to construct and operates with unusually high duty cycle. These advantages should be useful in many other applications.

By duty cycle is meant the fraction of time that resonant ions are represented in the output signal of the instrument when a steady beam of ions is fed into the input. Since a high duty cycle is a necessary (but of course not sufficient) condition for high sensitivity in time-of-flight spectrometers, the instrument to be described here should have advantages in applications where there is a limited number of ions to work with.

In Fig. 1 ions are accelerated to equal initial energies of 3000 ev between the ion source and the entrance of the drift tube. A relatively small sine voltage at radio frequency is applied at the entrance and exit gaps of the drift tube in such a way that the field at the entrance is the negative of that at the exit. Therefore, ions that pass through both the entrance and exit gaps as the same phase lose the energy at the exit gap which they received at the entrance. In other words, ions which pass through the drift tube in a whole number of rf cycles experience a minimum of energy change from the rf fields. These ions will be referred to as resonant ions, and it is these ions which are predominantly represented in the instrument's output signal. After leaving the drift tube, the ions are decelerated by 3000 ev as they pass through the barrier located just in front of the collector.

The retarding potential method [2] is used to distinguish the resonant ions from the nonresonant ions. Fig. 2 shows a plot of the ion current collected as a function of the barrier voltage, for a resonant and nonresonant ion beam. As the barrier increases, the number of ions reaching the collector decreases. It can be shown that the number of ions at a particular energy is proportional to the negative of the slope of this curve [3]. The nonresonant beam has a wider distribution of energies and therefore does not cut off as sharply as does the resonant beam.

The slope of the cut-off curve is measured over a narrow energy range by raising and lowering the barrier height with a square wave at 1 kc, as shown. The square wave is actually applied to the source in order to avoid the capacitive current between the barrier electrode and collector which would be encountered if the square wave were applied to the barrier electrode.

The signal at the collector produced by the square wave is amplified by ac amplifiers and then rectified by a synchronous detector. The mass is swept by changing the frequency of the rf voltage. For a given mass, a peak occurs at every frequency for which the ion takes a whole number of cycles to traverse the drift tube. Fig. 3 shows the output from the synchronous detector versus the frequency of the applied rf voltage for a beam of Cl negative ions formed from CCl_4. Here "n" is defined as the number of rf cycles an ion takes to travel through the drift tube and Δf is the difference in frequency between successive peaks of a particular mass. Δf is inversely proportional to the square root of the mass. C.F. is a calibration factor which includes the length of the drift tube and the voltage through which the ions have been accelerated before entering the drift tube. This instrument has a resolution of about 40 at 60% maximum duty cycle. However, its accuracy is such that the mass of heavier ions can be found if the ion beam is composed of a small number of masses. The instrument has identified the negative ion produced with low energy electrons in $Fe(CO)_5$ as $Fe(CO)_4$ or mass 168 with a 0.1% error in mass.

There are several advantages in utilizing ions which experience no change in energy that may not be immediately apparent. In other time-of-flight mass spectrometers where the resonant ions are given sufficient energy to overcome a barrier, there is a strong dependence between rf voltage height and resolution. For constant resolution the rf voltage must be carefully maintained constant. The strong dependence between resolution and rf voltage height does not exist in the instrument described here since the collector system selects the ions which have experienced zero energy change. Second, ions formed by collisions in the drift tube and in the initial accelerating area of the source are not represented in the output signal,

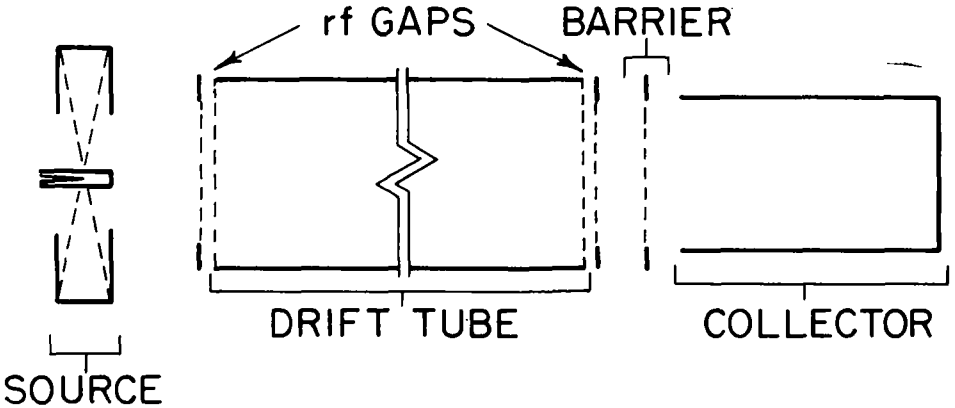
rf GAPS
BARRIER
DRIFT TUBE
COLLECTOR
SOURCE

FIG. 1

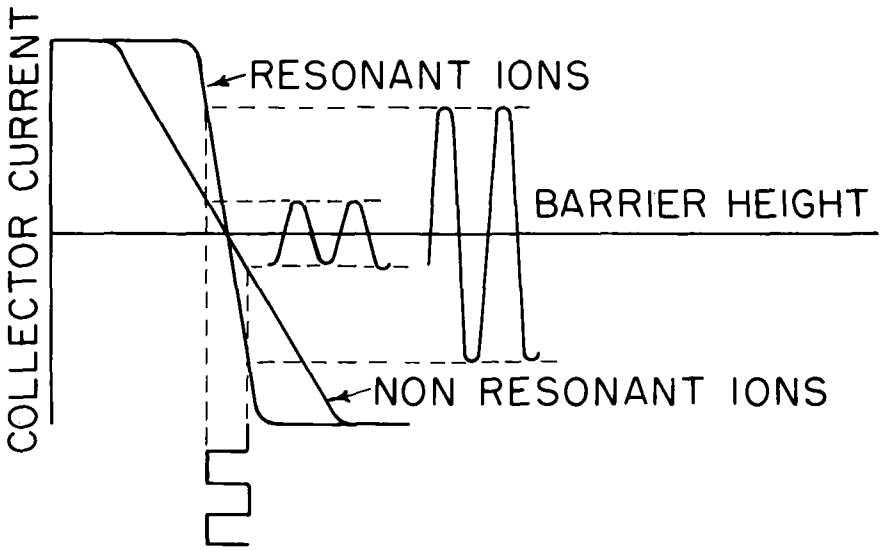
COLLECTOR CURRENT
RESONANT IONS
BARRIER HEIGHT
NON RESONANT IONS

FIG. 2

since they are not formed in the energy interval within which the collector system is sensitive, that is, the interval corresponding to the square wave in Fig. 2. In addition to this, the ac amplifiers have advantages in stability. And, the instrument, as a whole, offers electrical and mechanical simplicity. There are no critical alignments or spacings. The mass spectrometer which is described above has been built and is now operating.

The instrument has two serious limitations. If there are many different masses in the ion beam, the xy recorder plot becomes cluttered with a large number of harmonic peaks, making the measurement of a Δf for a particular mass difficult. Secondly, the instrument's resolution is only moderate. It has been shown that the resolution is limited by the influence of the rf voltage on the velocity of the ions as they travel through the drift tube [1]. The peak-to-peak rf voltage is only about 2% of the dc accelerating voltage. However, this is enough to cause significant variations in flight times through the drift tube, and the resulting energy spread is the factor which limits the resolution.

Studies show that by using an rf voltage of special wave shape, it should be possible to improve resolution and, at the same time, reduce the cluttering due to the presence of the harmonics [3]. In this scheme, saw-tooth waves are applied so that the rf fields rise linearly with time at both the entrance and exit gaps. As seen in Fig. 4, ions passing through the first gap late receive more acceleration, enabling them to catch up in the drift tube with ions which leave earlier. The effect is similar to the electron bunching in the klystron. With this scheme, however, the ions are allowed to continue their flight through the drift tube. By the proper choice of the ratio of rf to dc voltages, resonant ions that leave ahead of a reference ion by a time interval, OA, can be made to arrive behind the reference ion by the same time interval, BC. In other words, resonant ions passing through the entrance at "O" may be considered to be reference ions, and they exit at "C." Other resonant ions which happen to enter the drift tube at "A" exit at "B." It can be seen that, as before, the rf voltages are cancelled out and the resonant ions receive a minimum of energy change from the rf fields. Thus, the same collector system can be used.

By using the saw-tooth waves, the resolution is increased since a larger rf voltage can be applied. The velocity modulation, which limited the resolution in the previous scheme, is incorporated in the operation of this instrument. Details of the calculations made are given elsewhere [3]. Only the results will be given here. To the first approximation, the resolution and maximum duty cycle are given by the expressions shown in Fig. 5. V_{dc} is the applied dc accelerating voltage, δ is the amplitude of differentiating square wave, and V_{st} is the peak-to-peak saw-tooth voltage.

Fig. 6 shows the calculated peak shapes. n_o is defined as the number of rf cycles which an unmodulated ion takes to travel the drift tube. The ratio of rf to dc voltage is chosen so that the maximum duty cycle occurs at $n_o = 40$. Notice that the peak heights decrease for other whole number values of n_o. For values of n_o which are quite different from 40, the harmonic peaks disappear. Thus the cluttering problem is reduced, but not eliminated. The resolution in Fig. 6 is about 650, and the maximum duty cycle is about 80%.

Two modifications of the scheme which uses velocity modulation have been studied and are discussed in detail in [3]. It is shown there that it will be desirable to build the instrument with a third rf gap at the center of the drift tube. Otherwise either the instrument source or collector will have to be maintained above rf ground. The third gap also has the important advantage of eliminating the harmonics at the odd values of n_o. No change results in the expressions for maximum duty cycle and resolution when the extra gap is used. Further increases in resolution may be possible by applying a special correctional wave to the exit rf gap [3].

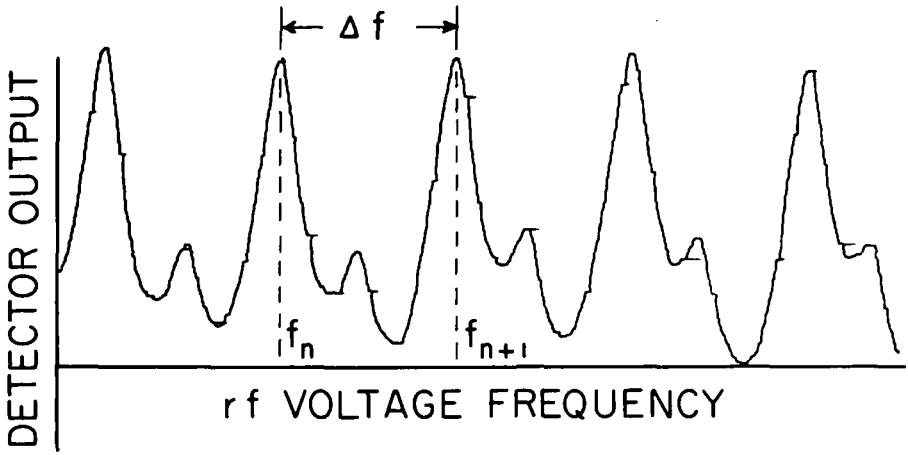

FIG. 3

$$\Delta f = \frac{f_n}{n} = \frac{C.F.}{\sqrt{m}}$$

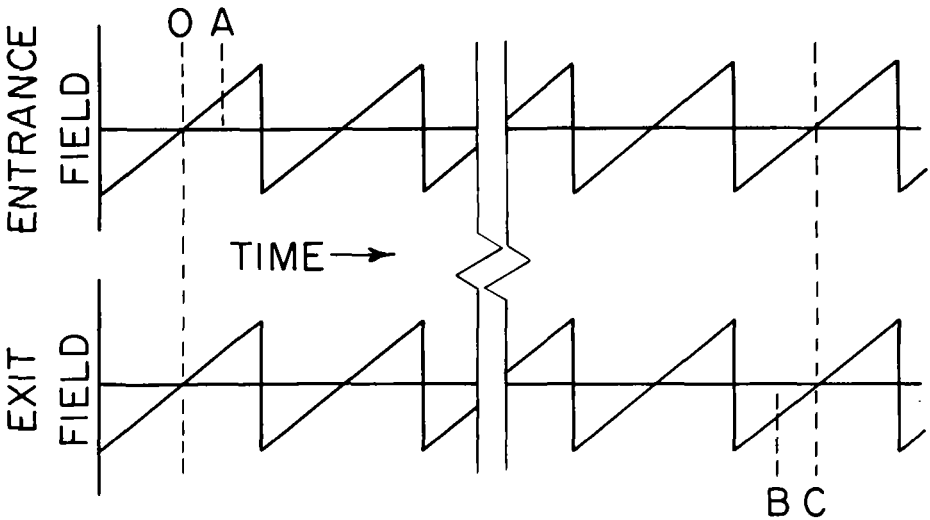

FIG. 4

References

[1] R. M. Mills, Journal of Research of the National Bureau of Standards, 67C, 283, (1962).

[2] J. A. Simpson, Rev. Sci. Instr., 32, 1283 (1961).

H. D. Hagstrum, Rev. Mod. Phys., 23, 185 (1951).

[3] R. M. Mills, Improvements in a Time-of-Flight Mass Spectromety, Master Thesis submitted to George Washington University School of Engineering, Feb. 22, 1964.

Figure Captions

Figure 1 - Simplified diagram of the TOF Mass Spectrometer

Figure 2 - The cut-off curve is differentiated by a square wave, producing a larger response from the resonant ions than from the non-resonant ions.

Figure 3 - X-Y Recorder peaks for negative chlorine ions produced by low energy electron bombardment in CCl_4.

Figure 4 - The rf fields in the proposed instrument utilizing velocity modulation. A resonant ion starting late by some time interval OA arrives at the exit gap early by the same time interval BC.

Figure 5 - Approximate theoretical expressions for the resolution and maximum duty cycle of the proposed velocity modulated instrument.

Figure 6 - Calculated peak shapes for the velocity modulated instrument.

$$\text{RESOLUTION} \cong \frac{3}{2} \frac{V_{dc}}{\delta}$$

$$\text{MAXIMUM DUTY CYCLE} \cong \frac{4}{V_{st}} \sqrt{\frac{\delta V_{dc}}{6}}$$

FIG. 5

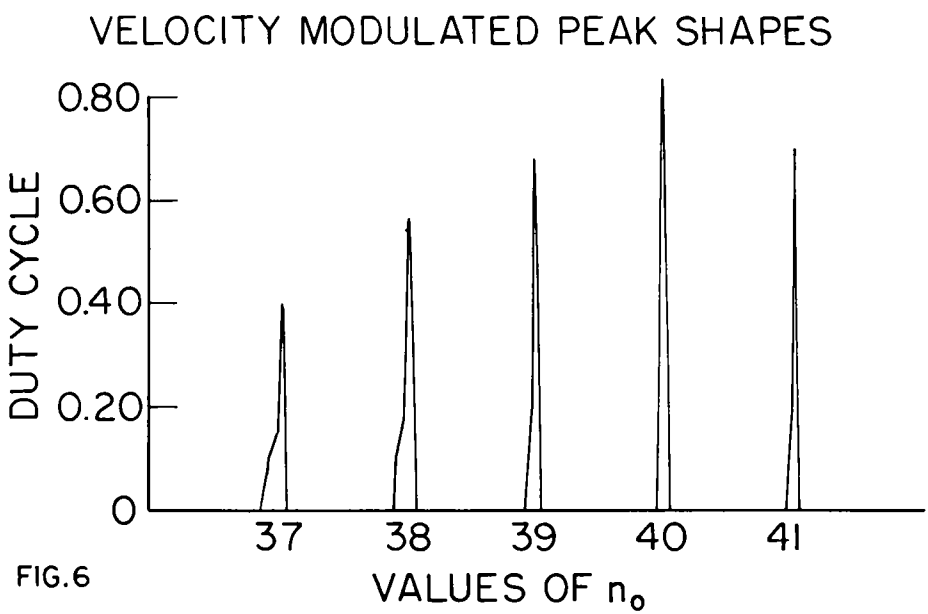

FIG. 6

ANALYZER SENSITIVITY PARAMETERS IN A DOUBLE FOCUSING MASS SPECTROGRAPH

By: C. W. Hull
Consolidated Electrodynamics Corporation
Pasadena, California

ABSTRACT

An analyst using a double focusing mass spectrograph is interested in the relationship between sensitivity and resolution. For some problems one would be willing to sacrifice sensitivity for resolution, or vice versa. And for any given resolution one would like to have maximum sensitivity.

The specific case of the Mattauch-Herzog-Robinson geometry is considered. The aberrations are presented in terms of the instrument slits and stops. From these the beam width function is derived. Then, using a "figure of merit" criteria the optimum instrument transmission for a given beam width is derived. Under these optimum conditions the relationship between resolution and instrument sensitivity is shown.

Also, sensitivity as it relates to accelerating voltage and scattered background is discussed.

In a mass spectrograph an ion leaves the source with a position displacement w, an angular dispersion α, and an energy dispersion β. The beam width at the photo-plate can be determined in terms of the w, α, and β that the analyzer will accept. In a double focusing instrument with complete first order focusing, the displacement that an ion has from the central ray position at the photo-plate is given by the expression[1]

(1) $$y = r_m (A_{00} w + A_{20} \alpha^2 + A_{11} \alpha\beta + A_{02} \beta^2)$$

where the A's are abberation coefficients that are determined by the geometry of the instrument.

Consider a specific analyzer. The Mattauch-Herzog-Robinson geometry is shown in Figure 1. The abberation coefficients for the geometry are [1]

(2a) $$A_{00} = 1/r_e$$

(2b) $$A_{20} = 1.416 - 1/2\,(r_e/r_m)^2 (1 - r_m/\rho)$$

(2c) $$A_{11} = -3.218 - r_e/r_m - r_e/r_m\,(0.293\, r_e/r_m + d/r_m)(1 - r_m/\rho)$$

(2d) $$A_{02} = -0.389 - (0.293\, r_e/r_m + d/r_m)\left[1 + \tfrac{1}{2}(0.293\, r_e/r_m + d/r_m)(1 - r_m/\rho)\right]$$

We can define the limits of w, α, and β in terms of the physical slits and stops in the instrument. Let w be limited by the object slit S_1, that is

(3a) $$-S_1/2 \leq w \leq S_1/2$$

We can define two new variables, x and z, similarly to w, such that

(3b) $$-S_2/2 \leq x \leq S_2/2$$

(3c) $$-S_3/2 \leq z \leq S_3/2$$

TABULATION 1 - VARIOUS LINE WIDTH PARAMETERS VS. r_m

r_m	m_{rel}	D	A	B	-C	$\frac{2A}{B}$	$\frac{-B}{2C}$
2	1.0	0.0794	0.0336	0.0696	0.1961	0.966	0.1774
4	4.0	0.1588	0.0672	0.0560	0.0738	2.40	0.3794
6	9.0	0.2382	0.1009	0.0423	0.0348	4.77	0.6078
8	16.0	0.3176	0.1345	0.0287	0.0169	9.37	0.8490
10	25.0	0.3970	0.1681	0.0150	0.00688	22.40	1.090
12	36.0	0.4764	0.2017	0.0014	0.00125	288.1	0.560

r_m	$\frac{B^2-4AC}{-16C}$	$\frac{B^2}{-16C}$	$\frac{B^2-4AC}{16A}$	$\frac{B^2}{16A}$	W_{opt4}	W_{opt6}	W_{opt8}
2	0.00994	0.00154	0.0580		0.490	1.165	2.791
4	0.01946	0.00266	0.02137		0.464	0.722	1.374
6	0.02844		0.00980		0.571	0.689	0.986
8	0.03714		0.00467	0.00038	0.712	0.764	0.903
10	0.04407		0.00180	0.00008	0.853	0.873	0.920
12	0.05050		0.00031		1.000	1.000	1.000

TABULATION 2
OPTIMUM SLIT SETTINGS FOR
VARIOUS RESOLVING POWERS

			mils		inches	
Opt r_m	R_{max}	W_{12}	S_1	S_2	S_3
8	1000	6.0	8.53	0.191	0.539
8	2000	3.0	4.26	0.135	0.381
8	3000	2.0	2.84	0.110	0.311
8	4000	1.5	2.13	0.095	0.269
8	5000	1.2	1.71	0.085	0.241
8	10000	0.6	0.853	0.060	0.170
8	20000	0.3	0.426	0.043	0.120
6	10000	0.6	0.868	0.060	0.103
6	15000	0.4	0.579	0.049	0.084
6	20000	0.3	0.434	0.043	0.073
4	10000	0.6	0.877	0.019	0.018
4	15000	0.4	0.584	0.015	0.015
4	20000	0.3	0.438	0.013	0.013

From figure 1,

(4a) $$\alpha = x / l_e' = c x$$

(4b) $$c = 1 / l_e' = \sqrt{2} / r_e$$

Energy dispersion is both a function of z and α.[1]

(5a) $$\beta = \frac{r_e \alpha - z}{0.293 r_e + d} = \frac{\sqrt{2}\, x - z}{0.293 r_e + d} = a x + b z$$

where

(5b) $$a = \sqrt{2} / (0.293 r_e + d)$$

(5c) $$b = -1 / (0.293 r_e + d)$$

Now we can write y in terms of w, x, and z. From equations 1, 2, 4 and 5.

(6a) $$y = D w + A x^2 + B x z + C z^2$$

where

(6b) $$D = r_m / r_e$$

(6c) $$A = r_m \left[\frac{2.832}{r_e^2} + \frac{6.436}{(0.293 r_e + d) r_e} + \frac{0.778}{(0.293 r_e + d)^2} \right]$$

(6d) $$B = \frac{\sqrt{2}}{0.293 r_e + d} \left[1 + r_m \left(\frac{0.778}{0.293 r_e + d} - \frac{3.218}{r_e} \right) \right]$$

(6e) $$C = \frac{-1}{0.293 r_e + d} - \frac{0.389\, r_m}{(0.293 r_e + d)^2} + \frac{1}{2} \left(\frac{1}{\rho} - \frac{1}{r_m} \right)$$

In the Robinson geometry r_e = 25.188 inches, d = 9.600 inches, and ρ = 4.329 inches.[1] Hence, A, B, C and D can be reduced to numerical functions of r_m.

(7a) $D = 3.970 \times 10^{-2} r_m$

(7b) $A = 1.681 \times 10^{-2} r_m$

(7c) $B = 8.329 \times 10^{-2} - 6.825 \times 10^{-3} r_m$

(7d) $C = 5.661 \times 10^{-2} - 1.349 \times 10^{-3} r_m - 1/2\, r_m$

A, B, C and D are plotted in Figure 2.

Now $y = f(w, x, z, r_m)$ is known. We are interested in determining the beam width function W in term of S_1, S_2 and S_3.

The beam width at the photo-plate is

(8) $$W = | y_{MAX} - y_{MIN} |$$

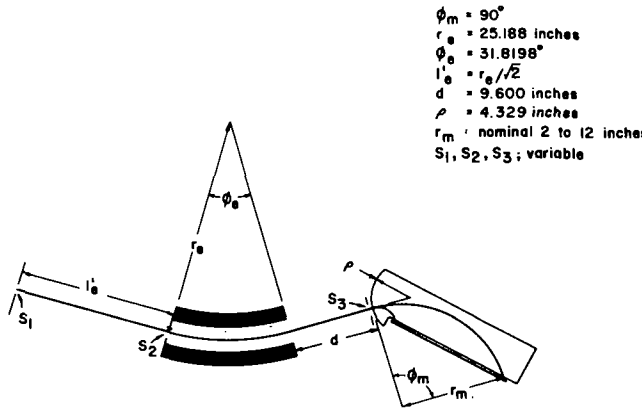

FIGURE 1 - MATTAUCH-HERZOG-ROBINSON GEOMETRY

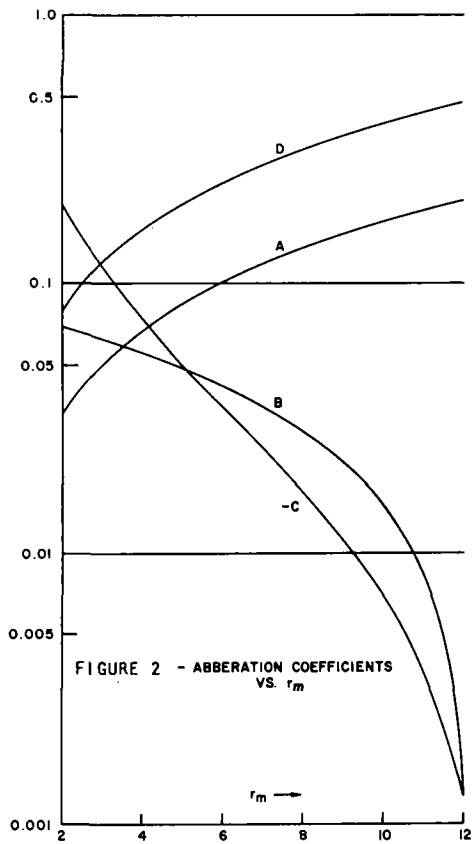

FIGURE 2 - ABBERATION COEFFICIENTS VS. r_m

The simplest approach is to consider y and W as each being composed of two functions. That is

(9a) $y = f(w, x, z, r_m) = g(w, r_m) + h(x, z, r_m)$

or

(9b) $y_i = f_i(w, x, z) = g_i(w) + h_i(x, z)$, where $r_m = i$

and

(10a) $W = F(S_1, S_2, S_3, r_m) = G(S_1, r_m) + H(S_2, S_3, r_m)$

or

(10b) $W_i = F_i(S_1, S_2, S_3) = G_i(S_1) + H_i(S_2, S_3)$, where $r_m = i$

where G and H are defined as

(11a) $G = |g_{max} - g_{min}|$

(11b) $H = |h_{max} - h_{min}|$

This approach is only valid of S_1 is small compared to S_2, which is the case. If it were not the case, we would have to relate α to S_1 in the manner that β was related to S_2. However, $g = Dw$, and then $g_{max} = D(S_1/2)$, $g_{min} = D(-S_1/2)$ so that

(12) $G = D\,S_1$.

H is not so easily found. The function h is not necessarily a maximum when S_2 and S_3 are maximum, nor is the minimum necessarily related to the maximum.

Consider the family of curves h = constant. This is a set of hyperbolae, asymptotic to the two lines generated by h = 0. These lines are

(13) $$X = \frac{-B \pm (B^2 - 4AC)^{1/2}}{2A} Z$$

Figure 3 shows a plot of this set, along with the limits of x and z from equations 3b and 3c. Each hyperbola is at some point parallel to either the x or the z axis. At these points $\partial z/\partial x = 0$ and $\partial x/\partial z = 0$ respectively. The set of points determined by these criteria form two straight lines

(14) $$Z = \frac{-B}{2C} X$$

(15) $$Z = \frac{-2A}{B} X$$

and these are also plotted in figure three. Now, in looking at this diagram, it is seen that h_{max} lies either at the intersection of $x = S_2/2$, and $z = \frac{-B}{2C} x = \frac{-BS_2}{4C}$ or at the intersection of $x = S_2/2$, and $z = S_3/2$, depending whether S_3/S_2 is greater or less than $\frac{-B}{2C}$. Thus

(16) $$h_{max} = \left(\frac{S_2}{2}\right)^2 \left(\frac{B^2 - 4AC}{-4C}\right) \quad \text{if } \frac{S_3}{S_2} \geq \frac{-B}{2C}$$

(17) $$h_{max} = \left(\frac{S_2}{2}\right)^2 A + \frac{S_2 S_3}{4} B + \left(\frac{S_3}{2}\right)^2 C \quad \text{if } \frac{S_3}{S_2} \leq \frac{-B}{2C}$$

Similarly, h_{min} lies either at the intersection of $z = \frac{S_3}{2}$ and $x = \frac{-Bz}{2A} = \frac{-B}{2A}\frac{S_3}{2}$ or at $z = \frac{S_3}{2}$, $x = \frac{-S_2}{2}$, depending on whether S_3/S_2 is less or greater than $2A/B$. So that

(18) $$h_{min} = \left(\frac{S_3}{2}\right)^2 \left(\frac{B^2 - 4AC}{-4A}\right) \quad \text{if } \frac{S_3}{S_2} \leq \frac{2A}{B}$$

(19) $$h_{min} = \left(\frac{S_2}{2}\right)^2 A - \frac{S_2 S_3}{4} B + \left(\frac{S_3}{2}\right)^2 C \quad \text{if } \frac{S_3}{S_2} \geq \frac{2A}{B}$$

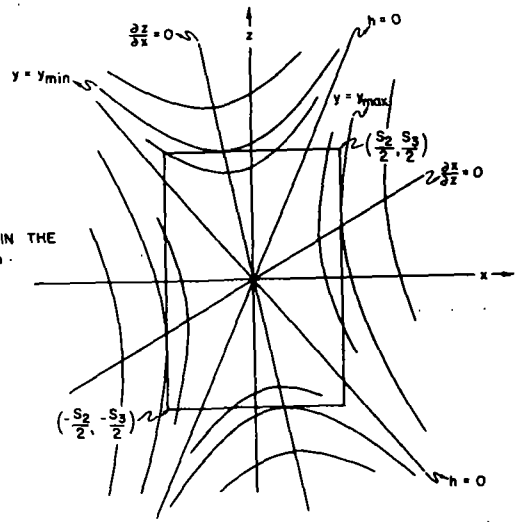

FIGURE 3 - THE FUNCTION h IN THE x, z PLANE AT SOME r_m.

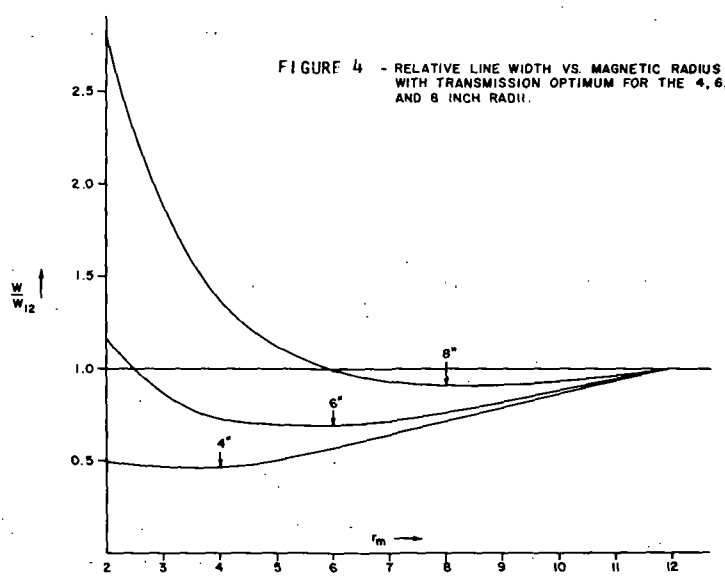

FIGURE 4 - RELATIVE LINE WIDTH VS. MAGNETIC RADIUS WITH TRANSMISSION OPTIMUM FOR THE 4, 6, AND 8 INCH RADII.

Now, from equation 11b

$$(20) \quad H = \frac{B^2 - 4AC}{-16C} S_2^2 + \frac{B^2 - 4AC}{16A} S_3^2 \qquad \text{if } \frac{-B}{2C} \leq \frac{S_3}{S_2} \leq \frac{2A}{B}$$

$$(21) \quad H = \frac{-B^2}{16C} S_2^2 + \frac{B}{4} S_2 S_3 - \frac{C}{4} S_3^2 \qquad \text{if } \frac{-B}{2C} \leq \frac{S_3}{S_2} \not\leq \frac{2A}{B} \leq \frac{S_3}{S_2}$$

$$(22) \quad H = \frac{A}{4} S_2^2 + \frac{B}{4} S_2 S_3 + \frac{B^2}{16A} S_3^2 \qquad \text{if } \frac{S_3}{S_2} \leq \frac{-B}{2C} \not\leq \frac{S_3}{S_2} \leq \frac{2A}{B}$$

The condition $2A/B \leq S_3/S_2 \leq -B/2C$ is never met in the system.

Thus, H, can have three forms, depending on the ratio S_3 to S_2, and upon A, B and C, which are functions of r_m. From equations 10a, 12, 20, 21 and 22, we may now write W as a function of S_1, S_2 and S_3.

$$(23) \qquad W = DS_1 + JS_2^2 + KS_2S_3 + LS_3^2$$

where J, K and L are defined in equations 20, 21 and 22. Tabulation 1 shows these various parameters versus r_m.

Equation 23 can now be examined to find what combination of S_1, S_2 and S_3 will give maximum transmission for a given W. To the extent that each stop is uniformly filled, the instrument transmission is proportional to that stop. Hence we may define transmission T, as

$$(24) \quad T = S_1 \cdot S_2 \cdot S_3$$

realizing that S_3 is filled only if a source with enough energy spread is used. Of course the same condition holds for equation 23 for W. Equations 23 and 24 can now be evaluated with Lagrange's method[2] to find a maximum T. Let W = constant and define

$$(25) \qquad u = T + \lambda W$$

Then

$$(26) \qquad \frac{\partial u}{\partial S_1} = S_2 S_3 + \lambda D = 0$$

$$(27) \qquad \frac{\partial u}{\partial S_2} = S_1 S_3 + \lambda(2JS_2 + KS_3) = 0$$

$$(28) \qquad \frac{\partial u}{\partial S_3} = S_1 S_2 + \lambda(2LS_3 + KS_2) = 0$$

When these equations are solved they yield

$$(29) \qquad S_1 = \frac{W}{2D}$$

$$(30) \qquad S_2 = \left[\frac{W}{4} \frac{1}{J + \frac{K}{2}\left(\frac{J}{L}\right)^{1/2}}\right]^{1/2}$$

$$(31) \qquad S_3 = \left[\frac{W}{4} \frac{1}{J + \frac{K}{2}\left(\frac{L}{J}\right)^{1/2}}\right]^{1/2}$$

Or, in the most common case K = 0 so

(32) $$S_2 = \left(\frac{W}{4J}\right)^{1/2}$$

(33) $$S_3 = \left(\frac{W}{4L}\right)^{1/2}$$

(34) $$\frac{S_3}{S_2} = \left(\frac{J}{L}\right)^{1/2} = \left(\frac{A}{-C}\right)^{1/2}$$

We are now interested in the relationship between resolution and instrument sensitivity under these optimum conditions. Sensitivity is proportional to the ratio of transmission to line width,

(35) $$S_T = \frac{T}{W}$$

and under optimum conditions, from equations 24, 29, 32 and 33

(36) $$T = S_1 S_2 S_3$$
$$= \frac{W^2}{8D}\left(\frac{1}{JL}\right)^{1/2}$$

so that

(37) $$S_T = \frac{W}{8D}\left(\frac{1}{JL}\right)^{1/2}$$

Equations 36 and 37 say that transmission varies with the square of line width, and that sensitivity is proportional to line width. Since resolving power R is

(38) $$R = \frac{r_m}{2W}$$

sensitivity is inversely proportional to resolving power.

Equations 29, 32 and 33 require that the D, J and L for some specific radius be used. Tabulation 1 shows how W varies with r_m if T is optimized for the 4, 6 or 8 inch radius.

Figure 4 shows this variation, and Figure 5 shows how this W varies with mass. The curve for 4 inches is useful if one wants to maintain high resolution across the plate, with a sacrifice in sensitivity at higher mass. With a spark source one would rather have uniform sensitivity, with resolution being a secondary consideration. The curve for 8 inches gives good sensitivity except at very low mass. Since low mass tends to be photographically more sensitive, and thus compensating, this curve is generally used. Tabulation 2 lists S_1, S_2 and S_3 corresponding to these curves for various maximum resolutions, R_{max}.

There are two more important sensitivity parameters: Accelerating voltage, and background. Sensitivity is dependent on ion energy in three ways. The source output increases with voltage. Also, since

(39) $$\bar{\beta} = \frac{\Delta V}{V}$$

where $\overline{\beta}$ is the maximum energy spread passed by the instrument, the ΔV passed by the instrument increases with V, and hence the number of particles accepted by the analyzer from the source is increased with voltage. And, finally, the response of the photoplate increases with voltage. Hence, to the extent that each of these effects is linear, sensitivity is cubic with accelerating voltage. Experiments show the relationship to be more closely parabolic.

Background has several sources. Gas scattering and charge exchange backgrounds are proportional to analyzer pressures and the number of incident ions. Ion scattering, and secondary electron, and photon backgrounds are proportional to the number of incident ions. In any case

$$E_B = kN \tag{40}$$

that is, the background exposure is proportional to the number of incident ions. Then from equation 37 it is seen that an increase in S_T corresponds to an increase in E_B, so that for maximum sensitivity some balance must be made between these two.

REFERENCES

1. R. L. Heath, G. D. Perkins, D. H. Pollock, A Mathematical Survey of the Tandem Mass Spectrograph, Bell & Howell Research Report II - 539, April 17, 1961.

2. Advanced Calculus, A. E. Taylor, Ginn & Company, New York, 1955, P. 198 - 201.

3. C. E. Berry, Remarks on High Resolution Mass Spectroscopy, ASTM E-14 May, 1963, San Francisco.

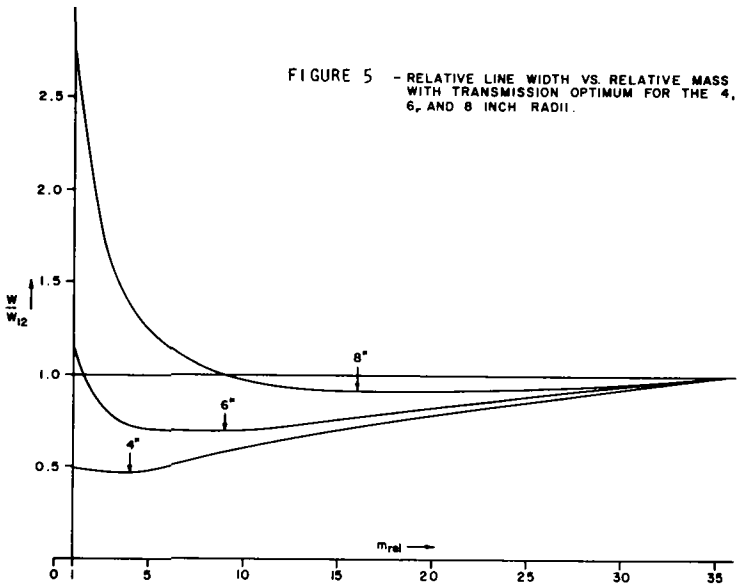

FIGURE 5 - RELATIVE LINE WIDTH VS. RELATIVE MASS WITH TRANSMISSION OPTIMUM FOR THE 4, 6, AND 8 INCH RADII.

A COLD ELECTRON MASS SPECTROMETER ION SOURCE

M. K. Testerman, B. E. Gilliland and E. M. King
Department of Electronics and Instrumentation
University of Arkansas
Graduate Institute of Technology
Little Rock, Arkansas

The results described below are a continuation of the study originally reported at the Eight Annual ASTM E-14 Meeting, Atlantic City, New Jersey, 1960, and discussed further at the Eleventh Annual Meeting at San Francisco, California, 1963.

A cold electron device has been incorporated in a radio-frequency mass spectrometer as a source of ionizing electrons. The source consists of a resistance strip electron multiplier in conjunction with a photocathode or Pm^{147} activating electron source. Data showing the performance of the source will be presented. The data will include the discussion of: (1) stability of the source; (2) effect of gain variations on cracking pattern; (3) effect of system gases on gain and lifetime; (4) efficiency of ionization; and (5) emission regulation. Other potential applications of the cold source, including use as an ultra-high vacuum ionization gauge, are also discussed. It is to be remembered that cold electron sources require appreciably less power for operation, possess negligible outgassing and gettering effects, and have much less emission fluctuation when compared with conventional temperature-limited thermionic emitters.

MONOPOLE MASS SPECTROMETER

Richard F. Herzog
Geophysics Corporation of America
Bedford, Massachusetts

(Manuscript Withdrawn)

A SIMPLE MASS SPECTROMETER FOR ANALYSIS OF ARGON AT ULTRA-HIGH VACUUM.

E. Farrar, R. M. MacIntyre, Derek York
Geophysics Laboratory, University of Toronto

ABSTRACT

A simple, inexpensive, leak-detecting device, the MS10, (from A.E.I.) has been examined to ascertain its value as a means of determining volumes of A^{40} occupying less than 10^{-3} cc n.t.p. The instrument which has a 2" radius of curvature and employs electrostatic scanning is in fact capable of routinely producing reliable measurements on such A^{40} volumes, the isotopic dilution method being employed with A^{38} as a tracer. Most notably there appears to be no "memory" effect.

INTRODUCTION

Much research is currently being pursued in Physics, Geophysics and Geology Departments to determine accurately the ages of rock formations. The modern methods are all based on radioactivity,[1,2] perhaps the most widely used technique so far being that employing the decay of K^{40} to A^{40}. K^{40} is a long-lived rare isotope of K (0.0119% atomic) and by virtue of a branching decay produces both A^{40} and Ca^{40}. Table 1 shows the various amounts of A^{40} that a typical K-containing mineral would generate over different time intervals. It is immediately apparent that a detection system capable of accurate measurements on gas samples of the order 10^{-5} cc n.t.p. is required for an age determination on a rock sample.

TABLE I.

TABLE TO ILLUSTRATE VOLUME OF RADIOGENIC A^{40} GENERATED BY TYPICAL BIOTITE (7% K) DURING DIFFERENT TIME INTERVALS

TIME INTERVAL (m.y.)	A^{40} (ccs. n.t.p./gm.
1,000	3.69×10^{-4}
500	1.60×10^{-4}
100	2.87×10^{-5}
50	1.42×10^{-5}
10	2.80×10^{-6}
1	2.80×10^{-7}

MASS SPECTROMETRY

Employment of the static method[3] of analysis in mass spectrometry produces a great increase in sensitivity over the more usual dynamic mode. In the former technique the vacuum in the mass spectrometer tube has to be sufficiently good so that when the tube is isolated from the pumps no significant rise in pressure is produced during the time required for an analysis. A small fraction of the gas from the inlet system is admitted to the tube where it is then completely isolated and analysed.

VACUUM SYSTEM

In this work the MS10 has been set up for such work at ultra-high vacuum and use in static analysis. The instrument as arranged by the authors is shown in fig.1. Although the instrument is designed for regular baking out at temperatures up to 400°C, we have not needed to exceed 200°C. With overnight baking little difficulty has been experienced in producing pressures of about $5\ 10^{-10}$ mm Hg and these have been maintained, without further baking, over periods of several months. A silicone oil, Dow Corning 705, has been used in the metal diffusion pump which has a liquid air cold trap. No difficulty has been experienced in reducing background at the critical mass 36 to zero. Apiezon (B) oil was not too satisfactory in this respect. A scan of the background in the tube, sealed off from the pumps with the MCV4 (Edwards) isolation valve, when the pressure was $6\ 10^{-10}$ mm Hg is shown in fig.2. At such pressures the only significant peak occurs at mass 28, presumed to be due to N_2 and CO.

INLET SYSTEM

A very simple inlet system has been employed and this may be seen in fig. 1. Even with Apiezon -T- greased stop-cocks it is a simple matter to evacuate the inlet side so that any background contributions in the inlet at masses 36, and 38 are not detectable by the mass spectrometer and any at 40 is only just seen on the most sensitive range. Samples left overnight in the inlet system show no variation in 36/38 and 40/38 ratios with time.

MASS SPECTROMETER CONSTRUCTION

The MS10 is shown in fig. 1. A small permanent magnet supplies the field of 1830 gauss. Electrostatic Scanning of the various beams is used -a motor driven potentiometer in the source controls causing the appropriate variations in accelerating voltage. A^{40} is focused onto the collector slit when the accelerating voltage is about 100 volts.

Ionization of the gas molecules is produced by the usual electron impact source[4], the electrons being emitted from a heated Rhenium filament, prior to being accelerated by falling through a potential difference of 70 volts. Regulation of trap current is employed, the current being stabilized at 50μA. A D.C. amplifier with a grid resistor of 10^{11} ohms is used to detect the ion currents, the output being fed to a Honeywell-Brown potentiometric pen recorder. The noise level is less than an equivalent ion current of 2×10^{15} amperes.

SCHEMATIC DIAGRAM OF EXPERIMENTAL ARRANGEMENT FOR STATIC ANALYSIS OF SMALL VOLUMES OF ARGON ON MS 10 MASS SPECTROMETER

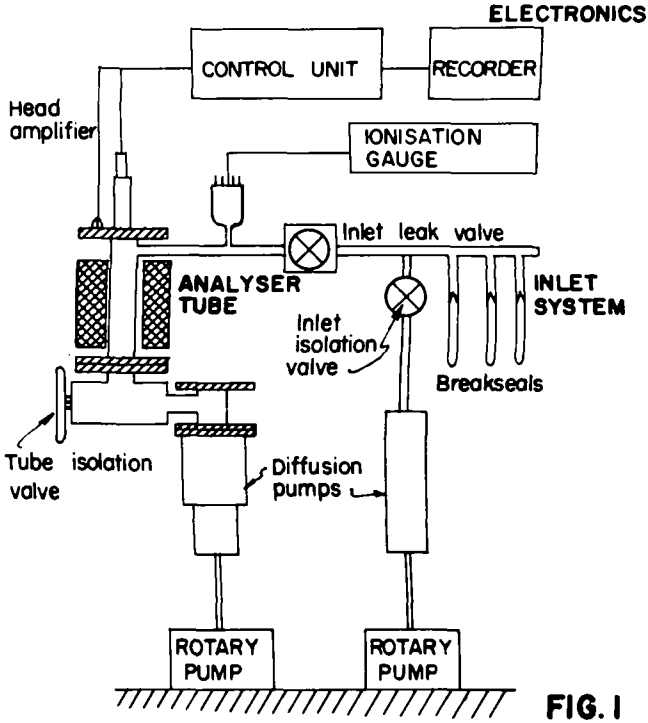

FIG. 1

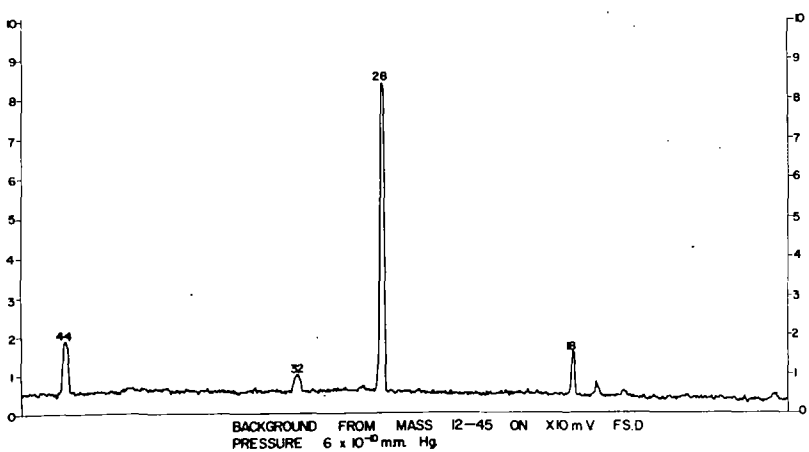

FIG. 2.

SENSITIVITY

This is claimed by the manufacturers to be $5\ 10^{-5}$ A/torr for argon, and a figure of this order has been found in our investigations, although no attempt at an accurate estimate of sensitivity has been made.

COMPARATIVE ANALYSES

Table II shows the results of analyses carried out on mineral samples varying in argon contents from 0.019 p.p.m. to 2.76 p.p.m. Generally about 2 gms. of biotite were fused in vacuum to release the argon, giving radiogenic A^{40} volumes ranging from $1.07\ 10^{-5}$ cc n.t.p. to $1.54\ 10^{-3}$ cc n.t.p. which were analysed statically on the MS10 after purification and mixing with accurately known quantities of A^{38}. (Typically the A^{38} volume would be about 9×10^{-6} cc n.t.p.) The very high sensitivity made the static analysis of these samples extremely simple. Table II also shows our results compared with those obtained on the same samples by other workers.

TABLE II.

TABLE SHOWING COMPARISON OF ANALYSES CARRIED OUT IN TORONTO WITH OTHERS MADE IN VARIOUS LABORATORIES ON SAME MINERAL SAMPLE.

SAMPLE	K %	Atmo. (%)	A^{40} (p.p.m).	LAB.	AGE (m.y.)
BAIL HILL	3.44	17.8	0.126	Toronto	455
BIOTITE No.1	3.39	2.0	0.121	Cambridge	445
	3.31	10.7	0.116	Oxford	437
COLMONELL	5.44	36.0	0.213	Toronto	483
BIOTITE No.3	5.34	1.5	0.203	Cambridge	467
COLMONELL	4.98	10.3	0.192	Toronto	476
BIOTITE No.4	4.85	2.7	0.186	Cambridge	477
COLM.BI.No.5	6.13	3.0	0.238	Toronto	479
MUSCOVITE XXII		3.9	0.704	Toronto	
			0.710	Geochron	
		2.8-	2.76	Toronto	
MUSCOVITE X		6.5	2.76	Geochron	
		1.7	2.73	Geochron	
LAXFORDIAN		0.9	1.353	Toronto	
BIOTITE 20165		0.6	1.376	Oxford	
BIOTITE XXIII	7.09	3.5	0.6096	Toronto	933
HORNBLENDE XXIII	0.221	53.0	0.0192	Toronto	940

$$\lambda_\beta = 4.72\ 10^{-10}\ yr^{-1}$$

$$\lambda_e = 0.584\ 10^{-10}\ yr^{-1}$$

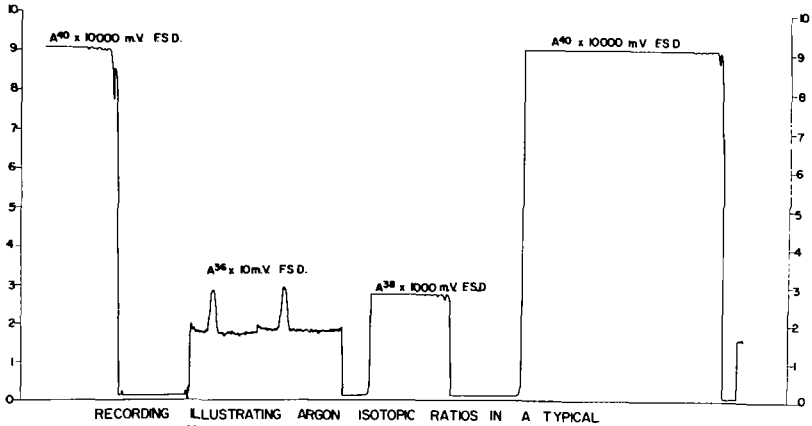

RECORDING ILLUSTRATING ARGON ISOTOPIC RATIOS IN A TYPICAL ANALYSIS OF A GRENVILLE BIOTITE

FIG. 3.

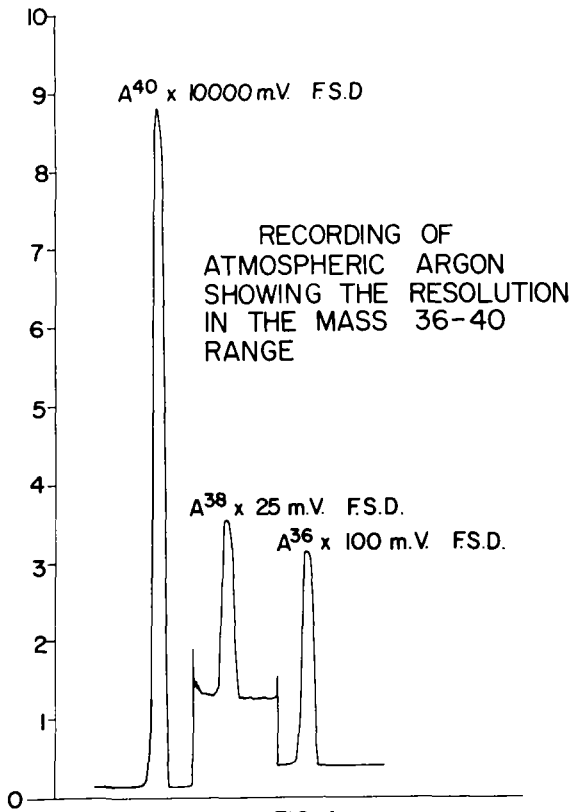

FIG. 4.

In Fig. 3 may be seen a reproduction of an actual chart recording. A^{40} was recorded on a range requiring 10 volts for full scale deflection, A^{38} on 1 volt full scale deflection and A^{36} on 10 mv. full scale deflection.

SCANNING

The isotope ratios may be taken by scanning the ion beams back and forth across the slit by automatic variation of the accelerating voltage to produce the sequence A^{36}, A^{38}, A^{40}, A^{36}, A^{38}, A^{40},..... Alternatively one can sit on top of the individual peaks for short periods by adjusting the scanning potentiometer manually. No difference is found in measurements made by both procedures on the same sample.

MEMORY EFFECT

It has frequently been reported that in static analysis the gases being analysed during a particular run are contaminated by a previous sample. Reynolds[3] has suggested that during an analysis ions are driven into the walls of the mass spectrometer tube. The composition of the embedded gases would then be representative of that sample. During a subsequent analysis it appears that ion bombardment of the walls causes the embedded gases to be re-emitted into the scaled-off chamber thus contaminating the new analysis and causing changes of the measured ratios with time. This "memory" effect has long been troublesome to many workers, and apparently is not removed completely by baking. In the MS10, for argon analysis, we find no trace at all of a memory effect. Measurements of the isotope ratios on an argon sample trapped in the tube for several hours show no variation with time. Peak heights barely change. This is an extreme advantage possessed by the instrument. We attribute this effect to the low accelerating voltage (100 volts) used when examining the argon isotopes. That is, in this instrument the positive ions bombard the walls of the mass spectrometer with a much lower energy than is usual. In most mass spectrometers several thousand volts are used for ion acceleration.

DISCRIMINATION

The isotope ratios obtained with the MS10 are critically dependent on the ion repeller voltage in the source. Ratios of A^{40}/A^{36} varying from about 300 to 220 may be reproducibly produced by systematic settings of the repeller plate voltage. However, the measured ratio remains fixed, for a given gas with a given repeller voltage setting. Thus as there is no call to adjust the repeller voltage the discrimination is constant and easily found from analyses of atmospheric argon samples. The results of static analyses give good agreement with dynamic runs when the former are submitted to a root-mass correction to allow for fractionation through the Granville-Phillips variable leak-valve.

RESOLUTION

For argon analyses of this nature it is merely necessary to be able to resolve completely the peaks at mass 40, 38 and 36. This is not a severe requirement and the MS10 is able to meet it easily. The resolving power is about 50. A typical recording of the mass spectrum of atmospheric argon is shown in Fig. 4. Clearly the A^{40} and A^{38} beams contribute no significant amount to each other. A more important feature to consider is the possible existence of tailing of the A^{38} beam at the mass 36 position. As can be seen from fig. 4 this is a negligible effect - the contribution two mass numbers away due to a beam at mass 38 is approximately 10^{-4} times the size of the A^{38} beam.

CONCLUSIONS

It has proved straightforward to use the MS10 mass analyser for isotopic dilution determination of the minute amounts of A^{40} generated in rocks by the radioactive decay of K^{40}.

Isotope ratios may be measured with an accuracy of $\pm$ 0.5%, or better, after calibration of the amplifier and recorder system. We have been achieving this simply and routinely and have carried out accurate argon analyses on over fifty mineral samples in the course of three and a half months work. The youngest sample we have analysed so far is a 50 m.y. old biotite. It is clear from our experiments, however, that one gram of a biotite 1 m.y. in age would definitely yield sufficient argon to be measured by the MS10.

This demonstration could have far-reaching consequences. Laboratories presently unable to afford the usually employed more elaborate mass spectrometers could doubtless now consider the variety of simple background analysers available of which one at least has been shown to be entirely suitable.

REFERENCES

1/ Hamilton, E.I., Dodson, M.H., and Snelling, N.J., 1962, Int. Jour. App. Rad. and Iso. 13, 587-610.

2/ Miller, J.A., and Brown, P.E., 1964, Adv. Sci.

3/ Reynolds, J.H., 1956, Rev. Sci. Inst., 27, 928.

4/ Nier, A.O., 1947, Rev. Sci. Inst., 18, 398.

APPARATUS FOR THE SIMULTANEOUS OBSERVATION OF ELECTRICAL CONDUCTIVITY AND GAS DIFFUSION IN CRYSTALS

by

P. P. Pronko and H. R. Krouse

Physics Department,

University of Alberta,

Edmonton, Alberta.

This paper involves an experimental approach to the simultaneous measurement of gas diffusion and electrical conductivity in solids.

Although the method can be applied to any solid, attention is currently being directed toward ionic conductivity and diffusion of Ar^{40} in dielectric minerals. This is of interest in radioactive age dating since Ar^{40} is the decay product of K^{40}.

The purpose of the present research is to determine the mechanisms of atomic movement for various temperature ranges. Thus far efforts have been confined to studying ionic transport in thin slabs of a single crystal of the mineral of interest. These slabs are a fraction of a millimeter thick and approximately one square centimeter in area. This geometry was chosen so that one dimensional diffusion could be observed. In the future attempts will be made to investigate atomic transport as a function of crystallographic direction using this method.

Figure 1: Diffusion-Conductivity Cell

The cell is made of high resistivity quartz to minimize alternative paths for the electrical conduction. Cooling jackets around the cell keep this conductivity to a negligible value. All metal to glass junctions are made through kovar seals. A graded transition of pyrex is used to connect the quartz to the kovar.

The sample is loaded between the electrodes as indicated and its temperature monitored by an alumel-chromel thermocouple located immediately adjacent to the crystal slab but not touching it. The electrical resistance of the crystal can be measured with a range of applied voltages from 0 to a few thousand volts. The temperature of the oven is set and the temperature, argon flux, and electrical resistance are simultaneously recorded as a function of time.

Figure 2: Block Diagram.

The gas from the diffusion cell goes directly into a 6-inch radius 60° magnetic sector mass spectrometer. The recorder cycles through the three channels corresponding to argon flux, conductivity, and temperature. All three curves are recorded on the same chart paper. A system is under development whereby the data is also punched on IBM cards concurrent with its visual recording. All data has been analysed on an IBM 1620 computer.

Figure 3: Chart Paper.

The following 3 curves show the temperature, argon flux, and electrical conductivity.

Note that as the temperature increases, both the conductivity and flux increase rapidly, the conductivity approaching a steady value as the temperature stabilizes. The argon flux increases with temperature, but also decreases with time. It is for this reason that it rises to a maximum and then drops off. It decreases in time with some character-

DIFFUSION-CONDUCTIVITY CELL

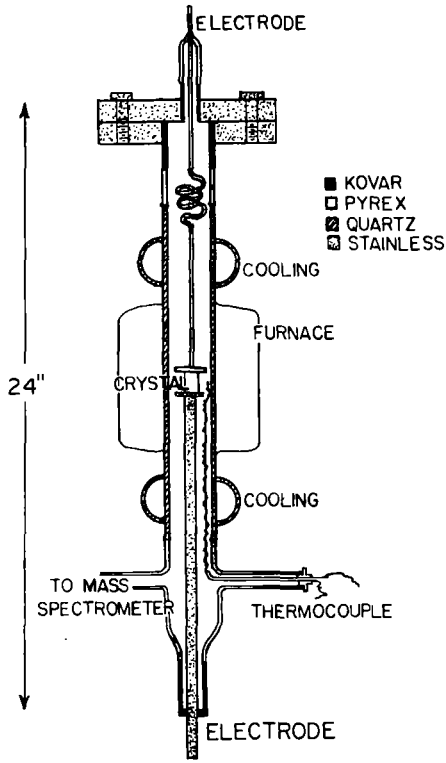

Fig. 1

DIFFUSION-CONDUCTIVITY EXPERIMENT

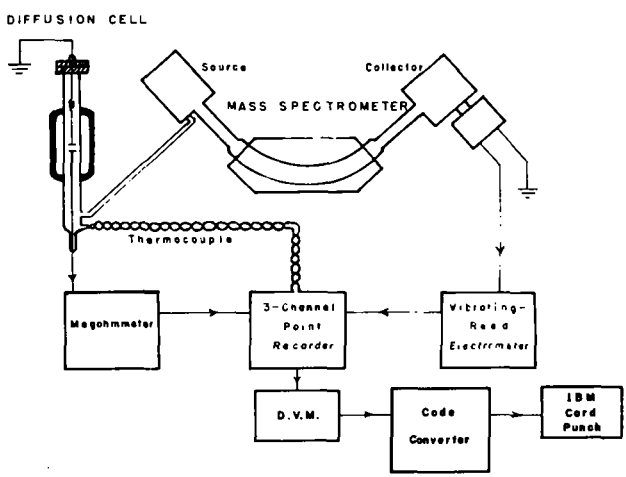

Fig. 2

istic curvature which is dictated by the nature of the diffusion process. Most previous investigators have used the area under the flux curve as indicative of the fraction of gas released and thereby determined the diffusion coefficient for a particular temperature. In the present investigation we attempt to find a theoretical equation, based on some assumed model, which will predict the shape of the flux-time curve and thus, by making a least squares fit, determine the diffusion coefficient. We have met with moderate success in this approach; however, a large amount of work still remains to be done.

Before going into the curve fitting procedure, I would like to discuss a certain correlation which was found between the conductivity and diffusion which suggests the kind of model to be chosen for temperatures in the neighborhood of 430° C.

As indicated in Figure 3, the conductivity increases with temperature and tends to stabilize as the temperature comes to a constant value. This procedure is indicative of a semi-conduction process.

Figure 4: (Cond-Diffusion Correlation) These are idealized plots.

The upper left hand diagram shows the conductivity as a constant in time for temperatures below 365° C. The upper right hand diagram shows the effect observed at 436° C. Here we see a marked dependance of the conductivity on the time. It will be noted that as the Ar^{40} flux goes into its asymptotic decay region the conductivity begins to flatten out. If the Ar^{40} atoms were leaving ionic lattice sites, then as each Ar^{40} atom came out of the crystal it would leave a vacant lattice site which would act as a single charge carrier for the ionic conduction process. If this were the case, it is noted that the conductivity is given as $\sigma = \mu N'q$ where N' is the density of charge carriers, q is the charge of each, and μ the mobility.

If vacancy conduction is the dominant mode then N' will correspond to the density of vacant lattice sites and should be proportional to the total number of Ar^{40} atoms leaving the sample. Thus a plot of the conductivity versus the accumulated area under the Ar^{40} curve should give a straight line if the process is as outlined.

Figure 5: (Cond. vs. Area)

Figure 5 shows the results of such a plot for the experimental data at 436° C.

In terms of a correlation one can fit a linear regression to these points quite nicely. It seems possible that in the neighborhood of 436° C the diffusion and conduction are dominantly vacancy-migration processes corresponding to volume diffusion.

For higher temperatures in the neighborhood of 500° C and above an entirely different effect is observed. Here the conductivity and Ar^{40} flux have the same sort of time dependence. They both decay characteristically with time. (See Figure 3; note that the Ar^{40} flux and σ rise and fall in the same fashion.)

This behavior of the conductivity suggests that the charge carriers are subject to the same type of concentration gradient as the neutral Ar^{40} atoms and are subject to the same diffusion laws. On the basis of this observation we might conclude that for temperatures above 500° C the crystal contains a large concentration of Frenkel defects and the charge carriers are the associated ions as opposed to vacancy conduction for lower temperatures. For the feldspar group, which we are studying, one would expect that potassium and aluminum ions are the principle conduction ions. Work is presently under way to establish this more definitely.

An interesting effect which has also been observed is that for these higher temperatures the Ar^{40} flux is quite sensitive to the applied voltage. Since the argon is supposedly neutral, one possible explanation is to attribute this to a collision process between the ions which are accelerated by the electric field and the argon atoms. If this can be demonstrated as a collision process one could then possibly use this effect to determine crystal parameters such as mean free paths and drift velocities of the charge carriers.

FIG. 3 TYPICAL SIMULTANEOUS RECORDING OF ARGON FLUX, TEMPERATURE, & ELECTRICAL CONDUCTIVITY

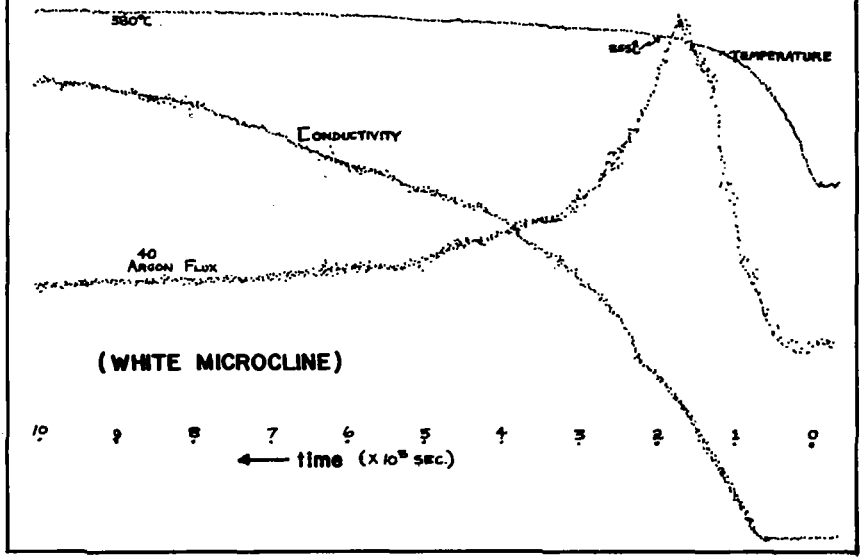

CONDUCTIVITY-DIFFUSION CORRELATION

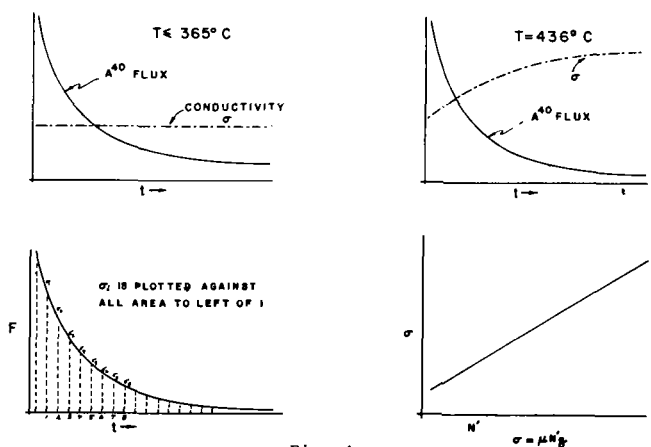

Fig. 4

Returning now to the lower temperatures and using the model for volume diffusion from a thin slab we shall develop the equations which predict the flux time curve.

ONE-DIMENSIONAL DIFFUSION $[C = C(x,t)]$

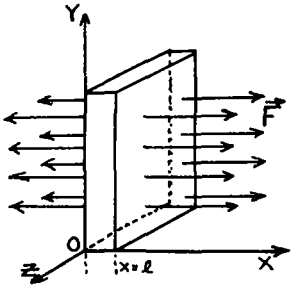

Fick's first law $\vec{F} = -D\frac{\partial C}{\partial x}\,\vec{i}$ (1)

Continuity Eq. $\frac{\partial C}{\partial t} = -\nabla \cdot \vec{F}$ (2)

Diffusion Eq. $\frac{\partial C}{\partial t} = D\,\frac{\partial^2 C}{\partial x^2}$ (3)

Boundary Conditions :— Thin slab-boundaries at o and ℓ

Concentration

$$C(x,t) = \frac{4\,C_o}{\pi} \sum_{n=0}^{\infty} \frac{1}{2n+1} \cdot \sin\left(\frac{2n+1}{\ell}\right)\pi x \exp\left[\frac{-D(2n+1)^2\pi^2}{\ell^2}t\right] \quad (4)$$

Flux $F = -D\,\frac{\partial C}{\partial x}$ (5)

Evaluate at $x = o$ and ℓ

$$F_{surface} = 8\,\frac{C_o D}{\ell} \sum_{n=0}^{\infty} e^{-D(2n+1)^2 \frac{\pi^2}{\ell^2} t} \quad (6)$$

Voltage flux relation $V = \beta F$ β = Proportionality constant

Time dependence of Mass Spec.

$$V = 8\,C_o\,\frac{\beta D}{\ell} \sum_{n=0}^{\infty} \exp\left[-D(2n+1)^2 \frac{\pi^2}{\ell^2} t\right] \quad (7)$$

Converting to Hyperbolic Fctns. $V_{detector} = \beta\,F_{surface}$

$$V_{detector} = 4\,\frac{\beta C_o D}{\ell}\ \mathrm{cosech}\,\frac{D\pi^2}{\ell^2}\,t \quad (8)$$

Normalized data expressed as

$$\frac{V}{V_{max}} = \frac{\mathrm{cosech}\,\frac{D\pi^2}{\ell^2}\,t}{\mathrm{cosech}\,\frac{D\pi^2}{\ell^2}\,t'} = A\ \mathrm{cosech}\ g\ t \quad (9)$$

where $g = \frac{D\pi^2}{\ell^2}$

Taking Inverse Cosech gives st. line

$$\mathrm{Cosech}^{-1}\left(\frac{V}{V_m}\,\frac{1}{A}\right) = g\ t \quad (10)$$

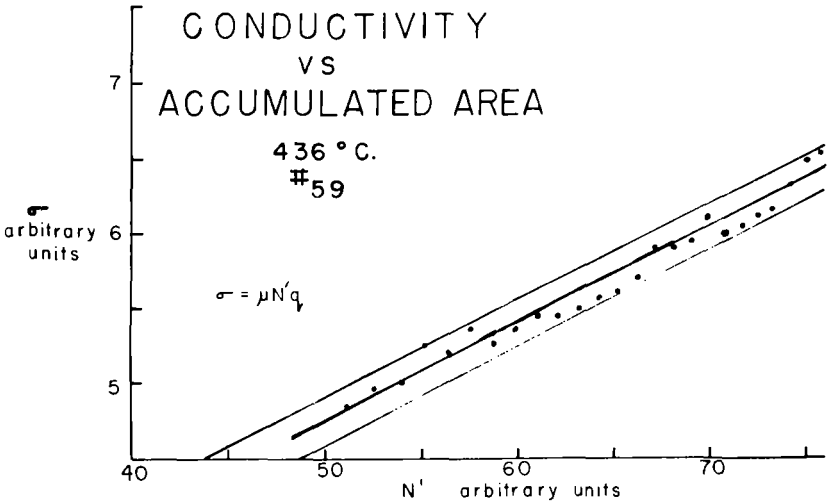
CONDUCTIVITY
VS
ACCUMULATED AREA
436 °C.
#59
σ
arbitrary units
σ = μN'q
7
6
5
40
50
60
70
N' arbitrary units

Fig. 5

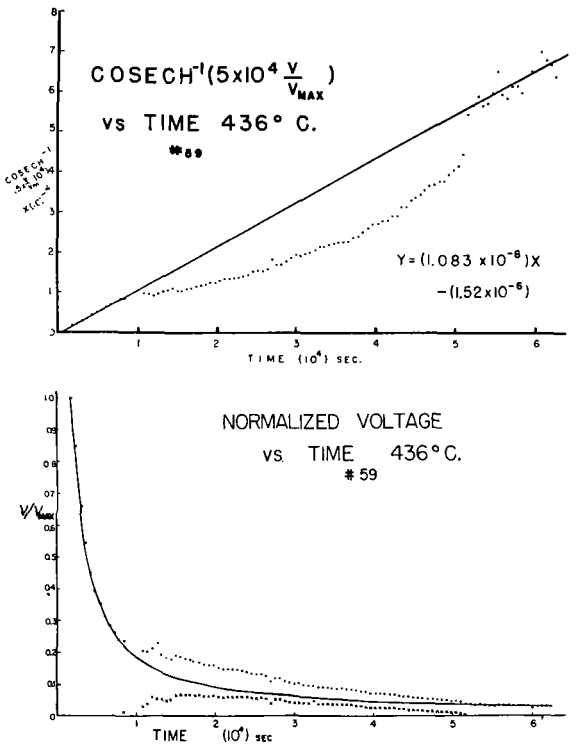
COSECH⁻¹(5x10⁴ V/V_MAX)
vs TIME 436° C.
#59
Y = (1.083 x10⁻⁶)X
-(1.52x10⁻⁶)
TIME (10⁴) SEC.
NORMALIZED VOLTAGE
vs TIME 436°C.
59
V/V_MAX
TIME (10⁴) SEC

Fig. 6

Thus a plot of $\text{Cosech}^{-1}\left(\frac{V}{V_m}\ \frac{1}{A}\right)$ vs. t will give a straight line if the process is truly volume diffusion according to the model chosen.

We thus look for this linearity when analyzing the inverse Cosech plots of the experimental data.

Figure 6: Experimental Flux Time Curves.

The following data were obtained from a white microcline cut along an arbitrary direction. The upper graph shows the inverse Cosech versus time. The lower graph shows the separated flux time curve.

Fixing our attention on the upper graph, we are concerned with departures of the experimental results from linearity and their possible causes.

The parts which do conform to linearity we attribute to volume diffusion effects. Those parts which depart from linearity must be attributed to some other mechanism or phenomena. We are not at this time prepared to identify these segments positively and will therefore simply acknowledge their existence and suggest that possibly this may be due to grain boundary diffusion.

Converting back to V/V_{max} vs. t allows one to see which portions of the decay curve correspond to simple volume diffusion and which portions contain the anomalous flux.

The black circles represent the experimental points, the solid line is the best fit theoretical curve to the volume diffusion portion. The x's are the anomalous flux as determined by subtracting the experimental from the theoretical results. A further knowledge of this anomalous flux may be obtained by investigating its growth and decay properties. In so doing we hope to be able to account for all possible mechanisms of argon loss from these crystals.

A NEW COUNTING METHOD FOR HIGH SENSITIVITY MASS SPECTROMETRY; SUBSTITUTION OF A VOLTAGE TO FREQUENCY CONVERTER FOR THE DISCRIMINATOR*

George W. Barton, Jr., Ronald Jene Dupzyk, and Laurin F. Tolman
Lawrence Radiation Laboratory, University of California
Livermore, California

In a previous paper[1] we reported on the use of pulse counting together with a modified nuclear pulse analyser in order to obtain high sensitivity together with high precision in our uranium isotope ratio work. Since then, analyser manufacturers have come to call this modification a multichannel scaler and list it as a catalog item. Pulse counting techniques are in limited, but not widespread use in mass spectrometry partly because they require tricky, and sometimes unreliable circuits.[2] Figure 1 is a redrawing, with some modifications, of the block diagram in reference 1. The important one for this presentation is the replacement of the wide band amplifiers and discriminator with a DC amplifier and voltage to frequency converter. The magnetic field sweep has been previously described[3] and the current refinement of it will be mentioned by Dupzyk at this meeting.

The replacement of the discriminator is a welcome outgrowth of some work done with Klein[4] on enhancement of signal-to-noise ratio in nuclear magnetic resonance. In mass spectrometry one of the major problems is random fluctuations in the average ion intensity. These have been reduced to manageable proportions in electron impact sources, but are bad in surface ionization sources, and almost catastrophic in spark sources. *The problem in nuclear magnetic resonance is a little different, in that* the fluctuations occur in the baseline or background rather than the signal. Yet it is easy to see qualitatively (much harder quantitatively) that a system which takes many spectra and averages them together will improve the precision of either measurement by something like the square root of the number of spectra averaged. In NMR, however, we had no ready source of pulses, as we do from ions striking an electron multiplier, which could be added into a multichannel scaler swept in synchronism with the spectrometer. Fortunately, the state of the art in voltage-to-frequency converters has been advancing rapidly. At the time of the work with Klein, three years ago, 100 kc/s units were available. At the present time, units with a maximum conversion rate exceeding 1 Mc/s are available.

The importance of the maximum conversion rate must not be overlooked. If we can collect only 25,000 counts in our standard counting interval, and we cannot identify fewer than one count as a signal at all, our dynamic range of signals is only 25,000 to 1 and we have no precision in our measurement of the smaller signal. For 1% precision, our dynamic range is 250 to 1 or about as good as a chart recorder without a range switch. The commercial mass spectrometer digitizers have dealt with this by a technique adapted from pinball machines, automatic range changing. With a 1 Mc/s voltage to frequency converter, the inherent dynamic range is 40 times as large, and one can do away with pinball relays in most experiments.

Aside from its disadvantages of unreliability, the pulse discriminator has an inherent limitation, its nonlinear response. If two pulses have too close a spacing in time, it ignores the second of the two. Continuous averaging assumes that all the spectra can be added together linearly. If the dead time correction is less than 10%, one can estimate it to adequate precision, make the correction, and get good answers. By taking exceedingly painful precautions we have obtained good answers up to a 50% dead time correction, but I never could develop a real feeling of confidence in those results. Thus, even with 10 Mc/s scalers and discriminators we are limited to a maximum accumulation rate of 1 Mc/s and all the dynamic range considerations of the previous paragraph apply. The voltage to frequency converter does not have this dead time limitation, because it has the ability to remember the second pulse for a short while, and does not spit it out until the counting circuits are ready to accept it. Hence there is no dead time correction.

Figure 3 shows the stability of the measured potassium isotope ratio over a range of current from 10^{-15} amp to 10^{-7} amp. This illustrates that the differential linearity is better than 2 1/2% over eight orders of magnitude. We have results that are more difficult to display leading us to believe that this behavior holds to at least 10^{-18} amperes, and we have no reason to believe that it should not hold to much larger currents.

This system has been in use for a year now on two 60° sector 12 inch radius instruments of our own design. As Dupzyk will discuss later in the meeting it is now in use on a CEC 21-110 spark source instrument with results we are very proud of. Then, just to prove it could be done, we borrowed a friend's CEC 21-103 and without mechanical or electronic modification of his instrument obtained direct data digitization, and in a different experiment, continuous averaging as well as data digitization. For highest sensitivity, an electron multiplier will be needed, but the remaining virtues can be achieved without internal modification of the 21-103.

References

*Work was performed under the auspices of the U. S. Atomic Energy Commission.

1. G. W. Barton, Jr., L. E. Gibson and L. F. Tolman, Anal. Chem. 32, 1599 (Nov. 1960).
2. R. A. White and T. L. Collins, Appl. Spectroscopy, 8, 17 (1954).
3. G. W. Barton, Jr., L. F. Tolman, and R. E. Roulette, Rev. Sci. Instr. 31, 995 (1960), and the paper by Dupzyk at this meeting.
4. M. P. Klein, and G. W. Barton, Jr., Rev. Sci. Instr. 34, 754 (1963).

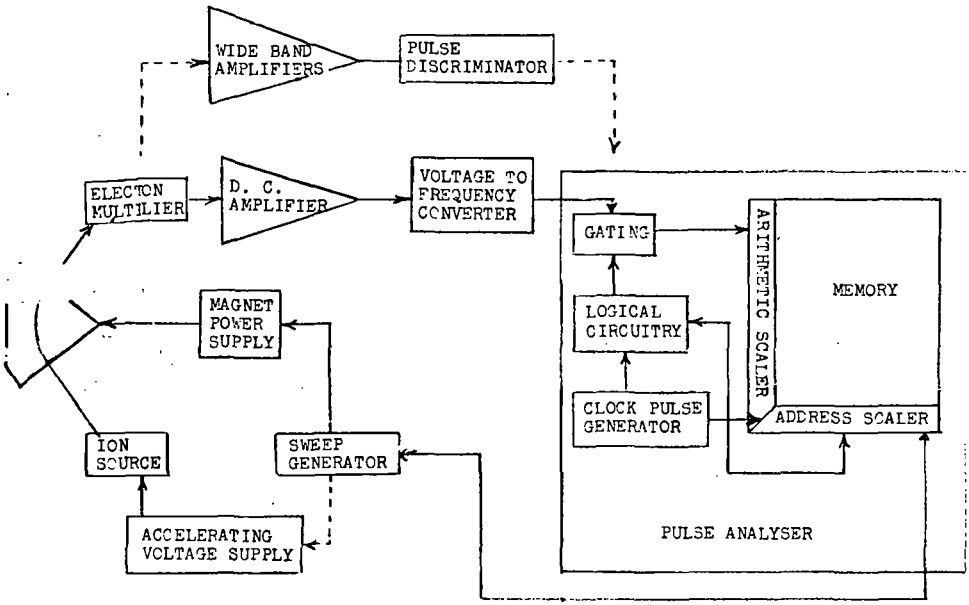

Fig. 1. Block diagram of the counting system. The previously reported system is indicated by the dotted lines. The currently installed system is indicated by solid lines.

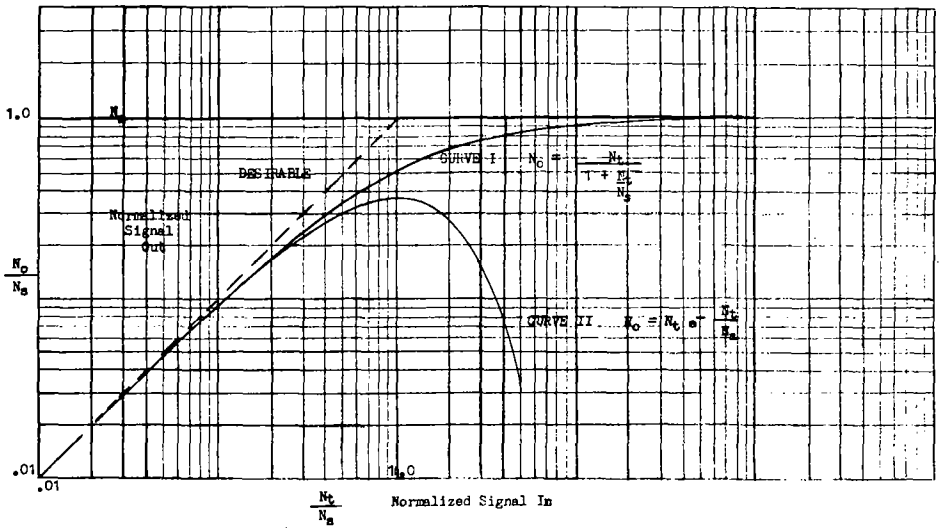

Fig. 2. Nonlinear response of counting circuits. Well behaved counting circuits fall between curve I and curve II. The voltage-to-frequency converter follows the ideal curve very closely.

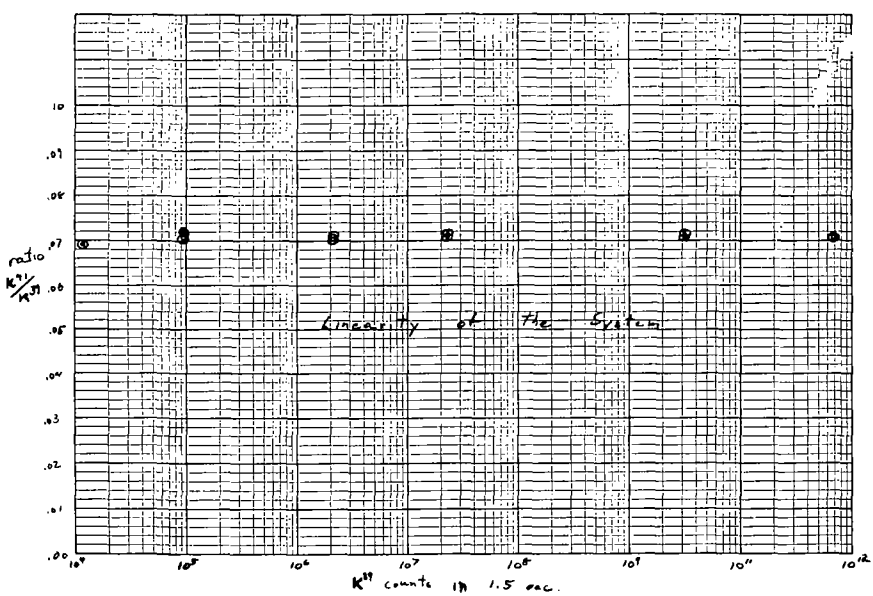

Fig. 3. Plot of the stability of the potassium isotope ratio as total ion current is changed, illustrating the differential linearity of the system.

ELECTRON MULTIPLIERS FOR USE IN MASS SPECTROMETRY

B. R. F. Kendall*
Nuclide Corporation
State College, Pennsylvania

ABSTRACT

Factors influencing the design of electron multiplier particle detectors are reviewed. Experimental results are presented which show that, in addition to meeting the normal requirements of stable high gain with a low noise level, it is necessary in ultra-high-vacuum applications to minimize gas evolution effects caused by internal dynode resistor heating and by electron currents passing between successive dynodes. A brief description is given of the construction and performance of a small venetion-blind electron multiplier designed in accordance with these principles. The basic multiplier design is suitable for use in magnetic sector-field, quadrupole, time-of-flight and other types of mass spectrometers.

1. INTRODUCTION

Electron multipliers are most frequently used in mass spectrometry for measuring currents of positive or negative ions. They may also be used to measure fluxes of energetic neutral particles, such as those formed in charge exchange experiments. An electron multiplier may have separate dynodes, as in the Allen and venetian-blind types, or continuous dynode surfaces, as in the various magnetic crossed-field and tubular electrostatic types. Either output current or output count rate may be used to indicate the magnitude of the input signal.

Whatever the type of electron multiplier and the details of its use for the direct detection of ions in mass spectrometry, there are several characteristics which are necessary if good all-round performance is to be achieved. This paper is concerned with the means by which these characteristics may be obtained, and in particular with certain requirements which must be met in order to avoid errors in gas analysis at low pressures.

2. DESIGN CONSIDERATIONS

The design of a typical electron multiplier for use in mass spectrometry is influenced by the need for the following characteristics:

1. High Gain, usually obtained by using between 15 and 20 stages, by activating the dynodes for maximum secondary emission yield, and by operating at fairly high interstage voltages.

2. Stable Gain, obtained by careful choice of activation procedures and dynode materials, by avoiding operation at high internal currents, by careful shielding of internal insulators, and by maintaining a constant supply voltage. Beryllium-copper is generally considered superior to other dynode materials if the system is often opened to air. Automatic gain stabilization has also been used successfully.

3. Low Noise Level, obtained by ensuring a smooth surface finish on all dynodes, avoidance of excessive interstage potentials, avoidance of glasses and other construction materials with radioactive impurities, and sometimes by cooling the dynodes.

4. Accurate Reproduction of Peak Shapes, implying constant gain as the ion beam is scanned across the first dynode. It appears that this can be achieved either by defocusing the incoming beam so that the gain is averaged over an area larger than the beam cross-section, or by focusing the incoming beam continuously onto the same region of the conversion dynode.

*Present Address: Department of Physics and Ionosphere Research Laboratory
Pennsylvania State University
University Park, Pa.

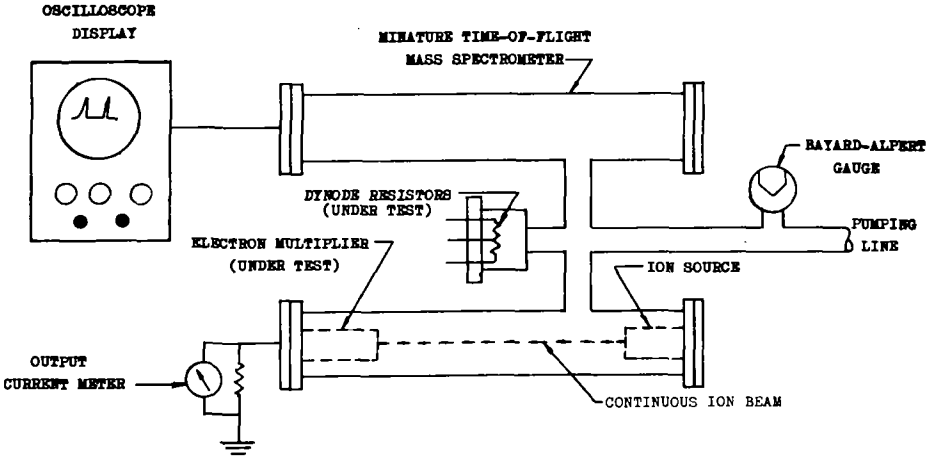

Fig. 1 Ultra-high Vacuum System used for Resistor and Multiplier Tests

POWER DISSIPATION (Milliwatts)	TEMPERATURE (°C)	GAS EVOLUTION RATE R (See text) Baked	Unbaked	GASES EVOLVED Baked	Unbaked
2	27				
18	30	5×10^{-12} (below detn. limit)	$<5\times10^{-10}$		
56	43				
225	95		Increasing Rapidly		
400	142	$<10^{-10}$ Increasing Rapidly		CH_4	
550	170		5×10^{-8}		CO_2, H_2O, CO, CH_4
900	240	10^{-10}		CH_4	

Fig. 2 Gas evolution from I. R. C. type VDCC internal dynode resistors

5. Negligible (or accurately predictable)Mass Discrimination, obtained by ensuring that ion beams always strike the conversion dynode at the same point,and by operation only under conditions for which the detector system has been calibrated.

6. Ability to Operate in Stray Magnetic Fields, obtained by internal or external magnetic shielding, or by the use of a comparatively field-insensitive dynode arrangement such as the venetian-blind layout.

7. Demountable Structure,to allow cleaning or repair.

8. Ability to withstand repeated 400°C Bakeouts, an essential requirement for ultra-high-vacuum applications, Correct mechanical design and choice of materials are necessary.

9. Miscellaneous Requirements for special applications, e.g., peak height distributions and pulse shapes suitable for use with counting circuits; or a large active area and low output capacitance, for use in Time-of-Flight mass spectrometry.

10. Good vacuum properties

The extensive literature on electron multipliers covers all but the last of these characteristics in considerable detail. General treatments of the subject are given in the books by Bruining,[1] Chenka[2], and Rodda[3], while reviews by Akishin[4] and by Inghram and Hayden[5] deal specifically with applications to mass spectrometry. Stability and fatigue effects are discussed by Keene and others[6-8]. Noise characteristics and gain statistics are dealt with by Pertsev[9] and several other workers[10-14]. Variations in gain over dynode surfaces and electrostatic design are described by Tyutikov[15], while Delaney and Walton[16] have successfully demonstrated an automatic gain control for electron multipliers. Isotope discrimination is discussed by White and Collins[17] and others[18, 19].

The tenth requirement, that of obtaining good vacuum properties, has received less attention. It has usually been assumed that it is sufficient to use materials which by themselves have good vacuum properties.

Experiments with a sensitive time-of-flight mass spectrometer described at a previous conference[20] showed that, at total pressures in the low 10^{-10} torr range, significant changes in pressure and gas composition could be produced by varying the multiplier output current or the applied voltage. It was assumed that gases were being produced by electron bombardment of the dynode surfaces, and probably also by the heating of the internal resistors connected between each pair of dynodes.

Recently it has been possible to test these assumptions using a special vacuum system fitted with a partial-pressure analyzer and total-pressure gauge and to obtain a more complete understanding of the ways in which an operating electron multiplier can act as a source of gas.

3. APPARATUS FOR STUDYING GAS EVOLUTION

The getter-ion pumped vacuum system used in these experiments is shown in Figure 1. Construction was mainly of 304 stainless steel with copper sealing gaskets. The system was baked overnight at 400°C before each experiment. Normal operating pressure was about 5×10^{-9} torr with all of the internal equipment in operation.

The electron multiplier under test was exposed to a continuous ion current of about 5×10^{-12} amp from a conventional ion source. The multiplier output current could be set to any current up to 20 microamp by varying the total applied voltage. A Bayard-Alpert gauge monitored the total pressure in the system while a small time-of-flight mass spectrometer recorded the changes in gas composition. Internal electron currents in the electron multiplier in the mass spectrometer were kept much smaller than the electron currents in the multiplier under test, and were kept as constant as possible as the total pressure changed.

A separate small chamber contained sample dynode resistors which could be heated by passing currents through them.

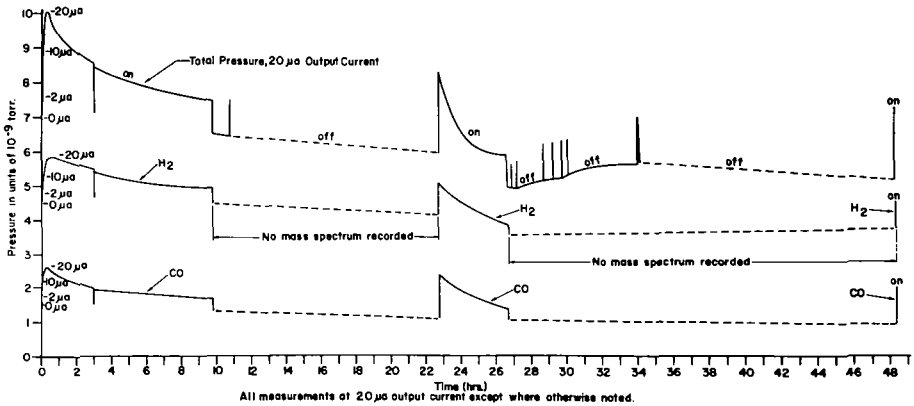

Fig. 3 Gas evolution caused by Electron Bombardment of dynodes.

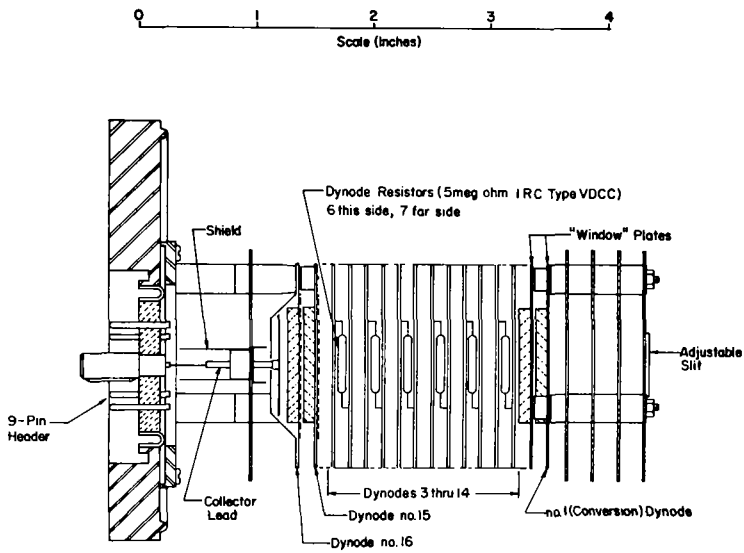

Fig. 4 Experimental Venetian-Blind Electron Multiplier.

4. GAS EVOLUTION FROM INTERNAL DYNODE RESISTORS

In order to make sure that results obtained in the later experiments would not be significantly affected by dynode resistor outgassing, these measurements were undertaken first. The test samples were groups of 400 kilohm and 5 megohm 1/2 watt IRC Type VDCC Pyrolytic resistors, which are used in several commercial multipliers.

Calibration in a separate vacuum system gave a temperature vs power dissipation curve for these resistors. As expected from their similar physical dimensions, the curves were essentially identical for the two resistance values at low power dissipations. Temperatures rose from 34°C at 32 mw dissipation to 170°C at 550 mw.

Figure 2 summarizes the results obtained when the resistors were heated in the main vacuum system. The quantity R is the magnitude of the pressure increase divided by the number of test resistors. If constant pumping speed is assumed, it is proportional to the rate of gas evolution per resistor.

As the power dissipation rose above about 200 milliwatts, outgassing began to increase rapidly. The main constituent of the gases given off was methane. For a previously-baked system which had then been exposed to air, noticeable gas evolution started at a much lower temperature and again rose rapidly, the main constituents being CO_2, H_2O, CO and CH_4 in that order.

These experiments show that, to prevent substantial temperature increases and resulting gas evolution from internal dynode resistors of this type, they should be operated at power dissipations much lower (preferably by a factor of 10 or more) than the rated values. For a maximum interstage voltage of 300 volts, this implies the use of resistors with values preferably greater than about 2 megohm. If lower interstage resistances are needed, as they may be in the final stages where electron currents are greatest, the necessary potentials must be supplied from an external resistor chain.

In the remainder of the gas evolution experiments, 5 megohm internal resistors were used on the first 13 stages of the 16-stage multiplier under test, and direct leads from an external low-resistance chain for the final three stages. The same arrangement was used on the multiplier in the partial-pressure analyzer. Gas evolution from the dynode resistors can therefore be assumed negligible in the later experiments.

No tests were made on glass-encased dynode resistors. However, it appears that they are subject to an additional gas evolution process, resulting from electrolysis of the heated glass envelope. Lichtman[21] has observed substantial oxygen evolution at low pressures when voltage was applied to glass-encased resistors.

5: GAS EVOLUTION FROM DYNODE AND COLLECTOR SURFACES

The test multiplier was a 16 stage venetian-blind type using E. M. I. beryllium-copper dynodes. The results of a typical experiment are shown in Figure 3. The three traces show variations in the total pressure, hydrogen partial pressure and carbon monoxide partial pressure. Because the partial pressure analyzer had not been calibrated within a synthetic gas mixture, the gas composition measurements should only be considered approximate.

The output electron current was first increased in steps to 2, 5, 10 and 20 microamps, operated continuously at 20 microamps to study cleanup effects, switched off to observe the buildup of gases on the surface, and then operated for one further "on" cycle and one additional "off" cycle. At the end of the experiment the multiplier was again switched "on" at 20 microamp output current. The momentary upward and downward deflections of the traces show where the "on" or "off" periods were interrupted to measure background pressures or gas evolution rates.

The results of this and similar experiments can be summarized qualitatively as follows:-

a) Gas evolution rate: Substantial amounts of gas are given off, at a rate which increases roughly linearly with the multiplier output current.

b) Cleanup Effect: The evolution rate fell roughly exponentially with time. The time constant was somewhat shorter for the second "on" cycle.

c) Gas Composition: The main gases given off early in the "on" cycle were CO and H_2, with traces of CH_4 and CO_2. Towards the end of the "on" cycle, CO predominated in most experiments.

d) Re-adsorption Effects: After the multiplier was turned off, the rate of gas evolution resulting from momentary switching on increased steadily with time for many hours. Unless gas diffusion from within the dynode was occurring, this phenomenon suggests a slow pumping action at the dynode surfaces.

e) Origins of the Evolved Gases: By suppressing electron currents to the collector and various dynodes while keeping other conditions constant, it was established that at the beginning of an "on" cycle the collector was the main source of gas (H_2 and CO). After some tens of minutes, the gas evolution from the collector had fallen considerably (mainly CO) and the last dynode was the main source of gas. In each case dynodes numbers 15 and 14 made only minor contributions to the total gas load. Contributions from the other dynodes were negligible.

It can be concluded from these experiments that the output electron current should be kept below about 1 microamp whenever precise measurements are being attempted at very low pressures, if errors due to gas evolution (and possible slow pumping action when the multiplier is switched off) are to be avoided.

6. EXPERIMENTAL ELECTRON MULTIPLIERS

An example of one of several experimental general-purpose electron multipliers is shown in Figure 4. It was designed in accordance with the principles laid down previously in this paper, with special attention being paid to the reduction of gas evolution.

The multiplier is of the venetian-blind type, using 16 beryllium-copper dynodes similar to those used in the E. M. I. 9603 electron multiplier. It is fitted with its own adjustable entrance slit so that it constitutes a complete ion detection system suitable for magnetic mass spectrometers. By omitting the slit and making minor structural changes, it can be converted into a form which, because of its 2 cm diameter active area, is ideally suited to quadruple, time-of-flight and Bennett mass analyzers.

Materials used in the construction are mainly ceramics, molybdenum, stainless steel and nickel. Repeated bakeouts to 400-425°C are therefore possible.

Performance characteristics were as follows:-

1. Gain: 10^6-10^7 for 16-stage multipliers at 270 v/stage. A 20-stage version gave a gain in excess of 10^8.

2. Gain Stability: Stable to within a few percent over periods of several days. A large internal active area, careful insulator shielding, and use of BeCu dynode material probably contributed to this performance. To eliminate ion feedback the individual "slats" of the venetion-blind dynodes were all checked for overlap before assembly, and successive dynodes had their "slats" facing in opposite directions.

3. Noise Level: Equivalent input noise of 10^{-18} to 10^{-19} amp at full gain with a simple electrometer detector, falling to about 10^{-20} amp if pulse-height discrimination was used. Emission from the large unused active areas in the first few stages of the multiplier were minimized by the use of windows of successively increasing size which blanked off all but the central portions of the first three dynodes. The shielded collector lead was supported from a grounded plate to minimize leakage currents, and the collector was supported within the final dynode assembly at a point where vibration would cause a minimum ac component in the output signal.

4. Sensitivity to Stray Magnetic Fields: Considerably less sensitive than conventional Allen-type multipliers, presumably because of the unfocused venetian-blind design and the limited internal shielding built into the dynode supports.

Other features included replacement of the shield mesh on the first dynode by electrodes providing suitable repelling fields, so that a narrow ion beam scanned across the entrance slit would not be subject to intermittent interception by strands of the mesh.

To minimize gas evolution, 5 megohm dynode resistors were used, operating at essentially room temperature because of the low power dissipation. The last three dynodes were connected directly to an external supply, as on the multiplier used in the gas evolution tests.

The first experimental multiplier used a flat-plate collector with an area of several square centimeters. However, recent tests with a fine mesh collector having a very much smaller surface area suggest that the small-area collector can be more quickly "cleaned up" by running the multiplier at high output currents, and also offers unexpected freedom from fatigue effects. Experiments are continuing in an effort to explain this phenomenon.

REFERENCES

1. Bruining, H., "Physics and Applications of Secondary Electron Emission", Pergamon Press, London (1954).
2. Chenka, N.O. et al, "Electron Multipliers" (Acad. Sci. USSR).
3. Rodda, S., "Photo-electric Multipliers", Macdonald, London, (1953).
4. Akishin, A.I., Soviet Physics Uspekhi, 66 (1), 113 (1958).
5. Inghram, M.G. and Hayden, R.J., "A Handbook on Mass Spectroscopy", U.S.N.R.C. Publication 311,(1954).
6. Keene, J.P., Rev. Sci. Instr., 34, 1220 (1963).
7. Cathey, L., AEC Report DP-642 (1961).
8. Vildgrube, G.S., et al, Prib. i Tekh. Eksper No.5, 167 (1963).
9. Pertsev A.N., et al, Prib. i Tekh. Eksper, No.5, 173 (1963).
10. Hyman, L.G., et al, Rev. Sci. Instr. 35, 393, (1964).
11. Lombard, F.J. and Martin, F., Rev. Sci. Instr., 32, 200, (1961)
12. Brault, M., and Gazier, C., J. Phys. Rad., 24, 345, (1963).
13. Tusting, R.F., et al, I.R.E. Trans. Nucl. Sci., NS-9, No. 3, 118, (1962).
14. Fleischer, V.G., Instr. & Exper. Techs. No.2, 336, (1962).
15. Tyutikov, A.M., Instr. & Exper. Techs. No.1, 112, (1963).
16. Delaney, C.F., and Walton, A.J., Nature, 186, 625, (1960).
17. White, F.A., and Collins, T.L., Applied Spectroscopy, 8, 17, (1954).
18. Campbell, B.L. and Whittem, R.N., Jour. Sci. Instr., 38, 516, (1961).
19. Sugiura, T., Bull. Chem. Soc. Japan, 35, 1257 (1962)
20. Kendall, B.R.F., Proceedings of Ninth ASTM E-14 Meeting on Mass Spectrometry, Chicago, Ill. (1961), p.158.
21. Lichtman, D., Private communication.

Comparison of 21-103 Electrometer and Electron Multiplier Spectra

R. A. Meyer
North American Aviation Science Center

The recent availability of an Electron Multiplier conversion kit for the 21-103 Mass Spectrometer has opened many new fields of usage for an old and well proven instrument. The greatly increased sensitivity has permitted the use of very narrow beam defining slits with an attendant increase in resolution. Another feature, the very rapid response of the multiplier, has opened the rapid scan field so valuable in gas chromatographic work. In both of these usages it still is desirable to be able to apply the standard spectra library to the data gathered by the multiplier. A study of the multiplier generated spectra was indicated.

The CEC Multiplier kit has provision for interposing an electrometer collector by manipulation of an external magnet. Thus, provision was made for a direct comparison of the two collectors using the same ion beam. The normal magnet operating parameters for our laboratory are shown in Table 1. The timing schedule for this investigation is shown in Table 2. Due to the wide range of molecular weights and attendant scan duration, no effort was made to maintain a rigid time schedule but rather the times at the various indicated points were measured.

The leak rate for each individual run was calculated from the base peak heights at T_0, T_1, and T_4. The time from T_0 was calculated for each peak by combining the time at the start of the scan and the chart distance from scan start to the peak when converted to time units. These data permit calculation of each peak height to its height at T_0. A direct comparison of the electrometer and multiplier generated spectra was now possible. A list of some of the compounds run includes: Hydrogen, Deuterium, Argon, Methane, Acetone, Normal Butane, Carbon Dioxide, Toluene, Xylene, Cyclohexane, 1-Hexene, Perfluorocyclohexene, Perfluorotoluene, Hexadecane, Terphenyl. Where convenient, divergent compound types of similar molecular weight were chosen. Fig. 1 shows data from two normal butane runs. The ratio of multiplier peak height to electrometer peak height when both are calculated to zero time is plotted against m/e. As can be seen, a definite bias is impressed upon the spectra by the multiplier-Wein filter combination. The difference is most apparent in the 12 m/e area, but even in the 27 area the electrometer pattern coefficient is 41.5% and the multiplier shows 82%.

The normal location of the electrometer collector within the magnetic field made some kind of ion beam extraction technique mandatory. CEC chose to use a Wein filter for this purpose. (Private comment at the meeting indicated that a true "Wein filter" is much more complex than the CEC version. This statement has in no way been confirmed and is included only as comment.) Five sets of electrostatic deflection plates within the filter guide the beam to its termination on the conversion dinode or electrometer collector. The voltages for these plates are drawn from the accelerating voltage through a resistor network. Potentiometers are provided for locating the beam on the conversion dinode. The operating instructions call for presetting the voltages and subsequent optimization upon the electrometer collector using the 43 peak. The peak height under these conditions is quite insensitive to focus potentiometer position. When the multiplier was activated and the electrometer collector removed, the Wein filter was found to be almost completely defocused for multiplier operation. The Wein filter potentiometers were once more optimized. Upon returning to electrometer operation no peak height sensitivity change from the previous settings was found. The focus for the Fig. 1 runs was a month old, but we anticipated only a general lowering of sensitivity at worst. Low sensitivity for ions in the 200+ range led to an experimental refocusing of the Wein filter. Fig. 2 shows data for the average of several runs using the early focus (the solid line) as well as two made after refocusing the filter for the high mass range. The refocusing of the Wein filter resulted in a large sensitivity increase. A rerun of normal butane at the new focus setting showed that a large amount of the discrimination had been removed. For example, quoting 27 peak pattern coefficient, with the old setting the multiplier gave a 82% and the electrometer 41% while the new focus settings pattern coefficients were 42 and 40.

A study of the Wein filter focusing parameters was made. There are 4 potentiometers each controlling the voltage distribution between a pair of deflection plates. With the controls for plates 3, 4, and 5 to their center of rotation, it was possible to adjust the first (also connected to the second) plate potentiometer to cause the peak height to pass through a maximum.

Fig. 3 shows good reproducibility in plots of peak height variation as the focus potentiometer is adjusted. These data are for two independent runs on the 4

peak of deuterium at a magnet current of 0.062 amps. When the magnet current is raised to 0.344 amps where we scan the 24-100 range, the focus plots for several accelerating voltages fall upon one another (Fig. 4). Unfortunately, this is not the case for a magnet current of 0.684 amps (Fig. 5). There, focusing at high accelerating voltage would cause a significant attenuation by the time the accelerating voltage had decayed to 600 volts. Note that the low voltage required the larger amount of rotation. When the magnet current is 0.062 amps, Fig. 8, rotational requirements are reversed and the lower voltage requires less rotation of the pot. However, the discrimination problem is as severe at this magnet current as it is at the high current. A reasonable focus for the 2 peak could almost eliminate the 4 peak.

Argon, although run at 0.244 amps where agreement is normally good, showed an interesting pair of curves for the single and double ionized peaks, Fig. 6. This is not thought due to the previously mentioned discrimination problem but rather to the difference in ions since a run on normal butane at the same magnet current (Fig. 7) showed good coincidence of curves. This phenomena is merely noted in passing and could be of considerable academic interest.

The sizes of the deflection plates were calculated on the basis of a particular 103's field. There is, of course, no guarantee that the fringing fields of other instruments are identical or even similar. In fact, it is quite possible that the fringe effect would be changed by a slight alteration in anaylzer position within the gap. We wish tc emphasize that these results are from a single 21-103C, a single Wein filter and multiplier. We have no evidence that the problem is general, suggest no theoretical solution or empirical cure. The purpose of this report is to alert other mass spectroscopists to a potential problem.

One last short study is worthy of report. The power supply has a meter displaying the volts per stage applied to the multiplier. It was noted that when a large peak passed the collector, the volts/stage decreased as much as 10 volts. This could well have a serious effect on the gain of the multiplier. However, a plot of peak height vs. ionizing current, Fig. 9, proved to be linear despite the registered voltage decrease at high output currents. (CEC says this is not unexpected in view of our 5×10^5 ohm input resistor's current requirements.)

In conclusion, for our particular mass spectrometer, although there is the expected discrimination by the multiplier a potentially more serious source of spectra alteration lies in the "Wein" filter. We plan frequent attention to the focus and perhaps even a look at the focus characteristics for several peaks when maximum agreement with published electrometer spectra is necessary.

A purely qualitative investigation of the Wein filter problem by CEC just prior to submission of this paper indicates a possible effect of the deflection control located on the multiplier power supply. Data for the paper were obtained with the control set to approximately 60% of its travel. When it was set to zero, the focus of the Wein filter controls appeared much less critical.

Table 1
NORMAL M. S.
OPERATING PARAMETERS

m/e	magnet amps
1-4	.166
12-24	.244
24-105	.344
105 +	.685

Table 2
OPERATING SCHEDULE

T_0	Base Peak "E"
T_1	Scan "E"
T_2	Base Peak "E"
T_3	Scan "M"
T_4	Base Peak "E"
"E"	Electrometer
"M"	Multiplier

Fig. 1

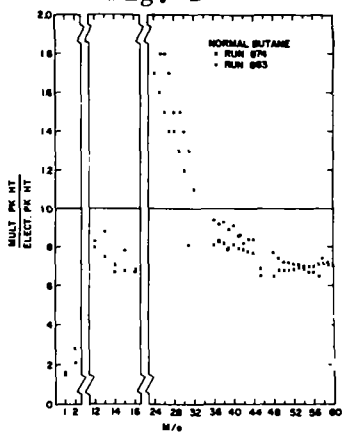

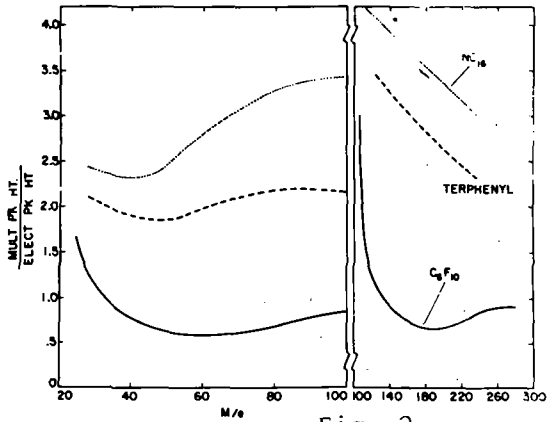

Fig. 2

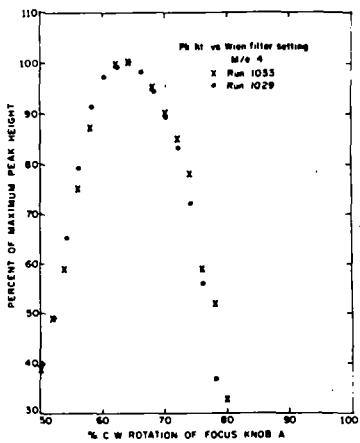

Fig. 3

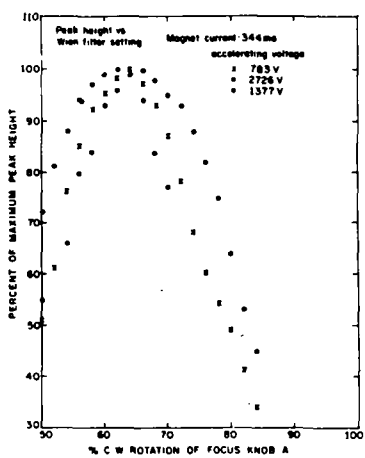

Fig. 4

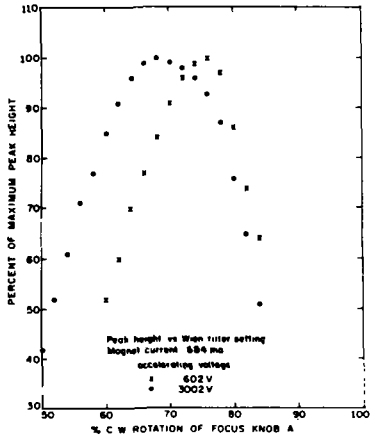

Fig. 5

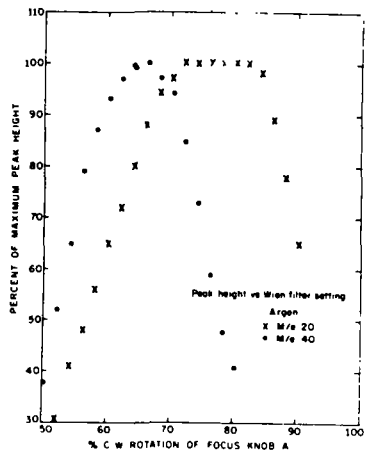

Fig. 6

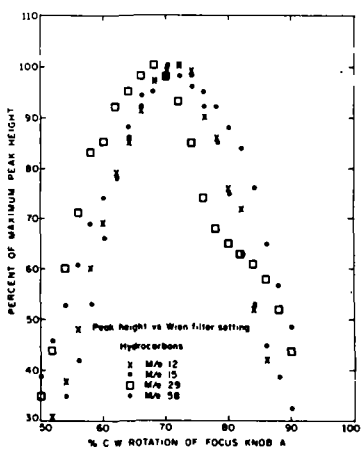

Fig. 7

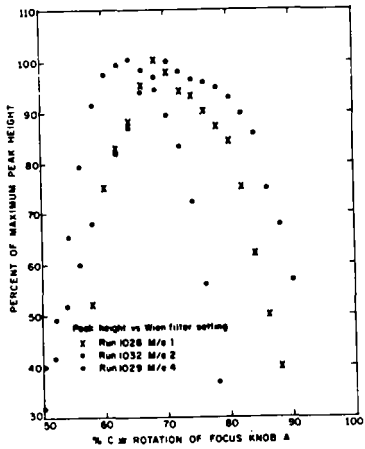
PERCENT OF MAXIMUM PEAK HEIGHT
% C ROTATION OF FOCUS KNOB A
Peak height vs Wien filter setting
Run 1028 M/e 1
Run 1032 M/e 2
Run 1029 M/e 4

Fig. 8

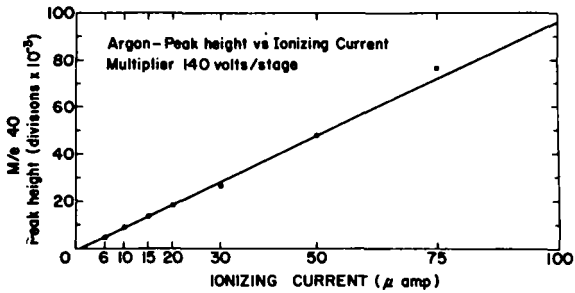
Argon – Peak height vs Ionizing Current
Multiplier 140 volts/stage
M/e 40
Peak height (divisions x 10⁻³)
IONIZING CURRENT (μ amp)

Fig. 9

ELECTRON MULTIPLIER DETECTORS IN MASS SPECTROMETRY

by

Heinz G. Boettger - CEC, Pasadena, California

Recent advances in the field of mass spectrometry and particularly of organic compounds require increasingly higher resolution and faster speed of response at high sensitivity. As a result more and more instruments are being equipped with electron multipliers. The basic advantages of these detectors are well known and have been reported in the literature. It is general knowledge that gains in the order of 10^7 are possible over conventional electrometers and that increases in speed of response of at least a factor of 10^3 can be achieved readily. (See Beynon: Mass Spectrometry, p. 206.) Considerably less has been published about a number of questions which are of importance for the analytical chemist, questions such as:

(1) What is the maximum useful gain that can be achieved in an operating mass spectrometer with multiplier detection? Where will it be limited by electrical noise and instrument background?

(2) How much mass discrimination due to the electron multiplier is there?

(3) How much, if any, "chemical" discrimination is there? "Chemical" discrimination being defined as variation in response due to different composition of ions of the same mass to charge ratio.

(4) What are the effects of fringing magnetic fields?

(5) What effects do large amounts of inert gases and monatomic gases have upon the multiplier, since one of the areas of application is monitoring of gas chromatographic effluents where large amounts of He, Argon, Nitrogen or Hydrogen have to be admitted into the mass spectrometer.

The purpose of this investigation was to find some answers to these questions and determine the limitations which had to be imposed upon the performance specifications of the CEC Type 21-103C and 21-110B Mass Spectrometers when used in conjunction with an electron multiplier.

EXPERIMENTAL

The experimental work was carried out on two instruments. A 21-103C was fitted with a commercial Wien Filter-Electron Multiplier Kit of our own design as shown in Figure 1. Since we were interested in high resolution and high speed scanning, the following changes were made:

(1) The standard Isatron was replaced by narrow slit Isatrons having 0.002" and 0.001" source slits respectively.

(2) The Wien-filter was fitted with 0.0025" and 0.0015" slits.

(3) The low sensitivity input resistor of the standard D.C. amplifier was changed from $5.10^9\,\Omega$ to $.10^7\,\Omega$.

(4) An alternate high speed amplifier of 1,000 cycle response was designed and installed in parallel for high speed G.C. monitoring during the last part of the investigation.

(5) A 5-124 Direct-Writing oscillograph was used in place of the standard oscillograph for all high speed work.

(6) The scan circuit was changed to allow rates as fast as 0.5 sec/octave.

The double focussing instrument, which was used in some parts of the investigation was a standard Type 21-110B mass spectrometer of the Mattauch-Herzog configuration.

Resolution of the 21-103C was demonstrated with the $CO/N_2/C_2H_4$ triplet (1/1120) at m/e = 28, the C_3H_4/A (1/682) doublet at m/e = 40, and C_3H_8/CO_2 (1/605) doublet at m/e = 44. Resolution at high masses was shown with PFK at m/e = 700. Beam width and sensitivity measurements were made with normal-butane at m/e = 43 and 58.

Mass and chemical discrimination was checked with a large variety of compounds over the mass range from 12 to approximately 700 (21-103C) and 1,000 (21-110B) respectively. These compounds included halocarbons, aromatic and aliphatic hydrocarbons, Amines, Nitriles, Esters, Ethers, Pyridines , Ketones and Alcohols. Spectra were taken with the electrometer detector and the multiplier and patterns were calculated as % of ΣH. In order to eliminate discriminatory effects outside the multiplier, all instrument variables, such as source pressure, ionizing current, isatron and Wien Filter controls, etc., were held constant.

RESULTS

At the beginning of the investigation it was hoped that the resolving power of the 21-103C could be increased to at least 1/1120, resolve $N_2^+/C_2H_4^+$ at m/e = 28 without loss of sensitivity relative to normal "narrow slit" operation. Also we desired to achieve this at less than maximum multiplier gain. We found early that we were not limited by electrical noise. Even at system gains of 10^6, electrical noise, in absence of an ion beam, was not visible. However, the useful gain of the system is limited by instrument background. In a reasonably clean system, which shows no background at maximum electrometer sensitivity there will be an off-scale xl peak at almost every mass at a gain of 10^6. Thus we had to limit the system gain to 1,000-10,000 by reducing the input resistor to 10^7 or $10^8\Omega$. For most of the work reported here a $1.10^7\Omega$ input resistor was used. At this level the instrument background of a reasonably clean vacuum system is negligible. Higher useful gains may be possible with an extremely clean, "dry-vacuum" system.

Another advantage is gained by reducing the input resistors to the $10^7\Omega$ level. The speed of response of the standard amplifier system is increased significantly.

Figure 2 shows the average gain for the major peaks of n-butane and perfluoro-cyclobutane which was obtained consistently with several production type multipliers.

The increase in sensitivity, which was achieved through the use of the multiplier, permitted us to increase the resolution of the 21-103C from a previous maximum of 1/400 to 1/700 with 0.002" and 0.0025" source and collector slits and to 1/1300 with 0.001" and 0.0015" slits. Under these conditions the A/C_3H_4 doublet at m/e = 40 and the N_2/C_2H_4 doublet at m/e = 28 were completely resolved. Figure 3 shows the doublet at m/e = 28. With a resolution of 1/1200 the butane sensitivity of the instrument was slightly better than normal narrow slit operation. Figure 4 shows the sensitivities which were obtained in the various modes of operation using 1 and 1.5 mil slits. Approximately twice the above values are obtained using 2 and 2.5 mil slits at 60% valleys for m/e = 28 doublet

Figure 5 shows the mass discrimination that was found in the multiplier. As expected there is a small amount of discrimination with increasing mass to charge ratio. The experimental values follow closely the predicted curve where discrimination is proportional to the square root of Δm. Thus the effect is within tolerable limits and does not interfere with the analytical function of the instrument. Furthermore, it was found that chemical discrimination was not detectable under the conditions of our experiment. This means that discrimination of the multiplier is a function of mass, but not a function of ion composition. Therefore it is possible to mathematically correct the mass spectral pattern either automatically or manually where this is desired in order to utilize existing reference spectra.

Figure 6 shows the results of the effects of changes of the magnetic field upon the Wien filter-multiplier combination in the 21-103C. As can be seen in all cases the sensitivity is a function of the magnetic field. With no shielding the sensitivity of the multiplier reaches a fairly sharp peak at about 240 m-Amp ($\sim$ 2,000 Gauss). As external magnetic shielding is increased the maximum moves towards lower magnetic fields and, at the same time, the curve flattens out. Again this effect is of little analytical significance, since scans are made at constant magnetic field. In case of the 21-110B no fringing magnetic field effects were found, because the multiplier is far enough removed from the field boundaries.

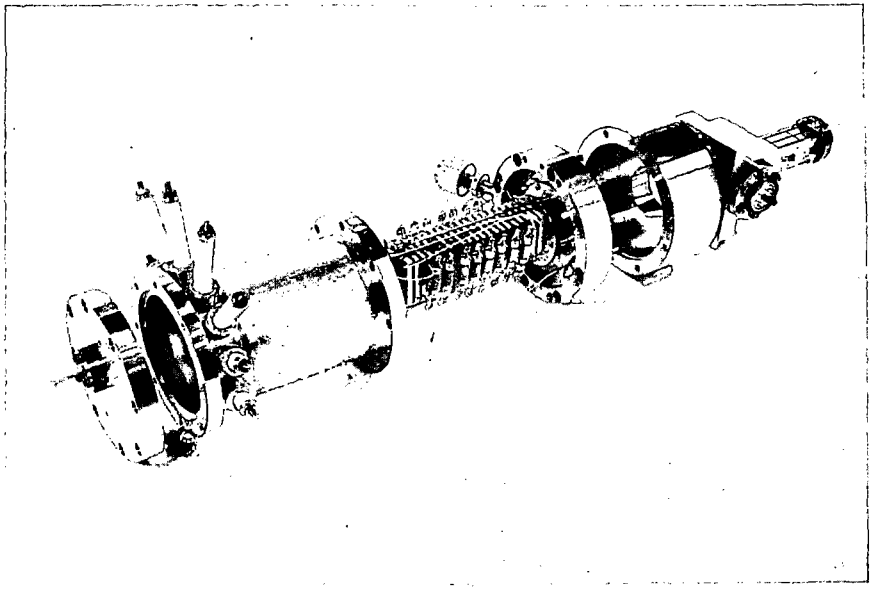

Figure 1

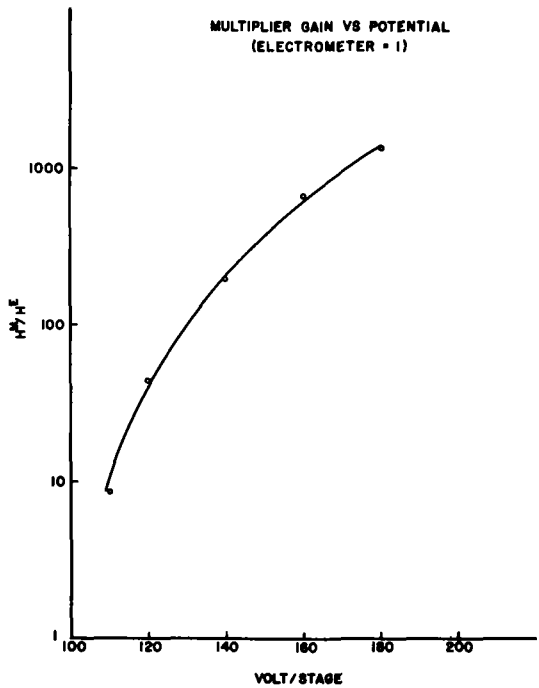

Figure 2

In both instruments the electron multiplier was exposed to large over-pressures of helium and nitrogen for long periods of time during the analysis of G.C. effluents. At times pressures at the exhaust vacuum gauges reached 5.10^{-5} mm Hg, but no ill effects were observed. Thus, the multiplier proved suitable for G.C. monitoring applications. Figure 7 shows the effect of peak and valley clipping when the multiplier was used with the standard amplifier. At a resolution of 1/1100 and a scan rate of 17 sec/octave peak and valley clipping amounts to approximately 30% of the original peak height. At 10 sec/octave this value rises to about 50%. It might be added here that peak broadening due to the over-pressure is included in these values. However, its contribution is negligible at pressures which are commonly employed.

Despite the fact that useful spectra can be obtained under these conditions, a new high speed amplifier was designed and installed. This amplifier is capable of driving five 1,000 cps galvanometers and has a linear response in excess of 1,000 cycles. It now enables us to scan at a maximum rate of 0.5 sec/octave, and 1/1000 resolution without peak and valley clipping.

In conclusion it can be said that a properly designed multiplier detector greatly widens the range of applications of a mass spectrometer without sacrifice in normal performance. As demonstrated on the 21-103C the use of the multiplier has allowed us to triple resolution and raise the scan rate by more than 2 orders of magnitude without loss of sensitivity. Alternately, at normal resolution we were able to raise the sensitivity by at least a factor of a thousand while still scanning at high speeds ten to a hundred times faster than normal.

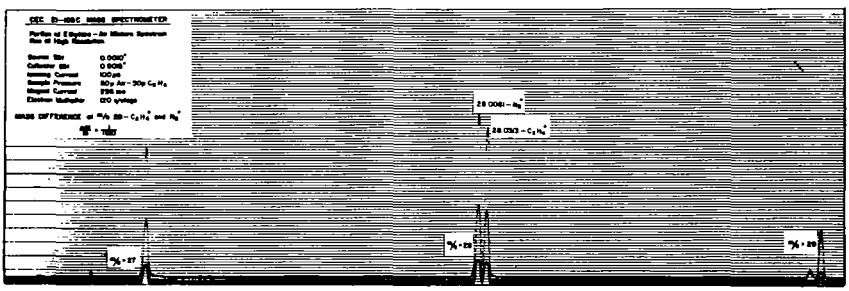

Figure 3

MODE OF OPERATION	b (mil)	m (m/e)	S (Div/u/10uAmp)
"FOCUSSED ELECTROMETER	14.6	310	0.077
"NON-FOCUSSED" ELECTROMETER	5.3	735	0.804
"FOCUSSED" MULTIPLIER (110 VOLT/STAGE)	8.8	500	6.08
"NON-FOCUSSED" MULTIPLIER (110 VOLT/STAGE)	2.8	1160	0.624
"NON-FOCUSSED" MULTIPLIER (180 VOLT/STAGE)	-	-	100 (Extrapol)
"FOCUSSED" MULTIPLIER (180 VOLT/STAGE)	-	-	900 (Extrapol)

Figure 4

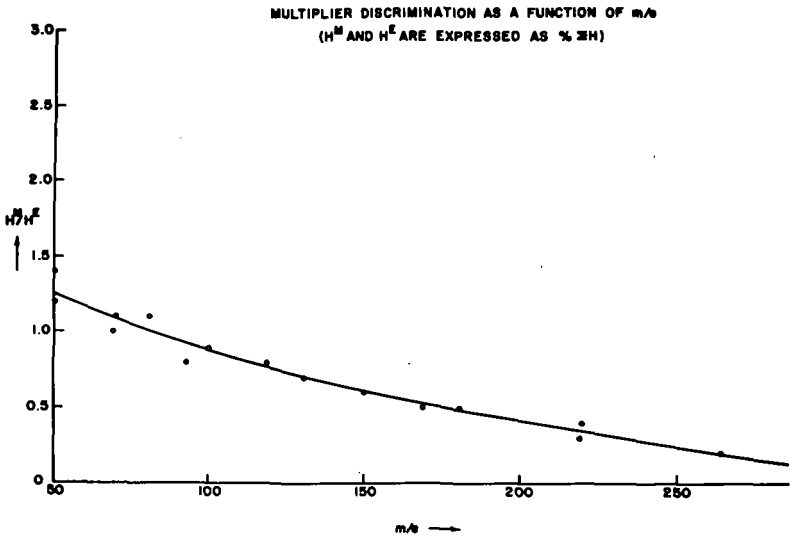

Figure 5

MAGNET CURRENT (Milli-Amp)	PEAK HEIGHT (cm)					
	No Shield	0.015" Shield		0.065" Shield	0.125" Shield	
200	440	510	520	234	204	204
220	630	600	610	-	-	-
240	680	660	610	237	204	192
260	620	670	525	-	-	-
280	560	640	530	204	174	156
300	470	600	490	-	-	-
320	380	550	440	168	168	168
340	300	490	380	-	-	-
360	-	-	-	136	157	143
400	213	-	310	89	124	120

Figure 6

SCAN RATE (Sec/Oct)	PEAK HEIGHT, H (cm)	VALLEY (cm)	VALLEY (% of H)
500	34.8	1.0	2.9
250	33.3	1.5	4.5
170	24.0	1.6	6.7
85	22.5	2.1	9.3
17	22.2	8.5	38.5

Figure 7

SIMPLE DATA DISPLAY SYSTEM FOR FAST-SCANNING MASS SPECTROMETER

D.G.H. Marsden*, W. Forst, K.K. Feng, Department of Chemistry, Université Laval, Québec, Canada, and K. Park, C.A.R.D.E., P.O.Box 1427, Québec, Canada.

Abstract

A very simple display device is described that makes use of two independent time bases provided by some types of oscilloscopes. The device consists essentially of a diode gate driven from the oscilloscope by means of some rather simple associated circuitry. The ion beam signal is chopped, or sampled, peak after peak, smoothed by an RC filter and displayed by means of a pen recorder, a recording galvanometer or another oscilloscope. Most of the statistical fluctuation in peak height is thus eliminated.

INTRODUCTION

The fast-scanning mass spectrometer developed at Laval University for the study of fast reactions[1,2,3] operates in conjunction with an oscilloscope, as indicated schematically in Fig. 1. The oscilloscope time base (Time Base B in Fig. 1) provides by means of its gate an impulse that triggers the scanning pulse, i.e. a hyperbolic decrease in voltage with time. As a result, ions of a certain mass range are scanned, depending on the setting of the analyser magnet. Ions are collected in an ion-electron multiplier and the signal is fed via a cathode follower to the vertical amplifier of an oscilloscope. Associated with gate B is a sweep (Sweep B) so that ions arriving at the collector are displayed as peaks on the oscilloscope screen.

Owing to the statistics of multiplication and the relatively small number of ions collected per scan, the peak heights are subject to a certain amount of statistical variation. The present display device was developed to reduce this statistical fluctuation in peak heights in cases where the half-life of the reaction studied was such that the maximum speed of the machine (500 scans/sec) was not needed. While this device offers little that is new as far as electronics is concerned, it has the virtue of being exceedingly simple, and consequently also cheap. Two similar devices described earlier[4,5] are much more complicated.

PRINCIPLE OF OPERATION

The display device requires an oscilloscope having two independent time bases (Tektronix 545A, for example). One time base (for example Time Base B in Fig. 1) operates in exactly the same way as in the absence of the display device. The other time base (Time Base A in Fig. 1) operates in association with Time Base B, a setting that on the Tektronix oscilloscope is called "B intensified by A", for reasons that will be apparent shortly. This time base has its own sweep (Sweep A) and gate (Gate A). The "length" or duration of sweep A can be set independently of sweep B ; in addition, sweep A can be made to start simultaneously with sweep B, or to run behind sweep B, i.e. start some interval of time after sweep B, the interval being variable. On the Tektronix oscilloscope the part of the displayed signal (or of the base line if there is no signal) where sweep B is coincident with sweep A appears as an intensified trace, which provides a quick visual check on the relative seetings of the two sweeps. If the signal displayed by sweep B consists of five peaks, as in the upper illustration in Fig.1, and if the relation of the two sweeps is as shown, the second peak from left will appear "brighter" or intensified.

Now sweep A has associated with it a gate (Gate A) that drives a transistorised Schmitt trigger, thus providing push-pull voltages necessary to turn on and off a diode gate (Fig. 1). This diode gate is normally closed, i.e. it opens only when gate A provides a pulse, so that it is, in effect, synchronised with sweep A. As a result, the diode gate passes only the part of the signal that corresponds to the intensified portion of the signal seen on the oscilloscope screen. Note that this screen is no longer the main recording device ; it acts merely as a monitoring device. If conditions are as

* Present address : Department of Aerospace and Mechanical Sciences, Princeton University, Princeton, N.J.

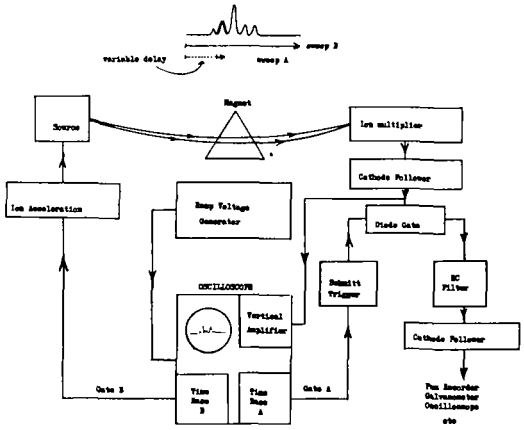

Fig. 1 - Schematic diagram of mass spectrometer and associated circuits.

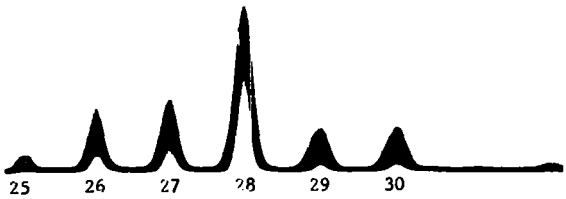

Fig. 2 - Group of ethane peaks in the mass 30 region taken without the averaging device. The photograph shows 500 superimposed spectra.

schematically indicated in the upper illustration in Fig. 1, the diode gate will pass only the second peak from left. Any variations in the height of this peak are smoothed in an RC filter and the smoothed signal is then fed via a cathode follower to a recording device. Thus the data display system is in effect an averaging or "integrating" device.

If the peaks seen on the oscilloscope screen are evenly spaced, and if Time Base A is adjusted so that the intensified portion of the displayed signal is visually no more than the width of a single peak, then by varying the delay time each peak in turn can be intensified, i.e. allowed to pass through the diode gate. In this way the ion beam signal is chopped, or sampled, peak by peak, and the recording device (a conventional strip-chart recorder, for instance) will write out the smoothed signal, peak by peak, at a speed equal to the speed at which the intensified trace moves across the oscilloscope screen, i.e. in unison with the sampling scan.

A ramp voltage generator (Fig. 1) using a neon lamp boot-strap circuit[6] has been built to replace, or rather by-pass, the Helipot used on the Tektronix oscilloscope to vary the delay time. By varying the time constant of this generator, delay time can be increased linearly from zero at a rate varying from one sampling scan in a fraction of a second to one sampling scan in a minute. The sampling scan can be made repetitive, and adjustments are also provided to confine the sampling scan to any desired portion of the mass spectrum as seen on the oscilloscope screen.

RESULTS

The appearance on the main oscilloscope screen of a typical spectrum without the use of the averaging device is shown in Fig. 2. It shows a group of ethane peaks in the mass 30 region (highest peak is at mass 28 ; there is one mass-number difference between peaks). This is a high-contrast print made from a Polaroid photograph. Exposure time 1 sec, 500 sweeps/sec, so that the photograph shows 500 superimposed spectra. The tip of each peak dissolves in a more or less vague halo that is not very well rendered in the print but which is nevertheless indicative of the uncertainty in peak height. Fig. 3 shows the ethane spectrum with the use of the averaging device, as photographed from the screen of a second oscilloscope. Here the mass range scanned is larger, the small peaks to the left being in the 15 region. Mass spectrometer speed is 500 sweeps/sec, exposure time 3 sec, sampling speed one scan in three seconds, which equals roughly to a sampling scan of 0.1 sec/mass unit, so that each peak is an average of something like 50 sweeps. The tip of each peak is seen to be very well defined. This is a rather sensitive test, since in a strip-chart recorder any residual fluctuation in peak height would tend to be smoothed out by the inertia of the pen and balancing motor. Fig. 4 shows nine successive sampling scans of the group of ethane peaks in the mass 30 region as recorded by an ultraviolet galvanometer. The negative peak at the end of each scan is a kick of the galvanometer associated with the ramp voltage generator returning to starting position. The time scale is one second between negative peaks, mass spectrometer speed 500 sweeps/sec, so that each peak is an average of slightly under 100 sweeps. The lack of any appreciable peak height variation over a period of about 10 sec (~ 5000 sweeps) is here clearly demonstrated.

The data display system described here thus offers great flexibility that permits recording the mass spectrum at any desired rate consistent with the time scale of the reaction studied. At the same time, the quantitative significance of the results is greatly improved when the mass spectrum is recorded at a rate that permits averaging several individual sweeps when the machine is running at its maximum sweep rate.

ACKNOWLEDGEMENT

The authors are indebted to the National Research Council of Canada for financial assistance. K.K. Feng is grateful to Université Laval for the award of a postdoctoral fellowship.

References

(1) E.G. Léger, Can. J. Phys., 33, 74 (1955).
(2) L.P. Blanchard, J.B. Farmer and C. Ouellet, Can. J. Chem., 35, 115 (1957).
(3) D.G.H. Marsden, Rev. Sci. Instr., 33, 388 (1962).
(4) B.R.F. Kendall, J. Sc. Instr., 39, 267 (1962).
(5) B.R.F. Kendall, paper presented at the 10th Annual Meeting on Mass Spectrometry of ASTM Committee E-14, New Orleans, La. (1962).
(6) R.E. Miller and W.R. Kincheloe, Jr., Tech. Rept. 10, Electronic Res. Lab., Stanford Univ. (1952).

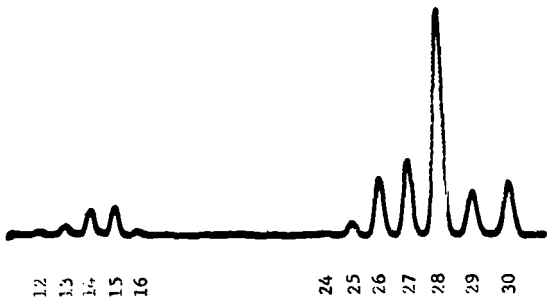

Fig. 3 - Ethane spectrum taken with the averaging device. Machine speed 500 sweeps/sed, one sampling scan in 3 sec.

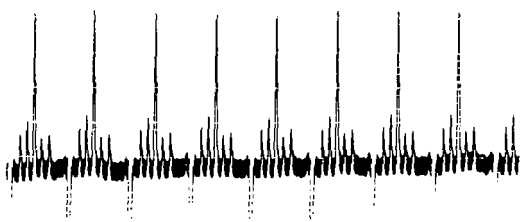

Fig. 4 - Averaging device used to obtain successive sampling scans of the five largest ethane peaks in the mass 30 region. Machine speed 500 sweeps/sec, one second per sampling scan.

ON THE PRODUCTION OF POSITIVE IONS FROM SOLIDS*

by

Richard E. Honig

RCA Laboratories

Princeton, N. J.

ABSTRACT

This paper reviews the major methods used to produce ions from inorganic solids. It describes in detail several vacuum discharge methods which combine adequate performance with good, reasonably uniform detection sensitivity suitable for mass spectrometric analyses.

INTRODUCTION

To study and analyze solids in a mass spectrometer, the sample material must be vaporized and ionized, preferably in such a way that the ionized vapor composition represents accurately that of the solid. Some of the methods used today were described already in early papers by Dempster(1), others have been developed more recently. This review will describe briefly all major methods used to produce positive ions from solids, and present in detail the functioning of the various vacuum discharge sources. The discussion applies primarily to INORGANIC solids in elemental or compound form, which often contain impurities at a low level of concentration.

To survey the different types of ion sources, it is useful to classify them according to the method employed, but it should be realized that systematizing is always a subjective matter. Table I shows the five major methods used today for the production of ions from solids, and quotes for each source order-of-magnitude values of three important characteristics:

1) the width ΔV, in volts, of the ion energy distribution;
2) the distribution among major charged species; and
3) relative elemental sensitivities, expressed in terms of "selectivity".

The magnitude of ΔV determines what type of instrument is required for mass analysis. For $\Delta V < 10$ V, a simple magnetic filter is adequate, while $\Delta V > 10$ V necessitates the use of a double-focusing machine. The relative concentrations of singly-and multiply-charged species shown in the charge distribution columns indicate the character of the mass spectrum. For maximum simplicity and minimum interference, a spectrum consisting solely of singly-charged species would be preferable, but this is obtained only in conjunction with an undesirably strong selectivity. The last column marked "selectivity" makes a qualitative statement about relative sensitivities which, even in the cases marked "W", can vary by a factor of three. Table I does not include either the "exploding wire" technique, which is limited to a single shot and therefore not very practical, or to the field emission source which applies to adsorbed gases. In the following, the various methods listed in Table I will be discussed in detail.

A. DIRECT HEATING

Since the two methods to be discussed under this heading produce ions with thermal energy spreads of less than 0.3 eV, a simple magnetic filter is adequate for mass analysis.

a Thermal Ions

The method of thermal ionization has been the subject of several recent reviews, e. g. by Wilson and Daly(2), and by Webster(3), and will therefore be

* The research reported in this paper was sponsored, in part, by the Air Force Cambridge Research Laboratories, Office of Aerospace Research, under Contract No. AF19(628)-446.

TABLE I
SURVEY OF ION SOURCES

METHOD	ΔV (VOLTS)	CHARGE DISTRIBUTION			SELECTIVITY*
		+	2+	3+	
(A) DIRECT HEATING					
a) Thermal Ions	10^{-1}	S	–	–	S
b) Neutral Vapor Ionized by Electron Impact	10^{-1}	S	W	–	W
(B) ELECTRON BOMBARDMENT	10^{2}	S	M	W	W
(C) FOCUSED RADIATION					
1) Arc Image Furnace					
2) Laser Source					
a) Thermal Ions	10^{0}	S	–	–	M
b) Neutral Vapor Ionized in Arc	10^{2}	S	S	M	W
(D) ION BOMBARDMENT					
a) Secondary Ions	10^{1}	S	–	–	M
b) Neutral Vapor Ionized by Electron Impact	10^{0}	S	W	–	W
(E) VACUUM DISCHARGES					
1) RF Spark	10^{3}	S	M	W	W
2) Vibrating Arc	10^{2}	S	S	M	W
3) Pulsed dc Arc	10^{2}	S	S	M	W

S – Strong
M – Medium
W – Weak

TABLE II
ELECTRICAL BREAKDOWN IN HIGH VACUUM: METHODS

A. CHARGE TRANSFER (Electrometer, Oscilloscope)
1) With/without magnetic field B: I^{+}, I_G (Pivovar and Gordienko)
2) Electron field emission
   a) Fowler-Nordheim plot: log I vs. $1/V_o$
   b) X-ray emission from A (Goldman)
   c) Anode fluorescence } (DeGeeter)
   d) Anode incandescence }
3) Small particles (Rozanova)

B. MATERIAL TRANSFER
1) Radioactivity, e.g. Cu^{64} (Tarasova and Razin)
2) Emission spectroscopy (Schwabe)
3) Mass spectrometry (RCA)

C. INSPECTION OF ELECTRODES
1) Microscope } (Little and Whitney)
2) Electron microscope }

discussed only briefly. The basic process was thoroughly investigated about 40 years ago and has been described by the Langmuir-Saha Equation(4). The relative intensities for positive ions and neutrals are given by

$$I^+/I^o = \exp\,(e(W - IP)/kT) = \exp\,(11606(W-IP)/T) \qquad (1)$$

and for negative ions and neutrals by the equivalent expression

$$I^-/I^o = \exp\,(e(EA - W)/kT) = \exp\,(11606(EA - W)/T) \qquad (2)$$

where

I^+ = number of positive ions
I^o = number of neutrals
I^- = number of negative ions
e = electronic charge, = 1.6021×10^{-19} coulomb
W = work function of surface, in electron-volts (eV)
IP = ionization potential, in eV
EA = electron affinity, in eV
k = the Boltzmann constant = 1.3804×10^{-23} joule/°
T = temperature of hot surface, in °K.

It is clear from Eqs. (1) and (2) that elements with a low ionization potential will be emitted largely as positive ions, while for elements with high electron affinity the production of negative ions is very efficient. For the case that IP > W, or EA < W, it is evidently advantageous to operate at the highest temperature possible, in order to enhance the emission, respectively, of positive ions or negative ions. This consideration led to the development of the multiple-filament source(5) in which one filament is heated to a temperature suitable to vaporize the material under study, while a second, much hotter, filament is employed to ionize the particles emitted by the first. To avoid excessive vaporization of the ionizing filament, its temperature should be kept below 2800°K. More recently, a thermal ion source was developed by Voshage and Hintenberger(6), which combines the advantage of the multiple-filament system with the efficiency of a double furnace that is completely enclosed except for the exit slit. The charge of material to be studied is vaporized at one end, at an appropriate temperature produced by external electron bombardment, and diffuses to the other end where it ionizes at a surface kept at a very high temperature.

Positive ions can be obtained by this method from all elements with ionization potentials below 9 eV, i,e. about two thirds of the periodic table. Similarly, negative ions are formed from all elements with an electron affinity > 1 eV. All species formed are singly-charged. Since individual ion currents depend exponentially on ionization potential (or electron affinity), sensitivity variations of many orders of magnitude are observed, resulting in strong selectivity.

b Neutral Vapor Ionized by Electron Impact

This well-known method, generally used in gas analysis, can be applied to solids by the addition of a crucible which is heated electrically to temperatures such that the concentration of neutrals vaporized in the ionization region produces measurable ion currents. If it is desired to maximize this concentration(7), and thereby the detection sensitivity, a source geometry such as shown in Fig. 1 is chosen, but two other orientations are possible. Hickam(8) analyzed Cu samples for Ag impurities with this method, while this author(9) studied semiconductors with the source shown in Fig. 1. To perform meaningful analyses with this system, the sample must be completely vaporized and ion currents integrated over time, in order to eliminate the effects of vapor pressure differences. Furthermore, the choice of crucible material is of great importance, so as to minimize reactions between sample and crucible. Impurities on the parts per million level are readily determined with this system. For studies in high temperature chemistry, the crucible is replaced by a Knudsen cell(10), allowing equilibrium to be established between solid and vapor.

B. ELECTRON BOMBARDMENT

In recent years, techniques have been developed to vaporize refractory solids by electron bombardment. With its supporting end water-cooled, the sample serves as its own crucible, which avoids the undesirable side reactions encountered with direct heating, as mentioned above. It seems logical to use the same bombarding electron beam to ionize the vaporized species, and draw out axially the ions formed. A suggested geometry is shown in Fig. 2: electrons from an annular

TABLE III

CHARGE DISTRIBUTION FOR IONS FROM $SnNb_3$

SYSTEM	PULSE LENGTH τ (μsec)	GAP CURRENT I_G (amp)	Sn			Nb		
			+	2+	3+	+	2+	3+
RF Spark	25-200	~ 0.1	1.0	0.3	0.05	1.0	0.3	0.05
Simple Trigger	~ 1	4	1.0	0.4		1.0	0.4	0.07
	~ 4	30	1.0	1.5	0.5	1.0	1.5	0.7
Triggered L.V. Discharge	20-100	30	1.0	1.5	0.3	1.0	1.5	0.6
Vibrating Arc	20	30	1.0	1.3	0.5	1.0	1.4	0.7

TABLE IV

DISSIMILAR ELECTRODE STUDIES

ANODE: Ni; CATHODE: Cu

SYSTEM	PULSE LENGTH τ (μsec)	SERIES RESISTANCE R_S (ohm)	GAP CURRENT I_G (amp)	RATIOS		
				Ni^+/Cu^+	Ni^{2+}/Ni^+	Cu^{2+}/Cu^+
Simple Trigger	~ 4	20,000	0.1 (est.)	6	0.1	
		0	30	0.2		0.4
Triggered L.V. Discharge	20-100	200	4	0.3	0.4	0.8
		0	30	0.2	0.9	1.1

TABLE V

COMPARISON OF SOURCE PERFORMANCE: TRIGGERED LOW-VOLTAGE VS. R. F.

PARAMETER	TRIGGERED LOW VOLTAGE		R. F.
	TRIGGER	T.L.V.	
MONITOR CURRENT			
STABILITY	ACCEPTABLE	ACCEPTABLE	POOR
MAX. VALUE, AVE.	10^{-9}	10^{-8}	10^{-9}
MAX. VALUE, PULSE	10^{-8}	10^{-7}	10^{-8}
MINIMUM TIME FOR 10^{-6} COUL. EXPOSURE (MIN.)	60	6	30
SHORTEST EXPOSURE (COUL.)	$< 10^{-14}$	10^{-12}	$3 \cdot 10^{-14}$
SHORTEST EXPOSURE (IONS)	$< 6 \cdot 10^4$	$6 \cdot 10^6$	$2 \cdot 10^5$
EN. DISTR.: 10% WIDTH (KV)	0.6	0.2	1 – 2.5
USEABLE FRACTION OF EN. BAND	1	1	0.2 – 0.5
RATIO ATOMS/ION	10^7	10^7	$5 \cdot 10^7$
GAP CURRENT (AMP)	10	10	(0.1)

filament are accelerated toward the free end of the solid sample, attaining energies of about 1000 V. An electrode placed between filament and sample serves to shield optically the latter from material vaporizing from the filament. The neutral species coming from the sample are, in part, ionized by electrons from the bombarding beam and drawn out axially into the mass analyzer. Depending on where they were formed, the ions will have initial energies that range over the full electron accelerating potential. Thus a double-focusing instrument is required for mass analysis. This system appears to have the advantage of simplicity, since the same electron beam efficiently performs the two functions of vaporization and ionization, yet, to the best of the author's knowledge, has yet to be tried.

C. FOCUSED RADIATION

The heating of solids by focused radiation from an arc-image furnace to temperatures near 4000°K is a well-established technique which, however, has been applied to mass spectrometric problems only recently. To go beyond 4000°K would be of special interest not only for high temperature chemistry studies, but also for the production of thermal ions from elements with relatively high ionization potentials.

1) Arc-image Furnace

The design of an arc-image furnace to be used in conjunction with a 60° mass spectrometer was discussed by Goldfinger(11) several years ago, but no published results have come to the writer's attention. Due to the rapid vaporization rate, it was expected that the sample would remain in focus only for short periods of time, and that it might be difficult to pump adequately the gases released.

Recently, Burns and collaborators(12) have reported on the vaporization of Al_2O_3 and of graphite, utilizing an arc-image furnace to heat the samples to intermediate temperatures. Due to the moderate vaporization rates used, neither gas pressure nor focusing on the sample surface seemed to present any problems. The upper temperature limit attainable by this method appears to be about 3600°K.

2) Laser Source

The nearly parallel light beam obtainable from pulsed lasers can readily be focused onto very small areas, yielding very high radiation densities and producing extremely high surface temperatures. In this fashion, well-defined microvolumes, ranging from 20 to 100 μ in diameter and up to 1000 μ deep have been vaporized from metals, semiconductors, and even sintered insulators(13,14) with an energy input of about one joule. Concurrent with the vaporization of neutral particles, there are observed large pulses of thermal electrons (up to 10 A, 100 μsec long) and of thermal ions (about 100 mA, 100 μsec long). These pulses are found to be made up of individual spikes, 0.1 to 1 μsec wide which coalesce into a single pulse if the energy density is sufficiently great. The energy distribution of the emitted electrons indicates surface temperatures of about 10,000°K for metals, and 6000°K for semiconductors.

Fig. 3 shows in diagrammatic form how a laser source was incorporated into a double-focusing mass spectrograph (AEI Type "MS7"). The nearly parallel laser beam entering through window W is focused internally by lens L onto target T. To optimize focusing and target location in the source, both L and T can be positioned independently with vacuum manipulators. The shield SH prevents the ions formed from being drained off to the vacuum housing which is at ground potential. Preliminary focusing adjustments are made with the help of a light beam on ground glass backing plate G, while target T is removed. After each laser pulse, the target can be moved sideways (normal to the paper plane) if a fresh surface is desired. The positive ions produced are accelerated into the double-focusing mass spectrograph, selected according to energy, mass-analyzed, and recorded on a photographic plate, which is the ideal detector for a short, single pulse. Each material is investigated in two ways:

a) With an ion-accelerating potential applied between T and S_1, particles emitted from the target as <u>thermal ions</u> are detected. Singly charged thermal ions are found for all cases, while multiply charged species are not detected. For different elements, relative intensities appear to depend on the work function of the surface and on the ionization potential of the species in question, as predicted by the Langmuir-Saha formula. So far, the photographic plate has recorded up to 10^8 ions produced from a single laser pulse.

b) With an electron-accelerating potential applied between T and S_1, a low-voltage arc discharge of the type to be discussed in Section E is produced in the source, yielding large ion currents by electron impact ionization of <u>vaporized neutrals</u>. The ion spectra obtained in this fashion include considerable

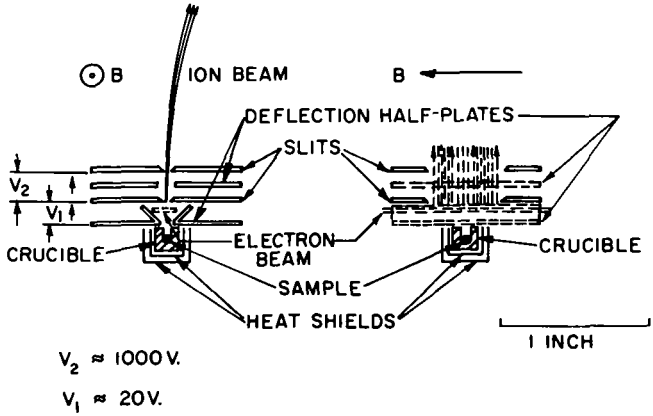

Fig. 1 ION SOURCE GEOMETRY

ELECTRON BOMBARDMENT SOURCE

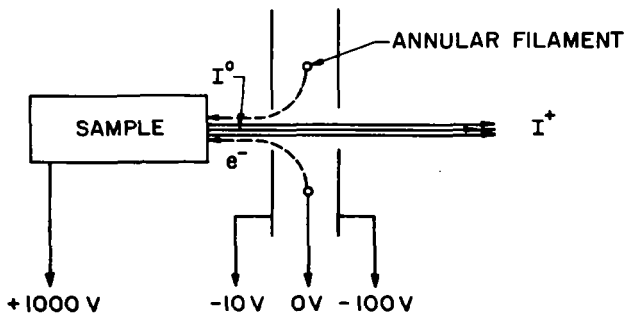

$$I^o + e^- \longrightarrow I^+ + 2e^-$$

Fig. 2

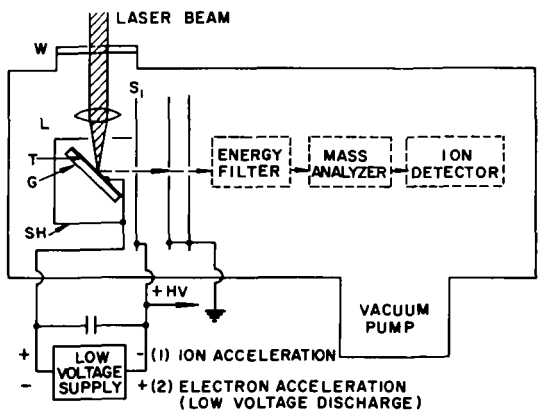

GEOMETRY AND SCHEMATIC DIAGRAM FOR MODIFIED ION SOURCE OF MS7 MASS SPECTROGRAPH

Fig. 3

concentrations of singly-and multiply-charged species typical of the target, and also species representing background gases. The considerable energy spread of these ions (about 100 eV) requires the use of a double-focusing machine. Approximately 10^{10} ions per laser pulse have been observed, corresponding to a maximum ion current of about 10^{-5} A. For currents of such magnitude, space-charge effects become serious in the focused regions, in particular on the photographic plate. Inspection of these spectra shows indeed severe space-charge broadening of the major lines, whereas the weaker lines are not affected. To make quantitative measurements, it therefore will be necessary to integrate over the line area. With the ion beam intensities obtained to date, it is possible to detect impurities down to a level of several parts per million.

Very recently, a study has been published(15) in which the neutral vapor ejected from several solids by a focused laser beam is ionized by electron impact, mass analyzed, and detected with an electron multiplier. By indirect means, a temperature of about 4000°K is deduced which is characteristic of the expanded vapor cloud and is clearly much lower than the initial surface temperature.

D. ION BOMBARDMENT

If it is desired to study surfaces rather than bulk material, the production of ions by ion bombardment (sputtering) should be considered. This method requires complex equipment, but has the advantage that the sample can be kept at room temperature, as is desirable for the investigation of organic monolayers.

The geometry of a simple ion bombardment source(16) is shown in Fig. 4. Rare gas ions are produced by electron impact in box B_o, are accelerated and decelerated in lens system 1-2-3, and focused onto target T (typical current densities: 10^{-5} A/cm^2, for energies between 50 and 600 eV). The secondary neutrals emitted are ionized by electron beam I^-, while secondary ions enter directly the source region (S_1, S_2) and are subsequently mass analyzed in a single-focusing instrument. Many metals and semiconductors, elements as well as compounds, have been investigated with this geometry and with similar sources(16,17,18). Recently, significant advances have been made by Liebl and Herzog(19), Castaign and Slodzian (20), and Smith and coworkers(21) which will be discussed in more detail below.

a Secondary Ions

Qualitatively, the emission of secondary ions, positive as well as negative, can be predicted from the two forms of the Langmuir-Saha formula presented in Section A, even though these equations apply quantitatively only to solid-gas systems in equilibrium at temperature T. In the present case, one can determine an "apparent" local temperature T which lies between 10,000 and 50,000°K. Positive ions are obtained from all elements whose ionization potentials are below about 10 eV, while negative ions are found for elements with electron affinities larger than 1 eV. Energy distribution measurements for the secondary ions yield values between 2 and 30 eV, the values being proportional to primary energy.

Liebl and Herzog(19) have described an improved sputtering source that utilizes a 1-mA primary ion beam of about 10 keV. Since this represents a power of 10 watts, the target has to be water-cooled to avoid thermal vaporization. The primary ion source and the target region are pumped by separate vacuum systems, so that the target will be at a low pressure while it is being bombarded by the high-intensity ion beam. The high energy of the primary ion beam increases the yield of secondary ions and helps reduce selectivity. The secondary ions are mass-analyzed in a small double-focusing machine of special design. A variety of samples, ranging from metals to insulators, have been investigated.

A "microanalyzer" has been designed and constructed by Castaing and Slodzian (20) who combined a sputtering source, mass spectrometer, and ion microscope into a single instrument, as follows: a small surface region of a solid sample is bombarded with a primary beam ($\sim 10^{-5}$ amp) of rare gas ions of 10 keV energy. The secondary ions produced are mass-analyzed in a magnetic field and refocused onto an exit slit. The mass-separated ion bundle is post-accelerated and falls onto an image converter where tertiary electrons are produced, accelerated in the opposite direction, and fall on a fluorescent screen. Thus the screen images the spatial distribution of a given component existing at a given time in the top three atomic layers of the sample surface, over an area of about 10^{-2} cm^2. The magnification of the system is about 300, the sensitivity depends strongly on the ionization potential of the atom in question. It is particularly promising in the low-mass region where an "electron microprobe" cannot be employed. Because elemental sensitivities differ widely, the analyzer is not suited for

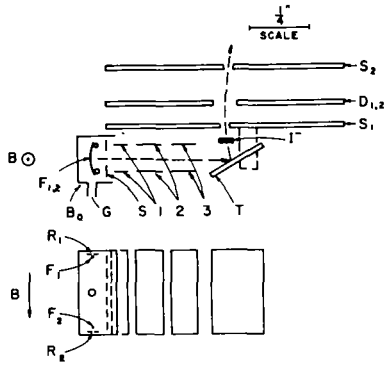

B_0 = BOX
$F_{1,2}$ = FILAMENTS
S = SLIT PLATE
$R_{1,2}$ = REPELLERS
1,2,3 = PAIRS OF EXTRACTION ELECTRODES
T = TARGET
G = GAS INLET
S_1 = PLATE OF FIRST SLIT (0.010" x 0.5")
$D_{1,2}$ = DEFLECTOR HALF PLATES
S_2 = PLATE OF SECOND SLIT (0.005" x 0.5")
I^- = IONIZING ELECTRON BEAM
B = MAGNETIC FIELD INTENSITY

Fig. 4

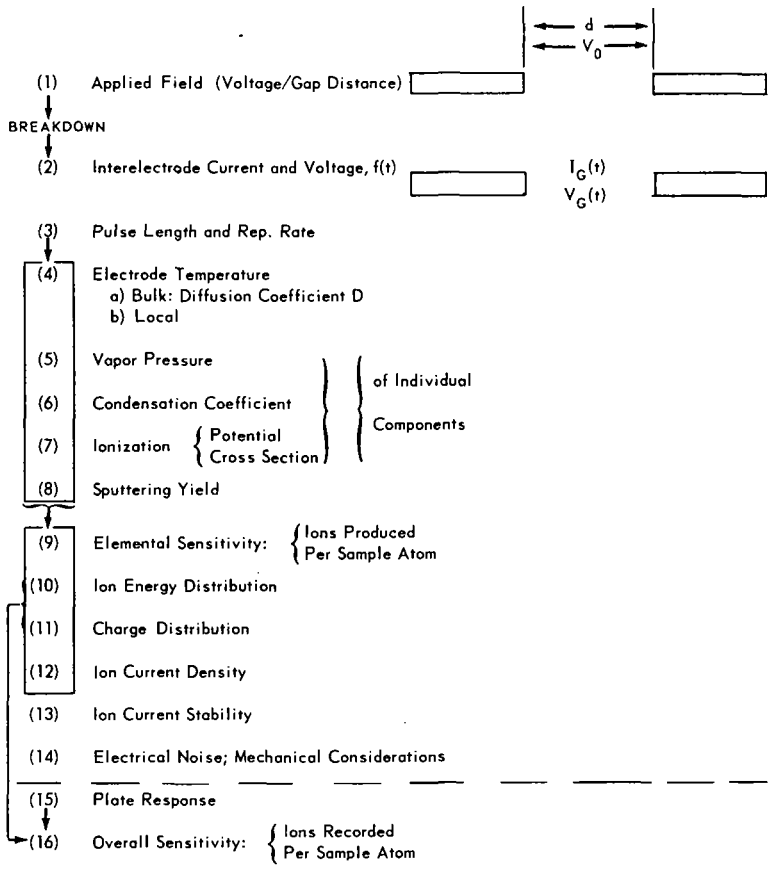

Fig. 5

quantitative work, unless it is calibrated with known samples.

b Secondary Neutrals

The selectivity encountered with secondary ions can readily be avoided by using secondary neutrals, but then another problem appears: usually, the pressure of background gases present in the sputtering source exceeds by many orders of magnitude that of the neutral beam. The logical answer is to use a pulsed primary ion beam together with a synchronous detection system which reduces the background gas signal by many orders of magnitude. Such a system has been successfully employed by Smith and coworkers(21) who use a relatively weak primary ion beam (about 10^{-6} A, energy up to 5 keV), a single-focusing mass spectrometer, and an electron multiplier. The sputtered neutrals are ionized by electron impact and yield currents of about 10^{-15} A. Although the sputtered neutrals are known to have an energy distribution of about 10 eV, their spectrum obtained after electron impact ionization displays an energy spread much smaller than expected. This is believed to be due to the relatively small probability of ionization of the more energetic neutrals.

E. VACUUM DISCHARGES

There are several methods of ion production that are based on vacuum breakdown in a gap between two electrodes: the rf spark, the vibrating arc, and the pulsed dc arc. Two of these systems were already investigated by Dempster(1) who, on the basis of equipment and circuitry available at that time, decided that the rf spark suited his purposes best. This Section will begin with a general discussion of the quantities that determine the performance of a given ion source. Next, it will define the basic terms used in vacuum breakdown and list the major parameters. This will be followed by a discussion of the breakdown mechanism and, lastly, a detailed description of the three types of vacuum discharge sources.

Fig. 5 shows in diagrammatic form a gap of width d formed by two electrodes between which an initial voltage V_0 is applied. When the average field $E_{AVE} = V_0/d$ becomes large enough, breakdown occurs (as discussed below), and gap current and voltage change rapidly with time. The length of the current pulse produced and its repetition rate determine the electrode temperature. This parameter, together with vapor pressure, condensation coefficient, ionization cross-section, and sputtering yield of the individual components, determines the elemental sensitivity, which is defined as the ratio of ions produced in the source per sample atom vaporized. While this quantity characterizes the basic efficiency of a given source, there are other parameters to be considered if an evaluation is to be made. These include: ion energy distribution, distribution among charged species, ion current density, geometry of the mass spectrograph, and the plate response (a function of mass and energy). When combined with the elemental sensitivity, they produce the overall sensitivity, which is defined as the ratio of ions recorded on the plate per sample atom vaporized. In addition, there are other factors, such as ion current stability, electrical noise, mechanical considerations, etc. that must be evaluated if the performance of different ion sources is to be compared.

1. Vacuum Breakdown

Before summarizing present-day theories of electrical breakdown in vacuum, it is desirable to define briefly the terms used, particularly since quite often the words "spark" and "arc" have been employed loosely and interchangeably. Fig. 6 shows qualitatively the three major regions of vacuum breakdown on a voltage-current plot. As the potential applied between two electrodes is raised gradually, prebreakdown currents appear, up to values of about a milliampere. In this prebreakdown region, the process is fully reversible. A further increase in potential produces catastrophic results, namely the spark breakdown, which, according to definitions given by Compton and Loeb, is a region of negative resistance and instability which produces an irreversible current increase. In this region, the interelectrode potential drops sharply by about three orders of magnitude. If the external circuit has a sufficiently low impedance and enough energy has been stored, the spark breakdown leads to the arc discharge region which is characterized by currents of 10 to 100 or more amperes and a potential drop, occurring near the cathode, of a value close to the ionization potential of the vapor.

The more important parameters to be considered for a detailed discussion of vacuum breakdown are summarized in Fig. 7. To have breakdown across a typical "narrow" gap ($d < 0.1$ cm), a voltage of 10^4 V or more is applied, which corresponds to an average field E_{AVE} of about 10^5 V/cm. Since field emission of

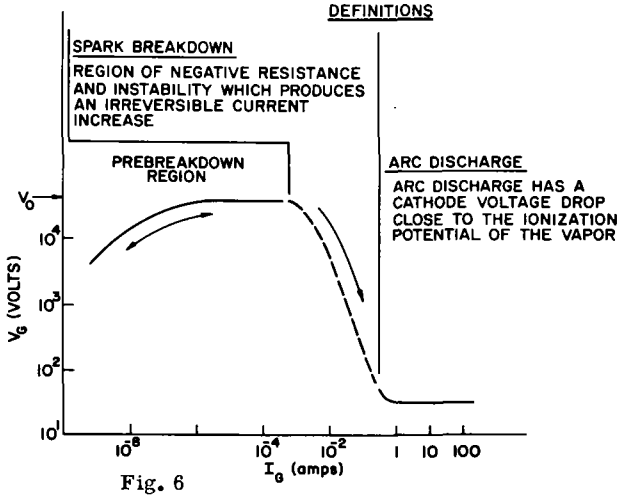

Fig. 6

APPLIED VOLTAGE	V_o: $10^4 - 10^5$ volts
GAP: NARROW	$d < 0.1$ cm
WIDE	$d > 0.1$ cm
AVERAGE FIELD	$E_{AVE} = V_o/d \cong 10^5$ v/cm
EFFECTIVE FIELDS	E_C, E_A
GAP CURRENT	$I_G = I^+ + I^-$
RESIDUAL PRESSURE	p: $10^{-6} - 10^{-9}$ torr

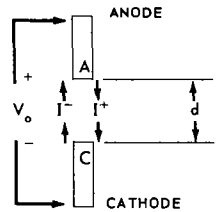

ELECTRODE CHARACTERISTICS:

- bulk temperature T °K
- gas content: bulk, surface
- mechanical strength
- vapor pressure
- microstructure (whiskers)

Fig. 7

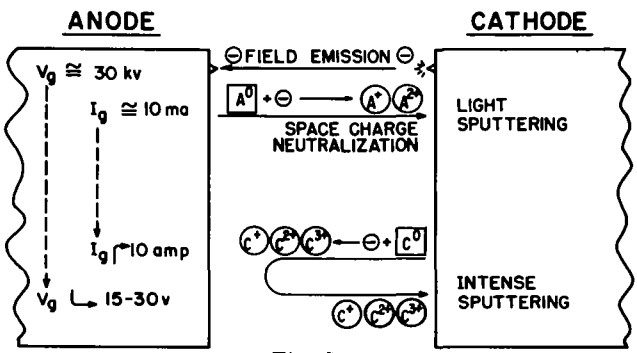

Fig. 8

electrons, which will be shown to initiate breakdown (see below), requires fields much larger, the effective field at the cathode, E_c, must be several orders of magnitude higher, presumably due to whisker growth. It is important to identify the charge carriers making up the gap current, and to determine their relative concentrations, in order to understand the breakdown details. While residual gases do not seem to play an important role once the pressure is less than 10^{-6} torr, the content of gases adsorbed on the electrodes, in the bulk as well as on the surface, does influence the breakdown voltage. Other parameters to be investigated are the mechanical strength of the electrode material in strong electric fields, its vapor pressure, and the growth of microstructures or "whiskers".

Since 1950, an enormous volume of work has been published in an effort to understand the breakdown mechanism, yet until recently there were several hypotheses, apparently conflicting, that beclouded the issue. While it is not possible within the framework of this paper to review adequately the complex situation, the more significant recent studies will be briefly mentioned. There seem to exist two regimes with two different breakdown mechanisms. For wide gaps, Cranberg's "clump hypothesis"(22) may apply which postulates that the electrical stress, if sufficiently great, can remove charged microscopic aggregates or clumps from either electrode. These clumps are then accelerated across the gap and produce heating and vaporization of the opposite electrode. However, for narrow gaps, which are of interest here, the field emission theory proposed by Boyle, Kisliuk, and Germer(23) is borne out by many different experiments. The most significant of these are listed in Table II, according to the method employed. Pivovar and Gordienko (23a) proved with the help of a magnetic field that during the prebreakdown stage charge transfer occurs largely through electron flow. Many experimenters, among them Boyle et al.(23), showed that on a Fowler-Nordheim plot the prebreakdown currents follow a straight line, thus must be due to the field emission process. The electronic nature of these currents has also been studied by Goldman(24) who observed X-ray flashes typical of the anode material in the early breakdown stages. With the help of photomicrographs, DeGeeter(25) showed that at a critical voltage luminous patches appear on the anode surface, and ascribed their bluish glow to ionization by electrons; at higher voltages, incandescent spots appeared, followed by breakdown. Similar observations have been made by Little and Whitney(26) who saw fluorescent spots during prebreakdown on a transparent anode coated with a conducting layer and a phosphor.

To explain the disparity between the average applied field and the effective field required for field emission, Little and Whitney(26) inspected electrode surfaces with optical and electron microscopes. They found projections (whiskers) that were about one μ high and 0.1 μ wide, approximately of the right size to produce the necessary field enhancement of 100. This has recently been confirmed by the studies of Tomaschke(27) who used electron and field emission microscopes for the same purpose.

The initial step of electron emission from the cathode is followed by heating of the anode, as established by several material transfer studies. Tarasova and Razin(28) used irradiated Cu electrodes to show that, during prebreakdown, there is material transfer mainly from anode to cathode. Similar results were obtained by Schwabe(29) who used two dissimilar electrodes and determined by emission spectrography the preferred direction of transfer. Recently, this author and coworkers(30) have used mass spectrometry to show that in dc arc pulses of one μsec duration the vapor consists largely of anode material.

Combining the bits of information presented above, one can postulate the following sequence of events occurring during the breakdown of a narrow gap, which is shown in diagrammatic form in Fig. 8. As the average field between electrodes is raised to about 10^5 volts/cm, a small predischarge current begins to flow which is due to field emission from one or more whiskers on the cathode surface. If the current density is sufficiently high, the whisker will partially vaporize, thereby contributing some cathode atoms to the vapor phase. Electron bombardment of the anode produces neutral atoms which probably come from anode whiskers, as well as O^+ ions(31) from adsorbed CO. These neutral atoms from anode and cathode are ionized by cathode electrons and help increase the electron current intensity by space charge neutralization. Furthermore, the ions bombard the cathode, producing mainly sputtered neutrals and some secondary electrons. As the electron and ion currents build up in intensity, the interelectrode potential drops, as shown qualitatively in Fig. 6. During this spark breakdown stage, the production of singly-charged ions predominates, but multiply-charged species are also found. If there is enough energy stored in the external circuit, the current build-up continues through heavy sputtering, ending in the arc discharge defined above. In this mode, gap voltages of between 15 and 30 volts are measured,

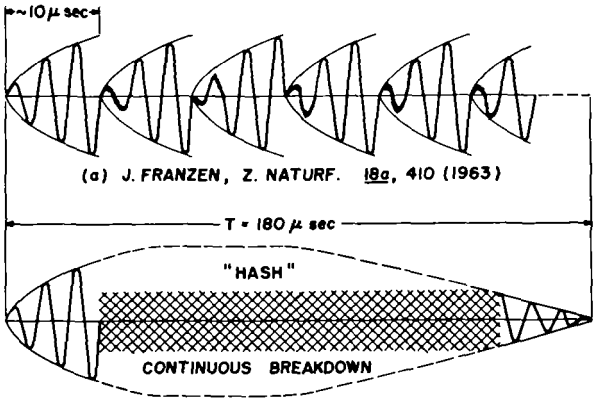

(b) RCA (MS7)

COMPARISON OF RF BREAKDOWN PATTERNS

Fig. 9

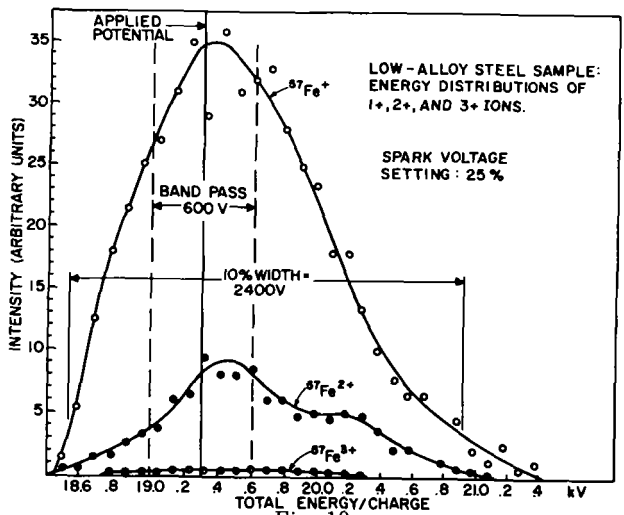

Fig. 10

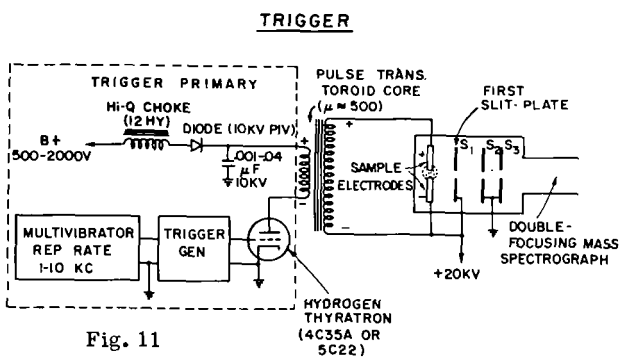

Fig. 11

and high concentrations of multiply-charged ions are observed, typical of plasma conditions.

2. The rf Spark

Although the rf spark is, to date, the most widely used vacuum discharge method, relatively few studies have been made to investigate its basic properties. Franzen(32) obtained oscillograms of the gap voltage which showed that the rf spark consists of a sequence of individual breakdowns, occurring only during selected half-cycles (see Fig. 9a). The rf voltage (f = 1 Mc/sec) builds up during a period of about 10 μsec to a point where breakdown occurs, as indicated by the heavy, wiggly trace which persists for about two half-cycles. When the energy stored in the Tesla coil circuit(33) has been exhausted, the breakdown terminates, but in the meantime the rf voltage is building up again, and the process is repeated several times during the duration of the pulse. Fig. 9b shows a different pattern, observed for the MS7 used at RCA Laboratories. After an initial build-up at the beginning of the pulse, continuous breakdown occurs which appears as "hash" and which terminates a few cycles before the end of the pulse. It is presumed that the breakdown is continuous because the coil circuit (typical impedance: $\sim$20,000 ohms) is capable of storing sufficient energy. In a paper which follows, Hickam and Sweeney(34) present evidence that in their instrument breakdown can occur once every half-cycle during most of the pulse.

Franzen(32) has presented a model for the acceleration of ions in the increasing rf field which permits an estimate of their initial energy in terms of time and place of origin. Actual measurements of ion energy distributions have been made by Woolston and Honig for total ion beams(35) and mass-resolved ion beams(36). Fig. 10 presents typical energy distributions, about 2400 V wide, for various iron ions from a low-alloy steel sample. The distributions have maxima close to the applied potential and close to each other, which is significantly different from the situation presented by Franzen and Hintenberger (Ref. 33, Fig. 5), who find a strong dependence on accelerating potential. It is believed that this dependence is caused by the special ion lens system used in their source.

3. The Vibrating Arc

This ion source, after being rejected initially by Dempster(1) because it presumably did not yield enough multiply-charged species, has enjoyed a sudden revival within the last two years(37,38,39,40,41,42). In most of these studies, a very simple electro-mechanical low-voltage system, similar to that of a doorbell circuit, was employed. The functioning of the vibrating arc has recently been described in detail by Schuy and Franzen(43) who investigated the time dependence of gap current and voltage, as well as ion- and light-emission with the help of a dual-trace oscilloscope. While the gap is open, the gap voltage is the applied voltage, say 6 V. When the gap closes, the voltage drops to zero, while the current increases exponentially which, in turn, gradually reduces the contact pressure to zero. At this point, the contact resistance becomes very large, produces melting of the contact areas, and results in a "liquid bridge" as the electrodes move apart. When the liquid bridge breaks, an arc keeps the current of about 15 A flowing, at a voltage of about 20 V. Ion and light emission are observed only during this arcing period. In some cases, the liquid bridge is reformed, and the arcing process may be repeated several times. When the arc finally goes out, an inductive voltage kick is observed.

The vibrating arc works well with conducting electrodes, but not with high-resistivity semiconductors. Furthermore, it clearly is not applicable to materials of insufficient mechanical strength, such as compressed powders or brittle materials. Among the ions produced, the doubly- and triply-charged species predominate over singly-charged ions, the distribution being typical of an arc discharge. When dissimilar electrodes are employed, the spectrum shows mostly cathode ions, indicating heavy sputtering. These aspects will be discussed in more detail in the following Section.

4. The Pulsed dc Arc

Recently, work has been done at RCA Laboratories(30) to utilize dc pulsed voltages for vacuum breakdown and produce intense ion beams with moderate energy distributions. This Section will first deal with the short "trigger" pulse, discuss the circuitry developed and results obtained, then describe the longer low-voltage discharge.

a Simple Trigger

The most convenient means of producing a trigger pulse of a few μsec

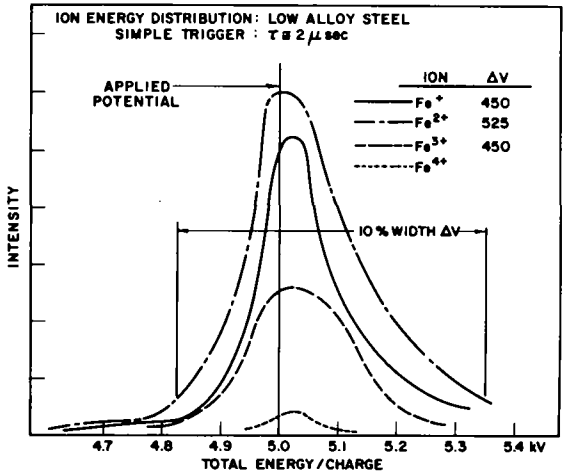

Fig. 12

TRIGGER AND SERIES LOW VOLTAGE DISCHARGE

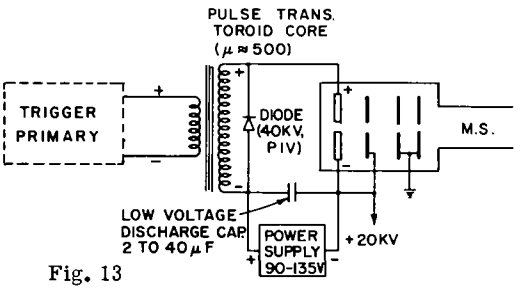

Fig. 13

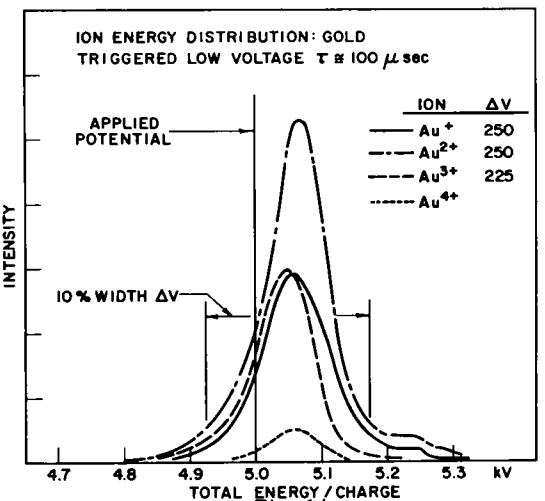

Fig. 14

duration between two sample electrodes is a pulse transformer since it isolates the associated circuitry from the high potential (+ 20 kV) of the mass spectrograph source. Fig. 11 is a block diagram of the system used. It delivers, at repetition rates up to 3000 cps, a high-voltage pulse of up to 60 kV which causes breakdown of the vacuum gap and results in a current pulse of from 5 to 50 A, between 1 and 4 μsec wide, depending on the value of the capacitor in the trigger primary circuit. Positive ion pulses (up to 10 mA) produced in the expanding discharge reach the first slit plate S_1 where a small fraction enters the mass spectrograph to be energy-selected and mass-analyzed. Fig. 12 presents some mass-analyzed energy distribution plots obtained for the various iron ions from a low-alloy steel. The relative intensities shown, while not yet corrected for plate response, indicate that Fe^+, Fe^{2+}, and F^{3+} are the three important species, and that their ΔV is near 500 V.

b Triggered Low-Voltage Discharge

Fig. 13 is a block diagram of the first and simplest variant of various triggered low-voltage systems tried to date. It consists of an adjustable low-voltage supply connected in series with the pulse transformer secondary. In its simplest form, the low-voltage supply is a 90 volt battery in parallel with a set of capacitors ranging from 2 to 40 μF. It yields a gap current pulse that decreases exponentially and is adjustable in width from about 10 to 200 μsec. If a true square pulse is desired, the simple low-voltage supply is replaced by a pulser of suitable design. The diode shown in Fig. 13 shorts out the high impedance of the pulse transformer secondary during the low-voltage pulse, allowing the low-voltage supply to furnish the gap current necessary to sustain the discharge. A portion of the positive ions formed in the discharge arrive at S_1 and pass into the mass spectrograph.

The energy distribution of the ions produced from gold electrodes in the low-voltage discharge is shown in Fig. 14. Relative intensities (not corrected for plate response) of the doubly- and triply-charged species, compared to singly-charged ions, have increased significantly, and their ΔV of about 250 V is considerably smaller, when compared to the simple trigger case. Still, the observed ΔV is almost three times larger than the applied voltage of 90 V, which is probably due to the fact that the ion accelerating potential of 20 kV can readily drop by several hundred volts when the trigger pulse is applied.

5. Comparison

To compare the performance of the three vacuum discharge methods and, at the same time, arrive at a better understanding of the basic processes involved, a number of tests have been carried out which will be described below.

a Charge Distribution

In an extended series of runs, the distribution among singly- and multiply-charged species was studied for the compound $SnNb_3$, employing the different vacuum discharge methods. Single pulses were used in all cases except for the rf spark where this was not possible. It was found that the relative intensities of the various species changed widely from pulse to pulse, but that the average values shown in Table III correlate reasonably well with the gap currents. For all intensity values, the plate response was taken into account, based on the assumption that response varies linearly with energy(44,45). The results shown in Table III confirm the well-known fact that in the rf spark the singly-charged species predominate, and it is interesting to note that this is still true for the shortest obtainable trigger pulse of 1 μsec duration. While only the singly-, doubly-, and triply-charged species are shown for the rf spark, ions with up to fourteen charges could be seen for some of the elements on heavy exposures. If these ions are produced by electron impact in a single ionizing process, the electron energy required would amount to from 400 to 900 V.

When the simple trigger pulse is lengthened to 4 μsec, the ion spectrum changes to the distribution typical of the arc discharge, with the doubly-charged species becoming predominant. It is seen that the distribution is the same for the 4 μsec-long simple trigger, the triggered low-voltage discharge, and the vibrating arc, all of which have approximately the same gap current of 30 A. Incidentally, the vibrating arc data were obtained by manually closing and opening the gap. It should be noted that, in the arc discharge, ion spectrum intensities fall off very rapidly for X^{4+}, and that the more highly ionized species are barely visible. Since during the arc discharge the gap voltage is 30 V or less, it is probable that the multiply-charged species are produced from the singly-charged ions in the dense plasma by multiple ionization processes.

Since the different low-voltage systems produce doubly- and triply-charged

species in large concentrations (Lines 3, 4, and 5, Table III), it is necessary to take these species as well as singly-charged ions into account for analytical applications. If their relative intensities are fixed, any single major species can be used, if not, it is necessary to add up intensities. In a recent study, Franzen and collaborators(46) have investigated the charge distribution in a triggered dc arc. With the help of a time-gating circuit, they observed that in the early discharge stage the distribution resembles that of the rf spark, while later on the typical arc distribution is found, in agreement with the results presented in Tables III and IV (see below).

b Dissimilar Electrode Studies

In order to study the material transport between electrodes and to establish the breakdown hypothesis presented above, runs were made with two dissimilar electrodes. In earlier work, Au and Pt electrode pairs were used which have neighboring masses, but do not match well in isotopic abundances. For this reason, a Ni anode Cu cathode pair was found to be more suitable, and has been used subsequently. By placing a series resistance of appropriate value in the electrode circuit, it was possible to limit the discharge to its early stage (Table IV, top line). Ions produced mostly from the anode material were observed, together with a charge distribution similar to that of the rf spark. With the series resistance removed (Table IV, second line), cathode ions become predominant over anode ions, by a factor of five to one. Qualitatively, these ratios agree with observations reported earlier(30) for a Au-Pt electrode pair. Attempts to change the gap current in a triggered low-voltage discharge with a series resistance were partially successful, but showed only a slight, though significant increase of cathode ions with gap current (lines 3 and 4, Table IV).

c Comparison

Table V summarizes the performance of the pulsed dc arc sources and compares them to the rf source. The vibrating arc characteristics are very similar to those shown in the third column for the triggered low-voltage system. It is of interest to note that the ion currents produced in the low-voltage sources are more stable than those from the rf source, and that the sample position needs to be readjusted less frequently, which is of considerable practical value. For analytical applications, it is important that exposures can be made short enough to make the lines of the matrix material just visible. Table V shows that the simple trigger readily fulfills this requirement. Energy distributions have been compared in terms of the "10 per cent width", i. e. the separation, in eV, of the two points where the intensity has dropped off to 10 per cent of its maximum value. This is a convenient parameter because the 10 per cent width includes approximately 90 per cent of the total ions. Since the monitor system accepts an energy band of 600 eV, essentially all the ions formed in the pulsed dc arc sources can be utilized. In contrast, the ions formed in the rf source have much larger energy distributions (1 - 2.5 kV), which limits the fraction of ions that can be used.

An estimate of the overall efficiency of a given ion source used in conjunction with the mass spectrograph is obtained from the ratio of sample atoms vaporized per ion arriving at the photographic plate. This is readily computed from weight measurements made on the sample rods before and after a given exposure recorded by the integrator. The integrated monitor current yields the total number of ions arriving at the plate, provided monitor current and plate current are equal. The ratios of atoms per ion shown in Table V for the low-voltage sources indicate a sample consumption that is considerably lower than that of the rf source. Under optimum conditions, all vacuum discharge sources can, in conjunction with a double-focusing mass spectrograph, detect impurities on the parts per billion level.

The last line of Table V quotes typical gap currents. Practical considerations limit low-voltage operation to electrodes with room-temperature resistivities of less than 0.1 ohm-cm, but this range can be extended several orders of magnitude if the samples are allowed to heat up a few hundred degrees during operation.

CONCLUSIONS

This review has discussed the many methods available to produce ions from solids. To select the method best suited for a particular application, it is necessary to evaluate its advantages and limitations. While no single method is outstanding in all respects, the vacuum discharge methods appear most appropriate for a broad, semi-quantitative survey of low level impurities. If surface impurities are to be determined, the ion bombardment method is useful because it does not materially raise the bulk temperature of the sample. Finally, it is possible to investigate microvolumes of inhomogeneous samples with the help of focused radiation sources, such as the laser source.

ACKNOWLEDGMENTS

The author is grateful to J. R. Woolston for his collaboration in much of the original work reported here, and to S. S. Glass who designed the triggered low-voltage circuitry and thereby made this method practicable. It is a pleasure to acknowledge the competent assistance of E. N. Botnick and H. H. Whitaker in various phases of the work.

REFERENCES

1) A. J. Dempster, Nature 135, 542 (1935); Rev. Sci. Instr. 7, 46 (1936).

2) H. W. Wilson and N. R. Daly, J. Sci. Instr. 40, 273 (1963).

3) R. K. Webster, in "Methods in Geochemistry", A. A. Smales and L. R. Wagner, Editors (Interscience Publishers, Inc., New York, 1960), pp. 203 - 246.

4) I. Langmuir and K. H. Kingdon, Proc. Roy. Soc. (London) 107, 61 (1925).

5) M. G. Inghram and W. A. Chupka, Rev. Sci. Instr. 24, 518 (1953).

6) H. Voshage and H. Hintenberger, Z. Naturforsch. 14a, 216 (1959).

7) R. E. Honig, in "Trace Analysis of Semiconductor Materials", J. P. Cali, Editor, (Pergamon Press, Oxford, 1964), pp. 169 - 205.

8) W. M. Hickam, Phys. Rev. 74, 1222A (1948); ASTM Bull. 149, 17 (1953).

9) R. E. Honig, Anal. Chem. 25, 1530 (1953); J. Chem. Phys. 22, 1610/11 (1954).

10) W. A. Chupka and M. G. Inghram, J. Phys. Chem. 59, 100 (1955).

11) P. Goldfinger, Paper 1, ASTM E-14 Meeting on Mass Spectrometry, Chicago (1961).

12) R. P. Burns, A. J. Jason, and M. G. Inghram, J. Chem. Phys. 40, 1161; 2739 (1964).

13) R. E. Honig and J. R. Woolston, Appl. Phys. Letters 2, 138 (1963).

14) R. E. Honig, Appl. Phys. Letters 3, 8 (1963).

15) J. Berkowitz and W. A. Chupka, J. Chem. Phys. 40, 2735 (1964).

16) R. E. Honig, in "Advances in Mass Spectrometry", Vol. 2, R. M. Elliott, Editor (Pergamon Press, Oxford, 1963), pp. 25 - 37.

17) R. C. Bradley, J. Appl. Phys. 30, 1 (1959); R. C. Bradley, A. Arking, and D. S. Beers, J. Chem. Phys. 33, 764 (1960); R. C. Bradley and E. Ruedl, J. Appl. Phys. 33, 880 (1962).

18) H. E. Stanton, J. Appl. Phys. 31, 678 (1960).

19) H. J. Liebl and R. F. K. Herzog, J. Appl. Phys. 34, 2893 (1963).

20) R. Castaing and G. Slodzian, J. Microscopie 1, 395 (1962).

21) A. J. Smith, L. A. Cambey, and D. J. Marshall, J. Appl. Phys. 34, 2489 (1963).

22) L. Cranberg, J. Appl. Phys. 23, 518 (1952).

23) W. S. Boyle, P. Kisliuk, and L. H. Germer, J. Appl. Phys. 26, 720 (1955).

24) M. Goldman and A. Goldman, J. Physique 24, 303 (1963).

25) D. J. DeGeeter. J. Appl. Phys. 34, 919 (1963).

26) R. P. Little and W. T. Whitney, J. Appl. Phys. 34, 2430 (1963).

27) H. E. Tomaschke, Coordinated Science Laboratory Report R-192, U. of Illinois (1964).

28) L. V. Tarasova and A. A. Razin, Soviet Phys. - Tech. Phys. 4, 879 (1960).

23a) L. I. Povovar and V. I. Gordienko, Soviet Phys. - Tech. Phys. 3, 2101 (1958); 7, 908 (1963).

29) S. Schwabe, Z. Angew. Phys. 12, 244 (1960).

30) R. E. Honig, S. S. Glass, and J. R. Woolston, Proc. Sixth Intern. Conf. on Ionization Phenomena in Gases, Vol. 2, pp. 209 - 216 (Paris, 1964).

31) J. R. Young, J. Appl. Phys. 31, 921 (1960).

32) J. Franzen, Z. Naturforsch. 18a, 410 (1963).

33) J. Franzen and H. Hintenberger, Z. Naturforsch. 18a, 397 (1963).

34) W. M. Hickam and G. S. Sweeney, Paper 41, Twelfth Annual Conference on Mass Spectrometry and Allied Topics, Montreal (1964).

35) J. R. Woolston and R. E. Honig, Rev. Sci. Instr. 35, 69 (1964).

36) J. R. Woolston and R. E. Honig, Paper 57, Twelfth Annual Conference on Mass Spectrometry and Allied Topics, Montreal (1964).

37) V. S. Venkatasubramanian and H. E. Duckworth, Can. J. Phys. 41, 234 (1963).

38) K. D. Schuy and H. Hintenberger, Z. Naturforsch. 18a, 95 (1963).

39) F. Rau and H. Ewald, Z. Anal. Chem. 197, 106 (1963).

40) E. B. Owens and N. A. Giardino, Lincoln Laboratory Report ESD-TDR-63-584 (1963)

41) L. A. Cambey, Report ML-TDR-64-75 (1964).

42) R. D. Craig and A. Riddoch, Paper 56, Twelfth Annual Conference on Mass Spectrometry and Allied Topics, Montreal (1964).

43) K. D. Schuy and J. Franzen, talk presented at the Bad Nauheim Meeting of the German Physical Society (April 1964).

44) E. Burlefinger and H. Ewald, Z. Naturforsch. 16a, 430 (1961).

45) E. B. Owens, Appl. Spectry. 16, 148 (1962).

46) J. Franzen, K. D. Schuy, and H. Hintenberger, Paper 39, Twelfth Annual Meeting on Mass Spectrometry and Allied Topics, Montreal (1964).

LIST OF FIGURE CAPTIONS

Fig. 1. Geometry of electron impact source.

Fig. 2. Diagram of electron bombardment source.

Fig. 3. Geometry and schematic diagram for laser ion source.

Fig. 4. Geometry of a simple ion bombardment source.

Fig. 5. List of parameters for a vacuum discharge source.

Fig. 6. Definitions and diagram for vacuum breakdown.

Fig. 7. Summary of parameters essential for vacuum breakdown.

Fig. 8. Steps leading to high voltage breakdown of a narrow gap.

Fig. 9. Comparison of breakdown patterns for the rf spark.

Fig. 10. Energy distributions for Fe ions produced in the rf spark from a low-alloy steel sample.

Fig. 11. Diagram of simple trigger circuit.

Fig. 12. Energy distributions for Fe ions produced in a simple trigger discharge from a low-alloy steel sample.

Fig. 13. Diagram of triggered low-voltage circuit.

Fig. 14. Energy distributions for Au ions produced in a triggered low-voltage discharge.

SOURCES OF FLUCTUATIONS IN THE MASS SPECTROSCOPIC ANALYSIS OF SOLIDS BY VACUUM DISCHARGE TECHNIQUES

J.FRANZEN, K.D.SCHUY, and H.HINTENBERGER
Max Planck-Institut für Chemie (Otto Hahn-Institut)
Mainz, West-Germany

I. Introduction

In 1935, DEMPSTER[1] investigated three types of vacuum discharges between solids: the r.f.spark, the vacuum vibrator (drawn arc), and the condensed discharge. In his later analytical work[2], DEMPSTER exclusively favoured the r.f.spark. Due to this fact, the r.f.spark has in the past predominantly been used in the mass spectrographic analysis of solids.

Until now, all but a few of the papers published in the field of the analysis of solids by vacuum discharges are empirical in nature, and aimed to prove the feasability of the method. Comparatively little effort went toward the elucidation of ion formation processes by the various discharge mechanisms. Pertinent investigations in bordering fields, as optical spectroscopy, the physics of contacts, plasma physics, etc., have not been evaluated to any extent with regard to the mass spectrographic analysis of solids.

We have attempted to reexamine various kinds of vacuum discharges as to their ion formation properties. We paid particular attention to factors affecting analytical errors.

The method of analysis consists of the following: The atoms of the solid are ionized in the discharge. A fraction of the ions is gathered, accelerated, and focused by electrostatic fields. The ions are analyzed by a mass spectroscope, and usually detected by a photographic plate. The mass spectra of vacuum discharges mainly show the lines of singly and multiply charged atomic ions of the electrode material, and relatively few lines due to molecular ions. The composition of the ion beam is very similar but not entirely equal to that of the electrode material. Standard-independent analyses can be carried out with limited accuracy. Accuracy can be improved by comparing the spectrum of the unknown sample with a spectrum of a standard sample on the same photographic plate, or by employing sensitivity factors determined previously.

As is customary, the accuracy of the method is determined by the standard error of a number of repeated analyses. It is found to be necessary to introduce standard error factors, since the logarithms of the analytical values lie on a normal distribution, and not the analytical values themselves.[3] However, for small deviations up to about 30 %, the standard errors are usually given in percent. Thus, a standard deviation of 10 or 20 % corresponds to an error factor of 1.10 and 1.20, respectively.

From the analysis procedure there follow four groups of error sources:

1. Electrode inhomogeneities and surface deposits lead to fluctuations of analytical results since the composition of the analyzed material changes with successively consumed volume. Requirements on electrode homogeneity are the higher the lower the sample consumption in the given type of discharge, and the higher the elemental concentration in the sample. In both cases, the analyzed volume is small. Inhomogeneous samples can be analyzed using special methods: Discharge scanning of a larger electrode area results in a more representative analysis of the sample than point-to-point discharges. Different discharge types consume different amounts of material and are therefore affected in different degrees by inhomogeneities. On the other hand, the analyzed volume can be increased by permitting only ions of, say, every fifth or tenth discharge to pass the mass spectrograph. Furthermore, by the application of time-resolved mass

Phase of analysis	Process	Possible factors relevant to analysis
electrodes from solids		
	evaporation	partial evaporation → changes of concentration with time
vapour		
	ionization, by impact or thermal	impact energy or plasma temperature varies with time
plasma		
	effusion of ions from discharge	time-dependent acceleration → ion-specific primary energy
ions of different primary energies in radial motion		
	ion-acceleration and -focussing	ion-specific focal points and beam divergencies
ion beam at entrance slit of M.S.		
	local ion selection	ion-specific selection due to different focal points
aperture slit		
	angular ion selection	ion-specific selection due to different beam divergencies
energy slit		
	energy ion selection	ion-specific selection due to different primary energies
beam monitor		
	exposure control	varying fractions of ion current due to ion-specific z-divergencies measured
photographic plate		

Fig. 1

Phase of cycle	Fieldstrength at cathode	Fieldemission from cathode	Anode evaporation	Ion yield	Kinetic ion energy
1. start	$0 \rightarrow 10^7$ V/cm	none	none	none	-
2. pre-breakdown	$\sim 10^7$ V/cm	$0 \rightarrow 100\ \mu$A	spot heating	none	-
3. transition region	space charge induced increase	100μA → 10 mA	low boiling point materials	highly charged ions	high
4. breakdown	cathode drop by space charge	10 mA → 10 A	high boiling point materials	singly charged ions	low
5. end after $\sim 10^{-7}$ s from pre-breakdown	drops to 0	none	cooling off	none	-

Fig. 2

spectroscopy as discussed below, only ions from a small time interval of the total discharge may be analyzed, thus averaging over a larger sample volume.

2. Changes in the process of ion formation as well as variations of the ion transmission properties of the mass spectrograph lead to considerable fluctuations of analyses. These phenomena shall constitute the main topic of this paper.

3. Local sensitivity variations of the photographic emulsion cause analytical errors. These variations are affected by inhomogeneous grain density, changes in thickness of the grain-screening gelatine, and changing processing conditions. The sensitivity fluctuations limit the reproducibility of analysis. The present state of the art of photoplate manufacturing apparently sets an absolute limit of 3 to 5 % to the accuracy of the method. According to our present knowledge, the law of reciprocity holds in good approximation; however, the accuracy of trace analysis may be impeded by neglecting a small reciprocity failure.

4. The densitometric evaluation of the photographic mass spectra, the application of factors correcting for the variation of line width and line height with ion mass, the corrections necessary to compensate for the variation of photographic sensitivity with ion mass and ion energy, and the calculation of final analytical results contain many possibilities for serious errors which, however, can be minimized by suitable methods.

In the present paper we confine ourselves to a discussion of the error sources given in group 2 above. In the following, we shall treat different sources of analytical errors hypothetically. We shall then proceed to demonstrate their actual occurrence in practical work.

II. Error Possibilities During Ion Formation and Ion Beam Analysis.

The process of ion formation and ion beam analysis starts with the ignition of a discharge between the sample electrodes in vacuum. It extends to the detection of individual ion species by the photographic plate. The whole process can be divided into a number of sub-processes as shown in fig.1.

The discharge converts the solid material, through its vapour phase, to its plasma from which ions of different primary energies emerge. After acceleration, the further fate of the ions from the discharge is solely determined by the external parameters of the mass spectrograph.

For the analysis of solids, r.f.-sparks and repeated d.c.-arcs are frequently employed. During one discharge cycle, the electrode surface must be heated from a bulk temperature in the order of a few hundred ^{o}C to spot temperatures of a few thousand ^{o}C. During this temperature rise, preferential evaporation might occur, resulting in a time variation of electrode vapour composition during the discharge cycle.

Depending on the particle density in different types of discharges, ionization might occur either by single impact with highly accelerated electrons, or thermally, i.e. by multiple collisions with low energy particles in a plasma of temperature up to about 60.000 ^{o}K. The ratio of singly-to-multiply-charged ions and the intensity ratio of ions from different elements changes either with the energy of the ionizing electrons or with the plasma temperature. The mean impact energy of the ionizing electrons depends on their mean free path and on the electric field strength in the gap. Both these parameters may alter during the discharge cycle so that the composition of the ion cloud may also vary with time. Experimentally, ions from the discharge exhibit certain primary energy spreads, between thermal energies up to some Kev. The mechanism of ion acceleration in the discharge is not yet completely understood. The models proposed[24,25] still leave some questions unanswered. It appears that the ions are accelerated by steady or r.f.electric fields in the gap. The electric field affects both the

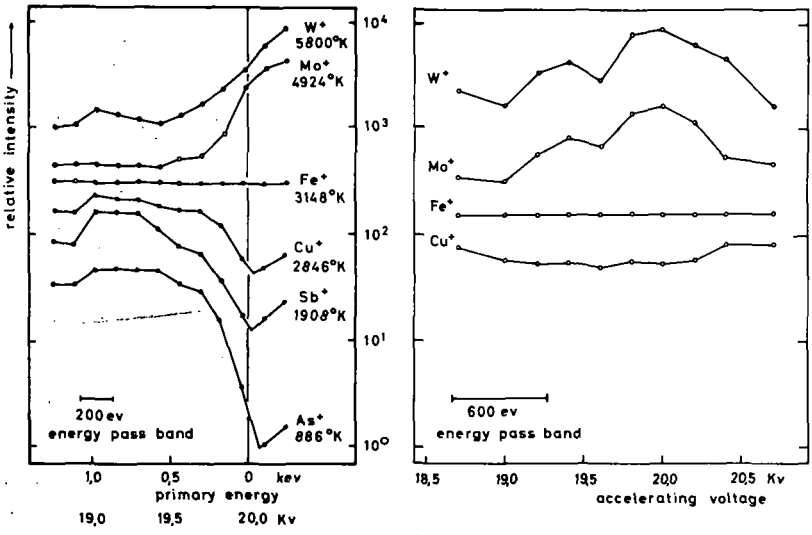

(own measurements).

(by courtesy of J.S. HALLIDAY, AEI., Manchester)

Fig. 3

Fig. 4

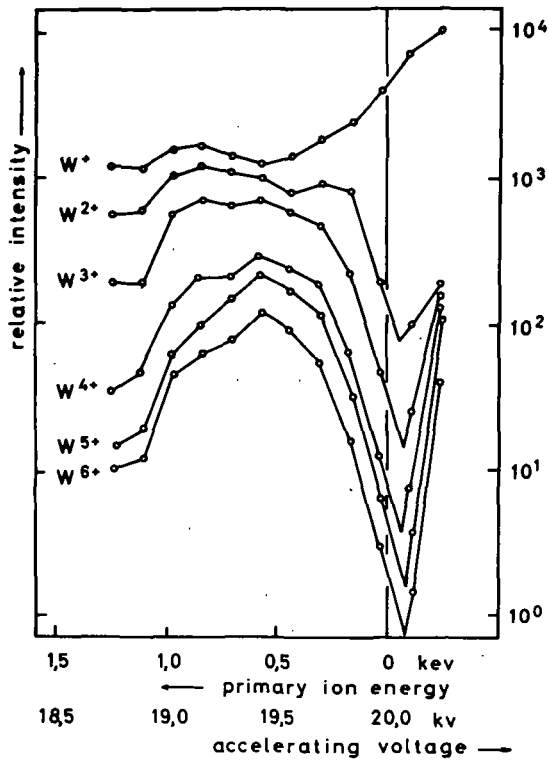

vapour ionization efficiency and the rate of electrode surface temperature rise. Therefore, surface temperature, mean electron impact energy and ion acceleration are mutually connected. This results in different energy distributions for different ion species[26,27].

The ions of different primary energies are electrostatically accelerated and focused. Due to the achromatism of any electrostatic lens system, ions with different primary energies are focused not on a point but on a focal line. Ion beam composition changes along this line. Ions from different points on the focal line have different angles of divergence, resulting in an ion-specific angular distribution.- Both the location of the focal line and the angular distribution of the ions depend on the location of the discharge with respect to the optical axis of the ion source, and on the alignment of the ion source with respect to the main slit. The energy distribution of the ion beam depends on both applied accelerating potential and discharge conditions.

The ion beam, showing both ion-specific energy and angular distribution, is now subjected to three different ion selection processes in the mass spectrograph. Every one of these processes may decisively alter the ion beam composition.

The main slit of the apparatus causes a selection of ions due to the different focal points of the acceleration system. Since the beam composition alters along the focal line, this selection process significantly influences the composition of the total ion beam in the spectrograph.- The aperture prior to the electric field affects an ion-specific angular selection. Finally, the energy slit prior to the magnetic field leads to an ion-specific energy separation. Therefore, in order to improve analyses, discharge conditions, accelerating potential and source geometry, must be held as constant as possible. Particular attention should be given to the discharge conditions with respect to analyses. This will be done in the following.

III. The Two Kinds of Vacuum Discharges.

Up to the present, several types of vacuum discharges between solid electrodes have been investigated: the r.f.spark[4,5,6], the d.c. drawn arc of the vacuum vibrator[7,8,9], the triggered condensed discharge[10,11,12], and the LASER-ignited discharge[11]. However, according to our present knowledge, all these discharge types contain two basically different mechanisms only, first the high voltage breakdown, and second the low voltage discharge. The high voltage breakdown is a strongly dynamical process, and the designation "high voltage spark" seems appropriate. In contrast, the low voltage discharge is almost stationary, and may extend over considerable periods of time: a plasma in thermal equilibrium is built up. We shall therefore use the term "low voltage arc" for this discharge, but we should like to point out that these terms somewhat collide with those customary in emission spectroscopy. There the word "spark" defines a strongly ion-forming process (spark spectrum), while the "arc" designates a discharge giving rise to the "arc spectrum" of neutral excited atoms or molecules.

a) The High Voltage Spark (Electrical Vacuum Breakdown)

We observe the high voltage spark in the r.f.spark as well as in the ignition phase of the triggered condensed discharge. First we shall limit ourselves to a discussion of the r.f.spark.

If just one cycle of operation of this discharge type is considered, then the entire process may be classified as in fig.2. The spark mechanism described is rather similar to that proposed by HONIG, GLASS, and WOOLSTON[10], and is based mainly on work performed by BOYLE, KISLIUK, and GERMER[13].

After some 10^{-7} s, when the field strength in the electrode gap has reached a value of about 10^7 v/cm, field electron emission commences at cathode asperities. The field electrons, highly accelerated in the

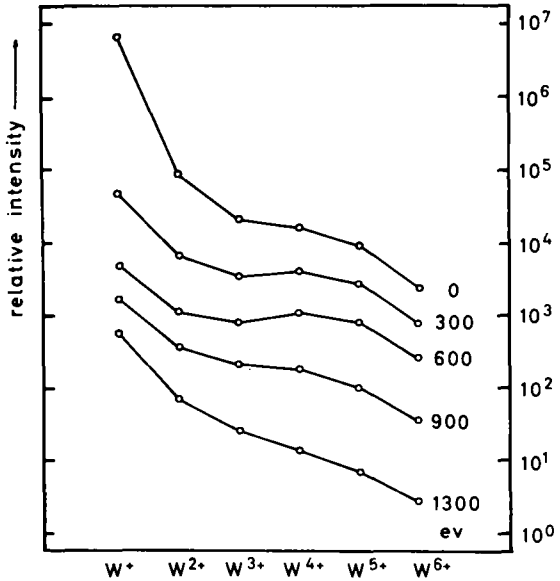
relative intensity
10^7
10^6
10^5
10^4
10^3
10^2
10^1
10^0
0
300
600
900
1300
ev
W^+
W^{2+}
W^{3+}
W^{4+}
W^{5+}
W^{6+}

Fig. 5

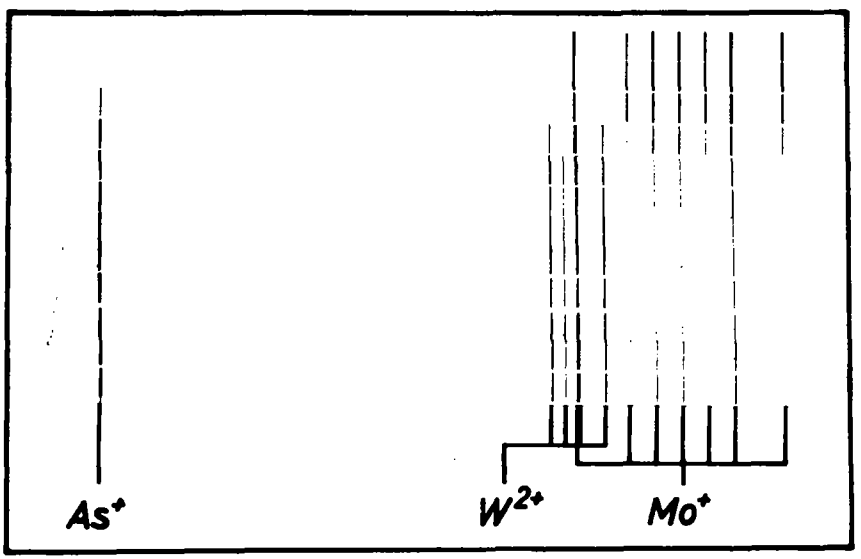
As^+
W^{2+}
Mo^+

Fig. 6

gap, form weakly divergent beams impinging on the anode surface. Small areas of the surface, some µm in diameter, are heated up by these beams and anode material starts to vaporize. Anode vapour is ionized by further field electrons. The gap is increasingly filled with these ions, representing a positive space charge. The space charge very strongly increases the field emission at the cathode. This process is cumulative and eventually diverges, leading to voltage breakdown of the gap. The initiating mechanism of vacuum breakdown has been a subject of speculation. DeGEETER[14] has recently succeeded to photograph anode spots which were heated up by electron streams and which could be held stationary for several hours. Any further minute voltage increase resulted in voltage breakdown of the gap at the glowing anode spots. Breakdown conditions have been calculated[13].

From this model we draw the following conclusions which, however, need further experimental confirmation.

In the r.f.spark, all breakdown phases just discussed rapidly follow each other. The temperature of the anode spot continuously rises, causing a variation of the vapour composition due to the different vapour pressures of the individual components. During the temperature rise of the anode surface, the mean impact energy of the ionizing electrons decreases, as a consequence of the electric field in the gap breaking down, and the acceleration of the ions emerging from the discharge also decreases. Therefore, at the beginning of breakdown, there should be more ions from volatile materials, and the ratio of multiply- to singly-charged ions should be high. Due to the high electric field in this phase, ions are highly accelerated and gain much kinetic energy in this process. As breakdown proceeds, ions of high vapour pressure materials should appear, and the ratio of multiply- to singly-charged ions should be much lower. At this stage, the emerging ions are subjected to lesser accelerations; consequently, their kinetic energies should be low.

The kinetic energy acquired by the ions due to acceleration in the gap shall henceforth be denoted by "primary ion energy", in contrast to the energy of the ions after passing through the acceleration region of the ion source.

Summarizing, amongst the ions of high primary energies we expect ions of volatile materials as well as many ions of high charge number. In contrast, ions of low energies should preferentially consist of singly charged ions. High boiling point materials should dominate.

Experimentally, fig.3 shows the change of intensity of some singly charged ions with different primary energies, as measured by varying the ion accelerating potential. The measurements on the lefthand side of the fig. were performed at an energy pass band of the mass spectrograph of 200 ev. Measurements were made on an iron sample, and normalized to Fe^+-ions. The plot thus depicts the variation of the ratio of the ion concentrations of various ion species to the main constituent (Fe^+) of the ion beam. The curves are arbitrarily displaced in the ordinate, but they are ordered according to the boiling points of the various elements. The plot does not indicate the ratio of the different element concentrations in the sample. It is apparent that volatile components preferentially occur with higher primary energies (about 1 Kev). High boiling point components of the sample favorably appear as ions with low primary energies.

Ions having apparent negative primary energies do not originate in the spark. They are produced from neutral vapour diffused into the acceleration region of the ion source by secondary electron ionization. Since these ions do not traverse the entire acceleration region, they appear at values of accelerating potential which are greater than the transmission energy of the mass spectrograph.

If the energy pass band of the spectrograph is broadened, the intensity changes are smoothed out. The improved accuracy of analyses

Fig. 7

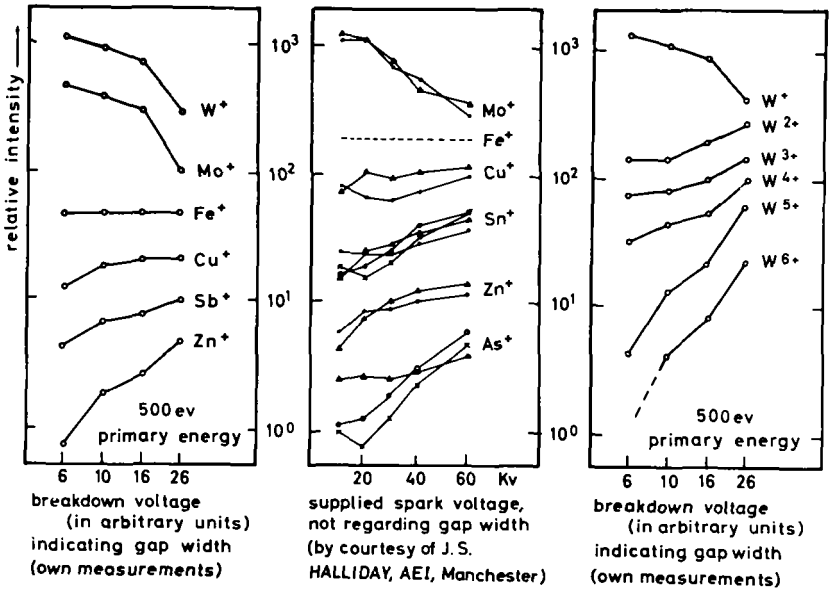
relative intensity
10^3
10^2
10^1
10^0
W+
Mo+
Fe+
Cu+
Sb+
Zn+
500 ev
primary energy
6 10 16 26
breakdown voltage
(in arbitrary units)
indicating gap width
(own measurements)
Mo+
Fe+
Cu+
Sn+
Zn+
As+
20 40 60 Kv
supplied spark voltage,
not regarding gap width
(by courtesy of J. S.
HALLIDAY, AEI, Manchester)
W+
W 2+
W 3+
W 4+
W 5+
W 6+
500 ev
primary energy
6 10 16 26
breakdown voltage
(in arbitrary units)
indicating gap width
(own measurements)

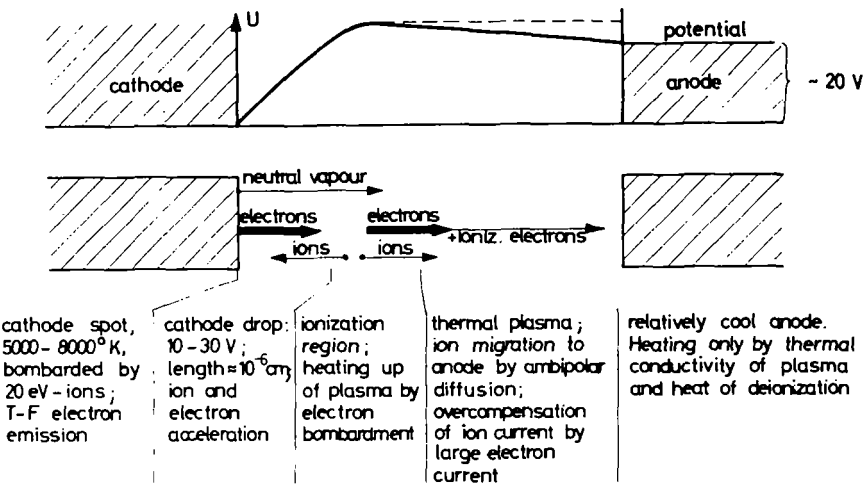
U
potential
cathode
anode
- 20 V
neutral vapour
electrons
ions
electrons
ions
+ioniz. electrons
cathode spot, 5000 - 8000° K, bombarded by 20 eV - ions; T-F electron emission
cathode drop: 10 - 30 V; length ≈ 10^{-6} cm; ion and electron acceleration
ionization region; heating up of plasma by electron bombardment
thermal plasma; ion migration to anode by ambipolar diffusion; overcompensation of ion current by large electron current
relatively cool anode. Heating only by thermal conductivity of plasma and heat of deionization

Fig. 8

reported by HALLIDAY[15] can probably be attributed to the wider energy pass band used. In addition, our measurements were performed employing an ion acceleration system consisting of cylindrical tubes, whereas HALLIDAY used an aperture system made up of a circular hole and a grounded slit arrangement.

Fig.4 shows that, for example, the multiply charged tungsten ions from a stainless steel sample appear at primary energies of about 500 ev, whereas singly charged species preferably have zero primary energy. The corresponding curves of the other elements contained in the steel sample also have the general appearance of those shown in fig.4.- In order to avoid overlapping, the curves are again arbitrarily displaced in the ordinate, and ordered according to their charge. Therefore, the intensity ratios of multiply- to singly-charged ions cannot be taken from the figure. The absolute intensity ratios of multiply- to singly-charged tungsten ions of five primary energies can be taken from fig.5. The portion of a stainless steel mass spectrum displayed in fig.6 indicates the large variation of As^+-, Mo^+-, and W^{++}- ion composition with primary energy. All exposures were made to equal total monitor charge, while the ion accelerating potential was varied for each exposure. The ratio of As^+ to Mo^+ changes as much as a factor of 300 with variations of the acceleration potential by about 600 volts.

From the above curves and from the mass spectrum it is evident that the constancy of the accelerating potential is imperative to avoid these unforeseeable intensity variations. Our 20 Kv- 30 ma power supply used for ion acceleration did not suffice for this purpose, so that a 1 µf condenser had to be connected directly across the high voltage terminals. We have estimated transient loads on the power supply up to 100 ma due to giant ion pulses from the discharge. Although the use of such condensers is rather hazardous, we found that they constituted the only effective remedy, since power supplies with the required short-time regulation (10^{-7} s) had not been available to us. However, even if the accelerating voltage is sufficiently constant, it turnes out that yet another parameter causes intensity variations in the same order of magnitude: the electrode gap width.

Fig.7 shows that with increasing gap width ions of volatile elements become more abundant relative to those of the high boiling point elements. The intensity of multiply charged ions also increases with increasing gap width.

In our own measurements, we controlled the gap width by monitoring the breakdown voltage displayed by an oscilloscope. This voltage was taken from a small antenna loop coupled to the tesla transformer of the r.f.generator. During each measurement, the breakdown voltage was held constant by continuous adjustment of the electrodes from the outside, thus keeping the gap width constant. In fig.7, the change of intensity of different ion species relative to the intensity of the main ion beam constituent (Fe^+) is plotted on an arbitrary ordinate scale.

HALLIDAYS's measurements were obtained in a somewhat different manner. This author did not monitor the gap width but, for each measurement, varied the setting of the r.f.spark voltage, adjusting the gap in accordance with the applied voltage. From HALLIDAY's measurements it cannot unambiguously be deduced whether the observed effects are due to the variation of gap width or to the variation of the applied r.f.voltage. However, we found that neither the ion composition nor the breakdown voltage substantially depended on the setting of the r.f.power supply voltage, provided the gap width remained constant. Therefore, we feel that HALLIDAY's measurements are indicative for the variation of ion composition with gap width, in good agreement with our measurements.

The change of ion composition with gap width can easily be understood by the breakdown concept developed above. If the gap is increased to two or three times its original value, the anode spot assumes its four- or ninefold area, respectively, as a consequence of the

Fig. 9

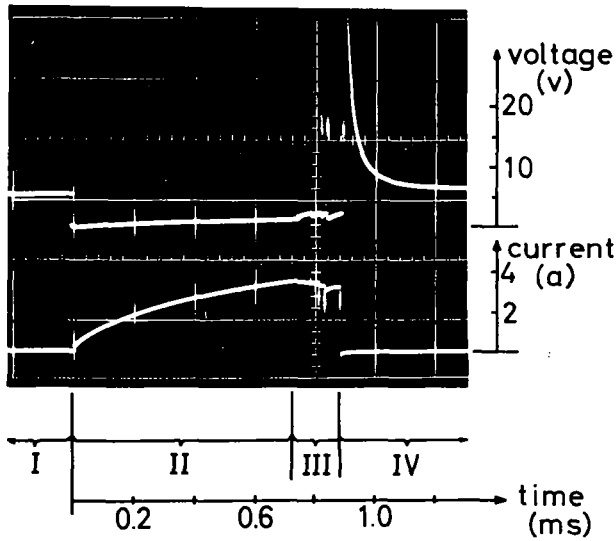
voltage
(v)
20
10
current
4 (a)
2
I
II
III
IV
0.2
0.6
1.0
time
(ms)

Fig. 10

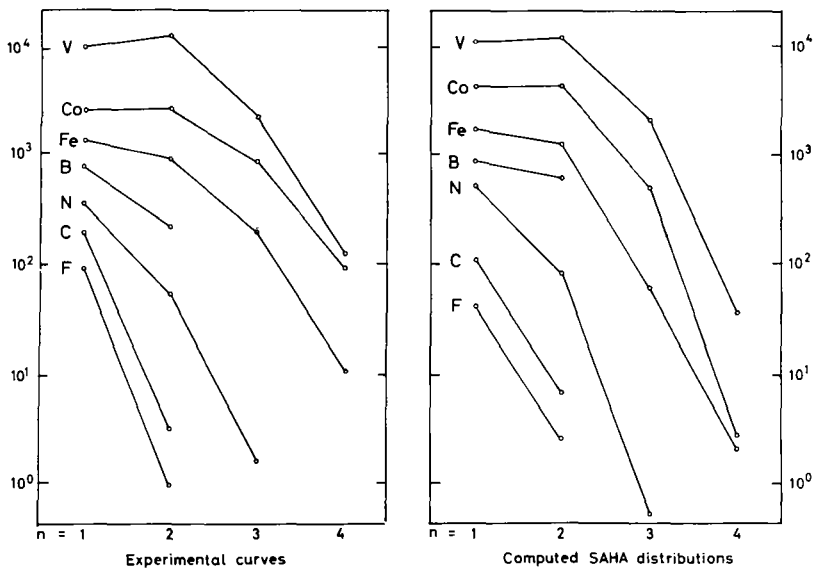
V
Co
Fe
B
N
C
F
10^4
10^3
10^2
10^1
10^0
n = 1
2
3
4
Experimental curves
Computed SAHA distributions

divergent field electron beam. Therefore, with increasing gap width, the power density at the anode spot decreases. The anode spot area heats up more slowly. In addition, wider gaps necessitate more time to become filled with positive space charge. Thus, for largergaps, the pre-breakdown interval as well as the transition interval is longer. According to fig.2, for large electrode gaps, we expect the preferential occurrence of ions of the volatile elements as well as highly charged ions.

b) The Low Voltage Arc

The quasi-stationary nature of the low voltage arc contrasts sharply with the dynamical behaviour of the high voltage spark just discussed. The low voltage arc occurs in the d.c.drawn arc discharge, in the triggered condensed discharge, and in the LASER-ignited discharge. However, unlike the high voltage spark, the low voltage arc always requires some auxiliary initiating mechanism.

In the following, we shall discuss the low voltage arc on the example of the d.c.arc. Here the initiating mechanism of the discharge is generally supplied by the vaporization of a liquid bridge of the electrode material, which is formed when the electrodes are drawn apart[16,8,9].

Fig.8 schematically shows the potential distribution and the various particle currents in the electrode gap of the low voltage arc discharge. The present model was developed using the theory of cathode drops in vacuum arcs by LEE and GREENWOOD[17], and the theory of particle currents in the negative column of a glow discharge by WEIZEL[18]. For reasons of clarity, the dimensions of the drawing are distorted. Actually, the cathode drop is only about one mean free electron path wide and somewhat resembles an electrical double layer.

From a hot cathode spot[16,17], cathode material evaporates. Simultaneously, electrons are extracted from the spot by the field strength existing in the cathodedrop region, a process known as temperature-field emission (T-F-emission)[19]. The electrons are accelerated to about 20 ev in the cathode drop. In the ionization region bordering the cathode drop region, the electrons heat up the cathode vapour by multiple collisions, and generate a plasma, of temperature up to 60000 °K. This plasma is neutral and in thermal equilibrium.

Charged particles within the neutral plasma are set in motion by ambipolar diffusion. The cathode fall boundary as well as the anode surface constitute complete sinks for the ion particle currents. Therefore, the ion particle current separates into two halves, moving in opposite directions: ions directed towards the cathode are accelerated in the cathode drop region and heat up the cathode spot. Ions migrating to the anode are responsible for the net transfer of cathode material to the anode, as observed experimentally.

For a neutral plasma in thermal equilibrium, the distribution of any given element is governed by SAHA's equation, and is uniquely determined by the plasma temperature and the electron pressure[28]:

$$\frac{N_{r+1}}{N_r} = \frac{1}{p_e} \cdot \frac{2 z_{r+1}}{z_r} \cdot \frac{(2\pi m)^{3/2} (kT)^{5/2}}{h^3} \cdot \exp\left[-\frac{eU_r}{kT}\right] ,$$

where

N_r = the number of ions with charge r, per unit volume,
p_e = electron pressure,
z_r = partition function for ions of charge r,
m = mass of electron,
k = BOLTZMANN factor,
h = PLANCK's constant,
T = plasma temperature,
U_r = ionization potential for ions of charge r

Fig. 11

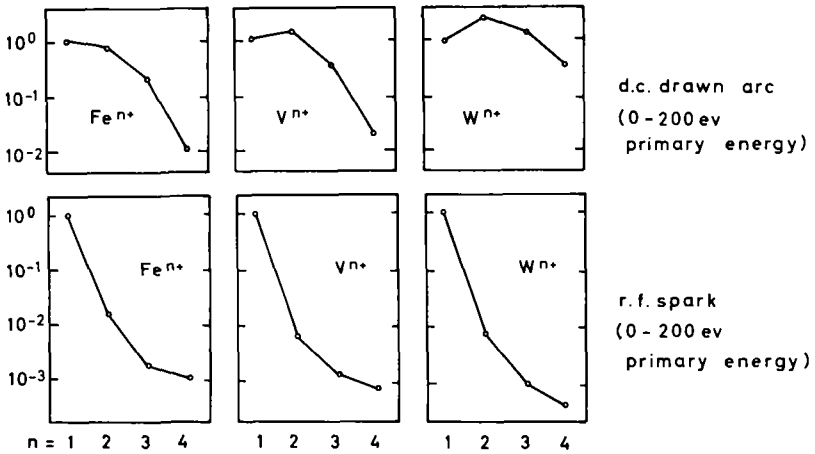
10^0
10^{-1}
10^{-2}
Fe^{n+}
V^{n+}
W^{n+}
d.c. drawn arc
(0 - 200 ev
primary energy)
10^0
10^{-1}
10^{-2}
10^{-3}
Fe^{n+}
V^{n+}
W^{n+}
r.f. spark
(0 - 200 ev
primary energy)
n = 1 2 3 4
1 2 3 4
1 2 3 4

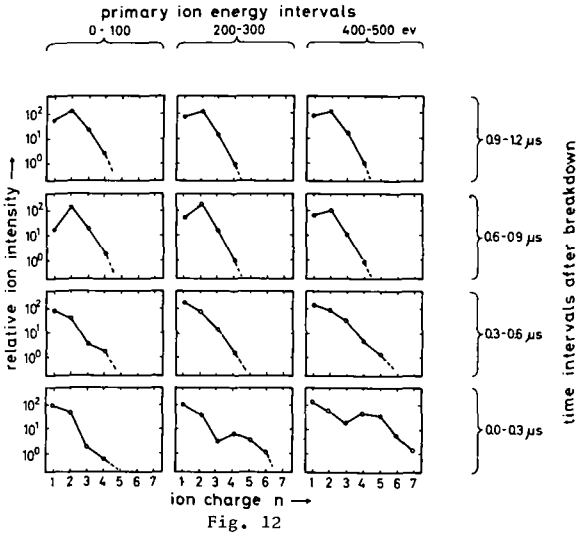
primary ion energy intervals
0 - 100
200-300
400-500 ev
relative ion intensity →
10^2
10^1
10^0
0.9-1.2 μs
0.6-0.9 μs
0.3-0.6 μs
0.0-0.3 μs
time intervals after breakdown
1 2 3 4 5 6 7
ion charge n →

Fig. 12

The electron pressure in the neutral plasma is determined uniquely by the particle vapour pressure and by the degree of ionization in the plasma. The particle pressure in the plasma can be estimated by the vapour pressure of the cathode material at cathode spot temperatures. Cathode spot temperatures are in the order of 3000 to 6000 °K [16], resulting in a vapour pressure in the cathode spot region between 1 and 100 atm. Due to the high temperature in the plasma, the ratio of electrons to the remaining particles is somewhat higher than unity, because of the large number of highly charged particles in the plasma. Therefore, the electron pressure is in the same order as the particle pressure, i.e. between 1 and 100 atm.

In agreement with this model we observed that in the drawn arc ions are preferentially formed from cathode material[20]. Similar observations were made by HONIG et al.[10] on the triggered condensed discharge.

Fig.9 shows a voltage and current oscillogram of one discharge cycle of the d.c.drawn arc discharge between nickel electrodes. Details of the discharge are explained in the figure. We took similar oscillograms with a number of different electrode materials and combinations of different electrode materials. Arc voltages fluctuate statistically above a minimum value. The measured minimum arc voltages agree well with the minimum voltages of arcs burning in gases[16,21]. The value of the arc voltage is determined by the cathode material[16].

According to measurements of similar arcs in gases in optical spectroscopy[22,23], the time necessary to reach thermal equilibrium is in the order of 10^{-8} to 10^{-7} s. Since from our oscillograms the average duration of arc intervals is in the order of 10^{-6} to 10^{-4} s, we considered the notion of the existence of a thermal plasma during the drawn arc discharge. To prove the point, we applied SAHA's equation to the measured distributions of various elements among their ionization states.

Fig.10 shows on the left-hand side for a number of elements the abundance distributions among the observed ionization states[7]. To avoid overlapping, all curves were arbitrarily displaced along the ordinate. Thus, the figure allows only the evaluation of the abundance ratios of ions of the same element. All abundance distributions were taken from a stainless steel mass spectrum, and originated in the same plasma. The distributions are corrected for different line widths, line lengths, and photographic sensitivities. On the right-hand side of fig.10, the computed SAHA distributions of the same elements are given. We started by using the measured intensity ratios V^{++}: V^{+}, and V^{+++}: V^{++} for the calculation of the plasma temperature T and the electron pressure p_e. Then T and p_e were used to calculate all other ratios shown. However, in the present tentative calculations only the statistical weights $g_{r,1}$ of the ground states were employed, and not the complete partition functions

$$z_r = \sum_i g_{r,i} \cdot \exp(eU_{r,i}/kT) \ ,$$

where

z_r = partition function of ions with charge r,
$g_{r,i}$ = statistical weight of the i-th excitation state, for ions of charge r,
$U_{r,i}$ = excitation potential of the i-th excitation state, for ions of charge r.

Neglecting the complete partition functions may lead to large errors when high temperatures are considered. In spite of the rough tentative treatment the experimental and computed curves agree reasonably well, confirming our notion on the existence of a thermal plasma in the low voltage vacuum arc.

We should not conceal that our preliminary approximated computation of the SAHA distributions yielded values of T and p_e too high to be very likely. The calculated plasma temperature was 1.2×10^5 °K, whereas

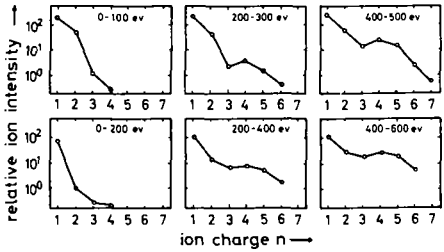

Fe^{n+} from ignition phase of the triggered condensed discharge (0-0.3 μs after breakdown)

W^{n+} from the r.f. spark

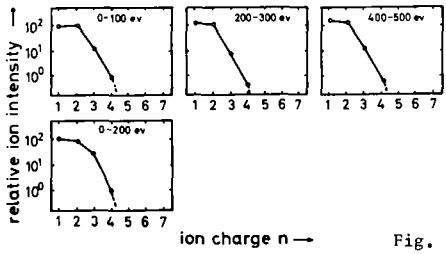

Fe^{n+} from low voltage phase of the triggered condensed discharge (0.9-1.2 μs after breakdown)

Fe^{n+} from the d.c. drawn arc discharge

Fig. 13

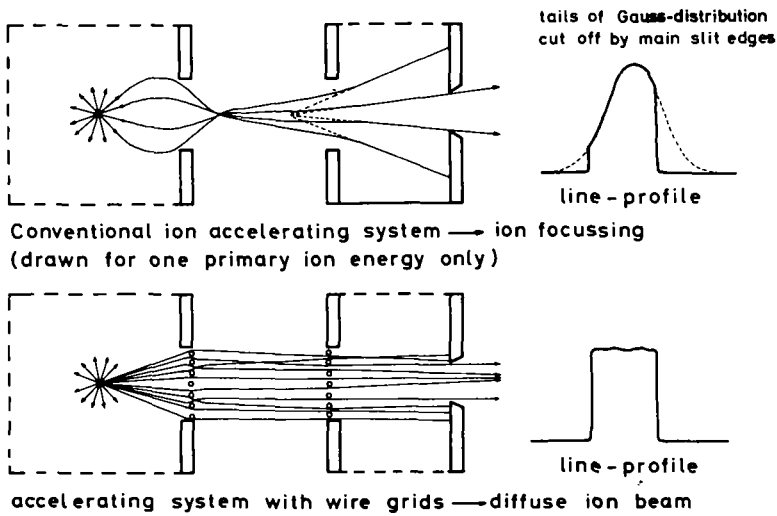

Fig. 14

spectroscopical measurements on comparable arcs in gases yielded temperatures up to 6×10^4 °K only. Our calculations resulted in an electron pressure of 9×10^5 atm, whereas from vapour pressure data we would expect pressures of 1 to 100 atm only. Furthermore, the computed SAHA distributions increasingly deviate from the experimental distributions with higher ion charges.

Calculations in progress at the present time indicate a possible reason for the remaining discrepancies. The temperature of the low voltage arc plasma is not constant in time and space, contrary to what we had anticipated in the computations of the SAHA distributions of fig.10. We hope that we shall obtain much better agreement between experimental and theoretical results when we introduce a weighted temperature distribution, between 2×10^4 and 6×10^4 °K, into our calculations. As an auxiliary result, this method will reduce the electron pressure of the plasma to a more probable value of 10 to 100 atm, as compared to 9×10^5 atm obtained above.

Provided our calculations are successfull, then there is a chance to compute the sensitivity factors of any given element from its SAHA distribution. This would make the analysis of solids with the low voltage vacuum arc standard-independent, and solve the vexatious question of procuring suitable standard samples.

The difference between the high voltage spark and the low voltage arc is apparent from fig.11, where the abundance distributions among their ionization states of Fe, V, and W were measured in discharges between stainless steel electrodes. From the shape of the distributions we assume that the ratio of neutral to charged atoms is, at least for the elements considered, much lower in the d.c.drawn arc than in the r.f.spark.

IV. The Triggered Condensed Discharge

We shall now show that there exist only two basically different types of discharges considered for ion production in this paper. The triggered condensed discharge is particularly useful for this comparison in as much as in this discharge type a high voltage breakdown of short duration ignites the longer low voltage arc.

We have developed a method to both time-resolve and energy-resolve the ions from the triggered condensed discharge. In order to time-resolve the ions, we installed two plane deflection plates (4 by 8 mm area, plate distance 1 mm) between the grounded end of the acceleration region and the main slit of the spectrograph. A voltage of about 100 volts was applied to the plates such that the ion beam passing between the plates was deflected away from the main slit. The platescould be grounded for a short time interval during each discharge. Both the length of the time interval and the delay of the interval with respect to the instant of ignition of the discharge could be adjusted to any given length with an accuracy of better than 10^{-7} s. During the interval, the ion beam passed the main slit. Time-resolution in the order of 10^{-7} s was achieved.

Energy-resolution was obtained by narrowing both the energy slit and the aperture prior to the electric field, thus decreasing the energy pass band of the spectrograph to about 100 ev. Ions of the considered primary energy are analyzed by adjusting the ion accelerating voltage to its respective value.

This method enabled us to expose a single photographic plate with ions having different primary energies, and having originated at different time phases of the discharge.

In fig.12, one such plate has been evaluated. Every spectrum was exposed to equal total monitor charge. The monitored ion currents differed from each other by several orders of magnitude for different exposures. Therefore, arbitrary units are used for each diagram. Thus,

fig.12 only allows to determine the intensity ratios within one diagram. The large difference in the shape of the ionization state distributions between the ignition phase (0 to 0.3 µs) and the low voltage arc phase (0.6 to 1.2 µs) is obvious. For the low voltage phase, we notice a SAHA distribution of ionization states typical for a thermal plasma.

In fig.13, plotted in a similar manner as fig.12, we compare the ionization state distributions of the triggered condensed discharge with those of the r.f.spark and of the d.c.drawn arc. We notice the close similarity between the two kinds of high voltage sparks (above) and the two low voltage arcs (below). However, some ions from the low voltage arc phase of the triggered discharge seem to be superimposed to the ions from the ignition phase, since the ignition phase cannot be clearly separated from the arc.

We should point to the fact that in the case of the low voltage arc there is a minimum change of ion composition with primary ion energy. In addition, the primary energy spread is very low; only very few ions lie in the primary energy interval of 400 to 500 ev. The exposure times required to obtain a distribution in this energy range were extremely long. The currents of 400-500 ev ions were lower by approximately 3 orders of magnitude than the currents of ions within the energy interval 0-100 ev. For the d.c.drawn arc, currents of high energy ions are still lower, and have not been measured until now.

V. Measures to Increase the Accuracy of Analysis

We recognized the variation of ion beam composition with primary ion energy as being one of the main factors influencing the accuracy of analysis. Fig.13 revealed the preponderance of the low voltage arc over the high voltage spark in this respect.

A further advantage of the low voltage arc is the higher total ion current, speeding up analyses. Despite of the increased mean ion currents, the maximum ion density in the beam is lower than in the high voltage spark since the discharge intervals are considerably longer. This leads to improved mass resolution on the photoplate. The r.f.stray fields are reduced by several orders of magnitude. In the thermal plasma of the low voltage arc, the intensity ratios of doubly- and triply-charged ions of most elements to their singly-charged ions are in the order of unity, and are very reproducible.

A disadvantage of the low voltage arc is its limitation to electrode materials of reasonably good electrical conductivity and mechanical rigidity, whereas high voltage spark discharges can sometimes be produced even between insulators when use is made of dielectric displacement currents. In the following, we shall therefore discuss some possible measures to increase the analytical accuracy of the high voltage spark, in particular that of the r.f.spark.

A first measure is to largely increase the energy transmission interval of the mass spectrograph. As shown in fig.3, with an energy pass band of 3 %, the primary ion energy has relatively little effect on the ion beam composition, so that fluctuations of the ion accelerating potential show no striking change of analyses. HALLIDAY thus succeeded in maintaining variations of analyses at about 25 %[15]. In contrast, we obtained mean error factors of 1.4 to 1.8 for an energy pass band of 1 %, with the same sample.

Continuous readjustment of the gap width is necessary to compensate for the consumption of electrode material during sparking. No servomechanism for this purpose is known up to now. In our experiments (fig.7), we employed the spark voltage to manually control the gap width.

The ion acceleration potential must be held as constant as possible. The transient load on the voltage supply may be as high as 100 ma. Therefore, the voltage supply should be powerful, and, if possible, be

equipped with extremely short-time regulation facilities.

To improve the accuracy of analysis, it is also necessary to improve the line profile of the mass lines on the photographic plate over that sufficient for visual and qualitative work. These profiles were found to be influenced by ion source geometry. In order to obtain mass lines suitable for quantitative evaluation, we have developed a new ion source geometry.

VI. Improved Ion Source Design

In a double focusing mass spectrograph, the lines on the photographic plate ought to be true images of the main slit, as a consequence of the first order focusing properties of the apparatus. Thus the lines on the photoplate should show rectangular profiles. Line widths must not increase with increasing exposures, contrary to the lines obtained in optical spectroscopy. However, using very narrow main slits, line profiles differ from the rectangular shape due to second order image defects, and for other reasons, e.g. residual gas scattering.

Rectangular line profiles would considerably reduce errors in photometry and enable more accurate line width corrections. Since often an extremely high mass resolution is not imperative, we attempted to procure such profiles by using wider main slits, up to 100 µm. However, we found that it is insufficient to just widen the main slit, because then not the mechanical main slit is focused on the photographic plate but the individual focal points on the focal line located in the vicinity of the main slit. This results in a profile similar to a standard distribution, cut off at its edges by the main slit, as is shown in fig.14, top portion.

After recognizing these phenomena, we succeeded in obtaining a parallel ion beam by employing curved apertures in the accelerating region of the ion source. This measure gave the desired line profile to some but not all lines of the mass spectrum. However, the analysis proved to be extremely sensitive to changes of the location of the discharge within the discharge chamber, as well as on the angle of rotation of the ion source about the main slit.

In contrast, we found that the design shown in fig.14, bottom portion, gave optimum results. Two wire grids (wire diameter 30 µm, effective mesh size 40 by 40 µm) produce a diffuse ion beam, and nearly rectangular line profiles for all lines of the mass spectrum result. In addition, this design proved to be rather insensitive to all changes of ion source alignments; ion currents are cut down by a factor of about 0.5 by the grids. In our case, we welcomed this ion current decrease since for wide main slits there appears the danger of line broadening due to space charge forces arising in the ion beam, at ion currents in the order of some 10^{-9} amps. The effects of the platinum wire grids on the analyses still remain to be investigated.

References

1 DEMPSTER, A.J., Proc.Am.Phil.Soc. 75, 755 (1935)
Rev.Scient.Instr. 7, 46 (1936)

2 DEMPSTER, A.J., MDDG 370, US Dept.Commerce (1946)

3 DÖRNENBURG, E., PhD-Thesis,"D 77", Mainz,Germany, 1959

4 FRANZEN,J., PhD-Thesis, "D 77", Mainz,Germany, 1963

5 see e.g. R.D.CRAIG et al., in "Advances in Mass Spectrometry", Vol.1, Pergamon Press,London, 1959, p.136

6 WOOLSTON, J.R. and R.E.HONIG, XIth Ann.Meet.ASTM,E-14, San Francisco, 1963

7 SCHUY, K.D. and H.HINTENBERGER, Z.Naturfg.18a, 926 (1963)
Z.Anal.Chem. 197,98 (1963)

8 VENKATASUBRAMANIAN, V.S., and H.E.DUCKWORTH, Can.J.Phys. 41, 234 (1963)

9 SCHUY, K.D., and J.FRANZEN, Reg.Meet.HMS-DPG, Bad-Nauheim, Germany, April 1964

10 HONIG, R.E., S.S.GLASS, and J.R.WOOLSTON, Conf.Paper, VIth Intern. Conference on Ionization Phenomena in Gases, Paris, 1963

11 HONIG, R.E., Appl.Phys.Letters 2, 138 (1963)
Appl.Phys.Letters 3, 8 (1963)

12 FRANZEN, J., and K.D.SCHUY, Reg.Meeting HMS-DPG, Bad-Nauheim, Germany, April 1964

13 BOYLE, W.S., P.KISLIUK, and L.H.GERMER, J.Appl.Phys. 26, 720 (1955)

14 De GEETER, D.J., J.Appl.Phys. 34, 919 (1963)

15 HALLIDAY, J.S., Reg.Meeting HMS-DPG, Bad-Nauheim, Germany, April 1963

16 HOLM, R., Electrical Contacts Handbook, Springer Verl., Berlin 1958

17 LEE, T.H., and A.GREENWOOD, J.Appl.Phys. 32, 916 (1961)

18 WEIZEL, W., Lehrbuch d.theor.Physik, Vol.2, Springer Berlin, 1952

19 LEE, T.H., J.Appl.Phys. 30, 166 (1959)

20 SCHUY, K.D., PhD-Thesis, "D 77", Mainz, Germany, 1963

21 REECE, M.P., Nature 177, 1089 (1956)

22 MANDELSTAM, S., Spectrochim.Acta 15, 255 (1955)

23 KREMPL, H., Z.Phys. 167, 302 (1962)

24 FRANZEN, J., Z.Naturfg. 18a, 410 (1963)

25 PLYUTTO, A.A., Soviet Phys. JETP (USA), 12, 1106 (1961)
Original: J.Exptl.Theoret.Fiz.(USSR) 39, 1589 (1960)

26 WOOLSTON, J.R., and R.E.HONIG, XIIth Ann.Meet. ASTM, E-14, Montreal, Canada, June 1964

27 FRANZEN, J., and H.HINTENBERGER, Z.Naturfg. 18a, 397 (1963)

28 UNSÖLD, A., Physik der Sternatmosphären, Springer-Verlag, Berlin ^{2}1955.

Fig.1 : Some possible sources of error in different phases of mass spectroscopic analysis of solids.

Fig.2 : Proposed qualitative model of high voltage spark mechanism. Ions are preferentially formed from anode material.

Fig.3 : r.f.spark: change of relative ion abundances in the ion beam with primary ion energy. Ions of different primary energies were allowed to pass the energy slit of the mass spectrograph by varying the accelerating potential, keeping the radial field constant. All curves were evaluated from r.f.spark mass spectra of a stainless steel sample. Since all exposures were made to equal total monitor charge, the curves just show the relative abundance change of these singly-charged ions with regard to the main constituent of the beam (Fe^+). To avoid overlapping, the curves were ordered according to the boiling points of the various elements, therefore, only abundance ratios of ions of the same element may be taken from this diagram.

Fig.4 : r.f.spark: change of relative abundances of multiply-charged tungsten ions in the ion beam with primary ion energy. Measurements were obtained from the r.f.spectra used in fig.3. The abundance changes are again plotted relative to Fe^+-ions. In order to avoid overlapping, the curves are arbitrarily displaced in the ordinate, and ordered according to ion charge numbers. The true ratios of tungsten ions of different charge numbers may be taken from fig.5.

Fig.5 : r.f.spark: Abundance ratios of tungsten ions of different charges, for ions of five different primary energies. Values were obtained from the mass spectra used in figs. 3 and 4. To avoid overlapping, the curves were again arbitrarily displaced in the ordinate.

Fig.6 : Portion of one of the plates used in figs. 3,4 and 5, demonstrating the change of relative ion abundances with primary ion energy. All exposures were made to equal total monitor charge. Beginning at the top exposure, the accelerating potential was decreased ba 140 volts for each exposure, from 20.25 to 18.71 Kv.

Fig.7 : r.f.spark: change of the relative ion abundances in the ion beam with electrode gap width. The experimental technique employed to obtain the curves is described in the text. The curves were evaluated from r.f.mass spectra of a stainless steel sample, and give the change of ion abundances relative to the matrix ion (Fe^+). The curves are arbitrarily displaced in the ordinate, and ordered according to the boiling points of the different elements.

Fig.8 : Proposed qualitative model of the low voltage arc discharge mechanism. Ions are preferentially formed from cathode material.

Fig. 9: d.c.drawn arc discharge: simultaneous voltage- and current oscillogram of one cycle of operation of the vacuum vibrator.
I: Electrode contact is open.
II: Contact closed. Metallic conduction. The apparent voltage increase is caused by a small resistor in the arc circuit.
III: Liquid bridge and arc phase. Liquid bridge is interrupted three times by low voltage arcs. Average arc duration 10 µs.
IV: Contact open after cessation of last arc. A induction peak

appears in the voltage oscillogram.

Fig.10: d.c.drawn arc:

left hand side: experimental abundance distributions of some elements among their ionization states. All distributions were taken from a stainless steel mass spectrum. To avoid overlapping, the curves were arbitrarily displaced in the ordinate. Thus, abundance ratios of ions of one element only may be taken from the figure.

right hand side: computed SAHA distributions for the same elements. See text for details.

Fig.11: Comparison of d.c.drawn arc and r.f.spark: abundance distributions of the elements Fe, V, and W among their ionization states, obtained from stainless steel mass spectra. All curves are normalized to the corresponding singly charged ions.

Fig.12: Triggered condensed discharge: energy- and time-resolved abundance distributions of Fe among its ionization states, from stainless steel mass spectra. (Intensities are not corrected for photographic sensitivity in this plotting). Arbitrary units were used for each curve.

Fig.13: Comparison of triggered condensed discharge, with the r.f.spark, and d.c.drawn arc, respectively: abundance distributions among the ionization states of ions originated within different time phases of the triggered condensed discharge are compared with those of the r.f.spark and the d.c.drawn arc. Arbitrary units are used for each curve.

Fig.14: Two ion source geometries, resulting in different line profiles on the photographic plate.

PHOTOGRAPHIC EMULSIONS AS ION DETECTORS IN QUANTITATIVE MASS SPECTROGRAPHY

Edward B. Owens
Lincoln Laboratory,* Massachusetts Institute of Technology
Lexington 73, Massachusetts

HISTORY

The first detection of rays of positive ions was made in 1886 by Goldstein[1] when in conducting experiments with a perforated cathode, he noticed streamers of light behind the perforations. Subsequent investigations by Thompson[2] showed that these streamers or rays normally carried a positive charge. Thompson called the streamers positive rays. As early as 1907, Thompson[3] was detecting the positive rays with screens of powdered willemite which luminesced when struck by the ions. The first use of photography was an indirect use in which Dechend and Hammer[4] in 1910 photographed the luminescent screen. That same year also saw the first direct use of photographic emulsion as ion detector when Koenigsberger and Kutschewski[5] put the plate inside the evacuated apparatus and let the ions strike the emulsion. By 1911, Thompson[6] was using the photographic plate for direct ion detection in his parabola positive ray apparatus.

NATURE OF ION DETECTION WITH PHOTOGRAPHIC EMULSION

When an ion strikes a silver halide grain, electrons are liberated in the silver halide crystal. The halide crystals always contain within the crystal lattice a number of free positive silver ions. The crystals also contain a small number of silver sulfide specks known as sensitivity specks for reasons that will soon be apparent. The electrons that are liberated by the ion collisions diffuse into the silver sulfide specks imparting a negative charge to the specks. The free silver positive ions migrate to the negatively charged sulfide specks and neutralize their negative charges by precipitation as metallic silver. The resultant small deposit of metallic silver on the activated silver halide grain serves as a nucleus in the following reduction of the entire grain by the developing solution.

The gelatine was first thought to serve simply as a means for mechanically suspending the silver halide grains. The permeability of the gelatine permits the chemical components of the developing solution to reach and react with the halide crystals without changing the crystals' position on the plate. It was later found that the gelatine contains trace impurities of sulfur which play a role in providing the active silver sulfide sensitivity specks. The gelatine also plays an important role in determining the sensitivity of an emulsion by limiting the penetration of the positive ions into the suspension of halide crystals. As early as 1921 Thompson[7] realized that the penetration of positive rays into the emulsion was small. He found that the most sensitive plate available at that time was the Schumann plate which contained only enough gelatine to keep the silver halide grains stuck to the plate.

The amount of gelatine in an emulsion and the size of the silver grains affect the nature of the curve relating the response of the emulsion to ion bombardment. With large grains in a gelatine-poor emulsion, a thin coating of the emulsion consists essentially of a layer of grains adhered to the glass plate with gelatine. There is little gelatine shielding the crystals from the on-coming ions. With fine grains, a coating of the same thickness as above consists of a suspension of grains within a layer of gelatine. Some of the fine grains are near the surface, and others lie deeper within the layer and are shielded from the on-coming ions.

Consider now the case of ions striking the surface of a thin emulsion layer which consists of large crystal grains and relatively little gelatine. An on-coming ion may strike a crystal lying on the emulsion surface and relatively free of gelatine covering. The collision alters the grain and makes it developable by the mechanism described previously. On the other hand, it is possible that the ion will not strike a surface grain but land on the gelatine surface instead. If the ion has sufficient velocity, it may penetrate the gelatine until it strikes a crystal grain lying beneath the surface. If the ion has sufficient energy after penetrating the gelatine, the collision will render the grain developable in the same manner as it did the surface grains. In either case, one ion is enough to make one grain developable. If the emulsion thickness is less than the effective penetration range of the ion and if the grains are closely spaced on the plate, it is easy to see that the blackening will be directly proportional to the number of ions per unit area striking the plate. (Here the effective range of an ion is defined

*Operated with support from the U. S. Air Force.

as the maximum depth to which an ion can penetrate and still have sufficient energy to render a crystal grain developable.) Brix[8] has stated that for the thin, gelatine-poor emulsion, this ion-crystal collision is the "primary" blackening mechanism. The maximum darkening caused by this mechanism will be reached when all of the crystal grains lying within the ion penetration range have been struck by ions.

The situation is somewhat different when the ion beam strikes the surface of an emulsion containing more gelatine and fine grains. In this case many of the silver halide grains lie beyond the effective penetration range of an ion. Those grains that are within the ion range are rendered developable by the "primary" blackening process, but those grains lying deeper within the emulsion are darkened by a "secondary" process. Brix[8] concludes that this "secondary" process is due to the light emitted by ion collisions with the gelatine within the outer layers of the emulsion. Thus this secondary process is not due to an ion-grain collision but to luminescence caused by the ion-gelatine reaction. This agrees with an earlier statement by Jakobson[9] that much of the photographic effect of ions is due to light emitted near the surface of the emulsion. In this "secondary" process, one ion does not release enough light energy to render one crystal grain developable. Several or more ion-gelatine collisions are required to make one crystal grain developable. Since the light energy is emitted spherically from the point of collision, there is overlap of areas of influence. A single crystal is affected by a number of ion-gelatine collisions, and the contribution made by a given collision to the developability of a given crystal depends on the energy of the ion upon collision and upon the distance of the grain from the point of collision. The properties of this "secondary" blackening mechanism are quite similar to the effects of light striking the emulsion, and the response curve for this "secondary" mechanism is quite similar to the curves obtained for light photography. Brix has drawn response curves for emulsions which show in order: a threshold, a rising straight line portion for the "primary" blackening, a flattening of the curve to form something of a plateau at the exposure level at which the "primary" mechanism has saturated the outer layers, another rising straight line portion caused by the luminescence from the continued ion exposure, and finally another flattening of the curve as the luminescent light saturates the halides grains lying deep within the gelatine. A fine grain emulsion will have a response curve that combines the simultaneous effects of both the "primary" and "secondary" blackening processes. If a large proportion of the grains lies deep within the gelatine, the "secondary" mechanism will have more effect and contribute more to the combined response curve. It is clear that emulsions can have response curves varying from the pure ion-grain collision type to a form that is very much like light photography response curves. Later in this paper it will be shown how this varying combination of "primary" and "secondary" blackening mechanisms affects other properties of the emulsion.

SENSITIVITY AND SENSITIZATION

As previously mentioned, Thompson learned quite early that the ions did not penetrate very far into the emulsion. He found that the thin layer, gelatine-poor Schumann plates were the most sensitive plates then available. The Schumann plates were so non-uniform that they could not be used quantitatively,[10] and the search continued for other emulsions. In 1919 Aston[11] found that the Paget Half Tone plates were both uniform and sensitive, though not as sensitive as the Schumann plates.

For the thin emulsion, gelatine-poor plates it has already been shown in this paper that in large grain emulsions the grains protrude from the emulsion with relatively little gelatine between the crystal and the on-coming ion. This results in the most efficient use of ions for making crystal grains developable. Consequently, for thin layers it is safe to say that the larger grained emulsions are the most sensitive for ion detection.

One of the first methods of sensitizing plates for ion detection was to remove much of the gelatine from the plate. Aston[12] used such a method which had been reported by Ducleaux and Jeantet[13] to increase the sensitivity of Paget Half Tone plates. The removal of the gelatine made the plates quite similar to Schumann plates and so this method of sensitization was called "Schumannizing". Aston found that Schumannizing did not increase emulsion sensitivity much for light ions but greatly increased the sensitivity for the heavier ions. This is quite understandable since we now know that the effect of an ion depends on its penetrating power, and it has been shown by Bainbridge[10] that lighter particles penetrate deeper into the emulsion. The removal of the gelatine would diminish the effect of differing penetrating power and thereby tend to equalize the sensitivity of the emulsion to light and heavy ions. Bainbridge[10] also attempted to sensitize plates by removing the gelatine with dilute sulfuric acid. He too found that the gelatine removal was especially effective for the heavy ions.

The fact that the luminescence of the gelatine causes blackening leads to the idea that increased sensitivity might be obtained by coating the emulsion with material having especially good luminescent properties. Schönheit[13] sensitized Perutz-Perulith and Perutz-Perenzo plates by dipping them in a benzene solution of Apiezon oil F. After exposure and before development this oil was removed with pure benzene. The unsensitized Perutz-Perenzo was appreciably more sensitive to light and to the ion beam. This is to be expected since the usual properties of a light sensitive emulsion, namely large grains and low gelatine content, are the same properties that favor ion detection. The "primary" blackening mechanism apparently dominates in the exposure of this emulsion. After sensitization with the fluorescent oil the Perutz-Perenzo was still the more sensitive emulsion, but the gain in sensitivity was greater for the Perutz-Perulith (gain factor of 17 for the Perenzo and 76 for the Perulith). This difference in the sensitization effectiveness is also to be expected, since the Perulith depends more upon the "secondary" blackening process, i.e. a luminescent process, and so would be affected more by sensitization which enhances the luminescence.

Rudloff[14] used an indirect sensitization technique reminiscent of the detection method Dechend and Hammer used in 1910 in which they photographed a luminescent screen. Rudloff made a luminescent screen by coating a clear piece of thin glass with a layer of silver activated zinc sulfide. The photographic film, Agfa Fluorapid X ray film, was put directly behind the zinc sulfide screen in the plate holder of the mass spectrograph. It was found that the shape and slope of the darkening curve is independent of the mass of the ion; but the intercept of the curve, and therefore the relative sensitivity are strongly dependent upon mass. At mass two this "sensitizing" system has a sensitivity equal to that of SWR films. The luminescent output decreases sharply with increasing ion mass, and at mass 40 and above the SWR film is the more sensitive. Rudloff states that this silver activated zinc sulfide is the most efficient producer of light of all known luminescent materials.

A system of sensitizing that has been used in light photography is to expose uniformly the total surface of the plate to light before making the exposures for the experiment at hand. This pre-exposure serves to bring the exposure level of the total plate to a point just above threshold level and close to the straight line portion of the response curve. With this prefogging the smallest darkening above the fogged level can be measured more accurately. The effect improves the minimum detection limit if the prefogging produces the density level which optimizes the signal to noise ratio, that is the spectral line to grain fluctuation ratio. The thought that this technique could be applied similarly to ion detection stems from a statement by Bainbridge[10] that for ion detection the effect of exposure of the plate to stray light before use is similar to sensitizing for light photography by prefogging. However, this writer knows of no experiments that have been made to evaluate or use this method of sensitization.

RECIPROCITY LAW

The measuring of relative film darkening to obtain relative exposures assumes that the exposure is truly equal to the product of the light (or ion beam) intensity times the time interval of exposure. That is to say it is assumed the $E = IT$, where E is the exposure, I is the intensity, and T equals the length in time of exposure. This assumption is called the Reciprocity Law; and if it is valid, doubling the time of exposure for a given intensity would have the same effect as doubling the intensity while keeping the exposure time constant. It has long been known that this reciprocal relationship between time and intensity does not hold for many of the emulsions used in light photography. Schwarzschild found that a general expression for the relationship was that $E = IT^{\rho}$, exposure is equal to the intensity multiplied by the exposure time to the rho power. If for a given emulsion rho is equal to 1, the reciprocity law is valid. If rho is much different from 1 the reciprocity law is said to be invalid, and we have reciprocity failure.

The previous discussion of emulsion blackening caused by ion bombardment can now be extended to the consideration of the reciprocity law. It has been shown that for emulsions in which the "primary" blackening mechanism is predominant, one ion collision is sufficient to render the total grain developable. The nearest neighboring crystal will not be made developable until it too suffers an ion collision, and it makes no difference whether the two grains were hit at the same time or many seconds apart. It is reasonable to predict, therefore, that those emulsions for which the "primary" mechanism is dominant will obey the reciprocity law. On the other hand, we have seen that for the "secondary" blackening mechanism more than one ion collision is required to render a single crystal grain developable. Since the effect is accumulative, it seems quite likely that the rate at which the luminescent energy is accumulated may be significant. This appears even more probable for the luminescent phenomenon when it is remembered that many emulsions have shown reciprocity failure in light photography. So, it seems that the degree to which an emulsion obeys the reciprocity law depends upon the relative contribution of

the "primary" and "secondary" blackening to the overall emulsion response. Some data for individual emulsions will be given at a later point in this paper.

CHOICE OF EMULSION FOR ION DETECTION

The choice of emulsions to use for ion detection should be based upon the general emulsion characteristics that have been reviewed in this paper. High sensitivity requires large silver halide grains, a low gelatine content, and a thin emulsion layer on the plate. Since the large grains impart a grainy appearance to the spectral lines, a finer grain emulsion might be desired for high resolution work. This better image resolution would be obtained at the expense of some sensitivity. It is preferable to use an emulsion that obeys the reciprocity law; but for those that do not, appropriate calibration enables one to evaluate and correct for the reciprocity failure. Better uniformity has been achieved generally with medium and fine grain emulsions, but again this is done with the loss of some sensitivity. The choice of the latitude of the emulsion (that is the difference between the threshold and the saturation exposure levels) will depend upon the intended use. A wide latitude is desirable for general survey analyses covering many orders of magnitude of concentrations. A smaller latitude with its steeper response curve will give better quantitative results. The single emulsion ideally suited for all purposes is impossible since some of the desirable characteristics are mutually exclusive. Some of today's emulsions are compromises, and some are designed to favor one characteristic at the expense of the other.

The number of emulsions suitable for ion detection is somewhat limited today. A review of mass spectrographic papers published during the past ten years shows only five different emulsions being used. The properties of these five emulsions have been compared in an excellent paper by Rudloff.[14] The five emulsions are the three Ilford Q plates, Eastman SWR, and Agfa Schumann plates.

The Ilford Q emulsions are by far the most widely used for ion detection today. The Q_1 emulsion has low speed, fine grains, and high contrast; Q_3 has high speed, large grain, and low contrast; and Q_2 has properties somewhere between those of Q_1 and Q_3. According to Rudloff[14] and Franzen and Hebeda[15] all three Q emulsions obey the reciprocity law. Despite the popularity of the Ilford Q plates it may be that the Eastman SWR emulsion is superior. According to Rudloff's report SWR is about equal to the Q emulsions in threshold exposure level (minimum detection limit) but superior in the slope and latitude of the response curve.

In the last several years this writer has heard a number of complaints about the lack of uniformity in the Ilford Q_2 plates. Upon inquiry, Ilford Inc. has stated[16,17] that the non-uniformity was found only in the field of low ion exposures. When they heard of these complaints Ilford investigated the problem and started a project to modify the Q_2 emulsions to meet the new, more exacting requirements. As a result, Ilford has recently made available new Q emulsions which they state are suitable for low ion exposures and which have lower background fog, higher sensitivity, higher maximum density, and better keeping qualities than the previous unimproved emulsions. These new emulsions completely supersede the old Q emulsions and will be supplied on all future orders for Ilford Q plates. The new Q_2 emulsion has been tested by Guthrie,[18] who found that compared with the previously supplied Q_2, the new Q_2 emulsion had lower and more uniform background fog, more contrast, about equal maximum density, and greater dynamic range.

DARKROOM PROCESSING

The best general rule about developing plates is to follow the instructions of the emulsion manufacturer, but it should be emphasized that controlled developing procedures are essential for quantitative or even semi-quantitative work. The parameters that must be controlled are the strength and temperature of the developing solution, the time duration of development, and the agitation of the plate or solution during development. A paper by this writer[19] describes a simple, homemade apparatus to accomplish this control. There are a number of satisfactory plate processors commercially available, although most of the commercial processors are limited to a plate length of up to 10 inches and cannot be used for the 15 inch plates used in some mass spectrographs.

The Ilford Company[20] recommends that the Q plates be developed in ID-19 for 3 1/2 to 5 minutes at 20°C, or in ID-13 for 2 1/2 to 3 minutes at 20°C. Recent work by Woolston[21] shows the effect of increased developing time and temperature. Woolston's data show that increasing either the temperature or the developing time shifts the response curve toward lower exposures without markedly changing its slope or shape. The change of developing conditions from 3 minutes at 68°F to 10 minutes at 68°F increased the sensitivity by a factor of 3. Going from 3 minutes at 68°F to 6 minutes at 75°F also gave a gain of a factor of 3. In both changes there was only a slight increase in the gamma of the calibration curve. The increase in fog was barely perceptible.

Because of their thinness the emulsions used for ion detection do not require as much fixing and washing as do the emulsions used for light photography. Ilford recommends that one-third to one-half the fixing and washing times allotted for ordinary plates be used for Ilford Q plates. Excessive fixing will decrease the image blackness.

EMULSION CALIBRATION

The degree of darkening of a spectral line cannot be used to determine the number of ions causing that line unless the emulsion has been calibrated. It is desirable that the calibration cover the exposure range from barely measurable images to just below film saturation. The data for calibration are usually obtained by putting on a single plate a series of spectral lines having known relative exposure values. Lichtblau and Mattauch[22] used a source that generated a steady source of ions, I, and varied the exposure duration, t, to obtain the required known variation in exposure, I x t. This is an excellent method if one has the steady source of ions and if the emulsion obeys the reciprocity law. Mattauch and Ewald[23] used a single exposure of the hafnium isotope pattern. The known relative abundance of the isotopes gave the required relative exposures. There are only six elements with enough isotopes covering the range of abundance desired for this purpose. This method is satisfactory except that it is difficult to cover adequately the full latitude of an emulsion with six or seven points. Geerk and Brix[24] and Hickam[25] have used a stepped aperture at the entrance to the magnet section to obtain the desired relative exposures. This method is open to grave doubt because it requires a) that the image width (i.e. line width) on the plate remain constant while the aperture width varies by a factor of as much as ten, and b) it assumes that the ion beam is of uniform density over the height and width of the total stepped aperture. Geerk and Brix used this system on a Thompson parabolic spectrograph and measured the ion beam coming through each step. These measured values were the data used in emulsion. Hickam used the step aperture on the Mattauch-Herzog double focusing instrument.

Some workers have obtained their calibration data by using the total ion beam monitor to measure the relative exposure. Dörnenburg and Hintenberger[26] state that the ion beam monitor generally is not precise enough for this and have used the relative abundance values of carbon polymers for calibration data. A somewhat similar method used by Duke[27] and this writer[28] is based on the two-line technique described by Churchill[29] for use in optical spectrography. The calibration data for the two-line method in mass spectrography are obtained by measuring the lines of two isotopes of a given element in a series of exposures ranging over the total emulsion latitude. The element is chosen so as to have two isotopes with an abundance ratio between 1.2 and 2.0. This writer prefers this two-line method for several reasons. First, as many points as desired can be obtained for the calibration curve by simply having one spectrum for each point. Second, many elements have isotopes with the appropriate abundance ratio, and the calibration data can often be extracted from the spectra of the sample being analyzed. Third, reciprocity law validity is not required.

All of the above calibration methods show the relationship between relative exposure and film response. Any of these methods can be made absolute if the absolute number of ions forming one of the spectral lines can be determined accurately. A method for making this measurement is illustrated in Fig. 1. The apparatus permits the electrometric measurement of one isotope of a given element while another isotope of the same element falls upon the photographic plate.

The relationship between exposure and emulsion darkening has been shown in a number of ways. The darkening of the plate has been expressed in units of transmission - T, opacity - O, optical density - D, darkening (schwarzung) - S, and Seidel function Δ. Considering the definitions of these units and the fact that they all are concerned with the same physical measurements, it is easy to see that all of the units are interrelated and that any one is as valid as any other. Table I shows the definition and interrelation of these units. The only basis for preference among these units is ease of handling, either graphically or mathematically. For example, the relationship reported by Hull[30]

$$E_x = \left(\frac{1 - T_x}{T_x - T_\infty}\right)^{1/R}$$

(where E_x is the exposure causing a line whose transmission is T_x, T_∞ is the transmission of the saturated emulsion, and R is an experiment constant between 1 and 1.5) has been used by Woolston[21] in a computer program which converts relative transmission measurements into concentrations.

DENSITOMETRY

The densitometric measurement of the spectrum on the photographic plate is quite straightforward with the usual precautions to be observed. The densitometer slit should be not wider than one-third the width of the smallest spectral line to be measured. A wider slit would cause error in the measurement of line width. The rate of scan on the densitometer should be chosen so that the limit imposed by the response time of the recorder does not decrease the peak reading for sharp, dark lines. The appropriate scan time can be determined by making repeated scans of a sharp, dark line increasing the scan rate one step each scan. All scan rates will give the same peak value until the response time limitation is exceeded. The fastest scan to be used is the fastest rate that gave a peak deflection that agreed with those obtained with slower scan rates.

A common practice among spectrographers is to set the gain on the densitometer so as to obtain full scale deflection (100% transmission) for the clearest area of the plate. This is valid only for the rather limited case in which the general fog level of the plate is low and is approximately equal to the fog level that existed on the plate from which the calibration data were obtained. When these criteria are not met, the correct technique is to adjust the gain to give 100% transmission for the plate whose transmission is equal to or less than the lowest fog ever encountered on your plates. Rudloff[14] used for this purpose an unexposed plate which had been fixed and washed but had not been in the developer solution. A constant setting of the gain for the setting of the zero transmission can be obtained by putting an opaque plate in the light path of the densitometer. Use of these constant, reproducible densitometer settings makes all of the data compatible regardless of fog level. It is theoretically unsound to attempt to correct for variations in fog and spectral background by varying the densitometer gain to give 100% transmission at the fog or background level. Measuring transmission while varying the densitometer is analogous to measuring length with a rubber ruler; increasing the gain stretches the ruler. In addition, the pronounced curvature at the lower part of the H and D curves makes the analogy that of measuring with a rubber ruler that does not stretch uniformly over its length.

CALCULATIONS

Several corrections must be made on the data obtained from the above calibration and densitometer procedures before relative darkening of two lines can be related to the relative numbers of ions causing the two lines. Corrections must be made for background, line width, effect of ion energy on sensitivity, and effect of ion mass on sensitivity. Lichtblau and Mattauch,[22] and Dornenburg and Hintenberger[26] corrected for line width by using the theoretical relationship that the line width increases with the square root of the mass. This relationship is based on the design characteristics of the Mattauch-Herzog double focusing spectrograph and presumes perfect focusing and no line broadening from space charge or scatter. This writer prefers the method that he recently published with Giardino[28] in which the line is always measured and the width is taken from the densitometer trace at the one-half exposure level. The instrument can be out of focus and no theoretical design features need be known, since all line broadening effects are measured in the line width measurement and automatically corrected for.

Lichtblau[31] made background corrections by subtracting the optical density of the background from the optical density of the line. Brix[8] subtracted the blackening, S, of the background from the blackening of the line and stated that this method caused only 2% errors. Subtraction of neither optical densities nor blackening is theoretically correct, since these are not linear functions, although such practice may cause only small errors. The theoretically correct method has been used by Mattauch and Ewald[23] and by Owens and Giardino.[28] In this method the exposure causing the background is subtracted from the exposure causing this line after the non-linear densitometer readings have been converted to linear exposure values by means of the calibration curve.

It has been shown by various workers (8)(10)(28)(32)(34) that the sensitivity of an emulsion to ion bombardment increases with increasing ion energy. The data of Owens and Giardino[28] indicate that the photographic response for Ilford Q_2 is directly proportional to the ion energy. Within a single spectrum this energy correction is applied only to the multi-charged ions, since the singly charged ions all have approximately the same energy.

A number of papers (10)(28)(31)(33)(34) have reported on the effect of ion mass on emulsion sensitivity. The relative sensitivity of Q_2 emulsion to ions is approximately inversely proportional to the square root of their masses. Fig. 2 shows the fit of the data to the $S = M_{Pt}/M$ function. The intensity of constant Pt exposures was used for normalization. It can be seen from the figure that the correction for mass is appreciable.

THE INFLUENCE OF THE DETECTOR ON ANALYTICAL RESULTS

The discussion up to this point has not dealt with analytical results. Instead, the concern has been with the ability of the photographic plate to detect ions and the proper method whereby the photographic image is used to determine the number of ions that created that image. Now let us consider the relationship between the detector and the analytical results obtained in mass spectrography.

As previously stated, the apparatus shown in Fig. 1 makes possible the absolute calibration of the photographic plate. Using this system this writer has determined that with ions of mass of 100 a.m.u. and energy of 15,000 e.v., about 10^5 ions per sq. mm. are required to make a detectable image on Ilford Q_2 plates - this is the Q_2 emulsion before the recent improvements were made. The lines measured for these ions actually had an area of about 0.1 sq. mm. So the minimum detectable line was caused by 10^4 ions landing on the area of the line. If the total number of ions reaching the detector is 10^{13}, this particular line represents 1 part in 10^9 sensitivity. If all of the ions generated from a given element in the sample fall in this one line, this element can be said to have a one part per billion sensitivity in an exposure of 10^{13} ions. Most elements have several isotopes; and if the most abundant isotope has an abundance of 25%, 4×10^4 ions of that element will be required to put 10^4 ions at the position of the strongest line for the element. This element has a sensitivity of 4 p.p.b. in a 10^{13} ions exposure. It has been shown that the emulsion is more sensitive to lighter ions. Consequently, in a 10^{13} ions exposure boron may have a sensitivity of 0.3 p.p.b. compared with an indium sensitivity of 1 p.p.b. in the same exposure. Since the emulsion darkening depends on the number of ions per unit area of the plate, it follows that more ions are required to make a wide line detectable than for a narrow line.

All of the above assumes that all elements are ionized with equal efficiency. It has been shown that this assumption is only approximately true. However, this is not a problem associated with the detector. The sensitivity of the detector can be and has been stated in precise terms. The conversion of detector sensitivity to analytical sensitivity requires that all of the above factors be considered.

Much the same statement can be made about analytical accuracy. Valid calibration techniques have been described, and it has been shown[23,28] that with these techniques isotope ratios can be determined to within a few per cent of the known values. However, the overall errors in an element concentration determination must include ionization efficiency, ion transmission of the instrument, as well as ion detection. It is this writer's opinion that the detection errors constitute a small part of the total analytical errors experienced in solids mass spectrography today.

TABLE I

I_o = incident light

I_t = light transmitted through image

I_s = light stopped by image

Transmission, $T = \frac{I_t}{I_o}$

Opacity, $O = \frac{I_o}{I_t} = \frac{1}{T}$

Optical Density or Density, $D = \log \frac{1}{T} = -\log T = \log \frac{I_o}{I_t}$

Blackening or Schwarzung, $S = \frac{I_s}{I_o} = \frac{I_o - I_t}{I_o} = 1 - T$

Seidel Function, $\Delta = \log \left[\left(\frac{1}{T}\right) - 1 \right] = \log (\text{Opacity} - 1)$

Units Used in Densitometry

REFERENCES

1. Goldstein, Berl. Ber. 39, 691 (1886).
2. J. J. Thompson, Rays of Positive Electricity and their Application to Chemical Analysis, (Longmans, Green, 1913).
3. J. J. Thompson, Phil. Mag. 13, 561 (1907).
4. Dechend and Hammer, Proc. Heidelberg Acad. Sci. 21, 12 (1910).
5. Koenigsberger and Kutschewski, Physikal Zeitschrift 11, 666 (1910).
6. J. J. Thompson, Phil. Mag. 21, 225 (1911).
7. J. J. Thompson, Rays of Positive Electricity, second ed., p. 4 (1921).
8. P. Brix, Z. Phys. 126, 35 (1949).
9. Jakobson, quoted in Bainbridge (10).
10. K. T. Bainbridge, J. Franklin Inst. 212, 489 (1931).
11. F. W. Aston, Mass Spectra and Isotopes (Arnold, 1941) second ed., p. 87.
12. F. W. Aston, Proc. Camb. Phil. Soc. 22, 548 (1925).
13. E. Schönheit, Die Natunwirrenschaften 9, 278 (1957).
14. W. Rudloff, Z. Naturforschg. 17a, 414 (1962).
15. J. Franzen and E. Hebeda, Z. Naturforsch 17a, 476 (1962).
16. J. V. Baccoli, Jr., Ilford Inc., New York, private communication, April 1964.
17. J. A. Zimmer, Ilford Inc., New York, private communication, April 1964.
18. J. W. Guthrie, Sandia Corp. Report SC-DC-64-262, Sandia Laboratory, Albuquerque, New Mexico (April 1964).
19. E. B. Owens, Rev. Sci. Instr. 32, 1420 (1961).
20. Ilford, Ltd., London, Tech. Inform. Sheet B, 524 (April 1953).
21. J. R. Woolston, RCA Laboratories, Princeton, New Jersey, private communication, January 1964.
22. H. Lichtblau and J. Mattauch, Z. Phys. 117, 502 (1941).
23. J. Mattauch and H. Ewald, Naturwiss. 41, 487 (1943).
24. J. Geerk and P. Brix, Z. Phys. 125, 767 (1949).
25. W. M. Hickam and G. G. Sweeney, A.C.S. Meeting, Washington, D. C. (March 1962).
26. E. Dornenburg and H. Hintenberger, Z. Naturforsch 16a, 676 (1961).
27. J. F. Duke, Ultrapurification of Semiconductor Materials, M. S. Brooks and J. K. Kennedy, eds., p. 279 (Macmillan, New York, 1962).
28. E. B. Owens and N. A. Giardino, Anal. Chem. 35, 1172 (1963).
29. J. R. Churchill, Ind. Eng. Chem., Anal. Ed. 16, 653 (1944).
30. C. W. Hull, 10th Mass Spectrometry Conf., New Orleans, La. (June 1962).
31. H. Lichtblau, Z. Phys. 41, 82 (1940).
32. P. Brix and H.-G. Dehmelt, Z. Phys. 126, 728 (1949).

33. E. Burlefinger and H. Ewald, Z. Naturforsch 16a, 430 (1961).

34. E. Burlefinger and H. Ewald, ibid 18a, 1116 (1963).

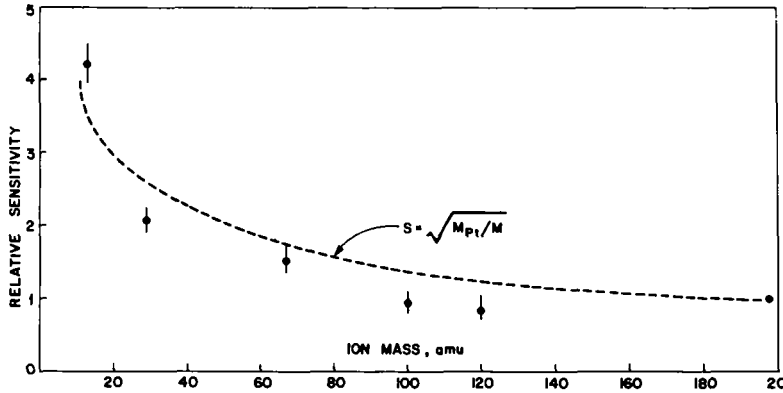

Fig. 1 Technique for Absolute Calibration

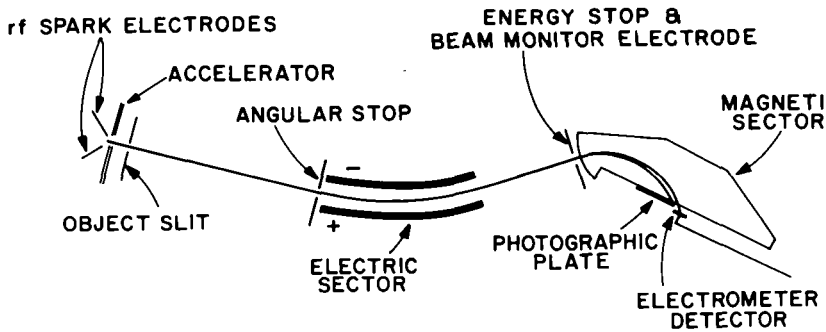

Fig. 2 Photographic Sensitivity vs Ion Mass

MASS SPECTROGRAPHIC MICROPROBE ANALYSIS

W. M. Hickman and G. G. Sweeney
Westinghouse Research Laboratories
Pittsburgh 35, Pennsylvania

The high sensitivity, wide elemental coverage, and large concentration range achievable with the spark source mass spectrograph make it a useful tool for microanalysis. The usefulness of the instrument as a microprobe depends upon the controlled sampling and analysis of specified small volumes of various geometries.

A study has been made of microsampling and analysis using three electrode configurations: (1) stationary point to stationary plane sample, (2) stationary point to manually translated plane sample, (3) stationary point to a 200 cm/sec translated plane sample. The use of each of the configurations as a source for a mass spectrographic microprobe will be described.

Special consideration will be given to configuration (3) with which sampled depths of the order of 2000 A are achieved. Electronmicrographs of the sampled geometry provide information on the spark operation. The technique offers a number of advantages in analyzing thin films.

MASS SPECTRA OF ORTHO-SUBSTITUTED DIARYLMETHANES

by

Seymour Meyerson

Research and Development Department, American Oil Company

and

H. J. Drews and E. K. Fields

Research Department, Amoco Chemicals Corporation

Whiting, Indiana

ABSTRACT

Mass spectra of ortho-methyldiarylmethanes show a characteristic intense peak corresponding to the rearrangement:

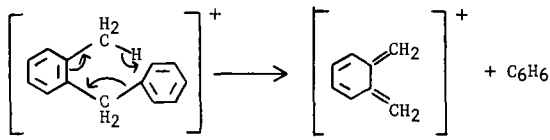

Precise parallels occur in the spectra of ortho-hydroxydiarylmethanes and ortho-methyldiaryl ethers. The reaction is another member of a large class of ionic unimolecular rearrangement-dissociation processes that are highly sensitive to molecular structure and insensitive to interchange of O, CH_2, and other such atoms and groups.

* * * * * * * *

Among the prominent features of mass spectra of hydrocarbons generally -- and for that matter, of derivatives containing any of the common heteroatoms other than nitrogen -- is a pattern of alternating intensities: high at odd mass numbers, low at even. This pattern has been rationalized on the basis that hydrocarbon ions of odd mass number contain even numbers of electrons that can be paired to yield relatively stable configurations.[1,2] Ions of even mass number, on the contrary, contain odd numbers of electrons and so are all free radicals. Moreover, a fragment ion arising by fission of a single bond in a hydrocarbon molecule necessarily has an odd mass number. Formation of a fragment ion of even mass number must involve fission of at least two bonds and often bond-making also; thus entropy considerations might well discriminate against such ions. Against this background, any even-mass-number peak of intensity close to or greater than that of adjacent odd-mass-number peaks is anomalous and suggests that some special factors favor the reaction giving rise to the ion in question. Investigation of such rearrangement-dissociation processes -- analogous to the photochemist's "molecular" decompositions -- has proved especially fruitful in revealing underlying relationships between mass spectra and molecular structure, and thus in facilitating construction of a systematic chemistry of gaseous ions.[3,4] Incidentally, many of these processes find close parallels in radiolytic, photolytic, and pyrolytic systems.[3]

Such a process was indicated by an intense even-mass-number peak in the spectra of products from pyrolysis of ortho-methyldiaryl sulfones. These sulfones eliminate sulfur dioxide on pyrolysis to give hydrocarbons composed of the elements of the two aryl groups.[5] Spectra of the first two such products investigated, those derived from dimesityl and di-para-xylyl sulfones, clearly ruled out the originally suspected biaryls. The spectrum of the former showed an intense peak at mass 132, corresponding to a $C_{10}H_{12}^+$ ion; that of the latter showed a similarly intense peak at 118, corresponding to $C_9H_{10}^+$. Each of these ions contains one carbon atom more than an aryl group of the original sulfone; thus, the two aryl groups appeared to be bonded via a side-chain carbon atom rather than directly. Further investigation confirmed the diarylmethane structure so inferred. Moreover, the products from pyrolysis of dimesityl and di-para-xylyl sulfones were both found to be ortho-methyldiarylmethanes and the decomposition process that gave rise to the $C_{10}H_{12}^+$ and $C_9H_{10}^+$ ions, to be characteristic of this class of compounds.

Table I shows partial spectra of diphenylmethane and ten methylated derivatives. Included in the spectra are the parent and parent-less-CH_3 ions and all fragment ions of even mass number having intensities greater than 35% that of the parent ion. In the unsubstituted compound, the parent ion yields the most intense peak. In the derivatives, loss of CH_3 -- to give most likely a phenyltropylium ion, by analogy with loss of CH_3 from xylene to give tropylium[6] -- produces an intense peak, often the most intense in the spectrum. Relative intensity of the parent-less-CH_3 ion is markedly higher in the spec-

TABLE I - PARTIAL SPECTRA OF METHYLATED DIPHENYLMETHANES $ArCH_2Ar'$

Positions of Methyl Groups in:												
	Ar	--	2	2,4	2,5	2,6	3,4	2,4,6	2,5	3,4	2,4,6	2,3,4,5
	Ar'	--	--	3	4	3	2	4	3,5	3,4	3,5	2,3,4,5
Molecular Weight		168	182	210	210	210	210	224	224	224	238	280
Mass	Ion											
Parent	Parent	100.0	100.0	100.0	100.0	100.0	100.0	100.0	100.0	100.0	100.0	100.0
Parent less 15	Parent less CH_3	14.2	134.	159.	159.	133.	139.	159.	130.	218.	130.	114.
104	$C_8H_8^+$	--	46.4	--	--	--	140.	--	--	--	--	--
118	$C_9H_{10}^+$	--	--	40.9	96.6	89.8	--	--	107.	--	--	--
132	$C_{10}H_{12}^+$	--	--	--	--	--	--	95.6	--	--	88.7	--
146	$C_{11}H_{14}^+$	--	--	--	--	--	--	--	--	--	--	229.

TABLE II - LABEL RETENTION IN $C_8H_8^+$ FROM 2-METHYL-d-DIPHENYLMETHANE

A. Partial spectra, 70 e.v.

Mass	Ion[a]	Unlabeled Relative Intensity	Labeled Relative Intensity
103	$C_8H_7^+$	8.5	3.6
104	$C_8H_8^+$	47.4	19.6
105	$C_8H_9^+$	11.0	30.5
106	...	...	10.6
Parent	$C_{14}H_{14}^+$	100.0	100.0

Retention = 30.5/47.4 = 64%

B. Voltage dependence at electron energies near appearance potential.

Nominal electron energy, e.v.	8.5	8.9	9.4	9.8	10.2	10.6
Peak height, arbitrary scale units						
104	0.3	0.8	1.2	1.9	2.7	3.7
105	1.0	1.7	2.3	3.7	5.3	7.3
Label retention, %	83	68	66	66	66	66

[a] Formulas listed correspond to unlabeled ions of indicated masses.

trum of the 3,4,3',4'-tetramethyl compound, the only one with no ortho substitution, than in any of the other spectra studied. The reason lies apparently in the absence of competition in this one case from the rearrangement-dissociation process evidenced by intense even-mass-number peaks. One such peak appears in the spectrum of each ortho-substituted compound. In each case it has a mass 13 units greater than that of the original ortho-substituted aryl group. Moreover, in each case the spectrum contains a metastable peak[3] that establishes the parent ion as an immediate precursor of the even-mass-number fragment ion.

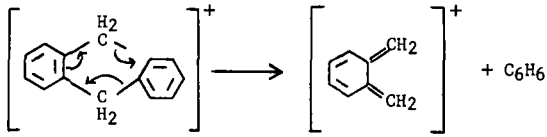

To confirm the ortho-methyl group as the source of the migrating hydrogen atom, we measured the spectra of ortho-methyldiphenylmethane unlabeled and singly deuterated in the methyl group. The pertinent spectral data, given in Table II, show that deuterium retention in the $C_8H_8^+$ ion is 66%, in agreement with the value expected if the migrating atom comes solely from the methyl group and no isotope effect is involved.

The precise structure written for the resultant ion is arbitrary; it could be formulated just as plausibly as benzocyclobutene. The structure of the apparently similar $C_8H_8^+$ ion produced by loss of C_2H_4 from tetralin is also not certain, but available data furnish some basis for a choice in that case. The dominant primary decomposition reaction of 2-methyltetralin under electron impact is loss of C_3H_6 to give $C_8H_8^+$, the same product as in the unsubstituted compound; that of 1-methyltetralin, on the contrary, is loss of CH_3, with loss of C_2H_4 appearing as a minor competing process.[7] Thus, loss of C_2H_4 from tetralin almost certainly occurs by rupture of the two β carbon-carbon bonds. An energetics argument, based on the appearance potential of the $C_8H_8^+$ ion in the spectrum of tetralin, has been advanced for the ortho-quinodimethane structure in preference to that of benzocyclobutene.[8] Elimination of ethylene from tetralin is most simply formulated as occurring by a reverse Diels-Alder reaction, apparently a favored path in molecules that satisfy the structural requirements.[9-11]

The even-mass-number peak that distinguishes ortho-substituted from non-ortho-substituted diarylmethanes has a precise parallel in diaryl ethers.[12] The underlying reaction has been formulated analogously; thus, the ionic product from ortho-tolyl ethers, for example, is represented as:

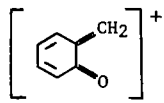

Both reactions fall into a larger class of ortho-rearrangements typified by respective loss of H_2O, CH_3OH, and H_2O from ortho-methylated aryl acids, derived methyl esters,[13,14] and benzyl alcohols.[15]

A structure problem originating in another investigation[16] furnished an opportunity to test the usefulness of the correlation and raised a question which, in turn, led to extension of the correlation to still another class of related compounds. The major product from a reaction of 2-chloromesitylene with peroxytrifluoroacetic acid and boron fluoride gave a mass spectrum with parent peaks at masses 322-324-326, with an isotopic distribution indicating a dichloro compound.[17] The molecular weight was right for a dichloro-monohydroxy-pentamethyl-diphenylmethane, as suggested by other evidence. The most abundant ion occurred at masses 166-168 (1 chlorine atom), indicating an ortho-methyldiarylmethane and establishing the formula:

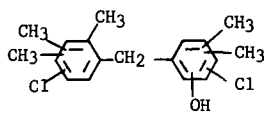

ortho-Methyl substitution in the second ring would lead to intense peaks at masses 168-170 (1 chlorine atom); only a tiny peak occurs at 170, ruling out such a structure. Peaks at 169-171 (1 chlorine atom) correspond to loss, without rearrangement, of the first aryl group -- $C_6HCl(CH_3)_3$. If the mesitylene carbon skeleton is assumed to remain unchanged, the possible structures can be narrowed to:

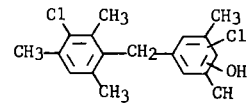

If an ortho-hydroxyl group resembles -- and is able to compete effectively with -- ortho-methyl in facilitating the rearrangement-dissociation,[18] only one structure remains:

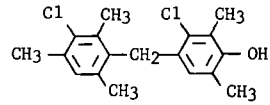

in satisfactory agreement with evidence from n.m.r. and i.r. spectroscopy.[16] Similar evidence led independently to the structure assignment:

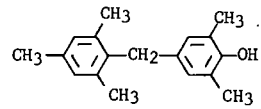

for the dechlorinated derivative.[16] Partial spectra of both are shown in Table III. Again, both spectra contain metastable peaks establishing the parent ions as precursors of the even-mass-number fragment ions.

TABLE III - PARTIAL SPECTRA OF CHLOROMESITYLENE OXIDATION PRODUCT AND DECHLORINATED DERIVATIVE

Diarylmethane		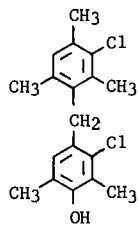	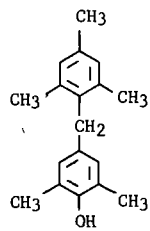
Molecular Weight[a]		332	254
Mass[a]	Ion	Relative Intensity	
Parent	Parent	100.0	100.0
Parent less 15	Parent less CH_3	32.0	94.1
Parent less 35	Parent less Cl	47.9	--
132[b]	$C_{10}H_{12}^+$	--	227
166	$C_{10}H_{11}Cl^+$	448	--

[a] Heavy-isotopic peaks due to ions containing ^{37}Cl are omitted.
[b] As in Table I, all even-mass-number peaks are shown that have intensities greater than 35% that of the parent ion.

To test the ability of ortho-hydroxyl to replace ortho-methyl as the hydrogen donor group, spectra were measured of 2-hydroxy-5-methyl- and 2-hydroxy-5-chloro-diphenylmethanes. These are shown in Table IV. Each spectrum contains the expected even-mass-number peak -- as well as the associated metastable peak, not shown in the table -- plus a second intense even-mass-number peak corresponding to further loss of a neutral particle of 28 mass units. The reaction sequence is apparently:

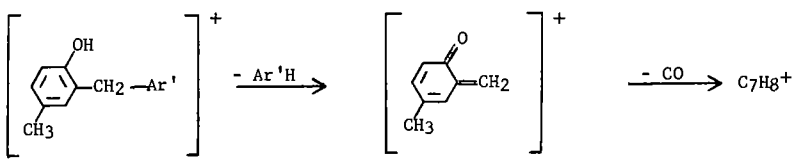

TABLE IV - PARTIAL SPECTRA OF ORTHO-HYDROXYDIARYLMETHANES

Diarylmethane		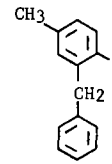	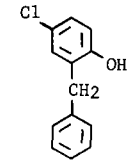
Molecular Weight[a]		198	218
Mass[a]	Ion	Relative Intensity	
Parent	Parent	100.0	100.0
Parent less 15	Parent less CH_3	37.0	0.8
Parent less 35	Parent less Cl	--	76.9
92[b]	$C_7H_8^+$	39.1	--
112	$C_6H_5Cl^+$	--	40.3
120	$C_8H_8O^+$	65.2	--
140	$C_7H_5ClO^+$	--	78.0

[a] See footnote a, Table III.
[b] See footnote b, Table III.

Subsequent loss of CO from the primary product was suggested also by the spectra of ortho-methyldiaryl ethers,[12] and is to be expected by analogy with ions of similar structure in other systems.[19-21] The peak arising from this secondary reaction is analytically useful in that it signals the presence of an oxygen atom, either in the ortho substituent or as the connecting link between the two aryl groups.

The reaction is thus common to diarylmethanes and diaryl ethers containing an ortho-methyl or -hydroxyl substituent. It is another member of a large class of ionic unimolecular rearrangement-dissociation reactions that are essentially unaffected by interchanging O, CH_2, and, no doubt, other groups such as NH and S.[3,4,7] These reactions, which seem to be energetically favored, are highly sensitive to molecular structure. Whether such a reaction will occur in a specific instance is determined largely by whether the molecule satisfies the geometric requirements needed to form the appropriate bridged cyclic intermediate or transition state.

EXPERIMENTAL

Materials

Table V summarizes the preparation and physical properties of the diarylmethanes studied. Method 1 consists of benzylation of an aromatic hydrocarbon by a benzylic halide in the presence of a mild Lewis acid, usually ferric chloride or zinc chloride[22]; aluminum chloride leads to extensive transbenzylation. Method 2 consists of the pyrolysis of a methylated diphenyl sulfone.[5]

In addition to the preparation listed, compound 1 was purchased from Matheson, Coleman and Bell. Compound 5 was obtained as the forecut from distillation of compound 3 on a 100-plate spinning-band column, and was purified by gas chromatography. The mass spectrum clearly indicated the 2,6,3'-structure rather than the 3,5,3'-, which might have been expected to be favored by steric considerations. Compound 6 was separated by fractional distillation from the pyrolysis products of di-ortho-xylyl sulfone. It was derived evidently from the 3,4,2',3'-isomer in the tetramethyldiphenyl sulfone mixture. Compound 7 was formed by reaction of para-xylyl bromide with mesitylene, catalyzed by zinc chloride in acetic acid. The mass spectrum of the pyrolysis product of mesityl para-xylyl sulfone indicated a mixture of the two predictable[5] isomeric tetramethyldiphenylmethanes. The peak at mass 132 was attributed to compound 7 and its spectral contributions were removed; the residual spectrum was attributed to compound 8. Compound 9 was formed along with other isomers by the condensation of formaldehyde with ortho-xylene, catalyzed by toluenesulfonic acid.[23] The dixylylmethanes were separated from more-highly condensed material by distillation. Compound 9, being the highest-melting isomer, crystallized first and was isolated in about 99% purity, as estimated by gas chromatography. Compounds 11 and 13 resulted from reactions of peroxytrifluoroacetic acid with prehnitene and chloromesitylene, respectively.[16] Compound 12 was obtained by dechlorination of compound 13.[16] Compounds 14 and 15 were purchased from Aldrich Chemical Company.

TABLE V - PREPARATION AND PROPERTIES OF DIARYLMETHANES

Compound Number	Positions of Methyl Groups	Method of Prep.[a]	Lit. Ref.	Yield, Mole %	B.P., °C./Torr	M.P., °C.
1	--	2	5	20	--	26
2	2	a	--	--	--	3-4
3	2,4,3'	1	22	30	123/1	--
		2	5	41	106/0.5	--
4	2,5,4'	1	22	69	104/0.5	--
		2	5	50	106/0.5	--
5	2,6,3'[b]	1	22	10	123/1	--
6	3,4,2'	2	5	8	98/0.2	--
7	2,4,6,4'[b]	1	22	60	--	50-52
8	2,5,3',5'[b]	2	5	20	127/1	--
9	3,4,3',4'	--	23	18	113-115/2	32-34
10	2,4,6,3',5'	1	22	52	--	67
		2	5	95	--	67
11	2,3,4,5,2',3',4',5'	--	16	--	--	150
12	4-OH-3,5,2',4',6'	--	16	--	--	121-123
13	2,3'-Cl_2-4-OH-3,5,2',4',6'	--	16	--	--	143-144
14	2-OH-5	--	c	--	184-186/13	--
15	2-OH-5-Cl	--	c	--	198-199/13	48.5

a See test.
b New compound.
c See K. Kindler, German Patent 824,058, December 10, 1951.

Preparation of ortho-Methyl-d-diphenylmethane

ortho-Benzylbenzoic Acid was prepared by reduction of ortho-benzoylbenzoic acid with zinc dust and ammonium hydroxide.[24] The yield of white acid, melting at 114-115°, was 26%; in addition, there resulted a 50% yield of the lactone of 2-carboxybenzhydrol.

ortho-Benzylbenzyl Bromide -- Refluxing 7.3 g. (0.0344 mole) ortho-benzylbenzoic acid and 1.31 g. (0.0344 mole) lithium aluminum hydride in 150 ml. ether for 1 hour gave, after the usual workup, 3.2 g. (51%) ortho-benzylbenzyl alcohol as a colorless oil. Treatment with concentrated hydrobromic acid[25] converted it to ortho-benzylbenzyl bromide, m.p. 44-45°, in 69% yield.

ortho-Methyl-d-diphenylmethane -- A mixture of 1.31 g. (0.005 mole) ortho-benzylbenzyl bromide and 0.44 g. (0.01 mole) lithium aluminum deuteride in 50 ml. ether was stirred and refluxed 3 hours. The mixture was cautiously treated with 10% sulfuric acid; the ether solution was dried and evaporated, leaving 0.9 g. (98%) of ortho-methyl-d-diphenylmethane, melting at 5-6°. The literature melting point for the undeuterated ortho-methyldiphenylmethane is 6.61°[26]; our undeuterated compound, obtained by the above reduction using lithium aluminum hydride, melted at 3-4°.

N.m.r. spectra of the unlabeled and labeled ortho-methyldiphenylmethanes were measured in deuteriochloroform with tetramethylsilane as the internal standard in the cavity of a Varian DP 60 machine. The peaks in τ units for the unlabeled compound were: aromatic hydrogens at 2.94, methylene hydrogens at 6.14, and methyl hydrogens at 7.89. The ratio of the integrated areas was 9:2:3. The hydrogens of the labeled compound gave peaks at the same τ values, and were in the ratio 9:2:2. Thus, the deuterium atom was clearly in the methyl group and no exchange with the hydrogens of the methylene group had occurred during the reduction with lithium aluminum deuteride.

Mass Spectrometry

Mass spectra were measured with 70-volt electrons on a modified[27] Consolidated model 21-103c instrument with the inlet system at 250°. Low-voltage measurements were made with the repeller plates at an average potential of 3 volts; actual settings, adjusted for maximum ion current, were 3.80 volts on the inner repeller and 2.20 volts on the outer one.

Corrections for naturally occurring heavy isotopes -- as well as for the isotopic impurity, 5.6% of the unlabeled species, estimated at low voltage[28] -- have been made only on the data in Table II. Such correction is required in calculating label retention.[7] Low-voltage measurements -- below the appearance potential of $C_8H_9^+$ -- were made to eliminate possible interference from unlabeled $C_8H_9^+$ ions and to check for possible dependence of label retention on ionizing voltage.[29] The 70-volt spectra show that the label is retained quantitatively in the $C_8H_9^+$ ion. The finding that retention is independent of ionizing voltage supports the assumption that $C_8H_8^+$ arises by only one path.

ACKNOWLEDGMENTS

We are indebted for the preparation of 2,4,6,4'-tetramethyldiphenylmethane to J. G. Hendrickson; of the 2,5,3',5'-isomer to D. H. Meyer; of the 3,4,3',4'-isomer to C. Serres, Jr.; and of 2,3,4,5,2',3',4',5'-octamethyl-, 4-hydroxy-3,5,2',4',6'-pentamethyl-, and 2,3'-dichloro-4-hydroxy-3,5,2',4',6'-pentamethyldiphenylmethanes to C. A. Buehler and Harold Hart, of Michigan State University. The assistance of D. K. Albert with gas-chromatographic purification and of E. M. Banas with n.m.r. spectroscopy is gratefully acknowledged.

REFERENCES

(1) M. Magat, Disc. Faraday Soc., 10, 113 (1951).
(2) F. W. McLafferty, in "Mass Spectrometry of Organic Ions," F. W. McLafferty, ed., Academic Press, New York, 1963, p. 309.
(3) S. Meyerson and J. D. McCollum, Advances in Analytical Chemistry and Instrumentation, 2, 179 (1963); S. Meyerson, J. Phys. Chem., 68, 968 (1964).
(4) K. Biemann, "Mass Spectrometry," McGraw-Hill Book Co., Inc., New York, 1962, pp. 107ff.
(5) H. Drews, E. K. Fields, and S. Meyerson, Chem. and Ind. (London), 1403 (1961).
(6) S. Meyerson and P. N. Rylander, J. Phys. Chem., 62, 2 (1958).
(7) H. M. Grubb and S. Meyerson, in "Mass Spectrometry of Organic Ions," F. W. McLafferty, ed., Academic Press, New York, 1963, p. 453.
(8) H. Wincel and Z. Kecki, Nukleonika, 8, 216 (1963).
(9) S. Meyerson, J. D. McCollum, and P. N. Rylander, J. Am. Chem. Soc., 83, 1401 (1961).
(10) K. Biemann, Angew. Chem. Intern. Ed., 1, 98 (1962).
(11) H. Audier, M. Fétizon, and W. Vetter, Bull. Soc. Chim. France, 1971 (1963).
(12) R. I. Reed and J. M. Wilson, Chem. and Ind. (London), 1428 (1962).
(13) F. W. McLafferty and R. S. Gohlke, Anal. Chem., 31, 2076 (1959).
(14) T. Aczel and H. E. Lumpkin, Anal. Chem., 33, 386 (1961).
(15) T. Aczel and H. E. Lumpkin, Anal. Chem., 32, 1819 (1960).
(16) C. A. Buehler and H. Hart, J. Am. Chem. Soc., 85, 2177 (1963).
(17) J. H. Beynon, "Mass Spectrometry and its Applications to Organic Chemistry," D. Van Nostrand Co., New York, 1960, p. 298.
(18) In substituted benzoate esters, for example, either a hydroxyl or methyl group in the ortho position can furnish the hydrogen atom needed for the analogous reaction. Thus, the mass spectra of alkyl salicylates are characterized by an intense peak at mass 120, attributed to an ion with the structure:

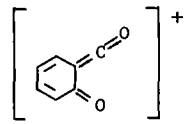

[See E. M. Emery, Anal. Chem., 32, 1495 (1960)].
(19) J. H. Beynon, G. R. Lester, and A. E. Williams, J. Phys. Chem., 63, 1861 (1959).
(20) J. H. Beynon and A. E. Williams, Appl. Spectroscopy, 14, 156 (1960).
(21) J. D. McCollum and S. Meyerson, J. Am. Chem. Soc., 85, 1739 (1963).
(22) C. Serres and E. K. Fields, J. Am. Chem. Soc., 82, 4685 (1960).
(23) J. G. Hendrickson and F. T. Wadsworth, Ind. Eng. Chem., 50, 877 (1958).
(24) R. Scholl and W. Neovius, Ber., 44, 1080 Anm. (1911).
(25) N. J. Leonard, A. J. Kresge, and M. Oki, J. Am. Chem. Soc., 77, 5078 (1955).
(26) I. H. Lammeck, Jr., and P. H. Wise, Natl. Advisory Comm. Aeronaut. Tech. Note 2230, 17 pp (1950); C. A., 45, 6609h (1951).
(27) H. M. Grubb, C. H. Ehrhardt, R. W. Vander Haar, and W. H. Moeller, 7th Annual Meeting of ASTM Committee E-14 on Mass Spectrometry, Los Angeles, California, May, 1959.
(28) D. P. Stevenson and C. D. Wagner, J. Am. Chem. Soc., 72, 5612 (1950); R. E. Honig, Anal. Chem., 22, 1474 (1950).
(29) S. Meyerson, J. Chem. Phys., 34, 2046 (1961); S. Meyerson, T. D. Nevitt, and P. N. Rylander, in "Advances in Mass Spectrometry," Vol. II, R. M. Elliott, ed., Pergamon Press, London, 1963, p. 313; S. Meyerson and H. Hart, J. Am. Chem. Soc., 85, 2358 (1963).

MASS SPECTRAL FRAGMENTATION OF PHENYL-N-ALKANES

A. Bruce King
Gulf Research & Development Company
Pittsburgh, Pennsylvania

ABSTRACT

The phenyl-n-alkanes with the phenyl group two or more carbon atoms from the terminal atom is characterized by two competing primary fragmentation reactions involving loss of either alkyl group on the α carbon atom. The loss of the smaller alkyl group has the lower appearance potential, but the competing reaction to lose the larger alkyl group increases in yield more rapidly at the higher electron energies and it has greater intensity at 70 eV. The ratio of intensities of these two ions correlates with the relative position of the phenyl group from the center of the chain for phenyl alkanes of different carbon numbers. Subsequent decomposition of these primary ions is by successive loss of olefins of C_3 through C_6. Attempts to explain the higher yield of the higher energy primary path within the framework of current theoretical models were unsuccessful. It is suggested that the usual method of applying the quasi-equilibrium assumption is not valid for molecules of this size and degree of localization of charge and energy.

INTRODUCTION

Although extensive studies of the fragmentation mechanisms for the lower alkyl benzenes have been reported by Meyerson and co-workers and others,[1] very little work of this type has been reported for the higher molecular weight compounds. Meyerson sometime ago related quantitative trends of the major ions in the 1-phenyl alkanes with carbon number.[2] Recently Boyer, et al,[3] reported on studies of hydrogen atom rearrangements in the fragmentation of the phenyl-n-alkanes at the α-β bond. The purpose of this paper is to report on more detailed studies of a number of phenyl-n-alkanes in the carbon number range through C_{26}.

Another aspect of this work is the possible use of the information on the fragmentation of large molecule-ions in a test of the quasi-equilibrium theory using the newly reformulated equations for the rate constants.[4] The point of interest here is to test for large molecules the validity of the basic assumption of the theory, i.e., that the rate of redistribution of energy in the newly formed molecule-ion is faster than the fragmentation reaction rates. Attempts to do this with n-paraffins for example are made difficult by the variety of paths that lead to the principal ions in the spectra. The alkyl benzenes would seem to be more suited for such a test as the charge is highly localized and all the major ions contain the phenyl group and thus their mode of formation is frequently quite apparent. In addition previous studies[1] with labeled compounds of the lower members of the series have given important insight into the principal reaction paths.

EXPERIMENTAL

All spectra were taken on a Consolidated 21-103C Mass Spectrometer equipped with an all glass heated inlet system that was operated at temperatures up to 350°C. Sample introduction was through a gallium covered glass frit[5] and the valve to the inlet pumps was of the gallium-umbrella type.[6] Thus the only surfaces exposed to the sample in the inlet system were glass and gallium and pyrolysis was thus avoided.

The high and low voltage spectra were obtained with electrostatic scanning on both photographic charts and IBM cards using the CEC MASCOT digitizer. Scans at two magnetic field strengths were required to obtain the entire spectra. A computer program was used to calculate the per cent of total ionization and to correct intensity differences between the two mass ranges. In addition, the program made first and second order isotope corrections for C^{13} and D. The energy scale for the low voltage patterns was based on the linear extrapolated ionization efficiency curve of the parent ion as the "internal" standard. Repeller voltages for the low voltage spectra and the appearance potential measurements were fixed at 1.5 volts. Appearance potentials were determined by the extrapolated voltage difference method as previously described[7] with krypton as the internal standard. The reproducibility of the appearance

potentials is about .02 eV although the absolute accuracy is considered to be no better than 0.1 eV.

The phenyl eicosanes reported in this study and 7-phenyl tridecane were obtained from API Project 42 and 3-phenyl dodecane from Eastman Kodak. The other phenyl dodecanes were GLC cuts of product synthesized in our laboratory.

RESULTS AND DISCUSSION

It was found that the 1-phenyl and 2-phenyl compounds have distinctly different fragmentation mechanisms from those substituted two or more atoms from the terminal atom. Treatment of the former compounds will be deferred to a later more detailed paper and this paper shall deal only with the latter group, the compounds with $n \geq 2$ (where n is the number of carbon atoms of the shorter alkyl group on the α carbon, m is the number for the larger group, and $n+m+1 = N$, the total number of carbon atoms in the alkane chain).

The fractional yields at 70 eV of the principal ions of the phenyl eicosanes and several lower carbon number compounds are listed in Table I. In Table II the metastable transitions observed for the same compounds are listed. Except for 9-phenyl eicosane the fragmentation reaction to lose the shorter alkyl group is the only decomposition reaction of the parent ion observed. This observation suggests the loss of the larger group occurs with a significantly greater activation energy which is confirmed by the appearance potential data in Table III. The relative intensities (Table I) of these two primary ions are seen to vary with the position of the substituent, with the $C_m\text{-}\overset{+}{C}HC_6H_5$ intensity being nearly constant and the $C_n\text{-}\overset{+}{C}HC_6H_5$ increasing markedly as n decreases. An examination of the ratio of intensities of the $C_n\text{-}\overset{+}{C}HC_6H_5$ to $C_m\text{-}\overset{+}{C}HC_6H_5$ with the distance of the phenyl group from the end of the chain relative to the distance of the center of the chain is shown in Figure 1. One notes a nearly logarithmic increase of the intensity ratio with the relative position for the phenyl eicosanes and an identical fit of the data for the phenyl dodecanes. Results consistent with Figure 1 were found for other phenyl alkanes in the $C_{16}\text{-}C_{20}$ range.

The metastable transitions in Table II indicate that the lowest energy fragmentation reactions of the two primary ions ($C_m\text{-}\overset{+}{C}HC_6H_5$ and $C_n\text{-}\overset{+}{C}HC_6H_5$) are loss of olefins C_3H_6 thru C_6H_{12} and C_2H_4 from the $C_2H_5\overset{+}{C}HC_6H_5$ ion. No metastable transitions are observed for the ions $m>13$. This may be due to lack of sufficient intensity or to reaction rates at even the lowest energies above the threshold that are greater than 10^6 sec^{-1}. The yields of these secondary ions at the intermediate carbon numbers, i.e., $C_iH_{2i+1}\overset{+}{C}HC_6H_5$ where $i<m$, are shown in Figure 2 for several of the phenyl alkanes substituted near the end of the chain. One notes that the yield decreases linearly as the carbon number of the remaining alkyl group increases and that the data extrapolates to zero yield for $i \cong m-2$. This is taken as further evidence that decomposition is by loss of olefin molecules of C_3 or greater from $C_m\text{-}\overset{+}{C}HC_6H_5$. At the lower values of i, the observed yield continues to rise presumably due to repeated loss of olefin molecules in units of C_3 to C_6. When $i<7$ the yields begin to rise more abruptly and this is attributed to the accumulation of products in this carbon number range due to the lower reaction rates and fewer paths for further decomposition. Naturally extrapolation of the data for $i>n$ in Figure 2 does not fit the data for $i = n$ and $i<n-2$, where additional contributions from the $C_nH_{2n+1}\overset{+}{C}HC_6H_5$ and its decomposition products are found, but the fit for $i = n-1$ and $n-2$ are readily seen in series such as the 5-phenyl and 7-phenyl eicosane spectra (Figure 2 and Table I). Thus for $i<n-2$ contributions from decomposition of the smaller primary ion is observed with much the same behavior.

The "rearrangement ions",[3] i.e. alkyl benzene ions of lower carbon number, are found to be about 4-5% of the alkyl benzyl ion one mass lower (after isotope correction) when the carbon number corresponds to loss of one of the alkyl groups on the α carbon (except for loss of C_2H_4 from 3-phenyl compounds which is not observed). At the intermediate carbon numbers, the rearrangement ions are generally less than 2% of the corresponding benzyl ion. This is similar to the data of Boyer, et al.[3]

TABLE I. Partial Spectra Of Some Phenyl n-Alkanes (n>2) At 70 eV
(% Of Total Ionization - C^{13} And D Corrected)

m/e	3-φ C_{12}	7-φ C_{13}	3-φ C_{20}	4-φ C_{20}	5-φ C_{20}	7-φ C_{20}	9-φ C_{20}
91	25.94	33.03	23.98	32.16	31.02	31.49	30.99
92	.48	.38	.39	.47	.48	.55	.54
105	2.63	4.79	2.52	2.41	3.51	4.52	4.76
119	15.08	1.995	20.83	.908	.876	1.904	2.24
133	.858	.813	.688	16.10	.630	1.090	1.666
147	.695	.066	.566	.550	14.18	.619	1.352
161	.441	.030	.472	.418	.446	.504	.838
175	.18	13.45	.340	.336	.350	10.345	.402
189	.033	.039	.262	.246	.278	.317	.238
190	.010	.015	.003	.004	---	.019	.006
203	---	.018	.214	.197	.220	.218	7.79
217	4.54	.024	.174	.160	.166	.151	.031
231	---	---	.152	.130	.118	.084	---
245	---	---	.124	.095	.084	---	5.54
259	---	---	.092	.064	---	---	---
273	---	---	.066	.046	---	4.55	---
287	---	---	.050	---	---	---	---
301	---	---	---	---	4.21	---	---
315	---	---	---	4.19	---	---	---
329	---	---	4.90	.024	---	---	---
Parent	3.28	3.40	3.01	2.98	2.83	3.00	3.08
$\frac{C_m\text{-}CH\varphi}{C_m\text{-}CH\varphi}$	3.32	1.00	4.25	3.84	3.37	2.27	1.406

TABLE II
Major Metastable Transitions Observed For Phenyl-n-Alkanes For n≥2
(Observed Mass In Parentheses)

Compound	Parent To $C_m\text{-}\overset{+}{C}H\varphi$ or $C_n\text{-}\overset{+}{C}H\varphi$	Loss Of Olefin From $C_m\text{-}\overset{+}{C}H\varphi$	Loss Of Olefin From $C_n\text{-}\overset{+}{C}H\varphi$
3φ-C_{12}	246 → 217 (192)	217 → 133 (81.6) → 147 (99.8) → 161 (119.5) → 175 (141.7)	119 → 91 (69.8)
7φ-C_{13}	n.o.	175 → 91 (47.4) → 105 (63.1) → 119 (81.1) → 133 (101.5) 119 → 91 (69.8)	Same
3φ-C_{20}	358 → 329 (303)	n.o.	119 → 91 (69.8)
4φ-C_{20}	358 → 315 (278)	n.o.	133 → 91 (62.4)
5φ-C_{20}	358 → 301 (253)	n.o.	147 → 91 (56.3) → 105 (75.3)
7φ-C_{20}	358 → 273 (209)	? 273 → 189 (131) 273 → 203 (151.5)	175 → 105 (63.2) → 119 (81.1) → 133 (101.5)
9φ-C_{20}	358 → 245 (168.5) ? 358 → 203 (115.5)	245 → 175 (125+) → 189 (146+)	203 → 119 (69.8) → 133 (88) → 147 (106.8)

Other Transitions Observed In Most Of The Spectra

71 → 43 (26.2)	{103 → 77, 106 → 78}	(57.4)
57 → 41 (29.5)		
43 → 41 (39.1)	105 → 104	(103+)
91 → 65 (46.8)	119 → 117	(113-115)

n.o. -- not observed

The ionization potentials of the phenyl eicosanes for $n \geqslant 2$ are seen to be the same within the experimental error (Table III). The method of group equivalents[8] predicts that the heats of formation of the 3- thru 9-phenyl eicosanes are the same, and thus the heats of formation of the ions are also the same. The appearance potentials of the ions for loss of the smaller alkyl group are always less than that for loss of the larger group with the difference becoming smaller as the phenyl group is moved towards the center of the chain. Figure 3 shows a plot of the appearance potential in excess of the ionization potential for these pairs of ions in the phenyl eicosanes studied. From the slope of the plot, a decrease of .058 eV per carbon atom in the appearance potential is found. This slope may be attributed to $d[\Delta H_f(C_nH_{2n+1}\overset{+}{C}HC_6H_5)]/dn - d[\Delta H_f(C_nH_{2n+1})]/dn$ caused by a greater rate of decrease in the heat of formation of the alkyl benzyl ion with carbon number than for the accompanying alkyl radical. This conclusion is however contrary to the predictions of the method of group equivalents[8] which would assign identical values to the heats of reaction to form all of the ions listed in Figure 3. None the less, if one assumes that the differences in Figure 3 are the result of heats of formation of the ions that are different from those predicted by group equivalents, one should still expect the same ion to have identical appearance potentials from different carbon number precursors. Examination of Table III reveals that the ions formed from 3-phenyl dodecane and 7-phenyl tridecane give appearance potentials somewhat less than that observed for the same ions interpolated from the phenyl eicosane data (Figure 3). This is especially true for $C_9H_{19}\overset{+}{C}HC_6H_5$. The conclusion is thus that excess energy is required for the loss of the larger alkyl group with the amount of the excess energy increasing with the size of the group lost. It should be noted that the quasi-equilibrium theory may interpret this excess energy as a consequence of the "kinetic shift". This point will be discussed further in the following section.

An attempt was made to estimate the magnitude of the excess energy by calculating the effective heat of formation of an ion for comparison with other available data. The heat of formation of $(C_2H_5\overset{+}{C}HC_6H_5)$ was calculated from the appearance potential data for 3-phenyl dodecane and 3-phenyl eicosane using known heats of formation.[8,10*] The reactions considered are:

$$C_2H_5\text{-}\underset{\underset{C_6H_5}{|}}{\overset{+}{C}}H\text{-}C_9H_{19} \longrightarrow C_2H_5\overset{+}{C}HC_6H_5 + C_9H_{19}\cdot \qquad (1)$$

$$C_2H_5\text{-}\underset{\underset{C_6H_5}{|}}{\overset{+}{C}}H\text{-}C_{17}H_{35} \longrightarrow C_2H_5\overset{+}{C}HC_6H_5 + C_{17}H_{35}\cdot \qquad (2)$$

The results were 203 and 209 kcal/mole, respectively. The expected excess energy from Figure 3 of ~1 eV would predict the actual heat of formation is ~180 kcal/mole. This is considerably less than the value of 199 kcal/mole calculated[8] from the isomeric ion $C_6H_5\overset{+}{C}(CH_3)_2$ from t-butyl benzene,[11] which may of course involve some excess energy as well. It would seem however that at least a portion of the activation energy change shown in Figure 3 may be due to a greater rate of decrease of ΔH_f of the alkyl benzyl ion with carbon number.

Spectra at low electron voltages were obtained on all of the compounds under study in order to gain information on the fragmentation mechanisms. The plots of relative yields vs. electron energy for the various ions were qualitatively similar and thus only the 3-phenyl eicosane data is shown to exemplify the behavior (Figures 4 and 5). Only the parent ion exhibits asymptotic decrease of yield with increasing electron energy. The $C_m\text{-}\overset{+}{C}HC_6H_5$ ion (m/e 329) exhibits a maximum at very low voltages with significant drop in yield at higher voltages. By contrast, the $C_n\text{-}\overset{+}{C}HC_6H_5$ (m/e 119) rises more gradually and levels off at much higher energies. The tropylium ion and m/e 105 continue to rise over the entire voltage range while the benzyl ions of the intermediate carbon numbers exhibit a broad maximum at ~5 eV. These results clearly demonstrate that the higher carbon number ions precede m/e 91 and 105 in the fragmentation scheme. As the phenyl group is moved toward the center of the chain, the shape of the curves for the $C_m\text{-}\overset{+}{C}HC_6H_5$ and $C_n\text{-}\overset{+}{C}HC_6H_5$ ions

* Based on calculation of $\Delta H_f(C_nH_{2n+1}\cdot)$ assuming D(R-H) = 100 kcal/mole for the primary bond.

TABLE III. Appearance Potential Data In eV
(Reproducibility ± .02 eV, Probable Uncertainty ± 0.1 eV)

Compound Type	Compound	Parent Ion	$C_mH_{2m+1}\overset{+}{C}HC_6H_5$	$C_nH_{2n+1}\overset{+}{C}HC_6H_5$	$C_7H_7^+$	Other	
n≥2	3-φ C_{12}	8.95	9.26	10.42	12.05		
	7-φ C_{13}	8.91	10.15	---	12.21		
	3-φ C_{20}	8.95	9.68	10.69	12.24	105:	11.28
	4-φ C_{20}	9.01	9.76	10.58	12.33	119:	11.36
	5-φ C_{20}	9.04	9.99	10.43	12.34		
	7-φ C_{20}	8.97	9.94	10.28	12.60		
	9-φ C_{20}	9.06	10.12	10.30	12.09		

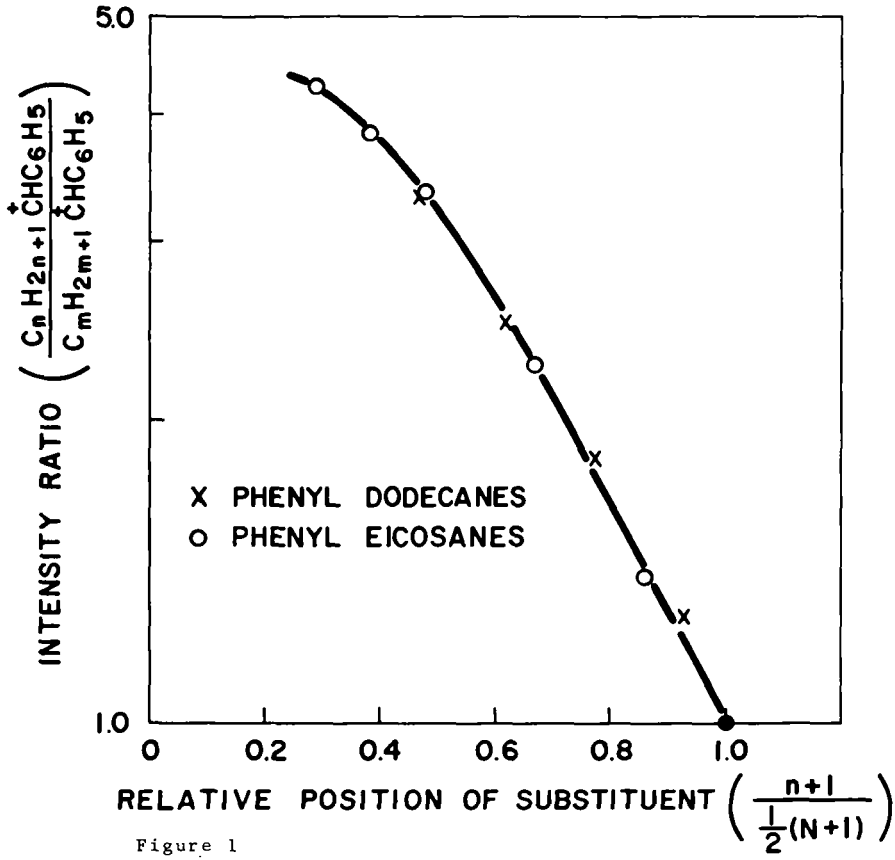

Figure 1

Semilog plot of the ratio of intensities of $C_nH_{2n+1}\overset{+}{C}HC_6H_5$ to $C_mH_{2m+1}\overset{+}{C}HC_6H_5$ vs. the relative position of the phenyl group in the chain for the phenyl dodecanes and phenyl eicosanes.

become similar but with the former always reaching a maxima before the latter and decreasing to a much lower level. The fragment ions $C_i\text{-}\overset{+}{C}HC_6H_5$ for $i<n-2$ continue to rise over the voltage range similar to that shown for m/e 105 in Figure 5. The behavior is presumably due to the fragmentation of the $C_n\text{-}\overset{+}{C}HC_6H_5$ which becomes important at higher voltages than the contributions from fragmentation of the $C_m\text{-}\overset{+}{C}HC_6H_5$.

The fragmentation mechanism of the phenyl-n-alkanes for $n\geqslant 2$ (Mechanism 1) is thus seen from the above observations to consist of two competing primary reactions involving loss of the alkyl groups on the α carbon. Subsequent decomposition of these ions is by repeated loss of C_3-C_6 olefins until the ionic fragment is $C_7H_7^+$, $C_8H_9^+$, or $C_9H_{11}^+$ (the latter will partially decompose further to $C_7H_7^+ + C_2H_4$ -- note metastable ions for this reaction in Table II). For the purpose of this discussion, the modes of formation of the minor alkyl ions (they are stronger in branched phenyl alkanes than the phenyl-n-alkanes) and the ring fragment ions (e.g., $C_3H_3^+$ and $C_5H_5^+$) will not be considered.

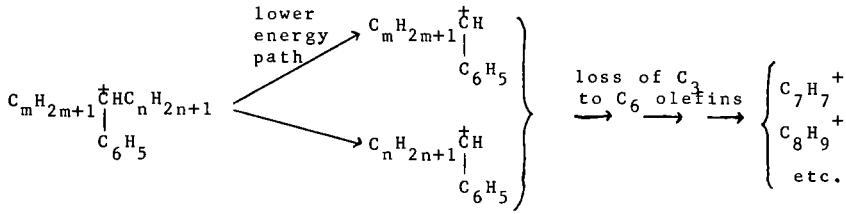

Mechanism 1. Fragmentation Mechanism for the phenyl-n-alkanes with $n\geqslant 2$

Two features of this mechanism and its relation to the experimental observations merit emphasis. The two primary reaction paths should involve very similar activated complexes and thus the yield of the lower energy reaction should be greater for all electron energies. The striking increase of the yield of the higher energy path in Figure 4 presents a situation which current theoretical models are not able to explain. This point will be discussed further in the next section.

The other point of interest is the mechanism whereby olefins (or cycloparaffins) of C_3 to C_6 are lost from the alkyl benzyl ion. The fact that the size of olefin lost is fairly independent of the length of the alkyl group would seem to suggest that the portion of the chain lost is from the phenyl end. This is based on the premise that the site of reaction is dictated by the proximity of the α carbon (charge site). Thus as the length of the alkyl chain in the reactant ion is varied, a loss from the saturate end of the chain would tend to give a fixed chain length remaining on the ion rather than a fixed chain length lost as the neutral product. The fact that the unit lost is C_3 to C_6 suggests a cyclic rearrangement is involved, similar to that suggested by Meyerson and co-workers from studies of labeled 3-phenyl pentane[12] and 3-phenyl, 3-ethyl pentane.[1] Labeled compound data is needed, however, to prove this suggestion.

EXAMINATION OF THE THEORETICAL MODEL

The most striking aspect of the above results is the much higher yield of the alkyl benzyl ions formed by the higher energy primary path ($C_n\text{-}\overset{+}{C}HC_6H_5$). One might argue that greater secondary decomposition of the ion with the larger alkyl group explains its lower yield. Several arguments may be offered against this explanation. First, at low voltages (Figures 4 and 5) where the yield of m/e 91 and other secondary decomposition products are small, the total yield of $C_m\text{-}\overset{+}{C}HC_6H_5$ and all of its decomposition products at the intermediate carbon numbers is still lower than the yield from the competing higher energy path ($C_n\text{-}\overset{+}{C}HC_6H_5$). Secondly, the yield of the intermediate carbon numbers do not extrapolate to high enough intensity at the lower carbon numbers and thus their combined yield will not explain the low yield of the precursor ion. Thirdly, a decrease is observed in the yield of $C_7H_7^+$ from 32% to 24% in going from the 4-phenyl to 3-phenyl eicosane where the only effect should be to retard slightly the yield of m/e 91 from the $C_n\text{-}\overset{+}{C}HC_6H_5$ ($119 \longrightarrow 91$ is however observed as a metastable transition). Thus a significant portion of m/e 91 arises from the smaller primary ion ($C_n\text{-}\overset{+}{C}HC_6H_5$) which appears to

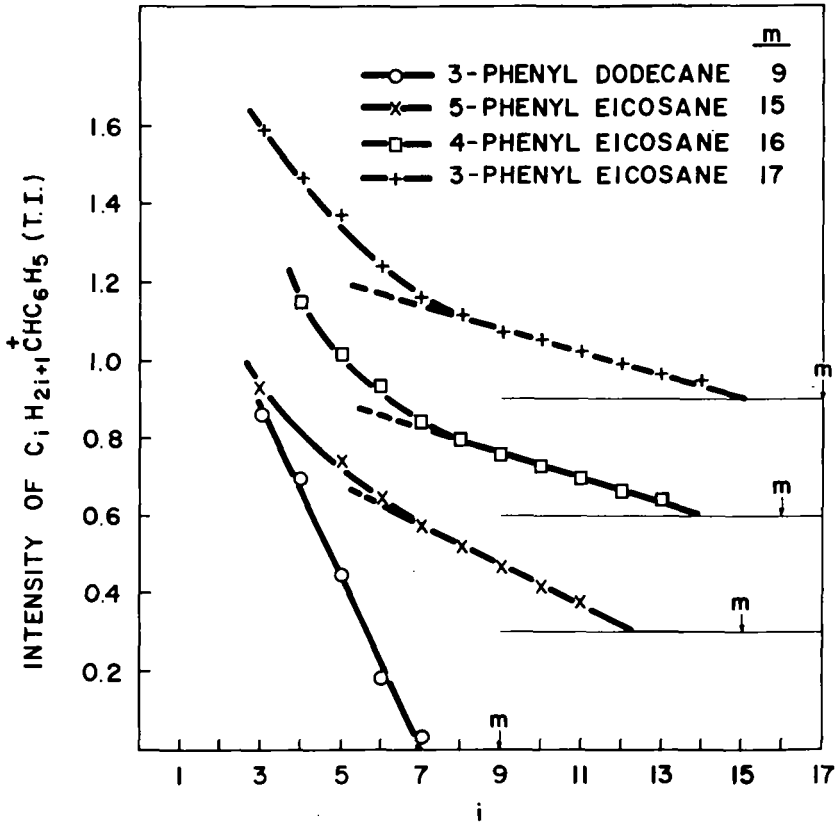

Figure 2

Intensities of $C_iH_{2i+1}\overset{+}{C}HC_6H_5$ at the intermediate carbon numbers (i<m) for several of the phenyl alkanes. The ordinate scales have been shifted for clarity.

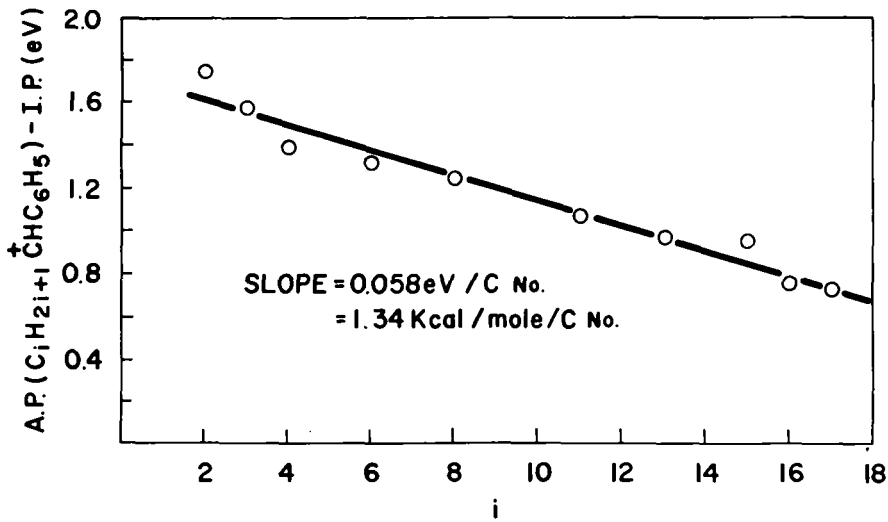

Figure 3 Appearance potential minus ionization potential for the $C_nH_{2n+1}\overset{+}{C}HC_6H_5$ and $C_mH_{2m+1}\overset{+}{C}HC_6H_5$ ions in the phenyl eicosanes. There are two points per compound: i = n and i = m.

undergo significant decomposition as well.

Since the two competing reactions both involve a simple α-β carbon bond break, it would be expected that the frequency distribution for the activated complex would be the same and any differences in rate constants would arise solely from the difference in the activation energies. Calculations were made of the rate constants for these reaction paths using the recently reformulated equations.[4*] The two competing primary reactions for 3-phenyl eicosane were selected for study because this isomer has the biggest difference in activation energies and yet the highest yield of the higher energy path. Various frequency distributions were studied to see if very minor differences in frequency distributions would account for the yields observed. The calculated rate constants for the various frequency distributions are summarized in Figures 6 and 7 for the lower and higher energy paths, respectively, where the activation energy (E_0) is assumed from the appearance potential. All the frequency distributions were based on three groups of identical frequencies in which the lower and upper group have a frequency 1/R and R times the frequency of the middle group. Changing the spread of the frequency group (increasing R from 3 to 10) lowers the rate constants slightly, especially at the lower energies. Lowering all of the frequencies by a factor of ten has a drastic reduction in the rate constant (Figure 6), while the use of a slightly asymmetric frequency distribution for the activated complex may alter the shape of the rate constant curve somewhat (not shown).

It is apparent from Figures 6 and 7 that the predicted rate of increase of the rate constants with energy is much less for the higher energy path. It is therefore necessary to correct for this effect in determining the activation energy from the appearance potential.** This correction has been termed the "kinetic shift"[13] and was determined by choosing an activation energy such that $k(A.P.-I.P.) = 10^6\ sec^{-1}$, where A.P. is the appearance potential and I.P. is the ionization potential. The results of rate constants calculated from activation energies thus determined are shown in Figures 8 and 9 for two of the frequency distributions considered. One notes that the magnitude of the kinetic shift is similar to the estimated excess energy implied in Figure 3. However, even after this correction, the calculated rate constants for the higher energy path are at least a factor of three less than those for the competing reaction at all values of the internal energy. In order to explain the higher yield of the higher energy path within this framework, it is necessary to choose significantly different frequency distributions for these two similar reactions. If this is done, the curve for the higher energy path may be made to cross the other one at higher energies. Although this procedure may predict the proper yields at higher voltages, it will not predict a rapid rise in yield of the higher energy path until the energy is reached where to two curves cross. This model would not predict the rapid rise observed at low voltages for m/e 119 as shown in Figure 4. One is forced to assume that even by choosing markedly different frequency distributions for these two similar reactions, it is not possible to get theoretical predictions consistent with the experimental observations.

It should be recalled that following the original introduction of the quasi-equilibrium theory[14] using the Kassel formulation, several objections[15,16] were raised that the theory predicted a much slower rate of rise of k(E) with E than the experimental data indicated. With the reformulation of the equations for the rate constants,[4] it was claimed that a better degree of agreement was now obtainable. Although the revised formulation does give a greater rate of rise of k(E) for the smaller values of E_0 and smaller number of the oscillators, the theory does not seem to be able to describe the decomposition rates observed in larger molecules for the higher activation energy reactions. The experimental data instead indicates that the shape and displacement of

---

* Computer calculations of the $\sigma_i^{\ddagger}$'s gave errors due to underflow for the higher terms. Thus $\sigma_1 - \sigma_{20}$ and $\sigma_1^{\ddagger} - \sigma_{20}^{\ddagger}$ were calculated exactly and the remaining terms were interpolated by a quadratic fit to the first twenty terms and σ_N and $\sigma^{\ddagger}_{N-1}$ equal to unity.

** The author is indebted to Dr. H. M. Rosenstock for making this suggestion.

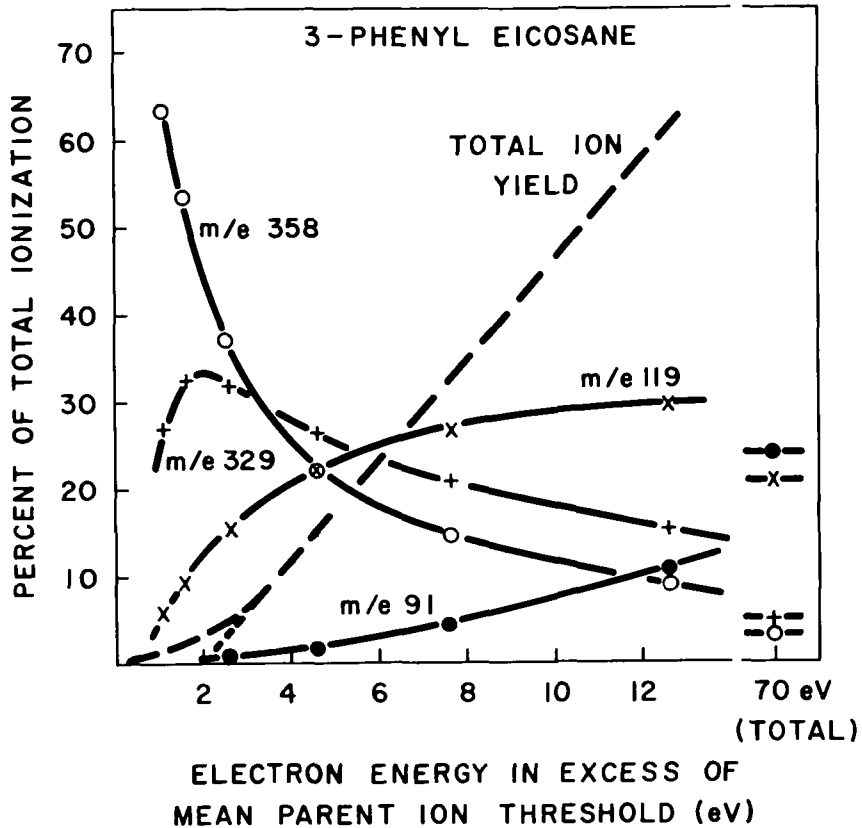

Figure 4 Low voltage yields of the major ions from 3-phenyl eicosane.

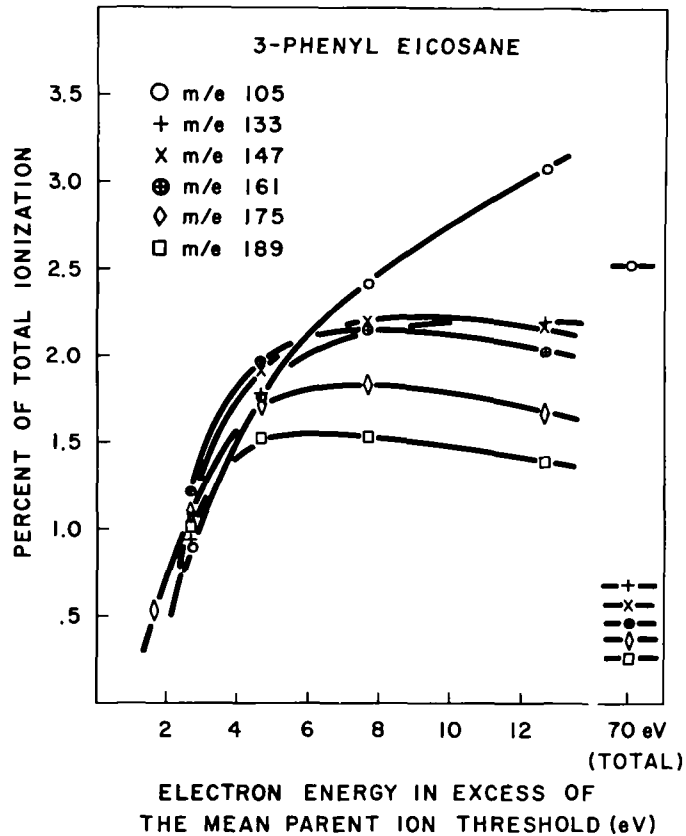

Figure 5
Low voltage yields of the minor fragment ions at the intermediate carbon numbers from 3-phenyl eicosane.

the k(E) vs. E curve is much less sensitive to the value of E_0 and the number of oscillators than the current theory would predict.

Although one may suggest that this disagreement between theory and experiment is due to significantly different activated complexes for these seemingly similar reactions, we suggest two other possible explanations: (1) the probability of radiationless transitions from excited states to other states of the ion is too small, and thus the effective zero of the energy scale for E and E_0 is not the ground state of the ion, or (2) the reaction may be described by a highly localized portion of the molecule-ion (i.e., highly reduced number of effective oscillators). Both of these explanations are equivalent to stating that the energy is not distributed throughout the entire molecule before reaction occurs, and both will explain the considerably greater rate of rise of k(E) with E that is implied by the experimental data than that predicted by the theory. Note that for the higher energies, the predicted rate constants in Figures 6 through 9 approach 10^{12}-10^{13} sec^{-1}. In this region the rate of reaction is surely comparable to the rate of energy redistribution among the vibrational degrees of freedom and the quasi-equilibrium assumption would not be valid. Although one is able to detect reactions with rates $\approx 10^6$ sec^{-1} as metastable transitions, if most of the fragmentation reactions occur at considerably faster rates, namely 10^{10}-10^{12} sec^{-1}, the use of the quasi-equilibrium assumption to describe the entire fragmentation mechanism is clearly open to question.

ACKNOWLEDGEMENTS

The author wishes to thank Dr. J. C. Schug for helpful discussions and assistance with computer calculation of the rate constants. He also wishes to thank Mr. J. Walter for supplying some of the compounds used and H. T. Best, J. P. Klems, and P. W. Mazak for obtaining the experimental data.

BIBLIOGRAPHY

1 See review: H. M. Grubb and S. Meyerson, in The Mass Spectrometry of Organic Ions, F. W. McLafferty, ed., Academic Press, New York, 1963, pp. 453-537.

2 S. Meyerson, Appl. Spectroscopy 9, 120 (1955).

3 E. W. Boyer, M. C. Hamming, and H. T. Ford, Anal. Chem. 35, 1168 (1963).

4 M. Vestal, A. L. Wahrhaftig, and W. H. Johnston, J. Chem. Phys. 37, 1276 (1962).

5 M. J. O'Neal, Jr., and T. P. Wier, Jr., Anal. Chem. 23, 830 (1951).

6 H. E. Lumpkin and B. H. Johnson, Anal. Chem. 26, 1719 (1954).

7 A. B. King, J. Phys. Chem. 68, 1409 (1964).

8 J. L. Franklin, Ind. and Eng. Chem. 41, 1070 (1949).

9 F. D. Rossini, et al., Selected Values of Physical and Thermodynamic Properties of Hydrocarbons and Related Compounds, Amer. Petrol. Inst., Carnegie Press, Pittsburgh, 1953.

10 F. D. Rossini, et al., Selected Values of Chemical Thermodynamic Properties, Natl. Bur. Standards Circ. 500 (1952).

11 F. H. Field and J. L. Franklin, Electron Impact Phenomena, Academic Press, New York, 1957.

12 S. Meyerson and H. Hart, J. Am. Chem. Soc. 85, 2358 (1963).

13 W. A. Chupka, J. Chem. Phys. 30, 191 (1959).

14 H. M. Rosenstock, M. B. Wallenstein, A. L. Wahrhaftig, and H. Eyring, Proc. Natl. Acad. Sci. U.S. 38, 667 (1952).

15 L. Friedman, F. A. Long, M. Wolfsberg, J. Chem. Phys. 26, 714 (1957).

16 A. B. King and F. A. Long, J. Chem. Phys. 29, 374 (1958).

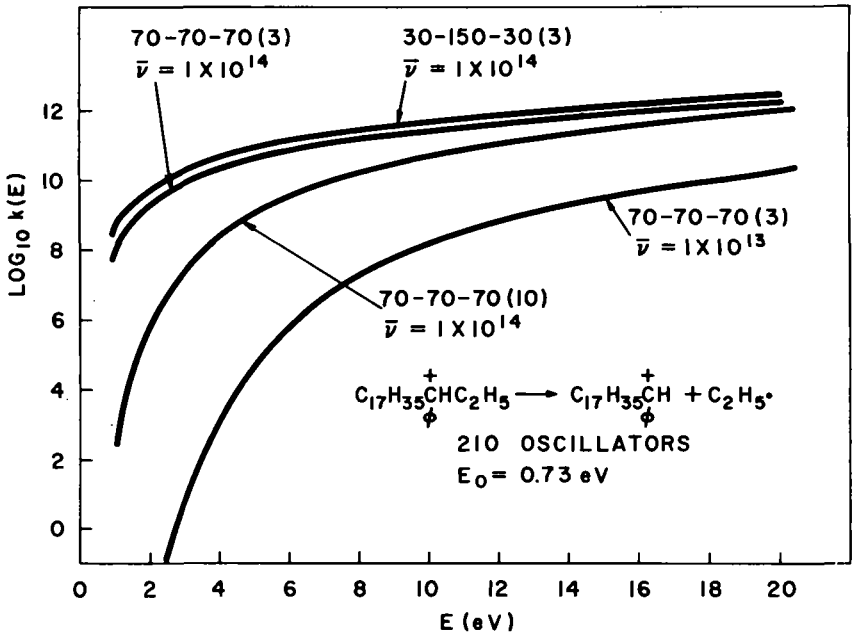

Figure 6 Calculated rate constants for the m/e 358 ⟶ m/e 329 for 3-phenyl eicosane. Frequency distributions indicated refer to the number of frequencies with the value $\bar{\nu}/R$, $\bar{\nu}$, and $R\bar{\nu}$, respectively, with the value of R in parenthesis.

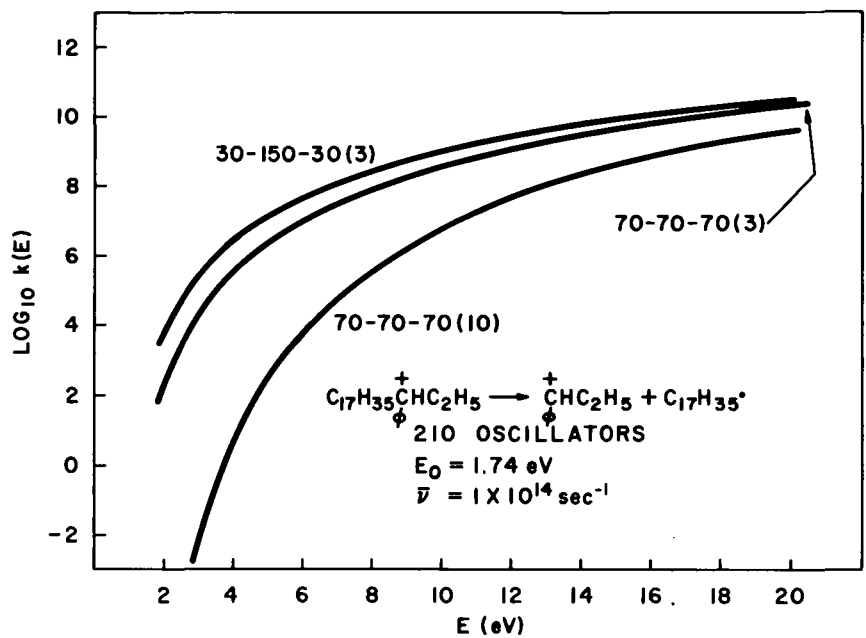

Figure 7 Calculated rate constants for the m/e 358 ⟶ m/e 119 for 3-phenyl eicosane. Frequency distributions indicated as in Figure 7.

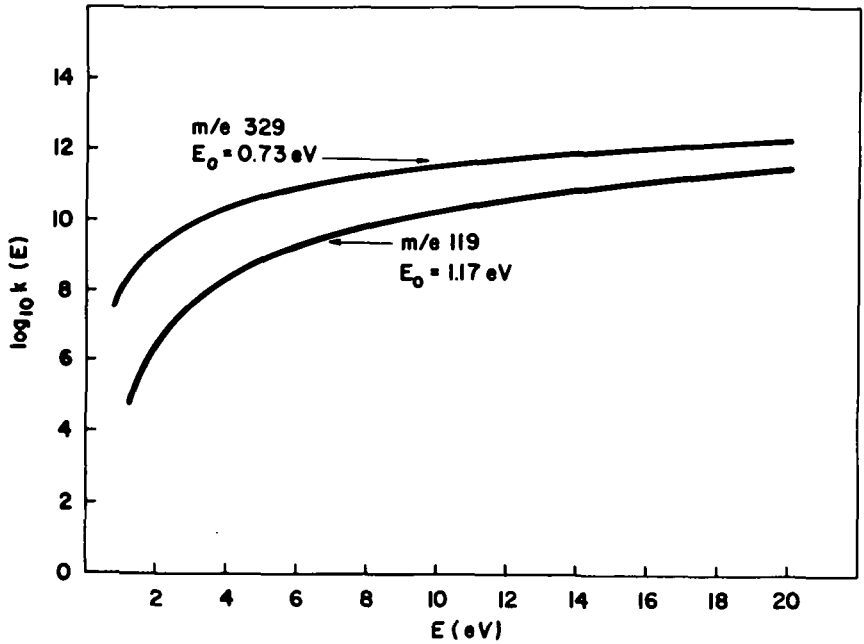

Figure 8 Calculated rate constants for the formation of m/e 329 and 119 from 3-phenyl eicosane based on activation energies corrected for kinetic shift and a frequency distribution of 70-70-70, with R = 3.0, and $\bar{\nu} = 1 \times 10^{14}$ sec^{-1}.

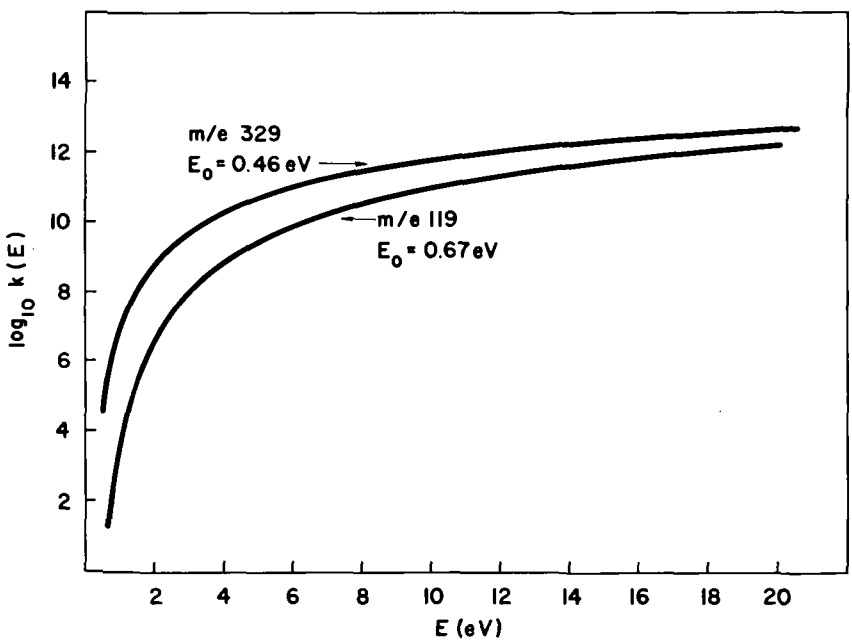

Figure 9 Calculated rate constants for the formation of m/e 329 and 119 from 3-phenyl eicosane based on activation energies corrected for kinetic shift and a frequency distribution of 70-70-70, with R = 10.0, and $\bar{\nu} = 1 \times 10^{14}$ sec^{-1}.

Mass Spectrometric Study of the Photoionization Of Acetylene, Acetylene-d_2, Benzene, and Benzene-d_6

Vernon H. Dibeler and Robert M. Reese
National Bureau of Standards
Washington, D.C.

Nearly monochromatic photon beams have been used for many years to study photoionization processes in low-pressure gaseous systems. Weissler[1] has reviewed the early work on atoms and small molecules and several authors[2] have discussed more recent work on larger molecules. Recently, Tanaka and co-workers have re-examined absorption spectra in the vacuum ultraviolet for rare gases[3] and other molecules[4]. Watanabe, et al [5] have also summarized measurements of ionization energies for many kinds of molecules.

Of major importance in the advancement of photoionization studies is the recent introduction of mass spectrometric techniques[6]. In principle, this development permits the identification of the ionization process and obviates uncertainty in the chemical composition of the species. However, previously reported systems either have incorporated a lithium fluoride window to separate the gas-discharge photon source from the monochromator (thus limiting the energy range) or have used a low-pressure repetitive spark source which provides a widely-spaced line spectrum. The latter frequently makes it impossible to determine the onset of ionization within several tenths of an electron-volt.

We have recently completed the construction of a combined mass spectrometer and vacuum ultraviolet monochromator designed to avoid these difficulties and are applying it to the study of photoionization processes in the energy range 2000 to 600Å (6 to 21 eV). The present report gives a brief description of the arrangement and the results of initial measurements on ordinary and completely deuterated acetylene and benzene. More nearly complete details appear elsewhere[7].

EXPERIMENTAL

A schematic diagram of the apparatus is shown in Figure 1. A photon source, L; a Seya-Namioka type [8] monochromator, M; and a conventional 6" radius of curvature sector-field mass spectrometer, N, are combined essentially in the manner first described by Hurzeler, et al [6b]. An important exception, of course, is the absence of a window making the entire vacuum ultraviolet region accessible.

The monochromator has a focal length of 1 meter and with a grating of 600 grooves/mm gives a first-order dispersion of 16.6Å/mm. The grating (Gr) is rotated manually or by synchronous motor and can be set to better than 1Å when travelling in one direction. Slits S_1 and S_4 are the optical entrance and exit slits. Replaceable slits of 0.05, 0.1 and 0.5 mm are available. Slits S_L, S_2, and S_3 separate the differential pumping ports, P_L, P_1, and P_2. These are pumped by 80 liter /sec mechanical, 400 ℓ/sec Heraeus-Roots, and 700 ℓ/sec oil diffusion pumps, respectively. The monochromator is pumped (P_3) by a 1400 ℓ/sec oil diffusion pump.

The base pressure of the monochromator is about 3 X10^{-7} torr. With the lamp operating at 200 torr and with 0.1 mm slits at S_1 and S_4, the present system maintains a pressure of 2 X10^{-4} torr in the monochromator.

Slit S_5 represents the ion-defining slit of the mass spectrometer. The ion source housing and analyser tube are pumped separately by mercury diffusion pumps. Under the above conditions, these pumps maintain

pressures of 10^{-6} and 10^{-7} torr in the source housing and analyser tube, respectively.

A conventional Nier-type ion source was modified for this application, taking particular care so that the photon beam could enter and leave the ionization chamber without illuminating any metal surfaces before reaching the photon detector. The latter consists of two parallel sheets of tungsten 10 X 40 X 0.1 mm separated by a few mms and mounted at a 70° angle with the photon beam. The anode plate is biased + 45v with respect to the cathode. Photoelectrons leaving the cathode are measured by means of a vibrating reed electrometer.

Two types of photon sources were used. The first is a Hinteregger-type[9] in which a hydrogen or rare-gas discharge is excited by a d.c. supply. Figure 2 shows a tracing of the photoelectric current for the familiar many-line spectrum of hydrogen obtained at a pressure of a few torr. The broad energy range makes this generally useful but the rapid change in intensity with wavelength is a disadvantage.

Figure 3. shows the well-known argon continuum[10] obtained at 400 mm using a 2450 MHz microwave discharge. A similar curve for the helium continuum extending to 600Å is obtained with the Hinteregger lamp. As yet, we have been unable to excite the He continuum using the microwave discharge. The slow variation of intensity with wavelength and the continuous nature of these emission spectra are of particular advantage in this work.

RESULTS AND DISCUSSION

The photoionization efficiency curve for the $C_2H_2^+$ ion of acetylene obtained with a H_2-discharge is shown in Figure 4. The photon yield (ions/photon) is plotted as a function of the wavelength in angstroms. The first sharp rise is interpreted as the 0-0 transition for the lowest energy electron. This is followed at nearly uniform intervals by several well-defined onsets taken to be the vibrational levels of the ground state of the ion. Figure 5 shows a very similar curve for the $C_2D_2^+$ ion of acetylene-d_2.

The observed ionization energies are summarized in Table I. For C_2H_2, the arithmetic mean of five determinations of the first ionization energy is 1087±0.6Å or 11.406 ±0.006 eV. The analogous values for C_2D_2 are 1086±0.6Å or 11.416 ± 0.006 eV.

From two Rydberg series in C_2H_2, Price [11] determines I (C_2H_2)= 11.41 eV. Watanabe [12] obtains an identical value by photoionization. Lossing, Tickner, and Bryce [13], using electron impact, report 11.40 v for C_2H_2 and 11.39 for C_2D_2. However, they consider the ionization potentials identical within the limits of their measurements. From the present results it would appear that I (C_2D_2) is greater than I(C_2H_2) by about 0.01 eV as expected from differences in zero-point energy.

The nearly uniform vibrational energy differences for $C_2H_2^+$ (0.23 eV or 1855 cm^{-1}) and for $C_2D_2^+$(0.22 eV or 1775 cm^{-1}) are in good agreement with the ν_2 (carbon-carbon stretching frequency) of the 3R state of the acetylenes determined by Wilkinson[14] to be 1848cm^{-1} and 1720 cm^{-1}, respectively.

There have been several calculations of the ionization energies of the $1\pi_u$ and the $3\sigma_g$ orbitals in acetylene [15]. In addition, Collin[16] reports RPD measurements of 11.50, 13.25, 14.40, and 16.95 eV for the ionization energies. Lindholm, et al [17], using a charge-exchange

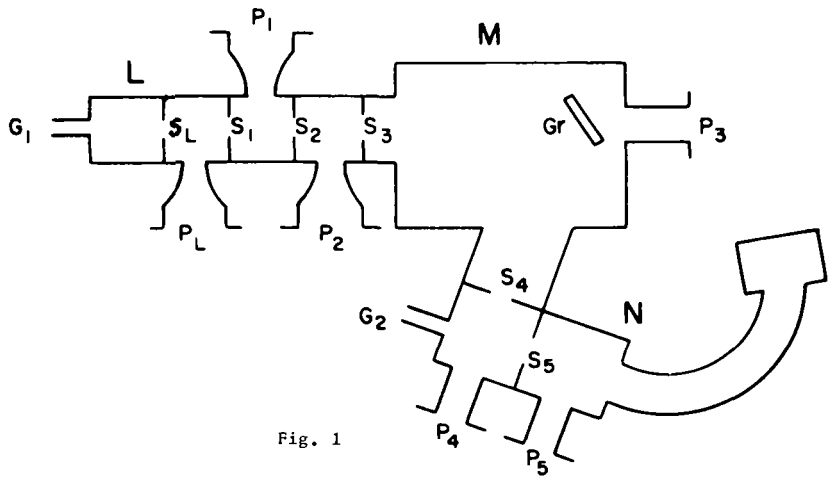
P1
M
L
G1
SL
S1
S2
S3
Gr
P3
PL
P2
S4
G2
N
S5
P4
P5

Fig. 1

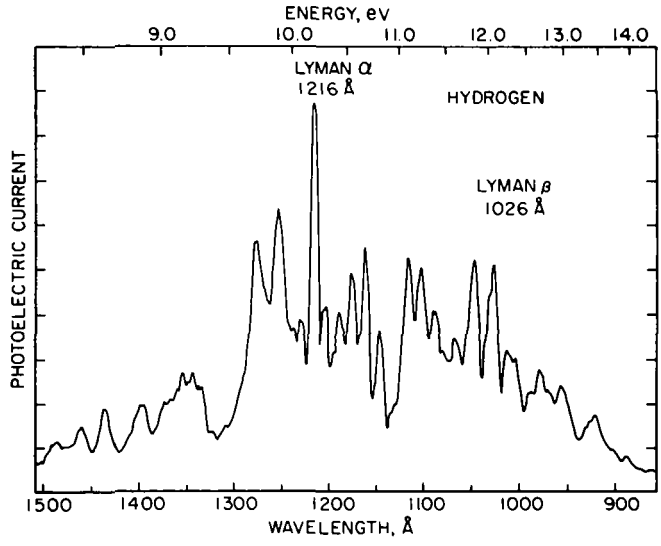
ENERGY, eV
9.0
10.0
11.0
12.0
13.0
14.0
LYMAN α
1216 Å
HYDROGEN
LYMAN β
1026 Å
PHOTOELECTRIC CURRENT
1500
1400
1300
1200
1100
1000
900
WAVELENGTH, Å

Fig. 2

method, obtained only 11.4 and 15.5 eV. In the present work there is little evidence for more than the first ionization energy below 13.75eV which supports Lindholm's observations. There is a suggestion of a low-intensity band about 13.5 eV which could be autoionizing Rydberg levels leading to a second onset at about 15.5 eV. If the excited state were bent, these levels might be expected to be diffuse and very weak.

The ionization efficiency curves for the $C_6H_6^+$ and the $C_6D_6^+$ ions obtained by means of the argon continuum and the H_2-discharge are shown in Figure 6. Although only shown to 1000Å, the curves are continuous, smooth and slowly rising to 900Å. The first ionization energies are $9.24_2 \pm 0.01$ eV for C_6H_6 and $9.24_5 \pm 0.01$ eV for C_6D_6. Wilkinson[18] identified four Rydberg series in the benzenes all leading to the ionization energies 9.247 ± 0.002 eV (C_6H_6) and 9.251 ± 0.002 eV (C_6D_6). Recent photoionization measurements are essentially identical [19].

Comparison of the curves with that obtained by Fox and Hickam [20] using the RPD method shows considerable agreement. The first Rydberg bands at 10.4 eV and the subsequent onset in the 11 eV region are observed in both cases. Fox did resolve an additional onset below the first Rydberg level which does not appear in our work. However, this may be observed by the sharply rising continuum in this region.

There are four interesting features of the benzene curves that should be noted:

1. Observation of partially resolved vibrational excitation at threshold,
2. A sharp rise in the continuum originating at or near the threshold of ionization,
3. Autoionization resonance bands beginning at 10.4 eV and merging into an unresolved structure, and
4. The onset of at least one new continuum at 11.5 eV.

Possibly the most interesting feature is the sharply rising continuum. This could be attributed to a second ionization continuum to a state with a much different geometric configuration. Such a transition would certainly be the removal of a σ framework electron from the 2 e_{2g} orbital. This could be construed as support for the recent conclusion by Hoffmann[21], based on a Hückel calculation including σ and π electrons, that the 2 e_{2g} orbital has a low ionization energy almost equal to that of the 1 e_{1g} orbital. The latter, of course, is usually considered to be by far the lowest energy orbital.

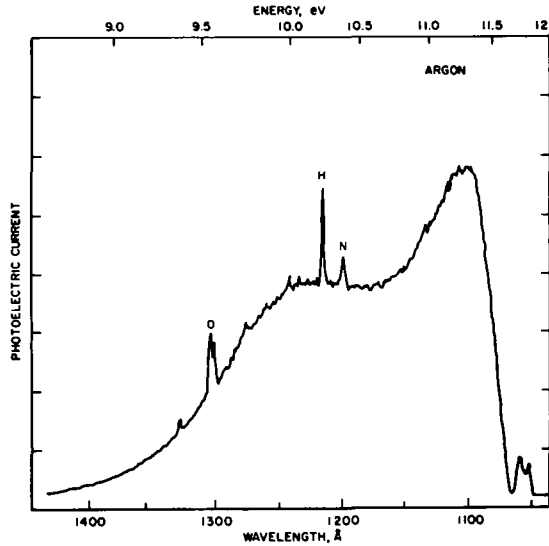
ENERGY, eV
9.0
9.5
10.0
10.5
11.0
11.5
12.0
ARGON
H
N
O
PHOTOELECTRIC CURRENT
1400
1300
1200
1100
WAVELENGTH, Å

Fig. 3

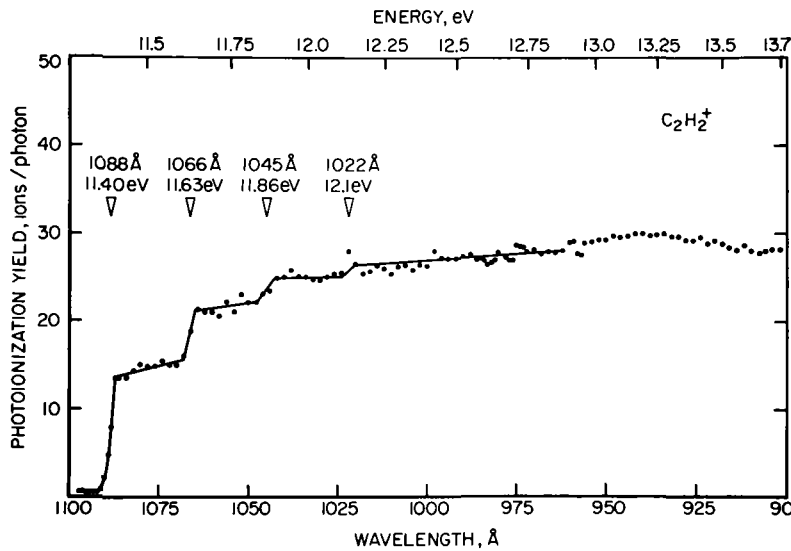
ENERGY, eV
11.5
11.75
12.0
12.25
12.5
12.75
13.0
13.25
13.5
13.75
$C_2H_2^+$
1088Å
11.40eV
1066Å
11.63eV
1045Å
11.86eV
1022Å
12.1eV
PHOTOIONIZATION YIELD, ions / photon
50
40
30
20
10
1100
1075
1050
1025
1000
975
950
925
900
WAVELENGTH, Å

Fig. 4

References

[1] G.L. Weissler, Handbuch der Physik, Springer-Verlag Berlin, 1956. Vol. 21, p.304.

[2]a. E.C.Y. Inn, Spectrochimica Acta, 7, 65 (1955).

b. W.C. Price, Advances in Spectroscopy, Vol.1 Interscience Publishers, New York, 1959. p.56.

[3] Absorption coefficients of xenon and argon in the 600-1025Å wavelength regions. R.E. Huffman, Y. Tanaka, and J.C. Larrabee, J.Chem. Phys. 39, 902 (1963).

[4] R.E. Huffman, Y. Tanaka, J. C. Larrabee, J.Chem.Phys.39,910(1963)

[5] K. Watanabe, T. Nakayama, and J. Mottl, J. Quant.Spectrosc. Radiat. Transfer, 2 , 369 (1962).

[6]a. F.P. Lossing and I. Tanaka, J. Chem. Phys. 25, 1031 (1956).

b. H. Hurzeler, M.G. Inghram, and J.D. Morrison, J. Chem. Phys. 28, 76 (1958).

c. G.L. Weissler, J.A. R. Samson, M. Ogawa, and G.R. Cook, J. Opt. Soc. Am. 49, 338 (1959).

[7] V.H. Dibeler and R. M. Reese, J.Research, Natl. Bur. of Standards, 68A, 409 (1964).

[8] M. Seya, Sci. of Light 2, 8 (1952), T. Namioka, ibid 3, 15 (1954).

[9] R. J. Huffman, Y. Tanaka, and J.C. Larrabee, J. Opt. Soc. Am. 52, 851 (1962).

[10] Y. Tanaka, A.S. Jursa, and F. J. LeBlanc, J. Opt. Soc. Am. 48, 304 (1958).

[11] W.C. Price, Phys. Rev. 47, 444 (1935)

[12] T. Nakayama and K.Watanabe, J. Chem. Phys.40, 558 (1964).

[13] F.P. Lossing, A.W. Tickner, and W. A. Bryce, J. Chem. Phys. 19, 1254 (1951).

[14] P.G. Wilkinson, J. Mol. Spectroscopy 2, 387(1958).

[15] A.D.McLean, J. Chem.Phys. 32, 1595 (1960).

[16] J.E. Collin, Bull. Soc. Chim. Belges 71, 15 (1962).

[17] E. Lindholm, I. Azabo, and P. Wilmenius, Arkiv Fysik 25, 417 (1963).

[18] P.G. Wilkinson, Can. J. Phys. 34, 596 (1956).

[19] M.F. Amr El-Sayed, M. Kasha, and Y.Tanaka, J. Chem. Phys. 34, 334 (1961).

[20] R.E. Fox and W. M. Hickam J. Chem. Phys. 22, 2059 (1954).

[21] R.Hoffmann, J. Chem. Phys.

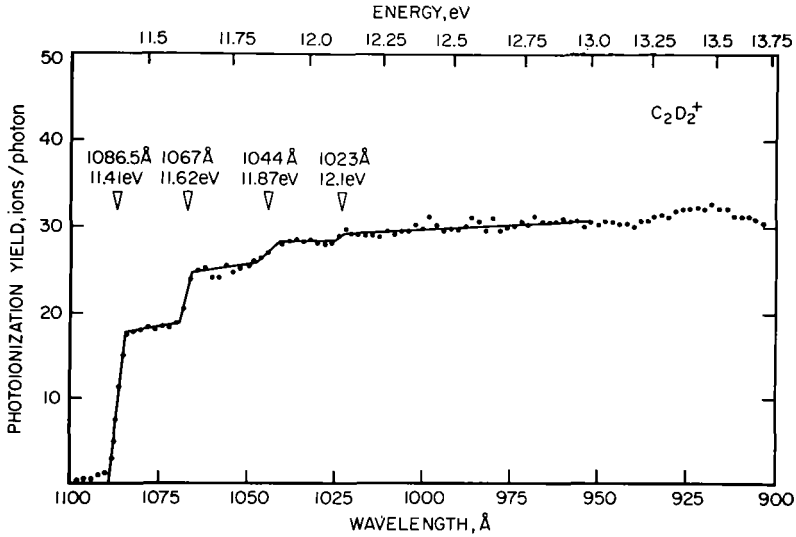
ENERGY, eV
11.5
11.75
12.0
12.25
12.5
12.75
13.0
13.25
13.5
13.75
50
40
30
20
10
PHOTOIONIZATION YIELD, ions / photon
$C_2D_2^+$
1086.5Å 11.41eV
1067Å 11.62eV
1044 Å 11.87eV
1023Å 12.1eV
1100
1075
1050
1025
1000
975
950
925
900
WAVELENGTH, Å

Fig. 5

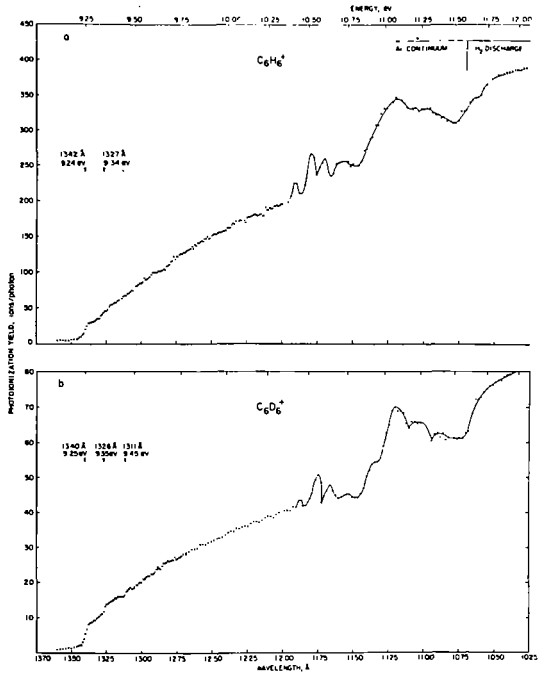
ENERGY, eV
a
$C_6H_6^+$
b
$C_6D_6^+$
PHOTOIONIZATION YIELD, ions/photon
WAVELENGTH, Å

Fig. 6

TABLE 1

Summary of ionization energies for acetylene and acteylene-d_2

Transition	Ionization Energy (eV) C_2H_2	C_2D_2
0-0	11.406±0.006	11.416±0.006
0-1	11.63 ±0.05	11.62 ±0.05
0-2	11.86 ±0.05	11.87 ±0.05
0-3	12.1 ±0.1	12.1 ±0.1

Figure Captions

Figure 1. Schematic diagram of apparatus showing arrangement of photon source (L), monochromator (M), mass spectrometer (N); slits (S), and pumping ports (P).

Figure 2. Tracing of recorded photoelectric current from photon detector as a function of wavelength for a dc H_2-discharge at a few torr. Entrance and exit slits are 0.1 mm and scan rate is 100Å/min.

Figure 3. Tracing of the recorded photoelectric current as a function of wavelength for the argon continuum at 400 torr using a microwave discharge.

Figure 4. Photoionization efficiency curve for the $C_2H_2^+$ ion of acetylene. The ordinate scale is in arbitrary units.

Figure 5. Photoionization efficiency curve for the $C_2D_2^+$ ion of acetylene-d_2. The ordinate scale is in arbitrary units.

Figure 6. Photoionization efficiency curves for the $C_6H_6^+$ and the $C_6D_6^+$ ions of benzene and benzene-d_6 using the argon continuum. The ordinates are in arbitrary units.

Ionization of Polyatomic Molecules in Collisions with Excited Metastable Noble Gas Atoms.[1]

V. Čermák and Z. Herman*
Institute of Physical Chemistry,
Czechoslovak Academy of Science, Prague

During the past decade there has been a considerable amount of data gathered from the studies of electron impact ionization, photoionization and ionization by charge-transfer, which have given better insight into the processes of ionization and fragmentation of polyatomic molecules and have provided a basis for testing the validity of theoretical description of decomposition of excited molecular ions. However, little attention has been hitherto paid to another type of ionization, namely ionization in collisions with excited neutral particles, though such phenomena as the Penning effect in gaseous electronics, or the Jesse effect in radiation chemistry were known for a considerable period of time.

We studied ionization and fragmentation of lower hydrocarbons, methanol and ethanol in collisions with excited metastable helium, neon and argon atoms by means of mass spectrometric techniques. We feel that these studies are useful in connection with the theories of decomposition of excited molecular ions and with the studies of elementary reactions in highly energized systems. There are several features, in which this ionization differs from other types of ionization: first, the ionization occurs in collisions of two uncharged particles of thermal energy; second, the time of collision is several orders of magnitude longer than that for electrons and photons, and the collision has an adiabatic character; third, one electron only is involved in the ionization process.

The mass spectrometer was an ordinary Nier-type apparatus with a modified ion source using molecular beams (Fig.1): the beam of noble gas atoms emerges from a multichannel molecular jet, T_A, and the particles are excited by electron impact (electron energy was usually 1.0 ev below the particular ionization potential). If necessary, ions were removed from the beam by collecting them on a negatively biased repeller-like plate, C, by positive barrier of the grid, G, and by the potential difference applied across the deflecting plates, P_1,P_2. After about 10^{-5} sec., which is the time necessary for thermal atoms to travel to the collision region, B, the atomic beam contains practically only excited atoms in long-lived metastable states. Across the collision region the beam of molecules to be studied is directed from another molecular jet, T_B. Reactions between particles of both beams occur and their charged product are extracted and mass-analyzed. The pressure in the collision region varied between $5.10^{-5} - 5.10^{-4}$ mm. Hg. The reactions observed are of two types:

$$R^*_m + ABC \rightarrow R + ABC^+ + e \qquad \text{ionization}$$

$$R^*_m + ABC \rightarrow R + AB^+ + C + e \qquad \text{dissociative ionization}$$

The energy transferred from the metastable atoms appears both as the excitation energy of the molecular ion and the kinetic energy of the released electron etc.

$$E(R^*_m) = E_i\ (ABC) + E_e\ (ABC^+) + E_{el}$$

A certain distribution of the excitation energy of the molecular ion is therefore to be expected, that is the probability of absorption of particular energy by the molecular ion. Table I shows abundances of ionic species from n-butane, bombarded by metastable argon, neon and helium. It can be seen that the higher the maximum energy transferable, the larger the extent of fragmentation. The question now arises, what form has the distribution function for the excitation energy of the molecular ion? We determined it indirectly from the extent of fragmentation in our mass pattern and the break-down curves known from charge-transfer studies of Lindholm, et.al.[2-5] We constructed by trial and error a stepwise distribution function, which gave us the best agreement of total ionic abundances, calculated and experimental. The results for n-butane with argon, neon and helium are in Fig. 2. The shape of the distribution function is practically the same for He and Ne, and that of Ar exhibits also a similar increase at the beginning. The curves are, of course, cut away at the maximum energy available from the particular metastable atom. The function falls away at higher energies and exhibits two maxima. An interesting comparison is available with the distribution function for butane ion, obtained by Chupka and Kaminski[6] from second-derivative electron-impact ionization curve: the first maximum compares well, but the second is much more pronounced in our case. Both maxima are located where theory predicts excited states in the molecular ion, as is shown in the lower portion of the figure. Similar results hold for propane: Table II shows experimental ionic abundances from metastable atom impacts, compared with calculated abundances, using the described procedure with chosen distribution functions, as can be seen in Fig. 3.

Again - two maxima, the first, at about 1 ev of excitation energy at the same position as on Chupka's second derivative electron-impact curve (and at the same place as the first maximum in n-butane), the second hump again much more pronounced. The distribution functions for ethanol, obtained in the same way, can be seen in Fig. 4 where the positions of maxima can be correlated with theoretically calculated positions of the excited levels in the molecular ion.[7] In Fig. 5 there are distribution functions for methanol. The first maximum corresponds probably to ionization of electrons in π- and y^1- orbitals (13 ev), the second to removal of electron from antisymmetrical π- and z^1- orbitals (about 15 ev).[3] In all four cases the shape of the distribution functions resemble that of energy distribution functions determined by means of a quite different technique in electron-impact experiments, and the maxima can be correlated with energies of molecular orbitals. This is a very encouraging result, as our energy distribution functions were determined without any a priori assumption about their shape. The pronounced second maxima are significant in this respect. It turns out that if polyatomic molecules are ionized by excited neutrals, more excitation energy is imparted to molecular ions than in impact of electrons of the same energy. This was confirmed by comparing the ionic abundances with mass spectra obtained separately with electrons of the energy 11.7, 16.6 and 20 ev, the energies of metastable Ar, Ne and He respectively. (Tables I, II and III.) It seems, therefore, that the transfer of higher energy is characteristic for collisions, in which neutral particles come fairly close to each other in the moment of reaction.

Table III summarizes ionic abundances in methane, bombarded by excited neon and helium. The ionic abundances in both spectra are very similar. We have used our older data on charge-transfer between noble gas ions and methane molecules, and have constructed approximate break-down curves for methane (Fig. 6).

We were then able to construct a rough energy distribution function, which fits the ionic abundances. It can be seen that for excitation energies above 3 ev there is very small probability of energy absorption. There is probably again an absorption region at about 7 ev, around the reported excited state of methane ion.[8] Conclusions, pointing to separate electronic states in molecular ions, can be drawn from our experiments with acetylene and ethylene.[1]

There are several interesting aspects of studies of ionizing reactions between excited metastable particles and molecules:

1. If the energy of the released electron is measured, direct data on energy distribution in molecular ions may be obtained; we have started these experiments already, but no sufficient data are available as yet;
2. The adiabatic character of the collision gives the possibility to obtain upper limits of appearance potentials of certain ions: thus we were able to show that the appearance potential of propyl-ion from propane and ethylene-ion from ethane and propane is lower than 11.7 ev;
3. On the other hand, extent of fragmentation or ionization in a mixture of suitably chosen gases can reveal the existence of long-lived metastable excited states in neutral particles: this was one of our methods, by which we demonstrated the existence of highly excited, long-lived states of noble gas atoms;
4. As the cross section of these processes is presumably quite high just above the ionization potential of the struck particle, an interesting possibility arises of selective ionization of free radicals by low-energy metastables, like xenon or krypton.

References:

1. V. Čermák, Z. Herman: to be published in Coll. Czech. Chem. Comm.
2. Koch von H., Lindholm E.: Arkiv for Fysik, 19, 123(1961).
3. Wilmenius P., Lindholm E.: ibid 21, 97 (1962).
4. Petterson E., Lindholm E.: ibid 24, 49 (1963).
5. Chupka W.A., Lindholm E.: ibid 25, 349(1963).
6. Chupka W.A., Kaminski M.: J. Chem. Phys. 35, 1991(1961).
7. Rosenstock H.M., Krauss M.: in Mass Spectrometry of Organic Ions, (McLafferty F.W., Ed.) Academic Press, New York, 1963.
8. Frost D.C., McDowell C.A.: Proc. Roy. Soc.(London) 241A, 194(1957).

*) Present address: Sterling Chemistry Laboratory, Yale University, New Haven, Connecticut

TABLE I

Ion Abundances in % from Reactions of Excited Atoms with n-butane.

		Experiment			Calc.			Electron impact			
m/e	A.P., V	Ar*	Ne*	He*	Ar*	Ne*	He*	11.5-12ev	16.5ev	20ev	50ev
58	10.8	18.3	2.8	2.9	18.4	2.9	3.4	36.0	18.9	11.4	4.7
57	12.1		1.0	0.5		1.8	1.5		2.7	2.0	0.9
43	10.9	69.4	31.7	24.9	69.6	32.3	26.4	49.8	41.3	54.2	37.9
42	10.9_7	12.3	3.8	4.1	12.0	4.2	3.3	13.3	11.7	7.6	4.7
41	13.1		20.2	16.6		18.1	17.4_5		7.7	8.4	10.4
40				0.8							
39	15.9			7.6			2.6		0.4	0.6	4.0
29	12.1		20.0	21.3		21.3	21.4		7.7	7.5	14.9
28	11.4		10.0	8.4		9.3	9.1	0.9	8.5	5.9	10.9
27	14.4		10.5	12.9		10.2	14.1		1.1	1.8	10.8
15	16.5						0.7			0.3	0.6

TABLE II

Ion Abundances in % from Reactions of Excited Atoms with Propane

		Experimental			Calc.			Electron Impact			
m/e	A.P., V	Ar*	Ne*	He*	Ar*	Ne*	He*	11.5-12ev	16.5ev	20.5ev	50ev
44	11.2	72.6	6.0	4.2	72.5	5.6	4.2	74.4	24.6	19.8	8.9
43	11.5-11.7 -12.0	16.2	5.7	4.1	16.3	7.0	5.8	16.3	18.7	16.0	7.5
42	12.2		1.8	2.2		1.7	1.5		3.2	3.4	1.9
41	13.7		6.8	8.1		7.8	9.6		1.6	4.0	4.3
40	14.8		1.0	1.5						0.4	0.9
39	15.7		0.6	10.2			3.3			0.1	6.1
29	12.0		37.1	24.7		37.0	28.9		29.3	32.4	32.4
28	11.6-11.75 -12.3	11.2	20.0	16.6	11.2	20.0	18.3	9.3	21.8	19.6	19.0
27	14.0		19.6	25.0		19.5	25.3		0.8	4.1	13.6
26	14.5		1.4	1.5		1.3	2.3		0	0.1	2.9
15	17.0			0.5			0.7			0	2.3

TABLE III

Ion Abundances in % from Reactions of Excited Atoms with Methane

		Experiment		Calc.	Electron Impact		
m/e	A.P., V	Ne*	He*	Ne*	16.5ev	20ev	70ev
16	13.1	44.1	39.5	44.3	74.2	62.7	46.8
15	14.4	52.6	56.6	52.4	25.4	36.1	40.0
14	15.6	3.3	4.8	3.3	0.4	1.2	8.0
13	23.0						4.0

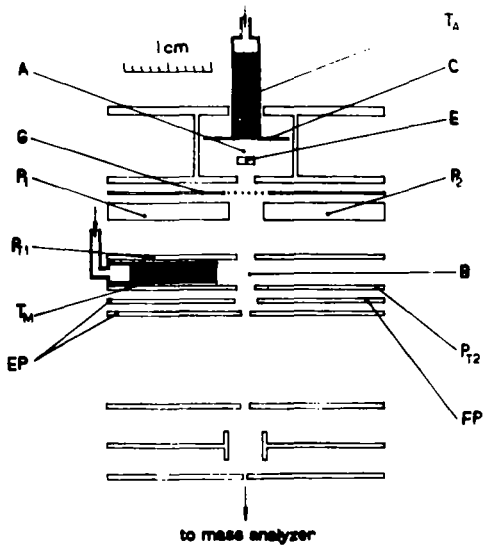
1cm
A
C
E
G
P_1
P_2
P_{T1}
B
T_M
EP
P_{T2}
FP
to mass analyzer

Fig. 1

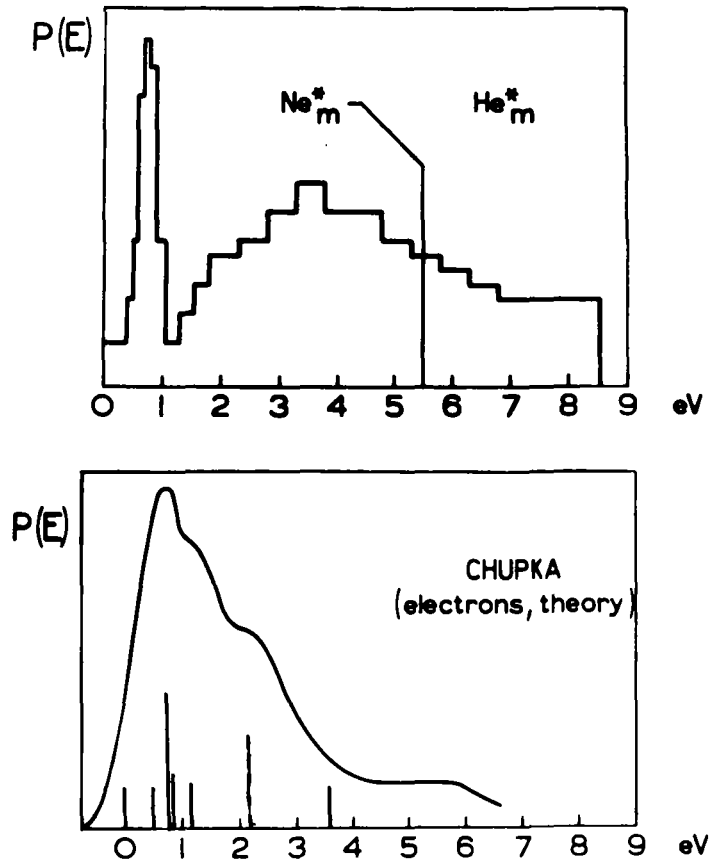
P(E)
Ne^*_m
He^*_m
0 1 2 3 4 5 6 7 8 9 eV
P(E)
CHUPKA
(electrons, theory)
0 1 2 3 4 5 6 7 8 9 eV

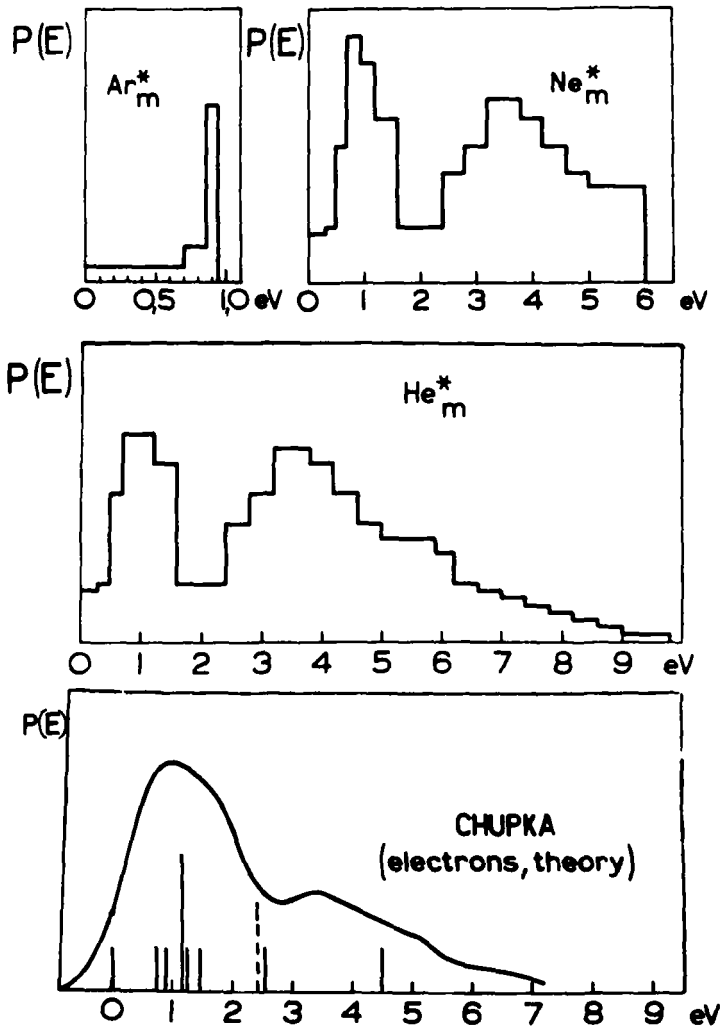
P(E)
Ar*m
0
0,5
1,0
eV
P(E)
Ne*m
0
1
2
3
4
5
6
eV
P(E)
He*m
0
1
2
3
4
5
6
7
8
9
eV
P(E)
CHUPKA
(electrons, theory)
0
1
2
3
4
5
6
7
8
9
eV

Fig. 2

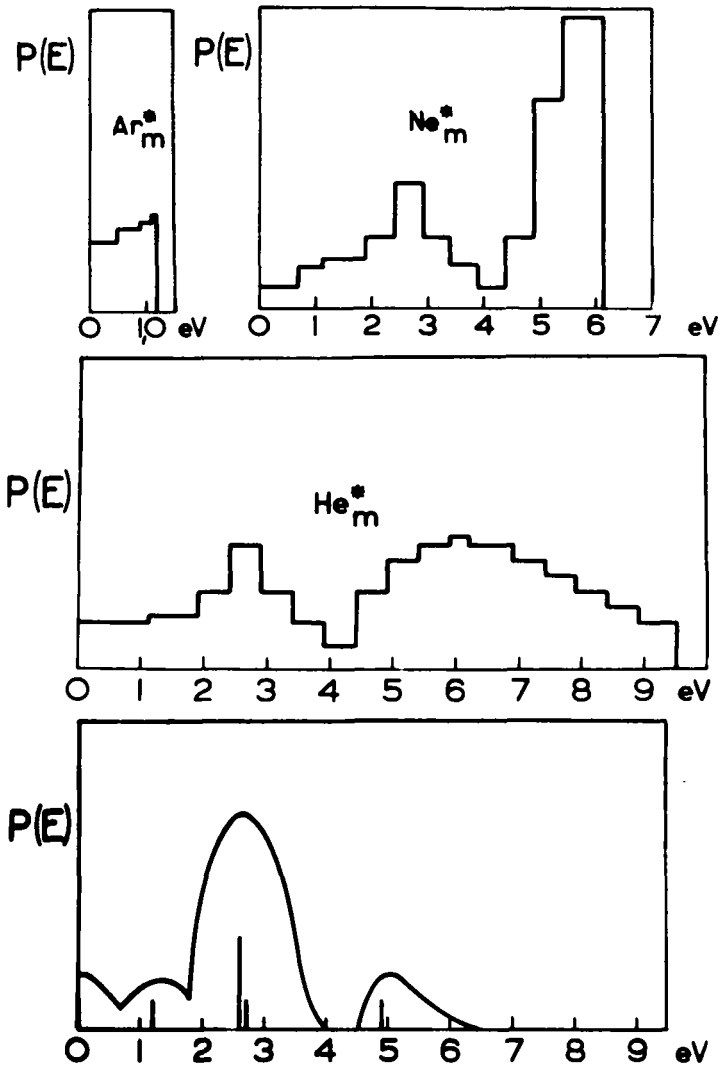
P(E)
Ar*m
0 1,0 eV
P(E)
Ne*m
0 1 2 3 4 5 6 7 eV
P(E)
He*m
0 1 2 3 4 5 6 7 8 9 eV
P(E)
0 1 2 3 4 5 6 7 8 9 eV

Fig. 4

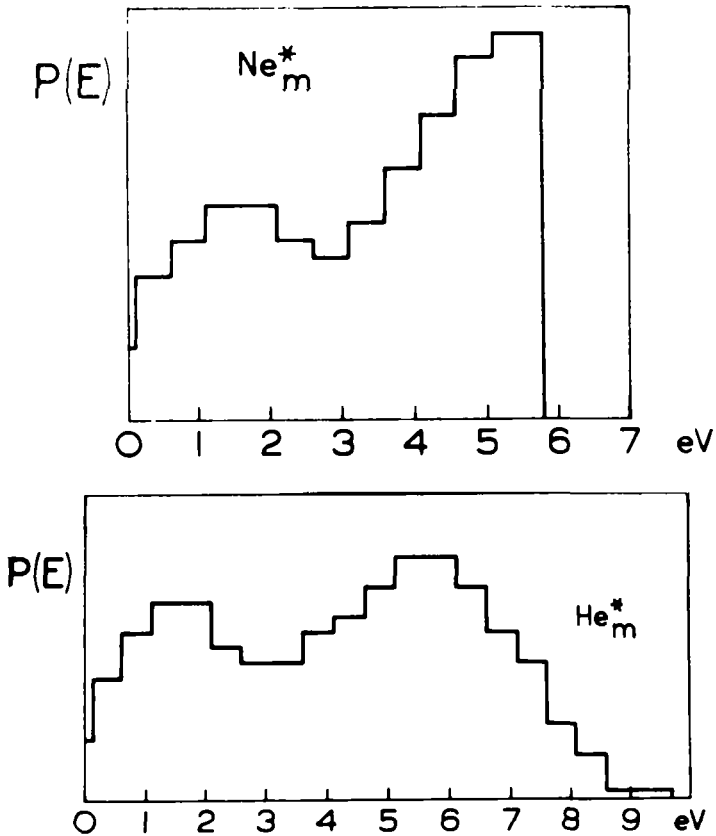
P(E)
Ne*m
0 1 2 3 4 5 6 7 eV
P(E)
He*m
0 1 2 3 4 5 6 7 8 9 eV

Fig. 5

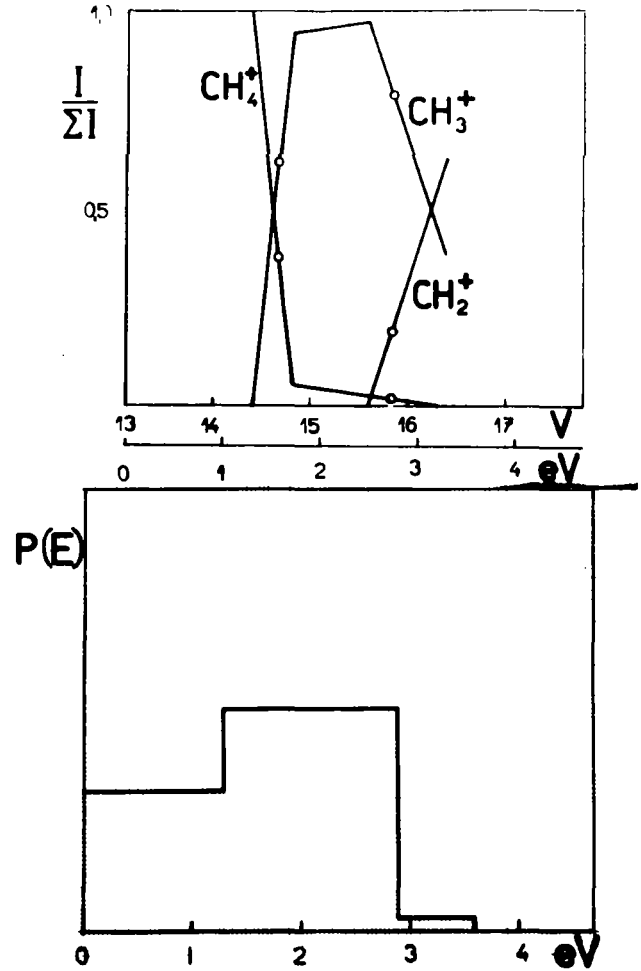
I/ΣI
1,0
0,5
CH4+
CH3+
CH2+
13 14 15 16 17 V
0 1 2 3 4 eV
P(E)
0 1 2 3 4 eV

Fig. 6

RARE GAS ION REACTIONS WITH PENTABORANE-9

G. R. Hertel and W. S. Koski
Department of Chemistry
The Johns Hopkins University
Baltimore, Maryland 21218

INTRODUCTION

Recent studies[1-3] of radiolyses of the boron hydrides have reported the formation of higher hydrides as a result of the coupling of hydride fragments. When 2 Mev. deuterons were used to irradiate pentaborane-9 in the gas phase, the products included decaborane-16, diborane, hydrogen, and polymeric materials. Experiments in which the rare gases were used as sensitizers varied the relative yields of the products and, in the cases of helium, neon, and argon sensitization, produced small amounts of tetraborane-10 and hexaborane-10. From these studies and others, involving iodine as a scavanger and deuterium as a tracer, a mechanism was proposed in which BH, postulated as a fragmentation product, abstracts hydrogen from pentaborane, stepwise, giving B_5H_8 and BH_3 radicals. Decaborane-16 and diborane are believed to result from dimerization of these radicals.

The use of rare gases as sensitizers enables a controlled amount of energy to be imparted to the pentaborane molecule. The ionizing radiation excites and ionizes the rare gas atoms which subsequently transfer energy to the pentaborane molecules through charge-exchange or collisions. The pentaborane molecules, thus, will be ionized and possibly fragmented, depending on the amount of energy transferred. Xenon, with a recombination energy of 12.13 ev., should produce very little fragmentation, while helium, with a recombination energy of 24.58 ev., should highly fragment the pentaborane molecules. The obvious effect of this on the relative yields would be a maximum yield of diborane with helium and a minimum with xenon, as was observed in the radiolysis experiment[3].

A study of the ionic products of rare gas ion-pentaborane-9 reactions was undertaken in an attempt to acquire detailed information about the mechanism of rare gas sensitization.

Such studies of positive ion bombardment of polyatomic molecules are also of interest to the mass spectroscopist. Lindholm and his co-workers[4-6] have carried out extensive investigations of mass spectra produced by positive ion bombardment. They obtain breakdown curves, experimentally, for some polyatomic molecule (e.g. ethanol) by bombarding it with a large variety of singly and doubly charged positive ions, recording the relative abundances of the fragmented ionic products, and plotting these abundances versus the recombination energies of the bombarding ions. Thus, they are able to make direct comparisons with the breakdown curves calculated from the quasi-equilibrium theory of mass spectra.[7]

Although no calculations have been attempted for the rather peculiar boron hydrides, the application of Lindholm's technique to the data yielded an interesting, although rough, estimate of the probable breakdown pattern.

EXPERIMENTAL

The instrument used in this experiment has been described previously.[8] There have been a few minor modifications which have improved the selection and focusing of the primary ion beam.

Basically, the instrument consists of two mass spectrometers in a tandem arrangement similar to that used by Lindholm.[9] The primary mass spectrometer is a 180°, 1 cm. radius of curvature commercial instrument known as a Diatron and manufactured by Consolidated Electrodynamics Corporation. A specially designed permanent magnet, constructed by Indiana General Corporation, produces a field strength of approximately 2500 gauss for the Diatron. This enabled selection of Xe^+ at an accelerating voltage of approximately 2 volts, Kr^+ at a voltage of about 3.5 volts, etc. After magnetic selection, this primary beam was focused, accelerated or decelerated to the desired energy, and refocused into the reaction chamber. The ionic products were extracted from the reaction chamber at an angle of 90° to the primary beam direction, accelerated and focused by a Nier-type lens, which has been modified by the addition of z-directional focusing plates, and magnetically analyzed by an 8" radius of curvature, 60° sector electromagnet. Detection was accomplished by an electron multiplier and suitable pulse counting equipment. Spectra were obtained by sweeping the secondary magnetic field and recording the output of a count-rate meter.

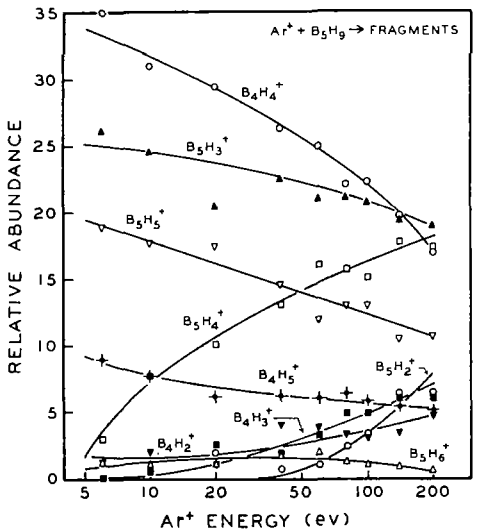

Fig. 1

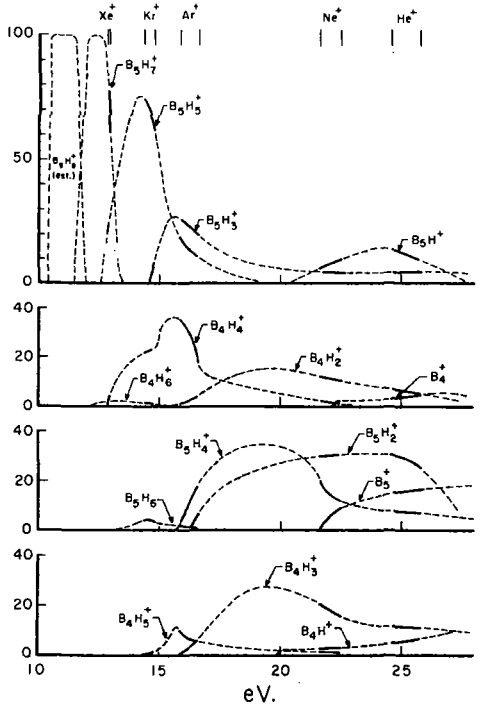

Fig. 2

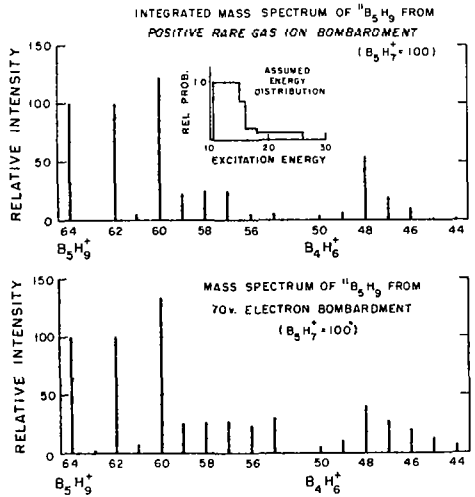

Fig. 3

The rare gases used in these experiments were research grade from various companies: helium from Airco Company; argon from Linde Company; and neon, krypton, and xenon from The Matheson Company. The pentaborane-9, purchased from the Callery Chemical Corporation, was distilled from trap to trap until no significant impurities were observed by mass spectrometric analysis.

The intensity of the primary beam passing through the reaction chamber could be measured by means of a Faraday cup connected to a Keithley Electrometer. Normal operating intensities were in the range of 10^{-12}-10^{-11} amperes. Secondary ion intensities were typically less than 100,000 counts per minute. The pressure in the vacuum manifold surrounding the source was nominally 1-2 x 10^{-5} Torr. during operation. The pressure in the reaction chamber is estimated to be a factor of 10 to 100 greater than the manifold pressure, or roughly 10^{-4}-10^{-3} Torr.

Since the pentaborane-9 contained the normal isotopic distribution of B-10 and B-11, the spectra had to be reduced to the corresponding monoisotopic spectra in order to determine the relative abundances of the ions produced. This was accomplished in the usual manner. The highest mass peak observed (M) was attributed to the ion containing five boron-11 atoms plus the appropriate number of hydrogens to give the observed mass. The contributions of this $B_5H_n^+$ ion to lower mass peaks were calculated and subtracted out. The remaining intensity of the M-1 peak was then due to the boron-11 contribution of the $B_5H_{n-1}^+$ ion. The procedure was repeated until the entire spectrum has been analyzed and the resulting monoisotopic spectrum deduced.

RESULTS AND DISCUSSION

Xenon bombardment produced relatively few ions, as expected, since the recombination energy is relatively low and the excess energy available to the $B_5H_9^+$ ion is less than 2 ev. Krypton changed the distribution of ions and produced more fragmentation. With argon, the major product was $B_4H_4^+$ and the fragmentation was quite extensive. Neon and helium continued this trend producing large amounts of highly fragmented species. Table I lists the relative abundances of the major products observed to illustrate the increasing fragmentation as the bombarding ion varied from xenon to helium.

It is obvious that one can qualitatively reconcile the observed data with the proposed mechanism. With xenon very few ions containing four boron atoms are produced which implies that very few BH radicals are formed. Thus, production of the radicals necessary for diborane and decaborane-16 formation is severely limited. As the rare gas is varied, the production of BH becomes more probable and thus the yields of the products should increase.

The mechanism attributes B_5H_8 formation to the abstraction of hydrogen by BH and BH_2, but only those B_5H_8 radicals which have had an apical hydrogen removed can couple to form decaborane-16. Therefore, for every decaborane-16 molecule formed, eight "useless" B_5H_8 radicals (assuming equal probability for removal of any one of the five terminal hydrogens) and five BH_3 radicals (or 2.5 diborane molecules) are formed. The ratio of diborane to decaborane-16 should be 2.5, then, if this mechanism is correct. The observed ratio in irradiation of pure pentaborane-9 was 2.83. In the rare gas sensitization experiments, the ratio varied from approximately 1 (for Xe) to over 10 (for He). For the cases where the ratio is greater than 2.5, it is possible to explain the increase in the diborane yield as due to more fragmentation and thus more BH radicals. The decrease in decaborane-16 could conceivably be due to a less quantitative production of B_5H_8 from the BH abstraction mechanism. With the large amounts of hydrogen-deficient fragments produced with He, Ne and Ar, a large amount of hydrogen must be present and readily available to the BH radicals.

In the Kr and Xe reactions, where the ratio is below 2.5, one must postulate an alternate mechanism for the production of decaborane-16. There is evidence that some of the $B_5H_n^+$ ions react rapidly to produce $B_{10}H_m^+$ ions ($m \leq 10$). A group of peaks in the $B_{10}H_m^+$ mass range were observed in the Xe^+ - B_5H_9 reactions when the pressure in the reaction chamber was increased two to five times the normal operating pressure. Similar $B_{10}H_m^+$ peaks and traces of $B_9H_n^+$ peaks were observed in the Kr^+ - B_5H_9 reactions under the same conditions of higher pressure. It is not inconceivable that such $B_{10}H_m^+$ ions would lead to decaborane-16 by hydrogen abstraction and finally neutralization. When the same "high" pressure conditions were produced in the Ar, Ne and He reactions, no peaks corresponding to ions higher than $B_5H_n^+$ were observed.

The bulk of the ions produced in all cases most probably end up in the polymeric solid material always found in the radiolysis.

The tetraborane-10 and hexaborane-10, observed with Ar, Ne, and He sensitization, can be attributed to some reaction or chain of reactions induced by some ion or ions produced by the higher recombination energies of these rare gases; e.g., possibly some $B_3H_n^+$ ion.

TABLE I

Relative abundances of pentaborane-9 fragment ions produced by rare gas ion bombardment. (Kinetic energy of rare gas ions = 10 ev.)

Ion	Xe	Kr	Ar	Ne	He
B_5H_7	73				
B_5H_6		2	1		
B_5H_5	20	76	18		
B_5H_4			8	11	7
B_5H_3	<1		25	8	7
B_5H_2				24	23
B_5H			3	3	8
B_5				6	15
B_4H_6	3	<1			
B_4H_5	<1	2	8		
B_4H_4	2	20	31	3	
B_4H_3			<1	19	11
B_4H_2		<1	2	11	4
B_4H			<1	1	13
B_4				1	3
B_3H_4			<1	2	
B_3H_3			2	4	4
B_3H_2			<1	6	3
B_3H					2

TABLE II

Important Recombination Energies of singly charged rare gas ions.

He	24.58 ev.
Ne	21.56 and 21.66 ev.
Ar	15.76 and 15.94 ev.
Kr	14.00 and 14.67 ev.
Xe	12.13 and 13.44 ev.

FIGURE CAPTIONS

FIGURE 1; Relative abundances of major products of Ar^+-B_5H_9 reactions as a function of the Ar^+ kinetic energy.

FIGURE 2; Breakdown curves of B_5H_9 as a function of the excitation energy. Solid line segments represent the experimentally determined points.

FIGURE 3; (Upper) Mass Spectra from integration of breakdown curves (Fig. 2). Assumed energy distribution shown in insert. (Lower) Mass Spectra from 70 v. electron impact data (Ref. 11).

It appears, however, that little can be said quantitatively about the detailed mechanisms of the reactions which give rise to the observed products. It seems likely that the radical mechanism, proposed by Subbanna, et al.,[3] is a possible, even probable, path which leads to the products. It also seems likely that ion-molecule reactions may contribute significantly to the observed yields.

When one is faced with the fragmentation of a complex, polyatomic molecule such as pentaborane-9, one is tempted to search for an approach which will add meaning to the observations made and perhaps indicate a logical pattern of decomposition. The procedure used by Lindholm, as outlined above, was applied to the rare gas ion-pentaborane-9 data. Although only five points were available for the breakdown curves, it had been observed that the relative abundances of the ions varied slowly with the kinetic energy of the primary ion beam, indicating that some reactions were being observed in which the relative kinetic energy of the colliding ion and molecule was contributing to the excitation energy imparted to the pentaborane. An example of this is shown in Fig. 1 where the relative abundances of secondary ions produced in the Ar^+ - B_5H_9 reactions are plotted as a function of the bombarding energy of the argon ions.

Lambert[10] has reported a simple empirical relationship between the frequency of the lowest fundamental mode and the average number of collisions required to produce a vibrational-translational transition in polyatomic gases. The experimental data indicates that the probability of a transition is determined mainly by the size of the vibrational quantum and the kinetic energy of the collision. Assuming that the implications of this relationship hold for the interaction of low velocity ions and molecules, a similar relationship was found for the energy transferred (E_{tr}) which varied logarithmically with the relative kinetic energy of the colliding species,

$$E_{tr} \sim \log\left(C \frac{h\nu}{E_{rel}}\right).$$

A value of 10^{14} was assumed for ν. C is a constant based on the assumption that our instrument is capable of detecting only those secondary ions having momentum vectors within an angle of 70°-110° from the primary beam direction. Admittedly, this is an empirical formula whose merit is that it fits the experimental data quite well. It appears to be based upon vibrational excitation only, overlooking any possibility of rotational excitation--a possibility which should probably not be ignored.

By taking into account the possibility of additional excitation energy as the relative kinetic energy increased, it was possible to construct breakdown curves for pentaborane-9 as shown in Fig. 2. The solid line segments are the experimentally determined abundances plotted as a function of the excitation energy.

Imagination was a great assist in filling in the dotted portions of the curves, but there were other factors available to guide the construction work. For example, the appearance potentials for several of these ions have been reported in the literature.[11] Also, one of the initially surprising observations--that no detectable parent ion was seen even with Xe^+ bombardment at low energies--must mean that the probability of producing $B_5H_9^+$ ions has decayed to essentially zero when the excitation energy is less than 2 ev. above the ionization potential of 10.4 ev. Thus, it is possible to estimate the parent ion curve. Beginning at 10.4 ev., the parent ion is the only ion produced. At the appearance potential of $B_5H_7^+$(11.4), the probability of producing the parent ion must drop rapidly as the $B_5H_7^+$ abundance rises. At the excitation energy supplied by Xe^+ ions, small amounts of $B_4H_6^+$ and $B_4H_4^+$ are present, the $B_5H_7^+$ abundance is already decreasing rapidly and the $B_5H_5^+$ intensity is increasing. At an energy corresponding to krypton excitation, the probability of producing $B_5H_7^+$ has vanished, the $B_5H_5^+$ is decreasing, and the intensities of other ions are gaining significance. Thus, it is possible to logically follow the growth and decay of the various ions as a function of the excitation energy imparted to the pentaborane molecule and construct reasonable breakdown curves.

In most cases where the appearance potentials were known, it was possible to use these values as the starting points of the curves. Exceptions were $B_4H_4^+$ (reported AP is 14.0 ev.), $B_4H_2^+$ (AP = 17.9 ev.), and $B_5H_4^+$ (AP = 13.0 ev.). The $B_5H_4^+$ curve does not seem to appear until well above 15 ev.; however, there may be an undetected low energy tail which actually extends down to the appearance potential. In the other two cases, the ions appeared with significant intensity at energies well below the reported appearance potentials. There is the possibility, of course, that the reported appearance potentials are incorrect. However, it is more probable that the mechanism responsible for producing these ions varies according to the excitation process employed. Any variations between positive ion and electron bombardment must be minor in this case since only two or three ions seem to show anomolous behavior.

A complication in applying this method is the existence in many cases of more than one important recombination energy for an ion. This is true for all rare gases except helium. The recombination energies are given in Table II. The two values arise from ions in the $^2P_{3/2}$ and $^2P_{1/2}$ states. For the purpose of constructing the breakdown curves, the two values for each ion were averaged. The only case in which the difference is sizable enough to create a problem is xenon. The resulting curves do not reflect any anomalies due to the averaging procedure although it is recognized that an accurate representation would require more rigorous consideration of the specific contributions of the individual recombination energies. It might be worthwhile to point out that one could decrease the disparity between the reported AP and the observation that Xe^+ bombardment produces $B_4H_4^+$ by assuming that the $B_4H_4^+$ arises due to excitation from the higher RE of xenon.

A comparison may be made between the mass spectrum obtained from electron impact studies and the curves in Fig. 2 by integrating the breakdown curves, assuming a proper energy distribution function. Chupka and Kaminsky[12] have determined, experimentally, the ionization efficiency curves for electron impact work on propane and n-butane and compared them with the assumed energy distributions which have been used in mass spectral calculations for these molecules. Using their curves as a guide, an energy distribution was assumed and an integrated mass spectrum was calculated from our data. The results are shown, along with the 70 v. electron impact spectrum[11] in Fig. 3. The agreement is generally satisfactory. The poor agreement at masses 55 and 56 (corresponding to B_5^+ and B_5H^+) is attributed to the upper limit of our data. Above 26 ev., extrapolation of the breakdown curves became very hazardous. Therefore, 26 ev. was taken as the upper limit of our integrations. As a result, ions requiring large amounts of energy are poorly represented. Also, the anomolous behavior of the $B_4H_4^+$ curve again is evident. The intensity of the integrated peak is 35% greater than the electron impact peak.

CONCLUSIONS

The mass spectrometer studies reported here indicate that the proposed radiolysis mechanism is qualitatively correct, but that fragmentation is greater than predicted. Initial loss of a hydrogen molecule, followed by loss of a second hydrogen molecule, appears to be the most probable decomposition path of pentaborane-9, after which loss of BH, H, or H_2 seem almost equally likely.

Of perhaps greater interest is the fact that reasonable breakdown curves can be constructed from charge-exchange data. A desired extension of this work would be further experimentation using a variety of bombarding ions, as Lindholm has done, to gain a better, more complete picture of the experimental curves. Ultimately, it would be of interest to compare the experimentally determined breakdown curves with those calculated from the statistical theory of mass spectra.

ACKNOWLEDGMENTS

This work was done under the auspices of the United States Atomic Energy Commission. G. R. H. is indebted to the Lever Brothers Co. Foundation for its support through a graduate fellowship. The authors wish to express their appreciation to Marsha S. Hertel who undertook the tedious task of reducing the original data to the monoisotopic spectra.

REFERENCES

1. H. Schmied and W. S. Koski, 38M abstract of papers, 135th meeting ACS, 1959.
2. L. H. Hall and W. S. Koski, J. Am. Chem. Soc., 84, 4205 (1962).
3. V. V. Subbanna, L. H. Hall, and W. S. Koski, J. Am. Chem. Soc., 86, 1304 (1964).
4. H. von Koch and E. Lindholm, Arkiv Fysik, 19, 123 (1961).
5. P. Wilmenius and E. Lindholm, Arkiv Fysik, 21, 97 (1962).
6. E. Pettersson and E. Lindholm, Arkiv Fysik, 24, 49 (1963).
7. H. M. Rosenstock, M. B. Wallenstein, A. L. Wahrhaftig, and H. Eyring, Proc. Nat. Acad. Sci. U. S., 38, 667 (1952).
8. E. R. Weiner, G. R. Hertel, and W. S. Koski, J. Am. Chem. Soc., 86, 788 (1964).
9. E. Lindholm, Z. Naturforsch, 9a, 535 (1954).
10. J. D. Lambert, "Atomic and Molecular Processes," ed. D. R. Bates, Academic Press, New York, 1962, p. 798.
11. Joyce J. Kaufman, W. S. Koski, L. J. Kuhns, and Sally S. Wright, J. Am. Chem. Soc., 85, 1369 (1963).
12. W. A. Chupka and M. Kaminsky, J. Chem. Phys., 35, 1991 (1961).

The Migration of Oxygen Atom In Unimolecular Ion Decomposition

I. Omura

Hitachi Central Research Laboratory,

Tokyo, Japan

Y. Nakajima and H. Sato

Scientific Instrument Dept., Naka Works,

Hitachi Ltd., Ibaragi Prefecture, Japan

INTRODUCTION

Detailed phenomena concerning hydrogen atom migration in unimolecular decomposition of organic molecular ions have been studied in analysing the fragmentation processes. Recently, also, the alkyl migration in esters has been studied from mass spectral analysis of benzoic acid.[1)]

New types of migration of oxygen atom and phenyl radical were obserbed in the mass spectral analysis of the organic molecules which have semipolar bond between nitrogen and oxygen atoms ($N \rightarrow O$).

In the mass spectra of organic molecules used as sample, there were the most interesting spectral peaks resulted from phenyl or oxygen migration, and they are assigned to diphenyl, diphenylmethane and benzophenone group ions when the sample was α-diphenyl-N-methylnitrone. The compound, α-diphenyl-N-phenylnitrone, also gave spectral peaks assigned to diphenyl and triphenylmethane group ions which were considered to be stable fragment ions. Such fragment ion may be considered theoretically to be resulted from the phenyl radical and oxygen atom migration in unimolecular ion decomposition. We have estimated the unimolecular decomposition rate constant for oxygen atom migration from peak intensities of the concerned fragment ions.

EXPERIMENTAL

The instrument used is a Hitachi ultra-high vacuum type mass spectrometer: modified RMU-6A, of a single focusing, 90° sector type with a radius of 200mm. The ion detector used are the electron multiplier with the total gain 5×10^6 and the D. C. amplifier with the corner frequency at 7kc/s. The recorder unit have one galvanometer with a natural frequency of 4000 cycles per second. Therefore, the mass range m/e 10~500 can be scanned magnetically within about one second. In addition, when one scan over the whole range mentioned above finished, electron accelerating voltage can be elevated automatically from low voltage to the high. Therefore, the total ion yield can be calculated as a function of the electron voltages.

The chemical formula of three kinds of samples used are shown by:

α-phenyl-N-methylnitrone

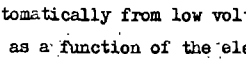

m. p. 83.5~84°C

α-diphenyl-N-methylnitrone

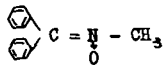

m. p. 105~108°C

α-diphenyl-N-phenylnitrone

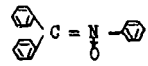

m. p. 210~215°C

The characteristic point in the three molecular structures is the semipolar bond N→O, in which oxygen atom can easily be migrated and can make a bond to the terminal methyl group under ultraviolet irradiation. Therefore, the sample charging were made in a dark room to prevent it from photoisomerization, and direct sample inlet into ionization chamber was applied.

Figure 1 shows the mass spectrum of α-phenyl-N-methylnitrone. The indication p means parent ion. According to the mass spectral analysis the oxygen atom migration causes terminal methyl radical to appear as the spectral peak at m/e 31 (CH_2OH) and a phenyl radical as the peak at m/e = 93 (C_6H_5O). On the other hand, the other peaks at m/e = 107, 106, 91, 78, 60 and 50 come from the hydrogen atom migration in the unimolecular ion decomposition. The peak at m/e = 91 in the spectrum is assigned to the tropylium ion the seven ring structure.

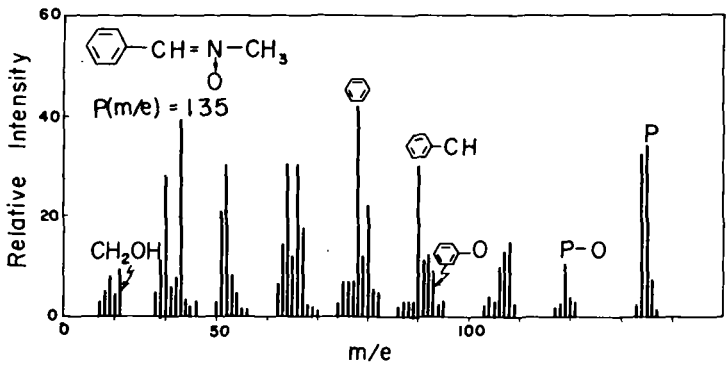

Fig. 1. The mass spectrum of the α-phenyl-N-methylnitrone.

Figure 2 shows the mass spectrum of α-diphenyl-N-methylnitrone. The migration of the oxygen atom gives ion peaks at m/e 31 (CH_2OH), 93 (C_6H_5-O), 106 ($C_6H_5CH=O$), and 182 ($(C_6H_5)_2C=O$). There are additional interesting rearrangement peaks at m/e 152 ($C_6H_4-C_6H_4$) and at m/e 167 ($(C_6H_4)_2CH_2$). Vinylacetylene ion (m/e = 52, $H_2C=CH-C\equiv CH$) was also observed in the mass spectra of α-phenyl and α-diphenyl-N-methylnitrone. The other ion peaks are given by the hydrogen atom migration and the simple fragmentation processes. The most distinguished peaks are of the radical ions. The fragment involving the phenyl radical ion gives informations convenient for analysis of the molecular structures because of excellent chemical stability. The peaks at masses 92 (C_6H_5O) and 181 ($\begin{matrix}C_6H_5\\C_6H_5\end{matrix}>C=O$) are the most interesting ion peaks involving phenyl radical and oxgyen atom.

Figure 3 shows the mass spectrum of α-diphenyl-N-phenylnitrone. The most important ion peaks are those at masses 106 ($C_6H_5CH=O$) and 182 ($(C_6H_5)_2C=O$). The peak at mass 259 is considered to be of the ion ($(C_6H_5)_2C-O-C_6H_5$) resulting from the fragmentation process involving oxygen atom migration. On the other hand, the ion peaks at masses 243, 166 and 92 are the ions having the structure ($(C_6H_5)_n\ C_4-n$.

Figure 4 shows the mass spectrum recorded over the mass range m/e 12~300 in about 2 seconds at electron accelerating voltage of 20V.

DISCUSSION

It has been believed that the statistical theory of unimolecular reaction can be applied to the interpretation of decomposition of molecular ions by the impact of electrons with comparativele high energies. The theory is based on the presumption that molecular ion do not decompose instantaneously into ionized and neutral fragments, but the electron energies are uniformly distributed to whole bonds of molecular ions and then they are concentrated in a specific bond. Denote the unimolecular rate constant for the rupture of bons i by K_i. Let I_i be the intensity of the ion produced by this primary dissociation, then

$$\frac{dI_i}{dt} = K_i I_o \qquad (1)$$

Here, relative intensities of principal ions may be determined from the expression

$$I_i = \frac{K_i I_o}{\Sigma K_i}\left[1 - \exp - (K_i)\ t\right] \qquad (2)$$

Here, I_o is the amount of parent ion at the begining. In practical calculation, the time, t, is usually assumed to be a certain constant value of the order of 10^{-5} sec. according to the dimension of the ion source as well as to the ion-accelerating voltage. The ratio of fragment ion to parent ion detecded are given according to the following equation:

$$\frac{I_i}{I_o} = \frac{K_i}{K_o} \qquad (3)$$

In this section, the discussion are carried out on the principal ions resulted from the migration of oxygen atom and phenyl radical. The migration probabilty of the oxygen atom and the phenyl radical can be estimated through a decomposition given by

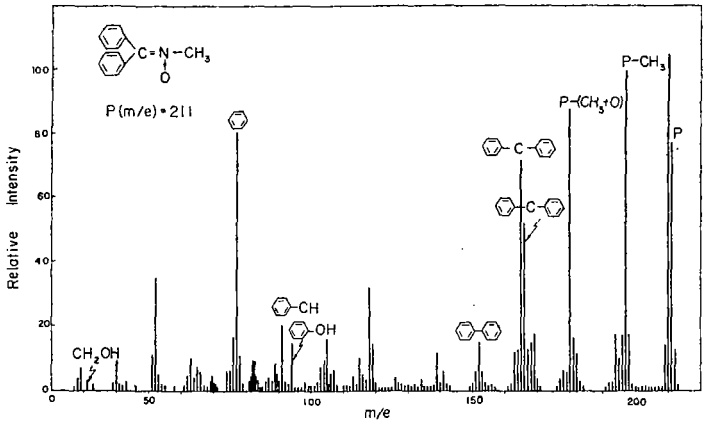

Fig. 2. The mass spectrum of the -diphenyl-N-methylnitrone.

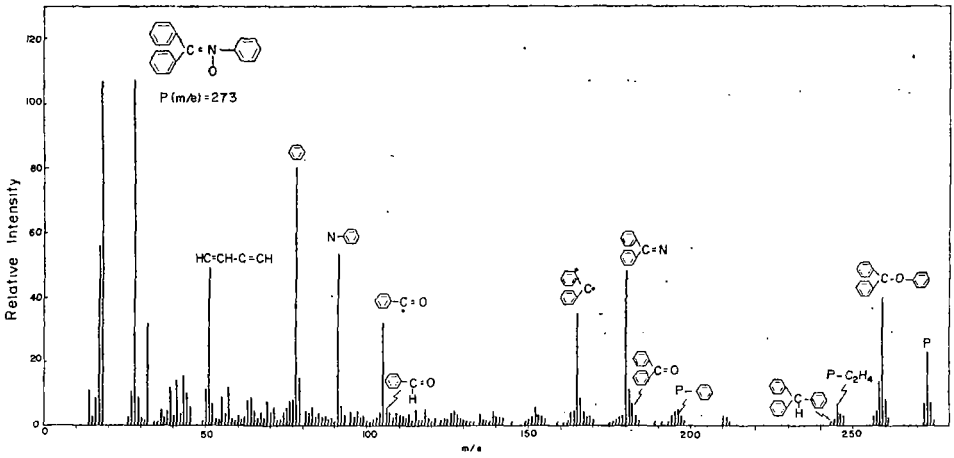

Fig. 3. The mass spectrum of the -diphenyl-N-phenylnitrone.

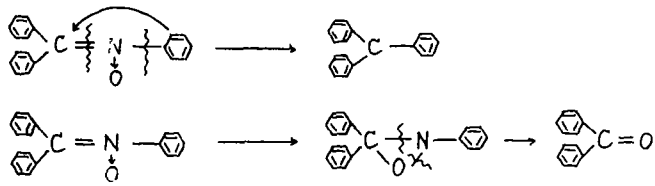

As shown in the processes, three-menber ring transient state can be posturated according to a logical explanation of the photochemical isomerization. The energy stabirization by the migration may also take place between a neutral migration atom and a resonant ion. Table 1 shows the most characteristic fragment ions producted from the parent ion of three kinds. The benzophenone type ions are expected to be formed through a unimolecular decomposition as follows:

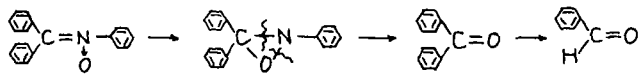

In this reaction, the energy stabirization of the final state may be given from the bond rearrangement of the oxygen atom. The energy necessary for the formation of benzophenone type ions may be calculated from the following energy values.,
D(CH_3- NH_2) = 3.46 ev, D(H_2C = O) = 7.8 ev, D(C_6H_5 - NH_2) = 2.7 ev, D(C_6H_5- C H O) = 3.4 ev.
In the region of comparatively low electron energy, the bond rearrangement by the migration of the nutral atom gives the large stabilization energy to a resonant ion. This ionic structures are based on the migration of the oxygen atom in three-menber ring transition state, though unfortunately their energy relation has not been exactly proved by experiment.

On the other hand, the migration of the oxygen atom can be estimated from the mass spectra obtained as a function of the electron accelerating voltage. The following unimolecular decomposition can be estimated from Figures 2 and 3.

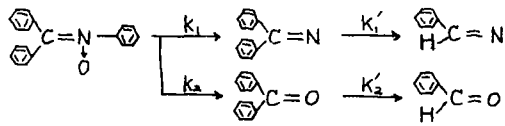

Here, unimolecular rate constant (K_i) for each process can be calculated according to the theory of unimolecular reaction. Figure 5 shows the ratios K_2/K_1 and K_2'/K_1' as a function of the electron accelerating voltage. The mass spectrum at each electron voltage was obtained by the fast recording method. As shown in Figure 5, the value K_2/K_1 is greater than unity in the range of the low electron energies and decreases rapidly with the increase of the electron energy. The reaction for K_2 and K_3 are shown by the following process:

Table I

RATIO OF FRAGMENT TO PARENT IONS OF THE MOLECULES

Recording method	Molecules \ m/e	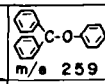 m/e 259	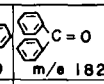 m/e 182	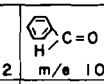 m/e 106	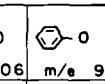 m/e 93
Slow	α-phenyl – N – methylnitrone			28.5	26
	α-Diphenyl-N-methylnitrone		15	8	2
Fast	α-Diphenyl-N-methylnitrone		17	7	5
	α-Diphenyl-N-phenylnitrone	170	28	24	13

Recording method	Molecules \ m/e	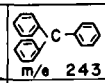 m/e 243	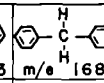 m/e 168	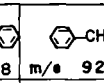 m/e 92
Slow	α-phenyl – N – methylnitrone			36
	α-Diphenyl-N-methylnitrone		20	4
Fast	α-Diphenyl-N-methylnitrone		22	7
	α-Diphenyl-N-phenylnitrone	4	15	28

Recording method	Molecules \ m/e	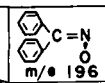 m/e 196	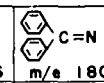 m/e 180	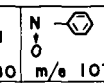 m/e 107	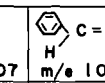 m/e 104	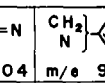 m/e 91
Slow	α-phenyl-N-methylnitrone				7	33
	α-Diphenyl-N-methylnitrone	22	113		10	26
Fast	α-Diphenyl-N-methylnitrone	29	150		20	39
	α-Diphenyl-N-phenylnitrone	23	210	17	10	232

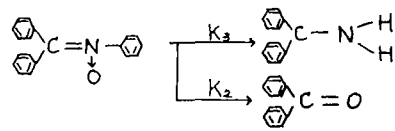

As mentioned above, the stabirization due to the transfer of the oxygen atom is a little larger than that due to the energy transfer of the hydrogen atoms. In the region of the low electron energies, the reaction for the K_2 occurs in preference to one for K_3.

In Figures 6 and 7, total ion yields of principal ions are shown as a function of the ionizing voltage. In the case of paraffins and olefins, these curves for the total ion yield can be clasified into four types. In the present molecular ions, it is difficult to classify into sevral types, because they show the complex rearrangement ions. However, the fragment ions due to simple bond rupture can be clasified into four types, as in the case of the paraffins and olefins.

As shown in Figures 1 and 2, the ion peak at mass 31 (CH_2OH) shows the migration of the oxygen atom from the semipolar bond to the terminal methyl. The CH_2OH ion formed from parent ion is expected through a primary decomposition as follows:

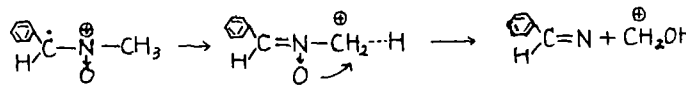

On the other hand, benzoxi ion (C_6H_5- OH) peak was observed in the mass spectrum providing an additional evidence for oxygen atom migration. In this reaction process, the hydrogen atom is rearranged from the bonding phenyl to the ruptured phenyl and further the oxygen atom is rearranged in the ruptured phenyl ion. The reaction processes are produced through both or either of the following process:

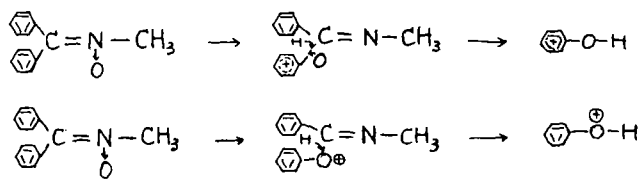

As mentioned above, the rate constants (Ki , i = 4~7) for the unimolecular decomposition processes of the α-phenyl-N-methylnitrone and α-diphenyl-N-methylnitrone are given by following processes,

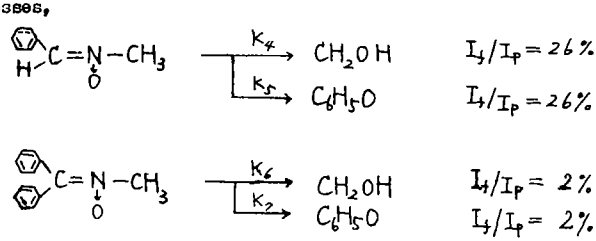

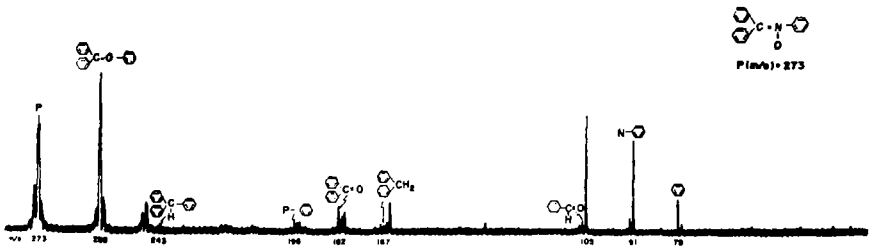

Fig. 4. The mass spectrum of the α-diphenyl-N-phenylnitrone (fast scanning method).

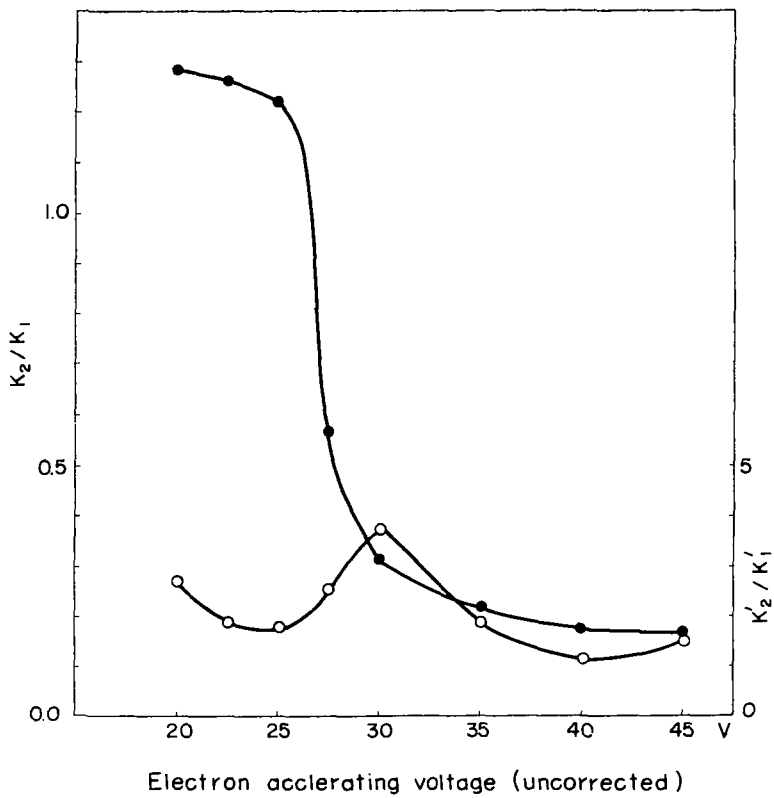

Fig. 5. The values k_2/k_1 and k'_2/k'_1 as a function of the electron accelerating voltage for α-diphenyl-N-phenylnitrone.

Where K_γ and K_δ mean the unimolecular rate constant for rupture of carbon-nitrogen bonds, and K_ζ and K_η for carbon-carbon bonds.

The unimolecular rate constant for the formation of each ion can be calculated from the spectral peak intensity by Eq (3). In these molecules, the ratios of the unimolecular rate constant, K_δ and K_γ, for the C - N bond rupture is 0.77 and K_η and K_ζ for C - C bond rupture is 0.77

CONCLUSION

In the unimolecular ion decomposition process, not only oxygen atom migration but also phenyl migration peakes takes place resulting the respective fragment ions. The concerned fragments are such as benzoxi radical group, methoxi group and triphenyl methane group. All of them are products of new type migration processes. In addition, it was found that rate constants of unimolecular reactions are nealy equivalent for the α-phenyl-N-methylnitrone and α-diphenyl-N-methylnitrone (for, m/e 31, 94). On the other hand, the rate constants of the reaction which produce fragments of mass number 180 and 182 are affected by the stabilization energies by the oxygen atom migration.

REFERENCES

1) F. W. Mclafferty, "Mass Spectrometry of Organic Ions" P. 542, Academic Press, New York (1963).

2) N. Hata and I. Tanaka, J. Chem. Phys., 36, 2072 (1962); Bull. Chem. Soc. Japan, 34, 1440, 1444 (1961).

3) H. M. Rosenstock, M. B. Wallenstein, A. L. Wahrhaftig and H. Eyring, Proc. Natl. Acad. Sci. U. S. 38, 667 (1952).

4) K. Shinzawa and I. Tanaka, J. Phys. Chem., 68, 1205 (1964).

5) T. L. Cottrell, "The Strengths of Chemical Bonds" London (1954).

6) I. Omura, Bull. Chem. Soc. Japan, 34, 1227 (1961); 35, 1845 (1962).

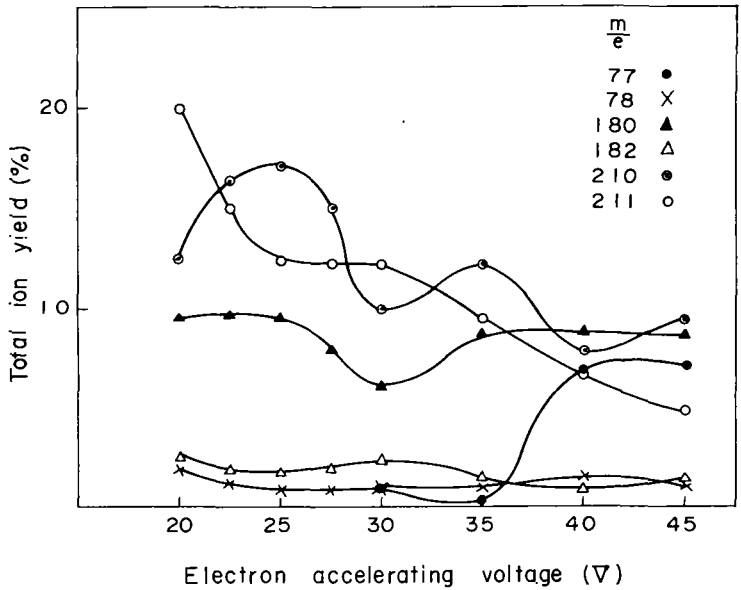

Fig. 6. Low voltage yield of ions from α-diphenyl-N-methylnitrone.

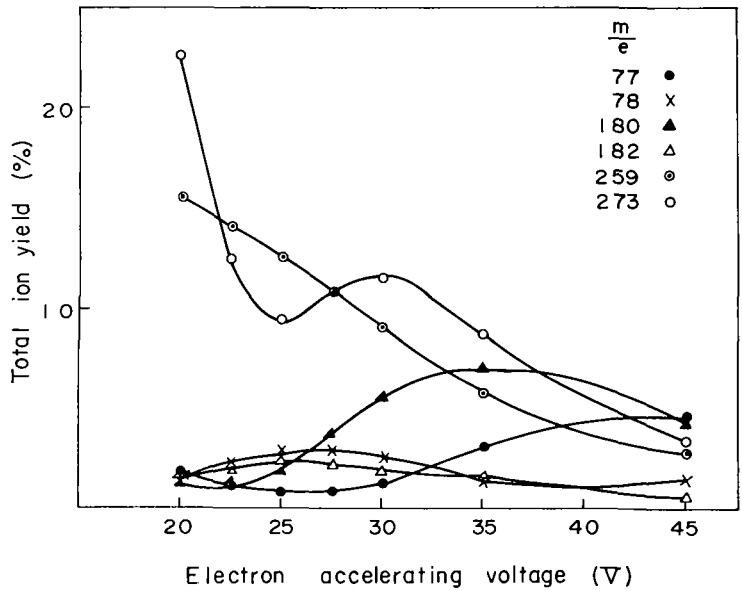

Fig. 7. Low voltage yield of ions from α-diphenyl-N-phenylnitrone.

ION DECOMPOSITION MECHANISMS

F. W. McLafferty*, R. S. Gohlke, and
R. C. Golesworthy, The Dow Chemical Co., Eastern Research Lab., Framingham, Mass.

* Present address: Dept. of Chemistry, Purdue Univ., W. Lafayette, Ind.

In the last few years, considerable progress has been made in the elucidation of ion fragmentation mechanisms through further mass spectral correlations, high resolution spectra, and the mass spectra of isotopically- labeled molecules. A new tool for such problems which has proved valuable in this laboratory is the determination of metastable transitions in the time-of-flight mass spectrometer. With this technique the parent ion for the observed metastable transition can be determined unequivocally, and ion residence times in the ionization chamber and flight tube can be varied over a large range. This paper presents a simplified equation allowing rapid calculation of the daughter and neutral fragment masses, and describes applications of the technique to particular fragmentation mechanisms. Wacks and Wahrhaftig (1) first proposed this method, which has been studied further at the National Bureau of Standards (2), by Hunt and coworkers (3, 4), and by Gohlke, Dauerman, and Golesworthy in this laboratory. In the T-O-F spectrometer an ion bunch is accelerated out of the ionization chamber and separated into individual bunches of particular m/e by their differing times of flight down a long drift tube. Any daughter ions and neutral fragments formed by decompositions during flight usually receive so little extra kinetic energy that they stay with the remaining parent (precursor) ions and are thus not distinguishable. By placing a region of separate electrostatic potential near the end of the flight tube, such a daughter ion formed in an individual bunch can be preferentially retarded (or accelerated) by an amount related to its new mass, and thus be identified. The neutrals are also separated by this retarder region, as their flight time is uneffected by the auxiliary retarding potential. In observing ions of a particular m/e in an oscilloscopic presentation of the spectrum, changing the retarder potential to a value different from the drift region causes displacement of the ions from the neutral fragments, with the daughter ions displaced to a greater degree than the parent ions. Thus the parent ion of the metastable transition is clearly established, a fact not always clear with magnetic instruments. The diffuse metastable ion peaks from the latter often cannot be measured with sufficient accuracy for this, for example:

transition	metastable m/e
m/e 100 → m/e 50	25.0
m/e 99 → m/e 50	25.2
m/e 64 → m/e 40	25.0

While the T-O-F method is advantageous for this example, it is poor for identifying a transition in which the parent and daughter are nearly the same m/e, such as m/e 100 → m/e 99.

A significant drawback in applying the method previously was that the complex equation necessitated solutions by a computer. This can be simplified to permit slide rule calculation in the following manner. The effective voltages in the flight tube, V_A, and retarder region, V_R, are not exactly those fed in from the power supplies. The effective V_A-V_R can be determined by plotting $1/V_R^{-1/2}$ versus $t_p - t_n$, where t_p and t_n are the flight times (measured as distance on the spectrum) of the parents and neutrals, respectively. This should produce a straight line with $V_R = V_A$ when $t_p = t_n$. Since the m/e of the parent is known, the effect of fringe electrostatic fields and similar aberrations can be effectively eliminated by comparing t_d, the flight time of the daughter, with t_p. The equation becomes:

$$\frac{t_d - t_n}{t_p - t_n} = \frac{\left[1 - \sqrt{1 - \frac{m_p}{m_d}\left(1 - \frac{V_R}{V_A}\right)}\right]}{\sqrt{1 - \frac{m_p}{m_d}\left(1 - \frac{V_R}{V_A}\right)}} \cdot \frac{\sqrt{\frac{V_R}{V_A}}}{\left[1 - \sqrt{\frac{V_R}{V_A}}\right]}$$

One application of this technique has been to the problem of the sequence of two degradation steps necessary to form a particular ion. When an abundant ion containing an even number of bonding electrons (E. E.) (5) is formed from one of an odd number (O. E.) by separate losses of a radical (O. E.) and a molecule (E. E.), is there a preferred order for these losses?

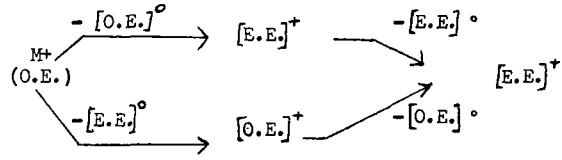

(All molecular ions, M+, are "O.E.").

Thus, the first step of the upper path should be favored by the formation of the more stable (E.E.)+, but this stability will slow the subsequent decomposition step as compared to the lower path.

The excellent detailed study by Professor Djerassi and his coworkers of amides (6) offers an opportunity to test this. In N,N-diethylacetamide at least three prominent fragment peaks (m/e 44, 58, and 72) should arise in such a two-step process. Two metastable transitions were noted in the spectrum from the magnetic instrument (6), while one of these plus six others were identified by the T-O-F method. The latter was especially valuable in defining metastables from prominent peaks at the adjacent masses 86 and 87.
The summarized results

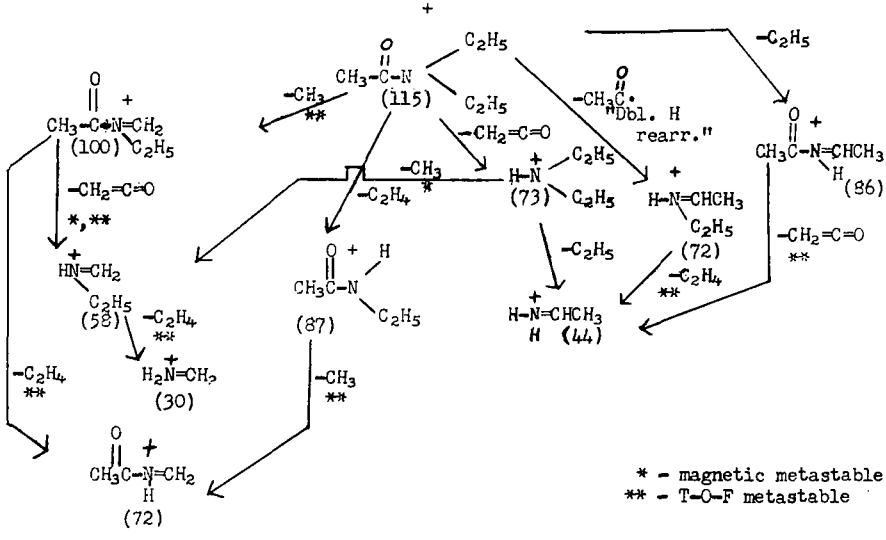

show that the formations of m/e 44, 58, and 72 procede simultaneously through both the possible paths.

Recent definitive research on the mass spectrum of benzyl alcohol, C_7H_8O, has greatly clarified the ion degradation mechanisms involved (7,8). Our study of the metastable transitions by T-O-F was hampered by a temporary instrument configuration causing high collision-induced dissociations, but the transitions of $C_7H_8O^+$ to $C_7H_7^+$, $C_6H_7^+$, $C_5H_5^+$, and $C_4H_3^+$, and of $C_7H_7O^+$ to $C_6H_7^+$, were indicated. Isotopic labeling experiments of Eliel et al (7) were explained well by the postulation that the most abundant ion, $C_6H_7^+$, was formed both by direct loss of the formyl radical with little scrambling of the hydrogen atoms, and by initial loss of H· with H atom scrambling followed by loss of CO. We sought to check this with metastable transition evidence for the following possible reaction paths using α, α-d_2-benzyl alcohol:

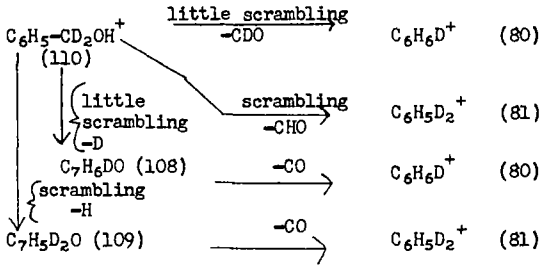

Obviously these would not be distinguishable utilizing metastable peaks on a magnetic instrument. Unfortunately, because of the instrumental difficulties mentioned above, our results are not definitive, but they are consistent with the theory of Eliel et al (7).

As a further part of our investigation of this system, the mass spectrum of α-C^{13}-benzyl alcohol was determined. The following abundance ratios were found:

m/e	C^{13}_O	C^{13}_1
80/79	$0.14_0 \pm 0.01$	$0.16_4 \pm 0.01$

Thus the formation of the $C_6H_7^+$ ion involves mainly, but not entirely, the loss of the alpha carbon atom.

The recent work of Rosenstock et al (9) emphasizes the need for and usefulness of better metastable ion data (see also Barber and Elliott, Paper No. 22, this meeting). The increased quality and quantity of such data possible with the T-O-F instrument should prove valuable in elucidation of ion decomposition mechanisms and of molecular structure by mass spectrometry.

Literature Cited

1. Morton Wacks, Ph.D. Thesis, Univ. of Utah, 1959.
2. R. E. Ferguson, K. E. McCulloh, H. M. Rosenstock, ASTM E-14 Meeting on Mass Spectrometry, New Orleans, 1962.
3. W. W. Hunt, Jr., et al, Rev. Sci. Instr., 35:1, 82, 88 (1964).
4. W. W. Hunt, Jr., AFCRL-64-383 (May, 1964).
5. F. W. McLafferty, "Mass Spectrometry of Organic Ions", p. 309, Academic Press, New York, 1963.
6. Z. Pelah, M. A. Kielczewski, J. M. Wilson, M. Ohashi, H. Budzikiewicz and Carl Djerassi, J. Am. Chem. Soc., 85, 2470 (1963).
7. E. L. Eliel, J. D. McCollum, Seymour Meyerson, and D. N. Rylander, J. Am. Chem. Soc., 83, 2481 (1961).
8. J. S. Shannon, Austr. J. Chem., 15, 265 (1962).
9. H. M. Rosenstock, V. H. Dibeler, F. N. Harllee, J. Chem. Phys., 40, 591 (1964).

"Mass Spectrometry in Carbohydrate Chemistry:
Dithioacetal-Peracetate Derivatives"

by

Don C. DeJongh
Wayne State University
Detroit, Michigan

Introduction. -- The potential importance of mass spectrometry as a technique for structure determination in the carbohydrate field has recently been demonstrated. The mass spectra of the peracetates of hexoses and pentoses[1] and their partially O-methylated derivatives,[2] of the O-isopropylidene derivatives of hexoses and pentoses,[3] and of various carbohydrate methyl ethers[4,5] have been interpretated in terms of molecular weight, ring size, variation in the type and degree of substitution, ketose or aldose structure, and stereochemistry. The structure of a newly isolated di-O-isopropylidene derivative of D-galactose was determined by applying this technique.[3]

(1) K. Biemann, D. C. DeJongh, and H. K. Schnoes, J. Am. Chem. Soc., 85, 1763 (1963).

(2) Don C. DeJongh and K. Biemann, ibid., 85, 2289 (1963).

(3) Don C. DeJongh and K. Biemann, ibid., 86, 67 (1964).

(4) N. K. Kochetkov, N. S. Wulfson, O. S. Chizhov, and B. M. Zolotarev, Tetrahedron, 19, 2209 (1963).

(5) K. Heyns and H. Scharmann, Ann., 667, 183 (1963).

Dithioacetal derivatives are very useful for the characterization of monosaccharides because of their stability and ease of preparation. They also are useful intermediates for the preparation of acyclic derivatives of sugars. The peracetates of these compounds, which usually are crystalline, are sufficiently volatile and thermally stable to be introduced directly into a conventional inlet system of the mass spectrometer.

Since the diethyl dithioacetal peracetates are monosaccharide derivatives in the acyclic structure, their mass spectra need not be interpreted in terms of ring size and exhibit only minor intensity differences with a change in stereochemistry. Structural differences which express themselves in the size of substituents and of the entire molecule and in the position of the carbonyl group lead to significant variation in their mass spectra; this is borne out in the following discussion by a comparison of the mass spectra of the corresponding diethyl dithioacetal peracetate derivatives of hexoses, pentoses, and deoxyhexoses.

The mass spectra of typical representatives of these derivatives are presented and interpreted. The fragmentation schemes proposed have been substantiated by the

mass spectra of deuteriated analogs, obtained by acetylation with acetic anhydride-d_6. Perhaps the most valuable aspect of these mass spectra is the presence of a sizeable molecular-ion peak which allows direct determination of the molecular weight. In all the mass spectra of carbohydrate derivatives published previously the molecular weight must be determined from a fragment peak resulting from the loss of a substituent on a carbon atom of the pyranose or furanose ring[1,2,4,5] or from the loss of a methyl group from an O-isopropylidene ring.[3]

The mass spectra of D-arabinose diethyl dithioacetal tetraacetate (I) and its d_{12}-analog (II) will be discussed in detail to elucidate the fragmentation processes characteristic of this class of compound. This shall be followed by a discussion of the influence of adding a CH_2OCOCH_3-group to form an aldohexose and of adding a CH_2-group to form a 2- and a 6-deoxyaldohexose.

D-Arabinose Diethyl Dithioacetal Tetraacetate (1). -- The peak at m/e-424(436)[6]

(6) Throughout this article, the m/e-assignments are followed by parentheses containing the location of the peak in the mass spectrum of the deuteriated analog, when known.

corresponds to the molecular weight of this compound. Elimination of a molecule of acetic acid[1] from the molecular ion forms fragment 364(373). The peak at m/e-363(375) arises from the fission of a carbon-sulfur bond in the molecular ion, leading to fragment 1a containing the four acetoxyl groups and to a thioethoxyl radical:

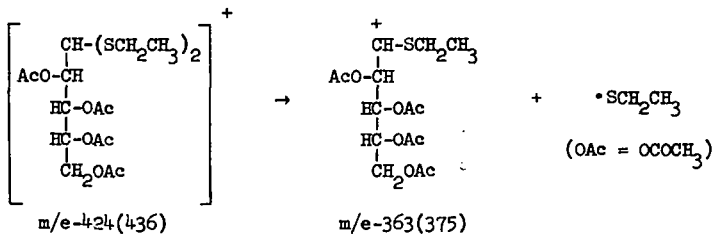

1a

This is analogous to the carbon-oxygen bond cleavage found in the mass spectra of diethyl acetals[7] and the carbon-sulfur bond cleavage characteristic of thioethers.[8,9]

(7) R. A. Friedel and A. G. Sharkey, Anal. Chem., 28, 940 (1956).

(8) E. J. Levy and W. A. Stahl, ibid., 33, 707 (1961).

(9) B. G. Hobrock and R. W. Kiser, J. Phys. Chem., 66, 1648 (1962).

Fragment 1b at m/e-303(312) forms by expulsion of a molecule of acetic acid from fragment 1a or of a thioethoxyl radical from the fragment at m/e-364(373). Loss of acetic acid [60(63)m.u.], ketene [42(44)m.u.], and acetic anhydride [102(108)m.u.] is a very important mode of fragmentation of peracetyl derivatives of carbohydrates[1,2]; fragments 1c-f at m/e-261(267,268), 201(204,205), 159(160,161), and 141(141,142), arise from the elimination of combinations of these stable molecules. The most intense peak in the mass spectra of these diethyl dithioacetal peracetates is at m/e-43(46), corresponding to the acetyl ion, CH_3CO +. Many of the fragmentations proposed throughout this

discussion are corroborated by metastable peaks in the mass spectra.

In the diethyl dithioacetal portion of the molecule, two carbon-carbon bond cleavages next to a sulfur atom are possible. Fission of the carbon-carbon bond of the thioethoxyl groups is not important, but fission of the C-1-C-2 bond of the arabinose forms fragment 2 at m/e-135(135). Stabilization of the charge by two neighboring sulfur atoms accounts for the preference for the latter fission. Fragment 2 is abundant in

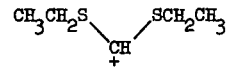

m/e-135(135)

2

the mass spectra of all the diethyl dithioacetal peracetates studied with the exception of the derivative of 2-deoxy-D-glucose (III); the corresponding radical formed from compound III by C-1-C-2 cleavage is primary and is not stabilized by a neighboring heteroatom. The corresponding peak from ethylene dithioacetal peracetates is found at m/e-105(105). Fragment 3 at m/e-107(107) results from ethylene expulsion from fragment 2 with hydrogen migration:

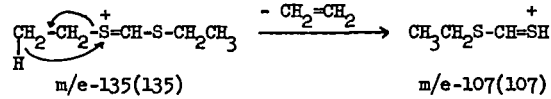

m/e-135(135) m/e-107(107)

2 3

A metastable peak at m/e-84.9(calcd. 84.8) substantiates this mechanism. Olefin elimination is a common decomposition of thioethers.[8]

Fragment 4 at m/e-75 also appears to be related to fragment 2. In those mass spectra where m/e-135 is small or absent, and in the mass spectra of ethylene dithioacetal peracetates, peak 75 is also small. The following mechanism tentatively can be proposed for fragment 4:

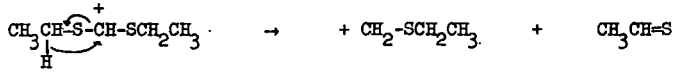

m/e-135(135) m/e-75(75)

2 4 5

An elimination of this type does not appear favorable for thioethers,[8,9] there being no α-sulfur atom remaining to stabilize the charge.

A thioaldehydo ion (6) can account for the major fragment at m/e-45(45). Fragment 7 at m/e-61(61) is a thioethoxyl ion rather than protonated acetic acid[1] since it does not shift in the deuteriated analog.

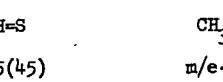

m/e-45(45) m/e-61(61)

6 7

Elimination of a molecule of acetic acid from the C-1-C-2 bond of the molecular

ion, followed by C-2-C-3 bond fission leads to fragment 9a found at m/e-219(222). Fragment 9b results from ketene expulsion:

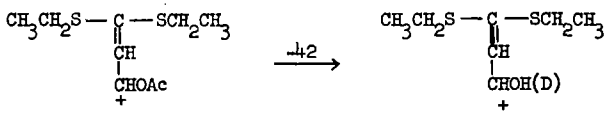

m/e-219(222) m/e-177(178)

9a 9b

Series 9 is not found in the mass spectra of the 2-deoxy-glucose derivative, indicating its formation is sensitive to changes at C-2 of the carbohydrate. A stable olefin containing C-1 and C-2 of the monosaccharide accounts for fragment 10 at m/e-104(105):

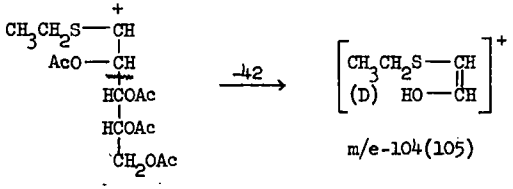

m/e-104(105)

1a 10

<u>Deoxyhexose Diethyl Dithioacetal Tetraacetates</u>. -- The molecular weight of 2-deoxy-D-glucose diethyl dithioacetal tetraacetate (III), its d_{12}-analog (IV), and 6-deoxy-L-mannose diethyl dithioacetal tetraacetate (V) can be directly determined from the molecular ion and are found 14 m.u. higher than the molecular weight of the pentose derivative. Also present in these mass spectra are "M+1"-peaks resulting from ion-molecule collision. Series 1 is a prominent fragmentation path for both the 2-deoxy and the 6-deoxy derivatives. In fact, the most intense peak in the mass spectrum of 2-deoxy-D-glucose diethyl dithioacetal tetraacetate, with the exception of m/e-43(46), is fragment 1f. The following scheme shows two pathways leading to fragment 1f; most of the steps are substantiated by metastable peaks:

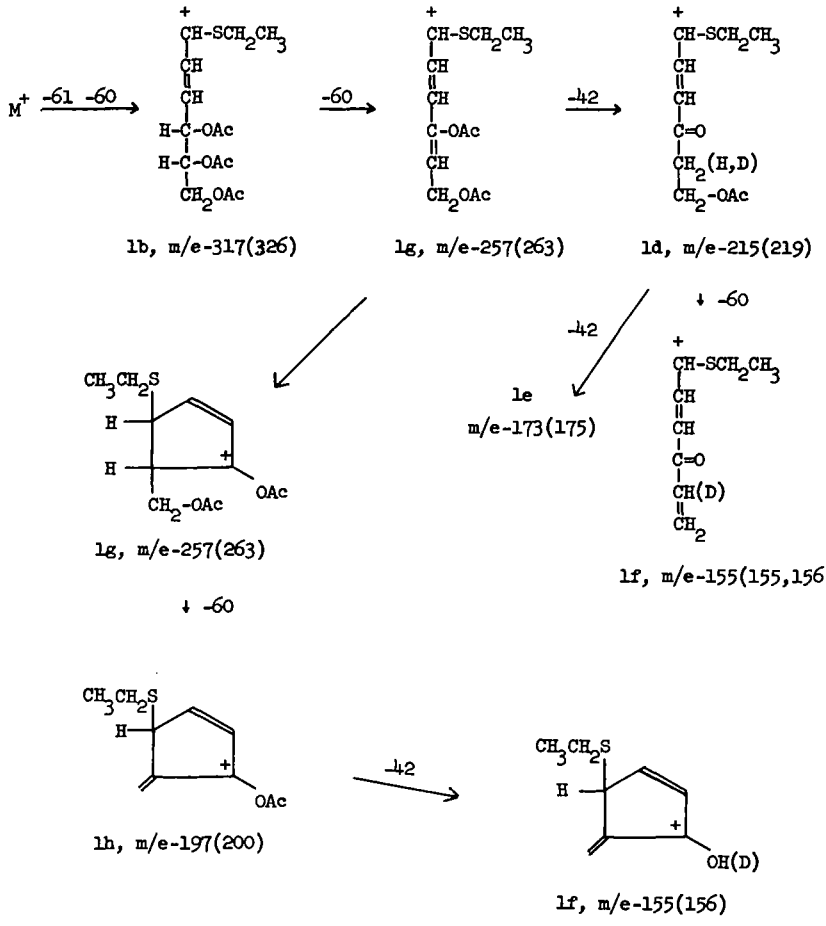

The mass spectrum of 6-deoxy-L-galactose diethyl dithioacetal tetraacetate is identical to the mass spectrum of 6-deoxy-L-mannose diethyl dithioacetal tetraacetate except for some minor intensity differences. This makes it difficult to gain insight into the stereochemistry of such molecules.

Discussion. -- The data from the mass spectra of these diethyl dithioacetal peracetate derivatives will be useful for the characterization of a sugar and may be useful in the structure determination of a newly-discovered sugar. The mass spectra can be interpreted in terms of stabilization of positive charge by the sulfur atoms which direct fragmentation in a predictable manner. The peracetates of aldohexose, aldopentose, and 6-deoxyhexose diethyl dithioacetals can be differentiated from their 2-deoxy isomers by the intense peak for the former group at m/e-135(135), arising from C-1-C-2 cleavage with charge retention on C-1, and from each other by their molecular weights (H vs. CH_3 vs. CH_2OCOCH_3). Stereochemical differences are of little influence on the fragmentation.

Acknowledgments. -- I would like to thank Professor K. Biemann for allowing me to use the mass spectrometer in his laboratories. Acknowledgment is made to the donors of the Petroleum Research Fund, administered by the American Chemical Society, for support of this research.

MASS SPECTROMETRIC STUDIES OF UNSATURATED METHYL ESTERS

W. K. Rohwedder, A. F. Mabrouk, and E. Selke
Northern Regional Research Laboratory, Peoria, Illinois

Abstract

Mass spectra of methyl sorbate, methyl hexenoate isomers and some of their deuterated derivatives were determined. Ions of mass 59, 74, 87, and M -31 were found in accordance with the expected fragmentation of saturated methyl esters. Both methyl 2-hexenoate and methyl sorbate had characteristic peaks at M -15. The spectra of deuterium-labeled hexenoates and sorbate and of longer chain esters indicate that the fragment forms by cleavage at the 5-6 carbon-to-carbon bond. Formation of the mass 87 fragment of methyl 2-hexenoate appears to be due to cleavage of the 3-4 carbon-to-carbon bond and rearrangement of two hydrogen atoms rather than double bond migration followed by cleavage.

- - - - - - - -

Introduction

The mass spectra of methyl sorbate and the isomers of methyl hexenoate were measured along with some deuterated derivatives as part of a study on the mechanism of the catalytic hydrogenation of methyl sorbate in the presence of pentacyanocobaltate II ion (1,2).

The mass spectra of many esters have been published along with a discussion of the fragmentation patterns by Sharkey, Shultz and Friedel (3). Ryhage and Stenhagen have published many papers on esters and two excellent review articles (4-8).

Experimental

The trans-2, trans-3, and trans-4-hexenoic acids were prepared by the Knoevenagel condensation reaction (9-11); the trans-5-hexenoic acid, by the reaction of 1-bromo-3-butene with diethyl malonate in the presence of sodium ethoxide (11). Their melting or boiling points agreed well with those given in the literature as did the melting points of their p-toluidide derivatives. The trans-2-octanoate was synthesized by condensing n-hexanal with malonic acid according to the Doebner reaction (11). All the acids were purified by preparing their methyl esters and subjecting them to separation by preparative gas chromatography. This means of purification leads to the separation of the cis-4-hexenoate present in the trans-4-hexenoate preparation. Sorbic acid was purified by crystallization from aqueous solution. The methyl esters were prepared according to the method of Stoffel, Chu, and Ahrends (12); the ethyl esters, according to Vogel (13).

The deuterated sorbic acid was prepared by equilibrating the acid twice with deuterium oxide in the presence of KOH. Sorbic acid (5.2 grams) was dissolved in D_2O (99.7% isotopic purity) containing 3.1 grams of KOH, and the mixture was refluxed for 5 hours on a steam bath. The acid was extracted, refluxed for another 6 hours after dissolving it in 40 ml of 7.7% KOH in D_2O. Nuclear magnetic resonance studies indicated that there were 0.6 protons on the number 2 carbon atom; 1.29 protons on the 3-, 4-, and 5-carbon atoms; and 0.42 protons on the number 6 carbon atom. Deuterated 2-hexenoic acid is a product of the reduction of sorbic acid with deuterium in the presence of D_2O and pentacyanocobaltate II ion (2). Nuclear magnetic resonance studies on the deuterated methyl 2-hexenoate indicated that there were 1.0 protons on the number four carbon atom and 0.3 protons on the number 5 carbon atom with a full complement of protons on the rest of the molecule.

The mass spectra of the nondeuterated samples were measured in a Bendix* Model 12 time-of-flight mass spectrometer using a heated inlet at 150° C. Backgrounds were taken before each sample, and except for air peaks, the background peaks were not significant. The air background was quite reproducible, and was subtracted out of the spectrum almost completely. The deuterated esters were trapped from a gas chromatograph and were subjected to severe air leakage both during trapping and during injection into the heated inlet system. The spectra below mass 37 and the peaks at 40 and 44 have not been included because corrections could not be made for the air peaks.

---

* The mention of firm names or trade products does not imply that they are endorsed or recommended by the Department of Agriculture over other firms or similar products not mentioned.

Results and Discussion

The mass spectra are tabulated in Table 1. The molecular ion peaks are somewhat more intense for all the unsaturated esters than for the saturated. The mass spectra of methyl 3-, 4-, and 5-hexenoates exhibit the same general fragmentation pattern as saturated methyl esters. They have a small peak at mass 113 due to loss of a CH_3 group, not found in the spectrum of methyl hexanoate. They also have a 97 peak due to the loss of a methoxy group and a 59 peak due to the methoxy carbonyl group. The 74 peak, due to cleavage of the 2-3 carbon-to-carbon bond and rearrangement of a hydrogen atom, is the largest in the methyl 5-hexenoate spectrum. This peak is considerably smaller for the methyl 3- and 4-hexenoates. The 87 peak due to simple cleavage of the 3-4 carbon-to-carbon bond is quite small in the methyl 3-, 4-, and 5-hexenoate. The hydrocarbon fragments are more prominent for the methyl 3- and 4-hexenoates than they are for the other isomers. The spectrum of the methyl cis-4-hexenoate is almost identical to the methyl trans-4-hexenoate as would be expected (6).

The methyl 2-hexenoate has peaks at 74, 87, and 113 which cannot be explained by the usual fragmentation rules. The 113 peak is due to the cleavage of the 5-6 carbon-to-carbon bond and probably forms the ring structure proposed by McLafferty (14) to explain characteristic peaks in the spectra of methyl esters of α-unsaturated long-chain fatty acids.

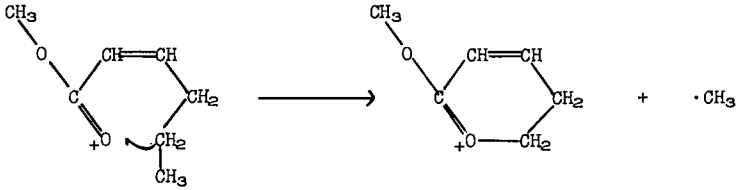

The 5-6 carbon-to-carbon bond cleavage is confirmed by the presence of a major peak at 113 in methyl 2-octenoate due to the loss of a C_3H_7 group, which is equivalent to the loss of CH_3 for the methyl 2-hexenoate. The peak at M -16 of ethyl 2-hexenoate indicates that the loss of CH_3 is not due to the loss of the methoxy CH_3. The loss of 16 rather than 15 is probably due to the CH_3 free radical removing a hydrogen atom from the molecule, probably from the ethyl group which can come quite close to the site of cleavage.

In saturated methyl esters the 74 peak is due to cleavage at the 2-3 carbon-to-carbon bond with rearrangement of a hydrogen atom (8); methyl 2-hexenoate would require cleavage of a double bond and rearrangement of two hydrogen atoms. Possibly, the double bond migrates to some other position and then fragments in the usual way to form the 74 peak.

The 87 peak of methyl 2-hexenoate is also difficult to explain. For saturated methyl esters the 87 peak is caused by simple cleavage of the 3-4 carbon-to-carbon bond, a mechanism that would give an 85 peak for methyl 2-hexenoate rather than the 87 peak actually found. The 87 peak cannot be explained by double bond migration because the other isomers have a much smaller 87 peak. The mass spectrum of methyl trans-2-methyleicosenoate investigated by Ryhage and Stenhagen (5,8) has a peak at 101, which is equivalent to the 87 mass fragment plus the methyl group on the number 2 carbon atom. This fragment would appear to be formed by the same mechanism as the 87 peak in methyl 2-hexenoate and would tend to prove that the basic skeleton of the fragment is the methoxy carbonyl group with the number 2 and 3 carbon atoms. Examination of the deuterated methyl 2-hexenoate shows the respective mass 87, 88 and 89 peaks to have intensities of 37.3, 48.6 and 12.3. The nuclear magnetic resonance data show that only the number 4 and 5 carbon atoms contain deuterium with 1.0 deuterium atoms on the number 4 carbon atom and 1.7 deuterium atoms on the number 5 carbon atom. The mass spectrum data would be explained if the molecule cleaved at the 3-4 carbon-to-carbon bond with the rearrangement of one hydrogen from the number 4 carbon and one hydrogen from the number 6 carbon with a certain probability of the rearrangement of one hydrogen from the number 5 carbon atom rather than the number 6 carbon atom.

The methyl sorbate spectrum is somewhat simpler than the hexenoate spectra. There are no 74 or 87 peaks. The peak at 95 is due to the loss of the methoxy group and the peak at 67 is the hydrocarbon ion after cleavage of the 1-2 carbon-to-carbon bond. The large peak at 111 appears to be formed by the same mechanism as the 113 peak in the methyl 2-hexenoate spectrum.

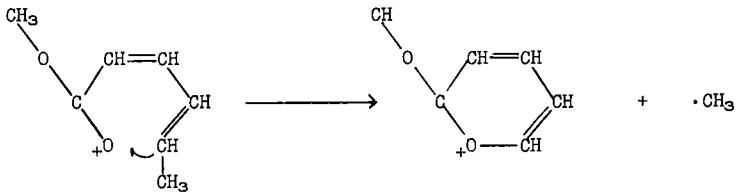

Since the mass spectrum of ethyl sorbate has an M -15 peak identical to the M -15 peak of methyl sorbate, the CH_3 lost must not be from the methoxy group. It is interesting that the ethyl sorbate has an M -15 peak, whereas ethyl 2-hexenoate has an M -16 peak. Holman (15) has observed that the mass spectrum of methyl 2,4-decadienoate has an important peak at mass 111 indicating a cleavage at the 5-6 carbon-to-carbon bond probably due to formation of a cyclic ion as suggested here for methyl sorbate. Further proof that the carbon atom lost is the number 6 is seen in the spectrum of the deuterated methyl sorbate. The intensities of the parent peaks at masses 129, 130, and 131 are 40.5, 64.2, and 40.5; accordingly, the molecules contain 3, 4, and 5 atoms of deuterium, respectively. The peaks at 112 and 113 are equivalent to M -17 and M -18 or the loss of CHD_2 and CD_3. The only carbon atom in methyl sorbate which could contain that much deuterium is the sixth.

Acknowledgment

We thank Mr. C. Glass for the nuclear magnetic resonance data.

Literature Cited

(1) A. F. Mabrouk, H. J. Dutton, and J. C. Cowan, J. Am. Oil Chemists' Soc., 41, 153 (1964).

(2) A. F. Mabrouk, E. Selke, W. K. Rohwedder, and H. J. Dutton. Presented at the 37th Fall meeting, American Oil Chemists' Society, Minneapolis, Minnesota, October 2, 1963.

(3) A. G. Sharkey, Janet L. Shultz, and R. A. Friedel, Anal. Chem., 31, 87 (1959).

(4) R. Ryhage and E. Stenhagen, Arkiv Kemi, 13, 523 (1959).

(5) R. Ryhage, Stina Stallberg-Stenhagen, and E. Stenhagen, Arkiv. Kemi, 18, 179 (1961).

(6) N. Dinh-Nguyen, R. Ryhage, and Stina Stallberg-Stenhagen, Arkiv. Kemi, 15, 433 (1960).

(7) R. Ryhage and E. Stenhagen, Arkiv. Kemi, 15, 291 (1960).

(8) R. Ryhage and E. Stenhagen, in "Mass Spectrometry of Organic Ions," (F. W. McLafferty, ed.) Academic Press, New York, 1963, Chapter 9.

(9) A. A. Goldberg and R. P. Linstead, J. Chem. Soc. 2343 (1928).

(10) R. P. Linstead, E. G. Noble, and E. J. Boorman, J. Chem. Soc., 557 (1933).

(11) R. P. Linstead and H. N. Rydon, J. Chem. Soc., 1995 (1934).

(12) W. Stoffel, Florence Chu, and E. H. Ahrends, Jr., Anal. Chem., 31, 307 (1959).

(13) A. I. Vogel, "A Textbook of Practical Organic Chemistry," 3rd ed. Longmans, Green and Company, Inc., New York, 1959, page 381.

(14) F. W. McLafferty, in "Mass Spectrometry of Organic Ions," (F. W. McLafferty, ed.) Academic Press, New York, 1963, Chapter 7.

(15) R. Holman. Private communication.

Table 1. Normalized Mass Spectra

Mass Number	(1) Methyl 2-Hexenoate	(2) Methyl 3-Hexenoate	(3) Methyl 4-Hexenoate	(4) Methyl 4-Hexenoate (cis)	(5) Methyl 5-Hexenoate	(6) Methyl Sorbate	(7) Ethyl 2-Hexenoate	(8) Ethyl 3-Hexenoate	(9) Ethyl Sorbate	(10) Methyl 2-Octenoate	(11) Methyl 2-Hexenoate $d_1^4 d_2^5$	(12) Methyl Sorbate d_5
15	28.2	27.0	37.6	28.0	30.1	26.3	5.8	4.1	6.6	20.2		
26	7.3	3.5	5.9	5.0	5.0	5.1	8.0	4.9	8.5	4.0		
27	53.8	28.6	49.4	43.8	33.2	20.6	67.7	39.3	44.6	49.7		
28	13.5	9.3	17.3	16.7	17.3	8.3	15.8	11.1	15.1	14.3		
29	35.9	14.7	35.5	34.9	18.0	15.5	81.8	100.0	47.3	69.2		
30	2.5	1.8	3.3	2.8	2.4	3.2	2.8	3.3	3.6	2.5		
31	3.9	3.6	7.5	6.3	7.8	3.8	3.0	2.4	1.9	2.9		
31.5						0.40			0.10			
32	0.16	0.17	0.26		0.29	0.72				0.07		
32.5		0.08	0.10	0.04	0.03	0.67		0.08	0.35			
33	0.64	0.60	1.2	0.89	0.69	0.54		0.10	0.21	0.52		
33.5		0.16	0.10	0.04	0.03	0.27		0.08	0.21			
34			0.41	0.19	0.22			0.08				
37	2.0	0.95	1.8	1.3	1.1	4.0	0.93	0.49	2.2	0.56	1.1	2.4
38	7.7	4.1	6.5	5.7	4.4	14.2	4.3	2.2	9.5	2.9	6.0	8.1
39	65.7	38.9	69.1	62.0	53.9	88.5	52.9	29.4	78.3	50.0	41.1	25.2
40	21.1	7.1	14.2	12.2	10.3	19.0	14.7	5.8	17.9	17.0		
41	89.1	100.0	100.0	96.9	76.2	83.1	76.3	92.3	81.3	81.5	67.4	92.4
42	32.1	12.9	23.0	22.5	16.4	4.9	21.7	11.7	6.2	29.8	71.4	59.6
43	14.1	14.3	39.2	44.5	62.8	5.4	21.2	8.6	14.0	19.9	77.7	70.5
44	1.3	1.2	3.1	3.5	6.0	0.54	2.9	0.95	1.5	1.3		
45	4.8	2.2	5.8	5.4	5.2	2.0	7.0	3.4	3.9	5.1	24.0	42.4
46	0.16		0.14		0.26	0.27	0.18	0.12	0.27	0.20	8.6	12.4
46.5									0.04			
47	0.32		0.06			0.27	0.18	0.11	0.42	0.35	2.5	1.4
47.5									0.02			

--continued

Table 1. Normalized Mass Spectra--continued

Mass Number	(1)	(2)	(3)	(4)	(5)	(6)	(7)	(8)	(9)	(10)	(11)	(12)
48			0.18		0.06			0.02		0.07	0.86	
49	0.32	0.19	0.24		0.11	1.1	0.14	0.02	0.27	0.10		1.0
50	2.9	2.4	3.6	2.9	1.6	5.9	2.5	1.3	4.0	1.4	1.4	4.3
51	5.6	4.7	7.1	5.8	3.2	11.4	5.9	3.0	9.5	4.5	4.6	10.0
52	2.6	2.6	3.9	3.1	1.7	5.4	2.9	1.9	5.4	2.8	5.2	15.2
53	18.9	15.1	23.8	23.3	10.3	7.7	16.1	11.4	5.8	22.2	11.8	15.2
54	5.9	8.6	15.7	15.1	15.1	1.9	5.4	7.7	1.5	11.9	10.4	10.0
55	100.0	17.8	79.3	67.1	31.4	12.8	100.0	14.6	11.5	100.0	80.6	7.6
56	6.3	1.9	5.3	5.1	2.7	0.91	10.7	4.4	2.5	16.1	100.0	10.5
57	3.0	1.1	2.7	2.6	1.6	1.1	11.8	3.4	1.0	16.2	31.4	8.1
58	1.4	0.54	0.89	0.78	1.3	0.27	1.6	0.39	1.4	2.1	11.4	5.7
59	24.4	27.0	27.3	27.1	21.4	8.7	3.0	0.36	0.10	31.5	32.0	22.8
60	0.64	0.86	1.1	1.2	0.78	0.46	3.6	5.4	0.17	1.2	5.1	4.3
61	0.48	0.48	0.85	0.78	0.45	2.0	0.91	1.4	0.81	0.52	2.3	1.4
62	0.80	0.46	0.98	0.78	0.45	4.0	0.68	0.34	2.5	0.17	0.57	2.4
63	1.4	1.1	1.8	1.5	0.89	8.2	1.4	0.61	6.2	0.87	1.7	3.8
64	0.42	0.29	0.41	0.27	0.16	2.3	0.32	0.15	2.1	0.17	1.0	5.7
65	2.9	2.9	3.7	3.2	1.9	24.1	3.1	1.6	20.4	2.7	1.7	6.2
66	2.0	1.3	2.4	2.1	1.1	35.4	2.0	1.0	28.8	2.6	2.1	4.7
67	10.6	10.4	23.4	23.0	9.3	100.0	10.9	8.1	100.0	13.6	5.7	13.6
68	49.7	54.0	96.8	100.0	47.7	10.0	24.8	31.1	14.8	34.3	14.9	29.5
69	30.4	48.9	60.2	64.0	25.2	2.4	21.8	80.1	5.4	22.1	45.7	46.7
70	2.6	3.6	4.5	4.8	2.6	0.32	5.5	8.7	1.5	12.9	32.0	76.2
71	11.2	12.1	15.7	15.3	3.6	0.80	6.2	9.7	0.83	8.7	28.6	100.0
72	2.1	1.1	1.6	1.6	0.76	3.7	1.7	1.1	0.06	2.9	28.3	57.2
73	7.7	0.67	0.85	0.97	0.70	0.27	25.0	2.6	0.17	1.0	12.7	8.5
74	30.8	41.3	79.7	83.3	100.0		1.4	0.24	0.02	29.4	34.3	3.8
75	1.3	1.8	3.0	3.3	4.1		0.3			2.3	28.3	6.2
76		0.32	0.49	0.39	0.71					0.14	9.3	3.3
77		0.08	0.24	0.19	0.13	0.80	2.1		0.54	1.4	2.9	0.50
78					0.03	0.21	0.45		0.25	0.45	1.8	0.50
79	0.42	0.29	0.28	0.31	0.45	2.4	2.5		1.7	1.8	1.7	1.0

--continued

Table 1. Normalized Mass Spectra--continued

Mass Number	(1)	(2)	(3)	(4)	(5)	(6)	(7)	(8)	(9)	(10)	(11)	(12)
80					0.03	0.40	0.45		0.21	1.1	0.57	1.9
81	15.0	3.2	4.7	4.7	0.23	2.9	6.8	1.6	3.3	18.2	4.6	1.4
82	1.3	0.40	0.43	0.39	0.14	1.2	1.6	0.64	0.87	31.4	3.4	2.4
83	0.96	0.37	0.41	0.39	0.17	5.6	6.3	1.0	3.8	12.6	12.5	2.9
84		0.16	0.26	0.39	0.11	1.3	2.3	0.12	5.1	1.3	10.6	3.3
85	8.1	2.4	5.1	4.1	2.0	1.3	7.5	1.8	0.37	7.6	13.3	4.3
86	1.3	1.6	1.4	1.3	0.56		3.2	0.34	0.62	0.80	5.3	5.7
87	57.4	3.7	6.0	6.2	5.4	0.03	1.7	0.06		79.0	37.3	5.2
88	3.2	1.9	0.41	0.47	0.33		3.9	11.2		7.6	48.6	3.8
89	0.45						0.23	0.51		0.70	12.3	1.0
90								0.04			2.3	
91							0.86			0.03		
92						0.21	0.07		0.04	0.17		
93						2.1	3.8		1.7	0.52		
94						3.5	0.48		4.3	0.17		0.5
95	2.6	0.95	2.4	2.2	0.67	64.1	2.7	0.75	89.6	6.3	1.1	1.4
96	6.6	3.8	6.8	7.4	9.3	6.7	4.4	3.5	9.5	22.4	3.4	4.8
97	53.5	6.7	23.6	25.5	24.5	2.9	74.5	7.8	63.3	4.5	11.4	15.2
98	4.8	0.70	2.2	2.1	2.4	1.9	7.2	0.89	4.9	0.87	8.0	47.2
99	2.9	1.2	1.2	1.2	0.67	0.43	42.1	1.5	1.1	2.7	21.3	85.7
100	2.6	0.48	0.57	0.78	0.78		4.5	0.46	0.37	16.0	74.9	54.8
101	0.32	0.16	0.20	0.39	0.17		7.6	0.36	0.17	20.2	13.6	7.6
102							0.73			1.7	4.2	1.9
103										0.14	2.9	1.0
109						0.59	0.14			0.70		
110							0.05		0.02			0.50
111	0.48	0.32	0.41	0.47	0.13	68.9	7.3	0.07	6.8	0.49	0.86	11.4
112			0.16			5.9	0.95	0.16	8.5	0.35	0.97	84.7
113	32.1	4.22	6.7	7.2	2.4	0.80	3.0	2.4	1.0	31.2	6.6	84.7
114	2.9	0.37	0.59	0.85	0.33		8.8	2.4	0.21	10.2	4.1	11.4
115	0.16						2.1	0.3		2.1	11.4	3.8
116							0.39			0.24	42.9	1.4

--continued

Table 1. Normalized Mass Spectra--continued

Mass Number	(1)	(2)	(3)	(4)	(5)	(6)	(7)	(8)	(9)	(10)	(11)	(12)
117											8.0	
124						0.43				27.6		
125						4.7	0.84	0.08	20.9	29.4		
126	0.10			0.19		41.3	14.5		2.5	3.8		0.50
127	2.2	0.56	1.0	1.2		4.5	2.8	0.34	0.02	4.7		1.9
128	43.3	22.7	37.4	39.5	16.0	0.80	0.32	0.04		1.1	6.9	12.4
129	5.5	2.2	3.9	4.3	2.6					0.28	4.4	40.5
130	0.80	0.24	0.47	0.70	0.39						15.7	64.2
131											57.1	40.5
132											11.0	4.8
133											2.4	1.0
134											1.71	
135											3.43	
138									0.21			
139									1.4			
140							0.07	0.18	38.1			
141							0.59	0.49	4.8	1.01		
142							7.5	15.8	0.62	0.07		
143							1.3	2.2				
144							0.18	0.36				
155										0.77		
156										7.6		
157										1.8		
158										0.38		

Radio-Frequency Absorption Experiments in the Omegatron

P. M. Llewellyn and D. P. Littlejohn
Analytical Instrument Research, Varian Associates
Palo Alto, California

A mass spectrometer which measures the mass of an ion by the periodic nature of its motion in a magnetic field has been described by a number of authors. The discussion by Sommer, Thomas, and Hipple contains most of the important aspects of this type of mass spectrometry. Sommer, Thomas, and Hipple called their device the omegatron. The name has been accepted and we shall call our device the same.

The conditions for the observation of a mass spectrum in an omegatron differ in a number of important aspects from other methods. In the experiments to be described the path taken by ions under the action of an oscillating electric field at the cyclotron frequency and a static magnetic field is an archimedes spiral when projected onto a plane at right angles to the direction of the magnetic field. The path length may approach 100 meters and the flight time many milliseconds. Inherent in these two quantities are the two main differences from more conventional spectrometers. Firstly, to avoid collisions which would adversely affect the resolution, the pressure must be kept low. Secondly, the time during which fragments may be observed from an ionized molecule is very long. The possible applications of these conditions to aspects of the ionization and dissociation of molecules by electron impact has been suggested by Sommer, Thomas, and Hipple and also by Beynon. To the best of our knowledge up to this date only the mass spectra of some hydrocarbons up to butane have been examined with the omegatron.

The omegatron in general use for the analysis of low molecular weight gases usually consists of a small cell or box through which passes an electron beam to produce ionized fragments. The detection of the presence of cyclotron resonance is a means of a target electrode which is placed in the cell to collect only resonant ions. At the cyclotron resonant frequency the resonant ions gain energy at the expense of the oscillating electric field. Thus the resonant condition may then be observed by detecting the loss in coherent radio-frequency energy. This absorption technique was suggested by Sommer, Thomas, and Hipple. The energy possessed by an ion moving in a circular orbit in a magnetic field is given by:

$$E = \frac{1}{2} mr^2 \omega^2$$

From this simple expression it can be seen that the usefulness of an absorption technique will increase at high masses and for large cells. In fact, for cyclotron frequencies in the region of 100 kc/s (corresponding to 15u/kg) the absorption technique is more sensitive.

Fig. 1 shows the cross section of an omegatron. 70 v electrons ionize the sample vapor in a region of oscillating electric field. In order to provide a means of containing the ions for sufficient time for analysis a small positive voltage, typically a few tenths of a volt, is applied to electrodes at opposite ends of the cell to provide a trapping electric field in the direction of the magnetic field. The magnetic field itself is a very effective trap for unwanted motions at right angles to the magnetic field. A resonant ion then starts its motion on the axis and some hundreds of periods later will discharge upon hitting one of the electrodes. It is unimportant where this discharge takes place as the total ion current is very small, typically less than 10^{-12}A.

The typical conditions of an experiment will depend on the desired resolution. The mass spectrum is most conveniently examined by sweeping the field and keeping the radio-frequency constant. The resolution (50% width definition) is given by:

$$\rho \cong \frac{5.10^{-5} B^2 r^2}{V_{rf}\, m}$$

Where r is the maximum radius available for the motion of the ion. The cell now in operation has $r \cong 2$ cm and for $V_{rf} = 100$ mV, $B = 10^4$ gauss, and m = 200u; $\rho \cong 1{,}000$.

The limitations of the device are essentially set by electrical effects of the ions on each other and the effect of this on the motion. The pressure of the sample is usually set at $\cong 10^{-7}$ torr and the electron current between 0.1 and 1 μA.

Figures 2, 3 and 4 show a part of the mass spectrum of two substances toluene and bromoform. In order to detect any absorption of radio-frequency energy that may be occurring, it is useful to modulate the conditions of the experiment. In Fig. 2 this modulation has been carried out by sweeping the magnetic field at a low audio-frequency over a range of the order of the width of a resonance. The absorption signal will then occur at an audio-frequency and the absorption as detected by a phase sensitive detector will appear as a derivative curve. In order to present the spectrum directly as an absorption the resonance was periodically destroyed at an audio-frequency by reversing the electrostatic voltages used for trapping the ions. The resulting shape of a mass peak is shown in Fig. 3 and 4.

The basic reason for carrying out these experiments was a curiosity as to the form a fragmentation pattern would take if the time for analysis were greater by a factor of at least 1000 from that in a conventional sector mass spectrometer. This mass spectrometer shows a mass discrimination in that the absorbed energy is proportional to mass. As a start in the comparison of fragmentation patterns it was decided to look at the ratio of the peaks of 91 u and 92 u in a few compounds. With high energy electrons no changes outside a factor of two were found for toluene, xylene, and iso-butyl benzene in comparison with literature spectra. The selection of materials is at this state a little haphazard but as confidence in the apparatus grows a well defined investigation can be undertaken. A number of other compounds have been examined up to a molecular weight of 250.

REFERENCES

J. H. Beynon, Mass Spectrometry and Its Applications to Organic Chemistry, Elsevier 1960.

H. Sommer, H. A. Thomas, and J. A. Hipple; Phys. Rev. 82, 697 (1951).

FIGURE CAPTIONS

Fig. 1 The basic elements of the omegatron.
Fig. 2 The mass peaks 91 and 92 for toluene using an audio-frequency modulation of the magnetic field.
Fig. 3 The mass peaks 91 and 92 for toluene using an audio-frequency modulation of the electrostatic voltages.
Fig. 4 Some mass peaks in bromoform.

CYCLOTRON RESONANCE

$$\omega = \frac{e\,B}{M}$$

THE OMEGATRON

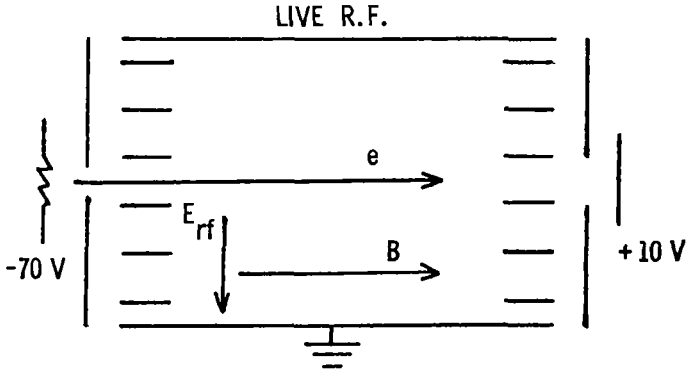

Fig. 1

Fig. 2

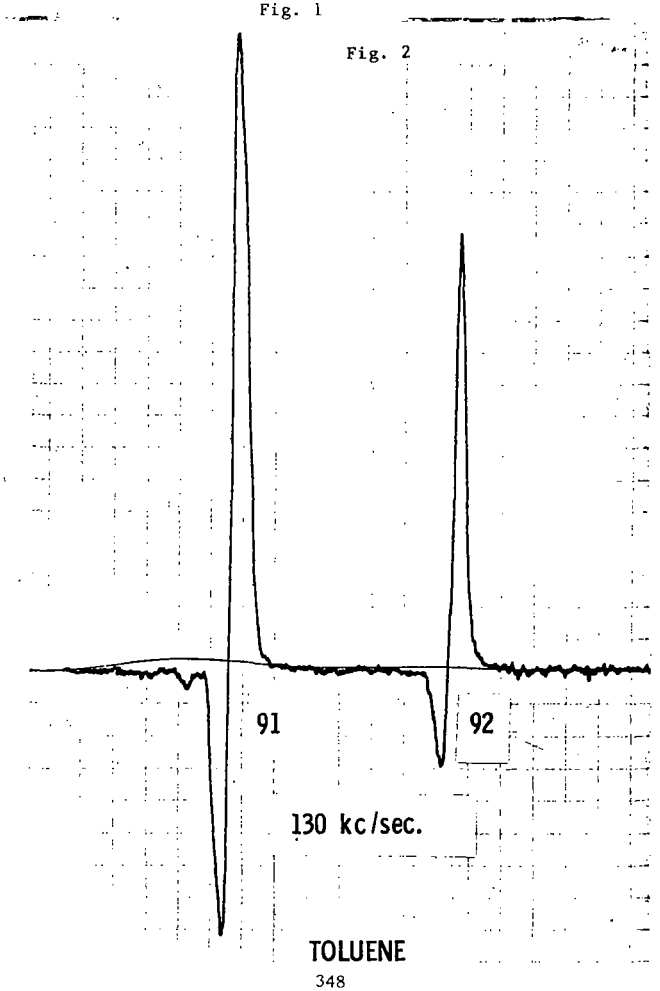

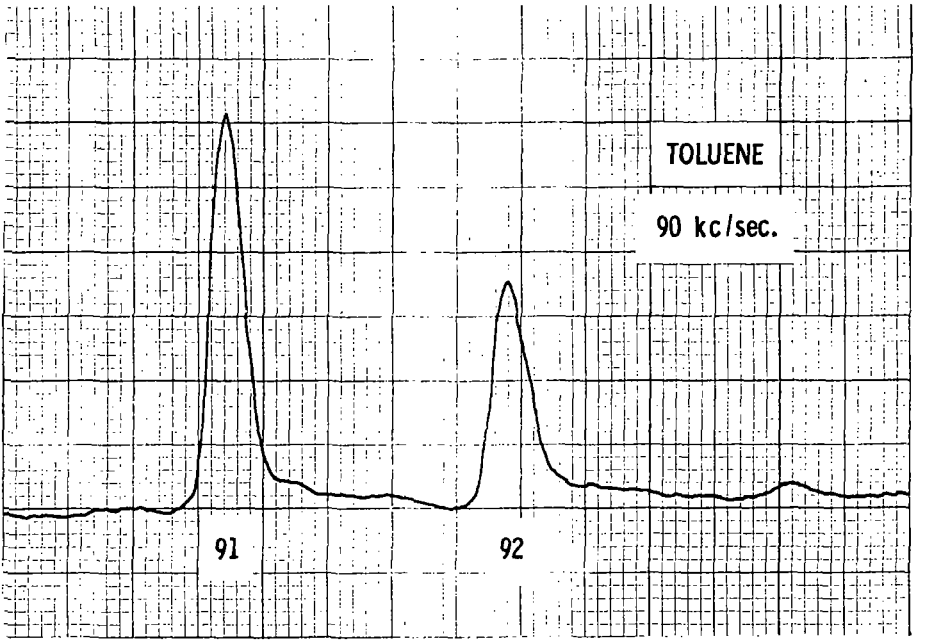

Fig. 3

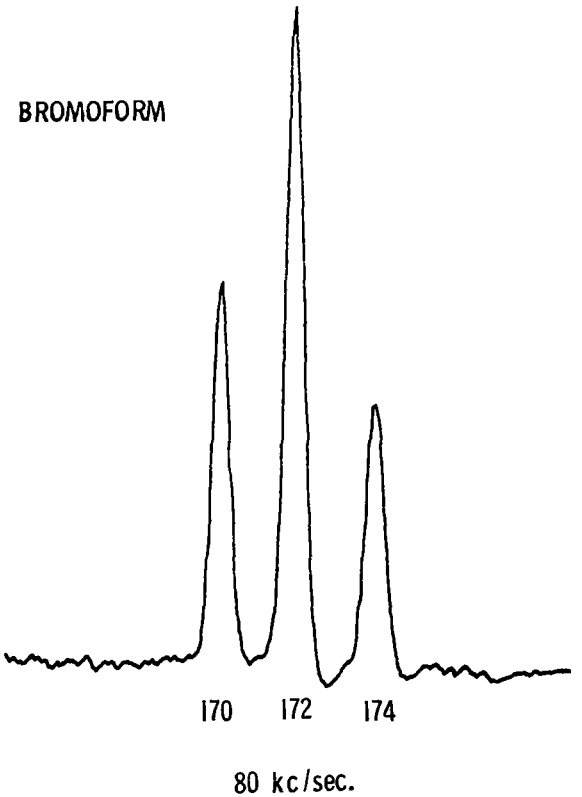

Fig. 4

INTERATOMIC PROPERTIES OF SOLIDS DEMONSTRATED IN SPARK ION SOURCE

BY

Berge B. Goshgarian & Andreas V. Jensen

Air Force Rocket Propulsion Laboratory, Research & Technology Division

Propellant Division, Chemical & Materials Branch

Edwards, California

ABSTRACT

The behavior of and analytical methods for inorganic compounds and metals were studied using a spark ion source solids mass spectrograph. Relative concentration of polyatomic species formed in the spark ionization of a compound are shown to be related to bond characteristics. Experimental relative sensitivities of ions in a compound and elements in an alloy are shown to agree within ± 20% with relative sensitivities calculated from values of lattice energy, ionic or atomic cross-section heat of sublimation, ionization energy, and electron affinity.

A number of representative cracking patterns for solid inorganic compounds, and analytical data for eight aluminum powder samples and an NBS Hastalloy C sample are presented and discussed. Results show that spark ion source mass spectrographic data can be used for qualitative analysis with an accuracy of ± 10% and to predict interatomic relationships in compounds.

INTRODUCTION

The spark ion source mass spectrograph has for some time been used for the analysis of metals, semi-condictors, and inorganic materials for major as well as trace constituents. Trace constituents can be detected to 0.001 ppm. The results obtained at these very low concentrations may be as much as 100% off, yet not greatly affect the analysis; however, when constituents present in greater than 100 ppm. are analyzed, discrepancies in the analytical results are observed. This may be attributable to differences in elemental and atomic sensitivities and irregularities of sample utilization in the spark. Therefore, spark analysis of known concentration standards and obtaining sensitivities are required. With matrices such as powders or alloys, which may contain a number of elements and atoms in the spark ion analysis from data given in literature was therefore desired.

Our investigations along this line suggest that values for lattice energy ionic or atomic cross-section, heat of sublimation, ionization energy, and electron affinity of atoms can be used to calculate relative sensitivities expected in a spark ion source. The calculated relative sensitivities will be shown to approximate experimentally derived sensitivities to within ± 20%. Also, these calculated relative sensitivities will be shown to be quite useful in the quantitative analysis of alloys and powders.

EXPERIMENTAL

A Mattauch-Herzog type double-focusing mass spectrograph equipped with an R-F spark ionization source and photoplate detection system was useful for this study. The instrument was a standard Consolidated Electronics Corporation 21-110 mass spectrograph. Ilford Q-2 photoplates were used for ion collection, and were developed in standard solutions for normal durations. Samples were packed in 1/8" x 3/4" spectrograde cupped electrodes. The electrode lines (Ag) on the photoplates were used as calibration lines. The ion line transmittancies were converted to normalized ion exposure values and corrected for line width variations similar to methods given by Hull (1) and Owens & Giardino (2).

PATTERNS

The ion exposure values obtained for a number of compounds were normalized to a standard ion in the compound. The resulting relative exposures gave patterns for the compounds as shown in Tables I, II, and III. As the percent ionic character of a bond increases, the intensity of polymolecular species decreases. This was especially noticeable for compounds as $AlCl_3$ (32% IC) as opposed to AlF_3 (62% IC), B_2O_3 (32% IC), as opposed to Al_2O_3(46% IC), $LiBH_4$(B-H ∿ 2% IC) as opposed to $LiAlH_4$(Al-H ∿ 11% IC), and

compounds like Al $(C_2H_3O_2)_3$, NH_4ClO_4.

Polymolecular species were not observed for characteristically ionic compounds, although high yield exposures may have given traces of the polymolecular species. Every compound studied gave a characteristic pattern, similar to conventional mass spectrometry; however, the elemental ion lines were generally the most intense.

EXPERIMENTAL RELATIVE SENSITIVITIES

The data obtained from the compounds fired was used to calculate relative sensitivities of the ion present using equation 1.

$$S_m = \frac{E_{cm}}{E_{cs}} \times \frac{I_s}{I_m} \times \frac{C_s}{C_m} \qquad (1)$$

Where

S_m = relative sensitivity of mass m to standard mass s.

E_{cm} = corrected ion mass exposure.

I_m, I_s = isotopic abundancies of mass ion m and standard mass ion s.

$C_m C_s$ = atom concentration of mass m and s.

E_{cs} = corrected standard ion mass exposure.

Once the relative sensitivities of the ions were determined, they could be used to calculate the concentration of elements in a matrix using equation 2.

$$C_m = \frac{E_{cm}}{I_m} \times \frac{1}{S_m} \qquad (2)$$

CALCULATED RELATIVE SENSITIVITIES

A. Ions in a Compound

The sensitivity of an anion relative to a cation in a compound was calculated using the basis of the Born-Haber Cycle (3) for positive ion formation. The reaction sequence for a simple ionic compound is:

$$MX_{(s)} \xrightarrow{U_o} M_{(g)}^+ + X_{(g)}^-$$

$$X_{(g)}^- \xrightarrow{EA} X_{(g)}^o$$

$$X_{(g)}^o \xrightarrow{I_p^+} X_{(g)}^+$$

The cation is released as soon as the lattice energy (U_o) is overcome. However, the anion must lose two electrons to assume a positive charge. Therefore, the energies of electron affinity (EA) and ionization (I_p^+) must be added. The ionic radii (IR) of the cation and anion are included in the overall process as ionic cross-section $(IR)^2$ available for electron collision. Relative sensitivities (S) of ions in a compound existing as MF, MCl, and MO are then calculated using equation 3.

$$S_{cation} = (IR)^2 \times \frac{1}{U_o} \qquad (3)$$

$$S_{anion} = (IR)^2 \times \frac{1}{U_o} \times \frac{1}{EA + I_p^+}$$

Of course, the lattice energies will cancel; however, it must be included when relating sensitivities among compounds. Experimental relative sensitivities (S_m) were then related to calculated data by multiplying the experimental number by the square root of the ion mass. The use of this square root function was suggested for photoplate ion detectors by Hintenburger (4) and Owens and Giardino (2).

Data given in Table IV show some correlation to exist.

LITHIUM CHLORIDE, LiCl

m/e	Specie	Relative Intensity
6	^{6}Li	8.0
7	^{7}Li	100.0
17.5	$^{35}Cl^{++}$	15.0
18.5	$^{37}Cl^{++}$	6.0
35	^{35}Cl	21.0
37	^{37}Cl	8.0
42	$^{7}Li^{35}Cl$	0.26
48	$^{6}Li^{7}Li^{35}Cl$	0.42
49	$^{7}Li_2{}^{35}Cl$	1.6
51	$^{7}Li_2{}^{37}Cl$	0.65

SODIUM CHLORIDE, NaCl

23	^{23}Na	100.0
35	^{35}Cl	13.0
37	^{37}Cl	5.7
58	$Na^{35}Cl$	0.09
60	$Na^{37}Cl$	0.05
81	$Na_2{}^{35}Cl$	0.90
83	$Na_2{}^{37}Cl$	0.32

POTASSIUM CHLORIDE, KCl

m/e	Specie	Relative Intensity
35	^{35}Cl	20.0
37	^{37}Cl	7.0
39	^{39}K	100.0
41	^{41}K	10.0
74	$^{39}K^{35}Cl$	0.05
113	$^{39}K_2{}^{35}Cl$	0.50
115	$^{39}K_2{}^{37}Cl$	0.20

BERYLLIUM FLUORIDE, BeF_2

9	Be	100.0
19	F	140.0

BERYLLIUM CHLORIDE, $BeCl_2$

9	Be	100.0
35	Cl	100.0
37	Cl	40.0
44	$Be^{35}Cl$	3.0
53	$Be_2{}^{35}Cl$	2.0
70	$^{35}Cl_2$	7.0
79	$Be^{35}Cl_2$	0.5

ALUMINUM FLUORIDE, AlF_3

19	^{19}F	105.0
27	^{27}Al	100.0
46	$^{27}Al^{19}F$	1.4
65	$^{27}Al^{19}F_2$	3.3

ALUMINUM CHLORIDE, $AlCl_3$

m/e	Specie	Relative Intensity
27	^{27}Al	100.0
35	^{35}Cl	32.0
36	^{35}ClH	2.0
37	^{37}Cl	8.0
38	^{37}ClH	0.26
62	$Al^{35}Cl$	2.0
64	$Al^{37}Cl$	0.70
70	$^{35}Cl_2{}^{35}Cl$	0.04
72	$^{35}Cl_2{}^{37}Cl$	0.016
89	$Al_2{}^{35}Cl$	0.05
91	$Al_2{}^{37}Cl$	0.017
97	$Al^{35}Cl_2$	1.4
99	$Al^{35}Cl^{37}Cl$	1.6
101	$Al^{37}Cl_2$	0.3
124	$Al_2{}^{35}Cl_2$	0.021
126	$Al_2{}^{35}Cl^{37}Cl$	0.02
132	$Al^{35}Cl_3$	0.13
134	$Al^{35}Cl_2{}^{37}Cl$	0.11
136	$Al^{35}Cl^{37}Cl_2$	0.043
159	$Al_2{}^{35}Cl_3$	0.056
161	$Al_2{}^{35}Cl_2{}^{37}Cl$	0.032

TABLE I

LITHIUM BOROHYDRIDE, $LiBH_2$

m/e	Specie	Relative Intensity
6	^{6}Li	19.0
7	^{7}Li	240.0
10	^{10}B	24.0
11	^{11}B	100.0
12	^{12}BH	4.0
12	$^{10}BH_2$	2.0
13	$^{11}BH_2$	4.3
14	$^{11}BH_3$	2.0
15	$^{11}BH_4$	7.0
20	$^{7}Li^{11}BH_2$	0.3

SODIUM BOROHYDRIDE, $NaBH_4$

10	^{10}B	25.0
11	^{11}B	100.0
12	^{11}BH	0.7
13	$^{11}BH_2$	0.4
23	Na	350.0

LITHIUM ALUMINUM HYDRIDE, $LiAlH_4$

m/e	Specie	Relative Intensity
6	^{6}Li	17.0
7	^{7}Li	270.0
27	Al	100.0
1	^{1}H	120.0
2	$^{1}H_2$	30.0
3	$^{1}H_3$	9.0
6	^{6}Li	40.0
7	^{7}Li	480.0
27	Al	100.0

SODIUM ALUMINUM HYDRIDE, $NaAlH_4$

23	Na	430.0
27	Al	100.0
28	AlH	4.0

ALUMINUM OXIDE, Al_2O_3

m/e	Specie	Relative Intensity
16	^{16}O	150.0
27	Al	100.0
32	$^{16}O_2{}^{16}O$	18.0

BORON OXIDE, B_2O_3

10	^{10}B	25.0
11	^{11}B	100.0
16	^{16}O	64.0
26	^{10}BO	4.0
27	^{11}BO	13.0
42	$^{10}BO_2$	0.5
43	$^{11}BO_2$	2.0
53	$^{10}B^{11}BO_2$	0.5
54	$^{11}B_2O_2$	2.0
69	$^{10}B^{11}BO_3$	3.0
70	$^{11}B_2O_3$	4.0
92	$^{11}B_4O_3$	3.0
96	$^{10}B^{11}B_2O_4$	2.0
97	$^{11}B_3O_4$	2.5

TABLE II

TABLE IV

RELATIVE SENSITIVITIES OF IONS IN COMPOUNDS

CALCULATED VS. EXPERIMENTAL

Compound	Ion	S. Calc.(1)	S. Exp.(2)	Compound	Ion	S. Calc.(1)	S.Exp.(2)
LiCl	Li	1.0	1.0	BeO	Be	1.0	1.0
	Cl	.54	.64		O	1.4	2.0(3)
NaCl	Na	1.0	1.0	BeF_2	Be	1.0	1.0
	Cl	.21	.21		F	.9	1.0
KCl	K	1.0	1.0	$BeCl_2$	Be	1.0	1.0
	Cl	.11	.25		Cl	2.0	1.4(4)
MgO	Mg	1.0	1.0				
	O	.32	.33				

(1) Calculated: $S_{cat} = (IR)^2 \times \frac{1}{U_o}$

$S_{an} = (IR)^2 \times \frac{1}{U_o} \times \frac{1}{EA + I_p+}$

(2) Experimental: $S_{cat} = S_m \sqrt{M}$

$S_{an} = S_m \sqrt{M}$

(3) $Be(OH)_2$ not accounted for.

(4) Be, BeO not accounted for.

When the cation is bonded to a standard atom, or the cations are bonded to a common anion (e.g., Mg-O relative to Al-O), the ionic cross-section $(IR)^2$ of the ion and first ionization energy (I_p+) are considered. This is based on the principle previously described and is shown by the following reaction sequence.

$$M - Al_{(s)} \xrightarrow{U_o} M^o_{(g)} + Al^o_{(g)}$$

$$M^o_{(g)} \xrightarrow{I_p+} M^+_{(g)}$$

$$Al^o_{(g)} \xrightarrow{I_p+} Al^+_{(g)}$$

Therefore, the two ions in the M-Al bond or cations in M-X, Al-X bond are related using equation 4.

$$S = (IR)^2 \times \frac{1}{I_p+}$$

[$\frac{1}{U_o}$ omitted as mentioned previously) (4)

The experimental data was then related to calculated data by multiplying experimental sensitivities by $\sqrt{M}$. Data given in Table V shows some correlation to exist.

TABLE V

SENSITIVITIES OF IONS RELATIVE TO ALUMINUM IN COMPOUNDS

Compound	Ion	S. Calc.(1)	S. Exp.(2)	Compound	Ion	S.Calc.(1)	S.Exp.(2)
$LiAlH_4$	Li	1.6	1.3	$BeO-AL_2O_3$	Be	.25	.24
	Al	1.0	1.0		Al	1.0	1.0
$NaAlH_4$	Na	4.2	4.0	BN-AlN	B	.12	.13
					Al	1.0	1.0
$KAl_2(AlSi_3O_{10})$	K	9.5	9.7	$MgO-Al_2O_3$	Mg	1.3	1.2
	Al	1.0	1.0		Al	1.0	1.0

(1) Calculated: $S = (IR) \times \frac{1}{I_p+}$

(2) Experimental: $S = S_m \sqrt{M}$

ALUMINUM ACETATE, $Al(C_2H_3O_2)_3$

m/e	Specie	Relative Intensity
12	C	160.0
13	CH	9.0
14	CH_2	8.0
15	CH_3	14.0
16	^{16}O	60.0
16	CH_4	3.5
24	C_2	1.5
25	C_2H	1.4
26	C_2H_2	4.5
27	Al	100.0
27	C_2H_3	5.0
28	CO	11.0
28	C_2H_4	2.5
29	COH	6.6
29	C_2H_5	1.1
30	COH_2	0.5
31	CH_2OH	1.2
39	AlC	1.3
40	C_2O	0.4
41	HC_2O	0.7
42	H_2C_2O	5.0
43	H_3C_2O	14.0
44	CO_2	8.5
45	HCO_2	4.5
60	$C_2H_3O_2H$	0.8
61	$C_2H_3O_2H_2$	0.9

ALUMINUM SULFATE, $Al_2(SO_4)_3$

m/e	Specie	Relative Intensity
16	^{16}O	510.0
17	^{16}OH	39.0
18	$^{16}OH_2$	129.0
27	Al	100.0
32	$^{16}O_2 + {}^{32}S$	390.0
33	$^{16}O,^{17}O$	21.0
34	$^{16}O,^{18}O$	24.0
48	$S^{16}O$	60.0
49	$S^{16}OH$	5.0
50	$S^{16}OH_2$	3.5
64	SO_2	30.0
80	SO_3	2.0
96	SO_4	1.5

AMMONIUM PERCHLORATE, NH_4ClO_4

m/e	Specie	Relative Intensity
14	N	100.0
15	NH	30.0
16	O	350.0
16	NH_2	100.0
17	OH	120.0
17	NH_3	300.0
18	HOH	280.0
18	NH_4	320.0
19	H_3O	120.0
28	N_2	40.0
30	NO	520.0
32	O_2	160.0
35	Cl	250.0
36	ClH	70.0
37	Cl	80.0
38	ClH	30.0
46	NO_2	50.0
51	^{35}ClO	180.0
67	$^{35}ClO_2$	170.0
70	$^{35}Cl_2$	50.0
83	$^{35}ClO_3$	30.0
99	$^{35}ClO_4$	6.0

TABLE III

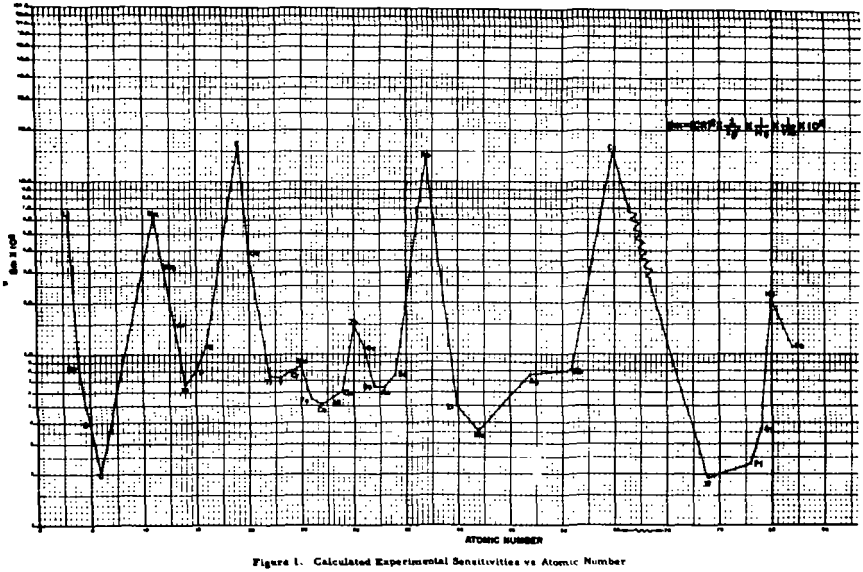

Figure 1. Calculated Experimental Sensitivities vs Atomic Number

B. Metallic Ions

The sensitivity of an ion originating from an alloy is shown to be related to its covalent radius squared $(CR)^2$, which approximates the atomic cross-section available for electron collision, its sublimation energy (Hs), and its ionization energy (I_p+). The following reaction sequence is proposed.

$$M^o_{(s)} \longrightarrow M^o_{(g)} - \Delta H_s$$
$$M^o_{(g)} \longrightarrow M+_{(g)} - I_p+$$

As the atomic cross-section of a metal atom increases, so does the probability of electron collusion and heat absorption. The concentration of metal atoms in the vapor after sublimation will be related to their inverse sublimation energies $[\frac{1}{\Delta H_s}]$. In other words, assuming a given electron energy, the concentration of a metal atom with a lower sublimation energy will be greater in the vapor. Consequently, as the energy required to ionize a metal atom in the vapor phase decreases, the intensity of the metal ion increases. The equation proposed for calculating sensitivities for metallic ions expected from an alloy is given by equation 5.

$$S = (CR)^2 \times \frac{1}{\Delta H_s} \times \frac{1}{I_p+} \qquad (5)$$

The data obtained using this equation for a number of elements is related to experimental data from a number of investigators (5,6,7,8,9) in Table VI by dividing the calculated sensitivity (s) by $\sqrt{M}$ to convert to an experimental sensitivity. Sensitivity data for a number of elements is shown in Figure I.

TABLE VI

CALCULATED VS. EXPERIMENTAL SENSITIVITIES OF ELEMENTS

m/e	Calc.* S_m	Hastalloy C.	Ref. 5	Ref. 6	Ref. 7	Ref. 8	Ref. 9
Be	1.5				.25		
B	.7						
C	.4	1.1					
Mg	5.8					2.4	
Al	2.7						
Si	1.2	1.1			.7		1.6
Ti	1.4						1.1
V	1.3	1.6					
Cr	1.4	1.4	1.7	1.5	1.2	1.4	
Mn	1.6	2.6	3.0		1.3	2.1	1.8
Fe	1.0	1.0	1.0	1.0	1.0	1.0	1.0
Co	.94	.94			.7		
Ni	1.02	.9	.9	.9	1.2	.83	.9
Cu	1.1		1.8			1.05	.8
Zn	2.8					1.9	5.5
Ga	2.0				1.2		
As	1.2				1.4		
Zr	.92						
Mo	.7	.72	.5				
Ag	1.4				2.7		
Sb	1.5				2.1		
W	.4	.68					
Pt	.4						

$$^*S_m = (CR)^2_m \times \frac{1}{\Delta H_{Sm}} \times \frac{1}{I_p+_m} \times \frac{1}{\sqrt{m}}$$

SAMPLE ANALYSIS

A. Hastalloy C

The data given in Table VII was obtained from five exposures of sample. The spread in ion intensity is approximately ± 20%; however, an average of five exposures gives a more meaningful value by decreasing the probability of selective sublimation and ionization of an element and sample non-homogeneity.

TABLE VII

HASTALLOY C - NBS STD.

Element	E_c Avg.	$(E_c)(MW)(10^2)$	Uncorrected Wt.%	Corrected Wt.%	NBS Wt.%
C	.012	14.4	.13	.30	.06
Si	.025	70.0	.61	.49	.51
V	.008	40.8	.35	.25	.2
Cr	.53	2750	23.9	16.5	15.7
Mn	.036	198	1.7	1.04	.6
Fe	.13	725	6.3	6.09	5.7
Ni	1.0	5871	51.0	48.4	52.6*
Co	.03	176	1.5	1.57	1.43
Mo	.16	1535	13.3	18.5	16.5
W	.017	330	2.9	6.9	3.4

*Includes impurities as Ca, K, Na.

The corrected analytical data from a photoplate agrees within ± 10% of the NBS analysis for most elements. Greater variation was observed when plate data was not corrected for relative sensitivities. The large difference in carbon is due to hydrocarbon background present in the instrument. Nickel concentration given by NBS included calcium, potassium, and sodium impurities as detected by mass spectrograph and can be expected to be higher than the experimental value. Tungsten concentration is found to be higher than the NBS value. Only two exposures showed faint tungsten lines, and the average exposure value may very well be invalid.

B. Aluminum Powders

The data presented in Table VIII is obtained from an average of four spectra per sample. Agreement between the two methods of analysis is better than expected when using the powder matrix. Calculations not using relative sensitivity values gave results for lithium which were as much as 300% greater than those obtained by wet chemical analysis. The value for chloride sensitivity was taken relative to lithium since the impurities included lithium chloride. If this was not done, chloride concentration was calculated to be a factor of 10 greater than found by wet chemical analysis.

TABLE VIII

ALUMINUM POWDERS - WT. % VALUES GIVEN

	1		2		3		4	
m/e	W/C	MS	W/C	MS	W/C	MS	W/C	MS
Li	.37	.2	.39	.2	.3	.2	.48	.2
B	--	.02	--	.01	--	.01	<0.1	.01
C	.12	.3	.2	.3	.39	.3	.3	.4
O	--	.35	--	.4	--	.6	--	.3
Na	--	.03	--	.04	--	.05	--	.07
Mg	--	.04	--	.06	--	.12	--	.15
Al	98.3	99.0	98.7	99.2	98.8	98.8	97.8	98.9
Cl	<0.1	0.02	<0.1	.04	.33	1.	.42	.2
Unk.	1.10	--	.60	--	--	--	.78	--
	5		6		7		8	
Li	.39	.4	.45	.3	.56	.4	.51	.5
B	--	.04	--	.03	--	.04	<0.1	.04
C	.4	.7	.32	.95	.42	.6	.3	.6
O	--	1.5	--	1.06	--	.6	--	.8
Na	--	.04	--	.2	--	.03	--	.05
Mg	--	.1	--	.05	--	.1	--	.08
Al	97.6	97.2	97.8	97.4	97.3	98.3	98.0	98.2
Cl	.25	.2	<0.1	.02	.18	.04	<0.1	.04
Unk.	1.4	--	1.3	--	1.55	--	1.00	--

CONCLUSION

Spark ion source mass spectrography can be used to obtain patterns for solid compounds. These patterns suggest an application for identification of the type of bonding of an ion, the ionic character of a bond, lattice energy, and other values.

The correlation of experimental with calculated relative sensitivities for atoms in a compound indicates that the reaction sequence proposed describes the process occurring in the spark reasonably well. Also, the correlation of experimental vs. calculated relative sensitivities for the elements indicates that the process occurring in the sparking of an alloy can be described as one of sublimation and ionization of the metallic atom with consideration given to its collision cross-sectional area.

Data presented for the analysis of Hastalloy C and eight Al powders illustrates the applicability of the spark ion mass spectrograph in quantitative analysis when relative sensitivities and plate calibrations are determined.

BIBLIOGRAPHY

1. Hull, C. W., Paper #72, Tenth Annual Conference, ASTM Committee E-14 on Mass Spectrometry (1962).

2. Owens, E. B. and Giardino, N. A., Anal. Chem., 35, No. 7, pp. 1172-1178 (1963).

3. Moeller, T., Inorganic Chemistry, John Wiley & Sons, New York (1955), pp. 184-186.

4. Hintenberger, H., Paper #41, Eleventh Annual Conference, ASTM Committee E-14 on Mass Spectrometry (1963).

5. Owens, E. B and Giardino, N. A., Lincoln Library, Massachusetts Institute of Technology, Report No. J.A. 2091.

6. Gorman, J. G., Jones, J. J., and Hipple, J. A., Anal. Chem, 23, 438 (1951).

7. Elliott, R. M., Craig, R. D., and Errock, G. A., Instruments and Measurements, Vol. 1, p. 271, edited by Helge von Koch and Gregory Ljungberg (1960).

8. Chakravarty, B., Venkatasubramanian, V. S., and Duckworth, H. E., Advances in Mass Spectrometry, Vol. 2, p. 128, edited by R. M. Elliot, Pergamon Press, New York (1963).

9. Craig, R. D., Errock, G. A., and Waldron, J. D., Advances in Mass Spectrometry, Vol. 1, pp. 136-156, edited by J. D. Waldron, Pergamon Press, New York (1961).

SPARK SOURCE MASS SPECTROGRAPHIC ANALYSIS OF SOME NICKEL AND IRON BASE ALLOYS

H. D. Cook, T. Kessler and L. T. Beeles
Westinghouse Electric Corporation
Bettic Atomic Power Laboratory
Box 1468
Pittsburgh 30, Pa.

Changes were observed in the metallurgical properties of various non-fuel alloys used to fabricate components for the Shippingport Atomic Power Plant. To explain the changes in metallurgical properties, variations in the chemical composition of the alloys were investigated. Because of the small size of the samples available, a spark source mass spectrographic method for the analysis of the alloys was developed. The analyses of all elements ranging in concentrations from 0.1 ppm to that of major constituents were accomplished on one plate.

Several instrumental techniques and methods of computation were used to increase the reliability of the determination of individual elements.

The results obtained by the spark source mass spectrographic method compared favorably with the results obtained by wet chemical analyses.

MASS SPECTROGRAPHIC ANALYSIS OF RARE EARTH METALS

J. W. Guthrie - Sandia Laboratory, Albuquerque, New Mexico

Introduction

A CEC 21-110 mass spectrograph equipped with an rf spark ion source and a photographic-plate, ion-detection system is being used to obtain semiquantitative analyses of homogeneous bulk impurities in several commercially available metal samples of scandium, yttrium, cerium, holmium, erbium, and lutetium. Partial results for three of these metals (erbium, cerium, and lutetium) are presented.

Positive ions with ratios of mass to charge values covering a range of 36 to 1 were collected simultaneously on 2 by 15 inch Ilford Q2 photographic plates.

No attempts were made to obtain extreme limits of detection (parts per billion range) because the effects of impurities in the 100 ppm range on experiments of interest are largely unknown. However, the results enable the researcher to choose the sample with the highest over-all purity or the highest purity with respect to one or several elements known to be present. This choice is not possible with the limited information often furnished with a sample. Also, the meaning of the term "rare earth 99.9%" that may be furnished with a sample for example, is often misleading, for it is not always clear if the percentage quoted is with respect to other rare earths, total non-gaseous impurities, or a combination of various impurity types.

As will be seen below, nonhomogeneity can be a major problem for some samples, especially when several small pieces are received in a shipment and designated by the supplier as being from one specific lot number. Since the quantity of sample used in the analysis is small (a few mg) nonhomogeneity in a piece weighing several grams can go undetected when only one sampling is made.

Even though the absolute accuracy is unknown, the relative values between samples for a given element present as a homogeneous impurity should be highly significant.

Results and Discussion

Erbium and Cerium

Erbium Sample A - Ingot (1 inch diameter)
B - Wire (0.040 inch diameter)
C - Ingot (1 inch diameter)
D - Wire (0.020 inch diameter)
E - Wire (0.050 inch diameter)
F - Sponge

Cerium Sample No. 1 - Ingot
No. 2 - Ingot

(No certificates of analyses were available from the suppliers since most samples were obtained from various laboratories which did not obtain analysis information from the supplier.)

An exposure range of 10^6 was covered in 13 separate exposures on each plate. The results were computed by an internal standard method, using visual and densitometer data, in which a comparison is made between the exposure required to produce two lines of equal optical density--one line from the impurity element and the other from the matrix element. Only singly charged ions were used, and allowances were made for plate-response differences for ions of different mass and for variations in spectrum - line widths.(1) The samples were given no special cleaning before analysis other than an alcohol rinse. The samples were "pre-sparked" to remove surface contaminants before analytical exposures were made. A minimum of two analyses was made for each sample, one analysis per plate. With the analytical method used, results could not be computed for elements present as nonhomogeneous bulk impurities. A nonhomogeneous impurity is detected by the erratic optical density of its spectrum as exposure increases.

Results(2) for the erbium and cerium samples are listed in Tables I and III. Additional information is given in the footnotes of the tables. Table II compares the mass spectrographic results for hydrogen, carbon, nitrogen and oxygen in five erbium samples with results from other methods. A microcombustion technique was used for analysis of hydrogen and carbon, and a neutron activation technique (not performed by Sandia) for the analysis of oxygen and nitrogen. An investigation is being made in an attempt to

TABLE I

Erbium Samples

Element	A	B	C	D	E	F	Detection Limit (a)
	Parts Per Million Atomic						
Th	130	90	ND(b)	5	2	ND	1
Au	1	3	ND	1	4	ND	1
Pt	ND	ND	ND	ND	150	ND	3
W	100	300	110	130	130	ND	3
Ta	650	830	440	1000	10	ND	1
Lu	ND	9	ND	3	35	ND	1
Yb	ND	ND	ND	3	ND	ND	3
Tm	500	10	100	170	10	15	1
Ho	1	300	3	100	330	4500	1
Dy	15	180	530	10	170	40	4
Tb	1	10	ND	10	10	15	1
Gd	50	20	7	7	20	75	7
Sm	5	ND	47	ND	ND	ND	5
Nd	700	3	5	12	20	190	2
Pr	2	6	0.6	6	60	ND	0.6
Ce	2	6	2	2	2	ND	0.7
La	2	20	10	2	20	ND	0.6
Ag	ND	64	ND	ND	230	ND	0.6
Pd	ND	11	ND	ND	ND	ND	1
Rh	ND	ND	ND	ND	5	ND	0.3
Ru	ND	ND	ND	ND	6	ND	1
Mo	ND	ND	275	ND	ND	ND	1
Nb	0.3	ND	0.4	0.8	ND	ND	0.3
Y	1	240	80	80	120	1300	0.2
As	ND	1	ND	ND	ND	ND	0.1
Ga	ND	0.6	ND	ND	ND	ND	0.2
Zn	14	ND	ND	ND	ND	ND	0.4
Cu	0.6	16	3	50	50	30	0.2
Ni	0.5	370	5	(c)	9	7	0.4
Fe	20	600	20	100	100	ND	0.1
Mn	1	13	13	3	0.2	5	0.1
V	ND	ND	ND	ND	ND	4	0.1
Cr	0.7	4	7	40	7	ND	0.1
Ti	2	2	(d)	2	2	700	0.2
Sc	ND	1	ND	ND	0.4	ND	0.1
Ca	1000	1	10	340	2	(c)	0.1
K	(c)	10	1	4	1	(c)	0.1
Cl	90	90	30	15	(c)	(c)	0.1
P	1	10	0.5	0.5	0.4	2	0.1
Si	10	800	110	(c)	40	ND	2
Al	10	90	30	(c)	50	1400	0.1
Mg	170	3	0.8	75	(c)	2	0.1
Na	(c)	32	(c)	(c)	(c)	5	0.1
F	830(e)	8	0.3	1300(e)	15	0.2	0.1
O(f)	3500	3500	1000	1200	1200	3500	0.1
N	300	30	100	200	1000	175	0.1
C	5000	900	300	1800	800	7000	0.1
B	0.5	1	0.4	25	0.8	0.2	0.1
Li	ND	ND	ND	ND	ND	(c)	0.1
H(g)	1300	2600	2600	5000	5000	(h)	0.03
Purity (per cent atomic)(i)	98.5	98.9	99.4	98.8	99.0	98.1 (j)	

(a) Limit of detection was computed from the longest exposure made, using the most abundant isotope of a given element free of interference from any isotope of any other element listed in Table I. The values listed can be decreased by increasing the exposure range. Because of slight differences in realized plate response between samples, the values listed may vary slightly from plate to plate and therefore the values are average.

(b) ND - none detected

(c) In the spectrum, but erratic in density with increasing exposure; therefore, it is considered nonhomogeneous.

explain the large discrepancies.

Lutetium

Sample I - Scrap-like pieces
II - " " "
III - " " "
IV - Ingot piece
V - " "

Three of the five samples (I, III, IV) all from different suppliers, were accompanied by certificates of analysis for Tm, Y, Si, Mg, and Ca. It is interesting to note that the results were identical. It is also very interesting that none listed Ta, which is the largest metal impurity. Three of the samples (II, III, IV) had identical lot numbers; and the evidence is that the three samples came from the same source even though they were received from different suppliers. Sample I had a different lot number assigned, but the results in Table IV indicate that it is very similar to III and IV.

Since better photographic plates[3] were available for the lutetium analyses than for the erbium and cerium work, a densitometer method similar to one described by Owens[1] was used. The mass spectrograph was also modified to allow 28 spectra to be placed on one plate instead of 15, thus enabling a duplicate analysis to be put on a single plate.

The lutetium samples were also rinsed in alcohol before placement in the spark source chamber and were "pre-sparked" before the analytical exposures were made. Samples IV and V required cutting-wheel operations to obtain suitably sized and shaped pieces. This procedure may explain some of the nonhomogeneities noted for these two samples.

Ion yields[1] were normalized to the longest exposure by using the ratio of beam monitor charges of the spectra from which ion yields were calculated and the longest exposure spectrum. The low-level impurities could usually be determined only once in each of the longest exposure spectrums of the duplicate run; however, for higher-level impurities, ion-yields were calculated in several exposures, normalized, and then averaged. An attempt was made to use lines whose optical densities were on the linear portion of the plate calibration curve. A previously prepared plate calibration curve[3] using ratios of erbium isotopes was used. The two lutetium isotopes (^{175}Lu - 97.41%, ^{176}Lu - 2.59%) have an undesirable (1) abundance ratio for use in plate calibrations.

A change in instrument slit widths, after the erbium and cerium analyses were made decreased the sensitivity at a given charge because of increases in line widths. Also, the exposure range used was less than that previously used. A 90% transmission was used as a basis for calculations of detection limit in the lutetium analyses. Results for the lutetium samples are listed in Table IV.

Conclusions

Because of significant differences found for some impurities in the analyzed samples, each lot or batch of material from a given supplier, from different suppliers, and following local efforts at purification should be analyzed when basic studies are made using the rare earth metals. (Based so far on the three rare earths analyzed.)

The purity value listed by a given supplier for a rare earth metal sample is often not reliable and at least needs clarification.

Nonhomogeneities may go undetected because of the small sample required for analysis and the small number of samplings usually made. One must exercise care and use explanations when listing the purity of a rare earth metal when the value listed is based on the type of mass spectrographic analysis described above. This is necessary due to the inability to calculate a value for nonhomogeneous impurities known to be present.

The mass spectrograph is a valuable instrument for the analysis of homogeneous bulk impurities and the detection of nonhomogeneous impurities in rare earth metals, and even though in its present state the results are only semiquantitative, it has the potential of yielding more accurate results.

Table I (cont'd)

(d) $^{48}Ti^{+}$ and $^{96}Mo^{++}$ with $M/\Delta M = 10561$ were not resolved and lines for other titanium isotopes were not visible.

(e) ErF^{+} was observed in the spectra in addition to F^{+}.

(f) It is assumed that all sources of Cl, F, O, N, C, and H in the material are sampled in the spark process.

(g) Separate exposures at a reduced magnetic field were used to record the H^{+} spectra.

(h) No analysis was made.

(i) Based on analyzed elements.

(j) Does not include a result for hydrogen.

TABLE II

Comparison Results

Sample	Hydrogen (ppm atomic) Mass spec.	Hydrogen (ppm atomic) Micro-comb.	Carbon (ppm atomic) Mass spec.	Carbon (ppm atomic) Micro-comb
A	1300	33,400	5000	2800
B	2600	66,800	900	5600
C	2600	33,400	300	1400
D	5000	100,000	1800	7000
E	5000	33,400	800	2800

Sample	Nitrogen (ppm atomic) Mass spec.	Nitrogen (ppm atomic) Neutron act.	Oxygen (ppm atomic) Mass spec.	Oxygen (ppm atomic) Neutron act.
A	300	ND,<8300*	3500	50,000±6200
B	30	ND,<83,000	3500	62,500±42,000
C	100	ND,<10,700	1000	15,700±4200
D	200	ND,<83,000	1200	52,000±31,000
E	1000	155,000±60,000**	1200	ND,<10,400

*ND - None detected. Limit established from one standard deviation of the oxygen or nitrogen blank value.

**The plus and minus values are standard deviations estimated from counting statistics only.

NOTE: The same sample pieces used for the nitrogen and oxygen analyses were used for the hydrogen and carbon analyses. Sample weights were: A - 1.6386 grams, B - 0.1615, C - 1.9265, D - 0.2524, E - 0.3968. Different sample pieces were used for mass spectrographic analyses, where less than 5 mg of each sample was consumed for the complete analyses of all elements listed in Table I.

TABLE III

Cerium Samples

Element	Parts Per Million Atomic No. 1	Parts Per Million Atomic No. 2	Detection Limit (a)
Th	325	350	3
Ta	(b)ND	80	3
Hg	80	30	10
Lu	2	ND	2
Yb	20	25	6
Tm	2	ND	2
Er	20	25	6
Ho	6	9	2
Dy	110	45	8
Tb	30	(c)	2
Gd	70	1000	15
Nd	320	100	7
Pr	175	30	2
La	175	570	2
Ba	250	ND	20
Mo	230	ND	6
Y	30	20	1

Table III (cont'd)

Element	No. 1	No. 2	Detection Limit (a)
Zn	75	5	2
Cu	100	164	1
Ni	70	3	1
Co	6	ND	1
Fe	630	50	1
Mn	30	6	1
Cr	30	2	1
V	3	(d)	1
Sc	2	ND	1
Ca	(d)	(d)	0.5
K	(d)	(d)	1
Cl	270	(d)	1
P	25	1	0.4
Si	75	10	5
Al	200	(d)	0.3
Mg	560	40	0.3
Na	(d)	(d)	0.3
F	50	650	0.2
O	(e)	(e)	0.2
N	570	65	0.3
C	6000	4400	0.2
B	3	0.4	0.3
Be	1	ND	0.3
Li	30	ND	0.3
H(f)	-	-	-
Purity (per cent atomic) (g)	98.9	99.2	

(a) See footnote (a) in Table I.

(b) ND - none detected.

(c) Could not be determined because of interference from $^{140}CeF^{+}$.

(d) Appears as "nonhomogeneous" in the spectrum.

(e) Value computed is probably meaningless since sample oxidation evidenced by considerable CeO^{+} was observed.

(f) No analysis made.

(g) Based on analyzed elements.

TABLE IV

Lutetium Samples

Parts Per Million Atomic

Element	I	II	III	IV	V	Detection Limit
Th	40		40	30	40	4
Ta	9,600	6-56%(c)	8,700	6,400	9,500	4
Lu	(97.8%(a) atomic)		(96.8% atomic)	(96.4% atomic)	(98.7% atomic)	-
Tm	230		240	215	20	4
Dy	15		ND	ND	ND	10
Nd	ND(b)		ND	ND	100	10
Pr	6		4	4	390	5
Ce	10		20	10	40	6
La	6		ND	ND	40	5
Y	20		15	10	160	2
Cu	45		30	40	4	2
Ni	30		25	25	15	3
Fe	170		140	150	300	1
Mn	6		4	4	10	1
Cr	15		10	15	(d)	2
Ti	8		7	7	20	2
Sc	15		10	10	40	2
Ca	20		35	ND	(b)	2
P	15		15	15	ND	1
Si	160		140	(d)	920	1
Al	100		80	(d)	50	1

Table IV (cont'd)

Element	I	II	III	IV	V	Detection Limit
Mg	ND		ND	ND	750	1
F	(d)		(d)	(d)	(d)	1
O	7,800		18,500	21,600	(d)	1
N	(d)		130	170	850	0.5
C	3,200		3,300	7,200	(d)	0.5
B	1		1	1	6	1

(a) Based on impurities considered to be homogeneous and listed in Table IV. Values indicated by the supplier in wt%: I-99.8; II-99.9; III-99.9; IV-99.9; V-not given.

(b) ND - None detected.

(c) Because of the high level nonhomogeneity of Ta, results for other impurities were not computed. Vacuum evaporation techniques and density measurements were used to confirm this serious nonhomogeneity situation.

(d) Nonhomogeneous.

References

(1) Owens, E. B. and Giardino, N. A., Analytical Chemistry 35, No. 9, August, 1963.

(2) Guthrie, J. W., Mass Spectrographic Analysis of Erbium and Cerium Metal, Sandia Laboratory SC-TM 343-63(14)

(3) Guthrie, J. W., Evaluation of a Modified Ilford Q2 Photographic Emulsion for Mass Spectrographic Uses, Sandia Laboratory SC-TM 64-534

THE ANALYSIS OF SOLIDS IN REACTOR MODERATOR BY SPARK SOURCE MASS SPECTROMETRY*

by

P. Chastagner

Savannah River Laboratory
E. I. du Pont de Nemours & Co.
Aiken, South Carolina

Introduction

The technique for detecting impurities in water developed by Dr. Ahearn[1] and reported at previous E-14 meetings is useful for analyzing a wide range of aqueous solutions. It is especially useful for the elemental analysis of solids in heavy water moderator from water-moderated nuclear reactors such as the Heavy Water Components Test Reactor (HWCTR). The moderator is extremely pure because it is produced by a distillation process and is circulated through deionizer beds in the reactor system. Under normal circumstances, the concentration level of most impurities is <100 ppb.

For detection and measurement of a 1-ppb impurity in a 30-mg drop of moderator, the bulk contamination of the electrode should be less than 1 ppm and the surface contamination should be less than 0.002 monolayer; therefore, the elimination of interfering impurities from electrodes and other materials is most important. Another consideration is that the moderator is radioactive. Tritium forms during neutron irradiation of heavy water, dissolved and suspended impurities may become neutron activated, and moderator samples taken immediately after a fuel tube failure usually contain fission products.

This technique is ideal for surveying impurities in moderator because most of the elements are determined simultaneously, and the small sample size obviates most of the problems associated with handling radioactive moderator.

Technique

The apparatus used for putting the drops of moderator on the electrodes and drying them is simple and inexpensive. It can be discarded if it becomes contaminated with radioactivity. A small stainless steel hood is mounted on a ring stand in a regular chemical fume hood and is connected to a special exhaust system for contaminated gases. The small hood has a metal stand that serves as a field plate, mounted at the same height as the exhaust port. The sample electrode is held by its shank in stainless steel hemostatic forceps that are in turn attached to the ring stand by an insulated clamp. The small hood and forceps are connected by clip leads to the chassis ground and positive terminals, respectively, of an adjustable 3000-volt power supply - a low current type usually used to power counting equipment. A 6000-volt supply would be preferable to the 3000-volt unit. A 250-watt reflector-type infrared lamp mounted on a second ring stand furnishes heat to dry the sample. The room air is filtered to minimize contamination of the electrode by airborne particulate matter.

*The information contained in this article was developed during the course of work under contract AT(07-2)-1 with the U. S. Atomic Energy Commission.

Samples are handled with micropipets made by drawing down 1/8"-O.D. polyethylene tubing. One-cc syringes are used as pipet controls. Polyethylene is used for the pipets and for containing samples of moderator to minimize the introduction of impurities. The amount of sample placed on the electrode is determined by measuring the length of the column of liquid dispensed from the pipet, which contains about 3.5 mg of water per mm.

The electrode is mounted in the forceps about 7 mm from the field plate and the power supply is adjusted to about 500 volts. The lamp is then turned on and a 10 to 30-mg drop is dispensed onto the bottom of the electrode. As the drop dries, the electrostatic field is increased to hold it in place. The sample can be concentrated by adding sample in approximately 10-mg increments to the evaporating liquid. With practice, an operator can learn to balance the applied voltage, drop size, and incremental additions so that sample is not lost from the electrode. When the electrode is dried, the power supply is turned off, and the electrode is transferred to the mass spectrometer where it is sparked against a counter electrode of the same material.

Electrodes

Electrode size and shape are quite important. The support electrode must be small enough to avoid losses due to self-shielding of the spark in the source, yet large enough to hold the drop of sample. The most efficient shape is the mushroom shape described by Ahearn, provided that it is not greater than about 1 mm in diameter. A chisel-shaped counter electrode is mounted with the edge on the axis of the ion source and is held in that position during the analysis. The support electrode is mounted so it can be swept past the edge of the counter electrode.

Electrode material should cause minimum interference with the analysis. The material should be as pure as is reasonably possible, easy to handle, easy to clean, and readily available. Impurities in the electrodes should not appear in the spectrum at the exposure used for the analysis. We have used silicon, indium, and gold electrodes. Transitor-grade silicon, though pure enough, is unsatisfactory because the polyatomic ions overlap most of the impurities being determined, including iron, nickel, and cobalt. The pure materials available from Johnson, Matthey and Co. in wire form are very convenient to work with but, as their analyses show, only their indium and gold are pure enough for use as electrodes. Indium is very soft and is of limited use. Gold is a reasonable compromise except that some of its impurities especially iron, copper, palladium, and silver show lines equivalent to an impurity in the sample. Transistor-grade germanium would be suitable for the iron determination, but the doubly charged ions would mask the chlorine lines at masses 35 and 37. Very pure tantalum would be best because tantalum is used extensively in the source.

When they can be used, hydrophobic materials such as silicon and germanium make convenient electrodes for analyzing solids in relatively pure water. The drop will dry in place on the tip of the electrode without the electrostatic field provided the surface is not electrically stressed. Garrett's work[2] establishing that electrocapillarity effects do occur suggests that the wetting Dr. Ahearn observed with silicon was due to electrocapillarity induced by electrical stresses in the high resistivity silicon he used. We avoided the problem by using relatively low resistivity (180 ohm-cm) boron doped, p-type silicon to allow electrical stresses to dissipate. The boron, which was at the 10 ppb level, did not appear in the subsequent spectra. This silicon was hydrophobic except immediately after sparking in the source when it exhibited electrocapillarity until the electrical stresses dissipated.

Sparking Conditions

Sparking conditions are selected such that all of the surface of the support electrode can be swept completely by the spark in a single scan past the counter electrode. In our work more than 75% of the deposits are removed by a scan that yields about a 3×10^{-9} coulomb exposure. After sparking the deposit, the exposure is repeated twice more on successive settings of the photoplate to provide a reference for the sample exposure. The third exposure is clear of all lines due to the sample.

After sparking the sample, a normal set of exposures is made with the electrodes to permit calibration of the photoplate emulsion.

Electrode Cleaning

Electrode cleaning is a critical step in the determination of impurities in moderator. Chemical cleaning with transistor-grade acids and deionized, distilled water leaves deposits that interfere with subsequent analyses. Argon etching in an alternating current field reduced some surface impurities, especially chlorine, but added as impurities the elements in the vacuum system. Better equipment might make argon etching satisfactory. Sparking in the source of the mass spectrometer completely removed surface deposits from the sparked areas, and was the most satisfactory technique.

A complete set of data obtained with gold electrodes is shown in Table I. The exposure was about 3×10^{-9} coulomb for each scan. Unit sensitivity was assumed in reading the photoplate.

Standardization

Because the moderator is radioactive, only small samples are analyzed, and because the moderator is very pure it is impractical to add an internal standard because the unavoidable addition of impurities will almost certainly ruin the sample. The best method of calibration is analysis of one of the impurities by another sensitive method. Manganese and the alkali metals can be determined accurately at low ppb levels by atomic absorption spectrophotometry, and chlorine can be measured with the Technicon AutoAnalyzer. After the measurement of one of the elements by another method, the mass spectrometer photoplate is read in the usual manner by either visual or densitometric methods relative to the element. The data in Table I were standardized by measuring the manganese in moderator by atomic absorption spectrophotometry.

Conclusion

Dr. Ahearn's technique is useful for analyzing solids in relatively pure aqueous solutions, such as reactor moderator. The use of purer electrode materials and better cleaning methods will improve the analytical procedure, but proper selection of support materials and concentration of the solution on the support electrode make the determination of fractional ppb impurities practical with present techniques.

Table I. Deposits on Gold Electrodes

(Exposure 3 x 10^{-9} coulomb; unit sensitivity assumed.)

Element	Bulk Impurities in Gold, ppm atomic	Surface Impurities after Chemical Cleaning[a,b]	Surface Impurities after Argon Etch[a,b]	Impurities in HWCTR Moderator, ppb atomic
U			0.3	
Bi		0.7		
Pb	0.06	1		
Hg			4	
W			1	
Ta			1	
In	7			
Ag	2	1		
Pd	30	3		
Rh	0.03	2		
Br		2		
Se	0.1	15		
Cu	0.3	3	0.3	
Ni	0.1	<2		
Fe	3	7	6	<0.7
Mn	1	0.7	2	<0.7
Cr	0.03	0.7	3	
V	0.03	0.7		<0.7
Ti	1	<0.7		
Ca	1	3	60	20
K	0.1		30	20
Cl	2	5	1	20
P	0.3	0.7	6	30
Si	100	60	9	70
Al	3	10	3	20
Mg	1	10	15	20
Na			1	7
F	1	5	6	10
B	0.03		3	20

(a) Corrected for impurities in gold.
(b) Listed as equivalent impurity in HWCTR moderator, ppb atomic.

References

(1) Ahearn, A. J., "Vacuum Spark Source Spectroscopy of Solids." Eleventh Annual Conference on Mass Spectrometry and Allied Topics. ASTM Committee E-14, May 19-24, 1963. Paper No. 42.

(2) Garrett, C. G. B., "Semiconductor Aspects of a Semiconductor Electrode." Chapter 3 in, "The Electrochemistry of Semiconductors," edited by P. J. Holmes. Academic Press, London, 1962.

MASS SPECTROMETRIC ANALYSIS USING A D.C. SPARK SOURCE

by

J.S. Halliday, A. Harrison and A. Riddoch

Associated Electrical Industries Limited
Manchester, England

INTRODUCTION

Analysis of solids by mass spectrometry commonly utilizes an ion source using a pulsed, high voltage, high frequency R.F. discharge between two electrodes of the material being analysed. However, interest has recently arisen in the low voltage D.C. interrupted arc source originally described by Dempster (1) and as used by Duckworth and Venkatasubramanian (2) and by Schuy and Hintenberger (3).

In this paper we describe comparative results obtained with these two types of source when fitted to an A.E.I. type MS7 double focusing mass spectrometer. The operating characteristics of the D.C. source used were as follows:

Operating frequency	100 c.p.s.
Maximum Operating Voltage	9 volts
Maximum Operating Current	9 amps
Interrupter inductance	15 microhenries
Separate Series inductance	200 microhenries
Spark duration	50 to 150 microseconds

COMPARISON OF SPECTRA OBTAINED USING D.C. AND R.F. SOURCES

The main difference between the D.C. and R.F. sources is that the D.C. source produces an ion beam with a greater proportion of multiply charged ions than the R.F. source, the doubly charged ions or the triply charged ions contributing most to the ion beam. Fig.(1) and Fig.(2) illustrate this characteristic. Fig.(1) shows the spectra obtained with a tungsten sample on the D.C. and R.F. sources and Fig.(2) shows the relative intensities of the singly and multiply charged ion beams in these spectra. It will be seen that for the D.C. source, the W^{3+} ion beam is the most intense and that the W^{2+}, W^{3+} and W^{4+} ion beam intensities are all higher than that for W^{+}. The intensity of the W^{6+} ion beam from the D.C. source is of the same order as that for W^{2+} from the R.F. source. Fig.(1) also shows the more intense charge transfer lines due to W^{2+} $(+e) \longrightarrow W^{+}$ at just below mass 140 and W^{3+} $(+e) \longrightarrow W^{2+}$ at just above mass 80 in the D.C. spectra, which are directly related to the increased intensity of the multiply charged ion beams from the D.C. source.

The intensity of the ion beam and the amount of material evaporated in laying down a given charge differ between the two sources. Table 1 shows the mean ion currents obtained and the numbers of atoms evaporated per ion reaching the monitor for the two sources. With the exception of copper, all the ion currents produced by the D.C. source were greater than the corresponding ones from the R.F. source. This effect was most pronounced for the high boiling point metals, niobium and tungsten, for which the increases were approximately factors of 100 and 10 respectively. In the case of the R.F. source the

TABLE 1

SOME TRANSMISSION MEASUREMENTS ON AN MS7

Specimen Material	Average ion current (amps x 10^{12})		Atoms consumed per ion delivered (x 10^{-7})	
	D.C. spark	R.F. spark	D.C. spark	R.F. spark
Aluminium	390	170	0.88	6.0
Copper	66	88	0.4	3.5
Steel	100–400	34	1.105	9.4
Niobium	390	4.2	0.28	9.5
Tungsten	61	4.7	0.72	1.8

TABLE 2

RELATIVE SENSITIVITIES AND REPRODUCIBILITY OF SPARK SOURCE ANALYSIS OF INHOMOGENEOUS ALUMINIUM JOHNSON MATTHEY AC1

					% STANDARD DEVIATIONS				
		RELATIVE SENSITIVITIES			8 SEPARATE ANALYSES			15 REPEAT EXPOSURES	
Impurity	Concentration given	D.C. spark		R.F. spark	D.C. spark		R.F. spark	D.C. spark	R.F. spark
		+	++		+	++			
Ti	70	0.61	-	0.31	73	-	60	20.5	59
Cr	600	4.7	-	0.47	76	-	52	15.5	12
Mn	2000	-	0.42	0.50	-	39	54	-	-
Fe	1800	0.58	2.3	0.34	56	61	55	20.5	-
Ni	120	1.33	-	0.23	125	145	86	-	18
Cu	150	4.88	1.2	0.25	67	72	99	23	44
Zn	80	1.3	-	0.30	80	-	68	13.5	-
Ga	-	-	-	-	-	38	-	-	14
V	-	-	-	-	-	-	-	-	29
Mg	15,200	2.6	3.3	-	12	32	-	-	-

MASS SPECTRA OF TUNGSTEN.

Fig. 1

order of decreasing ion current is the same as the order of increasing boiling point, the low ion currents given by the high boiling point metals is probably due to less metal being vaporized in the discharge. The results of Table 1 also indicate that less metal is lost from the electrode per ion reaching the monitor for the D.C. source than for the R.F. source. This will partly be due to the greater ion extraction efficiency in the source region resulting from the lower mean energy of the ions from the D.C. source. Another contributing factor will be the greater transmission efficiency through the energy defining slit in the monitor region, this arising from the narrower energy spread of the ions from the D.C. source. A further reason for the low material loss is that the electrodes were much closer together when sparking under D.C. conditions than under R.F. conditions and much of the metal evaporated from one electrode would be deposited on the other electrode. It is well known that in D.C. arc conditions metal is transferred from the anode to the cathode and it is therefore probable that the metal actually lost during an exposure was merely a sample from a larger amount which was transferred from one electrode to the other during the exposure.

REPRODUCIBILITY OF ANALYSIS

In order to investigate the reproducibility of analysis of the D.C. and R.F. sources three sets of eight separate analytical plates were exposed using standard samples of aluminium, copper and steel for both sources. The mean values for the concentrations of the impurity elements were determined and from these the relative sensitivity factors for the elements were calculated by dividing by the known concentrations. The standard deviations, expressed as percentages of the mean, were also calculated.

In another experiment which was performed twice for each sample with each source, a series of 15 equal exposures was taken across the photographic plate.

When lines due to doubly charged ions were used for analysis in the D.C. spectra an isotope of odd mass number was chosen whenever possible, so that the doubly charged species occurred at a fractional mass number, which would be free from spectral interference.

The results obtained for the aluminium, copper and steel samples are given in Tables 2, 3 and 4 respectively and the mean values of the standard deviations for each source and each sample are given in Table 5.

Relative Sensitivity Factors

For the aluminium samples the R.F. source gave low sensitivity factors with a narrow spread in the range 0.23 to 0.5 and the D.C. source gave factors having a wider spread, in the range 0.58 to 4.88 for singly charged ions and 0.42 to 3.3 for doubly charged ions. The D.C. factors are all larger, by factors between 1.5 and 20 than the R.F. sensitivity factors. The copper and steel samples give a similar range of sensitivity factors when used with the R.F. source and the D.C. source on doubly charged ions. The sensitivity factors on the singly charged ions had a greater spread than these.

Reproducibility

The mean standard deviations on separate analyses for aluminium determined for the D.C. and R.F. sources were very close to each other, the D.C. singly charged spectrum giving the largest value and the D.C. doubly charged spectrum giving the smallest value. The sample of aluminium used for these experi-

TABLE 3

RELATIVE SENSITIVITIES AND REPRODUCIBILITY OF SPARK SOURCE ANALYSIS OF JOHNSON MATTHEY COPPER CA2

Impurity	Concentration given	RELATIVE SENSITIVITIES D.C. spark +	RELATIVE SENSITIVITIES D.C. spark ++	RELATIVE SENSITIVITIES R.F. spark	% STANDARD DEVIATIONS 8 SEPARATE ANALYSES D.C. spark +	% STANDARD DEVIATIONS 8 SEPARATE ANALYSES D.C. spark ++	% STANDARD DEVIATIONS 8 SEPARATE ANALYSES R.F. spark	% STANDARD DEVIATIONS 15 REPEAT EXPOSURES D.C. spark	% STANDARD DEVIATIONS 15 REPEAT EXPOSURES R.F. spark
Bi	130	0.48	0.9	0.85	48	23	31	22.5	13
Pb	100	0.76	1.7	1.4	51	22	30	18	11
Sb	120	0.88	1.5	1.1	44	19	32	-	18
Sn	120	0.74	2.3	1.3	43	24	25	23	9.2
Ag	150	1.5	2.6	1.4	34	-	23	13.5	21
Ga	80	3.3	2.5	3.1	43	33	27	-	21
Cr	60	2.52	2.3	1.8	54	26	20	-	13

TABLE 4

RELATIVE SENSITIVITIES AND REPRODUCIBILITY OF SPARK SOURCE ANALYSIS OF STEEL - BUREAU OF ANALYSED STANDARDS LTD. MILD STEEL RESIDUAL SERIES SPECTROGRAPHIC STANDARD S.S.12.

Impurity	Concentration given	RELATIVE SENSITIVITIES D.C. spark +	RELATIVE SENSITIVITIES D.C. spark ++	RELATIVE SENSITIVITIES R.F. spark	% STANDARD DEVIATIONS 8 SEPARATE ANALYSES D.C. spark +	% STANDARD DEVIATIONS 8 SEPARATE ANALYSES D.C. spark ++	% STANDARD DEVIATIONS 8 SEPARATE ANALYSES R.F. spark	% STANDARD DEVIATIONS 15 REPEAT EXPOSURES D.C. spark	% STANDARD DEVIATIONS 15 REPEAT EXPOSURES R.F. spark
Cr	250	1.87	2.5	1.5	45	23	30	-	16
Co	2500	1.25	1.3	0.80	32	26	21	-	-
Ni	350	1.45	1.1	0.57	52	26	40	-	10
Zn	17	2.75	-	3.1	45	-	41	14.5	16
Zr	300	0.16	-	0.93	16.5	-	32	-	21
Sn	200	0.44	0.4	0.70	21	45	30	9.5	10
Pb	30	0.38	0.4	1.60	50	39	32	-	-
V	<10	1	-	-	37	-	27	-	10
Cu	150	1.4	1.8	0.85	27	40	29	9.0	9
Nb	(55)	1.4	-	(0.72)	44	-	29	-	-
Mo	1700	0.1	0.5	0.43	58	29	32	10.5	34

ments has been analysed in a scanning electron probe microanalyser (A.E.I. type SEM2) and was found to be inhomogeneous with respect to titanium and copper over volumes of the same order of size as the volume of material removed in an R.F. spark analysis, Fig.(3). The effects of this inhomogeneity are apparent in the repeat exposures made with the R.F. spark which gave standard deviations for titanium and copper of 59% and 44% respectively compared with the overall average of 29%. However, although the transmission results in Table 1 indicate that a smaller quantity of material is lost when using the D.C. source and the effects of inhomogeneity should be correspondingly greater, the repeat exposures for the D.C. source show no such effects. The standard deviations for Ti and Cu are 20.5% and 23% respectively, compared with the overall average of 19%. These results can be explained if, as postulated at the end of the last section, more metal is transferred from one electrode to the other than is lost from the electrodes; then if this volume of material is greater than the amount of material lost from the R.F. source this would explain the smaller standard deviations obtained with the D.C. source for the inhomogeneous impurities. These results indicate that the quantity of material transferred from one electrode to the other in the D.C. source is considerably greater than ten times the quantity of material consumed.

During the 8 repeat analyses of the aluminium sample using the D.C. source, the calculated concentration of nickel became progressively lower and the eighth analysis gave a result a factor of 20 lower than the first. The standard deviations for the results from the singly and doubly charged nickel isotopes are, therefore, high. This effect is indicative of dilution of the sample with respect to nickel in the region of the spark and it was observed, to a much lesser extent, for the other impurity elements with the exception of magnesium.

The mean standard deviations on separate analyses for copper are better than those obtained with aluminium samples, the R.F. and D.C. doubly charged spectra being very close and nearly twice as good as the D.C. singly charged spectra. The D.C. source gave slightly better standard deviations on repeat exposures than the R.F. source. For the steel samples the three standard deviations for repeat analyses were closer than those for copper, the D.C. singly charged spectrum again giving the largest standard deviation, the D.C. doubly charged spectrum and the R.F. spectrum giving nearly equal standard deviations.

Our results indicate that the reproducibilities of analysis of the R.F. source and D.C. source are comparable, the D.C. doubly charged spectrum giving the more reproducible of the D.C. analyses for lines of the spectrum which were free from interference from major component ion beams (Table 5).

Schuy and Hintenberger (3) found that the reproducibility of analysis with the R.F. source was much worse than the reproducibility of analysis with the D.C. source. However, the main difference between the results reported by Schuy and Hintenberger and the results presented above are in the R.F. results and may be due to greater dependence on source parameters in their mass spectrometer as the range of ion energies accepted by their mass spectrometer is 200 eV, compared with 600 eV for the A.E.I. type MS7.

TABLE 5

MEAN PERCENTAGE STANDARD DEVIATIONS OF ANALYSIS OF IMPURITIES USING SPARK SOURCE ANALYSIS

	SEPARATE ANALYSIS			REPEAT EXPOSURES	
Sample	R.F.	D.C.(+)	D.C.(++)	R.F.	D.C.(+)
Aluminium	65	70	61	29	19
Copper	27	45	24	15	19
Steel	33	41	35	16	11

TABLE 6

ACCURACY OF ANALYSIS AFTER CALIBRATION

BUREAU OF ANALYSED STANDARDS LIMITED MILD STEEL

S.S.14

Impurity	MS7 Corrected Values Using S.S.12. R.F.Spark	D.C.spark +	D.C.spark ++	Given Spectroscopic values
Cr	0.18	-	0.15	0.185
Ni	0.13	0.133	-	0.13
Cu	0.029	0.057	0.036	0.04
Zr	0.007	0.013	-	(0.005)
Nb	0.025	0.031	-	(0.05)
Mo	0.060	0.074	0.067	0.07
Sn	0.017	0.046	0.027	0.02
Co	0.18	-	0.16	0.19

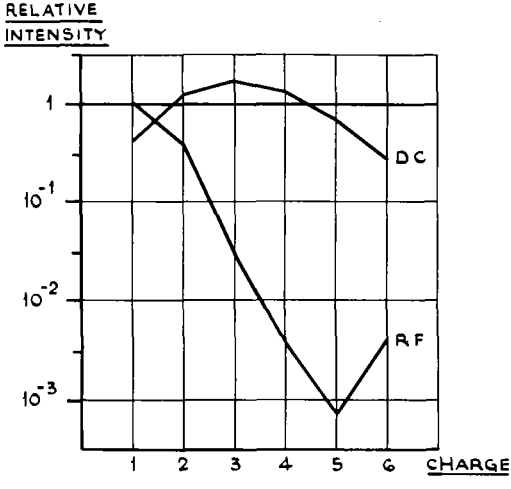

MULTIPLY CHARGED ION BEAMS FROM TUNGSTEN (PEAK INTENSITIES)

Fig. 2

ACCURACY OF ANALYSIS

Table 6 gives the results of an analysis of a steel sample (Bureau of Analytical Standards Ltd., Steel Standard SS14) using a standard steel sample (Bureau of Analytical Standards Ltd., Steel Standard SS12) from which to obtain sensitivity factors. Eight photographic plates were exposed on each sample for both the D.C. and R.F. analyses, the spark conditions being kept constant during each exposure and identical for the sample and the standard. The results of analysis using the R.F. and the D.C. doubly charged spectrum are equally close to the given values and both are slightly better than the analysis obtained using the D.C. singly charged spectrum.

DISCUSSION

The R.F. source can analyse a wide variety of samples, including semi-conductors and insulators, but the D.C. source is limited to the analysis of conducting samples and its performance may be limited by physical characteristics of the matrix elements, for example, in the experiments described above difficulty was experienced with welding of the copper samples. However, for hard, high boiling point materials, the ion currents obtainable are so much greater than those obtainable for the R.F. source that the D.C. source will be useful for the analysis of these metals, where the detection limit will be dependent on the time to make an exposure rather than on the background darkening of the photographic plate.

The relative sensitivities found for the impurity elements when using the D.C. source cover a greater range of values than those found for the R.F. source and will make the D.C. source less useful for semi-quantitative analysis, where no standards are available to establish relative sensitivity factors. When using a D.C. source the fact that each component of the sample contributes to three or more ion beams instead of only one means that, in general, the exposure must be increased by a factor of about three greater than the exposure to give a similar density and detection limit to those obtained using an R.F. source. This necessity for an increased exposure will be offset to some extent by the greater relative sensitivities obtained with some impurities and matrices for the D.C. source and the time taken to expose for a given detection limit will also be reduced because of the greater ion beams obtained with the D.C. source; in particular for the high boiling point metals, this time will be much shorter than the exposure time when using the R.F. source.

The detection limit is also worsened when using the D.C. source due to the greater background darkening of the photographic plate caused by (a) greater scattering on the major component lines because of the higher ion currents, (b) the hreater number of major component lines which provide a multiplicity of scattering centres and (c) the increased continuum resulting from pressure dependent charge transfer occurring in the increased multiply charged ion beams

Further work is necessary on the actual limits of detection possible with the D.C. source and on the advantages and disadvantages presented by the multiply charged ion beams of the D.C. source. The multiply charged ion beams are useful for identification purposes but are subject to interference by other component lines and a sample with many impurities can result in a very complex spectrum giving increased difficulties in interpretation. Further investigation of the apparent fractionation effect as formed with nickel in the aluminium sample is also required.

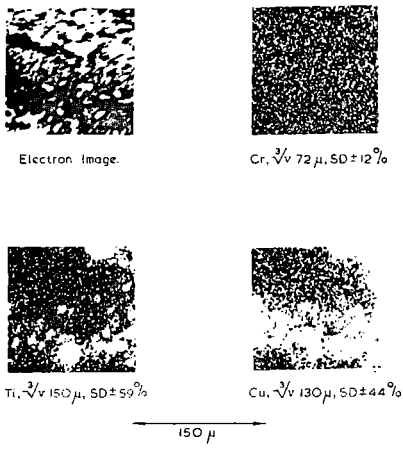

SURFACE DISTRIBUTION OF IMPURITY ELEMENTS, SHOWN BY SCANNING ELECTRON MICROPROBE X-RAY ANALYSER.

Local Ti and Cu concentrations found to be about 1000 times the spectroscopic mean.

Fig. 3

The authors wish to thank their colleagues, Mr. Wolstenholme, Mr. Swift for the results using the R.F. source, Mr. Wright for the SEM2 results and the Directors of A.E.I. for permission to publish this paper.

REFERENCES

(1) Dempster, A.J., MDDC 370 U.S. Dept. of Commerce 1946

(2) Duckworth, H.E. and Venkatasubramanian, V.S., Canadian J. of Phys. 41 234 , 1963

(3) Hintenberger, H. and Schuy, K.D. Z.F A.Chem. 197 98 1962
Z.F.Naturforsch 18a 926 1963

ENERGY DISTRIBUTION OF IONS FORMED IN THE RF SPARK SOURCE - II. INDIVIDUAL SPECIES *

by

J. Rogers Woolston and Richard E. Honig
RCA Laboratories
Princeton, N. J.

I - INTRODUCTION

Spark-source mass spectrography is now widely used for the qualitative and semi-quantitative analysis of a diverse range of solid materials. Its chief advantages are high sensitivity and complete coverage of the periodic table of the elements. Improvement is needed, however, in quantitative accuracy which is limited at present by two important instrumental factors:

1) the use of photographic plates as the ion detector, and
2) the behavior of the vacuum spark discharge.

This paper describes work directed at a better understanding of the vacuum spark.

In a previous paper[1)] the authors have shown that ion energy distributions can differ appreciably for various materials, and they depend on operating parameters in a complex manner. Serious analytical error may result if different elements in a given matrix exhibit dissimilar energy distributions. This is because double-focussing mass spectrographs utilized for such analyses transmit only those ions that fall within the energy and angular passbands of the instrument. The previous work showed that for most substances the energy distribution of the total ion beam which includes all ionic species present was much greater than the energy passband. In the present study, the energy distributions of the individual species present in the ion beam were determined, thus permitting an evaluation of their effect on quantitative analyses.

II - EXPERIMENTAL

This study was carried out in the same instrument used for the previous work: a double-focussing mass spectrograph of Mattauch-Herzog geometry (AEI type MS7). Fig. 1 shows the geometry pertaining to this work. As described more fully in the previous paper, the ion beam has at the entrance of the magnetic analyzer a width in the y-direction which is a function of α, the angular divergence of the beam, and β, its velocity deviation. By restricting suitably the slits which govern the magnitude of α, this width remains a nearly linear function of β. To accomplish this, slit S_9 at the entrance of the electrostatic analyzer was narrowed from its usual value of 0.080 in. to 0.001 in. which, in turn, reduced the magnitude of α_{max} from its normal value of 0.0047 radians to 0.0003 radians. To permit an energy range as large as possible to be examined without readjusting V_A or V_D, grounded masking slit S_{11} was increased from 0.100 in. to 0.700 in. Monitor-collector slit S_{13} retained its normal width of 0.500 in. In the previous study, a 1 in. by 2 in. photoplate was placed between S_{13} and the magnetic field boundary which graphically recorded the ion beam profile (in the y-direction), thus providing a direct measurement of the shape and width of the energy distribution of the ions in the beam. In the present work, this photoplate was replaced by a narrow slit whose position and width in the y-direction permitted only ions in a particular energy range to pass into the magnetic analyzer and be recorded on the usual photographic plate. By making this slit movable in the y-direction, the energy distribution could be "sam-

---

* The research reported in this paper was sponsored by the Air Force Cambridge Research Laboratories, Office of Aerospace Research, under Contract Number AF19(628)446.

1) J.R.Woolston and R.E.Honig, Proc. of the 11th Annual Conf. on Mass Spectrometry and Allied Topics - San Francisco, May 1963, paper no. 106, page 597, and Rev. Sci. Instr. 35, 69 (1964).

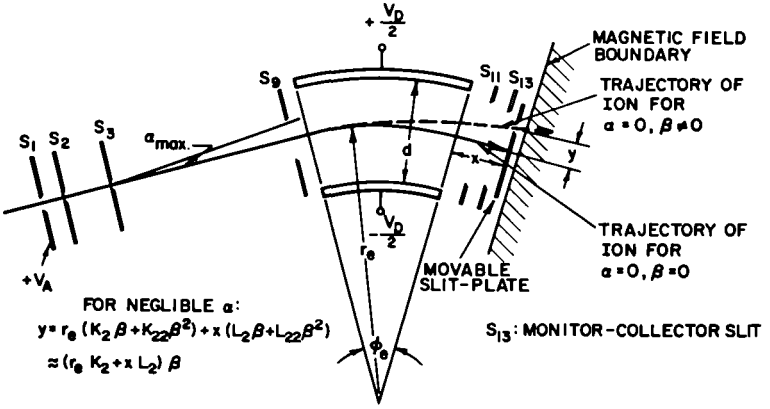

GEOMETRY USED FOR ENERGY DISTRIBUTION MEASUREMENTS

FIG. 1

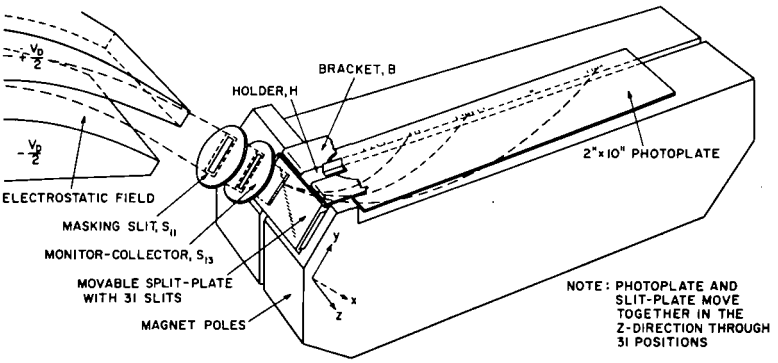

VIEW OF EXPERIMENTAL SET-UP

FIG. 2

SLIT GEOMETRY FOR ENERGY DISTRIBUTION MEASUREMENTS

	NORMAL	EN. DISTR.
S_3 - SOURCE EXIT SLIT	0.006"	0.006"
S_9 - ESA ENTRANCE SLIT	0.080"	0.001"
S_{11} - MASKING SLIT	0.100"	0.700"
α - ANGULAR BEAM DIVERGENCE	0.0047 RAD	0.0003 RAD

NOTE: Z-DIMENSIONS OF ALL SLITS REMAIN UNCHANGED

MOVABLE SLIT-PLATE DIMENSIONS:

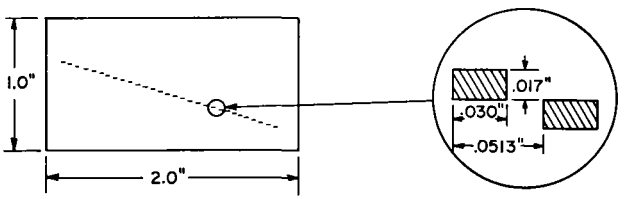

FIG. 3

pled" at any energy. As it was not practical to achieve this motion in the y-direction, the same result was produced by bringing a series of fixed slits sequentially into place. This was done by preparing a special 1 in. by 2 in. slit-plate containing 31 separate slits deployed on a diagonal and mounting it as shown in Fig. 2. This slit-plate, mounted in its holder, H, and attached to bracket, B, moved laterally (in the z-direction) together with the standard 2 in. by 10 in. photoplate. Thus 31 separate mass spectra were produced on the photoplate, each formed only by ions representing a particular energy range. The movable slit-plate was designed so that at an accelerating potential, V_A, of 20.0 kV the total energy range of 3100 V passed by the 0.500 in. monitor-collector opening could be sampled in contiguous 100 V increments. Details of the movable slit-plate are shown in Fig. 3. Identical exposures were made for each spectrum. These exposures, which are the time-integrated currents recorded by the monitor-collector, ranged from $1 \cdot 10^{-11}$C to $1 \cdot 10^{-9}$C for different experiments. The longer exposures were used to study the energy distributions of impurities in a matrix, the shorter ones to study the matrix itself.

The energy distribution of any ionic species was obtained by measuring the optical transmission of the lines on the photoplate corresponding to that species, converting these values to ion intensities by means of a calibration curve, and plotting the intensities versus the mean energy passed by the respective slit of the movable slit-plate.

A calibration of the mean ion energy transmitted by each slit was obtained by accelerating thermal ions to a known energy, and determining experimentally which slit transmitted them. The source of thermal ions used provided comparable numbers of Na^+, K^+, Rb^+, and Cs^+ ions. The range of masses represented by these four elements allowed a determination of the effect of the fringing magnetic field on the mean energy passed by each slit as a function of mass. Due to the proximity of the fringe field of the magnetic analyzer, some mass separation occurs before the ions reach the movable slit-plate. Therefore, the mean energy passed by each slit is a function of the mass to charge ratio.

The residual α, 0.0003 radians, was such that monoenergetic (thermal) ions displayed a width at the slit-plate equivalent to a 50 V energy spread. Considering the 100 V "width" of each slit, the energy resolution of the measurements was estimated to be approximately 125 V. This is considerably coarser than the 15 V resolution of the earlier work, and is due in part to the use of the standard 0.006 in. source exit slit, S_3, rather than the 0.001 in. slit used in the earlier work. The larger slit permitted much greater ion beam intensities for equivalent sparking conditions.

While in the earlier work only a single exposure was required, in the present study 31 separate exposures were needed to cover the entire energy range. It was, of course, essential that these 31 exposures be produced under conditions as nearly identical as possible, which, in fact, posed the most serious limitation of this technique. If a large exposure is chosen so that low-concentration impurities in the sample can be observed, much sample, time, and patience is consumed in making 31 exposures. For this reason, less than 31 exposures were made in many cases.

Highly stable power supplies for the accelerating voltage, electrostatic analyzer voltage, and magnet current are, of course, required. During the initial experiments of this study it became apparent that a 0.25 megohm series resistance in the accelerating voltage supply (part of an rf filter) was contributing a significant random voltage drop. This resistor was subsequently replaced by a low-resistance choke which eliminated this adverse effect.

In this study, Ilford Q2 photoplates were used which were processed in standard fashion with a JAco photoprocessor. They were developed for 3 min. in Kodak D19; development arrested with Kodak Indicator Stop Bath, 30 sec.; fixed for 2 min.; washed 30 min.; and force dried.

III - ENERGY DISTRIBUTIONS

A diverse range of materials was studied, including the following: Au; 90% Al - 10% Si alloy; Si; AgBr; a low-alloy steel standard, N.B.S. 461;

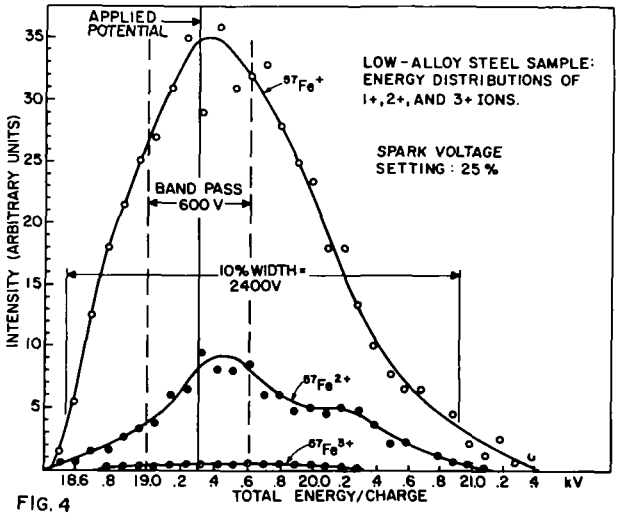

FIG. 4

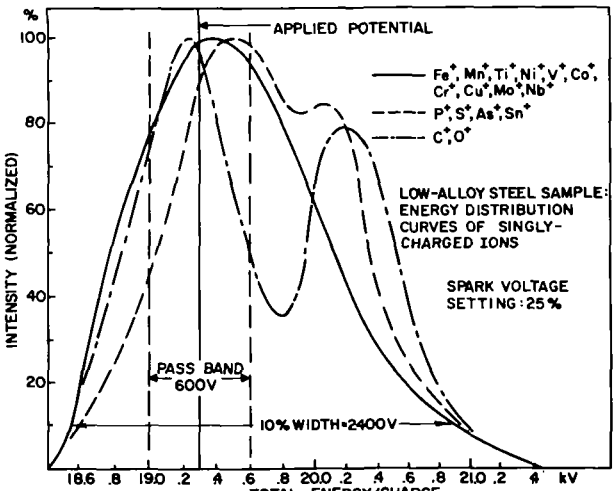

FIG. 5

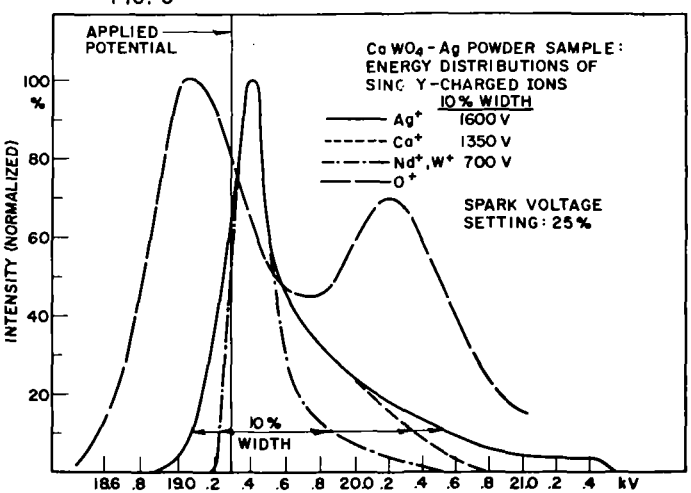

FIG. 6

and a briquetted powder sample consisting of 4 parts Ag powder, 1 part $CaWO_4$ doped with Nd. Runs were made with the Au and the Al-Si alloy samples at various rf spark voltages to determine the effect of this parameter on the energy distribution. Observations of both positive and negative ion energy distributions were made with the AgBr sample. The low-alloy steel sample contained many known impurities representing most columns of the periodic table. Finally, the Ag:$CaWO_4$ sample containing Nd permitted a comparison of major constituent elements of widely differing chemical and physical properties.

Energy distributions are shown graphically in Figures 4 through 9. As a typical example, Figure 4 shows the singly-, doubly-, and triply-charged ion energy distributions for Fe. It is seen that on the basis of energy per charge the distribution of multiply-charged ions is similar to that of the singly-charged ions. Of interest from the analytical point of view are the data shown in Fig. 5: the energy distributions of 16 components of a low-alloy steel sample. The distributions of ten of the metallic elements are sufficiently similar that, when normalized, they may be represented by a single curve. The elements with higher vapor pressures (P, S, and As) as well as Sn exhibit a two-peaked energy distribution. A more marked two-peaked distribution is seen for C and O which represent gas background of the ion source. All of these elements exhibit distributions whose width at 10% intensity is approximately 2400 V. At variance with this are the data shown in Fig. 6 for the Ag:$CaWO_4$ powder sample. Distribution widths from 700 V to about 2600 V are observed for the major constituents. Again, O exhibits a strongly double-peaked distribution. The distributions for Ag, Ca, and particularly for Nd and W display a marked asymmetry. In Fig. 7, the similarity of the two Si curves, one from a Si matrix, the other from an Al sample containing 10% Si, is apparent. The displacement of about 200 V is almost within experimental error and is not believed to be meaningful. Positive and negative ion energy distributions are compared in Fig. 8 for ions from AgBr. The positive ion curve (solid line) is the normalized response for both Ag and Br ions, singly- as well as doubly-charged. The negative ions of both Ag and Br are represented by the dashed curve. The apparent 200 V displacement between the two curves ($\sim$1% of the total energy) may well be experimental error incurred in reversing the polarities of all of the applied potentials. Fig. 9 illustrates the effect of rf spark voltage on the energy distributions of Al and Si ions. The shift of the maxima and the increase in width of the distributions is similar to that observed in the previous study for ions formed with a narrow spark gap between the two sample electrodes.

IV - DISCUSSION

As stated in the introduction, the objective of this work is to make spark-source mass spectrography a more quantitative analytical technique. This capability depends upon the reproducibility with which the composition of the sample may be determined from the output of the instrument, the photographic plate. With most analytical techniques, quantitative accuracy is achieved by preparing and analyzing known standards from which unknowns may be determined by interpolation or extrapolation. With the spark source technique, such standards are often impractical due to the nature of the samples and to the very low concentrations which are of interest. At levels below parts per million, contamination and inhomogeneity present formidable problems in the preparation of standards. Extrapolation from higher levels is possible if it can be proved that linearity exists over the range of interest, which in turn requires low-level standards. As a result of this paradox it seems prudent to approach the problem from a different direction, i.e. by determining the factors which affect a) the collection of the ions of the various elements present in the sample; and b) the calculation of the concentrations of those elements. These factors can be divided into several broad categories: those affecting the probability of ionization, including the extent of multiple ionization; those affecting the transmission of ions through the instrument; and those affecting the detection of ions. The energy distribution of the ions formed by the spark discharge in the ion source is the principal factor affecting the variability of transmission of ions through the instrument.

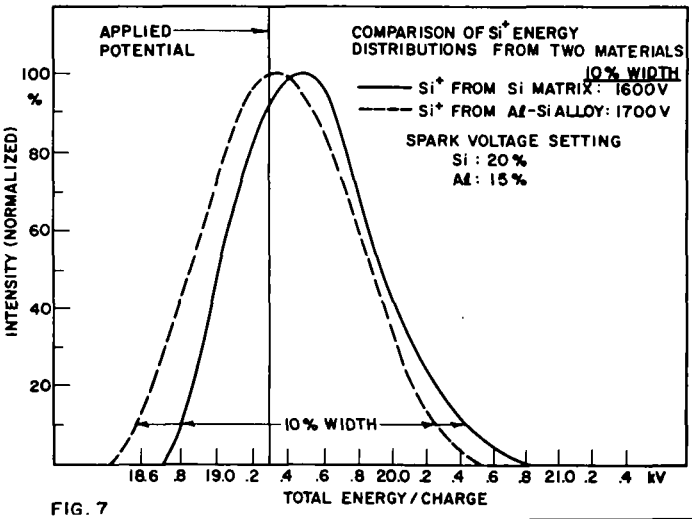

FIG. 7

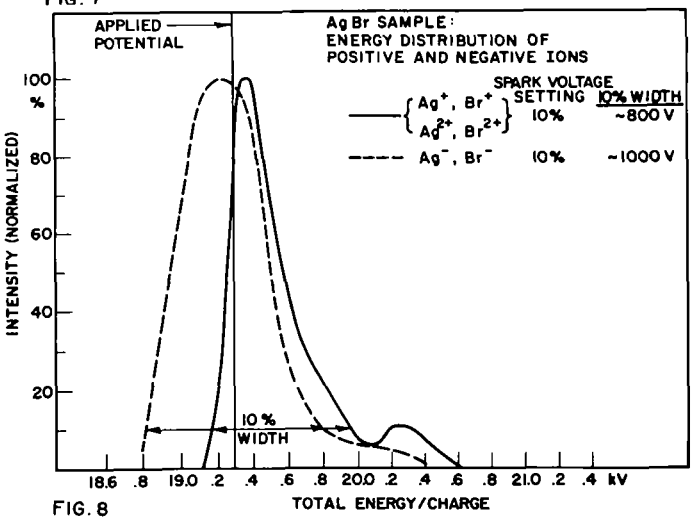

FIG. 8

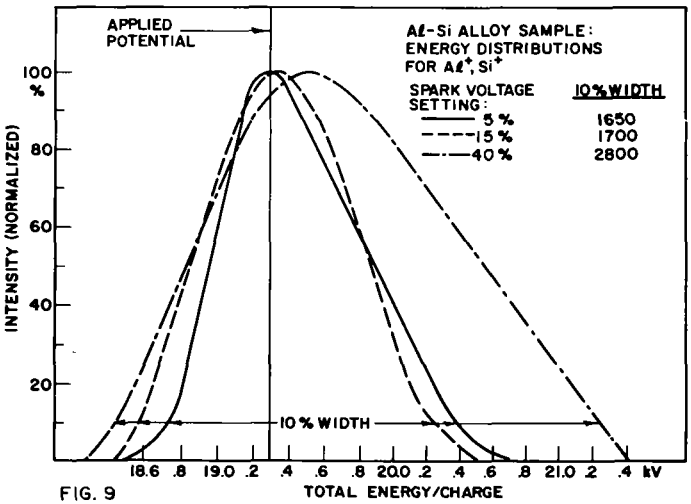

FIG. 9

All spark-source mass spectrographs employed for analytical work limit the ion energy range transmitted in order to preserve good mass resolution. The passband is customarily from 200 V to 600 V wide, and is dependent upon the geometry: the magnitude of α_{max}, and the y-dimension of a slit located between the electrostatic and magnetic analyzers. As the energy distribution width for most elements under most conditions considerably exceeds the passband, only a fraction of the ions emerging from the electrostatic analyzer will be admitted to the magnetic analyzer. The exact fraction transmitted depends not only on the shape of the energy distribution, but also on its location with respect to the passband. This latter factor is governed by the ratio of the accelerating potential, V_A, to the electrostatic analyzer potential, V_D. In Figures 4 and 5, a 600 V passband is shown in an arbitrary location. From Fig. 5 it is clear that were the passband shifted to a different location as a result of a change in either V_A or V_D, the relative fractions transmitted for ions with different energy distributions would change. For example, if the passband were centered at 20.2 kV the ratio of high vapor pressure and gaseous elements to the metallic elements in the sample would appear to have increased. Obviously, good regulation of the accelerating potential supply is required, as the current drawn from this supply fluctuates wildly during the course of an analysis, depending upon the instantaneous spark-gap width as well as the rf power input to the spark. As the calculation of concentrations involves measurements taken from several different exposures it is vital that all conditions be maintained as nearly constant as possible throughout all exposures.

In this work measurements of the energy distributions of rf spark-source ions have been made in order to assess their analytical significance. No attempts to explain the origin of the distributions observed will be given at this time. From the measurements several general conclusions can be drawn:

1) In a given sample, some components may exhibit markedly different energy distributions, which can lead to analytical error.
2) For a given element, very similar energy distributions are observed whether the element is the matrix or a minor constituent.
3) In agreement with previous work the energy distribution width increases with increasing rf spark voltage.
4) Similar energy distributions are observed for both negative and positive ions from a given substance.
5) Multiply-charged ions exhibit distributions very similar to singly-charged ions from the same substance.
6) The accelerating potential supply should be very well regulated.
7) Operating conditions should be maintained as nearly constant as possible throughout all analytical exposures.

ACKNOWLEDGMENTS

The authors gratefully acknowledge the very competent technical assistance with the experiment by E. M. Botnick. Special thanks are also due to S. Miszkowski for the photomechanical construction of the movable slit-plate.

ELECTRON INDUCED SURFACE IONIZATION MASS SPECTROMETRY

David Lichtman, Honeywell Research Center, Hopkins, Minnesota

Since the time of Dempster[1] people working with mass spectrometers have occasionally observed extraneous peaks which in some cases were shown to be related to surface phenomena. In recent years several people have studied ions produced at surfaces[2,3,4,5] generally considering a single type of ion or adsorbed molecule. In our program, studying beam surface interaction using mass spectrometer analysis, we have also observed ions desorbed from surfaces under electron bombardment. We have observed ion fragments which can be related to a very large variety of adsorbed molecules and can, therefore, be used to identify the type of molecule on a surface.

The work is being done in a sensitive 6" radius, 60° sector ultra high vacuum mass spectrometer system as shown schematically in Fig. 1. This system was described in some detail at last year's meeting[6]. In the original construction of the ionization chamber the slit systems were made rather large since we were more concerned with sensitivity than high resolution. Under these conditions and when the total pressure in the system was quite low, that is in the range of 10^{-9} torr and less, several satellite peaks became evident. A spectrum taken under these conditions is shown in Fig. 2. The normal gas phase fragments are seen for the residual gases in the system, such as methane, water vapor, carbon monoxide, etc. The satellite peaks marked S were shown to be originating on surfaces in the ionization chamber which were unintentionally struck by electrons from the primary ionizing electron beam.

Many of these satellite peaks have been observed by other experimenters at various times[7,8]. It is believed that the 16 peak is due to O^+ from adsorbed carbon monoxide. The 17 satellite peak we believe to be OH^+ from adsorbed water vapor. We observed a satellite peak at mass 1 (not shown in the figure) which we identify with adsorbed hydrogen. We observe satellite peaks at 19, 35, and 37, which we believe to be fluorine and chlorine respectively and at 23 and 39 which we believe to be sodium and potassium respectively. Observations of these latter peaks and their behavior with time seem to indicate that alkali-halide molecules exist on the surface and give rise to these fragment ions. Thus under these conditions one obtains a combination spectrum which simultaneously identifies the gas phase components as well as the surface phase adsorbed components. When the slit system in the ionization chamber was closed down, more closely approximating normal values, the satellites tended to disappear. It appears that the satellite positions are determined by the position of the site at which ions originate. These surface sites are removed from the normal ion trajectory path. When the acceptance angles through the ion focusing system were reduced, most of these ions were unable to get through to the collector. Thus, with most carefully designed mass spectrometer sources, existence of the satellite peaks will not be observed.

To study the effect still further, experiments were performed by bombarding a special target placed right behind the ionization chamber with a separate electron beam and analyzing the desorbed ions as these pass through the ionizing chamber and the analyzing region. A typical surface phase spectrum obtained from a stainless steel target at room temperature is shown in Fig. 3. The bombarding electron energy was 1 kev with an electron density of less than 1 μamp/sq cm so that thermal effects were negligible. Ion desorption has been observed with electron bombarding energies from 10 eV to 5000 eV. As one can see from the figure, a large number of ion species can be observed desorbing from the surface and producing fragment patterns which are quite different from that of the gas phase patterns. This effect is clearly seen in Fig. 4 showing the results obtained on bombarding a single crystal nickel target. The lower portion shows the spectrum obtained from the gas phase at a total pressure of about 10^{-9} torr as produced in the ionization chamber. In the upper portion are the surface ions produced by separately bombarding the nickel target.

The results obtained on a variety of targets under many environmental conditions indicate the following general observations. Ion fragments are observed which can be related to all the gas phase components other than the noble gases (helium, neon, argon, etc.). Ions of parent molecules are never observed. For example, we observe O^+ and C^+ but not CO^+; we observe OH^+ but not H_2O^+; we observe H^+ but not H_2^+, etc. The ratio of the fragments is also obviously different than the ratio of the fragments obtained in the gas phase. However, we have been able to definitely relate many of

the fragment ions to specific parent molecules. By determining the actual cross section values and the specific fragment patterns one should be able to build up calibrating data related to surface gases in much the same manner as one has in the case of the volume gas phase. Electron probing of the surface, coupled with mass spectrometry, then enables one to identify the specific components on a surface at any temperature in the same manner that one determines the components in the volume gas with the conventional ionization chamber.

Recent experiments have been performed in which this probing technique was compared with flash filament experiments and the correlation obtained was extremely good. This technique has the advantage, however, of providing continuous observation of adsorption and desorption since continuous data is obtained with a probing electron beam sufficiently small that it does not affect the conditions occurring at the surface. Experiments are continuing to obtain specific quantitative data on the cross section of these reactions as a function of bombarding electron energy, the type of adsorbed molecules, and the type and temperature of the substrate. It is hoped that this data will enable us to determine the specific mechanisms responsible for the electronically induced fragment ion desorption.

REFERENCES

1. A. J. Dempster, Phys. Rev. 11, 316 (1918)
2. R. H. Plumlee and L. P. Smith, J. Appl. Phys. 21, 811 (1950)
3. J. R. Young, J. Appl. Phys. 31, 921 (1960)
4. G. E. Moore, J. Appl. Phys. 30, 1086 (1959)
5. P. A. Redhead, Can. J. Phys. 42, 886 (1964)
6. D. Lichtman, Eleventh Annual Conference on Mass Spectrometry and Allied Topics 1963
7. W. D. Davis, Proc. of 9th National Vacuum Symposium 1962
8. T. E. Hartman, Rev. Sci. Instr. 34, 1190 (1963)

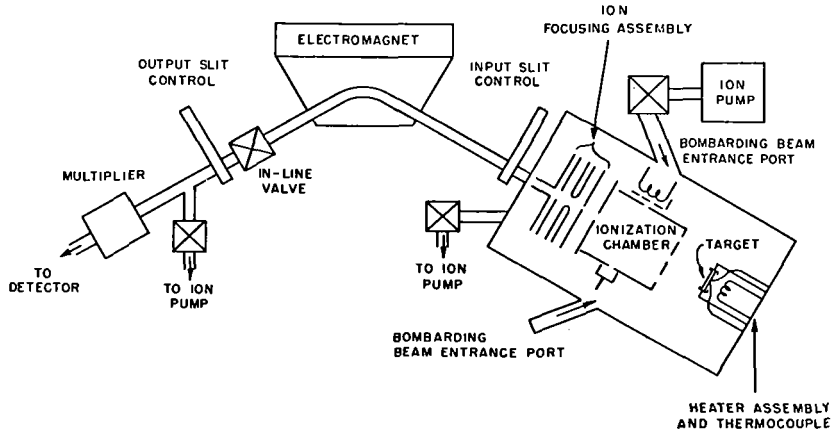

Figure 1. Schematic diagram showing essential features of the U. H. V. mass spectrometer system for beam-surface interaction studies.

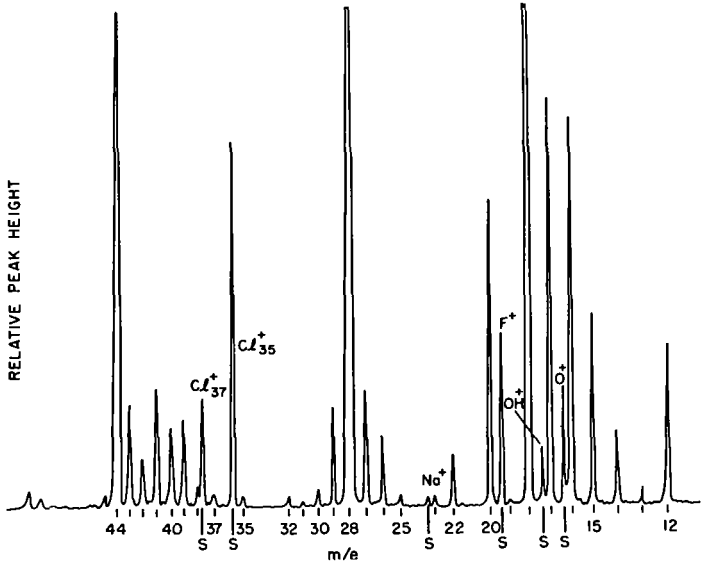

Figure 2. Portion of a typical spectrum of background gases at a gas phase total pressure of about 5×10^{-9} torr. Peaks marked "S" are produced by ions desorbed from surfaces in the ionization chamber struck by the ionizing beam.

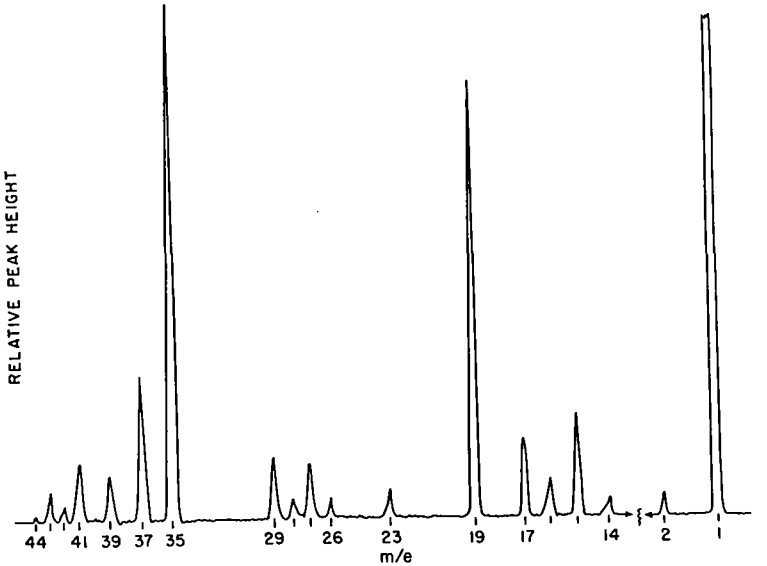

Figure 3. Spectrum of ions desorbed from the target surface by electron bombardment. Gas phase pressure is less than 1 x 10^{-9} torr and the target in this case was stainless steel. Electron bombarding energy was 1 kev with a total electron current of 1 μ ampere.

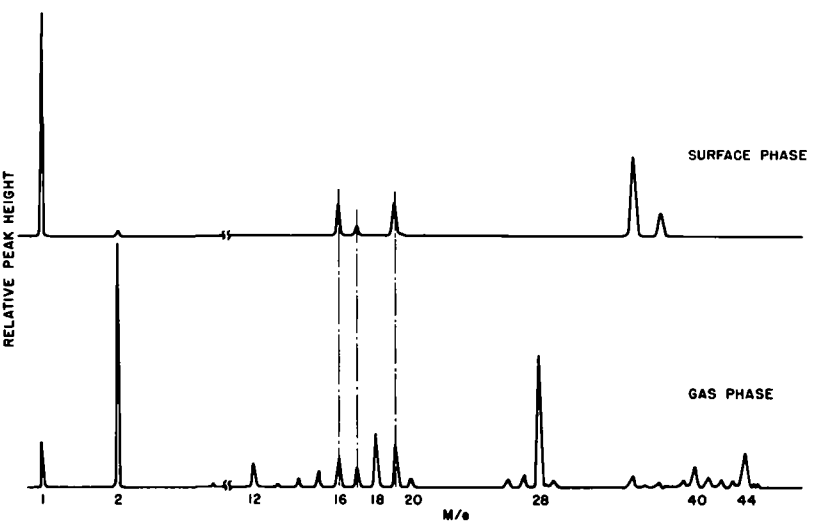

Figure 4. Lower portion indicates gas phase spectrum as produced in the ionization chamber. Upper portion is surface spectrum produced by bombardment of single crystal nickle target with 100eV electron beam. The nickle target is in the gaseous environment as indicated by the lower spectrum.

THE MASS ANALYSIS OF SMALL SAMPLES UTILIZING A SPUTTERING ION SOURCE

James A. McHugh and James C. Sheffield

General Electric Company
Knolls Atomic Power Laboratory*
Schenectady, New York

Abstract

An ion source that generates positive ions by sputtering has been shown to be of value for the isotope abundance analysis of small solid samples. The small sample efficiency of this source makes possible the mass analysis of a number of elements which perform poorly in thermal sources. The analysis of less than 10^{-8} grams of Be, B, Ni, Cu, Ag, and Sn has been accomplished.

INTRODUCTION

In solids mass spectrometry, the most common type of ion source employed for isotope abundance analysis is the surface or thermal ionization type source. The efficiencies of these sources are such that only a limited number of elements can be successfully analyzed from a 10^{-9} gram sample. The combination of factors governing source efficiency--ionization potential, sample form, volatility and sample environment--must possess the proper values and conditions, or the isotope abundance analysis of this size sample will be an impossibility. With this in mind, a series of experiments were undertaken to determine the small sample efficiency for a source which generates positive ions by sputtering. A number of elements that perform poorly in thermal sources have been investigated with this source. Some of the advantages and limitations of the method will be evident from this discussion.

EXPERIMENTAL

A detailed description of the cascade mass spectrometer used for this investigation has been reported previously.[1] A schematic diagram of the instrument is given in Fig. 1. The mass spectrometer provides for not only the selection of ions of a given m/e ratio from the primary source, but also for the identification and monitoring of secondary ions after the primary ion beam has interacted with a suitable target at the focal point of the first 180° 12-inch radius trajectory. Secondary ions from the target traverse a second 180° trajectory and are detected by a semiconductor magnetic electron multiplier,[2] which scans the focal plane of the second stage. The lower limit of ion current sensitivity for the detector in the pulse counting mode is 10^{-19} amp.

*Operated for the United States Atomic Energy Commission by the General Electric Company, Contract No. W-31-109 Eng52.

[1] F. A. White, J. C. Sheffield, and F. M. Rourke, Appl. Spectroscopy 17, 39 (1963).

[2] F. A. White, J. C. Sheffield, and W. D. Davis, Nucleonics 19, 58 (1961).

A quantity of the material to be investigated was evaporated on a flat tungsten ribbon filament (target) from an aqueous solution. The filament was mounted in what resembles a simple surface ionization source. A mass analyzed primary beam was normally incident on the filament surface, and produced beam densities in the range of 0.2 $\mu a/cm^2$ for currents of approximately 1×10^{-9} amp. The sputtering rate with these currents is sufficiently low that 10^{-9} gram samples have long lifetimes. The sample can be heated by passing a current through the ribbon filament. The pressure in the sample region was typically 2×10^{-7} torr.

Background Any material residing on the sample-filament surface is a potential source of secondary ions. Therefore, those substances which yield ions in the mass region of interest must be eliminated from the sample, or sample surface. Hydrocarbons present the most serious contamination problem. It is possible for hydrocarbons to be deposited on the filament along with the sample, or to deposit out from the vacuum system environment. Fig. 2 shows (a) the background peaks in the mass region of 9 to 150 amu for an untreated W filament, (b) the background peaks for a cold W filament which had been thoroughly outgassed by heating. The peaks observed represent contamination from the vacuum system, and (c) the background observed while the filament is maintained at 1000°C. From these results, it is clear that samples should be analyzed at elevated temperatures, or under ultra-high vacuum conditions if the contamination is due to hydrocarbons present in the vacuum system. The volatility of the sample compound will dictate whether heating can be employed. A sample filament temperature of 700°C is usually sufficient to eliminate the hydrocarbon background.

RESULTS AND DISCUSSION

A list of the elements investigated is given in Table I. The list is not meant to be comprehensive. However, it does include a number of elements which are difficult to analyze at the 10^{-9} gram sample level using thermal sources, and a few elements which can easily be handled by the thermal method. In addition, the results of the study are given in Table I along with the experimental conditions under which the observations were made.

Nickel and Copper There exists a large group of elements which perform poorly in thermal ion sources. Ni and Cu, as typical representatives of this group, have been investigated. Sample sizes for Cu and Ni of $5 - 10 \times 10^{-9}$ gram have yielded secondary ion beams considerably above any background impurities. However, the success of this operation is dependent for the most part on the conditions under which the sample is prepared and analyzed. The sample chemistry should involve no steps which would introduce hydrocarbon contaminants. The control of the sample filament temperature during the analysis is of extreme importance, both for eliminating surface contaminants and for maintaining a "clean" sample surface. Each element in the group investigated performed differently with temperature, and therefore, the best results for each were usually obtained under different temperature conditions. In the evaporation of the sample onto the filament, a temperature sufficient to convert the sample compounds to the oxides is advised. It was observed that if the sample filament was heated so that a noticeable amount of W was oxidized, the ion emission from the sample would be enhanced.

The best results for Cu were obtained when the sample filament temperature was maintained at approximately 1000°C. Additional heating would tend to deplete the sample (as was evidenced by a decrease in secondary ion current). The best Ni spectra, on the other hand, were obtained by flashing the filament to ~1400°C and returning to ~900°C for the analysis. The background peaks were, in both instances, reduced considerably. If needed, a fairly accurate correction can be made for any hydrocarbon contribution by utilizing the cracking patterns observed in Fig. 2. The mass spectra for Ni and Cu samples of $5 - 10 \times 10^{-9}$ gram are shown in Fig. 3.

TABLE I

Element	Ionization Potential (ev)	Sample Size (g x 10^9)	Secondary Ion Current[a] (ions/sec)	Primary Species and Ion Current	Energy Incident Particle (Kev)	Sample Temperature (°C)
Ni	7.61	10	8,000	Ar^+ - 1 x 10^{-10} amp.	3	900
Cu	7.68	10	13,000	Ar^+ - 1 x 10^{-10}	3	900
Ag	7.54	5	3,000	Ar^+ - 8 x 10^{-10}	5	450
Zr	6.9	5	18,000	Ar^+ - 8 x 10^{-10}	6	700
Sn	7.3	5	27,000	Ar^+ - 8 x 10^{-10}	6	700
Be	9.28	1	8,000	N_2^+ - 8 x 10^{-10}	3	750
B	8.25	10	10,000	N_2^+ - 1 x 10^{-9}	3	550
Li	5.36	1	50,000	CH_3^+ - 8 x 10^{-10}	4	450
Cs	3.87	0.1	88,000	Hg^+ - 3 x 10^{-10}	2.5	400
Ba	5.19	1	30,000	Hg^+ - 3 x 10^{-10}	2.5	400
Ce	6.54	5	18,000	Hg^+ - 3 x 10^{-10}	2.5	400
		(CeO^+)	180,000			
Zn	9.36	5	N.O.[b]	Hg^+ - 1 x 10^{-9}	3	--
I	10.6	10	N.O.	Ar^+ - 1 x 10^{-10}	7	--

[a]secondary ion current for the prominent isotope of the element, uncorrected for source transmission and detector efficiency.

[b]N.O. - not observed under prevailing experimental factors of sample size, primary beam intensity, primary energy and sample temperature.

Silver Silver peaks could be observed above background without having to heat the filament. The best ratio of Ag ion to hydrocarbon ion intensity was obtained when the sample filament was flashed to 1000°C and returned to 450°C. The secondary ion intensity of Ag was decreased by heating; however, the reduction of background peaks more than compensated for the loss in Ag^+ intensity. For example, the initial ratio of the major hydrocarbon in this region (mass 105) to Ag^{107} was approximately 1.0; upon heating, the ratio dropped to 0.01. The spectrum observed for a 5×10^{-9} gram sample of Ag is shown in Fig. 3.

Zirconium and Tin Zirconium and tin performed well at the $5 - 10 \times 10^{-9}$ gram sample level. Zirconium which is a good thermal emitter, performed as expected. In general, those materials which are good thermal emitters have high secondary ion yields. On the other hand, Sn performed much better than expected. The secondary ion intensities of the Sn isotopes were greater than the ion intensities of an equal sized Zr sample (see Fig. 3). The sample of Zr and Sn had been heated for 36 hours at 700°C. This treatment produced the best conditions for the Sn analysis. Increasing the temperature any further would only decrease the Sn ion intensity. Under these conditions Zr yielded both atomic and oxide ions in about equal abundance.

Beryllium A 1×10^{-9} gram sample of Be yielded a secondary Be^+ beam in excess of 8000 ions per second for a 2.7 kev - 8×10^{-10} amp N_2^+ primary beam. In this mass region one is not bothered by hydrocarbons, and the only possible interference could come from multiply-charged heavy mass ions. Multiply-charged species are not generated to any extent in this source with the primary particle energies employed (at least the yields are below our detection capability). A very temperature sensitive peak was observed at the mass 10 position. We are fairly certain from this and its behavior relative to Be that it can be attributed to HBe^+. The temperature dependence of the Be^+ emission was similar to the other species investigated. Maximum emission occurred when sample filament temperature was maintained at ~750°C.

Boron A 10^{-8} gram sample of boron gave a B^{11} current of 10,000 ions per second for a 2.8 kev - 1×10^{-9} amp N_2^+ primary beam. The sample was maintained at 550°C for 24 hours prior to the analysis. Fig. 4 shows (a) the boron mass region before placing a sample on the filament and (b) the spectrum obtained with a 10^{-8} gram sample of B on the sample filament.

CONCLUSIONS

The results reported herein indicate that the analytical technique of isotope dilution mass spectrometry may be extended to cover elements heretofore never seriously attempted because of their poor source efficiencies. With proper chemical separation techniques, and the ability to make an isotope abundance analysis on samples of $\lesssim 10^{-8}$ gram, there exists the possibility of measuring concentrations in the range of a ppb or less for a number of new elements. The possible applications for this source appear to be numerous. Its utilization coupled with existing mass spectrometric techniques will provide new analytical methods for the researcher.

FIGURE CAPTIONS

Figure 1. Schematic diagram of the cascade mass spectrometer. The primary ions are produced in a conventional electron-bombardment source.

Figure 2. Impurity peaks observed for (a) an untreated W sample filament, (b) a cold W filament which had been thoroughly outgassed by heating and (c) a W filament maintained at 1000°C.

Figure 3. Mass spectra obtained for (a) ten nanogram Cu and Ni samples and a 5 ng Ag sample (b) five ng Zr and Sn samples.

Figure 4. Mass spectra for (a) the boron mass region before placing sample on the filament and (b) the spectrum obtained with a 10 ng sample of natural B.

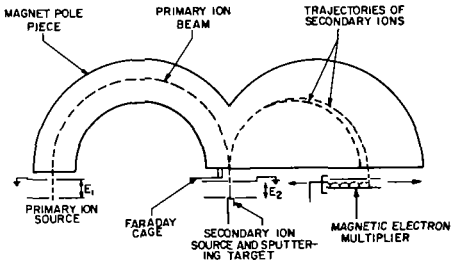

FIGURE 1

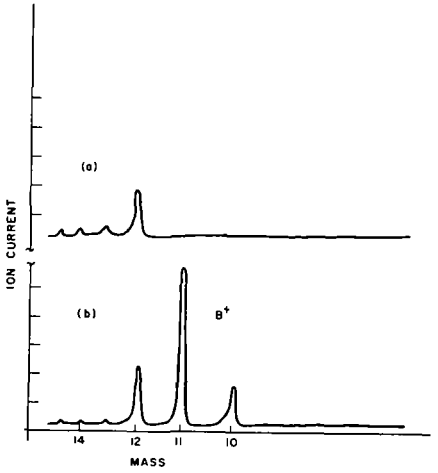

FIGURE 4

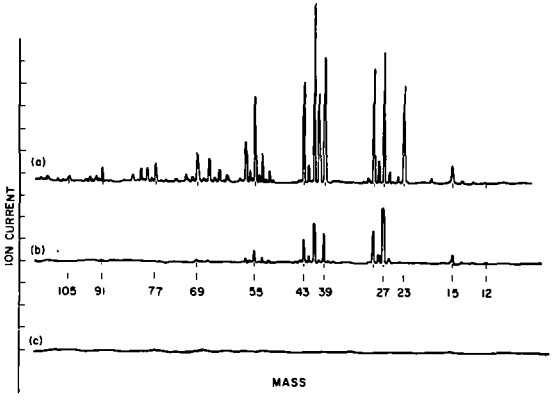

FIGURE 2

UNCLASSIFIED

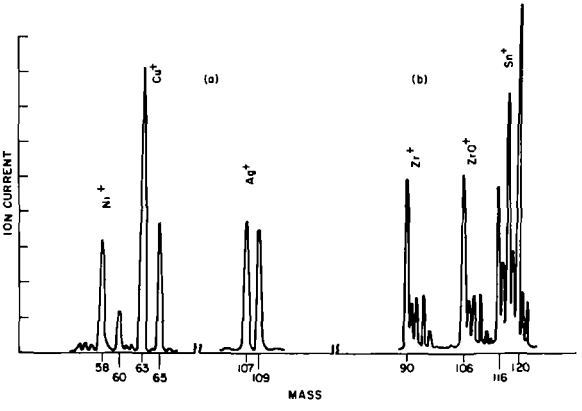

FIGURE 3

UNCLASSIFIED

SPUTTERING ION SOURCE FOR SOLIDS*

Helmut J. Liebl** and Richard F. K. Herzog
Physics Research Division
Geophysics Corporation of America
Bedford, Massachusetts

At last years conference, we reported about an ion source for solids, based on the sputtering principle. Figure 1 shows the latest version of the ion source: The primary ion source is a so-called duoplasmatron, where a magnetically constricted arc discharge burns in an argon atmosphere. Positive argon ions diffuse through a hole of 10 mil diameter in the anode and are accelerated to about 10 kv and focused on the specimen by an electrostatic lens. Two pairs of mutually perpendicular deflection plates are provided to adjust the beam. The secondary ions sputtered off the specimen are accelerated towards the left and focused onto the entrance slit of the mass spectrometer.

When the mass spectrometer was first equipped with an electron multiplier, a variety of instrumental background peaks appeared due to the increased sensitivity.

With this type of ion source there are three major sources of instrumental background. First, impurity ions coming with the primary beam out of the duoplasmatron; second, material which is sputtered by the fringe of the primary beam along its path and deposited on the sample and third, residual gases and vapors ionized on or close to the surface of the sample. The composition of the primary beam can be checked in a very simple manner by lowering the beam acceleration voltage to a value somewhat lower than the target potential. Then the field in front of the target acts as an "ion mirror" and reflects the ions. A good fraction of them are accelerated by the secondary ion optics and analysed in the mass spectrometer. In the original setup a variety of background peaks were found representing all the materials out of which the primary ion source and the primary ion optics was made, and also hydrocarbons, originating partly from the residual gas and partly from the duoplasmatron.

In this new design, therefore, the oil diffusion pump has been replaced by a mercury diffusion pump. No vacuum grease is used at all. The only sealing material used is Viton A. All parts close to the primary ion beam are made out of tantalum which is especially well suited for this purpose, since it is hard to sputter, has only one isotope to speak of at mass 181, multiply charged ions do not coincide with other mass numbers, and polymers are well beyond the highest nuclide masses.

Figure 2 shows the ion gun, consisting of the duoplasmatron, the electrostatic lens and the beam adjustment plates.

Figure 3 shows the sample mount. There are four samples mounted on a bar out of tantalum, held by miniature vices. They can be moved into the beam one after the other, and there are also adjustments parallel and perpendicular to their surface. Figure 4 shows a silver sample after a continuous bombardment of 2½ hours to illustrate the beam diameter which is about one-third of a millimeter.

In order to investigate the applicability of this ion source for quantitative analysis, the secondary ion spectra of a number of certified samples from the National Bureau of Standards were recorded. Figure 5 shows a typical recording obtained from the output of the multiplier. It had been noticed at the first preliminary runs that there was a rather wide variation of sensitivities for different elements and it was hoped that this discrimination could be reduced by using higher bombarding energies and thus increasing the so-called "apparent temperature". Figure 6 shows the results of two runs obtained with an iron base alloy. Here the sensitivities of the constituents relative to that of iron are plotted against the primary beam energy. Relative sensitivity is defined as the ratio of the sums of isotopic peak heights divided by the actual concentration, which in the ideal case should be unity for all constituents. At low voltages, the sensitivities of vanadium and chromium which are the highest of these four

* This work was supported by the National Aeronautics and Space Administration under NASA Contract No. NASw-839.

** New address: ARL Hasler Research Center, Goleta, California.

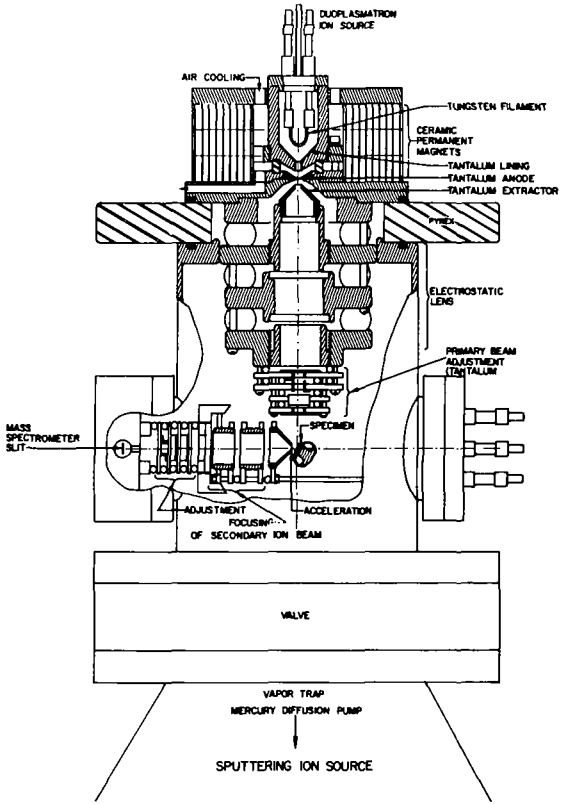

Figure 1.

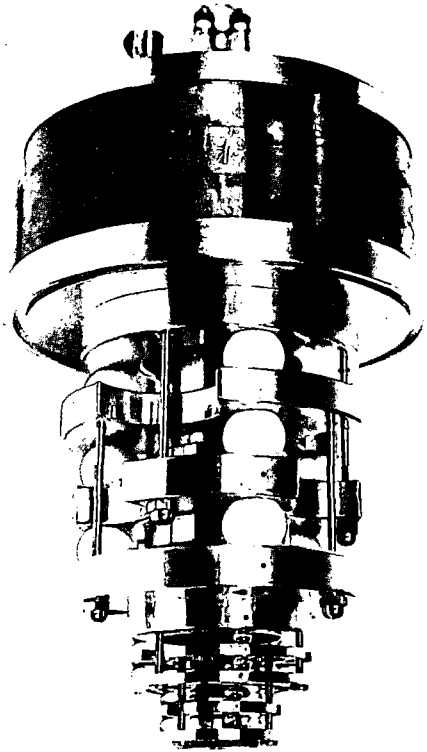

Figure 2.

constituents show indeed a decreasing tendency with increasing bombarding energy, but after passing a flat minimum between 15 and 20 kv they go up again. One explanation is that with higher energy the bombarding ions penetrate so deep into the lattice that actually less energy is dissipated on the surface where the ionization takes place. This result indicates that one does not gain anything as far as discrimination between different elements is concerned by increasing the bombarding energy from 10 to 25 kev. The question coming up immediately is whether these sensitivities depend to a great extent on the concentration or on the bulk material. Fortunately, this does not seem to be the case. Figure 7 shows how the sensitivities were found to depend on concentrations, measured with three different NBS Standards. Ideally, the curves should be horizontal lines. Actually, the deviations are within a factor of three with the exception of the manganese where the deviation is larger. It should be noted, however, that with new pieces cut from the same standards this large deviation did not appear, so that this deviation could be due to an inhomogeneity of one particular sample rod.

Some of the points on this plot in the region of low concentration are by far too high. This was apparently due to instrumental background since these measurements were made with the previous setup.

The determination of the detection limit for different impurities with the new setup is seriously hampered by the fact, that no really pure samples are available. The instrumental background cannot be observed independently of any sample. We have recorded secondary ion spectra from samples, in which impurities were less than 1 ppm according to the manufacturers analysis. We found no water peak and no hydrocarbon peaks, which indicates the cleanliness of the vacuum. However, we found some impurity metal peaks to be too high compared with the bulk material peak as to correspond to the 1 ppm impurity level, even after application of sensitivity factors. The striking fact is that the relative abundances of these metal impurities vary from sample to sample which suggests that they are not instrumental background. Besides of this situation which needs a more thorough investigation, it can be said that the limit for trace analysis is given by the noise level which, at the present, is in the order of ppm of the bulk peaks.

Concludingly, it can be stated that the sputtering ion source has proved itself a helpful new tool in the field of solids analysis. In several instances we had excellent success with the identification of unknown surface layers, and we feel that with appropriate calibration it has a future in the field of quantitative trace analysis. The obvious advantages are that it can accomodate a variety of sample sizes and shapes, and that the results are obtained immediately on a chart recorder.

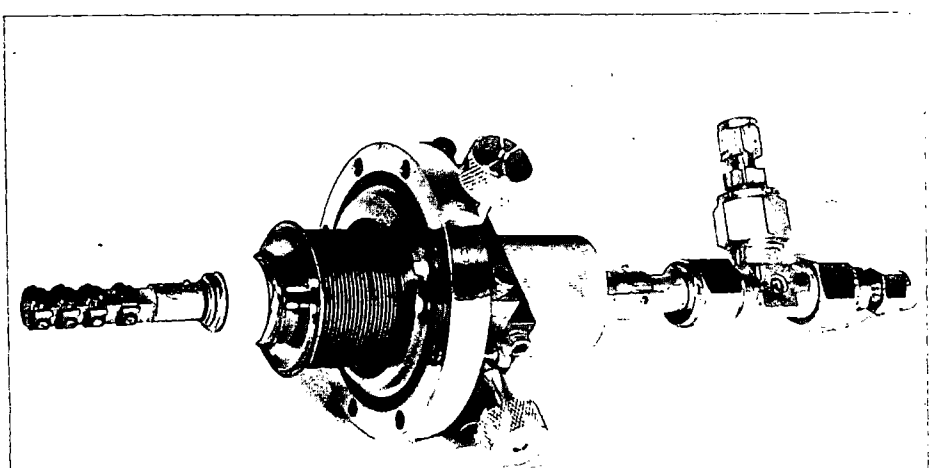

Figure 3.

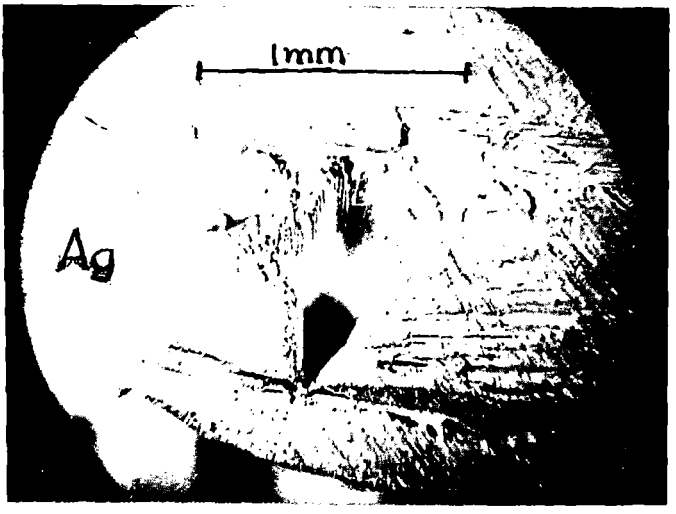

Figure 4.

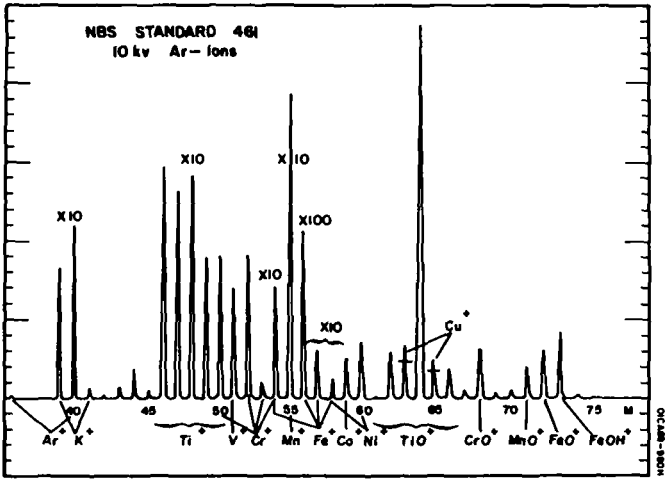

Figure 5.

Part of secondary ion spectrum from a surface of NBS Standard 461 (low alloy steel) bombarded with 10 kev argon ions, scanned by sweeping the magnetic field.

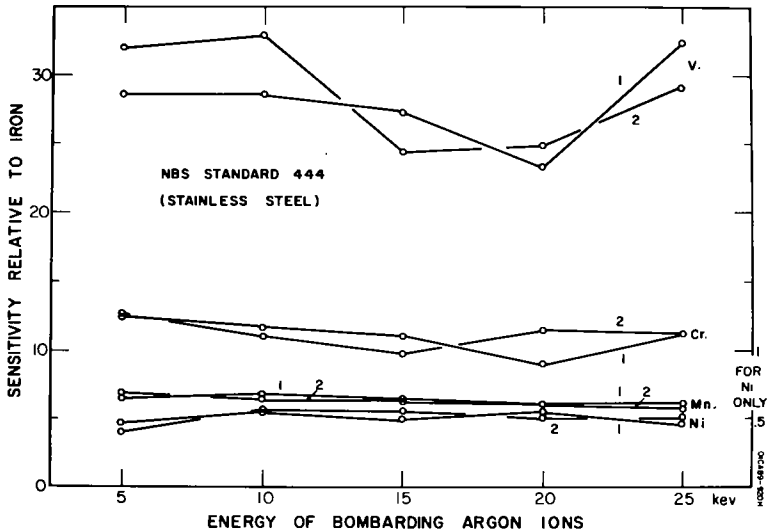

Figure 6. Effect of primary beam energy on relative spectral peak heights for NBS Standard 444 (stainless steel).

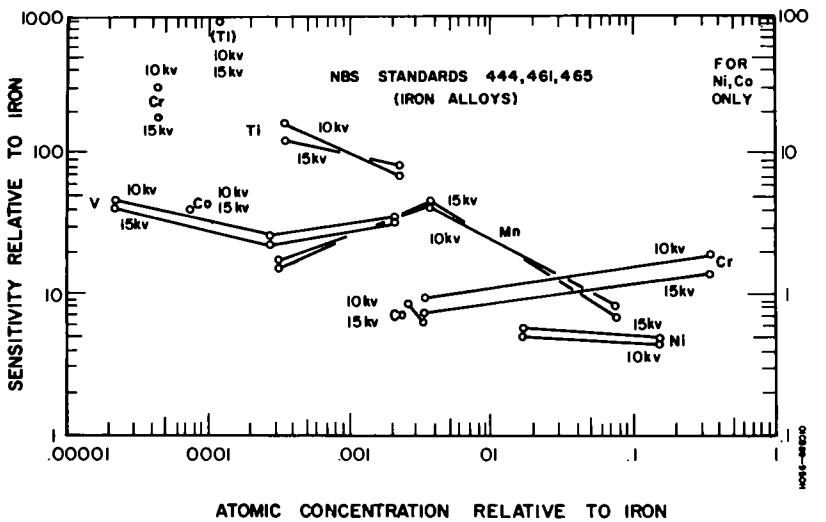

Figure 7. Effect of concentration on relative sensitivities for NBS Standards 444, 461 and 465 (iron alloys).

MASS SPECTROMETRIC STUDIES OF SPUTTERED PARTICLES FROM COPPER MONOCRYSTALS*

A. L. Southern
Solid State Division, Oak Ridge National Laboratory
Oak Ridge, Tennessee

As a part of a program for studying the sputtering from the surface of copper monocrystals bombarded with positive argon ions, the type, intensity, and energy of the sputtered particles is being investigated with a high-vacuum mass spectrometer. The results of some studies to determine techniques for obtaining clean surfaces are reported here, and some of the properties of the copper ions sputtered by 2.5 kev argon ions are described.

The dual-beam mass spectrometer used in this study has been described by the manufacturer.[1] Therefore, only a diagram of the bombarding ion source and the location of the solid angle for sputtered particles is shown in Fig. 1. The target could be rotated so as to obtain an angle of incidence of 0 to $\sim 90^{\circ}$ for the bombarding ion beam, and the particles sputtered at an angle 90° to the incidence ion beam were mass analyzed. This arrangement allowed only the sputtered particles to be analyzed for all angles of incidence, except for 45°, for which both sputtered and reflected particles were analyzed.

The target could be heated to approximately 900°C by electron bombardment of the target holder and the temperature could be monitored with a platinum-platinum rhodium thermocouple or by optical methods. The complete spectrometer could be baked out at 400°C by an oven. The best background pressure obtained was 1×10^{-9} torr, but pressures were generally in the range 3×10^{-9} to 1×10^{-8} torr. Typical pressures in the system during operation were 2×10^{-6} torr in the source, 3×10^{-7} in the target region, and 2×10^{-8} in the mass analyzer. The maximum bombarding Ar^{+} ion current density was 7 μa/cm^{2} at 3 kev energy and the minimum analyzer current measurable was 5×10^{-19} ampere.

The copper targets used in these experiments were sliced from a crystal with (100) surfaces by an acid saw (Fig. 2). When target A was rotated in the mass spectrometer the directions of incidence of the argon ion beam were in the [100] zone and for target B, the [110] zone. The (100) surfaces were chemically lapped, electropolished and washed to obtain a flat clean surface.

The degree of surface cleanliness was evaluated by comparing the spectra of the ejected positive ions. Table 1 shows the relative intensities of the positive ions ejected from the copper surface after various conditions of heat treatment. The intensities were normalized to mass 63 of the initial run, which was made from a target cleaned by electropolishing. The degree of cleanliness was found to be best after one system bake-out at 400°C and two target bake-outs at 600°C. System bake-outs appeared to drive impurities to the crystal surface, while bake-out of only the crystal removed these impurities. The In^{+} was due to indium contamination in the system and could easily be removed by target bake-out. The decrease in intensities of the copper ions with bake-out cannot be explained by a change in cleanliness. Ion bombardment of the surface should serve to clean the bombarded area, but the peak intensities during any one experiment were essentially constant. Also, note that CuO^{+} was absent for all cases.

The recording of the peaks of $^{63}Cu^{+}$ and $^{65}Cu^{+}$ of target A for an angle of incidence of 80° is shown in Fig. 3. Figures 4 and 5 show relative peak heights and area under the two peaks vs. angle of incidence for target A and B, respectively. The results from 84° to 90° are questionable since for these angles the target surface did not intercept the complete beam. The peak widths at half height of the $^{65}Cu^{+}$ and $^{63}Cu^{+}$ sputtered from target A are shown in Fig. 6. As can be seen for angles of incidence ϕ less than about 50° the peaks overlapped so much that information on the separate peaks could not be obtained.

Now, as can be seen from Figs. 4-6, the ratio of peak heights of $^{63}Cu^{+}$ and $^{65}Cu^{+}$ are equal to the isotopic ratio for only a small range of ϕ for target A (72°-80°);

* Research sponsored by the U. S. Atomic Energy Commission under contract with the Union Carbide Corporation.

never for target B. (As described above, only ions ejected 90° to the angle of incidence are collected.) Peak height is proportional to intensity only if (1) the peaks are separated, and (2) peak widths are either independent of or directly proportional to ϕ. For target A condition (1) is met only for $\phi > 72^{\circ}$, and since the ratio is not correct for $\phi > 80^{\circ}$, it must be concluded that condition (2) is not true. Therefore, any agreement in these experiments between the ratios of the peak heights and the isotopic ratio is fortuitous.

From Figs. 4 and 5 it is clear that the intensity of Cu ions ejected varies with ϕ, and in a very complicated way. (Only for ϕ greater than 70° are the peaks for $^{65}Cu^{+}$ and $^{63}Cu^{+}$ sufficiently separated to allow the areas under the individual peaks to be obtained.) With increasing ϕ the area under the peaks increases for target A and decreases for target B, though not monotonically in either case. Since the intensity is maximum for target A at $\phi = 45^{\circ}$, direction of incidence and direction of ejection both $\langle 011 \rangle$, and for target B at $\phi = 90^{\circ}$, direction of incidence approaching $[1\bar{1}0]$ and direction of ejection $[001]$, it can be concluded that the intensity of ions is greatest when a $[110]$ is involved, as has been shown for atoms ejected in sputtering. It appears that there may be some correlation between the other bumps in the area vs. ϕ curves and crystallographic directions, but if so, it is not thought to be significant at this time.

Calculations based on the Langmuir-Saha formula[2] of the ratio of sputtered ions to sputtered neutrals seem always to be smaller than experimental estimates. Using a value for the sputtering yield of 4 atoms/ion,[3] the ratio of sputtered ions to sputtered neutrals was estimated to be about 10^{-7}, while this ratio predicted from the Langmuir-Saha formula was about 10^{-54}.

References

1. A. J. Smith, L. A. Cambey, and D. J. Marshall, J. Appl. Phys. 34, 3489 (1963).

2. I. Langmuir and K. H. Kingdon, Proc. Roy. Soc. (London) 107, 61 (1925).

3. A. L. Southern, William R. Willis, and Mark T. Robinson, J. Appl. Phys. 34, 153 (1963).

TABLE I. POSITIVE IONS EJECTED FROM A (100) COPPER MONOCRYSTAL BY BOMBARDING WITH 3 kev Ar^+ IONS AT AN ANGLE OF INCIDENCE OF 75°

MASS	PROBABLE IDENTIFICATION	RELATIVE INTENSITIES			
		INITIAL RUN	SYSTEM BAKE-OUT	1st TARGET BAKE-OUT	2nd TARGET BAKE-OUT
1	H^+	26	7	1	1
23	Na^+	96	425	103	24
28	CO^+	13	28	62	2
39	K^+	68	500	73	13
41	K^+	9	32	5	1
52	Cr^+	3	3	10	1
63	Cu^+	1000	20	30	9
65	Cu^+	400	12	14	4
115	In^+	3	17	3	1

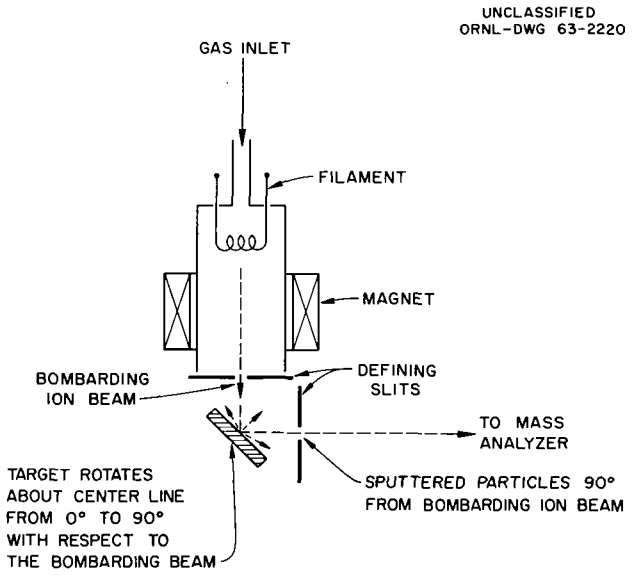

Fig. 1. Schematic diagram of the bombarding ion beam, target and section of the sputtered particles analyzed.

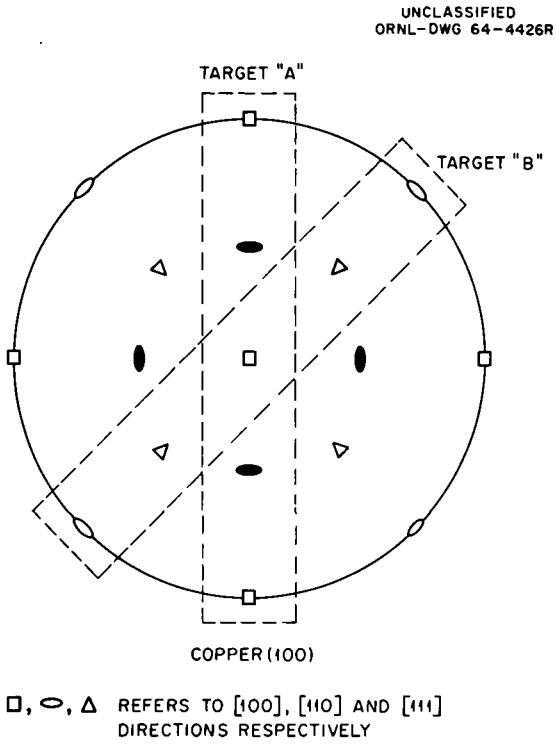

Fig. 2. Orientation of targets A and B.

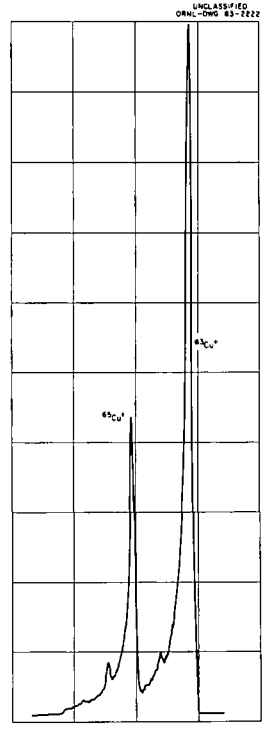

Fig. 3. $^{63}Cu^+$ and $^{65}Cu^+$ sputtered from copper monocrystal with 2.5 kev Ar^+ ion bombardment at an angle of incidence of 80°.

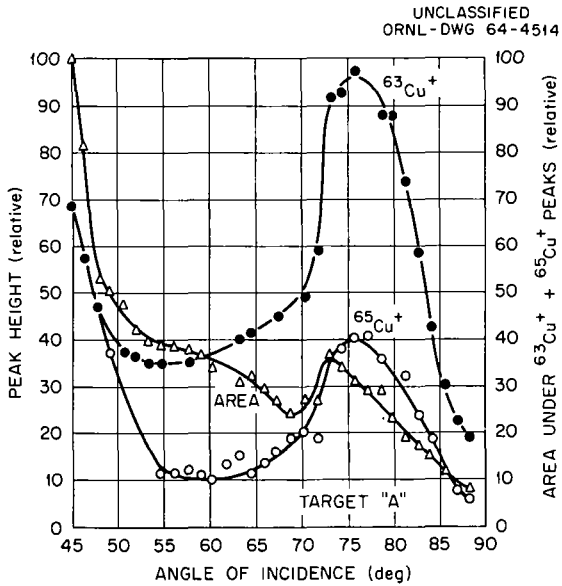

Fig. 4. Peak height and area under the peaks as a function of angle of incidence for $^{63}Cu^{+}$ and $^{65}Cu^{+}$ sputtered from target A with 2.5 kev Ar^{+} ion bombardment.

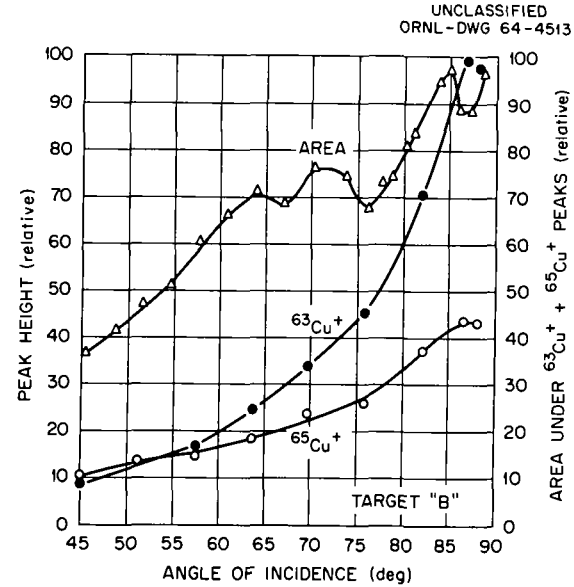

Fig. 5. Peak height and area under the peaks as a function of angle of incidence for $^{63}Cu^{+}$ and $^{65}Cu^{+}$ sputtered from target B with 2.5 kev Ar^{+} ion bombardment.

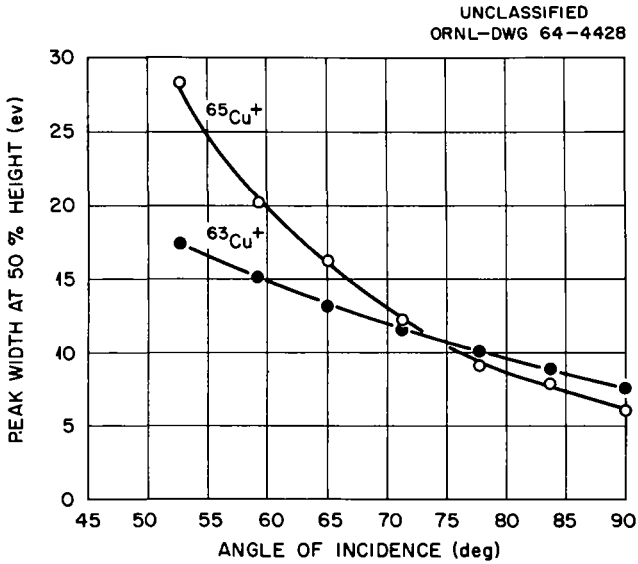

Fig. 6. Peak width at 50% level as a function of angle of incidence for $^{63}Cu^+$ and $^{65}Cu^+$ sputtered from target A with 2.5 kev Ar^+ ion bombardment.

SOME USES, MISUSES AND ABUSES OF THE TIME-OF-FLIGHT MASS SPECTROMETER

R. S. Gohlke
The Dow Chemical Company
Eastern Research Laboratory
Framingham, Massachusetts

Although over one hundred and fifty time-of-flight mass spectrometers have been in use for the last few years, surprisingly little has been published regarding their various applications.

This paper will attempt to provide a critical review of the time-of-flight mass spectrometer and the applications to which it has been put.

MASS SPECTROMETRIC INVESTIGATION OF GASES FROM FLASH AND LASER IRRADIATION OF COAL

By

A. G. Sharkey, Jr.,[a] J. L. Shultz,[b] and R. A. Friedel[c]

INTRODUCTION

Techniques for the rapid heating and subsequent rapid cooling of coal are being investigated at the Pittsburgh Coal Research Center of the Federal Bureau of Mines. The purpose of this investigation is to study the products from the flash and laser irradiation of coals.

This preliminary study was made with the samples irradiated external to the mass spectrometer to compare the stable end-products produced by these techniques with those from conventional high-temperature carbonization. Many of the parameters related to using laser energy to vaporize materials in the mass spectrometer can be studied in this manner. The objectives were to determine the pyrolysis products and their relationship to original structure and to explore the use of laser energy for vaporizing high-molecular weight organic materials in the mass spectrometer.

Techniques which have been used to study organic materials for structural and other information include conventional methods such as vacuum pyrolysis and Soxhlet extractions where the sample is exposed to temperatures of 100° to 1000°C for minutes to hours. In contrast to these types of studies, flash and laser irradiations produce extreme temperatures for milliseconds.

In a previous investigation at this laboratory, it was shown that the distribution of gaseous products produced by the flash irradiation of coal is different from that obtained by high-temperature carbonization.[1] Rau and Seglin have recently described a similar investigation which also included a study of the change in gas composition with the rank of the coal.[2] In a related study, Bond and others used an argon plasma-jet and reported that about 20 percent of the carbon in the coal appeared as acetylene in the gaseous product.[3] In these studies, only a solid residue, essentially soot, and gaseous products were produced. The amounts of liquid and tarry material were negligible if present at all.

Combined mass spectrometric and laser techniques have also been applied to a study of induced emission from solids by Honig and Woolston.[4] Since bituminous coals contain many aromatic hydrocarbons and their alkyl derivatives, the results described here should have applications in studies of other organic mixtures.

Apparatus and Methods

The experimental arrangement used in the laser irradiations is shown schematically in Figure 1. For the flash irradiations, the ruby rod was removed and the sample tube placed in the position shown for the rod. Energy from a 4000 joule supply was discharged through a xenon lamp for the flash irradiations. About 150 mg of powdered coal was placed in sample tubes 1/2 inch in diameter and 6 inches long. The tubes were evacuated and sealed and, prior to irradiation, rotated to deposit as much of the sample as possible on the inner surface of the tube in the direct path of the energy. An estimated 11 mg of powdered coal was irradiated.

A ruby crystal with an output of about 2 joules at 6943Å was used for the laser studies. For most of the experiments, energy from the 1 millisecond light pulses was focused, using a 3 cm focal length lens, on cubes of coal about 1/4" on a side. In one experiment coal particles <10 microns in size were used.

---

a. Supervisory Research Physicist
b. Research Mathematician
c. Project Coordinator
All authors are with the Pittsburgh Coal Research Center, Bureau of Mines, Pittsburgh, Pa.

Table 1.- Gaseous products from laser irradiation of Pittsburgh seam (hvab) coal, mole percent

Treatment	900° Carbonization	Flash	Laser
Sample form or particle size		<74 microns	cube
Atmosphere		vacuum	vacuum
Energy (joules)		4000	1.5
Number of shots			5
Compound			
H_2	55.6	69.2	42.5
CO	7.4	16.1	16.7
CO_2	0.4	0.5	15.4
CH_4	31.5	4.1	5.3
C_2H_2	0.05	7.8	16.0
C_2H_4	3.4	0.05	2.1
C_2H_6	1.2	0.1	0.5
HCN	-	1.7	0.1
Σ Hydrocarbons above C_2	0.5	0.4	1.4
Above gases as weight percent of coal irradiated	15	18	70

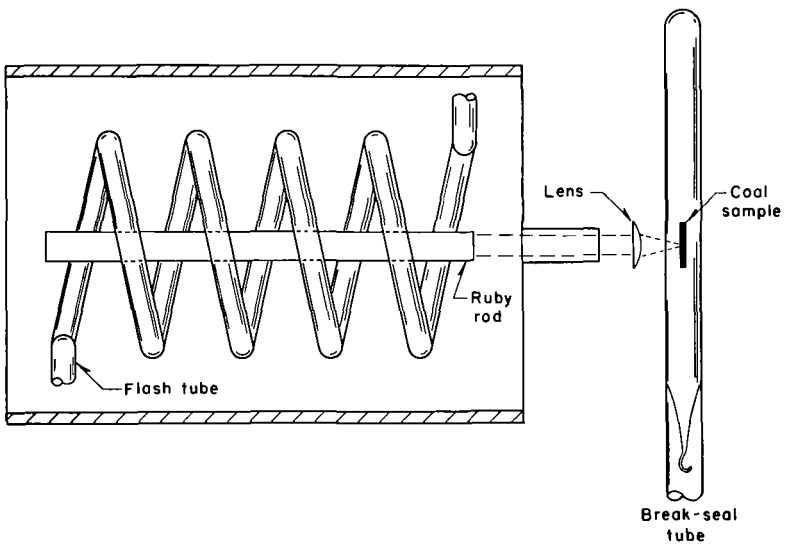

Figure 1.-Optical laser head.

Gases produced by the flash and laser irradiation were analyzed by mass spectrometry after fractionation using the following baths: Liquid nitrogen, dry ice, ice water, room temperature, and water at 60°C. The analyses of total gaseous products were obtained by combining data from the five fractions.

The temperature reached by the coal particles could not be determined but based on the average particle diameter and energy, the maximum temperature was estimated as greater than 1000°C with the flash irradiation. The coal in the path of the focused beam of laser light probably reached several thousand degrees centigrade. Laser irradiation of solids under similar experimental conditions has produced surface temperatures of approximately 7000°K as calculated from the Langmuir-Saha equation.[2]

Results and Discussion

Figure 2 shows the craters resulting from laser irradiation of a disk of coal. The periphery of the craters indicates some carbonization has occurred in the surrounding area. Figure 3 shows a replica of a crater produced at high-energy. The depth of the crater is approximately half the diameter. The volume of the crater was calculated assuming a conical shape and used to relate theyield of gas to the weight of the coal irradiated. These data are not considered valid since determination of the actual amount of material exposed to the light energy is difficult. There is evidence of carbonization around the periphery of the crater, Figure 2, and it is possible that some of the sample is simply blown from the crater. No evidence was found for liquid or tarry products.

Table 1 presents data from the flash and laser irradiation of bituminous coal and from the 900°C carbonization of the same coal. A comparison of gases from the flash irradiation and the high-temperature carbonization of coal confirms previously reported results that flash irradiation produces gas richer in acetylene, carbon monoxide, and hydrogen and poorer in methane and higher hydrocarbons.[1] In addition, hydrogen cyanide was also observed in the gas from the flash irradiation. Based on the estimate of 11 mg of powdered coal irradiated, the yield of gaseous product was about 18 percent.

Gases from the laser irradiations of coal showed higher yields of acetylene, and C_3 and higher hydrocarbons than the gaseous products from either flash irradiation or the 900°C carbonization of coal. Approximately the same concentrations of methane and carbon monoxide were produced in the flash and laser irradiations. Components with molecular weights up to 130 were found in the gas from laser irradiation. The yield of gaseous product, based on the volume of coal irradiated as determined from crater size, is estimated as 70 percent of the coal by weight.

As another phase of the investigation, gaseous products from the laser irradiation of coal were studied as a function of energy of irradiation, particle size of the coal, and atmosphere. These data are shown in table 2. The product from the laser irradiation of a cube of coal with 5 bursts 1.5 joule energy is considered the standard for the series of tests. One experiment was conducted with particles of <10 micron coal coating the inside of the tube. A second experiment, using a cube of coal, was conducted with a unit having an energy output of about 10 joules per burst. A third experiment was conducted in a helium atmosphere at 20 mm pressure, rather than in vacuo.

Product from the irradiation of the <10 micron particles of coal showed higher methane and lower acetylene than produce from cubes of coal. The temperature and acetylene percentage were expected to increase as the particle size of the coal was reduced. Other particle sizes will be studied.

Table 2.- Variation of gaseous products from laser irradiation of coals as a function of particle size, energy, and atmosphere, mole percent

Treatment	Laser	Laser	Laser	Laser
Sample form or particle size	Cube	<10 microns	Cube	Cube
Atmosphere	Vacuum	Vacuum	Vacuum	He
Energy (joules)	1.5	1.5	10	1.5
Number of shots	5	5	5	5
Compound				
H_2	42.5	46.0	42.8	30.7
CO	16.7	22.9	26.0	13.2
CO_2	15.4	7.6	2.6	23.5
CH_4	5.3	7.3	1.1	10.5
C_2H_2	16.0	9.4	25.9	6.2
C_2H_4	2.1	0.6	0.6	7.9
C_2H_6	0.5	1.0	0.03	1.9
HCN	0.1	2.4	0.1	0.2
Σ Hydrocarbons above C_2	1.4	2.8	0.9	5.9
Above gases as weight percent of coal irradiated	70	1/	92	1/

1/ Volume of coal irradiated could not be measured.

Table 3.- Laser irradiation of Pittsburgh seam coal (10 joules-5 shots) mole percent

GASEOUS HYDROCARBONS	
Acetylene	90.9
Methane	3.9
Diacetylene	2.8
Ethylene	2.1
Methylacetylene	.2
Ethane	.1

The highest acetylene content observed in these experiments, 25.9 percent, resulted when a cube of coal was subjected to 5 bursts of 10 joule energy. Ninety-five percent of the gaseous product from this irradiation consisted of hydrogen, carbon monoxide, and acetylene. As shown in table 3, acetylene accounted for approximately 91 percent of the hydrocarbon product; the yield of components having more than two carbon atoms was about 3 percent.

In a third experiment, helium was introduced prior to irradiation to determine if the inert gas would absorb some of the energy associated with the products and reduce secondary thermal effects. The gaseous product showed higher methane, lower acetylene, and more saturation in the higher hydrocarbons, indicative of lower temperatures. It is interesting that even though the distributions of the C_2 products--acetylene, ethylene, and ethane--are different for the standard and the experiment with the helium atmosphere, the total C_2 product is approximately the same.

Conclusions that can be drawn from this study of the irradiation of organic compounds under extreme temperatures are:

1. For the aromatic compounds found in coal, the products are gaseous and essentially a char, with little evidence of formation of liquids or tarry components.

2. The percent of vaporization is high, probably in excess of 70 percent.

3. The products obtained using high-energy for milliseconds are different from conventional pyrolysis at moderate temperatures for minutes or hours. The hydrocarbon products are richer in unsaturates with acetylene predominating.

4. The distribution of products appears to be a function of energy of irradiation, atmosphere and probably particle size of the sample.

5. While the high-energy, short-duration irradiation of coal produced a simple mixture of low molecular weight gases, it provided little information on the structure of coal.

Based on these preliminary studies, it appears that the laser will not be useful as a source of energy for vaporizing organic samples for analysis by mass spectrometry, as the degradation leads to many products too simple to allow them to be related to any pre-existing structure.

REFERENCES

1. Hawk, C. O., M. D. Schlesinger, and R. W. Hiteshue. BuMines Rept. of Inves. 6264, 1963, 7 pp.

2. Rau, E., and L. Seglin. Fuel 43, 1964, pp. 147-157.

3. Bond, R. L., I. F. Galbraith, W. R. Ladner, and G. I. T. McConnell. Nature, v. 200, 1963, pp. 1313-1314.

4. Honig, R. E., and J. R. Woolston. Appl. Phys. Letters, v. 2, 1963, pp. 138-139.

5. Honig, R. E. (Personal Communication).

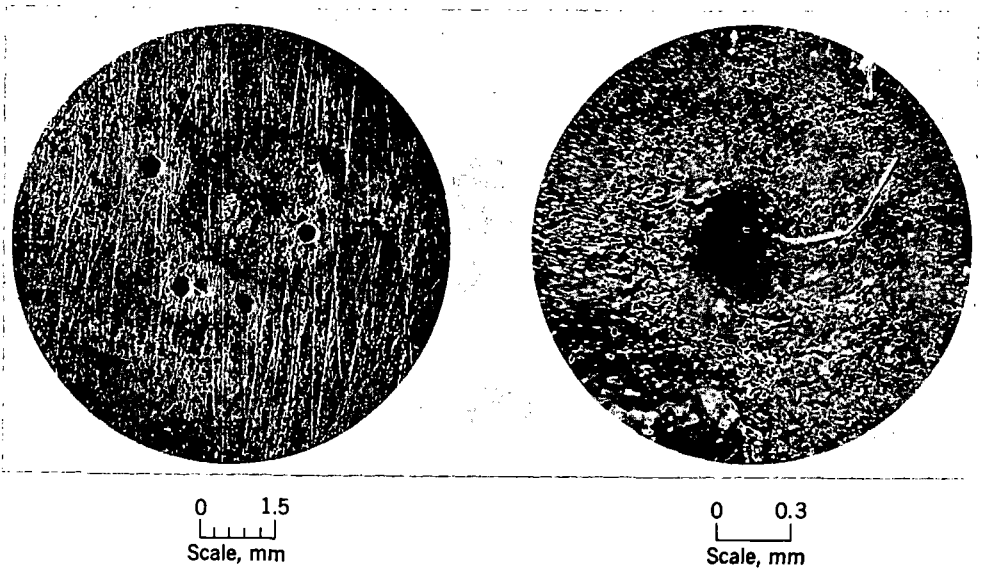

FIGURE 2. - Laser Irradiation of Pittsburgh Seam (hvab) 84 Percent Carbon, Coal. Section 0.9 mm Thick.

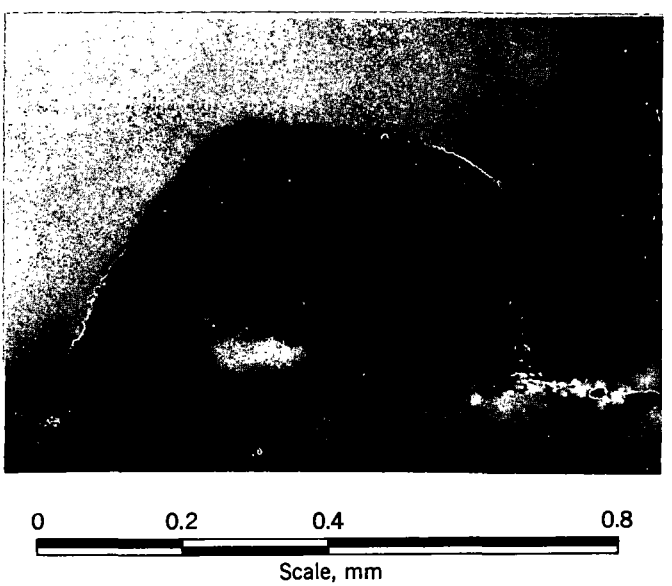

FIGURE 3. - Replica of Crater Produced by Laser Irradiation of Pittsburgh Seam (hvab) Coal.

USES OF THE MASS SPECTROMETER IN THE SPACE INDUSTRY

N.A. Mackie, C. P. Boebel
Spacecraft Department
General Electric Company
Valley Forge, Pennsylvania

INTRODUCTION:

Since the mass spectrometer is a vacuum oriented analytical instrument, one could say that this very sensitive tool was designed for use in the space industry. The vacuums of space and of space simulation chambers provide an ideal working environment for the mass spectrometer. Useful measurements which are directly provided by this instrument are leakage rates from sealed units, outgassing from materials, the quantity and quality of residual gases present in space simulators, as well as the background gases in space itself. Moreover, by using controlled leaks, the atmospheres of the various planets can be determined once spacecraft equipped with mass spectrometers are landed there.

The Missile and Space Division of the General Electric Company has used the mass spectrometer in all except the last of the aforementioned applications to some extent. Perhaps the most useful application of this instrument at General Electric has been in small vacuum chambers to determine the outgassing of materials at reduced pressure and at various temperatures.

OUTGASSING STUDIES:

Outgassing occurs as the result of the vapor pressure of dissolved gases or uncombined components becoming higher than the surrounding pressure. Consequently these dissolved gases or uncombined components volatilize. Whether some of organic's outgassing is due to vacuum destabilization of the compound is not known as yet. If this process does occur, it is certainly a secondary effect in the, relative to space, poor vacuums of small vacuum chambers.

Outgassing and sublimation can cause severe problems. The outgassing of toxic materials due to the reduced pressure in a manned spacecraft could be disasterous. For example, many of the epoxy compounds contain organic diluents and catalysts which cause severe allergic reactions in many people. If outgassing occurs in a partly enclosed electrical component, arc-over can result because the internal pressure remains higher than expected. When television camera lenses become clouded by condensed outgassed products, the image produced becomes very fuzzy and indeed, unrecognizable. Figure 1 shows the loss of resolving power caused by a condensed, degassed product. Since cloud cover or surface pictures are desired, such a loss of detail cannot be tolerated.

EXPERIMENTAL PROCEDURES AND RESULTS:

Outgassing studies were initiated at the General Electric Company to develop a list of materials which could be used on spacecraft so that the aforementioned problems are minimized. One of the vacuum chambers designed for the purpose of making outgassing studies was constructed around an automatic Recording Balance. A high speed 4" diffusion pump which is charged with Convalex-10, a polyphenyl ether pump fluid, serves as the high vacuum pump. The backing, roughing pump is filled with another diffusion pump oil, Convoil 20, as recommended by the manufacturer. Backstreaming from these oils is negligible. Pressures in the 10^{-7} torr range are quickly obtained.

The diagram, Figure 2, of the system shows the attachment of the mass spectrometer to the heater can. The sample of material under observation is usually cut or molded to a 1" x 1" x ½" shape and suspended from one arm of the balance within this can. Studies with various absorptivity/emissivity ratio materials suspended in this chamber show that the final equilibrium temperature of the material is always within 6°C of the wall of the can. In actual tests, therefore, the temperature of the wall of the can is used as the measure of the temperature of the sample.

The mass spectrometer used is a Consolidated Electrodynamics Corporation 21-611 residual gas analyzer. A 6060 gauss magnet is used with this instrument, and an additional potentiometer has been added in the scan circuit to expand the mass

TABLE 1. SPACECRAFT RADIATION ENVIRONMENT

Radiation Type	Energy Range	Penetrating Range in Aluminum, gms/cm^2	Dose Predicted in 6-Months	
			ergs/cm^2	Rads
Ultraviolet				
100 - 1,000 Å	124 - 12.4 ev	----	10^8	----
1,000 - 2,000 Å	12.4 - 6.2 ev	----	10^9	----
2,000 - 4,000 Å	6.2 - 3.1 ev	----	10^{12}	----
Protons	0.5 KEV - 1.0 MEV	~ 6×10^{-4}	3×10^6	10^{10}
	> 10 MEV	> 0.17	1.5×10^6	1.5×10^6
	> 20 MEV	> 0.58		7×10^3
	> 31 MEV	> 1.25		1.6×10^3
	> 43 MEV	> 2.3		0.15×10^3
Electrons(1)	0.1 - 6.3 MEV	0.43 avg @ 1 MEV	1.7×10^4	4×10^2

(1) Based on decay from measured 12/62 Starfish levels with an assumed 45-day half-life and a launch date of July, 1964.

Fig. 1

IMAGE DISTORTION

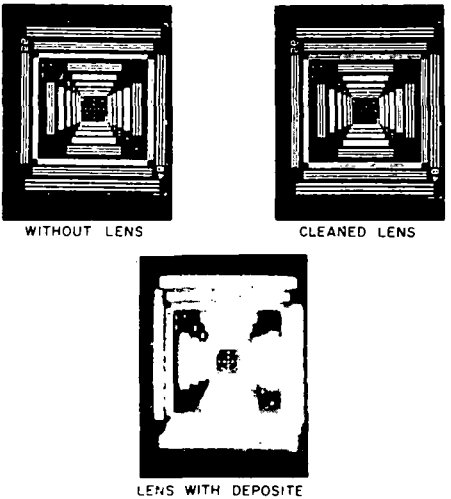

Fig. 2

ANALYTIC SYSTEM

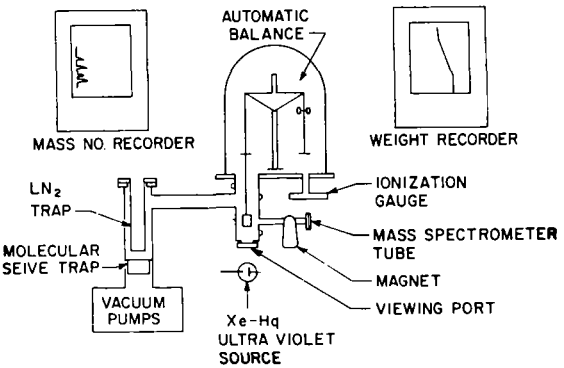

scale and facilitate low mass scanning. The time required to scan from a mass-to-charge ratio of 12 to 220 is ten minutes.

Although the mass spectrometer measures the partial pressures of the gases present in the chamber and hence the amount of each, the recording balance, which provides a record of weight loss as a function of time, is used to establish more accurately the quantity of each material present. The mass spectrometer is used to determine the relative amount of each of the desorbed gases. Then, this relative quantity is used with the total absolute weight loss to find the amount of each material lost.

Figure 3 shows a typical presentation of data. This format was chosen because it, in effect, shows the original data, the weight loss curve and the materials desorbed. Figure 4 shows a scan taken during the exposure of this material.

Using many curves similar to these, the mechanism of outgassing is being studied. As can be seen, the rates of outgassing of the various components of a material vary with time. All the data taken to date determined, perhaps during the manufacturing, proper procedures can be taken to minimize the outgassing problem. At present, a theoretical model for outgassing is in a formative stage. The model is based for the time being on internal pressures.

The interpretation of the mass spectra taken during the exposure of these samples to a thermal-vacuum environment is complicated by the fact that many components do evolve together from a given sample. There are usually two steps in the procedure used to determine what materials are represented by the mass spectra. The first step is to obtain a list of the component materials of the sample under study, and if possible, run spectra of the pure materials. The second is to notice in the long string of consecutive spectra which peaks vary in roughly the same proportions. In this way, the presence of a typical pattern, say of an amine, is pinpointed to a certain amine.

Two additional figures (5 and 6) show more of the data accumulated in this chamber. In the first figure, initial results, within the first half-hour of exposure, are shown for the relative amounts of each material lost for the various black paints mentioned. The organic compounds were grouped for convenience. One of the curves shows the typical moisture gain of a paint on exposure to atmosphere. Figure 6 summarizes some of the work done on organics to date. During these tests, a cold, $0^{o}C$ surface was held over the sample to observe whether or not any material condensed from the degassed products. In almost all cases some material did condense.

CONDENSATION OF ORGANICS:

In order to have a better correlation of mass spectral data with the amount of outgassed material which condenses on nearby optical systems, a larger vacuum chamber was used. The organic material under study was completely surrounded by a liquid nitrogen cold wall as shown in Figure 7. The arrangement used corresponds roughly to the actual arrangement of the organic materials surrounding the camera lenses of the Nimbus weather satellite. The liquid nitrogen cold wall simulates outer space, so that only outgassed products with straight line paths to the simulated lens could condense on the lens surface as would be the case in space.

A mass spectrometer was connected by means of a long (12") tube to the interior of this cryogenic enclosure. The use of such a tube complicates the measurements of the evolved gases. In an article on ion gauge characteristics in space simulation chambers, D. H. Hockeboer and D. J. Santeler described the difference in quantity measured by a tubulated ion gauge and by a nude ion gauge. Since the mass spectrometer is essentially a complicated ion gauge, several of their considerations were of use in the design of the connection to the interior of the cryogenic chamber.

Whether a measure of the emitted flux or of the emitted density was desired was an important design parameter. Of primary interest in the mass spectra measurements for this test was the length of time for the degassing to come to some constant value in addition to the density of the gases present in the chamber at any particular time. Knowing both, it may have been possible to relate the amount of condensation to the mass spectral analysis. The above-mentioned article pointed out that to sense density, the tube connecting the gauge to the chamber must be held at the same temperature as the chamber. For the purposes of this test, the chamber temperature

Figure 3 - Desorption of M&P-55

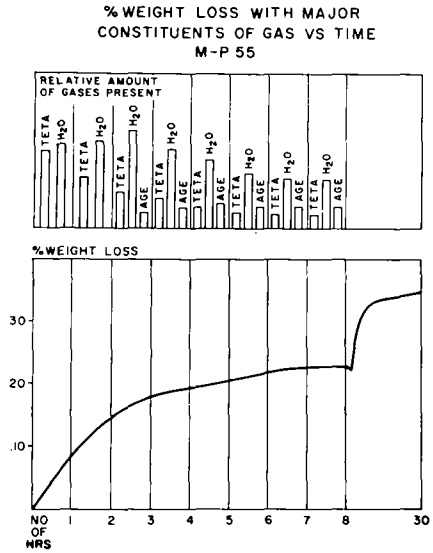

Figure 4 - Scan of M&P-55

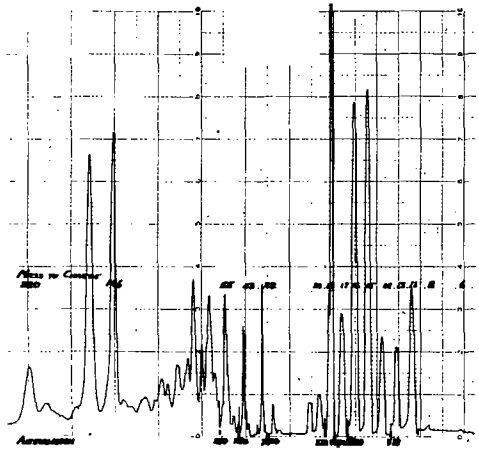

Figure 5 - Paint Desorption

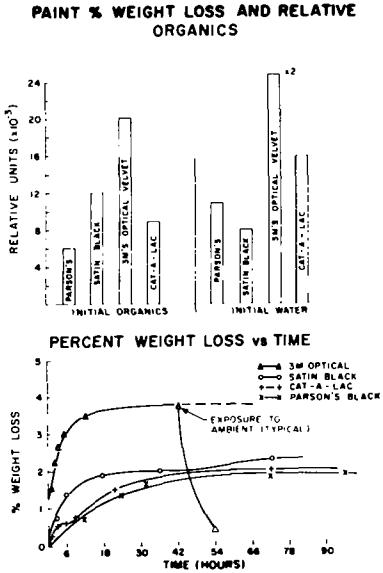

was taken as the temperature of the sample. Otherwise, the materials evolving from the organic present would have condensed along the tube before reaching the mass spectrometer. Since the molecules left the sample with approximately the sample's temperature or slightly lower, a good measure of the density of gases in the chamber should have been obtained.

The results of this test indicated that the material of the lens or the condensing surface was a more important consideration than the density of the gases present. Glass did not condense a film as readily as did potassium bromide and calcium fluoride. Later observations showed that coated lenses were more frequently coated with outgassed products than uncoated. Condensation then is a function to some extent of the crystal structure of the substrate of interest. An ionic substrate seems to serve as a better collector of condensible organics than an amorphous glass.

Since the outgassing studies in the small chambers indicated that exposure to thermal-vacuum caused materials to degas, rapidly at first and then more slowly, until a final leveling out period is reached, it was decided to degas in thermal vacuum the various spacecraft components which could be outgassed before assembling these into the final vehicle.

After assembly, the whole vehicle is evaluated for operation in large space simulation chambers. Several 39' spherical chambers, as shown in Figure 8, are available at General Electric. In these chambers thermal control, attitude control and the various sensing elements of the spacecraft are evaluated. Connected to these chambers and to other large simulation chambers at General Electric's Missile and Space Division are mass spectrometers. The instruments used include Consolidated Instruments, similar to the one described previously above, and General Electric partial pressure analyzers.

These instruments serve primarily to indicate the atmosphere within the chamber rather than to study outgassing from the vehicle. On a 10' x 24' simulation chamber a special attachment was designed to indicate as well as possible the density of particles striking the enclosed vehicles. The considerations of the ion gauge article mentioned previously were taken into account. A metal plate with 3/16" diameter holes cover the 4" intake port to the gas analyzer tube. This plate is held at the temperature of the surrounding walls simulating their pumping action. In this way, a good measure of the reflected particle density is obtained. An oven, which surrounds the whole intake port and analyzer tube and is capable of baking both at 250°C, was designed also.

This partial pressure analyzer was used to demonstrate that the lengths of cryogenic tybing used in the 10' x 24' space simulator did not leak. The total pressure in the chamber at this time was 1.7×10^{-8} torr. Liquid nitrogen was pumped through the cryogenic lines and the pressure in the lines varied from 5 psig to 70 psig by means of a pumping system. No difference in the heights of the nitrogen peaks was observed indicating that no leaks were present.

As a leak detector, both in large and small chambers, the mass spectrometer is an ideal instrument. Once calibrated by a standard leak, if corrections are made for the varying sensitivity to different molecule size, leakage rates from fuel tanks, batteries, infrared sensors and other sealed units can quickly be established. The useful life of each component can then be calculated.

To determine whether or not there was backstreaming from the diffusion pumps of the 39' space simulation chambers, sodium chloride lenses were suspended in the entrance ports of each pump. These lenses were then taken to a small vacuum chamber with mass spectrometer attached and heated to volatilize any material condensed on them. No material has been found to date eminating from the diffusion pumps. Sodium chloride lenses are used to enable infrared analysis of the deposit also. (Some people still don't trust the mass spectrometer).

Similarily, to study the outgassing properties of a completed vehicle in these chambers, small sodium chloride lenses are placed near suspected surfaces. In addition, swabs of any condensed films on the spacecraft are obtained using clean filter paper. In this way, the condensed films are traced to component materials such as silicone rubbers or to a certain paint by means of mass spectral analysis as above.

Figure 6

ORGANIC MATERIAL RESULTS

	SUBSTANCE (BASE RESIN)	TRADE NAME	PRINCIPAL FUNCTION	TOTAL EXPOSURE TIME (HRS)	OVER COAT (IF ANY)	% WEIGHT LOSS OF ORGANIC MATERIAL	MAJOR PRODUCTS	TEMP. (°F)	CONDENSATION RESULTS (IF ANY)
1	SILICONE RUBBER	RTU-60	POTTING/ ADHESIVE	32	NONE	0 38	CH_3, $S_i(CH_3)_2$	160-200	IMAGE DESTROYED
2	SILICONE RUBBER	RTU-60	POTTING/ ADHESIVE	30	MODIFIED EPOXY	0 06	WATER	160	NO EFFECT
3	SILICONE RUBBER	RTV-731	ADHESIVE	96	NONE	0 38	CH_3, $S_i[CH_3]_2$	160	IMAGE DESTROYED
4	POLYURETHANE	URALANE 241	CONFORMAL COAT	15	NONE	0 46	WATER		SLIGHT DEPOSIT
5	PHENOLIC-NYLON	91LD	HI-TEMP RESISTANCE		NONE	0 07		160	NO EFFECT
6	POLYESTER	HETRON 353	LAMINATE	21	NONE	0 25		160	IMAGE DAMAGED
7	POLYETHYLENE INSULATION	RACHEM	WIRE INSULATION	80		0 64	WATER + ETHYLENE FRAGMENTS	160	
8	PRE-BAKED INSULAT	RACHEM	WIRE INSULATION	120		0 05		160	
9	POLYSULPHIDE FORMULATION	PRC-1201Q	POTTING CONNECTORS	62		6 9	SULPHIDES	160	IMAGE DESTROYED
10	POLYSULPHIDE FORMULATION	PRC-1201Q	POTTING CONNECTORS	62	MODIFIED EPOXY	0 67	WATER CATALYST	160	IMAGE DAMAGED
11	POLYURETHANE	PRC-153B	POTTING CONNECTORS	120		0 38	50% WATER 50% CATAL	160	

Figure 7 - Cold Wall

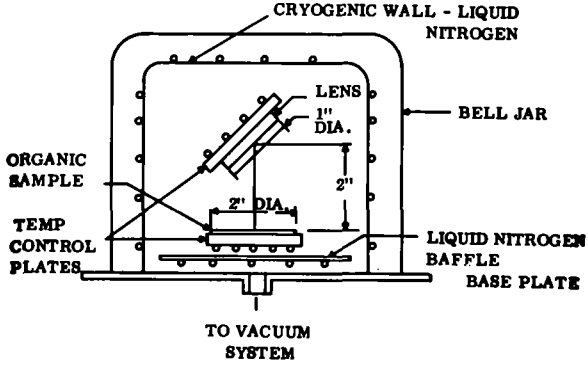

Figure 8 - 39' Chambers

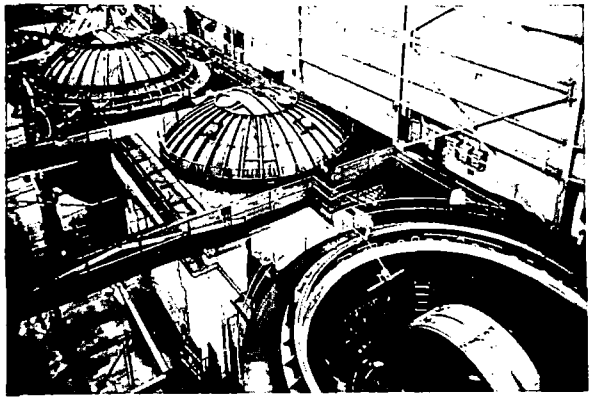

In addition to these mundane uses of the mass spectrometer, General Electric has flown a mass spectrometer as a part of the Explorer program. Others, including the Naval Research Laboratory, have also made significant contributions to an understanding of the constituents of the upper atmosphere as revealed in many publications on this subject using mass spectrometers flown on rockets.

FUTURE USES OF THE MASS SPECTROMETER

Hopefully, in the future, a more complete space simulation facility can be set up which more closely duplicates the environment shown in Table 1. A mass spectrometer attached to this facility can accurately measure the products volatilized from the material under study by any one of the radiation types. An electric barrier at the intake of this mass spectrograph tube can be used to distinguish which molecules are desorbed in an ionized state by rejecting charged particles before they enter the ionization chamber. The spectra of the neutral molecules can then be compared to the spectra of the ionized plus neutral molecules to determine the ionized molecule contribution and obtain a clearer understanding of the mechanism of radiation damage.

The authors hope to finish the outgassing model in the near future and to more fully understand some of the odd phenomenon which occur in the vacuum chambers. One of these phenomena of interest is rapid pressure burst. Mass spectra taken during these bursts indicate that they are due to carbon dioxide, but whether the burst comes from the pump fluid or from the chamber is not known. It has been observed, however, that ion gauges do produce carbon dioxide by observing the spectra with the gauges on and with the gauges off.

Such a brief paper cannot do justice to the many uses of the mass spectrometer in the space industry. Outgassing, leak detection, and residual gas studies are but a few of its uses. The mass spectrometer has been used to determine that moisture desorption was causing changes in capacitance of a thin dielectric material, that spilled tobacco was responsible for some black specs once found on a spacecraft component. Hopefully though, the wide and varied uses of the mass spectrometer in the space industry have at least been outlined.

The authors wish to gratefully acknowledge the help of John Jones, Thomas Neville and Curtis Quaintance in the preparation of this paper.

ALKANES-RECORDS OF PREHISTORIC LIFE

W. G. Meinschein
Esso Research and Engineering Company
Linden, New Jersey

Mass spectrometry has played a leading role in revealing the major structural types of biological and sedimental alkanes. Identifications of isoprenoid paraffins confirm the concept that former life has been an important source of certain hydrocarbons in sediments. Because these alkanes are probably the least altered and most widely distributed products of previous organisms, they may retain the most complete and legible records of life on earth and, perhaps, elsewhere. Alkane analyses may reveal the biochemical pathways of biologic evolution. Extensive research is a prerequisite of the full exploitation of alkanes in paleobiological investigations. Mass spectrometric analyses may provide the principal means for obtaining information about processes which control the structures and distributions of hydrocarbons in natural environments.

ANALYSIS OF SUB-MICROGRAM SAMPLES OF ORGANIC COMPOUNDS BY MASS SPECTROMETRY

R.M. Elliott, T.O. Merren and W.A. Wolstenholme.

Associated Electrical Industries Limited,
Manchester, England.

ABSTRACT

As a general means of identification of unknown organic compounds, mass spectrometry can deal with smaller quantities of sample than any other spectroscopic method. Techniques are described which extend the limit for identification to amounts in the sub-microgram range. Sufficient sensitivity is still achieved for high resolution spectra to be run and for sufficient mass measurements for structure determination to be carried out. The methods of handling such small quantities and introducing them into the ion source are described.

INTRODUCTION

Microgram quantities of organic compounds are encountered in the field of natural products during, for example, chemical degradation work and chromatographic separations, and the chemist is frequently faced with the problem of analysing qualitatively these very small quantities. It is well known that one of the main advantages of mass spectrometry for the analysis of organic compounds is that only a very small sample is required. Less than one microgram is sufficient for a mass spectrum to be run, and this applies equally to single and double focusing mass spectrometers operated at the same resolution. Furthermore, it has been shown that with a high resolution double focusing mass spectrometer at a resolution of 10,000 a considerable amount of further information including accurate mass measurements is obtainable on microgram amounts (1).

This paper describes some work carried out with sub-microgram amounts on the A.E.I. MS9 double-focusing mass spectrometer. The work was undertaken with two applications in mind, firstly identification of natural products which may be produced in minute quantities from laborious separation procedures and secondly the problem of identifying the very small amounts represented by the tails of chromatograph peaks, which are of particular interest in those cases where the peak consists of two overlapping components. The actual experiments were however more in the nature of an investigation of the technique and the limits of sample size and accuracy of mass measurement under various conditions.

EXPERIMENTAL

All the compounds examined were introduced into the ionization chamber by a direct admission technique, a particular example of the variety of systems used being shown in Fig.1. Samples were normally introduced into the re-entrant glass sample tube as a solution, usually in ethanol. With samples of this size great care was of course necessary to avoid contamination during sample loading but with reasonable precautions no trouble of this kind was encountered.

The assembly was then introduced into the ion source through a vacuum lock insertion system based on a ball valve and p.t.f.e. seals. Operation of this lock is particularly simple involving only straight line motion in one direction. A sample tube assembly could be introduced in less than 2 minutes with no

noticeable effect on the background spectrum and examination of the sample could be carried out without any further delay.

As shown in the figure the sample was evaporated directly from the glass tube into the ionization chamber through a channel immediately opposite the electron beam. In the form shown the system includes a sample tube heater. This arrangement was suitable for materials having the required vapour pressure (of the order of 10^{-6} torr) at temperatures above ambient, but controlled cooling could be used in the case of more volatile compounds.

Reduction of the background spectrum to a suitable level was achieved initially by bakeout of the whole ion source region to 200°C. Subsequently the ion source housing was kept at room temperature. In the cases examined there was no difficulty in removing traces of one compound before the next was run, but if necessary this would be achieved by bakeout of the ionization chamber. No other means was required over a period of a week to keep the background spectrum and memory of earlier samples to a sufficiently low level. The compounds studied were not particularly polar and even with the very small quantities used there was no indication of surface absorption in the sample tube.

Accurate mass measurements were carried out using the standard oscilloscope peak matching facilities of the MS9 mass spectrometer and with the instrument set for a resolution of 10,000. In all cases peaks in the spectrum of heptacosafluorotributylamine ($C_{12}F_{27}N$) were used as references for the mass measurements.

RESULTS

1. Unit Resolution Scans

Figure 2 shows a mass spectrum obtained from one tenth of a microgram of ibogaine with the resolving power set at 800. The associated blank spectrum, taken just before the sample was evaporated, is shown below the sample spectrum and is clearly insignificant. This conventional spectrum is included to show that in obtaining a good quality spectrum at unit mass resolution from a 10^{-7} gm. quantity there is a good deal in hand both in terms of signal to noise and of background.

A further 0.1 microgram sample was then used to carry out accurate mass determinations on several fragment ions. Four peaks were measured, covering a mass range of 20% and using the same reference mass for all the measurements. The results are summarised in Table I(a). The ions were all identified as containing one nitrogen atom and the observed masses were all within 10 parts per million of the calculated mass.

TABLE I. MASS MEASUREMENTS ON 0.1 MICROGRAM.

(a) Ibogaine (10^{-7} gm.)

Peak	Assigned Formula	Difference in ppm from measured mass
122	$C_8H_{12}N$	1
135	$C_9H_{13}N$	9
136	$C_{10}H_{14}N$	5
148	$C_{10}H_{15}N$	0

(b) Cholesterol (1.5×10^{-7} gm)

Peaks	Differences in ppm from measured mass
368, 369, 371, 386, 387	10, 1, 5, 4, 1 ppm.

(c) Alkaloid KA (10^{-7} gm).

Peak	Assigned Formula	Difference in ppm From measured mass
408 (parent)	$C_{28}H_{28}N_2O$	6
380 (p-28)	(i) $C_{26}H_{24}N_2O$ (p-C_2H_4)	5
	(ii) $C_{27}H_{28}N_2$ (p-CO)	7
379 (p-29)	(i) $C_{26}H_{23}N_2O$ (p-C_2H_5)	5
	(ii) $C_{27}H_{27}N_2$ (p-CHO)	6

A similar result shown in Table I(b) was obtained for 5 peaks in the parent region of the cholesterol spectrum. In this case there was little doubt as to the identity of the peaks but again the agreement between observed and calculated masses was within 10 ppm.

A more practical example is shown in Table I(c) where the sample was an alkaloid in which the presence of an aldelyde group was not certain so that the intensity and the identity of the (p-28) and (p-29) peaks would be of interest. In this case the peaks to be mass measured included doublets whose separation is 1 part in 11,000 so that a working resolution of over 10,000 was not only desirable but essential. Again a tenth of a microgram was used and all 5 observed masses agreed to within 10 ppm with the calculated values for the assigned formulae.

It should be noted the mass measurement accuracy of 10 ppm achieved in these cases is by no means the limit of the instrument and 5 ppm or even less, which may well be required in particular cases, can be achieved by taking a little more time. On the other hand, if an accuracy of 20 ppm is adequate this can be achieved for an even smaller expenditure of sample.

An even more economical use of sample is shown in the results of Table II, which demonstrates that a mass measurement of excellent accuracy can be made on one peak with as little as one two hundredth of a microgram. This is interesting in that the 225 peak, originally assigned the formula $C_{14}H_{13}N_2O$ when only a low resolving power spectrum was available, can here be shown unambiguously to have the formula $C_{15}H_{15}NO$ on this minute amount of material.

TABLE II. MASS MEASUREMENTS ON 5 MILLIMICROGRAMS

Ibogaine (5×10^{-9} gm.)

Peak	Assigned Formula	Difference in ppm from measured mass
310	$C_{20}H_{26}N_2O$	-2
310 (repeat)	"	+ 2
308 (impurity)	$C_{20}H_{24}N_2O$	+ 1
225	$C_{15}H_{15}NO$	- 2
225 (repeat)	"	- 7
136	$C_9H_{14}N$	+ 1

CONCLUSIONS

The results presented here demonstrate that a large amount of precise information including accurate mass measurements can be obtained from a fraction of a microgram, and hence that the techniques described are sufficiently sensitive for the identification of components present in a chromatograph stream at extremely low concentrations.

ACKNOWLEDGEMENTS

The authors wish to thank the Directors of Associated Electrical Industries Limited for permitting publication of this paper.

REFERENCE

(1) Barber, Craig, Elliott and Green, A.S.T.M. Mass Spectrometry Conference 1963.

FIGURE CAPTIONS

Fig.1. Inlet system for direct evaporation of small samples into the ion source.

Fig.2. (a) conventional mass spectrum and (b) corresponding blank spectrum for a 10^{-7} gm. sample of ibogaine.

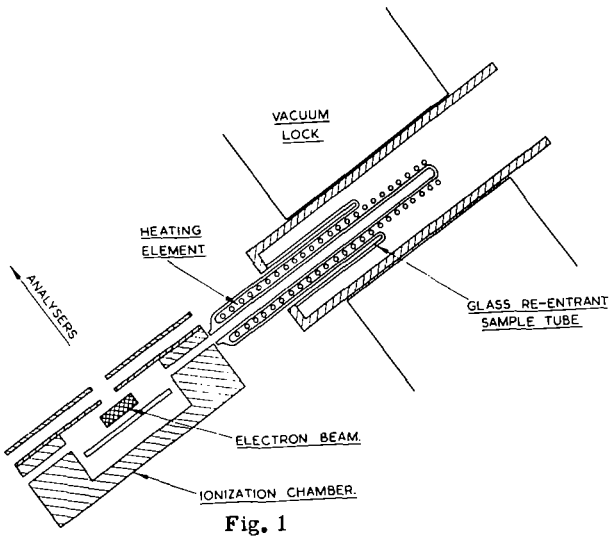

Fig. 1

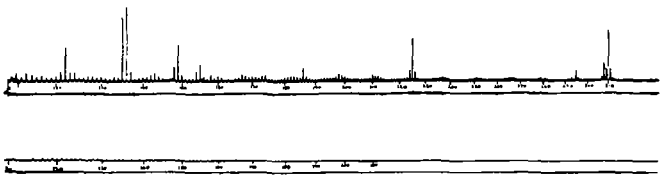

Fig. 2

Analysis of a Trinuclear Aromatic Petroleum Fraction by High Resolution Mass Spectrometry

H. E. Lumpkin
Humble Oil & Refining Company
Research and Development
Baytown, Texas

Abstract

The value of the low ionizing voltage technique for both qualitative and quantitative analyses of aromatic compounds has been repeatedly demonstrated. A difficulty of the method in the analysis of complex mixtures from petroleum with a low resolving power instrument is the ability to distinguish only seven classes of compounds. For example, alkyldibenzothiophenes cannot be distinguished from alkylnaphthalenes, as both form the same series of molecular ions in the C_nH_{2n-12} series. Thus, extensive separation by distillation and chromatographic methods are required prior to analysis. Even then, ambiguities still exist. However, when spectra are obtained at high resolving power and low voltage, these ambiguities disappear. Each molecular ion gives a separate peak, its mass can be measured, and its atomic constitution determined.

This paper describes the first use of high resolution mass spectrometry combined with the low ionizing voltage technique for the analysis of a complex mixture. Spectra recorded at these conditions from an instrument having a resolving power greater than 10,000 indicate that a series often has two and sometimes three classes of compounds at each mass. Identifications are achieved by:

1. Precise mass measurement of molecular ion.
2. Assumption of a reasonable structure.
3. Measurement of fragment ions to prove or disprove the assumed structure.

The analysis of a trinuclear aromatic fraction from the 347-360°C boiling range of a high sulfur and nitrogen crude is used as an example of these methods. In addition to the many condensed aromatic structures, a number of nonhydrocarbon molecules containing sulfur, nitrogen, and oxygen were found. A quantitative analysis for each of these types based on low voltage sensitivities is given; however, accuracy is limited to some extent by the availability of pure compounds.

Introduction

The major use of high resolution mass spectrometry has been the identification and structural determination of pure compounds, or of the major component of a single mixture. Beynon has pioneered this field and his book (1) is replete with examples of the use of this method. High resolution mass spectrometry and organic chemistry are happily joined in the excellent work of Biemann and his associates (2,3,4,8), particularly in the structural elucidation of many complex compounds encountered in natural products.

The low ionizing voltage method introduced by Field and Hastings (6) has continued to be developed in this laboratory (9,10) as well as by others (5) and is now in widespread use as an analytical technique. One of the major disadvantages of the technique when applied to complex petroleum mixtures is the ability to distinguish only seven classes of compounds. When high resolving power is available, however, this disadvantage no longer exists and the number of compound types which can be determined in admixture is limited only by the resolution and limits of detectability of the instrument. This paper describes the use of high resolution mass spectrometry with the low ionizing voltage technique for the analysis of a complex petroleum mixture.

Experimental

A sample from the trinuclear aromatic portion of a coker gas oil was selected for this study. The sample had been subjected to distillation, thermal diffusion, and chromatographic separation (Fig. 1) some years ago. Although it was not kept from contact with air during its separation, the fractions were tightly sealed during the interim periods.

A double focusing instrument having an electrostatic analyzer radius of 15 inches and a magnetic analyzer radius of 12 inches was used in this investigation. The instrument is capable of a resolution of over 1 in 10,000 and uses the Nier (12) peak matching system for mass measurement.

Table I

Summary Analysis of a Petroleum Fraction

Series	Compound Types	Wt. %
C_nH_{2n-8}	Indanothiophenes	4.2
-10	Indenothiophenes	1.8
	Indenes	0.4
-12	Dibenzothiophenes	39.7
	Naphthalenes	2.3
-14	Acenaphthenothiophenes	1.5
	Dibenzofurans	2.4
	Acenaphthenes	7.9
-15	Carbazoles	2.8
-16	Fluorenones	1.1
	Fluorenes	13.3
-18	Phenanthrenes	16.8
-20	Benzodithiophenes	2.8
	Cyclopentaphenanthrenes	3.0
		100.0

Table II

Mass Measurements in -14, -15 Series

Mol. Formula	Meas. Mass	Calc. Mass
$C_{13}H_{11}$	167.0866 ± 6	167.0861
$C_{13}H_9O$	181.0662 ± 9	181.0653
$C_{13}H_{11}N$	181.0897 ± 9	181.0891
$C_{14}H_{13}$	181.1021 ± 9	181.1017
$C_{13}H_7S$	195.0271 ± 6	195.0269
$C_{14}H_{11}O$	195.0812 ± 6	195.0810
$C_{14}H_{13}N$	195.1065 ± 8	195.1048
$C_{15}H_{15}$	195.1171 ± 6	195.1174
$C_{14}H_9S$	209.0421 ± 6	209.0425
$C_{15}H_{13}O$	209.0971 ± 10	209.0966
$C_{16}H_{17}$	209.1317 ± 10	209.1330
$C_{16}H_{14}S$	238.0816 ± 8	238.0816
$C_{17}H_{18}O$	238.1356 ± 10	238.1358
$C_{18}H_{22}$	238.1717 ± 7	238.1721

Recorded spectra of the sample were obtained at four operating modes: (1) low resolution high voltage (70 v. ionizing voltage), (2) low resolution low voltage (ca. 8 v. ionizing voltage), (3) high resolution high voltage, and (4) high resolution low voltage. Selection of parent peaks for further investigation was made from the low resolution low voltage run. However, mass measurements must be made at high resolution, and both high and low voltage spectra at high resolution were used to locate and recognize the mass desired and to select the peaks among the multiplets which were the molecular ions to be measured.

A minimum amount of low voltage sensitivity data on available pure compounds were obtained. These data indicated that the relative sensitivities among various classes of compounds was quite similar to those observed previously (10) on a 180° magnetic deflection instrument. From the sensitivity data and the high resolution low voltage scan, a quantitative analysis of the fraction was calculated by compound type and by carbon number. A summary of this analysis is given in Table I.

Discussion and Results

By far the most interesting as well as time consuming parts of the investigation were the mass measurements, calculations, and interpretations leading to the identifications of the compound types. Many mass measurements were necessary. Occasionally the instrument was noisy or the resolution was insufficient in a series of measurements and the measurements had to be repeated. Often a compound type could not be identified from its molecular formula alone and it was necessary to measure a series of fragment peaks. All of the mass measurements made in this study will not be given here; however, some selected measurements and assigned molecular formulae in the C_nH_{2n-14} and C_nH_{2n-15} series are given in Table II. These data indicate the precision of the measurements and will serve as a basis for identifications in these series, as discussed below.

The $C_nH_{2n-14,-15}$ series was one of the most interesting series of peaks in the sample. The low voltage high resolution spectra showed triplets in the C_nH_{2n-14} series at masses 224, 238, 252, 266, 280, 294. Mass measurements at 238, 266, and 294 established that the same compound types, one containing sulfur, one an oxygen, and the third a hydrocarbon, extended throughout the molecular weight range of the sample. An investigation of the fragment peaks was then necessary to establish as much structure as possible, at least to determine if the sulfur and oxygen were in side chains or in the nuclei. Mass measurements at masses 209 and 195 still revealed sulfur and oxygen; however, at mass 181 no sulfur containing ion in the series could be found. It was felt that the sulfur was in the nuclei and that a compound type of nuclear molecular weight of 196 or 210 was indicated. As the $C_{13}H_7S$ ion at mass 195 is likely due to the abundant dibenzothiophene class, the following structure was assigned to the sulfur compound type in the C_nH_{2n-14} series:

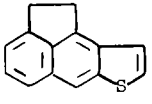

Acenaphthenothiophene
$C_{14}H_{10}S$ Mol. Wt. 210

On alkyl substitution parent peaks of 224, 238, etc. would result, the nucleus-H would give mass 209.

At mass 181 the oxygen and hydrocarbon ions were still present, but at mass 167 only the hydrocarbon ion, $C_{13}H_{11}$, was found. The oxygen compound type has been assigned as dibenzofuran. Benzofuran, an analogous 2-ring aromatic compound, was identified in a shale oil fraction by Van Meter et al. (11)

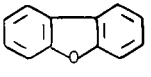

Dibenzofuran
$C_{12}H_8O$ Mol. Wt. 168

On alkyl substitution parent peaks of 224, 238, etc. would be formed, and β bond rupture would form an abundant mass 181. The absence of the mass 167 oxygen containing ion is not readily explained, but it may simply be due to low abundance.

The hydrocarbon is identified as the familiar acenaphthene.

Acenaphthene
$C_{12}H_{10}$ Mol. Wt. 154

An abundant peak due to $C_{13}H_{11}$ would be expected from alkyl acenaphthenes.

Fig. 1. Separation of a Trinuclear Aromatic Fraction.

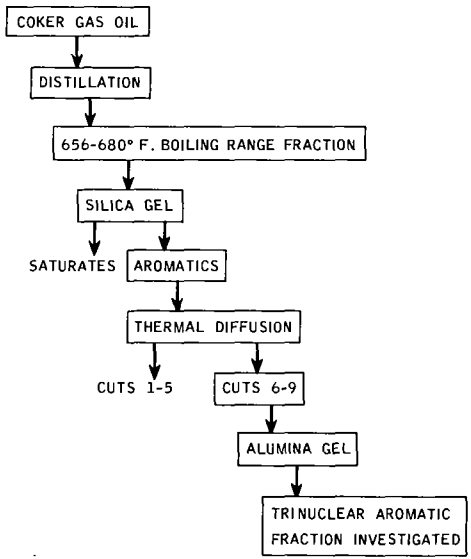

FIG. 2

HIGH RESOLUTION SPECTRA OF m/e 195

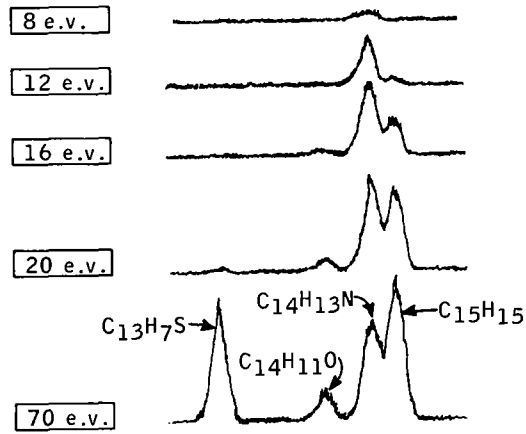

When the low voltage spectra were examined it was noted that parent peaks existed at masses 181 and 195. No combination of C, H, O, and S gives odd numbered compound molecular weights, whereas 1, 3, 5, etc. N atoms in combination with C, H, O, and S always give odd molecular weights. Mass measurements revealed a nitrogen compound type at mass 181 and 195. This leads to a proposed structure for the nitrogen compound type:

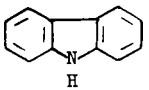

Carbazole

$C_{12}H_9N$ Mol. Wt. 167

Mass measurements made at mass 195 on the single peak still present at 8.0 e.v. showed it to be $C_{14}H_{13}N$, corresponding to ethyl or dimethyl carbazole. Helm et al (7) have shown that carbazoles are found in some crude sources.

The power of the low voltage technique in combination with high resolution is indicated in Fig. 2. At 8.0 e.v. only the molecular ion of the substituted carbazole appears at m/e 195. As the electron energy is increased, fragment ions from the other compound types appear in order of increasing appearance potential, until at the normal 70 volts, four peaks due to the sulfur-, oxygen- and nitrogen-containing, and the hydrocarbon molecules are seen.

Conclusions

High resolution mass spectrometry is applicable to complex mixtures. In combination with low ionizing voltage operations, 14 classes of compounds have been identified and determined in admixture in a separated petroleum sample. These include six hydrocarbon, five sulfur, two oxygenated, and one nitrogen compound types.

Literature Cited

1. Beynon, J. H., "Mass Spectrometry and Its Application to Organic Chemistry," Elsevier Publishing Co., Amsterdam, 1960 and references cited therein.

2. Biemann, K., Ann. Rev. Biochem. 32, 755-80 (1963).

3. Biemann, K., Bommer, P., Burlingame, A. L., and McMurray, W. J., Tetrahedron Letters 1963 (28), 1969-73.

4. Bommer, P., McMurray, W., and Biemann, K., J. Am. Chem. Soc. 86 (7), 1439-40 (1964).

5. Crable, G. F., Kearns, G. L., Norris, M. S., Anal. Chem. 32, 13 (1960).

6. Field, F. H., Hastings, S. H., ibid. 28, 1248 (1956).

7. Helm, R. V., Latham, D. R., Ferrin, C. R., and Ball, J. S., ibid. 32, 1765 (1960).

8. De Jongh, Don C., Biemann, K., J. Am. Chem. Soc. 86 (1) 67-74 (1964).

9. Lumpkin, H. E., Anal. Chem. 30, 321 (1958).

10. Lumpkin, H. E., Aczel, Thomas, ibid. 36, 181 (1964).

11. Van Meter, R. A., Bailey, C. W., Smith, J. R. Moore, R. T. Allbright, C. S., Jacobson, I. A., Jr., Hylton, V. M., and Ball, J. S., ibid. 24, 1758 (1952).

12. Nier, A. O., "Nuclear Masses and Their Determination" (Hintenberger, H., ed.), pp. 89-102, Pergamon Press, 1959.

Techniques in the High-Resolution Mass Spectrometry of Complex, Polyfunctional Organic Molecules

P. Bommer, W. McMurray and K. Biemann
Department of Chemistry, Massachusetts Institute of Technology
Cambridge, Massachusetts

During the past two years we have been concerned with the elaboration of techniques that would enable us to apply high resolution mass spectrometry to the solution of structural problems in organic chemistry. Due to the nature of these problems the research effort has to be directed toward the chemistry of the compounds and the interpretation of their spectra. The actual determination of the spectra should, therefore, be a reliable routine procedure leading to dependable, accurate data with a minimum amount of time spent on the adjustment of the instrument and repetitive attempts to get all the necessary data. One must remember that in this field frequently very little is known about the nature of the compound, its volatility, thermal stability, molecular size or important features of the mass spectrum. Not infrequently only very small amounts of substance, which may not even be highly purified, are available. For these and other[1] reasons, it is also important to determine the entire mass spectrum with the highest possible resolution in order to have available for the interpretation all data that can possibly be of importance.

Some results obtained[2] in the course of the determination of the structure of the alkaloid vinblastine will be discussed as an illustration. One of the major problems is the molecular size and complexity of this alkaloid, which in addition proved to be thermally labile and it was thus important to obtain a high resolution mass spectrum immediately at the beginning of its vaporization. As we use in our work a CEC 21-110 mass spectrometer, which is a Mattauch-Herzog type instrument that focuses all the ions simultaneously in one plane. With a photographic plate placed at the focal plane it is possible by taking consecutive exposures to obtain mass spectra showing the progress of the thermal transformation of the sample, which is important in order to be able to determine the nature of this process. For the interpretation, the accurate mass of a few hundred lines in these spectra are measured and a very small number of them are shown in Fig. 1. The line at 810 was a rather intense one in this exposure while those at 824 and 838 increased in the consecutive exposures at the expense of mass 810. Considering the differences in elemental composition, one sees the reaction taking place is a homologization due to selfalkylation of the molecules. The elemental composition of the species of mass 810 requires the formula $C_{46}H_{58}N_4O_9$, the calculated mass of which differs only by 1.5 millimass units (mmu) from the found one. Further details of the arguments, both chemical and mass spectrometric, which led to the final establishment of this structure are published elsewhere[2,3].

It should be noted that the determination of the elemental composition of this alkaloid was only possible by high resolution mass spectrometry and that the determination of masses in this range with an accuracy of 1 to 2 millimass units is possible. In order to achieve this it was, however, necessary to develop both sampling and measuring techniques and to test their reliability. With this and other problems encountered in our laboratory, it is particularly convenient to obtain the data in the form of a permanent record on the photographic plate and to be able to do this with a minimum amount of sample. In order to run such spectra it was necessary to modify the sample introduction system to permit introduction of the samples directly into the ion source and secondly, to develop a fast method to check and to adjust the resolution. Figure 2 shows a cross-section of the ion source with the introduction probe. The substances are brought directly into the ion source with a heatable probe from the left side of the source housing whereas more volatile substances and the calibration compound are introduced through a

conventional leak from the right. For the introduction of the sample the vacuum-lock is evacuated and after opening the ball-valve the probe with the sample can be pushed into the ion source. The whole procedure takes less than two minutes. The sample tube heater consists of a metal tube wrapped with heating wire. Just behind the sample tube, usually a glass capillary, sits the thermocouple for measuring the actual sample temperature.

To adjust and control the resolution for optimum performance we required a fast, repetitive scanning over a small mass range. Therefore the instrument was equipped with a scanning-system driven by a sawtooth generator as shown in Figure 3.

A sawtooth voltage, produced by a commercially available waveform generator (Tektronics) is superimposed to the d.c. voltage of the electric sector, which is already coupled with the acceleration-voltage. By varying the amplitude of the sawtooth voltage it is possible to sweep all masses within a region of 0.05% to 1% of the mass range. During each cycle a part of the ion beam is swept across the collector slit in front of the electronmultiplier. This signal is fed to the Y-axis of the oscilloscope which is triggered horizontally by the same sawtooth signal. By observing the line width and intensity of the peak or peaks displayed on the scope, one can adjust the instrument for maximum resolution and intensity. This modification made it possible to tune the instrument within a very short time and just before the spectrum is taken.

All spectra are run as a mixture of the calibration compound and the sample. In this manner the lines of known mass are by definition in the correct relationship with the sample lines which would be less reliable if the two compounds were introduced consecutively. It should be kept in mind that due to the high resolving power there is hardly any interference between compound spectrum and calibration spectrum if the calibration compound has a very different composition. To run a spectrum one adjusts the magnetic field to monitor with the Electronmultiplier a calibration ion, which is at least 15% heavier than the expected molecular ion of the sample. The reason for this difference is the distance between the high-mass end of the photographic plate and the collector slit. This signal is used for the final tuning of the instrument. In general, maximum intensity corresponds to best resolution. During the actual exposure the sawtooth sweep is turned off but the calibration ion beam is continued to be centered on the collector slit; in other words one sits on the top of the peak and monitors it with the scope. If the focus conditions should change during the sample introduction, the intensity of the ion beam focused on the collector slit and thus the signal on the scope would decrease. In this case the focus settings can quickly be corrected to restore maximum intensity and resolution.

Generally 3-4 exposures are taken, the time varying from five seconds to five minutes. These techniques permit us to run routine spectra with a resolving power of 1:20.000 in a reasonable amount of time. On a single plate we thus record a total of up to 29 spectra covering an average of five compounds. Each spectrum to be measured consists of a few hundred lines. Their reliable and speedy measuring requires a rather sophisticated system, which permits digital recording of all line positions and their densities directly on IBM cards. Besides the speed, the system outlined in Figure 4 avoids any manual notations of the data. For measuring the distances between the lines we use a commercially available comparator equipped with a line sensing device (Gaertner, Chicago). The precision screw is connected to an encoder which allows automatic printout of the distances to an accuracy of 0.5 microns. To measure the intensity of the line we mounted a photomultiplier of a Quantalog densitometer on the screen of the comparator which is also connected to an encoder. Both encoders feed an IBM-punch and depressing a single button prints positions and intensity on the card. With this system it is possible to measure an entire spectrum within about half an hour to two hours. The data obtained are still to be converted to accurate mass and elemental composition and this is conveniently done with a computer.[4]

Mass Found	Error (millimass units)	Composition of Ion	Elements lost (from mass 810)
838.4538	+2.4	$C_{48}H_{62}N_4O_9$	
824.4372	+1.2	$C_{47}H_{60}N_4O_9$	
811.4234	-0.3	$C_{45}C^{13}H_{58}N_4O_9$	
810.4219	+1.5	$C_{46}H_{58}N_4O_9$	
752.4153	+0.4	$C_{44}H_{56}N_4O_7$	$C_2H_2O_2$
751.4080	+1.0	$C_{44}H_{55}N_4O_7$	$C_2H_3O_2$
750.4014	+2.2	$C_{44}H_{54}N_4O_7$	$C_2H_4O_2$
651.3906	-0.5	$C_{40}H_{51}N_4O_4$	$C_6H_7O_5$
650.3858	+2.6	$C_{40}H_{50}N_4O_4$	$C_6H_8O_5$
591.3723	+2.6	$C_{38}H_{47}N_4O_2$	$C_8H_9O_7$
154.1219	-1.3	$C_9H_{16}NO$	$C_{37}H_{42}N_3O_8$

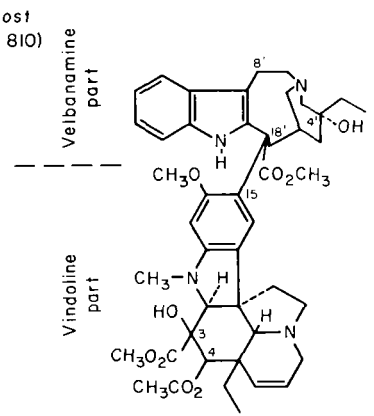

Fig. 1. Mass measurements on Vinblastine.[2]

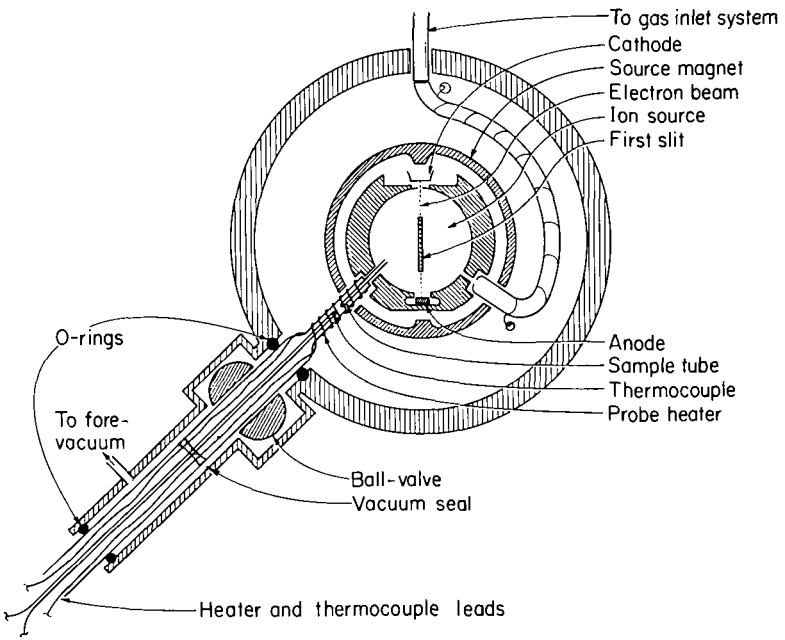

Fig. 2. SAMPLE INTRODUCTION SYSTEM

Acknowledgement: This work was supported by grants from the National Science Foundation (G-21037) and from the National Institutes of Health, Public Health Service (GM-09352).

References

(1) K. Biemann, W. McMurray and P. Bommer, Twelfth Annual Symposium on Mass Spectrometry, Montreal, June, 1964.
K. Biemann, P. Bommer and D. Desiderio, Tetrahedron Letters, No. 26, 1725 (1964).

(2) P. Bommer, W. McMurray and K. Biemann, J. Am. Chem. Soc., 86, 1439 (1964).

(3) N. Neuss, M. Gorman, W. Hargrove, N.J. Cone, K. Biemann, G. Buchi and R.E. Manning, J. Am. Chem. Soc., 86, 1440 (1964).

(4) D. Desiderio and K. Biemann, Twelfth Annual Symposium on Mass Spectrometry, Montreal, June, 1964.

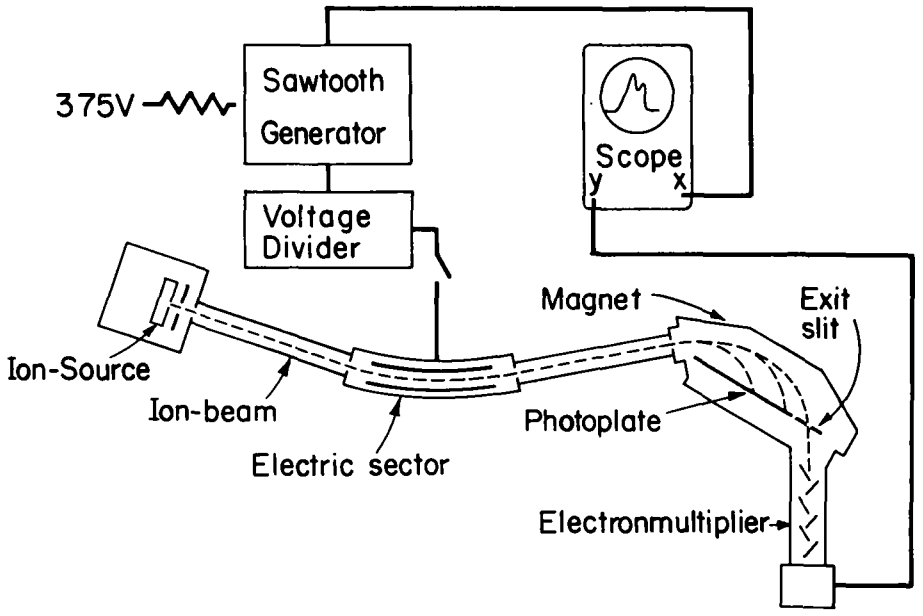

Fig. 3. ELECTRIC SCANNING SYSTEM

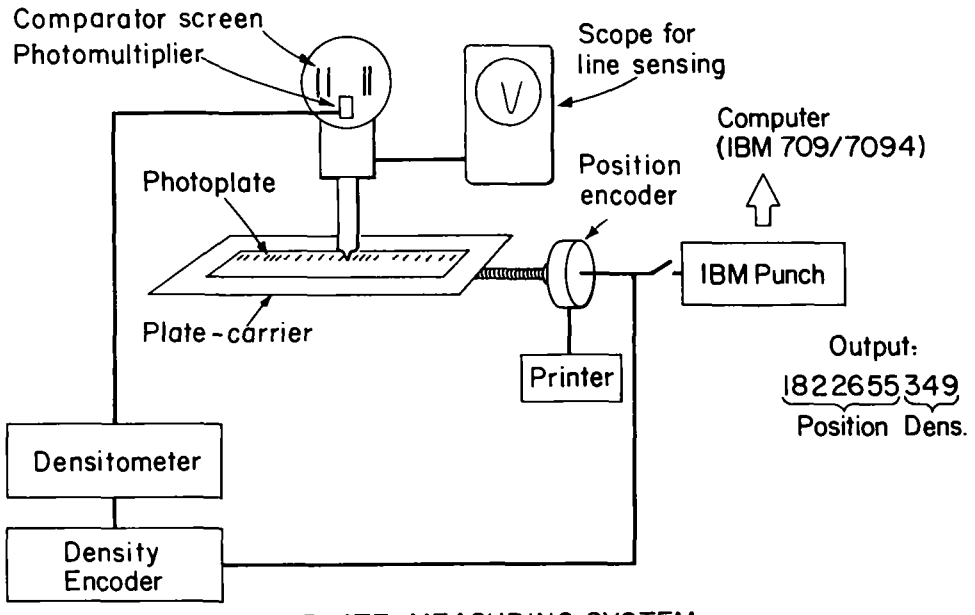

Fig. 4. PLATE-MEASURING SYSTEM

Computer Techniques for the Fast and Facile Conversion of Line Positions to Elemental Compositions of Ions Recorded on Photographic Plates

D. Desiderio and K. Biemann
Department of Chemistry, Massachusetts Institute of Technology
Cambridge, Massachusetts

Both the conversion of line positions into accurate masses as well as the correlation of the latter with the corresponding elemental composition of the ion are very simple mathematical operations. If required only occasionally, the masses could be calculated with a desk calculator and the elemental compositions could be looked up in Beynon's tabulation[1] or arrived at by one of the short cut methods recently published by Kendrick[2] or by Reid[3]. Anyone who has even tried to do this for more than a dozen of ions at a time will have realized how time consuming and tiring such a process is, not to mention the unavoidable errors associated with writing down large numbers.

As mentioned elsewhere[4] we have developed a system that permits to routinely measure not only dozens but a few hundred lines per spectrum but it soon became obvious that only a computer can handle this amount of data within a reasonable time. The problem is thus to convert these data, namely position and density of all lines regardless whether due to the sample itself or the calibration compound to the desired data, the elemental composition of the ions due to the sample only. Since the entire mass calculation is relative, at least two known masses have to be specified.

The individual steps involved in accomplishing this aim are as follows. First, one needs a set of calibration lines spread over the entire plate and spaced 12-20 mass units apart, a distance which we found to be sufficiently small to permit accurate results for the masses inbetween. Second, all masses are to be calculated; third, the lines due to the calibration compound are sorted out because their composition is known; fourth, all possible combinations for all compound lines are calculated within certain, narrow, specified limits (3-5 mmu.). In this process, a differentiation is made between singly and doubly charged species. Fifth, and finally, it is important to be able to rely on the obtained data, and thus, continuous checks are made in the various procedures and for deviations in the original data.

A FORTRAN program was written which achieves this and it is represented by the Flow diagram shown in Figure 1.

The primary data (positions and intensities) are read into the computer. Employing the two calibration masses manually identified at the low mass end, the intervening line positions are converted to the corresponding masses by a linear interpolation of the square root of the mass-to-charge ratio versus their distance along the photographic plate.

For each mass thus calculated, all of the possible elemental combinations are then compiled. This continues until no more lines are left between these two calibration lines.

At this point the mass of the lines beyond the second calibration line are calculated. This involves now extrapolation, which is not sufficiently accurate to produce final data but is certainly good enough to identify a line whose mass comes close to one of a set of previously specified calibration masses. Once this had been done, the accurate mass of all intervening lines is calculated and each one is checked against a list of additional masses arising from the calibration compound. If the two masses differ by less than 5 mmu., the line is stored for later print-out. If the calculated mass is not identical with the known mass, the fractional part of the mass is checked to see if it lies within the range 0.500-0.800. If so, then the calculated mass must be a doubly-charged ion and it is thus first multiplied by two before calculating its elemental composition. All other masses are

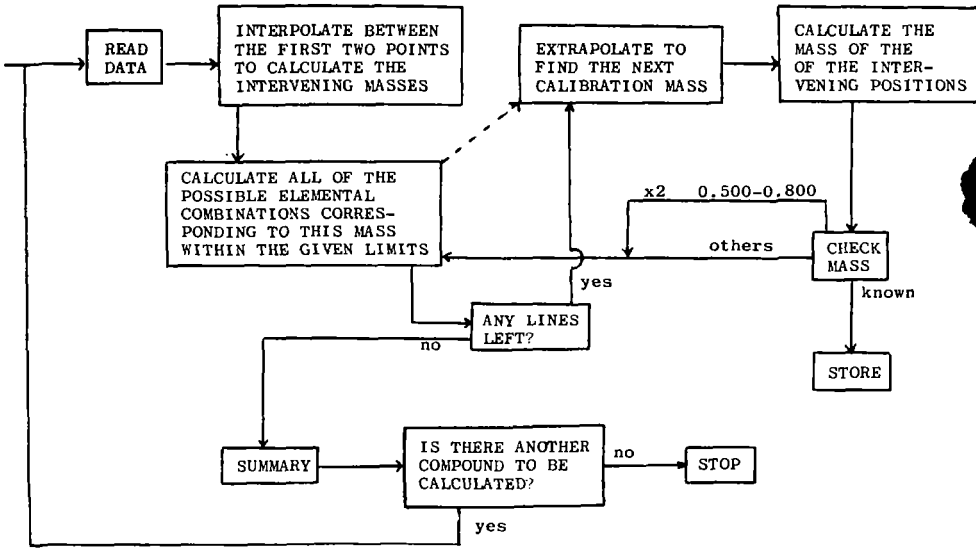

Fig. 1. Flow diagram of FORTRAN program for conversion of line positions to elemental composition.

VOACANGINE 145-25-2

MAXHET= 5 C-13= 2 N-14= 2 O-16= 3

A	B	DIFF	V	W	SLOPE	EXTRAP
216.98880	230.98560	-2.74	132.18400	141.72100	0.04903751	168.20927238

INT(ESTM)	DIST	DETM	CALC	ERROR	C12/13	H	N	O
**	135.6965	222.09295	222.09551	-2.57	14/2	12	0	1
			222.09189	1.05	15/0	12	1	1
			222.09149	1.45	9/2	12	2	3
*****	137.0720	224.10791	224.10754	0.37	15/0	14	1	1
			224.10714	0.77	9/2	14	2	3
*****	137.7340	225.08092	225.08260	-1.68	13/2	11	0	2
			225.07898	1.94	14/0	11	1	2
****	137.7550	225.11182	225.11089	0.93	14/1	14	1	1
***	138.4155	226.08479	226.08680	-2.01	14/0	12	1	2
			226.08233	2.46	13/1	11	1	2
**	138.4425	226.12461	226.12681	-2.21	14/2	16	0	1
			226.12319	1.42	15/0	16	1	1
			226.12727	-2.66	10/1	17	2	3
			226.12279	1.82	9/2	16	2	3
**	139.1015	227.09755	227.09825	-0.71	13/2	13	0	2
			227.09463	2.91	14/0	13	1	2
****	140.4610	229.11128	229.11390	-2.62	13/2	15	0	2
			229.11028	1.00	14/0	15	1	2

Fig. 2. Part of the computer-output for the alkaloid voacangine.

considered singly-charged ions of the sample and all of the possible elemental compositions for these masses are then compiled.

Two approaches could be considered for finding all possible combinations of elements that fit a certain mass: one could calculate all conceivable combinations once and put them on a tape which is searched by the computer, or, one lets the computer add the mass of atoms in all possible combinations, check each against the obtained mass, store those that fit within the desired limits but drop those which do not. This process must then be repeated from scratch for the next line.

We are using the second of the two approaches which is surprisingly fast, much more flexible, and avoids the calling for individual tapes. The sequence involves first checking the minimum number of carbon atoms ($\underline{n}$) possibly present without exceeding the value of $2\underline{n}+3$ for $\underline{m}$ (to account for protonated species), followed by increasing $\underline{n}$ by 1 until the sum of C exceeds the determined mass. At each point it is checked whether the difference between the sum of the carbon atoms and the obtained mass is divisible by the atomic weight of hydrogen. In the steps that follow one heteroatom after the other is first subtracted from the determined mass and the remainder is processed for C and H as mentioned before. ^{13}C is checked after each such sequence.

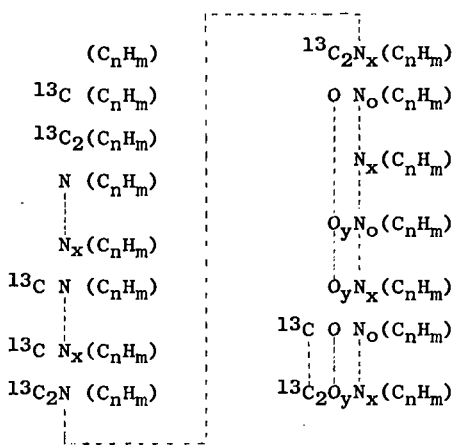

The sequence depicted above can be extended at will to any number of atoms of up to 20 different elements. Based on our experience during a year of use we found it safest to search for all compositions that fit within ± 3 mmu below mass 500 and ± 5 mmu. above that. Hardly any of our mass determinations were found to exceed this range.

Figure 2 shows part of the output of the computer, listing a small part of the results for the alkaloid voacangine. In the first column is found a logarithmic representation of the optical density of each line as denoted by the asterisks. Next is listed the line position (the original piece of data) followed in the third column by the mass corresponding to this line position, obtained by interpolation between A and B. The actual mass of the composition shown in the columns headed C12/13 H N O is listed in the fourth column, and the difference in millimass units between the theoretical and the determined mass is listed under "error".

After all of the masses and their corresponding elemental compositions have been calculated for all of those lines falling between the two calibration points, a check is made to see whether any other lines are present (see Figure 1). If more lines remain to be calculated, the next calibration mass is found by extrapolation and the loop is repeated. If there are no more lines a summary of various crucial values determined and used by the computer is printed and it then checks whether another compound is to be calculated. If there is one the new data is read in and the entire cycle is followed through again. After

SUMMARY

VOACANGINE 145-25-2

JELEM= 4 MAXHET= 5 ATOM(1)=C12 ATOM(2)=H PROGRAM 6.35

TITLE	LIM	JH	HET	AT.WT.
C-12	100	2	0	12.000000
H	200	0	0	1.007825
N-14	2	1	1	14.003074
O-16	3	0	1	15.994915

DENSITY FACTOR= 10

A	B	DIFF	V	W	SLOPE	EXTRAP	DIFSLO
142.99200	154.99200	0.	75.58350	85.62700	0.04895225	168.69381	0.
154.99200	166.99200	-2.11	85.62700	95.28700	0.04896069	168.65002	0.84
166.99200	180.98880	-3.55	95.28700	106.12300	0.04897281	168.58471	1.21
180.98880	192.98880	-6.45	106.12300	115.07900	0.04899878	168.43907	2.60
192.98880	204.98880	-3.71	115.07900	123.75800	0.04901360	168.35336	1.48
204.98880	216.98880	-3.57	123.75800	132.18400	0.04902797	168.26774	1.44
216.98880	230.98560	-2.74	132.18400	141.72100	0.04903751	168.20927	0.95
230.98560	242.98560	-3.40	141.72100	149.66750	0.04905114	168.12320	1.36
242.98560	254.98560	-5.59	149.66750	157.41650	0.04907385	167.97607	2.27
254.98560	266.98560	-1.99	157.41650	164.98400	0.04908162	167.92457	0.78
266.98560	280.98250	-7.41	164.98400	173.59450	0.04910733	167.75034	2.57
280.98250	292.98240	-3.65	173.59450	180.80500	0.04912227	167.64649	1.49
292.98240	304.98250	-2.42	180.80500	187.86800	0.04913201	167.57741	0.97
304.98250	316.98250	-5.71	187.86800	194.79000	0.04915548	167.40767	2.35
316.98250	330.97930	-0.54	194.79000	202.70000	0.04915730	167.39427	0.18
330.97930	342.97920	3.05	202.70000	209.35100	0.04914465	167.48953	-1.26
342.97920	354.97930	1.39	209.35100	215.88750	0.04913893	167.53351	-0.57
354.97930	366.97930	-2.46	215.88750	222.31300	0.04914939	167.45182	1.05
366.97930	380.97600	-0.56	222.31300	229.67600	0.04915153	167.43476	0.21

Fig. 3. Summary of important data fed into (e.g. atomic weights) or produced by (calibration lines) the computer.

the last compound, the program stops.

Part of the summary (Figure 3) lists for example, all the data involved in the extrapolations for finding the calibration masses. The first entries (142.9920 and 154.9920) show the first two calibration masses which are the only ones whose line positions had been identified by the operator while all others were found automatically by the computer; the second line shows the calibration mass (166.9920 of distance 95.2870) found by extrapolation using the first two points. Thus, using two points differing by 12 mass units, and extrapolating over 12 more mass units, the computer recognizes that line position due to the previously read-in accurate mass. The difference between this theoretical mass and the determined mass is -2.11 mmu. A ± 20 mmu. range is allowed to find the calibration masses. If no mass is found within this range the calculation would terminate, because this could only be the case if a calibration line measured incorrectly or not at all. Also, the difference in slope between this group and the previous group is found to be 0.0000084 (0.84×10^{-5}), a value well within the accuracy needed. If a slope would result which differs from the preceding one by more than 0.000050, then it would give rise to such a deviation that the next line found by extrapolation would be the wrong one and all the following mass calculations would be grossly incorrect. Thus, if DIFSLO exceeds 5.0, the calculation also stops.

Another check is made by comparing the masses found for the approximately 300 lines due to the calibration compound. These data serve as a check on the reliability of final line measurements and thus of the results. Since these masses are calculated in exactly the same manner and using exactly the same calibration data as the compound lines, the accuracy of the mass of the compound ions must be of the same order of magnitude as those of the ions of the calibration compound.

This computer program thus enables one to get all the final results directly in printed form. It requires only the measuring of one line line after the other on the comparator, without having to distinguish the lines of the sample from those of the calibration compound, or to recognize or identify any line but two, or to keep track of the mass scale during the measurement. If anyone of these operations would be necessary, the process would be too cumbersome to permit processing a large number of spectra routinely.

The volume of data involved in a single spectrum is revealed by the following example.

The measurement of all the 395 lines in a typical spectrum of a compound of molecular weight in the order of 400 took about one hour. 286 of these lines were found by the computer to be due to the sample and 109 to the calibration compound perfluorokerosene. For only 4 no elemental composition was found within the specified limits, when considering all compositions up to $C_{100}H_{200}N_2O_4$. The entire calculation took the IBM 7094 only 1.84 minutes.

Acknowledgement: The authors are indebted to the M.I.T. Computation Center for the use of the facilities.

References

(1) J.H. Beynon and A.E. Williams, "Mass and Abundance Tables for Use in Mass Spectrometry", Elsevier Publishing Company, Amsterdam, 1963.

(2) E. Kendrick, Anal. Chem., 35, 2146 (1963).

(3) W.K. Reid, W.L. Mead and A.R. West, Anal. Chem., 36, 1140 (1964).

(4) P. Bommer, W. McMurray and K. Biemann, Twelfth Annual Symposium on Mass Spectrometry, Montreal, June, 1964.

High-Resolution Mass Spectra of Compounds Emerging from a Gas Chromatograph

J.T. Watson and K. Biemann
Department of Chemistry, Massachusetts Institute of Technology
Cambridge, Massachusetts

The direct combination of a gas chromatograph with a conventional single focusing mass spectrometer has been used successfully in a number of laboratories.[1] The most sophisticated version of this principle may be the one recently described by Ryhage.[2]

Since the problems being investigated in our laboratories are concerned with somewhat more complex molecules such as amino acids, alkaloids, carbohydrates and steroids and are sometimes of unknown structure, we have explored the feasibility of obtaining complete high resolution mass spectra of compounds of this type while emerging from the gas chromatograph.

The most critical part in any such combination is the pressure reduction system connecting the gas chromatograph with the mass spectrometer. We are using an all glass pressure reduction system to keep the surface area small and free of metal to avoid catalytic decomposition of the more sensitive compounds. Figure 1 shows the apparatus[3] which involves a fritted glass tube instead of the metal valve generally used[1] to pump off the excess carrier gas (dimensions of orifice, porosity and performance differ somewhat from the earlier version[3]). The ultrafine porosity of the tube has the additional effect of permitting the helium carrier to be removed at a higher rate (due to preferential effusion) than the eluted sample. This results in the enrichment of sample in the remaining gas stream passing through a capillary constriction into the ion source of the spectrometer.

The magnitude of the enrichment has been found to be 50 times for diethyl ether (mol. wt. 74) and up to 200 times for perfluorokerosene which has an average molecular wt. of $\sim$800.

The opening of the pressure reduction system toward the gas chromatograph is a capillary restriction of about 0.1 mm. and accepts gas at $\sim$20 ml/min. when a good mechanical pump is connected to the evacuation jacket around the fritted glass tube.

The entire system is capable of being heated to 300-325°C before and 150°C after the second capillary orifice. The entire (longer) glass tube is mounted in a metal case. The part containing the pressure reduction system is placed in a cylindrical oven while the longer capillary fits into the vacuum lock of the spectrometer which is otherwise used to introduce samples directly into the ion source as was discussed earlier. By virtue of the vacuum lock arrangement it is possible to insert the pressure reduction system into the ion source of the spectrometer without venting it when one plans to use it in connection with the gas chromatograph.

The recording of the complete high resolution mass spectrum presents a particular problem as very fast scanning during the very short time of the emergence of the fraction from the gas chromatograph is incompatible with a consistent high resolution mass spectrum suitable for accurate mass measurement. The photographic plate that can be used in a Mattauch-Herzog type mass spectrometer permits one, however, to instantaneously and simultaneously record the entire spectrum in a quality that enables one to determine the masses of all the ions with almost the same accuracy as if the spectrum would have been obtained on a stationary sample. In addition, the disturbing effect of the change in sample concentration associated with gas chromatographic fractions is also eliminated, and a calibration compound can be fed continuously through the inlet system of the spectrometer to provide the mass standards necessary for the mass determinations to be performed later.

After the fraction is recorded, the plate can be moved about 1/30 of its usable height and the next fraction recorded. The result is shown in Figure 2. At the top is the gas chromatogram of an amino ester mixture during which 21 exposures were taken. These exposures consist of the mass spectra of both the background and the fraction. The ever-present calibration compound (perfluorokerosene) produces a microscopically visible mass scale as indicated on the bottom of the slide. The fifth exposure represents the mass spectrum of alanine ester, the sixth is background, the seventh glycine ester, etc. up to exp. 22 which is phenylalanine ester. The black line (at exposure 13) is always spoiled during the tuning procedure. The black spots are due to a strong ion beam that was on inadvertently for a few hours before starting the experiment.

The positions of the lines are then measured and the accurate masses calculated using the computer program discussed earlier.[4] Part of the results obtained with methionine ester (exposure #20) is shown in Figure 3.

At the top is shown for comparison a conventional mass spectrum[5] of methionine ethyl ester. Below is tabulated part of the high resolution data, namely just 20 lines of approximately 300 that had been measured from this single spectrum representing one gas chromatographic fraction. The elemental composition deduced from these accurate mass measurements which agree with the theoretical value by the amount in m.m.u. stated in parentheses confirms the correctness of the earlier interpretation of the low resolution mass spectrum. The photographic plate reveals, however, the multiplicity of many of the peaks and some of the examples are listed here, such as mass 56, 74 and 116. As an example, the origin of the two components of mass 116 is suggested to be the following.

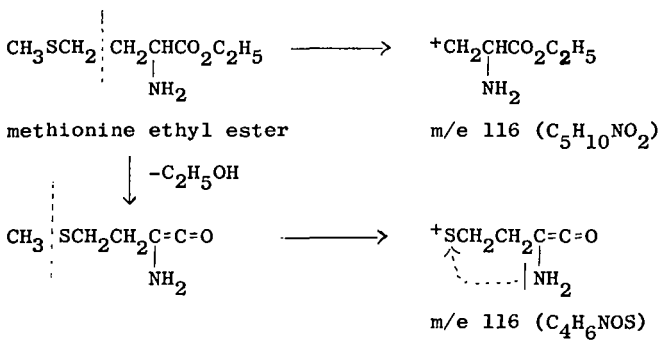

The sulfur free ion containing two oxygens and one nitrogen is due to cleavage of the bond between these two carbon atoms while the sulfur containing component seems to arise from the species at mass 131 which is due to loss of ethanol from the molecule followed by loss of the methyl group attached to sulfur.

It would be beyond the scope of this paper to go into some other interesting aspects of those few peaks listed on the previous slide, let alone the many others which were determined but not listed. The small fraction discussed here gives, however, an idea of the vast amount of data that is permanently recorded on the small piece of glass plate, which can contain 28 other spectra, in addition to the one discussed.

The information retained on the photographic plate can be represented in still another way.[3] In taking an automatic densitometer recording of an exposure, one obtains a trace which more closely resembles a conventional mass spectrum while still indicating the multiplicity of certain peaks. The superposition obtained by recording one densitometer scan (sample plus mass standard) on top of the next one (mass standard only) allows one to more easily distinguish peaks due to

the sample and those of the standard. Multiplets are clearly discernible if necessary at a slower densitometer speed which resolves them much better.

The simultaneous recording of the entire mass range on the photographic plate opens the possibility for recognizing the spectra of the components of an incompletely resolved gas chromatographic peak. If one constantly moves the plate during the exposure the spectra overlap in such a way that the slightly later fraction shows its lines slightly displaced vertically. If this is done a line that is missing at the top gradually appears toward the bottom of the exposure, i.e. at a later time of the exposure. The line position of such lines can still be measured with good accuracy. By measuring the line positions at the top as well as the bottom of this portion of the plate one can obtain the high resolution mass spectrum of both components.

It is hoped that this brief discussion of a few examples has illustrated the fact that high quality data can be obtained by direct connection of a gas chromatograph with a double focusing mass spectrometer. This technique may find its application when one deals with a compound whose more complex structure may defy quick identification based on a fast scanned conventional mass spectrum, but requires high resolution data for the solution of the problem.

Acknowledgement: The high resolution mass spectrometer used in this work was obtained with grants from the National Science Foundation (G-21037) and from the National Institutes of Health, Public Health Service (GM-09352).

References

(1) For references see those cited in (2) and (3).

(2) R. Ryhage, Anal. Chem. 36, 759 (1964).

(3) J.T. Watson and K. Biemann, Anal. Chem. 36, 1135 (1964).

(4) D. Desiderio and K. Biemann, Twelfth Annual Symposium on Mass Spectrometry, Montreal, June, 1964.

(5) K. Biemann, J. Seibl and F. Gapp, J. Am. Chem. Soc., 83, 3795, (1961).

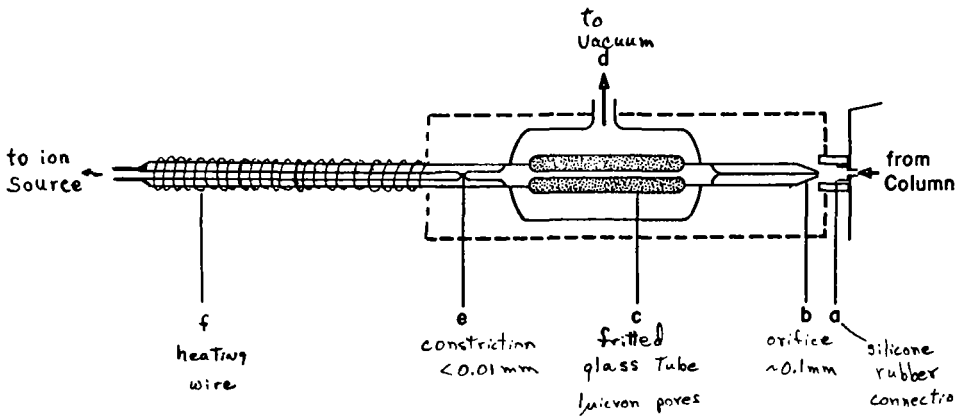

Fig. 1. Pressure reduction and enrichment system.

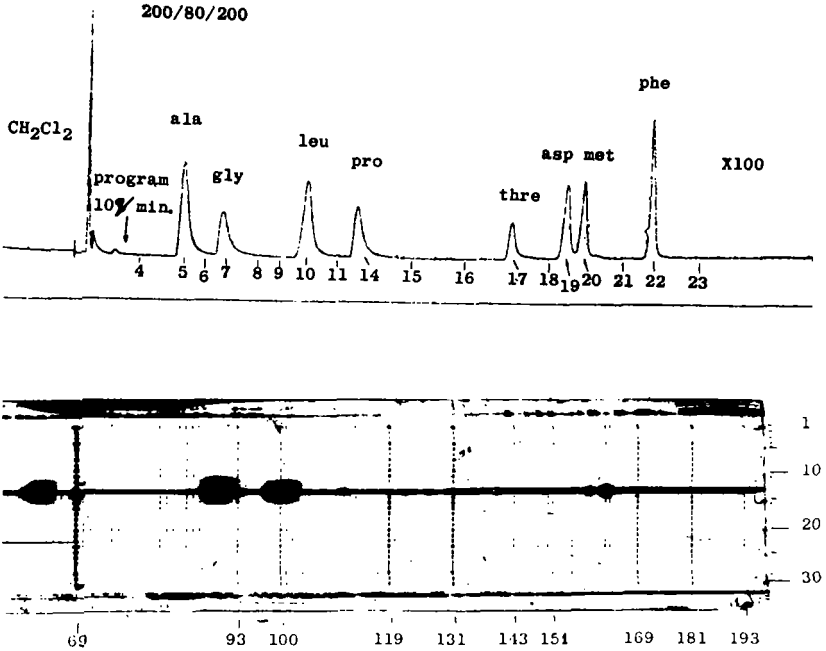

Fig. 2. Top: Gas chromatogram of amino ester mixture. Bottom: Part of the photographic plate on which the spectra of all the fractions were recorded.

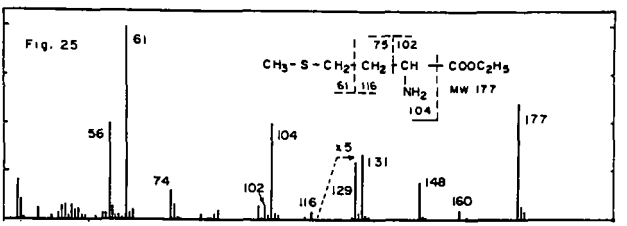

Ethyl Ester of Methionine

Mass determination	Elem. comp.	Mass determination	Elem. comp.
55.9722(0.1)	C_2S	102.0575(2.0)	$C_4H_8NO_2$
56.0121(-1.5)	C_2H_2NO	104.0531(-0.3)	$C_4H_{10}NS$
56.0494(0.0)	C_3H_6N	116.0171(0.1)	C_4H_6NOS
61.0106(-0.6)	C_2H_5S	116.0699(-1.3)	$C_5H_{10}NO_2$
74.0228(-1.4)	$C_2H_4NO_2$	129.0794(0.4)	$C_6H_{11}NO_2$
74.0379(1.1)	$C_3H_6O_2$	131.0395(-1.0)	C_5H_9NOS
75.0276(0.7)	C_3H_7S	148.0444(1.2)	$C_5H_{10}NO_2S$
87.0151(0.8)	C_3H_5NS	160.0585(2.7)	$C_7H_{12}O_2S$
87.0270(0.2)	C_4H_7S	177.0830(0.6)	$C_7H_{15}NO_2S$
88.0218(-0.3)	C_3H_6NS	178.0866(0.9)	$C_6{}^{13}CH_{15}NO_2S$
88.0525(0.1)	$C_4H_8O_2$	179.0800(1.9)	$C_7H_{15}NO_2{}^{34}S$

Fig. 3. Conventional mass spectrum of methionine ethyl ester and high resolution data obtained with a gas chromatographic fraction.

High Resolution Mass Spectra of Organic Molecules and their Use for Structure Determination

K. Biemann, W. McMurray and P. Bommer
Department of Chemistry, Massachusetts Institute of Technology
Cambridge, Massachusetts

Since the demonstration by J.H. Beynon[1] a number of years ago that high resolution mass spectrometry of organic compounds yields highly informative data not available with the conventional single focusing instruments, the techniques have been much discussed but very little actual data have been produced. This may be due to two factors, namely the scarcity of double focusing mass spectrometers available to organic chemists in the past, and the fact that the performance of a mass measurement of sufficient accuracy is a tedious task as compared with the scanning of a conventional low resolution mass spectrum.

The past practice was to first obtain a low resolution spectrum, then to select some peaks for accurate mass measurement and to perform this measurement with the aid of another peak of absolutely known mass that had previously been identified. It is obvious that such a technique cannot routinely be used to measure all the ions present in the mass spectrum of a reasonably complex organic molecule as this would involve a few hundred individual measurements while the compound resides in the mass spectrometer.

It is for this reason there are hardly any instances in which more than five peaks were measured in a mass spectrum. Only in a few instances[2] the entire mass spectrum has been recorded with a resolving power sufficient to distinguish between the various possible elemental compositions of the ions but this involved compounds of molecular weight below 150 which is small enough to record the entire spectrum within a reasonable amount of time.

This past practice represents, therefore, mainly low resolution mass spectrometry coupled with occasional mass measurement rather than true high resolution mass spectrometry which would imply the presentation of the entire spectrum with very high resolving power just as conventional mass spectrometry involves the determination of the entire mass spectrum displaying all the ions with respect to their nominal mass.

As was discussed earlier,[3] we have developed techniques that permit us to determine semi-automatically the mass of all the ions in a high resolution mass spectrum (using a CEC 21-110 spectrometer with photoplate detection) and to convert these data to the possible elemental compositions of these ions. The results obtained immediately revealed to us how much information is buried in this wealth of data, but also presented an exorbitant data handling problem because the evaluation and interpretation of the few hundred sets of elemental compositions was very tedious as long as the data were arranged by increasing mass. This is the presentation to which one is accustomed in conventional mass spectrometry but it soon became obvious that this is actually illogical and that it is the combination of atoms and their number which is of primary interest for the interpretation. As we are using a computer to produce these data it was relatively easy to extend the program in such a way that all the elemental compositions assigned to the various ions are first rearranged in terms of increasing heteroatom content and then printed out in a form which displays this feature. Thus, one obtains them in a form in which they can be most easily interpreted and, at the same time, have them available in a highly condensed form that can be looked at at one glance. This output is called an "element map"[4] for reasons that will become immediately apparent.

The principle of such element maps and their interpretation shall be outlined using a very simple compound, 3-octanone, as an example(Fig.1) In the first column is given the nominal mass of the various ions; the second column represents all ions containing only carbon and hydrogen, listing the number of carbons, hydrogens and the difference of found and

calculated mass, followed by an indication of the abundance (on a logarithmic scale) of this particular ion in the form of 1-10 asterisks. The second column lists all ions containing carbon, hydrogen and oxygen and the various numbers have the same significance as in the C,H column. Thus, the hetero-atom content of the ions increases from left to right while their mass and therefore the number of carbon and hydrogen atoms increases from top to bottom. It follows that the elemental composition of the molecule in question is found as the entry furthest down and to the right, in this case $C_8H_{16}O$.

In the C,H column one can follow the oxygen free species up to C_6 but it is significant to note that the largest ion of the C_nH_{2n+1} type is at n=5, pointing out that the largest saturated alkyl fragment is a pentyl group. The oxygen containing fragments indicate that of the $C_nH_{2n-1}O$ ions, i.e. acyl ions, those with n=2, 3 and 6 predominate. The last two representing the alkyl ions expected of a ketone with 8 carbon atoms and the carbonyl oxygen at C-3. The only $C_nH_{2n}O$ ion smaller than the molecular ion itself is found at n=4 which therefore must be the typical rearrangement peak of ketones, implying the presence of an α-unsubstituted ethyl ketone.

Without going further into the interpretation of the spectrum it should only be pointed out that many other features of the high resolution mass spectrum are easily discernible in this representation, for example, any multiplet gives rise, of course, to two entries at the same line which means two ions at the same nominal mass. Furthermore, various otherwise less obvious or perhaps unexpected features are brought to one's attention, such as, the peak at mass 81, which represents an ion of 6 carbon atoms but no oxygen, and must therefore arise by elimination of water from the acyl ion $C_6H_{11}O$. It goes without saying that the representation of the entire high resolution mass spectrum in such a form will make it easier to uncover fragmentation processes that have not been considered when inspecting low resolution spectra and thus would remain obscure if one were to measure only those ions which were thought to be of interest on the basis of the interpretation of a low resolution spectrum.

The full power of this approach is of course much more important in the case of more complex molecules and we have produced quite a number of element maps of natural products such as steroids, alkaloids and amino acids. A steroidal ketone can be element-mapped as easily as 3-octanone and, as to be expected, shows the presence of a large carbon skeleton by a highly populated C,H column. For androsterone acetate it goes to $C_{19}H_{26}$ implying the presence of a skeleton of at least 19 carbon atoms, uninterrupted by heteroatoms. Since these data have been published recently,[4] they shall not be discussed any further here.

On the other hand, the element map of a much more complex molecule, (Fig.2)voacangine (18-carbomethoxyibogaine), shall be presented as an illustration of a molecule containing quite a number of nitrogen and oxygen atoms spaced at various places all over the molecule. The lack of any C,H species above mass 143 implies the presence of a carbon skeleton into which heteroatoms are built rigidly. That this is not oxygen but nitrogen is borne out by the lack of C,H,O-ions and the presence of quite a number of C,H,N-ions. That there are two different nitrogens is not only displayed by the entry in the farthest lower right which gives the molecular composition ($C_{22}H_{28}N_2O_3$) but also by the fact that the C,H,N-ions have a high hydrogen content with respect to carbon up to C=10, but from there on, the C/H ratio is much higher. This implies that one of the nitrogen atoms in this molecule is associated with a non-aromatic portion of the molecule and the other one with an aromatic portion. The same can be said of the C,H,N,O_2-ions of which the saturated ones end at C 12, while the aromatic ones go to C 14. The C,H,N,O-column is so far of interest as it shows one oxygen and one nitrogen atom associated in aromatic ions (high C/H ratio) indicating an oxygenated substituent attached to the nitrogen-containing aromatic part.

ELEMENT MAP $CH_3CH_2CH_2CH_2CH_2CO-CH_2CH_3$

3-OCTANONE 17C-17-1

	CH	CHO	CHO2	CHO3
40	3/ 4 O**			
41	3/ 5 O*****			
42	3/ 6 C****			
43	3/ 7 O******	2/ 3 C*****		
44		2/ 4 C**		
45		2/ 5 C**		
50	4/ 2 O**			
51	4/ 3 O***			
52	4/ 4 O*			
53	4/ 5 O***			
54	4/ 6 O**			
55	4/ 7 1*****	3/ 3 1****		
56	4/ 8 1***	3/ 4-1****		
57	4/ 9 1****	3/ 5 1******		
58		3/ 6 C***		
59		3/ 7 O**		
62	5/ 2 1*			
63	5/ 3 C*			
65	5/ 5 O*			
67	5/ 7 O**			
68	5/ 8 O**			
69	5/ 9 O****	4/ 5 O****		
70	5/10 O***	4/ 6 C***		
71	5/11 C******	4/ 7 C****		
72		4/ 8 C******		
73		4/ 9-2*****		
75	6/ 3 1*			
79	6/ 7 O*			
80	6/ 8 O*			
81	6/ 9 O***			
83		5/ 7 O**		
84		5/ 8 C*		
85		5/ 9 1****		
86		5/10 C***		
97		6/ 9 O**		
98		6/10 C*		
99		6/11 O*****		
114		7/14 O*		
128		8/16 C*****		
	CH	CHO	CHO2	CHO3

Fig. 1. Element map of 3-octanone.

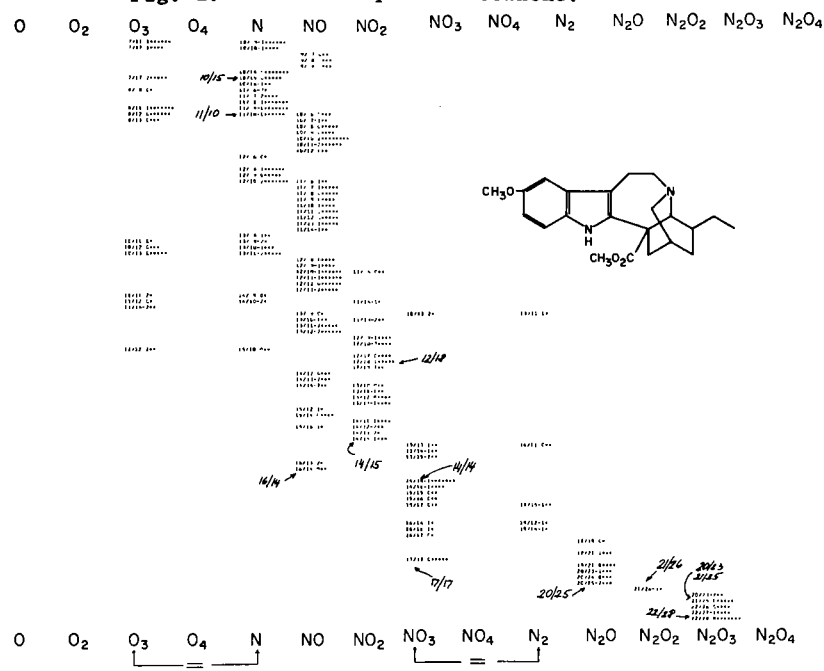

Fig. 2. Element map of voacangine.

Considering the ions of high heteroatom content it is obvious that the lack of ions with less than 20 carbon atoms in the N_2O_3 column indicates that only 2 carbon atoms can be eliminated (in the form of an ethyl group) without involving simultaneously the loss of heteroatoms.

One oxygen atom is lost much less easily than two and if so it involves at least two carbon atoms, i.e. there must be present such a substituent (i.e. the carbomethoxy group). The C,H,N,O_3 ions are also of rather high C/H ratio and this leads to the conclusion that the $C_2H_3O_2$-substituent is close to the aromatic part of the molecule, incorporating at least 13 and at most 17 carbon atoms. The $C_{14}H_{14}NO_3$-ion corresponds to the fragment of mass 186 in ibogaine[5] while the $C_{17}H_{17}NO_3$-fragment is the analog of mass 225 in ibogaine which in contrast to earlier assumptions[5] involves the loss of the alicyclic nitrogen.[6]

Two other features of the map are worth mentioning. First, there is the conspicuous lack of entries in the lower left and the upper right. This is due to the fact that voacangine does not contain all the heteroatoms concentrated in one corner of the molecule which would lead to the formation of either small fragments with many heteroatoms (thus appearing in the upper right) or of large fragments free of heteroatoms (thus appearing in the lower left) or, probably, both.

Second, there are entries on the same line (i.e. same nominal mass) in the C,H,O_3 column as well as the C,H,N group, indicating many doublets of this type. This is, however an artifact, because of the small mass difference (2.7 mmu.) between ions differing by C_3N vs. H_2O_3 and the mass found frequently fits both possibilities within ±3 mmu. (the limits we have set for element-mapping). Thus one has to decide for one of the two possibilities on the basis of other features of the map. The C,H,O_3 ions are, for example, much less likely than the C,H,N-type as we have already concluded (see above) that one oxygen atom seems to be strongly bound to the aromatic system containing a nitrogen atom while the two other oxygens are part of an easily eliminated small substituent. The formation of a nitrogen-free ion containing three oxygens is thus highly unlikely.

A similar set of such "imaginary" lines is found for C,H,N,O_3 vs. C,H,N_2. The latter can be excluded for purely logical reasons. Formation of $C_{19}H_{14}N_2$ from $C_{22}H_{28}N_2O_3$ would involve the loss of $C_3H_{14}O_3$, which is impossible.

It seems that this approach represents a valuable new technique in high resolution mass spectrometry which permits one to make use of the vast amount of highly sophisticated data produced by a high resolution mass spectrometer.

Acknowledgement: This work was supported by grants from the National Science Foundation (G-21037) and from the National Institutes of Health, Public Health Service(GM-09352). We are indebted to the M.I.T. Computation Center for the use of the facilities.

References

(1) J.H. Beynon, in J.D. Waldron (ed.) "Advances in Mass Spectrometry", Vol. I, Pergamon Press, 1959.

(2) For example, J.H. Beynon, R.A. Saunders and A.E. Williams, Anal. Chem., 33, 221 (1961).

(3) P. Bommer, W. McMurray and K. Biemann, Twelfth Annual Symposium on Mass Spectrometry, Montreal, June, 1964. D.Desiderio and K. Biemann, ibid.

(4) D. Desiderio, P. Bommer and K. Biemann, Tetrahedron Letters, No. 26, 1725 (1964).

(5) K. Biemann and M. Friedmann-Spiteller, J. Am. Chem. Soc., 83, 4805 (1961).

(6) K. Biemann, J. Pure Appl. Chem., (1964) in press.

Photographic Recording of Mass Spectra of Heavy Organic Molecules

N. Sasaki, Kyoto University, Emeritus Professor,
E. Watanabe, M. Naito, M. Samura, T. Aoyama, S. Enomoto, and M. Ishibashi,
Japan Electron Optics Laboratory Co., Ltd., Tokyo

Direct, simultaneous, and accumulative nature of photographic recording

Organic ions produced in a gas ion source by a controlled electron impact have been recorded usually peak by peak by some type or other of electrical method. An ion collector placed at a single focus point receives ions of differing masses successively. The height of the peak thus recorded represents fairly well the intensity of the ion beams. However, this advantage does not hold good unless the beams are resolved by an instrument exhibiting a high resolving power. Consider, for example, a high resolution instrument with a single focus point, such as a Johnson-Nier type double focusing mass spectrometer. This instrument requires a much smaller magnet and is easier to adjust than the instrument to be mentioned below. But it must be remembered that the higher the resolving power, the more time-consuming it is for scanning a given range of mass.

On the other hand, recording of the entire mass spectrum on a photographic plate by means of a Mattauch-Herzog type instrument exhibits many encouraging features inspite of many demerits inherent in the photographic method. To effectively apply the direct, simultaneous, and accumulative nature of this method of recording is a challenging problem.

Mass number determination

Methods for accurate measurement of isotopic masses have been developed and can be applied to the exact mass determination of organic ions. The mass number of an organic ion, the nearest whole number to the exact mass, may be obtained from a far less accurate mass value. However, the correct determination of mass number becomes difficult, if the extrapolation must be extended over a very wide mass range. In such a case the recording of a spectrum on a photographic plate is particularly valuable, for it is direct and simultaneous, so that the relative spacing between the spectral lines on the plate is less liable to distortion than the spacing between the peaks recorded peak by peak on a moving paper. Naturally deviation to some degree from the strict square root mass law may be unavoidable due to geometrical or other defects of the instrument.

Tentatively we extrapolated the mass number of line E on the basis of two spectral lines A and B, which were identified as $C_3F_5^{35}Cl$ and $C_4F_5^{35}Cl_2$, having masses of 165.961 and 212.930 respectively. The value obtained was 783.29 against the exact value 782.747, corresponding to the E ion composition of $C_{13}F_{20}^{35}Cl_6{}^{37}Cl$. Thus we get the correct mass number 783 for E. The mass value calculated on the basis of mass numbers of A and B was 783.62, giving a false mass number 784. However, even with mass numbers we can attain the correct mass number, if there are lines (C, D,...) at appropriate intervals between lines B and E. Extrapolation was first carried out for the nearest line C. The mass number 369 thus obtained will be certainly correct, for the mass range between B and C is not very large. We then proceeded to determine the mass number for the next line D on the basis of the mass numbers of C and either B or A and got 551. Finally the extrapolation on the basis of mass numbers of D and either C, B, or A gave 783.48 as the mass of E, from which follows the correct mass number 783 for E. In this stepwise approach each successive step corrects the error by rounding

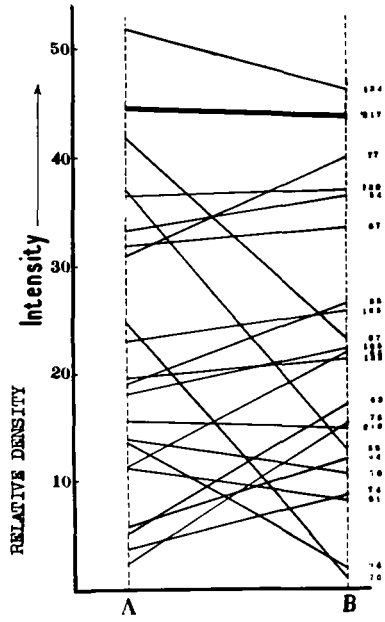

Fig.2. Classification of ions of allo-securinine by origin.
The spectrogram for A was taken at a lower vapor pressure and earlier than that for B.

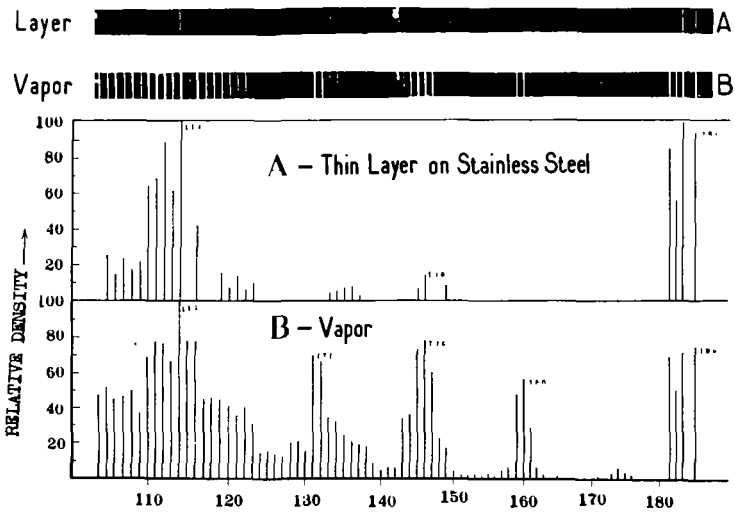

Fig.4. Mass spectra of vitamin B_{12} in a thin layer on stainless steel (A) and in a vapor state (B).

off the calculated mass value to the nearest whole number, before it surpasses one half. It is to be noted, however, that this approach may fail, if the mass number differs considerably from the exact mass.

Intensity measurement

A mass spectrogram taken on a photographic plate can by itself give a general idea of relative intensities of ions. If scanned with a micro-densitometer, it will furnish a peak spectrogram, similar to, but less quantitative than a conventional electric record. Another way of visualizing intensity relations is to take a series of spectrograms closely side by side in order of exponentially increasing exposure. Fig. 1 shows the spectrograms of tryptophan taken on a Q2 plate 35 cm long with our Mattauch-Herzog type mass spectrograph, model JMS-01S*. Strong and weak lines appear as large and small needles grown from the bottom spectrogram. This resembles the conventional segments diagram, the drawing made from the original peak-by-peak record obtained by an electrical method. However, all the lines over the entire spectrogram are highly resolved into multiplets and ready for later mass and intensity measurements.

An emulsion calibration curve can be obtained from the densitometric values of any line and the corresponding exposures in coulombs. Isotopic lines of platinum, for example, taken as mass marks may also be used for the purpose. Thus we tentatively measured the intensity ratio of mass number m+1 to m molecular ions of cholesterol ($C_{27}H_{46}O$ = 386) and found 0.275 ± 0.008 against the calculated value of 0.29951[1]. Accuracy may be improved still further. But this degree of accuracy may be of value in some cases to decide between two alternatives, for the m + 1/m intensity ratio extends from about 0.2 to about 0.35 for about 190 possible atomic combinations of C, H, N, and O[1].

A representative mass spectrogram obtainable with a small sample

As a consequence of the simultaneous and accumulative recording on a photographic plate we can always obtain sufficiently identical mass spectrograms of given sample material, even when the total ion current fluctuates uncontrollably during exposure. This is a great advantage not possessed by the conventional peak-by-peak recording method. By this reason a very small amount of a sample material, directly inserted into the ionization chamber, suffices to give an adequately representative mass spectrogram, because the exposure can be made throughout the whole period of specimen evaporation.

Convenient and effective study of all the ions over the entire spectrum

To be more precise, however, the perfect independence of the spectral pattern on the total ion current fluctuation holds true, for example, for a group of lines corresponding to primary ions that are produced primarily on electron impact. It also holds good for another group of lines corresponding to secondary ions that are produced secondarily by a molecular collision following electron impact. However, these two line groups behave differently toward pressure change, because the primary and secondary ions are produced at the rates proportional to the first and second vapor pressure powers respectively. There may also exist groups of lines originating from volatile impurities that are more or less quickly escaping from the specimen evaporating inside the ionization chamber.

This suggests an easy and effective method of classifying all the ions over the entire spectrogram into groups of different origins.

---

* The highest resolution recently obtained with this instrument is about 20,000.

The method is, for example, to plot the line intensity as a function of the sample material vapor pressure. Tentatively, to this end, two spectrograms A and B were chosen from our stock. A was taken at an early stage of sample evaporation, where the vapor pressure of the sample material was still low, whereas that of volatile impurities, if existed at all, might have well developed or begun to fall rapidly. B was taken at a later stage, where the sample vapor pressure and consequently the monitor current was higher. The total exposure in coulomb is the same for both A and B. In Fig. 2 the thick line corresponds to the molecular ion of allo-securinine. The ions may be classified roughly into three groups according to inclination. No serious study of the diagram has been attempted.

In quite a similar manner we can study the dependence of a mass spectrum over its whole length on thermal decomposition, on momentary change in the conditions inside the ionization chamber, on the intensity and energy of bombarding electrons, and others.

Dependence of a mass spectrum on the energy of bombarding electrons

The effect of bombarding electron energy on ionization and fragmentation can be most effectively studied by taking mass spectrograms one upon another in order of increasing electron energy, the exposure in coulomb being kept constant. Generally speaking, as the electron energy is increased, the molecular ions and heavy ions appear first and then soon begin to fade. The fragmentation shifts to the formation of lighter and lighter ions. There are also many exceptional ions that behave quite differently. In Fig. 3 the m/e 130 line of tryptophan corresponds to one of the exceptional ions. It appears as early and as profusely as the molecular ion of mass 204. We can thus easily find the optimum electron energy range for producing the highest mass (molecular) ion of a substance of unknown molecular weight.

Mass spectrum obtained by electron bombarding an organic substance on a solid surface

The mass spectrometric study may be extended to a class of organic substances possessing extremely low vapor pressure, if a reproducible and significant mass spectrum can be obtained by electron impact of an organic substance covering a solid (metal) surface. Better results would be obtained with a very thin layer or a monomolecular layer with molecular orientation. For this kind of study the simultaneous recording on a photographic plate is indispensable, for the consumption of the thin layer specimen by electron impact is rapid. A tentative attempt was made with vitamin B_{12}. In Fig. 4 the upper spectrogram taken with B_{12} in a thin layer terminates at m/e 186, whereas the lower one taken with B_{12} in a vapor state extends to about m/e 600. At the bottom are shown the corresponding segments diagrams drawn from the densitometric tracings. The large difference here revealed may be due at least to the following situation, firstly, that the interaction between the electron-bombarded molecule or ion thus formed and the neighbouring molecules in a thin layer may be quite different from that in the gas phase, secondly, that the thin layer reactions may be influenced by the substrate, and thirdly, that the part of the molecule exposed to bombarding electrons may be limited to a certain degree, if the molecules are at all oriented on the surface. Detailed comparison of the spectrograms from such a view point may be of value for elucidating the molecular structure.

Reference

1) Beynon and Williams, "Mass and Abundance Tables for Use in Mass Spectrometry", (1963).

A NEW HIGHLY RESOLVING COMMERCIAL MATTAUCH TYPE MASS SPECTROMETER FOR THE ANALYSIS OF ORGANIC AND INORGANIC SAMPLES

by

Karleugen Habfast
Atlas Meß- und Analysentechnik GmbH
Bremen, Germany

Last year at this conference we have given a first description of a new mass spectrometer. In the past year we have completed the development of this instrument. We will describe its performance in this paper.

Fig. 1 shows the ion optics: Mattauch Herzog Type double focusing mass spectrometer with spherical condenser and 76° magnetic deflection.

For this ion optic we have developed two spark ion sources and one electron bombardment ion source. For ion collection we have developed both, photographic and electric recording systems, which can be interchanged without breaking vacuum. Together with suitable additional equipment such as sample lock, inlet-system, peakmatching electronics a.s.o., we have an universal mass spectrometer, which can be used for the analysis of solids as well as for the analysis of organic compounds.

I. Spark source application

First we will describe the performance of this instrument for solids analysis.

We are using two types of ion sources:

1) the vacuum vibrator, similar to that, described by Hintenberger and Schuy (1)
2) a triggered DC-discharge, similar to that, described by Honig (2).

Some typical vibrator spectra are shown in Fig. 2. These are Iron standard samples, obtained from NBS and from Bureau of Analysed Samples. As you see and as Franzen (3) described in his paper, these spectra are quite different from RF-spectra. The multiply charged ions are much more predominant.

Fig. 3 shows on the top two spectra of a standard Iron sample, obtained with the triggered DC-discharge. These spectra are very similar to a vibrator spectrum.

In contrast to that, the spectrum of a Silicon sample at the bottom of Fig. 3, also obtained with the triggered DC-discharge, is very similar to a RF-spectrum. This is due to the fact, that the Iron is conductive and makes possible a low voltage discharge, while the Silicon is a semiconductor and prevents the low voltage discharge.

The Silicon spectra have been obtained with a large entrance slit width of 2 mm to get a high transmission. One can see lines of multiply charge Silicon atoms as well as lines of up to 7 atom clusters. The three spectra with the wide lines have been obtained by using 10, 100, and 1.000 discharges resp.

Three factors are important in the analysis of solids by the mass spectrometer:

1) The efficiency of the ion source should be high enough, to achieve a given detection limit without overlong exposure times.
2) The resolution should be high enough, to separate the sample spectrum from the background. If this is not so, interpretation of trace impurities is often very difficult.
3) The results should be reproducable.

How do we measure up to these three factors?

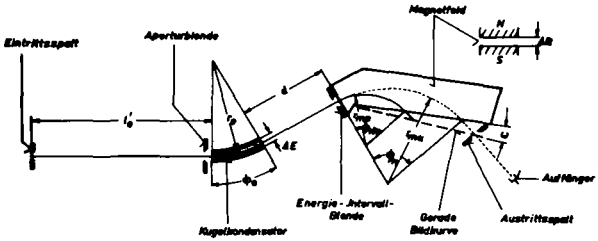

Φ_0	Φ_m	ε_0'	r_{ak}	ΔE	l_0'	d	ε_m'	r_{mo}	r_{mp}	ΔB	ω
29°	78°	0	154	12	350	173	0	194	40-240	5	5°

Fig. 1
Ion Optic

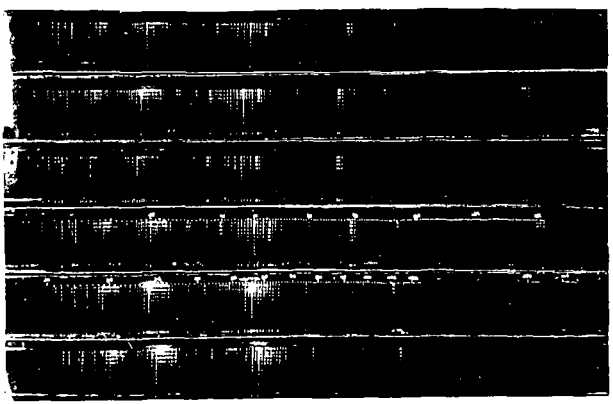

Fig. 2
Vibrator Spectra

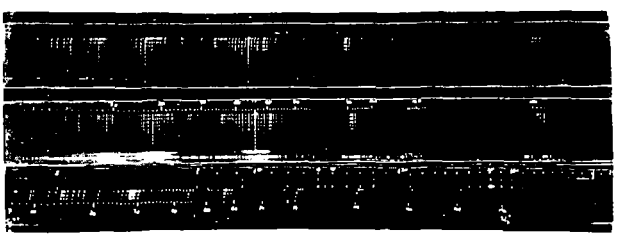

Fig. 3
DC Spark Spectra

With a slit width of 30 µm we get an ion current of about $5 \cdot 10^{-10}$Amp. onto the photographic plate. The mean area of our mass lines is 0.015 mm^2. A just detectable line needs about 10^5 ions/mm^2. A trace component, having a concentration of 10^{-8}, should therefore be detectable after an exposure time of 50 secs. Due to the fact, that the multiply charged ions contribute to the total ion current and that nearly no element has only one isotope, we need in fact a mean exposure time of about 1.000 secs., to detect a 10^{-8} component.

For instance, with a relatively pure Iron sample, which has been doped with 5ppm Oxygen, we were able to produce a just detectable line within an exposure time of 3 secs. This means, that an exposure time of 1.000 secs. would give a detection limit of about $2 \cdot 10^{-8}$ for Oxygen in Iron.

Fig. 4 shows resolution of the spark instrument. Some quantitative results taken with the spark source, are given in Fig. 5 and Table 1.

Fig. 5 shows sensitivities for 15 elements in an Iron matrix for the vibrator and for the triggered DC-discharge. They are reproducable to within 10 - 15% standard deviation and are quite the same for both types of ion sources except for Tin and Lead. The dotted line in Fig. 5 shows the sensitivities for 7 elements in a Nickel matrix. Here we were able to determine the sensitivity of Silicon in the presence of double ionized Iron at mass 28.

Table 1 shows analysis of two standard samples with fairly good reproducability.

II. Organic application

We have developed a new electron bombardment source which shows excellent transmission with a small ion beam divergence. With a Nitrogen pressure of 10^{-5} Torr in the ion source we get an ion current of $5 \cdot 10^{-10}$Amp. through an entrance slit 70 µ wide. This gives a sensitivity of $5 \cdot 10^{-5}$ Amp/Torr at a resolution of 1.000.

For the introduction of samples into the mass spectrometer we have used up to now a high temperature molecular leak inlet system. Our highest resolution results are quite recent.

Fig. 6 shows, as an example, the molecular peaks of

Anisol	(mol.-weight 108,057515) and
O-Phenylindiamin	(mol.-weight 108,068746)

Resolution is about 24.000 according to the 10% valley definition.

By oscilloscopic peakmatching we have measured the ratio of the two masses. All six measurements, which were made, were between 1.0001036 and 1.0001040. This means, reproducability was about 0,5 ppm.

REFERENCES

(1) K.D. Schuy and H. Hintenberger, Zeitschrift f. Naturforschung 18 (1963), 926

(2) R.E. Honig, S.S. Glass, and I.R. Woolston, Triggered Low-Voltage Sources for Positive Ions. International Conference on Ionisation Phenomena in Gases, Paris, 1963

(3) J. Franzen, K.D. Schuy, and H. Hintenberger, Conference on Mass Spectrometry, Montreal 1964, Paper No. 39.

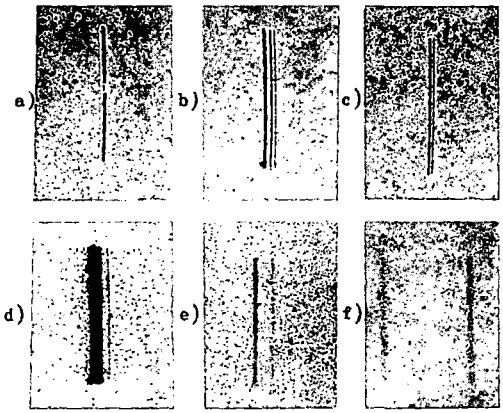

Fig. 4

Resolution

a) $^{26}Mg^{2+}$ - $^{13}C^{+}$ - $^{12}CH^{+}$

b) $^{56}Fe^{4+}$ - $^{14}N^{+}$ - $^{12}CH_2^{+}$

c) $^{12}C_2^{+}$ - $^{24}Mg^{+}$

d) $^{56}Fe^{2+}$ - $^{14}N_2^{+}$ - $^{12}C_2H_4^{+}$

e) $^{55}Mn^{+}$ - $C_4H_7^{+}$

f) $^{199}Hg^{+}$ - $^{200}Hg^{+}$

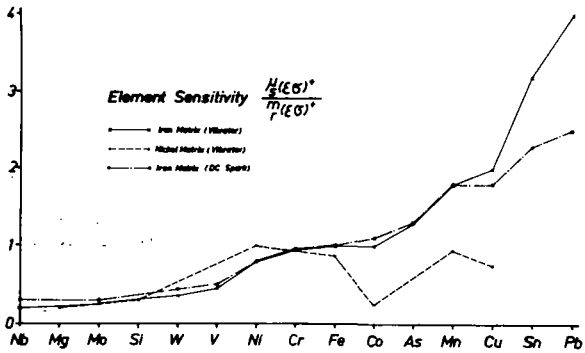

Fig. 5

Typical Analysis with Vacuum-Vibrator

(%, atomic)

Element	NBS Nr 461				BAS Nr SS 16			
	True	Measured			True	Measured		
Fe	100	100	100	100	100	100	100	100
V	0,027	0,03	0,025	0,03	0,055	0,073	0,070	0,072
Co	0,25	0,21	0,25	0,25	0,026	0,026	0,026	0,025
Cr	0,16	0,14	0,12	0,15	0,11	0,09	0,11	0,10
W	0,004	0,006	0,008	0,006	0,61	0,85	0,80	0,76
Cu	0,31	0,45	0,50	0,45	0,11	0,21	0,18	0,17
Mn	0,38	0,42	0,45	0,48	—	0,63	0,60	0,62
Mo	0,19	0,22	0,22	0,20	0,006	0,005	0,006	0,007

Table 1

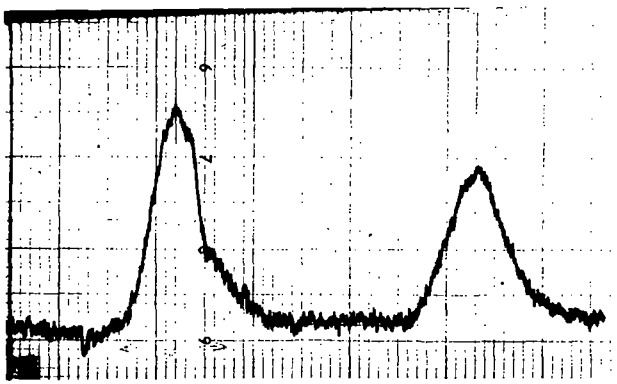

Fig. 6

High Resolution

QUADRUPOLE MASS SPECTROMETER FOR ATMOSPHERIC STUDIES IN THE 50- TO 90-KILOMETER RANGE*

Wilson M. Brubaker, Norton W. Bell and Frank B. Wiens

Bell & Howell Research Center, Pasadena, California

Abstract

A quadrupole mass spectrometer system has been designed for use on an atmosphere probing rocket (Nike-Cajun). Low pressure in the mass analyzer is maintained by a zeolite adsorption pump operating at liquid nitrogen temperature. The ionizing electron beam is concentrated at the aperture through which the sample is admitted. Thus the sensitivity of the source to incoming molecules is much higher than it is to the ambient molecules. Laboratory measurements with conventional pumps has shown a differential sensitivity in excess of one hundred. A complete mass scan of the components below mass 45 is made every two seconds. The ion current amplifier compresses the range from 10^{-12} amperes to 10^{-7} amperes into the 0- to 5-volt interval for telemetry.

Introduction

This paper describes the apparatus which was developed, designed, and constructed for the analysis of the earth's atmosphere in the 50- to 90-kilometer altitude range. A joint paper with Dr. Rocco Narcisi, to be presented later, will contain flight data. Only the description of the apparatus is contained here. The ambient pressure decreases from 600 microns to one micron as the rocket ascends through this interval. Since most mass analyzers require pressures lower than one micron for their proper functioning, this project presents a severe pressure reduction problem. When even very small apertures are used to admit the atmosphere for sampling, a vacuum pump with a speed of more than 100 liters per second is required to maintain the pressure within the operating range of the mass analyzer.

The project thus presents two problem areas: first, some means must be provided for maintaining as low a pressure as possible in the analyzer while the ambient gas is admitted; and second, a mass analyzer must be found which will perform satisfactorily at pressures higher than those usually used for mass analyses.

Solution of the Pumping Problem

At the outset, four potential solutions to the pumping problem were suggested. These include:

a. Gettering
b. Ion Pumping
c. Zeolite Adsorption
d. Liquid Helium Cryogenic Pumping.

While it is obvious that the liquid helium approach would do the job, it was hoped that an easier-to-use method could be devised.

With reference to gettering, it is easy to show that the amount of titanium required to react with the two atmosphere-cc's of air which is expected to enter the package on its flight is readily provided by the evaporation of a small filament. The adsorption of the gas on to a surface of reasonable area for this application would require the penetration of the molecules to tens of mono-layers. Preliminary experiments with the use of freshly deposited titanium films showed poor performance in a time comparable to that of the rocket flight.

---

* This project was supported in part by Air Force Cambridge Research Laboratories, Lawrence G. Hanscom Field, Bedford, Massachusetts under Contract AF 19(604)-8510, and monitored by Dr. Rocco Narcisi.

The requirement that the pump have a speed in excess of one hundred liters per second at pressures of the order of 10^{-4} torr removes ion pumps from serious consideration; the bulk and mass of the ion pump with this capacity exceed the volume and weight limits of the vehicle.

Preliminary experiments with zeolite at liquid nitrogen temperature were promising. The experiments quickly revealed that the air penetrated only a short distance into the zeolite during the first one hundred seconds of exposure. Thus, the depth of the exposed zeolite surface was made as thin as the mechanical bonding techniques would permit. In this manner it was possible to provide 2,000 square centimeters of zeolite-covered surface in a package of slightly over one liter volume.[1]

Because the pressure decreases nearly exponentially with time as the rocket ascends through the earth's atmosphere, it is easy to simulate in the laboratory the appropriate gas load for testing the performance of the pump. An atmosphere-cc sample of air is expanded rapidly into a volume of approximately one liter. From here it enters into the test chamber through a calibrated conductance. In this manner the gas is introduced at a rate which decays exponentially with time, just as it does on an actual flight. A plot of the pressure vs. time during one of these simulated tests is given in Figure 1.

The Quadrupole Mass Analyzer

The special requirements of this device are that it be small in size, light in weight, economical of power, and capable of resolving the neutral components of the atmosphere into the appropriate mass spectrum. In addition to these requirements, it must be able to operate at relatively high pressures. A quadrupole mass filter, Figure 2, about the size of an unfilled ice cream cone was found to fill these needs admirably. The operation of this unit at pressures above one micron was examined by using a thermal ion source. Increasing the pressure had only a small effect on the resolution. The transmission of ions through the quadrupole decreased as the pressure was increased above 10^{-4} torr, as is shown in Figure 3. It should be mentioned that the goal of this project is the analysis of the atmosphere, not the measurement of the pressure. The manner in which the quadrupole operates as a mass analyzer is seen in Figure 4.

A comparison of Figures 1 and 3 reveals that there is a comfortable overlap between the maximum pressure at which the quadrupole will operate and that reached by the chamber during flight.

The Ion Source

The unique parameters of this experiment present instrumentation problems which are unusual. In this instance the neutral molecules enter the package through a hole which is only 0.015 inches in diameter. As they expand into the vessel their density falls as $(X/0.015)^2$ where X is the distance from the hole. Because the density of the molecules falls so fast as they enter the package, it is very desirable that the ionizing electron beam be located as close to this aperture as possible. This is achieved through the use of the geometry of Figure 5. An electron emissive filament nearly surrounds the axis of the source. The electrons are prevented from leaking to the structural members and are directed to the electron accelerating screen by the potential applied to the filament shield. They are further accelerated by the positive potential on the combination anode and ion repeller. The density of the converging electron beam becomes a maximum in the immediate vicinity of the entrance aperture. This is also the place where the density of the incoming molecules is the greatest. The ion aperture limits the region from which the transmitted ions can originate to the vicinity of the entrance aperture.

Using 500 micro-amperes of total electron emission, ion currents in major resolved peaks exceeded 10^{-8} amperes.

---

1. 1962 Transactions of the American Vacuum Society, page 232.

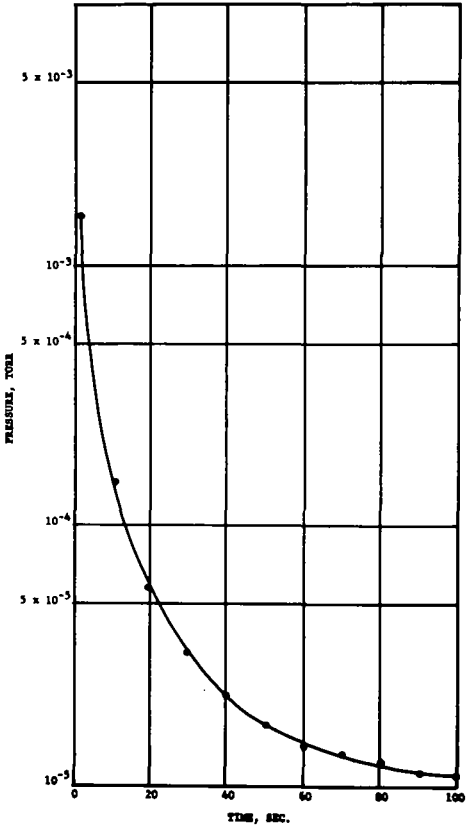

Figure 1.

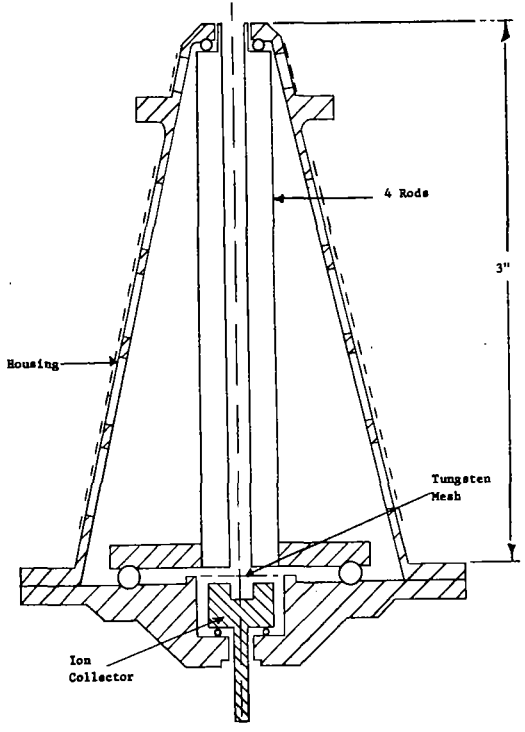

Figure 2

Quadrupole Mass Filter Assembly

The Electronic Components

A. The Ion Source Supply

This unit converts the 28-volt dc vehicle power source into the stabilized ion and electron accelerating potentials. Further, it regulates the total electron emission from the filament to the desired value of 500 microamperes. This emission is stabilized against variations in the emissivity of the filament and fluctuations in the power source potential.

B. Oscillator and Rectifiers to Provide Potentials for the Quadrupole

The six-megacycle oscillator is built around a trifilar (three winding) coil. The use of the three windings eliminates the need for radiofrequency chokes because the additional windings permit the application of the appropriate dc potentials at circuit points which are at ac ground.

The dc potentials for the rods are obtained by rectification of the potentials induced in the isolated windings. The influence of the cathode contact potentials in the rectifiers is essentially neutralized by similar, but oppositively directed contact potentials in companion diodes in the same envelope. This feature contributes substantially to the constancy of the dc/ac potential ratio over the wide voltage sweep.

Mass scanning is accomplished by varying the amplitudes of the ac and dc potentials while maintaining their ratio constant. A transistor-driven inverter transforms the vehicle 28-volt supply to the required potentials. A series regulator, using NUVISTOR tetrodes, stabilizes the B+ voltages. A motor-driven potentiometer causes the B+ potential to scan in a nearly exponential manner from 320 volts to a low value.

C. The Logarithmic Ion Current Amplifier

A logarithmic dc amplifier with a fast response and a dynamic range of five decades has been designed and fabricated for use with the quadrupole mass filter. Two pentode stages using ruggedized, reliable subminiature tubes provide a high input impedance and a bandwidth greater than 300 kc. A multisection RC filter at the amplifier input attenuates the radiofrequency voltage signal which is present at the ion collector due to electrostatic coupling from the rods of the quadrupole. The capacitance of this filter and the ion collector is about 100 pf. The dc transfer characteristic and the small signal response time are presented in Figure 6.

The small-signal response time is ten milliseconds. It provides an output signal of zero to five volts with input currents of 10^{-7} to 10^{-12} amperes. The transfer characteristic is nearly logarithmic for input currents of 10^{-7} to 10^{-11} amperes. To keep the input current above zero at all times (to avoid the resultant infinite response time) a small constant input current is provided through the use of a large resistor.

In-flight calibration of the electrometer amplifier is provided through the use of two relays. These disconnect the input from the ion collector and insert currents of 10^{-11} and 10^{-7} amperes in sequence. The relays are energized momentarily every fifth mass scan.

Description of the Assembled Package

A. The Zeolite Pump

The pumping package consists of a liquid nitrogen Dewar jacket made of stainless steel surrounding seven conical sections of 0.015-inch stainless steel onto which fine mesh zeolite is bonded by epoxy. Besides providing the necessary area in a compact and convenient arrangement, the conical structure also has high mechanical strength and a relatively uniform pumping speed to all zeolite surfaces. A section through this unit is shown in Figure 7. The cones are spot-welded to the wall for thermal conductivity.

Good thermal control is effected through the nearly complete enclosure of the zeolite covered surfaces by a copper heat shield which in turn, is in excellent thermal contact

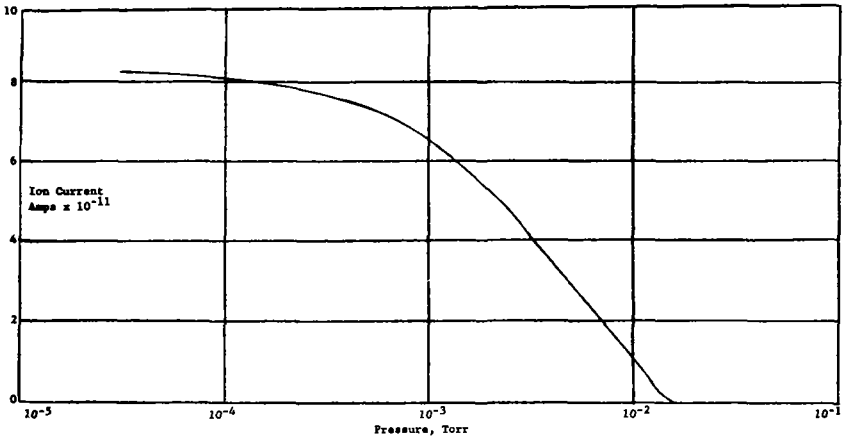

Figure 3

Operation of Quadrupole at High Pressures

Spectrum Obtained with Prototype Ion Source at High Resolution. Sensitivity: 3 x 10^{-11} amps full scale.

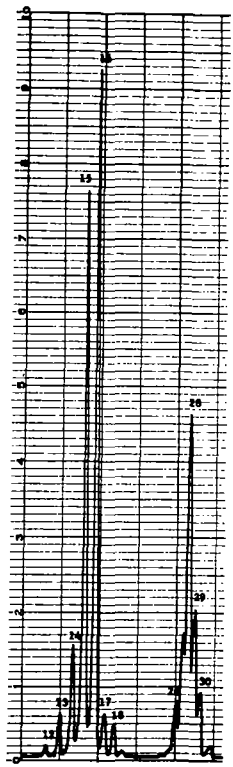

Figure 4.

with the liquid nitrogen. It also serves as a cold sink to maintain the temperature low during flight. Heat losses at the top of the vessel are diminished by the presence of urethane foam, which prevents the liquid nitrogen from coming into contact with the warm upper plate and lengthens the path for thermal conduction through the inner two of the three concentric cylinders which form the Dewar.

The cones which form the pumping surfaces all point toward the entrance aperture. This configuration enhances the chances of the incoming particles' penetrating to the bottom of the pumping volumes without making contact with the surfaces. Having once reached the lower regions of the pump, they are likely to make many contacts with the cold zeolite before they can escape back into the ionizing region. It is desired that they will be effectively trapped by the zeolite before they return to the ionizing region, as they may change from atomic to molecular species on contact with the surfaces. It is desired that the ionizing electron beam strike only the incoming molecules, before they contact a surface.

B. The Electronic Components

The electronic components were assembled onto chasses which would fit snugly inside a cylinder of six inches diameter. These are enclosed in an hermetically-sealed cylindrical package. In preparation for flight, the unit is evacuated and back-filled with dry nitrogen to atmospheric pressure. The elimination of most of the water vapor from the assembly maintains the leakage resistance high when the instrument is stored or used in hostile environmental conditions.

Summary and Conclusions

The problem of sampling the atmosphere between 50- and 90-kilometers has been solved by combining an effective pressure reduction system (adsorption pump) with a mass analyzer which will operate satisfactorily at high pressure (quadrupole mass filter).

A complete mass scan is made every two seconds. The scan starts above mass 44, and runs continuously to mass 11. It then jumps to masses 4, 2 and 1 in turn. In addition, advantage is taken of the unique characteristics of the quadrupole mass filter to observe the heavier masses as a group. The dc voltage is removed at the time of maximum ac voltage. Under these conditions all masses heavier than 38 are transmitted.

The wide range, logarithmic response electrometer amplifier is calibrated every ten seconds in flight. Two calibration points are given, in addition to the zero current signal between peaks. This sets the response fairly accurately.

The operation of the completed package is as expected with one exception: the zeolite has a lower pumping speed for oxygen than it has for nitrogen. This phenomenon is being explored in continuing experiments.

Acknowledgments

This contract was initiated by Mr. Lincoln R. Shedd and monitored by Dr. Rocco S. Narcisi of the Geophysics Research Directorate of the Electronic Systems Division of the Air Force Systems Command. The cooperation and assistance rendered by Mr. Shedd, and Dr. Narcisi and his entire group in the monitoring of this project and in many technical discussions is gratefully acknowledged.

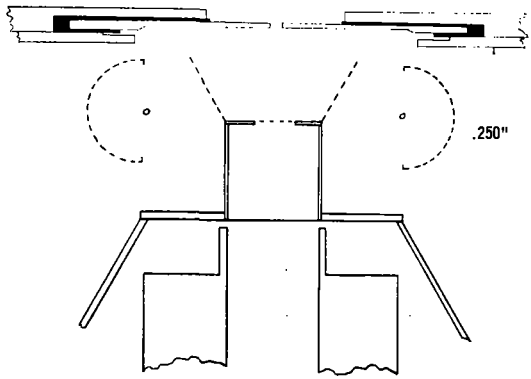

Figure 5. ION SOURCE GEOMETRY

DC TRANSFER CHARACTERISTICS AND SMALL-SIGNAL RESPONSE TIME OF LOGARITHMIC AMPLIFIER

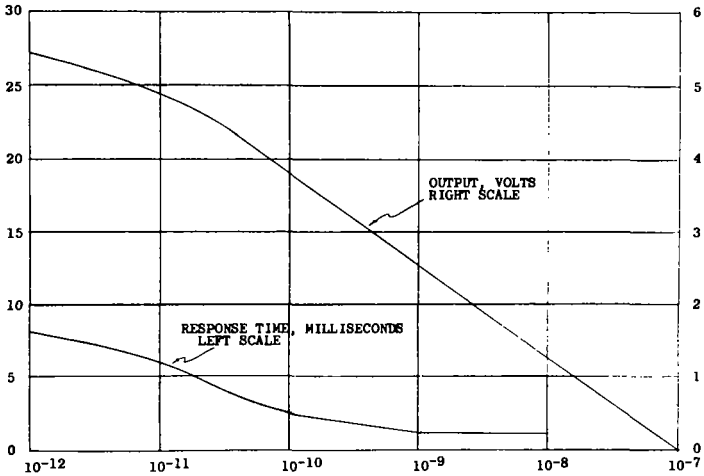

Figure 6. INPUT CURRENT, AMPS

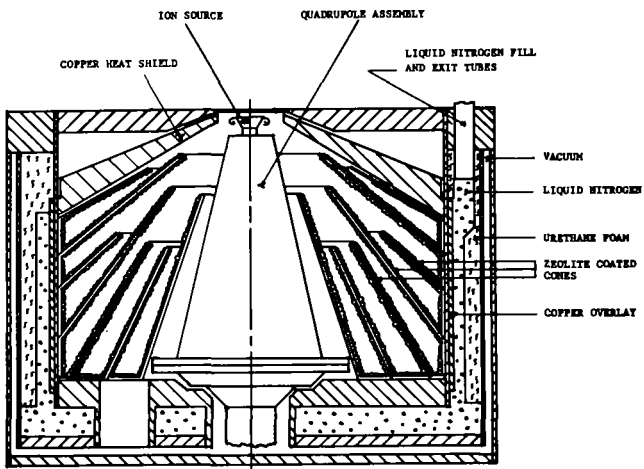

Figure 7.

QUADRUPOLE MASS SPECTROMETER

FOR ENERGETIC PARTICLE MEASUREMENTS*

by
L. G. Hall and M. R. Ruecker
Consolidated Systems Corporation
Monrovia, California

ABSTRACT

Analytical expressions are developed which define the initial conditions for 100% transmission of a quadrupole analyzer and which enable combination with equations for the focal properties of an ion source. The equation for the combined properties can be used to calculate the ion current intensity of the system as a function of the gas density, parameters of the mass spectrometer, and upper limits of acceptance of initial energy and initial angle. It is shown that the measurement of density may be, in principle, independent of the initial energy and initial angle at the time of ionization within the established upper limits. The equations are particularly useful in design of instruments for measurement in the upper atmosphere.

* * * * * *

INTRODUCTION

In terms of optimum performance, the design of any mass spectrometer considers the initial conditions under which the ions enter the analyzer. The initial condition of the ions, in turn, relates to the ion source properties. It is the purpose of this paper to present a means of analytically relating the quadrupole(1) analyzer with an ion source in one of two modes of focusing. For this purpose it is necessary to provide analytical expressions for both the analyzer and ion source operation.

QUADRUPOLE ANALYZER

The discussion of the quadrupole analyzer is limited here to operation in conditions of 100% transmission. This choice is dictated by a desire to: 1) obtain a more accurate absolute value for the ion current as related to gas density in the ion source; and 2) obtain "flat-topped" ion intensity peaks which can be measured by stepping from peak-to-peak. This method of measurement may be useful in space applications, where time or information capacity is limited and where the peak intensity must be independent of small changes in voltage or frequency. The discussion that follows thus treats the top width of the peak and the top to base ratio as important parameters of the operation.

The functional characteristics of the quadrupole analyzer have been adequately described by Paul, Reinhard and V. Zahn(1), and Brubaker (2). Their work is not extensively reviewed here.

It has been shown(1) that the maximum amplitudes of ion motion are inversely proportional to the stability parameters $(1 - \beta_x)$ and β_y. Paul, Reinhard, and V. Zahn have also computed the stability requirements as a function of entering phase angle under conditions that the initial transverse velocity is zero or that the initial position is zero. Here an analytical expression is required with all initial conditions (i.e., position, x_o, y_o, transverse velocity, $\dot{x}_o$, $\dot{y}_o$, and phase angle, ϕ) as variables. By retaining only the first few and important terms of the Fourier series solution of the Mathieu equation, the following approximate expressions for x and y motion are derived:

$$x \approx A_x \left\{ c_o \sin\left(\frac{\beta_x \omega t}{2} + \delta_x\right) - \left(c_{-2}\right)_x \sin \left[\left(1 - \frac{\beta_x}{2}\right)\omega t - \delta_x\right]\right\} \quad (1)$$

and

$$y \approx A_y \sin\left(\frac{\beta_y \omega t}{2} + \delta_y\right) \left[c_o + 2\left(\overline{c_2}\right)_y \cos\left(\omega t + \phi\right)\right] \quad (2)$$

* This work supported by the Jet Propulsion Laboratory and Goddard Space Flight Center of the National Aeronautics and Space Administration.

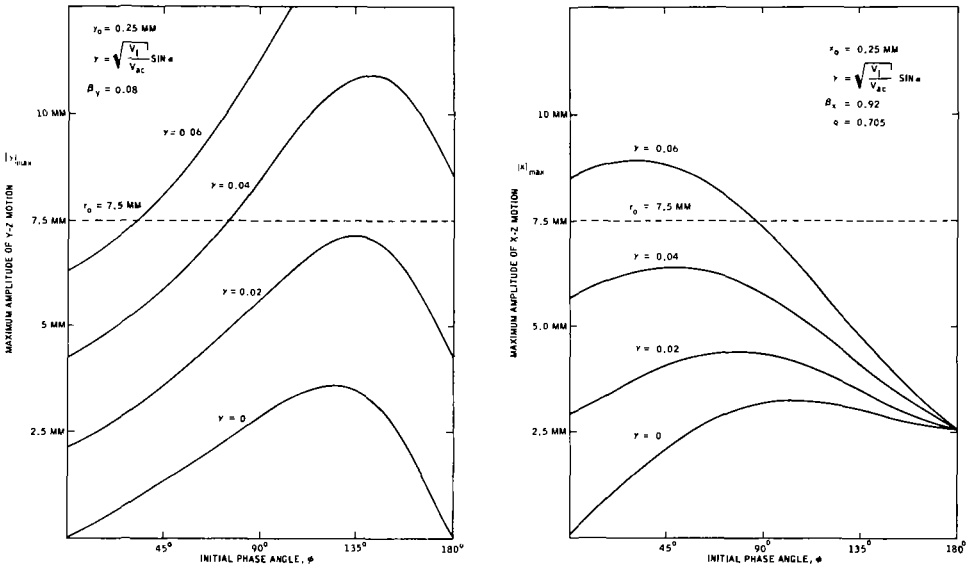

FIGURE 1
Maximum Amplitudes of Ion Motion in the y-z and x-z Planes vs Entering Phase Angle. Normalized Transverse Initial Velocity, γ, is the Parameter.

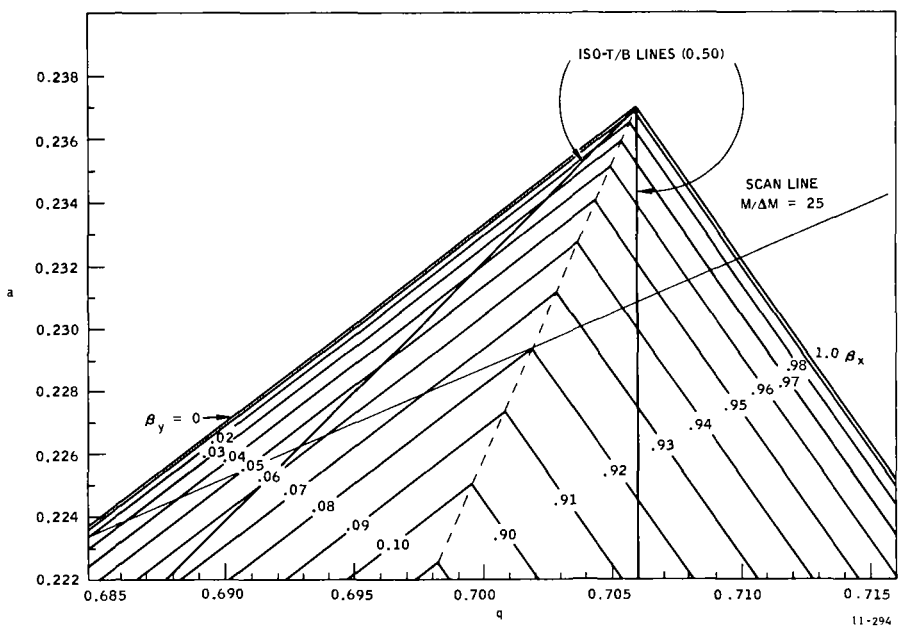

FIGURE 2
Quadrupole Stability Diagram Showing iso -β_x and iso - β_y Lines.

where

$$A_x, \ \delta_x = f\left(x_o, \mathring{x}_o, \phi\right)$$

$$A_y, \ \delta_y = f\left(y_o, \mathring{y}_o, \phi\right)$$

$$\phi = \text{Initial phase angle}$$

$$c_o = 1, \left(\overline{c_2}\right)_y = \frac{c_2 + c_{-2}}{2} = 0.168 \neq f\left(\beta_y\right)$$

$$\left(c_{-2}\right)_x = f\left(\beta_x\right), \quad 0.8 < \left(c_{-2}\right)_x < 1.0$$

It is noted in Equation (1) that when β_x is nearly 1 the arguments $\frac{\beta_x}{2}$ and $1 - \frac{\beta_x}{2}$ are each nearly 1/2 and since the coefficients[1] are of similar magnitude, an amplitude modulated wave is obtained without carrier, which is centered about the angular frequency $\frac{\omega}{2}$. On the other hand, when β_y is small the y motion is the low frequency wave $\sin \frac{\beta_y \omega t}{2}$, with superimposed fine motion $\left(1 + 0.336 \cos\left(\omega t + \phi\right)\right)$ Brubaker has shown the trajectories for both motions computed with specific conditions and has also derived the elements of Equation (2) by the integration of incremental forces on the ion. We differ from his constant which appears in the position of $2\left(c_2\right)_y$ in obtaining 0.336 instead of 0.353.

From Equations (1) and (2) the values of the maximum amplitude of motion in each plane are obtained as a function of initial conditions. Since the y motion is simpler we use this for an example as follows:

From (2),

$$y = A_y \sin\left(\frac{\beta_y \omega t}{2} + \delta_y\right)\left[1 + 0.336 \cos\left(\omega t + \phi\right)\right] \tag{3}$$

and we first observe that $(y_{max}) = 1.336\ A_y$. (4)

Evaluation of (3) and its time derivative at $t = 0$ gives:

$$y_o = A_y f_1 \sin \delta_y \tag{5}$$

and

$$\mathring{y}_o = A_y \left(f_1 \frac{\beta_y \omega}{2} \cos \delta_y - f_2\ \omega \sin \delta_y\right), \tag{6}$$

where

$$f_1 = \left(1 + 0.336 \cos \phi\right) \qquad \text{and}$$

$$f_2 = 0.336 \sin \phi .$$

Solving for A_y:

$$A_y^2 = \frac{1}{f_1^2}\left\{y_o^2 + \frac{4}{\beta_y^2}\left(\frac{\mathring{y}_o}{\omega} + y_o \frac{f_2}{f_1}\right)^2\right\} .$$

Substituting in (4) gives:

$$\left|y_{max}\right| = \frac{1.336}{f_1}\left\{y_o^2 + \frac{4}{\beta_y^2}\left(\frac{\mathring{y}_o}{\omega} + y_o \frac{f_2}{f_1}\right)^2\right\}^{\frac{1}{2}} . \tag{7}$$

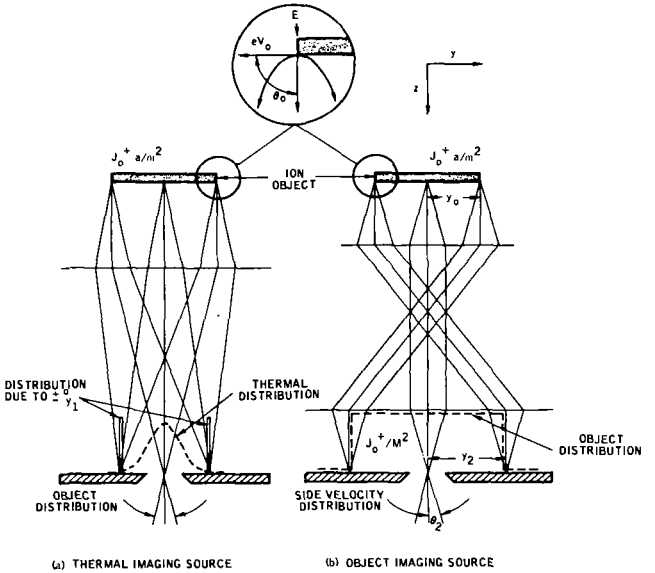

FIGURE 3
Schematic of Focusing of Two Generalized Types of Ion Sources.

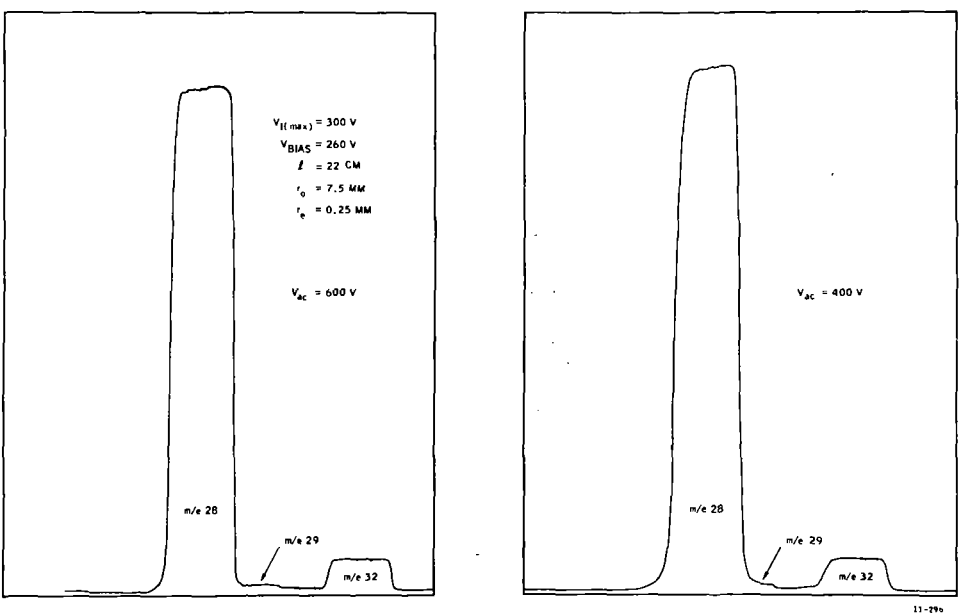

FIGURE 4
Effect of V_{ac} on the Top Width of Peak in a Study of Entrance Angle
from $V_I \sin^2 \alpha_{max} = 0.0095\, V_{ac} \frac{dm}{m} \left(1 - \frac{T}{B}\right)$

It can be easily shown that for resolution better than $\frac{m}{\Delta m} = 10$, the term y_o^2 can be neglected. Consequently,

$$\left|y_{max}\right| = \frac{2.672}{\beta_y f_1} \left| \frac{\dot{y}_o}{\omega} + y_o \frac{f_2}{f_1} \right| \tag{8}$$

where the absolute signs are obtained in the process of taking the square root.

By the method employed by Paul[1] an approximate equation for $\left|x_{max}\right|$ evaluated through coefficients C_{+2} and C_{-4} at $\beta_x = 0.92$ is;

$$\left|x_{max}\right|_{\beta_x = 0.92} = 16.35 \left(f_3 x_o^2 + f_4 \frac{x_o \dot{x}_o}{\omega} + f_5 \frac{\dot{x}_o^2}{\omega^2} \right)^{\frac{1}{2}} , \tag{9}$$

where

$$f_3 = 0.40 - 0.20 \cos \phi - 0.20 \cos 2\phi ,$$

$$f_4 = 0.93 \sin \phi + 0.26 \sin 2\phi , \text{ and}$$

$$f_5 = 1.63 + 1.86 \cos \phi + 0.26 \cos 2\phi .$$

The variable ω may be eliminated with the following substitutions:

$$\dot{y}_o = \left(\frac{2eV_I}{m}\right)^{\frac{1}{2}} \sin \alpha \tag{10}$$

where eV_I is the injection energy and α the entrance half-angle. Using the quadrupole equation:

$$\frac{e}{m} = \frac{q \omega^2 r_o^2}{4 V_{ac}} \tag{11}$$

and letting

$$\gamma = \left(\frac{V_I}{V_{ac}}\right)^{\frac{1}{2}} \sin \alpha , \tag{12}$$

equation (10) becomes:

$$\frac{\dot{y}_o}{\omega} = \left(\frac{q}{2}\right)^{\frac{1}{2}} r_o \gamma , \tag{13}$$

In the region of the apex of the stability diagram $q = 0.706$.

Thus dividing y_{max} by y_o in Equation (8) and substituting Equation (13):

$$\frac{\left|y_{max}\right|}{y_o} = \frac{2.672}{\beta_y f_1} \left| \frac{0.595\, r_o \gamma}{y_o} + \frac{f_2}{f_1} \right| \tag{14}$$

Similar substitutions may be made for $\left|x_{max}\right|$.

From these equations we can now show examples of combined initial position and angle in Figure 1 where (x_{max}) and (y_{max}) are plotted as a function of initial phase angle, ϕ, with γ as a parameter. The value $\frac{r_o}{r_e} = 30$ is used where $r_e = x_o = y_o$ is the radius of a round entrance aperture.

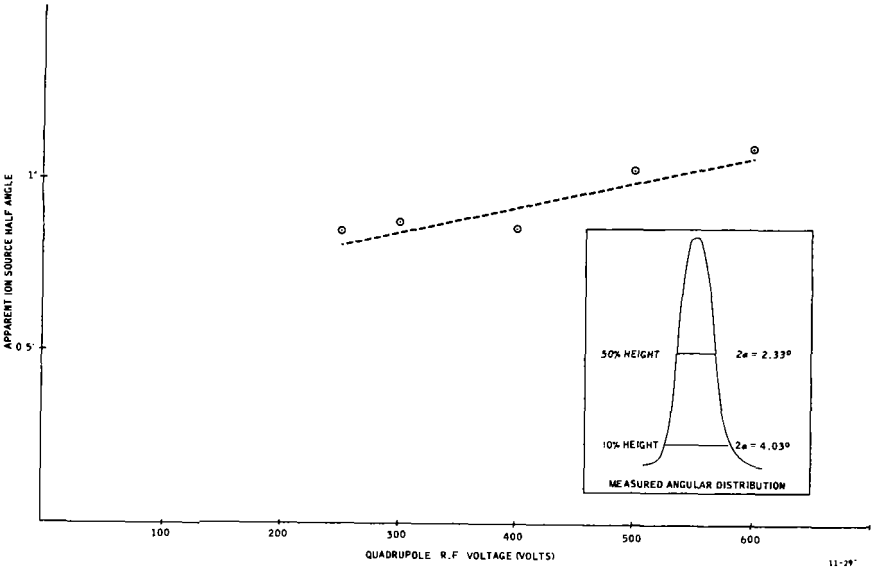

FIGURE 5
Apparent Entrance Angle vs V_{ac} Calculated from $V_I \sin^2 \alpha_{max} = 0.0095 V_{ac} \frac{dm}{m}\left(1 - \frac{T}{B}\right)$. Zero Slope is a Corroboration of the Form of the Equation.

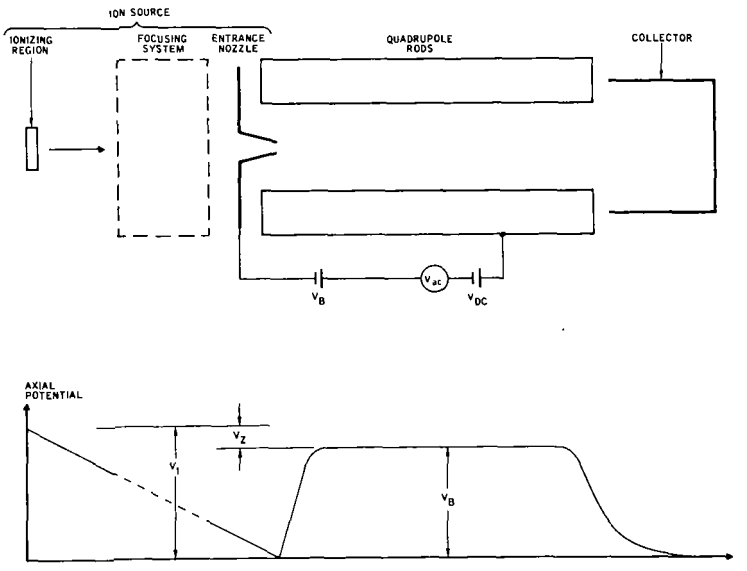

FIGURE 6
Quadrupole Mass Spectrometer Schematic and Axial Potential Distribution

Comparison with the curves which Paul has computed[3] for x_o, $y_o = 0$ or $\dot{x}_o$, $\dot{y}_o = 0$ indicate that the approximate solutions are in good agreement in the x - z plane where maxima are within 7% and the same shaped curve is obtained. In the y - z plane, ion motion reaches a maxima for a phase somewhat shifted from Paul's, however, maxima agree to better than 2%.

By comparing the $|x_{max}|$ and $|y_{max}|$ curves it is seen that for equal values of γ, $|y_{max}| > |x_{max}|$.

It should be noted that the maximum amplitude in y - z plane occurs in the useful region between $127° > \phi > 142°$. A study was made over a variety of conditions where it was found that for equal initial conditions in the two planes, nominal worst case condition is at $\phi = \frac{3\pi}{4}$ in the y - z plane. By choosing $\frac{3\pi}{4}$, up to a 3% amplitude change can occur. From the foregoing, it appears that the approximate expressions may be used with less than 10% error.

Consequently, the following generalizations are made:

For 100% transmission $\left|y_{max}\right|_{\phi = \frac{3\pi}{4}} \leq r_o$,

thus letting $y_{max} = r_o$ and $r_e = x_o = y_o$

$$\frac{r_o}{y_o} = \frac{r_o}{r_e} \geq \frac{2.672}{\beta_y f_1} \left| 0.595 \frac{r_o \gamma}{r_e} + \frac{f_2}{f_1} \right|_{\phi = \frac{3\pi}{4}}$$

where

$$(f_1)_{\frac{3\pi}{4}} = 0.763 \quad , \quad (f_2)_{\frac{3\pi}{4}} = 0.238.$$

$$\frac{r_o}{r_e} \geq \frac{1.09}{\beta_y} \left[1 + 1.9 \left| \gamma \right| \frac{r_o}{r_e} \right]$$

Solving explicitly for $\frac{r_o}{r_e}$ in the limiting case:

$$\frac{r_o}{r_e} = \frac{1.09}{\beta_y - 2.07 \left| \gamma \right|_{max}} \quad \text{or} \quad 1.09 \frac{r_e}{r_o} + 2.07 \left| \gamma \right|_{max} = \beta_y \tag{15}$$

Here then is a simple equation relating normalized transverse energy, normalized entrance position, and the position in the stability diagram. This assures 100% transmission regardless of entering phase and whether the ion enters in the x or y phase or a combination of both. This latter condition is satisfied since all conditions of entrance are less severe than the ones chosen. The value $(1-\beta_x)$ may be substituted for β_y when considering the x stability region.

Referring to Figure 2, the interpretation is as follows: As the scan line passes through the stability diagram, β_y is at first very small.

Consequently only low angle ions contained in low values of $\gamma = \left(\frac{V_I}{V_{ac}} \right)^{\frac{1}{2}} \sin \alpha$ are transmitted within a given $\frac{r_o}{r_e}$ ratio. As β_y increases, larger angles are accepted and transmitted by the analyzer with consequent increase in collected current until one of two conditions become predominant. If, by some means, γ is limited, a region of 100% transmission occurs with a resultant constant collected current or "flat-topped" peak. However, if γ is unlimited the x stability takes over at a position where $\beta_y = 1 - \beta_x$ at the tent peaks and by the same mechanism ions are lost to the x poles as $\beta_x \rightarrow 1$. In this condition, a pointed peak is produced.

The next question is: How should the entrance aperture be related to entrance angle for optimum performance. Therefore, we proceed to examine ion sources for an explicit relationship and from this to obtain a maximum in the ion current.

ION SOURCES

When reduced to their elements, most ion sources can be typified as focusing in one of two modes. Figure 3 shows the most common method wherein the source ion current is peaked up by producing the smallest line or point "image" and thus the highest density. However, it is noted that given some thermal distribution in the gas being ionized, those with higher side velocity are not transmitted. If only a specific side velocity $\pm\dot{y}_1$ is present such as encountered in satellite motion the line spectra are not transmitted at all.

An alternative mode of focusing is shown in Figure 3b where an image of the ion object is produced. In this case each position in the image correlates with a position in the object. Also, up to a limit determined by the lens aperture sizes, the position in the image is independent of initial energies of the ions. It is noted then that the distribution of initial energies lies in the angular distribution.

Since this mode of focusing is more appropriate for energetic particle measurements, we may proceed to describe the ion density more analytically. For a magnification, M the ion density at the image plane is $\frac{J_o^+}{M^2}$ for J_o^+ current per unit area produced is the ionizing beam. Thus the source current is

$$I_s^+ = \pi r_e^2 \frac{J_o^+}{M^2} , \qquad (16)$$

where r_e is the radius of a round aperture.

From Abbe's law[4], the bundle of rays produced within an included angle θ_o, at a point in the object plane, fall within an included angle θ_i at the image plane by the relationship;

$$y_o V_o^{\frac{1}{2}} \sin \theta_o = y_i V_i^{\frac{1}{2}} \sin \theta_i, \qquad (17)$$

where eV_o is the initial ion energy and eV_i the total ion energy at the image plane.

Letting $\theta_o = \frac{\pi}{2}$ to include a worst case angle and since $\frac{y_i}{y_o} = M$,

$$\sin \theta_i = \left(\frac{V_o}{V_i}\right)^{\frac{1}{2}} \left(\frac{1}{M}\right) \qquad (18)$$

From (18), for a given maximum of (V_o), we note that $\sin \theta_i$ can be kept within some upper limit acceptable for transmission by the analyzer by adjusting the magnification. Thus from (16) the ion source current becomes established. In the region of 100% transmission then, the collected current for the mass spectrometer becomes,

$$I_c^+ = \pi r_e^2 \frac{J_o^+}{M^2} \qquad (19)$$

Consequently for this mode of focusing we find that the measurement of partial density is, in principle, independent of initial conditions up to a maximum initial energy $(eV_{o\ max}$. It remains to establish r_e and $\sin \theta_i$ such that the maximum ion current is collected under the restraints of 100% transmission and limited initial energy.

Combining (18) and (19) by eliminating M yields

$$I_c^+ = \pi r_e^2 J_o^+ \left(\frac{V_I}{V_o}\right)_{max} \sin^2 \alpha_I \qquad (20)$$

in which the injection voltage V_I is used for the image plane energy V_i, and the maximum injection angle α_I is substituted for θ_i. In Equation (20), M is an implicit variable used to limit $\sin^2 \alpha$ as $(V_o)_{max}$ is chosen. Since this equation contains r_e and $\sin \alpha$ it may be solved simultaneously with the quadrupole equation.

Combined Quadrupole and Ion Source. By substituting for γ in (15) and solving for $V_I \sin^2 \alpha_{max}$, one obtains

$$V_I \sin^2 \alpha_{max} = 0.233\, V_{ac} \left(\beta_y - 1.09 \frac{r_e}{r_o} \right)^2, \tag{21}$$

where α_{max} is the largest acceptable angle for given values of β_y and $\frac{r_e}{r_o}$.

Angles less than this will be transmitted. Further, one may conclude for given α_I and $\frac{r_e}{r_o}$ that the collectable current, I_c^+, reaches a peak when $\alpha_{max} = \alpha_I$ and remain constant when $\alpha_{max} > \alpha_I$

Substituting in (20),

$$I_c^+ = \frac{0.233\, V_{ac}\, r_e^2\, J_o^+}{(V_o)_{max}} \left(\beta_y - 1.09 \frac{r_e}{r_o} \right)^2, \tag{22}$$

where we note that $I_c^+ = o$ at $r_e = o$ and at $1.09 \frac{r_e}{r_o} = \beta_y$.

These conditions represent zero aperture and zero acceptable angle respectively. Zero angle in turn implies infinite manification and thus zero current density.

By differentiating for a maximum, one finds that α_I and $\frac{r_e}{r_o}$ contribute equally to a hypothetical "beam width" when

$$\left(\frac{r_e}{r_o} \right)^2_{max} = 0.211\, \beta_y^2 \tag{23}$$

and from (21)

$$V_I \sin^2 \alpha_{max} = 0.0583\, V_{ac}\, \beta_y^2 . \tag{24}$$

With reference to Figure 2, for "flat topped" peaks the ion current arrives at a maximum before the scan line reaches the $\beta_y = 1 - \beta_x$ intercept. The base width, B, of the peak is defined to be that portion of the scan line within the stability diagram (i.e., the theoretical base width); and the top width, T, that portion lying between lines of $\beta_y = 1 - \beta_x$ (not at the intercept). By calculation of the intercepts,

$$\left(\beta_y^2 \right) = \left(1 - \beta_x \right)^2 = 0.164 \frac{dm}{m} \left(1 - \frac{T}{B} \right). \tag{25}$$

Equation (25) describes the β_y and β_x intercepts with the scan line where the current becomes constant. Iso $- \frac{T}{B}$ lines may be constructed by inspection.

We now require that the ion current reach maximum value at the above β_y - scan line intercept. This consequently defines the values of $\frac{r_e}{r_o}$ and $\sin^2 \alpha_{max}$ for maximum ion current as:

$$\left(\frac{r_e}{r_o} \right)^2_{max} = 0.0346 \frac{dm}{m} \left(1 - \frac{T}{B} \right) \tag{26}$$

and

$$V_I \sin^2 \alpha_{max} = 0.00955\, V_{ac} \frac{dm}{m} \left(1 - \frac{T}{B} \right) \tag{27}$$

From (22), (23) and (26).

$$I_{c\,max}^+ = 3.15 \times 10^{-4} \frac{V_{ac}}{(V_o)_{max}} \pi r_o^2 J_o^+ \left(\frac{dm}{m} \right)^2 \left(1 - \frac{T}{B} \right)^2 . \tag{28}$$

Throughout the T region then $I_{c\,max}^+$ is constant at this value since $\alpha_{max} > \alpha_I$.

Summarizing then: With given limits on the initial conditions and choice of the quadrupole parameters one may calculate the expected current of mass peaks meeting criteria of shape and resolution. The interesting result is that, for this mode of ion source focusing, the collected current is, in principle, a measure of partial density in the ionizing region independent of the initial energies up to $(V_o)_{max}$.

An instrument for atmospheric studies has been constructed along these lines having $r_o = 7.5$ mm, $r_e = 0.25$ mm and length $\ell = 22$ cm.

A check on Equation (27) was made however, to determine the validity of injection angle *versus resolution and* $\frac{T}{B}$ *ratio. Figure 4 shows two partial spectra typical of those* used to calculate the apparent injection angle, given measurements for the other variables. V_{ac} was the independent variable while $\frac{T}{B}$ was the primary dependent variable. The theoretical base width was used (i.e., without tails) measured by extending the peak sides. Figure 5 gives the apparent angle vs V_{ac} where the inset shows the directly measured angular distribution. The apparent angle is approximately constant over the range of V_{ac} however, with the density distribution shown is less than the measured angle by a factor of ~ 1.5. This contraction in apparent angle is believed to be due to the effect of quadrupole biasing.

Quadrupole Biasing. The length of the quadrupole rods is required to have a certain minimum value which depends upon the values of several parameters. von Zahn[5] stated this relationship in the simple form:

$$n \geq 3.5\sqrt{\frac{m}{\Delta m}} \qquad (29)$$

where n = number of cycles of the r.f. voltage which occur while the ion is in the quadrupole field. This equation implies that if a half height resolution of $\frac{m}{\Delta m}$ is required then n cycles must occur in order that the peak tails do not make an appreciable contribution to the width of the peak. By relating n to the axial ion energy, V_z, and using the quadrupole equation one obtains:

$$\frac{\ell}{r_o} = K\sqrt{\frac{13.9\ V_z}{V_{ac}}\ \frac{m}{\Delta m}} \qquad (30)$$

where ℓ is the length of the quadrupole rods, and K is a constant which depends upon the exact criterion used to measure the resolution and the contribution of the tail to the peak base width. If von Zahn's criterion is used, $K = 3.5$. For one percent peak height resolution $K \approx 7$.

In normal quadrupole operation the ion source injection voltage is equal to the axial kinetic energy of the ions in the quadrupole, i.e., $V_I = V_z$. When an ion source is required to capture and focus energetic particles which have an appreciable angle of incidence, the injection voltage, V_I, must be large. This implies that the length of the quadrupole rods will be excessive. It was found, however, that by placing a bias voltage V_B between the ion source and the quadrupole rods the mass spectrometer may be successfully operated in a mode where:

$$V_z = V_I - V_B \qquad (31)$$

A schematic of this technique, with an approximate axial potential distribution, is shown in Figure 6. The effect of the quadrupole bias voltage is shown in Figure 7. As the bias voltage is raised the peak tails are diminished. There is no observable decrease in sensitivity as V_B is increased until the least energetic ions are reflected. Even disregarding the contraction of the tails, the $\frac{T}{B}$ ratio apparently improves as the bias is applied. This may indicate that the field around the entrance nozzle is causing a contraction of the effective angle of injection.

REFERENCES

1. W. Paul, H. P. Reinhard and V. von Zahn; Z. Physik 152, 143 (1958).
2. W. M. Brubaker; Neuvieme Colloq. Spectroscopicum Intern., Lyon, France, 1961.
3. Reference 1, Fig. 4.
4. c.f.: Klemperer; Electron Optics, Cambridge University Press, 1953, p 14.
5. U. v. Zahn: Diplomarbeit Bonn, 1956 (unpublished).

A QUADRUPOLE MASS SPECTROMETER FOR ISOTOPE RATIO STUDIES OF PLASMA CONSTITUENTS*

by

M. A. Mosharrafa and H. J. Oskam
Department of Electrical Engineering
University of Minnesota

Abstract

A quadrupole mass spectrometer, bakeable at 350°C, has been constructed for studying plasma properties. The analyzing field, produced by 4 hyperbolic electrodes consisting of 124 molybdenum wires (diameter 0.5 mm), is 100 cm in length. A preliminary investigation of the properties of the mass spectrometer yielded a resolving power of at least 200. The inherent low background noise of the spectrometer permitted measurements of ion densities over a range of $1 - 10^6$.

The first studies were performed in pure argon and neon-argon systems, using an active plasma ion source and resulted in the definite establishment of the existence of the $(NeAr)^+$ molecular ion in an active gaseous plasma. The identification was achieved by determining the isotope ratio of $(NeAr)^+$. The relative number density of this hybrid molecular ion was also studied as a function of gas pressure.

Introduction

A thorough study of the behavior of different ionic species in gaseous discharges necessitates the use of a mass-analyzing instrument for accurate quantitative analysis and identification of plasma ions and their isotopes. A mass-spectrometer system utilizing plasma ion sources is desired to have the following features:

(1) Adequate resolving power. High resolution techniques are not necessary for most applications.

(2) High sensitivity.

(3) Large dynamic range. Features (2) and (3) are particularly desirable when studying disintegrating plasmas where it is important to observe the time decay of ion concentrations over several orders of magnitude. They also prove to be of great importance in the type of studies reported in this paper where minority ionic species and their isotopes are to be observed in a plasma.

(4) No energy discrimination in order to obtain true quantitative representation of plasma ionic constituents.

(5) High plasma-source pressure capabilities. The mass spectrometer should be capable of efficient operation throughout a large range of plasma ion-source pressure variation.

(6) Bakeable system, since it is well-known that impurity concentrations as small as 10^{-4}% have a large influence on plasma behavior.

* Work supported by the National Science Foundation and the Advanced Research Project Agency as part of Project Defender through the Office of Naval Research.

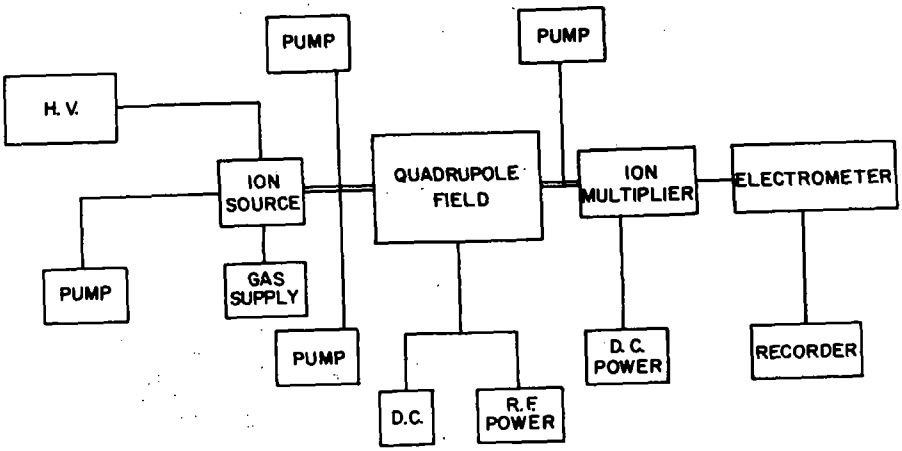

Fig. 1

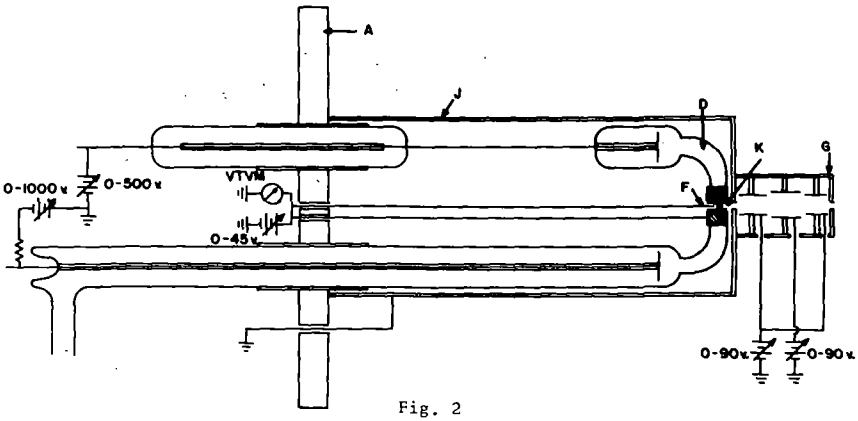

Fig. 2

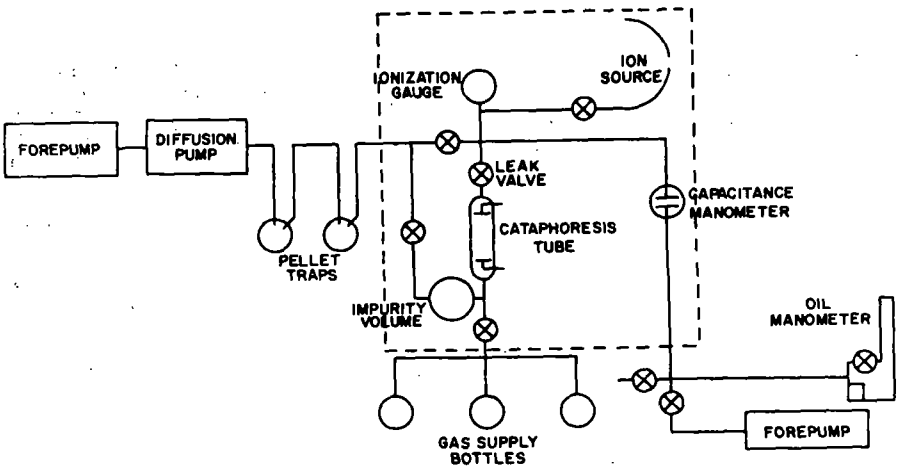

Fig. 3

(7) Minimal influence of the mass-spectrometer system on the plasma behavior. This is important in studies on undisturbed behavior of plasmas.

After a careful study had been made on different existing types of mass-spectrometers, the quadrupole "mass-filter" proposed and developed by Paul[1] appeared to be the most suitable type to be used since it offers the following distinct features:

(a) It has a very high transmission efficiency, especially at low resolving powers. This is due to the fact that the transmission characteristics of an ion are not changed (to a first approximation) by collisions with molecules of the residual gas (disregarding charge exchange) due to the strong focusing feature of the quadrupole field. This also permits the operation of the mass-spectrometer at higher residual pressures, a distinct advantage for "flow-through" systems.

(b) Elimination of magnetic field requirements for mass-spectrometer operation is extremely advantageous in plasma studies due to the difficulty of shielding plasmas from stray magnetic fields.

(c) Injection conditions (allowable radial energies, off axis injection, accelerating potentials, etc.) applied to the ion beam have a small influence on the transmission efficiency of the quadrupole field and are there fore noncritical.

(d) The cylindrical symmetry of the analyzing field. The most practical way of extracting ions from a plasma is via a small circular hole drilled through the plasma container. This produces an ion beam of cylindrical symmetry which matches the optimum injection requirements of the quadrupole field.

A quadrupole mass-spectrometer was designed[2] and built[3] for studying the behavior of ions and their isotopes in gaseous plasmas. The spectrometer was first used in an attempt to answer the question of the possible existence of rare-gas hybrid molecular ions in plasmas. All hybrid rare-gas molecular ions have been found to exist as products of the interaction of electron beams with rare-gas mixtures,[4,5,6] although no measurements of their isotopic abundances were reported. In plasmas, however, the only observed rare-gas hybrid molecular ion was the $(HeNe)^+$ ion. Oskam[7] postulated its existence in plasmas based on his observations in microwave studies of decaying plasmas containing a mixture of helium and neon. The existence of this molecular ion was at the same time established by Pahl and Weimer[8] using neon isotope measurements for proper identification. In Ne-Ar plasmas they did not find the $(NeAr)^+$ ion.[9] We have made a study of gaseous plasmas produced in neon, argon and their mixtures. Measurements were made, using the quadrupole mass-spectrometer, of the constituent ion densities and their isotopes. In this paper only the results relating to $(NeAr)^+$ will be presented.

Apparatus

Figure 1 shows a block diagram of the mass-spectrometer system. The quadrupole field of length 100 cm is obtained by 4 electrodes shaped to form two perpendicular equilateral hyperbolae having a field radius r_o = 2 cm. Each of the four hyperbolic electrodes is formed by stretching 31 molybdenum wires 0.508 mm in diameter along the field length; the cross-section of each set of wires thereby lying on an arc of the equilateral hyperbolae. The wires are fastened on each end by small stainless steel screws to two stainless steel plates each accurately machined to form one equilateral hyperbola. The quadrupole mass-filtering field specifications are as follows:

field radius = 2 cm
field length = 100 cm
range of mass analysis = 1 - 170
maximum resolving power = 1:200
operating r.f. frequencies: 0.5 Mc/s for complete mass range scanning
1.0 Mc/s for expanded mass range 1-50
2.0 Mc/s for expanded mass range 1-12

operating range of r.f. voltage: 0 - 1000 volts r.m.s.
maximum r.f. power requirement: 80 watts approximately
scanning: Is affected by varying the r.f. and dc voltage amplitudes simultaneously.
sensitivity: 5×10^{-17} amp
measureable ion density range: 10^6

One of the basic requirements which had to be taken into account in the design of the spectrometer, is the ability to bakeout the system at 400°C. This presented a problem in the quadrupole field region. Here, the difference in the thermal coefficient of expansion between the stainless steel casing of the field region and the molybdenum wires becomes quite serious. The wire tension will increase with increasing temperature up to the point where it will exceed the yield strength of molybdenum resulting in permanent sagging and deformation of the wires. The problem was solved by deliberately releasing the tension on the wires before bakeout and pulling the wires back to the required amount of tension after the system has cooled down to room temperature.

The plasma ion source is shown schematically in Fig. 2 and is constituted basically of a glass tube (D) 10 mm ϕ mounted on a 10" ϕ flange (A). A hole (K) 30 μ in diameter is drilled[10] through the glass wall midway between the 2 discharge electrodes allowing the escape of ions diffusing to the wall and therefore constituting the ion beam to be analyzed.

The ion source is enclosed in a metal cylinder (J) through which a longitudinal slit is cut to prevent r.f. heating of the cylinder and ion source. It also serves to shield the plasma from the r.f. quadrupole field and provides the reference for the accelerating potential applied to the ion beam. The cylindrical probe (F) lies on the same circumference as the hole. It measures approximately the wall potential of the plasma at the hole and thereby making it possible to monitor retarding or accelerating fields in the plasma region of ion extraction. (G) is the electrostatic lens focusing system used for limiting the radial energy of the ion beam. It constitutes an accurate symmetrical lens aimed at imaging the plasma source at the input of the quadrupole analyzing field.

The gas handling system shown in Fig. 3 provides a clean controlled-pressure flow-through system. Further purification of the gas is obtained by continuous effective cataphoretic action at a pressure independent of the gas pressure in the discharge ion source. With the existing ion source hole size (30 μ) and the available pumping speed of the mass-spectrometer vacuum system, it is possible to extend the gaseous discharge pressure over a range of 0.1 Torr to 40 Torr. At 40 Torr, the background pressure in the analyzing field region was found to be 9×10^{-4} Torr which had no effect whatsoever on its behavior. This was expected as explained previously.

Initial calibration of the mass-spectrometer was performed before bakeout in order to make use of the existing impurity ions. A dc argon discharge was used as the ion beam source at a pressure of about 5 Torr and a discharge current of 20 mA. A scan through the entire mass range indicated presence of ions corresponding to M = 12, 16, 17, 18, 19, 20, 21, 22, 36, 40, 76, 80 where M is the ratio of the mass in atomic units to the charge in electronic units. Calibration was made through identification of Ne^{20} and Ne^{22} isotopes. A second calibration was made after bakeout through observation of Ar^+ and Ar_2^+ peaks. The calibration agreed extremely well (within 2%) with that obtained from theoretical design calculations.

Results

Experiments were performed on a plasma produced in a neon-argon mixture, consisting of 60% argon and 40% neon. The ion beam was mass analyzed to determine the constituent ion species and their behavior as a function of pressure in the discharge ion source. The obtained results showed a strong behavior of the relative abundance of the ionic constituents in the plasma on pressure. Two pressure regions can be distinguished which are, of course, arbitrary since their spans are a very strong function of the sensitivity of the measurements and ion source geometry. They are as follows:

(a) High pressure region: ($p > 3.5$ Torr) Mass spectra were investigated at pressures up to 33 Torr, a typical spectrum is shown in Fig. 4. No neon ions or $(NeAr)^+$ hybrid molecular ions are observed, the spectra appears similar to that obtained from a pure argon discharge. The absence of ionized neon is understandably due to the high efficiency of the Penning process in this mixture.

(b) Low pressure region: As the pressure of the gas is decreased below 3.5 Torr mass M = 60 starts to appear in the spectrum (Fig. 5). It is impossible, however, to positively identify the M = 60 peak with $(NeAr)^+$ since the isotope abundance of this molecular ion (M = 62) is still below the threshold of sensitivity. Neon peaks are also not observable until the pressure is reduced to 1.2 Torr. At this pressure only Ne^{20} could be detected. At very low pressures (0.2 Torr - 0.6 Torr), the spectrum is "completed" by the observation of all isotopes of neon and the $(NeAr)^+$ isotope $(Ne^{22}Ar^{40})^+$ as shown in Fig. 6. In this pressure region measurement of the ratio of I^{62}/I^{60} was found to be equal to that of Ne^{22}/Ne^{20}.

In this pressure region, the existence of the $(NeAr)^+$ hybrid molecular ion in a plasma, therefore, is definitely established.

Assuming that $(NeAr)^+$ is produced in a plasma via the Hornbeck-Molnar process:[5]

$$Ne^* + Ar \longrightarrow (NeAr)^+ + e$$

The failure to observe this type of hybrid molecular ion at higher pressures may be due to:

(a) The decrease in number density of excited neon atoms with increasing pressure for the gas mixture used.

(b) $(NeAr)^+$ probably has a small dissociation energy which may involve a large dissociative recombination coefficient and/or effective dissociation by collisions with the gas molecules. This results in an increasing loss with increasing pressure.

In summary, the results of this work establish the existence of $(NeAr)^+$ in gaseous plasmas and we believe that the failure to observe this ion in previous studies by other investigators is due to the limited dynamic range of their mass-spectrometer systems.

References

1. W. Paul and H. Steinwedel, Z. Naturforschg 8a, 448 (1953).
2. M. Mosharrafa, Technical Report No. 2, Contract No. Nonr-710(37) (1961).
3. H. J. Oskam, Semi-Annual Technical Report No. 1, Contract No. Nonr-710(37), February, 1964.
4. R. Fuchs and W. Kaul, Z. Naturforschg 15a, 108 (1960).
5. W. Kaul, U. Lauterbach and R. Fuchs, Naturwiss 47, 353 (1960).
6. M. S. B. Munson, J. L. Franklin and F. H. Field, J. Phys. Chem. 67, 1542 (1963).
7. H. J. Oskam, Phillips Res. Reports 13, 401 (1958).
8. M. Pahl and U. Weimer, Naturwiss 44, 487 (1957).
9. M. Pahl and U. Weimer, Z. Naturforschg 12a, 926 (1957).
10. D. G. Andersen, R. A. Gerber and G. F. Sauter, Rev. Sci. Instr. March, 1964.

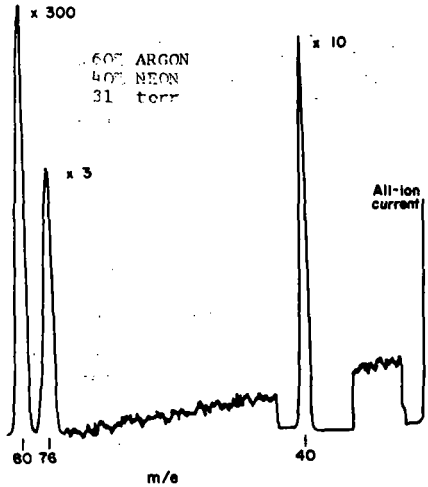

Fig. 4

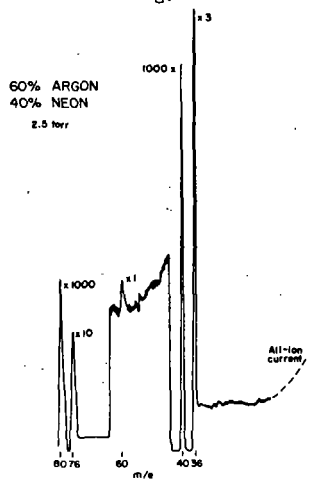

Fig. 5

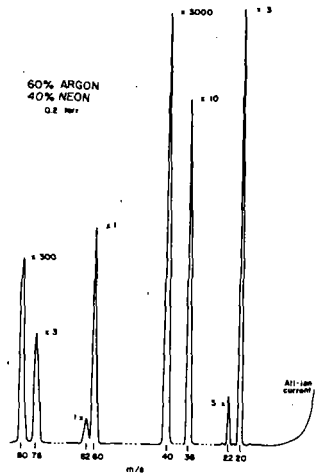

Fig. 6

TIME-OF-FLIGHT MASS SPECTROMETRIC ANALYSES OF A MULTI-KILOWATT PLASMA

G. J. O'Halloran and L. W. Walker
The Bendix Corporation
Research Laboratories Division
Southfield, Michigan

Results are presented of a recent experimental program[1] to extend and better define the capability of a Bendix Time-of-Flight Mass Spectrometer for the analysis of high energy density plasma. Data on reproducibility, species identification and particle density are included. Analyses using small amounts of seeded components to determine dynamic range are summarized.

(1) Part of the effort involved in conducting this program was supported by the Aeronautical Systems Division, United States Air Force, Wright-Patterson Air Force Base, Ohio, under Contract AF 33(657)-11018.

PERFORMANCE OF THE HIGH VOLTAGE ENGINEERING CORPORATION ISOTOPE SEPARATOR*

George W. Barton, Jr., Abe Tilles and J. R. Walton
Lawrence Radiation Laboratory
University of California
Livermore, California
and
Richard J. Connor and Thomas C. Smith
High Voltage Engineering Corporation
Burlington, Massachusetts

The performance of the Livermore isotope separator will be summarized as it has performed during and since its installation at Livermore. The magnet is a 160 cm radius homogeneous field 90° sector with a maximum field density in excess of 5000 gauss and capable of separating isotopes in the mass range of 1 to 400. The 80 kilovolt high voltage supply is normally run at 60 kv and has been successfully operated at 70 kv. The magnet and high voltage supplies are well regulated. Since at 60 kv and with a moderately clean accelerating structure, sparks occur only about once per half hour, isotopes can be collected without the use of beam feelers. The resolving power is normally in the range of 600 to 1200 with total beam currents from 5 to 130 microamperes. With sacrifice of total beam current to a few microamperes, a resolving power of 1700 is attainable.

* Work was performed under the auspices of the U. S. Atomic Energy Commission.

FLASH VAPORIZATION OF SOLID MATERIALS FOR MASS SPECTROMETRY BY INTENSE THERMAL RADIATION

Kenneth A. Lincoln
U. S. Naval Radiological Defense Laboratory
San Francisco, California 94135

Introduction

In more conventional mass spectrometry where fairly volatile materials are analyzed, the sample is vaporized in an external oven and the vapors are piped into the ion source via a calibrated leak or valve. On the other hand, materials having low vapor pressures are commonly vaporized in some type of small furnace within the ion source housing. Usually this is either in the form of a miniature furnace positioned close to the electron beam or a Knudsen cell from which the vapors effuse out as a molecular beam into the ion gun. The cell is situated usually within the vacuum of the ion source and is heated by a resistance wire or by bombardment from high-energy electrons. These techniques for studying solid samples suffer from several drawbacks which include the limited upper temperature available (1500° to 2200°C), reactions of some vapors with the hot metal structures, and frequent degassing problems.

The prevalent method for mass spectrometric analysis of inorganic solids is the radiofrequency spark ion source which ionizes the sample as it is vaporized from an electrode. There are two characteristics of this technique in particular which decrease its attractiveness: the ion beam has a very large velocity spread and it is quite unsteady. A less commonly used method for inorganic materials is thermal ionization of the solid from the surface of a heated filament, however, the ionization efficiencies with this technique vary with the chemical elements over several orders of magnitude.

In this paper attention is directed to a different heating method which has proved to be very successful for rapidly heating many types and kinds of solid materials to high temperatures. This technique utilizes the intense thermal radiation obtained from capacitor discharges through xenon flashtubes.[1] Nelson and Kuebler[2] have vaporized such refractory materials as tungsten by this technique, and have applied it to the vaporization of elements for atomic absorption spectroscopy.[3]

Described herein is a similar single-pulse method for vaporizing solid samples within the ion source housing of a time-of-flight mass spectrometer; also detailed is the solid-sample inlet which is an integral part of the system. We have utilized this technique of flash-vaporization mass spectrometry to study high-temperature decomposition of cellulose and have applied it to obtain mass spectra of several other low vapor pressure organic compounds as well as some inorganic compounds including meteoric fragments.

Radiant Flash Heating Considerations

It should be pointed out that a sample must possess certain physical characteristics to make this type of flash heating feasible. For maximum temperature rise, a material must have a high optical absorptance in the visible and near infrared plus a large surface-to-volume ratio; i.e., the greater the exposed surface the more energy absorbed by the material. Nelson[1] has shown that for spheres and rod-shaped particles a diameter of about 10 microns or less is advantageous; he has found that very thin metal foils are also readily vaporized in this manner. Where temperature requirements are not so high, e.g., vaporization of organic materials, the surface-to-volume ratio is not so critical. We have found that 2-mil sheets of cellulose made black by inclusion of 2% carbon black can be almost completely vaporized by radiant exposure as low as 2.0 cal/cm^2 incident on both surfaces. On the other hand the technique is not restricted to finely divided or thin samples; if the material has a low heat diffusivity and a reasonably good absorptance, each flash will vaporize enough of the surface layer from thick samples to provide a spectrum. Moreover this has the advantage of

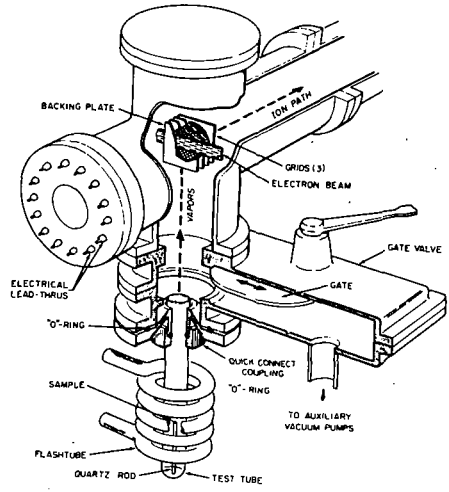

Fig. 1. Ion source of mass spectrometer with attached flash-heating inlet system.

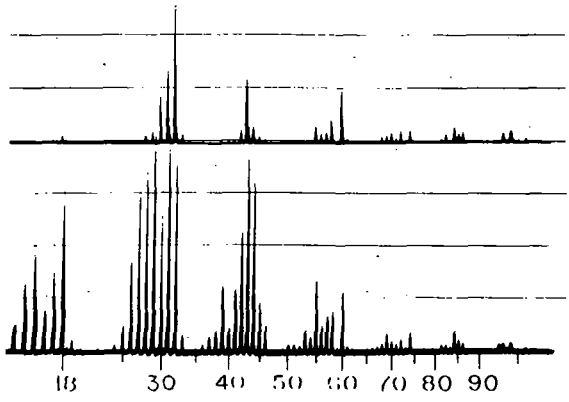

Fig. 2. Flash-vaporizatin mass spectra of cellulose. Upper: 15 electron-volt ionizing potential, Lower: 70 electron-volt ionizing potential.

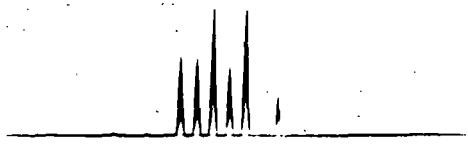

Fig. 3. Isotopes of cadmium from flash-heated CdS.

not requiring sample reloading for each spectrum obtained. One of the more striking features of the radiant flash-vaporization method is that the intense pulse of light heats only the sample; all of the surroundings remain cool and thus reactions with hot ion source structures are obviated.

Although the most difficult parameter to obtain is the temperature rise of the flash-heated material, an approximate upper temperature sometimes can be calculated[4]. On the other hand, the amount of energy per flash, and peak intensity incident on the samples, has been carefully measured for several flashtubes and it is easily varied by adjustment of the electrical parameters in the power supply of the flashtube.[5]

Instrumentation

The principal component of the flash-vaporization mass spectrometry system is a Bendix Model 14-107 time-of-flight mass spectrometer. Coupled to this is a flashtube thermal-radiation unit which has been fully described elsewhere[5], it is comprised of a General Electric type FT-625 xenon flashtube surrounded by an aluminum reflector and mounted in a compact enclosure which is readily attached to the mass spectrometer. Adaptation of the flash vaporization technique and solid-inlet system to the mass spectrometer required no modifications in the Bendix instrument itself; but rather, it required an appendage which included the following features:

1. Sample positioned where it can be irradiated from an external source of light. In this case it had to be located within a glass tube which inserts into the helix of the flashtube.

2. Line-of-sight path between sample and ionizing electron beam.

3. Close proximity between sample and electron beam--significantly less than a mean-free path.

4. Sample chamber contiguous with high vacuum of ion source.

5. Vacuum lock to expedite the introduction of samples into the instrument.

When a solid sample is introduced into the vacuum of the ion source, the instrument must be shut off electrically and the system brought up to atmospheric pressure during the transfer unless some kind of vacuum lock is employed. For this reason a combination sample tube and vacuum lock was incorporated onto the Bendix mass spectrometer by replacing the lower blank-off header on the ion source housing with a 2-in. gate valve and the glass sample tube attachment as shown in Fig. 1. The 3/4-in quick-connect vacuum coupling (Viton O-ring) permits easy removal of the glass tube to simplify sample reloading, and lipless Pyrex test tubes serve as convenient sample tubes. The sample rests on the end of a vertical, slender quartz rod so that when the flashtube is positioned coaxially around the glass tube, the sample is irradiated from all sides. The approximately half-millisecond thermal pulse vaporizes the sample directly into the ionizing beam from whence the resulting ions are immediately mass analyzed. It has been found that about 10 micrograms (of cellulose) is the maximum quantity of sample which can be instantaneously vaporized into the Bendix model 14 without raising the internal pressure of the mass spectrometer above its operating limit.

Before the gate valve is opened, the body of the valve and the sample tube are evacuated by an auxiliary pumping system which is comprised of a mechanical pump with a molecular sieve foreline trap and a 5-liter per second ion-getter pump. This vacuum-lock inlet has also proven to be very convenient for introducing samples in other than flash-heating applications, i.e., with materials which can be vaporized at lower temperatures. The sample is placed at the bottom of the glass tube which is then evacuated, the gate valve is opened, and the tube is warmed by an external heater to a temperature at which the vapor pressure of the material is adequate to obtain a mass spectrum. It is apparent that this application can be readily extened to slow low-temperature pyrolysis studies and mass spectrometric thermal analysis (MTA)[6] where the gaseous products are individually identified and measured as a function of temperature. This application necessitates attaching a thermocouple to the sample tube, but the results give much more information than thermal gravimetric analysis, especially for polymer decompositions.

Because of the short interval of time that the sample gases are in the ion source, oscilloscopic presentation of the spectrometer output is almost always required

for the recording of flash mass spectra. This is easily accomplished by a scope camera equipped with a flash-synchronized shutter. While the mass spectrometer is running continuously and the scope is displaying any spectra present (this, incidentally, monitors background spectra during degassing of the sample), the camera shutter is actuated, thereby triggering the flashtube power supply which, in turn, fires the flashtube. Thus, during the time the shutter is open the mass spectrum of the vaporized sample appears on the scope and is photographically recorded. A typical mass spectrum of a pyrolyzed polymer obtained in this manner is shown in Fig. 2. This is, of course, time-integrated over the brief interval of the event and is quite adequate for most applications of this type. Although oscilloscopic presentation is not as quantitative as the more typical strip chart presentation, it is evident from the photograph that relative peak heights can be established easily within a few percent.

Fig. 3 is an expanded portion of the mass spectrum from flash-heated CdS showing the Cd isotopes. Insofar as is discernible, the resolution is not affected by the abrupt heating of the sample within the ion source.

Discussion

Flash heating for mass spectrometry is, of course, not limited to flashtube thermal sources or to the particular ion-source configuration outlined here. Other possible radiant thermal sources include shuttered carbon arcs and high-intensity incandescent lamps, but the most promising extension of this work lies with pulsed lasers for flash heating. The coherent beam from a laser can be focused to concentrate the energy on a small area; therefore, the sample need not be prepared to a particular size, shape, or color to reach even higher temperature in a small spot and readily vaporize enough material to produce a spectrum. Thus, a unique method is practicable for performing analysis on minute areas of comparatively large pieces of inhomogenous materials. This concept has been carried out by Honig and Woolstron[7] who have incorporated a laser with the ion source of a mass spectrograph to produce spectra recorded on photographic plates. A similar technique can be achieved with the equipment described here, and an arrangement making effective use both of laser capabilities and the Bendix ion source configuration would be as follows (see Fig. 1): The sample could be inserted into the ion source through the vacuum lock via a vertically-sliding support probe and positioned between the backing plate and the first ion grid directly under and adjacent to the electron beam; the laser head would be located atop the ion-source housing with the beam directed downward through a window in the top header and focused onto a small spot on the sample. Such an arrangement should require only modest laser energy to provide extraordinarily high sensitivity (i.e., greatly reduce amount of sample needed for analysis), because nearly all of the vaporized material would erupt into the electron beam before it had a chance to disperse. Consequently, this arrangement would be optimum for observing thermally produced ions or free radicals because of the improved signal-to-noise ratio in the resulting mass spectrum, where, in this case, the signal is comprised of the spectrum derived from those species which had not collided with any surface prior to being ejected by the ion gun, and where the noise is the contribution from those species which had undergone collision.

We have chosen a time-of-flight instrument for this work in order to obtain time-resolved spectra, and the resultant merger of flash heating with time-resolved mass spectrometry has provided us with a powerful tool for detecting thermally-produced short-lived products of solid materials. The subject of time-resolved mass spectrometry (wherein the time sequence in which the various mass peaks occur is manifested) and the methods for achieving it have been delineated previously.[8,9]

REFERENCES

1. Nelson, L. S., "Intense Rapid Heating with Flash Discharge Lamps," Science, 135, No. 3513; 296-303 (April 1962).

2. Nelson, L. S. and Kuebler, N. A., "Vaporization of Tungsten Studied by Flash Heating and Kinetic Spectroscopy. I. Near Ultraviolet Region, " J. Chem. Phys., 39, 1055-61 (15 Aug. 63).

3. Nelson, L. S. and Kuebler, N. A., "Vaporization of Elements for Atomic Absorption Spectroscopy with Capacitor Discharge Lamps," Spectrochimica Acta, 19, 781-4 (1963).

4. Nelson, L. S. and Lundberg, J. L.,"Heterogeneous Flash Initiation of Thermal Reactions," J. Phys. Chem., 63, 433-6 (March 1959).

5. Lincoln, K. A., "Thermal Radiation Characteristics of Xenon Flashtubes" Applied Optics, 3, 405-12 (March 1964).

6. Langer, H. G. and Gohlke, R. S., "Mass Spectrometric Thermal Analysis (MTA)," Anal. Chem. 35, 1301-2 (August 1963).

7. Honig, R. E. and Woolstron, J. R., "Laser-Induced Emission of Electrons, Ions, and Neutral Atoms from Solid Surfaces" Appl. Phys. Letters, 2, 138-9 (1 Apr. 63).

8. Lincoln, K. A., "A Simple Display System for Recording Rapid Changes in Mass Spectra" Proceedings of A.S.T.M. Committee E-14 Conference on Mass Spectrometry, San Francisco (May 1963) pp. 149-52.

9. Meyer, R. T., "An Improved Oscillographic Camera Technique for Time-Resolved Mass Spectrometer Data Recording" Proceedings of A.S.T.M. Committee E-14 Conference on Mass Spectrometry, San Francisco (May 1963) pp. 489-95.

Negative Ions of I, II, and III Elements

Kumasaburo Kodera* and Tutomu Makita
Kyoto University, Kyoto, Japan
*Present Address: Brown University, Providence, R.I.

In a Mattauch-Herzog type double focusing mass spectrograph, solid samples are ionized by a high frequency discharge. In this type of ion source, negative ions are formed besides positive ions. We studied about negative ions of elements of 1st, 2nd, and 3rd groups of the periodic table. The instrument used was made by Mitsubishi Electric Company, Japan. Negative ions were measured by reversing both the electric and magnetic fields, and compared with the positive ions from the same sample. Frequency of the discharge was 1080 kc and applied to the sample electrodes as pulses of 200 μsec length and 60 c/sec. Maximun potential applied was about 20 kv. Accelerating potential was 15 kv both for positive and negative ions. Photographic plates used were Ilford Q-2 and exposure was measured by the charge collected by a monitor electrode placed in front of the magnetic field. Vacuum in the apparatus was about 2×10^{-6} torr, but during discharge, vacuum in the ion source chamber rose to about 1×10^{-5} torr, so that considerable back ground lines were observed especially in positive ion spectra.

Samples used were elements, alloys or compounds. For alkali metals, except rubidium, single crystals of high purity halides made for optical purpose were used. The sample of rubidium was a fused mass of rubidium chroride. Beryllium was laminar form powder and was more than 99.9% pure. Magnesium was an alloy of 92.2% magnesium content. (N.B.S. standard sample). Boron was powder and its purity was over 99.9%. For aluminum, 99.95% metal was used. (Johnson Mathey AA-1).

Ions detected are shown in Table 1. In the table, numbers in 2nd column show the number of charges of multi-charged ion and number of atoms of polyatomic or cluster ion. p and n show corresponding posotive and negative ions were detected. Symbols in parentheses mean that lines were found at corresponding position but because of the back ground or other reason, it is not certain that the corresponding ions are present or not.

For all the alkali metals, negative ions were detected. Positive ions have multiple charge ions, but we could not detected multiple charge negative ion. It is well kown that in vapor phase there are certain amount of diatomic molecules, but only Li_2^+ was detected, Li_2^- was not certain. For other alkali metals, positive ions of diatomic molecules may exist, but no sign of negative diatomic ion was seen. As to beryllium, negative ion Be^- was detected. For magnesium, as its isotopes have masses 24, 25, and 26 which coinside with the masses of C_2, C_2H, and C_2H_2, which are always seen as back ground ions, it is difficult to determine the existance of negative ion of magnesium. But, from the electron affinity of magnesium, it is probable that magnesium does not form negative ion. For boron, we found negative ion B^-, but we could

not found polyatomic negative ion such as found for aluminum, the element of the same group in the periodic table.

Aluminum forms many polyatomic negative ions as shown in the table. For positive ions, there are lines at the position of Al_2^+ and Al_3^+, but both lines have tails towards smaller mass side. These tails can be explained by the existance of charge transfer ions, that is, Al^{2+} to Al^+ and Al^{3+} to Al^+. To decide whether these lines contain Al_2^+ or Al_3^+ ion in addition to charge transfer ions, we take into consideration of our experiments on gallium, which has two isotopes 69 and 71. Three lines were found at the position of Ga_2^+, corresponding to $^{69}Ga_2^+$, $^{69}Ga^{71}Ga^+$, and $^{71}Ga_2^+$, respectively. Two lines corresponding to $^{69}Ga_2^+$ and $^{71}Ga_2^+$ have tails showing there are charge transfer ions, but no charge transfer ion can overlap to the position of $^{69}Ga^{71}Ga^+$. Therefore, the existance of Ga_2^+ ion was confirmed. It suggest that aluminum also has Al_2^+ ion and comparing the density distribution of Al_2^+ line to those of $^{69}Ga_2^+$ and $^{71}Ga_2^+$, we concluded that there is Al_2^+ ion in addition to the charge transfer ion. But for Al_3^+ ion, it was not possible to conclude its existance definitely. Table 2 shows the relative abundance of polyatomic negative ions. The values are given up to Al_8^-, it is because the position of Al_9^- was out of coverage of the photographic plate, so that it is very probable that there are polyatomic ions larger than Al_8^-. It is very interesting that for positive ions, we could not find any sign of existance of ions larger than Al_3^+.

For zinc and cadmium, zinc alloy and cadmium telluride single crystal were examined, but no negative ion was detected.

Electron affinities of these elements are shown in Table 3. Measurement of electron affinity is rather difficult and only those of some electro-negative elements have been measured up to the present. Therefore, these values are semi-empirical values. Values for alkali metals are those calculated by Edlén[1] by extraporation from the ionization potential of isoelectronic ion series. Other values are those of Ginsberg and Miller[2], which are calculated by their new method from a known electron affinity of an element in the same period of the periodic table. In the table, D means negative ion is detected and ND means not detected. It is seen that all the elements for which negative ions were detected have positive electron affinities. For beryllium, $2s^2 2p$ state has negative affinity, but $2s^2 3s$ state has positive affinity, therefore, it is supposed that the Be^- found was in the latter state.

1) B. Edlén, J. Chem. Phys., 33, 98 (1960)
2) A. P. Ginsberg, J. M. Miller, J. Inorg. Nucl. Chem., 7, 351 (1958)

Table 1. Detected Species of Positive and Negative Ions

Element		Li	Na	K	Rb	Cs	Be	Mg	B	Al
Atomic number		3	11	19	27	55	4	12	5	13
Isotopes		6 7	23	39 40 41	85 87	133	9	24 25 26	10 11	27
Multi-charge M^{n+} M^{n-}	6									
	5					p				
	4					p				p
	3		p	p	p	p	p	p	p	p
	2	p	p	p	p	p	p	p	p	p
Atomic, M^+ M^-		p n	p n	p n	p n	p n	p n	p (n)	p n	p n
Poly-atomic M_n^+ M_n^-	2	p (n)	(p)	(p)	(p)	(p)	(p)	(n)(p)	(p)	p n
	3									(p) n
	4									n
	5									n
	6									n
	7									n
	8									n
Sample		LiF	NaCl	KCl	RbCl	CsBr	Be	Mg-alloy	B	Al

Table 2. Relative Abundance of Polyatomic Negative Aluminum Ions

Al^-	Al_2^-	Al_3^-	Al_4^-	Al_5^-	Al_6^-	Al_7^-	Al_8^-
100.0	14.4	16.1	7.2	3.1	1.6	1.2	0.4

Table 3. Electron Affinity

Negative Ion	State	Electron Affinity (semi-empirical)	Present Work
Li^-	$2s^2$	0.82	D
Na^-	$3s^2$	0.41	D
K^-			D
Rb^-			D
Cs^-			D
Be^-	$2s^2 2p$	-0.12	
Be^-	$2s^2 3s$	0.90	D
Mg^-	$3s^2 3p$	-0.56	
Mg^-	$3s^2 4s$	-0.24	(ND)
Zn^-	$4s^2 4p$	-0.90	
Zn^-	$4s^2 5s$	-0.13	ND
Cd^-	$5s^2 5p$	-0.6	
Cd^-	$5s^2 6s$	0.0	ND
B^-	$2s^2 2p^2$	0.56	D
Al^-	$3s^2 3p^2$	0.45	D

MICROTRACE ANALYSIS OF LITHIUM ISOTOPE IN METAL TARGETS BOMBARDED BY HIGH ENERGY PROTONS

R. Bernas, M. Epherre, E. Gradsztajn, R. Klapisch, F. Yiou
Laboratoire Joliot-Curie, Faculté des Sciences
Orsay (Seine-et-Oise) France.

The work which we shall describe originated from the need to study the products of nuclear reactions occuring when targets of various elements are bombarded by high energy protons. The process by which light elements such as Lithium, Beryllium, up to Sodium are formed when a proton of say 1 GeV hits a heavy target such as Tantalum is not yet clearly understood, our aim was to examine whether the relative amounts of ^{7}Li and ^{6}Li isotopes formed depend on the N/Z of the target nucleus.

This type of experiment which is essentially a cross-section determination is usually done on radioactive isotopes produced in these reactions. However there are two reasons which make the mass-spectroscopic technique very valuable :

I - There are very few radioactive isotopes with convenient half-lives in the light masses (only ^{7}Be, ^{11}C, ^{19}F and ^{24}Na),

II - It is important to know whether the production of stable fragments is favored with respect to radioactives ones.

Moreover, the results we have obtained lead us to believe that the method may also be extended to the study of short lived radioactive isotopes.

In a first step, we have studied ^{7}Li and ^{6}Li production in various targets : C, V, Nb, Ta, Pt ; Sodium isotopes production is being investigated in the same manner.

Since it was expected that the lithium produced would be in extremely small amounts, a technique was developped to extract lithium without any chemical process so as to avoid contamination. The absolute amounts we were able to measure in the following report vary between 10^{-12} and 10^{-14} g corresponding to concentrations of the same order of magnitude.

Two values are of interest in these experiments :

1. the ratio of ^{7}Li/^{6}Li produced in the reaction,
2. the absolute amount of each isotope produced.

The first value is obtained by direct analysis in the mass-spectrometer just after the bombardment.

An isotope dilution method must be used for the second determination ; for this we use the fact that ^{7}Be produced in the target at the same time as ^{7}Li and ^{6}Li decays to ^{7}Li with a 54 day half-life ; so that the ^{7}Li/^{6}Li ratio measured after two months is different from that at t_0 by an amount which can be easily calculated knowing the ^{7}Be cross-section formation by usual methods.

We shall now describe briefly the experimental set up.

1) The ion source is a modification of the classical three filament thermionic emission source of Inghram and Chupka. It has to be demountable and easy to accurately readjust, each filament is mounted in a small block, and all 3 filaments blocks are ajusted exactly into grooves in a stainless steel structure. Anyone filament or all three can be taken apart and set back in the same position. (fig. 1 a - b).

The measured efficiency determined by integrated current measurement is of the order of 0.3% with Li ions (including the mass-spectrometer transmission which is not optimized in our case). A satisfactory isotopic analysis of 5 10^{-17} g. of lithium is possible without pulse counting technique (figure 2.).

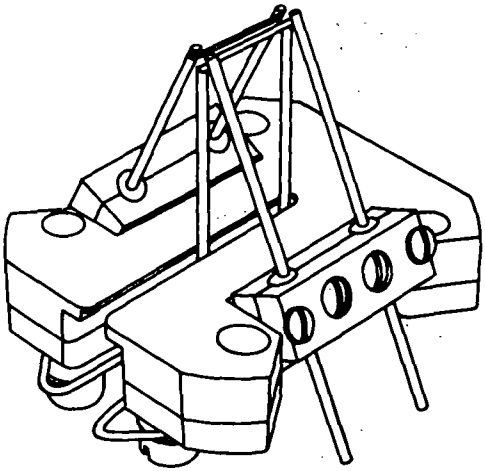

Fig. 1 b Source ELAL

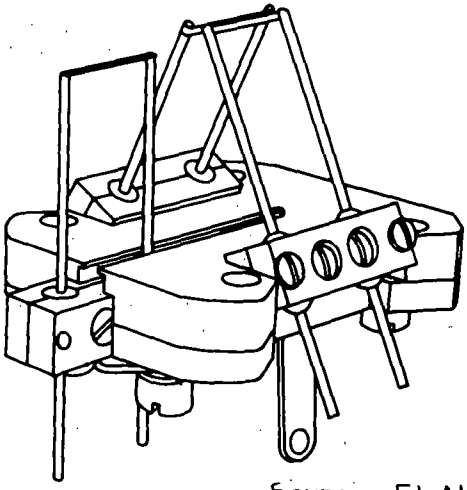

Fig. 1 a Source ELAL

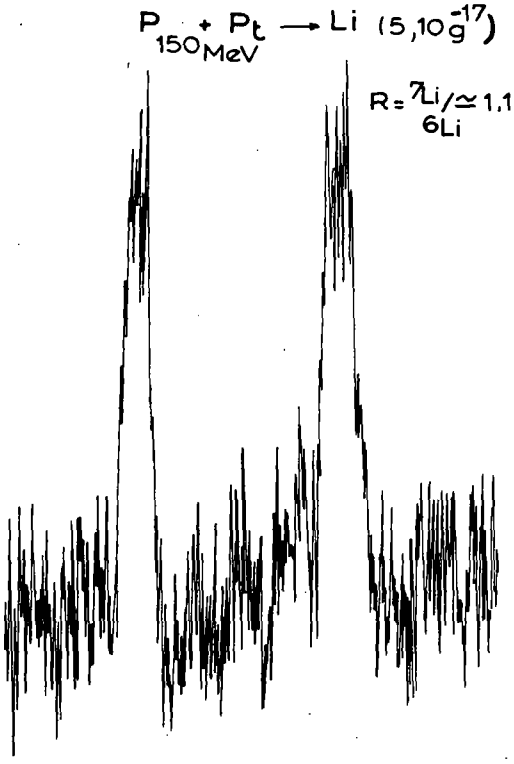

Fig. 2

2. The extraction and analysis of the lithium contained in the metal targets was at first done by the following method.

The sample was put into a small oven submitted to electron bombardment and the mass-spectrometer filament, cooled by contact with a silver block connected to a liquid N_2 vessel, was set immediateley above the oven. The diffusion of lithium from targets of a few 1/10 mm thickness can be achieved in a time varying from 1 minute to several hours at 1000°C depending on the crystalline structure of the target.

This technique is satisfactory but is more subject to contamination by traces of natural lithium than the one which we now use. (In particular oil traces from pumps or traces of moisture will condense on the cold filament).

In the present technique, it is the mass-spectrometer filament itself which is bombarded in the accelerator after ascertaining that it does not contain any detectable trace of natural lithium. After this bombardment, the filament is set back in place in the triple filament assembly where it is used as a "sample filament". With this method a one hour bombardment in the synchro-cyclotron with a 1 μA beam for example is quite sufficient to give a lithium ion beam lasting for several hours.

Since there is no direct handling of the filament itself contamination is very limited and the complete experiment may last only a few hours.

In the study of high energy nuclear reactions the fact that the mass-spectrometer filament constitutes a very thin target does not limit the amount of reaction products since the circulating proton beam will make up to 10.000 traversals of this target in the case of the CERN 25 GeV machine for example.

The mass-spectrometer we use, is a standard Nier type machine, home built, all stainless steel with 2 vacuum locks to isolate the source and the multiplier from the rest of the vacuum system. Two types of multiplier are used :

a) with the oven technique a low gain 12 stages Cu-Be non activated and with integration of the current,
b) with the filament technique, a 17 stage Cu-Be activated multiplier made in Zurich (ETH) with a gain of $> 10^8$ at 3,600 Volts which gives 4 Volts pulses. In this case a 10 MC scaler is employed, an automatic switching devices are used.

III - Experimental results

The following table indicates the results obtained.

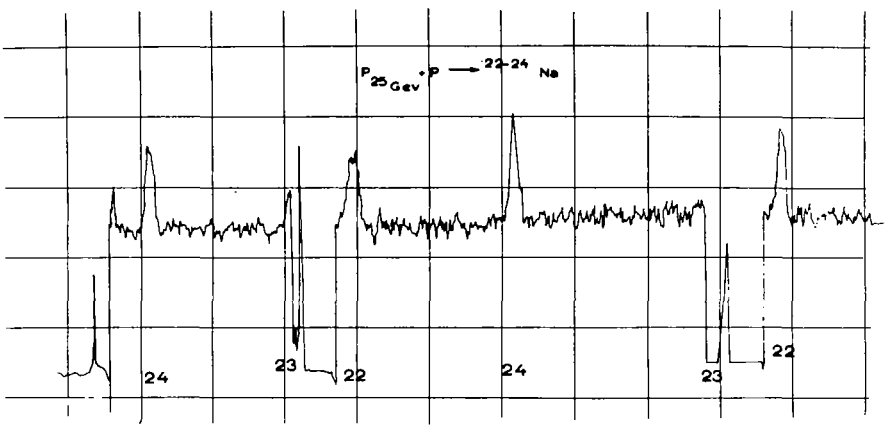

Fig. 3

TAB LE I

Relative abundance of the lithium isotopes produced in nuclear reaction induced by energetic protons on various targets

Target	Method	Proton energy	$R_1 = {}^7Li/{}^6Li$ at t = 0	$R_2 = {}^7Li/{}^6Li$ at $t = t_o + T$	T	$\sigma\ {}^7Li$ (mb)	Amount of Li analyzed
Carbon	oven	44 MeV	1.1 ± 0.1	3.14	∞	9.3 ± 1.9	10^{-12} g.
	"	50 MeV	0.77 ± 0.1	3.56	"	6.2 ± 1.3	"
	"	150 MeV	0.8 ± 0.1	2.03	"	7.4 ± 1.5	10^{-13} g.
	"	550 MeV	0.7 ± 0.1	2.25	"	5.6 ± 1.2	"
	"	25 GeV	-	1.2	25 d	-	"
Vanadium	"	150 MeV	-	1.3	222 d	0.4	"
	"	550 MeV	-	1.9	160 d	-	"
Niobium	"	150 MeV	-	1.25	368 d	-	"
Tantalum	"	150 MeV	-	2.3	180 d	0.04	"
	filament	25 GeV	-	1.4	180 d	20	10^{-11} g.
Platinum	"	150 MeV	1.1	-		0.03	5.10^{-17} g.
	"	25 GeV	-	1.4	30 d	20	10^{-12} g.

These experiments are now being continued by Mrs. Yiou in our laboratory who studies Na^{22}, Na^{23} and Na^{24} cross-sections in the same range of elements and energies ; fig. 3 is a mass-spectrum obtained after bombardment of a platinum filament for 15 minutes in the CERN P. S.

I would like to point out that Dr. Nguyen, in Orsay also, has been using the oven technique to determine nearly 100 cross-sections for 10 Cs isotopes (including the stable one) produced by spallation reactions in Lanthanum at proton energies varying from 40 to 150 MeV. The extension of this work to impurity analyses of $\leqslant$ 1 ppb has already been done by Dr. Nguyen, in the case of ^{23}Na in Al of high purity (2-3 10^{-9} g/g) and Cs in rare earth (2 - 3 10^{-10} g/g in La).

In conclusion I believe that this type of method, with due regard to the increased sensitivity of mass-spectrometer should in an increased number of occasions compete with the radioactive techniques in studying the products of nuclear reactions in a wide variety of experiments.

A Mass Spectrometer Method for Analysis of Alkylates for Bio-Soft Detergents

F. J. Galbraith, D. J. Skahan, N. P. Kilargis, P. J. Contino

This paper presents a comprehensive mass spectrometer method for analyzing alkylates used for making bio-soft detergents. With the increased emphasis on the production of bio-degradable detergents, a rapid and accurate analysis of alkylates was required. The mass spectrometer provides an ideal tool for the determination of a hydrocarbon type analysis as well as a molecular weight distribution of secondary phenyl alkanes. The necessary calibration data were obtained from pure compound API spectra and the laboratory alkylation of single carbon number 1-olefins.

The mass spectral data were calculated from runs on a Consolidated 21-103A instrument. The operating conditions are shown below:

M.S. Operating Conditions

Box temperature	301°C
Sintered Disc Temp.	315°C
Isatron Temp.	260°C
Magnet Current	1.30 amp
Ionizing Current	75 μ a
Ionizing Voltage	70 V
Scan Time	IAV 3000 --→ end 19'

The sample is introduced through a heated sintered disc sealed with indium. Due to the intensity of the major fragment peaks of the alkylbenzenes, care is exercised in charging the sample in order to eliminate amplifier overload. In practice, the ion source temperature is adjusted in order to maintain the n-hexadecane 127/226 peak ratio at 145 $\pm$ 2. Samples and calibrations are run at relatively constant pressures.

Gas chromatographic data were obtained on a Model 350 Aerograph. The operating conditions are shown below:

Operating Conditions
Wilkens Aerograph 350

Column	-	8 ft. x 1/4" - 10% Microwax Btms. on 80-100 mesh Chromasorb W
Carrier	-	Helium
Flow Rate	-	60 cc/min.
Temperature	-	Injector - 300°C Column - Initial 180°C, Final 300°C Programmed 1°C/min. Detector - 300°C
Detector Current	-	220 milliamps
Charge	-	10 microliters (analytical chg.) 50 microliters (prep. chg.)
Recorder	-	0-10 millivolt L & N Speedomax G
Sensitivity	-	1

The aerograph was used primarily for the cutting and collection of fractions from the laboratory alkylation of the pure olefins as well as for collecting predetermined fractions from the distillation cuts of a total sample.

Initial attempts to obtain calibrating material by distillation were surveyed with the 350 Aerograph. Due to the close boiling points of the individual isomers of the phenyl alkanes each cut contained a range of approximately five carbon numbers. It was evident that additional cutting by gas chromatography would be necessary to obtain closer boiling fractions and that the preparation of pure compounds by laboratory alkylation of single carbon number 1-olefins would also be required. Alkylation of benzene with 1-dodecene and 1-hexadecene subsequently supplied us with single carbon number isomeric phenyldodecanes and phenylhexadecanes. Heart cut fractions were further separated by gas chromatography for single isomer calibration data. Previous work on the alkylation of 1-dodecene has been reported by Olson (5).

Some knowledge of the starting material used in alkylation and a plot of the available boiling point information in the C_{14}-C_{22} range, $\sim$250-380°C, for the paraffins, cycloparaffins and/or olefins and the alkylbenzenes proved most helpful in

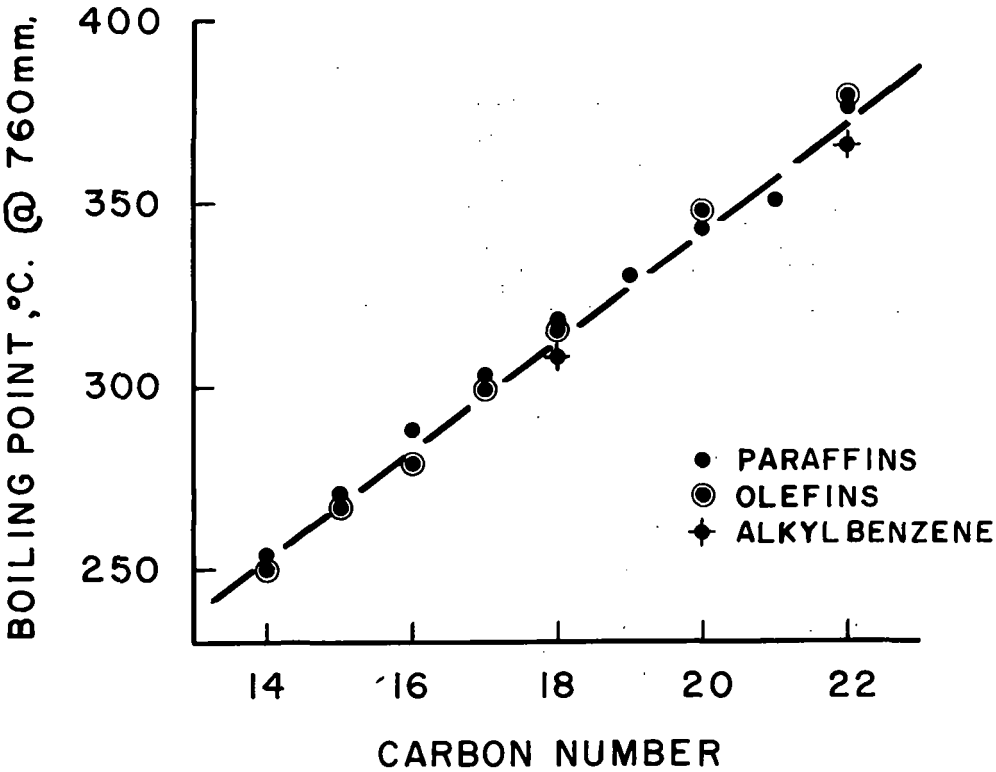
BOILING POINT, °C. @ 760mm.
400
350
300
250
PARAFFINS
OLEFINS
ALKYLBENZENE
14
16
18
20
22
CARBON NUMBER

Fig. 1

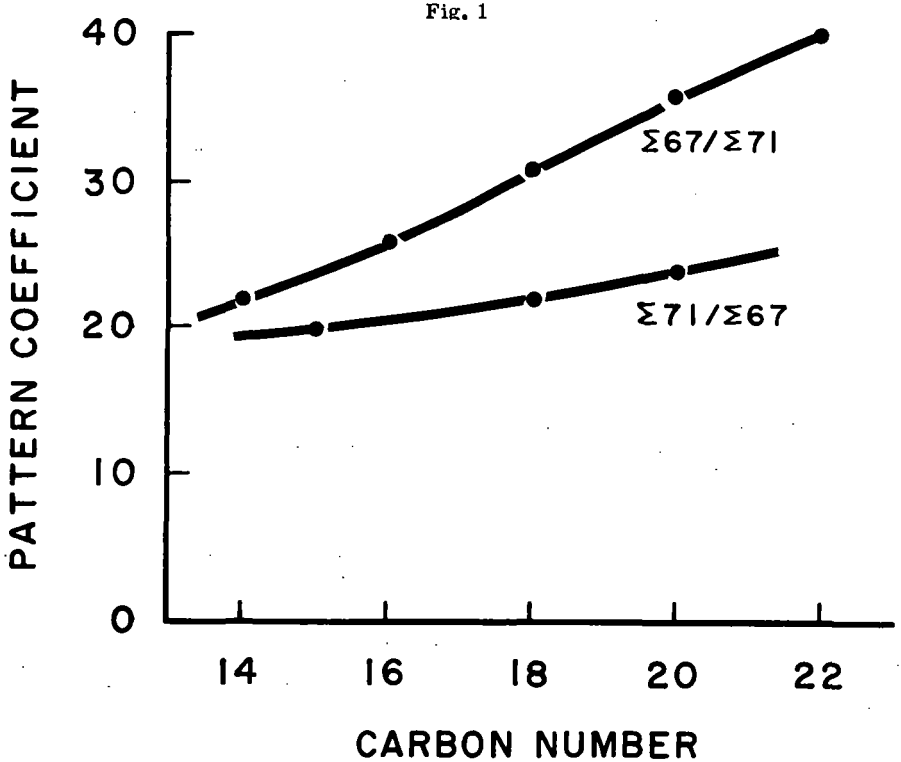
PATTERN COEFFICIENT
40
30
20
10
0
Σ67/Σ71
Σ71/Σ67
14
16
18
20
22
CARBON NUMBER

Fig. 2

the selection of matrices for the hydrocarbon type analysis. Figure 1 is a plot of the boiling point data. In addition to the types plotted, compounds of the Z number series, C_nH_{2n-8} are found. Their calculation is included in the matrix, however, sufficient boiling point data for specific hydrocarbons of this type were not available for reference.

Calculation

Samples are analyzed based on the summation of characteristic mass fragments to determine the concentration of the hydrocarbon types. In the range C_{15}-C_{23}, the paraffins have relatively weak parent ions, however, intense ions for all paraffin hydrocarbons occur at the C_nH_{2n+1} peaks. For calculation purposes pattern and sensitivity values for the peak summation 71 + 85 have been determined. They are the most intense peaks in paraffinic spectra for the operating conditions used in running this type sample. The cycloparaffin and/or olefin types have major fragment ions at the following masses: 67, 68, 69, 81, 82, 83, 96 and 97. They are grouped in the type analysis. Figure 2 illustrates the pattern coefficients used in the matrices. The pattern contributions of these classes of compounds to the sigma 77 used for calculating alkylbenzenes, and the sigma 103 for the calculation of C_nH_{2n-8} material is in the range 0 - 1 per cent. The pattern coefficients and sensitivity data for the sigma 67 have been weighted for predominately olefinic compounds.

Principal ions for the alkylbenzene compounds result from cleavage of bonds beta to the benzene ring. For the secondary phenyl alkane compounds, in the detergent alkylate range, relatively unique peaks occur at masses 105, 119, 133, 147 and 161. Alkylbenzenes posses molecular ions of a much greater intensity than the aliphatic series. The average molecular weight of the alkylbenzenes is used to determine the matrix for calculating the hydrocarbon type analysis. Figure 3 shows the pattern coefficients for the alkylbenzenes to the other sigmas used in the matrix for the type analysis. A very extensive study of alkylbenzene fragmentation has been reported by Meyerson (4).

The C_nH_{2n-8} series which includes Indans, Tetralins and Cycloparaffinic benzenes is characterized by the sigma 103. Major ions for the series occur at masses 117, 131, 145, 159 and 173. Average pattern and sensitivity data are used in the matrix. In order to precisely identify these hydrocarbons an extensive program would be necessary. Spectral data indicates a variety of structures are present. In addition to residual peak deltas at the above mentioned masses parent peaks are present in the sample spectrum at the p-2 peaks of the alkylbenzenes, indicating molecular ions of the C_nH_{2n-8} species. Due to the close boiling points of this type material to the alkylbenzenes and the relatively low concentration no efforts to date have been made to collect fractions. We anticipate additional cutting work by gas chromatography to obtain concentrates for mass identification. Figure #4 is a plot of the sensitivities for the mass groupings used in the calculation of the type analysis.

After the mass record has been read the parent peaks of the alkylbenzenes are corrected to a monoisotopic basis using factors from the Esso tables, McAdams (3). Correction factors for the range C_{15}-C_{22} with an illustration of the calculation of C_{18} alkylbenzenes mono peak are shown in Table I.

TABLE I

m/e	p-1	p-2	m/e	p-1	p-2
204	-.1655	+.0145	260	-.2099	+.0231
218	-.1766	+.0165	274	-.2210	+.0256
232	-.1877	+.0186	288	-.2321	+.0281
246	-.1988	+.0208	302	-.2432	+.0308

$$\text{mono } 246 = \text{poly } \overline{246} - \text{poly } \overline{245}\ (.1988) + \text{poly } \overline{244}\ (.0208)$$

The parent peak contributions and sensitivities calculated from API spectra (1) and gas chromatographic fractions are summarized in Table II. Although the contributions are low in the range of interest for detergent alkylate, the intensity of the parent peaks of the secondary phenyl alkanes made corrections necessary for calculating concentrations of lower molecular weight material. Starting with the highest molecular weight present the mono peaks are corrected and volume fractions at each carbon number calculated. The figures are mathematically combined to determine an average molecular weight for the alkylbenzenes. Figure 1 demonstrated the relationship of the average alkylbenzene carbon number to the average carbon number of the other components in the mixture.

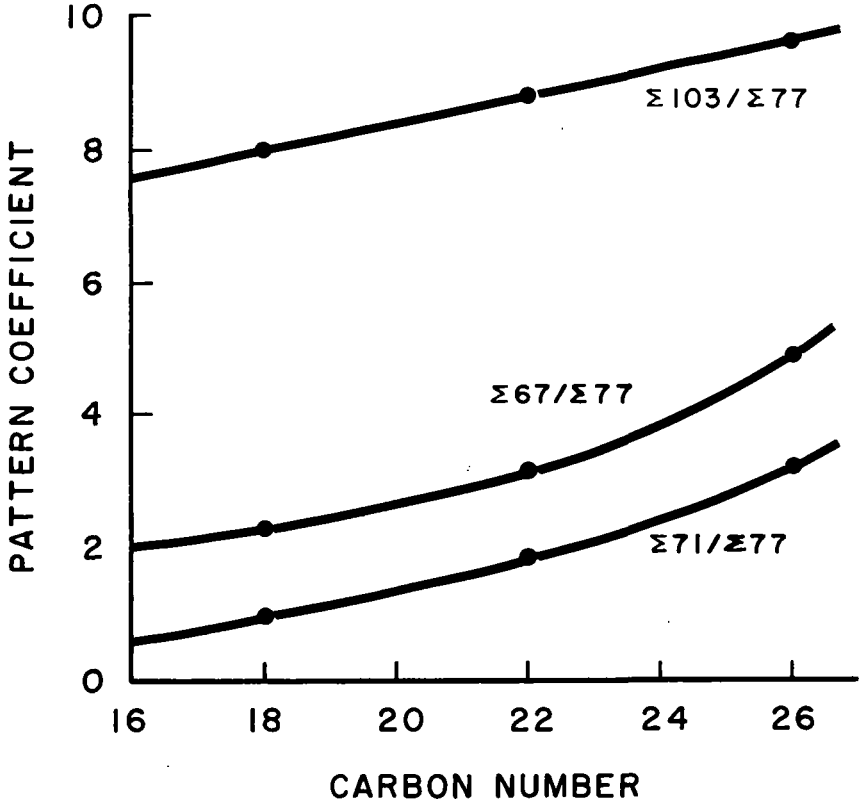
PATTERN COEFFICIENT
10
8
6
4
2
0
Σ103/Σ77
Σ67/Σ77
Σ71/Σ77
16
18
20
22
24
26
CARBON NUMBER

Fig. 3

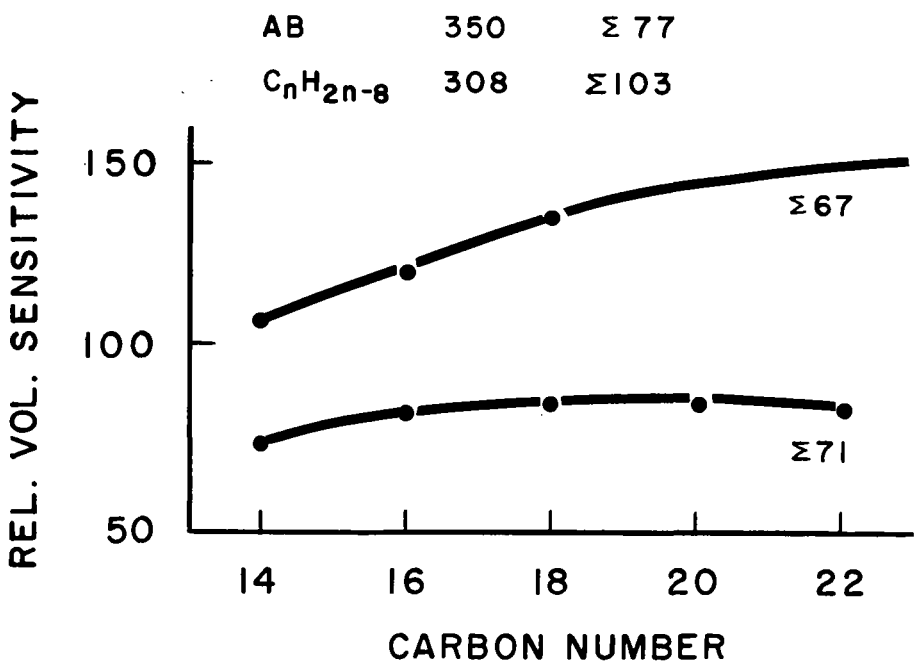
AB 350 Σ 77
C_nH_{2n-8} 308 Σ103
REL. VOL. SENSITIVITY
150
100
50
Σ67
Σ71
14
16
18
20
22
CARBON NUMBER

Fig. 4

TABLE II

C# m/e	15	16	17	18	19	20	21	22
204	100	-	1	1	1	1	1	1
218		100	-	1	1	1	1	1
232			100	-	1	1	1	1
246				100	-	1	1	1
260					100	-	1	1
274						100	-	1
288							100	-
302								100
Vol. Sens.	21.3	18.3	16.1	15	13	12	11	10

Table III shows the matrix used for an average C_{18} alkylbenzene sample. The molecular weight distribution of the alkylbenzenes is normalized to results from the type analysis. The table also includes a summary of the peaks read for sigma values.

The method has been applied to a large number of samples with satisfactory results obtained with a variation in alkylbenzene concentration from 85-100 volume per cent.

Table IV shows the molecular weight distribution of alkylbenzenes normalized to 100 per cent for comparison with gas chromatography and a published method of Dr. E. W. Boyer et al (2). The agreement between the two mass methods is within ± 2 per cent at all carbon numbers. The comparison with chromatographic results shows a wider variation which may be the result of the overlap of 2 phenyl with the internal phenyl isomers of the next higher molecular weight alkylbenzene.

TABLE III

Matrix for Type Analysis
C_{18} Alkylbenzene Samples

	Σ 71	Σ 67	Σ 77	Σ 103
Paraffins	100	20	1.0	2
Cycloparaffins and/or Olefins	31	100	2.3	4
Alkylbenzenes	0.4	0	100	25
C_nH_{2n-8}	0	0	8	100
Vol. Sens.	84	136	350	308

Characteristic Mass Groupings

Σ 71 = 71, 85.
Σ 67 = 67, 68, 69, 81, 82, 83, 96, 97.
Σ 77 = 77, 78, 79, 91, 92, 105, 106 to end of spectrum.
Σ 103 = 103, 104, 117, 118 to end of spectrum.

TABLE IV

Comparison Relative Distribution of Alkylbenzenes

	A			B			C			D		
	MS	GC	Lit.	MS	GC	Lit.	MS	GC	Lit.	MS	GC	Lit.
C_{15}							0.4		0.1			
C_{16}	2.4	2.5	2.5	18.3	19.0	18.1	1.2	1.8	1.4	17.4	20.8	17.0
C_{17}	25.3	25.6	25.5	20.3	19.4	20.4	28.6	28.6	29.6	31.5	31.5	31.3
C_{18}	24.3	25.5	25.6	16.7	19.0	18.0	25.5	27.4	27.3	26.9	27.8	28.4
C_{19}	25.1	24.4	24.5	17.0	17.8	16.6	23.0	23.1	21.5	20.2	17.0	19.5
C_{20}	22.3	22.0	21.3	17.4	15.9	16.6	19.1	19.1	17.9	3.8	2.9	3.6
C_{21}	0.6		0.6	9.0	8.9	9.1	2.2		2.2	0.2		0.2
C_{22}				1.3		1.2						

Conclusion

Advances in hydrocarbon analyses by mass spectrometry have extended the range of products which can be analyzed. This is of particular importance in the ever increasing number of petro-chemicals now manufactured by oil companies.

The mass spectrometer provides a unique tool for the calculation of a hydrocarbon type, molecular weight distribution and structural determination of detergent alkylate samples. The complete analysis can be done in about 2 man hours.

Acknowledgment

The authors wish to acknowledge the contributions made during this work by members of the Development Division, especially R. C. Taylor and W. J. DeWitt for helpful discussions and laboratory alkylation of the pure compounds. They also wish to thank S. Blittman for distillation and acid treat data, and members of the Analytical Chemistry Section for spectra used.

References

(1) American Petroleum Institute Project 42, Properties of Hydrocarbons of High Molecular Weight, September 1962.

(2) Boyer, E. W., Hamming, M. C., and Ford, H. T., Rearrangement Technique for Analysis of Alkylbenzenes by Mass Spectrometry, Analytical Chemistry, Vol. 35, No. 9, August 1963.

(3) McAdams, D. R., Isotope Correction Factors for Mass Spectra of Petroleum Fractions, Esso Research Laboratories, Baton Rouge, La., October 1957.

(4) Meyerson, S., Correlations of Alkylbenzene Structures with Mass Spectra, Applied Spectroscopy, 9, 120, 1955.

(5) Olson, A. C., Alkylation of Aromatics with 1-Alkenes, Industrial and Engineering Chemistry, Vol. 52, No. 10, October 1960.

DETERMINATION OF PHENYL POSITION DISTRIBUTION IN N-ALKYLBENZENES BY MASS SPECTROMETRY

Harrell T. Ford
Continental Oil Company
Ponca City, Oklahoma

Seventy electron volt mass spectra of pure n-alkylbenzenes show large peaks resulting from the cleavage of carbon-carbon bonds beta to the benzene ring. The beta bond adjacent to the larger segment of the alkyl chain is more labile. These spectral features have been used to determine the phenyl position distribution in C_{16} to C_{24} mixtures of n-alkylbenzenes. Positions one through nine can be determined by the use of conventional spectra such as ones used for determination of molecular distribution. About one man hour per analysis is required if an electronic computer can be used for computations.

ION CHAMBER MODIFICATIONS AND SAMPLING TECHNIQUES FOR OBTAINING THE MASS SPECTRA OF LOW VAPOR PRESSURE SUBSTANCES*

Gregor A. Junk and Harry J. Svec

Institute for Atomic Research and Department of Chemistry
Iowa State University, Ames, Iowa

Three phases of our research on sampling techniques will be covered in this report. First, two basic ion chamber designs will be described; secondly, the vacuum lock design which was fabricated will be explained; and finally, some of the data on the testing and operation of the system will be presented. Figure 1 is an exploded view of an ion chamber design used in our first successful attempts to obtain the mass spectra of amino acids and peptides.[1,2] With this system, it is necessary to vent the analyzer region of the mass spectrometer in order to place the sample into the ion chamber. This sample loading procedure is somewhat cumbersome and quite time-consuming. Under ideal conditions about one sample per 8 hr. day could be accurately assayed.

The desire to reduce the time per assay was one of the prime factors which influenced our decision to change the design to the system which is described in this report. The major design criteria for the new system are listed on Fig. 2.

A system was desired which:

1. would allow for samples to be cycled in a matter of minutes;
2. was readily adaptable to testing on the available General Electric instrument and ultimately adaptable to other commercial instrumentation;
3. was economical to fabricate from low cost components;
4. was conveniently usable for the alternate and the simultaneous use of the direct insertion technique and the introduction of a sample from a heated external system;
5. was simple in both operation and design.

These requirements of the design have been achieved using either a cylindrically shaped ion chamber or a more conventional enclosed box ion chamber.

The cylinder ion chamber which was tested is a slight modification of one shown in Fig. 1. A schematic of this modified chamber is shown in Fig. 3. Letter designations of the critical components appear in the figure and are identified as; A-furnace, B-furnace terminals, C-side arm (for connecting to external heated inlet), D-ceramic insulating sleeve, E-micro-miniature thermocouple and F-positioning screw for attaching ion chamber to first shield plate of ion source. The filament and trap assemblies which attach to the shield plate are not pictured but are identical to those shown in Fig. 1. One of the polished non-magnetic stainless steel rods (G) which are used to introduce samples is also pictured. The sample is retained in the hole (H) which is drilled into the end of the sample rod.

Figure 4 shows an exploded prospective drawing of the box ion chamber. This is a modification of the original General Electric gas chamber. The gas intake line located at the top of the ion chamber was removed. A T shaped adaptor (designated by D + E in the figure) was fabricated from non-magnetic stainless steel. One end of the T fits into the top of the chamber, where originally, the gas line was attached. The repeller plate (K) was also modified. About 20,0.005 in.diameter nichrome wires were spot welded over a hole which was drilled into the plate. This screened repeller allows for unrestricted passage of the sample vapor into the electron beam without appreciably distorting the electrical

* Work was performed in the Ames Laboratory of the U. S. Atomic Energy Commission.

field gradient in the ion box. Two components of the ion box assembly are not shown. At point H a bracket is attached which supports the terminals for the heater (F). A standard G.E. filament assembly is inserted at point G. B is a 1/4 in. length of expanded teflon which is used to secure the glass sample crucible (C) to the nipple on the end of the steel rod (A). The ion chamber is designated (I) and (J) is the trap.

A schematic cut-a-way of the vacuum lock and the box ion chamber is shown in Fig. 5. The entire vacuum lock consists of a modified Goddard, Series 600 straight through high vacuum valve. We have used a 1/2 in. stainless steel valve which sells for about $80.00 for this lock. However a lock was also fabricated from a 3/8 in. brass valve which sells for only $35.00. The body and bellows housing of the valve are not changed; the replacable end caps however are modified. The gland in the right hand end cap of the Goddard valve is machined so that the gland exactly receives a teflon disk which is cut from a 1/16 in. thick sheet of teflon. A sharp #7 cork borer is a convenient tool for cutting this disk. The inside hole in the teflon disk, which forms the dynamic seal, is made with either a 1/4 in. drill or a sharp 1/4 in. punch. An end plate fits over the teflon disk and is held in place with four bolts which screw into the end cap. The dynamic vacuum seal around the sample rod is achieved by tightening the bolts which position the end place. A 1/4 in. hole, drilled into the end cap, receives the vacuum line from the vacuum lock pumping station. A vacuum gland is also machined into the left hand end cap. This gland receives a short tubulation which projects from the mass spectrometer vacuum housing. When the sample rod is in the position shown the lock vacuum is isolated from the mass spectrometer vacuum by a plug seal. The plug is machined from teflon rod and is pressed into place. The operation of the vacuum lock and box ion chamber for the direct insertion technique is illustrated in Fig. 6.

Here is shown a graphic representation of the time required to change samples, eliminate memory effects of a previous sample and then stabilize the spectrum of the new sample. Base peak intensity using arbitrary units is plotted against time in minutes. On the far left is plotted the intensity of the 72^+ peak (base peak) from a sample of the amino acid valine. At point A the filament is turned off and naturally the peak drops to zero. During the time interval from B to C, several operations are performed. First, the heater is turned on. Then the valine sample is removed through the vacuum lock, and a new sample, leucine, is introduced into the high vacuum region. The heater is turned off and the filament of the mass spectrometer is again turned on. The 72^+ peak from the previous valine sample is shown at point C. It has gone to zero on the scale used here, although its actual intensity is about 1/10,000 of the intensity at point A. At the 12 minute point the crucible containing the leucine is translated into the ion chamber. At point D the 86^+ (base peak) from the amino acid leucine is focused on the collector. From point D to E is plotted the intensity of this peak as a function of time. The spectrum has stabilized at point E and the filament is again turned off. From points F to G is repeated the same cycle as described from points B to C, with the leucine sample being withdrawn from the system and valine reintroduced. The residual 86^+ is checked at point G. It's intensity is 1/20,000 of the 86^+ peak at point E. From points H to G is shown the rise of the 72^+ peak from valine.

Three main conclusions are drawn from a consideration of these data:

1. The residual peaks from a previous sample are reduced to a negligible level in less than 6 minutes.

2. The spectrum of these test samples begin to appear almost immediately after the sample is inserted in the ion chamber. It takes, however, about 20 minutes to completely stabilize the spectrum for exact quantitative work.

3. The vacuum lock operation is very satisfactory. One sample can be withdrawn and a new sample inserted within 5 minutes without incurring any loss in the instrument high vacuum.

The alternate and simultaneous use of the direct insertion technique and a Microtec external heated inlet system is shown in Fig. 7. Your attention is directed first to the schematic in the upper left-hand corner.

A box ion chamber is shown here but the operation is identical with the cylinder chamber. The numbers 1, 2, and 3 indicate the position of the end of the glass crucible which contains the sample. If only the direct insertion technique is used the sample crucible is at position 1 so that the side arm which connects to the external system is closed. If only the external system is being used an empty crucible is inserted to position 2 so that the side arm is open and the top of the chamber is closed by the crucible. If it is desired to introduce simultaneously a sample from both systems, a packed crucible is inserted to position 2. In this position some loss of sample vapor out the open side arm occurs. This effect is shown by the data on the slide where the 86^+ ion intensity from leucine is plotted at various positions of the crucible. At point B the crucible is in position 1. At point D the crucible has been raised to position 2. The 75% reduction in the sensitivity of the instrument to leucine is due to escape of the vapor through the side arm. This reduced sensitivity causes no serious problems if one is using the simultaneous system for either mass calibrating or appearance potential work.

We have tested the ion chambers extensively and have demonstrated that the mass spectra of amino acids are basically identical regardless of the chamber which is used. The spectra of valine using the box chamber (upper spectrum) and the venting procedure, described earlier (lower spectrum) are shown as the top pair of spectra in Fig. 8. One can see that the two spectra are virtually identical. These results for valine are representative of all of the amino acids.

We have also tested the box and cylinder ion chamber using samples which tend to thermally decompose, such as the dipeptides.[2] The data from glycylalanine (bottom pair of spectra in Fig. 8) is representative of all the dipeptides which were tested. The parent ion peak and the peak at mass 30 represent a greater fraction of the total ion yield using the box chamber vs the venting procedure. Also the peaks at 44, 57, 70, 85, 100 and 128 which are characteristic of a thermal decomposition product are reduced when the box chamber is used. The reduced thermal decomposition, using the box chamber, is attributed to fewer collisions of the sample molecules with hot metal walls when the sample is placed very close to the electron beam.

REFERENCES

1. G. A. Junk and H. J. Svec, J. Am. Chem. Soc. 85, 839 (1963).

2. H. J. Svec and G. A. Junk, J. Am. Chem. Soc. 86, 2278 (1964).

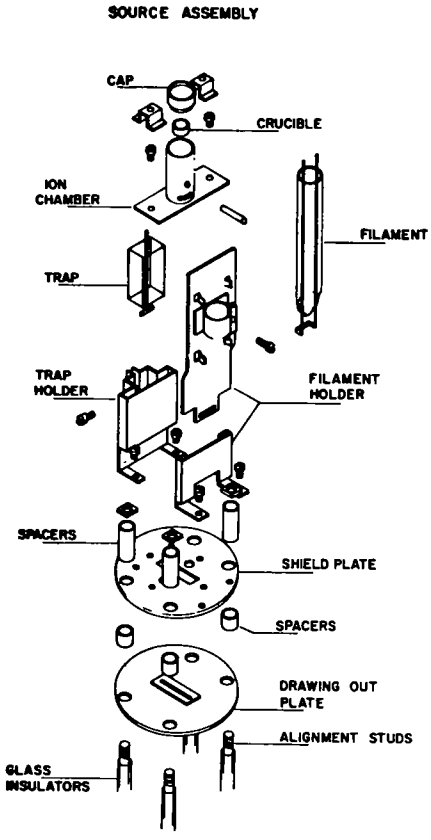

Fig. 1. Exploded view of original[1] cylinder ion chamber and G. E. ion source assembly.

1. FAST
2. ADAPTABLE
3. ECONOMICAL
4. VERSATILE
5. SIMPLE

Fig. 2. Design criteria for the vacuum lock and ion chamber.

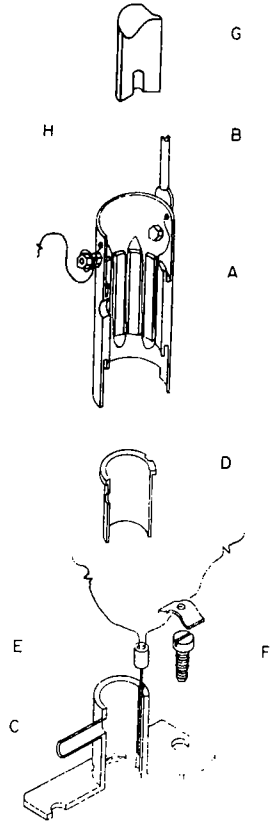

Fig. 3. Perspective drawing of modified cylinder ion chamber.

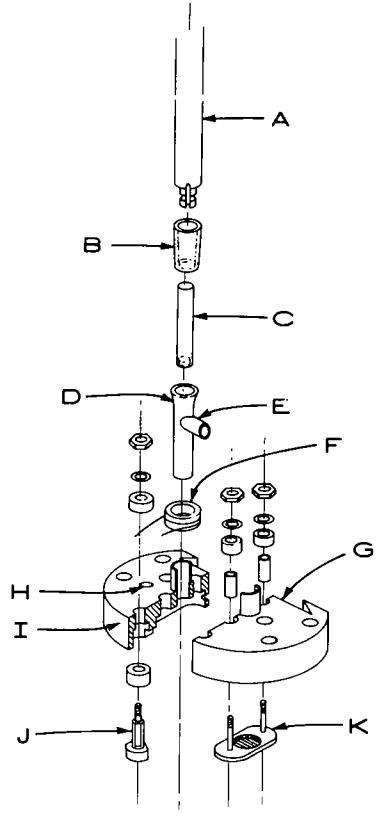

Fig. 4. Exploded view of box ion chamber

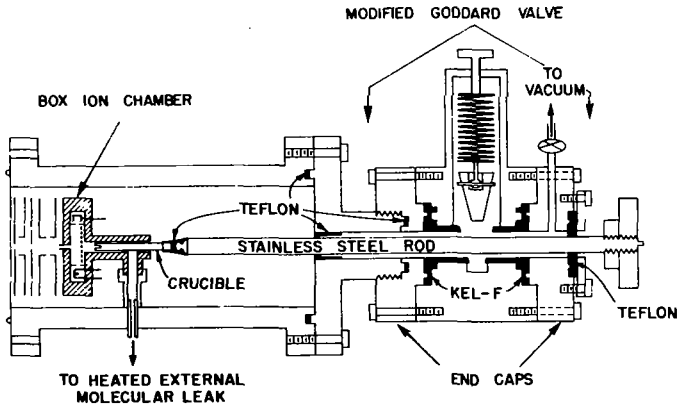

Fig. 5. Vacuum lock, box ion chamber and sampling tool for direct insertion technique.

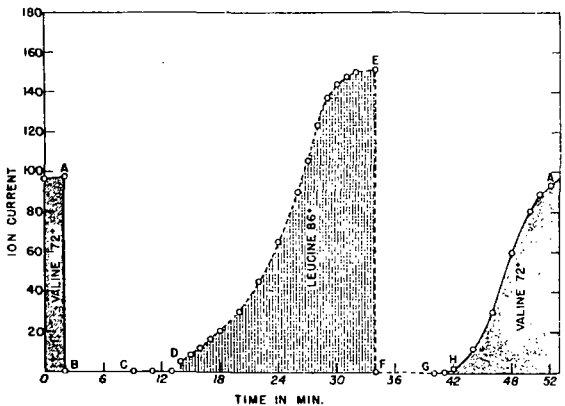

Fig. 6. Operational data using vacuum lock and box ion chamber.

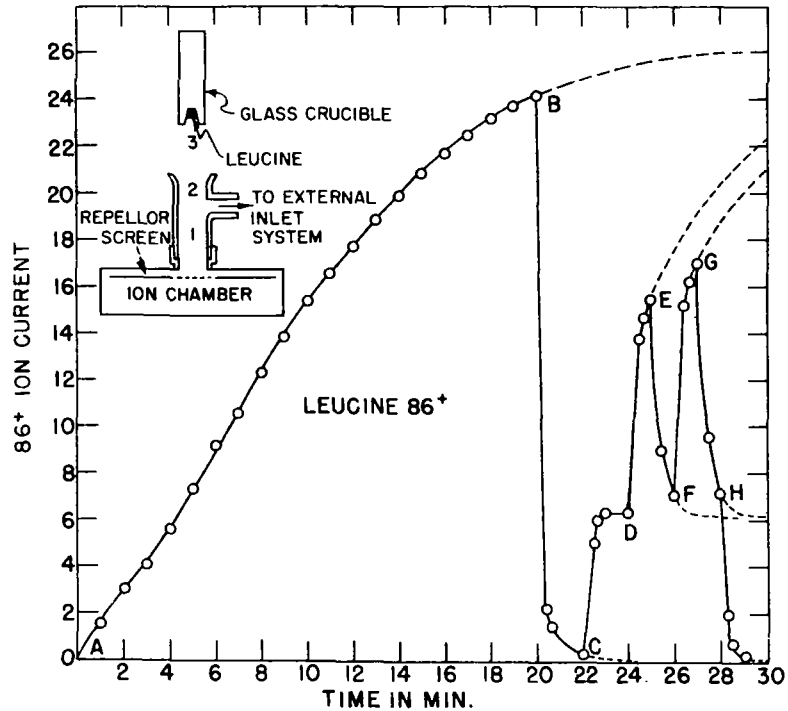

Fig. 7. Data on the alternate and simultaneous use of direct insertion technique and the use of an external system.

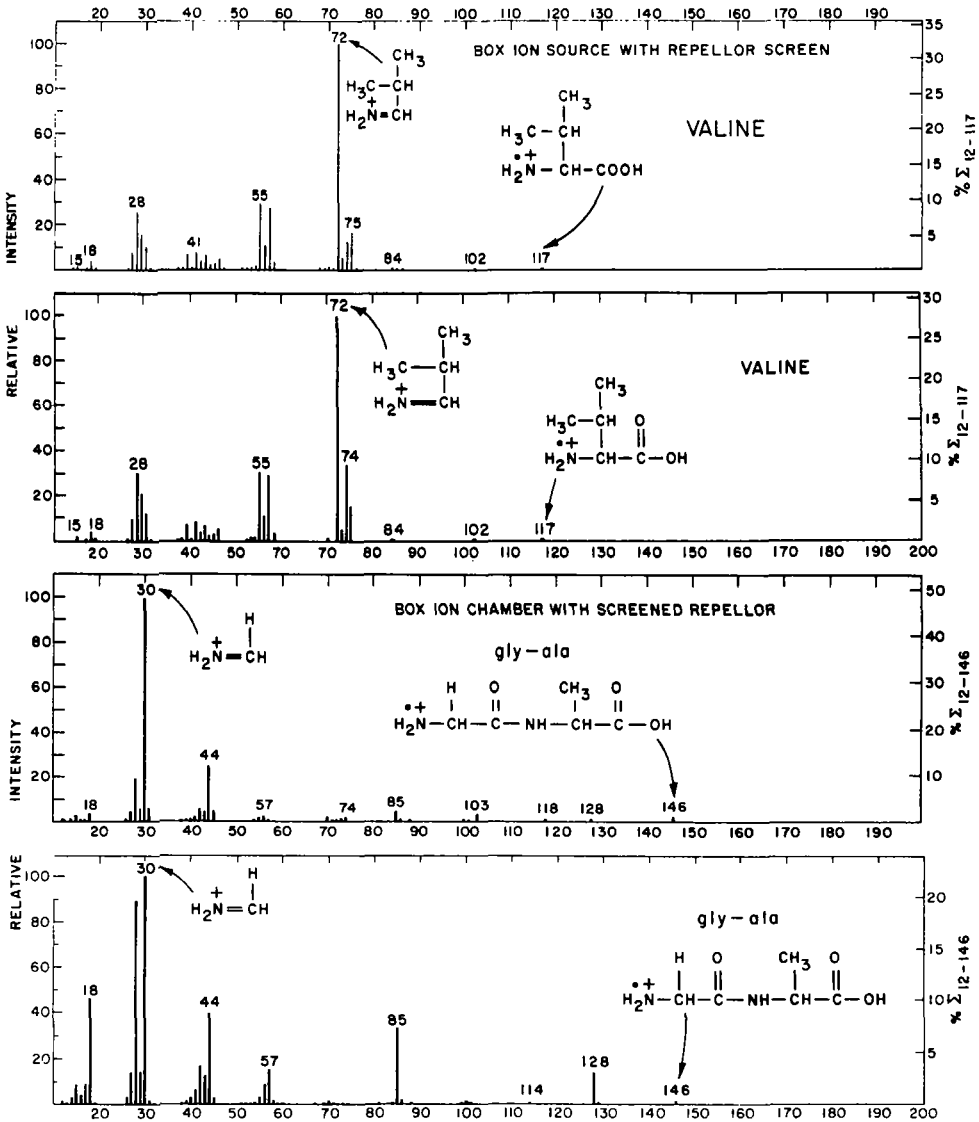

Fig. 8. Representative comparative spectra of amino acids and dipeptides.

CHROMATOGRAPHIC EFFICIENCIES DURING COMBINED MASS SPECTROMETRIC - GAS CHROMATOGRAPHIC ANALYSIS

W. H. McFadden, R. Teranishi, T. R. Mon, and Janet Wasserman
Western Regional Research Laboratory,* Albany, California

INTRODUCTION

One of the more important problems solved by direct introduction of gas chromatographic eluates into a mass spectrometer has been the qualitative analysis of very complex mixtures. Because such mixtures can generally be separated only on capillary columns, the problem of collecting and analyzing these submicro quantities is difficult. Techniques for coupling a capillary gas chromatograph to a mass spectrometer were first described in 1962 (1,2,3,4) and several applications have been demonstrated (4,5,6,7,8,9).

Because the interpretation of mass spectra thus obtained must often be made for types of compounds not catalogued or previously reported, it is extremely important that maximum chromatographic efficiency be maintained. The necessity of this requirement is convincingly shown by the chromatogram and mass spectra obtained during analysis of a strawberry oil (Figures 1 and 2). Figure 1 shows the chromatogram of the total mixture--approximately 150 peaks. On a packed column, only about 30 peaks are normally observed. Figure 2 shows the mass spectra obtained on the last large peak (eluted after 85 minutes at a temperature of 175°C.).

The mass spectra of Figure 2 were taken at approximately 10 sec. intervals. The first was taken about one-half way up the peak and shows the spectrum of trans-3-hexenyl caproate, component 149. The beginning of the spectrum of benzyl acetate, component 150 is apparent. The second spectrum was taken near the top of the peak and shows the spectrum of the benzyl acetate and the start of the mass spectrum of α-terpineol (151). In the third spectrum, the benzyl acetate has been effectively eluted but a fourth component, 2-hexenyl caproate (152), is apparent with the α-terpineol. Finally, as the small shoulder at the base of the large peak is traversed, the spectrum of a pentyl octanoate was obtained, clear of any serious interference from the other components.

Fortuitously, these components were all identified but the need for maintaining maximum chromatographic efficiency is obvious. To test this, theoretical plate measurements were made using ionization from the mass spectrometer for a chromatographic trace, thus obtaining a true representation of the rate of pump-out of the mass spectrometer. These are compared with the theoretical plate values obtained using a hydrogen flame detector. In addition, the chromatographic traces obtained from the mass spectrometer during analysis of oils extracted from orange juice are compared with the hydrogen flame chromatograms.

EXPERIMENTAL

The technique used in this work will be described briefly. Figure 3 shows a schematic diagram of the apparatus. The unique feature of the introduction is that the chromatographic column is operated with its outlet at vacuum (approximately 10^{-3} Torr). This has two advantages over a throttling technique in which the column exits at one atmosphere.

First, the very high linear velocities attained under vacuum conditions permit the use of awkward geometric construction and the possibility of eddies, which can seriously impair separations, are eliminated. Secondly, in order to have the same average linear velocity through the column and hence the same chromatographic efficiency (10), it is necessary to reduce the input pressure by one atmosphere. This significantly reduces the amount of carrier gas going through the column and permits introduction of a greater fraction of the eluate with no increased pumping requirement.

The disadvantages of the vacuum exit should be mentioned. If a steam splitter is used to facilitate sample injection, then operation of the column exit at vacuum and splitter exit at one atmosphere decreases the splitting ratio. This can be easily corrected but is very important if the normal pressure drop across the column is not significantly above 15 psi. Similarly, shorter columns (about 100 ft. 0.01") will normally be operated below a total pressure drop of 15 psi so that it is now necessary to operate the input of the column with a modest vacuum. Again, this can be easily accomplished but this is not usually encountered for very complex mixtures which require longer columns to effect separation.

---

* A laboratory of the Western Utilization Research and Development Division, Agricultural Research Service, U. S. Department of Agriculture.

Direct measure of the column plate efficiencies was made by setting gate 2 of the electron multiplier on a suitable mass and recording the chromatogram on a strip chart. The columns were 200 or 250 ft., 0.01" capillaries and were operated isothermally at 125°C. The average linear velocities were measured by injection of a gas (Argon or CH_4) and noting its elution time.

The sample size for the hydrogen flame detector was 0.2 μl. with a steam split of 1/200. The sample size for the mass spectrometer was 1.0 μl. with a steam split of 1/100.

RESULTS AND DISCUSSION

Table 1 shows the HETP values obtained for three different columns using the maximum efficiency average linear velocity of 15 cm. For the most part the values obtained on the mass spectrometer are comparable to those from the hydrogen flame detector. One or two cases show discrepancies of factors of two to three, but those are attributed to experimental error.

A comparison of van Deempter curves obtained by the two methods is given in Figures 4 and 5. Figure 4 shows the variation of HETP with average linear velocity as obtained from a Tween-20 column using the hydrogen flame detector. An optimum efficiency is indicated at 15 cm./sec. but, over this relatively narrow range, the differences were not extreme for this column. The van Deempter curve obtained using the mass spectrometer is shown in Figure 5. The optimum efficiency at approximately 15 cm./sec. is again evident and the HETP values at this point are essentially the same as the hydrogen flame values. However, at other flow rates the chromatographic efficiency is considerably impaired.

It must be emphatically pointed out that this difference in the van Deempter curves is not due to the mass spectral detection or the use of a vacuum exit. This difference was deliberately demonstrated by the use of a larger chromatographic charge. If the same sample size is used for both, then similar van Deempter curves are obtained. However, qualitative identification by mass spectrometry will usually require about 100 times more signal than is required for simple detection of a material. In order to obtain reasonable mass spectra for identification of the trace components of a mixture, it is almost always necessary to perform a second mass spectral-chromatographic run with an excess of the more abundant components. The need for operation at maximum efficiency is apparent.

Direct comparison of chromatographic traces obtained at higher temperatures during a temperature programmed run also provides a convincing test of the technique. Figure 6 shows the chromatogram of the first of two fractions separated from orange juice, free of peel oil. The first of these was more abundant in the water soluble components; the second in the terpene and sesquiterpene materials.

This chromatogram was obtained with a hydrogen flame detector. During the mass spectral run, mass 41 was selected on gate 2 to obtain a chromatographic trace. Figure 7 shows a comparison at 177°C. of this trace with the same region of the flame chromatogram. The eluates were sesquiterpene hydrocarbons (MW=204) and as the comparison shows, the chromatogramic efficiency has not been destroyed.

The chromatographic comparison shown in Figure 8 is of the region of the second fraction at 200°C. The eluates were sesquiterpene aldehydes and alcohols (MW=220-224). In this case the mass spectral chromatogram shows a slight, but not serious, broadening of the peaks. Possibly, this is an indication that the temperature of the mass spectrometer was at its lower limit (external temperature of the ionization chamber, 100°C.). In any event, the separations achieved were about the same as those obtained using a hydrogen flame detector.

It is concluded that no serious loss of chromatographic efficiency is realized when the eluate of a capillary chromatographic column is introduced directly into a mass spectrometer. Apparently, it is necessary that the temperature of the mass spectrometer is not more than 70-100 degrees below the column temperature.

Reference to a company or product name does not imply approval or recommendation of the product by the U. S. Department of Agriculture to the exclusion of others that may be suitable.

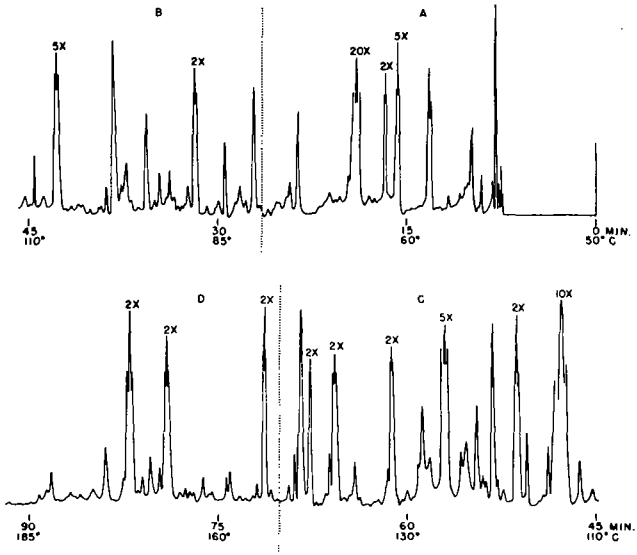

Fig. 1

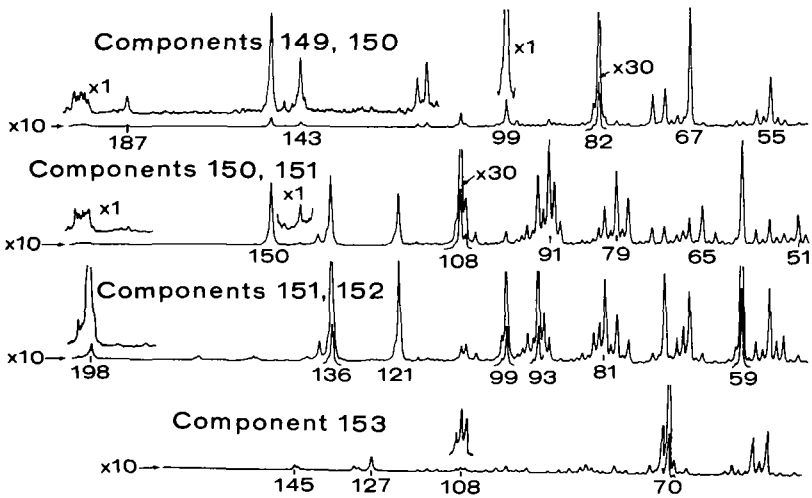

Fig. 2

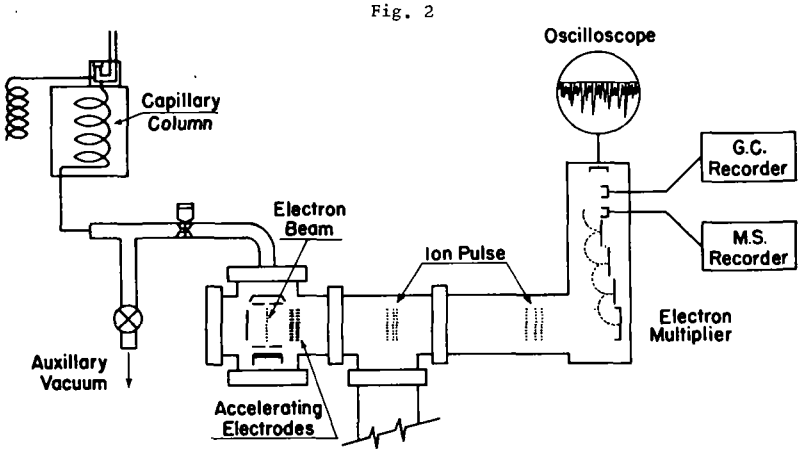

Fig. 3

TABLE 1

HETP (in cm.)

STATIONARY LIQUID	COMPOUND	HYDROGEN FLAME	MASS SPECTROMETER
SF 96-50	Limonene	0.08	0.18
	n-Amyl acetate	0.10	0.18
	n-Hexanol	0.18	0.21
Carbowax	Limonene	0.29	0.11
	n-Amyl acetate	0.12	0.14
	n-Hexanol	0.25	0.22
Tween-20	Limonene	0.20	0.15
	n-Amyl acetate	0.15	0.15
	n-Hexanol	1.0	0.80

Column Temperature 125°C. Helium Carrier Gas 15 cm./sec.

REFERENCES

(1) C. Brunnee, L. Jenkel, K. Kronenberger, paper given at the 10th Annual Meeting of ASTM Committee E-14, New Orleans, La., June 1962.

(2) W. H. McFadden, R. Teranishi, D. R. Black, J. C. Day, ibid.

(3) W. H. McFadden, R. Teranishi, Nature 200, 329 (1963).

(4) J. A. Dorsey, R. H. Hunt, M. J. O'Neal, Anal. Chem. 35, 511 (1963).

(5) R. Teranishi, R. G. Buttery, R. E. Lundin, W. H. McFadden, T. R. Mon, Proc. Amer. Soc. of Brewing Chemists, 52 (1963).

(6) R. G. Buttery, W. H. McFadden, R. Teranishi, Mary P. Kealy, T. R. Mon, Nature 200, 435 (1963).

(7) R. Teranishi, J. W. Corse, W. H. McFadden, D. R. Black, A. I. Morgan, Jr., J. Food Sci. 28, 478 (1963).

(8) E. A. Day, L. M. Libby, J. Food Sci., in press.

(9) E. A. Day, D. F. Anderson, J. Ag. and Food Chem., in press.

(10) R. Teranishi, R. G. Buttery, W. H. McFadden, T. R. Mon, Jan Wasserman, Anal. Chem., 36, 1509 (1964).

FIGURE CAPTIONS

Fig. 1. Capillary Chromatogram of Strawberry Oil. 200 ft., 0.01 in., Tween 20.

Fig. 2. Mass Spectra Obtained on Last Large Peak of Figure 1. Component 149, trans-3-hexenylcaproate; 150, benzylacetate; 151, α-terpineol; 152, 2-hexenylcaproate; 153, pentyloctanoate.

Fig. 3. Schematic Diagram of Mass Spectrometer - Gas Chromatograph.

Fig. 4. van Deempter Curves for Capillary Chromatograph Using H_2 Flame Detector. Limonene, +; n-amylacetate, △; n-hexanol, •; n-octanal, O. Sample size, 10^{-3} μl.

Fig. 5. van Deempter Curves for Capillary Chromatograph Using Mass Spectrometer. Legend same as Figure 4. Sample size, 10^{-2} μl.

Fig. 6. Capillary Chromatogram of Extract from Orange Juice. Column - 200 ft., 0.01 in., SF 96-50 silicone oil.

Fig. 7. Sample Comparison of H_2 Flame Detector Chromatogram with Mass Spectrometer (Mass 41) Chromatogram. Sesquiterpene hydrocarbons.

Fig. 8. Sample Comparison of H_2 Flame Detector Chromatogram with Mass Spectrometer (Mass 41) Chromatogram. Oxygenated sesquiterpenes.

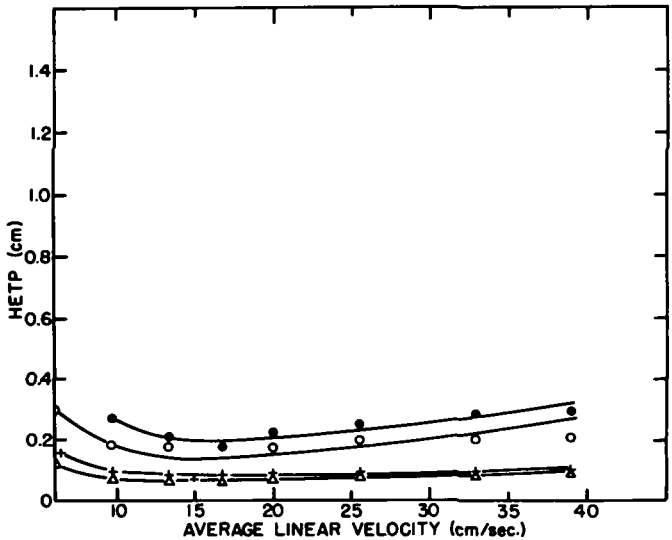
HETP (cm)
1.4
1.2
1.0
0.8
0.6
0.4
0.2
0
10
15
20
25
30
35
40
AVERAGE LINEAR VELOCITY (cm/sec.)
Fig. 4

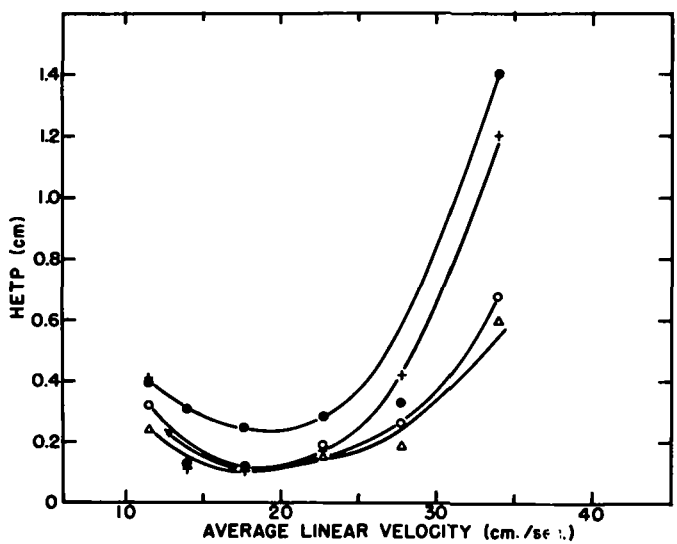
HETP (cm)
1.4
1.2
1.0
0.8
0.6
0.4
0.2
0
10
20
30
40
AVERAGE LINEAR VELOCITY (cm./sec.)
Fig. 5

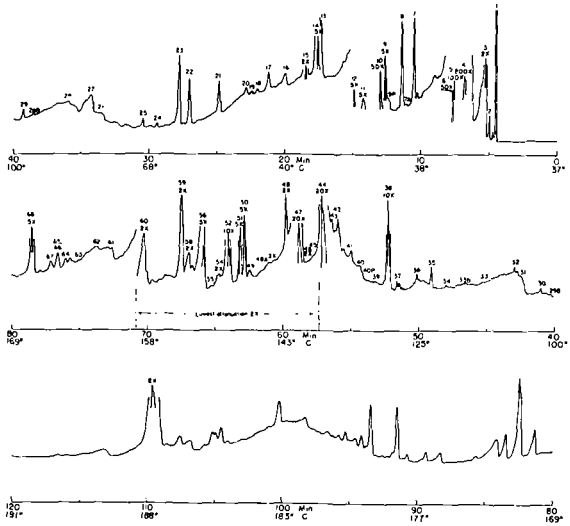

Fig. 6

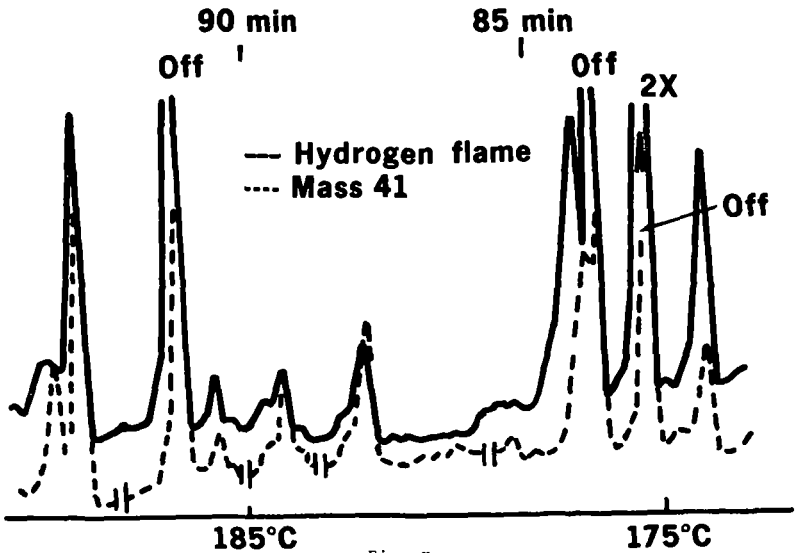

Fig. 7

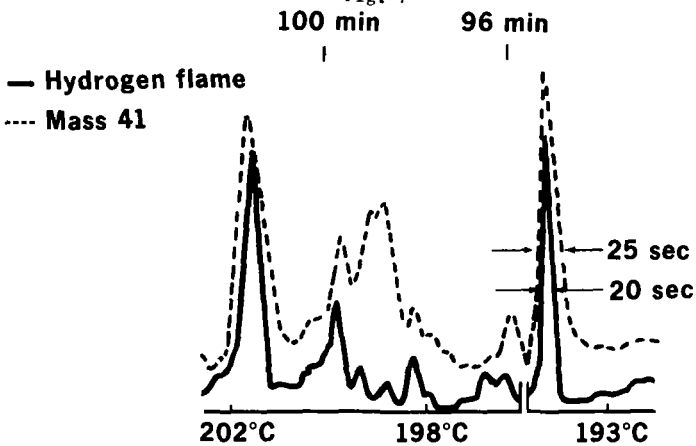

Fig. 8

A MASS SPECTROMETRIC PROCEDURE FOR THE IDENTIFICATION AND MEASUREMENT OF TRACE COMPONENTS IN NONCONDENSABLE MEDIA

W. J. Lambdin, Jr. and H. E. Persinger

Research and Development Department

Union Carbide Corporation, Chemicals Division

South Charleston, West Virginia

INTRODUCTION Advances in chemicals development and processing have resulted in an increasing demand for microanalytical techniques that are specific and quantitative. A mass spectrometric procedure has been developed for performing quantitative and qualitative analysis for condensable components in a noncondensable matrix in concentrations from 0.1 per cent to below 100 parts per billion. The procedure incorporates a static trapping system to collect the condensable components. Total recovery, and subsequent quantitative determination, has been achieved with materials boiling from -80° to 200°C.

Extensive use of the method can be predicted from the success of applications in the following categories.

(a) Identification of individual components eluted from a gas chromatograph after separation.

(b) Specific quantitative determinations for atmospheric pollutants.

(c) Analyses for trace components in noncondensable gaseous process streams.

Although the mass spectrometer is not usually considered a tool for the analysis of components below the 100 ppm level, the fact that it is an unexcelled identification tool urged the discovery of a means of applying it to trace analysis. This application depends on isolating the material to be analyzed from the matrix gas.

Approximately 1×10^{-10} moles of a compound is required to produce a usable mass spectrum. This amount should comprise at least 0.01 per cent of the material admitted to the instrument to prevent malfunction due to saturation in the ionization region. Various methods have been used to concentrate trace materials to this necessary level with only partial success. For instance, concentration from streams by use of cold traps usually have a maximum efficiency of about ten per cent for trace components, which precludes use of this method for quantitative determinations. Furthermore, other dynamic trapping techniques have not been entirely successful because of the following adverse phenomena.

(a) Dilution due to condensation of extreneous materials (e.g., water and carbon dioxide from the atmosphere).

(b) Loss by absorption in stopcock grease.

(c) Loss during prolonged exposure to high vacuum.

(d) Inefficient recovery due to aerosoling.

DISCUSSION The Consolidated Model 21-103 mass spectrometer has been modified to allow concentration of condensables with total recovery. A permanent cold trap has been incorporated into the inlet system of the instrument. The trap and auxiliary equipment were designed to eliminate the phenomena which have prevented previous use of condensation techniques.

An important advantage of the system is that the sample under investigation can usually be transferred by merely filling a dry hypodermic syringe. The sample is then injected directly into the modified inlet system through the silicone septum. This straightforward sampling procedure results in two decided benefits. The sample is representative since complex manipulations are unnecessary, and time consuming procedures are eliminated.

The design of the system is shown in Figure 1. Total recovery of condensables is possible because the condensation takes place in a static system, pump-out of the noncondensable matrix is rapid, highly absorbant surfaces (e.g., stopcocks, joints) have been eliminated, and contamination from condensation of extreneous materials is at a minimum.

The routine operating procedure is:

1. Isolate the evacuated trap from the inlet system.

2. Place a liquid-nitrogen bath around the trap.

3. Introduce the sample through the septum. The sample will be rapidly inspired.

4. After a condensing period of 30 seconds, a pumping period of 10 seconds will remove the noncondensables.

5. The condensables are then vaporized into the inlet system for analysis by replacing the liquid-nitrogen bath with a hot-water bath.

6. After vaporization the trap is evacuated with the hot-water bath in place, thus insuring a clean system for subsequent use.

In conjunction with the concentration procedure, the sensitivity of the detection system was increased by a factor of two. This was accomplished by increasing the preamplifier input resistance from 5×10^{10} ohms to 1×10^{11} ohms. Also, a high signal-to-noise ratio is desirable for the detection of small peaks.

Total recovery of condensables has been demonstrated by the analyses of known samples (Table I). A prepared mixture of 35 ppm ethylene dichloride in air analyzed 35 ppm. A sample of fresh air, which normally contains 317-320 ppm carbon dioxide, analyzed 315 ppm. The equivalent intensity of the mass 44 peak was 4 divisions for 1 ppm at 50 microamperes. Analyses for low molecular weight amines have not been successful, which indicates that critical applications should be evaluated.

Applications

Micro mass spectrometry has been applied successfully to analyses of process streams, the identification of compounds from gas chromatographic separations, and analyses for atmospheric pollutants.

Process Studies

Streams that are composed primarily of noncondensable materials can be effectively analyzed for most condensable organic components. These analyses provide information on processing efficiencies, reactions, and loss of materials. Two examples follow.

TABLE I

ANALYSES OF KNOWN CONCENTRATIONS IN AIR

	KNOWN, PPM	FOUND, PPM
BENZENE	37	38
ETHYLENE DICHLORIDE	35	35
ACETIC ACID	42	41
ACETONE	166	190
ETHYLENE OXIDE	50	60
MORPHOLINE	157	102
ETHYLAMINE	20	0

TABLE II

ANALYSIS FOR CONDENSABLES IN A NITROGEN STREAM

	PARTS PER MILLION
METHYL CHLORIDE	5
VINYL CHLORIDE	2
ETHYL CHLORIDE	4

TABLE III

ATMOSPHERIC POLLUTANTS

SPOT SAMPLES FROM A REFINERY PUMPING AREA

	PPM (MOLES)			
	III	IV	V	VI
DICYCLOPENTADIENE	1		2	1
NAPHTHALENE	0.1		0.2	0.03
INDAN	0.2		0.3	0.06
INDENE	0.2		0.3	0.2
XYLENES	1		2	0.6
STYRENE	2		5	2
TOLUENE	20	3	25	9
HEXENE	3			2
HEXADIENE	1	0.3	1	0.6
CYCLOHEXADIENE	5	1	6	2
BENZENE	120	15	140	42
PENTANE	9			8
PENTENE	40	3	5	7
PIPERYLENE	160	1	8	15
CYCLOPENTADIENE	260	2	7	23
BUTANE	30			
BUTENE	45			
BUTADIENE	80		5	6
CARBON DIOXIDE	470	490	370	860

First, vinyl chloride, methyl chloride, and ethyl chloride were identified in a N_2 stream in concentrations of 5 ppm or less (Table II). The identification and measurement of these products will assist in assigning losses in the process.

Second, the condensables from a hydrogen blowoff stream in a process were concentrated for identification prior to establishing activity coefficients for a water extraction.

Atmospheric Pollution

With the associated simplified sampling technique, this procedure provides an ideal method for analytical studies of atmospheric pollutants. The detectability limits are in a practical range that will provide maximum usable information. A series of atmospheric samples taken in an area of heavy contamination were successfully analyzed. Nineteen hydrocarbons were identified and measured in a refinery pumping area (Table III). The concentration of benzene was shown to be above the tolerable level of 35 ppm.

Gas Chromatography

Obviously, this procedure is ideally suitable to identification of unknown material from a gas chromatographic separation, since the effluent stream is noncondensable except for the compound to be identified. The material can be readily transferred from a chromatograph to the mass spectrometer by means of a hypodermic syringe. This transfer system has proven to be more efficient than those used previously and, consequently, is readily available to supplement the numerous gas chromatographic investigations in an area.

Gas chromatographic control analyses supplemented by this technique have been particularly useful in providing timely troubleshooting information for plant processes.

Special Problems

Table IV demonstrates the versatility of sampling with syringes. The off-gases from an automobile engine were readily examined without complex apparatus or procedures. The mass spectra show the loss of hydrocarbons in the blowby and in the exhaust gases during deceleration.

Odor problems can often be quickly solved by merely sampling the vapor space of a container or a particular area.

CONCLUSIONS

The incorporation of static trapping in the inlet system of a mass spectrometer greatly enhances its versatility insofar as trace analyses are concerned. The associated sampling and transfer method usually provides timely and more satisfactory data than more exotic procedures and apparatus.

TABLE IV

OFFGASES FROM AN AUTOMOBILE ENGINE

M/e	EXHAUST - UNDER LOAD	EXHAUST - DECELERATING	BLOWBY
18	812	2210	2790
26	36	270	190
27	40	580	1000
28	1410	1110	1080
29	36	410	760
30	9	17	22
39	28	470	790
40	14	87	136
41	40	780	1410
42	20	380	770
43	40	740	1445
44	10000	7700	6500
55	19	470	790
56	14	330	587
57	14	350	590
69	9	240	390
70	8	180	300
71	5	115	190
78	7	65	90
81	3	70	105
83	4	105	140
84	3	78	135
85	2	58	80
92	5	75	96
97	2	51	54
98	1	37	53

FIGURE 1

MASS SPECTROMETRIC ANALYSES OF TRACE COMPONENTS

ASSEMBLY FOR CONCENTRATING CONDENSABLES

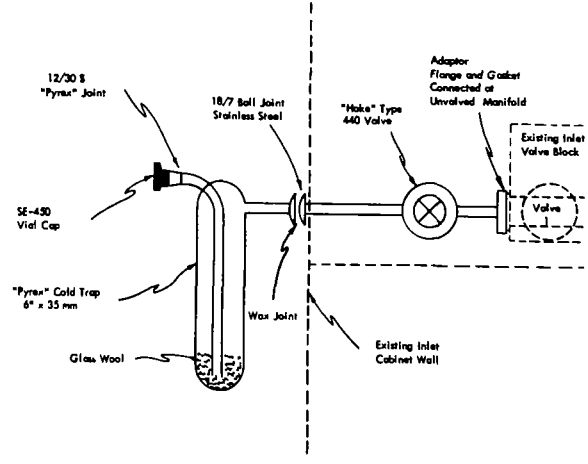

SIMPLIFIED MASS SPECTRA

Graham G. Wanless and George A. Glock, Jr.
Analytical Research Division
Esso Research & Engineering Company
P. O. Box 121
Linden, New Jersey

I. *Introduction*:

The examination of mixtures of compounds could be made easier if the mass spectra were less complex - that is, if the parent ions could be enhanced at the expense of fragment ions.

In the future such simplification may be accomplished best by field-emission mass spectra, or by certain kinds of negative ion mass spectra. Equipment for such studies is not widely available. This report summarizes what progress has been made in this direction, using conventional electron bombardment mass spectra. It is demonstrated with a series of aliphatic compounds.

II. Experimental:

(a) Basis for Comparing Spectra:

$$\text{"Gain"} = \frac{\text{Ratio Parent Ion/Base Peak - from simplified spectrum}}{\text{Ratio Parent Ion/Base Peak - from reference spectrum}}$$

Usually the "base" peak is the largest peak in the spectrum, but in those cases where the parent ion provides the largest peak, the "base" peak becomes the second largest peak in the spectrum.

Unless indicated otherwise, the "reference" spectra are 70 e.v. spectra, made with an ion chamber temperature of 220-250°C., and are taken from the API-44 compilation. The simplified spectra are designated MS-I or MS-II and defined below.

(b) Instrumental Conditions:

This work is an extension beyond conventional low-voltage mass spectra[4]. It was thought at first that this would be simply a matter of acquiring ion guns which would operate at lower temperatures, since parent ions are more temperature-sensitive than are fragment ions. However, some additional gains can improve the discrimination in favor of parent ions.

It is intended to present only practical data obtained under steady-state conditions on two modified General Electric 60°, magnetically scanned mass spectrometers. The parameters defined are for day-to-day operating conditions. No claim is made that the results represent the best that can be done. Nor is any advantage taken for special situations. Such is the result which can be obtained when a) the sample is charged, b) the filament is turned on, and c) the sample is scanned quickly before the ion chamber warms up. Such a procedure can improve the spectra, usually about two-fold over the results reported here.

The principal operating conditions for these two instruments are defined in Table I.

Table I.: MASS SPECTROMETER CONDITIONS

	MS-I	MS-II
Radius of 60° mass tube	6"	12"
Ion gun slit	0.008"	0.004"
First collimating slit	0.008"	0.004"
Second collimating slit	0.008"	0.004"
Accelerating voltage	1750V.	3500V.
Draw-out potential	1675V.	3120V.
Repeller field strength	1.5V/cm.	54V/cm.
Filament to shield voltage	10 ev.	15 ev.
Ion gun temperature	80°C.	110-130°C.
Sample system temperature	75°C.	150°C.
Mass range	to M 280	to M 450
Filament	Thoria coated iridium	Coiled thoriated tungsten

Yoke magnets optimized.

The 6" radius instrument (MS-I) which can operate at 80°C. has an ion chamber made of thin metal. The ion chamber of the 12" radius instrument is cut from a solid Nichrome V. block, and this causes it to operate at about 115°C. For this latter

Figure 1
M.S. CRACKING PATTERN OF n- HEXADECANE
RATIO M 226/M57

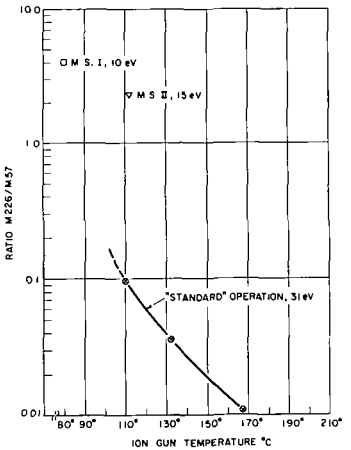

Figure 2
3-HEPTANONE

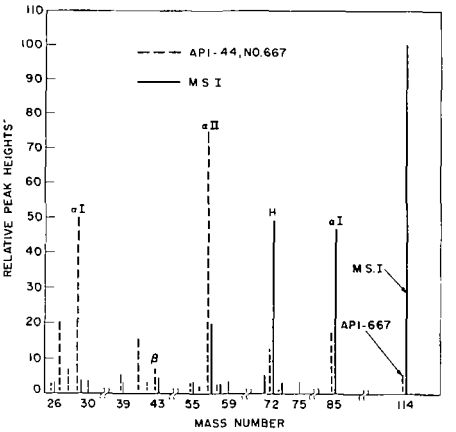

Figure 3
1-DECENE

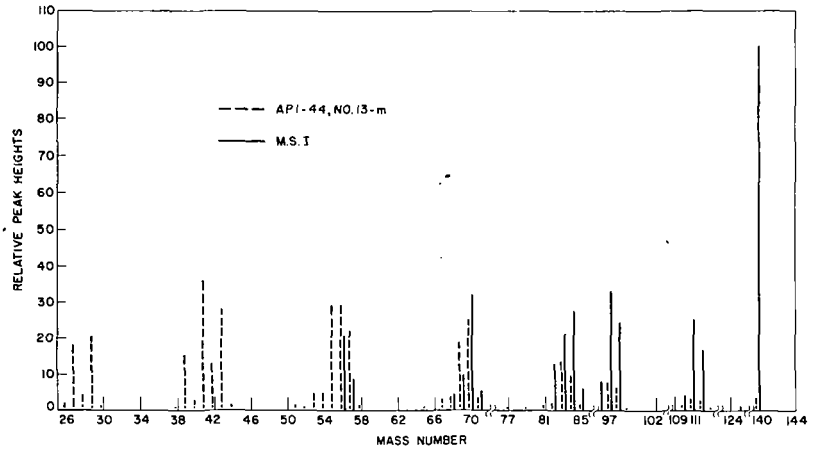

Figure 4
1-NONANE THIOL

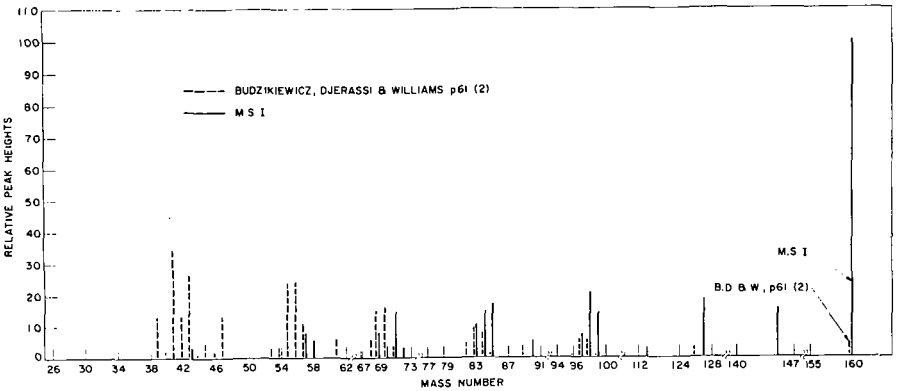

instrument the 15 ev. shield potential is a compromise choice. It gives parent ions which are about 35% as high as those which would be obtained with the usual "high" shield voltage (31V.).

The instruments are tuned by optimizing the cracking pattern of n-hexadecane (ratio M226/M57), at the particular shield voltage which has been selected. In Figure 1, the operating points for these two mass spectrometers are defined. The measure of improvement is shown in terms of the cracking pattern of n-hexadecane.

III. Results:

(a) Degree of Improvement for "MS-I" Conditions:

The gain is demonstrated in Table II in a series of 31 compounds, representing 13 classes of aliphatic compounds (linear and branched).

Table II.: SIMPLIFIED MASS SPECTRA OF ALPHATIC COMPOUNDS

COMPARISON WITH API-44 REFERENCE SPECTRA

Compound	(A) API-44	(B) MS-I	"Gain" = B/A
n-Hexane	0.155	0.903	5.8x
n-Heptane	0.122	1.05	8.6x
n-Octane	0.069	0.623	9.0x
n-Decane	0.060	1.16	19. x
n-Hexadecane	0.019	4.0	210. x
Neopentane	0.0001	0.0064	64. x
2,2-Dimethyl butane	0.0006	0.0073	12. x
2,3-Dimethyl butane	0.036	0.262	7.3x
3,3-Dimethyl pentane	0.0001	0.015	150. x
1-Decene	0.103	3.10	30. x
1-Tetradecene	0.060	4.2	70. x
3,3-Dimethyl-1-pentene	0.090	1.06	12. x
Cyclooctene	0.313(a)	2.02	6.5x
Cyclooctadiene	0.061(b)	0.421	6.9x
1-Pentyne	0.169	0.335	2.0x
2-Pentyne	1.10	2.86	2.6x
Propanal	0.389	22.1	57. x
Acetone	0.280	4.64	17. x
Methyl ethyl ketone	0.170	4.54	27. x
3-Heptanone	0.080	2.02	25. x
Diethyl ether	0.304	2.13	7.0x
1-Decanol	0.0002	0.402	2000. x
Silyl ether of 1-decanol	2.00(c)	22.7	11.4x
1-Decanoic acid	0.094(d)	0.512	5.4x
1-Hexane nitrile	0.0075	0.431	57. x
Succinonitrile	0.144(e)	0.750	5.2x
1-Bromohexane	0.023(f)	0.202	8.8x
2-Bromohexane	0.0011(g)	0.0051	4.6x
3-Bromohexane	0.0023(h)	0.012	5.2x
Erythro-3 phenyl-2-butyl chloride	0.096(i)	0.836	8.7x
1-Nonane thiol	0.143(j)	4.75	33. x

(a) Atlantic uncertified spectrum ARCO-109 (1688)
(b) Atlantic uncertified spectrum ARCO-110 (1699)
(c) E.R. & E. Co., spectrum 96-98-1, CEC-21-103c, ion gun 274°C., 70 ev.
(d) Dow uncertified spectrum No. 1926.
(e) B. F. Goodrich uncertified mass spectrum
(f) Dow uncertified spectrum No. 2188.
(g) Dow uncertified spectrum No. 3239.
(h) Dow uncertified spectrum No. 2902.
(i) E. R. & E. Co., spectrum 96-28, condns. as for footnote (c).
(j) See reference (2).

Figure 5
I - DECANOL

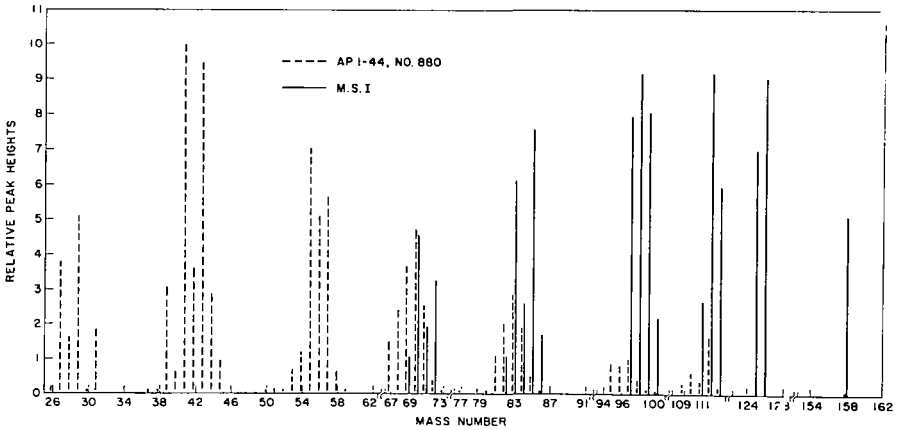

Figure 6
SILYL ETHER OF I-DECANOL

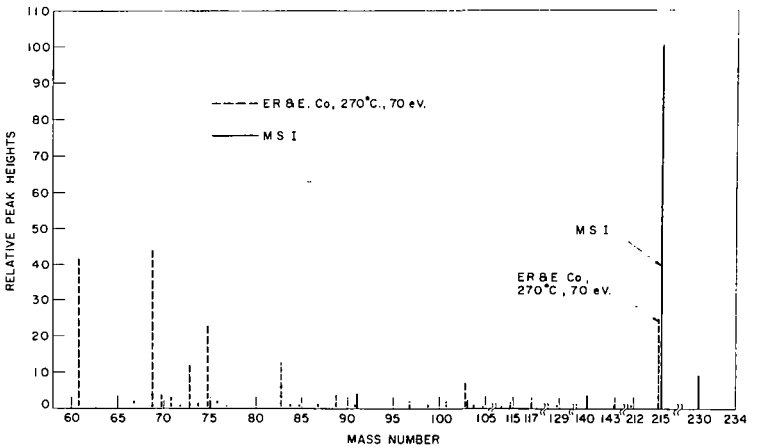

Figure 7
SILYL ETHER OF I-DECANOL

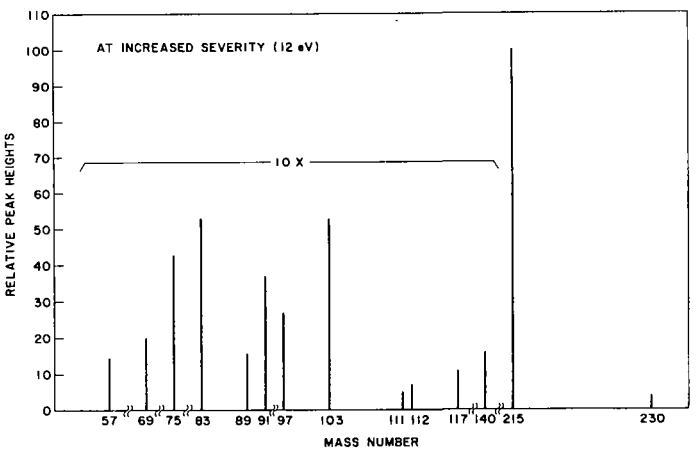

In summary, the gains vary widely from one compound class to another as well as within a given class of compounds (e.g. linear paraffins).

(b) Comparison of Two Sets of Instrumental Conditions:

For 25 cases reported in Table II, where direct cross-checks are available, the following comparison can be made between the two sets of conditions which are defined in Table I. (The example of 1-decanol is not used in this average):

Table III.: SIMPLIFIED MASS SPECTRA

	MS-I	MS-II
Mass tube radius	6"	12"
Shield voltage	10 ev.	15 ev.
Ion gun temperature	80°C.	120°C.
Ave. gain factor for 25 cpds.	34x	23x

(c) Comparison with Photoionization Spectra:

When this work was begun, it was thought that it would not be possible to obtain better results than can be obtained at room temperature by the photoionization method. In Table IV a comparison is made for six examples, with the photoionization data of Steiner, Giese and Inghram (1961)(5):

Table IV.: COMPARISON OF PHOTOIONIZATION SPECTRA AND SIMPLIFIED MASS SPECTRA

	Steiner, Giese and Inghram (5)		MS-I		
	Peak m/e	H't. Ratios (A)	Peak m/e	H't. Ratios (B)	Gain = B/A
Neopentane	72/57	0.0007	72/57	0.0064	9.0 x
n-Hexane	86/56	1.34	86/57	0.90	0.67x
2,3-Dimethyl butane	86/42	0.48	86/71	0.26	0.55x
2,2-Dimethyl butane	86/56	0.11	86/71	0.0073	0.66x
n-Heptane	100/70	0.26	100/71	1.05	4.0 x
n-Octane	114/85	1.19	114/85	0.62	0.52x

These data show results which vary from half as good to nine-fold better, for the case of neopentane. However, this latter improvement leaves much to be desired. Even with field emission spectra(1) a result only five-fold better than reported above for MS-I conditions may be expected.

(d) How Fragmentation Patterns are Altered - Five Examples:

In general i) the effects vary widely, ii) parent ions are enhanced, iii) peaks below m/e 56 are almost eliminated, iv) the relative abundances of larger fragments are increased, and v) new and useful features are revealed in the spectra. These latter differences and a wider knowledge of how they change with cracking severity should constitute a useful analytical tool.

Five examples will show some of the specific effects, (Figure 2 to 7). In each case, the reference spectrum (defined in Table II) is shown with dashed lines and the simplified spectrum with solid bar lines. The sum of the bar heights is the same for each spectrum.

1. 3-Heptanone: (Figure 2). For this compound we have come to expect two kinds of α-cleavage, β-cleavage and a rearrangement ion (type H) (2), at mass 72.

Table V summarizes the changes. It is found that in the competition i) one α-cleavage process is suppressed and the other enhanced, and ii) the rearrangement ion is increased four-fold.

(Table V on next page)

Table V.: 3-HEPTANONE

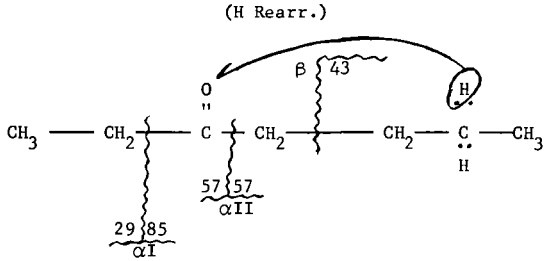

m/e	Cleavage Process or Rearrangement	Percent of Total Ionization (a) API-667	MS-I
29	αI	22%(a)	1.5%(a)
43	β	3.2	1.9
57	αII	32.	8.3
72	H Rearr.	5.6	21.
85	αI	7.5	20.
114	P	2.5	43.

(a) Percentages represent fraction of the sum of the ions in the spectrum. (Tables V, VI, VII).

The next group of examples compare four related compounds: 2. 1-Decene, 3. 1-Nonane thiol, 4. 1-Decanol, 5. Silyl ether of 1-decanol. The API spectra (dashed lines in Figures 2 to 7) of the first three compounds, show that when mass spectral conditions are severe enough, the spectra are more similar than they are dissimilar. They are characterized by a broad sweep of increasing fragmentation as one proceeds toward lower mass numbers. When treated more gently under conditions defined in this report, the three spectra develop substantial and characteristic differences:

2. 1-Decene: (Figure 3). The general "olefin" pattern is retained, i.e. the relative amounts of C_nH_{2n} and C_nH_{2n+1} peaks remain about the same - but the higher molecular weight fragments are more prominent.

3. 1-Nonane thiol: (Figure 4). In place of the general olefinic pattern, one obtains retention of charge on several alkyl fragments. These are summarized in Table VI.

Table VI.: 1-NONANE THIOL

m/e	Cleavage Process or Rearrangement	Percentage of Total Ionization B. D. & W., (3)	MS-I
57	$P-(CH_2)_5SH$ (a)	4.1%	3.0%
58	Rearr.	---	1.2
71	$P-(CH_2)_4SH$	1.4	5.4
85	$P-(CH_2)_3SH$	0.63	6.2
90	$P-(C_5H_{10})$	---	2.2
98	$P-C_2H_5SH$	2.1	7.7
99	$P-(CH_2)_2SH$	0.31	5.3
113	$P-CH_2$ SH	---	1.2
127	P-SH	---	6.8
145	$P-CH_3$	---	5.9
160	P	1.9%	37. %

(a) "P" = parent ion.

4. 1-Decanol: (Figure 5). This figure shows that the result is entirely changed for 1-decanol. Under the modified mass spectral conditions one obtains: i) Very large olefinic and alkyl peaks in the higher mass range. ii) Substantial rearrangement peaks at masses 72, 86, 100. Table VII summarizes the most important of these changes:

Table VII.: 1-DECANOL

m/e	Cleavage Process or Rearrangement	Percentage of Total Ionization API-44, #880	MS-I
84	Olefin	2.0 %	2.7%
85	Alkyl	0.53	7.9
86	Rearr.	0.09	1.8
98	Olefin	0.51	9.6
99	Alkyl	0.17	8.4
100	Rearr.	0.05	2.3
112	Olefin	1.7	9.6
113	Alkyl	0.2	6.2
125		---	7.3
126	Olefin	---	9.5
158	Parent Ion	0.002%	5.3%

5. Silyl ether of 1-Decanol: (Figure 6). The degree of improvement in the spectrum of 1-decanol (Figure 5) is quite substantial but falls far short of our desires. The difficulty can be rectified by using the silyl ether of 1-decanol. Figure 7 shows the large transformation which these modified operating conditions can make in the spectrum of this compound.

For once the situation is almost ideal. In order to observe structural features of the spectrum properly, one needs to increase cracking severity. This has been done in Figure 8, which is for a 12 ev. spectrum. Even so, all of the fragment peaks are displayed here, ten times larger than their actual size.

IV. Summary:

1. Simplified mass spectra are described which are an extension beyond conventional low-voltage mass spectra. They are for 31 products representing 13 different classes of alphatic compounds.

2. The simplification of these spectra are intended to show how far it has been possible to go using conventional and available equipment. Further advances in this direction are expected with the use of field-emission mass spectra. The presently available results are compared with photoionization mass spectra for 6 cases.

3. It is shown that

(a) The effects vary widely from one compound to another, even within a given class of compounds.

(b) Parent ions are enhanced.

(c) Mass peaks below m/e 56 are almost eliminated.

(d) The relative abundances of larger fragments are increased.

(e) New and useful features are revealed in the spectra. A wider knowledge of how these changes vary with cracking severity should constitute a useful analytical tool. Such changes are indicated for five of the 31 products cited.

V. References:

1. Beckey, H. D., "Advances in Mass Spectrometry", Vol. 2, R. M. Elliott, ed., Macmillan (New York) 1963, p. 22.

2. Biemann, K., "Mass Spectrometry - Organic Chemical Applications", McGraw-Hill (New York), 1962, p. 77.

3. Budzikiewicz, H., Djerassi, C., and Williams, D. H., "Interpretation of Mass Spectra of Organic Compounds", Holden-Day (San Francisco), 1964, p. 61.

4. Lumpkin, H. E., Analytical Chemistry, 30, 321 (1958).

5. Steiner, B., Giese, C. F., and Inghram, M. G., J. Chem. Phys. 34, 189 (1961).

This paper was presented at the "Twelfth Annual Conference on Mass Spectrometry and Allied Topics", McGill University, Montreal, Quebec, Canada, June 7 to 12, 1964.

THE RMU-6D - A VERSATILE SINGLE/DOUBLE FOCUSING MASS SPECTROMETER SYSTEM

Y. Nakajima, T. Noda
Hitachi Naka Works, Katsuta, Ibaraki, Japan

H. Tsuyama, J. Okamoto
Hitachi Central Research Lab., Tokyo, Japan

INTRODUCTION

The use of mass spectra for the study of molecular structures by Beynon, Biemann, Ryhage and others has generated a major field of application for mass spectrometry. The more recent use of exact mass measurements to characterize molecules requires a resolution capability greater than that available with single-focusing instruments. The Authors have developed a mass spectrometer system which includes a versatile, high-performance single-focussing instrument and provides for the addition of an electrostatic sector to give double-focusing operation. This combination retains the versatility of a single-focusing instrument, while providing the double-focusing resolution required for mass defect work. The system is designed so that the electrostatic sector can be field-installed at any time. The following is a brief description of the system including some operating performance data.

DESCRIPTION

The basic single-focusing instrument has a 90° magnetic sector with a 20 cm radius. The maximum accelerating voltage is 3600 volts. The instrument is magnetic scanning, with a maximum field strength of about 8000 gauss. The ion source slit and the collector slit can both be continuously varied by external controls from 1.0 to less than 0.01 mm. The ion collector is a combined Faraday cup electron multiplier system which allows both a very wide dynamic range and high sensitivity. The open type construction provides for ease of maintenance and modification. Automatic valves allow isolation of the pumping system and protection of the ion source in case of loss of power, cooling water, or vacuum.

Figure 1 shows the plan of the complete double-focussing instrument including the inlet unit, the electrostatic sector, the magnetic sector and the circuitry unit. The electrostatic sector angle is 45° and the radius is 25 cm. This unit is complete, containing its own vacuum pumping system, slit assemblies and power supplies and may be field-installed on any Hitachi Perkin-Elmer RMU-6D spectrometer.

The standard inlet system for both single and double-focusing operation is an all glass system shown schematically in Figure 2. It includes a room-temperature stopcock system as well as an all glass oven-enclosed section capable of being heated to 350°C. The construction of the five magnetically-operated ball and socket type glass valves contained in the heated inlet is shown in Figure 3. The standard inlet system includes another method of introduction not shown in the schematic. Provision is made for introducing samples on the low pressure side of the molecular leak, i.e. between the leak and the ion source. This is accomplished by using a standard Micro-tek 6000 Vacuum Lock Sample Introduction System. This inlet can be heated to 350°C and provides a convenient introduction point for low vapor pressure samples. It is also used for transferring gas chromatographic effluents directly to the ion source.

FIG. 1.

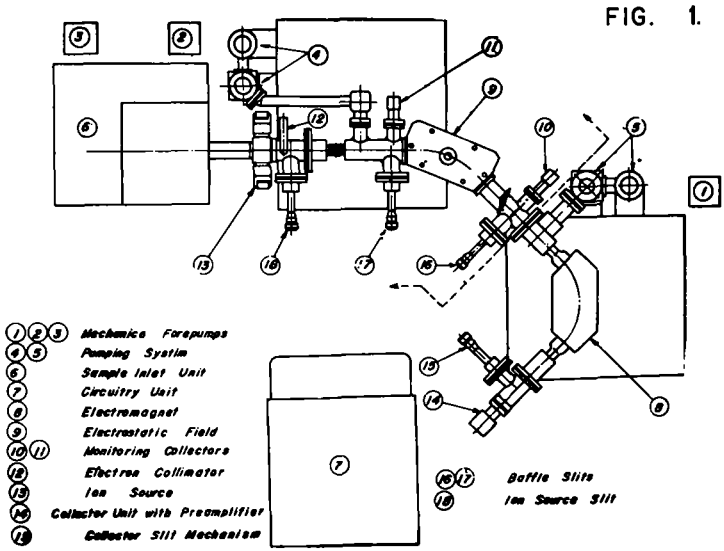

FIG. 2.

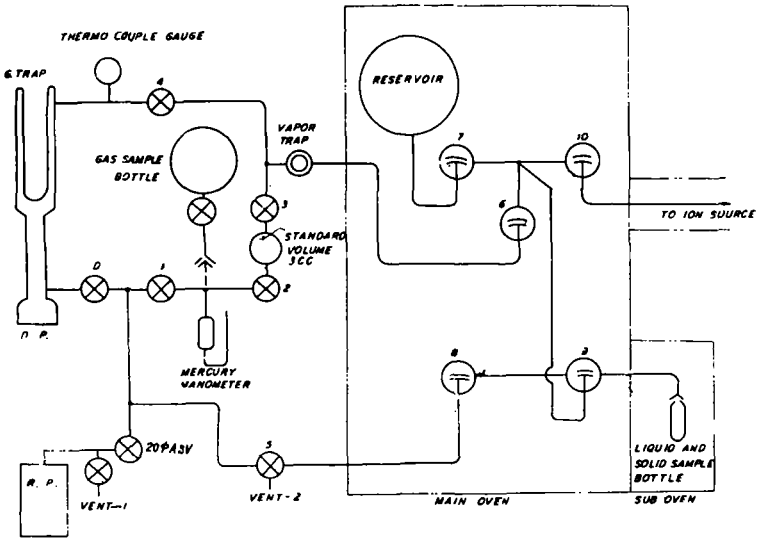
THERMO COUPLE GAUGE
G. TRAP
GAS SAMPLE BOTTLE
VAPOR TRAP
RESERVOIR
STANDARD VOLUME 5CC
TO ION SOURCE
MERCURY MANOMETER
D. P.
20φA3V
R. P.
VENT-1
VENT-2
MAIN OVEN
LIQUID AND SOLID SAMPLE BOTTLE
SUB OVEN

FIG. 3

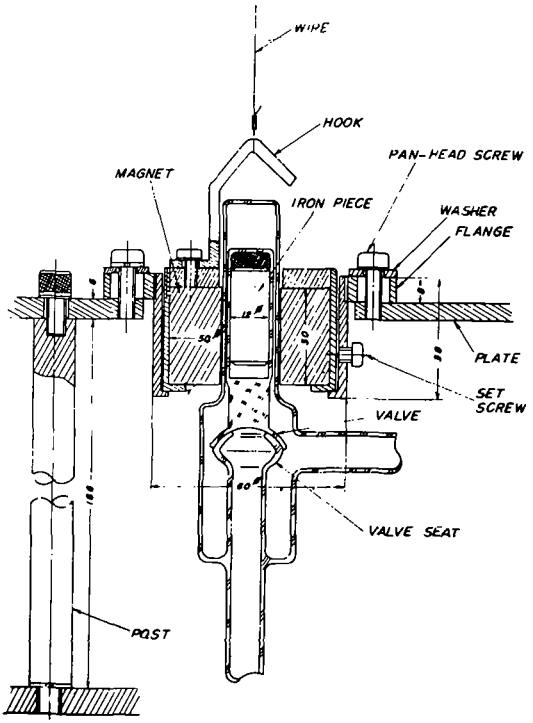
WIRE
HOOK
PAN-HEAD SCREW
MAGNET
IRON PIECE
WASHER
FLANGE
PLATE
SET SCREW
VALVE
VALVE SEAT
POST

In addition to the features included in the standard system, an optional inlet system is available for evaporating samples directly into the ionization region of the ion source. This is achieved by means of a vacuum lock system that provides for loading and evacuating a second sample while the first sample is being run. The sample temperature can be controlled between 40 and 350°C. This system parallels and does not interfere with the operation of the instrument with the standard inlet system.

PERFORMANCE

One of the features of the instrument is its fast scanning ability, without any serious loss of resolution or sensitivity. Figure 4 is a single-focusing 8.5 minute scan of methyl stearate from mass 25 to 300. Figure 5 is a 4 second scan of the same sample. The only change in operating parameters were the scanning rate and the chart speed. The fast scan shows some loss of peak height at the low mass end but this is not a serious problem and the more important high mass portion of the two spectra show good agreement. Figure 6 is an expansion of the parent peak region of the spectra from Figures 4 and 5. This shows the satisfactory reproduction of these peaks and demonstrates that there is no loss of resolution at the fast scanning rate.

Another important feature of the single-focusing version of the instrument is its excellent resolution. Figure 7 is a spectrum of the m/c 28 peaks of CO, N_2 and C_2H_4. There is a base line separation between the N_2 and C_2H_4 peaks with a difference of one part in 1100 and about a 25% valley between the peaks for N_2 and CO with a mass difference of one part in 2500.

An example of the increased resolution achieved by the addition of the electrostatic sector to make the instrument double focussing is shown in Figure 8. The doublet at mass 79 due to $^{13}C^{12}C_5H_6$ from benzene and C_5H_5N from pyridine with a mass difference of one part in 9700 is shown.

FIG. 4

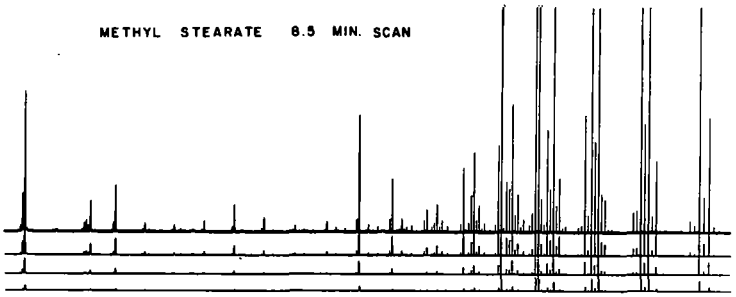

FIG. 5

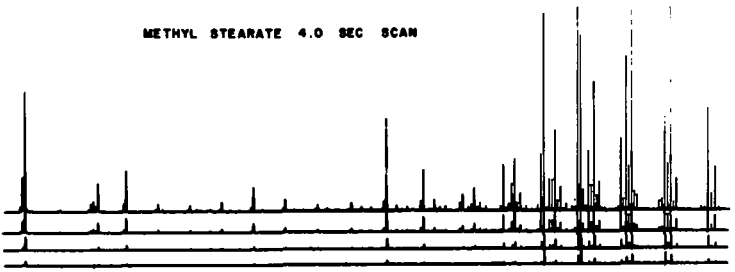

FIG. 6

298 PEAK OF METHYL STEARATE

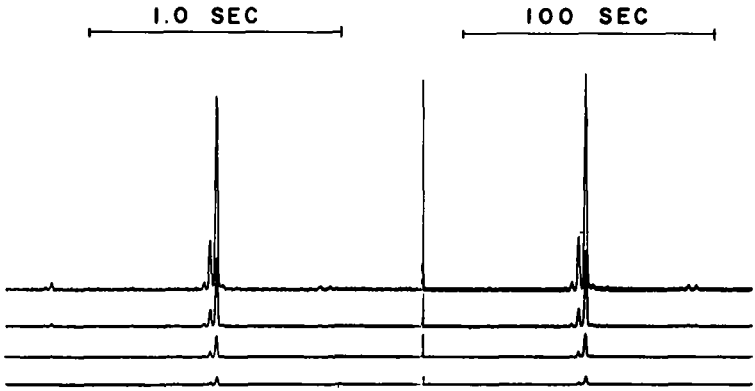

ACKNOWLEDGEMENT

The Authors are pleased to express their appreciation for the assistance and suggestions of:

Professor Ogata of Osaka University,
Professor Hayakawa of the University of Osaka Prefecture,
Professor Kitahara of Tohoku University, and
Professor Kanomata of Tokyo Metropolitan University

in the preparation of this paper.

FIG. 7

"HITACHI" MASS SPECTRAL DATA

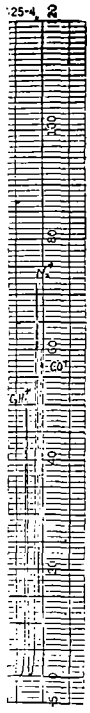

Type

RMU-6D

(Single focus mass spectrometer)

Sample

CO (Carbon monoxide) - 27,994914

$M/\Delta M$: 2500

N_2 (Nitrogene) - 28,006148

$M/\Delta M$: 1100

C_2H_4 (Ethylene) - 28,031300

FIG. 8

"HITACHI" MASS SPECTRAL DATA

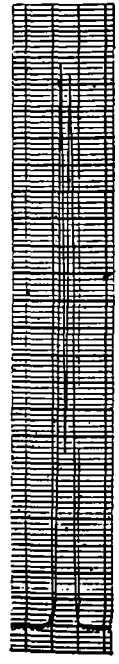

- Sample

C_5H_5N - 79,042199 (Pyridine)

$^{13}C_1C_5H_6$ - 79,050208 (Benzene)

M/ΔM : 990

Slit aperture

Main Slit : 0.008 ~ 0.004 mm

α Slit : 0.4 mm

β Slit : 0.05 mm

Collector Slit : 0.007 ~ 0.004 mm

- Secondary electron multiplier voltage

1300V (Gain : 1000 times)

- High resister of Amplifier

10^{10} Ω

- Amplifier sensitivity

$\frac{1}{3}$

- Sample amount

C_5H_5N - 1mcc (Pyridine)

C_6H_6 - 10mcc (Benzene)

Analyzer vacuum 2×10^{-6} mmHg

DESIGN CONSIDERATIONS FOR A MINIATURIZED TIME-OF-FLIGHT AEROSPACE PARTIAL PRESSURE SENSOR

J. F. Betts, G. J. O'Halloran and G. T. Wassell
The Bendix Corporation
Research Laboratories Division
Southfield, Michigan

The design problems associated with the development[1] of a small rapid response partial pressure gas sensor are discussed. The details of the method chosen to solve these problems are considered. The performance of the resulting time-of-flight gas analyzer is summarized.

(1) Part of the effort involved in conducting this program was supported by the Air Force Flight Test Center, United States Air Force, Edwards Air Force Base, California, Under Contract AF 04(611)-8171.

MASS SPECTROMETRIC ANALYSIS OF GASEOUS IMPURITIES IN REFRACTORY METALS

J. D. Reynolds

General Dynamics/Fort Worth

ABSTRACT

A method has been developed whereby a radiofrequency vacuum extraction cell coupled directly to the modified inlet of a C.E.C. 21-103C Mass Spectrometer may be utilized to observe the thermally induced evolution of gases from refractory metals.

Gaseous evolution data have been obtained as qualitative and quantitative functions of time and temperature.

Correlation of results of analyses by this technique with industrial standard methods has been achieved.

INTRODUCTION

The objective of this investigation was to develop techniques using the mass spectrometer to extract and analyze gaseous impurities in metals.

In order to perform an analysis of gases in metals, the first step is to remove the gases to determine the quantity present. These gases are then separated and identified to determine the component gases making up the evolved total. The mass spectrometer offers the unique ability to fulfill both of these analytical requirements.

Previously, mass spectrometric analysis of interstitual gases in metals has been limited to the analysis of gases first evolved and measured by various methods in separate systems and then transferred to the mass spectrometer(1). The technique described in this paper enables the quantitative and qualitative extraction and analysis of evolved gases for both static and dynamic studies to be accomplished with one apparatus integral to the mass spectrometer. The apparatus modifications involved do not impede normal operations of the mass spectrometer.

DISCUSSION

A vacuum diffusion-extraction cell was fabricated utilizing a 760 kc induction furnace as a heat source. This cell was coupled with a modified glass inlet system(2) on the Consolidated Electrodynamic Corporation 21-103C Mass Spectrometer. The extraction cell consists of a quartz furnace tube containing a molybdenum bucket suspended in an induction field. A viewing prism was installed above the furnace tube to enable temperature measurements using an optical pyrometer. The gas transfer tube leading to the modified mass spectrometer inlet also serves as a sample reservoir from which preweighed samples of refractory metals may be introduced into the sample bucket by means of a magnetic manipulator.

Gases evolved from samples heated in the molybdenum bucket are transferred into the inlet system using vacuum provided by the mass spectrometer pumping system. A cold trap in the inlet line allows freeze-out of undesirable contaminates. A three-way vacuum stopcock allows the evolved gases to be either directly introduced into the ionizing region of the mass spectrometer, by-passing the molecular leak, or expanded into a three liter volume in the inlet cabinet of the instrument. Direct introduction into the ionizing region reduces differential pumping through the molecular leak and increases instrument sensitivity. The three liter expansion volume contains a micromanometer which allows

the pressure of the expanded gas to be measured. The gases may then be introduced into the mass spectrometer through the molecular leak for analysis.

The volume of the system was determined by measuring pressure changes with the micromanometer as gas from a standard volume was expanded into the system. These data were necessary to determine the volume of interstitual gas evolved from the metal sample.

All specimens used in this program were 0.25 x 0.25 x 0.25 inch cubes sawed from the material being investigated. Sample weights varied from 0.3 to 0.5 grams.

Feasibility investigations on the new technique were accomplished using hydrogen diffusion-extraction from secondary standard titanium specimens previously analyzed with a National Research Corporation Type 917 Vacuum Hydrogen Determinator[3]. Four previously analyzed standard samples averaged 89.5 ppm hydrogen. Six samples analyzed using the mass spectrometer technique averaged 90.5 ppm hydrogen.

By increasing the output of the radio frequency generator in measured increments, total hydrogen evolution versus extraction temperature curves for two different titanium samples were obtained. Evolution of hydrogen from titanium appears to commence at 860°C and stabilizes at 1400°C.

At the optimum temperature of 1400°C, hydrogen evolution from titanium begins after 0.4 to 0.5 minutes and continues to completion in a total elapsed time of 1.5 minutes. Titanium samples were heated at 1400°C for three minutes, the evolved gas pressures measured on the micromanometer, and the gases then analyzed. All samples tested contained 99.6±0.2% hydrogen with trace amounts of nitrogen and carbon dioxide.

In analyzing samples of titanium weighing approximately 0.5 gram and containing about 100 ppm hydrogen, a pressure of 80 to 120 microns and a hydrogen peak 2500 to 3000 units high were observed. The micromanometer can accurately measure pressures in the 0.1 micron range, and peaks as low as 0.5 units are readily resolvable on the mass spectrometer. Thus, titanium samples weighing as little as 10 milligrams may be analyzed by this method.

Molybdenum samples heated to 1550°C in the diffusion-extraction cell evolved 32 ppm of a gaseous mixture composed of approximately 93% hydrogen, 7% nitrogen and a trace of carbon dioxide. Evolutions were completed in 0.7 minutes at 1550°C, the maximum temperature attainable with the 760 kc induction furnace. Lack of evolved oxygen is attributed to the apparatus' inability to attain the optimum diffusion-evolution temperature of 1800°C for molybdenum[4].

The gaseous diffusion-extraction of H-11 alloy steel at 1000°C produced a mixture of 58% hydrogen and 42% nitrogen in a series of three analyses. Hydrogen evolution begins after approximately one minute at temperature and continues for about three minutes. Total gas evolved from the sample was less than five ppm.

Optimum diffusion-extraction parameters for the previously mentioned metals are summarized below.

Metal	Temperature	Elapsed Time in Minutes Until: Evolution Starts	Elapsed Time in Minutes Until: Evolution is Complete
Titanium	1400°C	0.4 to 0.5	1.5
Molybdenum	1550°C*	0.2	0.7
H-11 alloy steel	1000°C	1.0	3.0

*Highest temperature attainable with existing apparatus. Actual optimum temperature for extraction of oxygen in molybdenum is 1800°C.

Limitations encountered stemmed from the inability of the available radio-frequency generator to reach the 1800 to 2000°C required for

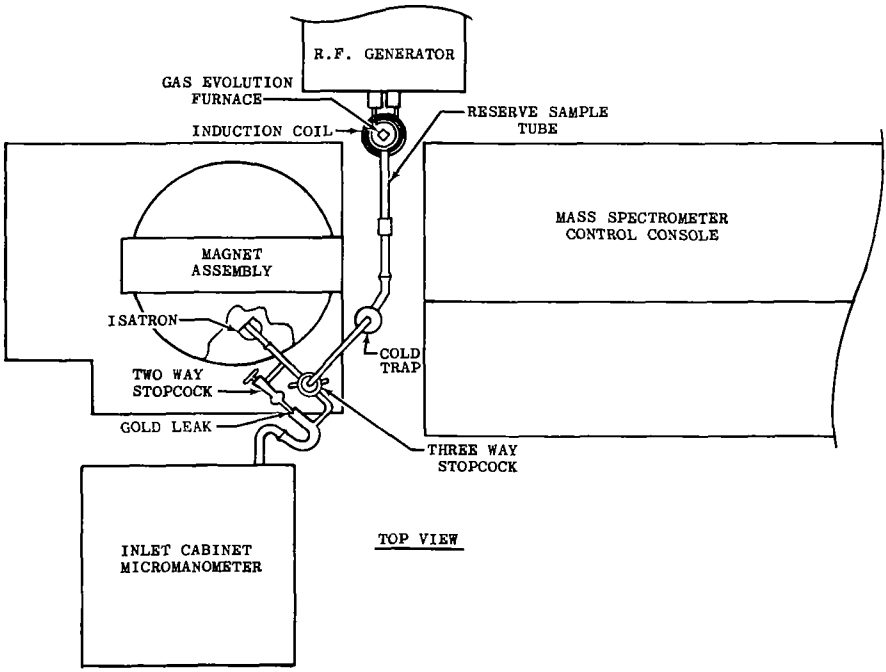

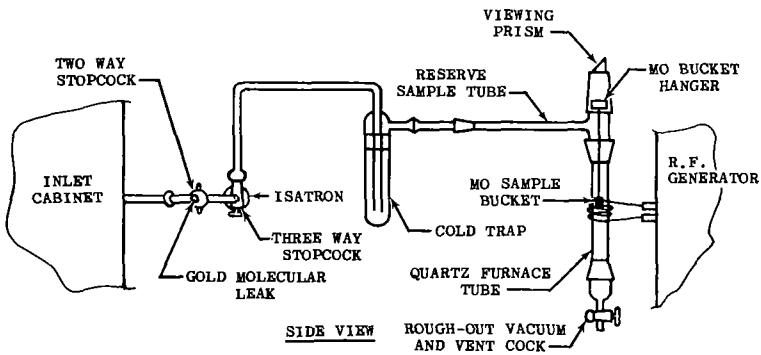

Figure 1. EXTRACTION CELL AND MODIFIED MASS SPECTROMETER INLET

optimum diffusion extraction of molybdenum, tungsten, tantalum and columbium[5]. Also certain refractory metals fail to yield all of their interstitual gases in a vacuum diffusion type extraction [6]. To fully utilize the potential of the mass spectrographic technique, a vacuum fusion type extraction apparatus[7] should be made available for alternate use with the diffusion-extraction cell.

REFERENCES

1. Manley W. Mallett, "The Determination of Interstitual Elements In The Refractory Metals," Talanta, Pergamon Press Lte., 1961, vol. 9, p. 135.

2. O. H. Hill and R. H. Johnston, "Gaseous Yields From X-Irradiated Polyethylenes," Bulletin The American Physical Society, Ser. 2, vol. 7, No. 1, Jan. 1962.

3. F. C. Benner, "Analytical Techniques for Vacuum Processed Metals and Alloys, Part IX, Analytical Techniques," Vacuum Metallurgy, R. F. Bunshas (Editor), Reinhold Publishing Corp., New York, 1958, p. 407.

4. Manley W. Mallett and C. B. Griffith, Trans American Society Of Metals, 1954, vol. 46, p 135.

5. M. W. Mallett, D. F. Kohler, R. B. Iden and B. G. Koehl, A Basic Study Of Vacuum Fusion Analysis Of Refractory Metals For Gases, Technical Report WAL TR 823/5, May 1962.

6. J. E. Fagel, R. F. Whitbeck and H. A. Smith, Analytical Chemistry, 1959, vol. 31, p 1115.

7. M. W. Mallett and W. R. Hansen, "Determination Of Gases in Molybdenum," The Metal Molybdenum, J. J. Harwood (Editor), American Society for Metals, 1958, chapter 16, p. 365.

ANALYSIS OF TRACE CONTAMINANTS IN PERMANENT GASES

by

John Roboz

Air Reduction Company, Inc.
Central Research Laboratories
Murray Hill, New Jersey

It is frequently desired to determine contaminants in permanent gases at the ppm or lower level in connection with their use in both industry and research. As a major producer of industrial gases, Air Reduction Company assures high purity standards through a rigorous product control program.

The objective of this work was to extend the concentrational sensitivity of our mass spectrometer into the ppb region for specific impurities, and to improve analytical techniques in cases where performance is limited by interferences. There are two approaches to the problem, one, to improve performance by modifying the instrument, and two, to develop pre-concentration techniques. We have been proceeding to explore both.

We have a CEC Model 21-130 mass spectrometer, a cycloidal focusing instrument with a unit resolution of about 200. Two modifications were made to improve performance. First, an additional input resistor was installed, its resistance, which is of the order of 10^{11} ohms, being ten times that of the standard resistor. Second, a one millivolt potentiometer recorder is used. The amplifier system was properly modified to accommodate these changes. Sensitivity, under these conditions, is such that a recorder width of one inch is equivalent to about one ppm for most impurities. Credit is due to Dr. Fred Gollob for most of this work.

Further modifications, such as rebuilding the vacuum system, or incorporation of an electron multiplier would be too costly and involved, considering that the final objective is to develop methods for routine use. In what follows, a few pre-concentration methods will be described by means of which various limitations could be overcome.

Perhaps the most unique is the one for the determination of certain impurities in hydrogen by, what we call the Pd-leak technique. There are no interferences between the matrix gas and the impurity peaks in the spectra, thus here the only objective was to improve sensitivity. Palladium-25% silver tubes are widely used to produce ultra-pure hydrogen. We use these tubes in a reverse manner. The hydrogen is pumped away from the sample, and the remaining impurities, highly concentrated, are analyzed. As long as there is no chemical reaction between the hot palladium and the impurity the method works perfectly and concentration factors of practically any desired magnitude can be obtained.

A schematic of the apparatus is shown in Fig. 1. The Pd-tube is a commercial model, manufactured by General Electric Company. Heating is accomplished by heater coils, embedded in a ceramic tube and using a standard variable a.c. power supply. The temperature is measured by a Chromel-Alumel thermocouple, attached to a Simplytrol type meter. Pumping speed is variable from 0 to 10^4 micronliter/sec. depending on the temperature of the tube and pressure of the hydrogen.

The whole assembly is mounted on the inlet system of the mass spectrometer so that samples can be directly expanded and no outside pumps are needed for the removal of the hydrogen.

Operation is simple. First, everything is evacuated by opening valves V1, V2 and V3. Next, V2 is closed and a known amount of sample, at 1 atm. pressure, is admitted into a known volume. The temperature is raised to 500°C, and the hydrogen is pumped away through the leak via V1 and V3. This, including slow warm-up, takes about 25 min. under our operating conditions, but can, if desired, be accomplished much faster. The sample to be analyzed is expanded into the reservoir by opening valves V2 and V5 after V1 and V3 had been closed. The pressure of the remaining hydrogen is of the order of 25 u. The final hydrogen pressure is not critical, as long as it is low enough to permit the expansion of all the remaining gases into the sample reservoir, and subsequently into the ionization chamber. This was proven by varying the pressure by as much as a full order of magnitude in both directions; it had no influence on the measured impurity content.

As mentioned already, the basic assumption of the method is that there is no interaction between the hot alloy and the impurities. We have found that oxygen-containing compounds cannot be concentrated on account of reactions on the hot surface. There is also evidence that carbon containing compounds interact with each other and hydrogen on the surface of Pd. For helium, neon, nitrogen and argon, however, no reaction of any kind was noticed and concentration could be obtained without difficulties.

Table I shows detection limits for these gases using both the regular and the Pd-leak techniques. The high sensitivity resistor can, of course, be used in either case, providing an additional factor of about eight. It is seen that the limits are extended by more than two orders of magnitude, down into the ppb range. By using larger samples, these values could, naturally, be further lowered. Presently, however, these limits are more than adequate.

The reproducibility of these measurements is conservatively estimated as ±10% of the value reported, in routine measurements. With proper instrument conditioning and special care, precision to as low as a few percent can be achieved.

These high sensitivity measurements are important not only in the analysis of samples of exceptional purity, but also in the analysis of the more-or-less ordinary high purity hydrogen, where the level of the various constituents lies in the low ppm region. An important case in point is that of the nitrogen, where one is always fighting the background, particularly after the analysis of a sample with high nitrogen content.

A second type of problem, where pre-concentration technique has been applied, is illustrated in the determination of nitrogen in carbon dioxide. Here the major problem is interference. Due to the contribution to the 28 peak by carbon dioxide, amounting to almost 10%, the 14 peak must be used to evaluate the nitrogen content. This reduces the threshold value by more than a factor of 10, and also decreases the reliability of the analysis, on account of possible pattern instability.

The solution is, obviously, to remove the carbon dioxide matrix by chemical reaction, by adsorption or by freezeout. We selected the freezeout technique. In principle it is simple, in practice, however, since one is looking for trace impurities, it took some time to establish the proper operating conditions.

Fig. 2 shows a simplified schematic of the apparatus. Neither carbon dioxide slush, nor liquid nitrogen could be used as refrigerant. The first is not cold enough, the second is too cold. Liquid oxygen, which has a boiling point of -297°F, 23 degrees higher than that of liquid nitrogen, is used to remove the carbon dioxide.

DETN. OF IMPURITIES IN H_2 (ppm/div.)				
	NORMAL DETN.		Pd - LEAK	
INPUT RESISTOR	NORMAL	HIGH SENS.	NORMAL	HIGH SENS.
He AND Ne	4	0.50	0.16	0.020
N_2 AND Ar	1	0.12	0.04	0.005

SMALLEST CHART DIVISION MEASURABLE: 3 DIV.
IONIZATION CURRENT: 80 μa

TABLE 1

DETECTION LIMITS IN CO_2 (ppm/div.)				
	REGULAR		FREEZEOUT	
INPUT RESISTOR	NORMAL	HIGH SENS.	NORMAL	HIGH SENS.
NITROGEN	32	4	0.13	0.016
ARGON	4	0.5	0.11	0.014

IONIZATION CURRENT: 80 μa
REGULAR DETN. OF N_2: BASED ON m/e 14

TABLE 2

The procedure is straightforward. The sample bottle is filled up with carbon dioxide at 1 atm pressure, the carbon dioxide is frozen out, the remaining gas expanded and analyzed. The carbon dioxide pressure in the sample reservoir after expansion is of the order of .5 micron. Its value, similarly, to the case of hydrogen, is not critical.

Detection limits are shown in Table II. It is seen that not only is the problem of CO_2 interference eliminated but also a concentration of the impurities is achieved. Argon, where there is no interference, can be used to check the concentration factor, and the values can, of course, be compared to gas chromatographic determinations. Reproducibility of these measurements was again better than 10% of the values reported, a value that can be significantly reduced if required.

Another similar problem, nitrogen in carbon monoxide, is an old one. In most cases gas chromatography is the simplest solution. When, however, only a small amount of gas is available, such as in the analysis of breakseal Pyrex flasks, and the impurity level is in the low or fractional ppm range, nitrogen can be separated and concentrated by a molecular sieve and analyzed subsequently in the mass spectrometer. While in the case of nitrogen in carbon dioxide, the matrix gas is removed and the impurity remains at low pressure, in the case of carbon monoxide the matrix gas is essentially replaced by helium, the carrier gas. Another alternative is to use CO_2 as the carrier gas and remove it subsequently by freezing.

To develop methods of this kind it is advantageous to connect a simple gas chromatograph to the mass spectrometer and to collect the individual fractions, in turn, in the inlet system. A schematic is shown in Fig. 3. The detector is mainly used for time programming and can eventually be eliminated in routine applications. Although a simple thermal conductivity cell is usually adequate, a detector which is less sensitive to gas flow, such as a β-ray detector, is better employed.

Acknowledgement: Thanks are due to Mr. Howard James for his competent technical assistance.

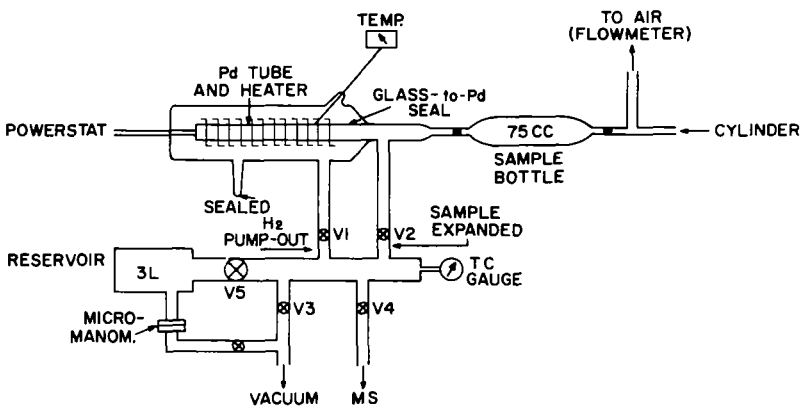

PRE-CONCENTRATION OF IMPURITIES IN HYDROGEN
(Pd-LEAK ASSEMBLY)

FIG. 1

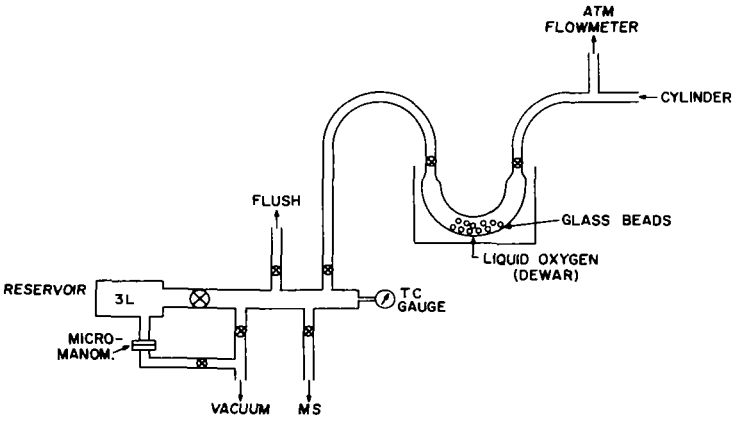

DETERMINATION OF N_2 IN CO_2
(FREEZEOUT OF CO_2)

FIG. 2

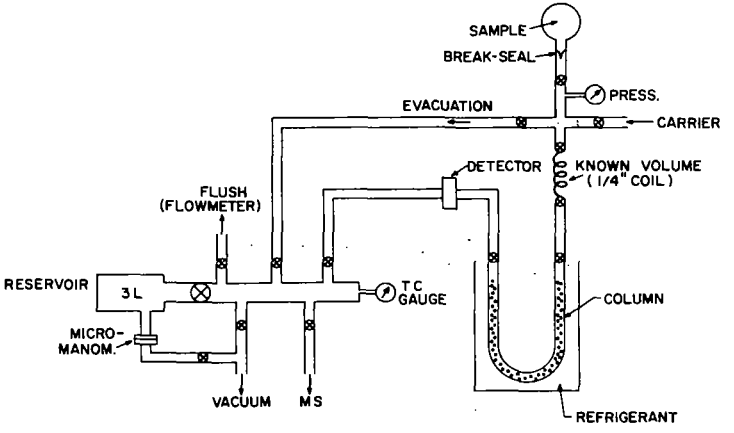

GC FRACTION COLLECTION IN MS INLET SYSTEM

FIG. 3

CHARACTERISTICS OF ION-SENSITIVE EMULSIONS FOR MASS SPECTROGRAPHY

J. M. McCrea
Applied Research Laboratory
United States Steel Corporation
Monroeville, Pennsylvania 15146

Abstract

As part of a research program in spark-source solids mass spectrometry, the photon and ion response characteristics of various types of detector plates have been determined. Outgassing behavior of the plates in high-vacuum service has also been evaluated by empirical tests in a mass-spectrometer system.

Conventional ion-sensitive plates are compared and contrasted on the basis of log-probability response curves. Various development procedures are classified by the nature of the response curves and by the extent of processing fog. Coating analyses and microstructure are related to the response properties of some emulsions. Development of an emulsion with much higher ion sensitivities than the present SWR and Q plates is forecast.

- - - - - - - -

Prologue

Monsieur le Président, Messieurs: Comme l'E-14 se réunit cette fois dans la belle province de Québec, nous considérons que l'un de nous doit prononcer quelques mots en français. Après cette introduction je continue ma communication en anglais. (Mr. Chairman, Gentlemen: This time E-14 is meeting here in the beautiful province of Quebec, and out of courtesy one of us ought to say a few words in French. After this introduction my paper continues in English.)

In an earlier paper (No. 40) at this meeting, Mr. Owens gave an excellent review of published data on plates for mass spectrography. This paper will present results of a new study which cover emulsion appearance and chemistry as well as a determination of relative ion and photon sensitivities.

Introduction

Photographic plates have been used for ion detection since the early days of mass spectrometry, and low-gelatin Q plates of Ilford Ltd. for this application have been commercially available since the mid 1930's. Various studies of the relationships between ion exposures and the resultant blackening of the developed image have been reported for one or other of the ion-sensitive plate types. Most recently, Owens has studied Ilford Q2 plates in detail (1). On the other hand, Rudloff has presented coordinated data for five types of low-gelatin plate (2). Although ion sensitivity is a highly important property of these plates, plate uniformity, outgassing characteristics, processing methods, and photon sensitivity all have an important bearing on the speed and precision with which quantitative analytical data can be obtained. As a natural sequel to earlier work on emulsion uniformity (3), plate types and handling techniques have been investigated with the aim of decreasing the time required for mass-spectrographic determination of trace-level impurities.

Composition and Appearance

Uniform regions of unprocessed 2- by 15-inch plates were used for the coating examinations. The weight of coating and silver per unit area of plate were determined by the simple expedient of measuring the weight loss of plate sections when the emulsion was removed by sulfuric acid digestion; the silver in the resulting solution was then determined by a dithizone colorimetric method. The appearance of the emulsion surface was recorded in X500 photomicrographs with transmitted light, Figure 1. Grain size, clustering, and porosity were estimated from measurements on the photomicrographs, Table I. The Type Q2 plates, emulsion numbers S4219 (control), S4219B (double coating weight), and S4358 (improved emulsion), were supplied for test purposes through the courtesy of Ilford Inc., New York. Specially cropped Q plates have normally been used for ion detectors in this Laboratory to avoid incidence of edge irregularities in normal production (3). The author has been advised that all Q2 plates of 2- by 15-inch size with the improved emulsion will be cut to eliminate edge irregularities (4).

The extent of porosity and grain clustering observed in Q2 and Q3 plates is the most unexpected and striking result of the coating study. Vanishing light transmission in processed plates simply cannot be attained with porous plates; thus porosity

TABLE I - COATING PROPERTIES OF ION SENSITIVE PLATES

Type and Emulsion No.	Special Properties	Coating, mg/cm^2 Total	Coating, mg/cm^2 Silver	Ratio, Silver/Total	Calculated Thickness, μ	Apparent Microstructure: Grains: Average Size, μ	Grains: Length/Width	Grains: Clustering	Pores: Average Size, μ	Pores: % Area Occupied
Q1 S4185		0.78	0.25	0.32	3.5	0.5	2	Slight	1	2.2
Q2 S4143	Specially cropped	0.55	0.22	0.40	2.0	0.8	1	Moderate	3	5.0
S4158		0.57	0.21	0.37	2.3	0.8	1	Moderate	3	4.6
S4173		0.62	0.22	0.36	2.6	0.8	1	Moderate	3	4.5
S4219	Control for S4219B	0.58	0.21	0.36	2.4	0.8	1	Limited	2	3.0
S4358	Improved product	0.53	0.19	0.36	2.2	0.8	1	Almost none	1	1.5
Q2 S4219B	Double coating weight	0.96	0.30	0.31	4.5	Not clearly seen			2	2.0
Q3 S4152	Specially cropped	0.88	0.26	0.30	4.3	1.0	1	Great	4	10
S4255	Specially cropped	1.04	0.29	0.28	5.2	1.0	1	Great	4	9
SWR SP0450	2 x 15" special size	2.61	0.12	0.046	19.4	0.5	3	None	No porosity	

TABLE II - ESSENTIAL FEATURES OF ARBITRARY PUMPING SCHEDULE

Time (min)	Operation or Requirements
-10	Ionization gauge reading $\leq 4 \times 10^{-7}$ torr with magnetic sector open to electric sector
-6	Isolate electric sector from magnetic sector
-5	Load plate holder, then identify plate by light marking
-1	Isolate and bypass magnetic-sector diffusion pump
-0.5	Admit air to magnetic sector, insert plate holder as soon as door can be opened, close door
0.0	Start evacuating magnetic sector by mechanical pump
2.5	Close bypass and cut in diffusion pump
3.5	Open sector isolation valve for 10 seconds to evacuate valve region
10.0	Open sector isolation valve; read ionization gauge, initially at 0.5 minute intervals, and thereafter at progressively longer intervals of 1, 2, 3, 5, and 10 minutes until at least 1 hour of pumping time has elapsed

is directly related to response data. Product improvement in the Q2 plate has been accompanied by reduction of porosity and clustering. Among other Q coating properties, the relatively constant proportion of silver is worthy of note. The coatings are distinctly thinner on the Q2 plates than on the Q1 and Q3 plates and are of different thicknesses on the two lots of Q3 plates.

The variation in coating thickness among Q plates is minor compared to the difference between them and the SWR plates. The coating is about five times heavier on the SWR plates than on Q2 plates, but the associated silver is less than half that on Q plates. Although a few isolated pores were noted, there is no general porosity in SWR plates. Because the silver on a wet processed SWR plate can be wiped off and leave a clear gelatin layer, the silver is effectively on the gelatin rather than in it. The SWR emulsion swells visibly when wetted with cold water and is readily dissolved and washed from the glass support by hot water. In contrast, Q emulsions do not swell visibly when wetted, are difficult to remove from the glass, and must be fully removed to complete removal of silver from an exposed region on a processed plate.

Outgassing in Vacuum

Outgassing properties were determined in the mass spectrometer of commercial design also used for the ion exposure work, a Consolidated Type 21-110 instrument with tandem electric and magnetic sectors arranged in the Mattauch-Herzog geometry (5). The essential features of the arbitrary pumping schedule used for these tests are given in Table II. Relative humidity, controlled below 50 percent by air conditioning, was spot-checked at the time of pumping experiments and appeared to have little influence on the results, although water absorption in gelatin varies considerably with relative humidity (6). Outgassing-test results for SWR and Q plates immediately reflected their differences in coating thickness and swellability; Figure 2 shows that the SWR plate outgasses extensively for much longer than Q plates that are specifically recommended for mass spectrometer service. Electron microscope plates (Kodak Projector Slide and Ilford Type N60) and direct electron recording film (Kodak Type 039-01) were also found to be slow in pumping. The curve for the Projector Slide Plate in Figure 2 was estimated from data for smaller areas in Figure 3.

The differences in pumping time for Q plates are also shown in Figures 2 and 3. The data for plate sections (Figure 3) suggest that, for a given emulsion number and thickness, pressures in the 0.7 to 4.0 x 10^{-6} torr range after 40 to 80 minutes of pumping are proportional to the area of emulsion pumped in the system. The pressures attained with the Q2 plates were in the approximate ratio of the amount of coating, whereas the pressures attained with the fine-grained Q1 and coarse-grained Q3 emulsions (Figure 2) were respectively lower and higher than would have been predicted by application of a proportionality rule. Thus pressure in a specified mass spectrometer system during pump-down of a Q plate is determined primarily by amount of emulsion, but is also affected by grain size and possibly, in thick emulsions, by diffusion limitations.

Response Data

The response data for processed plates can be divided into two parts, one dealing with maximum and minimum image transmissions obtainable regardless of exposure level, and the other relating intermediate transmissions to actual exposure levels. Plate-processing techniques affect both parts, but background fog (the maximum transmission obtainable in the absence of exposure) is dependent solely on emulsion characteristics, plate storage, and processing. Ion-sensitive emulsions are susceptible to high and nonuniform fog, and developing procedures should not accentuate these problems. Fog levels were examined systematically because Guthrie, who visited the Ilford plant, emphasized that fogging tendency was an important property of ion-sensitive plates (7). The author has adopted the practice of clearing a small end region on test plates with fixer just before processing. The cleared region serves as a transmission reference for the emulsion during photometry, and eliminates the effect of thickness and color variation in the glasses used for different plates from the study of emulsion properties.

Controlled light and 17-kv ion exposures for determination of response were applied to plates in the special illuminator and in the mass spectrometer mentioned earlier (3,5). Ilford Q plates were processed in a vertical-design processor, but for satisfactory processing the Kodak SWR plates were slightly shortened and handled in a commercial rocking-tray processor (Applied Research Laboratories, Inc.) (8). Conservative variations in processing conditions were tested on plates with essentially the same exposure history. Light transmission of the images on processed plates was measured with a Jarrell Ash microphotometer.

Transmission data for saturation photon exposure and for unexposed background were obtained from the microphotometer as percentages of the light transmitted through

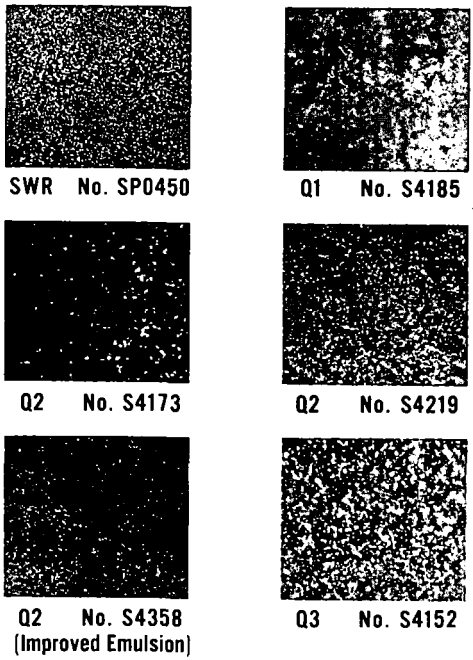

FIGURE 1
Photomicrographs of 100-X 110-Micron Areas
of Plate Surfaces, Transmitted Light

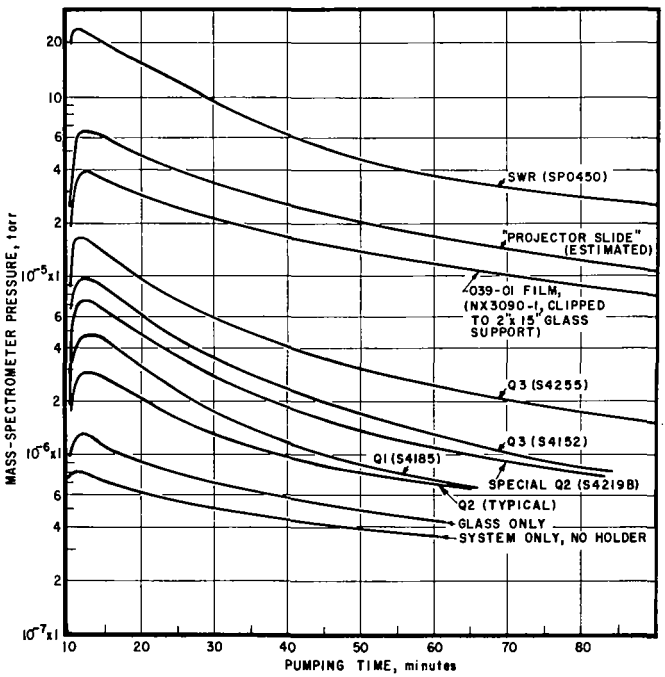

PRESSURE VERSUS PUMPING TIME FOR 2 BY 15-IN. PLATES
Fig. 2

the cleared region of each plate. For intermediate exposures, microphotometer readings were converted linearly to a relative transmission scale by assigning the values of 0 and 1, respectively, to saturation and background exposure levels. Relative transmission defined in this way is the same as the function T' used by Hull if the 100% level on the microphotometer is set at background (9). Response curves were obtained by plotting relative transmission and exposure on logarithmic probability paper. The probability-scale ruling is equivalent to a linearizing transformation based on the cumulative normal distribution function, and permits presentation of both photon and ion response data in linear or nearly linear form (10,11). Because the sensitivity of plates at low exposure is the primary factor governing the minimum concentration detected in analysis, the exposures required to produce a 95% relative transmission were obtained for tabulation from the response curves. These exposures are expressed in arbitrary units of seconds of light or picocoulombs of ion.

The term contrast generally denotes the steepness of a photographic response curve, and the term gamma (γ) used for contrast is measured quantitatively as the slope of the straight portion of a plot of optical density against logarithm of exposure (12). Because the slope of a nearly linear plot is far more meaningful than the slope of a limited straight section of a pronounced sigmoid curve, gamma was abandoned in favor of a new contrast measure G derived from the slope of the logarithmic probability plots, Figure 4. The units of G are transmission transform units per logarithmic unit of exposure. The transform unit is in a form numerically consistent with the Baker-Sampson-Seidel Δ of emission spectroscopy at a relative transmission of 0.5 (11).

Background and response data for seven types of plate are summarized in Table III.

TABLE III - RESPONSE CHARACTERISTICS OF ION-SENSITIVE PLATES

Emulsion Type	Emulsion Numbers	Emulsion Transmission % (Absolute): Typical Background	Emulsion Transmission % (Absolute): Saturation Photon Exposure	Exposure for 95% Relative Transmission: Seconds With Photons	Exposure for 95% Relative Transmission: Pico-coulombs of Ions	Exposure for 95% Relative Transmission: Ion Type Used	Contrast (G): Photons	Contrast (G): Ions
Q1	S4185	96	1.3	3.2	0.14	Pt^+	1.72	1.18
Q2	S4143 S4173 S4158 S4219	84	1.8	0.14	0.019	Pt^+	1.17	0.98
Q2	S4358	90	0.2	0.21	0.010	Fe^+	1.50	1.33
Q2	S4219B	83	1.7	0.18	0.12	Pt^+	1.18	0.67
Q3	S4152	89	9.5	0.053	0.0048 0.018	Fe^+ Pt^+	0.87	0.76 0.69
Q3	S4255	91	5.0	0.041	0.037	Fe^+	0.87	0.71*
SWR	SP0450	90	2.7	5.2	0.016	Pt^+	2.6	1.10
Slide	BER2D3 BER1H3	99.2	0.5	3.4	5100	Fe^+	3.6	2.04

Processing: All Q plates 2.5 min in ID19 at 25 C in vertical design processor. SWR plates 4.0 min in ID19 (1:1) at 20 C in rocking-tray processor. Projector slide plates 4.0 min in D11 at ambient temp in static bath, intermittent hand agitation.

Storage at ambient temp: <4 days except one Q1 plate stored 10 days.

* Plate characteristics abnormal, pseudo-saturation at 55% transmission and intermediate exposures.

- - - - - - - - - - - - - - - - - -

(No data are entered for the N60 plates, which were outdated, or for the direct electron recording film, 039-01, which has essentially no sensitivity to photons or ions under the test conditions.) The background in projector slide plates is most satisfactory, but these plates have such a small sensitivity for ions that they are useless as routine ion detectors. Their gelatin overcoat, readily penetrated by electrons in an electron microscope, effectively screens the emulsion from bombardment by positive ions. Among the Q plates, the slow Q1 plate has the best background and the early Q2 plates the worst. The improved Q2 plate and the Q3 plates have intermediate backgrounds. The background densities for Q plates reported by Rudloff (2) agree well with the transmission levels for Q1, early Q2, and Q3 plates given in Table III. In both studies, Ilford ID19 developer was used, but the processing times and temperatures differed.

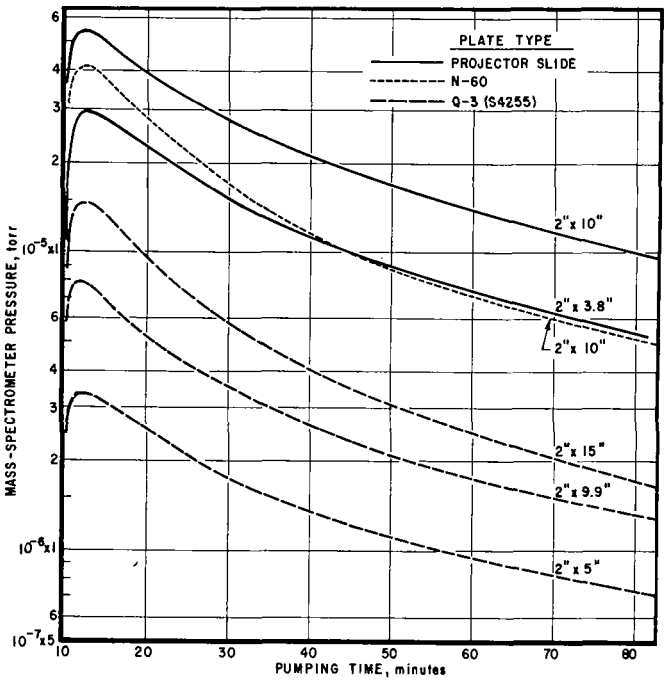

PRESSURE VERSUS PUMPING TIME FOR PLATES OF DIFFERENT AREAS

Fig. 3

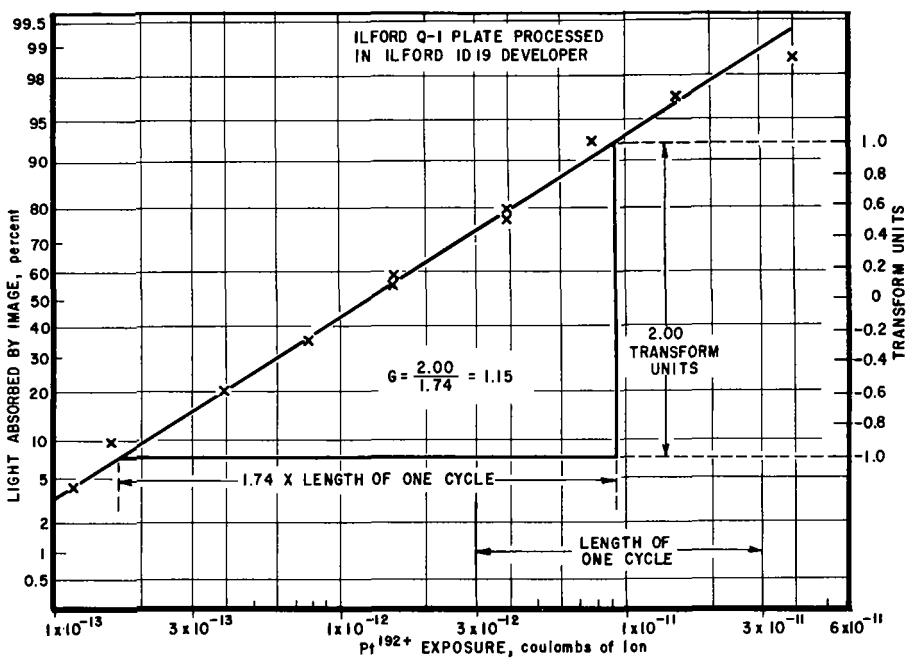

G AND LOG-PROBABILITY PRESENTATION OF ION RESPONSE

Fig. 4

Uniformity of the background was not studied extensively, but the author confirms Guthrie's finding that the background of the improved Q2 plate is more uniform as well as more light transmitting than that of the early Q2 plates (13). The background of the SWR plate is generally heavy and nonuniform, and considerable experimentation with processing conditions was required before results as satisfactory as those shown in Table III were obtained. Subsequently the manufacturer has recommended gelatin overcoating of exposed SWR emulsions prior to processing for improving background and for reducing abrasion marks (14). The overcoating technique was not used in the work reported here.

The performance of improved Q2 plates at saturation exposures is better than that of earlier Q2 plates, and very substantially better than that of Q3 plates. The microporosity given in Table I correlates roughly with light transmission at saturation, and the improvement in the Q2 plate is almost certainly a result of reduced microporosity.

The ion or photon exposure necessary to effect a small reduction in transmission on the exposed region of a processed plate is not very different for the Q2 and Q3 plates, although the Q3 is the more sensitive of the two. The Q1 plate is not nearly as sensitive as the other Q plates. The relationship among the 17-kv ion exposures required for an image of 95% light transmission is similar to that found by Rudloff with 9-kv ions at an optical density of 0.1 above background for Q1, Q2, and Q3, and SWR emulsions (2). The double-coating-weight Q2 product proved to be unsatisfactory because it was less sensitive to ions than normal Q2 plates.

The contrast G of Q3 and normally coated Q2 plates for ions is about 80 to 90% of that for photons. The greater contrast of the improved Q2 plates (S4358) compared with that of lower Q2 emulsion numbers is advantageous for quantitative analysis. Similar improvement of contrast in Q3 plates is needed. The SWR plate is again different from the Q plates; its contrast for ions is less than 50% of its contrast for photons.

A Possible High Sensitivity Plate

A comparison of SWR and Q plates leads readily to speculation about a hypothetical high-sensitivity plate with the best characteristics of each type. The grain sizes of SWR and Q1 are about the same, but the SWR is slower to photons than Q1. But the front-surface, low-silver coating of the SWR plate has a sensitivity for ions of the order of that of the Q2 coating. In terms of silver used, the SWR plate is more ion-sensitive than either Q2 or Q3. A front-surface coating with coarser grains and more silver should be yet more sensitive. Because there is roughly a factor of 10 difference in ion sensitivity between Q1 and Q2 plates, a plate with an ion sensitivity 10 times greater than that of present products is a reasonable expectation. With the same relationship between ion and photon sensitivity as the SWR plate, the ultrasensitive plate would require no more darkroom precautions than the present Q2 and Q3 plates. Availability of a highly ion-sensitive plate as a result of photographic research would be most welcome to investigators in mass spectrometry.

Processing Conditions

Background and photon response data obtained with various development conditions are given in Table IV. Among ID19, ID13, Ilford caustic hydroquinone developer (a developer similar to ID13 but made up by the user from prepackaged chemicals), and D19, the ID19 developer is most satisfactory and D19 is the least. ID19, ID13, and the caustic hydroquinone developer all have similar developing action in the background region, but D19 tends to reduce light transmission of the background. These observations are in accord with Guthrie's conclusion that ID13 is a more suitable developer for Q plates than D19 (13). The author prefers ID19 to ID13 or caustic hydroquinone because the last two tend to leave yellow stain marks on plates if washing is not fast and thorough. Of the three, ID19 has the best storage properties, is least corrosive, and gives plates with least deviation from logarithmic-probability plot linearity.

Development with ID19 is not very sensitive to developer dilution or temperature. A compromise must be made between excessive development of background and sensitivity of development for extremely weak exposures. Although extensive trials might yield better processing conditions, the choice of 25 C and 2.5 minutes in normal-strength ID19 gives reasonably satisfactory plates.

Plate Aging

Refrigerated storage of ion-sensitive plates before use is essential if satisfactory background transmission is to be obtained, Table V. Long storage at ambient temperatures virtually ruins plate quality, but storage of one or two days at ambient temperature is permissible. There may be an optimum storage period for which the sensitivity to small exposure is greatest. A systematic investigation of the effects of

ambient-temperature storage is planned for future shipments of plates received for routine analytical use.

TABLE IV - PHOTON RESPONSE AND PROCESSING FACTORS

Emulsion Type	Emulsion Number	Developing Time, min	Developing Developer Type	Developing Temp, C	Absolute % Transmission Typical Back-ground	Absolute % Transmission Saturation Photon Exposure	Photon Response Seconds for 95% Relative Transmission	Photon Response Contrast (G)
Q2	S4143	2.5	ID19	25	83	2.1	0.15	1.12
		3.0	ID19	20	87	3.1	0.14	1.05
		2.5	ID19 (1:1)	25	89	3.0	0.24	1.12
		3.0	ID19 (1:1)	20	88	3.0	0.19	1.16
		2.5	ID13	25	84	3.3	0.22	1.22
		2.5	D19	25	77	2.0	0.18	1.19
		3.0	D19	20	88	2.2	0.26	1.26
		2.5	D19 (1:1)	25	83	2.9	0.17	1.12
		2.5	Caustic	25	not measured		0.18	0.99
Q3	S4255	2.5	ID19	25	91	5.0	0.041	0.87
		3.0	ID19	20	96	6.9	0.088	1.03*
		2.5	ID19 (1:1)	25	95	5.9	0.070	0.90
		3.0	ID19 (1:1)	20	96	7.6	0.118	1.05
		2.5	ID13	25	91	5.3	0.088	0.87*
		2.5	D19	25	92	4.3	0.062	0.92*
		3.0	D19	20	92	5.2	0.066	0.92*
		2.5	D19 (1:1)	25	92	6.3	0.070	1.09

* Low-exposure end of log-probability plot is curved.

TABLE V - AGING OF ION-SENSITIVE PLATES

Emulsion Type	Emulsion Number	Ambient (72-77 F) Storage Days	Absolute % Transmission Typical Back-ground	Absolute % Transmission Saturation Photon Exposure	Photon Response Seconds for 95% Relative Transmission	Photon Response Contrast (G)	Developing Time, min	Developing Developer Type	Developing Temp, C
Q1	S4158	0	96	0.6	3.5	1.7	2.5	ID19	25
		89	56	0.6	1.2	2.5	2.5	ID19	25
Q2	S4143	0	87	3.1	0.14	1.05	3.0	ID19	20
		7	84	2.5	0.24	1.20	3.0	ID19	20
Q2	S4143	0	87	3.0	0.24	1.12	2.5	ID19 (1:1)	25
		7	84	2.0	0.21	1.23	2.5	ID19 (1:1)	25
Q2	S4143	0	88	3.0	0.19	1.16	3.0	ID19 (1:1)	20
		29	69	3.2	0.15	1.18	3.0	ID19 (1:1)	20
Q3	S4255	0	95	5.9	0.070	0.90	2.5	ID19 (1:1)	25
	S4183	34	82	6.8	0.048	0.87	2.5	ID19 (1:1)	25
	S4255	72	43	6.4	0.053	1.18	2.5	ID19 (1:1)	25

- - - - - - - - -

Ion Energy Effects

Lines for the multiply charged ions in Table VI show the effect of ion charge or energy on response of the Q1 plate.

TABLE VI - CHARGE DEPENDENCE OF ION RESPONSE FOR Q1 PLATES

Type of Exposure	Image Transmittance at Saturation, %	Exposure for 95% Relative Transmission*	Contrast (G)
Pt^{+}	51	0.14	1.18
Pt^{+2}	46	0.25	1.20
Pt^{+3}	39	1.0	1.04
Pt^{+4}	32	-	-
Pt^{+5}	26	-	-
Photon	2.0	3.0 sec	1.75

* Unit for ions is picocoulombs of an isotopic species of Pt summed for all charges.

As ion charge is increased, the transmission at saturation exposure tends towards the value for photons. The contrast G is not greatly influenced by charge level. These results and those of Lichtblau are consistent with his hypothesis that the ions are not fully penetrating the emulsion (15). Studies of Q1 plate response are thus primarily related to ion range in gelatin-silver emulsion. The results obtained are of little value for analytical application because the Q1 plate is simply too slow and too variable for analytical work.

Summary of Desired Characteristics

Because coating properties are relatively easy to measure and prove to correlate strikingly with some aspects of the response data, there can be little excuse for neglecting them in future response studies. Before the improved Q2 plate was introduced, the slightly higher outgassing and lower contrast of Q3 plates was not a great sacrifice for the investigator interested in high sensitivity. The low microporosity and high contrast of the improved Q2 plate are an almost compelling reason for selecting this plate unless the Q3 plate is similarly improved. Still in the future are plates more than ten times as sensitive as the Q2 or Q3 plate; such a development is forecast from the properties of the present Q and SWR plates, and would certainly be most appreciated for trace-level analytical work. An idealized ion-sensitive plate would have the following properties, which are listed in order of decreasing importance for trace-level quantitative or semiquantitative analysis:

- High sensitivity for ions.
- Fine grain for good resolution.
- Plates available in two contrast classes - moderate for wide concentration ranges and high for precision in a limited range.
- Low long-term outgassing in high vacuum.
- Uniformity - plate, batch, and product.
- Low fog level.
- Saturation optical density - high - same for ions and photons.
- Response curves - similar shape for ions and photons - linear-plotting transformation known - reciprocity behavior known.
- Relatively low photon sensitivity for easy processing.

The investigator of mass defects would revise this list to fit his prime requirement of high resolution.

In practice, compromises must be made between grain size and fog level to achieve the utmost sensitivity desired for trace-level analysis. Active investigation by plate users and cooperation of users in development work by the photographic industry will lead to improvement in ion-sensitive plates and consequently in quality and quantity of results emanating from spark-source mass spectrometers.

Acknowledgments

The author thanks Mr. J. A. Zimmer, Ilford Inc., New York, and Mr. W. T. Swanton, Eastman Kodak Co., Rochester, for arranging to supply samples of the experimental products tested as a part of this research. He acknowledges assistance of his associates at the U. S. Steel Research Center with the chemical analysis and micrographic studies, and the inspiration derived from frequent discussions of photographic products and emulsion making with Dr. C. F. Glick.

Literature Cited

(1) E. B. Owens, Applied Spectroscopy, 16, 148 (1962).
(2) W. Rudloff, Z. Naturforschung, 16a, 1263 (1961), 17a, 414 (1962).
(3) J. M. McCrea, 11th Annual Conference on Mass Spectrometry and Related Topics, San Francisco, May 19-24, 1963, Paper No. 105.
(4) J. A. Zimmer, Ilford Inc., New York, private communication.
(5) Bulletin 21110, Analytical and Control Division, Consolidated Electrodynamics Corporation, Pasadena (July 1960).
(6) C. E. K. Mees, The Theory of the Photographic Process, The MacMillan Co., New York (1944), p. 78.
(7) J. B. Guthrie, Sandia Corporation, Albuquerque, private communication.
(8) J. M. McCrea, Applied Spectroscopy (in press).
(9) C. W. Hull, 10th Annual Conference on Mass Spectrometry and Related Topics, New Orleans, June 3-8, 1962, Paper No. 72.
(10) J. M. McCrea (submitted to Spectrochimica Acta).
(11) J. M. McCrea, in Advances in Spectroscopy (to be published by Plenum Press).
(12) C. E. K. Mees, op. cit., p. 204, 408, 700.
(13) J. B. Guthrie, Technical Memorandum SC-TM 64-534, Sandia Laboratory, Albuquerque (1964).
(14) Tech Bits, 1964, No. 1, Eastman Kodak Co., Rochester.
(15) H. Lichtblau, Physik. Z., 41, 82 (1940).

A COMPUTER PROGRAM FOR THE QUANTITATIVE INTERPRETATION OF MASS SPECTROGRAPH PLATES

Philip R. Kennicott
General Electric Research Laboratory
Schenectady, New York

There are two methods for the quantitative interpretation of photographic plates produced by the mass spectrograph, a visual method in which densities are compared visually and impurity concentrations calculated from relative exposures, and the photometric method in which the plate is measured with a microdensitometer and the resulting data processed in order to obtain impurity concentrations.

This paper is not intended to argue in favor of one method over the other. I feel they both have their application. However, if the photometric method is to be used, the principles of Information Theory would dictate that all the information available on the plate should be included in the data processing. The proper utilization of all this information requires a large amount of routine computation. The labor is so great that, in fact, all the information is seldom, if ever, used. This routine computation can in principle be done best on a digital computer.

It is the purpose of this paper to describe a preliminary experiment using a digital computer in processing data for a mass spectrograph plate. Two things have become evident from this experiment. First, where the photometric method is to be used, the computer does offer real advantages. And second, this is only an initial experiment; much more work needs to be done. I hope in presenting this paper to interest others in the application of computers to the data processing of mass spectrographic plates.

The primary problem is to obtain the photoplate characteristic curve. Of the available methods, the Churchill[1] method, applied to mass spectrographic plates by Duke[2] and by Owens,[3] was chosen for the computer program. It was chosen because it seemed to offer the best compromise between the efficient use of the information on the plate and ease of programming. The method of Judson and Hull, in which the data is fit to an empirical curve, would have been easier to program, but it tends to force the data into a predetermined formula. I can see no point in postulating an empirical formula if not necessary, so I wished to avoid this method. The method of Mattauch and Ewald[4] uses an element with several isotopes covering a wide range of abundances to construct the characteristic curve. In principle it uses the available information more efficiently, but it would be much more difficult to program.

In implementing the Churchill method a preliminary curve is constructed which relates the optical densities of two isotopes of known relative abundance to each other at different exposures. The density of one isotope is plotted versus the density of the other isotope at the same exposure. This preliminary curve is related to the derivitive of the photoplate characteristic curve which we are trying to determine. It is nearly linear with most photoplates. It was found that it could be easily approximated by a second degree polynomial for purposes of computation.

The photoplate characteristic curve is constructed from the preliminary curve. This construction, which is done graphically in the Churchill method, is mathematically equivalent to the solution of the first order differential equation. Counting the constant of integration introduced in this solution, there are three parameters used to describe the characteristic curve. That is, two parameters describing the second order polynomial approximating the preliminary curve, and the constant of integration which is conveniently expressed as a relative sensitivity for the photoplate.

After reading the input data, the program computes and prints out the photoplate parameters - A1 and A2. A1 is the linear term in the preliminary curve divided by the ratio of the isotopic abundances. If it is equal to 1, the characteristic curve is a straight line. If it is not equal to 1, the characteristic curve has some curvature. A2 is a measure of the variation of curvature. If A2 is zero, the curvature is constant, and if A2 is not zero, the curvature varies along the photoplate characteristic curve. Typical values are A1 = 0.9 - 1.3, A2 = 10^{-3} - 10^{-4}.

These constants, A1 and A2, are next used to construct the characteristic curve. This construction in the computer program is mathematically identical to the graphical method. An arbitrary value of density and exposure is chosen for the starting point. The manner in which this point is put on an absolute basis is described below. From any point on the curve another point is found with the exposure reduced by the ratio of isotopic abundances, and with the density calculated from the preliminary curve. This procedure is repeated from point to point until the entire curve has been constructed. In the event that the user does not wish to use the Churchill method for constructing the curve, another curve can be read in as input data.

Following the construction of the characteristic curve and the printing out of the values in the curve, data are read in for the various lines one wishes to process. These data are corrected for the characteristic curve, for any background which may be present in the line, for isotopic abundance, and for relative exposure. The background correction is made by computing the total number of ions contributing to the line, and then subtracting the number of ions equivalent to the background density. As each datum is considered, an apparent total exposure is printed out in the output. After all the data for one element have been considered, the geometrical mean is taken of these data. Each datum is weighted according to its isotopic abundance. The geometrical mean is divided by the plate sensitivity factor described below in order to place the data on an absolute basis, and the resulting number printed out is the concentration of the impurity.

In order to place the characteristic curve on an absolute basis, an element from the matrix whose concentration is known is processed first. Its apparent total exposure is taken as the plate sensitivity factor (the "integration constant" mentioned above). Each subsequent total exposure is divided by this number.

The program was written about six months ago and has been working satisfactorily in our laboratory since then. It is written in the FORTRAN language, and it should be quite easy to compile it on any digital computer accepting this language. I have made an attempt to avoid special features peculiar to my own machine in an

effort to make it easier for others to use the program if they wish to do so.

We have found three advantages to using the computer for our mass spectrographic data processing. First, it saves time. A job which would have taken 4 or 5 hours by hand can be done in about 1 minute on the General Electric 225 computer which is a moderate speed computer, somewhat slower than the IBM 704. Secondly, accuracy of the data is increased. This is for two reasons. First of all, more information can be used resulting in a statistical improvement, and secondly, the chance for human error in using this information is less. Finally, a numerical characterization of each plate is available. This is useful in studying different emulsions or developing techniques. For example, we can see quite clearly the difference between the Ilford Q2 emulsion and the Kodak SWR emulsion.

The program does have its limitations. One of these is the fact that the Churchill method considers only information from a single element in constructing the characteristic curve. Another limitation is in the manner in which the density data from the densitometer must be integrated before being corrected for the characteristic curve. In principle one should correct this data point by point along the density curve obtained from the densitometer, subtract equivalent background exposure at each point, and finally accumulate the sum of the resulting data in order to obtain the integrated exposure from a single line. Work is currently in progress on a program which will correct these limitations. It will use a combination of the Churchill and the Mattauch-Ewald methods to obtain the characteristic curve and will have provision for considering the densitometer data point by point.

In summary, in an effort to utilize the information available on a mass spectrograph plate more efficiently, a program has been written to process this information on a digital computer using the Churchill method to construct the photographic plate characteristic curve. The program has been found to operate satisfactorily within its limitations. The computer processing of mass spectrographic data is only beginning, but it is apparent that there is a real advantage to using a computer for this type of data processing.

REFERENCES

1. Churchill, J.R., Ind. Eng. Chem., Anal. Ed. 16, 653 (1944)

2. Duke, J.F., Ultrapurification of Semiconductor Materials, M.S. Brooks, J.K. Kennedy, eds., p. 294 Macmillan, New York 1962.

3. E.B. Owens and N.A. Giardino, Anal. Chem. 35, 1172 (1963).

4. Mattauch, J.; Ewald, H.; Naturwissenschaften 31, 487 (1943).

PLATE READER FOR MASS SPECTROGRAPH*

George D. Perkins

Bell & Howell Research Center
Pasadena, California

Abstract

The output of a mass spectrograph is a photographic plate containing a large number of spectral lines. The two most important items of interest in each line are its position and opacity. From this information, an analysis of the sample can be made. An optical and mechanical system has been fabricated which will measure line position to 1/10,000 of an inch and relative light transmission to 0.1%. It is primarily intended to acquire line position and opacity data rapidly and easily, and thereby shorten the time of analysis of solid samples. Its accuracy has been tested on a few sample runs with satisfactory results being obtained.

Introduction

The output of a mass spectrograph is a photographic plate containing a large number of lines. A typical single high density exposure contains several hundred lines. Each one of these lines defines uniquely, by its position on the plate, the mass-to-charge ratio of the ions producing the line. The line density is a measure of the number of ions producing it and is thus a measure of the abundance of this ionic species in the sample being sparked. Sample analysis from the photoplate is therefore a fourfold problem: (1) measure accurately the position each ionic species occupies in the resolved spectrum; (2) measure the blackening of the photographic plate by each ionic species; (3) identify the ionic species; and (4) from this information, compute the analysis of the sample.

General Description

An instrument has been fabricated which will enable the operator to perform quickly and easily the measurements required in the first two items. It will measure the position of any line along a 15-inch plate with resolving power of one ten-thousandth of an inch and absolute accuracy of 10^{-4} inches in any 10-inch range. It will also measure the relative light transmission through a small selected area of the photographic plate to an accuracy of one-tenth of one percent. It is a single assembly approximately six feet long, three feet wide, and four feet high.

Four different types of information are displayed continuously on the main data panel: a projected and magnified image of a section of the photographic plate; a position measurement in digital form; digital presentation of percentage light transmission; and a line graph of the light transmission through a small area of the plate.

The projected image is visible on a ground glass screen 13" square and, as a zoom lens is used in the optical train, a magnification range from 11.5X to 55X is available. At minimum magnification three-quarters of the usable photographic plate width is visible on the screen. Manipulation of the plate carrier controls will place the image of any portion of a 2" x 15" photoplate at the center of the screen. A second projection system with a fixed magnification of 15 diameters is included for comparison of two plates. It is controlled by a push-pull knob. Pulling on this knob blanks out the upper half of the image from the primary plate and turns on the projection lamp for the secondary system. The second image then appears on the upper half of the screen.

The position measurement system is based on electronic counting of moire' fringes with each count representing a distance of 0.0001 inches. Automatic direction

* This work was supported in whole or in part by the United States Air Force under Contract AF 33(657)-8174, monitored by the Materials Central, Wright-Patterson Air Force Base, Ohio, and described in Technical Documentary Report No. RTD-TDR-63-4128.

sensing is included so the final reading is the number of 10^{-4} inch increments that lie between the reference position and the measured position. An accuracy of 1 in 10^5 is maintained at all plate transport speeds up to 10 inches per second in either direction.

Light transmission is measured by optically imaging a very small area of the photoplate on the cathode of a photomultiplier tube, the output of which goes to a sensitive voltmeter which presents the value digitally. The voltmeter operating speed is controllable up to repetition rates of 20 times per second. The measurement scale is divided into 1000 parts. The area measured by this system is adjustable both in length and width.

The analog of the variation of light transmission across a small area of the plate is displayed on a cathode ray tube. This signal is derived from an optically magnified image which is swept across a slit in front of a photomultiplier tube by a rotating square prism. The photomultiplier output is the vertical input to the oscilloscope and the horizontal input comes from a tachometer generator which rotates with the prism.

Visual Image Presentation

Visual examination of the spectra on an exposed photographic plate has been found to be of great value to the mass spectroscopist. Various techniques are used to derive information by this method but all are common to the extent that a magnified image is needed. In the present instrument the magnification is variable over a wide range. At minimum magnification the image of an area on the photographic plate approximately 1.1" square fills the 13" square ground glass screen. At maximum magnification the plate area displayed is about 0.235" square. The optical train for this section consists of the following items:

- Spherical Reflector
- Projection Lamp
- Heat Absorbing Glass Filter
- Condenser Lens Assembly
- Zoom Lens
- Field Lens
- Projection Lens
- Four Front Surface Mirrors
- Ground Glass Screen

The distance from object to image is 101-3/4".

The projection lamp filament is powered from a regulated d-c source to eliminate a-c modulation effects from the transmission measuring sections.

Plate Carriage

The plate carriage and its support are the most important components in the instrument. They establish the limits of accuracy which can be obtained in any measurement made by the system. Every effort has been made to make this assembly precise, stable, convenient, and sturdy.

The base is made from a stabilized cast aluminum jig plate. Two precision bars support the plate carriage which moves on rolling ball bushings. Throughout the entire length of travel the carriage maintains parallelism with respect to a point on the base plate to within less than 1/1000 of an inch. This keeps the photographic plate in focus at all times and establishes the required conditions for precise spacing of the gratings to get position measurement accuracy.

Each plate holder has three controls for changing its position on the main carriage. The knob on top is for lateral motion so any portion of the width of the plate can be brought to the center of the field. The knob on the side skews the plate to correct for non-parallelism between the edge of the plate and the spectrum along the plate. This adjustment also aligns the image of the spectral lines with the transmission measuring slits.

The third knob, on the end, is for vernier longitudinal motion of the plates for lining up spectra from two plates.

Manual movement of the carriage is controlled by rotation of two knobs, one of which is a vernier, on the control panel. The carriage can also be moved in either direction by a motor drive through a gear reduction system. The range of speeds can be varied from 2" per minute to 0.002" per minute in ten steps. The direction switch on the control panel indicates the direction the image will move on the ground glass viewing screen. Reversing is done by selecting either of two magnetic clutches whose input shafts are continually driven in opposite directions when the scan motor is operating, so that essentially instantaneous reversing is accomplished.

Position Measurement

The grating and pickup head along the left edge of the carriage are parts of a commercially-available measuring system.*

The measuring technique is an optical and electronic combination without any physical contact required between the moving carriage and the position sensor, based on a method of counting moire' fringes and simultaneously determining the direction of fringe motion.

When light passes through two diffraction gratings slightly misaligned, moire' fringes are produced. As far as its use in this measurement system is concerned a moire' fringe can be considered as a highly magnified image of one grating line. The skew angle between the gratings determines the effective magnification power. In the system used, the grating has 2500 blazed lines per inch and the angle between it and a small reference grating is set to produce a fringe 3/8 inch long. This fringe moves in a direction normal to the direction of travel of the main grating. The blazing of the lines causes the light intensity per fringe to have essentially a sinusoidal distribution. This distributed light is sensed by four silicon solar cells spaced equally in one complete fringe pattern. The silicon sensor outputs are interpreted electronically into information as to direction and amount of motion of the fringe. A change in light level of one quarter of the sinusoidal distribution produces a pulse which can be counted. Thus one complete cycle from a fringe motion of 3/8 inch gives four counts and as this is due to a grating motion of one line width the net result is one count for each 0.0001-inch movement of the carriage.

A six-digit reversible counter stores the interpreted information on motion and direction so the reading always represents the distance from the chosen zero position to the measured position in increments of 0.0001 inches. When the switch on the panel of the counter is in the HOLD position the number is not changed by moving the carriage. This feature permits the operator to choose any desired zero reference position arbitrarily. The procedure is to move the carriage until a desired number is reached (such as a previously determined convenient value for a particular mass line), switch to HOLD, move the carriage to center the reference point and return the switch to COUNT. The counter can always be set to zero by pressing the RESET button.

Transmission Measurement

The basic function of the light transmission measuring optical system is to position two magnified images of a spectrum line on separate slits each of which is in front of a photomultiplier tube. The light passing through the slits is thus converted to electrical signals, one of which is measured by a sensitive digital voltmeter. The slit for this signal is adjustable from the control panel both in width and length. The width can be any value from 0 to 0.050 inch but the length changes in five steps. The output signal is a direct function of the light striking the photomultiplier cathode and for a particular area on the plate it will vary as the slit size is changed. The sensitivity controls on the main control panel give a total range of about 100 to 1 by varying the voltage applied to the dynodes of the multiplier tube.

---

* Ferranti, Ltd., Plainview, New York

The second image path is through a cubic prism which is rotated 1675 times per minute. The refraction introduced by the prism causes the image to scan across the slit, which is 0.001 inch wide and 1 inch long. Only two of the cube faces are used so the image scans twice each revolution. A tachometer generator rotates with the prism. Its sinusoidal output voltage is therefore always in synchronization with the image scan.

The rapidly varying light level from the scanning system is converted by the photomultiplier into a voltage which is used as the vertical input to the oscilloscope. The tachometer supplies the horizontal sweep. There is an adjustable phasing control on the generator to get the desired relationship between vertical and horizontal signals.

Overall instrument alignment produces coincidence of the two views of the line image shown on the oscilloscope by the forward and reverse scans at the same plate position which gives a minimum reading on the digital voltmeter and the visual image of the line is at the cross-hairs of the ground glass screen.

This coincidence point is an extremely accurate and rapid means of standardizing the conditions for position measurement of the spectral lines.

Conclusion

Mass determination accuracy of around one part in 80,000 is the maximum permitted by the position measurement system. In practice, any condition which introduces difficulty in determining an exact line position will reduce this accuracy. Dense broad lines are an example of such a situation. Routinely, the accuracy is well above one in 25,000.

Qualitative and semi-quantitative analyses of samples become relatively easy with the information obtained by use of this system. Quantitative analysis is still beset by so many variables in both sample homogeneity and mass spectrograph operation and response that reliable and accurate methods still have to be evolved. In any quantitative work, however, the relative light transmission of the lines from each ionic species will be a basic part of the analysis so the reliability, accuracy, and ease of reading this parameter in this instrument will greatly assist in interpreting the output of a mass spectrograph into useful data for analytical computations.

AN ELECTRONIC DATA SYSTEM FOR SPARK SOURCE SPECTROMETRY*

R. J. Dupzyk, G. W. Barton, Jr., R. D. Carver and R. A. Thomas
Lawrence Radiation Laboratory, University of California
Livermore, California

A number of papers presented during the previous sessions have dealt with the problems involved in getting reliable data from a spark source spectrometer. Many of these problems always seem to be blamed on variations in photoplate sensitivity, emulsion thickness, background fogging, γ response curve and so on.

The use of a photoplate detector in spark source spectrometers has been necessary because of the extremely random nature of the spark. The integrating nature of the photoplates has allowed the resulting ion beam to be analyzed. Figure 1 shows the typical sort of data one gets from a photoplate. This is a series of exposures showing the iron region in a stainless steel sample (Mn, Cr, Fe, Ni). The multiple exposures are necessary because of the limited dynamic range of the photo emulsion. In order to interpret the data it is necessary to read each exposure with a microdensitometer. The percent transmission of each line which falls in a useable portion of the calibrated film response curve when combined with the exposure of the line gives the ion intensity. With these intensities and the aid of a computer one can calculate percent composition.

Because traditional electronic data collection systems are not applicable under these conditions, we decided to apply our knowledge of pulse systems[1] to the problem. This technique, enhancement of signal-to-noise by continuous averaging,[2] was described by Dr. George Barton of our laboratory on Tuesday.

A CEC 21-110 mass spectrometer was modified for direct data acquisition with an electron multiplier as shown in Figures 2, 3, and 4. Figure 2 shows the placement of the multiplier housing and the addition of Vac-Ion pump. If I might digress momentarily, this 15 ℓ/s Vac-Ion pump not only helped in our work with the multiplier, but also improved the appearance of our photoplates, especially in the low mass range.

Figure 3, shows the essentials of the spectrometer and the position of our electron multiplier. A DuMont SP-172 electron multiplier which was modified so it could be placed perpendicular to the ion beam was mounted in the housing shown in Figure 2. A large section of the plate holding device was removed to form a window and a triangular slit replaced the plate. This slit was about 20 mils at the top and tapered down to about 2 mils. By racking the plateholder up and down, we could obtain some variation in slit width.

The next step in our modifications was in the magnet power supply. In trying to apply a magnetic field sweep[3] we found that the CEC supply could not be swept at any reasonable speed. We put together our own power supply and control circuit as shown in Figure 4. A Belman-Invar Constant Voltage Supply controlled by a transistorized series gate provide power. The remainder of the circuit is a Hall-effect field control unit which was developed in our laboratory. This employs a Bell-240 differential gauss meter and three operational amplifiers. By adjusting the feedback control on the Bell instrument you essentially dial the magnetic field you want. The width of the sweep is controlled by R-5 and R-6.

A stable sweep can be obtained in the range of 0.005 c/s to about 10 c/s depending upon the width of the sweep. At the slow sweep rate we could observe the mass range of 6 to 250. The stability of this Hall-regulator as measured by the CO-N_2 doublet was better than 10^4/1 for one hour and an overnight reproducibility of better than 2×10^3/1. These are overall system stabilities and include major high voltage warm up effects.

Now with all these system modifications completed so that we had an electron multiplier and a magnet sweep, we hooked everything up to a Nuclear Data ND-160M-4096 channel multisumming scaler as shown in Figure 5. The current from the electron multiplier is amplified through a good quality D.C. amplifier and then converted into a train of pulses in a Vidar-Voltage to Frequency converter. These pulses are accumulated in the multisumming scaler which is being addressed synchronously with the magnet. Data can be accumulated in a one-way magnet sweep or both up and down field sweep. The digital data is read out of the scaler in one of four ways - oscilloscope, opticon, punch paper tape or magnetic tape.

Some of the typical data obtained with this system are shown on Figure 6.

1. Shows the Cu 65-63 peaks and the ratio agrees with the published ratio to better than one percent. Note that we get this in spite of the discontinuous spark.
2. Shows a platinum spectrum.

3 and 4. Show the iron region of the same stainless steel sample shown on the photoplate in Figure 1. These results agree with those obtained from the photoplate. The Ni-61 indicates a sensitivity of about 1000 ppm. This can easily be extended to 100 ppm on reasonably good sparking materials.

In conclusion we have described the modification and additions necessary to obtain on-line digital data from a spark source spectrometer. At present we have demonstrated that continuous averaging of the random ion signal to enhance the signal to noise ratio is feasible and does work over a limited mass range. How far this system will go towards completely replacing the photoplate is now under study. Even at its present state of development it is very good as a survey method to find out what is present in a sample. We have not determined the ultimate sensitivity yet but in part it will be dependent upon how much patience one has to sit and keep the spark going.

References

*Work was performed under the auspices of the U. S. Atomic Energy Commission.

1. G. W. Barton, Jr., L. E. Gibson and L. F. Tolman. Anal. Chem. 32, p 1599 (Nov. 1960) and the paper by Barton at this meeting.
2. M. P. Klein and G. W. Barton, Jr., Rev. Sci. Instr. 34, 754 (1963).
3. G. W. Barton, Jr., L. F. Tolman and R. E. Roulette, Rev. Sci. Instr. 31, 995 (1960).

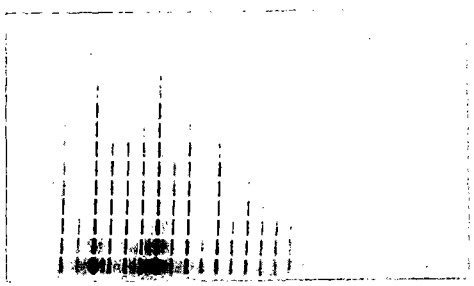

Fig. 1. Typical photoplate exposure of the stainless steel sample - Mn, Cr, Fe, Ni region.

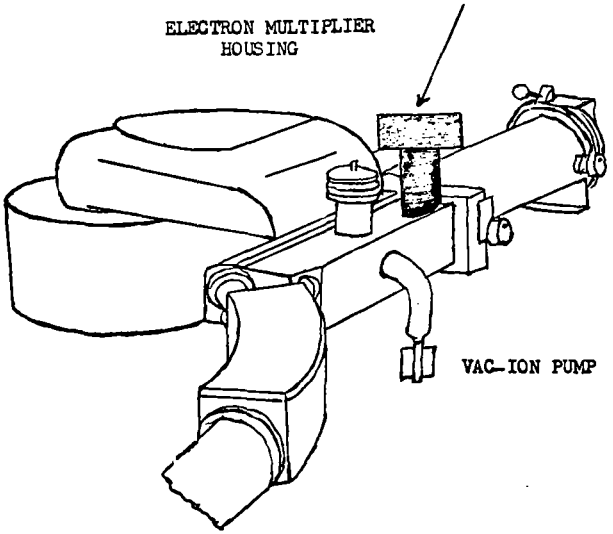

Fig. 2. Electron multiplier housing placement and added Vac-Ion pump.

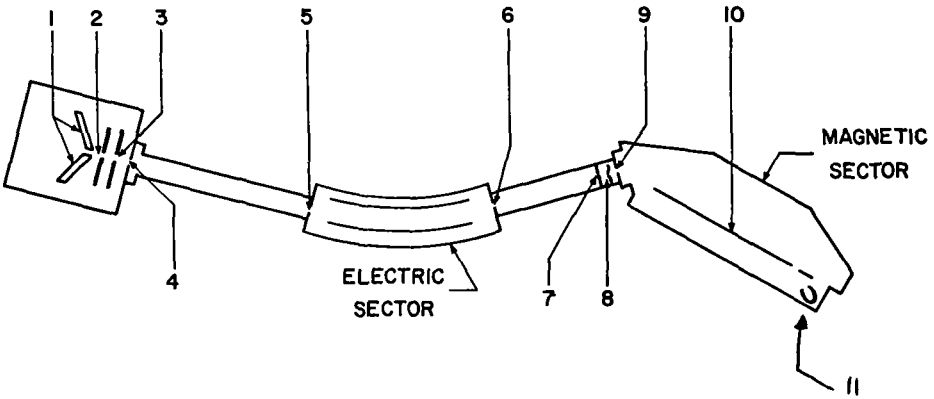

1. SAMPLE ELECTRODES
2. FIRST APERTURE
3. SECOND APERTURE
4. OBJECT SLIT
5. ELECTRIC SECTOR ENTRANCE SLIT
6. ELECTRIC SECTOR EXIT SLIT
7. MAGNET SHUNT
8. BEAM MONITOR ELECTRODES
9. ENERGY RESOLVING SLIT
10. PHOTOGRAPHIC PLATE MASK
11. ELECTRON MULTIPLIER

Fig. 3. Diagram of working parts of spark source spectrometer showing placement of electron multiplier and slit.

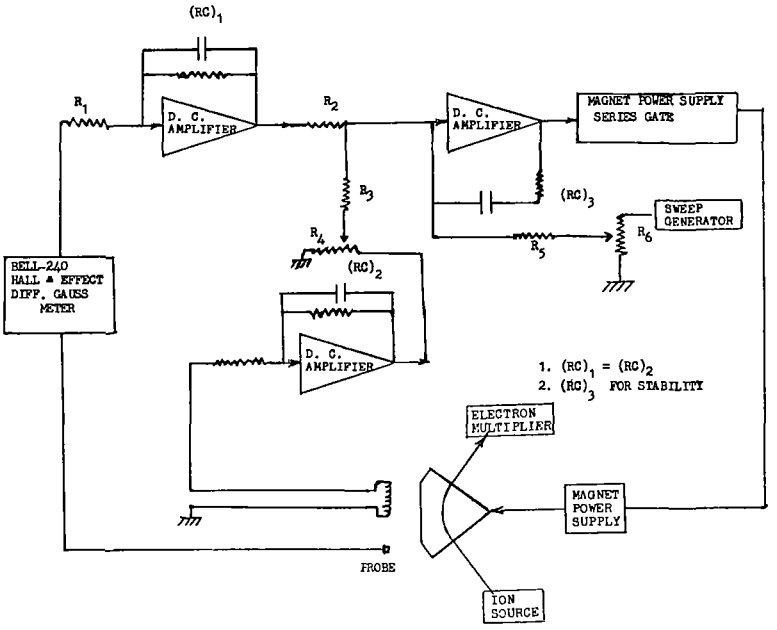

Fig. 4. Block diagram of the magnet field sweep control circuit.

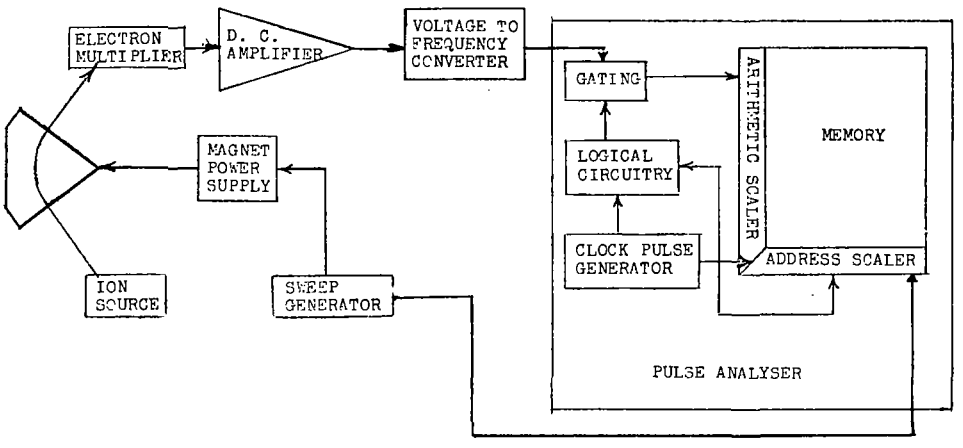

Fig. 5. Block diagram of the counting circuit as an integral part of the synchronously swept system.

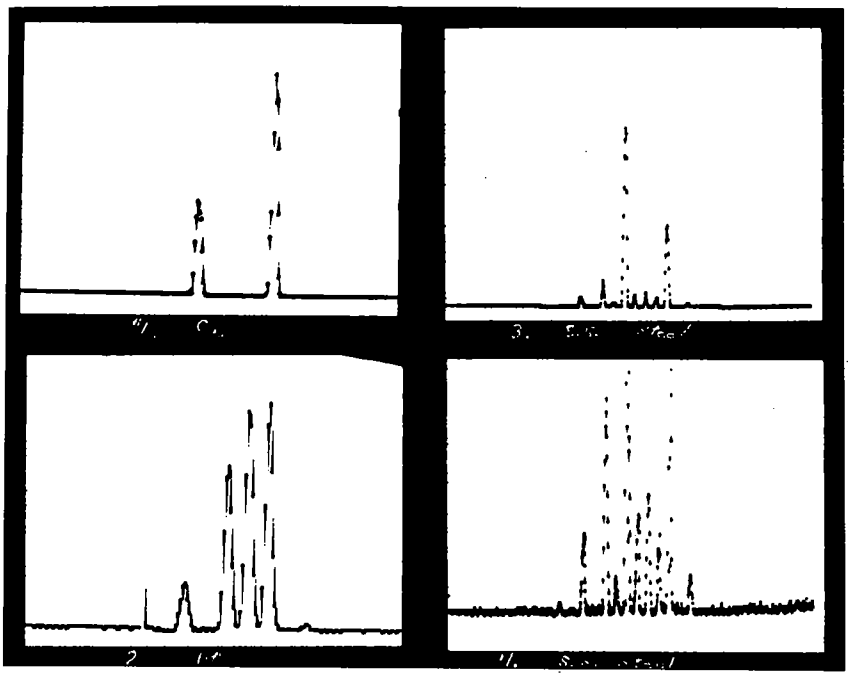

Fig. 6. Oscilloscope read out of digital data.
1. Copper 63/65 ratio good to better than 1%.
2. Platinum spectrum.
3 and 4. Stainless steel in digital form as contrast to photoplate. No. 4 is taken on an eight times more sensitive scale to show detail.

MASS SPECTROMETRIC STUDY OF THE FRAGMENTS IN Pu^{241} THERMAL NEUTRON FISSION

H. FARRAR

Atomics International, Canoga Park, California, U.S.A.

W.B. CLARKE

University of California, La Jolla, California, U.S.A.

R. H. TOMLINSON and H. G. THODE

Hamilton College, McMaster University, Hamilton, Canada

ABSTRACT

The relative yields of forty-five isotopes of ten elements formed by the thermal neutron fission of Pu^{241} have been obtained by mass spectrometric methods. The relative yields of the elements were normalized by means of the isotope dilution and isobaric techniques and absolute cumulative yields were determined by summing the relative yields of the heavy fragments to 100%. The curve obtained for Pu^{241} is compared with other mass-yield curves. The general shape of the heavy fragment mass-yield curve is similar to that for Pu^{239}, yet the fine structure shows greater similarity to that for U^{235} thermal neutron fission.

INTRODUCTION

In the past few years, a large amount of experimental data on the mass yields resulting from the fission of various heavy nuclides has been accumulated. Observation of systematic variations in the general shape and fine structure of the mass-yield curves has resulted in a better understanding, and some explanations for various facets of the fission process. It has become increasingly important in calculations of reactivity for high burn-up reactor fuels to know the fission yields of heavy elements such as Pu^{241}. This paper describes mass spectrometric measurements of the yields of the fragments resulting from the thermal neutron fission of Pu^{241}. Although the relative yields of isotopes of each of the elements krypton, strontium, xenon, cesium, barium, cerium, neodymium and samarium have been obtained with a precision of 1% or better, the normalization of each element to the others has somewhat greater uncertainty. Absolute yields were obtained by imposing the condition that the sum of all the relative yields of the heavy fragments, including interpolated and extrapolated values, must equal 100%. The absolute yields should be accurate to at least 5%. The fact that the yield of each isotope was determined relative to its adjacent masses, makes this work particularly suitable for the study of fine structure. From these measurements, it has been found that the general shape of the heavy mass-yield curve is quite different from that predicted by Walker[1], having a considerable amount of fine structure remarkably similar to that on the mass-yield curve for U^{235} thermal fission[2]. The general shape of the heavy mass-yield curve however, is similar to the shape of the corresponding Pu^{239} mass-yield curve[3]. Evidence for fine structure in the primary fission act has been found from observation of an unexpectedly low yield at mass 141 and also at its complementary primary fragment for the thermal neutron fission of Pu^{241}, Pu^{239}, U^{235} and U^{233}. In addition, it has been found that the yields between masses 143 and 154 decrease with increasing mass more slowly than they do for Pu^{239} fission. This follows a systematic trend of slower decrease of yield with increase in mass progressing from U^{233} through U^{235} and Pu^{239} to Pu^{241} thermal neutron fission.

EXPERIMENTAL METHODS

Twelve samples were prepared from 2.4 mg of plutonium containing 87% Pu^{241} which was purified by anion exchange. The eluant was divided into drops which were placed on small pieces of aluminum foil. The solutions were evaporated to dryness, the foils were tightly wrapped to help contain the fission products and to dissipate the heat generated during irradiation, and then these

were sealed in small quartz vials. One sample was irradiated in the thermal column and two in an x-rod position in the NRX reactor, Chalk River, the remaining samples were irradiated at various positions adjacent to the core of the McMaster University (swimming pool) reactor.

Various procedures were employed to separate the plutonium and americium from the solid fission products, including the method described by Surls and Choppin[4] in which a Dowex 1 anion exchange column was eluted with 2 M NH_4SCN and the method of Allison and Hart[5] in which the plutonium was eluted from a similar column with a solution of 5% HCl 2% H_2SO_3. In each case, the solid fission products were finally dissolved in water and were placed altogether upon a tungsten filament for mass spectrometric analysis.

The quartz vials containing the samples from which krypton and xenon isotopes were analysed were sealed either directly to the sample handling system of the gas-analysis mass spectrometer or to a separate vacuum line. In each case, the tip of the vial was broken with a glass-covered iron slug and the vial was then heated to 1100° C, which was sufficient to melt the aluminum foil. Reheating experiments showed that at least 99.5% of the available fission product xenon was released during the first heating. The krypton and xenon samples, after purification by exposure to titanium "sponge" heated to 800° C either were admitted immediately to the mass spectrometer or were condensed in sample tubes which were sealed and kept for subsequent analysis.

The fission products were analysed in two 10" radius 90° sector direction-focusing mass spectrometers using 10-stage Allen-type electron multipliers for ion detection. For the analysis of small quantities of krypton and xenon, the electron bombardment source mass spectrometer was operated in the "static mode" wherein samples were introduced to the mass spectrometer volume after it had been completely sealed from the pumps by magnetically operated valves. Two quartz furnaces containing a few grams of titanium "sponge" heated to 800° C were sealed to the closed system. The hot titanium served to maintain a vacuum of approximately 1×10^{-8} torr and to remove traces of chemically active gases in the sample. This method allowed the successful isotopic analysis of 6×10^{-13} g. of fission product xenon. Separation of the various solid fission-product elements was accomplished within the solid-source mass spectrometer by suitable adjustment of the temperatures of the sample and ionization filaments. Although it was possible to perform an isotopic analysis of rare earth elements in quantities less than 10^{-9} g, better results were obtained with larger samples. Unfortunately the observed rare earth spectra were generally of a composite nature. However, it was always possible to make one element predominant either in its metal or oxide form. Calculation of the corrections due to the contribution to the peaks from isobars could be made by measuring the abundance of an isotope of the other element not isobaric with an isotope of the predominant element. Figure 1 shows an example of the spectra that appeared simultaneously during a measurement of the relative abundances of $Ce^{141}O^{16}$ and $Ce^{142}O^{16}$. First, the contribution to the mass 157 peak due to $Ba^{138}F^{19}$ and $Pr^{141}O^{16}$ was found. The barium contribution was determined by measurement of $Ba^{135}F^{19}$ and the praseodymium contribution was determined from $Pr^{143}O^{16}$, and a knowledge of the barium and praseodymium isotopic abundances in the sample. It was also necessary however, to subtract Sm^{154} from the mass 154 peak and both $Nd^{143}O^{16}$ and $Ba^{140}F^{19}$ from the 159 peak. Such corrections must be applied individually to each spectrogram due to the changing proportions of the contributing elements. The validity of the corrections was always verified by making the measurements at times when different proportions of the various elements were present. When these corrections were applied they were usually very small and their uncertainty did not contribute appreciable uncertainty to the final results. Each ratio was measured under a variety of filament temperature conditions in order to ensure that the ratio measured was representative of the sample. No systematic change in any ratio other than that due to radioactive decay was observed during the course of expenditure of the sample, indicating that mass discrimination in the source did not occur. Moreover, the measured ratios of the isotopes of cesium, barium and neodymium remained unchanged within experimental error, when the electron-multiplier detector was quickly replaced by a Faraday cup detector with repeller grid, during the course of a measurement. The final uncertainties take into account the statistical errors in the mass spectrometric determinations as well as the estimated uncertainties in the half-lives and other nuclear data used.

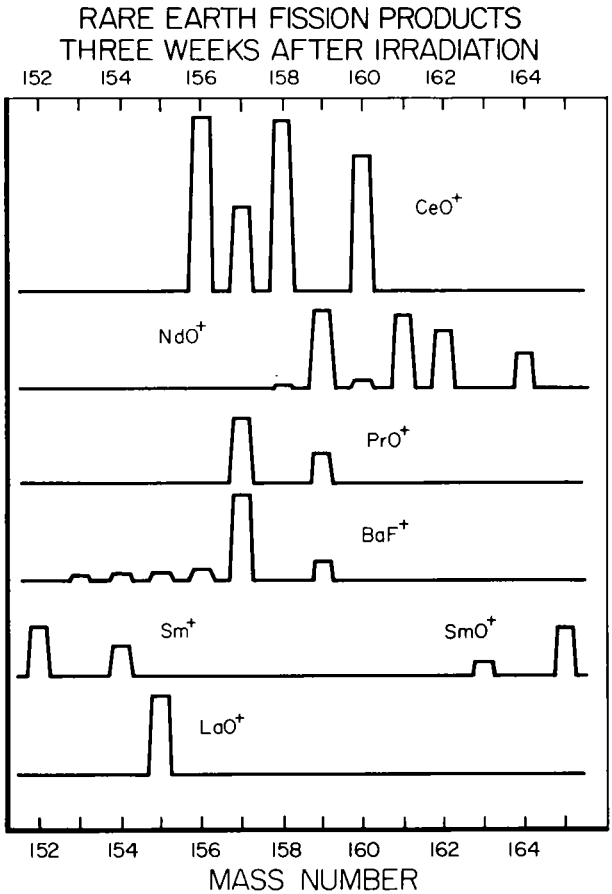
RARE EARTH FISSION PRODUCTS
THREE WEEKS AFTER IRRADIATION
152 154 156 158 160 162 164
CeO+
NdO+
PrO+
BaF+
Sm+
SmO+
LaO+
152 154 156 158 160 162 164
MASS NUMBER

Fig. 1

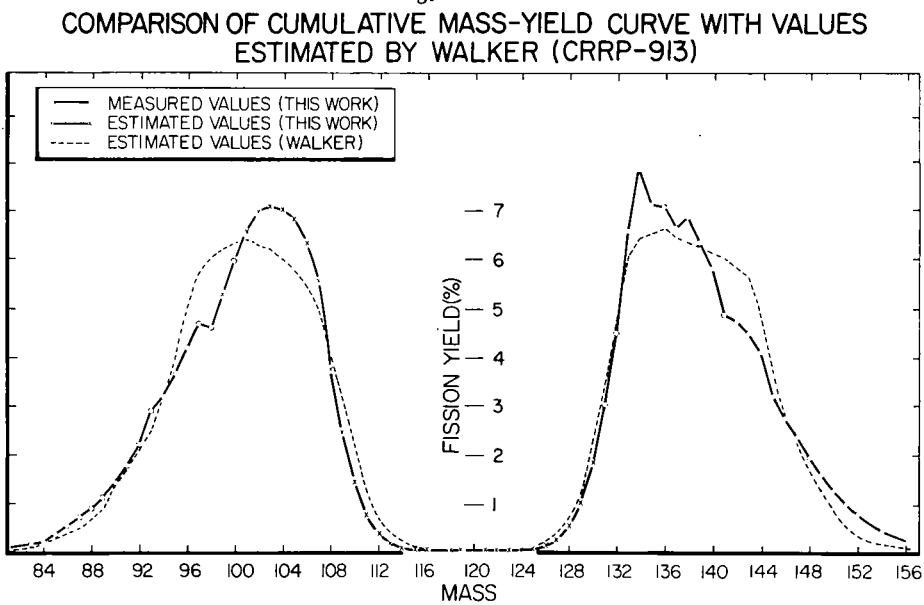
COMPARISON OF CUMULATIVE MASS-YIELD CURVE WITH VALUES
ESTIMATED BY WALKER (CRRP-913)
MEASURED VALUES (THIS WORK)
ESTIMATED VALUES (THIS WORK)
ESTIMATED VALUES (WALKER)
FISSION YIELD(%)
1 2 3 4 5 6 7
84 88 92 96 100 104 108 112 116 120 124 128 132 136 140 144 148 152 156
MASS

Fig. 2

RESULTS

By analysing some fission products a few minutes after an irradiation lasting less than half an hour, the yields of such isotopes as Kr^{87} and Xe^{138} could be determined relative to the yields of stable krypton and xenon isotopes with small uncertainty due to half-life corrections. The relative yields of Sr^{88}, Sr^{89} and Sr^{90} were obtained after making a small correction for natural strontium contamination, determined from the presence of Sr^{86}. Isotopes of zirconium were measured as ZrO^+ and contained varying amounts of natural contamination which were found from the abundance of Zr^{90}. Yields of the molybdenum isotopes were obtained from Mo^+ spectra. An unsuccessful attempt was made to measure small peaks of Ru^+.

Measurements of the heavy mass-fragment yields were far more precise. The ratio of Xe^{133}/Xe^{134} was measured in four young samples to permit normalization of the relative yields of the xenon isotopes to the cesium isotopes at mass 133. Isotopes of cesium were analysed in three samples, but only in the thermal column sample was the yield of Cs^{135} obtained without a large and uncertain correction due to neutron capture in Xe^{135}. The averages of the ratio Cs^{133}/Cs^{137} represented more than 200 measurements. Because the averages differ from the weighted mean by less than 0.7%, the authors believe that the cesium in the samples was essentially free from natural contamination. The abundances of barium isotopes were measured in three independent groups at different times approximately 29 d after the end of irradiation. The contribution of natural barium to the sample was determined from measurements of the abundance of the Ba^{136}, after corrections had been made for a small amount of Ba^{136} resulting from the decay of Cs^{136} formed directly in fission. The abundances of the cerium isotopes were measured as cerium oxide with more than seventy complete spectra under seven different filament conditions. Peaks due to praseodymium oxide and barium flouride were large enough to make some of the first ratios too uncertain to be used. For subsequent spectra very small amounts of oxides of lanthanum, praseodymium and neodymium were generally present, but as described above, accurate corrections could be made. After the corrections, which included allowance for the contribution of O^{17} and O^{18} to the peaks had been made, good consistency was achieved for the cerium isotope abundances. Uncertainty in the isotopic composition of the praseodymium led to an estimated uncertainty of 2.5% in the Ce^{141} yield. Due to growth of Ce^{140} resulting from Ba^{140} decay, the relative abundance of Ce^{140} increased until after the complete loss of barium from the filament. From these measurements it is impossible to tell whether or not there was any contribution from natural cerium, although such is likely to be small since there was little natural neodymium or samarium contamination in this sample. It should nevertheless be noted that the principal effect of natural cerium contamination would be to lower the yield of mass 140 with respect to mass 144. There is another way, however, to obtain the ratio of the yields of masses 140 and 144 and thus to ascertain the amount of natural cerium contamination. This method employs the isotope dilution of cesium to neodymium and will be described later. Isotopes of neodymium were measured both as Nd^+ and NdO^+ in several samples. The results, after very small corrections for natural neodymium contamination had been made, were consistent to better than 1%. The relative abundances of the samarium isotopes were measured in four groups from three samples, all of which were subjected to different chemical treatments. For the last three groups, a small residue of natural Sm^{148} remained after the observed abundance was corrected for Sm^{148} produced as a result of neutron capture in Pm^{147}. Because the mass 150 chain decays to stable Nd^{150}, all the Sm^{150} left after subtaction of natural Sm^{150} should be due to neutron capture in Sm^{149} and therefore the mass 149 chain yield was obtained by direct summation of the abundances of Sm^{149} and Sm^{150}. Also, the neutron fluxes could be determined and used to calculate the depletion of Sm^{151} and corresponding increase of Sm^{152}. The relative abundances of Cs^{137} and Nd^{145} were determined by a single isotope dilution using natural cesium and neodymium. Since both Nd^{145} and Nd^{146} exist in nature as well as in fission in proportions that are not greatly different, there is a 5% uncertainty in the Cs^{137}/Nd^{145} ratio even though the standard deviations of the measured ratios were less than 1%.

Because masses 133 and 135 were measured both as xenon and cesium, it was possible to normalize these two elements by three methods. The first method, considered the most reliable, is to equate the yield of the 133 mass chain determined from xenon measurements to the yield of the same mass chain determined from cesium measurements. The second method is to equate the yield of the 135 mass chain obtained from measurements in a low-burnup sample, to the yield of this mass chain determined from cesium measurements in the thermal column sample. The greater uncertainty in the yield of mass 135 resulting from half-life and

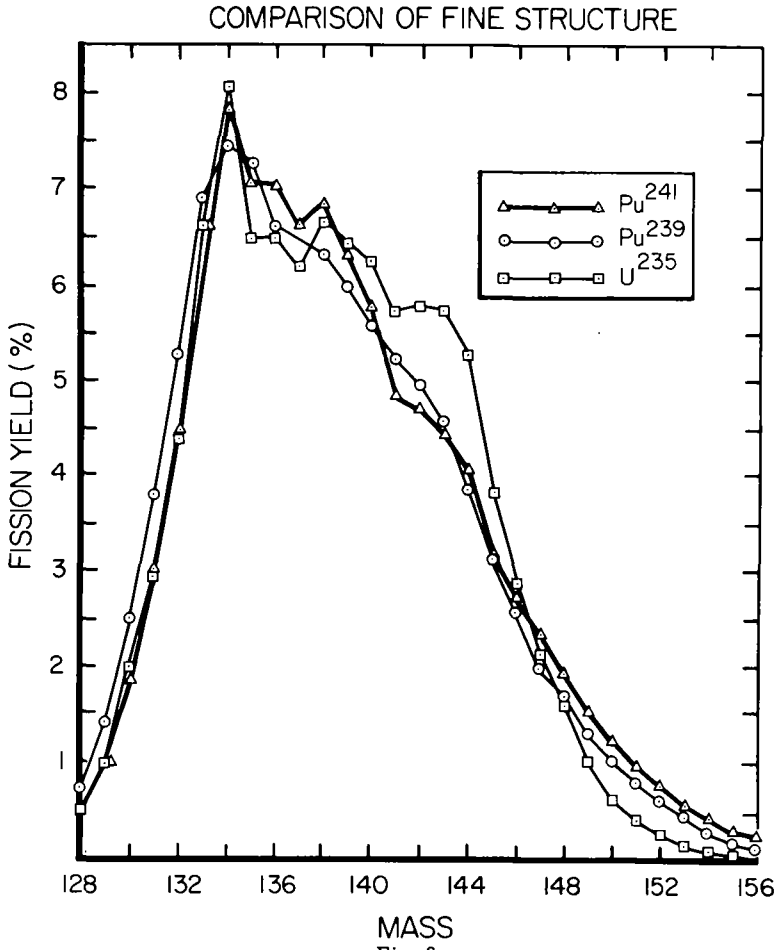
COMPARISON OF FINE STRUCTURE
FISSION YIELD (%)
8
7
6
5
4
3
2
1
128
132
136
140
144
148
152
156
MASS
Pu241
Pu239
U235

Fig. 3

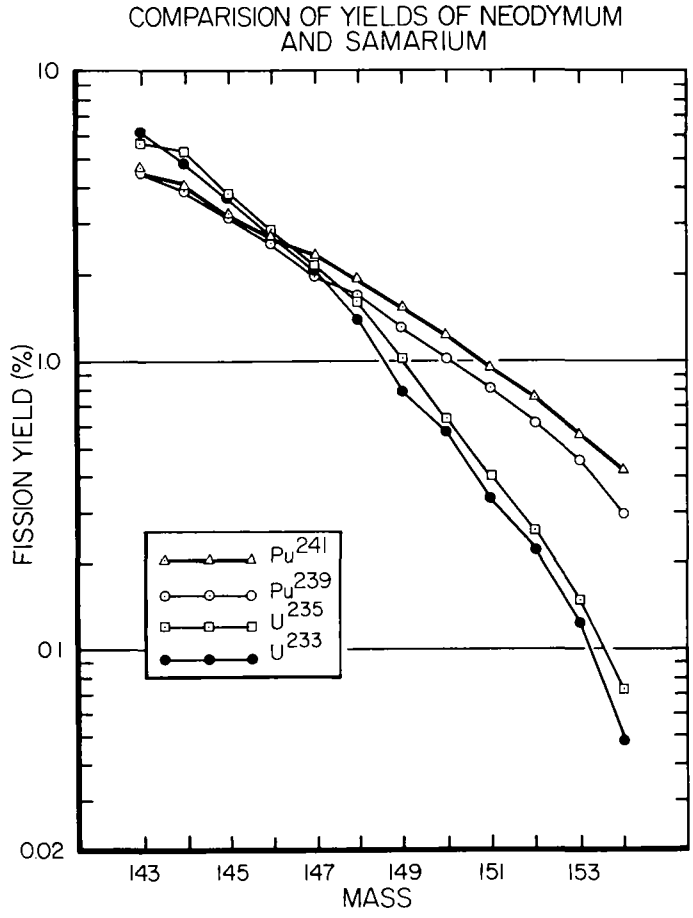
COMPARISION OF YIELDS OF NEODYMUM AND SAMARIUM
FISSION YIELD (%)
10
1.0
0.1
0.02
143
145
147
149
151
153
MASS
Pu241
Pu239
U235
U233

Fig. 4

burn-up corrections make this method less attractive. The third method normalizes xenon to cesium by noting that in the thermal column sample, loss of Cs^{135} must equal the gain in Xe^{136}. Within the estimated uncertainties the results of the latter methods confirm the results of the first.

Isotopes of barium were normalized to those of xenon at mass 138 and cerium at mass 140. Similarly cerium was normalized to neodymium at mass 144. Neodymium and samarium measurements unfortunately did not include a pair of isobars, and since no isotope dilution was performed on samarium, their normalization could only be estimated. Examination of the relative yields reveals that the neodymium isotope abundances decrease faster with increasing mass, and that the samarium isotopes follow the same trend. The samarium isotopes have been normalized to the neodymium isotopes so that Sm^{149} has a value between those of Nd^{148} and Nd^{150} interpolated with regard to change of slope of the other neodymium isotopes. This value for mass 149 is averaged with the value obtained by interpolating Sm^{147} between Nd^{146} and Nd^{148} and with the values obtained by placing Nd^{148} and Nd^{150} between their adjacent samarium isotopes. The four combinations result in values of Sm^{149}/Nd^{145} differing by much less than 1%. The fact that this normalization produces a smooth curve by no means proves that this normalization is correct, but in view of the smooth transitions from neodymium to samarium found in the fission mass-yield curves of U^{233}, U^{235} and Pu^{239}, the authors believe that it is improbable that fine structure should exist in this region for Pu^{241} fission, especially since the neodymium and samarium isotopes by themselves decrease remarkably uniformly. In the same way, the isotopes of krypton and strontium, which were normalized to each other through their isobars at mass 88, were normalized to zirconium and molybdenum by assuming a smooth increase of yield with mass observed in the isotope ratios by themselves.

All the isotopes between masses 131 and 146 have thus been normalized to each other by the isobaric technique. As mentioned above, there is a possibility that the fission-product cerium was contaminated with a small amount of natural cerium. For this reason, the abundance of Cs^{137} was measured relative to Nd^{145} by isotope dilution. The ratio Cs^{137}/Nd^{145} resulting from the isotope dilution is 1.99 whereas the value obtained from the isobaric technique is 2.19. The average value, 2.09, lies within the 5% estimated uncertainties of each of the methods and has been used in the final normalization. The cerium ratios have been modified slightly assuming that the difference between the isobaric technique normalization value of 2.19 and the average value of 2.09 is due to a small amount of natural contamination. The relative yields of the light fragments were converted to absolute yields by observing the relative peak heights of Xe^{134} and Kr^{86} and comparing them numerous times with known mixtures of xenon and krypton. Due to the 3% estimated uncertainty in the Kr^{86}/Xe^{134} ratio thus obtained, and due to the uncertainty in the strontium-zirconium-molybdenum normalizations, the absolute values of the measured light yields are considered somewhat less accurate than the heavy yield values. The sixty percent of the light mass chain yields that were not measured at all were chosen so that the light yields summed to 100% and so that the slope of the curve above mass 107 matched the complementary yields on the heavy mass-yield curve assuming an average neutron emission of 2.5 in this mass region.

Analysis of the plutonium isotopes before and after the irradiations indicated that the ratio Pu^{241}/Pu^{239} decreased from 14.3 in the first samples to 12.9 in later samples. Thus the corresponding estimated percentage of fissions attributed to Pu^{239} increased from 5.3% to 5.8%. To correct for this, the normalized relative yields were added to 105.82% preparatory to the subtraction of a 5.5% contribution from Pu^{239} fission. The subtraction of the Pu^{239} contribution made negligible changes to the absolute yields.

Figure 2 shows the measured absolute cumulative yields along with extrapolated values between masses 101 and 130 and between masses 155 and 160, plus interpolated values for masses 99, 139 and 153. The yields of masses higher than 154 were estimated by assuming a continuation of the trend of decrease of yield noted between masses 143 and 154. This assumption has been shown to be true for the fission of U^{235} and Pu^{239}. Yields in the valley between masses 114 and 126 have been extrapolated taking into account the systematic variations between the mass-yield curves resulting from the thermal neutron fission of U^{233}, U^{235} and Pu^{239}.

DISCUSSION

The absolute yields of the measured heavy mass fragments are considered to be accurate to within 5%. The uncertainty arises mainly from the uncertainty of the cesium-neodymium normalization, as discussed above. It should be noted that if the cesium-neodymium normalization were in error by 5%, the absolute yields would change only by 1.8% between masses 120 and 140, and 3.4% between masses 141 and 160. Because the yield of each mass is known relative to the adjacent masses in most cases to better than 2%, the resulting curve is most suitable for the study of fine structure. There can be no doubt that the pronounced peak on the mass-yield curve at mass 134 and the dips at masses 98, 137 and 141 are real and that they would not change appreciably if the cesium to neodymium normalization were changed.

The yields shown in figure 2 are compared with the yields for Pu^{241} thermal neutron fission predicted by Walker[1] from extrapolations of systematic changes in the U^{233}, U^{235} and Pu^{239} fission yields.

The heavy fragment mass-yield curves for U^{235}, Pu^{239} and Pu^{241} thermal neutron fission are compared in Figure 3. It can be seen that the average masses for the three curves are very nearly the same and that all three curves have a maximum yield at mass 134. It must further be noted that although the Pu^{241} curve has a general shape very similar to the Pu^{239} curve, the structure upon the curve is strikingly similar to that of U^{235}. An important difference can be seen from Figure 4 in which the yields of masses 143 to 154 from U^{233}, U^{235}, Pu^{239} and Pu^{241} fission are compared. It is clear that there is a systematic change in the rate of decrease of the yields; the rate being largest for U^{233} and smallest for Pu^{241}.

It has been previously shown[6,7] that the prominent peak at mass 134 in U^{235} thermal fission can be explained by the neutron yield changing slowly as a function of mass of the primary fission fragments. The fact that there were no peaks at the fragment masses complementary to the peak at mass 134 in U^{233} and Pu^{239} fission supported this idea. The dip in the Pu^{241} curve at mass 141, also noticeable in Pu^{239} fission but even more pronounced in U^{235} fission, would seem to require a different explanation. The complementary fragments to mass 141: mass 91 in U^{233} fission, 92 in U^{235} fission, 96 in Pu^{239} fission and 98 in Pu^{241} fission are in unexpectedly low yield. Thus it would appear that this fine structure must be due in part to a preference in the primary fission act. This conclusion is borne out by recent time-of-flight prompt-yield measurements by Milton and Fraser[8] in which the yields of the primary fragments in U^{233}, U^{235} and Pu^{239} fission around mass 142 appear noticeably low.

A possible reason for the striking similarity between the structure in the U^{235} and Pu^{241} mass-yield curves and the fact that the Pu^{239} shows little structure is that the primary fragments from Pu^{241} and U^{235} fission contain, on the average, a greater neutron-to-proton ratio than do the fragments from Pu^{239} fission. Thus the β-decay chain lengths at any given mass are shorter for Pu^{239} than for U^{235} and Pu^{241} where they are almost equal. Since it has been shown that most of the fine structure can result from a change in neutron emitting properties of the primary fragments[6,7], it is reasonable to expect the structure of Pu^{241} to be similar to that of U^{235} and to expect Pu^{239} and U^{233}, which do not have the same set of primary fragments, to have less.

ACKNOWLEDGMENTS

The authors wish to thank Atomic Energy of Canada Ltd. for some of the neutron irradiations and the National Research Council of Canada for financial assistance. The Pu^{241} was supplied by Atomic Energy Research Establishment, Harwell, England.

1. WALKER, W. H. Chalk River Report AECL 1054, 19. (1960)
2. FARRAR, H. and TOMLINSON, R. H. Nuclear Physics 34, 367, (1962)
3. FICKEL, H. R. and TOMLINSON, R. H. Can. J. Phys. 37, 926 (1959)
4. SURLS Jr., J. P. and CHOPPIN, G. R. J. Inorg. & Nucl. Chem. 4, 62 (1957)
5. ALLISON, G. M. and HART, R. G. Chalk River Report AECL 1372 (1961)
6. FARRAR, H. and TOMLINSON, R. H. Can. J. Phys. 40, 943 (1962)
7. TERRELL, J. Phys. Rev. 127, 880 (1962)
8. MILTON, J. C. D. and FRASER, J. S. Can. J. Phys. 40, 1626 (1962)

Mass Spectrometric Determination of the Ratio of the Neutron Capture to Fission Cross Sections of U-235

M. Lounsbury, I.H. Crocker, R.W. Durham and A. Okazaki

Atomic Energy of Canada Limited, Chalk River, Ontario

A: INTRODUCTION

Alpha, the ratio of the neutron capture to fission cross sections of the fissile nuclide U-235, is related to other nuclear parameters as shown in the following equation.

$$1 + \alpha = 1 + \frac{\sigma_c}{\sigma_f} = \frac{\sigma_a}{\sigma_f} = \frac{\nu}{\eta}$$

where, σ_c = capture cross section
σ_f = fission cross section
σ_a = absorption cross section $= \sigma_c + \sigma_f$
ν = no. neutrons emitted per fission
η = no. neutrons emitted per neutron absorbed
α = σ_c/σ_f

High accuracy in the measurement of α can lead to high accuracy in the other inter-related nuclear parameters, which must form a self-consistent set.

Alpha for U-235 has been measured a number of times during the past 20 years. Various authors (1-6) have reviewed the data and arrived at best values of α_o, the value at the standard neutron velocity of 2200 m/sec, which range from 0.171 to 0.184.

This paper describes a new measurement α for U-235 irradiated in the NRU reactor at Chalk River, using isotope dilution and thermal emission mass spectrometry. A value of $\alpha_o = 0.1718 \pm 0.0006$ was obtained.

B: EXPERIMENTAL PROCEDURE

Three samples (I, II and III) were made from an alloy of 99.7% U-235 in super-pure aluminum in the form of right circular cylinders, 1.5 cm. diameter and 12 cm. long, and sheathed in aluminum 0.25 mm. thick. Each alloy core contained about 1.5 gms. of U-235 in 57 gms. of aluminum.

The relative uranium contents of the three samples were first compared by a non-destructive method involving measurement of their relative reactivities in the Pool Test Reactor (PTR) at Chalk River. The isotopic composition and absolute uranium content of Sample I was then determined mass spectrometrically by the isotope dilution method, using natural uranium as a spike. This combined with the PTR measurements gave the absolute initial uranium content of the two remaining Samples II and III.

These two samples were then irradiated to 75% burnup of the U-235 in a vacant lattice site of the NRU reactor. After irradiation, the isotopic composition and the uranium content of the samples were determined mass spectrometrically by the isotope dilution method, using natural uranium as a spike.

For this purpose, a Consolidated mass spectrometer Model 21-702B, with a 2-stage vacuum lock for inserting the triple filament assembly, was used. Duplicate analyses were performed on each sample and on each of the duplicate spikings of each sample.

C: RESULTS

The value of α may be calculated using the following equation:

$$\frac{\alpha}{1+\alpha} = \frac{\sigma_c}{\sigma_a} = \frac{N_6 + N_7 + N_8 - N_6^o}{N_5^o - N_5}$$

The number of U-235 atoms destroyed by neutron capture is equal to the final number of U-236 atoms N_6 in the irradiated sample, plus the number of Np-237 atoms N_7 produced by neutron capture in U-236, plus the number of Pu-238 atoms N_8 produced by neutron capture in Np-237, less the initial number of U-236 atoms N_6^o present in the sample before irradiation. The total number of U-235 atoms destroyed by both capture and fission in the irradiation is equal to the initial number N_5^o in the sample before irradiation less the final number N_5 after irradiation. The ratio of these two quantities is the ratio of the capture to the absorption cross section, σ_c/σ_a which is equal to $\alpha/(1+\alpha)$.

In the above equation, the four terms N_5^o, N_5, N_6^o and N_6 were determined by the mass spectrometer analyses. The term N_7, the Np-237 produced by neutron capture in U-236 was determined radiochemically by alpha counting and pulse height analysis. The yield of Np-237 was determined by measuring the 105 keV γ-ray of Np-239 which was used as a spike. The calculated value of N_8 was small, being about 0.2% of capture in U-235. The amount of U-235 produced by neutron capture in U-234 was small (~0.05% of N_5) and has been neglected. A summary of the results for Samples II and III is given in Table 1.

TABLE 1

Summary of Results

	Sample II	Sample III
N_5^o	3.995 ± 0.005 ($\times 10^{21}$)	4.000 ± 0.005 ($\times 10^{21}$)
N_6^o	0.00264 ± 0.00008 "	0.00265 ± 0.00008 "
N_5	1.0364 ± 0.0012 "	0.8904 ± 0.0014 "
N_6	0.4368 ± 0.0006 "	0.4579 ± 0.0009 "
N_7	0.0064 ± 0.0003 "	0.0073 ± 0.0004 "
N_8	0.0010 ± 0.0001 "	0.0011 ± 0.0001 "
n/kb	2.031	2.261
α	0.1753 ± 0.0006	0.1753 ± 0.0006
α_o	0.1718 ± 0.0006	0.1718 ± 0.0006

The effective value of α obtained from these measurements is:

$\alpha = 0.1753 \pm 0.0006$ Sample II
$\alpha = 0.1753 \pm 0.0006$ Sample III

The error is based on the standard error of the mass spectrometer results.

D: DISCUSSION

Since the value of α is a function of the neutron energy spectrum in which it is measured, then in order to compare the present result with other measurements, it is necessary to calculate

the value, α_o, at the standard neutron velocity of 2200 m/sec.

The conversion from α to α_o may be made using the following equation:

$$\alpha_o = \alpha(g_f + rs_f)/(g_c + rs_c)$$

where g and s are functions of the neutron temperature and describe the departure of the capture and fission cross sections from an inverse velocity dependence in the thermal and epithermal regions respectively, and r is the ratio of the epithermal to thermal neutron densities. For these irradiations, the value of r was estimated to be 0.022 ± 0.004, and the neutron temperature 40°C. The g and s factors for this temperature were taken from Critoph's tables (7).

The value of α_o for U-235 obtained from these measurements is 0.1718 ± 0.0006. The error is based on the standard error of the mass spectrometric results, and does not include any error arising from the conversion of α to α_o, i.e. from uncertainty in the value of the r, g and s factors.

In Table 2, this value is compared with various estimates of the best value and with other recent measurements. The Westcott value of 0.184 was used at Chalk River until 1963 when Hanna recommended the adoption of the lower value of 0.176. This value is somewhat higher than other recommended values, but is the weighted mean of the first three experimental values listed in the table. The first two of these were not weighted very heavily because of the high epithermal index and neutron temperatures.

The most accurate value of α_o will be obtained from measurements of α made in a well-defined neutron spectrum with a low epithermal index and a low neutron temperature. From this point of view, our measurements of 1963 and 1964 should be of equal reliability. However our measurement of 1964 is in good agreement with the lower experimental and recommended values, whereas the measurement of 1963 is not.

If one takes all of the experimental results of Table 2 into consideration, the best value of α_o for U-235 would be 0.173 ± 0.002. The uncertainty of 1% in α_o then leads to an uncertainty of less than 0.2% in the ratio of σ_a/σ_f and of ν/η.

Table 2

Summary of Values of α_o

RECOMMENDED VALUES		
Safford and Havens, 1959	0.172 ± 0.010	Ref. (1)
Westcott, 1960	0.184 ± 0.010	(2)
Leonard, 1961	0.172 ± 0.007	(3)
Sjostrand & Storey, 1961	0.173 ± 0.005	(4)
Sher & Felderbaum, 1962	0.171 ± 0.003	(5)
Hanna, 1963	0.176 ± 0.002	(6)
EXPERIMENTAL VALUES		
Jones et al, 1961	0.173 ± 0.004	(8)
Cabell & Slee, 1962	0.1715 ± 0.0034	(9)
Durham et al, 1963	0.1767 ± 0.0025	(10)
This work, 1964	0.1718 ± 0.0006	(11)

A more complete description of this work is given in Atomic Energy of Canada Limited publication AECL-1965.

E: REFERENCES

(1) G.J. Safford and W.W. Havens, Nucleonics 17, (11), 134 (1959)

(2) C.H. Westcott, AECL publication AECL-1101 (1960)
(3) B.R. Leonard, USAEC report HW-69342 (1961)
(4) N.G. Sjostrand and J.S. Storey, UKAEA report AEEW-M125 (1961)
(5) R. Sher and J. Felderbaum, USAEC report BNL-722 (1962)
(6) G.C. Hanna, AECL report NDC-51 (1963)
(7) E. Critoph, AECL publication AECL-1101 (Addendum) (1964)
(8) R.W. Jones, M. Lounsbury, R.G. Hart and G.C. Hanna, AECL report EANDC(Can)-11 (1961)
(9) M.J. Cabell and L.J. Slee, J. Inorg. Nucl. Chem. 24, 1493 (1962)
(10) R.W. Durham, R.G. Hart, M. Lounsbury and G.C. Hanna, AECL report EANDC(Can)-17 (1963)
(11) A. Okazaki, M. Lounsbury, R.W. Durham and I.H. Crocker, AECL publication AECL-1965 (1964)

The Effect of an Axial Temperature Gradient on the Apparent Pressure in a Knudsen Effusion Cell*

by

Edmund K. Storms

Most workers who have used a Knudsen cell to obtain thermodynamic data have worried about the errors a temperature gradient might introduce, and have made efforts to minimize these gradients. However, they are difficult to eliminate completely. This study was undertaken in order to learn how serious the resulting error might be and to obtain some additional insight into the evaporation mechanism within a Knudsen cell. An electron bombardment furnace was designed which would allow the gradient to be changed by employing three filaments, shown in Figure 1, each of which is independently heated. Actually, the top and bottom filaments are in series and a shunt is placed in parallel with either one to change its relative temperature. Power to the center filament is controlled by a separate series resistor. The tungsten filament wire is bent to produce a more uniform heating profile than is usually used, and the wires are clamped to the support posts to facilitate their replacement or alignment. A water cooled base, which can be moved from the outside, supports the crucible assembly, and the entire oven is surrounded by a series of tantalum radiation shields.

Graphite was chosen as a crucible material because it is non-reactive to the systems of interest and, when heated bare, severe temperature gradients can be produced quite easily. A number of crucible designs were tried; the first is shown as drawing B in Figure 2. In this case, if a uniform gradient was maintained along the wall of the cell, at about 1400°C, the lid was found to be about 30° colder than the sides. This naturally resulted in considerable condensation on the lid. Although the use of graphite produces an extreme case, a metal crucible would still show this effect. For example, Büchler and Berkowitz-Mattuch (1) observed that all of the silver contained in such a metal crucible was quickly transferred to the lid. This experience and the observations to follow make it clear that the use of such a crucible design can introduce significant errors in the pressure measurements and should be avoided. In order to eliminate this abrupt temperature change, the top and bottom were screwed together as depicted in drawing C. A uniformly varying gradient was achieved, but temperature measurements and fabrication procedures were inconvenient. The design shown as A, having a conical shaped interior, was finally chosen. The massive top near the orifice not only allows accurate sampling of the temperature, but the heat generated at the side is more easily conducted to the orifice area where it is being radiated. In addition, by using the conical shape, the hole size can be changed simply by removing some length from the end. Temperatures were measured by a pyro optical pyrometer which was sighted into 0.022" diameter black-body holes drilled as indicated in the drawing. The holes drilled into the midplane were abandoned when it was found that the temperature profile was very insensitive to the center filament power. However, this does not mean that the center filament is unnecessary. By tapering the crucible bottom to mate with the crucible stand, the crucibles could be interchanged easily and, by using a jig, each could be returned to exactly the same position. Radiation shields were placed in the hollow bottom to lessen radial gradients.

This assembly was placed onto a 60° sector mass-spectrometer. From the relationship between the crucible and the detection region of the spectrometer, shown in Figure 3, one can see that the detection slit projects onto the crucible bottom in the same way as an image in a pin hole camera. It follows that only those atoms which pass through the orifice after leaving from this area will be detected. Therefore, neither the inner shape nor the length of the crucible will affect the beam intensity, provided the image projects only onto the bottom.

Most of the gradient studies were made using gold, however, the behavior of other materials will also be described. When only a small quantity of gold is used it resides as a ball at the lower edge of the crucible. Thus, the detected atoms leave from a graphite surface, not from the primary source of the vapor. In a few experiments, sufficient metal was added to completely cover the bottom. There was no basic difference between the behavior in the two cases.

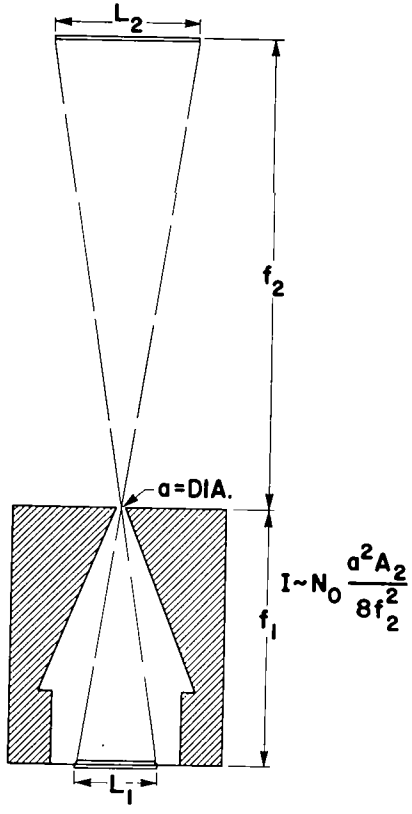

Fig. 3 - Relationship between the Detector and the Crucible

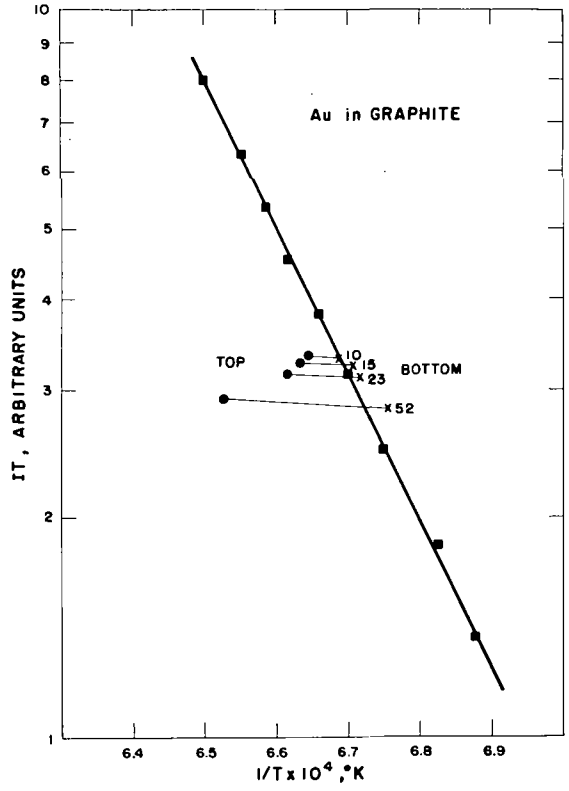

Fig. 4 - Relationship between 1/T and log IT with the top colder than the bottom.

The effect of the gradient depends on which is colder, the top or the bottom. The situation which occurs when the top is the warmer of the two will be described first. The behavior is best seen in Figure 4, where the data is plotted as log IT vs. 1/T. A straight line was drawn through the values obtained when there was no gradient, i.e., less than 3°. You will notice that all of the points fall within 3° and most within 1° of the line. I will assume that the pressure and temperature which determine this line represent the thermodynamic properties of the system. When a gradient is produced, the temperature of the top and bottom, suitably plotted, falls on either side of the thermodynamic line. The fact that the thermodynamic temperature lies near the bottom and that the deviation from the line increases regularly with the total gradient, suggests that there is a location within the cell which is independent of the gradient and, therefore, determines the thermodynamic properties of the system. One would expect that it is the temperature at the surface of the gold bead. In order to understand a little better the situation within the cell, the following procedure was adopted. Plugs of graphite of various thickness were placed in the crucible well, with the gold bead on top. In each case a plot like Figure 4 was constructed from the data. If a temperature is calculated from the measured pressure (IT) using the thermodynamic line, and the difference between this temperature and that measured at the bottom is plotted against the total temperature gradient, Figure 5 results. In other words, the pressure is used to determine the temperature of that portion of the cell which creates the pressure. The three top curves were obtained with the indicated number of inches of graphite between the gold bead and the black-body hole. As expected, the greater the distance between where the temperature is measured and the source of the vapor, the greater the effect of the gradient. However, when a semicircular plug of greater thickness than used previously was placed in the crucible, but this time with the gold resting on the bottom and the detector image projecting onto the top, the lower line in Figure 5 resulted. As you can see, the effect was smaller than when the bead simply rested on the bottom. It is clear that the gold surface has the pressure-determining temperature. The semicircular plug, in this case, partially surrounded the gold bead and protected it from the radiation coming from the hotter top. Consequently the effect of the gradient was reduced. The effect of graphite thickness can be seen more clearly in Figure 6 where the difference between the bottom temperature and thermodynamic temperature, resulting when a total gradient of 50° existed, is plotted against the graphite thickness. When the resulting line is extrapolated to zero graphite thickness, one finds that a temperature difference still remains. This is probably due to the temperature gradient across the gold-graphite innerface. When the bead was shielded from the top the residual gradient was reduced almost by 1/2.

While the semicircular plug was in place, an additional interesting observation was made. Gold was caused to condense onto the upper part of the crucible, including the surface of the plug at the detector image, by making the top colder than the bottom. When the gradient was reversed, the beam intensity was found to be consistent with the temperature at the detector image until all of the gold had evaporated from this area. The intensity then dropped abruptly to correspond to the temperature of the gold bead in the well.

Several conclusions can now be made. When the top is hotter than the bottom, the rate at which particles enter a detector above a Knudsen cell will be determined by the temperature at the detector image if this is a primary source of vapor. If a primary source is not located at the detector image, the temperature of the source, wherever it is located, will determine the collection rate. For example, Büchler and Berkowitz-Mattuck (1) found that after all of the silver in their cell had condensed on the lid, it was the lid temperature which gave the best thermodynamic values. Of course these conclusions assume that the temperature is uniform within the detector image and that no other perturbations are occurring to the system.

When the top is colder than the bottom the collection rate is affected not only by the gradient as described previously, but also by the nonequilibrium condition caused by condensation onto the colder top. Figure 7 shows the relationship between the thermodynamic properties of the system and those produced by a gradient. Notice that there are two groups of points. In changing the gradient within the upper group, the beam current changed in a regular way, but when the gradient was made greater than about 25°, the current suddenly began to drop and became fairly steady only after about 15 min. This is shown graphically in Figure 8 where the total gradient is plotted against ΔI. ΔI was obtained by taking the difference between the measured beam current and the

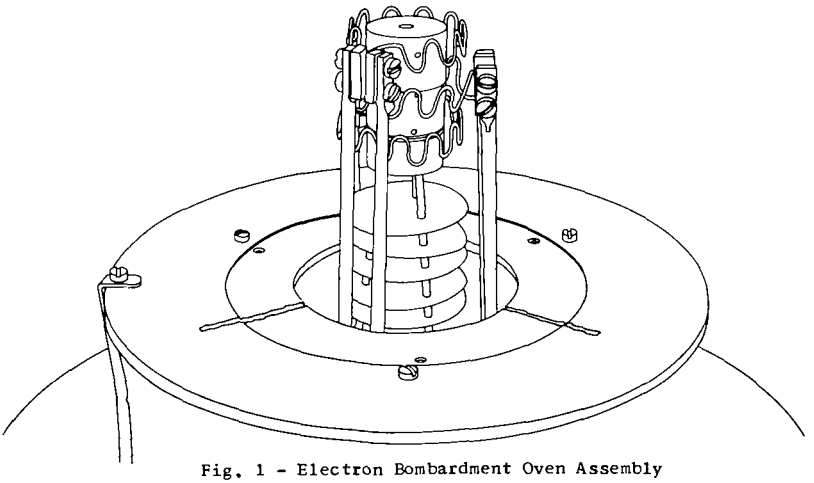

Fig. 1 - Electron Bombardment Oven Assembly

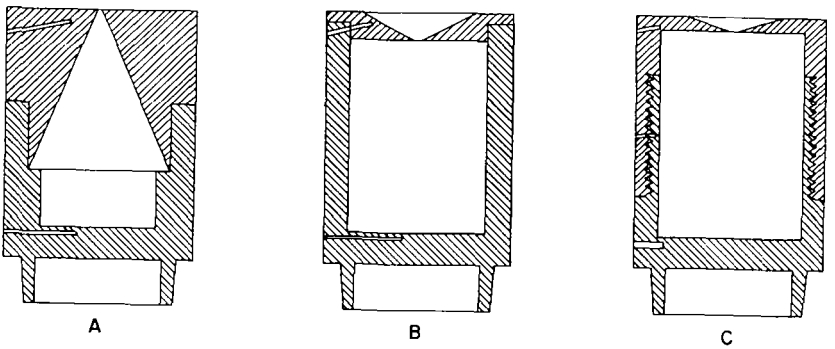

Fig. 2 - Crucible Designs

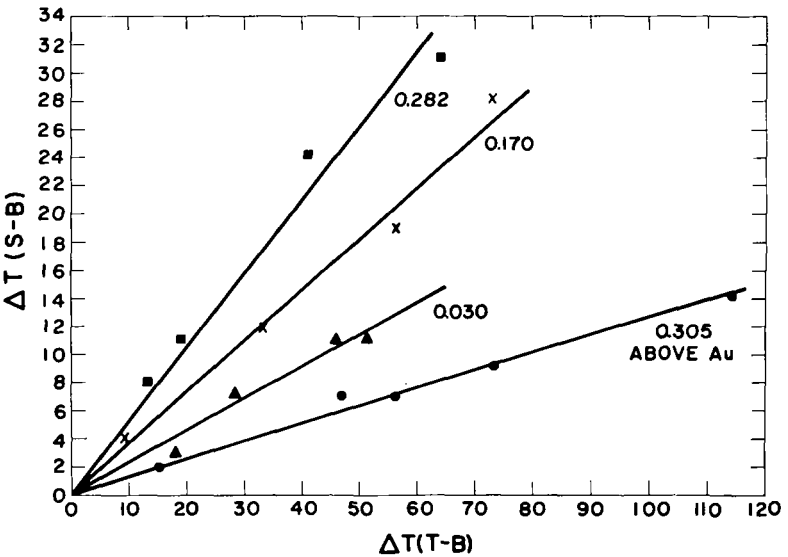

Fig. 5 - The Temperature Error Produced by Various Graphite Plugs.

current that would result if the gold had a temperature one would expect from the previously measured gradient effect. Thus, up to a ~25° gradient, the system behaves as one would expect. However, at high gradients the beam current drops drastically. Examination of the crucible showed a band of condensation covering about 1/2 of the cone length to within ~1 mm of the hole. This effect was not observed in all crucibles. In some cases the onset of condensation did not occur as abruptly and did not cover so large an area. When this happened, the change in beam current was not as pronounced. No difference was observed when the bottom was completely covered by gold. It can be concluded that so long as condensation does not take place within the crucible, the system behaves in the same way as described previously. However, as long as condensation is occurring, the collection rate will not be related uniquely to the sample temperature, but will depend, among other things, on the evaporation coefficient.

Some generalities are worth making at this point. In order to obtain the best data from a Knudsen cell, one should measure the temperature as near the source of vapor as practical and, if a gradient is unavoidable, the top should be hotter than the bottom. These are actually common sense rules that have been applied to most Knudsen measurements. However, one would want to know how much gradient to expect in an electron bombardment furnace such as that commonly used, and how much error this gradient would introduce. If a crucible is heated uniformly by electron bombardment there will be a tendency for the top to be hotter than the bottom. For a bare graphite crucible this can amount to as much as 50°. When the graphite was surrounded by a Ta crucible having ~1/16" walls, no observable gradient could be produced. A condition between these extremes will result if an unlined metal crucible of poor design is used. Furthermore, an interesting side light resulted when a crucible containing uranium was heated. After heating the crucible for ~10 min above 1800°C, the top filament was found to have become such a good emitter that its temperature had to be reduced substantially in order to keep a uniform temperature. Therefore, the nature of the material in the crucible can play a role. Also, when a current was drawn from the radiation shield the gradient was made worse, with the top hotter than the bottom. Although the gradient effect is fairly insensitive to the total temperature, the amount of the gradient was found to change with temperature, usually becoming worse as the temperature was increased.

The error that a gradient would introduce will depend on the crucible material and its design. For bare graphite, Figure 5 shows that a 30° gradient would create a 6-10° error in the measured temperature at about 1400°C. This error may not seem large, but since it will become greater as the temperature is raised, a significant error can be introduced into the second law heat of vaporization. As Büchler and Berkowitz-Mattuck (1) point out, a 15° change in the temperature error over a 150° range will produce a 10% error in ΔH. The use of a metal crucible, with its larger heat conductivity, will reduce this error.

The systems C-saturated U, UC_2 and VC, all in graphite, were examined and found to behave in essentially the same way as gold. The only difference being that when the top was made colder than the bottom no condensation was observed. In the case of liquid uranium, apparently most of the atoms striking the graphite top reacted to form UC or UC_2 no matter what the temperature. Thus, the observed pressure was unexpectedly low. One could view this situation as being one of chemical condensation.

Pressure measurements using Knudsen cells have become more common in the last few years and the resulting errors have been reduced as the technique has become better understood. This study shows that a major source of remaining error can be eliminated if the axial temperature gradient is reduced.

(1) A. Büchler and J. Berkowitz-Mattuck, J. Chem. Phys. 39, 296 (1963).

***Work done under the auspices of the U. S. Atomic Energy Commission at the Los Alamos Scientific Laboratory, University of California, Los Alamos, New Mexico.**

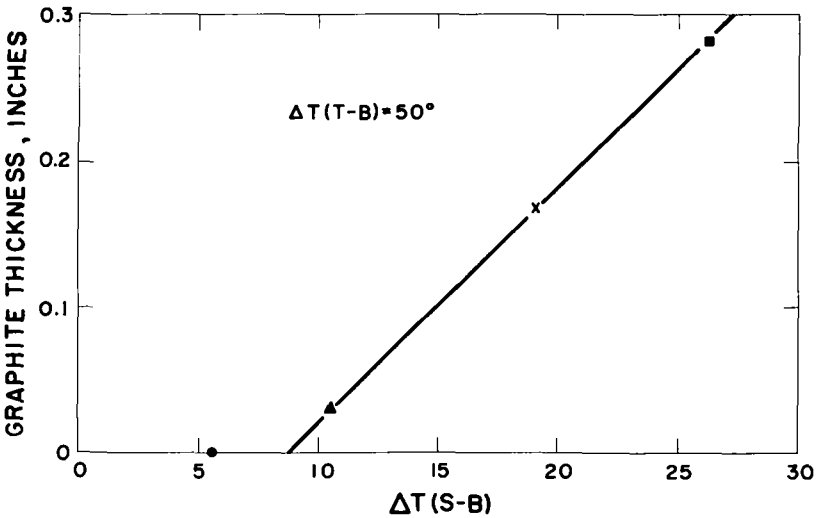

Fig. 6 - The Effect of Graphite Thickness on the Temperature Error

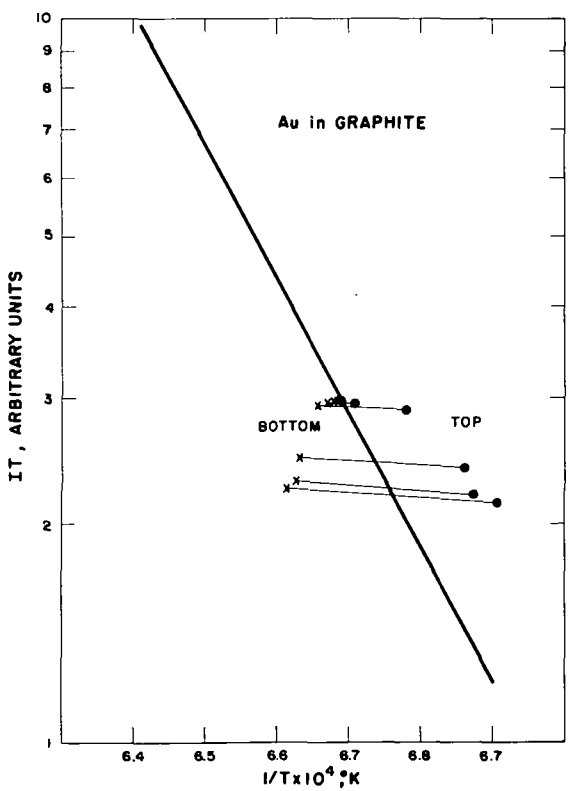

Fig. 7 - Relationship Between I/T and log IT with the Top colder than the Bottom

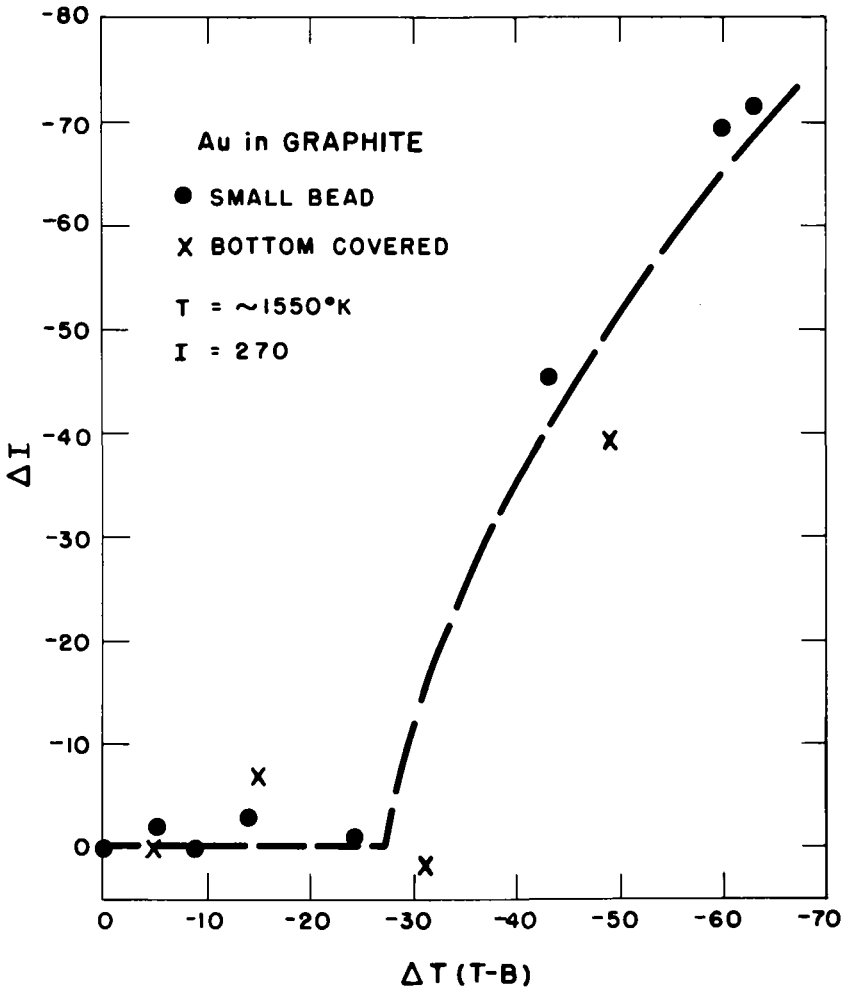

Fig. 8 - The Effect of Condensation on the Collection Rate.

MASS SPECTROMETRY AND THE PROPERTIES OF CONDENSED SYSTEMS AT HIGH TEMPERATURES

P. Breisacher
Aerospace Corporation
El Segundo, California

(Manuscript Withdrawn)

THE USE OF A MASS SPECTROMETER TO DEMONSTRATE THE EXISTENCE OF GASEOUS $Ba(OH)_2$*

R. S. Newbury, A. W. Searcy, and G. W. Barton, Jr.

Lawrence Radiation Laboratory, University of California
Livermore, California

A mass spectrometer has been modified to allow studies of solid-gas reactions at pressures up to several millimeters. This was accomplished by multiple differential pumping between the sample and the source regions. In a typical run, the pressures were: 2 mm at the sample, 10^{-5} mm around the sample container, and 10^{-6} – 10^{-7} mm in the source region.

The $BaO_{(s)} - H_2O_{(g)}$ system was studied using this instrument. The water vapor was introduced into a Knudsen-cell in the spectrometer up to pressures of a few millimeters. The ion most easily observed under these conditions was $BaOH^+$, but the technique of continuous averaging indicates that $Ba(OH)_{2(g)}$ is the parent molecule. This is in agreement with thermodynamic considerations.

---

*Work was performed under the auspices of the U. S. Atomic Energy Commission and the Department of Mineral Technology, College of Engineering, University of California at Berkeley, California.

A TWIN-CRUCIBLE STUDY OF THE LITHIUM FLUORIDE-BERYLLIUM FLUORIDE SYSTEM*

Alfred Büchler and James L. Stauffer
Arthur D. Little, Inc., Cambridge, Massachusetts

INTRODUCTION

The work described in this note forms part of a continuing investigation of the thermodynamics of light-metal compounds. The first study of the lithium fluoride-beryllium fluoride system was published by Berkowitz and Chupka,[1] who examined briefly a 50% LiF-50% BeF_2 composition and identified the mixed dimer $LiBeF_3(g)$. In the present work, the first composition examined was an LiF-BeF_2 melt saturated with LiF. Comparison of its mass spectrum with that of pure LiF showed that a large part of the Li^+ ion current in the mass spectrum of an LiF-BeF_2 mixture could be contributed by fragmentation of $LiBeF_3$, and thus could not be used as a measure of LiF activity. Careful comparative measurements at various compositions were found necessary for a satisfactory analysis of this system. In order to increase the reliability of such measurements, the twin-crucible source described in this paper was designed. This source permits the direct comparison, in a single experiment, of the mass spectra of the vapors above, say, a pure compound and a mixture. Using this crucible design it has been possible to obtain information concerning

1. the activities of LiF and BeF_2 in the solutions examined;
2. the fragmentation patterns of the mixed lithium-beryllium species $LiBeF_3$ and Li_2BeF_4;
3. the composition of the vapors;
4. the heats of formation of the mixed species.

The remainder of this paper will be devoted to the discussion of points 1 and 2.

EXPERIMENTAL

The instrument used in these experiments was a Nuclide Corporation 12" radius, 60°-sector high-temperature mass-spectrometer. The twin-crucible source was placed in the Knudsen cell section of the mass spectrometer. A schematic drawing of the source is shown in Figure 1. The assembly consists of 2 crucible chambers in a resistively heated block. The samples are contained in platinum cups, each of which has a thermocouple welded to its bottom. Another pair of thermocouples is located near the top of the oven chambers. The oven block can be moved from outside the vacuum chamber so that first one and then the other crucible is brought into the line of sight of the ion source entrance slit. In a typical experiment the crucible block is brought to temperature and mass spectra of first, say, the solution and then of the pure compound are obtained. The design was tested by placing pure lithium fluoride in both chambers. A log I^+T vs 1/T plot using data from the two crucibles, and using in each case the temperature given by the bottom thermometer (the temperature of the top being in general about 20° higher) gave a single straight line.

RESULTS

Fragmentation Pattern of Mixed Species

Data for three experiments are compared for a single temperature in Table I. The first set of data compares the mass spectrum of pure LiF with that of an LiF-BeF_2 melt in equilibrium with LiF. As can be seen from the table, Li^+, LiF^+ and Li_2F^+ ion intensities are higher in the mass spectrum of the vapor above the solution than in the mass spectrum of pure lithium fluoride. Since the lithium fluoride activity in the LiF-BeF_2 melt cannot be greater than that of pure LiF, the excess Li^+, LiF^+ and Li_2F^+

---

*This research was sponsored by the Advanced Research Projects Agency, U.S. Department of Defense, under Contract No. DA-19-020-ORD-5584, ARPA Order No. 40-62, monitored by U.S. Army Research Office.

ion current must be derived from the fragmentation of mixed lithium-beryllium species. That the differences observed are real is demonstrated by the data of Figure 2, which gives log I^+T vs 1/T plots for Li^+, Li_2F^+ and $Li_3F_2^+$. For both Li^+ and Li_2F^+ the points representing solution data fall above those representing pure LiF. In the case of the $Li_3F_2^+$ ion, however, there is only a single neutral precursor, the lithium fluoride trimer Li_3F_3; and in this case the points derived from the two crucibles fall on a single straight line. It is therefore reasonable to assign Li^+ and LiF^+ to the mixed dimer $LiBeF_3$, and Li_2F^+ to the mixed trimer Li_2BeF_4. This assignment is substantiated by the mass spectrum in the vapor above a 67% BeF_2-33% LiF solution (Table I, set 3). In this manner we obtain the fragmentation patterns of $LiBeF_3$ and Li_2BeF_4 shown in Table II. The very large degree of fragmentation of the mixed trimer should be noted.

TABLE II

FRAGMENTATION PATTERNS OF MIXED SPECIES

$LiBeF_3$:	Li^+	2.7
	$LiBeF_2^+$	1
	LiF^+	0.06
Li_2BeF_4:	Li_2F^+	32
	$Li_2BeF_3^+$	1

The fact that Li_2F^+ is the principal higher-polymer fragment supports the conclusion that the higher polymer is indeed the mixed trimer Li_2BeF_4 with the structure

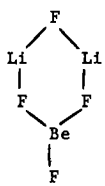

Activity Measurements

In Experiment 1, the LiF activity was set at unity through the use of a solution saturated with LiF. The BeF_2 activity in the LiF-saturated melt is given by the ratio of BeF_2^+ ion intensities in Experiment 2, where its mass spectrum is compared to the mass spectrum of pure BeF_2. The resultant BeF_2 activity is shown in Table III.

TABLE III

BeF_2-LiF SOLUTIONS, 604°C
ACTIVITIES (a) AND ACTIVITY COEFFICIENTS (γ)

	26% BeF_2-74% LiF		67% BeF_2-33% LiF	
	a	γ	a	γ
BeF_2	0.016	0.06	0.86	1.3
LiF	1	1	0.076	0.23

For LiF activities other than 1, a simple comparison does not work since the lithium fluoride ion intensities contain contributions of mixed-species fragment. However, the $LiBeF_3$ concentration may be used as a measurement of LiF activity. This has been done in Table III for the data of Experiment 3, where a 67% BeF_2-33% LiF melt was compared to pure BeF_2. For this composition nearly all the intensity of the lithium-containing

TABLE I

LiF-BeF_2 TWIN-CRUCIBLE EXPERIMENTS
MASS SPECTRA AT 604°C; ION CURRENTS IN ARBITRARY UNITS

	Experiment 1			Experiment 2		Experiment 3	
	Crucible 1	Crucible 2	Contribution of Mixed Species	Crucible 1	Crucible 2	Crucible 1	Crucible 2
	LiF(c)	26% BeF_2-74% LiF solution + LiF(c)		26% BeF_2-74% LiF solution + LiF(c)	$BeF_2(\ell)$	$BeF_2(\ell)$	67% BeF_2-33% LiF solution
BeF_2^+	.	36		37	2200	2100	1800
$Be_2F_3^+$	.	-		-	(1.7)	1.9	1.4
$LiBeF_2^+$	.	2.1		2.3	.	.	8
$Li_2BeF_3^+$	.	0.015		-	.	.	-
Li^+	0.20	5.4	(5.2)	5.4	.	.	24
LiF^+	0.18	0.30	(0.12)	-	.	.	0.5
Li_2F^+	0.32	0.80	(0.48)	0.86	.	.	0.23
$Li_3F_2^+$	0.019	0.019	(0)	-	.	.	-

ion species derives from mixed lithium-beryllium compounds. The activity a_{LiF} was obtained by means of the equilibrium constant

$$K = \frac{(LiF)(BeF_2)}{(LiBeF_3)}$$

evaluated in the form

$$K^* = \frac{a_{LiF}\, I^+_{BeF_2^+}}{I^+_{LiBeF_2^+}}$$

For a given temperature K* can be evaluated from the data of Experiment 1, for which $a_{LiF} = 1$. The values of a_{LiF} at other concentrations can then be derived from the BeF_2^+ and $LiBeF_2^+$ ion intensities.

Table III shows that the LiF-BeF_2 system is highly non-ideal. The BeF_2 activity coefficient goes from less than 0.1 to greater than 1 in a concentration range from 26 to 67% BeF_2. In particular, it may be noted that the vapor pressure over the 26% solution is less than 0.1 of the vapor pressure which would be obtained for an ideal solution, and that possibly as much as 15% of the vapor is contributed by the mixed dimer $LiBeF_3$. These results, as well as the fragmentation patterns shown in Table II, demonstrate the care which must be exercised if the correct vapor composition and activities are to be derived from the mass spectra of mixed systems.

REFERENCE

1. J. Berkowitz and W. A. Chupka, Annals N. Y. Acad. Sci. 79, 1073 (1960).

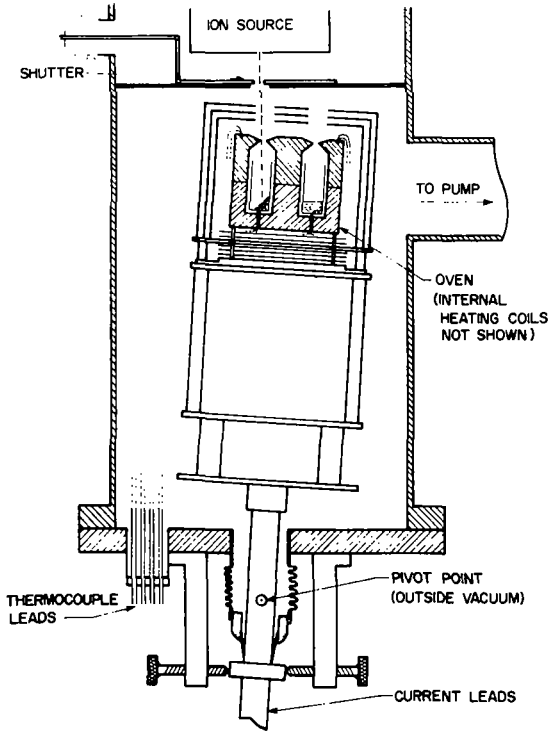

FIGURE 1 TWIN CRUCIBLE SOURCE ASSEMBLY

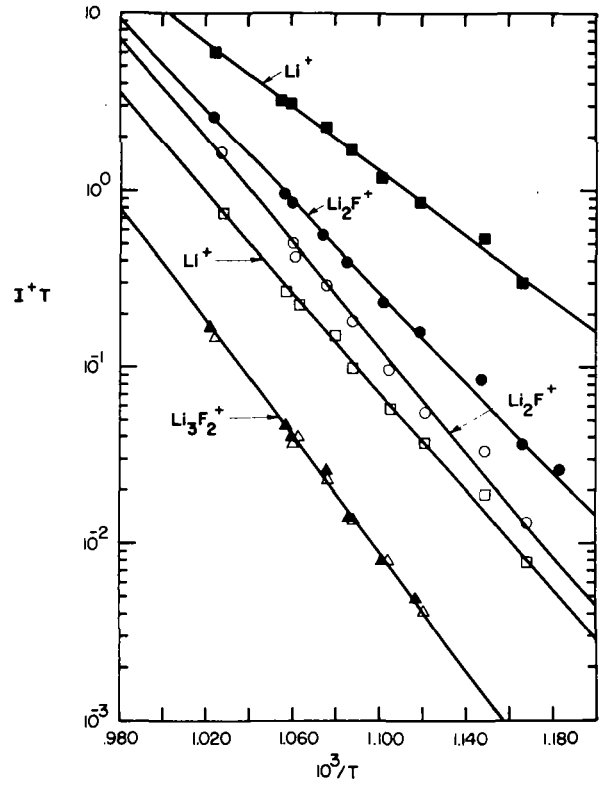

FIGURE 2 TWIN CRUCIBLE EXPERIMENT
OPEN SYMBOLS — LIF (c) PURE,
FULL SYMBOLS — LIF (c) + LIF - BeF_2 MELT,

Bibliography of Published and Unpublished Papers on Mass Spectrometry for 1963

The following pages were prepared by Subcommittees II, III, and V as part of the Annual Report of Subcommittees, covering activities in their fields of interest. As was done in previous years, these bibliographies are included with the papers to provide a broader and more useful distribution of such information. In the present list, no specific attempt has been made to avoid multiple listings of papers of interest in several fields.

1963 (and early 1964) Bibliography

Fundamental and Theoretical Aspects of Mass Spectrometry

Prepared by Subcommittee 2

Ionization and Appearance Potentials---------- R.W. Kiser

Gaseous Negative Ions ---------- B. Steiner and N. Wells

Photoionization and Related Studies---------- V.H.Dibeler and R.M.Reese

Charge Exchange ---------- B.Steiner and N.Wells

Ion Molecule Reactions---------- B.Steiner and N.Wells

Inelastic Electron Scattering and
Recombination ---------- B.Steiner and N.Wells

Inelastic Heavy Particle Collisions ---------- B.Steiner and N.Wells

Elastic Scattering ---------- B.Steiner and N.Wells

Free Radicals and Chemical Kinetics---------- J.T.Herron

Isotopic Abundance ---------- E.J.Catanzaro

Miscellaneous and Addenda---------- H.M.Rosenstock

In all references, where no date is given the year is 1963.

IONIZATION AND APPEARANCE POTENTIALS

Robert W. Kiser

(Review was completed 30 April 1964)

1. Ackermann, R.J., Rauh, E.G., and Thorn, R.J., J. Chem. Phys., 40, 883 (1964). THERMODYNAMIC PROPERTIES OF GASEOUS YTTRIUM MONOXIDE. CORRELATION OF BONDING IN GROUP III TRANSITION-METAL MONOXIDES.

2. Altenburg, K., Z. Phys. Chem. (Leipzig), 219, 271 (1962). IONIZATION POTENTIALS OF BRANCHED ALKANES.

3. Asundi, R.K., Craggs, J.D., and Kurepa, M.V., Proc. Phys. Soc. (London), 82, 967 (1963). ELECTRON ATTACHMENT AND IONIZATION IN OXYGEN, CARBON MONOXIDE AND CARBON DIOXIDE.

4. Asundi, R.K. and Kurepa, M.V., J. Electron Control, 15, 41 (1963). IONIZATION CROSS SECTIONS IN He, Ne, Ar, Kr AND Xe BY ELECTRON IMPACT.

5. Asundi, R.K. and Kurepa, M.V., J. Sci. Instr. 40, 183 (1963). THE CALIBRATION OF THE ELECTRON ENERGY SCALE FOR IONIZATION POTENTIAL MEASUREMENTS.

6. Babeliowsky, T.P.J.H., Physica, 28, 1160 (1962). MASS SPECTROMETRIC DETERMINATION OF THE HEAT OF VAPORIZATION OF SOME SOLID ELEMENTS.

7. Babeliowsky, T.P.J.H., Boerboom, A.J.H., and Kistemaker, J., Physica, 28, 1155 (1962). MASS SPECTROMETRIC DETERMINATION OF THE HEAT OF VAPORIZATION OF CaO.

8. Baker, C.E., McGuire, J.M., and Muschlitz, E.E., J. Chem. Phys. 37, 2571 (1962). LOW-ENERGY COLLISION CROSS SECTIONS OF H^- and OH^- IONS IN OXYGEN.

9. Baker, F.S. and Brink, G.O., U.S. At. Energy Comm., UCRL-7087 (1962). 52 pp. IONIZATION OF ALKALI ATOMS BY ELECTRON BOMBARDMENT.

10. Basila, M.R. and Clancy, D.J., J. Phys. Chem. 67, 1551 (1963). THE IONIZATION POTENTIALS OF MONOSUBSTITUTED PYRIDINES BY ELECTRON IMPACT.

11. Becker, R.S. and Wentworth, W.E., J. Am. Chem. Soc., 85, 2210 (1963). ELECTRON AFFINITIES AND IONIZATION POTENTIALS OF AROMATIC HYDROCARBONS.

12. Berkowitz, J. and Chupka, W.A., J.Chem. Phys., 40, 287 (1964). VAPORIZATION PROCESSES INVOLVING SULFUR.

13. Berkowitz, J. and Marquart, J.R., J. Chem. Phys., 39, 275 (1963). EQUILIBRIUM COMPOSITION OF SULFUR VAPOR.

14. Bernecker, R.R., Doctoral Dissertation, Cornell University, 1962. MASS SPECTRA STUDIES OF MOLECULAR ION DECOMPOSITIONS OF SIMPLE ESTERS AND ACIDS.

15. Bernecker, R.R. and Long, F.A., J. Chem. Phys., 39, 253 (1963). REARRANGEMENT PROCESSES FOR FORMING OXONIUM IONS FROM ALIPHATIC ESTER IONS.

16. Berthelot, C., J. Phys. Radium, 23, 447 (1962). IONIZATION POTENTIAL AND NUCLEAR MAGNETIC MOMENTS OF PLUTONIUM.

17. Bibby, M.M. and Carter, G., Trans. Faraday Soc., 59, 2455 (1963). IONIZATION AND DISSOCIATION IN SOME FLUOROCARBON GASES.

18. Bishop, D.M., J. Chem. Phys. 40, 432 (1964). STABILITY OF THE AMMONIUM RADICAL (NH_4).

19. Blaise, J. and Vetter, R., Compt. Rend., 256, 630 (1963). DETERMINATION OF THE IONIZATION POTENTIAL OF THULIUM FROM ARC SPECTRA.

20. Blue, G.D., Doctoral Dissertation, University of Wisconsin, 1963. 149 pp. MASS SPECTROMETRIC STUDIES OF THE STABILITIES OF GASEOUS ALKALINE EARTH MONOFLUORIDES.

21. Blue, G.D., Green, J.W., Bautista, R.G., and Margrave, J.L., J. Phys. Chem., 67, 877 (1963). THE SUBLIMATION PRESSURE OF CALCIUM (II) FLUORIDE AND THE DISSOCIATION ENERGY OF CALCIUM (I) FLUORIDE.

22. Botter, R., Advances in Mass Spectrometry, vol.2, edited by R.M. Elliott, Pergamon Press, England, 1963. pp. 540-554. CARBON SUB-OXIDE.

23. Brion, C.E. and Dunning, W.J., Trans. Faraday Soc. 59, 647 (1963). ELECTRON IMPACT STUDIES OF SIMPLE CARBOXYLIC ESTERS.

24. Boudreaux, E.A., J. Chem. Phys., 40, 246 (1964). ELECTRONIC STRUCTURE AND SPECTRUM OF XeF_4. A SEMIEMPIRICAL MO TREATMENT.

25. Burns, J.F., Nature, 192, 651 (1961). EXPERIMENTAL DETECTION OF AUTOIONIZING TRANSITIONS IN KRYPTON BY ELECTRON IMPACT.

26. Burns, R.P., DeMaria, G., Drowart, J., Inghram, M.G., J. Chem. Phys., 38, 1035 (1963). MASS SPECTROMETRIC INVESTIGATION OF THE VAPORIZATION OF In_2O_3.

27. Chelobov, F.N., Dubov, S.S., Tikhomirov, M.V., and Dobrovitskii, M.I., Dokl. Akad. Nauk S.S.S.R., 151, 631 (1963). IONIZATION AND DISSOCIATION OF HEXAFLUOROPROPYLENE BY ELECTRONS OF VARIOUS ENERGY.

28. Colin, R. and Drowart, J., J. Phys. Chem. 68, 428 (1964). THERMODYNAMIC STUDY OF GERMANIUM MONOTELLURIDE USING A MASS SPECTROMETER.

29. Collin, J.E., Colloq. Spectros. Intern. 9th, Lyons, 3, 596 (1961). (Publ. 1962). IONIZATION AND DISSOCIATION OF METHANE, METHYLAMINE, AND METHYL ALCOHOL BY MONOENERGETIC ELECTRONS.

30. Collin, J.E., Bull. Soc. Chim. Belges, 71, 15 (1962). IONIZATION AND DISSOCIATION OF MOLECULES BY MONOENERGETIC ELECTRONS.

31. Collin, J.E., Can. J. Chem., 40, 2172 (1962). THE FRANCK-CONDON PRINCIPLE AND THE IONIZATION OF MOLECULES.

32. Collin, J., Ind. Chim. Belge, 28, 943 (1963). STUDY OF THE IONIZATION AND EXCITATION OF MOLECULES BY MASS SPECTROMETRY.

33. Collin, J. E., Bull. Soc. Roy. Sci. Liege, 32, 133 (1963). IONIZATION AND DISSOCIATION OF ETHYL NITRATE UNDER ELECTRON IMPACT, AND THE IONIZATION POTENTIAL OF NITROGEN DIOXIDE.

34. Craggs, J.D. and Meek, J.M., Gas Discharge Elec. Supply Ind., Proc. Intern. Conf., Leatherhead, Surrey, Engl., 1962, 338. ELECTRICAL DISCHARGES IN SULFUR HEXAFLUORIDE.

35. Cubiciotti, D., J. Phys.Chem. 67, 1385 (1963). MASS SPECTROMETRIC STUDY OF THE VAPORS OVER BISMUTH-SULFUR MELTS.

36. Curran, R.K., J. Chem. Phys., 38, 2974 (1963). MASS SPECTROMETER INVESTIGATION OF ELECTRON-IMPACT PROCESSES AT PRESSURES TO 1 mm Hg.

37. Dibeler, V.H. and Rosenstock, H.M., J. Chem. Phys. 39, 3106 (1963). MASS SPECTRA AND METASTABLE TRANSITIONS OF H_2S, HDS and D_2S.

38. Dolejsek, Z., Hanus, V. and Prinzbach, H., Angew.Chem., 74, 902 (1962). MASS SPECTROMETRIC BEHAVIOR OF QUADRICYCLENE.

39. D'Or, L. Momigny, J. and Natalis, P., Advances in Mass Spectrometry, vol. 2, edited by R.M. Elliott, Pergamon Press, Oxford, England, 1963. pp. 370-376. MASS SPECTRA AND GEOMETRICAL ISOMERISM.

40. Dorman, F.H. and Morrison, J.D., J. Chem.Phys., 39, 1906 (1963). IONIZATION POTENTIALS OF DOUBLY CHARGED OXYGEN AND NITROGEN.

41. Earnshaw, D.G., Cook, G.L. and Dinneen, G. U., J. Phys. Chem., 68, 296 (1964). A STUDY OF SELECTED IONS IN THE MASS SPECTRA OF BENZENETHIOL AND DEUTERATED BENZENETHIOL.

42. Ehlet, T. C., Doctoral Dissertation, University of Wisconsin, 1963. MASS SPECTROMETRIC STUDIES AT HIGH TEMPERATURE.

43. Erikson, K.B.S. and Isberg, H.B.S., Arkiv Fysik, 23, 527 (1963). THE SPECTRUM OF ATOMIC ALUMINUM, Al(I).

44. Fehlner, T.P. and Koski, W.S., J. Am. Chem. Soc. 85, 1905 (1963). FRAGMENTATION OF TETRABORANE BY ELECTRON IMPACT.

45. Fehlner, T.P. and Koski, W.S., J. Am. Chem. Soc., 86, 581 (1964). THE FRAGMENTATION OF SOME BORON HYDRIDES BY ELECTRON IMPACT.

46. Fiquet-Fayard, F., J. Chim. Phys. 59, 439 (1962). MULTIPLE IONIZATION OF ARGON BY ELECTRON IMPACT OF C-500 v.

47. Fiquet-Fayard, F. and Lahmani, M., J. Chim. Phys., 59, 1050 (1962). AUGER EFFECT IN MULTIPLE IONIZATION OF ARGON POTASSIUM AND CALCIUM BY ELECTRON IMPACT.

48. Fiquet-Fayard, F. and Ziesel, J.P., Compt. Rend., 256, 4885 (1963). MULTIPLE IONIZATION OF ZINC BY ELECTRON (0-500v.)

49. Fischler, J. and Halmann,M., J. Chem. Soc., 1964, 31. ELECTRON IMPACT STUDIES OF PHOSPHORUS COMPOUNDS.

50. Fisher, I.P. and Lossing, F.P., J. Am. Chem. Soc., 85, 1018 (1963). IONIZATION POTENTIAL OF BENZYNE.

51. Fisher, I.P. and Lossing, F.P., presented before the 11th Annual Conference on Mass Spectrometry and Allied Topics, ASTM Committee E-14, San Francisco, California, May 19-24, 1963. RELATION BETWEEN IONIZATION POTENTIAL AND ELECTRONEGATIVITY IN ISOELECTRONIC FREE RADICALS.

52. Foffani, A., Pignataro, S., Cantone, B. and Grasso, F., Nuovo Cimento, 29, 918 (1963). MASS SPECTRA OF DIAZO COMPOUNDS. I. DIAZOCARBONYL COMPOUNDS.

53. Gerdzhikov, D., Compt. Rend. Acad. Bulgare Sci., 15, 621 (1962). CORRELATION BETWEEN IONIZATION POTENTIAL AND POLARIZATION COEFFICIENT OF ATOMS OF RARE GASES.

54. Gillis, R.G. and Occolowitz, J.L., J. Org. Chem., 28, 2924 (1963). ISOCYANIDES. III. ELECTRON IMPACT STUDY OF ALIPHATIC ISOCYANIDES.

55. Glick, R.E. and Llewellyn, J.A., presented before the 11th Annual Conference on Mass Spectrometry and Allied Topics, ASTM Committee E-14, San Francisco, California, May 19-24, 1963. IONIZATION CROSS SECTIONS.

56. Gowenlock, B.G., Kay, J. and Majer, J.R., Trans. Faraday Soc., 59, 2463 (1963). ELECTRON IMPACT STUDIES OF SOME SULFIDES AND DISULFIDES.

57. Hagemann, R., Compt. Rend., 255, 899 (1962). MASS SPECTROMETRIC STUDY OF S_2O.

58. Hagemann, R., Compt. Rend., 255, 1102 (1962). DETERMINATION OF THE HEAT OF FORMATION OF S_2O by MASS SPECTROMETRY.

59. Hanus, V. and Dolejsek, Z., Coll. Czech. Chem. Comm., 28, 652 (1963). SOME EXPERIMENTAL DATA RELATED TO THEORIES OF THE ORIGIN OF MASS SPECTRA.

60. Hassan, G.E.M.A., Physica, 29, 1119 (1963). THE ATOMIC SPECTRUM OF NEODYMIUM. I. PRELIMINARY ANALYSIS AND IONIZATION POTENTIAL OF Nd (I).

61. Hildenbrand, D.L., Theard, L.P. and Saul, A.M., J. Chem. Phys., 39, 1973 (1963). TRANSPIRATION AND MASS SPECTROMETRIC STUDIES OF EQUILIBRIA INVOLVING BOF(g) AND $(BOF)_3(g)$.

62. Hobrock, B.G., Doctoral Dissertation, Kansas State University, 1963. MASS SPECTROMETRIC INVESTIGATIONS OF ORGANIC MONO-, DI-, AND TRI-SULFIDES.

63. Hobrock, B.G. and Kiser, R.W., J.Phys. Chem., 67, 648 (1963). ELECTRON IMPACT INVESTIGATIONS OF SULFUR COMPOUNDS. II. 3-METHYL-2-THIABUTANE, 4-THIA-1-PENTENE, AND 3,4-DITHIAHEXANE.

64. Hobrock, B.G. and Kiser, R.W., J. Phys. Chem., 67, 1283 (1963). ELECTRON IMPACT INVESTIGATIONS OF SULFUR COMPOUNDS. III. 2-THIAPROPANE, 3-THIAPENTANE, AND 2,3,4-TRITHIAPENTANE.

65. Hobrock, B.G., Shenkel, R.C. and Kiser, E.W., J. Phys. Chem., 67, 1684 (1963). SINGLY-AND DOUBLY -CHARGED IONS FROM METHYL AND ETHYL ISOTHIOCYANATES BY ELECTRON IMPACT.

66. Hobrock, D.L. and Kiser, R.W. J. Phys. Chem., 68, 575 (1964). ELECTRON IMPACT STUDIES OF SOME TRIHALOMETHANES. TRICHLOROMETHANE, DICHLOROFLUOROMETHANE, CHLORODIFLUOROMETHANE, AND TRIFLUOROMETHANE.

67. Humphries, C.M., Walsh, A.D. and Warsop, P.A., Discussions Faraday Soc., 35, 148 (1963). ABSORPTION SPECTRA OF THE HYDRIDES, DEUTERIDES AND HALIDES OF GROUP 5 ELEMENTS.

68. James, L.H. and Carter, G., J. Electron Control, 13, 213 (1962). MASS SPECTROMETRIC STUDY OF IONIZATION AND DISSOCIATION BY ELECTRON IMPACT OF PERFLUOROMETHYLCYCLOHEXANE.

69. Junk, G. and Svec, H., J. Am. Chem. Soc., 85, 839 (1963). THE MASS SPECTRA OF -AMINO ACIDS.

70. Kaneko, Y. and Kanomata, I., J. Phys. S c. Japan, 18, 1822 (1963). SINGLE AND DOUBLE IONIZATION OF CALCIUM BY ELECTRON IMPACT.

71. Kaufman, J.J., J. Am. Chem. Sec., 85, 1576 (1963). THE EFFECT OF SUBSTITUTION ON THE IONIZATION POTENTIALS OF FREE RADICALS AND MOLECULES. II. THEORETICAL INTERPRETATION OF $_K$ VALUES FOR ALKYL RADICALS AND AMINES.

72. Kaufman, J.J., Koski, W.S., Kuhns, L.J., and Wright, S.S., J. Am. Chem. Soc., 85, 1369 (1963). APPEARANCE AND IONIZATION POTENTIALS OF SELECTED FRAGMENTS FROM ISOTOPICALLY LABELED PENTABORANES.

73. Kennedy, A. and Colburn, C.B., J. Chem. Phys., 35, 1892 (1961). STRENGTH OF THE N-F BONDS IN NF_3 AND OF N-F and N-N BONDS IN N_2F_4.

74. Khvostenko, V.I., Zh. Fiz. Khim., 36, 384 (1962). IONIZATION OF THIOPHENE AND SOME OF ITS DERIVATIVES BY ELECTRON IMPACT.

75. Krauss, M. and Dibeler, V.H., in Mass Spectrometry of Organic Ions, edited by F.W. McLafferty, Academic Press, New York, 1963. pp. 117-161. APPEARANCE POTENTIAL DATA OF ORGANIC MOLECULES.

76. Krishna, V.G. and Chowdhury, M., J. Phys. Chem., 67, 1067 (1963). CHARGE TRANSFER INTERACTION BETWEEN IODINE AND AZINES: IONIZATION POTENTIALS OF AZINES.

77. Kuppermann, A. and Raff, L.M., Discussions Faraday Soc., 35, 30 (1963). ELECTRON-IMPACT SPECTROSCOPY.

78. Kupriyanov, S.E., Zh. Fiz. Khim., 36, 218 (1962). DISSOCIATION OF EXCITED IONS.

79. Kupriyanov, S.E. and Latypov, Z.Z., Zh. Eksperim. i Teoret. Fiz., 45, 815 (1963). IONIZATION OF POSITIVE IONS BY ELECTRONS.

80. Larin, N.V., Devyatykh, G.G. and Agafonov, I.L.,Zh. Neorgan.Khim., 9, 205 (1964). MASS SPECTRA FOR PHOSPHINE AND ARSINE.

81. Lifshitz, C. and Bauer, S.H., J.Phys. Chem., 67, 1629 (1963). MASS SPECTRA OF VALENCE TAUTOMERS.

82. Lifshitz, C. and Long, F.A., J. Phys. Chem., 67, 2463 (1963). APPEARANCE POTENTIALS AND MASS SPECTRA OF FLUORINATED ETHYLENES. I. DECOMPOSITION MECHANISMS AND THEIR ENERGETICS.

83. Majer, J.R., in Advances in Fluorine Chemistry, vol. 2, edited by M. Stacey, J.C. Tatlow and A.G. Sharpe, Butterworths, London, 1961. pp. 55-103. MASS SPECTROMETRY OF FLUORINE COMPOUNDS.

84. Majer, J.R. and Patrick, C.R., Nature, 193, 161 (1962). IONIZATION POTENTIALS OF PERFLUOROCYCLOALKANES.

85. Majer, J.R. and Patrick, C.R., in Advances in Mass Spectrometry, vol. 2, edited by R.M. Elliott, Pergamon Press, Oxford, England, 1963. pp. 555-559. ELECTRON IMPACT STUDIES ON AROMATIC HALOGEN COMPOUNDS.

86. Majer, J.R. and Patrick, C.R., Trans. Faraday Soc., 59, 1274 (1963). APPEARANCE POTENTIALS OF THE BENZOYL RADICAL-ION.

87. Maksimova, I.N., Zh. Strukt. Khim., 3, 208 (1962). IONIZATION POTENTIALS AND HEATS OF FORMATION OF COMPOUNDS.

88. Mann, J.B., J. Chim. Phys., 40, 1632 (1964). IONIZATION OF U, UO and UO_2 BY ELECTRON IMPACT.

89. Marquart, J.R. and Berkowitz, J., J. Chem. Phys., 39, 283 (1963). DISSOCIATION ENERGIES OF SOME METAL SULFIDES.

90. Maslov, P.G. Proc. Intern. Meeting Mol. Spectry., 4th, Bologna, 1959, 1, 266 (Publ. 1962). APPLICATION OF THE ADDITIVE STATISTICAL METHOD FOR THE STUDY OF FLUORESCENT AND ABSORPTION SPECTRA.

91. McGowan, J.W. and Kerwin, L., Can. J. Phys., 41, 1535 (1963). METASTABLE Ar^+ IONS NEAR THE Ar^{++} THRESHOLD.

92. Momigny, J., Bull. Soc. Chim. Belges, 70, 291 (1961). RATE CONSTANTS FOR THE DECOMPOSITION OF METASTABLE POLYATOMIC IONS.

93. Momigny, J., Nature, 191, 1089 (1961). IONIZATION POTENTIALS OF cis- AND trans-DICHLORO- AND -DIBROMO-ETHYLENES.

94. Momigny, J., Brakier, L. and D'Or, L., Bull. Classe Sci., Acad. Roy. Belg., 48, 1002 (1962). COMPARISON OF THE EFFECT OF ELECTRON IMPACT ON BENZENE AND ON ITS OPEN CHAIN ISOMERS.

95. Momigny, J. and Wirtz-Cordier, A.M., Ann. Soc. Sci. Bruxelles, Ser. I., 76, 164 (1962). ELECTRON IMPACT ON DIHALOGENATED DERIVATIVES OF BENZENE.

96. Morrison, J.D., J. Chem. Phys., 39, 200 (1963). THE OPTIMUM USE OF IONIZATION-EFFICIENCY DATA.

97. Muccini, G.A., Hamill, W.H. and Barker, R., J. Phys. Chem., 68, 261 (1964). METASTABLE IONS IN MASS SPECTROMETRY.

98. Natalis, P., Bull. Soc. Chim. Belges, 72, 264 (1963). THE BEHAVIOR OF GEOMETRICAL ISOMERS UNDER ELECTRON IMPACT. I. THE cis- AND trans-DECALINS.

99. Natalis, P., Nature, 200, 881 (1963). EFFECT OG GEOMETRICAL ISOMERISM ON THE BEHAVIOR OF cis- AND trans- HEXAHYDROINDANS UNDER ELECTRON IMPACT.

100. Neale, R.S., J. Phys. Chem., 68, 143 (1964). A CORRELATION OF BOND DISSOCIATION ENERGY WITH IONIZATION POTENTIAL AND ELECTRON AFFINITY.

101. Newton, A.S., J. Chem. Phys., 40, 607 (1964). TRIPLE IONIZATION IN SMALL MOLECULES.

102. Newton, A.S. and Sciamanna, A.F., J. Chem. Phys., 40, 718 (1964). METASTABLE STATE OF THE DOUBLY CHARGED CARBON DIOXIDE ION.

103. Nikitin, O.T. and Akishin, P.A., Dokl. Akad. Nauk S.S.S.R., 145, 1294 (1962). DETERMINATION OF THE HEAT OF EVAPORATION OF BORON OXIDE BY MASS SPECTROMETRY.

104. Norman, J.H., Staley, H.G. and Bell, W.E., J. Phys. Chem., 68, 662 (1964). MASS SPECTROMETRIC STUDY OF GASEOUS OXIDES OF RHODIUM AND PALLADIUM.

105. Olmsted, J.A., U.S. At. Energy Comm. UCRL-10687 (1963). 127 pp. FORMATION OF ENERGETIC FRAGMENT IONS BY BOMBARDMENT OF ORGANIC MOLECULES WITH SLOW ELECTRONS.

106. Olmsted, J. III., Street, K. Jr., and Newton, A.S., J. Chem. Phys., 40, 2114 (1964). EXCESS-KINETIC-ENERGY IONS IN ORGANIC MASS SPECTRA.

107. Palmer, T.F. and Lossing, F.P., J. Am. Chem. Soc., 84, 4661 (1962). FREE RADICALS BY MASS SPECTROMETRY. XXVIII. THE HS, CH_3S, AND PHENYL-S RADICALS: IONIZATION POTENTIALS AND HEATS OF FORMATION.

108. Palmer, T.F. and Lossing, F.P., J. Am.Chem. Soc., 85, 1733 (1963). FREE RADICALS BY MASS SPECTROMETRY. XXX. IONIZATION POTENTIALS OF ANILINO-AND 2-, 3- AND 4-PYRIDYLMETHYL RADICALS.

109. Paulett, G.S, and Ettinger, R., J. Chem. Phys., 39, 825 and 3535 (1963). MASS SPECTRA AND APPEARANCE POTENTIALS OF DIAZIRINE AND DIAZOMETHANE.

110. Polyakova, A.A., Khmel'nitskii, R.A. and Petrov, A.A., Zh. Obshch. Khim., 33, 2518 (1963). MASS SPECTRA AND STRUCTURES OF ORGANIC COMPOUNDS. VIII. MASS SPECTRA OF SOME ALLENE HYDROCARBONS WITH A tert-BUTYL RADICAL.

111. Pottie, R.F. and Lossing, F.P., J. Am. Chem. Soc., 85, 269 (1963). FREE RADICALS BY MASS SPECTROMETRY. XXIX. IONIZATION POTENTIALS OF SUBSTITUTED CYCLOPENTADIENYL RADICALS.

112. Prophet, H., J. Chem. Phys., 38, 2345 (1963). HEAT OF FORMATION OF METHYLENE.

113. Reynolds, F.L., J. Chem. Phys., 39, 1107 (1963). IONIZATION ON TUNGSTEN SINGLE-CRYSTAL SURFACES.

114. Sazhinov, Yu.G. and Kupriyanov., S.E., Zh. Fiz. Khim., 36, 1969 (1962). EXCITATION OF IONS FORMED IN THE IONIZATION OF MOLECULES BY ELECTRONS.

115. Schexnayder, G.J., N.A.S.A. Tech. Note TN-D-1791 (1963). 62 pp. TABULATED VALUES OF BOND IDSSOCIATION ENERGIES, IONIZATION POTENTIALS, AND ELECTRON AFFINITIES FOR SOME MOLECULES FOUND IN HIGH-TEMPERATURE CHEMICAL REACTIONS.

116. Shchukarev, S.A., Semenov, G.A., Frantseva, K.E., Izv. Vysshikh Uchebn. Zavedenii, Khim. i Khim. Tekhnol., 5, 691 (1962). MASS SPECTROMETRIC INVESTIGATION OF NbO EVAPORATION.

117. Sholette, W.P. and Porter, R.F., J. Phys. Chem., 67, 177 (1963). MASS SPECTROMETRIC STUDY OF HIGH TEMPERATURE REACTIONS IN THE BORON-HYDROGEN-OXYGEN SYSTEM.

118. Sjogren, H. and Lindholm, E., Phys. Rev. Letters, 4, 85 (1963). HIGHER IONIZATION POTENTIALS IN ALCOHOLS AND WATER MEASURED BY ELECTRON IMPACT.

119. Stevens, M.R., presented before the 11th Annual Conference on Mass Spectrometry and Allied Topics, ASTM Committee E-14, San Francisco, California, May 19-24, 1963. IONIZATION POTENTIAL STUDY OF HIGH MOLECULAR WEIGHT COMPOUNDS.

120. Svec. H.J. and Flesch, G.D., Science, 142, 954 (1963). THERMO-CHEMICAL PROPERTIES OF XENON DIFLUORIDE AND XENON TETRAFLUORIDE FROM MASS SPECTRA.

121 Thrush, B.A. and Zwolenik, J.J., Discussions Faraday Soc., 35, 196 (1963). SPECTRUM OF THE TROPYL RADICAL.

122. Tunitskii, N.N., Kupriyanov, S.E. and Perov, A.A., Izv. Akad. Nauk S.S.S.R., Otdel. Khim. Nauk, 1962, 1945. THE MASS SPECTRA OF MOLECULES AND RADIATION CHEMISTRY.

123. Utterback, N.G., Phys. Rev., 129, 219 (1963). IONIZATION OF NITROGEN AND OXYGEN MOLECULES BY NITROGEN AND OXYGEN MOLECULES.

124. Van Raalte, D. and Harrison, A.G., Can. J. Chem., 41, 2054 (1963). IONIZATION AND DISSOCIATION OF FORMATE ESTERS BY ELECTRON IMPACT.

125. Van Raalte, D. and Harrison, A.G., Can. J. Chem., 41, 3118 (1963). ENERGETICS AND MECHANISM OF HYDRONIUM ION FORMATION BY ELECTRON IMPACT.

126. Vedeneev, V.I., Gurich, L.V., Kondrat'ev, V.N., Medvedev, V.A., and Frankevich, E.L., Published by the Academy of Science, Institute of Chemical Physics, U.S.S.R., Moscow, 1962. 215 pp. DISSOCIATION ENERGIES OF CHEMICAL BONDS. IONIZATION POTENTIALS AND ELECTRON AFFINITIES. HANDBOOK.

127. Vergaegen, G., Stafford, F.E., and Drowart, J., J. Chem. Phys., 40, 1622 (1964). MASS SPECTROMETRIC STUDY OF THE SYSTEMS BORON-CARBON AND BORON-CARBON-SILICON.

128. Wada, Y. and Kiser, R.W., Inorg. Chem., 3, 174 (1964). MASS SPECTROMETRIC STUDY OF PHOSPHINE AND DIPHOSPHINE.

129. Westmore, J.B., Mann, K.H., and Tickner, A.W., J. Phys. Chem., 68, 606 (1964). MASS SPECTROMETRIC STUDY OF THE NONSTOICHIOMETRIC VAPORIZATION OF CADMIM ARSENIDE.

130. White, D., Sommer, A., Walsh, P.N., and Goldstein, H.W., in Advances in Mass Spectrometry, vol. 2, edited by R.M. Elliott, Pergamon Press, Oxford, England, 1963. pp. 110-127. THE APPLICATION OF THE TIME-OF-FLIGHT MASS SPECTROMETER TO THE STUDY OF INORGANIC MATERIALS AT ELEVATED TEMPERATURES.

131. Wiberg, K.B., Bartley, W.J., and Lossing, F.P., J. Am. Chem. Soc., 84, 3980 (1962). STRAIN ENERGY IN CYCLOPROPENE AND THE HEAT OF THE $C_3H_3^+$ ION.

132. Wilkinson, P.G., Astrophys. J., 138, 778 (1963). DIATOMIC MOLECULES OF ASTROPHYSICAL INTEREST: IONIZATION POTENTIALS AND DISSOCIATION ENERGIES.

133. Wilson, E.G., Jortner, J.,and Rice, S.A., J. Am. Chem. Soc., 85, 813 (1963). A FAR-ULTRAVIOLET SPECTROSCOPIC STUDY OF XENON DIFLUORIDE.

134. Wincel, H. and Kecki, Z., Nukleonika, 8, 215 (1963). PRIMARY PROCESSES IN RADIATION CHEMISTRY AS STUDIED BY MASS SPECTROMETRY. II. THE STRUCTURE OF $C_7H_7^+$ AND $C_8H_8^+$ IONS FROM TETRAHYDRONAPHTHALENE IN THE GAS PHASE.

135. Zlotowski, I. and Wincel, H., Isotopen Tech., 2, 231 (1962). MASS SPECTROMETRIC STUDIES OF THE DISSOCIATION OF ETHYL HALIDES BY ELECTRON IMPACT.

136. Zmbov, K.F., Bull. Boris Kidrich Inst.Nucl. Sci., 13, 17 (1962). EFFECT OF FREON-12 ON THE THERMAL IONIZATION OF URANIUM ON TUNGSTEN.

1. Ahrens, J., Vacuum 13, 187. NEGATIVE IONS AND THEIR IMPORTANCE FOR THE ANALYSIS OF RESIDUAL GAS.

2. Albasiny, E.L. and Cooper, J.R.A., Proc. Phys. Soc. (London), 82, 289. THE CALCULATION OF ELECTRONIC PROPERTIES OF BH_4^-, CH_4 and NH_4^+ USING ONE-CENTRE SELF-CONSISTENT FIELD WAVE FUNCTIONS.

3. Albasiny, E.L. and Cooper, J.R.A., Proc. Phys. Soc. (London) 82, 801. AMENDMENTS TO THE CALCULATED POLARIZABILITIES OF BH_4^-, CH_4 AND NH_4^+.

4. von Ardenne, M., Steinfelder, K., and Tummler, R., Vakuum Tech. 12, 135. MOLEKUL-MASSENSPEKTROGRAPHISCHE UNTERSUCHUNGEN von DIFFUSIONSPUMPENOLEN.

5. Ardenne, M.V., Stenifelder, K., Tummler, R., and Schreiber, K., Experentia, 19, 178. MOLEKUL-MASSENSPEKTROGRAPHIE von NATURSTOFFEN STEROIDE.

6. Asundi, R.K., Craggs, J.D., and Kurepa, M.V., Proc.Phys. Soc. (London) 82, 967. ELECTRON ATTACHMENT AND IONIZATION IN OXYGEN, CARBON MONOXIDE, AND CARBON DIOXIDE.

7. Armstrong, B.H., Phys. Rev., 131, 1132. EMPIRICAL ANALYSIS OF THE H^- PHOTOCETACHMENT CROSS SECTION.

8. Barney, J.E. II, Stanley, C.W. and Cook, C.E., Anal. Chem. 35, 2206. BEHAVIOR OF DEMETON M ELECTRON AFFINITY DETECTORS.

9. Becker, R.S. and Wentworth, W.E., J. Am. Chem. Soc. 85, 2210. ELECTRON AFFINITIES AND IONIZATION POTENTIALS OF AROMATIC HYDROCARBONS.

10. Berry, R.S. and Reimann, C.W., J. Chem. Phys., 38, 1540 (1963). ABSORPTION SPECTRUM OF GASEOUS F^- AND ELECTRON AFFINITIES OF THE HALOGEN ATOMS.

11. Berry, R.S., Reimann, C.W., and Spokes, G.N., J. Chem. Phys., 37, 2278 (1962). ABSORPTION SPECTRA OF GASEOUS HALIDE IONS AND HALOGEN ELECTRON AFFINITIES: CHLORINE, BROMINE AND IODINE.

12. Booz, J. and Ebert, H.G., Z. Angew. Phys., 16, 180. ANFANGSREKOMBINATION VON IONEN IN LUFT.

13. Brooks, N.B., Roos, M., Bastide, R.P., Rose, P.H., and Wittkower, A.B., Phys. Letters 6, 169. FORMATION OF HYDROGEN NEGATIVE IONS IN MERCURY AND WATER VAPOURS.

14. Carlson, T.A. and White, R. M., J. Chem. Phys., 39, 1748. FRAGMENTATION OF THE EXCITED PARENT IONS, $(CH_3Kr^{82})^+$ AND $CH_3O^{18})^-$, FOLLOWING THE β^- DECAY OF CH_3Br^{82} AND THE β^+ DECAY OF CH_3F^{18}.

15. Clementi, E. and McLean, A.D., Phys. Rev., 133, 419 (1963). ATOMIC NEGATIVE IONS.

16. Clementi, E. and McLean, A.D., J. Chem. Phys., 39, 323. SELF-CONSISTENT-FIELD WAVEFUNCTIONS FOR THE N_3^- AND NO_2^+ MOLECULES.

17. Chen, J.C., Phys. Rev., 129, 202. THEORY OF ELECTRON CAPTURE BY MOLECULES: DISSOCIATIVE ATTACHMENT°

18. Crain, C.M., J. Geophys. Res., 68, 2167. DECAY OF IONIZATION IMPULSES IN THE D AND E REGIONS OF THE IONOSPHERE.

19. Crossley, R. J.S. and Coulson, C.A., Proc. Phys. Soc., (London) 81, 211. GLOCKLER'S EQUATION FOR IONIZATION POTENTIALS AND ELECTRON AFFINITIES.

20. Curran, R.K., J. Chem. Phys., 38, 780. FORMATION OF SF_6^- BY IELASTICALLY SCATTERED ELECTRONS.

21. Darewych, G. and NEAMTAN, S.M., Nucl. Inst. Methods, 21, 247. ON THE MEAN LIFE OF H^- IONS IN ACCELERATING DEVICES.

22. Donath, W.E., J. Chem. Phys. 39, 2685. ATOMIC CALCULATIONS. II. POLARIZABILITIES AND LONDON FORCE CONSTANTS FOR F^-, Ne, AND Na^+.

23. Donath, W.E., J. Chem. Phys., 38, 3032. ATOMIC WAVEFUNCTIONS FOR THE GROUND STATE OF Na^+, Ne, and F^-. ERRATUM.

24. Dunken, H. and Muller, H., Z. Chem. 3, 110. DIE HOMONUKLEAREN ZWEIATOMIGEN MOLEKULE A_2 DER HAUPTGRUPPENATOME A; XI. DIE EINFACH GELADENEN MOLEKULIONEN.

25. Dutton, J., Harris, F.M., and Llewellyn-Jones, F., Proc. Phys. Soc.(London) 81, 52. THE DETERMINATION OF ATTACHMENT AND IONIZATION COEFFICIENTS IN AIR.

26. Dutton, J., Harris, F.M., and Llewellyn-Jones, Proc. Phys. Soc. (London) 82, 581. THE INFLUENCE OF THE THREE-BODY PROCESS OF ELECTRON ATTACHMENT ON THE GROWTH OF IONIZATION IN AIR AT HIGH PRESSURE.

27. Dutton, J., Llewellyn-Jones, F., and Morgan, G.B., Nature 198, 680. ELECTRON ATTACHMENT IN OXYGEN.

28. Edelson, D., Griffiths, J.E., and McAfee, K.B., J. Chem. Phys. 37, 917 (1962). AUTODETACHMENT OF ELECTRONS IN SULFUR HEXAFLUORIDE.

29. Eiber, H., Z. Angew. Phys., 15, 103. UBER DAS VERHALTEN NEGATIVER UND POSITIVER IONEN IN REINEM SAUERSTOFF UND IN SAUERSTOFF-WASSENDAMPFGEMISCHEN.

30. Eiber, H., Z. Angew. Phys., 15, 461. BESTIMMUNG VON IONENMASSEN BEI GASDRUCKEN BIS ZU EINIGEN TORR MITTELS EINES HOCHFREQUEN-ZGSPEISTEN SIEBGITTERS.

31. Ellison, F.O. and Huff, N.T., J. Chem, Phys., 39, 2051. USE OF RESCALED EIGENFUNCTIONS AS VARIATIONAL WAVEFUNCTIONS IN CALCULATIONS ON ATOMS AND IONS.

32. Fischer, H. and Nurrell, J.N., Theoret. Chim. Acta 1, 463. THE INTERPRETATION OF THE STABILITY OF AROMATIC HYDROCARBON IONS BY VALENCE BOND THEORY.

33. Gaines, A.F. and Page, F.M., Trans. Faraday Soc., 59, 1266 (1963). DETERMINATION OF ELECTRON AFFINITIES. VI. PHENYL AND BENZYL RADICALS.

34. Garzo, G. and Til, F., Talenta 10, 583. ARGON IONIZATION DETECTOR IN GAS-LIQUID CHROMATOGRAPHY OF ORGANO-SILICON COMPOUNDS.

35. Geltman, S., Phys. Letters 4, 168. DOUBLE-PHOTON PHOTODETACHMENT OF NEGATIVE IONS.

36. Gentner, W and Hortig, G., Z. Physik 172, 353. EINE METHODE ZUR ERZENGUNG VON STRAHLEN NEGATIVE IONEN.

37. Grob, V.E., J. Chem. Phys., 39, 972 (1963). FORMATION OF NEGATIVE IONS IN $SbCl_3$.

38. Hintenberger, H., Franzen, J., and Schuy, K.P., Z. Naturforsch. 18a, 1236. DIE PERIODIZITATEN IN DEN HAUFIGKEITSVERTEILUNGEN DER POSITIV UND NEGATIV GELADENEN VIELATOMIGEN KOHLENSTOFFMOLEKULIONEN C_n^+ UND C_N^- IM HOCHFRENZFUNKEN ZWISCHEN GRAPHITELEKTRODEN.

39. Hinze, J. and Jaffe, H.M., Can. J. Chem. 41, 1315. ELECTRO-NEGATIVITY. III. ORBITAL ELECTRONEGATIVITIES AND ELECTRON AFFINITIES OF TRANSITION METALS.

40. Hoegl, A., Z. Angew. Phys., 16, 252. MESSUNG VON KONZENTRATION UND BEWEGLICHKEIT ATMOSPHARISCHER IONEN.

41. Hultquist, B., J.Atmosph. Terr. Phys., 25, 225. ON THE HEIGHT DISTRIBUTION OF THE RATIO OF NEGATIVE ION AND ELECTRON DENSITIES IN THE LOWEST IONOSPHERE.

42. Hurst, D.M. and Linnett, J.W., J. Chem. Soc. 1963, 1068. THE ALLYL RADICAL AND ANION.

43. Ionescu, T. V., Compt. Rend. 257, 2268. SUR LES CONDITIONS DE MESURE DES FREQUENCES PROPRES DES IONS NEGATIFS MOLECULAIRES.

44. Ionescu, T. V., Rev. physique 8, 347. SUR LE COEFFICIENT DE FROTTEMENT DES IONS NEGATIFS MOLECULAIRE D'HYDROGENE ET D'OXYGENE.

45. Kaplan, S.N., Paulikas, G.A., and Pyle, R.V., Phys. Rev. 131, 2574. ELECTRON DETACHMENT FROM 20-MEV D^- IONS BY A MAGNETIC FIELD.

46. Kaufman, M., Astrophys. J. 137, 1296. SEMI-EMPIRICAL ELECTRON AFFINITIES.

47. Klemm, W and Busmann, E., Z. Anorg. Allgem. Chem., 319, 297. VOLUMENINKREMENTE UND RADIEN EINIGER EINFACH NEGATIV GELADENER IONEN.

48. Kutselnigg, W., Theoret. Chim. Acta 1, 343. RESOLUTION DU PROBLEME A DEUX ELECTRONS EN MECANIQUE QUANTIQUE PAR DETERMINATION DIRECTE DES ORBITALES NATURELLES II. APPLICATION AUX ETATS FONDAMENTAUX DE HELIM ET DES IONS ISOELECTRONIQUES.

49. Latter, R. and LeLevier, R.E., J. Geophys. Res., 68, 1643. DETECTION OF IONIZATION EFFECTS FROM NUCLEAR EXPLOSIONS IN SPACE.

50. Lohr, L.L. Jr., and Allen, L.C., J.Chem. Phys., 39, 2106. WAVEFUNCTIONS AND CORRELATION ENERGIES FOR F, F^-, AND Ne.

51. Lory, J. and Desprez-Rebaud, S., Compt. Rend. 256, 4173. DETERMINATION DES FONCTIONS D'ONDE RADIALES DE L'ION Br^-.

52. Lowke, J.J. and Rees, J.A., Aust. J.Phys., 16, 447. THE DRIFT VELOCITIES OF FREE AND ATTACHED ELECTRONS IN WATER VAPOR.

53. McAfee, K.B.Jr., and Edelson, D.E., Proc. Phys. Soc. (London) 81, 382. IDENTIFICATION AND MOBILITY OF IONS IN A TOWNSEND DISCHARGE BY TIME-RESOLVED MASS SPECTROMETRY.

54. McDowell, M.R.C. and Williamson, J.H., Phys. Letter 3, 159. ELECTRON DETACHMENT FROM H^- BY ELECTRONS.

55. Molmud, P., J. Geophys. Res. 68, 5443. ALTERING THE ELECTRON DENSITY IN THE D REGION: A NEW TOOL FOR IONOSPHERIC D-LAYER RESEARCH.

56. Moruzzi, J.L. and Craggs, J.D., Proc.Phys. Soc. (London) 82, 979. MEASUREMENT OF IONIZATION AND ATTACHMENT COEFFICIENTS IN C_3F_8.

57. Napper, R. and Page, F.M., Trans. Faraday Soc.., 59, 1086 (1963). DETERMINATION OF ELECTRON AFFINITIES. V. CYANIDE AND THIOCYANATE RADICALS.

58. Page, F.M. and Kay, J., Nature, 199, 483 (1963). ELECTRON AFFINITY OF TETRACYANOETHYLENE.

59. Pekeris, C.L., Phys. Rev., 126, 1470 (1962). 1 ^1S, 2 ^1S, AND 2 ^3S STATES OF H^- AND OF He.

60. Person, W.B., J. Chem. Phys., 38, 109 (1963). ELECTRON AFFINITIES OF SOME HALOGEN MOLECULES AND THE CHARGE-TRANSFER FREQUENCY.

61. Roothaan, C.C.J. and Kelly, P.S., Phys. Rev., 131, 1177. ACCURATE ANALYTICAL SELF-CONSISTENT FIELD FUNCTIONS FOR ATOMS. III. THE $1s^2 2s^m 2p^n$ STATES OF NITROGEN AND OXYGEN AND THEIR IONS.

62. Ross, W. D., Anal. Chem. 35, 1596. DETECTION OF METAL CHELATES IN GAS LIQUID CHROMATOGRAPHY BY ELECTRON CAPTURE.

63. Schulz, C.J., U.S. Dept. Comm. Office Tech. Serv., AD-272,783. CROSS SECTIONS AND ELECTRON AFFINITY FOR O^- IONS FROM O_2, CO, AND CO_2 BY ELECTRON IMPACT.

64. Sears, R.D., J. Geophys. Res., 68, 5135. CONTRIBUTION OF ENERGETIC PHOTOELECTRONS TO D-REGION NONEQUILIBRIUM ELECTRON TEMPERATURES.

65. Slifkin, M.A., Nature 200, 877. MOLECULAR ORBITAL THEORY AND EXPERIMENTALLY DETERMINED ENERGY-LEVELS.

66. Taylor, H.W. and Harris, F.E., J. Chem. Phys., 39, 1012. POTENTIAL CURVE FOR THE $^2\Sigma_u^+$ STATE OF H_2^-.

67. Trepka, L.V. and Neuert, H., Z, Naturforsch, 18a, 1295. UBER DIE ENSTEHUNG VON NEGATIVER IONEN AUS EINIGEN KOHLENWASSERSTOFFEN UND ALKOHOLEN DURCH ELEKTRONENSTOSS.

68. Wentworth, W.E. and Becker, R.S., J. Am. Chem. Soc., 84, 4263 (1962). POTENTIAL METHOD FOR THE DETERMINATION OF ELECTRON AFFINITIES OF MOLECULES: APPLICATION TO SOME AROMATIC HYDROCARBONS.

69. Zacharias, B., Acta Chem. Scand. 17, 2221. DETECTION OF POSITIVE AND NEGATIVE GAS IONS IN ULTRAVIOLET IRRADIATED NITROGEN GAS AND THEIR EFFECT ON NITROGEN FIXATION IN CONTINUOUS CULTURES OF AZOTOBACTER VINELANDII.

70. Zacharias, B., Acta Chem. Scand. 17, 2225. EFFECT OF NITROGEN GAS, IRRADIATED WITH A BETA-RAY SOURCE, ON NITROGEN FIXATION IN CONTINUOUS CULTURES OF AZOTOBACTER VINELANDII.

Photoionization and Related Studies

V. H. Dibeler and R.M. Reese

1. Akopyan, M.Ye., and Vilesov, Kinetika i Kataliz 4, 39 (1963). DECOMPOSITION OF MOLECULAR IONS FORMED DURING PHOTOIONIZATION OF HYDRAZINE AND SOME OF ITS ALKYL DERIVATIES.

2. Akopyan, M. Ye., Vilesov, F.I., and Terenin, A.N., Isz. Akad. Nauk SSSR, Ser. Fiz. 27, 1083 (1963). MASS SPECTROMETRIC STUDY OF MOLECULAR PHOTOIONIZATION AND DISSOCIATION OF EXCITED MOLECULAR IONS.

3. Alexander, E. and Fraenkel, B.S., Rev. Sci. Instruments 34, 887 (1963). VACUUM ULTRAVIOLET SPECTROMETER.

4. Axelrod, N.N., J. Opt. Soc. Am. 53, 297 (1963). MICROWAVE LINE SOURCE FOR THE VACUUM ULTRAVIOLET.

5. Bates, D. R. (ed.), Academic Press, New York, 1962. ATOMIC AND MOLECULAR PROCESSES.

6. Branscomb, L.M., see reference 5, p. 100; PHOTODETACHMENT.

7. Cook, G.R., Samson, J.A. R. and Weissler, G.L., U.S. Dept. Comm., Office Tech. Serv., PB Rept. 145, 185 (1961). PHOTOIONIZATION INDUCED ION MOLECULE REACTIONS IN MASS SPECTROMETER.

8. CRTEF, Air Force Cambridge Research Lab., Bedford, Mass. PHOTOIONIZATION IN GASES. - COMPREHENSIVE REPORT ON SOVIET PERIODICAL LITERATURE. MARCH 1964.

9. Deslattes, R.D., Peterson, T.R.Jr., and Tomboulian, D.H., J. Opt. Soc. Am., 53, 302 (1963). PENNING DISCHARGE AS A SOURCE IN THE EXTREME ULTRAVIOLET.

10. Dibeler, V. H. and Reese, R. M., J. Chem.Phys. 40, 2034 (1964). MASS SPECTROMETRIC STUDY OF THE PHOTOIONIZATION OF ACETYLENE AND ACETYLENE-d_2.

11. Ditchburn, R.W., and Opik, U., Chapter in ref. 5, PHOTOIONIZATION.

12. Ederer, D. L., U.S. Dept. of Commerce, Office of Tech. Serv., AD 410, 574 (1963). THE PHOTOIONIZATION CROSS-SECTION OF NEON FROM 80 to 600 Å.

13. Hernandez, G.J., J. Chem. Phys. 38, 1644 (1963). VACUUM ULTRAVIOLET ABSORPTION SPECTRUM OF DIMETHYL ETHER.

14. Hernandez, G.J., J. Chem. Phys. 38,2233 (1963). VACUUM-ULTRAVIOLET ABSORPTION SPECTRA OF THE CYCLIC ETHERS: TRIMETHYLENE OXIDE, TETRAHYDROFURAN, AND TETRAHYDROPYRAN.

15. Hernandez, G. J., J. Chem. Phys. 39, 1355 (1963). VACUUM ULTRAVIOLET ABSORPTION SPECTRUM OF DIETHYL ETHER.

16. Hinnov. E. and Hofmann, F.W., J. Opt. Soc. Am. 53, 1259 (1963). MEASUREMENT OF ABSOLUTE INTENSITY IN THE VACUUM ULTRAVIOLET.

17. Huffman, R.E., Tanaka, Y., and Larrabee, J.C., Appl. Opt. 2, 617 (1963). HELLIUM-CONTINUUM LIGHT SOURCE FOR PHOTOELECTRIC SCANNING IN THE 600 -1100 Å REGION.

18. Huffman, R.E., Tanaka, Y., and Larrabee, J.C., J. Chem. Phys., 38, 1920 (1963). FLOURESENCE AND PRE-IONIZATION IN NITROGEN EXCITED BY VACUUM ULTRAVIOLET RADIATION.

19. Huffman, R.E., Tanaka, Y., and Larrabee, J.C., J. Chem. Phys. 39, 910 (1963). ABSORPTION COEFFICIENTS OF NITROGEN IN THE 1000-580 Å WAVELENGTH REGION.

20. Hunter, W.R. in "Proceedings of the Xth Colloquium Spectroscopicum Internationale," E.R. Lippincott and M. Margoshes (eds.), Spartan Books, Washington, D.C. 1963. A PULSED LIGHT SOURCE FOR THE EXTREME ULTRAVIOLET.

21. Jacobus, G.F., Madden, R.P., and Canfield, L.R., J. Opt. Soc. Am. 53, 1084 (1963). REFLECTING FILMS OF PLATINUM FOR THE VACUUM ULTRAVIOLET.

22. Johns, J.W.C., Can. J. Phys., 41, 209 (1963). THE ABSORPTION SPECTRUM OF H_2O AND D_2O IN THE VACUUM ULTRAVIOLET.

23. Krog, V., Ruppel, H., and Witt, H.T., Ber. Bunsengesellschaft Phys. Chemie 67, 795 (1963). PHOTOIONIZATION OF AROMATIC AMINES.

24. Madden, R.P., Canfield, L.R., and Hass, G., J. Opt. Soc. Am. 53, 620 (1963). ON THE VACUUM ULTRAVIOLET REFLECTANCE OF EVAPORATED ALUMINUM BEFORE AND DURING OXIDATION.

25. Madden, R.P. and K. Codling, Phys. Rev. Letters 10, 516 (1963). NEW AUTOIONIZING ATOMIC ENERGY LEVELS IN He, Ne, AND Ar.

26. Maecker, H. (ed.). Proc. Intern. Conf. Ionization Phenomena Gases, Munich, 1961 (Publ. 1962). North Holland Publishing Co. Amsterdam, Vol.2. p. 1884. SURVEY OF RECENT ADVANCES IN THE SPECTROSCOPY OF THE VACUUM ULTRAVIOLET.

27. Mohler, F. L., US. Dept. Fomm., Office Tech. Serv., PB Rept. 161,632 (1962). 43 pp. PHOTOIONIZATION OF ATOMS AND MOLECULES.

28. Momigny, J., Nature, 199, 1179 (1963). IONIZATION POTENTIALS AND THE STRUCTURES OF THE PHOTOIONIZATION YIELD CURVES OF ETHYLENE AND ITS HALOGENODERIVATIVES.

29. Momigny, J., Nature 199, 805 (1963). PREIONIZATION PHENOMENA IN THE APPEARANCE OF SOME POLYATOMIC MOLECULAR IONS.

30. Moskin, Yu. V., Optika i Spektroskopiya 15 (5), 582 (1963). PHOTOIONIZATION OF ATOMS AND RECOMBINATION OF IONS IN THE VAPORS OF ALKALI METALS.

31. Nakayama, T. and Watanabe, K., J. Chem. Phys., 40, 558 (1964). ABSORPTION AND PHOTOIONIZATION COEFFICIENTS OF ACETYLENE, PROPYNE AND 1-BUTYNE.

32. Nicholson, A. J. C., J. Chem. Phys. 39, 954 (1963). PHOTOIONIZATION EFFICIENCY CURVES. MEASUREMENT OF IONIZATION POTENTIALS AND INTERPRETATION OF FINE STRUCTURE.

33. Ogawa, M. and Tanaka, Y., Can. J. Phys., 40, 1593 (1962). RYDBERG ABSORPTION SERIES OF N_2.

34. Peterson, T. J. Jr., and Tomboulian, D. H., J. Quant. Spectros. Rod. Transf. 3, 285 (1963). A PHOTOMULTIPLIER INVESTIGATION OF THE LOW-ENERGY CONTINUOUS X-RAY SPECTRA.

35. Platzman, R. L., J. Chem. Phys., 38, 2775 (1963). SOME REMARKS ON THE NATURE OF IONIZATION, IONIZATION OF MOLECULES BY VARIOUS AGENCIES.

36. Price, W. C., Bralsford, R., and Roessler, D.M., Spectry. Rept. Conf. Organ. Hydrocarbon Res. Group. Inst. Petrol., London, 1962. pp. 279-287. VACUUM ULTRAVIOLET SPECTRA AND PHOTIONIZATION OF MOLECULES AND RADICALS.

37. Price, W. C., Passmore, T. R., and Roessler, D.M., Discussions Faraday Soc., 35, 201 (1963). IONIZATION AND DISSOCIATION ENERGIES OF THE HYDRIDES AND FLUORIDES OF THE FIRST ROW ELEMENTS IN RELATION TO THEIR ELECTRONIC STRUCTURES.

38. Reeves, E. M. and Parkinson, W. H., J. Opt. Soc. Am. 53, 941 (1963). EFFICIENCIES OF GOLD AND PLATINUM GRATINGS IN THE VACUUM ULTRAVIOLET.

39. Rendina, J.F., Rev. Sci. Instruments 34, 813 (1963). ALL-METAL VACUUM ULTRAVIOLET LAMP.

40. Samson, J.A.R. and Golomb, D., Rev. Sci. Instruments 34, 441 (1963). LYMAN-ALPHA DETECTOR.

41. Samson, J.A.R., Phys. Rev. 132(5), 2122 (1963). OBSERVED AND PREDICTED NEW AUTOIONIZED ENERGY LEVELS IN KRYPTON, ARGON, AND XENON.

42. Stewart, A. L. and Webb, T. G., Proc. Phys. Soc.(London) 82, 532 (1963). PHOTOIONIZATION OF HELIUM AND IONIZED LITHIUM.

43. Vilesov, F.I. and Akopyan, M.E., Pribory i Tekhn. Eksperim., 7, 145 (1962). PHOTOIONIZATION AND ITS APPLICATION IN ANALYTICAL MASS SPECTROSCOPY.

44. Vilesov, F.I. and Zaitsev, V.M., Dokl. Akad. Nauk S.S.S.R., 154, 886 (1964). PHOTOIONIZATION OF PHENYL DERIVATIVES OF THE GROUP V ELEMENTS.

45. Vilesov, F. I., Usp. Fiz. Nauk 81, 669 (1963)., Transl. Soviet Physics Uspekhi 6, 888 (1964). PHOTOIONIZATION OF GASES AND VAPORS BY VACUUM ULTRAVIOLET RADIATION.

46. Vilesov, F. I. and Karbatov, B.L., Izv. Akad. Nauk SSSR, Sery. Fiz. 27, No. 8. 1088 (1963). ENERGY SPECTRA OF ELECTRONS EJECTED DURING PHOTOIONIZATION OF MOLECULES.

47. Vodar, B., in Proceedings Xth Colloquium Spectroscopicum International, Lippincott and Margoshes (eds.) Spartan Books, Washington, D.C., 1963. EXTREME ULTRAVIOLET SPECTROSCOPY.

48. Watanabe, K., Natl. Aeron. Space Admin., Doc. N62-10947 (1962). 17 pp. PHOTOIONIZATION AND ULTRAVIOLET ABSORPTION PROCESSES.

49. Weissler, G.L., in"Handbrichder Physik," S. Flugge (ed.) Vol. 21, Springer, Berlin, 1956. PHOTOIONIZATION IN GASES AND PHOTOELECTRIC EMISSION FROM SOLIDS.

50. Wilkinson, P.G., J. Mol. Spectroscopy 6, 1 (1961). MOLECULAR SPECTRA IN THE VACUUM ULTRAVIOLET.

51. Yoshida, M., Nippon Kagaku Zasshi 84, 826 (1963). PHOTOIONIZATION OF ACETYLENE AND XENON.

52. Zhirnov., V.A., Zh. Eksperim. i Teoret. Fiz., 42, 1097 (1962).
EFFECTIVE CROSS SECTION FOR PHOTOIONIZATION OF Li IONS.

Charge Exchange

B. Steiner and N. Wells

1. Boersch, H., Forst, G., and Schweda, S., Z. Physik, 174, 446. ENERGIEVERLUSTE SCHNELLER LITHIUM- UND NATRIUM-IONEN BEI WECHSELWIRKUNG MIT EDELGASEN.

2. Bransden, B.H. and Cheshire, I.M., Proc. Phys. Soc. (London) 81, 820. ELECTRON CAPTURE FROM HELIUM BY FAST PRONTONS.

3. Cheshire, I.M., Proc. Phys. Soc.(London) 82, 113. ELECTRON CAPTURE BY FAST PROTONS ON HYDROGEN.

4. Chkuaseli, D.V., Guldamashivili, A.I. and Nikoleishvili, U.D., Bull. Acad. Sci. (USSR), Phys. Ser. 27, 999. CHARGE EXCHANGE BETWEEN ATOMS AND IONS OF ALKALINE EARTH ELEMENTS.

5. Chupka, W.A. and Lindholm, T., Arkiv Fysik, 25, 349 (1963). DISSOCIATION OF BUTANE MOLECULAR IONS FORMED IN CHARGE EXCHANGE COLLISIONS WITH POSITIVE IONS.

6. Cobic, B., Tosic, D., and Perovic, B. Nue. Inst. Methods 25, 157. ASTON BANDS IN THE ELECTROMAGNETIC MASS SEPARATOR.

7. Collin, J.E., Nature 197, 1197. IONIZATION BY CHARGE TRANSFER OF ABSORBED GASES IN A MASS SPECTROMETER.

8. Cook, C.J., Proc. Phys. Soc. (London) 81, 789. THE ASYMPTOTIC FORM OF THE ELECTRON CAPTURE CORSS SECTIONS.

9. Davis, W.D. and Vanderslice, T.A., Phys. Rev., 131, 219. ION ENERGIES AT THE CATHODE OF A GLOW DISCHARGE.

10. Demkov, Yu. N., Soviet Phys. JETP (English Transl) 18, 138 (1964); original: 45, 195 (1963). CHARGE TRANSFER AT SMALL RESONANCE DEFECTS.

11. Dmitriev, I.S. and Nikolaev, V.S., Soviet Phys. JETP (English Transl) 17, 447; original: 44, 660. CALCULATION OF THE CROSS SECTIONS FOR ELECTRON LOSS BY FAST IONS IN LIGHT MEDIA.

12. Everhart, E., Phys. Rev., 132, 2083. ANALYSIS OF THE He^+ ON He COLLISION.

13. Fite, W.L., Smith, A.C. H., Stebbings, R.F., and Rutherford, J.A., J. Geophys. Res. 68, 3225. COLLISIONS BETWEEN H_e^+ AND O_2.

14. Flaks, I.P. and Ogurtsov, G.N., Soviet Phys. Tech. Phys. (English Transl) 8, 560; original: 33, 748. CHARGE-EXCHANGE AND IONIZATION PROCESSES OCCURRING DURING THE COLLISION OF NITROGEN ATOMS AND IONS WITH HYDROGEN MOLECULES.

15. Futrell, J.H. and Tiernan, T.O., J. Chem. Phys., 38, 150. INHIBITION OF THE ARGON-SENSITIZED RADIOLYSIS OF PROPANE BY HYDROGEN.

16. Futrell, J. H. and Tiernan, T.O., J. Chem. Phys., 39, 2539. DISSOCIATIVE CHARGE-EXCHANGE REACTIONS OF RARE-GAS IONS WITH PROPANE.

17. Giese, C.F. and Maier, W.B., J. Chem.Phys., 39, 197 (1963). II, DISSOCIATIVE IONIZATION OF CO BY ION IMPACT.

18. Gilbody, H.B., Hasted, J.B., Ireland, J.V., Lee, A. R., Thomas, E.W., and Whiteman, A.S., Proc. Roy. Soc. (London) A274, 40. CHARGE TRANSFER AND IONIZATION BY POSITIVE IONS IN THE ENERGY RANGE 60 TO 450 keV.

19. Gilbody, H.B. and Lees, A.E., Proc. Roy. Soc. (London) A274, 365. IONIZATION BY PROTONS IN THE ENERGY RANGE 100 TO 450 keV.

20. Hanson, W.B. and Patterson, T.N.L., Planetary Space Sci., 11, 1035. DIURNAL VARIATION OF THE HYDROGEN CONCENTRATION IN THE EXOPHERE.

21. Hanson, W.B., Patterson, T.N.L., and Degaonkar, S.S., J. Geophys. Res. 68, 6203. SOME DEDUCTIONS FROM A MEASUREMENT OF THE HYDROGEN ION DISTRIBUTION IN THE HIGH ATMOSPHERE.

22. Henglein, A. and Muccini, G.A., Z. Naturforsch 18a, 753. MASS SPECTROMETRIC OBSERVATION OF ELECTRON AND PROTON TRANSFER REACTIONS BETWEEN POSITIVE IONS AND NEUTRAL MOLECULES. PART II.

23. Jones, P.R., Costigan, P., and Van Dyk, G., Phys. Rev., 129, 211. RESONANT ELECTRON CAPTURE AND STRIPPING IN Ne^+—Ne COLLISIONS AT ENERGIES OF SEVERAL keV.

24. Kocharts, G. and Nicolet, M., Ann. Geophys. 19, 370. L'HELIUM ET 1 HYDROGENE ATOMIQUE AU COURS D'UN MINIMUM DE 1'ACTIVITE SOLAIRE.

25. Kozlov, V.F., Fogel, Ya. M., and Stratienko, V.A., Soviet Phys. JETP (English Transl) 17, 1226; original: 44, 1823. TWO ELECTRON CHARGE EXCHANGE OF LOW-ENERGY PROTONS.

26. Kozhushner, M.A. and Sayasov, Yu. S., Opt. Spect.(USSR) (English Transl) 15, 399; original; 399. THE PROBABILITY OF INELASTIC ATOMIC COLLISIONS IN THE CASE OF SEVERAL POINTS OF INTERSECTION (OR PSEUDO-INTERSECTION) OF TERMS.

27. Lencher, A.M. and Singer, S.F., Planetary Space Sci., 11, 1151. THE ALBEDO NEUTRON THEORY OF GEOMAGNETICALLY TRAPPED PROTONS.

28. Lichten, W., Phys. Rev. 131, 229. RESONANT CHARGE EXCHANGE IN ATOMIC COLLISIONS.

29. Lockwood, G.J., Helbig, H.F., and Everhart, E., Phys. Rev., 132, 2078. MEASUREMENTS OF RESONANT ELECTRON CAPTURE IN He^+ ON He COLLISIONS.

30. McClure, G.W., Phys. Rev., 132, 1636. DOUBLE-ELECTRON CAPTURE BY PROTONS IN H_2 GAS.

31. McClure, G.W., Phys. Rev., 130, 1852. CHARGE EXCHANGE AND DISSOCIATION OF H^+, H_2^+, and H_3^+ IONS INCIDENT ON H_2 GAS.

32. McGowan, W. and Kerwin, L., Proc. Phys. Soc. (London) 82, 357. SOME CHARGE EXCHANGE AND DISSOCIATION COLLISIONS OF N_2^{2+} IONS.

33. McGowan, Wm. and Kerwin, L., Can. J. Phys. 41, 316. ON THE APPLICATION OF ASTON BANDS AND APPEARANCE POTENTIAL MEASUREMENTS TO ION COLLISION STUDIES.

34. McGowan, J. WM. and Kerwin, L., Can J. Phys. 41, 1535. METASTABLE Ar^+ IONS NEAR THE Ar^{++} THRESHOLD.

35. Mapleton, R.A., Phys. Rev., 130, 1839. ELECTRON CAPTURE FROM He($1s^2$) BY PROTONS. II.

36. Mapleton, R.A., Phys. Rev., 130, 1829. ELECTRON CAPTURE FROM ATOMIC NITROGEN AND OXYGEN BY PROTONS. I.

37. Melroy, M.B., Proc. Roy. Soc. (London) A272, 542. ELECTRON CAPTURE BY FAST PROTONS AND α-PARTICLES IN HYDROGEN.

38. Mittleman, M.H., Proc. Phys. Soc.(London) 81, 633. REARRANGEMENT COLLISIONS III. ELECTRON TRANSFER FROM ATOMS TO FAST PROTONS.

39. Nicolet, M. and Swider, W. Jr., Planetary Space Sci., 11, 1459. IONOSPHERIC CONDITIONS.

40. Nikitin, E.E., Bull. Acad. Sci. (USSR), Phys. Ser. 27, 996. PROBABILITY OF CHARGE EXCHANGE DURING ATOMIC COLLISIONS IN THE CASE OF RANDOM RESONANCE.

41. Nikolaev, V.S., Dmitriev, I.S., Teplova, IA.A., and Fateeva, L.N., Bull. Acad. Sci. (USSR), Phys. Ser., 27, 1078. DEPENDENCE OF THE MEAN CHARGE OF FAST IONS ON THE DENSITY OF THE MEDIUM.

42. Parzen, P., J. Appl. Phys. 34, 2322. MULTIPLE CHARGE EXCHANGE OF AN ACCELERATED POSITIVE-ION BEAM IN A NEUTRAL GAS.

43. Pettersson, E., Arkiv Fysik, 25, 181 (1964). DISSOCIATION OF n-PROPANOL MOLECULE IONS FORMED IN CHARGE EXCHANGE COLLISIONS WITH POSITIVE IONS.

44. Pilipenko, D.V. and Fogel, Ya. M., Soviet Phys. JETP (English Transl) 17, 1222; original: 44, 1818. ELECTRON CAPTURE AND LOSS ON PASSAGE OF FAST ATOMS THROUGH MOLECULAR GASES.

45. Pradhan, T., and Tripathy, D.N., Phys. Rev., 130, 2317. ELECTRON CAPTURE BY PROTONS PASSING THROUGH HYDROGEN.

46. Rapp, D., J. Geophys. Res. 68, 1773. ACCIDENTALLY RESONANT ASYMMETRIC CHARGE EXCHANGE IN THE PROTONOSHPERE.

47. Roth, W., J. Chem. Phys., 38, 1786. ERRATUM: CHARGE TRANSFER CROSS SECTION FOR ELECTRONICALLY EXCITED N_2^+ WITH O ATOMS AT LOW ENERGY.

48. Rydnik, V.I. and Lavorskii, B.M., Bull. Acad. Sci. (USSR), Phys. Ser. 27, 1005. CALCULATION OF NON-RESONANCE CHARGE EXCHANGE AND IONIZATION OF ATOMS IN COLLISIONS WITH SLOW IONS.

49. Sagalyn, R.S. and Smiddy, M., J. Geophys. Res. 68, 199. MEASURMENT AND INTERPRETATION OF ION DENSITY DISTRIBUTIONS IN THE DAYTIME F REGION.

50. Smirnov, B.M., Soviet Phys. JETP (English Transl) 16, 81; original: 43, 112 (1962). INELASTIC COLLISIONS OF LIGHT ATOMS IN THE ADIABATIC APPROXIMATION.

51. Stebbings, R.F., Turner, B.R., and Smith, A.C.H., J. Chem. Phys., 38, 2277. CHARGE TRANSFER IN OXYGEN, NITROGEN, AND NITRIC OXIDE.

52. Stebbings, R.F., Smith, A.C.H., and Gilbody, H.B., J. Chem. Phys., 38, 2280. CHARGE TRANSFER BETWEEN SOME ATMOSPHERIC IONS AND ATOMIC OXYGEN.

53. Stebbings, R.F., Smith, A.C.H., and Ehrhardt, H., J. Chem. Phys., 39, 968. DISSOCIATIVE CHARGE TRANSFER IN He^+ — O_2 and He^+—N_2 COLLISONS.

54. Uhler, J. and Rossi, J., Arkiv Fysik 24, 369. INVESTIGATIONS OF SOME PROPERTIES OF ISOTOPE SEPARATOR BEAMS OF DIFFERENT CHARGE STATES.

55. Weiner, E.R., Hertel, G.R., and Koski, W.S., J. Chem. Phys., 39, 3538. CROSS SECTIONS FOR SOME GAS-PHASE SINGLE-CHARGE TRANSFER REACTIONS OF N_2^{++} AND Ar^{++}.

56. Wexler, S. and Hess, D.C., J.Chem. Phys., 38, 2308. IONIZATION BY IONS IN THE MeV RANGE.

57. Yanow, G., J. Astronaut. Sci. 10, 75. PRELIMINARY REPORT ON THE CALCULATION OF UPPER ATMOSPHERE MODELS FROM FIRST PRINCIPLES; THE EARTH.

Ion-Molecule Reactions

B. Steiner and N. Wells

1. Anex, B.G., J. Chem. Phys., 38, 1651. GROUND STATE OF THE HeH^+ MOLECULE ION.

2. Ausloos, P., Lias, S.G., and Gordne, R. Jr., J. Chem. Phys., 39, 3341. EFFECT OF ADDITIVES ON THE IONIC REACTION MECHANISM IN THE RADIOLYSIS OF METHANE.

3. Babeliowsky, T.P.J.M. and Boelrijk, N.A.I.M., Physica 29, 405. NEGATIVE TEMPERATURE COEFFICIENTS OF ION-MOLECULE REACTIONS IN THE IONIZATION CHAMBER OF THE MASS SPECTROMETER. STATISTICAL CALCULATIONS BASED ON AN EXPERIMENTAL MODEL FOR THE VARIATION OF THE MICROSCOPIC REACTION CROSS-SECTION WITH RELATIVE VELOCITY.

4. Beaty, E.C. and Patterson, P., JILA Report 3. REACTION RATES FOR THE FORMATION OF He_2^+ AND Ne_2^+.

5. Block, A., in Advances in Mass Spectrometry, vol. 2, edited by R.M. Elliott, Pergamon Press, Oxford, 1963. pp. 48-50. MASS SPECTRA OF ACETYLENE UNDER HIGH PRESSURE IN THE ION SOURCE.

6. Comes, F.J., Z. Naturforsch 18a, 539. SEKUNDARIONENBILDUNG IN KRYPTON.

7. Comes, F.J., Z. Naturforsch., 17a, 1031 (1962). MECHANISM OF He_2^+ FORMATION.

8. Curran, R.K., J. Chem. Phys., 38, 2974. MASS-SPECTROMETER INVESTIGATION OF ELECTRON-IMPACT PROCESSES AT PRESSURES TO 1 mm Hg.

9. Derwish, G.A.W., Galli, A., Giardini-Guidoni, A., and Volpi, G.G., J. Chem. Phys., 39, 1599. ION-MOLECULE REACTIONS IN GASEOUS AMMONIA.

10. Eiber, H., Z. Angew, Phys., 15, 103. UBER DAS VERHALTEN NEGATIVER UND POSITIVER IONEN IN REINEM SAUERSTOFF UND IN SAUERSTOFF-WASSERDAMPFGEMISCHEN.

11. Eiber, H., Z. Angew. Phys., 15, 461. BESTIMMUNG von IONENMASSEN BEI GASDRUCKEN BIS ZU EINIGEN TORR MITTELS EINE HOCHFREQUEN-ZGESPEISTEN SIEBGITTERS.

12. Field, F.H., Franklin, J.L., and Munson, M.S.B., J. Am. Chem. Soc. 85, 3575. REACTIONS OF GASEOUS IONS XII. HIGH PRESSURE MASS SPECTROMETRIC STUDY OF METHANE.

13. Field, F.H., Franklin, J.L., and Munson, M.S.B., J. Am. Chem. Soc., 85, 3575 (1963). REACTIONS OF GASEOUS IONS. XII. HIGH PRESSURE MASS SPECTROMETRIC STUDY OF METHANE.

14. Fite, W.L., Smith, A.C.H., Stebbings, R.F., and Rutherford, J.A., J. Geophys. Res., 68, 3225. COLLISIONS BETWEEN He^+ AND O_2.

15. Freeman, G.R., J. Chem. Phys., 39, 988. YIELD OF "FREE IONS" IN GAMMA-IRRADIATED LIQUID SATURATED HYDROCARBONS.

16. Galli, A., Giardini-Guidoni, A., and Volpi, G.C., J. Chem. Phys., 39, 518. ION-MOLECULE REACTIONS LEADING TO NO^+ FORMATION.

17. Giese, C.F. and Maier, W.B. II., J. Chem. Phys., 39, 739. ENERGY DEPENDENCE OF CROSS SECTIONS FOR ION-MOLECULE REACTIONS. TRANSFER OF HYDROGEN ATOMS AND HYDROGEN IONS.

18. Harrison, A.G., Can. J. Chem. 41, 236. CONCURRENT ION-MOLECULE REACTIONS IN ETHYLENE AND PROPYLENE.

19. Henglein, A., Jacobs, G., and Muccini, G.A., Z. Naturforsch, 18a, 98. OBSERVATIONS ON THE REACTIONS OF NORMAL AND EXCITED IONS OF CYANOGEN AND THE PERSISTENT COMPLEX $C_4N_4^+$.

20. Henglein, A. and Muccini, G.A., Z. Naturforsch 18a, 753. MASS SPECTROMETRIC OBSERVATION OF ELECTRON AND PROTON TRANSFER REACTIONS BETWEEN POSITIVE IONS AND NEUTRAL MOLECULES. PART II.

21. Herman, Z. and Cermak, V., Collection Czech. Chem. Commun. 78, 799. MASS SPECTROMETRIC INVESTIGATION OF THE REACTIONS OF IONS AND EXCITED NEUTRAL PARTICLES IN MIXTURES CONTAINING MERCURY VAPOR.

22. Kebarle, P. and Codbole, E.W., J. Chem. Phys., 39, 1131. MASS-SPECTROMETRIC STUDY OF IONS FROM THE α-PARTICLE IRRADIATION OF GASES AT NEAR ATMOSPHERIC PRESSURES.

23. Kevan, L. and Libby, W.F., J. Chem. Phys., 39, 1288. CHEMISTRY OF POSITIVE IONS. III. THE RADIATION CHEMISTRY OF SOLID n-HEXANE AT 77°K.

24. Klots,C.E., J. Chem. Phys., 39, 1571. INTERPRETATION OF ION YIELDS IN BINARY MIXTURES.

25. von Koch, H and Friedman, L., J. Chem. Phys., 38, 1115. HYDROGEN-HELIUM ION-MOLECULE REACTIONS.

26. Kubose, D.A. and Hamill, W. H., J. Am. Chem. Soc., 85, 125. VELOCITY DEPENDENCE OF ION-MOLECULE REACTIONS REACTION CROSS SECTIONS IN A MASS SPECTROMETER.

27. Lindholm, E. and Wilmenius., Arkiv Kemi, 20, 255. ION-MOLECULE REACTIONS IN THE RADIOLYSIS OF METHANOL.

28. Lorquet, A.J. and Hamill, W.H., J. Phys. Chem. 67, 1709. THE ENERGY DEPENDENCE FOR REACTION CROSS SECTIONS OF ION-MOLECULE REACTIONS OF SOME PENTYL AND CYCLOPENTYL HALIDES.

29. Moran, T.F., and Hamill, W.H., J. Chem. Phys., 39, 1413. CROSS SECTIONS OF ION-PERMANENT-DIPOLE REACTIONS BY MASS SPECTROMETRY.

30. Moran, T.F. and Friedman, L., J. Chem. Phys., 39, 2491. NEON-HYDROGEN ION-MOLECULE REACTIONS.

31. Munson, M.S.B., Field, F.H., and Franklin, J.L., J. Am. Chem. Soc. 85, 3584. REACTIONS OF GASEOUS IONS XIII. THE SYSTEM METHANE-HYDROGEN.

32. Munson, M.S.B., J. Phys. Chem., 67, 1542 (1963). A MASS SPECTROMETRIC STUDY OF HOMONUCLEAR AND HETERONUCLEAR RARE GAS MOLECULE IONS.

33. Pahl, M., Z. Naturforsch., 18a, 1276. MASSENSPEKTROMETRISCHE UNTERSUCHUNGEN AN DER POSITIVEN SAULE IN Ar, Ar-He- UND Ar-H_2 GEMISCHEN.

34. Pettersson, E. and Lindholm, E., Arkiv Fysik, 23, 79. DISSOCIATION OF PROPANE MOLECULE IONS FORMED IN CHARGE EXCHANGE COLLISIONS WITH POSITIVE IONS. ION-MOLECULE REACTIONS OF PROPANE.

35. Schluter, H., Z. Naturforsch 18a, 439. REKOMBINATION UND IONISATION IN EINER STATIONAREN HOCHFREQUENZENTLADUNG.

36. Sieck, L.W. and Johnson, R.H., J. Phys. Chem. 67, 2281. SOME ASPECTS OF THE RADIATION CHEMISTRY OF METHANE.

37. von Trepka, L., Z. Naturforsch. 18a, 1122. UBER EINIGE DURCH NEGATIVE IONEN IN ALKOHOLEN AUGELOSTE IONEN-MOLEKULE-REAKTIONEN.

38. Volkov, V.M. and Levin, A.A., Zh. Strukt. Khim., 4, 114 (1963). THE MECHANISM OF THE ADDITION OF A PROTON TO METHANE.

39. Weiner, E.R., Hertel, G.R., and Koski, W.S., J. Am. Chem. Soc., 86, 788 (1964). GAS PHASE REACTIONS BETWEEN CARBON TETRACHLORIDE AND MASS ANALYZED IONS OF NITROGEN BETWEEN 3 AND 200 ev.

40. Wexler, S., J. Am. Chem. Soc., 85, 272. ON THE MECHANISM OF THE ISOTOPIC EXCHANGE OF TRITIUM WITH METHANE.

41. Yang, J-H. and Conway, D.C., J. Chem. Phys., 40, 1729 (1964). BONDING IN ION CLUSTERS. I. O_4^+.

1. Aleksandrov, E.B., Bonch-Bruevich, A.M., and Khodovoi, V.A., Bull. Acad. Sci., (USSR), Phys. Ser., 27, 1070. SPIN EXCHANGE.

2. Alfimov, M.V., Buden, N. Ya., Pristupa, A.I., and Shamshev, V.N., Bull. Acad. Sci. (USSR), Div. Chem. Sci., 1963, 1525. EXCITATION OF TRIPLET STATES OF NAPHTALENE AND BENZENE MOLECULES BY FAST ELECTRONS.

3. Altshuler, S., J. Geophys. Res., 68, 4707. EFFECTS OF INELASTIC COLLISIONS UPON ELECTRICAL CONDUCTIVITY AND ELECTRON HEATING IN THE LOWER IONOSPHERE.

4. Athay, R.G. and Hyder, C.L., Astrophys. J. 137, 21. CORONAL IONIZATION BY TWO-STEP COLLISION PROCESSES.

5. Baraff, G.A. and Buchsbaum, S.J., Phys. Rev., 130, 1007. ANISOTROPIC ELECTRON DISTRIBUTION AND THE dc AND MICROWAVE AVALANCHE BREAKDOWN IN HYDROGEN.

6. Becker, P.M. and Dahler, J.S., Phys. Rev. Letters, 10, 491. DOUBLE EXCITATION OF HELIUM BY ELECTRONIC IMPACT.

7. Beigman, I. and Vainshtein, L., Bull. Acad. Sci. (USSR), Phys. Ser., 27, 1018. EMPIRICAL FORMULAE FOR THE EFFECTIVE CROSS SECTIONS OF EXCITATION AND IONIZATION.

8. Bely, O., Tully, J. and Regemorter, H.V., Ann. Phys. (Paris) 8, 303. L'EXCITATION DES ATOMES PAR CHOCS ELECTRONIQUES. APPLICATION A L'EXCITATION DES TRANSITIONS DE RESONANCE DANS LES SERIES ISOELECTRONIQUES DU LITHIUM ET DU SODIUM.

9. Biberman, L.M., Toropkiw and Yanov, K.N., Yi., Soviet Phys. Tech.Phys. (English Transl) 7, 605; original: 32, 827 (1962). THE THEORY OF MULTISTAGE IONIZATION AND RECOMBINATION.

10. Biondi, M.A., Phys. Rev., 129, 1181. STUDIES OF THE MECHANISM OF ELECTRON-ION RECOMBINATION. I.

11. Bogdanova, I. P. and Geitsi, I.I., Bull. Acad. Sci. (USSR), Phys. Ser., 27, 1056. MEASURABILITY OF OPTICAL EXCITATION FUNCTIONS BY MEANS OF MODULATED ELECTRON BEAMS.

12. Bogdanova, I.P. and Geitsi, I.I., Opt. Spectry. (USSR)(English Transl) 14, 312; original: 588. USE OF MODULATED ELECTRON BEAMS IN THE STUDY OF THE OPTICAL EXCITATION FUNCTIONS OF ATOMS.

13. Bohn, W.L., Z. Physik 174, 383. IONISATIONSGLEICHUNG FUR PLASMEN DES MITTLEREN TEMPERATUR UND DICHTEBEREICHES.

14. Bonham, R.A. and Iijima, T., J. Phys. Chem., 67, 2266. THE THEORY OF ELECTRON SCATTERING FROM MOLECULES. II. MOLECULAR HYDROGEN.

15. Booz, J and Ebert, H.G., Z. Angew. Phys., 16, 180. ANFANGSREKOMBINATION von IONEN IN LUFT.

16. Brace, L.H., Spencer, N.W., and Carignan, G.R., J. Geophys. Res. 68, 5397. IONOSPHERE ELECTRON TEMPERATURE MEASUREMENTS AND THEIR IMPLICATIONS.

17. Burgess, A. and Rudge, M.R.H., Proc.Roy. Soc. (London) A273, 372. THE IONIZATION OF HYDROGENIC HYDROGEN IONS BY ELECTRON IMPACT.

18. Burke, P.G., Proc. Phys. Soc. (London) 82, 443. THE CONVERGENCE OF THE CLOSE COUPLING EXPANSION.

19. Burke, P.G., Schey, H.M. and Smith, K., Phys. Rev. 129, 1258. COLLISIONS OF SLOW ELECTRONS AND POSITRONS WITH ATOMIC HYDROGEN.

20. Caren, R.P., Phys. Rev., 131, 1904. MEASUREMENT OF ELECTRON MOBILITIES IN ARGON GAS IN A PURE VAPOR CLOUD CHAMBER.

21. Carlson, T.A., Phys. Rev., 131, 676. ELECTRON SHAKEOFF FOLLOWING THE β^-DECAY OF Ar^{41}.

22. Carlson, T. A. and White, R. M., J. Chem. Phys., 39. 1748. FRAGMENTATION OF THE EXCITED PARENT IONS, $(CH_3Kr^{82})^+$ and $(CH_3O^{18})^-$, FOLLOWING THE β^-DECAY OF CH_3Br^{82} AND THE β^+ DECAY OF CH_3F^{18}.

23. Chanin, L.M. and Rork, G.D., Phys. Rev., 132, 2547. MEASUREMENTS OF THE FIRST TOWNSEND IONIZATION COEFFICIENT IN NEON AND HYDROGEN.

24. Cook, C.J. and Peterson, J.R., Phys. Rev. Letters, 9, 164 (1962). DIRECT AND DISSOCIATIVE IONIZATION CROSS SECTIONS FOR ELECTRONS IN N_2.

25. Cottingham, W.B. and Buchsbaum, S.J., Phys. Rev., 130, 1002. ELECTRON IONIZATION FREQUENCY IN HYDROGEN.

26. Crain, C.M., J. Geophys. Res. 68, 2167. DECAY OF IONIZATION IMPULSES IN THE D AND E REGIONS OF THE IONOSPHERE.

27. Curran, R.K., J. Chem. Phys., 38, 780. FORMATION OF SF_6^- BY INELASTICALLY SCATTERED ELECTRONS.

28. Damburg, R. and Gailities, M., Proc. Phys. Soc.(London) 82, 1068. CALCULATIONS IN THE VICINITY OF THE 2s, 2p THRESHOLD OF THE CROSS SECTIONS FOR THE EXCITATION OF HYDROGEN ATOMS BY ELECTRONS.

29. Damburg, R. Ya. and Karule, E.M., Opt. Spectr. (USSR)(English Transl) 14, 165; original: 199. SCATTERING OF POSITRONS BY ATOMIC HYDROGEN.

30. Damburg, R. Ya. and Peterkop, R.K., Soviet Phys. JETP (English Tranl) 16, 1247; original: 43 1765 (1962). EXCITATION OF THE 2s and 2p LEVELS OF THE HYDROGEN ATOM BY SLOW ELECTRONS.

31. Danilov, A.D., Planetary Space Sci. 11, 1359. (Translated by H.S.M. Massey from Iskusstvennye Sputniki Zemil 15, 38). SOME QUESTIONS CONNECTED WITH RECOMBINATION AND IONIZATION PROCESSES IN THE EARTH'S ATMOSPHERE.

32. Dolder, K.T., Harrison, M.F.A. and Thonemann, P.C., Proc. Roy. Soc.(London) A274, 546. A MEASUREMENT OF THE IONIZATION CROSS-SECTION OF Ne^+ TO Ne^{2+} BY ELECTRON IMPACT.

33. Dunn, G.H. and Kieffer, L.J., Phys. Rev., 132, 2109. DISSOCIATIVE IONIZATION OF H_2: A STUDY OF ANGULAR DISTRIBUTIONS AND ENERGY DISTRIBUTIONS OF RESULTANT FAST PROTONS.

34. Dutton, J., Harris, F.M. and Llewellyn Jones, F., Proc. Phys. Soc. (London) 81, 52. THE DETERMINATION OF ATTACHMENT AND IONIZATION COEFFICIENTS IN AIR.

35. Ehrhardt, H. and Erbse, U., Z. Physik 172, 210. STREUUNG NIEDERENERGETISCHER ELEKTRONEN AN MOLEKULEN I.

36. Faure, A., Nedelec, O.,and Pebay-Peyroula, J-C., Compt. Rend. 256, 2145. DEPLORISATION MAGNETIQUE DE LA LUMIERE EMISE PAR BOMBARDMENT ELECTRONIQUE DE L'HELIUM 4.

37. Feldman, P. and Novick, R., Phys. Rev. Letters, 11, 278. AUTOIONIZING STATES IN THE ALKALI ATOMS WITH MICROSECOND LIFETIMES.

38. Ferguson, E., Ann. Phys. (N.Y.) 22, 351. STARK BROADENING OF PALMER LINES AT LOW ELECTRON DENSITIES.

39. Frish, S.E. and Revald, V.F., Opt. Spectry. (USSR) (English Transl) 15, 395; original: 726. EFFECTIVE CROSS SECTIONS FOR THE DIRECT AND STEPWISE EXCITATION OF NEON ATOMS.

40. Gailitis, M., Soviet Phys. JETP (English Transl) 17, 1325; original: 44, 1974. BEHAVIOR OF CROSS SECTIONS NEAR THRESHOLD OF A NEW REACTION IN THE CASE OF A COULOMB ATTRACTION FIELD.

41. Gailitis, M.K., Opt. Spectry. (USSR) (English Transl) 14, 249; CALCULATION OF THE EXCITATION OF IONS BY ELECTRONS USING COULOMBIC WAVE FUNCTIONS.

42. Gailitis, M. and Damburg, R., Proc. Phys. Soc. (London) 82, 192. THE INFLUENCE OF CLOSE COUPLING ON THE THRESHOLD BEHAVIOR OF CROSS SECTIONS OF ELECTRON-HYDROGEN SCATTERING.

43. Gailitis, M. and Damburg, R., Soviet Phys., JETP (English Transl) 17, 1107; original: 44, 1644. SOME FEATURES OF THE THRESHOLD BEHAVOIR OF THE CROSS SECTIONS FOR EXCITATION OF HYDROGEN BY ELECTRONS DUE TO THE EXISTENCE OF A LINEAR STARK EFFECT IN HYDROGEN.

44. Geiger, J., Z. Physik 175, 530. ELASTISCHE UND UNELASTISCHE STREUUNG von ELEKTRONEN AN GASEN I. STREUUNG AND HELIUM.

45. Geltman, S., Rudge, M.R.H., and Seaton, M.J., Proc. Phys. Soc. (London) 81, 375. ELECTRON IMPACT IONIZATION OF ATOMIC HYDROGEN.

46. Harrison, M.F.A., Dolder, K.T., and Thonemann, P.C., Proc. Phys. Soc. (London) 82, 368. A MEASUREMENT OF THE CROSS SECTION FOR THE IONIZATION OF N^+ TO N^{2+} BY ELECTRON IMPACT.

47. Heddle, D.W.U. and Lucas, C.B., Proc. Roy. Soc.(London) A271, 129. THE POLARIZATION OF ELECTRON IMPACT RADIATION IN HELIUM.

48. Heylen, A.E.D., J. Chem. Phys., 38, 765. INFLUENCE OF MOLECULAR BONDING ON THE TOWNSEND IONIZATION COEFFICIENTS OF HYDROCARBON GASES.

49. Heylen, A.E.D. and Lewis, T.J., Proc. Roy. Soc. (London) A271, 531. ELECTRON ENERGY DISTRIBUTION FUNCTIONS AND TRANSPORT CO-EFFICIENTS FOR THE RARE GASES.

50. Hsundi, R.K., Proc. Phys. Soc. (London)82, 372. ELECTRON PATH LENGTH IN COLLISION EXPERIMENTS.

51. Hurst, G.S., O'Kelly, L.B., Wagner, E.B., and Stockdale, J.A., J. Chem. Phys., 39, 1341. TIME-OF-FLIGHT INVESTIGATIONS OF ELECTRON TRANSPORT IN GASES.

52. Hughes, R.H., Kay, R.B., and Weaver, L.D., Phys. Rev., 129, 1630. POLARIZATION OF OPTICAL RADIATION INDUCED BY ELECTRON IMPACT ON HELIUM.

53. Hughes, R.H. and Weaver, L.D., Phys. Rev., 132, 710. EXCITATION OF THE He II λ4686 Å LINE BY ELECTRON IMPACT.

54. Iijima, T. and Bonham, R.A., J. Phys. Chem. 67, 2769. THE THEORY OF ELECTRON SCATTERING FROM MOLECULES. III. HYDROGEN MOLECULE ION.

55. Iijima, T., Bonham, R.A., and Ando, T., J. Phys. Chem., 67, 1472. THE THEORY OF ELECTRON SCATTERING FROM MOLECULES I. THEORETICAL DEVELOPMENT.

56. Jesse, W.P., J. Chem. Phys., 38, 2774. ISOTOPE EFFECT IN THE IONIZATION OF POLYATOMIC GASES BY BETA PARTICLES.

57. Kamenetskii, V.D., Fiz. Probl. Spektroskopii, Akad. Nauk S.S.S.R., Materialy 13-go (Trinadtsatogo) Soveshch., Leningrad, 1960-61 (Punl. 1962). pp. 25-28. THE THEORY OF IMPACT OF SLOW ELECTRONS WITH ATOMS.

58. Kamenetskii, V.D. and Murav'ev, V.T., Bull. Acad. Sci. (USSR), Phys. Ser., 27, 1027. GENERAL METHOD FOR THE DERIVATION OF TRIAL WAVE FUNCTIONS.

59. Kononovich, E.V., Soviet Astron. A.J. (English Transl) 6, 811; original: 39, 1045 (1962). THE PROBABILITY OF HYDROGEN IONIZATION BY ELECTRON IMPACT.

60. Kownacki, S., J. Geophys. Res. 68, 5461. IONIZATION OF THE ATMOSPHERE DUE TO BETA PARTICLES EMITTED BY FISSION PRODUCTS.

61. Kretchmer, C.B. and Petersen, H.L., J. Appl. Phys.,34, 3209. USE OF LANGMUIR PROBES TO STUDY ION-ELECTRON RECOMBINATION.

62. Kuppermann, A. and Raff, L.M., Disc. Faraday Soc., 35, 30. ELECTRON-IMPACT SPECTROSCOPY.

63. Kuppermann, A and Raff, L.M., J. Chem.Phys., 39, 1607. DIFFERENCES BETWEEN LOW-ENERGY ELECTRON-IMPACT SPECTRA AT 0° AND AT LARGE SCATTERING ANGLE.

64. Kuprianov, S.E. and Latypov, Z.Z., Soviet Phys., JETP (English Transl) 18, 558 (1964); original: 45, 815. IONIZATION OF POSITIVE IONS BY ELECTRONS.

65. Latter, R. and Lelevier, R.E., J. Geophys. Res., 58, 1643. DETECTION OF IONIZATION EFFECTS FROM NUCLEAR EXPLOSIONS IN SPACE.

66. Legler, W., Z. Physik. 173, 169. ANREGUNG von V-STRAHLUNG IN STICKSTOFF UND WASSERSTOFF DURCH EINEN ELEKTRONENSCHWARM.

67. Lewis, R.R., Phys. Rev., 130, 666. DISCUSSION OF ELECTRON OPTICS LIMIT OF OPTICALLY PUMPED ALKALI VAPOR.

68. Lowke, J.J., Australian J. Phys., 16, 115. THE DRIFT VELOCITY OF ELECTRONS IN HYDROGEN AND NITROGEN.

69. Liubimov, A.P., Pavlor, S.I., Ratchovoskii, V.I., and Zaitseva, N.G., Bull. Acad. Sci. (USSR), Phys. Ser., 27, 1060. METHOD FOR MEASURING THE EFFECTIVE IONIZATION CROSS SECTIONS AND IONIZATION COEFFICIENTS OF METAL ATOMS DURING AN ELECTRONIC IMPACT.

70. McCoyd, G.C.and Milford, S.N., Phys. Rev., 130, 206. BORN CROSS SECTIONS FOR INELASTIC SCATTERING OF ELECTRONS BY HYDROGEN ATOMS. IV. APPROXIMATE VALUES FOR ALLOWED TRANSITIONS UP TO n = 10.

71. McElroy, M.B. and Hirschfelder, J.O., Phys. Rev., 131, 1589. HYPERVIRIAL THEOREM FOR COLLISIONS BETWEEN ELECTRONS AND ATOMS.

72. McFarland, R.H., Phys., Rev. Letters, 10, 397. CAUSE OF THE OBSERVED POLARIZATION OF ELECTRON-INDUCED RADIATION FROM HELIUM.

73. McFarland, R. H. and Soltysik, E.A., Phys. Rev., 129, 2581. ALTERNATE METHOD OF MEASUREMENT OF THE POLARIZATION OF LIGHT EMITTED BY HELIUM ATOMS EXCITED BY ENERGETIC ELECTRONS.

74. Makin, B. and Keck, J.C., Phys. Rev. Letters, 11, 281. VARIATIONAL THEORY OF THREE-BODY ELECTRON-ION RECOMBINATION RATES.

75. De Maria,G., Guerra, R., and Malaspina, L., Ric. Sci. Rend.3, 689. SEZIONI D'URTO MOLECOLARI ALLA IONIZZAZIONE PER COLLISIONE ELECTRONICA IN BASE A DETERMINAZIONI MASSAPETTROMETRICHE. NOTA II: SEZIONE D'URTO DI ALCUNI IDROCARBURI.

76. De Maria, G., Malaspina, L., and Placente, V., Ric. Sci. Rend. 3, 681. SEZIONI D'URTO MOLECOLARI ALLA IONIZZAZIONE PER COLLISIONE ELECTTRONICA IN BASE A DETERMINAZIONI MASSASPETTRO-METRICHE. NOTA I: METODO E RISULTATI PRELIMINARI.

77. Matsuzawa, M., J. Phys. Soc., Japan 18, 1473. EXCITATION OF π ELECTRONS IN BENZENE BY ELECTRON IMPACT

78. Meadows-Reed, E. and Smith, C.R., NASA Tech. Note D-1851. MASS SPECTROMETRIC INVESTIGATIONS OF THE ATMOSPHERE BETWEEN 100 AND 227 KILOMETERS ABOVE WALLOPS ISLAND, VIRGINIA.

79. Mentzoni, M. H., J. Geophys. Res. 68, 4181. EFFECTIVE ELECTRON RECOMBINATION IN HEATED NITROGEN.

80. Mentzoni, M.H. and Row, R.V. Phys. Rev., 130, 2312. ROTATIONAL EXCITATION AND ELECTRON RELAXATION IN NITROGEN.

81. Morgulis, N.D. and Korchevoi, Yu. P., Soviet Phys. Tech. Phys. (English Transl) 7, 655; original: 82, 827 (1962). MOBILITY AND SCATTERING CROSS SECTIONS OF ELECTRONS IN WEAKLY IONIZED CESIUM PLASMA.

82. Moruzzi, J.L. and Craggs, J.D., Proc. Phys. Soc. (London) 82, 979. MEASUREMENT OF IONIZATION AND ATTACHMENT COEFFICIENTS IN C_3F_8.

83. Moskvin, Yu. V., Opt. Spectry. (USSR)(English Transl) 15, 316; original: 582. PHOTOIONIZATION OF ATOMS AND RECOMBINATION OF IONS IN THE VAPORS OF ALKALI METALS.

84. Murav'ev, V.T., Bull. Acad. Sci. (USSR), Phys. Ser. 27, 1030. COMPUTATION OF COLLISIONS OF SLOW ELECTRONS WITH HYDROGEN ATOMS USING THE METHOD OF TRIAL FUNCTIONS.

85. Nedelec, O., Deschizeaux, M-N., and Pebay-Peyroula, J-C., Compt. Rend. 257, 3130. OBSERVATION D'UNE PRECESSION COHERENTE LOSS DE L'EXCITATION DE NIVEAUX ATOMIQUES PAR BOMBARDMENT D' ELECTRONS PULSES.

86. Neynaber, R.H., Marino, L.L., Rothe, E.W., and Trujillo, S.M., Phys. Rev., 129, 2069. LOW-ENERGY ELECTRON SCATTERING FROM ATOMIC NITROGEN.

87. Nicolet, M. and Swider, W. Jr., Planetary Space Sci. 11, 1459. IONOSPHERIC CONDITIONS.

88. Nisbet, J.S. and Quinn, T.P., J. Geophys. Res. 68, 1031. THE RECOMBINATION COEFFICIENT OF THE NIGHTTIME F LAYER.

89. Ochkur, V.I. and Petrun'kin, A.M., Opt. Spectr. (USSR)(English transl) 14, 245; original: 457. THE CLASSICAL CALCULATION OF THE PROBABILITIES OF EXCITATION AND IONIZATION OF ATOMS BY ELECTRON IMPACT.

90. Olson, O.D. and Skarsbard, H.M., Can. J. Phys., 41, 391. PROBE STUDIES OF HELIUM AFTERGLOWS DOMINATED BY COULOMB INTERACTIONS.

91. O'Malley, T. F., Phys. Rev., 130, 1020. EXTRAPOLATION OF ELECTRON-RARE GAS ATOM CROSS SECTIONS TO ZERO ENERGY.

92. Oskam, H.J. and Mittelstadt, V.R., Phys. Rev., 132, 1445. RECOMBINATION COEFFICIENT OF MOLECULAR RARE-GAS IONS.

93. Parker, J.H. Jr., Phys. Rev., 132, 2096. SPATIALLY DEPENDENT ENERGY DISTRIBUTIONS FOR ELECTRONS DRIFTING THROUGH A GAS IN A UNIFORM ELECTRIC FIELD.

94. Peterkop, R.K., Bull. Acad. Sci. (USSR), Phys. Ser. 27, 1012. ASYMPTOTIC BEHAVIOR OF THE WAVE FUNCTION OF A SYSTEM OF NEUTRAL AND CHARGED PARTICLES.

95. Pilyankevich, A.N., Soviet Phys. Tech. Phys. (English Transl) 8, 938 (1964); original: 33, 1260. ON THE CALCULATION OF CROSS SECTIONS FOR INELASTIC ELECTRON SCATTERING.

96. Platzman, R.L., J. Chem. Phys., 38, 2775. SOME REMARKS ON THE NATURE OF IONIZATION, IONIZATION YIELDS, AND ISOTOPE EFFECTS IN THE IONIZATION OF MOLECULES BY VARIOUS AGENCIES.

97. Prasad, S.S. and Prasad, K., Proc. Phys. Soc. (London) 82, 655. CLASSICAL CALCULATIONS FOR IMPACT IONIZATION CROSS SECTIONS.

98. Read, F.H. and Whiterod, G.L., Proc. Phys. Soc. (London) 82, 434. ELECTRON IMPACT SPECTROSCOPY 1. THE DETERMINATION OF THE SYMMETRY SPECIES OF MOLECULAR EXCITED STATES.

99. Rees, M.H., Planetary Space Sic., 11, 1209. AURORAL IONIZATION AND EXCITATION BY INCIDENT ENERGETIC ELECTRONS.

100. Roach, F.E., J. Geophys. Res. 68, 1015. THE AURORA AND TRAPPED ELECTRONS.

101. Robben, F., Kunkel, W.B., and Talbot, L., Phys. Rev., 132, 2363. SPECTROSCOPIC STUDY OF ELECTRON RECOMBINATION WITH MONATOMIC IONS IN A HELIUM PLASMA.

102. Robinson, P.D., Proc. Phys. Soc. (London) 81, 15. THE EFFECTS OF DEGENERACY ONF THE INELASTIC SCATTERING OF ELECTRONS AND PROTONS BY HYDROGEN ATOMS.

103. Rother, H., Z. Physik 173, 441. GESCHWINDIGKEITSVERTEILUNG der ELEKTRONEN BEI UNELASTISCHEN STOSSEN.

104. Sagalyn, R.C. and Smiddy, M., J. Geophys. Res. 68, 199. MEASUREMENT AND INTERPRETATION OF ION DENSITY DISTRIBUTIONS IN THE DAYTIME F REGION.

105. Salmon, J., J. Phys. 24, 1118. MOBILITE ET TEMPERATURE DES IONS ET DES ELECTRONS DANS UN GAZ FAIBLEMENT IONISE.

106. Schluter, H., Z. Naturforsch 18a, 439. REKOMBINATION UND IONIZATION IN EINER STATIONAREN HOCHFREQUENZENTLADUNG.

107. Schmeltekopf, A.L. Jr., and Broida, H.P., J. Chem. Phys., 39, 1261. SHORT-DURATION VISIBLE AFTERGLOW IN HELIUM.

108. Sears, R. D., J. Geophys. Res. 68, 5135. CONTRIBUTION OF ENERGETIC PHOTOELECTRONS TO D-REGION NONEQUILIBRIUM ELECTRON TEMPERATURES.

109. Simpson, J.A. and Mielczarek, S.R., J. Chem. Phys., 39, 1606 (1963). DETERMINATION OF ELECTRONIC ENERGY LEVELS OF MOLECULES BY LOW-ENERGY ELECTRON-IMPACT SPECTROSCOPY.

110. Skinner, J.G. and Brady, J.J., Phys. Rev., 129, 2087. NET FREQUENCY OF IONIZATION IN OXYGEN.

111. Smit, C., Heidman, G.M., and Smit, J.A., Physica 29, 245. RELATIVE OPTICAL EXCITATION FUNCTIONS OF HELIUM (EXCITATION BY ELECTRONS).

112. Somerville, W.B., Proc. Phys. Soc. (London) 82, 446. CROSS SECTIONS FOR ELECTRON-HYDROGEN ATOM COLLISIONS IN THE BORN APPROXIMATION TO THE REACTANCE MATRIX.

113. Stabler, R.C., Phys. Rev., 131, 679. ROTATIONAL EXCITATION OF MOLECULAR IONS BY SLOW ELECTRONS.

114. Stabler, R.C., Phys. Rev., 131, 1578. CAPTURE OF ELECTRONS BY MOLECULAR IONS.

115. Stotz, K.C., NASA Tech. Note D-2226. INVESTIGATION OF PLASMA AFTERGLOWS WITH APPLICATION IN NITROGEN.

116. Trefftz, E., Proc. Roy. Soc. (London) A271, 379. THE CROSS SECTION FOR IONIZATION OF O^{5+} BY ELECTRON IMPACT.

117. Tsuchiya, T., Bull. Chem. Soc., Japan, 36, 1290. HIGH-KINETIC ENERGY FRAGMENT IONS FROM ELIPHATIC HYDROCARBONS UNDER ELECTRON IMPACT III. NINE HYDROCARBONS RANGING FROM C_2 TO C_4.

118. Twiddy, N.D., Proc. Roy. Soc. (London) A275, 338. ELECTRON ENERGY DISTRIBUTION IN PLASMAS V. A SEARCH FOR EVIDENCE OF A HIGH ANOMALOUS RATE OF ENERGY EXCHANGE BETWEEN ELECTRONS OF LOW-PRESSURE DISCHARGE.

119. Vainshtein, L., Presniakov, L., Sobel'man, I., Soviet Phys. JETP, 45, 1970. A CERTAIN MODEL FOR CALCULATION OF THE EFFECTIVE CROSS SECTIONS FOR EXCITATION OF ATOMS.

120. Varsavsky, C.M., Planetary Space Sci. 11, 1001. ATOMIC PARAMETERS FOR FIVE TIMES IONIZED OXYGEN.

121. Volkova, L.M. and Deviatov, A.M., Bull. Acad. Sci. (USSR), Phys. Ser. 27, 1052. DETERMINING THE EFFECTIVE EXCITATION CROSS SECTIONS OF RESONANCE LINES OF POTASSIUM ATOMS.

122. Wada, J.Y. and Knechtli, R.C., Phys. Rev. Letters, 10, 513. MEASUREMENTS OF ELECTRON-ION RECOMBINATION IN A THERMAL CESIUM PLASMA.

123. Watson, M.B., Ferguson, H.I.S., and Nicholls, R.W., Can. J. Phys., 41, 1405. ELECTRICAL AND OPTICAL STUDIES OF THE ARGON PLASMA JET

124. Weber, T.A., Deck, R.T. and Mullin, C.J., Phys. Rev., 130, 660. LOW-ENERGY SPECTRUM OF ELECTRONS SCATTERED ON BOUND ELECTRONS.

125. Yanow, G., J. Astronaut. Sci. 10, 75. PRELIMINARY REPORT ON THE CALCULATION OF UPPER ATMOSPHERE MODELS FROM FIRST PRINCIPLES; THE EARTH.

126. Young, B.G., Johnson, A.W., and Carruthers, J.A., Can J. Phys. 41, 625. THE LOSS OF FREE ELECTRONS IN IRRADIATED AIR.

127. Zapesochnyi, I.P. and Shimon, L.L., Bull. Acad. Sci. (USSR), Phys. Ser. 27, 1037. EXCITATION FUNCTIONS OF ATOMS OF CERTAIN ALKALI METALS.

128. Zapesochnyi, I.P. and Shpenik, O.B., Bull. Acad. Sci. (USSR), Phys. Ser. 27, 1033. NEW EXPERIMENTAL METHODS FOR STUDYING EXCITATION IN ELECTRON-ATOM COLLISIONS.

129. Zhdanov, A.B., Tret'Yakova, M.L., Tsytovich, V.W., and Shcher Bakova, M.N., Soviet Phys. JETP (English Transl) 16, 245; original: 43, 342 (1962). IONIZATION LOSSES OF ULTRARELATIVISTIC ELECTRONS.

130. Zipf, E.C. Jr., and Fastie, W.G., J. Geophys. Res. 68, 6208. AN OBSERVATION OF DAY AIRGLOW EMISSION AT 6300 Å.

Inelastic Heavy Particle Collisions

B. Steiner and N. Wells

1. Abramenkov, A. D., Rybalko, V.F., and Fogel' Ya. M., Russia 1963, 76. IONIZATION OF A SUPERSONIC JET OF MERCURY VAPOR BY A BEAM OF HYDROGEN IONS.

2. Bay, Z.and Pearlstein, R.M., Phys. Rev., 130, 223. SEARCH FOR A SLOW COMPONENT IN ALPHA IONIZATION.

3. Bobashev, S.V., Andreev, E.P. and Anjudinov, V.A., Soviet Phys. JETP 45, 1759. EXCITATION OF THE BALMER SERIES SPECTRAL LINES OF ATOMIC HYDROGEN UPON PASSAGE OF H^+, H_2^+ and H_3^+ ION BEAMS THROUGH HELIUM AND NEON.

4. Boersch, H., Forst, G., and Schweda, S., Z. Physik 174, 446. ENERGIEVERLUSTE SCHNELLER LITHIUM-UND NATRIUM-IONEN BEI WECHSELWIRKUNG MIT EDELGASEN.

5. Bowen, H.C. and Linnett, J.W., J. Chem. Soc. 1963, 1064. BINDING IN THE HYDROGEN MOLECULE AND ITS ION.

6. Breene, R.G. Jr., Phys. Rev. 131, 2560. PROTON SCATTERING BY MOLECULES. I. THE TWO-STATE OXYGEN CASE AND THE MULTISTATE CASE.

7. Caudano, R., Delfosse, J.M., and Steyaert, J., Ann. Soc. Sci. Bruxelles, Ser. I, 76, 127 (1962). DISSOCIATION OF H_2^+ AND D_2^+ PASSING THROUGH A GAS.

8. Chanin, L.M. and Steen, R.D., Phys. Rev. 132, 2554. MOBILITIES OF CESIUM IONS IN CESIUM.

9. Dahlquist, J.A., J. Chem. Phys., 39, 1203. DRIFT VELOCITIES OF IONS IN NITROGEN.

10. Davis, W.D. and Vanderslice, T.A., Phys. Rev., 131, 219. ION ENERGIES AT THE CATHODE OF A GLOW DISCHARGE.

11. Dmitriev, I.S., Bull. Acad. Sci. (USSR), Phys. Ser. 27, 1081. POSSIBILITY OF PRODUCING MULTIPLY CHARGED IONS IN A CYCLOTRON BY PROTON IMPACT.

12. Dmitriev, I.S., Nikolaev, V.S., Fateeva, L.N., and Teplova, Ya.A. Soviet Phys. JETP (English Transl) 16, 259; original: 43, 361 (1962). INVESTIGATION OF THE LOSS OF SEVERAL ELECTRONS BY FAST MULTIPLY CHARGED IONS.

13. van Eck, J., de Heer, F.J., and Kistemaker, J., Phys. Rev., 130, 656. EXCITATION OF Ne, Ar, and Kr induced by H^+ and He^+ IMPACT (5-35 keV).

14. Engelhardt, A.G. and Phelps, A.V., Phys. Rev., 131, 2115. ELASTIC AND INELASTIC COLLISION CROSS SECTIONS IN HYDROGEN AND DEUTERIUM FROM TRANSPORT COEFFICIENTS.

15. Fache, Janine, Compt. Rend., 256, 2145. SPECTRE D'EMISSION de He-Ne.

16. Fehsenfeld, F.C., J. Chem. Phys., 39, 1653. CYCLOTRON RESONANCE IN SLIGHTLY IONIZED GASES.

17. Golubev, V.S., Soviet Phys. JETP (English Transl) 16, 1399; original: 43, 1985 (1962). INVESTIGATION OF CHARGE DIFFUSION IN IONIZED GASES BY THE DIFFUSION-WAVE TECHNIQUES.

18. Gulyaev, R.A., Nikol'skaya, K.I., and Nikol'skii, G.M., Soviet Astron. A.J. (English Transl) 7, 332; original: 40, 433. THE STRUCTURE OF THE SOLAR ATMOSPHERE IN ACTIVE AND UNDISTRUBED REGIONS. IONIZATION OF HYDROGEN AND HELIUm.

19. Gurevich, D.B. and Podmoshenskii, I.V., Opt. Spectry. (USSR) (English Transl) 15, 319; original: 587. THE RELATIONSHIP BETWEEN THE EXCITATION TEMPERATURE AND THE GAS TEMPERATURE IN THE POSITIVE COLUMN OF AN ARC DISCHARGE.

20. Hacker, D.S. and Bloomberg, H., J. Chem.Phys., 39, 3263. INVESTIGATION OF EARLY IONIZATION PROCESSES IN SHOCKED XENON.

21. Hatfield, L.L. and Hughes, R.H., Phys. Rev., 131, 2556. BALMER EMISSIONS INDUCED BY H_2^+ AND H_3^+ IMPACT ON MOLECULAR HYDROGEN.

22. Hoegl, A., Z. Angew. Phys. 16, 252. MESSUNG von KONZENTRATION UND BEWEGLICHKEIT ATMOSPHARISCHER IONEN.

23. Hughes, R.H., Lin, S., and Hatfield, L.L., Phys. Rev., 130, 2318. BALMER EMISSIONS INDUCED BY PROTON IMPACT ON MOLECULAR HYDROGEN.

24. Kockarts, G. and Nicolet, M., Ann. Geophys. 19, 370. L'HELIUM ET L'HYDROGENE ATOMIQUE AU COURS D'UN MINIMUM D' ACTIVITE SOLAIRE.

25. Kozhushner, M.A. and Sayasov., Yu. S., Opt. Spectry. (USSR) (English Transl) 15, 313; original: 577. THE RELATION BETWEEN THE CROSS SECTIONS FOR ELASTIC AND INELASTIC SCATTERING IN NONADIABATIC ATOMIC COLLISIONS.

26. Kupriianov, S.E. and Perov, A.A., Bull. Acad. Sci. (USSR), Phys. Ser. 27, 1102. DISSOCIATION OF POLYATOMIC IONS IN COLLISIONS WITH ATOMS AND MOLECULES OF GASES.

27. Kupriyanov, S.E. and Perov, A.A., Soviet Phys. Tech. Phys. (English Transl) 8, 618; original: 33, 823. THE DISSOCIATION OF IONS FROM METHANE, AMMONIA, AND WATER DUE TO COLLISIONS WITH MOLECULES IN THE 3.5-100 keV ENERGY RANGE.

28. Kupriyanov, S.E. and Perov, A.A., Doklady Phys. Chem. (English Transl) 149, 351: original: 1368. SPONTANEOUS AND INDUCED DECOMPOSITION OF DOUBLY CHARGED IONS.

29. Kupriyanov, S.E., Perov, A.A., and Tunitskii, N.N., Soviet Phys. JETP (English Transl) 16, 539; original: 43, 763 (1962). CROSS SECTIONS FOR DISSOCIATION OF D_3^+ IONS INTO D_2^+ AND D^+ IONS IN COLLISIONS WITH DEUTERIUM MOLECULES.

30. Kupriyanov, S.E., Perov, A.A., and Tunitskii, N.N., Soviet Phys. JETP (English Transl) 16, 1152; original: 43 , 1636 (1962). CROSS SECTIONS FOR DISSOCIATION OF D_2^+ IONS IN COLLISION WITH D_2 MOLECULES IN THE ENERGY RANGE FROM 3.5 TO 100 keV.

31. Kupriyanov, S.E., Tunitskii, N.N., and Perov, A.A., Soviet Phys. Tech. Phys. (English Transl) 8, 932 (1964); original: 33, 1252. THE DISSOCIATION OF D_2^+ IONS WITH ENERGIES FROM 3.5 TO 100 keV COLLISION WITH MOLECULES.

32. Kuyatt, C.E. and Jorgensen, T. Jr., Phys. Rev., 130, 1444. ENERGY AND ANGULAR DEPENDENCE OF THE DIFFERENTIAL CROSS SECTION FOR PRODUCTION OF ELECTRONS BY 50-100 keV PROTONS IN HYDROGEN GAS.

33. Lencher, A.M. and Singer, S.F., Planetary Space Sci. 11, 1151. THE ALBEDO NEUTRON THEORY OF GEOMAGNETICALLY TRAPPED PROTONS.

34. Lindhard, J., Scharff, M., and Schitt, H.E., Mat. Fys. Medd. Dan. Vid. Selsk. 33, No. 14. RANGE CONCEPTS AND HEAVY ION RANGE.

35. McGowan, Wm. and Kerwin, L., Can, J. Phys. 41, 316. ON THE APPLICATION OF ASTON BANDS AND APPEARANCE POTENTIAL MEASUREMENTS TO ION COLLISION STUDIES.

36. McGowan, J. Wm. and Kerwin, L., Can. J. Phys. 44, 1535. METASTABLE Ar^{+} IONS NEAR THE Ar^{++} THRESHOLD.

37. McDowell, M.R.C., NBS Tech. Note 185. LECTURES ON ION-ATOM COLLISIONS.

38. Meckbach, W. and Allison, S.K., Phys. Rev., 132, 294. RATIO OF THE EFFECTIVE CHARGE OF He BEAMS TRAVERSING GASEOUS AND METALLIC CADMIUM.

39. Mittleman, M.H., Phys. Rev., 129, 190. EXCITATION OF ATOMIC HYDROGEN BY FAST PROTONS.

40. Morgulis, N.D. and Korchevoi, Yu. P., Soviet Phys. Tech. Phys. (English Transl) 8, 853 (1964); original: 33, 1146. MOBILITY AND TRANSVERSE SCATTERING OF CESIUM IONS IN A WEEKLY IONIZED CESIUM PLASMA.

41. Ob"Edkov, V.D., Soviet Phys. JETP (English Transl) 16, 463; original: 43, 649 (1962). A VARIATIONAL METHOD FOR CONSTRUCTING THE POLARIZATION POTENTIAL IN COLLISION THEORY.

42. Ochkor, V.I., Soviet Phys. JETP (English Transl) 18, 503 (1964); original: 45, 734. THE BORN-OPPENHEIMER METHOD IN THE THEORY OF ATOMIC COLLISIONS .

43. Oskam, H. J. and Mittelstadt, V.R., Phys. Rev., 132, 1435. ION MOBILITIES IN HELIUM, NEON, AND ARGON.

44. Park, J.T. and Zimmerman, E.J., Phys. Rev., 131, 1611. STOPPING CROSS SECTIONS OF SOME HYDROCARBON GASES FOR 40-250 keV PROTONS AND HELIUM IONS.

45. Pretzer, D., Van Zyl, B., Geballe, R., Phys. Rev. Letters, 10, 340. LYMAN ALPHA PRODUCTION IN PROTON-RARE GAS COLLISIONS.

46. Rovinskii, R.E., Soviet Phys. Tech. Phys. 8, 361; original: 33, 489. ELECTRICAL CHARACTERISTICS OF A HIGH-PRESSURE XENON ARC.

47. Rudd, M.E. and Jorgensen, T. Jr., Phys. Rev. 131, 666. ENERGY AND ANGULAR DISTRIBUTION OF ELECTRONS EJECTED FROM HYDROGEN AND HELIUM GAS BY PROTONS.

48. Russek, A., Phys. Rev., 132, 246. IONIZATION PRODUCED BY HIGH-ENERGY ATOMIC COLLISIONS.

49. Smirnov, B.M., Soviet Phys. JETP (English Transl) 16, 81; original: 43, 112 (1962). INELASTIC COLLISIONS OF LIGHT ATOMS IN THE ADIABATIC APPROXIMATION.

50. Solov'ev, E.S., Il'in, R., Oparin, V.A., and Fedorenko, N.V., Soviet Phys. JETP (English Transl) 18, 342 (1964); original: 45, 401. IONIZATION OF GASES BY FAST HELIUM ATOMS AND SINGLY-CHARGED HELIUM IONS.

51. Strickler, T.D., J. Phys. Chem. 67, 825. IONIZATION BY ALPHA PARTICLES IN BINARY GAS MIXTURES.

52. Taylor, H.A. Jr., Brace, L.H., Brinton, H.C., and Smith, C.R., J. Geophys. Res. 68, 5339. DIRECT MEASUREMENTS OF HELIUM AND HYDROGEN ION CONCENTRATION AND TOTAL ION DENSITY TO AN ALTITUDE OF 940 KILOMETERS.

53. Temkin, A., J. Chem. Phys., 39, 161. RELATIVE PARTIAL WAVE THEORY OF DIATOMIC MOLECULES.

54. Vainshtein, L., Presnyakov, L., and Sobel'man, I., Soviet Phys. JETP (English Transl) 16, 370; original: 43, 518 (1962). EXCITATION OF ATOMS BY HEAVY PARTICLES.

55. Varob'ev, A.A., Komar, A.P., and Korolev., V.A., Soviet Phys. JETP (English Transl) 16, 306; original: 43 426 (1962). DECREASE OF FLUCTUATIONS OF THE IONIZATION PRODUCED BY ALPHA PARTICLES IN ARGON.

56. Wexler, S. and Hess, D.C., J. Chem. Phys., 38, 2308. IONIZATION BY IONS IN THE MeV RANGE.

57. Whyte, G.N., Radiation Res. 18, 265. ENERGY PER ION PAIR FOR CHARGED PARTICLES IN GASES.

58. Wobschall, D., Graham, J.R. Jr., and Malone, D.P., Phys. Rev., 131, 1565. ION CYCLOTRON RESONANCE AND THE DETERMINATION OF COLLISION CROSS SECTIONS.

59. Zozhushner, M.A. and Sayasov, Yu. S., Opt. Spectry (USSR) (English Transl) 15, 399; original: 399. THE PROBABILITY OF INELASTIC ATOMIC COLLISIONS IN THE CASE OF SEVERAL POINTS OF INTERSECTION (OR PSEUDO-INTERSECTIONS) OF TERMS.

1. Biberman, L.M. and Norman, E.G., Soviet Phys. JETP 45, 1970. SEMI-EMPIRICAL METHOD FOR THE CALCULATION OF THE ELASTIC SCATTERING CROSS SECTION OF SLOW ELECTRONS ON ATOMS.

2. Boersch, H. and Forst, G., Z. Physik 176, 221. STREUUNG von Li^+ -IONEN AN EDELGASEN.

3. Bogush, A.A. and Satsunkevich, I.S., Soviet Phys. JETP (English transl.) 16, 1375; original: 43, 1953 (1962). SCATTERING OF ELECTRONS ON PROTONS WITH ACCOUNT OF DIPOLE MOMENTS.

4. Bonham, R.A. and Iijima, T., J. Phys. Chem. 67, 2266. THE THEORY OF ELECTRON SCATTERING FROM MOLECULES. II. MOLECULAR HYDROGEN.

5. Burke, P.G., Proc. Phys. Soc. (London) 82, 443. THE CONVERGENCE OF THE CLOSE COUPLING EXPANSION.

6. Burke, P.G., Schey, H.M. and Smith, K., Phys. Rev., 129, 1258. COLLISIONS OF SLOW ELECTRONS AND POSITRONS WITH ATOMIC HYDROGEN.

7. Damburg, R. Ya. and Karule, E.M., Opt. Spect. (USSR)(English transl.) 14, 165; original: 199. SCATTERING OF POSITRONS BY ATOMIC HYDROGEN.

8. Damburg, R. Ya. and Peterkop, R.K., Soviet Phys. JETP (English transl.) 17, 167; original: 44, 244. RESONANCES IN THE SCATTERING OF ELECTRONS ON HYDROGEN ATOMS.

9. Dolique, J.M., Ann. Radioelec. 18, 167. COLLISIONS COULOMBIENNES, ET AUTRES COLLISIONS ELASTIQUES, DANS LES PLASMAS.

10. Ehrhardt, H. and Erbse, U., Z. Physik, 172, 210. STREUUNG NIEDERENERGETISCHER ELEKTRONEN AND MOLEKULEN I.

11. Engelhardt, A.G. and Phelps, A.V., Phys. Rev., 131, 2115. ELASTIC AND INELASTIC COLLISION CROSS SECTIONS IN HYDROGEN AND DEUTERIUM FROM TRANSPORT COEFFICIENTS.

12. Epstein, S.T. and Robinson, P.D., Phys. Rev., 129, 1396. HYPERVIRIAL THEOREMS FOR VARIATIONAL WAVE FUNCTIONS IN SCATTERING THEORY.

13. Fleming, R.J. and Higginson, G.S., Proc. Phys. Soc. (London) 81, 974. RESONANCE IN ELASTIC SCATTERING OF ELECTRONS BY HELIUM ATOMS.

14. Garrett, W.R. and Mann, R.A., Phys. Rev., 130, 658. MODEL FOR THE SCATTERING OF SLOW ELECTRONS BY CESIUM ATOMS.

15. Geiger, J., Z. Physik 175, 530. ELASTISCHE UND UNELASTISCHE STREUUNG von ELEKTRONE AN GASEN I. STREUUNG AN HELIUM.

16. Goldman, R. and Oster, L., Phys. Rev., 129, 1469. COULOMB INTERACTIONS IN A STRONG MAGNETIC FIELD.I. ADIABATIC CASE.

17. Hashino, T. and Matsuda, H., Prog. Theoret. Phys. (Koyoto) 89, 370. ON THE ELASTIC SCATTERING OF ELECTRONS OF NEARLY ZERO ENERGY BY HELIUM ATOMS.

18. Hashino, T. and Matsuda, H., Prog. Theoret. Phys. (Koyoto) 30, 918. ON THE ELASTIC SCATTERING OF SLOW ELECTRONS BY HELIUM ATOMS.

19. Hayess, E. and Wojaczek, K., Beitr. Plasma Phys. 3, 75. DIE ELEKTRONENBEWEGLICHKEIT IM QUECKSILBERDAMPFPLASMA.

20. Herzenberg, A. and Mandl, F., Proc. Roy. Soc.(London) A274, 253. RESONANT ELECTRON SCATTERING BY ATOMS.

21. Iijima, T., Bonham, R.A., and Ando, T., J. Phys. Chem., 67, 1472. THE THEORY OF ELECTRON SCATTERING FROM MOLECULES. I. THEORETICAL DEVELOPMENT.

22. Iijima, T. and Bonham, R.A., J. Phys. Chem. 67, 2769. THE THEORY OF ELECTRON SCATTERING FROM MOLECULES. III. HYDROGEN MOLECULE ION.

23. Jost, K. and Kessler, J., Z. Physik 176, 126. DIE ORTSVERTEILUNG MITTELSCHNELLER ELEKTRONEN BEI MEHRFACHSTREUUNG.

24. Kozhoshner, M.A. and Sayasov, Yu. S., Opt. Spect. (USSR) (English transl.) 15, 313; original: 577. THE RELATION BETWEEN THE CROSS SECTIONS FOR ELASTIC AND INELASTIC SCATTERING IN NONADIABATIC ATOMIC COLLISIONS.

25. Lindhard, J., Scharff, M., and Schitt, H.E., Mat. Fys. Medd. Dan. Vid. Selsk 33, No. 14. RANGE CONCEPTS AND HEAVY ION RANGES (NOTES ON ATOMIC COLLISIONS, II).

26. McElroy, M.B. and Hirschfelder, J.O., Phys., Rev. 131, 1589. HYPERVIRIAL THEOREM FOR COLLISIONS BETWEEN ELECTRONS AND ATOMS.

27. McEachran, R.P. and Fraser, P.A., Proc. Phys. Soc. (London) 82, 1038. EFFECT OF VIRTUAL EXCITATION OF THE 2s and 2p STATES ON THE ELASTIC SCATTERING BY ATOMIC HYDROGEN.

28. Martynenko, Yu. V., Firsov, O.B., and Chibisov, M.I., Soviet Phys. JETP (English transl) 17, 154; original: 44, 225. SCATTERING OF SLOW ELECTRONS ON ATOMS.

29. Moiseiwitsch, B.L., Proc. Phys. Soc. (London), 81, 35. QUANTUM DEFECTS AND SCATTERING LENGTHS.

30. Neynaber, R.H., Marino, L.L. Rothe, E. W., and Trujillo, S.M., Phys. Rev., 129, 2069. LOW-ENERGY ELECTRON SCATTERING FROM ATOMIC NITROGEN.

31. Ob"edkov, V.S., Soviet Phys. JETP (English transl.) 16, 473; original: 43, 649 (1962). A VARIATIONAL METHOD FOR CONSTRUCTING THE POLARIZATION POTENTIAL IN COLLISION THEORY.

32. Ohara, S., J. Phys. Soc.(Japan) 18, 852. NEGATIVE RESISTANCE IN RARE GASES.

33. O'Malley, T. F., Phys. Rev., 130, 1020. EXTRAPOLATION OF ELECTRON-RARE GAS ATOM CROSS SECTIONS TO ZERO ENERGY.

34. Reichert, E., Z. Physik 173, 392. DIE WINKELVERTEILUNG IM BEREICH 30 BIS 155° von ELASTISCH AN GOLDDAMPF GESTREUTEN ELEKTRONEN MIT ENERGIEN ZWISCHEN 150 and 1900 eV.

35. Robinson, P.D. and Hirschfelder, J.O., Phys. Rev., 129, 1391. VIRIAL THEOREM AND ITS GENERALIZATIONS IN SCATTERING THEORY.

36. Schulz, G.J., Phys. Rev. Letters, 10, 104. RESONANCE IN THE ELEASTIC SCATTERING OF ELECTRONS IN HELIUM.

37. Simpson, J.A. and Fano, U., Phys. Rev. Letters, 11, 158. CLASSIFICATION OF RESONANCES IN THE ELECTRON SCATTERING CROSS SECTIONS OF Ne AND He.

38. Stone, P.M. and Reitz, J.R., Phys. Rev., 131, 2101. ELASTIC SCATTERING OF SLOW ELECTRONS BY CESIUM ATOMS.

39. Temkin, A., NASA Tech. Note D-1849. POSITRON-HYDROGEN SCATTERING.

40. Temkin, A. and Pohle, R., Phys. Rev. Letters, 10, 22. ELECTRON-HYDROGEN PHASE SHIFTS JUST BELOW THE INELASTIC THRESHOLD.

41. Temkin, A. and Sullivan, E., Phys. Rev., 129, 1250. NONADIABATIC THEORY OF ELECTRON-HYDROGEN SCATTERING. II.

42. Tietz, T., J. Chem. Phys., 38, 1027. ELASTIC SCATTERING OF LOW-ENERGY ELECTRONS AND THE PERIODIC SYSTEM OF ELEMENTS.

43. Tietz, T. and Wojtczak, L., Soviet Phys. JETP (English transl.) 16, 63; original: 43, 87 (1962). FORMULA FOR CALCULATIONS OF PHASE SHIFTS IN CASE OF THOMAS-FERMI AND HARTREE POTENTIALS.

44. Twiddy, N.D., Proc. Roy. Soc. (London) A275, 338. ELECTRON ENERGY DISTRIBUTIONS IN PLASMAS V. A SEARCH FOR EVIDENCE OF A HIGH ANOMALOUS RATE OF ENERGY EXCHANGE BETWEEN THE ELECTRONS OF A LOW-PRESSURE DISCHARGE.

45. Uhler, J. and Rossi, J., Arkiv Fysik 24, 369. INVESTIGATIONS OF SOME PROPERTIES OF ISOTOPE SEPARATOR BEAMS OF DIFFERENT CHARGE STATES.

46. Veklenko, B.A., and Novobrantsev, I.V., Soviet Phys. JETP (English transl.) 16, 652; original: 43, 919 (1962). SINGLE ELECTRON APPROXIMATION IN COLLISION THEORY.

47. Veklenko, A. and Starostin, A.N., Soviet Phys. JETP (English transl.) 18, 182 (1964); original: 45, 260. OPTIMAL SYSTEM OF BASIS FUNCTIONS IN THE THEORY OF COLLISIONS BETWEEN ELECTRONS AND ATOMS.

Free Radicals and Chemical Kinetics

J.T. Herron

1. Avrahmi, M., and Kebarle, P., J. Phys. Chem., 67, 354 (1963). PRIMARY REACTIONS IN THE MERCURY-PHOTOSENSITIZED DECOMPOSITION OF PROPYLENE.

2. Avrahami, M., and Kebarle, P., Can. J. Chem., 41, 347 (1963). THE MERCURY-SENSITIZED PRIMARY DECOMPOSITION OF DEUTERATED PROPANES. A MASS SPECTROMETRIC STUDY AT LOW PRESSURES. PART II.

3. Barber, M., Cuthbert, J., Farren,J., and Linnett, J.W., Proc. Roy. Soc., 274A, 285, (1963). A MASS SPECTROMETER FOR STUDYING CHEMICAL REACTIONS.

4. Barber, M., Farren, J., and Linnett, J.W., Proc. Roy. Soc. 274A, 293 (1963). MASS SPECTROMETRIC SAMPLING THROUGH A SMALL HOLE IN THE ADIABATIC FLOW REGION.

5. Barber, M., Farren, J., and Linnett, J.W., Proc. Roy. Soc. 274A, 306 (1963). THE MASS SPECTROMETRIC STUDY OF THE REACTION OF METHYL RADICALS WITH OXYGEN.

6. Berkowitz-Mattuck, J.B., Buchler, A., Engelke, J.L., and Goldstein, S. N., J. Chem. Phys., 39, 2722 (1963). MASS-SPECTROMETRIC INVESTIGATION OF THE OXIDATION OF MOLYBDENUM AND TUNGSTEN.

7. Calcote, H. F. and Reuter, J. L., J. Chem. Phys. 38, 310 (1963). MASS-SPECTROMETRIC STUDY OF ION PROFILES IN LOW-PRESSURE FLAMES.

8. Campbell, J.S. and Kemball, C., Trans. Faraday Soc. 59, 2583 (1963). CATALYTIC FISSION OF THE CARBON-HALOGEN BOND. PART 2. REACTIONS OF TERTIARY BUTYL CHLORIDE WITH HYDROGEN AND DEUTERIUM ON EVAPORATED PLATINUM AND PALLADIUM FILMS.

9. Chiltz, G., Eckling, R., Goldfinger, P., Huybrechts, G., Johnston, H.S., Meyers, L., and Verbeke, G., J. Chem. Phys. 38, 1053 (1963). KINETIC ISOTOPE EFFECT IN PHOTOCHLORINATION OF H_2, CH_4, $CHCl_3$, AND C_2H_6.

10. Datz, S. and Taylor, E. H., J. Chem. Phys., 39, 1896 (1963). ATOM-MOLECULE REACTION OF HYDROGEN STUDIED BY MOLECULAR BEAMS.

11. Dong, P. and Cottin, M., J. Chim. Phys., 58, 803 (1961). STUDY BY MASS SPECTROMETRY OF THE PRODUCTS OF THERMAL DECOMPOSITION OF H_2, O_2, AND WATER VAPOR.

12. Diesen, R.W., J. Chem. Phys., 39, 2121 (1963). MASS SPECTRAL STUDIES OF KINETICS BEHIND SHOCK WAVES. II. THERMAL DECOMPOSITION OF HYDRAZINE.

13. Diesen, R.W. and Felmlee, W. J., J. Chem. Phys., 39, 2115 (1963). MASS SPECTRAL STUDIES OF KINETICS BEHIND SHOCK WAVES. I. THERMAL DISSOCIATION OF CHLORINE.

14. Fisher, I. P. and Lossing, F.P., J. Am. Chem. Soc. 85, 1018 (1963). IONIZATION POTENTIAL OF BENZYNE.

15. Foner, S.N., Science, 143, 441 (1964). FREE RADICALS AND UNSTABLE MOLECULES.

16. Fontijn, A. and Baughman, G.L., J. Chem. Phys., 38, 1784 (1963). CHEMI-IONIZATION IN THE ROOM-TEMPERATURE REACTION OF OXYGEN ATOMS WITH ACETYLENE.

17. Frasier, G.C. Jr., Fristrom, R.M., and Wehner, J.F., Am. I. Ch. E. Journal 9, 689 (1963). MICROSTRUCTURE OF A LOW-PRESSURE HYDROGEN-BROMINE FLAME.

18. Fristrom, R.M., Science, 140, 297, (1963). SCAVENGER PROBE SAMPLING: A METHOD FOR STUDYING GASEOUS FREE RADICALS.

19. Goldfinger, P., Huybrechts, G., and Verbeke, G., Adv. in Mass Spectrometry, 2, 302 (1963). MASS SPECTROMETRIC STUDY OF FAST REACTIONS AT ATMOSPHERIC PRESSURE.

20. Greene, F.T. and Milne, T.A., J. Chem. Phys. 39, 3150 (1963). MASS SPECTROMETRIC DETECTION OF POLYMERS IN SUPERSONIC MOLECULAR BEAMS.

21. Herron, J.T., J. Phys. Chem., 67, 2864 (1963). MASS SPECTROMETRIC STUDY OF THE RECOMBINATION OF BROMINE AND CHLORINE ATOMS ON PYREX.

22. Howlett, K.E., Sci. Progress, 51,429 (1963). THE USE OF MASS SPECTROMETRY IN CHEMISTRY AND ALLIED SUBJECTS.

23. Kaugman, J.J., J. Am. Chem. Soc. 85, 1576. THE EFFECT OF SUBSTITUTION ON THE IONIZATION POTENTIALS OF FREE RADICALS AND MOLECULES II. THEORETICAL INTERPRETATION OF δ_k VALUES FOR ALKYL RADICALS AND AMINES.

24. Kebarle, P., J. Phys. Chem., 67, 351 (1963). THE MERCURY-SENSITIZED DECOMPOSITION OF MERCURY DIMETHYL AT LOW PRESSURE.

25. Kebarle, P., J. Chem. Phys., 39, 2218 (1963). PRIMARY REACTIONS IN THE MERCURY-PHOTOSENSITIZED DECOMPOSITION OF 1-BUTYNE, PROPYNE, AND ACETYLENE AT LOW PRESSURES.

26. Kebarle, P., J. Phys. Chem., 67, 716 (1963). THE VINYL + H SPLIT IN THE MERCURY SENSITIZED PHOTOLYSIS OF ETHYLENE.

27. Kebarle, P. and Avrahami, M., J. Chem. Phys., 38, 700 (1963). PRIMARY REACTIONS IN THE MERCURY-PHOTOSENSITIZED DECOMPOSITION OF BUTENE-2 AT LOW PRESSURES.

28. Kebarle, P. and Avrahami, M., Can. J. Chem., 41, 335 (1963). THE MERCURY-PHOTOSENSITIZED DECOMPOSITION OF PROPANE. A MASS SPECTROMETRIC STUDY AT LOW PRESSURES. PART I.

29. Klein, F.S., Spindel, W., and Stern, M.J., J. Chim. Phys. 148 (1963). CATALYSIS OF ISOTOPIC EXCHANGE IN NITRIC OXIDE.

30. Knewstubb, P.F., Dawson, P.H., and Tickner, A.W., J. Chem. Phys. 38, 1031 (1963). MASS SPECTROMETRY OF IONS IN GLOW DISCHARGES. V. OXYGEN.

31. Knewstubb, P.F. and Tickner, A.W., J. Chem. Phys. 38, 464 (1963). MASS SPECTROMETRY OF IONS IN GLOW DISCHARGE. IV. WATER VAPOR.

32. Lee, R.W., J. Chem. Phys., 38, 448 (1963). DIFFUSION OF HYDROGEN IN NATURAL AND SYNTHETIC FUSED QUARTZ.

33. McAfee, K.B. Jr., and Edelson, D., Phys. Soc. 81, 382 (1963). IDENTIFICATION AND MOBILITY OF IONS IN A TOWNSEND DISCHARGE BY TIME-RESOLVED MASS SPECTROMETRY.

34. McGrath, W.D. and McGarvey, J.J., J. Chem. Phys., 37, 1574 (1962). ABSORPTION SPECTRUM AND DISSOCIATION ENERGY OF THE SO RADICAL.

35. McKinley, J.D., J. Chem. Phys., 40, 120 (1964). MASS SPECTROMETRIC INVESTIGATION OF THE HIGH-TEMPERATURE REACTION BETWEEN NICKEL AND CHLORINE.

36. Margrave, J.L., J, Phys. Chem., 66, 1209 (1962). THE HEAT OF FORMATION OF $BF_2(g)$.

37. Margrave, J.L., Nature, 197, 376 (1963). HEAT OF FORMATION OF THE DIFLUOROMETHYLENE RADICAL.

38. Narcissi, R.S., Schiff, H.I., Morgan, J.E., and Cohen, H.A., AFCRL-63-437, Air Force Cambridge Research Labs. (1963). CALIBRATION OF A FLYABLE MASS SPECTROMETER FOR N AND O ATOMS.

39. Onchi, M. and Ma, E., J. Phys. Chem., 67, 2240 (1963). AN APPLICATION OF THE OMEGATRON MASS SPECTROMETER TO THERMAL DECOMPOSITION STUDIES.

40. Pahl, M., Z. Naturforschg, 18a, 1276 (1963). MASSENSPEKTROMETRISCHE UNTERSUCHUNGEN AN DER POSITIVEN SAULE IN AR, AR-HE- UND AR-H_2-GEMISCHEN.

41. Palmer, T.F. and Lossing, F.P., J. Am. Chem. Soc. 85, 1733 (1963). FREE RADICALS BY MASS SPECTROMETRY. XXX. IONIZATION POTENTIALS OF ANILINO AND 2-,3- and 4- PYRIDYLMETHYL RADICALS.

42. Pottie, R. F. and Lossing, F.P., J. Am. Chem. Soc. 85, 269(1963). FREE RADICALS BY MASS SPECTROMETRY. XXIX. IONIZATION POTENTIALS OF SUBSTITUTED CYCLOPENTADIENYL RADICALS.

43. Prophet, H., J. Chem. Phys., 38, 2345 (1963). HEAT OF FORMATION OF METHYLENE.

44. Redmond, J.P., J.Phys. Chem., 67, 788 (1963). KINETICS OF THE LOW PRESSURE NITROUS OXIDE DECOMPOSITION ON A PLATINUM FILAMENT.

45. Schaefer, E.J., J. Geophys. Res. 68, 1175. THE DISSOCIATION OF OXYGEN MEASURED BY A ROCKET-BORNE MASS SPECTROMETER.

46. Schuler, H. and Arnold, G., Z. Naturforsch, 18a, 15. BEOBACHTUNG von ELEMENTARPROZESSEN AN ANGEREGTEN MOLEKULEN II. n-BUTAN.

47. Sholette, W.P. and Porter, R.F., J. Phys. Chem., 67, 177 (1963). MASS SPECTROMETRIC STUDY OF HIGH TEMPERATURE REACTIONS IN THE BORON-HYDROGEN-OXYGEN SYSTEM.

48. Smith, J.N. Jr., and Fite, W.L., 3rd International Rarefied Gas Dynamics Symp. 1, 430 (1963). RECENT INVESTIGATION OF GAS-SURFACE INTERACTIONS USING MODULATED-ATOMIC-BEAM TECHNIQUES.

49. Stebbings, R.F., Smith, A.C.H., and Gilbody, H.B., J. Chem. Phys., 38, 2280 (1963). CHARGE TRANSFER BETWEEN SOME ATMOSPHERIC IONS AND ATOMIC OXYGEN.

50. Vreeland, R.W., J. Am. Chem. Soc., 85, 3349 (1963). A MASS SPECTROMETRIC INVESTIGATION OF THE THERMAL DECOMPOSITION OF CYCLOBUTANE AT LOW PRESSURES.

51. Wong, E.L. and Potter, A.E. Jr., J. Chem. Phys., 39, 2211 (1963). REACTION RATES OF HYDROGEN, AMMONIA, AND METHANE WITH MIXTURES OF ATOMIC AND MOLECULAR OXYGEN.

1. Baker, B.H. and Miller, J.A., Nature, 199, 346 (1963). GEOLOGY AND GEOCHRONOLOGY OF THE SEYCHELLES ISLANDS AND STRUCTURE OF THE FLOOR OF THE ARABIAN SEA.

2. Bauer, C.A., J. Geophys. Res., 68, 6043 (1963). THE HELIUM CONTENTS OF METALIC METEORITES.

3. Beall, G.H., Hurley, P.M., Fairbairn, H.W., and Pinson, W.H., Am. Journal of Sci., 261, 571, (1963). COMPARISON OF K-Ar AND WHOLE ROCK R6-Sr DATING IN NEW QUEBEC AND LABRADOR.

4. Binns, R.A. and Miller, J.A., Nature, 199, 274 (1963). POTASSIUM-ARGON AGE DETERMINATIONS ON SOME ROCKS FROM THE BROKEN HILL REGION OF NEW SOUTH WALES.

5. Broecker, W.S., J. Geophys. Res., 68, 2817 (1963). A PRELIMINARY EVALUATION OF URANIUM SERIES INEQUILIBRIUM AS A TOOL FOR ABSOLUTE AGE MEASUREMENTS ON MARINE CARBONATES.

6. Butler, W.A., Jeffery, P.M., Reynolds, J.H., and Wasserburg, G.J., J. Geophys. Res., 68, 3282 (1963). ISOTOPIC VARIATIONS IN TERRESTRIAL XENON.

7. Catanzaro, E.J. and Kulp, J.L., Geochimica et Cosomochimica Acta, 28, 87, (1964). DISCORDANT ZIRCONS FROM THE LITTLE BELT (MONTANA) BEARTOOTH (MONTANA) AND SANTA CATALINA (ARIZONA) MOUNTAINS.

8. Chakraburtty, A.K., Stevens, C.M., Rushing, H.C., and Anders, E., J. Geophys. Res., 69, 505 (1964). ISOTOPIC COMPOSITION OF SILVER IN IRON METEORITES.

9. Clarke, W.B., and Thode, H.G., Canadian Journal of Physics, 42, 213 (1964). MASS SPECTROMETER MEASUREMENTS OF THE HALF LIVES OF Kr^{87}, Kr^{88}, Xe^{135}, and Xe^{138}.

10. Clayton, D.D., J. Geophys. Res., 68, 3714 (1963). A CALCULATION OF THE ABUNDANCES OF URANIUM AND THORIUM FROM THE PRIMORDIAL Pb^{206}/Pb^{207} RATIO.

11. Cooper, J.A., Richards, J.R., and Webbs, A.W., J. Geological Soc. of Australia, 10, 313 (1963). SOME POTASSIUM-ARGON AGES IN NEW ENGLAND, NEW SOUTH WALES.

12. Craig, H., Gordon, L.I., and Horibe, Y., J. Geophys. Res., 68, 5079 (1963). ISOTOPIC EXCHANGE EFFECTS IN THE EVAPORATION OF WATER. 1. LOW-TEMPERATURE EXPERIMENTAL RESULTS.

13. Craig, H., and Keeling, C.D., Geochimica et Cosmochimica Acta, 27, 549 (1963). THE EFFECTS OF ATMOSPHERIC N_2O ON THE MEASURED ISOTOPIC COMPOSITION OF ATMOSPHERIC CO_2.

14. DeFelice, J., Fazio, G.G., and Fireman, E.L., Science, 142, 673 (1963). COSMIC RAY EXPOSURE AGE OF THE FARMINGTON METEORITE FROM RADIOACTIVE ISOTOPES.

15. Doe, B.R., and Hart, S.R., J. Geophys. Res., 68, 3521 (1963). THE EFFECT OF CONTACT METAMORPHISM ON LEAD IN POTASSIUM FELDSPARS NEAR THE ELDORA STOCK, COLORADO.

16. Emiliani, C. and Mayeda, T., Am. Journal of Sci., 262, 107, (1964). OXYGEN ISOTOPIC ANALYSIS OF SOME MOLLUSCAN SHELLS FROM FOSSIL LITTORAL DEPOSITS OF PLEISTOCENE AGE.

17. Epstein, S., Sharp, R.P., and Goddard, I., J. of Geology, 71, 698 (1963. OXYGEN-ISOTOPE RATIOS IN ANTARCTIC SNOW, FIRN AND ICE.

18. Evernden, J.F. and Richards, J.R., Australia Nat. Univ. Pub. No. 206, 9, 1 (1962). POTASSIUM-ARGON AGES IN EASTERN AUSTRALIA.

19. Evernden, J.F., Savage, D.E., Curtis, G.H., and James, G.T., Am. Journal of Sci., 262, 145 (1964). POTASSIUM- ARGON DATES AND THE CENOZORI MAMMALIAN CHRONOLOGY OF NORTH AMERICA.

20. Fahrig, W.H. and Wanless, R.K., Nature, 200, 934 (1963). AGE AND SIGNIFICANT OF DIABASE DYKE SWARMS OF THE CANADIAN SHIELD.

21. Fairbairn, H.W., Faure, G., Pinson, W.H., Hurle, P.M., and Powell, J.L., J. Geophys. Res., 68, 6575 (1963). INITIAL RATIO OF STRONTIUM 87 TO STRONTIUM 86, WHOLE ROACK AGE, AND DISCORDANT BIOTITE IN THE MONTEREGIAN IGNEOUS PROVINCE°

22. Farquhar, R.M. and Russell, R.D., Geochimica et Cosmochimica Acta, 27, 1143 (1963). A NOMOGRAPH FOR THE INTERPRETATION OF ANOMALOUS LEAD ISOTOPE ABUNDANCE.

23. Faul, H. and Jager, E., J. Geophys. Res., 68, 3293 (1963). AGES OF SOME GRANITIC ROCKS IN THE VOSGES, SCHWARZWALD AND THE MASSIF CENTRAL.

24. Faure, G. and Hurley, P.M., J. Petrology 4, 31 (1963). THE ISOTOPIC COMPOSITION OF STRONTIUM IN OCEANIC AND CONTINENTAL BASSETS: APPLICATION TO THE ORIGIN OF IGNEOUS ROCKS.

25. Faure, G., Hurley, P.M., Fairbairn, H.W., and Pinson, W.H., Nature, 200, 769 (1963). AGE OF THE GREAT DYKE OF SOUTHERN RHODESIA.

26. Fitch, F.J., Miller, J.A., and Menisy, M.Y., Nature, 199, 449 (1963). GEOCHRONOLOGICAL INVESTIGATIONS ON ROCKS FROM NORTH WALES.

27. Friedman, I., Redfield, A.C., Schoen, B., and Harris, J., Reviews of Geophysics, 2, 177, (1964). THE VARIATION OF THE DEUTERIUM CONTENT OF NATURAL WATERS IN THE HYDROLOGIS CYCLE.

28. Hamilton, E.I. and Deans, T., Nature, 198, 776 (1963). ISOTOPIC COMPOSITION OF STRONTIUM IN SOME AFRICAN CARBONATITES AND LIMESTONES AND IN STRONTIUM MINERLAS.

29. Jensen, M.L., Utah Geological and Mineralogical Survey Bulletin 54, (1963). THE BEARING OG SULFUR ISOTOPES ON COLORADO PLATEAU URANIUM AND PETROLEUM DEPOSITS.

30. Jensen, M.L. and Dechow, E., Trans. Geological Soc. of S. Africa, 65, 1 (1962). THE BEARING OF SULPHUR ISOTOPES ON THE ORIGIN OF THE RHODESIAN COPPER DEPOSITS.

31. Kulp, J.L., Kologrivov, R., Engels, J., Catanzaro, E.J., Neuman, H., and Nilssen, B., Geochimica at Cosmochimica Acta, 27, 847 (1963). AGE OF THE TORDAL, NORWAY PEGMATITE- A CORRECTION.

32. Leipziger, F.D., Applied Spectroscopy, 17, 158, (1963). SOME NEW UPPER LIMITS OF ISOTOPIC ABUNDANCE BY MASS SPECTROMETRY.

33. Lepp, H., Goldich, S.S., and Kistler, R.W., Am. Journal of Sci., 261, 693 (1963). A GRENVILLE CROSS SECTION FROM PORT CARTIER TO MT. REED, QUEBEC, CANADA.

34. McDougall, I., Nature, 198, 677 (1963). POTASSIUM-ARGON AGES OF SOME ROCKS FROM VITI LEVU, FIJI.

35. McDougall, I., Compston, W., and Hawkes, D.D., Nature, 198, 564 (1963). LEAKAGE OF RADIOGENIC ARGON AND STRONTIUM FROM MINERALS IN PROTEROZOLIC DOLERITES FROM BRITISH GUIANA.

36. McDougall, I. and Tarling, D.H., Nature, 200, 54 (1963). DATING OF POLARITY ZONES IN THE HAWAIIAN ISLANDS.

37. Murthy, V.R., Geochimica at Cosmochimica Acta, 27, 1171 (1963). ELEMENTAL AND ISOTOPIC ABUNDANCES OF MOLYBDENUM IN SOME METEORITES.

38. Nicolaysen, L.O., Burger, A.J., and Johnson, R.L., Trans. Geolog. Soc. of S. Africa (1962). THE AGE OF THE SHAWA CARBONATITE COMPLEX.

39. Ostic, R.G., Russell, R.D., and Reynodls, P.H., Nature, 199, 1150 (1963). A NEW CALCULATION FOR THE AGE OF THE EARTH FROM ABUNDANCES OF LEAD ISOTOPES.

40. Patterson, C. and Duffield, B., Geochimica et Cosmochimica Acta, 27, 1180 (1963). THE ISOTOPIC COMPOSITION OF LEAD IN EASTERN ISLAND RHYOLITE.

41. Peterman, Z. and Hedge, C.E., U.S. Geol. Survey Prof. Paper 474-D, D100 (1964). AGE OF BASEMENT ROCKS FROM THE WILLISTON BASIN OF NORTH DAKOTA AND ADJACENT AREAS.

42. Poole, W.H., Beland, J., and Wanless, R.K., Geological Soc. America Bulletin, 74, 1063 (1963). MINIMUM AGE OF MIDDLE ORDOVICIAN ROCKS IN SOUTHERN QUEBEC.

43. Reynolds, J.H., J. Geophys. Res., 68, 2939, (1963). XENOLOGY.

44. Richards, J.R., Cooper, J.A., and Webb, A.W., J. Geol. Soc. Australia, 10, 299 (1963). POTASSIUM-ARGON AGES ON MICAS FROM THE PRECAMBRIAN REGION OF NORTH-WESTERN QUEENSLAND.

45. Richards, J.R. and Pidgeon, R.T., J. Geol. Soc. Australia, 10, 243 (1963). SOME AGE MEASUREMENTS OF MICAS FROM BROKEN HILL, AUSTRALIA.

46. Robinson, S.C., Loveridge, W.D., Rimsaite, J., and van Peteghem, J., The Canadian Mineralogist, 7, 533 (1963). FACTORS INVOLVED IN DISCORDANT AGES OF EUXENITE FROM A GRENVILLE PEGMATITE.

47. Shima, M., Geochimica at Cosmochimica Acta, 27, 911 (1963). GEOCHEMICAL STUDY OF BORON ISOTOPES.

48. Shima, M., J. Geophys. Res., 68, 4289 (1963). ISOTOPIC COMPOSITION OF GERMANIUM IN METEORITES.

49. Silver, L.T., I AEC Vienna 1963, Radioactive Dating. THE USE OF COGENETIC URANIUM-LEAD ISOTOPE SYSTEMS IN ZIRCONS IN GEOCHRONOLOGY.

50. Silver, L.T., Nuclear Geophys. - NAS-NRC Pub. 1075. THE RELATION BETWEEN RADIOACTIVITY AND DISCORDANCE IN ZIRCONS.

51. Silver, L.T. and Deutsch, S., J. Geology, 71, 721 (1963). URANIUM-LEAD ISOTOPIC VARIATIONS IN ZIRCONS: A CASE STUDY.

52. Silver, L.T., McKinney, C.R., Deutsch, S., and Bolinger, J., J. Geology, 71, 196 (1963). PRECAMBRIAN AGE DETERMINATIONS IN THE WESTERN SAN GABRIEL MOUNTAINS, CALIFORNIA.

53. Slawson, W.F., Kanasewich, E.R., Ostic, R.G., and Farquhar, R.M., Nature, 200, 413, (1963). AGE OF THE NORTH AMERICAN CRUST.

54. Smitheringale, W.G. and Jensen, M.L., Geochimica at Cosmochimica Acta, 27, 1183 (1963). SULFUR ISOTOPIC COMPOSITION OF THE TRIASSIC IGNEOUS ROCKS OF EASTERN UNITED STATES.

55. Stuiver, M., Am. Journal of Science, 262, 377 (1964). CARBON ISOTOPIC DISTRIBUTION AND CORRELATED CHRONOLOGY OF SEARLES LAKE SEDIMENTS.

56. Tatsumoto, M. and Patterson, C.C., Earth Science and Meteorites, North-Holland Pub. Co. 1963. THE CONCENTRATION OF COMMON LEAD IN SEA WATER.

57. Tatsumoto, M. and Patterson, C.C., Nature, 199, 350 (1963). CONCENTRATIONS OF COMMON LEAD IN SOME ATLANTIC AND MEDITERRANEAN WATERS AND IN SNOW.

58. Taylor, H.P., Albee, A.L., and Epstein, S., J. Geology, 71, 513 (1963). O^{18}. O^{16} RATIOS OF COEXISTING MINERALS IN THREE ASSEMBLAGES OF KYANITE-ZONE PELITIC SCHIST.

59. Taylor, H.P. and Epstein, S., J. of Petrology, 4, 51 (1963). O^{18}/O^{16} RATIOS IN ROCKS AND COEXISTING MINERALS OF THE SKAERGAARD INTRUSION, EAST GREENLAND.

60. Ulrych, T.J., Nature, 200, 561 (1963). DISCORDANT LEAD-URANIUM AGES DUE TO CONTINUOUS LOSS OF LEAD.

61. van Schmus, W.R., Wetherill, G.W., and Bickford, M.E., J. Geophys. Res., 68, 5589 (1963). R6-Sr AGE DETERMINATIONS OF THE NIPISSING DIABASE, NORTH SHORE OF LAKE HURON, ONTARIO, CANADA.

62. Wasserburg, G.J., J. Geophys. Res., 68, 4823 (1963). DIFFUSION PROCESSES IN LEAD-URANIUM SYSTEMS.

63. Wasserburg, G.J., Craig, H., Menard, H.W., Engel, A.E.J., and Engel, C.G., J. Geology, 71, 785 (1963). AGE AND COMPOSITION OF A BOUNTY ISLANDS GRANITE AND AGE OF A SEYCHELLES ISLAND GRANITE.

64. Webb, A.W., Cooper, J.A., and Richards, J.R., J. Geological Soc. Australia, 10, 317 (1963). K-Ar AGES ON SOME CENTRAL QUEENSLAND GRANITES.

65. Webb, A.A., McDougall, I. and Cooper, J.A., Nature, 199, 270 (1963). RETENTION OF RADIOGENIC ARGON IN GLAUCONITES FROM PROTEROZOIC SEDIMENTS, NORTHERN TERRITORY, AUSTRALIA.

66. Weber, J.N., Nature, 201, 63 (1964). CARBON AND OXYGEN ISOTOPE RATIOS AS ENVIRONMENTAL INDICATORS: ANOMALOUS RESULTS FROM SHELLS FROM BEACH SEDIMENTS OF LAKE MANAGUA, NICARAGUA.

67. Wetherill, G.W., J. Geophys. Res., 68, 2957 (1963). DISCORDANT URANIUM-LEAD AGES. 2. DISCORDANT AGES RESULTING FROM DIFFUSION OF LEAD AND URANIUM.

68. York, D., Nature, 201, 383 (1964). ANOMALOUS GALLNAS AND THE CONTINUOUS DIFFUSION OF LEAD.

69. Zahringer, J., Radioactive Dating IAEC, Vienna, (1963). K-Ar MEASUREMENTS OF TEKTITES.

70. Zahringer, J. and Gentnre, W., Nature, 199, 583 (1963). RADIOGENIC AND ATMOSPHERIC ARGON CONTENT OF TEKTITES.

Miscellaneous and Addenda
H. M. Rosenstock

1. Abbe, J.-C. and Adloff, J.-P., Compt. Rend. 258, 3003 (1964). SUR LES REACTIONS D'IONS POSITIFS AVEC L'ETHYLENE ET L'ETHANE.

2. Aleksandrov, E.B., Optika i Spektroskopiya, 61, 377 (1964). COHERENT EXCITATION OF STATES BY ELECTRON IMPACT.

3. Bakulina, I.N. and Ionov, N.I., Doklad, Akad. Nauk SSSR, 155 , 309 (1964). THE ELECTRON AFFINITY ENERGY OF COPPER, SILVER, AND GOLD ATOMS AS DETERMINED BY SURFACE IONIZATION.

4. Bates, D.R., Cook, C.J., and Smith, F.J., Proc. Phys. Soc., 83, 49 (1964). CLASSICAL THEORY OF ION-MOLECULE REARRANGEMENT COLLISIONS AT HIGH IMPACT ENERGIES.

5. Beckey, H.D., Angew. Chem. 75, 100 (1963). FELDIONISATION-MASSENSPEKTREN ORGANISCHER MOLEKULE.

6. Becky, H.D., Z. Naturf. 19a, 71 (1964). MOLEKULDISSOZIATION durch HOHE FELDER.

7. Berkowitz, J. and Chupka, W.A., J. Chem. Phys. 40, 287 (1964). VAPORIZATION PROCESSES INVOLVING SULFUR.

8. Berkowitz, J, and Chupka, W.A., J. Chem. Phys. 40, 2735 (1964). MASS SPECTROMETRIC STUDY OF VAPOR EJECTED FROM GRAPHITE AND OTHER SOLIDS BY FOCUSED LASER BEAMS.

9. Bertin, E.P. and Hamill, W.H., J. Am. Chem. Soc.,86, 1301 (1964). ELECTRON CAPTURE PROCESSES IN THE GAMMA RADIATION OF ORGANIC HALIDES IN HYDROCARBON RIGID MATRICES.

10. Bhatnagar, V.P., Indian J. Pure Appl. Phys. 2, 160 (1964). AN ULTRASOMIC METHOD FOR DETERMINING ELECTRON AND ION TEMPERATURES OF PLASMA.

11. Biondi, M.A., Ann. de Geophysique, 20, 34 (1964). ELECTRON-ION AND ION-ION RECOMBINATION.

12. Branscomb, L.M., Ann. de Geophysique, 20, 88 (1964). A REVIEW OF PHOTODETACHMENT AND RELATED NEGATIVE ION PROCESSES RELEVANT TO AERONOMY.

13. Brink, G.O., Phys. Rev. 134, A345 (1964). ABSOLUTE IONIZATION CROSS SECTIONS OF THE ALKALI METALS.

14. Brewer, R.G. and Kester, F. L., J. Chem.Phys., 40, 812 (1964). DISSOCIATION ENERGY OF THE CH RADICAL.

15. Brion, C.E., J. Chem. Phys., 40, 2995 (1964). IONIZATION OF OXYGEN BY "MONOENERGETIC" ELECTRONS.

16. Brytov, I.A. and Lukirsky, A.P., Optika i Spektroskopiya 16, 363 (1964). ON THE PHOTOIONIZATION ABSORPTION CROSS SECTION OF BERYLLIUM.

17. Bunkin, F.V. and Prokhorov, A.M., Zh. Eksp. Teor. Fiz, 46, 1090 (1964). EXCITATION AND IONIZATION OF ATOMS IN A STRONG RADIATION FIELD.

18. Canfield, L.R., Hass, G., and Hunter, W.R., J de Physique,25 , 124 (1964). THE OPTICAL PROPERTIES OF EVAPORATED GOLD IN THE VACUUM ULTRAVIOLET FROM 300A TO 2000A.

19. Cermak, V. and Herman, Z., Coll. Czech. Chem. Commun. 29, 953 (1964). THE MASS SPECTROMETRIC DETECTION OF HIGHLY EXCITED LONG LIVED STATES OF NOBLE GAS ATOMS.

20. Chantry, P. J. and Schulz, G.J., Phys. Rev. Letters, 12, 449 (1964). INTERPRETATION OF EXPERIMENTS ON DISSOCIATIVE ATTACHMENT ON IONIZATION OF MOLECULES.

21. Chen, J.C.Y., Physics Letters, 8, 183 (1964). ANHARMONICITY EFFECTS IN VIBRATIONAL EXCITATION OF MOLECULES BY SLOW ELECTRON IMPACT.

22. Comes, F.J. and Lessman, W., Z. Naturf. 19A, 508 (1964). DIE PHOTOIONISATION des WASSERSTOFFMOLEKULS.

23. Dubrovsky, G.V., Zh. Eksp. Teor. Fiz. 46, 863 (1964). NONADIABATIC TRANSITIONS IN SLOW COLLISIONS BETWEEN HEAVY PARTICLES.

24. Demkov, Yu. N., Zh. Eksp. Teor. Fix. 46, 1126 (1964). DETACHMENT OF ELECTRONS IN SLOW COLLISIONS BETWEEN NEGATIVE IONS AND ATOMS.

25. Earnshaw, D.G., Cook, G.L. and Dinneen, G.V., J. Phys. Chem. 68, 296 (1964). A STUDY OF SELECTED IONS IN THE MASS SPECTRA OF BENZENETHIOL AND DEUTERATED BENZENETHIOL.

26. Ebinghavs, H. and Nevert, H., Naturwissenschaften 51, 83 (1964). UBER die ELEKTRONENAFFINITAETEN der ALKALIMETALLE.

27. Ederer, D. L. and Tomboulian, D.H., Phys. Rev. 133, A1525. PHOTOIONIZATION CROSS SECTION OF NEON IN THE 80 TO 600A REGION.

28. Evans, D.F., Chem. Soc. Proceedings Dec. 1963, pg.378. EFFECT OF NITROGEN UNDER PRESSURE ON THE RYDBERG SPECTRA OF POLYATOMIC MOLECULES; THE NATURE OF THE LONG-WAVELENGTH OLEFIN BANDS.

29. Fite, W.L., Ann. de Geophysique, 20, 47 (1964). CHARGE TRANSFER AND ION-ATOM INTERCHANGE COLLISIONS ABOVE THERMAL ENERGIES.

30. Fuchs, R. and Taubert, R., Z. Naturf. 19A, 494 (1964). DIE KINETISCHE ENERGIE IONISIERTER MOLEKULFRAGMENTE. II UNTERSUCHUNGEN AN EINFACHEN PARAFFINEN.

31. Galli, A., Giardini-Guidoni, A., and Volpi, G.G., Il Nuovo Cimento 31, 1145 (1964). CHARGE EXCHANGE PROCESSES BETWEEN RARE GAS IONS AND SOME MOLECULES.

32. Gordeev, Yu. S, and Panov, M.M., Zh. Tekhn. Fiz. 34, 857 (1964). IONIZATION AND CAPTURE OF ELECTRONS BY THE COLLISIONS OF THE HYDROGEN IONS WITH THE ATOMS AND MOLECULES OF A GAS.

33. Goudsmit, S.A. and Richards, P.I., Proc. Nat. Acad. Sci., 51, 664 (1964). THE ORDER OF ELECTRON SHELLS IN IONIZED ATOMS.

34. Green, J.H. and Pinkerton, D.M., J. Phys. Chem. 68, 1107 (1964). HYDRIDE ION TRANSFER AND RADIOLYSIS REACTIONS IN PENTANE AND ISOPENTANE.

35. Gruen, N., Z. Naturf. 19A, 358 (1964). ZUSTANDSFUNKTIONEN UND ELEKTRONENAFFINITAETEN EINFACH NEGATIVER IONER.

36. Gurgev, M.V., Somin, L.V., and Tunitskii, N.N., Zhurnal Tekh. Fiz., 34, 535 (1964). ON THE MEASURE OF THE KINETIC ENERGY OF THE FRAGMENT IONS IN A MASS SPECTROMETER. I. ANALYSIS OF A LINE SHAPE.

37. Haarhoff, P.C., Molecular Physics, 6, 337 (1963). SEMI-CLASSICAL APPROXIMATION TO DENSITY OF VIBRATIONAL ENERGY LEVELS.

38. Haarhoff, P.C., Mol. Phys. 7, 101 (1963). THE DENSITY OF VIBRATIONAL ENERGY LEVELS OF POLYATOMIC MOLECULES.

39. Hand, C.W. and von Weissenhoff, H., Can. J. Chem., 42, 195(1964). ION-MOLECULE REACTIONS STUDIED BY TIME-OF-FLIGHT MASS SPECTROMETRY.

40. Hasted, J.B., Butterworths, Washington (L964). PHYSICS OF ATOMIC COLLISIONS.

41. Herron, J.T. and Klein, F.S., J. Chem. Phys. 40, 2731 (1964). MASS SPECTROMETRIC STUDY OF THE ISOTOPIC EXCHANGE RATE OF OXYGEN ATOMS WITH O_2, NO and NO_2.

42. Hirt, R.C. and Schmidt, R.G., Applied Spectroscopy 18, 30 (1964). BIBLIOGRAPHY OF VACUUM ULTRAVIOLET SPECTROSCOPY°

43. Homer, J.B., Lehrle, R.S., Robb, J.C., and THOMAS, D.W., Nature, 202, 795 (1964). GAS PHASE ION-MOLECULE INTERACTIONS INVOLVING ATOM TRANSFER; LIMITATIONS OF THE ORBITING THEORY IN ACCOUNTING FOR THE VARIATION OF CROSS SECTION WITH ENERGY.

44. Huffman, E., Larrabee, J.C., and Tanaka, Y., J. Chem. Phys., 40, 356 (1964). ABSORPTION COEFFICIENTS OF OXYGEN IN THE 1060-580A WAVELENGTH REGION.

45. Huffman, R.E., Larrabee, J.C. and Tanaka, Y., J. Chem. Phys. 40, 2261 (1964). ABSORPTION COEFFICIENTS OF CARBON MONOXIDE IN THE 1006 - 600A WAVELENGTH REGION.

46. Hunter, W.R. and Tousey, R., J. de Physique 25, 148 (1964). TRANSMITTANCE OF THIN FILMS IN THE EXTREME ULTRAVIOLET.

47. Koyano, I., Tanaka, I., and Omura, I., J. Chem. Phys. 40, 2734 (1964). CHEMI-IONIZATION IN PHOTOEXCITED ACETYLENE.

48. KROG, U., Rueppel, H., and Witt, H.T., Ber. Bunsengesellschaft f. Physik. Chem. 68, 115 (1964). ERGANZUNG wu der ARBEIT "PHOTOIONIZATION AN AROMATISCHEN AMINEN."

49. Kuprijanov, S.E., Zh. Tekhn. Fiz. 34, 861 (L964). INVESITAGTION OF THE DISSOCIATION OF THE DOUBLY CHARGED IONS. DISSOCIATION OF IONS OF CO^{++}

50. Kuroda, H., Nature, 201, 1214 (1964). IONIZATION POTENTIALS OF POLYCYCLIC HYDROCARBONS.

51. Kuyatt, C.E., Mielczarek, S.R., and Simpson, J.A., Phys. Rev. Letters, 12, 293 (1964). ENERGY LOSSES AND ELASTIC RESONANCES IN ELECTRON SCATTERING FROM H_2.

52. Latypov, Z.Z., Kuprianov, S.E., Tunitskii, N.N., Zh. Eksp. Teor. Fiz. 46, 833 (1964). IONIZATION ENCOUNTERS OF ELECTRONS WITH IONS AND ATOMS.

53. Lofthus, A. and Miescher, E., Can. J. Phys. 42, 848 (1964). ABSORPTION SPECTRUM OF THE NO MOLECULE.

54. Madden, R.P. and Codling, K., J. Opt. Soc. 54, 268 (1964). RECENTLY DISCOVERED AUTOIONIZING STATES OF KRYPTON AND XENON IN THE 380-600A REGION.

55. McGowan, J.W. and Kerwin, L., Can. J. Phys. 42, 972 (1964). THE EFFECT OF VIBRATIONAL EXCITATION OF H_2^+ ON ITS COLLISION INDUCED DISSOCIATION.

56. Meyerson, S., J. Phys. Chem. 68, 968 (1964). MASS SPECTRA RADIOLYSIS AND PHOTOLYSIS OF PENYL ALKYL KETONES°

57. Mori, M., Watanabe, T., Katsuura, K., J. Phys. Soc. Japan 19, 380 (1964). COLLISIONAL EXCITATION TRANSFER BETWEEN ATOMS IN THE RESONANT PROCESS.

58. Morrison, J.O. J. Chem. Phys. 40, 2488 (1964). THRESHOLD LAWS FOR PROCESSES OF AUTOIONIZATION.

60. Muccini, G.A., Hamill, W.H. and Barker, R., J. Phys. Chem. 68, 261 (1964). METASTABLE IONS IN MASS SPECTROMETRY°

61. Nagakura, Kaya, K, and Tsubomura, H., J. Mol. Spectr. 13, 1 (1964). VACUUM ULTRAVIOLET ABSORPTION SPECTRA AND ELECTRONIC STRUCTURES OF FORMIC ACID, ACETIC ACID AND ETHYL ACETATE.

62. Newton, A.S., J. Chem. Phys. 40, 607 (1964). TRIPLE IONIZATION IN SMALL MOLECULES.

63. Newton, A.S. and Sciamanna, J. Chem. Phys. 40, 718 (1964). METASTABLE STATE OF THE DOUBLY CHARGED CARBON DIOXIDE ION.

64. Olmsted, J., Street, K. Jr., and Newton, A.S., J. Chem. Phys. 40, 2114 (1964). EXCESS KINETIC ENERGY IONS IN MASS SPECTRA.

65. Paulson, J.F., Ann. de Geophysique 20, 75 (1964). LOW ENERGY CHARGE EXCHANGE AND ION-MOLECULE REACTIONS.

66. Peek, J.M., Phys. Rev. 134, A877, (1964). INELASTIC SCATTERING OF ELECTRONS BY THE HYDROGEN MOLECULE ION.

67. Read, F.H., Proc. Phys. Soc. 83, 619 (1964). ELECTRON IMPACT SPECTROSCOPY II. VIBRONIC INTERACTIONS IN EXCITATION CROSS SECTIONS.

68. Reich, H.-J. and Schmoranzer, Physics Letters 9, 127 (1964). DURCH SCHNELLE ELEKTRONEN ANGEREGTE SCHWINGUNGSTERME des MOLEKULAREN WASSERSTOFFS.

69. de Reilhac, L. and Damany-Astoin, N., Compt. Rend. Acad. Sci., 258, 519 (1964). SUR le SPECTRE d'ABSORPTION de l'OXYGENE dans l'ULTRAVIOLET EXTREME.

70. Roth, B., Phys. Rev. 133, A1257 (1964). THEORY OF ELECTRON CAPTURE IN H^+- H COLLISIONS.

71. Rudge, M.R.H. and Seaton, M.J., Proc. Phys. Soc., 83, 680 (1964). THE THRESHOLD LAW FOR IONIZING COLLISIONS.

72. Saraph, H.E., Proc. Phys. Soc., 83, 763 (1964). CROSS SECTIONS FOR $n \rightarrow n+1$ TRANSITIONS IN HYDROGEN PRODUCED BY ELECTRONS IMPACT.

73 Schmidt, W.A., Z. Naturf. 19A, 318 (1964). MASSENSPEKTROMETRISCHE UNTERSUCHUNG de FELDIONISATION von WASSERDAMPF and SPITZEN aus WOLFRAM, PLATIN UND IRIDIUM.

74. Silverman, S.M. and Lassettre, E.N., J. Chem, Phys. 40, 2922 (1964) COLLISION CROSS SECTIONS FOR OXYGEN IN THE EXCITATION ENERGY RANGE 10 TO 80V.

75. Simpson, J.A., Mielczarek, S.R., and Cooper, J., J. Opt. Soc., 54, 269 (1964). OBSERVATION OF OPTICALLY FORBIDDEN TRANSITIONS IN THE CONTINUUM OF THE RARE GASES BY ELECTRON ENERGY LOSS MEASUREMENTS.

76. Smirnov, B.M., Zh. Eksp. Teor. Fiz., 46, 1017 (1964). RESONANCE CHARGE EXCHANGE IN SLOW COLLISIONS.

77. Stabler, R.C., Phys. Rev., 133, A1268 (1964). CLASSICAL IMPULSE APPROXIMATION FOR INELASTIC ELECTRON-ATOM COLLISIONS.

78. St.John, R.M., Miller, F.L. and Lin, C.C., Phys. Rev. 134, A888 (1964). ABSOLUTE EXCITATION CROSS SECTIONS OF HELIUM.

79. Taubert, R., Z. Naturf. 19A, 484 (1964). DIE KINETISCHE ENERGIE IONISIERTER MOLEKULFRAGMENTE. I. METHODIK.

80. Thiele, E., J.Chem.Phys. 39, 3258 (1963). SMOOTH CURVE APPROXIMATION TO THE ENERGY LEVEL DISTRIBUTION FOR QUANTUM HARMONIC OSCILLATORS.

81. Tietz, T and Nowak, W., Nuovo Cimento 32, 224 (1964). THE INELASTIC SCATTERING FACTOR FOR TRANSITIONS IN ATOMS.

82. Tikhomirov, M.V., Komarov, V.N., and Tunitskii, N.N., Zh. Fiz. Khim. 38, 955 (1964). FORMATION OF N_3^+ AND N_4^+ IONS IN THE MASS SPECTROMETER.

83. Tilford, S.G. and Wilkinson, P.G., J. Mol. Spect. 12, 231 (1964). THE EMISSION SPECTRUM OF MOLECULAR NITROGEN IN THE REGION 900-1130A.

84. Tsubomura, H., Kimura, K., Kaya, K., Tanaka, J., and Nagakura, S., Bull. Chem. Soc. Japan 37, 417 (1964). VACUUM ULTRAVIOLET ABSORPTION SPECTRA OF SATURATED ORGANIC COMPOUNDS WITH NON-BONDING ELECTRONS.

85. Tuzzolino, A.J., Phys.Rev., 134, A205 (1964). QUANTUM EFFICIENCY OF SILICON IN THE VACUUM ULTRAVIOLET.

86. Utterback, N.G., Phys. Rev. Letters 12, 295 (1964). RESONANT EXCITATION IN HELIUM ION-ATOM COLLISIONS.

87. Vriens, L., Physics Letters 8, 260 (1964). CALCULATION OF ABSOLUTE IONIZATION CROSS SECTION OF He, He^*, He^+, Ne, Ne^*, Ne^+, Ar, Ar^*, Hg and Hg^*.

88. Weingartshofer, A. and Clarke, E.M., Phys. Rev. Letters 12, 591 (1964). CROSS SECTION FOR THE ION-MOLECULE REACTION $H_2^{+*} + H_2 \longrightarrow H_3^+ + H$ AS A FUNCTION OF THE VIBRATION STATE OF THE H_2^+ ION.

89. Zazula, P. and Wilhelmsson, H., Arkiv F. Fysik 24, 511 (1963). SURFACE IONIZATION PHENOMENA INVESTIGATED BY MASS SPECTROMETRIC DETERMINATION OF THE ION INITIAL VELOCITY DISTRIBUTION.

90. Zhikhareva, T.V., Vest. Leningr. U., Fiz. Khim. Ser. 1, 21 (1964). THE NEAR-THRESHOLD BEHAVIOR OF INELASTIC SCATTERING.

BIBLIOGRAPHY OF MOLECULAR WEIGHT MASS SPECTROMETRY

PREPARED BY SUBCOMMITTEE III

E. M. Emery, M. C. Hamming, W. E. McKinstry, Wanda Wright

1. Andersson, Carl-Ove, Ryhage, Ragnar, Stallberg-Stenhagen, Stina, Stenhagen, Einar, MASS SPECTROMETRIC STUDIES IX, Methyl and Ethyl Esters of Some Aliphatic α-Amino Acids, Arkiv for Kemi 19, 405 (1962).

2. Andersson, Carl-Ove, Ryhage, Ragnar, Stenhagen, Einar, MASS SPECTROMETRIC STUDIES X, Methyl and Ethyl Esters of N-Acetylamino Acids, Arkiv for Kemi 19, 417 (1962).

3. Ardenne, M. V.; Steinfelder, K.; Tuemmler, R.; and Schreiber, K., MOLECULAR MASS SPECTROGRAPHY OF NATURALLY OCCURRING SUBSTANCES - STEROIDS, Experientia 18, No. 19, 178 (1962).

4. Audier, H.; Diara, A.; Durazo, M. J., Dr.; Fetizon, M.; Foy, P.; and Vetter, W., ORIENTATION OF THE FRAGMENTATION IN MASS SPECTROMETRY BY INTRODUCTION OF FUNCTIONAL GROUPS, Ethylene Ketals of Steroids, Bull. Soc. Chim. France, No. 12, 2827 (1963).

5. Audier, H.; Fetizon, M.; and Vetter, W., ORIENTATION OF THE FRAGMENTATION IN MASS SPECTROMETRY BY INTRODUCTION OF FUNCTIONAL GROUPS, Delta-2-Steroids, Terpenes, and Related Substances, Bull. Soc. Chim. France 1963, 1971.

6. Aulinger, F., and Reerink, W., MASS SPECTRA OF ADDITIONAL COMPOUNDS FROM THE PYROLYSIS OF METHYL-CHLORO-SILANE, Z. Anal. Chem. 197, 24 (1963).

7. Barnes, C. S., and Occolowitz, J. L., THE MASS SPECTRA OF PHENYL METHYL ESTERS, Australian J. Chem. 16, 219-224 (1963).

8. Beynon, J. H.; Saunders, R. A.; and Williams, A. E., MASS SPECTRUM OF TETRACHLORO COPPER PHTHALOCYANINE, Appli. Spec. 17, 63 (1963).

9. Bergstrom, Sune; Ryhage, Ragner; and Stenhagen, Einar, MASS SPECTROMETRIC STUDIES ON STEROLS AND BILE ACIDS, Svensk Kemisk Tidskrift 73, 566 (1961).

10. Bergstrom, Sune; Ryhage, R.; Samuelsson, B.; and Sjovall, J., DEGRADATION STUDIES ON PROSTAGLANDINS - PROSTAGLANDINS AND RELATED FACTORS 10, Acta Chemica Scandinavica 17, 2271 (1963).

11. Bergstrom, Sune; Ryhage, R.; Samuelsson, Bengt; and Sjovall, Jan, PROSTAGLANDINS AND RELATED FACTORS: 15. THE STRUCTURES OF PROSTAGLANDIN E_1, F_1 , AND F_1 , J. Biological Chem. 238, 3555 (1963).

12. Biemann, K.; Bommer, P.; Burlingame, A. L.; and McMurray, W. J., HIGH-RESOLUTION MASS SPECTRA OF AJMALIDINE AND RELATED SUBSTANCES, Tetrahedron Letters, 1963, Nos. 28-30, 1969.

13. Biemann, K.; DeJongh, D. C.; and Schnoes, H. K., APPLICATION OF MASS SPECTROMETRY TO STRUCTURE PROBLEMS XIII, Acetates of Pentoses and Hexoses, J. Am. Chem. Soc. 85, 1763 (1963).

14. Biemann, K.; Schnoes, H. K.; and McCloskey, J. A., APPLICATION OF MASS SPECTROMETRY TO STRUCTURE PROBLEMS, Carbohydrates and Their Derivatives, Chem. Ind. (London), 448 (1963).

15. Biemann, K.; Spiteller, F. M.; and Spiteller, G., APPLICATION OF MASS SPECTROMETRY TO STRUCTURAL PROBLEMS, Alkaloids of the Bark of Aspidosperma Quebracho Blancho, J. Am. Chem. Soc. 85, 631 (1963).

16. Boyer, E. W.; Hamming, M. C.; and Ford, H. T., REARRANGEMENT TECHNIQUE FOR ANALYSIS OF ALKYL BENZENES BY MASS SPECTROMETRY, Unique Inlet System, Anal. Chem. 35, 1168 (1963).

17. Brion, C. E., and Dunning, W. J., ELECTRON IMPACT STUDIES OF SIMPLE CARBOXYLIC ESTERS, Trans. Faraday Soc. 59, 647 (1963).

18. Brunnee, C.; Jenckel, L.; and Kronenberger, K., STUDY OF THE APPLICATION OF THE MASS SPECTROMETERS AS SPECIFICALLY INDICATING IONIZATION DETECTORS FOR GAS CHROMATOGRAPHY, Z. Anal. Chem. 197, 42 (1963).

19. Budzikiewicz, H., APPLICATIONS OF THE MASS SPECTROMETER TO THE PROBLEMS OF DETERMINING STRUCTURES AND STEREOCHEMISTRY, Bull. Soc. Chim. France 1963, 1899.

20. Budzikiewicz, H.; Djerassi, C.; Puisieux, F.; Percheron, F.; and Poisson, J., VOACANGA ALKALOIDS - STRUCTURE OF VOACANINE AND VOACORINE - MASS SPECTRA OF VOBASINE AND ITS DERIVATIVES, Application of the Mass Spectrometer to the Problems of Determining Structures and Stereochemistry, Bull. Soc. Chim. France 1963, 1899.

21. Budzikiewicz, H.; Wilson, J. M.; and Djerassi, Carl, MASS SPECTROMETRY IN STRUCTURAL AND STEREOCHEMICAL PROBLEMS - XXXII. PENTACYCLIC TRITERPENES, J. Am. Chem. Soc. 85, 3688 (1963).

22. Budzikiewicz, H.; Wilson, J. M.; Djerassi, C.; Levy, J.; Lemen, J.; and Janot, M. M., MASS SPECTROMETRY IN STRUCTURAL AND STEREOCHEMICAL PROBLEMS, Akuammicine and Related Alkaloids, Tetrahedron 19, 1265 (1963).

23. Buechler, A., Berkowitz - Mattuck, J. B., GASEOUS METAL BORATES - MASS SPECTROMETRIC STUDY OF THE VAPORIZATION OF LITHIUM AND SODIUM META BORATES, J. Chem. Phys. 39, 286 (1963).

24. Cawley, J. J., and Westheimer, F. H., ON THE MECHANISM OF THE OXIDATIVE CLEAVAGE OF PHENYL-t-BUTYL CARBINOL WITH CHRONIC ACID, J. Am. Chem. Soc. 85, 1771 (1963).

25. Clayton, E., and Reed, R. I., ELECTRON IMPACT AND MOLECULAR DISSOCIATION. MASS SPECTRA OF PHYSOSTIGMINE AND SOME RELATED COMPOUNDS, Tetrahedron 19, 1345-58 (1963).

26. Coggeshall, N. D., COMPARISON OF MASS SPECTRAL REGULARITIES FOR n-PARAFFINS AND n-TERMINAL OLEFINS, J. Phys. Chem. 67, 183 (1963).

27. Coggeshall, N. D., STUDIES OF METASTABLE ION TRANSITIONS WITH A 180-DEGREE MASS SPECTROMETER, J. Chem. Phys., 37, No. 10, 2167 (1962).

28. Collin, J., PROGRESS AND RECENT PROBLEMS OF MASS SPECTROMETRY, Ind. Chim. Belge 28, 621 (1963).

29. Courtney, J. L., and Shannon, J. S., STUDIES IN MASS SPECTROMETRY - TRITERPENOIDS - STRUCTURE ASSIGNMENT OF SOME FRIEDELANE DERIVATIVES, Tetrahedron Letters, 1963, 13.

30. Craig, R. D.; Green, B. N.; and Waldron, J. D., APPLICATION OF HIGH RESOLUTION MASS SPECTROMETRY IN ORGANIC CHEMISTRY, Chemis 17, No. 2, 33 (1963).

31. Davis, J. W.; Hirsch, D. E.; Foster, N. G.; and Schwartz, F. G., SEPARATION AND CHARACTERIZATION OF POLAR MATERIAL IN DISTILLATE FUEL, U.S. Bur. Mines Rept. Invest. 1963, No. 6298.

32. Deffner, G., REVIEW OF THE APPLICATION OF MASS SPECTROMETRY TO STRUCTURE DETERMINATION OF NATURALLY OCCURRING SUBSTANCES WITH SPECIAL REGARD TO FOOD ANALYSIS, 2 - Lebensm. Untersuch Forsch 120, 300 (1963).

33. DeJongh, Don C., and Biemann, K., APPLICATION OF MASS SPECTROMETRY TO STRUCTURE PROBLEMS - XIV. ACETATES OF PARTIALLY METHYLATED PENTOSES AND HEXOSES, J. Am. Chem. Soc. 85, 2289 (1963).

34. De-Maria, G., SPURIOUS IONS IN MASS SPECTROMETRY AT HIGH TEMPERATURE, Ann. Chim. (Rome) 53, 993 (1963).

35. Djerassi, Carl, ALKALOID STUDIES - XLI. STRUCTURE OF THE ASPIDOSPERMA ALKALOID COMPATINERVINE, Experientia 19, 467 (1963).

36. Djerassi, C., MASS SPECTROMETRIC INVESTIGATIONS IN THE STEROID, TERPENOID, AND ALKALOID FIELDS, Pure Appli. Chem. 6, 575 (1963).

37. Djerassi, Carl; Budzikiewicz, H.; Owellen, R. J.; Wilson, J. M.; Kump, W. G.; LeCount, D. J.; Battersby, A. R.; and Schmid, H., MASS SPECTROSCOPY AND ITS APPLICATION TO STRUCTURAL AND STEREOCHEMICAL PROBLEMS - MASS SPECTRA OF ALKALOIDS OF THE REFRACTIN PLEICARPIN CLASS..., Helv. Chim. Acta. 46, 742 (1963).

38. Dolejs, L.; Hanus, V.; Cerny, V.; and Sorm, F., STEROIDS. MASS SPECTRA OF HOLARRHENA ALKALOIDS, Coll. Czech. Chem. Commun. 28, 1584 (1963).

39. Elliott, R. M. (ed), Advances in Mass Spectrometry, Pergamon, London, 1963.

40. Fields, E. K., and Meyerson, S., PREPARATION AND MASS SPECTRUM OF HEXA CHLORO CYCLOPROPANE, J. Org. Chem. 28, 1915 (1963).

41. Foffani, A.; Pignataro, S.; Cantone, B.; and Grasso, F., MASS SPECTRA OF DI-AZO COMPOUNDS. DI-AZO CARBONYL COMPOUNDS, Nuovo Cimento 29, 918 (1963).

42. Funasaka, W., ASPECT OF ANALYSIS AND TESTING IN PETROLEUM INDUSTRIES - APPLICATION OF GAS CHROMATOGRAPHY, MASS SPECTROMETRY, AND INFRARED SPECTROSCOPY, Sekiyu Gakhai Shi 6, No. 10, 752 (1963).

43. Gilbert, B.; Brissolese, J. Aguayo; Finch, Neville; Taylor, W. I.; Budzikiewicz, H.; Wilson, J. M.; and Djerassi, Carl, MASS SPECTROMETRY IN STRUCTURAL AND STEREOCHEMICAL PROBLEMS - XX. CARAPANAUBINE, A NEW ALKALOID FROM ASPIDOSPERMA CARAPANAUBA AND SOME OBSERVATIONS ON MASS SPECTRA OF OXINDOLE ALKALOIDS, J. Am. Chem. Soc. 85, 1523 (1963).

44. Gillis, R. G., and Occolowitz, J. L., ISOCYANIDES. III. ELECTRON IMPACT STUDY OF ALIPHATIC ISOCYANIDES, J. Org. Chem. 28, 2924 (1963).

45. Gohlke, R. S., OBTAINING THE MASS SPECTRA OF NONVOLATILE OR THERMALLY UNSTABLE COMPOUNDS, Chem. Ind. (London) 1963, 946-7.

46. Goldfinger, P., and Jeunehomme, M., Service de Chimie Physique, Universite Libre de Bruxelles, Brussels, MASS SPECTROMETRIC AND KNUDSEN-CELL VAPORIZATION STUDIES OF GROUP 2B-6B COMPOUNDS, Trans. Faraday Soc. 59, 2851 (1963).

47. Gorman, M.; Burlingame, A. L.; and Biemann, K., APPLICATION OF MASS SPECTROMETRY TO STRUCTURE PROBLEMS, Structure of Quebrachidine, Tetrahedron Letters 1963, 39.

48. Greene, Frank T., and Milne, Thomas A., MASS SPECTROMETRIC DETECTION OF POLYMERS IN SUPERSONIC MOLECULAR BEAMS, J. Chem. Phys. 39, 3150 (1963).

49. Grogerov, I. P., and Turkina, M. Y., MECHANISM OF HOMOLYTIC REACTIONS IN SOLUTION BY THE ISOTOPE AND MASS SPECTROSCOPY METHODS, Zh. Obshch. Khim. 33, 1894 (1963), Zh. Obshch. Khim. 33, 1901 (1963), Zh. Obshch. Khim. 33, 1907 (1963), and Zh. Obshch. Khim. 33, 1910 (1963).

50. Hanus, V., and Dolejsek, Z., EXPERIMENTAL DATA RELATED TO THEORIES OF MASS SPECTRA ORIGIN, Collection Czech. Chem. Commun. 28, No. 3, 652 (1963).

51. Henneberg, D., and Schomburg, G., MASS SPECTROMETRIC IDENTIFICATION IN CAPILLARY GAS CHROMATOGRAPHY, Gas Chromatography Intern. Symp. 4, 191 (1963).

52. Heyns, K., and Grützmacher, H. F., MASS SPECTROMETRIC INVESTIGATIONS, Mass Spectra of Free and N-Acetylated Amino Sugars, Ann. Chem. 667, 194 (1963).

53. Heyns, K., and Grützmacher, H. F., MASS SPECTROMETRIC INVESTIGATION OF ACYLATED PEPTIDES, Tetrahedron Letters, 1963, 1671 (1963).

54. Heyns, K., and Grützmacher, H. F., MASS SPECTROMETRIC INVESTIGATIONS, Mass Spectra of n-Acetyl Peptides of Some Simple Mono-Amino Carboxylic Acids, Ann. Chem. 669 (1963), 189.

55. Heyns, K., and Scharmann, H., MASS SPECTROMETRIC INVESTIGATION, Mass Spectra of the Derivatives of Mono Saccharides and Amino Sugars, Ann. Chem. 667, 183 (1963).

56. Hill, H. C., and Reed, R. I., VOLATILIZATION OF HIGH MELTING SOLIDS IN A MASS SPECTROMETER, J. Sci. Instrs. 40,259 (1963).

57. Hobrock, Brice G., and Kiser, Robert W., ELECTRON IMPACT INVESTIGATIONS OF SULFUR COMPOUNDS. III. 2-THIAPROPANE, 3-THIAPENTANE, AND 2,3,4-TRITHIAPENTANE, J. Phys. Chem. 67, 1283 (1963).

58. Hobrock, Brice G.; Shenkel, Roger C.; and Kiser, Robert W., SINGLY- AND DOUBLY-CHARGED IONS FROM METHYL AND EHTYL ISOTHIOCYANATES BY ELECTRON IMPACT, J. Phys. Chem. 67, 1684 (1963).

59. Hodgson, F. N.; Desjardin, M.; and Baun, W. L., STUDY OF POLYNUCLEAR AROMATIC HYDROCARBONS USING THE VACUUM SPARK MASS SPECTROGRAPH, J. Phys. Chem. 67, 1250 (1963).

60. Junk, G. A., and Svec, H. J., MASS SPECTROMETRIC IDENTIFICATION OF DIPEPTIDES, Anal. Biochem. 6, 199 (1963).

61. Junk, G., and Svec, H., USE OF THE MASS SPECTROMETER FOR THE QUANTITATIVE ANALYSES OF MIXTURES OF AMINO ACIDS, Anal. Chim. Acta. 28, 164 (1963).

62. Junk, G., and Svec, H., MASS SPECTRA OF THE -AMINO ACIDS, J. Am. Chem. Soc., 85, No. 7, 839 (1963).

63. Kecki, Z., and Wincel, H., PRIMARY PROCESSES OF RADIATION CHEMISTRY AS STUDIED BY MASS SPECTROMETRY. I. FRAGMENTATION OF TETRAHYDRONAPHTHALENE ON ELECTRON IMPACT, Nukleonika 8, 117 (1963).

64. Kjaer, A.; Ottashi, M.; Wilson, J. M.; and Djerassi, C., MASS SPECTRA OF ISOTHIO CYANATES, Acta. Chem. Scand. 17, 2143 (1963).

65. Kochetkov, N. K.; Wulfson, N. S.; Chizhov, O. S.; and Zolotarev, B. M., MASS SPECTROMETRY OF CARBOHYDRATE DERIVATIVES, Tetrahedron, 19, No. 12, 2209 (1963).

66. Kochetkov, N. K.; Wulfson, N. S.; Chizkov, O. S.; and Zolotarev, B. M., MASS SPECTROMETER STUDY OF HYDROCARBONS, Methyl Ethers and Acetates of Glycosides, Dokl. Akad. Nauk SSSR, 151, 336 (1963).

67. Krylov, B. K., and Kamanovskii, V. I., IDENTIFICATION OF THE PRODUCTS OF CHROMATOGRAPHIC ANALYSIS USING THE MASS SPECTROMETER, Tr. Khim. i Khim. Tekhnol. 1961, 747, Anal. Abstr. 10, Abstr. 3288 (1963).

68. Lander, R. L., TEST OF MASS SPECTRA, Phys. Rev. Letters 10, 553 (1963).

69. Langer, F. B., and Gohlke, R. S., MASS SPECTROMETRIC THERMAL ANALYSIS, Anal. Chem. 35, 1301 (1963).

70. Lemmon, R. M., and Smith, M. A., ISOTOPIC STUDIES ON THE RADIATION DECOMPOSITION OF CRYSTALLINE CHOLINE CHLORIDE, J. Am. Chem. Soc. 85, 1395 (1963).

71. Lester, G. R., THEORY OF MASS SPECTRA, Brit. J. Appl. Phys. 14, 414 (1963).

72. Lifshitz, Chava, and Bauer, S. H., MASS SPECTRA OF VALENCE TAUTOMERS, J. Phys. Chem. 67, 1629 (1963).

73. Lund, E.; Budzikiewicz, H.; Wilson, J. M.; and Djerassi, Carl, MASS SPECTROMETRY IN STRUCTURAL AND STEREOCHEMICAL PROBLEMS - XXI. FRAGMENTATION AND HYDROGEN TRANSFER REACTIONS AFTER ELECTRON IMPACT ON -DECALONES, J. Am. Chem. Soc. 85, 1528 (1963).

74. Lund, E.; Budzikiewicz, H.; Wilson, J. M.; and Djerassi, Carl, MASS SPECTROMETRY IN STRUCTURAL AND STEREOCHEMICAL PROBLEMS - XVIII. FRAGMENTATION AND HYDROGEN TRANSFER REACTIONS AFTER ELECTRON IMPACT ON -DECALONES - SYNTHESIS OF POLYDEUTERATED -DECALONES, J. Am. Chem. Soc. 85, 941 (1963).

75. Lundin, R. E., and Black, D. R., VOLATILES FROM ORANGES - HYDROCARBONS, Identified by Infrared, NMR, and Mass Spectra, J. Food Sci. 28, 541 (1963).

76. Lynch, J. F.; Wilson, J. M.; Budzikiewicz, H.; and Djerassi, C., DETERMINATION OF MASS SPECTRA OF NONVOLATILE SUBSTANCES, Experientia, 18, No. 19, 211 (1962).

77. McCollum, J. D., and Meyerson, S., ORGANIC IONS IN THE GAS PHASE X, Decomposition of Benzaldehyde Under Electron Impact, J. Am. Chem. Soc. 85, 1739 (1963).

78. McFadden, W. H., and Teranishi, R., FAST-SCAN MASS SPECTROMETRY WITH CAPILLARY GAS-LIQUID CHROMATOGRAPHY IN INVESTIGATION OF FRUIT VOLATILES, Nature 200, 329 (1963).

79. McFadden, W. H.; Teranishi, R.; and Black, D. R., USE OF CAPILLARY GAS CHROMATOGRAPHY WITH A TIME OF FLIGHT MASS SPECTROMETER, J. Food Sci., 28, 316 (1963).

80. MacDonald, C. G., and Shannon, J. S., STUDIES IN MASS SPECTROMETRY - II. RANDOM HYDROGEN REARRANGEMENT IN AROMATIC MOLECULAR IONS, Australian J. Chem. 15, 771-785 (1962).

81. MacDonald, C. G.; Shannon, J. S.; and Sugowdz, G., MASS SPECTROMETRY, Stereochemistry and Elimination Reactions of Hydroxy and Acetoxy Compounds, Tetrahedron Letters, 1963, 807.

82. McDowell, C. A. (ed), Mass Spectrometry, McGraw-Hill, New York, 1963.

83. McLafferty, F. W. (ed), Mass Spectrometry of Organic Ions, Academic Press, New York, 1963.

84. McLafferty, F. W., Mass Spectral Correlations, American Chemical Society, Washington, D. C., 1963.

85. Maclean, D. B., LYCOPODIUM ALKALOIDS, Mass Spectra of Representative Alkaloids, Can. J. Chem. 41, 2654 (1963).

86. Marsel, J., and Vrsca, V., MASS SPECTROMETRIC MEASUREMENT OF XENON FLUORIDES, Croat. Chem. Acta. 34, No. 3, 191 (1962).

87. Merritt, C.; Bazinet, M. L.; Sullivan, J. H.; and Robertson, D. H., COFFEE AROMA, MASS SPECTROMETRIC DETERMINATION OF VOLATILE COMPONENTS FROM GROUND COFFEE, J. Agr. Food Chem. 11, 152 (1963).

88. Monahan, J. E., and Stanton, H. E., MASS SPECTRA RESULTING FROM HIGH-ENERGY ELECTRON IMPACT ON SOME HYDROCARBON MOLECULES, J. Chem. Phys. 37, Nos. 10 and 11, 2654 (1962).

89. Mutzenbecher, G. V.; Pelah, Z.; Williams, D. H.; Budzikiewicz, H.; and Djerassi, C., MASS SPECTROMETRY IN STRUCTURAL AND STEREOCHEMICAL PROBLEMS - MASS SPECTROMETRIC FRAGMENTATION OF STEROIDAL ETHYLENE KETALS AND ETHYLENE THIO KETALS, Steroids 2, 475 (1963).

90. Natalis, P., EFFECT OF GEOMETRICAL ISOMERISM ON THE BEHAVIOR OF CIS AND TRANS-HEXAHYDROINDANES UNDER ELECTRON IMPACT, Nature 200, 881 (1963).

91. Natalis, P., BEHAVIOR OF GEOMETRICAL ISOMERS UNDER ELECTRONIC BOMBARDMENT, Correlation Between Mass Spectra and Molecular Structure in a Series of 1,2-Dialkoylcyclohexanes, Bull. Soc. Chim. Belges 72, 416 (1963).

92. Natalis, P., BEHAVIOR OF GEOMETRICAL ISOMERS UNDER ELECTRONIC BOMBARDMENT, Cis and Trans-Hexahydoindanes, Bull. Soc. Chim. Belges 72, 374 (1963).

93. Occolowitz, J. L., and White, G. L., MASS SPECTROMETRY OF ESTERS OF PHOSPHORUS AND PHOSPHORIC ACIDS, Anal. Chem. 35, 1179 (1963).

94. Ohashi, M.; Budzikiewicz, H.; Wilson, J. M.; and Djerassi, C., MASS SPECTROMETRY IN STRUCTURAL AND STEREOCHEMICAL PROBLEMS, Alkaloids of Periwinkles - 27, The Mass Spectra of Stereo-Isomers of the Sarpagine-Akuammidine Group, Tetrahedron 19, No. 12, 2241 (1963).

95. Ohashi, M.; Wilson, J. M.; Budzikiewicz, H.; Shamma, M.; Slusarchyk, W. A.; and Djerassi, C., MASS SPECTROMETRY IN STRUCTURAL AND STEREOCHEMICAL PROBLEMS, Aporphines and Related Alkaloids, J. Am. Chem. Soc. 85, 2807 (1963).

96. Olivier, L., STRUCTURE OF P.S.I. - AKUAMMIGINE AND OF PICROLINE, ALKALOIDS OF PICRALIMA NITIDA - APPLICATION OF M.S. TO THE PROBLEMS OF STRUCTURE AND STEREOCHEMISTRY, Bull. Soc. Chim. France 1963, 646.

97. Oshima, Shozo, THE STRUCTURE OF ORGANIC COMPOUNDS AND ITS MASS SPECTRA, Nippon Kagaku Zasshi 84, 956 (1963).

98. Oshima, Shozo; Katsumata, Akira; and Fujii, Kinya, MASS SPECTROMETRIC INVESTIGATION OF PETROLEUM (11) MASS SPECTROMETRIC ANALYSIS OF MONOAROMATIC HYDROCARBON IN GAS OIL, Nippon Kagaku Zasshi 84, 646 (1963).

99. Oshima, S.; Nishishita, T.; and Fujii, K., MASS SPECTROMETRIC ANALYSIS OF AROMATIC HYDROCARBONS IN LUBRICATING OIL AND BY THE LOW ENERGY IONIZATION METHOD, Nippon Kagaku Zasshi 84, 646 (1963).

100. Owens, E. B., and Giardino, N. A., QUANTITATIVE MASS SPECTROMETRY OF SOLIDS, Anal. Chem. 35, 1172 (1963).

101. Paulett, Grover S., and Ettinger, Raymond, MASS SPECTRA AND APPEARANCE POTENTIALS OF DIAZIRINE AND DIAZOMETHANE, J. Chem. Phys. 39, 825 (1963) and J. Chem. Phys. 39, 3534C (1963).

102. Parello, J.; Longevialle, P.; Vetter, W.; and McCloskey, J. A., STRUCTURE OF PHYLLABINE, Application of Nuclear Magnetic Resonance and Mass Spectrometry to the Study of Tropane Derivatives, Bull. Soc. Chim. France 1963, 2787.

103. Pelah, Z.; Kielczewski, M. A.; Wilson, J. M.; Ohashi, M.; Budzikiewicz, H.; and Djerassi, C., MASS SPECTROMETRY IN STRUCTURAL AND STEREOCHEMICAL PROBLEMS - XXVII. MASS SPECTRAL FRAGMENTATION PROCESSES AND HYDROGEN TRANSFER REACTIONS OF AMIDES AND AMINES, J. Am. Chem. Soc. 85, 2470 (1963).

104. Pelah, Z.; Wilson, J. M.; Ohashi, M.; Budzikiewicz, H.; and Djerassi, C., MASS SPECTROMETRY IN STRUCTURAL AND STEREOCHEMICAL PROBLEMS - XXXIV, Tetrahedron 19, 2233 (1963).

105. Pelah, Z.; Wilson, J. M.; Ohashi, M.; Budzikiewicz, H.; and Djerassi, C., MASS SPECTROMETRY IN STRUCTURAL AND STEREOCHEMICAL PROBLEMS, Aromatic Methyl and Ethyl Ethers, Tetrahedron 19, No. 12, 2233 (1963).

106. Phillips, J. K., IDENTIFICATION OF RUBBER POLYMERS BY MASS SPECTROMETRY, Appli. Spec. 17, 9 (1963).

107. Plat, M.; Le-Men, J.; Janot, M. M.; Budzikiewicz, H.; Wilson, J. M.; Durham, L. J.; and Djerassi, C., STRUCTURE OF 4 ALKALOIDS OF THE SMALL PERIWINKLE (VINCA MINOR). (Minus) -VINCA-DIFFORMINE, MINOVINCINE, MINOVINCININE, AND 16-METHOXY-MINOVINCINE, Periwinkle Alkaloids - Application of Mass Spectrography to the Problem of Determining the Structure and Stereochemistry, Bull. Soc. Chim. France 1962, 2237.

108. Reed, R. I., and Reid, W. R., ELECTRON IMPACT AND MOLECULAR DISSOCIATION, Mass Spectra of Some Malonic Acids and Furan Compounds, J. Chem. Soc., Dec., 5933 (1963).

109. Reed, R. I., and Tabrizi, F. M., MASS SPECTRA OF SOME FERROCENES, Appli. Spectroscopy 17, 124 (1963).

110. Ryhage, R., and Sydow, E. von, MASS SPECTROMETRY OF TERPENES, Mono-Terpene Hydrocarbons, Acta. Chem. Scand. 17, 2025 (1963).

111. Ryhage, R., FAST RECORDING OF MASS SPECTRA OF ORGANIC COMPOUNDS OF HIGH MOLECULAR WEIGHT, Using Amounts of Material in the Microgram Range, Arkiv Kemi 20, Nos. 14-19, 185 (1962).

112. Sandoval, Antonio A.; Moser, H. C.; and Kiser, Robert W., IONIZATION AND DISSOCIATION PROCESSES IN PHOSPHORUS TRICHLORIDE AND DIPHOSPHORUS TETRACHLORIDE, J. Phys. Chem. 67, 124 (1963).

113. Sandulescu, D.; Hanes, A.; and Bulaceanu, R., MASS SPECTROMETRY, Rev. Chim. (Bucharest) 13, 735 (1963).

114. Schaefer, H., MASS TRANSFER BY WAY OF THE GAS PHASE, Naturwissenschaften 50, Nos. 3 and 4, 53 (1963).

115. Schumacher, Ernst, CHEMICAL REACTIONS IN THE MASS SPECTROMETER, Helv. Chim. Acta. 46, 1295 (1963).

116. Schug, John C., INVESTIGATION OF A FRAGMENTATION MODEL FOR N-PARAFFINS, J. Chem. Phys. 38, 2610 (1963).

117. Schumacher, E., CHEMICAL REACTIONS IN A MASS SPECTROMETER, Helv. Chim. Acta. 46, 1295 (1963).

118. Seibl, J., and Gaeumann, T., MASS SPECTRA OF ORGANIC COMPOUNDS, Cyclo Hexanone, Helv. Chim. Acta. 46, No. 7, 2857 (1963).

119. Seibl, J., and Gaeumann, T., MASS SPECTRA OF ORGANIC COMPOUNDS, Monocyclic Ketones, Z. Anal. Chem. 197, 33 (1963).

120. Shannon, J. S., MASS SPECTROMETRY, Triterpenoids Ifflaionic Acid, Australian J. Chem. 16, 683 (1963).

121. Shannon, J. S., MASS SPECTROMETRY, Sporidesmin and Sporidesmin B, Tetrahedron Letters 1963, 801.

122. Shannon, J. S.; MacDonald, C. G.; and Courtney, J. L., STUDIES IN MASS SPECTROMETRY, Tri Terpenoids - Structure Assignment to Friedelan-y-one (y-al) and Derivatives, Tetrahedron Letters, Nos. 3 and 4, 173 (1963).

123. Shapiro, R. H.; Wilson, J. M.; and Djerassi, C., MASS SPECTROMETRY IN STRUCTURAL AND STEREOCHEMICAL PROBLEMS, Mass Spectral Fragmentation of Delta-1 and Delta-4- 3-Keto Steroids, Steroids 1, 1 (1963).

124. Sharkey, Jr., A. G.; Shultz, J. L.; and Friedel, R. A., ADVANCES IN COAL SPECTROMETRY, U. S. Bur. Mines Rept. Invest. 1963, No. 6318.

125. Sidorov, L. N., and Akishin, P. A., MASS SPECTROMETRIC METHOD OF DETERMINING PARTIAL VAPOR PRESSURES AND RELATIVE IONIZATION CROSS-SECTIONS OF MOLECULES FROM TOTAL EVAPORATION ISOTHERMS, Dokl. Akad. Nauk SSSR 151, 136 (1963).

126. Snyder, L. R.; Howard, H. E.; and Ferguson, W. C., DIRECT MASS SPECTROMETRIC ANALYSIS OF PETROLEUM SAMPLES BOILING IN THE KEROSINE RANGE, Heavy Reformates and Hydro Dealkylated Products, Anal. Chem. 35, 1676 (1963).

127. Spiteller, G., RESEARCH ON THE STRUCTURE OF ORGANIC COMPOUNDS WITH THE AID OF MASS SPECTROMETRY, Chem. Weekblad 59, 205 (1963).

128. Spiteller, G., STRUCTURAL INVESTIGATION OF ORGANIC COMPOUNDS WITH THE AID OF MASS SPECTROMETRY, Z. Anal. Chem. (197), 1 (1963).

129. Spiteller, G., INVESTIGATIONS OF THE STRUCTURE OF ORGANIC COMPOUNDS USING MASS SPECTROMETRY, Chem. Weekblad 59, 205 (1963).

130. Spiteller, G., and Kaschnitz, R., USE OF MASS SPECTROMETRY FOR THE INVESTIGATION OF PHARMACEUTICALS, Sulfon Amides, Monatsh. Chem. 94, No. 5, 964 (1963).

131. Spiteller, G., and Spiteller, F. M., KEY FRAGMENTS IN THE MASS SPECTRA OF ALKALOIDS (GERMAN), Tetrahedron Letters, Nos. 3 and 4, 147 (1963).

132. Spiteller, G., and Spiteller, F. M., KEY FRAGMENTS IN THE MASS SPECTRA OF ALKALOIDS (GERMAN), Tetrahedron Letters, Nos. 3 and 4, 153 (1963).

133. Spiteller, G., and Spiteller, F. M., REARRANGEMENT OF AROMATIC COMPOUNDS IN A MASS SPECTROMETER, Monatsh. Chem. 93, 1395 (1962).

134. Spiteller, G., and Spiteller-Friedmann, M., MASS SPECTROMETRIC STUDY OF LABILE AND DIFFICULTY VOLATILE ORGANIC COMPOUNDS, Monatsh. Chem. 94, 742 (1963).

135. Spiteller, G., Spiteller-Friedmann, M., APPLICATION OF MASS SPECTROMETRY TO THE CLARIFICATION OF THE STRUCTURE OF ALKALOIDS, Secondary Alkaloids from the Bark of Aspidosperma Oblongum, Monatsh. Chem. 94, 779 (1963).

136. Steinfelder, K.; Tummler, R.; Schreiber, K.; and Ardenne, M. V., MOLECULAR MASS SPECTROGRAPHY OF NATURAL PRODUCTS, STEROIDS, Experientia 178 (1963).

137. Sydow, E. Von, MASS SPECTROMETRY OF TERPENES, Monoterpene Alcohols, Acta. Chem. Scand. 17, No. 9, 2504 (1963).

138. Teranishi, R.; Corse, J. W.; McFadden, W. H.; Black, D. R.; and Morgan, A. I., VOLATILES FROM STRAWBERRIES, Mass Spectral Identification of the More Volatile Components, J. Food Sci. 28, 478 (1963).

139. Traylor, T. G., OXYGEN-18 TRACER STUDIES OF ALKYL PER OXY RADICALS, Kinetic Technique with Mass Spectrometry, J. Am. Chem. Soc. 85, 2411 (1963).

140. Tsuchiya, T., MASS SPECTROMETRY OF FATTY ACIDS, Yukagaku 11, 600 (1962).

141. Ullman, E. F., and Buncel, E., AN APPROACH TO A BENZOCYCLOPROPENE, J. Am. Chem. Soc. 85, 2106 (1963).

142. Van Langermeersch, A., QUALITATIVE AND QUANTITATIVE METHODS FOR ANALYSIS OF HYDROCARBON TYPES, Chim. Anal. (Paris) 44, 148-152 (1962), Fuel Abstr. Current Titles 4, No. 1, 164 (January 1963).

143. Van Raalte, D., and Harrison, A. G., IONIZATION AND DISSOCIATION OF FORMATE ESTERS BY ELECTRON IMPACT, Can. J. Chem. 41, 2054 (1963).

144. Van-Peteghem, A. P., and Vanderkelen, G., MASS SPECTROMETRY IN THE STUDY OF CORROSION, Corrosion Anti-Corrosion 11, 41 (1963).

145. Vastel, J., SOME RECENT PROGRESS IN MASS SPECTROMETRY, Colloq. Spectros. Intern., 9th, Lyons 1961 3, 612 (1962).

146. Vetter, W.; Longevialle, P.; and Khuong-Huu-Laine, F., STEROIDAL ALKALOIDS, Mass Spectrometry in the Determination of the Structures of Amino Steroids, Bull. Soc. Chim. France 1963, No. 6, 1324.

147. Von Sydow, E., MASS SPECTROMETRY OF TERPENES - MONOTERPENE ALCOHOLS, Acta. Chem. Scand. 17, 2504 (1963).

148. Weygand, F.; Prox, A.; Koenig, W.; and Fessel, H. H., MASS SPECTROCHEMICAL AND GAS CHROMATOGRAPHIC SEQUENCE ANALYSIS OF PEPTIDES, Augew. Chem. 75, 724B (1963).

149. Willhalm, B.; Thomas, A. F.; Stoll, M.; and Hawkins, E. G. E., NUCLEAR MAGNETIC RESONANCE SPECTRA AND THE MASS SPECTRA OF SOME CHLORINATED DERIVATIVES OF METHYL-BUTANE AND RELATED SUBSTANCES, Helv. Chim. Acta. 46, 2098 (1963).

150. Williams, D. H.; Wilson, J. M.; Budzikiewicz, H.; and Djerassi, C., MASS SPECTROMETRY IN STRUCTURAL AND STEREOCHEMICAL PROBLEMS, XXIV. A Study of the Hydrogen Transfer Reactions Accompanying Fragmentation Processes of 11-Keto Steroids - Synthesis of Denterated Androstan-11-Ones, J. Am. Chem. Soc. 85, 2091 (1963).

151. Wilson, H. W., and Daly, N. R., MASS SPECTROMETRY OF SOLIDS, J. Sci. Instr. 40, 273 (1963).

152. Wilson, J. M.; Ohashi, M.; Budzikiewicz, H.; and Djerassi, C., MASS SPECTROMETRY IN STRUCTURAL AND STEREOCHEMICAL PROBLEMS, Tropone and Tropolone Derivatives, Tetrahedron 19, No. 12, 2247 (1963).

153. Wilson, J. M.; Ohashi, M.; Budzikiewicz, H.; Santavy, F.; and Djerassi, C., MASS SPECTROMETRY IN STRUCTURAL AND STEREOCHEMICAL PROBLEMS, Colchicine Alkaloids, Tetrahedron 19, No. 12, 2225 (1963).

154. Wulfson, N. S.; Stepanov, V. M.; Puchkov, V. A.; and Zjakun, A. M., MASS SPECTRA OF PHENYL THIO-HYDANTOINS OF THE AMINO ACIDS, IZV. Akad. Nauk. SSSR, Ser. Khim., 1963, No. 8, 1524B.

155. Wulfson, N. S.; Zardskii, V. I.; Puchkov, V. A.; Zaikin, V. G.; Shkrob, A. M.; Antonov, V. K.; and Shemiakin, M. M., MUTUAL TRANSFORMATION OF CYCLALS AND CYCLO DEPSI PEPTIDES, AS STUDIED BY MEANS OF FRAGMENTARY MASS SPECTROMETRY, Dokl. Akad. Nauk SSSR 153, 336 (1963).

156. Wulfson, N. S.; Zaretsky, V. I.; and Zaikin, V. G., MASS SPECTROMETRIC INVESTIGATION OF NATURAL COUMARINS, Izu. Akad. Nauk SSSR, Ser. Khim., 1963, 2215.

157. Young, Howard A., MASS SPECTROMETRY, NEW INSTRUMENTS, AND TECHNIQUES, MASS SPECTROMETRY, NEW INSTRUMENTS TECHNICAL REPORT 11, 7 pages (1962), pub. 63.

BIBLIOGRAPHY of published and unpublished material pertaining to new instruments and techniques in mass spectrometry for 1963.

Prepared by Subcommittee V
ASTM Committee E-14

1. Ackerman, M., Stafford, F. E., and Drowart, J., "Vaporization of Compounds and Alloys at High Temperature Part I, Mass Spectrometric Determination of the Dissociation Energies of the Molecules AgAu, AgCu, AuCu", Report for March, 1959 - March, 1960, on Refractory Inorganic Non-Metallic Materials, Contract AF 61 (052) 225, Proj. 7350.

2. Ackerman, R. J., and Rauh, E. G., "A Thermodynamic Study of the Tungsten-Oxygen System at High Temperatures", Journal of Physical Chemistry 67, pp. 2596-2601 (1963).

3. Anderson, H. U., "Mass Spectrometric Determination of Ionization Pressure Gauge Sensitivities", Rev. of Sci. Inst. 34, #6, p. 703 (1963).

4. Arikawa, Tatsuo, "Perfect Focusing Mass Spectrometer", Japanese Journal of Applied Physics, 2 - 7, 420-428 (1963).

5. Ausloos, P., Lias, S. G., and Gorden, R., Jr., "Effect of Additives on the Ionic Reaction Mechanism in the Radiolysis of Methane", Journal of Chemical Physics 39, No. 12, 3341-8 (1963).

6. Banick, C., Carothers, G., and Donaldson, W., "Determination of Americium-243 in Curium-244", Analytical Chemistry 35, 9, 1312-3, (1963).

7. Barber, M., Farren, J., and Linnett, J. W., "The Mass Spectrometric Study of the Reaction of Methyl Radicals with Oxygen", Proc. Roy. Soc. A, 274, 306-318 (1963).

8. Barber, M., Farren, J., and Linnett, J. W., "Mass Spectrometric Sampling Through a Small Hole in the Adiabatic Flow Region", Proc. Roy. Soc. A, 274, 293-305 (1963).

9. Barber, M., Cuthbert, J., Farren, J., and Linnett, J. W., "A Mass Spectrometer for Studying Chemical Reactions", Proc. Roy. Society A, 274, 285-292 (1963).

10. Bartlett, M. F., and Taylor, W. I., "Burnamicine, A Cryptopine-Like Analog of Corynantheol" (Communications to the Editor), Journal of American Chemical Society, 85, 1203, (1963).

11. Batelle Memorial Institute, "Development of Analytical Techniques for the Determination of Minute Quantities of Selected Elements in Beryllium", (Contract NOw 62-0629), p. 42 (1963).

12. Basila, Michael R., and Clancy, Donald J., "The Ionization Potentials of Monosubstituted Pyridines by Electron Impact", Journal of Physical Chemistry, 67, pp. 151-1554, (1963).

13. Baun, W. L., Hodgson, F. N., and Desjardins, M., "Mass Spectrographic Study of Molecular Carbon Ions Formed in a Spark Source", Journal of Chemical Physics 38, No. 11, pp 2787-8 (1963).

14. Betts, J. F., and O'Halloran, G. L., "Miniaturized Bendix Time-of-Flight Mass Spectrometers", Unpublished Work.

15. Berkowitz, J., "Equilibrium Composition of Sulfur Vapor", Journal of Chemical Physics 39, No. 2, 275-83, (1963)

16. Berkowitz-Mattuck, J. B., Buchler, A., Engelke, J. L., and Goldstein, S. N., "Mass Spectrometric Investigation of the Oxidation of Molybdenum and Tungsten", Journal of Chemical Physics 39, No. 10, 2722-30, (1963).

17. Beynon, J. H., Saunders, R. A., and Williams, A. E., "The Mass Spectrum of Tetrachloro Copper Phthalocyanine", Applied Spectroscopy 17, No. 3, 63-5 (1963).

18. Bibby, M.M., and Carter, G., "Ionization and Dissociation in Some Fluorcarbon Gases", Trans. Faraday Soc., 59, 2455-62 (1963).

19. Biemann, K., DeJongh, D. C., and Schnoes, H. K., "Application of Mass Spectrometry to Structure Problems. XIII. Acetates of Pentoses and Hexoses", Journal of the American Chemical Society 85, p. 1763 (1963).

20. Biemann, K., Spiteller-Friedmann, M., and Spiteller, G., "Application of Mass Spectrometry to Structure Problems. X. Alkaloids of the Bark of Aspidosperma quebracho blanco", Journal of the American Chemical Society 85, p. 631 (1963).

21. Bliven, C. M., and Florio, J. F., "Study of Adsorption of Gases on Solids in the High Vacuum Range", Scientific Report #4; TR 632554 (Contract AF 19(628) 331, Proj. 5634 Task 563405). AFCRL 63170, p. 19, (1963).

22. Bloom, J. H., Ludington, C. E., and Phipps, R. L., "Improved High Mass Range Resolution with an Omegatron Mass Spectrometer", Research Report, AFCRL 62 953, p. 17 (1962).

23. Blue, Gary D., Green, John W., Bautista, Renato G., and Margrave, John L., "The Sublimation Pressure of Calcium (II) Fluoride and the Dissociation Energy of Calcium (I) Fluoride", Journal of Physical Chemistry 67, pp. 877-882 (1963).

24. Brault, M., and Gazier, C., "Several Statistical Properties of Electron Photomultipliers", Comptes Rendus, 256, 1241-44 (1963).

25. Breisacher, P., Gibbins, S. G., and Giegel, B., "Propulsion Research Program. Hydride and Fluoride Investigations; Part I, Hydride Investigation", Semi-Annual Technical Report, (Contract AF04(647)930) (DCAS TDR 62-4), p. 93 (1962).

26. Brion, C. E., and Dunning, W. J., "Electron Impact Studies of Simple Carboxylic Esters", Trans. Faraday Society, 59, 647-56, (1963).

27. Buchler, A., and Berkowitz-Mattuck, J. B., "Gaseous Metaborates. I. Mass Spectrometric Study of the Vaporization of Lithium and Sodium Metaborates", Journal of Chemical Physics 39, No. 2, 286-91, (1963).

28. Buchler, A., Stauffer, J. L., Klemperer, W., and Wharton, L., "Determination of the Geometry of Lithium Oxide by Electric Deflection", Journal of Chemical Physics 39, No. 9, 2299-2303, (1963).

29. Budzikiewicz, H., Wilson, J. M., and Djerassi, C., "Mass Spectrometry in Structural and Stereochemical Problems. XXXII. Pentacyclic Triterpenes", Journal of the American Chemical Society 85, p. 3688 (1963).

30. Burns, R. P., DeMaria, G., Drowart, J., and Inghram, M. G., "Mass Spectrometric Investigation of the Vaporization of In_2O_3", Journal of Chemical Physics 38, No. 4, 1935-6, (1963).

31. Cady, G. H., Eggers, D. F., et al., "Difluoroamine, SF_5 NF_2, and Xenon Hexafluoride", (Contract NOnr-47716), Technical Reports 39 & 40, p. 7 (1963).

32. Calcote, H. F. and Reuter, J. L., "Mass Spectrometric Study of Ion Profiles in Low Pressure Flames", Journal of Chemical Physics 38, No. 2, 310-17, (1963).

33. Carlson, T. A. and White, R. M., "Fragmentation of the Excited Parent Ions, $[CH_3Kr^{82}]^+$ and $[CH_3O^{18}]^-$, Following the β-Decay of CH_3Br^{82} and the β^+ Decay of CH_3F^{18}", Journal of Chemical Physics 39, No. 7, 1748-52, (1963).

34. Carlson, T. A. and White, R. M., "Mass Spectrometric Analyses of the Ions Resulting from the Nuclear Decay of CH_3I^{130} and $C_2H_5I^{131}$. Study of Xenon-Hydrocarbon Ions. II", Journal of Chemical Physics 38, No. 9, 2075-81 (1963).

35. Chakravarty, V. S., Venkatasubramanian, and Duckworth, H. E., "Relative Ionization Efficiencies for Elements in a Spark Source", AFOSR Grant 62 33, AFOSR J745, p. 7, (1962).

36. Chapin, D. S., "Packless All-Metal Ultra-High Vacuum Valve for Temperatures from -196°C or below to 450°C", Review of Scientific Instruments, Vol. 34, No. 1, p. 47.

37. Chemical Engineering 70, No. 18, p. 58 (1963).

38. Coggeshall, Norman D., "Comparison of Mass Spectral Regularities for n-Paraffins and n-Terminal Olefins", Journal of Physical Chemistry 67, pp. 183-187 (1963).

39. Cornides, I., "Investigations of Some Reaction Mechanisms by the Use of the O-18 Tracer Techniques", Unpublished Work.

40. Crouch, E. A. and Webster, R. K., "Choice of the Optimum Quantity and Constitution of the Tracer Used for Isotopic Dilution Analysis", Journal of Chemical Society (British), No. 18, p. 118, (1963).

41. Cubicciotti, Daniel, "Mass Spectrometric Study of the Vapors over Bismuth-Sulfur Melts", Journal of Physical Chemistry, 67, p. 1385, (1963).

42. Curran, R. K., "Formation of SF_6^- by Inelastically Scattered Electrons", Journal of Chemical Physics 38, No. 3, pp. 780-1, (1963).

43. Curran, R. K., "Mass Spectrometer Investigation of Electron-Impact Processes at Pressures to 1mm Hg", Journal of Chemical Physics 38, No. 12, pp. 2974-8, (1963).

44. Daly, N. R., "New Type of Positive Ion Detector for the Simultaneous Measurement of Two Beams", Review of Scientific Instruments 34, No. 10, p. 1116 (1963).

45. Damerow, Richard A., Ries, Richard R., and Johnson, Walter H., Jr., "Atomic Masses from Ruthenium to Xenon", Physical Review 132, pp. 1673-1681 (1963).

46. Dattner, J. and Fischler, J., "Calculations of Oxygen Isotope Abundance Ratios in a Mass Spectrometer", British Journal of Applied Physics, 14-10, pp. 728-729 (1963).

47. Davies, E. A., and Gosling, D. S., "Mains-Operated Cold Trap Filler", Journal of Scientific Instruments, 40, p. 429 (1963).

48. DeJongh, D. C. and Biemann, K., "Application of Mass Spectrometry to Structure Problems. XIV. Acetates of Partially Methylated Pentoses and Hexoses", Journal of the American Chemical Society 85, p. 2289, (1963).

49. Derwish, G. A. W., Calli, A., Giardini-Guidoni, A., and Volpi, G. G., "Ion Molecule Reactions in Gaseous Ammonia", Journal of Chemical Physics 39, No. 6, pp. 1599-1605 (1963).

50. Diesen, R. W., "Mass Spectral Studies of Kinetics Behind Shock Waves. II. Thermal Decomposition of Hydrazine", Journal of Chemical Physics 39, No. 9, pp. 2121-8, (1963).

51. Diesen, R. W. and Felmlee, W. J., "Mass Spectral Studies of Kinetics Behind Shock Waves. I. Thermal Dissociation of Chlorine", Journal of Chemical Physics 39, No. 9, pp. 2115-20 (1963).

52. Diebeler, V. H. and Rosenstock, H. M., "Mass Spectra and Metastable Transitions of H_2S, HDS, and D_2S", Journal of Chemical Physics 39, No. 11, pp. 3106-11 (1963).

53. Dibeler, V. H. and Rosenstock, H. M., "Metastable Transitions in Mass Spectra of Methane and Deuteromethanes", Journal of Chemical Physics 39, No. 5, pp. 1326-9 (1963).

54. Dimitriev, I. S., Nikolaev, V. S., Fatteeva, L. N., and Teplova, Y. A., "Investigation of the Loss of Several Electrons by Fast Multiply-Charged Ions", Soviet Physics--JETP, 16, 259, (1963).

55. Dodson, M. H., "A Theoretical Study of the Use of Internal Standards for Precise Isotopic Analysis by the Surface Ionization Technique: Part I - General First-Order Algebraic Solutions", Journal of Scientific Instruments, 40, pp. 289-295, (1963).

56. Dolder, K. T., Harrison, M. F. A., Thonemann, P. C., "A Measurement of the Ionization Cross-Section of Ne^+ by Electron Impact", Proceedings of the Royal Society of London A, 274, pp. 256-551, (1963).

57. Dolejšek, Z., Hanuš, V., and Vokač, K., "A Study of the Formation of Fragment Ions in the Mass Spectra of Butin-1, Pentin-1, Hexin-1, Heptin-1 and Xoctin-1", Unpublished Work.

58. Dorman, F. H. and Morrison, J. D., "Ionization Potentials of Doubly Charged Oxygen and Nitrogen", Journal of Chemical Physics 39, No. 7, pp. 1906-7 (1963).

59. Epstein, L. and Kaufman, L. J., "Materials for and the Mechanism of Gettering Multiple Component Gases", Contract AF19 (604) 8430, Proj. 4619, ACFRL 63-7, p. 36, (1963).

60. Farnsworth, H. E., Marsh, J., and Shooter, D., "Study of Surface Properties of Atomically - Clean Metals and Semiconductors", Contract DA36-039-SC-78286, p. 44, (1962).

61. Field, F. H., Franklin, J. L., and Munson, M. S. B., "Reactions of Gaseoue Ions. XII. High Pressure Mass Spectrometric Study of Methane", Project Squid, Technical Report HUM2P, p. 38, (1963).

62. Fiquet-Fayard, F. and Ziesel, J. P., "Multiple Ionization of Zinc by Electron Impact of 0 to 500 Volts", Comptes Rendus, 256, pp. 4885-8, (1963).

63. Flesch, G. D. and Svec, H. J., "Model of Mass Spectrometer Which Simultaneously Collects Positive and Negative Ions", Review of Scientific Instruments 34, No. 8, p. 897, (1963).

64. Frankevich, E. L. and Tal'roze, V. L.; Translation by Zanis Stuberovskis, "A Mass Spectrometer for Investigating the Processes Which Occur When Electrons and Ions collide with Molecules", Translation from Pribory i Tekhnika Eksperimenta, Vol. 2, pp. 48-53, (1957).

65. Futrell, J. H. and Tiernan, T. O., "Dissociative Charge-Exchange Reactions of Rare-Gas Ions with Propane", Journal of Chemical Physics 39, No. 10, pp. 2539-45, (1963).

66. Galli, A., Giardini-Guidoni, A., and Volpi, G. G., "Ion-Molecule Reaction Leading to NO^+ Formation", Journal of Chemical Physics 39, No. 3, pp. 518-21, (1963).

67. Giese, C. F. and Maier, W. B., II, "Energy Dependence of Cross Sections for Ion-Molecule Reactions. Transfer of Hydrogen Atoms and Hydrogen Ions", Journal of Chemical Physics 39, pp. 739-48, (1963).

68. Giese, C. F. and Maier, W. B., II, "Dissociative Ionization of CO by Ion Impact", Journal of Chemical Physics 39, No. 1, pp. 197-200, (1963).

69. Gilbody, H. B., "Charge Transfer Between Some Atmospheric Ions and Atomic Oxygen", Journal of Chemical Physics 38, No. 9, pp. 2280-4, (1963).

70. Gilbert, B., Brissolese, J. A., Finch, N., Taylor, W. I., Budzikiewicz, H., Wilson, J. M., and Djerassi, C., "Mass Spectrometry in Structural and Stereochemical Problems. XX. Carapanaubine, a New Alkaloid from Aspidosperma Carapanauba and some observations on Mass Spectra of Oxindole Alkaloids", Journal of the American Chemical Society 85, p. 1523, (1963)

71. Gowenlock, B. G., Kay, J., and Majer, J. R., "Electron Impact Studies of Some Sulfides and Disulfides", Transactions of the Faraday Society 59, pp. 2463-8, (1963).

72. Greene, F. T. and Milne, T. A., "Mass Spectrometric Detection of Polymers in Supersonic Beams", Journal of Chemical Physics 39, No. 11, pp. 3150-1 (1963).

73. Grob, V. E., "Formation of Negative Ions in $SbCl_3$", Journal of Chemical Physics 39, No. 4, pp. 972-8, (1963).

74. Groth, W. E., "Photochemical Investigations in the Far Ultraviolet", AF CRL Report No. 63884, p. 11, (1963).

75. Haase, G., "Influence of the H-addition on the Precision of Mass Spectrometric Isotope Analyses", Unpublished Work.

76. Hanse, W. W. and Jennings, J. R., "Applied Research in Microminiature Field Emmision Tubes", Stanford Research Institute.

77. Harrison, M. F. A., Dolder, K. T., and Thonemann, P. C., "A Measurement of the Cross Section for the Ionization of N^+ to N^{2+} by Electron Impact", Proceedings of the Physical Society (London) 82, pp. 368-371, (1963).

78. Heath, G. A., and Hobson, R. M., "The Study of Complex Ions in a Modified Mass Spectrometer", Rocket Propulsion Establishment, Great Gritain, Technical Memo. No. 260, p. 17, (1962).

79. Herron, John T., "Mass Spectrometric Study of the Recombination of Bromine and Chlorine Atoms on Pyrex", Journal of Physical Chemistry 67, No. 12, pp. 2864-65 (1963).

80. Hickman, W. M., and Sweeney, G. G., "Mass Spectrograph for the Analysis of Solids", Review of Scientific Instruments 34, No. 7, p. 783, (1963).

81. Hildenbrand, D. L., Theard, L. P., and Saul, A. M., "Transpiration and Mass Spectrometric Studies of Equilibria Involving BOF and $(BOF)_3$", Journal of Chemical Physics 39, No. 8, pp. 1973-8, (1963).

82. Hill, H. C., and Reed, R. I., "The Volatilization of High Melting Solids in a Mass Spectrometer", Journal of Scientific Instruments 40, p. 259, (1963).

83. Hobrock, Brice G. and Kiser, Robert W., "Electron Impact Investigations in Sulfur Compounds. II. 3-Methyl-2-Thiabutane, 4-Thia-1-Pentene, and 3,4-Dithiahexane", Journal of Physicsl Chemistry 67, No. 3, pp. 648-650, (1963).

84. Hobson, J. P., Edwards, T., and Verreault, R., "Thermal Transpiration in Helium in the Pressure Range 10^{-8} to 20 Torr", Canadian Journal of Physics 41, p. 983, (1963).

85. Hoch, George and Kok, Bessel, "A Mass Spectrometer Inlet System for Sampling Gases Dissolved in Liquid Phases", Reprint from Archives of Biochemistry and Biophysics, 101:1, pp. 160-170, (1963).

86. Hodgson, F., Desjardins, M., and Baun, W., "A Convenient Mass Reference Plate for Use in Spark Source Mass Spectrometry", Analytical Chemistry 35, 9, p. 1112, (1963).

87. Hodgson, F. Neil, Desjardins, Michel, and Baun, William L., "A Study of Polynuclear Aromatic Hydrocarbons Using the Vacuum Spark Mass Spectromgraph", Journal of Physical Chemistry 67, No. 6, pp. 1250-1253, (1963).

88. Hou, K. C., and Anderson, Robbin C., "Comparative Studies of Pyrolysis of Acetylene, Vinylacetylene, and Diacetylene", Journal of Physical Chemistry 67, pp. 1579-1581, (1963).

89. Hunt, W. W., Jr., Stinnett, A. J., and Novack, R., "Charge Transfer Studies with a Time-of-Flight Mass Spectrometer: Cross Section for N_2^+ on N_2 at 2650 Electron Volts", Air Force Cambridge Research Labs, AFCRL-63-709, Upper Atmosphere Physics Laboratory Project 7635, Sept. 1963.

90. Jackson, Don M., Jr., "Epitaxial Control System", Scientific Report No. 2, Contract AF19(604)8351, Proj. 4608 (AFCRL 62-741), (1962).

91. James, L. H. and Carter, G., "Ion Bombardment Induced Re-Emission Studies of Argon in an Ionization Pump", British Journal of Applied Physics, 14-3, p. 147-154, (1963).

92. Jennings, Allen Louis, Jr., "A Mass Spectroscopic Study of Selected Heterocyclics", Master's Thesis from University of Texas, Austin, Texas, p. 65, June, 1963.

93. Jensen, A. V., Goshgarian, B. B., and Dane, N. E., "Mass Spectral Analysis of Rocket Engine Combustion Products Containing Boron Mitride", Space Systems Division, Air Force Systems Command, Report #SSD TDR 62-202, 10 p., (1962).

94. Johnston, W. H., Vestal, M., and Others, "Basic Studies in Radiation Effects on Materials. Part II. Ionic Fragmentation of Molecules by X-Rays and Secondary Electron Spectra from Bombardment of Gas with Electrons", Contract AF33(616)7678, Proj. 7360, ASD TDR 62-10, pt. 2, p. 67, (1962).

95. Junk, G. and Svec, H., "The Mass Spectra of the a-Amino Acids", Journal of the American Chemical Society 85, p. 839, (1963).

96. Junk, Gregor and Svec, Harry, "The Use of the Mass Spectrometer for the Quantitative Analysis of Mixtures of Amino Acids", Analytica Chimica Acta 28, pp. 164-69, (1963).

97. Kandel, R. J., "Methane-Tritium System. I. Mass Spectra of Tritium Substituted Methanes", Journal of Chemical Physics 39, No. 10, pp. 2581-7, (1963).

98. Kebarle, P. and Godbole, E. W., "Mass Spectrometric Study of Ions from the a-Particle Irradiation of Gases at Near Atmospheric Pressures", Journal of Chemical Physics 39, No. 4, pp. 1131-2, (1963).

99. Kiczkowski, R. L., Wilson, E. B., Jr., "Microwave and Mass Spectre of Sulfur Monofluoride (Communications to the Editor)", Journal of the American Chemical Society 85, p. 2028, (1963).

100. Kingdon, Kenneth H., "Enhancement of The Evaporation of Water by Foreign Molecules Adsorbed on the Surface", Journal of Physical Chemistry 67, No. 12, pp. 2732-2737, (1963).

101. Klots, Cornelius E. and Benson, Bruce B., "Thermodynamic Properties of the Atmospheric Gases in Aqueous Solutions", Journal of Physical Chemistry 67, pp. 933-934, (1963).

102. Knewstubb, P. F., Dawson, P. H., and Tickner, A. W., "Mass Spectrometry of Ions in Glow Discharges. V. Oxygen", Journal of Chemical Physics 38, No. 4, pp. 1031-2, (1963).

103. Knewstubb, P. F. and Tickner, A. W.,"Mass Spectrometry of Ions in Glow Discharges. IV. Water Vapor", Journal of Chemical Physics 38, No. 2, pp. 464-9, (1963).

104. Krebs, K. H., "Investigations Concerning the Use of Electron Multipliers to Ion Detection in Mass Spectrometers", Unpublished Work.

105. Kubose, D. A., and Hamill, W. H., "Velocity Dependence of Ion-Molecule Reaction Cross Sections in a Mass Spectrometer", Journal of the American Chemical Society 85, p. 125, (1963).

106. Kupriyanov, S. E., Perov, A. A., and Tunitskii, N. N., "Cross Sections for Dissociation of D_2^+ Ions in Collisions with D_2 Molecules in the Energy Range from 3.5 to 100 Kev", Soviet Physics-JETP 16, p. 1152, (1963).

107. Kupriyanov, S. E., Perov, A. A., and Tunitskii, N. N., "Cross Sections for Dissociation of D_3^+ and D^+ Ions in Collisions with Deuterium Molecules", Soviet Physics--JETP, 16, p. 539, (1963).

108. Langer, H. G., Cohlke, R. S., "Mass Spectrometric Thermal Analysis (MTA)", Analytical Chemistry 35, 9, pp. 1301-2, (1963).

109. Lee, T. G., "Electron Attachment Coefficients of Some Hydrocarbon Flame Inhibitors", Journal of Physical Chemistry 67, pp. 360-366, (1963).

110. Leipziger, F. D., "Some New Upper Limits of Isotopic Abundance by Mass Spectrometry", Applied Spectroscopy 17, No. 6, pp. 158-160, (1963).

111. Lester, G. R., "Theory of Mass Spectra", British Journal of Applied Physics, 14-7, pp. 414-421, (1963).

112. Levy, Joseph B. and Copeland, B. K. Wesley, "The Kinetics of the Thermal Hydrogen-Fluorine Reaction. I. Magnesium Reactor", Journal of Physical Chemistry 67, No. 10, pp. 2156-2159, (1963).

113. Liebl, Helmut J., and Herzog, F. K., "Sputtering Ion Source for Solids", Journal of Applied Physics 34-9, pp. 2893-2896, (1963).

114. Lewis, C., and Hokerecht, H., "A Gallium-Glass Heated Inlet Valve for Mass Spectrometry", Analytical Chemistry 35, 12, pp. 1991, (1963).

115. Lifshitz, Chava and Bauer, S. H., "Mass Spectra of Valence Tautomers", Journal of Physical Chemistry 67, pp. 1629-1635, (1963).

116. Logan, S. R., and More, Walter J., "Decomposition of Crystalline Nitrates by Light Ions at Kilovalt Energies", Journal of Physical Chemistry 67, pp. 1042-1068, (1963).

117. Lorquet, Andree J. and Hamill, William H., "The Energy Dependence for Reaction Cross Sections of Ion-Molecule Reactions of Some Pentyl and Cyclopentyl Halides", Journal of Physical Chemistry 67, pp. 1709-1712, (1963).

118. Lund, E., Budzilkiewicz, H., Wilson, J. M., and Djerassi, C., "Mass Spectrometry in Structural and Stereochemical Problems. XVIII. Fragmentation and Hydrogen Transfer Reactions after Electron Impact on a-Decalones. Synthesis of Polydeuterated a-Decalones", Journal of American Chemical Society 85, p. 941, (1963).

119. Lund, E., Budzikiewicz, H., Wilson, J. M., and Djerassi, C., "Mass Spectrometry in Structural and Stereochemical Problems. XXI. Fragmentation and Hydrogen Transfer Reactions after Electron Impact on b-Decalones", Journal of American Chemical Society 85, pp. 1528, (1963).

120. Major, J. R., and Patrick, C. R., "Appearance Potentials of the Benzoyl Radical-Ion", Transactions of the Faraday Society 59, pp. 1274-8, (1963).

121. Marquart, J. R. and Berkowitz, J., "Dissociation Energies of Some Metal Sulfides", Journal of Chemical Physics 39, No. 2, 283-5, (1963).

122. Marsden, D. G. H., "A Mass Spectrometric Study of the Oxidation of Hydrogen Sulphide", Canadian Journal of Chemistry 41, pp. 2607-20, (1963).

123. Massey, Sir Harrie, "The Physics of Space Research", British Journal of Applied Physics, 14-2, pp. 77-78, (1963).

124. McAfee, K. B., Jr., Edelson, D., "Identification and Mobility of Ions in a Townsend Discharge by Time-Resolved Mass Spectrometry", Proceedings of the Physical Society (London) 81, pp. 382-384, (1963).

125. McFadden, W. H., "The Mass Spectra of Three Deuterated Propenes", Journal of Physical Chemistry 67, pp. 1074-1077, (1963).

126. McFadden, W. H., Black, D. R., and Corse, J. W., "Further Studies on the Mass Spectra of Butanols. 3-Monodeuterio-1-Butanol and 4-Monodeuterio-1-Butanol", Journal of Physical Chemistry 67, pp. 1517-1519, (1963).

127. McGowan, J. Wm., and Kerwin, Larkin, "Metastable Ar^{+} Ions Near the Ar^{++} Threshold", Canadian Journal of Physics 41, p. 1535, (1963).

128. McGowan, Wm., and Kerwin, Larkin, "On the Application of Aston Bands and Appearance Potentials Measurements to Ion Collision Studies", Canadian Journal of Physics 41, p. 316, (1963).

129. McGowan, Wm., and Kerwin, Larkin, "Some Charge Exchange and Dissociation Collisions of N_2^{2+} Ions", Proceedings of the Physical Society (London) 82, pp. 357-367, (1963).

130. Meeting on Mass Spectrometry, London, December, 1962, British Journal of Applied Physics, 14-4, pp. 169-171, (1963).

131. Meyerson, S., "Organic Ions in the Gas Phase. XIII. Cycloheptatriene-7-d; Decomposition of $C_7H_8^{+}$ and $C_7H_8^{++}$ from Cycloheptatriene and Toluene", Journal of American Chemical Society 85, pp. 3340, (1963).

132. Meyerson, S., Grubb, H. M., and VanderHaar, R. W., "Effects of Isotopic Labeling and Molecular Structure on Probability of Ionization by Electron Impact", Journal of Chemical Physics 39, No. 6, pp. 1445-6, (1963).

133. Meyerson, S., and Hart, H., "Organic Ions in the Gas Phase. XI. Phenylated Cyclopropane Ion in the Decomposition of 3-Phenylpentane", Journal of American Chemical Society 85, pp. 2358, (1963).

134. Meyerson, S., and McCollum, J. D., "Organic Ions in the Gas Phase. X. Decomposition of Benzaldehyde Under Electron Impact", Journal of the American Chemical Society 85, p. 1739, (1963).

135. Moran, T. F. and Friedman, L., "Neon-Hydrogen Ion-Molecule Reactions", Journal of Chemical Physics 39, No. 10, pp. 2491-2500, (1963).

136. Moran, T. F. and Hamill, W. H., "Cross Sections of Ion-Permanent-Dipole Reactions by Mass Spectrometry", Journal of Chemical Physics 39, No. 6, pp. 1413-22, (1963).

137. Morrison, J. D., "On the Optimum Use of Ionization Efficiency Data", Journal of Chemical Physics 39, No. 1, pp. 200-7, (1963).

138. Munson, M. S. B. and Anderson, Robbin C., "Effects of Oxygen and Chlorine on Thermal Reactions of Acetylene", Journal of Physical Chemistry 67, pp. 1582-1586, (1963).

139. Munson, M. S. B., Field, F. H., and Franklin, J. L., "Reactions of Gaseous Ions. XIII. The System Methane-Hydrogen", Journal of the American Chemical Society 85, p. 1384, (1963).

140. Munson, M. S. B., Franklin, J. L., and Field, F. H., "A Mass Spectrometric Study of Homonuclear and Heteronuclear Rate Gas Molecule Ions", Journal of Physical Chemistry 67, pp. 1542-1548, (1963).

141. Narcissi, R. S., Schiff, H. I., Morgan, J. E., and Cohen, H. A., "Calibration of a Flyable Mass Spectrometer for N and O Atoms", Contract AF19(604)8807, Project 6687, 7676, Task 668700, 767302, (AFCRL 63-437), pp. 22, (1963).

142. Nelson, L. C., "An Automatic Liquid Level Controller for Use with Liquid Nitrogen", Journal of Scientific Instruments 40, p. 428, (1963).

143. Nevitt, T. O., and Rondeau, R. E., "Radiation Chemistry of Triple Bond Compounds. Part I: Acetonitrile and Butyne-2, Liquid Phase", Contract AF33(616) 8247, Project 7367, ASD TR 63-144, pt. 1, p. 26, (1963).

144. O'Halloran, G. J., and Fluegge, R. A., "Plasma Analysis with the Bendix Time-of-Flight Mass Spectrometer", Unpublished Work.

145. O'Halloran, G. J., and Wyess, W. R., "The Model 17-Series Bendix Time-of-Flight Mass Spectrometer", Unpublished Work.

146. Ohashi, M., Wilson, J. M., Budzikiewicz, H., Shamma, M., Slusarchyk, W. A., and Djerassi, C., "Mass Spectrometry in Structural and Stereochemical Problems. XXXI. Aporphines and Related Alkaloids", Journal of the American Chemical Society 85, p. 2807, (1963).

147. Onchi, M. and E.M.A., "An Application of the Omegatron Mass Spectrometer to Thermal Decomposition Studies", Journal of Physical Chemistry 67, pp. 2240-2242, (1963).

148. Opanszky, I., "Some Experiences with Different Types of Ion Sources Used for the Isotopic Analysis of the Uranium", Unpublished Work.

149. Opanszky, I. and Zmbov, K. F., Bulletin of the Boris Kidrich Institute of Nuclear Sciences, 14 - 1, p. 293, (1963).

150. Ormrod, J. H. and Duchworth, H. E., "Stopping Cross Sections in Carbon for Low Energy Atoms with $Z \leq 12$", Canadian Journal of Physics 41, p. 1424, (1963).

151. Owens, E. B. and Strauss, Alan J., "Mass Spectrographic Evidence for Deviations from Stoichiometry in GaSb", Lincoln Labs., M.I.T., Lexington, p. 9, (1962).

152. Panish, M. B. and Reif, L., "Thermodynamics of the Vaporization of Hf and HfO: Dissociation Energy of HfO", Journal of Chemical Physics 38, No. 1, pp. 253-6, (1963).

153. Pattillo, A. and Young, H., "Liquid Sample Introduction System for a Mass Spectrometer", Analytical Chemistry 35, 11, p. 1768, (1963).

154. Paulett, G. S. and Ettinger, R., "Mass Spectra and Appearance Potentials of Diazirine and Diazomethane", Journal of Chemical Physics 39, No. 3, pp. 825-7, (1963).

155. Pelah, I., Dattner, J. and Fischler, J., "Mass Abundance Ratiometer for a Single-Beam Mass Spectrometer", Review of Scientific Instruments 34, No. 8, p. 865, (1963).

156. Pelah, Z., Kielczewski, M. A., Wilson, J. M., Ohashi, M., Budzikiewicz, H., and Djerassi, C., "Mass Spectrometry in Structural and Stereochemical Problems. XVII. Mass Spectral Fragmentation Processes and Hydrogen Transfer Reactions of Amides and Amines", Journal of American Chemical Society 85, p. 2470, (1963).

157. Pennsylvania State University, "Crystal Preparation Research", Semi-Annual Technical Summary Report 1, Contract SD-132, p. 34, (1962).

158. Perie, M., Demay, J., and Chemla, M., "Isotopic Analysis of Boron by Thermionic Emission in the Mass Spectrometer", Journal de Chimie Physique 60, pp. 1231-35, (1963).

159. Perry, D. D., "Difluoramine Chemistry", Contract NOnr-187800, Report RMD 076-03-62, p. 23, (1962).

160. Phillips, J. K., "Identification of Rubber Polymers by Mass Spectrometry", Applied Spectroscopy 17, No. 1, pp. 9-11, (1963).

161. Ploch, Werner, Translated by Alan I. Ross, "Mass Dependence in the Emission of Electrons due to Isotopic Ions", Translation No. T-G-169 from Zeitschrift fur Physik 130: 174-195, 1951, Contract AF 19(605)6113, AFCRL 62-840.

162. Pottie, R. F., and Lossing, F. P., "Free Radicals by Mass Spectrometry. XXIX. Ionization Potentials of Substituted Cyclopentadienyl Radicals", Journal of the American Chemical Society 85, p. 269, (1963).

163. Rabideau, Sherman W., "The Oxygen Exchange Reactions of $N_pO_2^{+2}$ and $N_pO_2^{+}$ with Water", Journal of Physical Chemistry 67, pp. 2655-2659, (1963).

164. Rakhovskiy, V. I., Lyubimov, A. P., and Others, "A Device for Measuring Ion Currents in Mass Spectrometer Circuits", Translation No. FTD-TT-62-1529 from Soviet Patent No. 144559 (685696/26), (1960).

165. Redmond, John P., "Kinetics of the Low Pressure Nitrous Oxide Decomposition on Platinum Filament", Journal of Physical Chemistry 67, pp. 788-793, (1963).

166. Reed, R. I., "The Mass Spectra of Some Ferrocenes", Applied Spectroscopy 17, No. 5, p. 124, (1963).

167. Reynolds, F. L., "Ionization on Tungsten Single-Crystal Surfaces", Journal of Chemical Physics 39, No. 4, pp. 1107-8, (1963).

168. Rice, Philip, "Quadrupole Mass Spectrometer", Contract DA44009 Eng. 5127, p. 26, (1963).

169. Ries, Richard R., Damerow, Richard A., and Johnson, Walter H., Jr., "Atomic Masses from Gallium to Molybdenum", Physical Review 132, pp. 1662-1672, (1963).

170. Robertson, A. J. B., Viney, B. W., and Warrington, M., "The Production of Positive Ions by Field Ionization at the Surface of a Thin Wire", British Journal of Applied Physics, 14-5, pp. 278-283, (1963).

171. Robins, J. L., "Mass Peaks from Adsorbed Gases in a Single Focusing M.S.", Canadian Journal of Physics 41, p. 1385, (1963).

172. Rylander, P. M., Meyerson, S., Eliel, E. L., and McCollum, J. D., "Organic Ions in the Gas Phase. XII. Aniline", Journal of the American Chemical Society 85, p. 2723, (1963).

173. Schnabel, W. and Dole, M., "Radiation Chemistry of Isotactic and Atactic Polypropylene. I. Gas Evolution and Gel Studies", Journal of Physical Chemistry 67, pp. 295-299, (1963).

174. Schrader, C. D., "Moon and Planetary Measurements Research Program. Survey of Rocket and Satellite - Borne Mass Spectrometers", Report No. TDR-69(2260-30) TN-1, Contract AF04 (695)69, p. 13, (1962).

175. Schug, J. C., "Investigation of a Fragmentation Model for n-Paraffins", Journal of Chemical Physics 38, No. 11, pp. 2610-5, (1963).

176. Shapiro, I., Keilin, B., Williams, R. E., and Good, David G., "The Carborane Series: $B_nC_2H_{n+2}$. II. The Two Isomers of $B_4C_2H_6$", Journal of the American Chemical Society 85, p. 3167, (1963).

177. Sholette, William P. and Porter, Richard F., "Mass Spectrometric Study of High Temperature Reactions in the Boron-Hydrogen-Oxygen System", Journal of Physical Chemistry 67, pp. 177-182, (1963).

178. Shoonmaker, Richard C., Friedman, Alan H., and Porter, Richard F., "A Mass Spectrometric and Thermodynamic Study of Gaseous Transition Metals (II) Halides", Cornell University, AFOSR TN 59668, p. 14 (1963).

179. Shubin, L. D., Peterson, J. I., and Fitch, R. W., "Sampling of Gaseous Components Contained in Glass Bulbs in Mass Spectrometry", Applied Spectroscopy 17, No. 1, p. 25, (1963).

180. Shvidkovskii, E. G., Martynhevic, G. M., and Malyarova, G. V., "The Effect of Irradiation of Indium by Thermal Neutrons on the Molecular Composition of Its Vapor", Doklady 8-4, pp. 354-371, (1963).

181. Smith, D. F., "Xenon Difluoride", Journal of Chemical Physics 38, No. 1, pp. 270-1, (1963).

182. Snow, W. R., "Research Studies on Analysis of Ionized Gases", Contract DA 49-146-XZ-049, Report #GA-3358, p. 16, (1962).

183. Spittler, E. G., Jordan, P., Dorfman, Leon M., and Sauer, Myran C., Jr., "Isotope Effects in the Mercury-Photosensitized Decomposition and the Direct Radiolysis of the Systems Methane, Methand-d_4 and Butane, Butane-d_{10}", Journal of Physical Chemistry 67, pp. 2235-2237, (1963).

184. Stebbings, R. F., Smith, A. C. H., and Ehrhardt, H., "Dissociative Charge Transfer in He-O_2 and He-N_2 Collisions", Journal of Chemical Physics 39, No. 4, pp. 968-71, (1963).

185. Studier, M., "Continuous Ion Source for a Time-of-Flight Mass Spectrometer", Review of Scientific Instruments 34, 12, pp. 1367-70, (1963).

186. Tracerlab, Inc., "A Study of Techniques for Reactor Effluent Analysis. Tracerlab West Analysis by Methods Including Mass Spectroscopy for U, Be, Mo, Sr, Ru, Cs, Ba, Y, Cd, Np", Contract AF29(601)2852, Proj. 1448, AFSWC, TDR 62-146, p. 70, (1962).

187. Traylor, T. G., "Oxygen-18 Tracer Studies of Alkylperoxy Radicals. II. Kinetic Technique with Mass Spectrometry", Journal of the American Chemical Society 85, p. 2411, (1963).

188. Tsuchiya, T., "Mass Spectrometric Study of Positive Ion Emissions from Iron Oxide Catalysts Containing Alkali Metals", Journal of Chemical Physics 39, No. 3, pp. 828-30.

189. Venkatsubamanian, U. S., and Duckworth, H. E., "The Vacuum Vibrator as a Source of Ions for M.S.", Canadian Journal of Physics 41, p. 234, (1963).

190. Von Zahn, U., "Monopole Spectrometer, a New Electric Field Mass Spectrometer", Review of Scientific Instruments 34, No. 1, p. 1, (1963).

191. vonKoch, H. and Friedman, L., "Hydrogen-Hellium Ion-Molecule Reactions", Journal of Chemical Physics 38, No. 5, pp. 1115-22, (1963).

192. Vreeland, R. W., and Swinehard, D. F., "A Mass Spectrometric Investigation of the Thermal Decomposition of Cyclobutane at Low Pressures", Journal of the American Chemical Society 85, p. 3349, (1963).

193. Warnecke, R. J., "Investigation and Development of a Mass Spectrometer of the Omegatron Type. Its Use for the Detection of Leaks and Analysis of Gases at Low Pressures", Admiralty Centre for Scientific Information and Liaison, 1 Vol. (1962).

194. Wendt, John F. and Cambel, Ali Bulent, "Surface Ionization of Potassium on Tungsten", Journal of Applied Physics 34 - 1, pp. 176-178, (1963).

195. Wexler, S. and Hess, D. C., "Ionization by Ions in the MeV Range", Journal of Chemical Physics 38, No. 9, pp. 2308-9, (1963).

196. White, D., Seshadri, K. S., Dever, D. F., Mann, D. E., and Linevsky, M. J., "Infrared Spectra and the Thermodynamics of Gaseous LiO, Li_2O and Li_2O_2", Journal of Chemical Physics 39, No. 10, pp. 2463-73, (1963).

197. White, F. A., Sheffield, J. C., Rourke, F. M., "A Cascade Mass Spectrometer", Applied Spectroscopy 17, No. 2, pp. 39-44, (1963).

198. Williams, D. H., Wilson, J. M., Budzikiewicz, H., and Djerassi, C., "Mass Spectrometry in Structural and Stereochemical Problems. XXIV. A Study of the Hydrogen Transfer Reactions Accompanying Fragmentation Processes of 11-Keto Steroids. Synthesis of Deuterated Androstan-11-ones", Journal of the American Chemical Society 85, p. 2091, (1963).

199. Wilson, H. W., and Daly, N. R., "Mass Spectrometry of Solids", Journal of Scientific Instruments 40, pp. 273-285, (1963).

200. Wolstenholme, W. A., "Analysis of Gallium by Spark Source Mass Spectrometry", Applied Spectroscopy 17, No. 2, p. 51, (1963).

201. Wong, E. L. and Potter, A. E., Jr., "Reaction Rates of Hydrogen, Ammonia, and Methane with Mixtures of Atomic and Molecular Oxygen", Journal of Chemical Physics 39, No. 9, pp. 2211-7, (1963).

202. Woodward, R. B., "Structural and Synthetic Studies of Tetrodotoxin", Harvard University, Grant DA-CML-18-108-G-45, p. 18, (1962).

203. Woolston, J. R., "Silver Halide Mass Spectrography", David Sarnoff Research Center, Contract DA 36-034-AMC-3789, p. 41, (1962).

204. Zahn, U. V., "An Electric Quadrupole Spectrometer for Precision Mass Determinations", Zeitschr.f.Physik, 168, pp. 129-142, (1962).

205. Zmbov, K. F., "Mass Spectrometric Analysis of Uranium with a Surface Ionization Ion Source", Unpublished Work.

206. Zmbov, K. F., Matic-Vukmirovic, B., and Ilic, M. D., "Investigation of the Active Surface of Zinc Oxide with Oxygen Isotope Exchange with Carbon Dioxide", Unpublished Work.